PROPERTY OF
CHICAGO MIDWAY LABORATORIES

QC
1
P5

PROCEEDINGS

OF THE

PHYSICAL SOCIETY

JULY TO DECEMBER 1959

VOLUME 74

Published by
THE PHYSICAL SOCIETY
1 Lowther Gardens, Prince Consort Road,
London S.W. 7

OFFICERS AND COUNCIL 1959–60

PRESIDENT

J. A. Ratcliffe, C.B.E., M.A., F.R.S.

VICE-PRESIDENTS

who have filled the office of President

Sir Frank Smith, G.C.B., G.B.E., D.Sc., LL.D., F.R.S. (1924–26)
W. H. Eccles, D.Sc., M.I.E.E., F.R.S. (1928–30)
T. Smith, M.A., F.R.S. (1936–38)
Sir Charles Darwin, K.B.E., M.C., M.A., Sc.D., F.R.S. (1941–43)
E. N. da C. Andrade, Ph.D., D.Sc., LL.D., F.R.S. (1943–45)
Sir David Brunt, K.B.E., M.A., Sc.D., F.R.S. (1945–47)
G. I. Finch, M.B.E., D.Sc., F.R.S. (1947–49)
S. Chapman, M.A., D.Sc., F.R.S. (1949–50)
L. F. Bates, D.Sc., Ph.D., F.R.S. (1950–52)
R. Whiddington, C.B.E., M.A., D.Sc., F.R.S. (1952–54)
H. S. W. Massey, B.A., Ph.D., D.Sc., LL.D., F.R.S. (1954–56)
N. F. Mott, M.A., D.Sc., F.R.S. (1956–58)

VICE-PRESIDENTS

K. Mendelssohn, M.A., D.Phil., F.R.S.
R. W. Ditchburn, M.A., B.Sc., Ph.D.
A. J. Philpot, C.B.E., M.A., B.Sc.
G. B. B. M. Sutherland, Sc.D., LL.D., F.R.S.

HONORARY SECRETARIES

C. G. Wynne, B.A., Ph.D. (*Business*)
H. H. Hopkins, D.Sc. (*Papers*)
A. G. Peacock, B.Sc. (*Exhibition*)

HONORARY FOREIGN SECRETARY

E. N. da C. Andrade, Ph.D., D.Sc., LL.D., F.R.S.

HONORARY TREASURER

D. A. Wright, D.Sc.

HONORARY LIBRARIAN

R. W. B. Pearse, D.Sc., Ph.D.

ORDINARY MEMBERS OF COUNCIL

D. Gabor, Dr.Ing., F.R.S.
J. G. Wilson, M.A., Ph.D.
B. H. Flowers, M.A., D.Sc.
M. H. L. Pryce, M.A., Ph.D., F.R.S.
E. W. H. Selwyn, B.Sc.
N. Kemmer, M.A., Dr. Phil., F.R.S.
W. H. George, M.Sc., Ph.D.
R. L. F. Boyd, B.Sc., Ph.D.
W. E. Burcham, Ph.D., F.R.S.
V. E. Cosslett, M.A., M.Sc., Ph.D.
R. A. Smith, M.A., Ph.D.
D. H. Wilkinson, M.A., Ph.D., F.R.S.

OFFICERS OF THE SPECIALIST GROUPS

COLOUR GROUP

Chairman
G. J. Chamberlin
Honorary Secretary
A. W. S. Tarrant

LOW TEMPERATURE GROUP

Chairman
P. H. Sykes, M.Sc., Ph.D.
Honorary Secretary
R. W. Powell, Ph.D., D.Sc.

OPTICAL GROUP

Chairman
K. J. Habell, M.Sc.
Honorary Secretary
W. T. Welford, B.Sc., Ph.D.

ACOUSTICS GROUP

Chairman
T. Somerville, B.Sc.
Honorary Secretaries
G. G. Parfitt, B.Sc., Ph.D., and
R. W. B. Stephens, B.Sc., Ph.D.

SECRETARY-EDITOR

Miss A. C. Stickland, M.Sc., Ph.D.
1 Lowther Gardens, Prince Consort Road, London, S.W.7
(Telephone : KENsington 0048, 0049)

CONTENTS

Part 1 *July* 1959

PAGE

Dr. J. S. Greenhow and Dr. E. L. Neufeld. Measurements of turbulence in the upper atmosphere 1

Mr. J. Maybank and Dr. B. J. Mason. The production of ice crystals by large adiabatic expansions of water vapour 11

Dr. M. Blackman. On the lattice theory of expansion 17

Dr. W. T. Doyle. The selective photoelectric effect 27

Mr. A. N. Prasad. Measurement of ionization and attachment coefficients in dry air in uniform fields and the mechanism of breakdown. 33

Mr. Chatar Singh. Noise spectra of a probe in a hot-cathode discharge . . 42

Dr. V. R. Howes. The critical stress for the production of pressure crack figures on diamond faces 48

Prof. L. F. Bates and Dr. D. J. Sansom. Magnetothermal effects in iron and silicon–iron 53

Dr. J. P. Llewellyn and Dr. T. Smith. The magnetic susceptibility of iron ditelluride. Part I 65

Dr. D. M. Finlayson, Dr. J. P. Llewellyn and Dr. T. Smith. The magnetic susceptibility of iron ditelluride. Part II 75

Mr. C. Hilsum. Properties of p-type indium antimonide. II: Photoelectric properties and carrier lifetime 81

Prof. R. W. Nicholls, Mr. E. M. Reeves and Dr. D. A. Bromley. Excitation of N_2 and O_2 by 1/2 and 1 mev protons 87

Prof. J. M. Cassels, Mr. D. P. Jones, Dr. P. G. Murphy and Mr. P. L. O'Neill. Neutral pions. 92

Dr. L. I. Maissel. Selective pressure broadening and the stark effect . . 97

Dr. A. H. Moussa. The effect of polarization on the elastic scattering of positrons by hydrogen atoms 101

Dr. J. McK. Ellison and Mrs. C. V. Peetz. The forward scattering of light by spheres according to geometrical optics 105

Mr. J. D. Prentice, Dr. E. H. Bellamy and Dr. W. S. C. Williams. The spin of the neutral pion 124

Research Notes:

Dr. T. S. Moss and Mr. A. K. Walton. Determination of the effective electron mass in GaAs by the infra-red Faraday effect 131

Prof. R. W. Nicholls and Mr. W. R. Jarmain. On r-centroids of molecular transitions, equilibrium internuclear separations and oscillator turning points 133

Dr. B. H. Armstrong. Use of fractional parentage coefficients in the calculation of photoelectric cross sections 136

Letters to the Editor:

Mr. A. Lempicki. The reflection spectrum of CdS 138

Corrigendum: Dr. R. S. Longhurst 140

Reviews of Books 141

Part 2 *August* 1959 PAGE

Mr. E. R. Harrison and Dr. W. B. Thompson. The low pressure plane symmetric discharge 145

Mr. R. M. May and the late Dr. M. R. Schafroth. Susceptibility of superconducting spheres 153

Dr. R. D. Connor and Dr. I. L. Fairweather. The β-decay of ^{239}Np . . 161

Prof. L. F. Bates and Dr. P. F. Davis. Direct measurement of domain wall energy 170

Dr. G. D. Archard. Trajectory plotting in electron guns 177

Dr. H. N. V. Temperley. Application of the Mayer method to the melting problem 183

Dr. S. Hinds and Dr. R. Middleton. An investigation of the protons, deuterons and tritons from the bombardment of ^{9}Be with 5·7 MeV ^{3}He 196

Prof. R. Eisenschitz and Mr. A. R. Boot. The thermal conductivity of monatomic dielectric liquids 208

Research Notes:

Dr. B. K. Agarwal. On the thickness of helium films 217

Reviews of Books 219

Part 3 *September* 1959

Dr. L. Mandel. Fluctuations of photon beams: The distribution of the photo-electrons 233

Dr. J. C. Woolley, Mr. J. A. Evans and Mr. C. M. Gillett. Optical energy gap variation in the GaSb–InSb system 244

Mr. D. A. Jones, Dr. J. M. Baker and Mr. D. F. D. Pope. Electron spin resonance of Gd^{3+} in lanthanum fluoride 249

Dr. K. Phillips and Mr. K. R. Allen. The scattering of fast charged particles: V—Multiple scattering of fast electrons and positrons in xenon 257

Prof. E. Wolf. A scalar representation of electromagnetic fields: II . . 269

Dr. P. Roman. A scalar representation of electromagnetic fields: III . . 281

Dr. M. M. Newmann and Prof. K. W. H. Stevens. Magnetic susceptibilities of iron–chromium alloys 290

Mr. E. Kuffel. Electron attachment coefficients in oxygen, dry air, humid air and water vapour 297

Prof. J. M. Somerville and Mr. J. F. Williams. The early stages of spark channel expansion 309

Mr. M. Nunn and Dr. C. G. Wynne. Lens designing by electronic digital computer: II 316

Dr. B. R. Judd. The matrix elements of tensor operators for the electronic configurations f^n 330

Dr. G. L. Sewell. The Meissner effect, gauge invariance and electron correlations 340

Dr. S. P. Rosen. On the electron coincidence spectrum in double beta decay . 350

Mr. R. T. Bate and Mr. R. K. Willardson. Hall coefficient and magnetoresistance in semiconducting diamond 363

Dr. R. Cade. The equilibrium of a double layer 368

Research Notes:

Prof. J. M. Somerville. A method of generating pairs of millimicrosecond current pulses separated by a variable interval 378

Reviews of Books 380

Part 4 *October* 1959

PAGE

Dr. T. E. Peacock and Dr. R. McWeeny. A self-consistent calculation of the graphite π band 385

Mr. D. H. Lindley and Dr. P. C. Banbury. Recombination relaxation effects in germanium surfaces 395

Dr. G. P. Srivastava. Absorption of microwaves in ethyl chloride 401

Dr. K. Luszczynski and Dr. J. G. Powles. Proton magnetic resonance in liquid *iso*-butyl bromide 408

Dr. J. C. Walling and Mr. P. B. Bunn. The electronic specific heats of some nickel–cobalt alloys 417

Dr. A. P. Stone. Interpretation of isotope shifts in the rare gases 424

Dr. H. N. V. Temperley. On the asymptotic behaviour of the Mayer cluster series in the antiferromagnetic problem 432

Dr. H. N. V. Temperley. Can the ' lattice ' model of a gas describe both liquefaction and solidification ? 444

Mr. N. J. Freeman. The decay of ^{144}Ce 449

Mr. A. F. Ferguson and Dr. B. L. Moiseiwitsch. Double charge transfer and the mobility of He^{2+} ions in helium 457

Dr. M. R. C. McDowell and Miss G. Peach. Electron loss from fast negative ions of atomic hydrogen passing through atomic hydrogen 463

Dr. D. T. Stewart and Mr. E. Gabathuler. Electron Collision Cross Sections in Helium 473

Research Notes:

Mr. R. Jakeways and Dr. W. G. V. Rosser. The decay of ^{147}Pm . . 478

Mr. J. G. Gilson. Vacuum polarization due to charged bosons 480

Mr. J. V. Allaby, Dr. A. Ashmore, Dr. A. N. Diddens and Mr. J. Eades. A measurement of the spin correlation coefficient C_{nn} in p–p scattering at 320 mev, for 90° centre of mass scattering angle 482

Mr. H. C. Evans and Dr. E. H. Bellamy. The response of plastic scintillators to protons 483

Dr. P. T. Landsberg. The entropy of a non-equilibrium ideal quantum gas 486

Letters to the Editor:

Mr. C. H. L. Goodman. Bonding in cadmium telluride 489

Dr. T. S. Moss. The extent of ionic binding in cadmium telluride . . 490

Mr. J. W. Searl, Mr. R. C. Smith and Dr. S. J. Wyard. Electron spin resonance for polycrystalline substances 491

Corrigendum : Prof. B. Bleaney 493

Reviews of Books 494

Part 5 *November* 1959

Dr. R. W. Crompton and Dr. M. T. Elford. The mobility of potassium ions in nitrogen and neon at 29° K 497

Dr. R. F. Pearson. The magnetocrystalline anisotropy of cobalt-substituted manganese ferrite 505

Dr. J. G. Park. The principal g values of ytterbium ions in yttrium acetate, a triclinic crystal 513

Mr. T. Honda and Dr. M. Nagasaki. On the angular distribution of (d, p) stripping reactions 517

Mr. A. C. Butcher and Mr. J. M. McNamee. The scattering of alpha particles by helium 529

PAGE

Dr. W. T. Doyle, Dr. D. J. E. Ingram and Mr. M. J. A. Smith. Electron spin resonance of colloid centres in lithium hydride 540

Dr. P. G. Harper. Electron–lattice interaction in metals. 545

Dr. E. W. Kellermann and Dr. N. Dickinson. On the structure of extensive cosmic ray air showers : The penetrating component 554

Prof. K. W. H. Stevens and Dr. B. Josephson, Jr. The coupling of a spin system to a cavity mode 561

Mr. M. G. Haines. The inverse skin effect 576

Dr. R. B. J. Palmer and Dr. H. A. B. Simons. The experimental determination of the range–energy relations for alpha particles in water and water vapour, and the stopping power of water and water vapour for alpha particles at energies below 8·78 Mev 585

Dr. R. Mansfield. The magnetic susceptibility of bismuth telluride . . 599

Mr. A. K. Dutta. An analysis of the soft x-ray emission spectroscopy of graphite and an appropriate electronic picture of it 604

Dr. J. Spreadborough and Dr. J. W. Christian. The measurement of the lattice expansions and Debye temperatures of titanium and silver by x-ray methods . 609

Dr. V. R. Howes. Observations on the development of electroplating deposit structures on single crystals of copper 616

Dr. J. D. Dowell, Mr. W. R. Frisken, Dr. G. Martelli and Dr. B. Musgrave. Proton–proton elastic interactions at 930 Mev 625

Mr. J. F. Barry, Mr. R. F. Coleman, Mr. B. E. Hawker and Dr. J. L. Perkin. Cross sections for some (n, pn) reactions with heavy nuclides 632

Research Notes :

Mr. G. N. Spokes and Dr. A. G. Gaydon. Flame spectra : the effect of deuteration on the hydrocarbon flame bands 639

Dr. Lee Sang Soo. Ageing effect in evaporated films of zinc sulphide . . 641

Prof. H. Fröhlich and Dr. G. L. Sewell. Electric conduction in semiconductors 643

Dr. F. A. Raal. A strong absorption system in type I diamonds . . . 647

Dr. P. Roman. Decomposition of 3×3 matrices. 649

Dr. R. J. N. Phillips. Nucleon polarization from charge-exchange reactions in deuterium 652

Dr. K. Phillips and Mr. C. Ambasankaran. The scattering of fast charged particles VI : The multiple scattering of 10 Mev electrons and positrons in nuclear emulsions 655

Dr. K. W. Allen, Dr. D. Eccleshall and Mr. M. J. L. Yates. 1·12 Mev level in ^{18}F 660

Letters to the Editor :

Mr. D. Boakes, Dr. G. Garton, Mr. D. Ryan and Dr. W. P. Wolf. Paramagnetic resonance of Yb^{3+} in yttrium gallium garnet 663

Dr. W. P. Wolf. Magnetic properties of rare earth ions in garnets . . 665

Dr. C. Hilsum. The absorption edge of arsenic–sulphur–selenium mixtures . 667

Mr. A. Trainor and Mr. P. T. Harris. The control of resistivity in pulled silicon crystals 669

Dr. J. A. Lee, M. G. T. Meaden and Dr. K. Mendelssohn. Low temperature resistivity of plutonium and neptunium 671

Corrigendum : Dr. R. D. Connor and Dr. I. L. Fairweather 671

Reviews of Books 671

PAGE

Dr. D. K. Thomas and Mr. T. W. Baker. An x-ray study of the factors causing variation in the heats of solution of magnesium oxide 673

Dr. D. C. Champeney and Mr. C. A. Miller. Measurements of atomic velocity distributions in Hg and HgO by the nuclear resonant scattering of gamma rays. 680

Dr. J. F. Barry, Mr. L. P. O'Connor and Dr. J. L. Perkin. The radiative capture cross section of ^{232}Th for neutrons in the energy range 300 to 1200 kev . . 685

Dr. F. M. Kelly and Mr. E. Tomchuk. Isotope shift in the CdI intercombination resonance line λ 3261 Å 689

Dr. R. E. Meads and Mr. J. E. G. McIldowie. The decay of arsenic 80 . . 693

Mr. N. J. Phillips. The current sheet in a gas discharge 700

Mr. M. A. Al-Jeboori, Mr. M. S. Bokhari, Dr. B. Hird and Mr. A. Strzałkowski. The polarization of protons elastically scattered from oxygen at 8·7 mev . . 705

Mr. A. S. Chakravarty. On the magnetic susceptibility and anisotropy of trivalent vanadium alum under the crystalline electric field having predominantly cubic symmetry with a small trigonal symmetry 711

Mr. A. S. Marathay. Geometrical optical calculation of frequency response for systems with coma 721

Dr. A. K. Head. Aplanatic lenses 731

Dr. G. B. F. Niblett and Dr. T. S. Green. Radial hydromagnetic oscillations . 737

Dr. B. J. Mason and Mr. A. P. van den Heuvel. The properties and behaviour of some artificial ice nuclei 744

Dr. D. C. Northrop. Conduction processes in condensed aromatic hydrocarbons. 756

Dr. S. Hinds and Dr. R. Middleton. The angular distribution of some proton groups from the reaction ^{16}O(^{3}He, p)^{18}F 762

Research Notes:

Mr. W. R. George, Dr. R. Sharples and Dr. J. E. Thompson. The sintering of bismuth telluride 768

Prof. D. V. Gogate and Mr. H. S. Desai. Heat transfer by forced convection. 770

Dr. L. Mackinnon, Dr. A. Myers and Mr. M. T. Taylor. The effect of the direction of a transverse magnetic field on the electronic component of ultrasonic absorption in a lead single crystal. 773

Dr. S. Hinds and Dr. R. Middleton. Some angular distribution measurements on the reactions ^{16}O(^{3}He, d)^{17}F and ^{16}O(^{3}He, α)^{15}O . . . 775

Dr. S. Hinds and Dr. R. Middleton. The energy levels of ^{21}Ne . . 779

Dr. V. L. Telegdi and Dr. R. Winston. Comments on Faragó's treatment of spin precession in crossed magnetic and electric fields 782

Mr. E. D. Isaac. Domain structures on thin sheets of magnetoplumbite . 786

Letters to the Editor:

Dr. J. N. Dodd, Mr. W. N. Fox, Dr. G. W. Series and Mr. M. J. Taylor. Light beats as indicators of structure in atomic energy levels . . . 789

Dr. A. H. Cooke, Dr. D. T. Edmonds, Mr. C. B. P. Finn and Dr. W. P. Wolf. Dipolar ferromagnetism in dysprosium ethyl sulphate 791

Dr. R. Parker and Mr. H. Lord. The electrical resistivity of oxygen deficient nickel ferrite 793

Corrigendum : Dr. G. L. Rogers 795

Reviews of Books 796

Subject Index, Vol. 74 801

Index to Authors (with Titles), Vol. 74 806

Index to Reviews of Books, Vol. 74 813

PROCEEDINGS OF
THE PHYSICAL SOCIETY

VOL 74, PART 1 1 July 1959 No. 475

Measurements of Turbulence in the Upper Atmosphere

BY J. S. GREENHOW AND E. L. NEUFELD
Jodrell Bank Experimental Station, University of Manchester

Communicated by A. C. B. Lovell; MS. received 30th January 1959

Abstract. The structure of turbulence in the 80–100 km region above the earth has been investigated by the simultaneous measurement of wind velocities at two points along a meteor trail. The fall off in correlation between the wind velocities at the two points, as their separation is increased, has been used to obtain a measure of the eddy size. The turbulence is found to be distinctly anisotropic, the vertical scale of the large eddies being 7 km whilst their horizontal extent is of the order of 150 km. The size of the smallest eddies is found to be approximately 50 m. Mean wind shears of 10 m sec^{-1} km^{-1} are found with a maximum of 140 m sec^{-1} km^{-1}. No significant difference between day and night time turbulence is found.

§ 1. INTRODUCTION

THE visual observation of noctilucent clouds and persistent meteor trains has shown that turbulent winds exist at heights of 80–100 km. These events are rare, and it is difficult to make quantitative measurements of turbulence using such effects.

Radio echo observations, on the other hand, have provided a powerful method of investigating both the uniform and irregular winds in the 80–100 km region (Greenhow 1950, 1952, 1954, Elford and Robertson 1953, Greenhow and Neufeld 1955 a). Mean wind speeds of the order of 30 m sec^{-1} are observed, yet at any instant the velocities at points separated by a few kilometres may differ by as much as 50 m sec^{-1}. Turbulent winds of r.m.s. velocity 25 m sec^{-1} are generally present, even when the mean wind speed is zero. Similar results have been obtained by the photographic observations of bright meteors (Liller and Whipple 1954).

This paper describes an experiment designed to investigate the turbulent structure by the simultaneous measurement of wind velocity at two points of variable separation in space. The fall off in correlation between the velocities as the separation of the points is increased gives a measure of the large scale eddy size, whilst the difference between the velocities gives the magnitude of the wind shear.

§ 2. TECHNIQUE

2.1. *Use of Two Stations*

The measurement of wind velocity simultaneously at two points in space may be achieved by observation of the drift of two points on the same meteor trail. In order to obtain radio echoes from different parts of the same trail it is necessary to employ widely spaced receiving stations. Therefore, in addition to the home station at Jodrell Bank, one of two remote stations at Siddington (3·6 km to the East) and at the Cat and Fiddle Inn (20 km to the East) was used.

In figure 1, consider any meteor travelling along the path AB. Due to the specular reflecting properties of meteor trails, the echoes received at O and C will come from points X and Y respectively. If V is the velocity of the meteor and T the time taken for it to travel from X to Y, the separation along the trail of the echoing points is $XY = VT$.

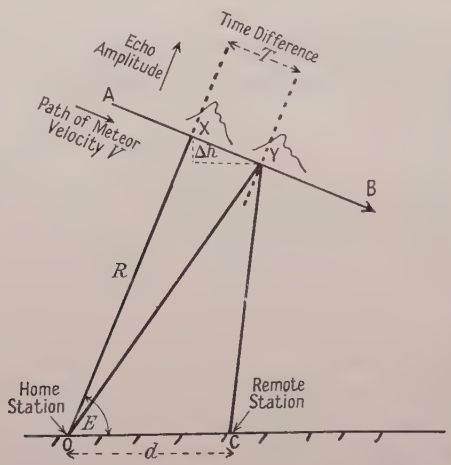

Figure 1. Diagram illustrating the reception of radio echoes from a single trail at two receiving stations.

A narrow beamed transmitting aerial will restrict the majority of echoes to approximately easterly azimuths. In this case, the height separation Δh between X and Y for a meteor trail at any inclination to the vertical east–west plane is given by

$$\Delta h = \frac{2(VT)^2}{d} \cot E \qquad \ldots\ldots (1)$$

where d is the distance between O and C, and E the elevation of the echoing points.

It can be seen that VT may vary between zero for a vertical trail or for one at right angles to the vertical east–west plane, and $d/2$ for a horizontally travelling meteor in the east–west plane. Δh, however, is zero for both these cases and reaches a maximum at $E = 45°$. For the Siddington spacing the maximum value of Δh is 0·9 km and for the Cat and Fiddle it is 5 km.

For this system echoes at O should always be received before those at C with a time difference T between reception of the echoes. (The efficiency of the system is shown by the fact that only 5% of the echoes were received at C before appearing at O. This shows that side-lobes of the aerial system were of negligible importance.) A few random coincidences due to the two separate meteor trails were also obtained, but these could be distinguished by differences in range and were rejected.

The velocity V of the meteor is obtained to an accuracy of about $\pm 20\%$ by measuring the rate of rise of echo amplitude as the meteor crosses the specular reflecting point and, in the cases of the slower meteors only (due to the low pulse repetition frequency used), from the diffraction fluctuations (Davies and Ellyett 1949).

The elevation E is obtained to within 2 or 3° from the range and height of the echo, the height being estimated from the echo decay times (Greenhow and Neufeld 1955 b).

2.2. *Apparatus*

A coherent pulse transmitter was situated at the home station (O in figure 1) and operated at a pulse repetition frequency of 300 per second with a 30 μsec pulse length. The peak power was 50 kilowatts and the frequency 36·3 Mc/s. The transmitting aerial pointed eastward over the remote stations and consisted of an array of four Yagis inclined at 45° to the horizontal, giving a beamwidth of $\pm 25°$ to the first zero. The receiving aerials at the home station and at the remote station (C in figure 1) consisted of identical single half-wave folded dipoles with reflectors, looking eastward. These aerials were horizontally polarized and were at heights of half a wavelength above the ground.

Measurements of wind velocity entail the comparison of the phase of successive echo pulses with a reference signal of fixed phase (Greenhow 1954). Thus it was necessary to preserve the phase of the echo signal received at the remote station, while transmitting it to the home station by radio link for phase comparison with the transmitted wave.

The receiver at C was a conventional superheterodyne, the local oscillator being crystal controlled. The final stage of the i.f. amplifier was coupled directly to an aerial, and the undetected signal transmitted back to O. To preserve coherency it was also necessary to send back the local oscillator frequency, so that the original 36·3 Mc/s could be reproduced. The local oscillator frequency F was chosen so that its second harmonic lay within the i.f. bandwidth of the receiver at C. Thus the second harmonic of the local oscillator was also transmitted to O via the same transmitting aerial and receiver output.

At O the second harmonic continuous wave signal was frequency divided and, after re-combining with the incoming i.f. signal, a signal coherent with the original 36·3 Mc/s signal was obtained. Beyond this point the receiving and phase measuring systems were similar to that used for single station work (Greenhow 1954).

A switched pre-amplifier enabled echo pulses received at O and C to be accepted alternately. After passing through the same amplifying, phase reference and video channels, they were recorded on switched beam cathode ray tubes. The recording system was similar to that described previously apart from the beam-switching. Alternate pulses from O and C thus appeared at 150 pulse repetition frequency on the upper and lower traces of each tube respectively as shown in figure 2. Tube K shows the range of the echoes, 50 km markers also appearing on the trace. Tube L shows the amplitudes of the echoes received at O (upper trace) and at C (lower trace). The markers at the base of the signals correspond to 1/50 second. The time difference between the amplitude maxima for echo P at O and C is $T = 0{\cdot}05$ second. The velocity of the meteor calculated from the rate of rise and range is $V = 24$ km sec^{-1}. The mean elevation of the reflecting points, obtained from the range $R = 190$ km and duration of the echo, is 30°. Hence, $VT = 3{\cdot}4$ km and $\Delta h = 2{\cdot}1$ km. Tube M shows the changes in phase of the echoes at O and C and enables the wind velocities to be calculated. The reference signal at M is in phase quadrature with that at N so that the direction of the drift—to or from the station—can be determined (Manning, Villard and

Peterson 1950). This echo shows a drift of 0·0 m sec^{-1} for the home station and 55 m sec^{-1} for the remote station, a wind shear of 26 m sec^{-1} km^{-1}. The wind shear of 4 m sec^{-1} km^{-1} determined from echo Q is very much less than this, as the two velocity measurements differ by only 16 m sec^{-1} over a height difference of 4 km.

§ 3. Results

3.1. *Correlation between Velocities at the two Echoing Points*

3.1.1. *Definition and determination of correlation coefficients.*

In order to obtain a measure of the largest eddy size it is necessary to find statistically the correlation between the velocities at two points in space, and to observe how the correlation falls off as the separation of the points is increased. The separation corresponding to zero correlation coefficient gives an estimate of the eddy size.

Apart from the turbulent winds present there are also the quasi-steady horizontal components. In order to allow for these, the mean horizontal wind $\bar{u}$ during one hour is obtained by averaging all the measured velocities. The deviations of the individual wind velocity components at O and C from the radial components $\bar{u}_r$ of the steady wind along their directions are then obtained for each echo pair in that hour.

This gives values for the turbulent wind components

$$\delta u_O = \bar{u}_r - u_O \qquad \text{and} \qquad \delta u_C = \bar{u}_r - u_C$$

where u_O, u_C are the velocities at O and C respectively and δu_O and δu_C their deviations from the mean component $\bar{u}_r$.

The lateral correlation coefficient g is then given by

$$g = \frac{\Sigma \delta u_O \delta u_C}{(\Sigma \delta u_O{}^2 \Sigma \delta u_C{}^2)^{1/2}} \qquad \ldots\ldots (2)$$

and the experimental error in g is

$$\delta g = \frac{1-g^2}{(n-1)^{1/2}} \qquad \ldots\ldots (3)$$

where n is the number of values of δu_O, δu_C.

3.1.2. *Variation of correlation coefficient with spatial separation.*

Approximately 600 echo pairs were obtained between the home and Cat and Fiddle stations and 300 pairs for the home and Siddington stations. For Siddington a mean separation VT of 0·67 km was taken, while for the Cat and Fiddle eight different separations between 0·6 and 7·8 km were used. A list of separations VT and corresponding values of correlation coefficient is given in the table. g is plotted against VT in figure 3 (*a*).

g is seen to decrease as VT increases up to a separation of approximately 6 km. For separations greater than this g remains constant at 0·2. For the case of isotropic turbulence, g would be expected to fall off steadily to zero and then become slightly negative, as the separation is increased. This behaviour is apparently not observed for turbulence in the 80–100 km region. In order to investigate any

anisotropy, the variation of g with vertical separation, irrespective of horizontal separation, will now be considered.

Correlation Coefficient g as a Function of Spatial Separation and Height Separation of Pairs of Reflecting Points

(1)	(2)	(3)	(4)	(5)
0·6	0·25	39	0·96	±0·01
0·67†	0·43†	319†	0·92†	±0·01†
1·5	0·6	76	0·85	±0·02
2·5	1·3	88	0·63	±0·04
3·5	2·2	101	0·51	±0·05
4·5	3·3	104	0·34	±0·07
5·5	4·3	86	0·22	±0·09
6·5	4·5	44	0·22	±0·11
7·8	4·3	72	0·28	±0·08

(1) Separation along a trail VT (km); (2) height differences Δh (km); (3) number of values (n); (4) correlation coefficient g; (5) error in g. † Siddington.

3.1.3. *Variation of correlation coefficient with height separation.*

As shown in § 2.1. the maximum possible height differences for pairs of meteor echoes are observed for meteor trails at an elevation of 45°. At elevations below 45° both the spatial and vertical separations fall to zero. Above 45°, on the other hand, although the spatial separation continues to increase to a maximum of 10 km for a horizontally travelling meteor, the height separation Δh decreases to zero.

If g is now plotted against Δh the correlation curve of figure 3 (*b*) is obtained. The three points corresponding to $VT = 5{\cdot}5$, 6·5, 7·8 km show no significant differences in their values of Δh (i.e. 4·5 km) and the unusual behaviour of the correlation curve is removed. Extrapolation of the curve in figure 3 (*b*) shows that the vertical extent of the eddies is approximately 7 km. The behaviour of the correlation curve in figure 3 (*a*) can thus be explained if the fall off in correlation with horizontal separation is less rapid than with vertical separation.

Because of this slow fall off in correlation horizontally, compared with the vertical fall off, it is difficult to make an accurate estimate of the horizontal dimensions of the eddies. However if echo pairs of the same height difference but different spatial separations are compared, an estimate of the rate of fall off in correlation horizontally may be made. This shows that there is a 75% probability that the horizontal extent of the eddies exceeds 60 km with a most probable size of the order of 150 km. This is an order of magnitude greater than the vertical depth. (Further evidence for the existence of eddies of this type will be given in a later paper on large scale wind systems.)

3.1.4. *Diurnal variation of turbulence.*

The variation of g with height separation for daytime and night time is shown in figure 4. The mean curve of figure 3 (*b*) is superimposed for comparison. In view of the errors of measurement, there are no significant differences between the two sets of points and the mean curve. Thus the scale of turbulence is appreciably the same during the night as during the daytime. Similarly, the observed wind shears do not differ significantly between day and night.

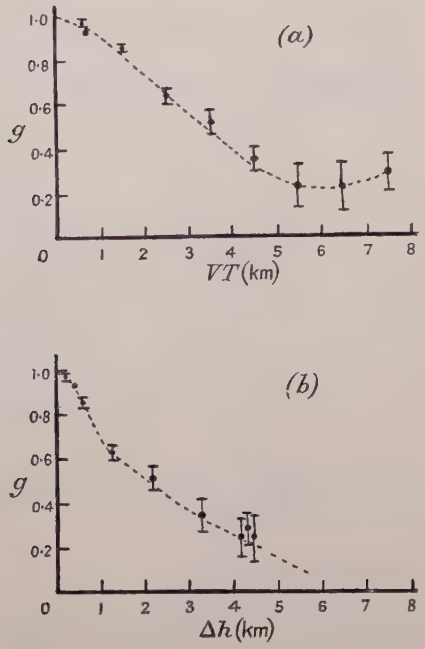

Figure 3. Variation of correlation coefficient g with (*a*) spatial separation VT, (*b*) difference in height Δh.

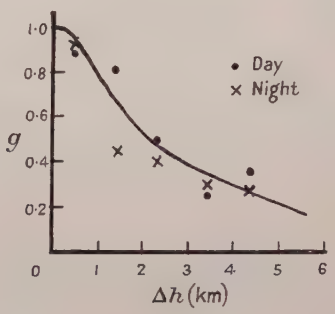

Figure 4. Variation of correlation coefficient g with height difference during day and night. The mean curve of figure 3 is shown for comparison with the day and night time points.

3.1.5. *The small scale turbulence.*

The separation over which the correlation falls significantly from unity gives a measure of the smaller eddies. In particular the dissipation length parameter λ is given by fitting a parabola of the form

$$g = 1 - \frac{(\text{Separation})^2}{\lambda^2} \qquad \ldots\ldots (4)$$

to the first part of the correlation curve. Although the large scale turbulence is distinctly anisotropic, the anisotropy will decrease for smaller eddy sizes. If the smaller eddies of scale λ are isotropic, then the value of λ can be derived from figure 3 (*a*). If some degree of anisotropy is still present, this value will give a lower limit for λ.

The dissipation length parameter λ may be used to relate the scale of the smallest eddies η to that of the largest eddies L, using the relation (Townsend 1956)

$$\eta^2 = \lambda^3/10\sqrt{15}\,L. \qquad \ldots\ldots (5)$$

λ is found to be 2·4 km and for a value of L of 150 km, η is approximately 50 metres.

3.2. *Dependence of Turbulent Velocity upon Mean Wind Shear and Mean Wind Speed*

The turbulent velocities cover a wide spectrum from large positive to large negative values. The r.m.s. turbulent velocity V can be calculated from values of $\Sigma\delta u_0^2$ and $\Sigma\delta u_c^2$ (§ 3.1.1) and the mean values are found to be 28 m sec^{-1} for daytime and 23 m sec^{-1} for night observations, with an average of 25 m sec^{-1}.

A search was made for any dependence of r.m.s. turbulent velocity upon (i) mean hourly wind speed at a given height (ii) height gradient of the mean hourly wind speed. Scatter diagrams relating the turbulent wind velocity to wind speed and wind gradient are given in figure 5 (*a*) and (*b*). It can be

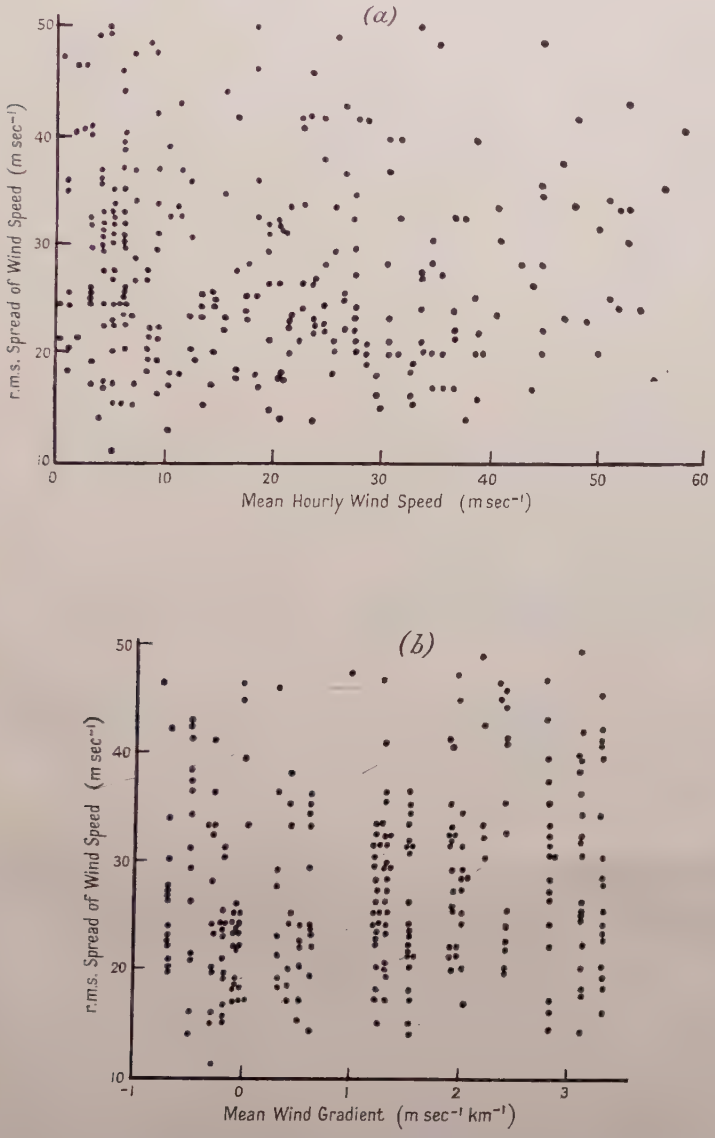
(a)
r.m.s. Spread of Wind Speed (m sec⁻¹)
Mean Hourly Wind Speed (m sec⁻¹)
(b)
r.m.s. Spread of Wind Speed (m sec⁻¹)
Mean Wind Gradient (m sec⁻¹ km⁻¹)

Figure 5. Scatter diagrams showing lack of correlation between r.m.s. turbulent velocity and (*a*) mean wind speed, (*b*) mean height gradient of wind.

seen that there is no variation of r.m.s. turbulent velocity for variations of mean wind speed from 0 to 50 m sec^{-1}; thus even when the mean wind speed is zero turbulent velocities as high as 40 m sec^{-1} are observed. Similarly, there is no dependence of turbulent velocity upon height gradient of the mean wind for negative gradients of 1 m sec^{-1} km^{-1} up to positive gradients of 3 m sec^{-1} km^{-1}.

3.3. *Wind Shears*

In the previous section we have been concerned only with the scale of the turbulence and the r.m.s. velocities. The wind shears associated with the turbulence will now be considered. 750 pairs of echoes for the Siddington base-line have been used to investigate the velocity differences across a mean height separation of 0·43 km. A histogram of the wind shears measured in this way, expressed in m sec^{-1} km^{-1}, is shown in figure 6. The velocity differences are taken irrespective of sign. Wind shears between 0 and 140 m sec^{-1} are observed, with a median value of 10 m sec^{-1} km^{-1}. Of the 750 shears, 7% are greater than 36 m sec^{-1} km^{-1} and approximately 1% greater than 72 m sec^{-1} km^{-1}.

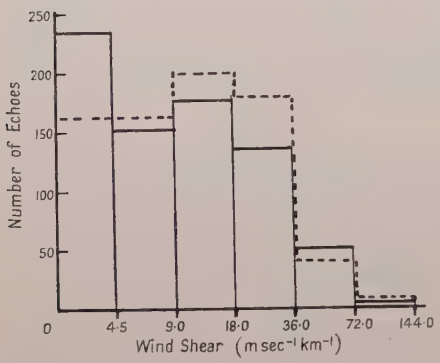

Figure 6. Wind shears in m sec^{-1} km^{-1} measured over a height separation of 0·43 km: continuous lines, radio echo observations; broken lines, photographic meteor observations.

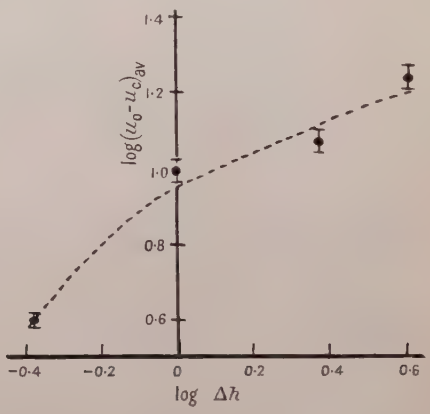

Figure 7. Variation of $\log (u_O - u_C)_{av}$ with $\log \Delta h$. $(u_O - u_C)_{av}$ is in m sec^{-1} and Δh is in km.

The wind shear is not independent of the height difference, as the mean velocity difference between two points is not a linear function of the height separation. Clearly a wind shear of 30 m sec^{-1} km^{-1} could not persist over a very large height range. The echoes obtained for the Cat and Fiddle baseline have therefore been used to plot similar histograms of velocity differences for height separations up to 4·0 km. The variation of the mean velocity difference $(u_O - u_C)_{av}$ with Δh can then be investigated, and $\log (u_O - u_C)_{av}$ is plotted against $\log \Delta h$ in figure 7. A smooth curve has been drawn through the points. For the case of isotropic turbulence, Kolmogoroff's spectrum law (1942) is expected to hold for large values of Reynolds number, where Reynolds number is given by $R = (LV/\nu)$ where L is the eddy size and ν the kinematic viscosity. In this region $\nu \sim 10^5$ cm^2 sec^{-1}. Hence $R \sim 2 \times 10^4$. We would thus expect the Kolmogoroff Law to be obeyed. Von Weizsäcker (1949) has shown that if the law holds $(u_O - u_C)_{av} \propto \Delta h^{1/3}$.

It thus appears from the broken line in figure 7, that the turbulence does not follow Kolmogoroff's law closely. This behaviour might be expected from the distinctly anisotropic nature of the eddies discussed in § 3.1.

3.4. *Comparison with Other Observations*

From the photographic observation of the distortion occurring in the trains of bright meteors, Liller and Whipple (1954) have investigated turbulence in the 80 to 100 km region. Estimates of the scale of the larger eddies are similar to those discussed in § 3, but figures quoted for the wind shear are considerably larger than the median value of 10 m sec $^{-1}$ km $^{-1}$ found by radio observations. An average maximum wind shear of 50 m sec^{-1} km^{-1} is given. However, if the Liller and Whipple plots of wind velocity against height are analysed to give values of the wind shear over the same separation as the Siddington echo pairs (0·43 km) the dotted histogram in figure 6 is obtained. It can be seen that there is very little difference between the two histograms. Thus the figure of 50 m sec^{-1} km^{-1} is somewhat misleading unless it is borne in mind that such a shear may only be observed at one point along an individual meteor trail, which may be 30 km in length. Thus the probability of observing a wind shear as high as 50 m sec^{-1} km^{-1}, at any given time and place, is less than 0·05.

§ 4. Discussion

It has been shown that the region between altitudes 80 to 100 km is extremely turbulent. The large scale turbulence is anisotropic, the vertical scale being of the order of 7 km while the horizontal scale is of the order of 150 km. In this height region there exists a high positive temperature gradient. Thus it would be expected that turbulence would be severely inhibited and that conditions would be quite stable. The presence of such intense irregular winds is therefore surprising. The energy associated with the turbulence of r.m.s. velocity 25 m sec^{-1} is of the same order as the uniform wind components, which have similar velocities. However, at times when the mean wind speed is zero, the r.m.s. velocity is still as high as 25 m sec^{-1} and on these occasions all the energy is associated with the turbulent winds. Similarly, there is no correlation between the degree of turbulence and the mean wind shears, as might be expected. Thus the turbulence is of a very unusual form and this is shown by the extremely anisotropic nature of the large eddies. Vertical wind components are extremely small and it is only possible to set an upper limit of 1 to 2 m sec^{-1} for the r.m.s. vertical velocities. Vertical mixing is therefore largely inhibited, although the wind velocities in horizontal planes separated by only 0·4 km may differ by up to 20 m sec^{-1}. In view of these observations it seems likely that the large flat eddies are caused by horizontal disturbances, due for example to horizontal temperature gradients, while the vertical turbulence remains severely damped.

Acknowledgments

This work was carried out at the Jodrell Bank Experimental Station, of the University of Manchester. The authors wish to thank the Director of the Station, Professor A. C. B. Lovell, for his interest in the investigation, and their colleague Dr. H. P. Palmer for his cooperation at the distant site.

References

Davies, J. G., and Ellyett, C. D., 1949, *Phil. Mag.*, **40**, 614.
Elford, W. G., and Robertson, D. S., 1953, *J. Atmos. Terr. Phys.*, **4**, 271.
Greenhow, J. S., 1950, *Phil. Mag.*, **41**, 682.
—— 1952, *J. Atmos. Terr. Phys.*, **2**, 282.
—— 1954, *Phil. Mag.*, **45**, 471.
Greenhow, J. S., and Neufeld, E. L., 1955 a, *Phil. Mag.*, **46**, 549.
—— 1955 b, *J. Atmos. Terr. Phys.*, **6**, 133.
Kolmogoroff, A. N., 1941, *C. R. Acad. Sci. U.S.S.R.*, **30**, 301.
Liller, W., and Whipple, F. L., 1954, *Spec. Suppl., J. Atmos. Terr. Phys.*, **1**, 112.
Manning, L. A., Villard, O. G., and Peterson, A. M., 1950, *Proc. Inst. Radio Engrs, N. Y.*, **38**, 877.
Townsend, A. A., 1956, *The Structure of Turbulent Shear Flow* (Cambridge: University Press).
von Weizsäcker, C. F., 1949, *Proceedings of the Symposium on the Motions of Gaseous Masses of Cosmical Dimensions*, Paris (U.S. Central Air Documents Office).

The Production of Ice Crystals by Large Adiabatic Expansions of Water Vapour

By J. MAYBANK and B. J. MASON
Imperial College, London

MS. received 5th March 1959

Abstract. The numbers of ice crystals produced by the explosive expansion of a small volume of moist air have been determined for various values of the terminal temperature and supersaturation. In clean air crystals, formed by spontaneous condensation followed by homogeneous crystallization, appeared only when the supersaturation exceeded 400% and the terminal temperature fell below $-40°$C. Thereafter, the crystal concentration continuously increased up to a maximum of $4 \times 10^6/\text{cm}^3$ and not to about $10^{11}/\text{cm}^3$ as reported by Schaefer. The appearance of crystals at temperatures above $-40°$C in room air may be attributed to the presence of ice nuclei. No evidence was obtained for a sudden increase in the crystal production or a change in their mode of formation at about $-65°$C as suggested by expansion chamber experiments of other workers.

§ 1. Introduction

These experiments, in which ice crystals were produced by the explosive expansion of a small volume of moist air, were carried out for the following reasons:

(i) To ascertain whether a new phase transition occurs when water-saturated air is suddenly cooled below $-60°$C, i.e. well below the $-40°$C limit associated with the homogeneous nucleation of micron-size water droplets. Suggestions that ice crystals may be formed direct from the vapour phase have arisen from the experiments of Sander and Damköhler (1943), Rau (1954), and Pound, Madonna and Sciulli (1955).

(ii) To check whether rapid expansions of small volumes of moist air can produce ice crystals in concentrations of order $10^{11}/\text{cm}^3$ as reported by Schaefer (1954).

In precipitating water vapour by rapid expansions in cloud chambers, Sander and Damköhler, and also Pound, Madonna and Sciulli reported that, until terminal temperatures of $-62°$C to $-65°$C were reached, the condensate appeared as spherical particles but, at lower temperatures, as a cloud of angular, glittering ice crystals. Sander and Damköhler suggested that either the crystals were formed by direct sublimation of ice from the vapour, or that $-62°$C represented the crystallization temperature of what, at higher temperatures, had been liquid droplets. Pound *et al.* suggested that because homogeneous nucleation of liquid water droplets at $-40°$C had been well established, the particles appearing between this temperature and $-65°$C were frozen spheres which had not developed crystalline faces. A similar suggestion was made earlier by Mason (1952) to account for the appearance of iridescent mother-of-pearl clouds which occur at temperatures of about $-80°$C in the stratosphere. Although the cloud chamber operators

report a change in the optical properties of the fog, with the appearance of glittering crystals below $-65°$C, they do not observe a marked increase in particle concentration. On the other hand, Rau (1954) reported that when samples of atmospheric air were cooled isobarically to low temperatures in a mixing-cloud chamber, the crystal concentration, which remained steady at about 200/cm^3 from $-40°$C to $-65°$C, thereafter rose rapidly to about 10^4/cm^3.

§ 2. Experimental Procedure

A small volume, 3 cm^3, of air, sealed in a pressure capsule, was rapidly expanded to atmospheric pressure into a water-saturated environment held either at $-10°$C or $-20°$C. Using room air, and also clean, filtered air in the capsule, the total number of ice crystals produced was determined for various values of its initial temperature, pressure, and water-vapour content, the final temperature and nominal supersaturation being calculated on the assumption of adiabatic expansion.

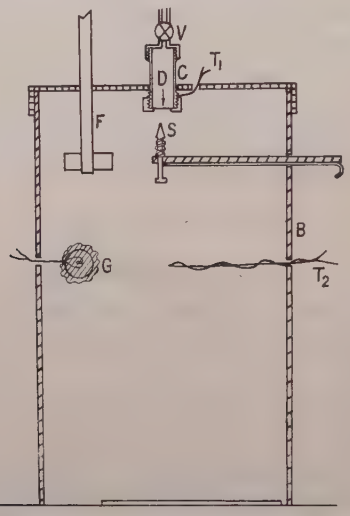

Figure 1. Apparatus used to detect ice crystals produced by adiabatic expansions.

The apparatus is shown in figure 1. One end of the brass pressure capsule C was connected through a valve V to a compressed air supply, the other end being sealed with a thin metal or plastic diaphragm D which could be suddenly shattered by a spring-fired striking pin S. The capsule was sealed into the lid of a cylindrical brass chamber B, 30 cm high × 10 cm diameter, the air in which was saturated with water vapour evaporated from an electrically heated, water-soaked gauze G. The whole chamber was immersed in a thermostatically controlled refrigerator, the air inside it being stirred by a small fan F and maintained at a fairly uniform temperature recorded by the thermocouple T_2. A second thermocouple T_1 measured the initial temperature of the air sample in the pressure capsule.

In a typical trial, the capsule was sealed with a diaphragm, filled with air to the desired pressure, and allowed to attain temperature equilibrium with the rest of the chamber. With the vaporizer on, the collectors in position and the valve closed, the striker was released.

Ice crystals produced by the expansion grew in the water-saturated environment and, with the fan off, settled to the bottom of the chamber where they were

collected and counted. Sampling was continued for at least three minutes after the expansion, by which time they had all reached the collectors. At least three trials were carried out for each set of conditions.

Subsidiary tests established that no crystals were produced by the action of the striker and the fan which, in any case, were coated with glycerol to prevent frost formation. Nor were crystals detected after the passage through the supercooled cloud of the shock wave produced by exploding the capsule just outside the refrigerator. It could therefore be assumed that the crystals appearing in the main tests were produced only by expansion and cooling of the air samples.

The relatively low concentrations of crystals produced by small expansions were collected in a dish of supercooled sugar solution in which they quickly grew to visible size and were easily counted (see Bigg 1956). With larger expansions, the sugar solution was replaced by glass slides on which the average number of crystals per mm^2 were counted under a microscope placed in the refrigerator. When the crystal concentrations were so high that more than 10^3 crystals, 3–10 μ in diameter, appeared on 1 mm^2, successive slides were exposed until all the crystals had settled. Very little coagulation and overlap of crystals was observed on the slides, and loss of crystals by evaporation, which occurred only within a few millimetres of the chamber walls, was less than 5%, and was allowed for. The total count per unit area of collector, multiplied by the base area of the chamber, and divided by the capacity of the capsule, gave the number of crystals produced by each cubic centimetre of the original air sample.

§ 3. Results

The number of ice crystals produced by 1 cm^3 of air, initially at temperature T_1 and the pressure p_1, after adiabatic expansion to temperature T_2 and a fixed pressure p_2, where $\log T_1/T_2 = 0{\cdot}286 \log p_1/p_2$, may be related to either the final temperature or the initial pressure. Another relevant parameter is the nominal saturation ratio attained at the end of the expansion, given by $S_n = e_1 p_2/e_2 p_1$, where e_1 is the initial vapour pressure of the air sample and e_2 the equilibrium vapour pressure relative to ice at the final temperature T_2. In large expansions, producing high concentrations of crystals, the maximum supersaturation actually achieved will be much lower than this nominal value because of the abstraction of vapour by the growing crystals. In calculating the final temperature, allowance has been made for warming of the air by the release of latent heat of sublimation; with final temperatures of -40 °C, this correction amounts to 2–3 °C under the conditions of the present experiments.

The numbers of crystals produced by a sample of room air, initially saturated relative to ice at either -10 °C or -20 °C, and expanded from various initial pressures to atmospheric pressure are shown in figure 2. Crystal production increases rapidly as the initial pressure increases from 1·2 to 2·0 atmospheres but thereafter becomes constant at about $4 \times 10^6/cm^3$. Schaefer's results, which are shown for comparison, are greatly different in that they show maximum concentrations of nearly $10^{11}/cm^3$.

It is, however, more instructive to plot the crystal numbers against the final temperature reached at the end of the expansion, as in figure 3. The number of crystals produced by the expansion of room air, which is not very sensitive to the initial temperature, increases rapidly from about $10^2/cm^3$ at -30 °C to a maximum, steady value of $4 \times 10^6/cm^3$ at final temperatures below -60 °C. Expansion of

moist, filtered air produced no crystals until the terminal temperature fell below $-40°C$ beyond which the numbers increased rapidly to reach the same maximum limiting value as before. When the air was dried to about 10% relative humidity

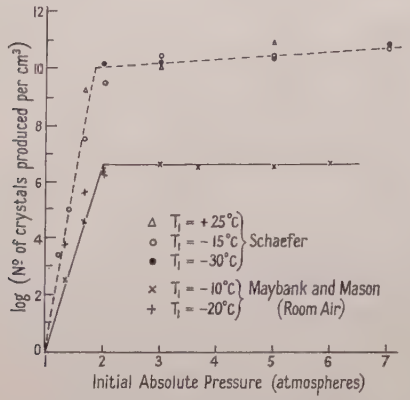
log (No of crystals produced per cm³)
Initial Absolute Pressure (atmospheres)
Δ T_i = +25°C
o T_i = −15°C } Schaefer
• T_i = −30°C
× T_i = −10°C
+ T_i = −20°C } Maybank and Mason (Room Air)

Figure 2. The number of ice crystals produced by adiabatic expansions of moist air from various initial pressures.

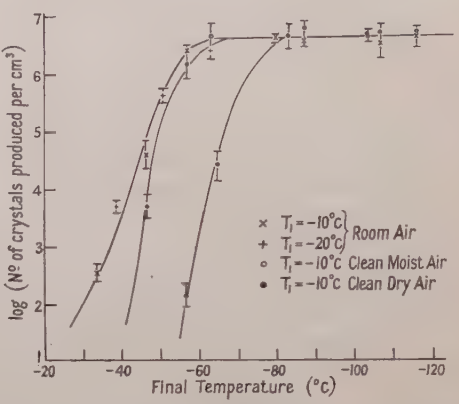

Figure 3. The number of crystals produced as a function of the final temperature attained by the expansion.

at $-10°C$, crystals did not appear until the final temperature fell below $-50°C$, at which stage it achieved four-fold supersaturation and allowed condensation to commence on small ions.

§ 4. Discussion of Results

Expansion of clean, filtered air produces ice crystals only if the supersaturation exceeds values at which condensation can occur either spontaneously or on ions, and if the terminal temperature falls below $-40°C$. This is strong evidence that the crystal formation is a two-stage process—condensation followed by homogeneous nucleation of the tiny droplets at temperatures below $-40°C$. The appearance of ice crystals at temperatures above $-40°C$ in room air may be attributed to the presence of ice nuclei.

Although nucleus concentrations of order $10^2/cm^3$ active at $-30°C$ are rarely observed in the free atmosphere (Mason 1957), such concentrations are present in our laboratory, through the generation of artificial ice nuclei.

Schaefer's claim that up to 10^{11} crystals/cm^3 are produced by the method of this experiment is not confirmed. His result is indeed surprising because, with increasingly large expansions, the concentration of droplets in cloud chambers reaches a maximum limiting value, observed by Frey (1941) and calculated by Mason (1951) to be about $3 \times 10^6/cm^3$, as a consequence of the supersaturation being limited by the release of latent heat and the abstraction of water vapour by the growing droplets. On the other hand, our maximum crystal concentrations of $4 \times 10^6/cm^3$ accord very well with these facts and support the view that the crystals resulted from the freezing of supercooled droplets.

In attempting to account for the large discrepancy between the present results and those of Schaefer, his technique, by which compressed air was suddenly released by shattering a small glass bulb, may be criticized on the following grounds.

After shattering of the glass capsule, air from the high pressure line continued to escape through a small orifice and, at the end of his paper, Schaefer admits that this produced copious ice crystals. We have confirmed this by testing a copy of the system described by Schaefer. Moist air, initially at room temperture and 4 atmospheres pressure, after expansion through the orifice of about 200 μ diameter, produced about 10^6 crystals/sec in a supercooled cloud at -10°C. Left on for only 10 sec, the jet produced about as many crystals as could be formed by explosion of the pressure capsule; in Schaefer's experiment, in which the volume of the exploding bulb was only 0·1 cm^3, the crystals may have been formed almost entirely by the expanding jet.

His method of determining ice crystal concentrations of up to 10/mm^3 by visual estimation of their average separation, in only a very small volume of the cloud, is not considered reliable. Furthermore, his assertion that ice crystals were formed only when the final temperture fell below -40°C does not tally with his tabulated experimental data. For example, he reports that crystal production of 10^9/cm^3 was achieved by the expansion of air initially at 1·7 atmospheres and 25°C to atmospheric pressure; under these conditions, adiabatic expansion would produce a final temperature of only -16°C.

With regard to Rau's (1954) work, figure 3 fails to show a *sudden* increase in crystal production as the terminal temperature falls below -65°C. Rau's experiment is different in that a sample of *atmospheric* air was cooled *isobarically* by injecting it into a pre-cooled chamber. As the air cooled, condensation of water vapour upon atmospheric nuclei produced droplets, few of which froze until the temperature fell below -40°C, when crystals appeared in concentrations of about 200/cm^3. With the chamber held at a temperature well below -40°C, cooling beyond that point was probably sufficiently rapid to release vapour at a rate faster than it could condense on to the growing particles and the walls of the chamber. The supersaturation would therefore rise and allow condensation, followed be immediate freezing, on the smaller nuclei. It is suggested that these conditions were obtained when Rau's chamber temperature was below -65°C, and were responsible for the rapid increase in crystal numbers which he observed below this temperature.

The observations of Sander and Damköhler and of Pound *et al.* that expansion of clean, particle-free air to six-fold supersaturation produced glittering ice crystals below about -65°C, but not at higher temperatures, is not easy to explain. In our experiments, which differed essentially only in that there was much more time available for particle growth, there was a gradual increase in the production of crystals via the freezing of droplets as the temperature fell from -40°C to -65°C. The non-appearance of glittering crystals in the cloud chambers between -40°C and -65°C is therefore most readily explained by the particles failing, in the short time available, to develop faces large enough ($d > 1\mu$) to facilitate specular reflection. Since for a given degree of supersaturation, the flux of vapour molecules towards a growing crystal is less at low temperatures, a more rapid growth to visible size at these temperatures would seem to require an over-compensating increase in the accommodation coefficient of the growing ice surfaces.

But whatever be the true explanation of the change in the visual appearance of the condensate below -65°C in the cloud chambers, there appears to be no evidence nor necessity to assume that this temperature marks a new phase transition by which crystals form by direct sublimation of the vapour. It does not seem

likely that molecules will condense directly into the ice lattice without first going through the less ordered liquid structure.

References

Bigg, E. K., 1956, *Aust. J. Phys.*, **9**, 561.
Frey, F., 1941, *Z. phys. Chem.* B, **49**, 83.
Mason, B. J., 1951, *Proc. Phys. Soc.* B, **64**, 773.
—— 1952, *Quart. J. R. Met. Soc.*, **78**, 22.
—— 1957, *The Physics of Clouds* (Oxford : Clarendon Press), p. 139.
Pound, G. M., Madonna, L. A., and Sciulli, C. M., 1955, *Proc. Conf. on Interfacial Phenomena and Nucleation*, Airforce Cambridge Research Center, Geophys. Res. Pap. No. 37.
Rau, W., 1954, *Geofis. Pur. Appl.*, **28**, 201.
Sander, A., and Damköhler, G., 1943, *Naturwissenschaften*, **31**, 460.
Schaefer, V. J., 1954, *J. Colloid Sci.*, **9**, 175.

On The Lattice Theory of Expansion

By M. BLACKMAN
Physics Department, Imperial College, London, S.W.7

MS. received 8th January 1959, in final form 3rd March 1959

Abstract. An investigation has been made of the expansion coefficient of two-dimensional lattices—ionic lattices and the close packed hexagonal lattice with central forces. A survey has been made of the Grüneisen constants γ_ν of a representative set of vibrations in reciprocal space. From these a set of functions are constructed from which the variation of the Grüneisen constant γ can be calculated, and which also permit one to see the reasons for the variation. It is shown that the ionic lattices are characterized by a large spread in γ_ν values, this being in the main due to the lower of the two frequency branches. In the hexagonal lattice the distribution of γ_ν values is, in comparison, very limited and the Grüneisen assumption of a single constant can be justified in this case.

§ 1. Introduction

In the theory of the expansion of crystals, an important part is played by the Grüneisen relation

$$\gamma = \frac{V\beta}{\kappa C_V} \qquad \ldots\ldots(1)$$

where V is the volume of the solid, C_V the heat capacity, κ the compressibility, β the volume expansion coefficient and γ is a constant. This relation can be derived from thermodynamic considerations if certain assumptions are made as to the properties of the vibrations of the solid. The more general result which is also well known and is derived in standard textbooks is that a relation of the form (1) holds where, however, γ is not a constant, but is defined in the following manner:

$$\gamma = \frac{\Sigma\gamma_\nu E(h\nu/kT)}{\Sigma E(h\nu/kT)} \qquad \ldots\ldots(2)$$

where $\gamma_\nu = -d\ (\log \nu)/d\ (\log V)$, E is the Einstein function for the heat capacity of a linear oscillator of frequency ν, and the summation is taken over all frequencies.

In the limit of low frequencies γ tends to a constant γ_0, as has been indicated by Born (1923) and discussed recently in more detail by Barron (1955), while at high temperatures the value γ_∞ is an average over all γ_ν values for the lattice. The form of $\gamma(T)$ between these limits depends on details which cannot be described in a simple manner.

There are two comparatively simple assumptions about the γ_ν values under which the relation (1) would hold. The first is that all γ_ν values are equal. Though this appears to be most unlikely, it does in fact occur in the case of the linear chain with nearest neighbour forces between the particles. Here the

frequencies are known to be given by the expression $\nu = \nu_0 |\sin \phi|$, where ϕ has a set of discrete values. The quantities $\gamma_\nu' = -d(\log \nu)/d(\log r)$, where r is the distance between neighbouring particles, are hence independent of the frequency.

One can next proceed to the assumption that that distribution function of γ_ν values is sharply peaked around an average value, and then the relation will hold to a good approximation.

A second assumption depends on forming a quantity $\overline{\gamma_\nu}$ which is the average value of γ_ν taken between neighbouring frequency contours. Then (2) can be written as (Blackman 1957)

$$\gamma = \frac{\int \overline{\gamma_\nu} \rho(\nu) E(h\nu/kT) d\nu}{\int \rho(\nu) E(h\nu/kT) d\nu} \qquad \ldots\ldots (2a)$$

where $\rho(\nu)$ is the distribution function for the frequencies. If this $\overline{\gamma_\nu}$ value is independent of the frequency, the relation (1) will also follow. Since this is a less stringent condition than a constant γ_ν value, it seems a reasonable one to assume as a starting point. A graph of $\overline{\gamma_\nu}$ against frequency allows one to judge the behaviour in a convenient manner, as a straight line parallel to the frequency axis means that the Grüneisen relation holds exactly.

So far the theoretical data on the behaviour of lattices is rather meagre. The only case in which $\gamma(T)$ has been examined in some detail is that of a face centred cubic lattice with short-range central forces (Barron 1955). The value of γ_0 and the high temperature part of the $\gamma(T)$ curve from a value of $T/\theta_D \simeq 0{\cdot}15$ onwards were obtained. In this the properties of the secular determinant of the frequencies were used and neither the vibrational spectrum nor the individual γ_ν values were needed. While the investigation is not complete, the analysis does suggest that the total variation of $\gamma(T)$ is not likely to be more than a few per cent, in the case where a Lennard-Jones potential is used. It was also shown that the main part of the γ_ν value for any of the vibrations is independent of frequency and it is therefore probable that one is dealing here with a case in which each frequency branch will contribute a sharply peaked function to the distribution of γ_ν values. The total distribution will then have a small spread about a mean value. The $\overline{\gamma_\nu}$ curve in this case would also show little variation in magnitude and the $\gamma(T)$ curve even less since this is obtained as a weighted average (cf. (2*a*)) over the $\overline{\gamma_\nu}$ curve.

A partial investigation has also been made (Barron 1957, Blackman 1957) of ionic crystals of the rocksalt type. Here the study of γ_ν values in the elastic region shows a very large variation from large positive values to appreciable negative values. It does not seem likely that a single γ_ν value would be a good approximation in this case and a complete examination would certainly be instructive.

Such experiments as have been carried out on alkali halides (Adenstedt 1936) suggest changes of about 25% in the γ values (these decreasing with temperature), but measurements do not extend to really low temperatures and there is no reason to suppose that the limit of change has been reached at the lowest measured values.

In order to obtain a better understanding of the relation between the $\gamma(T)$ curves and the dynamical quantities γ_ν, an examination has been made of two-dimensional lattices for which a complete survey can be obtained without

a very lengthy set of calculations. The lattices examined are of two types: (*a*) the ionic lattice consisting of a square array of alternately positive and negative ions, (*b*) the hexagonal lattice with a short-range central force interaction. The results of these investigations should provide the basis for a good qualitative picture of what happens in corresponding three-dimensional lattices.

The general formula (2) will apply in two dimensions if appropriate changes are made in the definition of the γ_ν values. In three dimensions one can write γ_ν in the form $-\frac{1}{3}d(\log \nu)/d(\log r)$, where r is a characteristic lattice distance. In two dimensions the corresponding quantity will be $-\frac{1}{2}d(\log \nu)/d(\log r)$.

§ 2. The Two-dimensional Ionic Lattice

In this type of lattice the ions, of equal mass, are distributed as on the cube face of rocksalt. The vibrational properties and the vibrational spectrum of this lattice have been worked out by Smollett (1952) and need only brief comment. If M is the mass of an ion and ν the frequency it follows that

$$4\pi^2 M\nu^2 = \tfrac{1}{2}\{-(A_{xx}+A_{yy}) \pm [(A_{xx}-A_{yy})^2+4A_{xy}{}^2]^{1/2}\} \quad \ldots\ldots (3)$$

where

$$A_{\alpha\beta} = \sum_{m_1 m_2} \phi_{\alpha\beta}^{m_1 m_2} \exp\{-i\tau(\mathbf{r}_{m_1 m_2} \cdot \mathbf{s})\}. \quad \ldots\ldots (4)$$

Here $\phi_{\alpha\beta}^{m_1 m_2}$ is the second derivative of the potential energy of a pair of ions, one in the cell of index zero and the other in the cell whose index is (m_1, m_2). The Coulomb part of the interaction has the form $e^2(-1)^{m_1+m_2}|\mathbf{r}_{m_1 m_2}|^{-1}$, where $\mathbf{r}_{m_1 m_2}$ is the vector distance of the two particles, and the repulsive part of the interaction the form $b|\mathbf{r}_{m_1 m_2}|^{-n}$. The unit vector $\mathbf{s}$ is the wave vector and $\tau = 2\pi/\lambda$, where λ is the wavelength.

The methods of evaluating the Coulomb part of the lattice sums (4) have been discussed by Smollett and Blackman (1951) and the numerical values of the $A_{\alpha\beta}$ (Coulomb) have been tabulated by Smollett (1951) for a representative set of points in reciprocal space.

These values have been used by the author and the corresponding values for the repulsive interaction were obtained by direct summation. The γ_ν values were obtained by differentiating (3) with respect to r, where r is the closest distance between positive and negative ions. The equilibrium conditions for the lattice are used after this procedure has been carried out. It is also necessary to calculate the frequencies. The required quantities were evaluated for all the points in reciprocal space used originally by Smollett with the value of $n=9$, and the same frequency contours were used, i.e. fourteen contours in the lower frequency branch and sixteen in the upper frequency branch.

The γ_ν values at low frequencies were evaluated separately. Here the value depends on the direction of propagation of elastic waves in the two-dimensional elastic continuum and not on the frequency itself. If we write

$$\nu^2 = c^2/\lambda^2 \sim c^2/r^2 \quad \ldots\ldots (5)$$

where c is the velocity, it follows that

$$\gamma_\nu = -\frac{r}{4\nu^2}\frac{d\nu^2}{dr} = -\frac{r^3}{4c^2}\frac{d}{dr}\left(\frac{c^2}{r^2}\right) \quad \ldots\ldots (6)$$

$$= -\frac{1}{4}\frac{r}{\rho c^2}\frac{d}{dr}(\rho c^2) = \gamma^c$$

where $\rho = M/r^2$ is the density in the two-dimensional case.

The value of γ^c will of course depend on the elastic constants in terms of which ρc^2 can be expressed, and for each direction of propagation there will be two values of γ^c. The elastic constants have the following form (Smollett and Blackman 1951):

$$\left.\begin{aligned} c_{11} &= -1{\cdot}46\frac{e^2}{r^3} + 92{\cdot}0\frac{b}{r^{11}} \\ c_{12} &= 0{\cdot}228\frac{e^2}{r^3} + 11{\cdot}7\frac{b}{r^{11}} \\ c_{44} &= 1{\cdot}047\frac{e^2}{r^3} - 7{\cdot}19\frac{b}{r^{11}}. \end{aligned}\right\} \qquad \ldots\ldots(7)$$

The parameter b can be eliminated after the appropriate differentiations have been carried out. The potential energy per ion has the form

$$\Phi = -1{\cdot}616\frac{e^2}{r} + \frac{4.191b}{r^9} \qquad \ldots\ldots(8)$$

and the condition $d\Phi/dr = 0$ gives the equilibrium condition for the lattice. Typical values of γ^c are given for certain special directions in the lattice; $n = 9$.

Direction	Elastic Constant	γ^c
[10]	c_{44}	−0·076
[10]	c_{11}	4·00
[11]	$\frac{1}{2}(c_{11}-c_{12})$	4·50
[11]	$\frac{1}{2}(c_{11}+c_{12}+2c_{44})$	2·30

The average value which is again termed γ_0 is obtained by numerical integration of the $\gamma_j{}^c$ values in reciprocal space. It follows from (6) and (2) that in the two-dimensional case

$$\gamma_0 = \sum_{j=1,2}\int\frac{\gamma_j{}^c}{c_j{}^2}\frac{d\theta}{2\pi}\Big/\sum_j\int\frac{1}{c_j{}^2}\frac{d\theta}{2\pi} \qquad \ldots\ldots(9)$$

where c_j is a function of the angle θ in reciprocal space.

The γ_ν values (for each frequency branch) which lie between given neighbouring frequency contours are averaged and these averages produce the curves $\overline{\gamma_\nu{}^{(1)}}$, $\overline{\gamma_\nu{}^{(2)}}$ as a function of frequency. Here the index (1) refers to the lower frequency branch, the index (2) to the upper frequency branch. The $\overline{\gamma_\nu}$ value needed in the calculation of $\gamma(T)$ (see (2 *a*)) is the average obtained from all the γ_ν values in both branches associated with the two frequency contours. In addition, the distribution function of the γ_ν values was found. This is denoted by $f(\gamma_\nu)$ where $\int f(\gamma_\nu)d\gamma_\nu$ is the total number of vibrations in a frequency branch, the indices (1) and (2) being used, as before, to distinguish between the two frequency branches.

The results of the calculations for the ionic lattice with $n = 9$ are plotted in a set of diagrams. Figure 1 shows the variation of $\overline{\gamma_\nu{}^{(1)}}$ and of $\overline{\gamma_\nu{}^{(2)}}$ with frequency, figure 2 that of $\overline{\gamma_\nu}$. It will be seen that $\overline{\gamma_\nu{}^{(2)}}$ does not vary much from a constant value, while the deviation of $\overline{\gamma_\nu{}^{(1)}}$ is considerable. The upper frequency branch, index (2), contains vibrations which are mainly longitudinal, the lower frequency branch those which are mainly transverse. The singularities in the $\overline{\gamma_\nu}$ curves are associated with the logarithmic infinities in the vibrational spectrum (Smollett 1952).

Using these curves and the vibrational spectrum one can calculate the γ value (see (1)) as a function of temperature (figure 3). The reduced temperature T/θ_0 is used, θ_0 being the Debye temperature obtained from the elastic constants for the two-dimensional lattice. The small dip in the curve at low temperatures follows from the corresponding larger feature in the $\overline{\gamma_\nu^{(2)}}$ curve. The general tendency is, however, an increasing γ value with temperature with a total variation of about 20%.

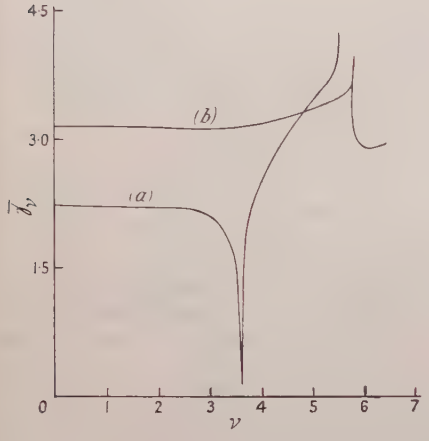

Figure 1. Variation with frequency of the the averaged γ_ν value of the two-dimensional ionic lattice with $n=9$, (*a*) for the lower frequency branch, (*b*) for the upper frequency branch. The frequency is in arbitrary units.

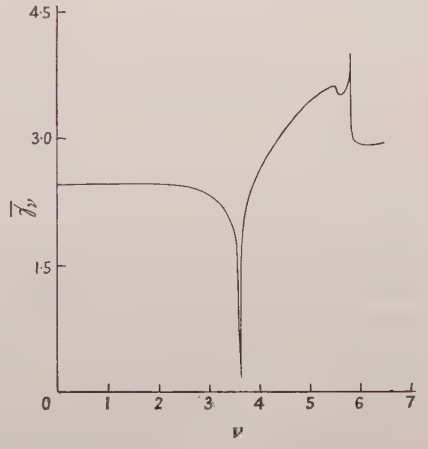

Figure 2. Variation with frequency of $\overline{\gamma_\nu}$ value for the two-dimensional ionic lattice.

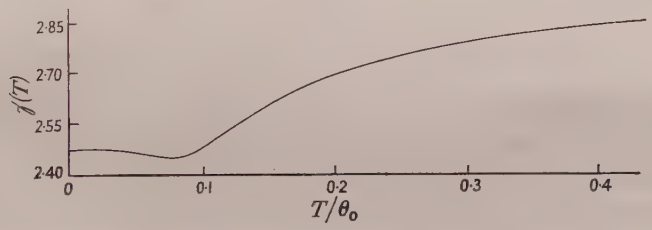

Figure 3. The Grüneisen parameter as a function of the reduced temperature (ionic lattice, $n=9$). θ_0 is the Debye temperature deduced from the elastic constants. ($\gamma_\infty = 2{\cdot}90$).

The distribution function for the γ_ν values can also be obtained from the same data. It is instructive to consider the individual distribution functions $f(\gamma_\nu^{(1)})$, $f(\gamma_\nu^{(2)})$ for the two frequency branches. These are shown in figures 4 and 5, where again it is the 'transverse' branch for which a very broad distribution is found. The longitudinal branch gives a distribution which is limited and which could be approximated by a single γ_ν value without a large error.

It should also be noted that the negative γ_ν values represent only a small part of the distribution function, and their influence is not apparent in the $\overline{\gamma_\nu}$ curves.

A corresponding calculation was carried out for the case of $n=20$, which leads to strongly anisotropic behaviour at low frequencies of the type characterized

by a small value of the ratio of the elastic constants c_{44} and c_{11}. Only the (γ, T) curve for this case is shown (figure 6) and the other results will be described in brief. The γ_ν and the $f(\gamma_\nu)$ curves have a similar character to those for the

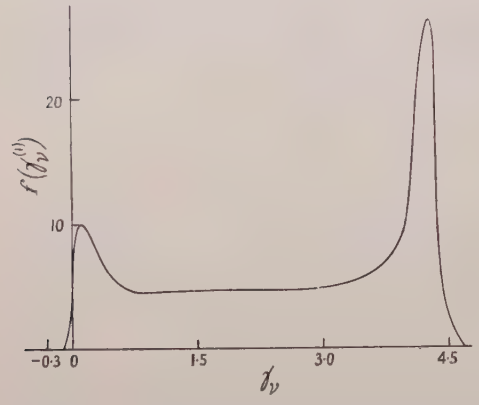

Figure 4. The distribution function of the γ_ν values for the lower frequency branch (ionic lattice, $n=9$).

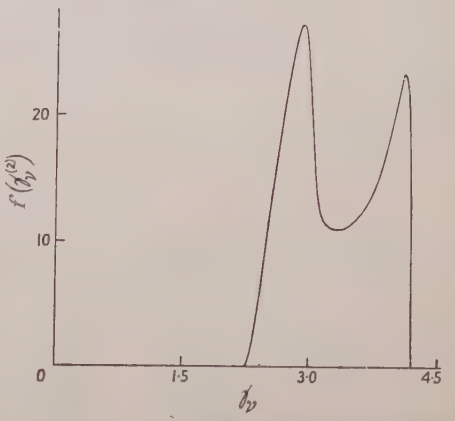

Figure 5. The distribution function of the γ_ν values for the upper frequency branch (ionic lattice, $n=9$).

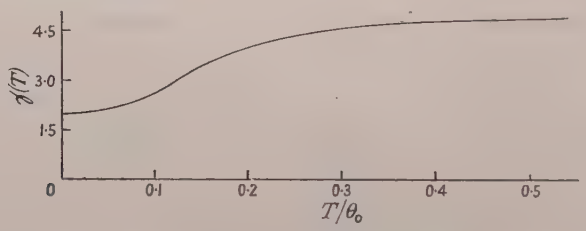

Figure 6. The Grüneisen parameter as a function of the reduced temperature (ionic lattice, $n=20$).

previous case. The chief feature is the increase in the region in reciprocal space associated with negative γ_ν values. These are concentrated, as before, in a narrow angular region around the rectangular axes of the reciprocal lattice cell, but extend further out; they are also still confined to the lower frequency branch. The dip corresponding to that in figure 1 (*a*), now extends to negative values. The (γ, T) curve is, however, affected only in that the variation in γ is appreciably larger, and this is also a consequence of the larger magnitude of the positive γ_ν values.

A further point which was examined was the effect of increasing the value of n to larger values. This does not lead to any radical change in the (γ, T) curve and in particular does not lead to negative γ values at low temperatures.

§ 3. The Two-dimensional Hexagonal Lattice

Here the lattice cell can be chosen so as to contain one particle of mass m per cell. A central force potential interaction $\phi(r)$ is assumed, this to act between nearest neighbours only. Standard methods then lead to an expression for the angular frequencies ω of the lattice in the form

$$2m\omega^2 = A(2P + r^2Q) \pm r^2Q(B^2 + 3C^2)^{1/2} \qquad \ldots\ldots (10)$$

where

$$P=\frac{1}{r}\frac{d\phi}{dr},\quad Q=\frac{1}{r}\frac{d}{dr}\left(\frac{1}{r}\frac{d\phi}{dr}\right)$$

$$\left.\begin{aligned}A&=6-2\cos\phi_1-2\cos\phi_2-2\cos(\phi_1+\phi_2)\\B&=\cos\phi_1+\cos\phi_2-2\cos(\phi_1+\phi_2)\\C&=(\cos\phi_1-\cos\phi_2).\end{aligned}\right\}\quad\ldots\ldots(11)$$

The phase angles $\phi_i=2\pi(\mathbf{a}_i\cdot\mathbf{s})/\lambda$ where the $\mathbf{a}_i$ are the basic lattice vectors, $\mathbf{s}$ the wave vector and λ the wavelength and (ϕ_1, ϕ_2) would define a point (h_1, h_2) in reciprocal space if one omits the factor 2π.

The Grüneisen parameters γ_ν can be calculated directly from (10)

$$\gamma_\nu=-\tfrac{1}{4}\frac{r}{(2m\omega^2)}\frac{d}{dr}(2m\omega^2)$$

$$=-\tfrac{1}{4}\left(2+\frac{r}{Q}\frac{dQ}{dr}+\frac{2A}{A\pm(B^2+3C^2)^{1/2}}\right).\quad\ldots\ldots(12)$$

If one takes the interaction in the form

$$\phi(r)=-\frac{a}{r^6}+\frac{b}{r^{12}}\quad\ldots\ldots(13)$$

the quantity $(r/Q)dQ/dr$ has the value -24, and the main part of the magnitude of γ_ν comes from this term, the remainder contributing at most about 25%.

The rest of the calculation follows the same lines as for the ionic lattices, the frequencies and γ_ν values being evaluated for a representative set of points in reciprocal space.

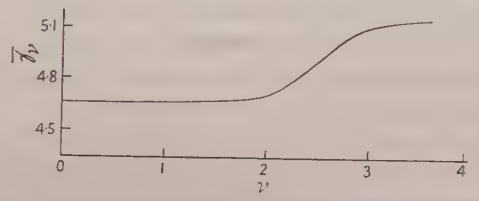

Figure 7. Variation with frequency of the $\overline{\gamma_\nu}$ value for the two-dimensional hexagonal lattice.

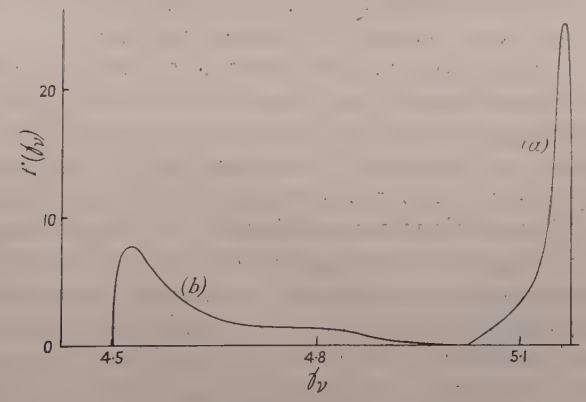

Figure 8. The distribution functions of the γ_ν values for (*a*) the upper frequency branch (*b*) the lower frequency branch (hexagonal lattice).

The main results are shown in a set of curves. In the $\overline{\gamma_\nu}$ curve (figure 7) the singularities are omitted as they are unimportant here. The main variation comes again chiefly from the lower frequency branch. The distribution functions $f(\gamma_\nu^{(1)})$ and $f(\gamma_\nu^{(2)})$ have been plotted separately (figure 8), and show in a striking manner how close to a constant γ_ν value the distribution can be in a special case.

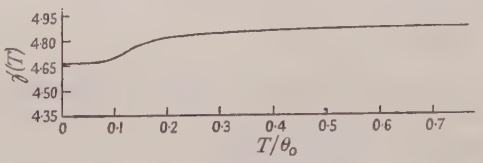

Figure 9. The Grüneisen parameter as a function of the reduced temperature (hexagonal lattice). ($\gamma_\infty = 4{\cdot}89$.)

Finally, the (γ, T) curve for the lattice is given in figure 9. As is to be expected, the variation in γ is a good deal less than that in $\overline{\gamma_\nu}$ and amounts in the extreme case to only 5%.

§ 4. Discussion and General Comments

The results for the hexagonal lattice show a completely different character to those for the ionic lattices. The narrow variation of the γ_ν values in the former case will in all probability be repeated in the corresponding cases in three dimensions—the close packed hexagonal and cubic lattices with a nearest neighbour central force interaction (or for that matter, if the nearest neighbour assumption is not used). There is strong evidence for this statement in the work of Barron (1955) on the latter case; a relation for the γ_ν value is found in this case which is not essentially dissimilar to (12). It has, however, sometimes been assumed that this calculation can also be applied to face-centred cubic metals and of course experimental measurements on these metals show a small $\gamma(T)$ variation in the region of temperature investigated. It cannot be assumed *a priori* that γ_ν values for such metals will necessarily be the same as for the central force cases, even if specific heat measurements appear to indicate a very similar vibrational spectrum. Experimental measurements at very low temperatures and a theoretical investigation of a typical metal are both needed before it will be clear if and why there is a similarity.

The main feature of the results on the two-dimensional ionic lattices is the very large spread of the γ_ν values in the lower frequency branch. It is likely that this property will also be found in the ionic crystals, probably in the two acoustic frequency branches which are mainly transverse in character.

A second feature of interest is the appearance of negative γ_ν values, which had already been noted (Barron 1957, Blackman 1957) in the long-wave region of the vibrational spectrum of ionic lattices of the rocksalt type. In the two-dimensional case it is possible to see that these γ_ν values are confined to a region of reciprocal space around the rectangular axes; also that both the magnitude of these γ_ν values and the size of the region increases as the value of the parameter n of the repulsive potential is increased. The question as to whether it is possible to obtain an overall negative γ_0 value has been considered in some detail, using the methods discussed above. It is found that the γ_0 value always remains positive however large n is made. This differs from the result obtained in the corresponding three-dimensional ionic lattice (Blackman 1958). In the

three-dimensional case, the negative γ_j^c values (cf. equation (6)) are relatively large in magnitude for the same value of n and there are also two transverse branches contributing to the effect. In addition one is weighting the γ_j^c values with c_j^{-3} instead of c_j^{-2} as in (9) and the negative values are again associated with the smallest values of the velocity.

A property common to the two types of lattices investigated is to be found in the distribution functions $f(\gamma_\nu)$. The component $f(\gamma_\nu^{(2)})$ for the 'longitudinal', or upper, frequency branch extends over a comparatively small region of values and could be approximated reasonably well by a single γ_ν value. It would be of interest to know how far this is a general feature for either monatomic crystals or for those without a pronounced molecular character.

The three (γ, T) curves which have been calculated, all show a general rise with increasing temperature. The rate of change is greatest at a point where $T/\theta_D = 0{\cdot}14$ for the ionic lattices and 0·12 for the hexagonal lattice. A value of 0·2 was suggested by Barron (1955) as the point at which a rapid change in γ took place when the temperature was decreased.

It is doubtful whether any of these features of the (γ, T) curve have a general validity. For instance, there is no reason to suppose that $\gamma_0 < \gamma_\infty$ in all cases. This might appear to follow from the cases studied here. In fact, γ_0 depends on elastic properties of the lattice, i.e. on the very low frequencies, whereas the magnitude of γ_∞ depends mainly on the properties of the high-frequency vibrations. There is therefore (as in the case of the heat capacity) no direct relation between the high temperature and low temperature properties and the (γ, T) curve is governed by at least two parameters. The γ_0 value can on this argument be larger as well as smaller than the γ_∞ value and the form of the (γ, T) curve can be as varied as (θ_D, T) curves in specific heat theory—more so in fact since γ_0 can be negative in some cases (Adenstedt 1936, Blackman 1958).

The occurrence of these negative values alters considerably the status of the Grüneisen relation (1). As long as the γ values are positive the relation can be justified as a useful general approximate formula, but once negative values are admitted the Grüneisen relation loses its general character.

That γ itself will vary with temperature has been recognized for a long time. Grüneisen (1926) suggested a set of three γ values for solids with different properties in different directions. He also pointed out that where the solid contains molecular groups, there will be at high temperatures a variation of γ characteristic of the group (as well as of the lattice vibrations), whereas at low temperatures the γ value will be expected to conform to that for a monatomic lattice. While the γ value for the monatomic lattice would not now be regarded as necessarily constant or approximately constant, it still remains correct that the complex lattices will have a special character at temperatures where the molecular groups give an appreciable contribution. From the point of view of lattice theory, these groups contribute vibrations which form 'optical branches'. For these it is likely that the γ_ν value will be practically constant, particularly if the frequencies are well removed from those of the acoustic branches. These optical γ_ν values may in certain special cases be negative (for the transverse or mainly transverse vibrations). This could then lead to low overall γ values or even negative γ values at relatively high temperatures.

References

Adenstedt, H., 1936, *Ann. Phys., Lpz.*, **26**, 29.
Barron, T. H. K., 1955, *Phil. Mag.*, **46**, 720.
—— 1957, *Annals of Physics*, **1**, 77.
Blackman, M., 1957, *Proc. Phys. Soc.* B, **70**, 827.
—— 1958, *Phil. Mag.*, **3**, 831.
Born, M., 1923, *Atomtheorie des festen Zustandes* (Berlin: Teubner).
Grüneisen, E., 1926, *Geiger–Scheel Handbuch der Physik*, **10**, 1.
Smollett, M., 1951, *Ph.D. thesis*, University of London.
—— 1952, *Proc. Phys. Soc.* A, **65**, 109.
Smollett, M., and Blackman, M., 1951, *Proc. Phys. Soc.* A, **64**, 683.

The Selective Photoelectric Effect

By W. T. DOYLE†
Department of Electronics, University of Southampton

MS. received 12th February 1959

Abstract. The spectral selective photoelectric effect in alkali metals is considered as a local field phenomenon taking place in a colloidal surface structure. Treating the colloidal particles as spheroids containing a mixture of bound ion core and free valence electrons, an expression is derived for the wavelength for peak photoemission which is compared with the experiments on hydride cells and on thin films.

§ 1. Introduction

The alkali metals display two remarkable optical properties: they are transparent to ultraviolet light (Wood 1933) and they exhibit a marked spectral selectivity in their photoelectric emission (Pohl and Pringsheim 1910). The critical wavelength for the onset of ultra-violet transparency has been calculated by Zener (1933) using the free electron theory of metals. It is the purpose of this note to show that the wavelength for maximum photoelectric emission also follows from the free electron theory.

Actually, there is not one selective photoelectric effect, but many. A myriad of selective effects appear with the complex cathodes which have been developed for practical photocells (Olpin 1930, 1931). The spectral sensitivity of these cells depends in detail upon the chemical and thermal sensitization procedures used. Such cells will not be considered here. At the other extreme of surface conditions, even specular surfaces of pure bulk metal are expected to exhibit a spectral selectivity (Mitchell 1934, 1936). The predicted maxima are broader and occur at shorter wavelengths than do the experimental peaks. However, in view of the difficulty in preparing uncontaminated surfaces of bulk alkali metal, it is possible that the predicted effect has never been observed free of disturbing influences (Hill 1938). In any event, there is considerable evidence (Hughes and DuBridge 1932, Boutry 1936) that the distinctive selective effects discovered by Pohl and Pringsheim arise from a surface structure which, while lacking the simplicity of a specular surface, is not so complicated as that of the composite cathodes in commercial cells.

In spite of large and erratic variations in the magnitude of the selective effect, the wavelength for maximum emission is characteristic of the alkali metal and varies little from cell to cell (Boutry 1936). This is most strikingly revealed in the process of 'sensitization'. Elster and Geitel (1910, 1911) found that the selective photoelectric yield is enormously enhanced in cells formed by exposing a fresh alkali metal surface to a low pressure hydrogen discharge. The wavelength for maximum emission is the same as for Pohl and Pringsheim's bulk metal cells

† National Science Foundation Postdoctoral Fellow. On leave from Dartmouth College, Hanover, New Hampshire, U.S.A.

(see table 1). The sensitized hydride cells thus exhibit, in prominent and reproducible form, the peaks which were accidently present in the older work on bulk metal.

Elster and Geitel noticed that during sensitization the metal became coated with a strongly coloured film of alkali hydride. They attributed the strong increase in selectivity and concomitant coloration to the presence of colloidal alkali metal. This same assumption will be made here. Since the term 'colloidal' as applied to these cells has come to be regarded more as a convenient name (Hughes and DuBridge 1932, p. 172) than as indicating a specific surface structure, it will be well to review some of the evidence which points to this form of coloration, as opposed to an atomic dispersal of colour and photoelectric centres.

It is clear from the method of formation of the hydride surface that alkali metal will be present in excess. From the well-known behaviour of additively coloured alkali-halides (Seitz 1954) it is to be expected that the stoichiometric excess of alkali will be present either in the form of colour centres or as colloidal metal. If the excess metal were present as colour centres the position of the peaks in photoemission and optical absorption would be strongly dependent upon the nature of the host crystal. It is found, however, that the selective peak is virtually identical for cells sensitized with water vapour instead of hydrogen (Tykociner and Bloom 1941). Moreover, there is no change in peak shape or position as the temperature is lowered to that of liquid air (Ives 1924), in strong contrast with the behaviour to be expected from atomically dispersed centres (Fröhlich and Sack 1947). The behaviour, in fact, is just what one expects from the coagulated colloidal aggregates which occur in strongly coloured unquenched crystals.

§ 2. Theoretical Model

Turning now to a specific model of the hydride cell, it will be assumed that the electrons associated with the strong selective peak all originate in colloidal particles of alkali metal located on the outer surface of the hydride film. The hydride acts simply as a supporting surface. The colloidal particles will be assumed to be much smaller than the wavelength of visible light. For simplicity they will be assumed spheroidal in shape with the symmetry axis along the normal to the surface of the metal. We neglect the interaction between the colloid particle and the hydride surface. The metal surface behind the hydride will be considered simply as a reflector which serves to suppress components of the electric field not normal to its surface. Image effects will also be neglected.

The probability that an electron will be ejected from the colloid particle, will, in general, be a complicated function of wavelength. Whatever the relationship, it will contain the square of the electric field inside the particle as a factor. Now the electric field inside a spheroidal particle E' may be expressed in terms of the field outside, E. Thus (Gans 1912)

$$E' = \frac{E}{1+(n^2-1)P/4\pi} \qquad \ldots\ldots(1)$$

where n is the index of refraction of the metal and P is the depolarization factor along the symmetry axis. Treating the alkali metal as a mixture of bound ion core electrons and free valence electrons, and neglecting damping, the index of refraction of the metal is given by (Mott and Jones 1936)

$$n^2 = 1 + 4\pi N\alpha - \frac{4Ne^2}{m^*\omega^2} \qquad \ldots\ldots(2)$$

where N is the number of metal atoms per unit volume, e and m^* are the charge and effective mass of the valence electrons, α is the ion core polarizability and ω is the angular frequency of the light. Putting the index of refraction (2) into equation (1) one finds that the internal field E' becomes infinite (neglecting damping) for light of angular frequency ω_0 where

$$\omega_0^2 = \frac{4\pi Ne^2/m^*}{4\pi/P + 4\pi N\alpha}. \qquad \ldots\ldots (3)$$

Since other factors influencing the photoelectric yield may be considered slowly varying functions of frequency we identify $\lambda_0 = 2\pi C/\omega_0$ as the wavelength for maximum photoelectric emission. Equation (3) contains only one unknown parameter, the depolarization factor P, which depends upon the shape of the particles. For spherical particles $P = 4\pi/3$. For this case equation (3) reduces to $\omega_0 = (4\pi Ne^2/3m)^{1/2}$, if ion core polarizability and effective mass corrections are ignored. It is of interest to note that this relation was derived many years ago by Lindemann (1911). Lindemann's formula has often been regarded as a useful rule (Olpin 1931) even though the reasoning behind his derivation has been rejected.

§ 3. Hydride Cells

Equation (3) has been used to compute the wavelength for peak emission for hydride cells assuming spherical particles. The theoretical effective masses calculated by Brooks (quoted by Pines 1955) have been used in obtaining the peak positions displaced in the fifth column of table 1. The ionic polarizabilities were taken from the compilation of Tessmann, Kahn and Shockley (1953). For comparison the observed values of the wavelength for peak emission are also shown. The right trend is certainly evident, but all the calculated values are uniformly too high. This may be taken to indicate that the particles are not perfectly spherical. Since the particles reside upon a surface with which some attractive forces must operate it is natural to assume that the spheroids are somewhat oblate, with the symmetry axis normal to the surface. In the absence of further information it is not possible to state what degree of eccentricity will exist. However, a useful further approximation may be obtained by assuming that the particle shape, while not spherical, is still the same for all members of the series. Then, using the photoelectric data for one member of the series to obtain P, one may compare calculated and observed values of λ_0 for all the others. This has been done in the last column of table 1. The experimental value of λ_0 for sodium was used to find P. The choice was made because both theory and experiment indicate that the effective mass ratio is very nearly unity for sodium. The agreement between the observed and calculated values is quite good. A single value of P serves to fit the entire series of alkali metals. The empirical depolarization factor $P/4\pi$ is 0·41, corresponding to an axial ratio of 0·75. The fact that lithium fits into the pattern merits special notice, since the predicted effective mass ratio, 1·45, differs most from unity. For lithium other optical data are scanty.

It has long been thought that an intimate connection exists between the photoelectric effect and optical absorption (Boutry 1936). Indeed, this was the motivation behind the original designation of hydride cells as colloidal. It is apparent that some connection must exist, since the photoemission itself

Table 1. Wavelength for Maximum Photoelectric Emission for Hydride Photocells

Photocathode (hydride cells)	m^*/m [1]	$4\pi N\alpha$ [2]	λ_0(Å), exp. [3]	λ_0(Å), eqn. (3) $P/4\pi=\frac{1}{3}$	λ_0(Å), eqn. (3) $P/4\pi=0{\cdot}41$
LiH–Li	1·45	0·02	2800	3200	2900
NaH–Na	0·98	0·13	3300	3700	3300
KH–K	0·93	0·22	4350	5000	4500
RbH–Rb	0·89	0·27	4800	5500	5000
CsH–Cs	0·83	0·37	5400	6000	5400

For bulk metal cells the corresponding peaks for maximum emission are: 2800, 3400, 4400, 4700 and 5500 Å respectively (Hughes and DuBridge 1932, p. 161). The calculated values were obtained using the indicated depolarization factors. The corresponding axial ratios are 1·0 and 0·75 respectively (Osborne 1945). [1] Pines (1955); [2] Tessmann, Kahn and Shockley (1953); [3] Olpin (1931).

extracts energy from the light beam. However, even when this is a negligible fraction of the total absorbed light one may still expect the correlation to be manifest. All transitions depend, in common, upon the square of the local electric field, if nothing else. In the present model there should be a strong absorption of light due to induced currents in the colloid particle. Using the theory of Gans (1912) for the absorption of light by spheroidal particles together with equation (2) for the index of refraction of the metal one can show that this absorption exists and that the photoemission and optical absorption peaks should coincide.

There do not seem to be any measurements on the optical absorption of hydride cells. However, Kaiser (1952) has observed absorption peaks in films obtained by simultaneous evaporation of alkali halides and alkali metal, which he attributes to colloidal metal deposited on the surface of the films. He finds absorption maxima at 3350 and 4380 ångströms for sodium and potassium respectively presumably corresponding to the photoemission peaks at 3400 and 4500 ångströms in the respective hydride cells.

§ 4. Thin Films

The colloid theory may also be compared with the experiments which have been carried out on thin films. Ives and Briggs (1938) have measured the photoelectric response of thin films of alkali metal spontaneously deposited upon platinum–iridium mirrors. They analysed their data using Fry's theory (1927, 1928, 1932) for the absorption of light by thin absorbing films on a metal backing, together with the empirical optical constants which they had recently obtained (Ives and Briggs 1936, 1937) for this purpose. Table 2 shows Ives and Briggs experimental wavelengths for peak emission together with their calculated values.

Equation (3) may also be applied to the thin film experiment by assuming that the oblate spheroids degenerate into discs ($P=4\pi$). The predicted maxima occur when

$$\omega^2=4\pi Ne^2/m^*(1+4\pi N\alpha). \qquad \ldots\ldots(4)$$

This is just the Wood–Zener critical frequency, corrected for core polarization and effective mass. The calculated values are also listed in table 2. The

differences between Ives and Briggs calculated values and those obtained using equation (3) arise because Ives and Briggs used empirical optical constants, while the free electron theory has been used here. Both treatments predict that peak photo-emission from thin films on a reflecting backing should occur at the Wood–Zener wavelength.

Table 2. Wavelength for Maximum Photoelectric Emission for Thin Films on Pt–Ir Mirrors

Photocathode	Ives and Briggs (1938)		Equation (3)	
	Observed	Calculated	$P/4\pi=1$	$P/4\pi=0{\cdot}85$
K	3450	3400	3200	3450
Rb	3800	3950	3400	3700
Cs	4000	4350	3800	4100

Effective mass and core polarization corrections are tabulated in table 1. $P/4\pi=1$ corresponds to disc of zero height. $P/4\pi=0{\cdot}85$ corresponds to an axial ratio 0·1 (Osborne 1945).

Ives and Briggs consider that the discrepancy between observed and calculated values may be attributed to the finite thickness of the film, which they treat as a uniform lamina. They achieve agreement with experiment by using the thickness of the film as an adjustable parameter. The present treatment, on the other hand, treats the film as composed of numerous disc-shaped spheroids. The experiments of Sennett and Scott (1950) show that this is probably a more accurate picture of the actual state of a thin film. On this assumption, agreement may be obtained, as before, by adjusting the axial ratio (and thus the depolarization factor) of the spheroids. It is significant that in the present case the assumption of extreme disc shape leads to too high a frequency. Assuming an axial ratio of 1/10, rather than zero, the predicted wavelengths become those shown in the last column of table 2. Again only moderate departures from the ideal shape are required to bring the predicted values into agreement with experiment.

§ 5. Conclusion

The selective photoelectric effect has been considered as a frequency dependent local field phenomenon occurring in a colloidal surface structure. Applying the free electron theory to the metal particles an expression for the wavelength of maximum photoelectric emission has been obtained. The theory is compared with experimental results for hydride photocells and for thin films. In both cases the agreement with experiment is satisfactory.

Since the distinction between longitudinal and transverse oscillations vanishes for the systems considered here, it would have been possible to give the discussion a somewhat different appearance by treating the matter from the standpoint of plasma oscillations. However, it seemed preferable to approach the problem using the simpler concepts of the Drude theory, while relying upon its intimate connection with the newly developed analysis of collective modes of behaviour (Pines 1955) for a deeper understanding of the reasons for its success.

Acknowledgments

This work was undertaken while the author was a guest of the Microwave Physics group of the Department of Electronics at the University of Southampton. The auther wishes to express his gratitude for the kind hospitality shown him by Professor E. E. Zepler and Dr. D. J. E. Ingram.

References

Boutry, G. A., 1936, *Les phénomènes photoélectriques et leurs applications* (Paris : Hermann), part II.

Elster, J. T., and Geitel, H., 1910, *Phys. Z.*, **11,** 257, 1082.

—— 1911, *Ibid.*, **12,** 609.

Fröhlich, H., and Sack, R. A., 1947, *Proc. Phys. Soc.*, **59,** 30.

Fry, T. C., 1927, *J. Opt. Soc. Amer.*, **15,** 137.

—— 1928, *Ibid.*, **16,** 1.

—— 1932, *Ibid.*, **22,** 307.

Gans, R., 1912, *Ann. Phys., Lpz.*, **37,** 881.

Hill, A. G., 1938, *Phys. Rev.*, **53,** 184.

Hughes, A. L., and DuBridge, L. A., 1932, *Photoelectric Phenomena* (New York: McGraw-Hill).

Ives, H. E., 1924, *J. Opt. Soc. Amer.*, **8,** 551.

Ives, H. E., and Briggs, H. B., 1936, *J. Opt. Soc. Amer.*, **26,** 238.

—— 1937, *Ibid.*, **27,** 181, 395.

—— 1938, *Ibid.*, **28,** 330.

Kaiser, R., 1952, *Z. Phys.*, **132,** 482.

Lindemann, F. A., 1911, *Verh. dtsch. phys. Ges.*, **13,** 482, 1107.

Mitchell, K., 1934, *Proc. Roy. Soc.*, **146,** 442.

—— 1936, *Ibid.*, **153,** 513.

Mott, N. F., and Jones, H., 1936, *The Theory of the Properties of Metals and Alloys* (London : Oxford University Press), p. 105.

Olpin, A. R., 1930, *Phys. Rev.*, **36,** 251.

—— 1931, *Ibid.*, **38,** 1745.

Osborne, J. A., 1945, *Phys. Rev.*, **67,** 351.

Pines, D., 1955, *Solid State Physics* (New York : Academic Press), Vol. I.

Pohl, R., and Pringsheim, P., 1910, *Verh. dtsch. phys. Ges.*, **11,** 1039.

—— 1910, *Ibid.*, **12,** 697.

Seitz, F., 1954, *Rev. Mod. Phys.*, **26,** 7.

Sennett, R. S., and Scott, G. D., 1950, *J. Opt. Soc. Amer.*, **40,** 203.

Tessmann, J. R., Kahn, A. H., and Shockley, W., 1953, *Phys. Rev.*, **92,** 890.

Tykociner, J. T., and Bloom, L. R., 1941, *J. Opt. Soc. Amer.*, **31,** 689.

Wood, R. W., 1933, *Phys. Rev.*, **44,** 353.

Zener, C., 1933, *Nature, Lond.*, **132,** 968.

Measurement of Ionization and Attachment Coefficients in Dry Air in Uniform Fields and the Mechanism of Breakdown

By A. N. PRASAD
Department of Electrical Engineering, The University of Liverpool

Communicated by J. D. Craggs; MS. received 13th January 1959

Abstract. Measurements of pre-breakdown currents in uniform field conditions in dry air in the E/p range of 25 to 45v cm^{-1} (mm Hg)$^{-1}$ over the pressure range 60—700 mm Hg indicate the presence of appreciable attachment. Assuming dissociative attachment as the mechanism of negative ion formation, it is shown that the growth of current at constant E/p can be represented by the Townsend equation corrected for the removal of electrons from the swarm by attachment. From the semi-logarithmic plots of current against electrode separation, employing this equation the Townsend ionization coefficients α and γ and an attachment coefficient η are evaluated by curve fitting techniques. From the values of attachment coefficient, assuming a Maxwellian distribution, attachment cross sections for various mean electron energies have been evaluated and agree well with earlier measurements. Further, static breakdown potentials have been measured up to $pd \sim 1200$ mm Hg cm. Employing the values of α, γ and η, and the breakdown criterion as derived from the modified Townsend equation, static breakdown potentials have been derived and agree well with measured values, thus confirming the validity of the Townsend build up mechanism.

§ 1. Introduction

In the study of the mechanism of breakdown under static uniform field conditions in non-attaching gases, the Townsend equations,

$$I_d = \frac{I_0 e^{\alpha d}}{1-\gamma(e^{\alpha d}-1)} \qquad \ldots\ldots(1)$$

and

$$\gamma(e^{\alpha d}-1)=1 \qquad \ldots\ldots(2)$$

giving the growth of pre-breakdown current and the criterion for breakdown have been known to be very satisfactory (Llewellyn Jones and Parker 1952, Hopwood, Peacock and Wilkes 1956). In these equations α and γ represent the primary and secondary ionization processes respectively, and d the electrode separation.

In the case of ionization in an attaching gas, however, a new parameter (or parameters) is necessary in the charge transport equations, to account for the removal of electrons from the avalanche due to various attachment processes. Confining ourselves to the case of oxygen (and air), Harrison and Geballe (1953) and Craggs, Thorburn and Tozer (1957) have suggested that the attachment processes are due primarily to dissociative attachment resulting from resonance capture, the cross section for which has been measured to be $2{\cdot}25 \pm 0{\cdot}3 \times 10^{-18}$ cm^2 at 6·7 ev (Craggs, Thorburn and Tozer 1957). In this case, defining a new

parameter η describing the mean number of attachments per centimetre of drift in the field direction, Harrison and Geballe (1953) have derived the following equation for the growth of current under constant field conditions:

$$\frac{I_d}{I_0} = \left[\frac{\alpha}{\alpha-\eta} e^{(\alpha-\eta)d} - \frac{\eta}{\alpha-\eta}\right]. \qquad \ldots\ldots(3)$$

This obviously indicates that the semi-logarithmic plot of current against electrode separation is not linear and also that at comparable magnitudes of the parameters η and α, the current tends to ' saturate '. This equation however does not consider any secondary process at all and implies that all current measurements should be confined to conditions where contributions due to secondary processes are negligible. Consideration of secondary processes yields the following equation for the growth of current:—

$$\frac{I_d}{I_0} = \left[\frac{\alpha}{\alpha-\eta} e^{(\alpha-\eta)d} - \frac{\eta}{\alpha-\eta}\right] \Big/ \left[1 - \frac{\gamma\alpha}{\alpha-\eta}(e^{(\alpha-\eta)d}-1)\right] \qquad \ldots\ldots(4)$$

and the corresponding criterion for breakdown as

$$\frac{\gamma\alpha}{\alpha-\eta}(e^{(\alpha-\eta)d}-1) = 1. \qquad \ldots\ldots(5)$$

The author finds that measurements of pre-breakdown currents in air over a wide range of pressures conform to the above theory, and demonstrate the presence of appreciable attachment in the E/p range of 25 to 45 v cm^{-1} (mm Hg)$^{-1}$.

From the semi-logarithmic plots of current against electrode separation, by a careful process of curve fitting the parameters α, η and γ can be evaluated, employing equations (3) and (4). Further, from values of η so obtained, using the known values of drift and agitation velocities, the cross section for the attachment process can be computed at various mean energies using the relationship

$$\sigma = \frac{1}{N_0}\frac{W}{U}\frac{\eta}{p} \qquad \ldots\ldots(6)$$

where N_0 is the number of molecules/cm^3 at 0°c and 1 mm Hg pressure and W and U are the drift and agitation velocities respectively.

§ 2. Experimental Method and Results

The apparatus used has been previously described by Hopwood, Peacock and Wilkes (1956) and is indicated schematically in figure 1. It essentially consists of the following: A large ionization chamber of approximately 80 litres capacity which can be evacuated to 10^{-5} mm Hg, with an apparent leak rate of 1 μ/hour, by means of an oil diffusion pump. The electrodes are of aluminium alloy, machined to a Rogowski profile, with an overall diameter of 15 cm, the anode being perforated and mounted on a tubular high-voltage bushing with built-in quartz lenses to facilitate the ultra-violet irradiation of the cathode. The ultra-violet source is a low pressure mercury discharge lamp situated directly above the bushing and fed from a stabilized a.c. supply. A quartz envelope photocell of Type QVA-39, incorporated in the lamp assembly, indicates variations of the intensity of the lamp. The gas pressures are measured either on an oil manometer using silicone oil of specific gravity of 1·09 to within 0·1 mm Hg or

a micromanometer utilizing metal bellows as a pressure sensitive element to within $\pm 0{\cdot}5$ mm Hg. The electrode separation is measured to within $\pm 0{\cdot}005$ mm by means of a rigidly supported micrometer. The h.t. needed is supplied from an r.f. power unit and a potential divider system with a short term stability of 2 parts in 10 000. The voltage applied to the chamber, variable in steps of 20v, is calculated to 0·4% by measuring to 0·1% the current flowing down the potential divider chain and using predetermined values of the resistance of the potential divider up to various tapping points obtained under working conditions to within 0·3%.

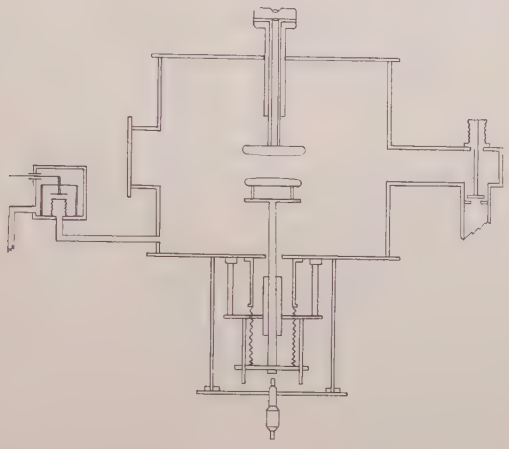

Figure 1. Schematic diagram of the ionization chamber.

The ionization currents are measured by a balanced electrometer bridge comprising two electrometer triodes of Type ET1 of G.E.C. with a set of high stability resistances in the range 10^6 to 10^{11} ohms on each. The values of these resistances were measured to within 1% using a Weston Standard Cell and the electrometer circuit. A high sensitivity Tinsley galvanometer is used as the null detector of the bridge. By carefully balancing the heater currents of the two electrometer triodes, zero drift of the bridge was reduced to the order of 1 cm for 8 to 10 working hours, while the sensitivity of the bridge was of the order of 3·5 cm mv^{-1} input. The bridge is supplied from a set of special high stability low leakage batteries.

All current measurements were repeatedly checked for reproducibility to within 5% at all pressures. The intensity of the ultra-violet lamp, as indicated by the output of the photocell was also carefully watched for any possible variations. It was found that the discharge lamp took approximately 60 to 90 minutes to stabilize, after which period variations in the intensity of the lamp were negligible. A similar time was needed for ultimate stabilization of the h.t. unit and the photo emission from the cathode as well. Hence a period of 90 minutes was allowed as the warming up time before measurements were commenced. The air was never left in the chamber for longer than 48 hours, during which time the rise in pressure, as indicated by the oil manometer, which was used differentially for this purpose, was negligible.

The measurements of pre-breakdown currents were first made in cylinder air free from water vapour and carbon dioxide supplied by the B.O.G. Ltd. The air, however, was passed through a cold trap using a mixture of acetone and solid carbon dioxide to be certain of its dryness. The experiments were conducted over a pressure range of 60 to 700 mm Hg (corrected to 20°c) and an E/p range of 25 to 60 v cm^{-1} (mm Hg)$^{-1}$. Breakdown voltage measurements were then made at 700 and 300 mm Hg (corrected to 20°c) up to a maximum pd of 1190 mm Hg cm. The cathode was then 'cleaned' by running a low pressure glow discharge in an atmosphere of oxygen-free hydrogen in the chamber for approximately 30 minutes.

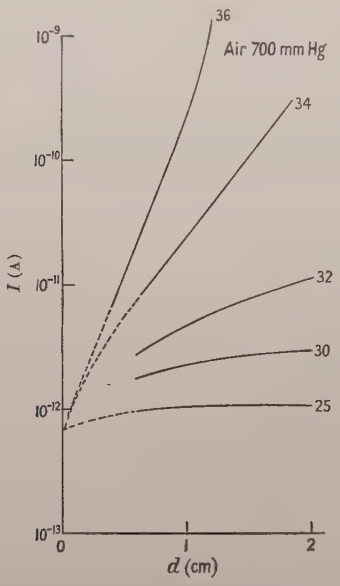

Figure 2. Ionization currents in dry air at 700 mm Hg pressure for various constant values of the parameter E/p (v cm^{-1} (mm Hg)$^{-1}$).

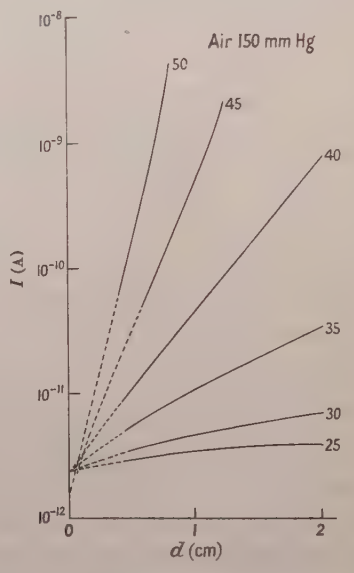

Figure 3. Ionization currents in dry air at 150 mm Hg pressure for various constant values of the parameter E/p.

The entire range of experiments was then repeated in room air filtered over a plug of cotton wool and dried in a liquid nitrogen cold trap. Breakdown measurements were made at 300 mm Hg (corrected to 20°c).

For the sake of brevity, (log I, d) plots at two pressures only are given in figures 2 and 3 which exhibit curvatures characteristic of equations (3) and (4). It was found, however, that beyond a particular value of E/p, for each pressure, the curvature of the (log I, d) plot ceased to be apparent and the plot was linear, with an upcurving at high voltages, as in a non-attaching gas. Further some of the plots had an elongated S shape, indicating the simultaneous presence of α, η and γ mechanisms (cf. equation (4)). (Current measurements have since been made in argon and indicated no curvature in the (log I, d) plots, thus confirming the accuracy of the equipment and technique.) The results of this entire study can be broadly grouped under two headings: (*a*) the evaluation of the coefficients α and η and (*b*) breakdown measurements. It was found that there was good agreement in the values to be reported of the parameters α and η and

the measured values of the breakdown voltages V_s, between those of dried cylinder air and dried room air within the experimental scatter, proving that there was no difference in fundamental properties of the two types of air used.

(*a*) *Evaluation of* α *and* η.

From the non-linear plots of (log I, d) at various pressures, the coefficients α and η were evaluated by a careful process of curve fitting, employing equation (3). The values of α/p obtained at pressures of 150 and 300 mm Hg agree within the experimental scatter and have been taken for computing the mean (α/p, E/p) curve, as indicated in figure 4, curve (*a*). It is suggested that the large scatter in the α/p values at low E/p, particularly at low pressures, is due to the limitations of the technique of evaluation of the coefficients by curve fitting, when the amplification of the current is small and the current tends to 'saturate'. Under

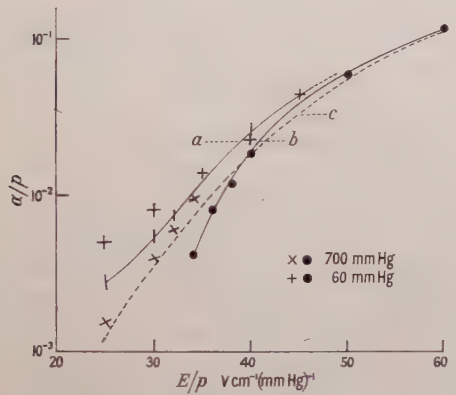

Figure 4. Values of α/p as a function of E/p in dry air. *a*, α/p values corrected for attachment from the present study; *b*, α/p values uncorrected for attachment from the present study; *c*, earlier measurements of α/p (Harrison and Geballe 1953).

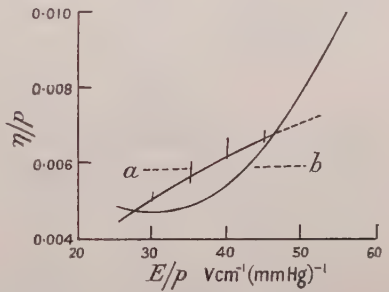

Figure 5. Attachment coefficient η/p as a function of E/p in dry air. *a*, present study; *b*, earlier work (Harrison and Geballe 1953).

these conditions only η can be evaluated with any degree of accuracy. These points are indicated along with those obtained at 700 mm Hg in figure 4, curve (*a*). It was found that the values of η/p for any particular value of E/p, at various pressures, agreed within the experimental scatter as indicated in figure 5, curve *a*. This suggests that there is no pressure effect in the attachment mechanism as such, thus confirming that dissociative attachment is the process leading to the negative ion formation in this case. The mean values of α/p and η/p from this study further differ appreciably from the previous measurements of Harrison and Geballe (1953) which are indicated in figures 4, curve *c*, and 5, curve *b*, for comparison.

'Apparent' values of α/p were evaluated from the linear plots of (log I, d) on the assumption that equation (1), which does not consider attachment, and hence represents a linear plot, was operative and are indicated in figure 4, curve *b*, where again the values obtained at 150 and 300 mm Hg were taken to compute the mean curve. It was found that these values, which were uncorrected for attachment, were consistently below those obtained from the non-linear plots

and further agree with the earlier measurements of Sanders (1932), Llewellyn Jones and Parker (1952) (see § 4). Mean values of α/p (true and apparent) and η/p from this study are summarized in table 1.

Table 1

E/p	Mean Value of α/p		Mean Value of η/p
(v cm^{-1} (mm Hg)$^{-1}$)	True Value†	Apparent Value‡	
25	$2{\cdot}8 \times 10^{-3}$	—	$4{\cdot}5 \times 10^{-3}$
30	$5{\cdot}45 \times 10^{-3}$	$1{\cdot}00 \times 10^{-3}$ (extrapolated)	$5{\cdot}1 \times 10^{-3}$
35	$1{\cdot}26 \times 10^{-2}$	$5{\cdot}7 \times 10^{-3}$	$5{\cdot}7 \times 10^{-3}$
40	$2{\cdot}63 \times 10^{-2}$	$2{\cdot}0 \times 10^{-2}$	$6{\cdot}3 \times 10^{-3}$
45	$4{\cdot}60 \times 10^{-2}$	$4{\cdot}0 \times 10^{-2}$	$6{\cdot}75 \times 10^{-3}$
50	—	$6{\cdot}40 \times 10^{-2}$	—
55	—	$9{\cdot}05 \times 10^{-2}$	—
60	—	$1{\cdot}23 \times 10^{-1}$	—

† Evaluated from non-linear plots of log I against d.
‡ Evaluated from linear plots of log I against d, uncorrected for attachment.

§ 3. Mean Cross Section for Attachment

The mean cross sections for attachment have been computed for various mean electron energies from the measurements of η/p using Townsend's measurement of drift and agitation velocities (Healey and Reed 1941) and are plotted in figure 6, curve *a* together with recent measurements of Harrison and Geballe (1953) and Kuffel (1958) (curves *b* and *c*). Calculated values of cross section (Tozer 1958, private communication) at various mean energies for dissociative attachment assuming a Maxwellian distribution are also indicated.

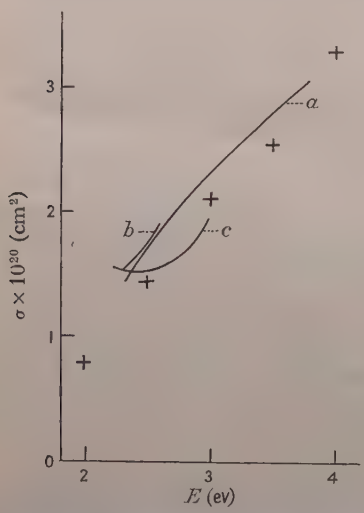

Figure 6. Attachment cross sections in dry air as a function of mean energy. *a*, present study; *b*, Kuffel (1958); *c*, Harrison and Geballe (1953); crosses, calculated values (Tozer 1958).

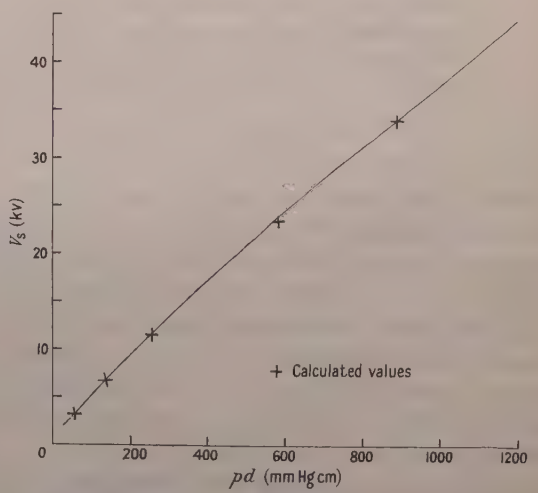

Figure 7. Observed breakdown potentials in dry air as a function of pd.

(*b*) *Breakdown measurements.*

Breakdown voltages as measured at 700 and 300 mm Hg showed no pressure dependence for any particular value of *pd* and are plotted together in figure 7, while table 2 summarizes the measurements of earlier work. Values of breakdown potential have been calculated from both the linear and the non-linear plots of log *I* against *d* using the appropriate breakdown criteria (equations (2) and (5)) and agree with the measured values to within 1 to 2% as indicated in figure 7. Table 3 summarizes the values of α (true and apparent), d_s the calculated value of the breakdown gap and γ from this study as calculated for various runs.

Table 2

	Breakdown Potential (kv)						
pd (mm Hg cm)†	(1)	(2)	(3)	(4)	(5)	(6)	(7)
380	19·8	17·4	16·41	16·9	16·6	16·3	16·25
760	31·55	31·7	30·3	30·1	30·2	29·4	29·6
1140	—	—	—	—	43·2	—	42·3
1520	—	59·6	57·04	55·7	55·8	—	—

† $p = 760$ mm Hg at 20°c.

(1) Spath
(2) Schumann } Fisher (1947)
(4) Fisher

(3) Bruce (1947)
(5) Köhrmann and Raether (1954)
(6) Llewellyn Jones and Parker (1952)
(7) Present study.

Table 3

p (mm Hg at 20°c)	*E*/*p*†	α/p	η/p	γ	d_s (cm)	V_s (kv) calc.	V_s (kv) meas.
700	40	$1{\cdot}65\times10^{-2}$	—	$6{\cdot}57\times10^{-5}$	0·835	23·4	23·7
	38	$1{\cdot}19\times10^{-2}$	—	$2{\cdot}53\times10^{-5}$	1·27	33·8	33·7
300	45	$4{\cdot}25\times10^{-2}$	—	$2{\cdot}98\times10^{-5}$	0·836	11·3	11·2
150	50	$6{\cdot}15\times10^{-2}$	—	$2{\cdot}48\times10^{-4}$	0·902	6·76	6·7
	45	$4{\cdot}4\times10^{-2}$	$6{\cdot}8\times10^{-3}$	$7{\cdot}85\times10^{-5}$	1·663	11·23	11·2
60	60	$1{\cdot}16\times10^{-1}$	—	$2{\cdot}02\times10^{-3}$	0·89	3·21	3·2
	50	$5{\cdot}9\times10^{-2}$	—	$4{\cdot}13\times10^{-4}$	2·205	6·615	6·6

†E/p in units v cm^{-1} $(mm\ Hg)^{-1}$

§ 4. Discussion

The discrepancy in the α/p values from the linear and the non-linear plots of log *I* against *d* can be explained from the following considerations. From equation (3) the slope at any particular value of electrode separation, *d*, of the log *I* against *d* plot is

$$\frac{\partial\,(\log I)}{\partial d} = \frac{\alpha\, e^{(\alpha-\eta)d}}{[\alpha/(\alpha-\eta)]\, e^{(\alpha-\eta)d} - \eta/(\alpha-\eta)}.$$

When the magnitudes of α (and or *d*) are such that

$$\frac{\alpha}{\alpha-\eta}\, e^{(\alpha-\eta)d} \gg \frac{\eta}{\alpha-\eta}$$

the above equation can be approximated to a constant ($=\alpha-\eta$). The interpretation, however, of the slope at medium values of α is complex and the slope does not represent any simple quantity. Further when α is large compared with η, the curvature of the plot is apparent only at small electrode separations ($d<1$ cm) and hence if the plot is confined to electrode separations greater than 1 cm, the straight line drawn through the points is apt to represent a quantity of the order of $\alpha-\eta$ and the extrapolated value of the current would not represent the true value of I_0. The former conclusion is borne out from the present measurements and explains the observed linearity of the (log I, d) plots. The 'apparent' values of α/p from the linear plots in the E/p range of 35 to 45 v cm^{-1} (mm Hg)$^{-1}$ agree with those of $(\alpha-\eta)/p$ from the non-linear plots (of table 1 and figures 4 and 5). This could not be tested for the apparent values of α/p for $E/p>45$, since the measurements of true values of α/p were available only up to $E/p=45$. There is however a pronounced gap between the extrapolated values of the true (α/p, E/p) curve and the apparent (α/p, E/p) curve.

Regarding the criterion for breakdown, however, consideration of a 'linear' plot with the slope of $\alpha-\eta$ yields

$$\gamma(e^{(\alpha-\eta)d}-1)=1$$

as the criterion, whereas the true criterion is given by equation (5). In the latter, since $\alpha/(\alpha-\eta)$, when $\alpha\gg\eta$, is of the order of unity, there is no appreciable error in d_s, the calculated value of the breakdown gap. Hence the breakdown voltages calculated from the linear plots would yield nearly correct values, as borne out in the present study and the earlier work of Llewellyn Jones and Parker (1952).

The satisfactory agreement between the values of the cross section for attachment from this study, and the recent measurements and the calculated values, and the absence of any pressure effect in the η/p measurements in this study, justifies the assumption of the dissociative attachment being operative under the conditions of present study. Further no 'upcurving' at low values of E/p in the (η/p, E/p) curve has been observed in the present study, contrary to the earlier measurements (Harrison and Geballe 1953) (figure 5) and the cross section values at these values of E/p agree well with the recent measurements of Kuffel (1958) on a modified Bradbury apparatus, as shown in figure 6.

§ 5. Conclusions

The good agreement between the measured and calculated values of breakdown potential confirms the view as held by the previous workers (Llewellyn Jones and Parker 1952, Bandel 1954, Fisher 1956) that the static breakdown in air is brought about by the Townsend build-up processes up to a pd of 1200 mm Hg cm and that no new mechanism need be postulated to explain the breakdown in air. Further the author submits that dissociative attachment is appreciable in air up to pressure of the order of one atmosphere and that the values of α/p evaluated from linear plots of log I against d are apt to be in appreciable error unless corrected for attachment.

Acknowledgments

The work described in this paper has been directed by Professor J. D. Craggs. The author is indebted to Mr. B. A. Tozer for valuable discussions and suggestions

and is further grateful to the University of Liverpool for the award of a Fellowship and to the Electrical Research Association for a supplementary grant, and permission to publish this paper, a copy of which has earlier been submitted for publication as E.R.A. Report No. L/T378.

References

Bandel, H. W., 1954, *Phys. Rev.*, **95**, 1117.
Bruce, F. M., 1947, *J. Instn Elect. Engrs*, Pt. II, **94**, 138.
Craggs, J. D., Thorburn, R., and Tozer, B. A., 1957, *Proc. Roy. Soc.* A, **240**, 473.
Fisher, L. H., 1947, *Phys. Rev.*, **72**, 423.
—— 1955–56, *Appl. Sci. Res., Hague*, B, **5**, 281.
Harrison, M. A., and Geballe, R., 1953, *Phys. Rev.*, **91**, 1.
Healey, R. H., and Reed, J. W., 1941, *The Behaviour of Slow Electrons in Gases* (Australasia: Amalgamated Wireless).
Hopwood, W., Peacock, N. J., and Wilkes, A., 1956, *Proc. Roy. Soc.* A, **235**, 334.
Köhrmann, W., and Raether, H., 1954, *Naturwissenschaften*, **41**, 400.
Kuffell, E., 1958, *Proc. Phys. Soc.*, **71**, 516.
Llewellyn Jones, F., and Parker, A. B., 1952, *Proc. Roy. Soc.* A, **213**, 185.
Sanders, F. H., 1932, *Phys. Rev.*, **41**, 667.

Noise Spectra of a Probe in a Hot-Cathode Discharge

By CHATAR SINGH†
Department of Physics, University of Malaya, Singapore

Communicated by J. A. Ratcliffe; MS. received 24th February 1959

Abstract. Measurements have been made with a floating and a biased probe of the low-frequency noise which occurs in hot-cathode discharges through mercury vapour at low pressures. As previously reported by Cobine and Gallagher, and Martin and Woods, the spectrum is continuous but there are no superimposed peaks of oscillation. The spectra agree with that of the tube noise in their general shape. It has been shown that the primary electrons from the cathode are not essential for the noise to be recorded from the probe.

§ 1. Introduction

Low-frequency tube noise emanating from low-pressure gas discharges has been investigated by Cobine and Gallagher (1947 a), Martin and Woods (1952), Thong Saw Pak (1955) and others. The noise spectrum extends up to frequencies of several megacycles per second; above 10 kc/s there is a rapid decrease in amplitude with increase in frequency. Integrated noise at a floating probe, i.e. one which is at the potential of the tube wall, and a biased probe has been measured by Thong Saw Pak (1954, 1955) and its relationship with the probe characteristic curve established.

The present investigation was undertaken primarily to analyse the frequency spectrum of the discharge noise at a floating and a biased probe, for the collecting plate perpendicular to and along the anode–cathode line, with the probe shielded and unshielded; secondly, to see if this spectrum bears any relationship with that of the tube noise; and finally, to find out the possible source of the observed noise.

§ 2. Experimental Arrangements

The experimental tube, which contained mercury vapour at pressures between 2×10^{-6} and 2×10^{-3} mm Hg, is shown in figure 1. The vacuum was maintained by an oil-diffusion pump backed by a Speedivac high vacuum rotary pump. The

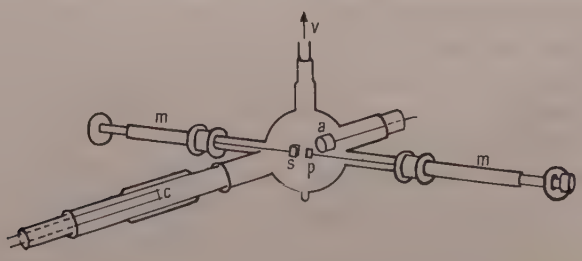

Figure 1. The discharge tube. a, anode; c, cathode; p, probe; s, shield; m, movable probe device; v, to vacuum train.

† Now at Cavendish Laboratory, Cambridge.

anode was a hollow nickel cylinder open at both ends, 3 cm long and 2·5 cm in diameter. The cathode was a 200 micron tungsten filament, 2 cm in length. The cathode was about 37 cm away from the anode and current saturation was obtained at approximately 40 v. The probe was a nickel plate 8 mm square and 0·2 mm thick, spot-welded edge-on to a 0·3 mm tungsten wire which was in turn spot-welded to a 1 mm tungsten rod. The tungsten wire and rod were electrically shielded by a glass sleeve. The end of the tungsten rod was silver-soldered to a slide rod of a movable-probe device which permitted forward and backward motion of the probe. The probe collector plate was about 5 cm from the anode. It could be set at any desired angle to the anode–cathode line by rotating the ground-glass cone which carried the movable-probe mechanism. The probe shield was made of 0·2 mm nickel plate bent into a U-shape. Its dimensions were 1·5 cm × 1·5 cm × 0·5 cm. The shield was soldered to the slide rod of another movable-probe device. The probe could be shielded completely by advancing the U-shield sufficiently.

Accumulators were used for the h.t. and the l.t. supplies, in conventional tube and probe circuits. The anode was earthed. The circuit for obtaining the tube noise spectra was connected directly to the cathode. The output leads of the probe were connected to a two-pole four-way switch to give the required selections of a floating or a baised probe to the cathode-ray oscilloscope or the noise analyser. A Furzehill cathode-ray oscilloscope, type 0·100 was used, which gave a uniform response to within 0·5 dB in the frequency range of 0 to 1 Mc/s.

Two analysers capable of covering the frequency range of 30 c/s to 1 Mc/s were used to obtain the noise spectra. The first was built on the lines of Scott's harmonic wave analyser (Scott 1938). This circuit consisted of a straightforward three-valve amplifier with inverse feedback from the output to the input. A parallel-T resistance–capacitance network was used in the feedback loop. The feedback network balanced at a null frequency equal to $(2\pi RC)^{-1}$. This analyser covered a frequency range from 30 c/s to 10 kc/s. For frequencies up to 1 Mc/s an extension was built which could be attached to the first analyser. The circuit was identical with a superheterodyne circuit used by Cobine and Curry (1946). The heterodyne system used the first analyser as a tuned detector set at 2 kc/s.

Following the practice of other workers on this subject, the noise level has been expressed in decibels relative to a zero level of $10\,\mu\text{v}/(\text{kc/s})^{1/2}$.

§ 3. Experimental Results

With the hollow cylindrical anode, a very stable discharge was obtained and the tube was filled with plasma.

The results of Martin and Woods (1952) and Thong Saw Pak (1955) concerning the relationship between integrated tube noise and the tube characteristic curve were confirmed. Noise was found to be generally high in the non-saturated part of the characteristic curve.

The low frequency tube noise spectra agreed with those reported by Cobine and Gallagher (1947 b) and by Martin and Woods (1952) in their general shape and noise level, but differed strongly in that there were no large amplitude oscillations superimposed on the random noise. A typical example is given in figure 2, set A, *c*.

The results of Thong Saw Pak (1954) concerning the relationship between the tube characteristic curve and the integrated noise from a floating probe in a

current-saturated discharge were confirmed and extended in several respects. In the infra current saturated region of the tube characteristic, the tube noise level was greater than that of the floating probe. As current saturation set in, the tube noise died down and the noise of the floating probe started to build up rapidly until it reached a maximum and then remained fairly constant up to the highest voltages applied, 480 v. The noise level at a floating probe was measured

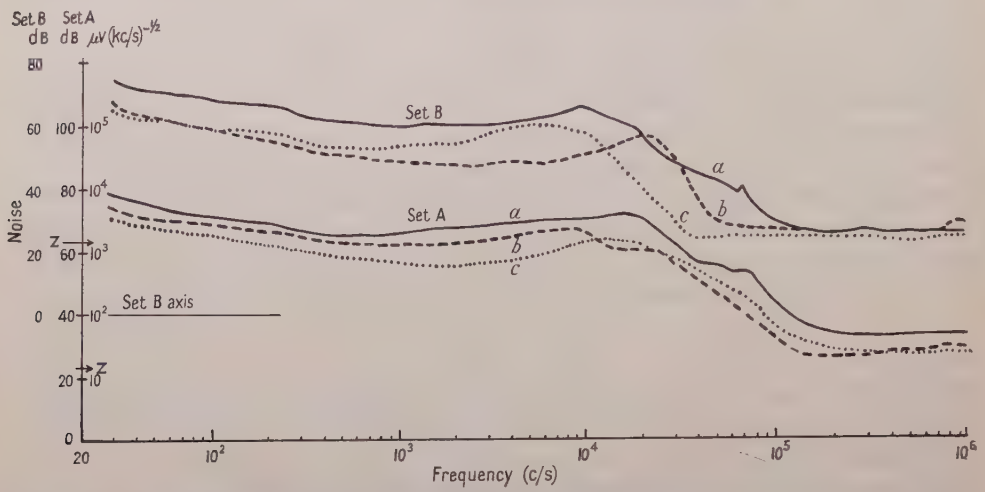

Figure 2. Set A, comparison of the unshielded floating probe noise spectra with tube noise, *c*; set B, noise spectra of the unshielded biased probe at three different probe potentials. (Z = zero level of instruments).

	Set A			Set B		
	a	*b*	*c*	*a*	*b*	*c*
Room temperature (°C)	27·8	29·0	28·0	27·3	28·5	29·0
Filament current (A)	4·64	4·38	4·45	3·25	4·55	4·42
Tube voltage (v)	160	140	56	310	244	78
Tube current (mA)	68·4	44	56	8·6	8·8	4·9
Probe voltage (v)	—	—	—	−8·8	−10·7	−21·0
Probe current (mA)	—	—	—	0·7	0·5	0
Probe position	perp.	par[1]	perp.	peak	space	wall

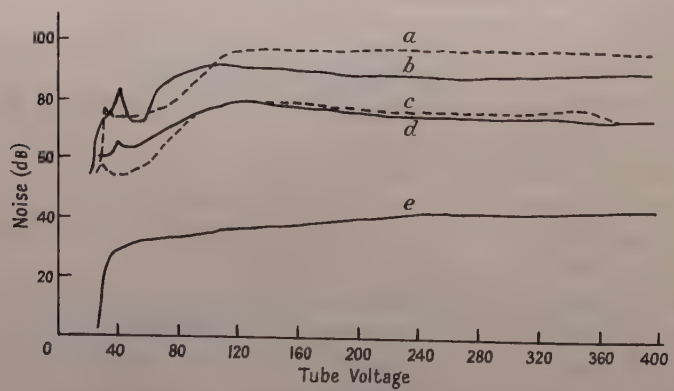

Figure 3. Noise curves from a floating probe; *a*, *b*, unshielded probe in perpendicular and parallel position respectively; *c*, *d* shielded probe in perpendicular and parallel position respectively; *e* typical tube characteristic curve.
Room temperature = 27·0°C; filament current = 4·5 amp.

for different orientations of the collector plate, with the plate shielded and unshielded. It was found that the noise picked up was a maximum when the plate was perpendicular to the anode–cathode line and when it was not shielded. Figure 3 shows a set of noise curves from a floating probe.

With the floating probe in the 'perpendicular' and 'parallel' positions, the noise from the current saturated discharge again had a broad continuous spectrum without any superimposed peaks. The spectrum extended from audio frequencies into at least the megacycle region. A general decrease in noise level was observed when the probe was in the parallel position and when the collector-plate was shielded, otherwise the spectra were identical. The application of two widely differing tube voltages also did not alter the general shape and level of the spectra. Figure 2, set A, shows the striking similarity in the general shape of the tube noise spectrum and the floating probe noise spectra for the unshielded collector plate in the perpendicular and parallel positions.

Additional results were obtained by using a biased probe. The results reported by Thong Saw Pak (1954) concerning the relationship between the probe characteristic curve and the integrated noise at a probe for different values of the probe bias were confirmed and extended by shielding and orientating the collector-plate at various angles to the anode–cathode line. The probe characteristic curve was parallel to the voltage axis from -160 v to wall potential, -30 v. Between wall and space potential there was a gradual increase in the current but after space potential the curve rose very steeply and continued rising even after the probe had taken over the discharge.

For the probe in the perpendicular and parallel positions, the noise curve was practically flat for large negative bias (~ -140 v). As the probe in the perpendicular position was made more and more positive a small drop in noise level was followed by a steep increase on approaching wall potential. The noise attained a maximum value at space potential and remained steady until the probe took over the discharge. No striking difference was observed on shielding the probe. However, an interesting observation was made with the probe in the parallel position. A sharp and well-defined noise peak which did not alter on shielding the collector-plate appeared at approximately the wall potential. A typical example of the above observations is given in figure 4.

Figure 2, set B, shows the noise spectra of the biased probe (perpendicular position) taken at wall potential, at space potential and at the noise maximum just past the space potential. Note that even the noise at a probe biased to different potentials has a broad continuous spectrum without a single oscillation peak. These spectra agree with that of the tube noise spectrum in their general shape. The noise spectra of the probe at space and wall potentials have a lower noise level but the amplitude decreases more rapidly at the transition frequency region.

A second set of spectra were obtained at the same three positions mentioned above but with the probe rotated through 90°. The spectra were again continuous and similar to that of the tube noise. Even shielding the collector-plate made no difference to their general shape though there was a decrease in the noise level.

In an attempt to find if the primary electrons from the cathode were responsible for the noise at a probe, the probe was made more negative (-160 v) than the applied anode voltage (70 v). No electrons emitted by the cathode could then reach the probe's surface. On comparing the spectra obtained with that of the tube noise it was found that there was no clear-cut difference between these.

However, the fact that the noise persisted at the probe and had a spectrum similar to that of the tube noise, suggested that reception of the direct primary electrons at the probe was not essential for the noise to be recorded from the probe.

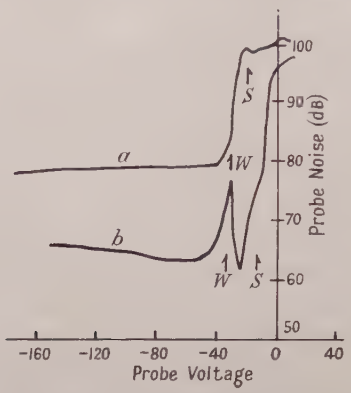

Figure 4. Noise curves of a shielded biased probe in the *a*, perpendicular and *b*, parallel position.

	a	*b*
Room temperature (°C)	28·8	28·1
Filament current (A)	4·43	3·93
Tube voltage (V)	330	137
Tube current (mA)	40·0	17·9
Wall potential, *W* (V)	−29·5	−32·5
Space potential, *S* (V)	−21·0	−13·0

§ 4. Discussion

The work has confirmed and extended the experimental results of previous workers.

A floating probe is about 15 V negative to space potential and has an ion sheath surrounding its collector plate. The vibration of this ion sheath could possibly be responsible for the noise. From results obtained by placing a probe close to the cathode, thereby increasing the number of primary electrons reaching the collector, Thong (1954) concluded that the ion sheath surrounding the floating probe in a current-saturated discharge was being disturbed by the bombardment of the direct primary electrons from the cathode. The observations now made of the integrated noise at a floating probe (perpendicular position) shielded to cut off the direct primary electrons from the cathode suggest that the direct primary electrons are not responsible for disturbing the probe ion sheath, since the integrated noise curve obtained was similar to that of an unshielded probe, apart from the initial drop of about 20 dB. Further evidence for this was obtained on comparing the noise spectra of a shielded floating probe with that from an unshielded one, operated under similar conditions. With the probe biased to a negative potential greater than that of the anode, a noise spectrum not much different from that of the tube noise or noise from an unshielded probe was obtained. This gives further weight to the view that the noise at a floating or biased probe does not arise from the probe ion sheath being disturbed by bombardment from the direct primary electrons emitted by the cathode. Instead, it is suggested that the ion sheath is caused to vibrate by a series of irregular pulses from, or transmitted by, the surrounding plasma.

As already stated it was observed that shielding and orientating the collector plate of a floating probe caused no difference in the general trend of the integrated noise curves. This suggests that the mechanism causing the probe ion sheath to vibrate and produce noise was effective from all directions. Again it also leads one to suppose that the fluctuations of the space charge potential in the homogeneous plasma surrounding the probe are responsible for the disturbances, or that the plasma assists in transferring the actual mechanism actuating the probe ion sheath. This latter view would be compatible with the vibration of the ion sheath between the tube wall and the plasma being a possible source of the disturbances (cf. Gabor, Ash and Dracott 1955).

The close similarity between the noise spectra from a probe biased to space potential and to wall potential, which is effectively the potential of the floating probe indicates that there is only one type of noise affecting the probe in the two positions. Comparison of the tube noise spectrum with the spectra obtained from a floating and a biased probe in the perpendicular and parallel positions again reveals the close similarity in their general shape and regions of transition frequencies, thus indicating that the noise at the probe resembles that across the discharge electrodes. It is suggested, therefore, that plasma space charge fluctuation could cause the discharge noise, both across the tube and at the probe.

Acknowledgments

This work was carried out under the supervision of Dr. Thong Saw Pak whilst the author was a Shell Research Fellow of the University of Malaya. The author is indebted to Professor K. G. Emeléus for his interest and advice.

References

Cobine, J. D., and Gallagher, C. J., 1947 a, *J. Franklin Inst.*, **243,** 41.
—— 1947 b, *J. Appl. Phys.*, **18,** 110.
Cobine, J. D., and Curry, J. R., 1946, *Rev. Sci. Instrum.*, **17,** 190.
Gabor, D., Ash, E. A., and Dracott, D., 1955, *Nature, Lond.*, **176,** 916.
Martin, H., and Woods, H. A., 1952, *Proc. Phys. Soc.* B, **65,** 281.
Scott, H. H., 1938, *Proc. Inst. Radio Engrs, N.Y.*, **26,** 226.
Thong Saw Pak, 1954, *Ph.D. Thesis*, Queen's University of Belfast.
—— 1955, *Proc. Phys. Soc.* B, **68,** 292.

The Critical Stress for the Production of Pressure Crack Figures on Diamond Faces

By V. R. HOWES
Royal Holloway College (University of London), Egham, Surrey

Communicated by S. Tolansky; MS. received 3rd March 1959

Abstract. In recent papers static impact tests carried out on different diamond surfaces have been described. Here the quantitative results from these experiments are collected together and are then compared with theoretically derived values for the critical average stress for cracking to be initiated on the different diamond surfaces.

Both theoretical and experimental results show that the octahedral face is less resistant to cracking than the cubic face; but theoretical values obtained are of the order of 100 times greater than the corresponding experimental values.

This, together with other considerations, is thought to indicate experimentally some sort of flaw distribution in diamond.

§ 1. Introduction

In recent investigations (Howes and Tolansky 1955, Tolansky and Howes 1957) static impact experiments have been described which have been carried out on different diamond surfaces, with the consequent production of pressure crack figures on the faces. From these experiments average pressures could be directly deduced and, from the values of load and area for the particular condition at which the crack figures were initiated, the corresponding critical average stresses could be found.

In the earlier experiments the load was applied first and the surface studied after its consequent removal, no areas of contact being measured. Here the quantity calculated was called the *nominal* average stress for the production of cracking and this is defined as being the maximum load applied divided by the greatest surface crack area for any particular test. In later experiments observation was possible *during* the application of the load so that the value of the load and the area of the circle of contact could be evaluated at the precise moment when the crack figure first appeared. Here the calculated quantity is called the *real* critical average stress and is the load at the initiation of cracking divided by the corresponding circular area of contact.

It would be possible to derive from this experimental value a fundamental physical quantity by making the necessary theoretical assumptions, but it has been thought better to compare directly the experimental critical average stress value with a corresponding theoretical one derived from fundamental physical data by using certain theoretical assumptions.

In the derivation of a theoretical value for the critical average stress, the main assumption made is that the stress field in diamond below the circular area of contact of a sphere on the diamond face is isotropic, conforming with the theoretical stress field derived by Hertz. The value derived will be approximate

only, but at least should be of the right order of magnitude and on this basis can be compared with the experimental results.

§ 2. The Theoretical Derivation

It has been definitely established (Howes and Tolansky 1955) that whatever face of diamond is slowly impacted, the cracks form along the intersections of (111) planes with the face, i.e. the initial cracking is in the (111) planes of easy cleavage.

Ramasesham (1946) calculated the cleavage energy per unit area for different planes of diamond, using a value of the c-c bond energy of $6{\cdot}22\times10^{-12}$ erg (Harkins 1942). For the (111) plane this energy was found to be 11 330 erg cm^{-2}.

Now, after Orowan (1948–9), where fracture begins the critical fracture (tensile) stress σ_c is obtainable as follows:

$$\begin{aligned}\text{cleavage energy} &= \text{elastic energy available for tensile fracture}\\ &= \text{energy density}\times\text{volume}\end{aligned}$$

hence $$e=\tfrac{1}{2}\sigma_c^2/E\times(1\times a) \qquad \text{or} \qquad \sigma_c^2=2Ee/a$$

where E is the Young's modulus, a is the atomic spacing, and e is the cleavage energy of the surface of fracture; for diamond a is 1·54 Å (Bragg and Bragg 1913), and e is 11 330 erg cm^{-2} for a (111) plane. The elastic constants of diamond given by Bhagavantam and Bhimasenachar (1945) are $c_{11}=9{\cdot}5$, $c_{12}=3{\cdot}9$ and $c_{44}=4{\cdot}3\times10^{12}$ dyn cm^{-2}; and from these, the Young's modulus perpendicular to a (111) plane, i.e. along the diagonal of the cubic cell is $10{\cdot}2\times10^{12}$ dyn cm^{-2}. By inserting this value for E in the above equation, a value of $3{\cdot}8\times10^{12}$ dyn cm^{-2} is obtained for the (111) cleavage stress of diamond.

To derive from this quantity a value of the critical average stress, the Hertzian stress field (Hertz 1881) for a sphere pressing on an isotropic material has to be assumed for an anisotropic crystal—diamond—under similar pressure. Making this assumption, the maximum tensile stress which will occur at the perimeter of the area of contact will act parallel to the undisturbed surface and will have the value given by the equation (Timoshenko 1934)

$$\text{MTS}=\tfrac{1}{3}(1-2\nu)p_0$$

where ν is Poisson's ratio and p_0 is the pressure at the centre of the area of contact, and is equal to $3p/2$ where p is the average pressure applied. For diamond, Poisson's ratio is 0·3, i.e. $c_{12}/(c_{11}+c_{12})=3{\cdot}9/13{\cdot}4$; this gives $\text{MTS}=0{\cdot}2p$.

By considering the critical value when fracture occurs and remembering that it occurs not in the direction normal to the surface where the tensile stress is maximum, but along (111) planes inclined to this normal, then by applying Sohncke's law, it is seen that the cleavage stress is

$$\sigma_c=(\text{MTS})_c\sin^2\theta$$

hence $\sigma_c=0{\cdot}2p_c\sin^2\theta$ and $p_c=19\times10^{12}/\sin^2\theta$ dyn cm^{-2} where θ is the angle of inclination of the (111) plane to the particular diamond face concerned.

Thus, for the octahedral face where $\theta=70^\circ32'$, the calculated theoretical value for the critical average stress p_c is 21×10^{12} dyn cm^{-2}, for the cubic face ($\theta=54^\circ44'$) p_c is 29×10^{12} dyn cm^{-2}, and for the dodecahedral face, where there are two sets of intersecting (111) planes, $p_c=19\times10^{12}$ dyn cm^{-2} for the set for which θ is largest, i.e. 90° (the other value of θ is 35°16′).

§ 3. Experimental Values from the Various Tests

The numerical data derived from the experimental tests on diamond are collected together in the table.

Similar experiments using a tungsten carbide ball of 1 mm diameter on glass surfaces gave critical average stress values of between 200 and 250 kg mm^{-2}, which, compared with the value of 1100 kg mm^{-2} for the octahedral face of diamond shows the latter to be about five times more resistant to pressure cracking than glass.

It is seen from the table that the octahedral face is the least resistant on diamond, the real critical average stress being two and a half times less than that for the truncated cubic face in comparable tests.

§ 4. Discussion

Both experimental and theoretical results indicate that the cubic plane has greater resistance to cracking than the octahedral. The results for the dodecahedral plane are less definite, experimentally because only a value for the *nominal* critical average stress was obtained, and theoretically because of the complication of there being two sets of intersecting (111) planes at different angles to the face, the onset of cracking being influenced presumably by the stress conditions at both sets.

From the tests with a diamond ball it is seen in comparison that the ratio of the theoretical to the experimental values for the critical average stress is 150 for the octahedral face and 90 for the cubic plane. Thus the theoretical resistance to cracking of diamond is of the order of 100 times greater than the experimental value obtained.

This may have significance when it is remembered that similar strength discrepancies in other materials have been explained by the supposed presence of localized surface and body weaknesses, e.g. Griffith cracks in the case of glass, and dislocations in cases of materials with a crystal structure.

There are two other indications of a possible flaw distribution; on the diamond octahedral face the critical average stress was found to be $1{\cdot}4 \times 10^{11}$ dyn cm^{-2} in the diamond ball test, and $1{\cdot}1 \times 10^{11}$ dyn cm^{-2} in the tungsten carbide ball test. There is no definite reason why the latter value should be less, but it is notable that the pressure figure in this case is very much bigger than in the diamond ball test (i.e. the area of contact was bigger before cracks occurred, due to the greater elastic deformation of the tungsten carbide ball); this is a possible indication that the strength of the surface, found experimentally, depends upon the scale of the experiment—analogous to the strength–area relationship well known in strength of glass testing, due to the Griffith crack distribution (Haward 1949). Also it has already been noted elsewhere (Howes and Tolansky 1955) that the pressure figures formed on diamond faces are initiated at one point, which thus must be weaker than surrounding points on the surface.

It is seen above that there is some evidence which indicates the distribution over the diamond surfaces of some type of localized flaw. If this is valid, then it is important to note that the cubic plane, for which experimental values are given above, is an artificial face produced by truncating an octahedral stone by sawing and polishing; so that localized weaknesses in this surface would have been within the body of the original octahedral stone.

(1)	(2)	(3)	(4)	(5)	(6)	(7)
Octahedral face of octahedral stone	Diamond 0·78	primary crack at 5	35	44	1·4	1·1
Octahedral face of octahedral stone	Diamond 0·78	primary crack at 3·5, increased up to 12	25	87	1·4	1·3
Octahedral face of octahedral stone	Sapphire 1·0	—	—	55	—	—
Octahedral face of octahedral stone	Tungsten carbide 1·0	primary crack at 16, increased up to 30	142	261	1·1	1·1
Dodecahedral plane of octahedral stone	Diamond 0·78	7–10–13–24–24	—	46–51–80 196–131	—	1·8
Cubic plane of cubic stone after polishing	Diamond 0·78	20–26–30–30	—	108–119–140–161	—	2·0
Cubic plane of octahedral stone	Diamond 0·78	29	86	210	3·3	1·4

(1) Face of diamond and type of stone; (2) spherical impactor used and diameter (mm); (3) loads for different cracks formed (kg); (4) circular area of contact at cracking $\times 10^{-6}$ (cm^2); (5) area of the crack figure $\times 10^{-6}$ (cm^2); (6) real critical average stress $\times 10^{11}$ (dyn cm^{-2}); (7) nominal critical average stress $\times 10^{11}$ (dyn cm^{-2}).

Acknowledgment

The author wishes to gratefully acknowledge the helpful advice and encouragement received from Professor S. Tolansky.

References

Bhagavantam, S., and Bhimasenachar, J., 1945, *Proc. Roy. Soc.* A, **187,** 381.
Bragg, W. H., and Bragg, W. L., 1913, *Proc. Roy. Soc.* A, **89,** 277.
Harkins, W. D., 1942, *J. Chem. Phys.* **10,** 268.
Haward, R. N., 1949, *The Strength of Plastics and Glass* (London : Cleaver-Hume).
Hertz, H., 1881, *English translation of Miscellaneous Papers* (London : Macmillan 1896).
Howes, V. R., and Tolansky, S., 1955, *Proc. Roy. Soc.* A, **230,** 287, parts I and II.
Orowan, E., 1948–9, *Rep. Progr. Phys.*, **12,** 185 (London : Physical Society).
Ramasesham, S., 1946, *Proc. Indian Acad. Sci.* A, **24,** No. 1, 114.
Timoshenko, S., 1934, *Theory of Elasticity* (New York and London : McGraw-Hill).
Tolansky, S., and Howes, V. R., 1957, *Proc. Phys. Soc.* B, **70,** 521.

Magnetothermal Effects in Iron and Silicon–Iron

By L. F. BATES and D. J. SANSOM
University of Nottingham

MS. received 12*th January* 1959, *in final form* 23*rd February* 1959

Abstract. The thermal changes accompanying the magnetization of specimens of iron and 0·5% silicon–iron and of a single crystal of 2·7% silicon–iron were measured by the direct method in fields between ±1000 oersteds. Agreement with the Stoner and Rhodes theory was found for the range 1000 to 20 oersteds. The coefficient a of their notation was measured for each specimen; for the single crystal specimen the coefficient b was found from a comparison of the theoretical and the experimental magnetization curves taken at two different temperatures. An estimate made of the effect of including the anisotropy coefficient K_2 in theoretical calculations showed it to have little effect in the case of iron at room temperature.

An alternative, indirect, method of making magnetothermal measurements was devised for use with the single crystal specimen. In low fields measurements by the direct and indirect methods do not agree and it is not possible to give a reliable account of magnetization processes in these regions.

§ 1. Introduction

While much valuable information has been obtained over a long period concerning the magnetothermal behaviour of iron, nickel and cobalt and their alloys, considerable experimental difficulties have been encountered in the case of iron and silicon–iron (Bates and Healey 1943). Moreover, several physical properties, known to be necessary for a full analysis of the magnetothermal measurements, were not measured with the actual specimens used in earlier measurements, and it appears that the field range employed in them was too restricted (Bates and Marshall 1953).

We therefore considered it worth while to make new measurements on a specimen of iron of greater purity than any previously used in such work, obtaining data for proper analysis from experiments on the specimen itself, and employing fields up to 1000 oersteds, so that technical saturation was definitely exceeded. Due to improved techniques, the accuracy of the new measurements is much greater than that of earlier work. At the same time, we have repeated the work of Bates and Marshall on their specimen of 0·5% silicon–iron over a greater field range. We have also made measurements with a single crystal specimen of 2·7% silicon–iron magnetized along a difficult direction of magnetization; in fact, this work preceeded that of Bates *et al.* (1957) who used a 3·5% specimen magnetized along an easy direction.

The analysis of magnetothermal measurements made with polycrystalline metals is complicated because the various magnetic processes are superimposed. With a single crystal it may be arranged that practically only one process occurs in a given field, so that the measurements may be more readily interpreted.

Prior to our work, no previous magnetothermal measurements had been made on single crystals, except those by Okamura (1936) on a single crystal of iron. Unfortunately, he recorded insufficient data for an adequate comparison of his results with modern theory.

§ 2. Details of Specimens

The specimen of iron was in the form of a rod 40 cm long and 0·414 cm in diameter. It was kindly supplied by the British Iron and Steel Research Association and was stated to contain 0·001% C, 0·002% Si and 0·01% Ni as impurities. The 0·5% silicon–iron specimen was the rod 37·9 cm long and 0·487 cm in diameter used by Bates and Marshall. The 2·7% silicon–iron single crystal specimen consisted generally of two strips, placed side by side, cut from a large single crystal in a sheet of transformer iron; each strip was 21·5 cm long, 0·35 cm wide and 0·024 cm thick. As shown in figure 1, the long axis of the

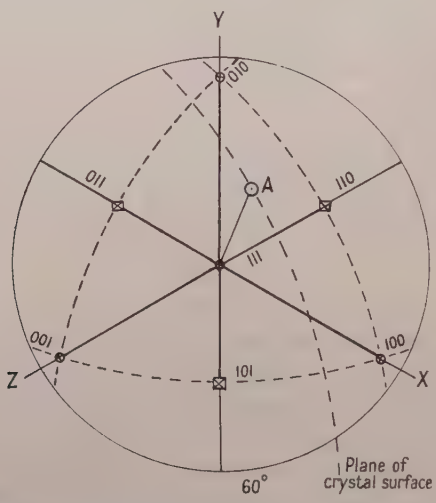

Figure 1. Orientation of single crystal specimen.

composite specimen was inclined at angles of 32·5°, 61° and 76·5° to the three [100] directions of easy magnetization, 22° from the nearest [110] axis and 25·5° from the nearest [111] axis. The orientation of the surface of the specimen is shown in the figure, where the direction A on the plane of this surface gives the direction of the long axis of the specimen. All the specimens were in the annealed state, so that irreversible heating was small and confined to low fields.

The magnetization curves were obtained by the usual induction coil and ballistic galvanometer method, using a long water-cooled solenoid to produce the magnetizing fields. The demagnetization factors for the above three specimens were respectively $4{\cdot}7\times10^{-3}$, $7{\cdot}0\times10^{-3}$ and $1{\cdot}4\times10^{-3}$ per strip. The relevant portions of the magnetization curves, corrected for demagnetization field as the applied field was reduced from 1000 oersteds to zero, are shown in figure 2. The curve labelled $3a$ was calculated for the single crystal specimen by the method of Lawton and Stewart (1948). In the section from the origin to the point A domain wall movements occur in such a way that at A three types

of domain exist, each with its magnetization vector pointing along the [100] direction nearest to the applied field. In the section from A to B the three vectors rotate towards the [111] direction. At B only two vectors are left, and in the section from B to C these rotate towards the direction of the applied field. Finally, in the region of C there is a small section in which only one vector rotates.

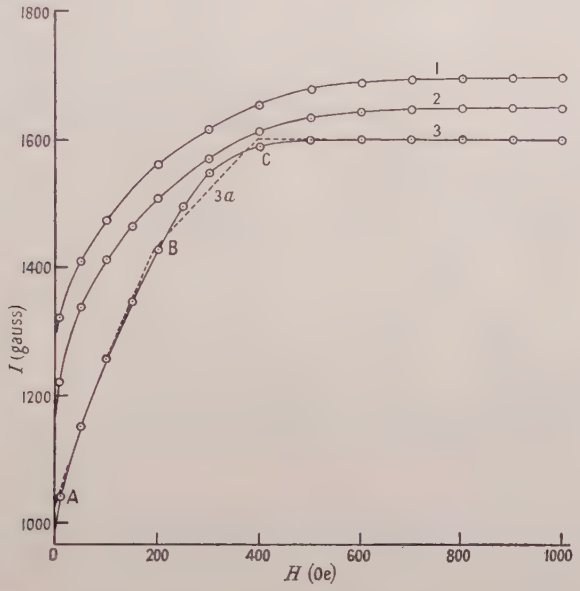

Figure 2. Magnetization curves for 1000 Oe cycles: 1, pure iron ; 2, 0·5% silicon–iron; 3, single crystal 2·7% silicon–iron; 3*a*, theoretical curve for single crystal with $I_0=1606$, $K_1=3{\cdot}9\times10^5$ erg cm^{-3} and $K_2=\frac{1}{2}K_1$.

As Lawton and Stewart assumed that the demagnetizing factor in the direction perpendicular to the long axis of their specimen was 2π, exact agreement between the calculated and the experimental curves is not to be expected. Nevertheless, in the three-vector region, for fields below 180 oersteds, the two curves coincide reasonably well.

Curve 3 *a* was calculated from the equation

$$H=\frac{K_1}{I_0}f_1\left(\frac{I}{I_0}\right)+\frac{K_2}{I_0}f_2\left(\frac{I}{I_0}\right) \qquad \ldots\ldots(1)$$

where K_1 and K_2 are the first and second order anisotropy constants, respectively. A table of values of $f_1(I/I_0)$ and $f_2(I/I_0)$ for a crystal when the field is applied along the [110] and [111] directions, respectively, and when the field is applied parallel to the long axis of the crystal used in the present work, is given in Appendix I (cf. Lawton and Stewart 1948).

§ 3. Thermodynamical Considerations

The thermal change $\Delta Q'$ in erg cm^{-3} which accompanies a reversible change in magnetization dI_R was shown by Stoner and Rhodes (1949) to obey the equation

$$\Delta Q'=a\int d(HI)+b\int HdI_R \qquad \ldots\ldots(2)$$

In this equation

$$a = -\frac{T}{I_0}\frac{dI_0}{dT} \quad \text{and} \quad b = \frac{T}{K}\frac{dK}{dT},$$

where K is the appropriate anisotropy constant. The first term on the right in equation (2) represents the thermal effect due to changes in intrinsic or spontaneous magnetization, and may be termed the intrinsic effect. The second term represents the thermal changes due to rotation of domain magnetization against the crystal anisotropy. If the coefficient a is known, the intrinsic effect may be subtracted from the observed thermal change $\Delta Q'$ to leave the effects due to the remaining magnetization processes; and these, in general, are not those of rotation alone.

Accordingly, we define the quantity Q_R'', where

$$\Delta Q_R'' = \Delta Q_R' - a\int d(HI_R), \qquad \ldots\ldots (3)$$

Q_R' being the reversible part of the experimentally observed thermal change. We also define the quantity b'', the experimental counterpart or equivalent of the theoretical coefficient b, such that $\Delta Q'' = \int b'' H dI_R$. In practice, b'' varies with H, and we may test the applicability of the Stoner and Rhodes theory by comparing b'' with b.

In Appendix II the effect upon b of the inclusion of the second anisotropy constant K_2 is calculated by a method which, while less general than that of Teale and Rowlands (1957), is more conveniently applicable to our work. It is found that

$$b = b_1 + \frac{K_2 f_2(I/I_0)}{K_1 f_1(I/I_0) + K_2 f_2(I/I_0)}(b_2 - b_1)$$

where

$$b_1 = \frac{T}{K_1}\frac{\partial K_1}{\partial T} \quad \text{and} \quad b_2 = \frac{T}{K_2}\frac{\partial K_2}{\partial T}.$$

The variation of b/b_1 with field strength was calculated for the single crystal specimen as used here, and also for a crystal with the field applied parallel to a [111] direction. The relevant curves, A and B respectively, are given in figure 3; as no reliable measurements of the variation of K_2 with temperature are available, it has been assumed that $K_2 = \frac{1}{2}K_1$ and that b_2 lies between 0 and $2b_1$. The

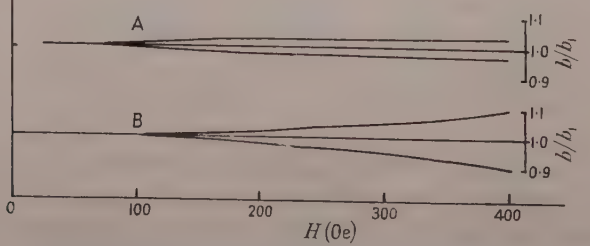

Figure 3. Variation of b/b_1 with field strength for single crystal: A, specimen as described; B, with field parallel to [111] direction.

curves show that it is unlikely that the effect of K_2 will be apparent in the experimental measurements described below.

§ 4. Direct Thermal Measurements

Thermal measurements were made on the three specimens by the direct method normally used in Nottingham. By means of 20 thermojunctions attached to the specimen, the temperature changes were recorded as it was taken step by step round a hysteresis cycle. Small reverse steps were also taken (Bates and Sherry 1955) to enable the separation of reversible from irreversible thermal changes. For convenience, these are expressed in erg cm^{-3}. Calibration of the system was effected by the method of loading and also by electrical heating. The former method requires a knowledge of the coefficient of linear expansion α, and the latter a knowledge of the resistivity ρ; these quantities were measured on the actual specimens and the data are recorded in the table. The

(1)	(2)	(3)	(4)	(5)	(6)	(7)	(8)
Iron	52·9[1]	0·037[2]	0·038	−0·34[3]	−0·29	10·9	9·9
		0·039[4]					
0·5% Si–Fe	50·0[1]	0·043[4]	0·044	—	−0·37	11·1	17·1
2·7% Si–Fe	38·5[1]	0·046[4]	0·047	−0·37[4]	−0·39	11·0	36
Single crystal	39·2[4]						

(1) Material; (2) $K_1 \times 10^{-4}$(erg cm^{-3}); (3) $(T/I)_0 \partial I_0/\partial T$; (4) a from thermal curve; (5) $(T/K_1)\partial K_1/\partial T$; (6) b from thermal curve; (7) $\alpha \times 10^6$ (deg^{-1}); (8) $\rho \times 10^6$ (ohm cm).

[1] Tarasov (1939); [2] Weiss and Forrer (1929); [3] Honda, Masumoto and Kaya (1929) as analysed by Czerlinsky (1932); [4] present work.

calibration constants found by the two methods were in good agreement, the sensitivity of the system being 26·8 and 27·0 erg cm^{-3} per mm scale deflection for the pure iron and the silicon–iron specimens respectively. In the case of the single crystal specimen only 10 thermojunctions could be attached to the thin specimen and the sensitivity was 220 in the same units.

The rate of change of the saturation magnetization with temperature was measured, by a method similar to that of Weiss and Forrer (1929), in order to obtain the coefficient a. A value of this coefficient for iron was also deduced from the linear graphs of the specific magnetization σ against T^2 given by these authors; using the relation

$$a = \frac{T}{I_0}\frac{dI_0}{dT} = \frac{2T^2}{\sigma}\frac{d\sigma}{d(T^2)}$$

the value found was $0{\cdot}037 \pm 0{\cdot}002$ for the two specimens of iron used by them. This is distinctly higher than the value 0·034 assumed in earlier work (cf. Bates and Marshall 1953).

A value of K_1 was obtained by comparing the calculated magnetization curve with the experimental curve in the case of the single crystal specimen. In addition, a value of b was obtained by comparing magnetization curves at 20° and 100°C with the theoretical curve, over the range 0 to 180 oersteds, where agreement between experiment and theory was closest. The results are given in the table, with results obtained by other workers for comparison.

The thermal measurements are reproduced in figures 4, 5 and 6. By convention we record only the measurements made in one half cycle as the field is reduced from its maximum (negative) value to zero, reversed, and then increased

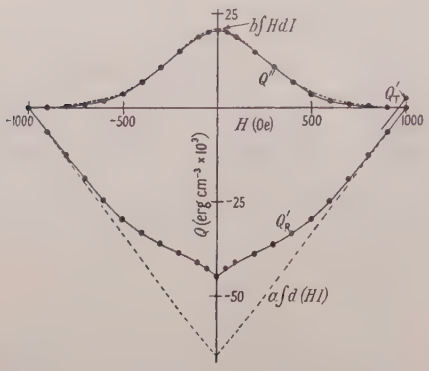

Figure 4. Thermal curves for pure iron for 1000 Oe cycles; $a=0{\cdot}0385$, $b=-0{\cdot}29$.

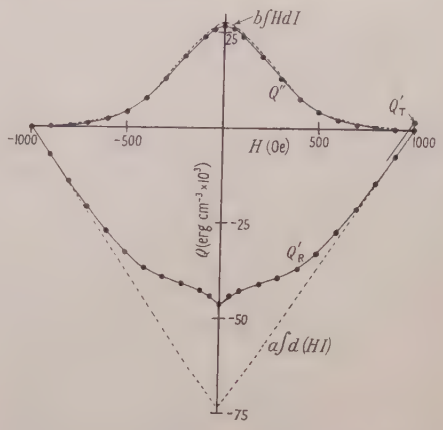

Figure 5. Thermal curves for 0·5% silicon–iron for 1000 Oe cycles; $a=0{\cdot}044$, $b=-0{\cdot}37$.

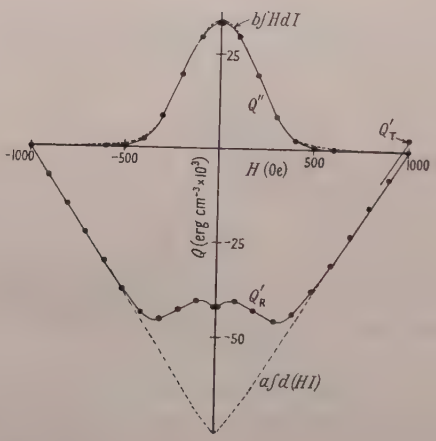

Figure 6. Thermal curves for single crystal 2·7% silicon–iron for 1000 Oe cycles; $a=0{\cdot}047$, $b=-0{\cdot}39$.

to the same maximum (positive) value. The overall irreversible heating was approximately 2000 erg cm^{-3} for one half cycle, compared with the large reversible heating of over 40 000 erg cm^{-3}. Almost the whole of the irreversible heating occurred in the field range -20 to $+20$ oersteds.

In the low field range the measurements had to be corrected for heating due to eddy currents which arose when comparatively large changes in magnetization took place. The correction was made in the usual manner (Bates and Marshall 1953). Results for half cycles extending between -20 and $+20$ oersteds are shown in figures 7 and 8 for the iron and 0·5% silicon–iron specimens, where the broken lines in figures 7 (*a*) and 8 (*a*) give the uncorrected results, while

the curves Q_T' give the total thermal changes after correction for eddy current heating. The irreversible contributions are shown in figures 7 (*b*) and 8 (*b*) respectively.

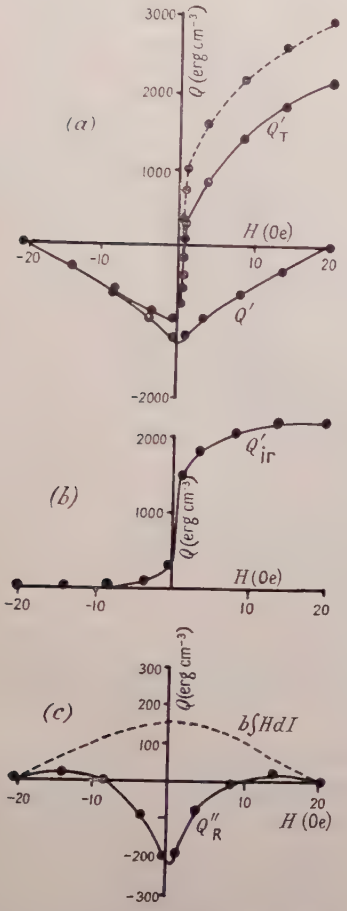

Figure 7. Thermal curves for pure iron for 20 Oe cycles; (*a*), experimental results; (*b*), irreversible contribution; (*c*), Q_R'' curves.

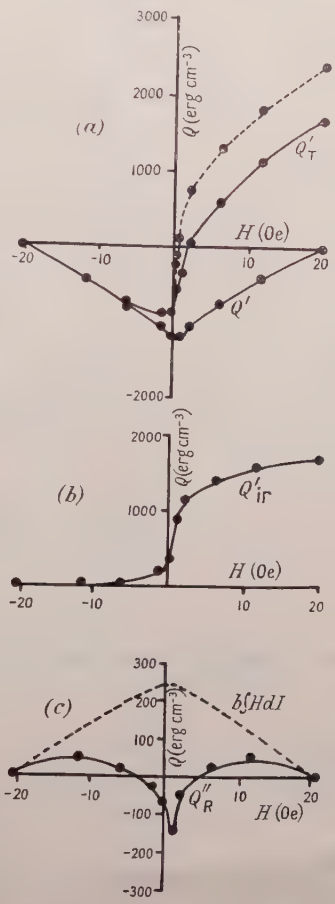

Figure 8. Thermal curves for 0·5% silicon–iron for 20 Oe cycles: (*a*), experimental results; (*b*) irreversible contribution; (*c*), Q_R'' curves.

By assuming suitable values for the coefficients *a* and *b* a very good fit may be obtained between the calculated results obtained from the Stoner and Rhodes expression and those obtained by direct experiment for fields greater than 50 oersteds. In fields less than 30 oersteds, as shown in figures 7 (*c*) and 8 (*c*), there are very marked depressions or 'dips' in the curves of Q_R'' against field which are apparently due to domain wall movements. Such 'dips' in low fields have been observed for many specimens and they have not yet received an adequate explanation. The experimental results for the single crystal in low fields were not very accurate, but they showed some evidence of a 'dip.'

The variation of b'' with field for the several specimens is shown in figure 9. In high fields b'' has a constant negative value corresponding to *b* in the Stoner

and Rhodes equation. In fields less than 50 oersteds b'' becomes less negative and rises to a large positive value in very low fields, presumably due to the increasing effect of wall movements. In the case of the single crystal specimen the effect of the second anisotropy constant on the variation of b'' could not be

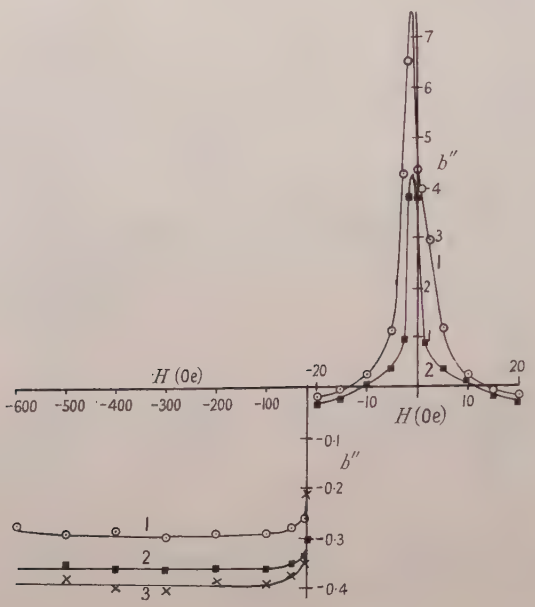

Figure 9. Curves of b'' against H obtained by the direct method. 1, Pure iron; 2, 0·5% silicon–iron; 3, single crystal 2·7% silicon–iron.

distinguished from experimental error and it was thought desirable to obtain the thermal curves by another, indirect method of measurement. Because of limitations of accuracy low field values of b'' are not reproduced in figure 9.

§ 5. Indirect Thermal Measurements

The indirect method of thermal measurement was similar to that of Tebble, Wood and Florentin (1952). It is based on the thermodynamic relation $(\partial Q/\partial H)_S = -T(\partial I/\partial T)_H$. Instead of measuring $\Delta Q'$ directly, the rate of change of magnetization with temperature is found at various points on the magnetization cycle and used to calculate $(\partial Q/\partial H)_S$. An increment of temperature must be of the order of 1°c if the corresponding change in magnetization is to be reversible, so that the latter is only of the order of 0·1 e.m.u. Tebble, Wood and Florentin measured such changes in magnetization by means of an astatic magnetometer; they had to use ellipsoidal specimens and the sensitivity of their apparatus was limited.

In the present work a search coil of 2000 effective turns was used with either a sensitive ballistic galvanometer or an electronic fluxmeter. The specimen was heated electrically. As the passage of current through the specimen would disturb its magnetic state, it was sandwiched between non-inductive heaters. The heaters consisted of four layers of constantin strip 0·0025 cm thick and slightly wider than the specimen, insulated by 'Durofix' cement. It was

calculated that they produced a maximum field of less than 0·001 oersted over the specimen. Changes in temperature were measured by the junction of a fine wire thermocouple attached to one edge of the specimen.

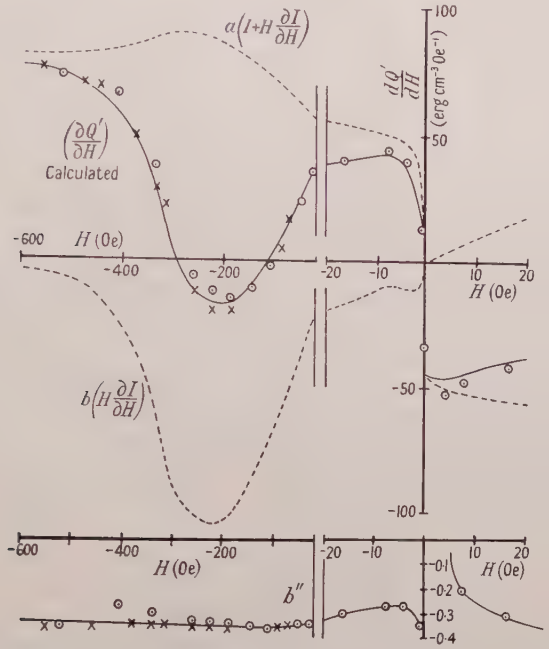

Figure 10. Thermal curves and b'' curves for single crystal 2·7% silicon–iron by the indirect method. (Note change of scale at 20 Oe.)

The maximum change in magnetization observed in the region of magnetic saturation was 0·25 e.m.u. which produced a scale deflection of 90 mm. The results are plotted in figure 10, the encircled points representing measurements made on one strip, and the crosses those made on two strips of crystal. Good agreement is found between the experimental results and the thermal curve calulated, with the assumption of appropriate values of a and b, from the differential form of the Stoner and Rhodes equation, viz.

$$(\partial Q'/\partial H)_S = a[I + H(\partial I/\partial H)_T] + bH(\partial I/\partial H)_T.$$

The values for best fit thus found for a and b were 0·050 and $-0{\cdot}35$ respectively whereas the corresponding values obtained by the direct method were 0·047 and $-0{\cdot}39$. The differences between the two sets of values may, of course, be due to the failure of the thermojunction to record the average temperature of the specimen. However, the two sets of values certainly agree within the limits of experimental error.

Values of b'' were obtained using the calculated curve of $a[I + HdI/dH]$ and the experimental values of dQ'/dH; these are shown in the lower portion of figure 10. It is thought that the value of b'' so obtained from high field measurements is more accurate than that obtained from the results of the direct method recorded in the lower portion of figure 9. In figure 10 the behaviour of b'' in very low fields provides no evidence of a 'dip' which would require a large positive value of b'' in these fields.

§ 6. Conclusions

The measurements made with all three specimens were sufficiently accurate and extensive to permit the definite statement that, over the field ranges where rotation processes determine changes in magnetization, the Stoner and Rhodes theory holds completely, the values of b'' being reasonably constant over these ranges. The coefficients a and b are thus seen to be of primary importance. The measurements with the single crystal specimen show that the effect of the second anisotropy constant was too small to be measured, and therefore $b=(T/K_1)dK_1/dT$ to the present order of accuracy.

'Dips' were found in the low field regions with the iron and 0·5% silicon–iron specimens and they are attributed to domain wall movements. A 'dip' was not found in the indirect measurements on the single crystal. It may be that in the direct method we have not succeeded in properly disentangling the reversible and irreversible thermal changes in low fields. Further measurements by both methods on the same specimen are clearly needed. So far we have only observed a similar discrepancy in measurements on a grain-oriented nickel–iron alloy, known as H.C.R. alloy (cf. Bates 1957) where a large 'dip', i.e. a very large positive value of b'' in low fields, was observed by the direct method in contrast with an approximately constant value of $b''=-0{\cdot}5$ over the whole field range by the indirect method.

Acknowledgments

D. J. S. thanks the Department of Scientific and Industrial Research for a maintenance grant which made this work possible. We are indebted to Mr. H. Clow for helpful discussion.

References

Bates, L. F., 1957, *Bull. Acad. Sci. USSR*, **21**, 1175.
Bates, L. F., Christoffel, D. A., Clow, H., and Davis, P. F., 1957, *Proc. Roy. Soc.* A, **243**, 160.
Bates, L. F., and Healey, D. P., 1943, *Proc. Phys. Soc.*, **55**, 188.
Bates, L. F., and Marshall, G., 1953, *Rev. Mod. Phys.*, **25**, 17.
Bates, L. F., and Sherry, N. P. R., 1955, *Proc. Phys. Soc.* B, **68**, 642.
Czerlinsky, E., 1932, *Ann. Phys., Lpz.*, **13**, 80.
Honda, K., Masumoto, H., and Kaya, S., 1928, *Sci. Rep. Tohoku Univ.*, **17**, 112.
Lawton, H., and Stewart, K. H., 1948, *Proc. Roy. Soc.* A, **193**, 72.
Okamura, T., 1936, *Sci. Rep. Tohoku Univ.*, **24**, 745.
Stoner, E. C., and Rhodes, P., 1949, *Phil. Mag.*, **40**, 481.
Tarasov, L. P., 1939, *Phys. Rev.*, **56**, 1231.
Teale, R. W., and Rowlands, G., 1957, *Proc. Phys. Soc.* B, **70**, 1123.
Tebble, R. S., Wood, J. E., and Florentin, J. J., 1952, *Proc. Phys. Soc.* B, **65**, 858.
Weiss, P., and Forrer, R., 1929, *Ann. Phys., Paris*, **12**, 297.

APPENDIX I

Calculation of Magnetization Curves

Table of Values for use in equation (1)

Field applied in direction [110]			Field applied in direction [111]			Crystal used in present work		
I/I_0	f_1	f_2	I/I_0	f_1	f_2	I/I_0	f_1	f_2
0·707	0	0	0·578	0	0	0·64	0	0
0·72	0·053	0	0·60	0·070	0	0·66	0·050	0
0·74	0·141	0	0·62	0·135	0	0·68	0·102	0
0·76	0·236	0	0·64	0·201	0·001	0·70	0·158	0
0·78	0·338	0	0·66	0·273	0·002	0·72	0·213	0·001
0·80	0·449	0	0·68	0·347	0·003	0·74	0·272	0·002
0·82	0·566	0	0·70	0·425	0·005	0·76	0·332	0·003
0·84	0·691	0	0·72	0·503	0·008	0·78	0·396	0·005
0·86	0·824	0	0·74	0·582	0·014	0·80	0·460	0·009
0·88	0·966	0	0·76	0·665	0·020	0·82	0·526	0·013
0·90	1·116	0	0·78	0·751	0·028	0·84	0·593	0·018
0·92	1·275	0	0·80	0·838	0·040	0·86	0·662	0·024
0·94	1·442	0	0·82	0·922	0·058	0·88	0·735	0·03
0·96	1·619	0	0·84	1·007	0·080	0·90	0·86	0·04
0·98	1·805	0	0·86	1·094	0·104	0·92	0·99	0·05
1·00	2·00	0	0·88	1·178	0·132	0·94	1·12	0·06
			0·90	1·261	0·164	0·96	1·27	0·07
			0·92	1·338	0·202	0·98	1·42	0·08
			0·94	1·406	0·244	1·00	1·58	0·10
			0·96	1·459	0·296			
			0·98	1·483	0·355			
			1·00	1·333	0·445			

APPENDIX II

Calculation of Effect of the Second Order Anisotropy Constant on the Value of b

By thermodynamic reasoning

$$\left(\frac{\partial Q'}{\partial I}\right)_S = T\left(\frac{\partial H}{\partial T}\right)_I \qquad \ldots\ldots(A1)$$

From Lawton and Stewart,

$$H = \frac{K_1}{I_0} f_1\left(\frac{I}{I_0}\right) + \frac{K_2}{I_0} f_2\left(\frac{I}{I_0}\right) \qquad \ldots\ldots(A2)$$

which we now write as

$$H = \frac{K_1}{I_0} f_1 + \frac{K_2}{I_0} f_2.$$

Therefore

$$\left(\frac{\partial H}{\partial T}\right)_I = -\frac{1}{I_0}\frac{dI_0}{dT}\left(\frac{K_1}{I_0} f_1 + \frac{K_2}{I_0} f_2\right) - \frac{I}{I_0}\frac{dI_0}{dT}\left(\frac{K_1}{I_0^2} f_1' + \frac{K_2}{I_0^2} f_2'\right) + \frac{1}{I_0}\left(\frac{dK_1}{dT} f_1 + \frac{dK_2}{dT} f_2\right) \qquad \ldots\ldots(A3)$$

and

$$\left(\frac{\partial H}{\partial I}\right)_T = \frac{K_1}{I_0^2} f_1' + \frac{K_2}{I_0^2} f_2'. \qquad \ldots\ldots(A4)$$

Simplifying (A3) we have

$$\left(\frac{\partial H}{\partial T}\right)_{\mathrm{I}} = -\frac{H}{I_0}\frac{dI_0}{dT} - \frac{I}{I_0}\frac{dI_0}{dT}\left(\frac{\partial H}{\partial I}\right)_{\mathrm{T}} + \frac{1}{I_0}\frac{dK_1}{dT}f_1 + \frac{1}{I_0}\frac{dK_2}{dT}f_2 \quad \ldots\ldots (A5)$$

whence substituting in (A1) gives

$$\left(\frac{\partial Q'}{\partial I}\right)_{\mathrm{S}} = -\frac{T}{I_0}\frac{dI_0}{dT}\left[H + I\left(\frac{\partial H}{\partial I}\right)_{\mathrm{T}}\right] + \frac{T}{K_1}\frac{dK_1}{dT}H_1 + \frac{T}{K_2}\frac{dK_2}{dT}H$$

where

$$H_1 = \frac{K_1}{I_0}f_1 \quad \text{and} \quad H_2 = \frac{K_2}{I_0}f_2.$$

In integral form we have

$$\Delta Q_{\mathrm{R}}' = a\int d(HI) + b_1\int H_1 dI + b_2\int H_2 dI$$

where

$$a = -\frac{T}{I_0}\frac{dI_0}{dT}, \quad b_1 = \frac{T}{K_1}\frac{dK_2}{dT} \quad \text{and} \quad b_2 = \frac{T}{K_2}\frac{dK_2}{dT}.$$

This is very similar to the Stoner and Rhodes equation.

Let

$$b\int H dI = b_1\int H_1 dI + b_2\int H_2 dI$$

then

$$b\int H dI = \int\left[b_1 + \frac{H_2}{H}(b_2 - b_1)\right]H dI$$

as b_1 and b_2 are constants; or

$$b = b_1 + \frac{H_2}{H}(b_2 - b_1)$$

i.e.

$$b = b_1 + \frac{K_2 f_2}{K_1 f_1 + K_2 f_2}(b_2 - b_1).$$

The Magnetic Susceptibility of Iron Ditelluride: I

By J. P. LLEWELLYN† and T. SMITH
Marischal College, Aberdeen

MS. received 19*th November* 1958, *in revised form* 16*th February* 1959

Abstract. The magnetic susceptibility of three compositions of the ditelluride phase of the Fe–Te system have been measured between 100° and 1200°K. This temperature range can conveniently be divided into three regions: above 700°K the susceptibility variations of all the three compositions can be interpreted in terms of the phase diagram, while below 300°K the variations follow the Curie–Weiss law. Between these temperatures the susceptibilities deviate from the Curie–Weiss values and this has been explained in terms of an increasing concentration of defects. A discussion of the bonding in the three compositions has been given by considering the estimated values of the Curie constants.

§ 1. Introduction

A measurement of the magnetic susceptibility of the ditelluride phase of the Fe–Te system has been carried out over a large temperature range. $FeTe_2$ was selected as a little investigated example of the intermediate ionic-covalent compounds formed between a metal and a metalloid from the fourth, fifth or sixth group of the periodic table. It was hoped that a combined measurement of the thermal expansion (Llewellyn and Smith 1957) and susceptibility, reported here, would throw some light on the bonding in this compound. The phase $FeTe_2$ has the advantage of a wide homogeneity range so that material can be prepared containing interstitial iron atoms ($FeTe_{1\cdot95}$) and vacant iron sites ($FeTe_{2\cdot10}$) (Grønvold, Haraldsen and Vihovde 1954). Thus the changes in the bonding associated with the different defects can be investigated.

In this paper measurements between 100° and 1200°K will be discussed in terms of the phase diagram, the bonding in the perfect and defect materials, and the change in the number of thermal defects with temperature.

The anomalous antiferromagnetic behaviour of the compound below 100°K is discussed elsewhere (Finlayson, Llewellyn and Smith 1959, to be referred to as II).

§ 2. Preparation of Samples

Compounds with compositions corresponding to $FeTe_{1\cdot95}$, $FeTe_{2\cdot00}$ and $FeTe_{2\cdot10}$ were prepared from spectrographically standardized iron and tellurium supplied by Johnson, Matthey and Co. Ltd. Both these elementary substances were reduced in purified hydrogen immediately before use in order to minimize the formation of magnetite (Fe_3O_4), small quantities of which would make any measurement of the paramagnetic susceptibility of the iron ditelluride extremely difficult; the iron was not exposed to the atmosphere again after this reduction.

† Now at University College of North Wales, Bangor, Caerns.

Appropriate quantities of the freshly reduced elements were sealed into a silica tube, which had been carefully degassed, at a pressure of about $1/10\,\mu$. This was heated in an electric furnace for 24 hours at a temperature of 950°C, which is well above the melting point of the iron ditelluride (780°C); the temperature was then lowered to that of the surroundings over a period of about three days. The compound formed was then ground and small particles of ferromagnetic impurity removed magnetically.

In spite of the care taken to prevent the formation of magnetite, preliminary magnetic measurements showed that a detectable quantity of this compound was still present in the samples. A similar difficulty was experienced by Uchida (1955) and Chiba (1955) in removing traces of magnetite from compounds of the Fe–Te system: they finally overcame the difficulty by adding manganese to their samples in a concentration of about 0·5 atomic % of the iron present. This procedure was not adopted in the present investigation because of the unknown effect the comparatively massive manganese atoms might have on the iron ditelluride itself. Instead it was decided to reduce the amount of magnetite present in the compounds by heating them in the presence of a small quantity of hydrogen which, it was felt, would not affect the parent lattice, and to accept the necessity of making a correction for any magnetite that might remain.

A known mass of the finely ground powder was therefore loaded into a silica tube suitable for use on the magnetic balance. After evacuation, one third of an atmosphere of purified hydrogen was introduced into this tube which was then sealed and heated to 1200°K. It was found that this treatment reduced the amount of magnetite so that the correction could be more easily made.

§ 3. Apparatus

The high temperature susceptibility measurements were made on a Sucksmith type of magnetic balance used in conjunction with an electric furnace. For specimen temperatures between room temperature and about −120°C the furnace was replaced by a cryostat; this temperature region was also covered by the measurements described in II. The specimen temperature was measured with a 13% platinum–platinum-rhodium thermocouple.

Vibrations transmitted from the floor were found to be troublesome and the balance was therefore mounted on a dural anti-vibration platform suspended by beryllium–copper springs and damped by vanes moving in oil. With the period of the platform oscillations adjusted to be about 1 second it was found that the vibrations of the balance transmitted from the floor were reduced to an acceptable level.

The magnet used was similar to that described by Hudson (1949). The pole-pieces were 10 cm in diameter and flat ended, the pole gap being 4·2 cm. For a normal reading of the specimen deflection the field at the centre of the pole gap was 6350 oersteds; some readings were taken at a reduced field strength to enable the ferromagnetic component of the susceptibility to be estimated.

§ 4. Experimental Results

For the region above room temperature, readings of the specimen deflection were taken at 10 degree intervals as the temperature was reduced from around 950°C to room temperature; in order to ensure that the specimen remained in thermal equilibrium, a slow cooling rate, about 40 deg per hour, was used.

While a detailed curve was obtained at the normal field strength, a less detailed curve was obtained at a reduced field to enable the ferromagnetic component of the susceptibility to be estimated.

Before obtaining the susceptibility from the balance deflection, corrections were made for the silica sample container and for the ferromagnetic component of the deflection. The ferromagnetic correction–temperature graph, deduced from the readings taken at two field strengths, shows a Curie point at about 570°c, which is what would be expected if the impurity were magnetite. To enable these corrected deflections to be converted into susceptibilities the balance was calibrated with a sample of $NiSO_4 . 7H_2O$, which was assumed to have a susceptibility of $15{\cdot}8 \times 10^{-6}$ g^{-1} at room temperature.

Finally, the paramagnetic susceptibilities of the samples were found by subtracting the estimated diamagnetic susceptibilities. The diamagnetic susceptibilities were estimated by the method suggested by Slater (1930), the value obtained being $-0{\cdot}44 \times 10^{-6}$ g^{-1}.

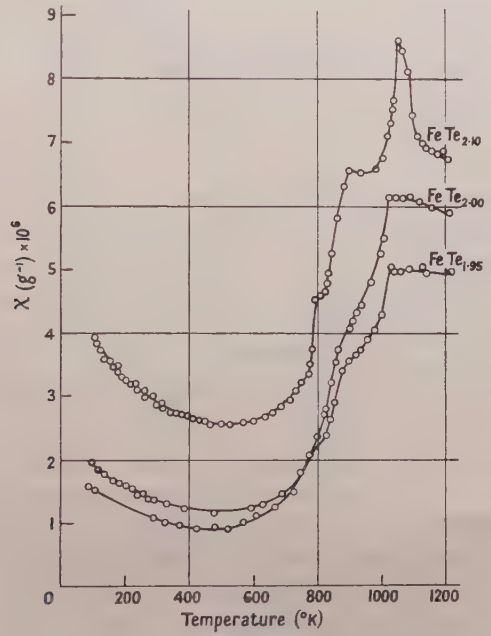

Figure 1. Susceptibility curves for iron ditelluride.

The susceptibility curves obtained for the three samples of iron ditelluride are shown in figure 1. Included on this graph are some points taken below room temperature with the furnace replaced by the cryostat, and some taken on the apparatus described in II.

The maximum error in these susceptibility curves is about 10%; this error is due almost entirely to the uncertainty in determining the ferromagnetic correction terms. The relative values for a given sample are correct to about 2%.

§ 5. The Temperature Region above 770°K

In the temperature region above 770°K the changes in the susceptibilities shown in figure 1 can be interpreted in terms of the phase diagram. However,

in order to do this, slight alterations have to be made to the diagram given by Chiba (1955); this is the only phase diagram of the Fe–Te system to have been published, although Grønvold, Haraldsen and Vihovde (1954) have made an x-ray study of the system. These alterations were first suggested by the appearance on a high temperature x-ray powder photograph of $FeTe_{2\cdot10}$ of lines corresponding to a hexagonal phase at 943°K (Llewellyn and Smith 1957); according to Chiba's phase diagram, this photograph should be representative of the two phase region 'δ + liquid', where δ is a NiAs type phase. (Note: the symbols used to represent the phases are those suggested

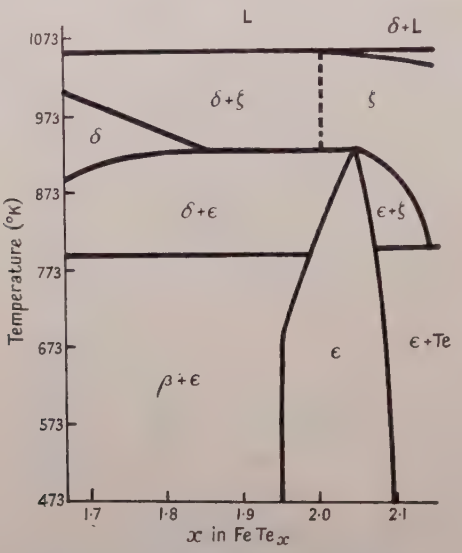

Figure 2. The modified phase diagram in the region of $FeTe_2$ (ϵ).

by Grønvold *et al.* (1954) and differ from those used by Chiba.) The quality of this powder photograph, however, makes it seem improbable that there would be a significant amount of liquid present in the sample. It is therefore suggested that this photograph is of a previously undetected phase ζ which is either of an NiAs structure with 50% of the metal atoms missing or of a CdI_2 structure. A comparison of the present system with those of Co–Te and Ni–Te (Tengnér 1938) would suggest that the latter alternative is the more probable. Figure 2 shows Chiba's phase diagram modified to accommodate this new phase ζ. It can be seen that with this modified phase diagram the changes in the susceptibilities above about 770°K are explained.

§ 6. The Temperature Region from 90°K to 300°K

In the temperature region below about room temperature the susceptibility variations of all three compositions follow the Curie–Weiss law

$$\chi_M = C_M/(T-\theta) \qquad \ldots\ldots(1)$$

where χ_M is the molecular susceptibility and T is the temperature. Danielian and Stevens (1957) have shown that for an antiferromagnetic substance on a face-centred cubic lattice, the susceptibility variations would not be expected

to follow the Curie–Weiss law until temperatures of the order of ten times the Néel temperature are reached; this does not appear to be the case in the present situation. Here the lattice is of the marcasite type, and the susceptibility changes can be described by equation (1) to within a degree or two of the Néel point (see II).

Table 1. The Variation of C_M and θ with Composition

	$FeTe_{1.95}$	$FeTe_{2.00}$	$FeTe_{2.10}$
C	0·265	0·194	0·601
ΔC	0·027	0·028	0·096
θ (°K)	−350	−320	−400
$\Delta\theta$ (deg)	50	50	50

From a graph of the inverse molecular susceptibility against the temperature the values of the constants θ and C_M can be found; the values obtained are shown in table 1. Included in this table are the maximum errors in θ and C_M, which correspond to a maximum error of 10% in the level of the susceptibility curves.

It should be noted that the presence of either vacancies or interstitials increases the value of C_M. A discussion of this effect in terms of the interatomic bonding will be given in § 8.

§ 7. The Temperature Region from 300°K to 770°K

Although the Curie–Weiss law is followed at temperatures below 300°K, above this temperature the susceptibility curves of all the three compositions of iron ditelluride depart from the predicted values. While this departure may be explained in terms of the phase diagram for $FeTe_{2.10}$, it seems very improbable that this explanation can be applied to the other two compositions. It is therefore suggested that the departure from the Curie–Weiss law is due to the introduction of an increasing number of defects; on this hypothesis the concentration of defects can be estimated as a function of temperature, since the change produced in C_M by known numbers of defects is known (table 1).

The problem, therefore, is to deduce from the observed values of C_M the defect concentrations. This is done by making the simplifying assumption that only those defect types which occur in the non-stoichiometric compositions at room temperature need be considered (i.e. interstitial Fe atoms and Fe vacancies); the law of mass action is then applied to the quasi-chemical reactions involving these defects in a closed vapour–solid system (Kroger and Vink 1956). Two of these equations involving vacancies v and interstitials i are

$$i \rightleftharpoons Fe_g \qquad \ldots\ldots (2a)$$

and

$$v + i \rightleftharpoons 1 \qquad \ldots\ldots (2b)$$

where Fe_g represents an atom of iron in the vapour state and 1 represents an occupied iron lattice site. Applying the law of mass action to these equations

$$[i]/[Fe_g] = K_1 \qquad \ldots\ldots (3a)$$

$$[i] \,.\, [v] = K_2 \qquad \ldots\ldots (3b)$$

where K_1 and K_2 are functions of temperature, and the square brackets indicate concentrations.

Since the total number of Fe atoms in the solid–vapour system remains constant at N_0, then

$$a[N]+a[i]-a[v]+b[\mathrm{Fe_g}]=N_0 \qquad \ldots\ldots(4)$$

where a and b are the volumes of the solid and vapour respectively and $[N]$ is the concentration of Fe lattice sites. A solution of equations (3) and (4) gives

$$[v]=\frac{D+\{D^2+4aK_2(a+b/K_1)\}^{1/2}}{2a} \qquad \ldots\ldots(5)$$

where D is the difference between the total number of Fe lattice sites and the total number of Fe atoms in the system (i.e. $D=a[N]-N_0$). Although it is not convenient to estimate the actual values of D for any given system, the difference δ between the number of Fe lattice sites and the total number of Fe atoms in the volume c occupied by 100 Fe lattice sites can be estimated from the data given by Grønvold *et al.* (1954). It is found that δ is $-2{\cdot}56$ for $FeTe_{1\cdot95}$, 4·76 for $FeTe_{2\cdot10}$ and zero for $FeTe_{2\cdot00}$.

$$\left.\begin{aligned}&\text{Since} \quad D=\frac{a}{c}\delta \qquad \ldots\ldots(6a)\\ &\text{and} \quad [v]=\frac{(v)}{c} \qquad \ldots\ldots(6b)\end{aligned}\right\}$$

where (v) is the number of vacant Fe lattice sites per 100 sites, equation (5) can be written in the form

$$(v)=\frac{\delta}{2}+\left\{\frac{\delta^2}{4}+\frac{K_2}{c^2}\left(1+\frac{b}{a}K_1\right)\right\}^{1/2}.$$

This expression can be simplified since it is known that for $FeTe_{2\cdot00}$ δ is zero, so that

$$(v)_{2\cdot00}=\left\{\frac{K_2}{c^2}\left(1+\frac{b}{a}K_1\right)\right\}^{1/2}. \qquad \ldots\ldots(7a)$$

Thus

$$(v) \quad =\tfrac{1}{2}\delta+\{\tfrac{1}{4}\delta^2+(v)^2_{2\cdot00}\}^{1/2} \qquad \ldots\ldots(7b)$$

To enable the concentrations of vacancies and interstitials to be calculated from equations (3*b*) and (7*b*) and the observed Curie constants, it is necessary to propose a relation between the defect concentrations and the Curie constants. It has already been shown (§ 6) that the Curie constant is increased by the introduction of either vacancies or interstitials; if there is no interaction between the two types of defects when both are present, then the Curie constant C may be represented by

$$C=\alpha(v)+\beta(i)+A_0 \qquad \ldots\ldots(8)$$

where the constants α and β can be deduced from the susceptibility data in the region where there are assumed to be no thermal defects (i.e. between 90°K and 300°K) and A_0 is the Curie constant of the stoichiometric composition in this region; (v) and (i) represent the numbers of vacancies and interstitials per 100 Fe lattice sites. It is worth noting that equation (7) in II implies that the Curie constant is a linear function of the concentration of the magnetic ions.

If the Curie constants A and B of the stoichiometric and a non-stoichiometric composition are estimated as a function of temperature from equation (1), it can

then be shown by substituting from equations (3 *b*), (6 *b*) and (7 *b*) in equation (8) that

$$(v)_{2\cdot00}=\delta\frac{A-A_0}{B-A_0-\alpha\delta}\Big/\left[\left\{\frac{A-A_0}{B-A_0-\alpha\delta}\right\}^2-1\right] \qquad \ldots\ldots (9\,a)$$

$$(i)_{2\cdot00}=\frac{1}{\beta}\left\{A-A_0-\alpha(v)_{2\cdot00}\right\} \qquad \ldots\ldots (9\,b)$$

Thus the defect concentrations in the stoichiometric composition can be calculated. If this calculation is made using the estimated Curie constants of $FeTe_{2\cdot00}$ and $FeTe_{1\cdot95}$ the values of $(v)_{2\cdot00}$ and $(i)_{2\cdot00}$ obtained are those shown in figure 3:

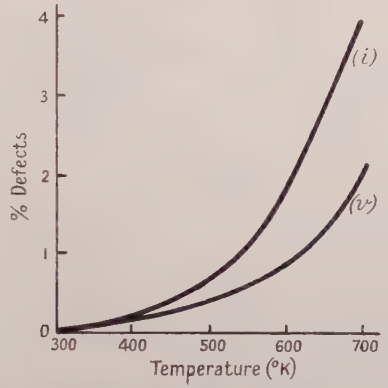

Figure 3. The estimated variation of the concentration of vacancies v and interstitials with temperature.

the maximum error of the points shown in this graph is 10%. These variations of concentration imply activation energies of $0{\cdot}21\pm0{\cdot}02$ ev and $0{\cdot}26\pm0{\cdot}03$ ev for the vacancies and interstitials respectively; these values may be compared with the defect energies found in some metals. Fumi (1955) has found that the activation energy of vacancies in Li, K, Rb, Cs and Na lie in the range 0·26 ev to 0·85 ev, while Pneth (1950) has estimated that the activation energy of interstitials in Na, aassuming a ' crowdion ' configuration, is less than 0·3 ev. No data are available on the defect energies in compounds similar to iron ditelluride.

The deviations of the susceptibility curves of $FeTe_{2\cdot00}$ and $FeTe_{1\cdot95}$ from the values predicted by the Curie–Weiss law are thus adequately explained in terms of an increasing concentration of defects. However, this explanation alone is not sufficient to account for the susceptibility curve of $FeTe_{2\cdot10}$ in the temperature range under consideration; this can be seen by calculating $(v)_{2\cdot00}$ from the susceptibility data of $FeTe_{2\cdot00}$ and $FeTe_{2\cdot10}$ instead of $FeTe_{2\cdot00}$ and $FeTe_{1\cdot95}$, which gives the meaningless result that $(v)_{2\cdot00}$ is negative. This anomaly confirms the original suspicion that the Te-rich composition $FeTe_{2\cdot10}$ passes into the two-phase region $\epsilon+Te$ at temperatures only a little above room temperature; the presence of free tellurium in the compound could be responsible for an increase in the Curie constant, in the same way that the defects already considered produce this type of change, thus accounting for the anomaly.

§ 8. The Bonding in Iron Ditelluride

Below 300°K the Curie–Weiss law is followed, and the differences between the three compositions are presumably associated with differences in their band structures. In the absence of any detailed information on the electrical properties,

however, it is not justifiable to develop a model based on the band structure at the present time. Instead the results will be discussed on a molecular bonding model.

If the orbital moment is quenched, then the number of electron spins per molecule n can be found from the values of the Curie constants C_M given in table 1, as $n(n+2)=8{\cdot}060C_M$. The value of n obtained in this way limits the number of possible bonding arrangements which can be accepted.

The calculated values of n are given in table 2. It is evident from the fact that these values are non-integral that a mixture of molecular types must be

Table 2. The Variation of n with Composition

	$FeTe_{1.95}$	$FeTe_{2.00}$	$FeTe_{2.10}$
n	0·77	0·59	1·42
Δn	0·06	0·07	0·16

present in all the three compositions of iron ditelluride; molecules with no unpaired electron spins must be considered, as must molecules with two or perhaps a multiple of two spins. The possibility of molecules with an odd number of unpaired spins is excluded since both iron and tellurium in the neutral state contain even numbers of electrons.

The different molecular states with the different numbers of unpaired electron spins will now be considered. A possible arrangement of the electrons in a molecule with no uncompensated electron spins can be represented as in figure 4 (a). The full lines represent the formation of covalent bonds. This molecule is very similar to the FeS_2 molecule described by Benoit (1955); however, whereas FeS_2 is a semiconductor, qualitative resistivity measurements have shown that $FeTe_2$ has a marked metallic nature. This might be expected if the 4s and 4p orbitals of the Fe atoms are used as metallic orbitals.

The molecule described above is not the only possible one with no uncompensated electron spins: the partially ionic molecule of the type shown in figure 4 (*b*) could be formed. The bonds represented by the broken lines are shown for convenience to be formed between the Fe^{2-} ion and the Te^{+} ions; in fact they would be formed between the Fe^{2-} ion and two different neighbouring Te^{+} ions. It should be noted that the formation of a molecule of this type was suggested by the x-ray results (Llewellyn and Smith 1957).

If the formation of Te^{-} ions is not considered (Llewellyn and Smith 1957) the above two are the only possible arrangements in which there are no unpaired electron spins. There are also two possible arrangements in which $n=2$; these are shown in figure 4 (*c*) and (*d*). The formation of molecules with n greater than 2 does not seem probable.

The concentrations of molecules with $n=0$ and $n=2$ can be found since the average values of n are known (see table 2): it is not possible, however, to distinguish molecules of type (*a*) from those of type (*b*), or type (*c*) from type (*d*). It is found that in $FeTe_{2.00}$ there is 1 molecule of types (*c*) or (*d*) in every 3·4 molecules, while in $FeTe_{1.95}$ and $FeTe_{2.10}$ the concentrations of these molecular types are 1 in 2·6 and 1 in 1·4 respectively. Since the concentration of defects in the non-stoichiometric compositions is known (Grønvold *et al.* 1954) it can be shown that 1 interstitial Fe atom introduces 3·5 molecules with $n=2$ while a

vacant Fe site has 8·7 such molecules associated with it. It should be noted that the thermal expansion measurements (Llewellyn and Smith 1957) also suggest that there is a change of bond type in the neighbourhood of a defect.

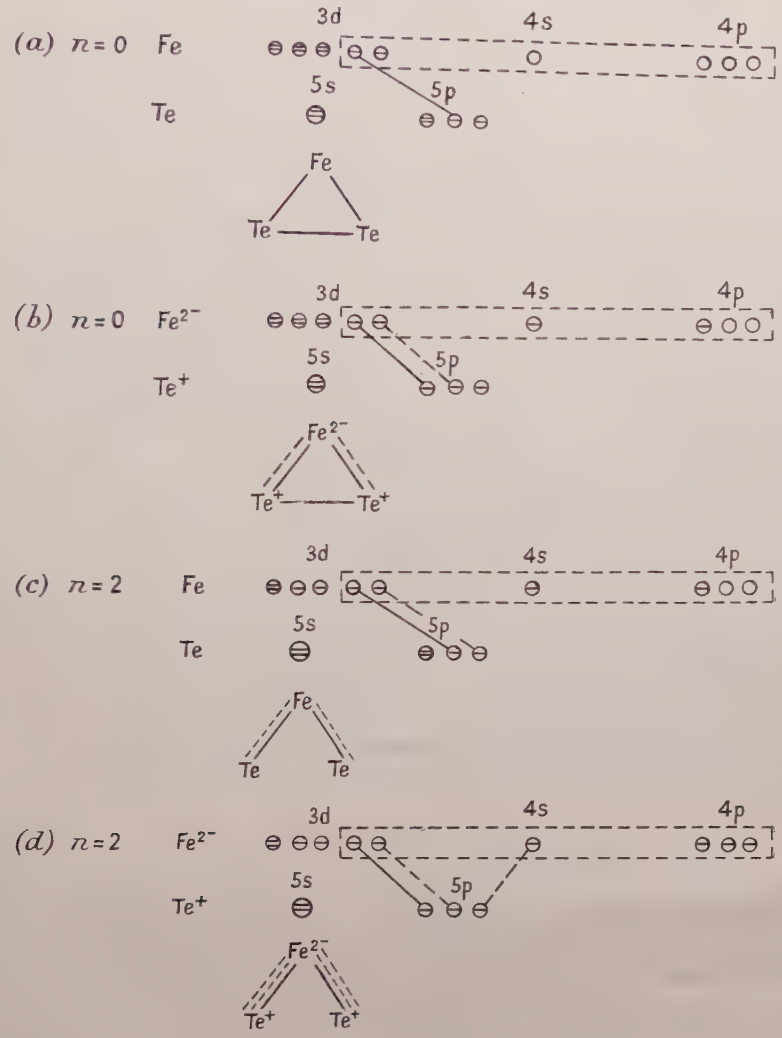

Figure 4.

Besides accounting for the high electrical conductivity of iron ditelluride, the use of two of the 3d and the 4s and 4p iron orbitals as metallic orbitals explains why each Fe atom is surrounded octahedrally by six Te atoms. Pauling (1940) has shown that when these orbitals, which are bracketed together in the diagrams of the molecular types, are used for bonding purposes six bonds of equal strength are formed and that they are directed towards the corners of a regular octahedron. In the molecular schemes already described not all these octahedral bonds will

be formed simultaneously, but the use of the orbitals as metallic orbitals enables the existing bonds to move between any of the six possible positions.

§ 9. Summary

The susceptibilities of three compositions of the ϵ phase of the Fe–Te system, $FeTe_{1\cdot95}$, $FeTe_{2\cdot00}$ and $FeTe_{2\cdot10}$, have been measured in the temperature region from about 90°K to 1200°K. The susceptibility curves of all the compounds follow the Curie–Weiss law between about 100°K and 300°K; at higher temperatures the susceptibilities increase above the predicted values, reaching a maximum at about 1030°K, the melting point of the phase.

The susceptibility variations between 700°K and 1200°K have been explained in terms of the phase diagram. Between 300°K and 700°K it has been shown that the susceptibility curves of $FeTe_{1\cdot95}$ and $FeTe_{2\cdot00}$ can be interpreted in terms of an increasing concentration of vacancies and interstitials; this interpretation suggests that the sample of $FeTe_{2\cdot10}$ passes into the two-phase region $\epsilon + Te$ at temperatures only a little above room temperature. The activation energies of the vacancies and interstitials in the stoichiometric composition have been found to be 0·21 ev and 0·26 ev respectively.

From the susceptibility variations in the region where the Curie–Weiss law is obeyed, it has been deduced that two distinct molecular classes exist in the compound, one with no unpaired electron spins and the other with two such spins. It has been found that vacant Fe lattice sites and interstitial Fe atoms each produce an increase in concentration of the latter class of molecule. A discussion on the bonding within the possible molecular types has been given; it has been suggested that while the molecules are predominantly covalent, they possess a partially ionic character. The atomic distribution in the compound has been qualitatively explained by assuming that the covalent bonds formed by the Fe atoms exhibit the characteristics of metallic bonds.

References

Benoit, R., 1955, *J. Chim. Phys.*, **52,** 201.
Chiba, S., 1955, *J. Phys. Soc. Japan*, **10,** 837.
Danielian, A., and Stevens, K. W. H., 1957, *Proc. Phys. Soc.* B, **70,** 326.
Finlayson, D. M., Llewellyn, J. P., and Smith, T., 1959, *Proc. Phys. Soc.*, **74,** 75.
Fumi, F. G., 1955, *Phil. Mag.*, **46,** 1007.
Grønvold, F., Haraldsen, H., and Vihovde, J., 1954, *Acta Chem. Scand.*, **8,** 1927.
Hudson, R. P., 1949, *J. Sci. Instrum.*, **26,** 401.
Kroger, F. A., and Vink, H. J., 1956, *Solid State Physics*, Vol. 3 (New York : Academic Press Inc.).
Llewellyn, J. P., and Smith, T., 1957, *Proc. Phys. Soc.* B, **70,** 1113.
Paneth, H. R., 1950, *Phys. Rev.*, **80,** 710.
Pauling, L., 1940, *The Nature of the Chemical Bond* (Oxford : University Press).
Slater, J. C., 1930, *Phys. Rev.*, **36,** 57.
Tengnér, S., 1938, *Z. anorg. Chem.*, **239,** 126.
Uchida, E., 1955, *J. Phys. Soc. Japan*, **16,** 357.

The Magnetic Susceptibility of Iron Ditelluride : II

By D. M. FINLAYSON, J. P. LLEWELLYN† and T. SMITH
Marischal College, Aberdeen

MS. received 19*th November* 1958, *in revised form* 16*th February* 1959

Abstract. The magnetic susceptibility of stoichiometric iron ditelluride has been measured between 15° and 100°K. The material appears to be antiferromagnetic with a Néel temperature at about 85°K. The curve is anomalous in that the susceptibility at 15°K is greater than that at the Néel temperature. This behaviour can be explained by a simple model of an antiferromagnetic containing some non-magnetic ions, provided that the concentration of the latter changes as a result of the ordering process.

The susceptibility of samples of $FeTe_{1\cdot95}$ and $FeTe_{2\cdot10}$ is also given.

§ 1. Introduction

Measurements of the magnetic susceptibility of iron ditelluride above 100°K have already been reported (Llewellyn and Smith 1959, to be referred to as I). In the region between 100° and 300° K these measurements are characteristic of an antiferromagnetic material above its Néel temperature. Measurements at lower temperatures described here were undertaken to verify the existence of an antiferromagnetic transition and to examine possible ferimragnetic behaviour in the non-stoichiometric materials.

§ 2. Experimental Measurements

A Sucksmith balance was used in conjunction with a hydrogen–helium liquefier of the type described by Chester and Jones (1953).

The vibration mounting used for measurements at higher temperatures could not be used since a fairly rigid coupling was now required between the liquefier and the balance enclosure. Two vibration platforms were therefore mounted in series within the vacuum enclosure. The first was supported by compression springs from the base plate and was oil damped, and the second was supported by tension springs from the first. The transmission of vibrations to the base plate was minimized by a syphon bellows, and electromagnetic damping was provided by an annular magnet.

The specimen holder was suspended from the balance ring by a silica rod 1 mm diameter and 3 ft long. The temperature of the surrounding calorimeter was measured by a helium thermometer and thermal contact between the specimen and calorimeter was provided by filling the calorimeter with dry helium gas.

The balance was calibrated and used in a manner similar to that described in I.

† Now at University College of North Wales, Bangor, Caerns.

§ 3. Results

The magnetic susceptibilities of the samples of $FeTe_{1.95}$, $FeTe_{2.00}$ and $FeTe_{2.10}$ used in I were measured down to 15 °K. The ferromagnetic correction was again determined by measurements in different field strengths; the correction curve obtained did not agree with that obtained by Uchida (1955) for magnetite containing both tellurium and manganese as impurities. A check on the correction curve was therefore made by preparing an enriched sample of the ferromagnetic impurity by magnetic separation and noting balance deflections at various temperatures (figure 1).

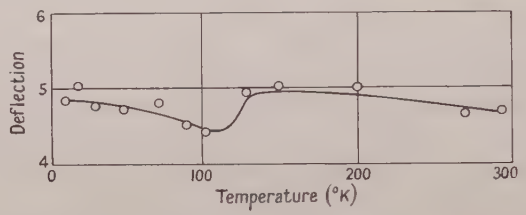

Figure 1. Balance deflection plotted against temperature for ferromagnetic impurity.

The susceptibility curves after all corrections, including the diamagnetic correction, had been applied are shown in figure 2. Measurements were carried out in fields ranging from 1300 to 4500 oersteds and no variation of the susceptibility was found. The maximum error in the susceptibility is about 10% and is mainly due to the uncertainty in determining the ferromagnetic correction terms, the relative values for a given sample being correct to 2%.

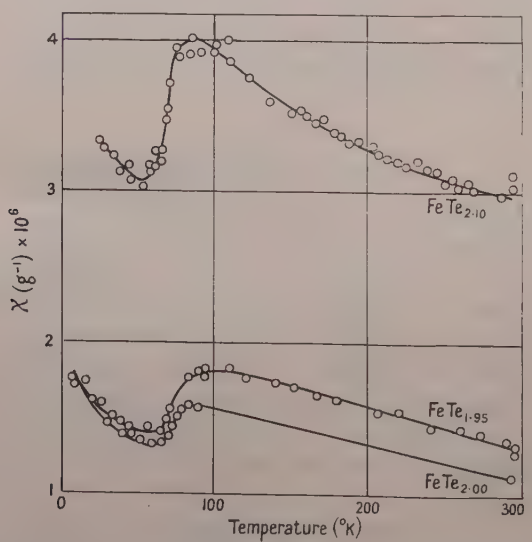

Figure 2. Susceptibility curves for iron ditelluride.

§ 4. Discussion of Results

The susceptibility curves have a maximum at about 85 °K which is interpreted as being the Néel temperature. Two departures from the curves expected for an antiferromagnetic powder are found. Firstly, the susceptibility at low

temperatures increases considerably, and secondly, the peak near the Néel temperature is broad.

Curves showing an anomalous increase at low temperatures have been reported for $MnCl_2$ (Murray and Roberts 1955), UMn_2 (Lin and Kaufmann 1957), CoO (Singer 1956) and dysprosium (Hendrickson and Keller 1956). Singer suggests that the increase in CoO is due to paramagnetic islands forming round defects. In dysprosium the increase has been explained as due to transitions to different states of ordering on the sublattices. It is interesting that both the transitions and the resulting increase are predicted only if the interaction coefficients between nearest and next nearest neighbours are temperature dependent. A consequence of the model is that the susceptibility below the Néel point is field dependent. In iron ditelluride there is no indication of such a change over the range of fields used (1300 Oe to 4500 Oe). Also the introduction of temperature dependent interaction coefficients introduces a great deal of freedom into the theory and before this is done for $FeTe_2$ it would seem desirable to try a simple development of conventional theory.

An obvious possibility is that the low temperature increase results from an approach to a ferrimagnetic ordering. As the increase is particularly marked in the stoichiometric material, the ferrimagnetism is not associated with vacancies or interstitials. However, some of the iron and tellurium ions carry a magnetic moment and some do not (I); and it is possible that ordering between the two types of ions is taking place. A similar problem has been investigated by Elcock (1954) who considered an antiferromagnetic substance with vacant lattice sites and nearest neighbour interaction. A minimum in the susceptibility curve was predicted for small concentrations of defects, but not for the higher concentrations of zero-moment ions found in $FeTe_2$. The problem has therefore been re-examined for a two-sublattice antiferromagnetic substance with both nearest and next nearest neighbour interactions considered, and with the number of zero moment ions varying with temperature. This temperature dependence is supposed to arise for the following reasons. It is envisaged that the energy of a configuration of the crystal can be written in the form

$$E(i_1 i_2) = E_1(i_1 i_2) + E_2(i_2)$$

where i_1 symbolizes the variables specifying the spin ordering of the magnetic ions and i_2 symbolizes the variables specifying the numbers of ions of the two different kinds in the configuration of interest. It has been shown by Elcock and Landsberg (1957) that for a decomposable system of this kind, and where interest centres only on the variables symbolized by i_1, it is possible to suppose a prior summation over i_2 to be performed in a part of the system, and then to restrict attention to a part system with energy levels given by

$$E_1(i_1, i_2(T))$$

where $i_2(T_2)$ now plays the part of a temperature dependent parameter.

On this basis, the equilibrium magnetic susceptibility has been worked out in the Bragg–Williams approximation. It is found that the total magnetic internal energy (E) is given by

$$E = \frac{-1}{2\mathcal{N}}\left[\frac{J_{11}z_{11}}{2}\{N_1^2(1+\zeta_1^2)+N_2^2(1+\zeta_2^2)\}+J_{12}z_{12}N_1N_2\{1+\zeta_1\zeta_2\cos(\eta_2-\eta_1)\}\right.$$
$$\left.-\mu H\{N_1\zeta_1\cos\eta_1+N_2\zeta_2\cos\eta_2\}\right] \qquad \ldots\ldots(1)$$

where $\mathcal{N}$ is the number of sites on each sublattice, N_1 and N_2 are the number of magnetic ions on sublattices A and B, J_{11} and J_{12} are the interaction parameters between z_{11} next nearest and z_{12} nearest neighbours, ζ_1 and ζ_2 are the relative magnetization of the two sublattices, μ the magnetic moment of a magnetic ion, H the field, and η_1 and η_2 are the angles between ζ_1 and ζ_2 and H. The partition function for the spin system is

$$Z(\zeta_1\zeta_2N_1N_2)=h(\zeta_1\zeta_2N_1N_2)\exp\left\{\frac{-E(\zeta_1\zeta_2N_1N_2)}{\boldsymbol{k}T}\right\} \qquad \ldots\ldots(2)$$

where $E(\zeta_1\zeta_2N_1N_2)$ is given by equation (1) and the weighing factor $h(\zeta_1\zeta_2N_1N_2)$ is

$$h(\zeta_1\zeta_2N_1N_2)=\frac{2\mathcal{N}!}{[\tfrac{1}{2}N_1(1+\zeta_1)]!\,[\tfrac{1}{2}N_1(1-\zeta_1)]!\,[\tfrac{1}{2}N_2(1+\zeta_2)]!\,[\tfrac{1}{2}N_2(1-\zeta_2)]!\,[\mathcal{N}-N_1]!\,[\mathcal{N}-N_2]!} \qquad \ldots\ldots(3)$$

and N_1 and N_2 are supposed temperature dependent for the reasons stated above. The equilibrium state of the system is now obtained by differentiation of the partition function (with respect to N_1, N_2, ζ_1, ζ_2, η_1 and η_2). From the resulting equation it follows that $\eta_2-\eta_1=\pi$ i.e. the two sublattices are magnetized in opposite directions, and the expressions for the Néel temperature T_1, the susceptibility parallel to the antiferromagnetic axis $\chi_{\parallel}$ and perpendicular to the axis $\chi_{\perp}$ and the susceptibility above the Néel temperature χ, are given by

$$T_1=\frac{d_1}{2\boldsymbol{k}}(J_{11}z_{11}-J_{12}z_{12}) \qquad \ldots\ldots(4)$$

$$\frac{1}{\chi_{\parallel}}\frac{\mu^2}{\boldsymbol{k}T_1}d_1=\frac{T_2}{T_1}\left\{\frac{T}{T_2}\left[\frac{d_T}{d_1}(1-\zeta^2)-\frac{\zeta^2}{T_1/T-[d_T(1-d_T)/d]^{-1}}\right]^{-1}-1\right\} \qquad \ldots\ldots(5)$$

$$\frac{1}{\chi_{\perp}}\frac{\mu^2}{\boldsymbol{k}T_1}d_1=\left(1-\frac{T_2}{T_1}\right) \qquad \ldots\ldots(6)$$

$$\frac{1}{\chi}\frac{\mu^2}{\boldsymbol{k}T_1}d_1=\frac{T}{T_1}-\frac{T_2}{T_1} \qquad \ldots\ldots(7)$$

where $$T_2=\frac{d_1}{2\boldsymbol{k}}(J_{11}z_{11}-J_{12}z_{12}),$$

d_T is the ratio of magnetic to non-magnetic ions at the temperature T, and $\zeta_1=\zeta_2=\zeta$ where

$$\tfrac{1}{2}\ln\left[\frac{1+\zeta}{1-\zeta}\right]=\frac{d_T}{d_1}\frac{T_1}{T}J.$$

In the derivation of equation (7) it is assumed that the number of magnetic ions is sensibly constant above the Néel temperature, i.e. $d_T=d_1$.

With a constant number of non-magnetic ions the model does not explain the minimum in the susceptibility of the $FeTe_{2\cdot00}$ material as can readily be verified by substituting the experimental values of d_1, T_1 and T_2 (Part I) in equations (5) and (6) and combining the results in the ratio of 1 : 2 to give the susceptibility of a powder χ_p. The result is shown in figure 3. Although

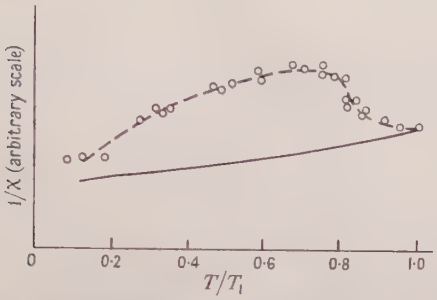

Figure 3. The calculated inverse susceptibility curve for $FeTe_{2\cdot00}$ with constant number of magnetic ions ($d_1=0\cdot29$ and $T_2/T_1=-3\cdot76$), and the experimental (broken) curve below the Néel temperature.

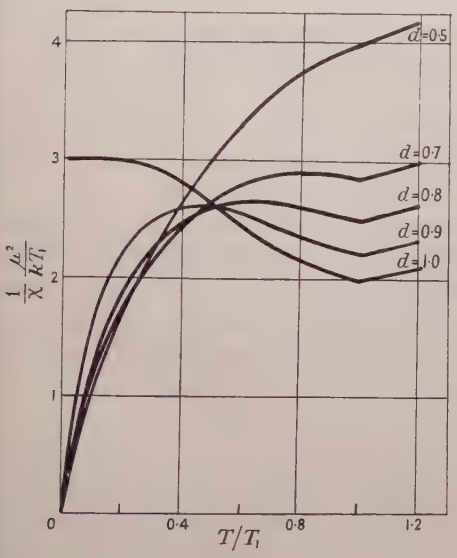

Figure 4. Calculated inverse susceptibility curves for $T_2=-T_1$.

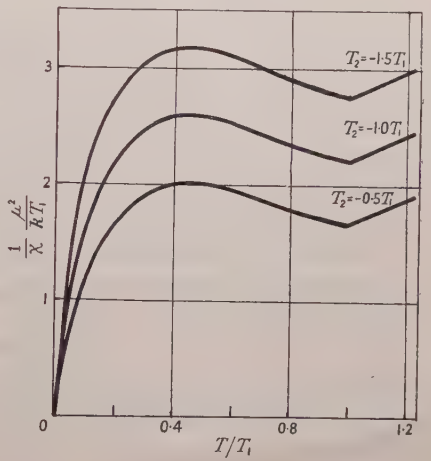

Figure 5. Calculated inverse susceptibility for $d=0\cdot9$ and different values of the ratio T_2/T_1.

this curve shows no maximum, peaks are obtained in $1/\chi_p$ for larger numbers of magnetic ions (figure 4). The next nearest neighbour interaction produces no substantial change in the character of the susceptibility curves, but displaces the $1/\chi_p$ curve along the inverse susceptibility axis (figure 5).

It appears, therefore, that the model would associate the peak with a change in the number of magnetic ions resulting from the ordering process. From equations (5) and (6) together with the subsidiary condition (8) the variation in d_T can be found (figure 6). An increase in the ratio of magnetic to non-magnetic ions from 0·29 at 90°K to 0·97 at 15°K is implied. Such a change should lead to anomalies in other physical characteristics, for instance a large negative coefficient of expansion of about 10^{-4} for the *a* and *b* axis, and a positive coefficient of 10^{-4} for the *c* axis would be expected below the Néel temperature where d_T is changing rapidly (Llewellyn and Smith 1957).

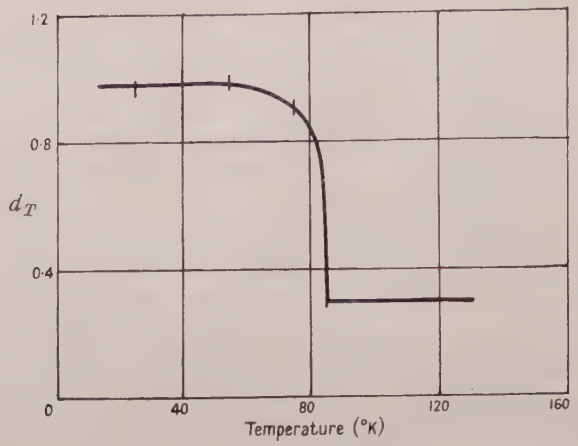

Figure 6. Apparent change in number of magnetic ions produced by ordering.

It is of interest to notice that the ratio of the values of χ_p at low temperatures to χ_p at the Néel temperature is greatest for $FeTe_{2\cdot00}$ ($d_1=0\cdot29$), next for $FeTe_{1\cdot95}$ ($d_1=0\cdot38$) and smallest for $FeTe_{2\cdot10}$ ($d=0\cdot71$). This is the sequence which would be expected from figure 4.

The above model neglects physical processes which may be important, in particular the electrostatic energy, but no fuller treatment is justified till neutron diffraction data become available. It serves to suggest, however, that the modification of the electronic configuration of the ions as the ordering develops is a mechanism which may be responsible for the low temperature increases in the susceptibilities of these materials.

Acknowledgments

We are grateful to Dr. E. W. Elcock for many useful discussions, and to Mr. T. Wratten for his skilful technical assistance.

References

Chester, P. F., and Jones, G. O., 1953, *Proc. Phys. Soc.* B, **66,** 296.
Elcock, E. W., 1954, *Proc. Roy. Soc.* A, **227,** 102.
Elcock, E. W., and Landsberg, P. T., 1957, *Proc. Phys. Soc.* B, **70,** 161.
Hendrickson, T. J., and Keller, J. M., 1956, *Thesis*, Iowa State University.
Lin, S. T., and Kaufmann, A. R., 1957, *Phys. Rev.*, **108,** 1171.
Llewellyn, J. P., and Smith, T., 1957, *Proc. Phys. Soc.* B, **70,** 1113.
—— 1959, *Proc. Phys. Soc.*, **74,** 65.
Murray, R. B., and Roberts, L. D., 1955, *Phys. Rev.*, **100,** 1067.
Singer, J. R., 1957, *Phys. Rev.*, **104,** 929.
Uchida, E., 1955, *J. Phys. Soc. Japan*, **16,** No. 5, 357.

Properties of p-type Indium Antimonide
II: Photoelectric Properties and Carrier Lifetime

By C. HILSUM
Services Electronics Research Laboratory, Baldock, Herts.

MS. received 22*nd December* 1958, *in final form* 3*rd March* 1959

Abstract. Photoconductive and photoelectromagnetic effects were studied on p-type specimens of InSb with impurity concentrations varying from 10^{15} to 2×10^{17} cm^{-3}. Results were consistent with a simple theory, which assumes that the carrier relaxation time is independent of energy. Values for carrier lifetime were deduced. The fall in lifetime with increasing impurity concentration is explained as the result of two recombination processes, radiative recombination and recombination via traps.

§ 1. Introduction

Measurements on intrinsic InSb have shown that at room temperature the carrier lifetime τ approaches the theoretical limit imposed by radiative recombination (Hilsum, Oliver and Rickayzen 1955). In most other semiconductors this process is much less important than recombination via traps. Information about the recombination processes can be obtained by studying τ as a function of either temperature or impurity concentration, and Wertheim (1956) has used the temperature dependence to establish that in InSb trapping is operative at temperatures below 250°K; his method of measuring τ would not work at higher temperatures. If we wish to investigate the variation of τ with impurity concentration at room temperature, it must be done by measuring the photoelectric effects, since the other standard methods have not proved successful (Avery and Jenkins 1955). The technique is then straightforward for intrinsic or n-type material, but for material with an excess of holes it is first necessary to develop a method for measuring the material parameters. In a previous paper (Hilsum and Barrie 1958 referred to as I), it was shown that this could be done by measuring the Hall coefficient and resistivity as a function of magnetic field. In the experiments now described the specimens studied in I were used again, and their photoelectric properties measured.

§ 2. Fundamental Relations

The results of I indicated that the electrical properties of p-type InSb are best explained by assuming that the relaxation time is independent of the energy of the carriers. The photoelectric effects are then given (Kurnick and Zitter 1956) by the following relations:

$$V_{PC}=DE\tau\frac{d}{tp}\frac{b+1}{bc+1}\frac{1}{F_1} \qquad \ldots\ldots(1)$$

$$V_{PEM}=DBL_D{}^*\frac{d}{tp}\frac{b+1}{bc+1}\frac{[1+\mu^2B^2(b+c)/b(1+bc)]^{1/2}}{1+\mu^2B^2[(1-c)/(1+bc)]^2}\frac{1}{F_2} \qquad \ldots\ldots(2)$$

where V_{PC} and V_{PEM} are the open circuit photoconductive and photoelectromagnetic voltages, E the electric field along the specimen, B the magnetic field, D the photon density, d the specimen length and t its thickness, p the hole concentration, c the ratio of electron to hole concentration, μ the electron mobility, b the mobility ratio, τ the carrier lifetime, L_D^* the ambipolar diffusion length, i.e.

$$\left(\tau\mu\frac{\boldsymbol{k}T}{\boldsymbol{e}}\frac{1+c}{1+bc}\right)^{1/2}$$

and

$$F_1=1+\frac{\tau s}{L_D^*},\quad F_2=1+\frac{\tau s}{L_D^*}\left[\frac{1+\mu^2B^2+bc(1+\mu^2B^2/b^2)}{1+bc}\right]^{1/2}$$

where s is the surface recombination velocity.

Photoelectric effects are sometimes expressed as the short-circuit current created by the radiation; in our experiments the resistance of the specimen is very small, and it is more convenient to measure the open-circuit photovoltages. The meaning of V_{PEM} is obvious; V_{PC} is the incremental change in voltage across the specimen at constant current. Each voltage is equal to the respective short circuit current multiplied by the specimen resistance.

The relations are valid for small D and it is assumed that the photons are absorbed with unit quantum efficiency in the front surface of the specimen, and that the thickness is large relative to the electron diffusion length.

If B is small we have

$$\tau=0{\cdot}026\left[\frac{V_{PC}}{V_{PEM}}\frac{B}{E}\right]^2\frac{\mu(c+1)}{bc+1}. \qquad \ldots\ldots(3)$$

This is independent of surface conditions and photon density.

§ 3. Experimental Procedure

The radiation source was a 6v, 108 watt strip filament lamp, and an image of it was focused on the specimen with a 3 in. F 1·2 lens. A rotating chopper disc modulated the radiation at 800 c/s. The specimens, rectangular blocks 15 mm × 3 mm × 1 mm, had their ends masked to prevent photovoltaic effects. The photovoltages were fed to a high gain tuned amplifier through a transformer and measured by comparison with a known voltage from an oscillator and calibrated attenuator.

The spectral output of the lamp–lens combination was measured, and no radiation could be detected at wavelengths beyond 2·5 microns; all the radiation was therefore of a suitable wavelength to be absorbed near the front face of the specimens. The radiation distribution in the image of the filament was measured with a Schwartz air thermopile, calibrated by the National Physical Laboratory, and a photon density deduced using the measured colour temperature of the filament. An allowance was made for the loss by reflection from the front face of the specimen. The photon density could be varied by an optical attenuator, consisting of two grids which could be moved across one another by a vernier screw motion. This was calibrated with the thermopile and gave a method of changing the photon density without altering the spectral distribution. The density could also be varied by altering the voltage across the filament, and calibrated as a function of voltage by measuring the colour temperature and radiation intensity at each setting.

For the photoconductive measurements, currents up to 100 mA were passed through the specimens, and E measured by a potential probe at 1 mm intervals along the length. All the specimens had been selected for their uniform resistivity.

The photoelectromagnetic voltages were obtained by applying a magnetic field of up to 12 000 gauss from a Newport Instruments Type A electromagnet, fitted with coned vanadium–permendur pole pieces.

The specimens used were, with one exception, the same as those mentioned in I. Specimen 5 had been broken so a substitute was cut from the same crystal, and denoted by 5a. All the material parameters are given in the table. Specimen 2 was the only polycrystalline one. To reduce the surface recombination velocity, the specimens were electrolytically etched using an electrolyte of 4% NHO_3 in ethylene glycol, and washed in acetone or toluene.

Specimen No.	p (cm^{-3})	$cm^2\ v^{-1}\ sec^{-1}$	b	c
1	$<10^{14}$†	78000	104	1·004
2	2×10^{15}†	75000	104	0·90
3	$5{\cdot}2\times10^{16}$	41000	62	0·097
4	7×10^{16}	37000	60	0·057
5a	$1{\cdot}4\times10^{17}$	27000	49	0·0165
6	$1{\cdot}86\times10^{17}$	24000	46	0·0084

† For specimens 1 and 2 the impurity concentration is given instead of the hole density.

§ 4. Results

4.1. *Photoelectric Effects*

Equations (1) and (2) predict simple proportionality between the two voltages and the photon density, and V_{PC} and the exciting current. For all specimens V_{PC} and V_{PEM} were proportional to D, whether this was changed by altering the optical attenuator or the lamp voltage (figure 1). V_{PC} was proportional to the current passing as long as the current was not large enough to give appreciable heating effects.

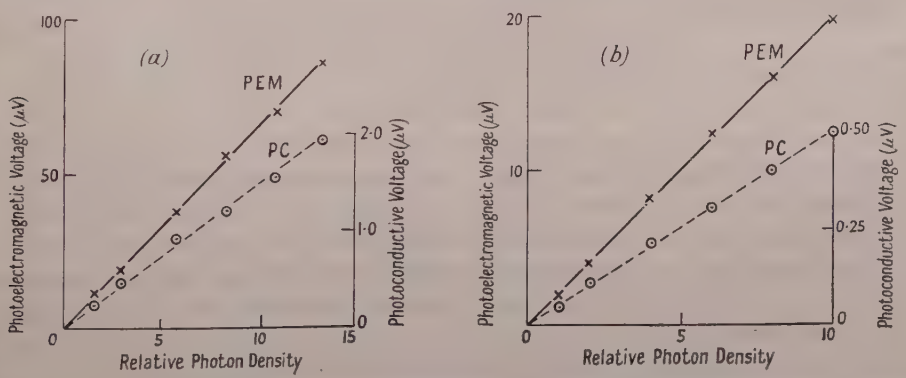

Figure 1. Dependence of photovoltages on photon density. (Specimen 4, $B=2270$ gauss, $I=54$ milliamps.)

(*a*) Density varied by altering voltage applied to source,

(*b*) Density varied by altering setting on optical attenuator.

The variation of V_{PEM} with the magnetic field depends on the impurity concentration of the specimen. In figure 2 the experimental values for five specimens are shown, together with the theoretical curves calculated from equation (2) using the material parameters of the table and assuming that surface

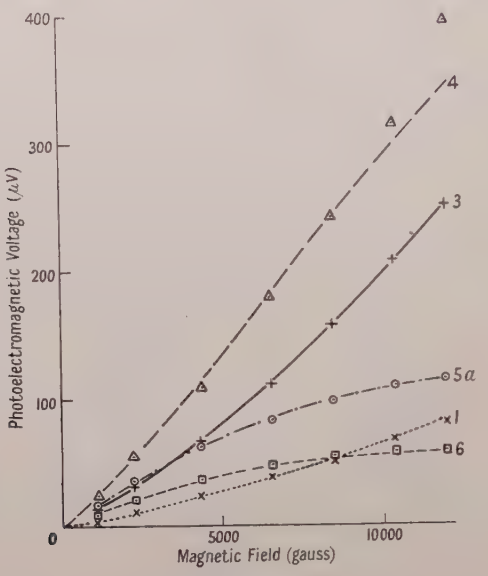

Figure 2. Photoelectromagnetic voltages as a function of magnetic field.

effects are negligible. The results for specimen 2 are not given, as the predicted and experimental values show a field dependence indistinguishable from specimen 1; the absolute values were smaller by a factor of about 2.

Figure 3 indicates how the photovoltages depend on impurity concentration. The factors of merit are the photovoltage for a standard photon flux and electric or magnetic field divided by the corresponding value for specimen 1, the intrinsic specimen. The photoelectromagnetic factor of merit increases as the material is made p-type to a maximum at a hole concentration of 6×10^{16} cm^{-3}, and then decreases. The photoconductive factor shows little variation with impurity concentration until this reaches 10^{17} cm^{-3}, and after this it drops rapidly.

4.2. *Carrier Lifetime*

We may deduce τ from any one of equations (1), (2) and (3). If we use equation (3) we must measure both of the photovoltages, but we need not know the photon density D or the surface conditions. This method is the preferred one since the accuracy of measuring D is estimated as only within $\pm 10\%$. In practice, however, the results deduced by all three methods were in good agreement, if it was assumed that the effects of surface recombination were negligible. This indicates that s was less than 100 m sec^{-1}, which is confirmed by the agreement between theory and experiment shown in figure 2. Appreciable surface recombination would have given lower photoelectromagnetic voltages at the higher magnetic fields. The results for τ are shown in figure 4. The method for obtaining the theoretical curve is discussed in the next section. The rapid decrease of τ with impurity concentration will be noted.

The polycrystalline specimen showed a lifetime of only 0·03 microsecond, which appears low for its impurity concentration of 2×10^{15} acceptors/cm^3; it has therefore been omitted from the graph.

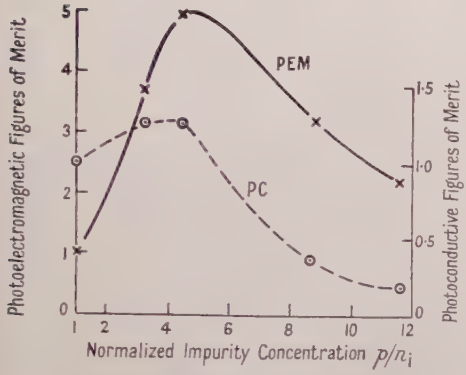

Figure 3. Photoelectromagnetic and photoconductive figures of merit as function of impurity concentration (normalized to unity for intrinsic material).

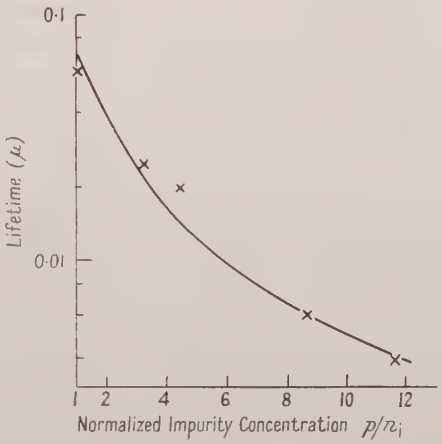

Figure 4. Dependence of lifetime on impurity concentration.
(× = experiment; — = theory.)

§ 5. Conclusions

The scattering processes in InSb were discussed fully in I. Here we have further confirmation that the assumption of an energy independent relaxation time predicts the room temperature behaviour very well. The five curves of figure 2 have quite different shapes, and the agreement between theory and experiment is very satisfactory.

The theoretical estimates (Mackintosh and Allen 1955, Moss and Hawkins 1956) of 'radiative-limited' lifetime in InSb are in the region of half a microsecond. Wertheim shows that below 250°K the dependence of τ on temperature can be explained by simultaneous action of two recombination processes, one radiative and the other via traps. When he extrapolated his results to room temperature they indicated that if τ were limited solely by radiative processes, it would be 0·17 μsec, rather lower than the predicted value. Our values are lower still. If we assume that some recombination via traps is also taking place at room temperature we may calculate from our results the trap depth, density and capture cross section. The lifetime given by equation (1) is that of the carrier with the longer lifetime, whereas equation (2) gives a diffusion length appropriate to the carrier with the shorter life (Rose 1955). When use of the two equations leads to equal values of τ, as it does throughout our results, we have $\tau_p = \tau_n$. Following Shockley and Read (1952) we obtain

$$\tau_p = \tau_n = \tau = \frac{\tau_{p0}[n+n_1] + \tau_{n0}[p+p_1]}{n+p}$$

where τ_{p0} = hole lifetime in very n-type material, τ_{n0} = electron lifetime in very p-type material, p_1 = hole concentration in valence band when Fermi level coincides with the trap level, n_1 = electron concentration in conduction band

when Fermi level coincides with the trap level, and the trap density is small compared with any one of n, n_1, p or p_1. We find our results can only be explained if $\tau_{p0} \gg \tau_{n0}$. The theoretical curve of figure 4 has been calculated on the assumptions that $\tau_{p0} = 0{\cdot}2\ \mu$sec and the trap level is half way between the full and conduction bands. We deduce from these assumptions that the trap density must be less than 4×10^{14} cm^{-3}, the cross-sectional area for hole capture greater than 6×10^{-16} cm^2, and for electron capture greater than 2×10^{-14} cm^2. The position of the trap level, and the value for τ_{p0} are not critically defined by our results, and slightly different combinations could give as good agreement with experiment.

The information contained in figure 4 is useful for the design of InSb photocells (Hilsum and Ross 1957, Avery, Goodwin and Rennie 1957). A photoconductive cell is usually operated with a high current and its performance is limited by the power which may be dissipated in it. Since the resistivity of InSb increases as it is made p-type it would be permissible to operate p-type units with a larger electric field, and so obtain a better sensitivity (in terms of volts per photon); however, the signal to noise ratio would not be improved since the Johnson noise would also be higher. For photoelectromagnetic cells there is a large gain to be obtained by using p-type material. The factor of merit is so much improved that both the sensitivity and signal to noise ratio would be higher.

Acknowledgments

The author is grateful to Mrs. A. Rayner for her help with these measurements, to Dr. O. Simpson for valuable discussions, and to the Admiralty for permission to publish.

References

Avery, D. G., Goodwin, D., and Rennie, A., 1957, *J. Sci. Instrum.*, **34**, 394.
Avery, D. G., and Jenkins, D. P., 1955, *J. Electronics*, **1**, 145.
Hilsum, C., and Barrie, R., 1958, *Proc. Phys. Soc.*, **71**, 676,
Hilsum, C., Oliver, D. J., and Rickayzen, G., 1955, *J. Electronics*, **1**, 134.
Hilsum, C., and Ross, I. M., 1957, *Nature, Lond.*, **179**, 146.
Kurnick, S. W., and Zitter, R. N., 1956, *J. Appl. Phys.*, **27**, 278.
Mackintosh, I. M., and Allen, J. W., 1955, *Proc. Phys. Soc.* B, **68**, 985.
Moss, T. S., and Hawkins, T. H., 1956, *Phys. Rev.*, **101**, 1609.
Rose, A., 1955, *Proc. Inst. Radio Engrs, N.Y.*, **43**, 1850.
Shockley, W., and Read, W. T., Jr., 1952, *Phys. Rev.*, **87**, 835.
Wertheim, G. K., 1956, *Phys. Rev.*, **104**, 662.

Excitation of N_2 and O_2 by 1/2 and 1 MeV Protons

By R. W. NICHOLLS†, E. M. REEVES† and D. A. BROMLEY‡

† Department of Physics, University of Western Ontario
‡ Physics Division, Atomic Energy of Canada Ltd., Chalk River, Ontario

MS. received 8th April 1958, in revised form 10th February 1959

Abstract. Spectroscopic observations have been made photographically, over the wavelength range from 3800–8000 Å, upon the luminosity produced by 1/2 and 1 MeV proton beams in N_2, over the pressure range 63 μ Hg to atmospheric, and in O_2 at atmospheric pressure. The spectra excited in N_2 consisted entirely of bands of the N_2 First Positive ($B^3\Pi$–$A^3\Sigma$) and Second Positive ($C^3\Pi$–$B^3\Pi$) systems, and of the N_2^+ First Negative ($B^2\Sigma$–$X^2\Sigma$) system. No atomic lines of HI, NI, or NII were found. In contrast, the spectra excited in O_2 consisted solely of lines of OI and OII. No bands of O_2 or O_2^+ were found. The probable excitation mechanisms of these spectral features are discussed.

§ 1. Introduction

The increasing importance in auroral and radiation physics of the luminosity excited by the passage of positive ions through gases has led to a number of spectroscopic observations being made on the luminosity during the past few years.

Fan and Meinel (1953) have studied the spectra arising from the ion bombardment of air with H^+, He^+, Ne^+ over the energy range from 46 to 400 kev, and Branscomb, Shalek and Bonner (1954) have made similar observations with 100 kev H^+ beams in N_2. In a lower energy range, Carleton (1957, 1958) has studied the luminosity arising from H^+ (1–5 kev) in N_2, while Nicholls and Pleiter (1956), and Nicholls, Reeves and Pleiter (to be published) have studied luminosities from Li^+ (2–4 kev) in N_2, O_2, A, CO. A few observations have also been made on the feeble luminosity of gas scintillations from high energy Po α-particles in air and other gases (Huggins 1903–6, Ortner and Salim 1952, Ward 1954, Brown and Miller 1957, Nicholls and Reeves 1957).

In this paper, results of the first of a series of experiments on the spectra of gases excited by proton beams are described. The work was performed at Atomic Energy of Canada Ltd., Chalk River, using the facilities of the 3 MeV Van de Graaff accelerator. In the survey experiments described below N_2 and O_2 at pressures from 63 μ Hg to atmospheric have been used as target gases for 0·5–1 MeV protons. Identifications of the spectra of the luminosities and their variations with pressure are discussed. Later papers will discuss spectral intensities and excitation cross sections.

§ 2. Experimental

Mono-ergic proton beams (0·25–0·5 μA) from 0·5 to 1 MeV energy were directed through a thin (0·001 in.) titanium foil into a 50 cm long collision chamber which was part of a dynamic vacuum system through which target

gas passed at controlled pressure. Spectra of a 0·5 cm luminous region, where the beam entered the gas, were photographed transversely to the beam through quartz windows in the chanber by an f/1·1 prism spectrograph (Reeves and Nicholls 1958) over the wavelength range 3800–8000 Å at a reciprocal dispersion of 130 Å mm $^{-1}$ at 4050 Å on Kodak HIR402 film (1-N emulsion). Exposure times, which increased with decreasing pressure, varied from one minute to two hours using a 200 μ slit width.

§ 3. Results

The experiments which were performed are summarized in table 1. The observed region of the beam was a well defined, compact, luminous cylinder of about 1 cm diameter which did not change in appearance over the pressure range

Table 1. Summary of Experiments

Proton Energy (MeV)	Gas	Pressure	Spectral Features†
1	N_2	63 to 150 μ Hg 5 to 20 mm Hg Atm.	N_2^+1N, $N_2$1P, $N_2$2P, N_2GG
1/2	N_2	150 μ Hg	N_2^+1N, $N_2$1P, $N_2$2P
1	O_2	Atm.	OI, OII

† 1P First Positive System of N_2, 2P Second Positive System of N_2, 1N First Negative System of N_2^+, GG Gaydon Green System of N_2.

encountered. At the lowest pressures the beam was collected by an electrode at the end of the chamber. At pressures greater than about 15 mm Hg the beam was stopped completely in the target gas, and at atmospheric pressure was about 2·5 cm long.

3.1. *Protons into Nitrogen*

The dominant spectral features are the band systems of N_2^+ (First Negative $B^2\Sigma - X^2\Sigma$) and N_2 (First Positive $B^3\Pi - A^3\Sigma$; and Second Positive $C^3\Pi - B^3\Pi$) as shown in figure 1 (plate), in which all the commonly excited bands of these systems (Pearse and Gaydon 1950) are present. No *lines* of H, N or N^+ were photographed. The dense coverage of bands over a wide spectral range is consistent with a relatively bright visual beam.

It was noted from a comparison of the proton induced spectra with those from gaseous discharges in N_2 that bands arising from the $v' = 0$, 1 levels of $N_2^+(B^2\Sigma)$ and from the $v' = 0$, 1, 2 levels of $N_2(C^3\Pi)$ appear to be enhanced in our spectra. Fan (1955) has reported a similar effect. The (8, 5)N_2 First Positive band in the proton-induced spectra was observed to be of much lower intensity, relative to its neighbours (7, 4), (6, 3), (5, 2), (4, 1) than in discharge excitation. The spectra recorded over the pressure range 5–20 mm Hg and at atmospheric pressure are superficially very similar to the above except for bands at 5040, 5309, 5327, 5575, and 5815 Å which were observed at atmospheric pressure. They have tentatively been attributed to the Gaydon Green system (Gaydon 1944)

The most evident change in spectrum with increasing pressure, up to atmospheric, is a steady increase in the intensity of the N_2 Second Positive bands relative to the adjacent N_2^+ bands, as judged from photographic blackening.

Furthermore, the blackening of the N_2 First Positive bands decreased between 63 μ and 5 mm Hg and then remained relatively unchanged up to atmospheric pressure. No variation in the above pattern was observed when 0·5 MeV protons were used.

3.2. *Protons into Oxygen*

The visual luminosity produced by the proton beam in oxygen was markedly less intense than that in nitrogen, and exposure times of the order of an hour were required to photograph the spectrum at atmospheric pressure. A typical

Table 2. Identification of Proton Induced Spectrum in O_2 at Atmospheric Pressure†

Wavelength (Å)	Identification	Wavelength (Å)	Identification
3947	OI(3)	4590–4596	OII(15)
3954	OI(30)	4641–4661 (5 lines)	OII(1)
4069–4076 (4 lines)	OII(10)	4699	OII(40)
4119	OII(20)	4699–4705	OII(25)
4185–4190 (2 lines)	OII(36)	7156	OI(38)
4275	OII(67)	7254 (3 lines)	OI(20)
4277	OII(68)	7473–7480 (4 lines)	OI(55)
4317–4319	OII(2)	7772–7775 (3 lines)	OI(1)
4347–4351	OII(16)	7943–7952 (4 lines)	OI(35)
4367	OII(2)	7981–7995 (3 lines)	OI(19)
4368	OII(5)	8221–8235 (7 lines)	OI(34)
4415–4417	OII(5)	8446–8447 (3 lines)	OI(4)
4465–4469	OII(94)		

† Multiplet numbers and wavelengths from *A Multiplet Table of Astrophysical Interest* (Moore 1945).

spectrum is given in figure 2 (plate), with identifications in table 2. The relatively weak lines of O and O^+ in the blue and near infra-red are consistent with the feeble luminosity. No H lines nor O_2 or O_2^+ bands were photographed.

§ 4. Discussion

A detailed discussion of the ion-induced luminosities in terms of excitation mechanisms must await a more complete quantitative study involving variations of spectral intensities with pressure, beam energy, and current. Nevertheless, the following general comments may be made upon the gross features of the spectra.

4.1. *Nitrogen Target*

The presence of N_2^+bands, and the absence of the Balmer lines of H indicate that ionization and excitation of N_2 without charge transfer, viz.

$$H^+ + N_2 \rightarrow N_2^{+*} + H^+ + e$$
$$N_2^{+*} \rightarrow N_2^+ + h\nu \text{ (bands)}$$

is a far more probable excitation mechanism, at these energies, than excitation with charge transfer, viz.

$$H^+ + N_2 \rightarrow N_2^{+*} + H^*$$

followed by

$$N_2^{+*} \rightarrow N_2^+ + h\nu \text{ (bands)}$$
$$H^* \rightarrow H + h\nu \text{ (lines)}$$

which was found by Carleton (1957) to be operative at lower energies. This is not surprising in view of the high proton velocity relative to orbital velocities.

It will be important in future experiments to look for H Balmer radiation at the end of the beam stopped in N_2 where proton velocities should be comparable with orbital velocities.

It is impossible to invoke proton excitation of the N_2 First Positive and Second Positive bands, which require a singlet–triplet excitation, and which almost certainly were excited by energetic electrons arising from the above ionization processes and by secondary electrons from the foil window through which the beam passed. The same electrons probably played some part in the excitation of the N_2^+ bands. However the apparent increase in N_2 band intensity with pressure relative to N_2^+ band intensity would favour preponderant proton excitation of N_2^+ and electron excitation of N_2. The relative decrease in the N_2 First Positive band intensity with pressure is probably due to collisional de-excitation of $N_2(B^3\Pi)$ levels by the small O_2 impurity present in the tank N_2 used. Such de-excitations are well known in electrical discharges (Pearse and Gaydon 1950, p. 169, Nicholls 1954).

Although the upper state of the Gaydon Green system is not known with certainty, its appearance at higher pressures, probably through electron excitation, is not surprising as the conditions are similar to those under which it is preferentially excited in discharges.

4.2. *Oxygen Target*

The domination of the spectrum in this case by lines of OI and OII, together with the complete absence of bands of O_2 and O_2^+, strongly suggests the operation of the dissociative ionizing collisions:

$$H^+ + O_2 \rightarrow H^+ + O^* + O^{+*} + e$$

followed by

$$O^* \rightarrow O + h\nu \text{ (OI lines)}$$
$$O^{+*} \rightarrow O^+ + h\nu \text{ (OII lines)}.$$

This is similar to the mechanism proposed by Feast (1949) in the case of dissociative electron collisions.

The atomic lines may also arise in a secondary manner from the preferential dissociation of O_2 into ground state $O(^3P)$ atoms and metastable $O(^1S)$ and $O(^1D)$ atoms, by the operation of the Franck–Condon principle, under the impact of the electrons produced by ionizing collisions or secondary electrons from the foil window.

Acknowledgments

Two of the authors (R.W.N. and E.M.R.) wish to acknowledge partial support of this research by the Geophysical Research Directorate, Air Force Cambridge Research Centre, Air Research and Development Command, under contract number AF 19(604)-1718 and by the National Cancer Institute of Canada and the Ontario Research Foundation through research grants. One of us (E.M.R.) gratefully acknowledges an Ontario Research Foundation Scholarship.

References

Branscomb, L. M., Shalek, R. J., and Bonner, T. W., 1954, *Trans. Amer. Geophys. Union*, **35**, 107.

Brown, L. O., and Miller, N., 1957, *Trans. Faraday Soc.*, **53**, 748.

Carleton, N. P., 1957, *Phys. Rev.*, **107**, 110.

—— 1958, Conference of Electronic and Atomic Collisions, held at New York University.

Fan, C. Y., 1955, *The Airglow and the Aurorae*, edited by E. B. Armstrong and A. Dalgarno, (London: Pergamon Press), p. 276.

Fan, C. Y., and Meinel, A. B., 1953, *Astrophys. J.*, **118**, 205.

Feast, M. W., 1949, *Proc. Phys. Soc.* A, **62**, 114.

Gaydon, A. G., 1944, *Proc. Phys. Soc.*, **56**, 85.

Huggins, Sir Wm. and Lady, 1903, *Proc. Roy. Soc.* A, **72**, 196.

—— 1905, *Ibid.*, A, **76**, 488.

—— 1906, *Ibid.*, A, **77**, 130.

Moore, C. E., 1945, *A Multiplet Table of Astrophysical Interest*, Revised Edition (Princeton: University Press).

Nicholls, R. W., 1954, *Nature, Lond.*, **173**, 495.

Nicholls, R. W., and Pleiter, D., 1956, *Nature, Lond.*, **178**, 1456.

Nicholls, R. W., and Reeves, E. M., 1957, *Nature, Lond.*, **180**, 1188.

Ortner, G., and Salim, S., 1952, *Nature, Lond.*, **169**, 1060.

Pearse, R. W. B., and Gaydon, A. G., 1950, *The Identification of Molecular Spectra* (London: Chapman and Hall).

Reeves, E. M., and Nicholls, R. W., 1958, *J. Opt. Soc. Amer.*, **48**, 358.

Ward, A., 1954, *Proc. Phys. Soc.* A, **67**, 841.

Neutral Pions

By J. M. CASSELS, D. P. JONES, P. G. MURPHY and P. L. O'NEILL

Nuclear Physics Research Laboratory, University of Liverpool

MS. received 11*th March* 1959

Abstract. The angular correlation between the γ-rays produced in Panofsky reactions has been measured. The results exclude one of the two possible ways of introducing the π_0^0 proposed by Baldin and Kabir. On the conventional assumption that there is only one π^0, it is found that $m_{\pi^-} - m_{\pi^0} = (8{\cdot}90 \pm 0{\cdot}14)m_e$; the lifetime of the π^0 must be greater than 3×10^{-22} sec.

§ 1. Introduction

Several years ago Anderson and Fermi (1952) pointed out that there was a simple theoretical relation between the cross sections for low-energy pion–nucleon scattering, the cross sections for pion photoproduction at threshold, and the Panofsky ratio. The numerical data which should be substituted into the relation have often been discussed (e.g. Cassels, Fidecaro, Wetherell and Wormald 1957, Moravcsik 1958, Baldin 1958, Cini, Gatto, Goldwasser and Ruderman 1958, Beneventano, Bernardini, Stoppini and Tau 1958). More often than not the experimental Panofsky ratio has turned out to be lower than the theoretically expected value, and this has led Baldin and Kabir (1958) to make the interesting suggestion that there are two kinds of neutral pion. The conventional pion of unit isobaric spin π_1^0 is retained, and a new pion of zero isobaric spin π_0^0 is proposed.

This idea brings two new parameters into low energy pion physics, a pion mass and an amplitude for charge exchange pion–nucleon scattering. There are two possible schemes, one of which Baldin and Kabir call 'revolutionary' and the other, by implication, 'evolutionary'. The revolutionary scheme envisages that one of the neutral pions is too heavy to be produced in the Panofsky reaction, and the experiment reported here has no bearing on this possibility (see, however, Cini *et al.* 1958). The evolutionary scheme involves the production of both neutral pions in Panofsky reactions:

$$\pi^- + \mathrm{p} \rightarrow \pi_0^0 + \mathrm{n} \rightarrow 2\gamma + \mathrm{n}(+Q_0^0) \qquad \ldots\ldots(1)$$

$$\pi^- + \mathrm{p} \rightarrow \pi_1^0 + \mathrm{n} \rightarrow 2\gamma + \mathrm{n}(+Q_1^0). \qquad \ldots\ldots(2)$$

An attempt has been made to separate experimentally the two groups of γ-rays which would be produced in these reactions. The angular correlation in laboratory space of the γ-ray pairs is a sensitive function of the neutral pion velocity, and hence of Q_0^0 or Q_1^0. The observed angular correlation should be a superposition of two correlation functions with the two Q values. The form of these functions has been given by Chinowsky and Steinberger (1953). For each π^0

$$\frac{dN}{d\omega} = \frac{(1-\beta^2)}{2\pi(1-\cos\phi)^{3/2}\beta[(1-\cos\phi)/(1-\beta^2)-2]^{1/2}} \qquad \ldots\ldots(3)$$

where ϕ is the angle between the two γ-rays, β is the velocity of the π^0 in units of c, $d\omega$ is an element of solid angle, and $dN/d\omega$ is the differential probability for the coincidences. A typical intensity distribution is plotted in figure 1, which shows a cut-off at an angle ϕ_c given by $\cos\phi_c = 2\beta^2 - 1$. The experiment of Chinowsky and Steinberger was designed simply to determine the largest ϕ_c, and their apparatus would not have been very sensitive to an admixture of

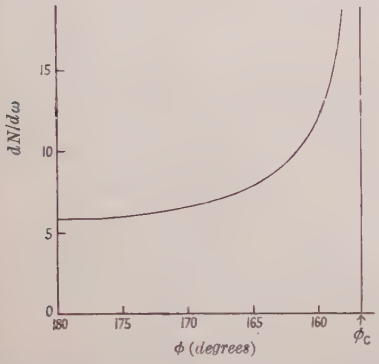

Figure 1. Angular correlation function for the two gamma rays in $\pi^0 \rightarrow 2\gamma$.

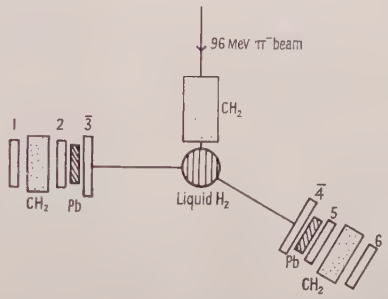

Figure 2. Schematic diagram of apparatus.

a second π^0 with a smaller ϕ_c. The experiment reported here was done with the highest practicable angular resolution over the whole range of ϕ in the hope of detecting such a second group. As will be seen this was not found and the experiment can be used to rule out the evolutionary proposal of Baldin and Kabir. An accurate value for the mass difference between the π^- and the conventional π^0 is obtained, however, together with a small lower limit for the π^0 lifetime.

§ 2. Experimental Procedure

The apparatus is shown schematically in figure 2. The 96 MeV π^- beam from the Liverpool synchrocyclotron was slowed down in a polyethylene absorber and stopped in liquid hydrogen contained in a copper cylinder 3 in. in diameter and 4 in. high, with $\frac{1}{16}$ in. thick walls. A cylindrical copper radiation shield $\frac{1}{32}$ in. thick surrounded the target and the whole structure, including the liquid hydrogen reservoir, was enclosed in an aluminium alloy vacuum tank with $\frac{1}{4}$ in. thick walls. The γ-rays were detected in counter telescopes each consisting of a lead converter $3\frac{1}{8}$ in. $\times 3\frac{3}{4}$ in. $\times \frac{1}{4}$ in. and two plastic scintillation counters $3\frac{1}{4}$ in. $\times 3\frac{7}{8}$ in. $\times \frac{1}{4}$ in. The lead converters were each 45 in. from the axis of the target. Each pair of counters was shielded from charged particles by large anticoincidence counters. One inch of polyethylene absorber was placed between each pair of counters to eliminate coincidences due to low energy γ-rays arising from nuclear reactions in the main absorber. Coincidences $(12\bar{3}\bar{4}56)$ were counted by means of a coincidence circuit with resolution time 2×10^{-8} second. The beam was monitored by counting the $(12\bar{3})$ coincidences.

The $(12\bar{3})$ telescope was kept fixed in position while counts were recorded for various angular settings of the $(\bar{4}56)$ telescope. Correlation angles between 150° and 210° were used. The results were combined on the assumption that the correlation function was symmetric about 180°; a small correction was applied to allow for the fact that the target was found not to be exactly in the centre of the

scale. Counts were recorded both with hydrogen in the target and with the target empty.

§ 3. Results

The experimental results are given in the table, where the uncertainties are the statistical standard deviations. The background counts for different angular settings have been added together on the assumption that the counting

Angle	Events/10^3 monitor counts	Events/10^3 monitor counts (Background subtracted)
179·45°	0·502	0·454 ± 0·074
175°	0·565	0·517 ± 0·069
170°	0·527	0·479 ± 0·066
165°	0·727	0·679 ± 0·077
162·5°	0·815	0·767 ± 0·081
160°	1·059	1·011 ± 0·093
157·5°	1·050	1·002 ± 0·091
155°	0·583	0·535 ± 0·069
152·5°	0·200	0·152 ± 0·040
150°	0·055	0·007 ± 0·029

rate with no hydrogen in the target was independent of angle over the range used. The counts could not have been accidental coincidences; they must have been due to coincident pairs of γ-rays. Pairs of γ-rays from successive decays of nuclear excited states with reasonable spin values should have correlation functions which are fairly constant over a range of 30°. The last column gives the counting rate after subtraction of the averaged background rate.

§ 4. Interpretation

As a first step the results were interpreted on the conventional assumption that only one π^0 exists. The angular resolution functions for the counters, which were calculated numerically by the method of Chinowsky and Steinberger (1953), had widths of about $6\frac{1}{2}°$ at half height. These resolution functions were folded into the theoretical correlation functions with various values of ϕ_c, and the best curve was selected by the least squares method (figure 3). The value of ϕ_c for the curve is 156·7°, and the corresponding difference between the π^- and π^0

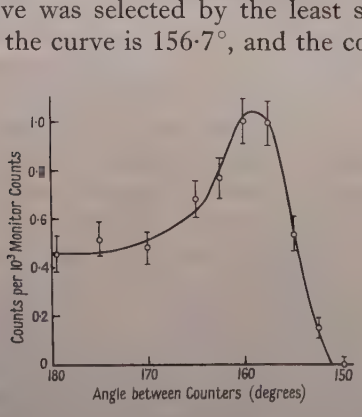

Figure 3. Experimental results, with background subtracted. The curve is the theoretical curve for $m_{\pi^-} - m_{\pi^0} = 8{\cdot}90 m_e$.

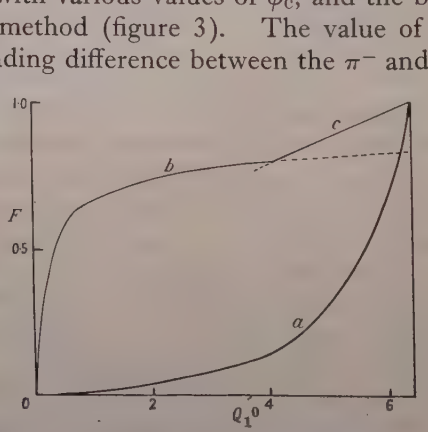

Figure 4. F = fraction of decays due to $\pi_1{}^0$, $Q_1{}^0$ = energy released in $\pi^- + p \rightarrow \pi_1{}^0 + n$ in units of m_e.

Curve a, experimental upper limit; curves b and c, theoretical lower limits.

masses is equal to $(8{\cdot}90 \pm 0{\cdot}14)m_e$. The standard deviation was evaluated by studying the variation with ϕ_c of the χ^2 sum. The result agrees excellently with the value $(8{\cdot}8 \pm 0{\cdot}6)m_e$ given by Chinowsky and Steinberger.

An attempt was then made to interpret the results in terms of the evolutionary proposal of Baldin and Kabir. In order to achieve a reduction in the theoretical Panofsky ratio it is necessary that $Q_0^0 > Q_1^0$. Thus the ϕ_c already given must be assigned to the π_0^0, and a superposed distribution with a smaller ϕ_c should arise from the π_1^0. Clearly figure 3 provides no positive evidence in favour of this, and figure 4 shows the upper limit (95% confidence) to the fraction F of the total number of γ-rays arising from the π_1^0 (curve *a*). The experiment cannot distinguish the π_1^0 γ-rays if $Q_0^0 = Q_1^0$; on the other hand it can place a low limit on F as $Q_1^0 \to 0$.

Also shown on figure 4 are the lower limits on F required by two other considerations:

(*a*) The purpose of introducing the π_0^0 is to lower the theoretical Panofsky ratio. In the notation of Baldin and Kabir, this means that

$$v_0^0 |a_0|^2 + \tfrac{2}{9} v_1^0 |a_1 - a_3|^2 < \tfrac{2}{9} v_0^0 |a_1 - a_3|^2 \qquad \ldots\ldots (4)$$

where v_0^0 and v_1^0 are the velocities of the π_0^0 and π_1^0, and a_0, a_1 ,and a_3 are scattering amplitudes. Now F is given by

$$F = \frac{\frac{2}{9} v_1^0 |a_1 - a_3|^2}{v_0^0 |a_0|^2 + \frac{2}{9} v_1^0 |a_1 - a_3|^2} \qquad \ldots\ldots (5)$$

and the combination of equation (5) with the inequality (4) means that

$$F > (Q_1^0/Q_0^0)^{1/2} \qquad \ldots\ldots (6)$$

since $Q_1^0/Q_0^0 = (v_1^0/v_0^0)^2$

(*b*) The introduction of the π_0^0 must not significantly increase the theoretical positive energy charge-exchange scattering at energies large compared to Q_1^0, Q_0^0. Nearly all this scattering is taken up by a term proportional to $|a_1 - a_3|^2$, where a_1 and a_3 are determined quite independently by the π^+ and direct π^- scattering. These experiments show in fact that

$$\frac{|a_0|^2}{\frac{2}{9}|a_1 - a_3|^2} < \tfrac{1}{5} \qquad \ldots\ldots (7)$$

which leads to the inequality

$$F > \frac{5}{5 + (Q_0^0/Q_1^0)^{1/2}} \qquad \ldots\ldots (8)$$

The lower limits to F provided by these two considerations are also shown in figure 4 (curves *b* and *c*). The experimental upper limit does not, for any Q_1^0, overlap the more stringent of the two lower limits. The evolutionary proposal of Baldin and Kabir therefore seems to be quite excluded.

Finally, it may be mentioned that the results can be used to give a lower limit to the lifetime of the conventional π^0. If τ is the lifetime of the π^0, its mass must be uncertain by an amount $\Delta m \sim \hbar/2\tau c^2$. Theoretical distributions were constructed for various values of Δm to replace the curve in figure 3, which assumes a sharp value. The results show that the fit becomes significantly bad when τ is assumed to be less than 3×10^{-22} second. In fact, of course, τ is believed to be more than 10^5 times larger than this.

Acknowledgments

We would like to thank Mr. B. Halliday and the cyclotron crew for their co-operation in running the experiment, and Mr. L. F. Leech for his skill in constructing the apparatus. We are also grateful to Dr. J. R. Wormald for much helpful advice, to him, Miss M. Rigby and Mr. T. W. O'Keeffe for help in recording the data, and to Mr. R. L. Plackett of the Department of Applied Mathematics for advice on statistical treatment of the results. One of us (P. G. M.) is indebted to I.C.I. Ltd., for a fellowship, and two of us (D. P. J. and P. L. O.'N.) to the Department of Scientific and Industrial Research for maintenance grants.

References

Anderson, H. L., and Fermi, E., 1952, *Phys. Rev.*, **86,** 794.
Baldin, A. M., 1958, *Nuovo Cim.*, **8,** 569.
Baldin, A. M., and Kabir, P. K., 1958, *Nuovo Cim.*, **9,** 547.
Beneventano, M., Bernardini, G., Stoppini, G., and Tau, L., 1958, *Nuovo Cim.*, **10,** 1109.
Cassels, J. M., Fidecaro, G., Wetherell, A. M., and Wormald, J. M., 1957, *Proc. Phys. Soc.* A, **70,** 405.
Chinowsky, W., and Steinberger, J., 1953, *Phys. Rev.*, **93,** 586.
Cini, M., Gatto, R., Goldwasser, E. L., and Ruderman, M., 1958, *Nuovo Cim.*, **10,** 243.
Moravcsik, M. J., 1958, *Nuovo Cim.*, **7,** 442.

Selective Pressure Broadening and the Stark Effect

By L. I. MAISSEL†
Imperial College of Science and Technology, London

Communicated by R. W. B. Pearse; MS. received 20th November 1958, in final form 2nd April 1959

Abstract. Broadening of the spark lines from a condensed discharge in neon and argon has been compared with their Stark effects and good correlation obtained, indicating that Stark effect is important as a cause of line broadening for other elements besides hydrogen and helium.

§ 1. Introduction

Soon after Stark had demonstrated the existence of an effect by electric fields on emission spectra, it was realized that the random interionic fields in a gaseous discharge might cause a broadening of the spectral lines. Holtsmark's (1919, 1924) and other more recent (Unsöld 1956) treatments of this phenomenon have found wide application in the study of stellar and discharge tube spectra. Such application has, however, been almost invariably confined to the spectrum of hydrogen (and occasionally helium), both because of this element's great abundance in the stars and because of its unusually large Stark effect. As a result of this, the impression has become widespread that Stark effect is of no importance as a cause of line broadening in other elements and alternative explanations such as Doppler effect etc. have been sought.

In the case of lines broadened by the ionic plasma of a condensed discharge, direct comparison between broadening and Stark effect has not been attempted before because of the scarcity of data concerning the latter. This, in turn, is due to the fact that the lines involved are always members of spark rather than arc spectra (as a result of the violent conditions prevailing within the condensed discharge). Stark effects of spark spectra are relatively difficult to measure.

§ 2. Selective Pressure Broadening in the Spark Spectrum of Neon

Neon is one of the rare cases where extensive data on the Stark effects of the spark lines have been published (see later). Except for Pretty's work (1931) on pressure shifts, however, this element does not appear to have been previously examined for selective pressure broadening. A suitable tube was therefore constructed and the spectrum of the condensed discharge photographed over the pressure range 0·5 mm to 35 cm. The rather low maximum pressure is due to the fact that the neon was stored in 1 litre flasks filled at a pressure of two thirds of an atmosphere (industrial high pressure cylinders, if obtainable at all, being prohibitively expensive).

The magnitude of the capacity used for condensing the discharge was 0·01 mF (at 20 kv), and the discharge was forced to pass through a capillary of 1 mm bore. Narayan's classification of lines (to be published) into three arbitrary classes according to their susceptibility to pressure has been retained for the sake of uniformity:—

† Now at the Philco Corporation, Philadelphia 34, Pa., U.S.A.

Class A lines are those which show the first signs of broadening at about 1 mm pressure and merge into the background continuum at about 3 cm. Class B lines begin to broaden at about 1 cm and vanish into the background at about 10 cm while class C lines show no signs of broadening until about 4 cm and are not completely submerged until about 50 cm. Lines still visible above this pressure are termed 'surviving'. In a few cases lines lying roughly between two classes have been designated A–B or B–C.

§ 3. Direct Comparison between Selective Pressure Broadening and Stark Effect

(*a*) Neon.

Stark effect shifts for Ne II have been published by Ishida, Tamura and Kamijima (1939) and by Ryde (1931). All shifts are in cm^{-1}.

Wavelength	Broadening Class	Broadening Dir^{n}	Ishida etc. ($F=100$ kv cm^{-1})	Ryde ($F=85$ kv cm^{-1}) P	Ryde ($F=85$ kv cm^{-1}) s
2537·4	surviving		0		
2538·7	A	R	−37		
2562·2	A	R	−35		
2586·3	surviving		0		
2621·0	A	V	45		
2623·2	A	R	−37	−25·0	−24·4
2636·14	A	sym.	−35	−29·6	−29·6
2638·2	A–B	–	−35	−19	−20
2897·6	B	R	−10	−6·9	−8·6
2915·2	A	–	−10	−7·9	−9·1
2922·0	B	–	−17		
2940·7	A	R	−11	−5·7	−7·1
2972·28	B	R		−3·5	−5·5
2973·03	A	R	−11	−6·3	−8·3
2976·63	A	R		−7·7	−11·2
2986·02	A	R	−10	−9·3	−10·3
2988·91	A	R	−10	−5·9	−6·2
2993·0	C	–		0·0	−2·3
2994·90	A	R	−13	−10·5	−11·1
3007·82	A	R	−13	−4·6	−6·5
3050·57	A	R	−11		
3060·6	A	–	15	14·4	11·1
3062·59	A	–	−16		
3063·39	A	R		−8·5	−9·1
3069·0	A	V	16	12·3	6·9
3071·50	A	R	−14	−9·7	−9·7
3075·67	A	sym.	−10	−5·0	−5·2
3115·72	A	sym.	−11	−9·0	−9·0
3123·7	A	V	15		
3124·12	A	R	−13	−9·9	−9·9
3138·12	A	R	−11	−8·7	−8·8
3148·8	A	R	−12	−12	−14

(*b*) Argon.

Stark effects for AII have been published by Minnhagen (1948) and by Maissel (1958). The broadening characteristics of the spark lines have been observed by Narayan (to be published). A few of the lines given below are not to be found in his lists; these were observed in the discharge tube described above (which was used for neon). All Stark shifts are in cm^{-1}.

Wave-length	Broadening Class	Broadening Dirⁿ	Maissel ($F=160$ kv cm^{-1})	Minnhagen ($F=100$ kv cm^{-1})
3464·14	B	R	−1·0	
3476·74	B	R	−1·0	
3491·54	B	R	−0·4	
3514·39	B	R	−0·8	
3535·33	B	R	−0·9	
3559·53	B	–	−1·3	
3567·67	B	R	−1·3	
3588·44	B	R	−1·3	
3622·15	B	R	−0·7	
3639·86	B	R	0·0	
3655·29	B	R	−1·4	
3660·44	B	R	0·0	
4237·22	B–C	R		−0·21
4448·88	B	R		−0·06
4474·76	B	R		−1·42
4502·93	B	R		−1·40
4530·55	B–C	R		−0·22
4537·65	B	R		−1·45
4598·76	B–C	R		−0·20

The following lines which have been classified as 'surviving', show no Stark effect up to 160 kv cm^{-1} :

4228·18	4400·09	4589·93	4879·90	5062·07
4266·53	4401·02	4609·60	4889·06	5141·84
4282·90	4426·01	4637·25	4904·75	5145·36
4331·90	4430·18	4657·94	4933·24	6114·92
4348·11	4481·83	4726·91	4965·12	6172·98
4352·23	4490·99	4735·90	4972·16	6243·13
4371·36	4545·08	4764·89	5009·35	6483·10
4375·96	4579·39	4827·90	5017·16	

The following lines, classified 'C to Red', also show no Stark effect up to 160 kv cm^{-1} :

4300·66 4460·56.

Even closer correspondence between broadening and Stark effect is obtained if one considers, not the lines themselves, but, instead, the upper level of the transition involved in each case (see C. E. Moore's *Revised Multiplet Table* (1945) and *Atomic Energy Levels* (1949)).

Where the j-value is not given, the shift represents the average for the multiplet.

Level	Broadening Class	Broadening Dirⁿ	Stark effect (cm^{-1}) at 160 kv cm^{-1}	Stark effect (cm^{-1}) at 100 kv cm^{-1}
$5s\,^4P$	B	R	−0·7	
$4d\,^4F$	B	R	−1·3	
$4d\,^4P$	B	R	−2·0	
$4d\,^2F$	B	R	−1·2	
$4d\,^4D$	B–C	R	−0·9	
$4p'\,^2p^0$	B–C	R		−0·20
$4p'\,^2p^0_{1\frac{1}{2}}$	A	R		−1·42
$3d'\,^2D_{1\frac{1}{2}}$	A	V		+1·4
$5s'\,^2D_{1\frac{1}{2}}$	B	R		−0·10

This improved correlation is certainly surprising and, contrary to present ideas, suggests that the selective pressure broadening of a line is more sensitive to the Stark effect of the upper level than to that of the line itself. In most cases, the Stark effect of the line largely reflects that of the upper level anyway, so that good correlation is still found between line broadening and line Stark effect. The following examples, however, illustrate instances when the upper level shows its domination:

Line	Transition	Stark effect at 100 kv cm^{-1} (cm^{-1}) Lower Level	Upper Level	Line	Broadening	Dir^n
4537·65	$3d'^2D_{1\frac{1}{2}}-4f^2F^0_{2\frac{1}{2}}$	+1·4	0·0	−1·4	B	R
4502·93	$3d'^2D_{1\frac{1}{2}}-X^0$	+1·4	0·0	−1·4	B	R
2890·38	$4s^2P_{1\frac{1}{2}}-3d'^2D_{1\frac{1}{2}}$	0·0	+1·4	+1·4	A	V
2977·86	$4s^2P_{\frac{1}{2}}-3d'^2D_{1\frac{1}{2}}$	0·0	+1·4	+1·4	A	V
3660·44	$4p'^2P^0-4d'^2D_{1\frac{1}{2}}$	−0·2	−0·2	0·0	B	R
3639·86	$4p'^2P^0-4d'^2D_{2\frac{1}{2}}$	−0·2	−0·2	0·0	B	R

We have no explanation for this unexpected result except to observe that for an electric field varying appreciably in strength across an ionic diameter, the intensity would, in general, be greater for the upper than the lower level. Stark effects, of course, are measured in relatively uniform fields. For a discussion of some of the difficulties associated with present day theories of the Stark effect see Sobelman (1954).

Acknowledgments

The author wishes to thank Dr. R. W. B. Pearse for his guidance and advice throughout.

References

Holtsmark, J., 1919, *Ann. Phys., Lpz.*, **58**, 577.
—— 1924, *Phys. Z.*, **25**, 73.
Ishida, Y., Tamura, T., and Kamijima, G., 1939, *Sci. Pap. Inst. Phys. Chem. Res. Tokyo*, **36**, 12.
Maissel, L. I., 1958, *J. Opt. Soc. Amer.*, **48**, 853.
Minnhagen, L., 1948, *Ark. Mat. Astr. Fys.*, **35** A, No. 16.
Moore, C. E., 1945, 'Revised Multiplet Table', *Contributions from the Princeton University Observatory*, No. 20.
—— 1949, 'Atomic Energy Levels', *Circ. Nat. Bur. Stand., Wash.*, No. 467.
Pretty, W. E., 1931, *Proc. Phys. Soc.*, **43**, 279.
Ryde, N., 1931, *Z. Phys.*, **71**, 124.
Sobelman, I. I., 1954, *Adv. Phys. Sci., Moscow*, **54**, 551.
Unsöld, A., 1956, *Physik der Sternatmosphären* (Berlin: Springer), Ch. 11.

The Effect of Polarization on the Elastic Scattering of Positrons by Hydrogen Atoms

By A. H. MOUSSA
University College, London

Communicated by H. S. W. Massey; MS. received 26th February 1959

Abstract. The Hulthén and Kohn variational methods are applied to a further consideration of the effect of polarization in the scattering of slow positrons by hydrogen atoms. A trial function is used which allows for virtual positronium formation. Although the results indicate a greater effect of polarization than those of previous calculations using a mathematically simpler but physically less appropriate trial function the effect is much less than seems to be required from the experimental results on the scattering of slow positrons by rare gas atoms.

§ 1. Introduction

In a recent paper Massey and Moussa (1958, to be referred to as I) have discussed the theoretical interpretation of the cross sections for elastic scattering of low energy positrons by helium, neon and argon atoms derived by Marder, Hughes, Wu and Bennett (1956) from the experimental study of the effect of an electric field on the formation of positronium in the respective gases.

It was shown that these cross sections are much smaller than would be expected for scattering by the undisturbed mean fields of the appropriate atoms. As this field is repulsive any polarization effect would act in the opposite sense and it is natural to seek an explanation of the low cross sections in terms of cancellation arising in this way. Empirical support for this was found by Massey and Moussa, based on a representation of the polarization potential $v_p(r)$ in the form

$$v_p(r) = -\tfrac{1}{2}\frac{\alpha e^2}{(r^2+l^2)^2} \qquad \ldots\ldots(1)$$

where α is the polarizability of the atom and l is a parameter of the order of magnitude of atomic dimensions. However, this procedure is very rough, particularly as the polarization cannot be represented adequately by a static potential. Massey and Moussa therefore investigated the importance of the polarization effect in the scattering of positrons by atomic hydrogen using the Hulthén and Kohn variational methods with trial functions of the same form as those used by Massey and Moiseiwitsch (1950) in a corresponding study of the scattering of slow electrons. In contrast to the empirical results no appreciable effect of polarization appeared in the variational calculations.

It is an unfortunate feature of variational calculations of scattering cross sections that one has little guidance about the accuracy of the results obtained. Although the trial functions used gave quite satisfactory results for the scattering by the static field there is no guarantee that the major effects of polarization were allowed for by the modifications of the trial functions which were introduced.

It is desirable therefore to examine whether some functions more appropriate on physical grounds could be used, and if so to test whether such functions yielded more marked polarization effects. This is the aim of the present paper.

§ 2. Trial Wave Function

One of the main features of elastic scattering of electrons by atoms is that it may include electron exchange. In the positron case (I) the possibility of forming real or virtual positronium is the only effect which could be compared with the exchange effect in electron collisions. The cross sections for real positronium formation in atomic hydrogen, as calculated by Massey and Mohr (1954) using Born's approximation, are quite large. This indicates that there may be considerable coupling between purely elastic scattering and positronium formation which may make a major contribution to the polarization, remembering that this arises eventually from the effect of the inelastically scattered waves on the elastic scattering. We therefore seek a trial wave function to introduce in the variational calculations which includes this effect as far as possible.

In the present work the energy of the positron is below the threshold for positronium formation, so we are dealing with the effect of virtual processes. We choose as trial function describing the scattering of slow positrons the form

$$\Psi_t = \psi_0(r_2) F_0(r_1) + \phi_0(\mathbf{r}_1, \mathbf{r}_2) \qquad \ldots\ldots (2)$$

where $\mathbf{r}_1$ and $\mathbf{r}_2$ are the respective coordinates of the positron and electron relative to the proton and $\psi_0(r_2)$ is the ground state wave function of the hydrogen atom. $F_0(r_1)$ represents the motion of the positron with wave number k and is taken to be of the form

$$F_0(r_1) = r_1^{-1}[\sin kr_1 + (a + b\, e^{-r_1})(1 - e^{-r_1}) \cos kr_1] \qquad \ldots\ldots (3)$$

which is the same as that used successfully in conjunction with the variational method to calculate the cross sections for elastic scattering of positrons by the static field of the atom (see I).

The additional term $\phi_0(\mathbf{r}_1, \mathbf{r}_2)$ allows for distortion of the atom during the collision. According to the above considerations we represent it by

$$\phi_0(\mathbf{r}_1, \mathbf{r}_2) = \chi(r_{12}) G(\tfrac{1}{2} |\mathbf{r}_1 + \mathbf{r}_2|) \qquad \ldots\ldots (4)$$

where $\chi(r_{12})$ is the wave function for the ground state of positronium and G represents the relative motion of the positronium in the field of the proton. As we are dealing with virtual formation of positronium we choose for G the form

$$G = c \exp(-\gamma |\mathbf{r}_1 + \mathbf{r}_2|); \qquad \ldots\ldots (5)$$

c and γ may be taken as further adjustable parameters. However, to decrease the very considerable labour involved in the calculations if γ is varied it was chosen once and for all in the following way.

The asymptotic form of the function G for large values of $|\mathbf{r}_1 + \mathbf{r}_2|$ is given by

$$G \sim \text{const.} |\mathbf{r}_1 + \mathbf{r}_2|^{-1} \exp(-\lambda |\mathbf{r}_1 + \mathbf{r}_2|), \qquad \ldots\ldots (6)$$

where, in atomic units,

$$\lambda^2 = \tfrac{1}{4} - \tfrac{1}{2}k^2. \qquad \ldots\ldots (7)$$

It is to be expected then that with the form (5) a fair approximation would be obtained by taking $\gamma = \lambda$ and this was adopted.

This differs very considerably from the procedure adopted in I in which the polarization effect was represented by taking

$$\Psi_t = \psi_0(r_2) F_0(r_1, r_{12}) \qquad \ldots\ldots (8)$$

with

$$F_0(r_1, r_{12}) = r_1^{-1}[\sin kr_1 + \{a + (b + cr_{12})e^{-r_1}\}(1 - e^{-r_1}) \cos kr_1]. \qquad \ldots\ldots (9)$$

If a large contribution actually comes from the possibility of virtual positronium formation the new form should represent a good approximation.

§ 3. Details of the Calculation

In applying the variational method we proceed from the integral

$$L = \int\int \Psi_t (H - E) \Psi_t d\tau_1 d\tau_2 \qquad \ldots\ldots (10)$$

where, in atomic units,

$$H = -(\nabla_1^2 + \nabla_2^2) + \frac{2}{r_1} - \frac{2}{r_2} - \frac{2}{r_{12}}, \qquad \ldots\ldots (11)$$

m being the mass of the electron or positron and

$$E = E_0 + \frac{k^2 h^2}{8\pi^2 m}$$

where E_0 is the energy of the ground state of the hydrogen atom.

Having calculated L as a function of the parameters a, b, and c which occur in Ψ_t, we obtain an approximate value for the phase shift η_0. According to Hulthén's method the equations to be solved are:

$$L = 0, \quad \frac{\partial L}{\partial b} = 0, \quad \frac{\partial L}{\partial c} = 0, \text{ and } \eta_0 = \arctan a, \qquad \ldots\ldots (12)$$

and according to Kohn

$$\frac{\partial L}{\partial a} = 4\pi k, \quad \frac{\partial L}{\partial b} = \frac{\partial L}{\partial c} = 0, \quad \eta_0 = \arctan\left(a - \frac{L}{4\pi k}\right). \qquad \ldots\ldots (13)$$

The evaluation of L involves some expressions which can be integrated analytically and for which the data obtained in I were used. It also involves other integrals which can only be evaluated by numerical methods. These are of the form

$$I = \int\int f(r_1, r_2) g(r_{12}, |\mathbf{r}_1 + \mathbf{r}_2|) d\tau_1 d\tau_2. \qquad \ldots\ldots (14)$$

The function g may be expanded in the form

$$g(r_{12}, |\mathbf{r}_1 + \mathbf{r}_2|) = \sum_n g_n(r_1, r_2) P_n(\cos\Theta) \qquad \ldots\ldots (15)$$

where Θ is the angle between $\mathbf{r}_1$ and $\mathbf{r}_2$, and

$$g_n(r_1, r_2) = \frac{2n+1}{2} \int_0^\pi g(r_{12}, |\mathbf{r}_1 + \mathbf{r}_2|) P_n(\cos\Theta \sin\Theta d\Theta. \qquad \ldots\ldots (16)$$

On substitution in (14) we have

$$I = 16\pi^2 \int_0^\infty \int_0^\infty f(r_1, r_2) g_0(r_1, r_2) r_1^2 r_2^2 dr_1 dr_2. \qquad \ldots\ldots (17)$$

The numerical evaluation of g_0 and thence of the double integral (17) was carried out using the DEUCE electronic computer at the English Electric Company's

office in London. Because of the length of the calculations it was confined to the case $k=0{\cdot}5$, corresponding to a positron energy of 3·4 ev.

Values of Parameters a, b and c, Phase shifts η_0 and Cross Sections Q_0

Method	Case	a	b	c	η_0 (rad.)	Q_0 (in πa_0^2)
Hulthén	$b\neq 0$	−0·232	−0·188	0·087	−0·228	0·817
Hulthén	$b\equiv 0$	−0·244	—	0·079	−0·239	0·897
Kohn	$b\equiv 0$	−0·012	—	0·028	−0·211	0·702
No polarization (exact solution)					−0·264	1·089
Polarization included using trial function of I					−0·251	0·987

§ 4. Discussion of Results

The results obtained are given in the table. For comparison the phase shifts η_0 and cross sections Q_0 obtained in I are also included.

It will be seen that the new trial function does indeed suggest that the polarization effect is rather larger than does the function (8) used in I. Nevertheless, even with the most extreme case in which Kohn's method is used with $b=0$, the cross section remains as high as 70% of the value it would have if polarization were completely absent. Although there are no experimental results with which to compare for atomic hydrogen it was shown in I that, in order to interpret the results for the rare gases, the polarization would need to be so large as nearly to cancel out the effect of the undisturbed mean atomic field. It seems that we have still no direct theoretical evidence that this can be so.

In view of this still unsatisfactory situation it is very desirable that the experimental work be repeated and extended. Further theoretical work is being undertaken in which the back coupling between virtual inelastic processes (including positronium formation) is being taken into account by the solution of coupled differential or integro-differential equations.

Acknowledgments

I am greatly indebted to Professor H. S. W. Massey for suggesting the problem and for valuable discussions on it. I am also indebted to Dr. M. J. Seaton for a discussion on the problem, to Dr. P. G. Burke for permission to use his programme for the electronic computer, and to the English Electric Company for allowing me to use the DEUCE electronic computer in London.

References

Marder, S., Hughes, V. W., Wu, C. S., and Bennett, W., 1956, *Phys. Rev.*, **103**, 1258.
Massey, H. S. W., and Mohr, C. B. O., 1954, *Proc. Phys. Soc.* A, **67**, 695.
Massey, H. S. W., and Moiseiwitsch, B. L., 1950, *Proc. Roy. Soc.* A, **205**, 483.
Massey, H. S. W., and Moussa, A. H. A., 1958, *Proc. Phys. Soc.*, **71**, 38.

The Forward Scattering of Light by Spheres according to Geometrical Optics

By J. McK. ELLISON† and C. V. PEETZ‡
Environmental Hygiene Research Unit, Medical Research Council, London School of Hygiene and Tropical Medicine, W.C.1

MS. received 13*th October* 1958, *in revised form* 16*th February* 1959

Abstract. If the light scattering by transparent spheres is calculated according to geometrical optics a large part of the scattered flux falls within a cone of half-angle $|m-1|$ radians around the forward direction, where m is the refractive index of the sphere relative to the surrounding medium. For many purposes it is this light which is of principal interest.

If $I(\theta)$ is the intensity scattered at angle θ and $\Delta E(\theta)$ the flux scattered within this angle, the light externally reflected (I_1) and that transmitted without internal reflection (I_2) normally predominate in the forward-scattered light. For $0{\cdot}75 \leqslant m \leqslant 2$ graphical methods of obtaining I_1 and I_2, and ΔE_1 and ΔE_2, are given: this is made possible by plotting I_1, I_2, and ΔE_1, ΔE_2, against functions of single variables which themselves depend on m and θ. For light internally reflected once (I_3) or twice (I_4) analytical expressions are not given, but the values over which they range are indicated. Light internally reflected more than twice is shown to be negligible.

The accuracy obtainable is within about 1% in each case, and the angular range over which approximation is possible increases as $|m-1|$ increases as long as $m<1{\cdot}65$: if $m>1{\cdot}65$ the range decreases as m increases. For more accurate computation exact expressions for I_1 and I_2, in terms of m and θ only, are given. Unless $m \gg 1$, $I_2(\theta) \gg I(\theta) - I_2(\theta)$ for small values of θ, and consequently if accurate values of I_1 and I_2 are combined with approximations to I_3 and I_4 the overall accuracy is fairly high.

To simplify the computation, from the approximations given, of I and ΔE respectively two tables show the procedures suggested in each case.

§ 1. Introduction

An exact solution of the equations giving the scattering of electromagnetic waves by spherical obstacles was first obtained by Mie (1908), and for spheres of radius comparable with the incident wavelength it is necessary to have recourse to this solution. For polydisperse clouds of water droplets much larger than this however Bricard (1946) showed that the light scattered forward could be treated as if it were comprised of two incoherent components, one resembling diffraction by opaque discs of the same cross-sectional areas and the other resembling scattering according to geometrical optics by clouds of transparent spheres of the same refractive index m relative to the surrounding medium. This approximation will be called Bricard's method. It is an adaptation of Mecke's method (1920) in which the phase of all rays is taken into account.

† Now at the Group for Research on Atmospheric Pollution, St. Bartholomew's Hospital, London E.C.1.

‡Now at the Group for Research on the General Effects of Radiation, Western General Hospital, Edinburgh 4.

A recent paper (Ellison 1957) described experiments showing that the angular distribution of forward-scattered light, for suspensions of silica dust of mean particle size down to about 2 microns, resembled that calculated by Bricard's method for clouds of spheres of the same relative refractive index. If this method is to be applied to clouds of particles of arbitrary m the geometrical scattering must be readily calculable. The formulae involved are simple to derive (see for example van de Hulst 1957, § 12.21) and are not intrinsically difficult to compute, but the process as normally done is laborious, and has been carried out for few values of m. The earliest detailed calculations appear to be those of Wiener (1907, 1909), for $m = 4/3$, but these are rejected by van de Hulst (1957) who presents his own figures for this refractive index (p. 233 and table 21). The only other published computations of which the authors are aware are those of Davis (1955) for a large air bubble in water ($m = 0{\cdot}75$). None of these computations is presented in a manner designed to facilitate interpolation with respect to m, and none gives the dependence of extinction coefficient on angle of acceptance.

The method presented here is intended to fill these gaps. It can be applied to the forward scattering and extinction by clouds of spheres up to the scattering angle within which about three-quarters of the incident flux is scattered if $0{\cdot}75 < m < 1{\cdot}65$, and to smaller angles if $1{\cdot}65 < m < 2{\cdot}0$. The observer is assumed to be at such a distance that the diameters of the spheres can be neglected.

The range $0{\cdot}75 \leqslant m \leqslant 2$ includes van de Hulst's region of spheres with refractive index near 1 (van de Hulst 1946, 1957), for which he gives an altitude chart of an amplitude function $|A|$ whose square is the total field: $|A|$ is plotted against two parameters $z = x\theta$ and $\rho = 2x(m-1)$, where $x = 2\pi a/\lambda$ (a = radius of sphere, λ = wavelength of incident light, and θ = scattering angle). Where valid, this method is certainly preferable to either Mecke's or Bricard's. Without integration however, it is not applicable to polydisperse clouds, for which Bricard's gives acceptable results (Bricard 1946). Moreover since the chart is only plotted to $z = 14$, $\rho = 28$, its range is severely restricted with respect to both x and θ. Van de Hulst does not state the maximum value of $m - 1$ for which it can be used, and for $m < 1{\cdot}33$ comparison with computations of Mie's theory is hampered by the scantiness of computed values of angular distribution of scattered light. For $m = 1{\cdot}33$ Gumprecht *et al.* (1952) give numerous computed values of Mie's theory, and those for $x = 20$ and $x = 40$ have previously been compared with values calculated by Mecke's method, the approximation appropriate to scattering by single spheres (Ellison 1954). To this comparison may be added one with the values derived from van de Hulst's chart, for those angles tabulated by Gumprecht *et al.* which are in the ranges of x and θ covered by the chart. As van de Hulst predicts, near $\theta = 0$ and near the minima of the Kirchhoff diffraction pattern both Mecke's approximation and van de Hulst's give considerable proportional errors, although near the minima the absolute errors are small. At other angles both methods are surprisingly successful; Mecke's is rather better for $x = 40$, and for $x = 20$ there is little to choose between them. The advantages claimed for the methods presented in this paper are therefore: (1) their ready applicability to polydisperse clouds; (2) the much greater range of x and θ as well as m which they cover; and (3) the ease with which the extinction can also be derived.

In general the methods suggested are approximate. For greater accuracy exact expressions, in terms of m and θ only, are given for the intensity of light externally reflected I_1 and of that passing through the sphere without internal reflection, I_2. I_2 is the most important part of the forward-scattered light and has hitherto always been expressed in terms of the three variables m, θ, and angle of incidence i (see for example Davis 1955, van de Hulst 1957): the elimination of i greatly simplifies the computation. If θ is small, then compared with I_1 and I_2 the intensities of internally reflected rays are small, and errors of approximations to them are negligible.

§ 2. General Characteristics of Geometrical Scattering by Spheres

The light scattered by a transparent sphere may be divided into components according to the number of times the scattered ray meets the surface of the sphere, and the various components characterized by this number. Light externally reflected will then be component 1, that passing through the sphere without internal reflection will be component 2, and that transmitted after $n-2$ reflections and 2 refractions will be component n. The path of any ray lies in the equatorial plane containing the corresponding incident ray, which is the plane of incidence, for all refractions† and reflections. If the sphere is in a

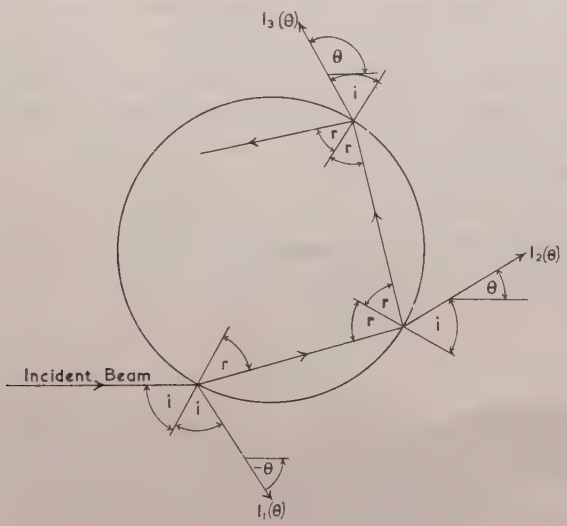

Figure 1. Reflection and refraction of light by transparent sphere.

parallel beam of incident light, and if $I(\theta)$ is the scattered flux per unit solid angle, per unit incident flux, at any angle θ from the direction of the incident beam, it is given by

$$I(\theta)=\sum_n I_n(\theta) \qquad \ldots\ldots (1)$$

where $I_n(\theta)$ is the contribution of the nth component. This subdivision into

† The fact that incident ray, refracted ray, and normal to the refracting surface lie in a plane is contained in Snell's law as it is often stated (see for example Jenkins and White 1957) and its discovery seems therefore to be attributed sometimes to Snell. It was in fact known very much earlier, and indeed the explanation of the rainbow by Qutb al-Din al-Shirazi, mentioned below, would not have been possible without it. It is stated quite unambiguously in Eugene of Palermo's translation (from the Arabic, itself translated much earlier from the Greek) of Ptolemy of Alexandria's *Optics*, (Ptolemaeus 1885). Eugene of Palermo's translation was made about A.D. 1160: Ptolemy himself flourished about A.D. 160.

components is implicit in the explanation of the rainbows, which is due to the Persian Qutb al-Din al-Shirazi (died 1311), and was discovered independently, probably slightly later, by Theodore of Freiburg (died *ca.* 1311) (Sarton 1947).

The derivation of the expression giving the intensity scattered by a sphere at an angle θ is well known (see for example van de Hulst 1957) and only the results needed will be given here. If i is the angle of incidence of the ray on the sphere and r the angle of refraction (see figure 1), then

$$\theta = 2i - 2(n-1)r + 2(n-2)\pi. \qquad \ldots\ldots (2)$$

Since $\theta, -\theta, 2k\pi+\theta$, and $2k\pi-\theta$ are all equivalent physically there may be several values of i corresponding to a given pair of values of n and θ. For each of these i, and for light polarized either in or perpendicular to the plane of incidence, $I_n(\theta)$ is given by

$$I_n(\theta) = \left| \frac{1}{2\pi} \frac{\sin 2i}{\sin \theta} \frac{di}{d\theta} \tau_n \right| \qquad \ldots\ldots (3)$$

Here τ_n is the overall transmission coefficient for the corresponding ray and is the cumulative product of n terms, two being the transmission factors at the surfaces at which the ray enters and leaves the sphere and the remaining $n-2$ being reflection coefficients at the surfaces at which it is reflected; if $n=1$ the single term is the reflection coefficient for external reflection. Hence for $n>1$

$$\tau_n = \rho^{2(n-2)}(1-\rho^2)^2 \qquad \ldots\ldots (3\,a)$$

where ρ^2 is the corresponding Fresnel reflection coefficient (see below). If the suffices 1 and 2 are used to denote respectively the components polarized in and perpendicular to the plane of incidence then T_n the effective value of the overall transmission coefficient will be

$$T_n = \tfrac{1}{2}(\tau_{n,1} + \tau_{n,2}) \qquad \ldots\ldots (3\,b)$$

In measuring $I(\theta)$ for small θ another quantity, the extinction $E(\theta)$, is useful. $E(\theta_0)$ is the fraction of the flux incident on the sphere which is scattered through angles greater than θ_0, and is given by

$$E(\theta_0) = 1 - \int_{\theta=0}^{\theta_0} \{I(\theta) \times 2\pi \sin\theta\} d\theta. \qquad \ldots\ldots (4)$$

Clearly $E(0)=1$ and $E(\pi)=0$. $E(\theta_0)$ can be split into components just as $I(\theta)$ can, each component being given by

$$E_n(\theta_0) = E_n(0) - \int_{\theta=0}^{\theta_0} \{I_n(\theta) \times 2\pi \sin\theta\} d\theta. \qquad \ldots\ldots (5)$$

$E_n(0)$ is difficult to evaluate, but in practice only the difference $E(0) - E(\theta_0)$ and therefore only the component differences $E_n(0) - E_n(\theta_0)$ are required; these will be denoted by ΔE and ΔE_n respectively.

If $0{\cdot}75 \leqslant m \leqslant 2$ the reflection coefficients ρ_1^2 and ρ_2^2 (see (6 *a*) and (6 *b*) below) are small unless $\frac{1}{2}\pi - i$ is small (or, if $m<1$, unless $\sin i > m$ or $\frac{1}{2}\pi - r$ is small). Consequently a large proportion of light penetrating the sphere ($n \geqslant 2$) is transmitted without internal reflection and is thus of $n=2$. At $\theta=0$ the term $\{|(\sin 2i/\sin\theta)(di/d\theta)|\}_{n=2}$ has a maximum which is very sharp if $|m-1|$ is small, but which flattens out as $|m-1|$ increases. Even for $m=2$ however the directly transmitted light near the forward direction is sufficiently intense to dominate the forward scattering, and a large proportion of the incident flux is scattered after direct transmission through the sphere, into a cone of half-angle of 60° about $\theta=0$. For this reason this component is treated very fully.

The externally reflected light ($n=1$), which is next in importance, is also mainly scattered forward, since the Fresnel reflection coefficients ρ_1^2 and ρ_2^2 are greatest near glancing incidence (or, if $m<1$, at angles near $i=\sin^{-1} m$; and if $\sin i > m$, $\rho_1^2=\rho_2^2=1$).

If $n>2$, each successive component includes a lower proportion of the incident flux, and the larger the number of reflections then in general the more widely is the light scattered. Moreover, unless $m<1{\cdot}02$ none of component 3 is scattered within the cone of $\theta<30°$, so that only the fourth and higher components need be considered. These form only a small part of the scattering and since $I_3(\theta)$, $I_4(\theta)$, ... are not readily expressed in terms of θ only, they are treated only approximately and discussed in general terms.

If $m<1$ and $n>2$, light striking the sphere near the limiting angle $i'=\sin^{-1} m$ will be scattered through small angles forward. $|di/d\theta|$ is however small and although the term $1/\sin\theta$ makes I large near $\theta=0$ the contribution to ΔE is small. Only if $\theta\to 0$ are I_3, I_4 . . . important; their relative importance increases as $1-m$ increases, and for $m=0{\cdot}75$ they cannot be neglected.

§ 3. Component 1: Externally Reflected Light

For externally reflected light $\theta=\pi-2i$ so that $|di/d\theta|=\frac{1}{2}$, $\sin 2i/|\sin\theta|=1$ and $I_1(\theta)=T_1/4\pi$.

If m is less than 1 then for scattering angles less than $2\sin^{-1}(1-m^2)^{1/2}$ incident light of both polarizations suffers total reflection and $T_1=1$. $2\sin^{-1}(1-m^2)^{1/2}$ is considerably greater than the maximum angle at which the approximation to I_2 given below can be applied. Consequently, no approximation to I_1 is required, and $I_1(\theta)=1/4\pi$ exactly. Hence by (5) $\Delta E_1=(1-\cos\theta)/2$.

If $m>1$ the two components $\tau_{1,1}$ and $\tau_{1,2}$ of T_1 must be considered separately. They are given by $\tau_{1,1}=\rho_1^2$ and $\tau_{1,2}=\rho_2^2$ where (see for example van de Hulst 1957)

$$\rho_1=\frac{\cos i-m\cos r}{\cos i+m\cos r}, \qquad \ldots\ldots(6a)$$

$$\rho_2=\frac{m\cos i-\cos r}{m\cos i+\cos r}. \qquad \ldots\ldots(6b)$$

Since $\cos i=\sin\frac{1}{2}\theta$ these may be put into the form

$$\tau_{1,1}=\left\{\frac{\sin\frac{1}{2}\theta-[m^2-1+\sin^2\frac{1}{2}\theta]^{1/2}}{\sin\frac{1}{2}\theta+[m^2-1+\sin^2\frac{1}{2}\theta]^{1/2}}\right\}^2 \qquad \ldots\ldots(6c)$$

$$\tau_{1,2}=\left\{\frac{m^2\sin\frac{1}{2}\theta-[m^2-1+\sin^2\frac{1}{2}\theta]^{1/2}}{m^2\sin\frac{1}{2}\theta+[m^2-1+\sin^2\frac{1}{2}\theta]^{1/2}}\right\}^2 \qquad \ldots\ldots(6d)$$

$\tau_{1,1}$ may be expressed in terms of a parameter $s=[\sin\frac{1}{2}\theta]/(m^2-1)^{1/2}$ and is given by

$$\tau_{1,1}=1-4s(1+2s^2)(1+s^2)^{1/2}+8s^2+8s^4 \qquad \ldots\ldots(7)$$

If $I_1=I_{1,1}+I_{1,2}$, where $I_{1,1}$ and $I_{1,2}$ are polarized in the planes corresponding to $\tau_{1,1}$ and $\tau_{1,2}$ respectively, then by (3) $I_{1,1}=\tau_{1,1}/8\pi$; this is plotted in figure 2.

No similarly simple and exact expression for $\tau_{1,2}$ is available. Algebraically the simplest is

$$\tau_{1,2}=\left(\frac{1-t}{1+t}\right)^2 \qquad \ldots\ldots(8)$$

where $t=m^2s/(1+s^2)^{1/2}$ but this is clumsy to compute. Probably it is easier to use (6*d*) above. If $m^2s<1$, $\tau_{1,2}$ can be expanded in powers of m and s and gives

$$\tau_{1,2}=1-4m^2s+8m^4s^2-(12m^6-2m^2)s^3 +(16m^8-8m^4)s^4-(20m^{10}-18m^6+\tfrac{3}{2}m^2)s^5. \qquad \ldots\ldots(8a)$$

The corresponding expansion of $\tau_{1,1}$ from (7) is

$$\tau_{1,1}=1-4s+8s^2-10s^3+8s^4-(7/2)s^5 \ldots . \qquad \ldots\ldots (7a)$$

so that

$$\tau_{1,2}=\tau_{1,1}(m^2s)-(m^4-1)[2m^2s^3-8m^4s^4+\tfrac{3}{2}(11m^4-1)m^2s^5] \ldots . \qquad \ldots\ldots (9)$$

For small values of m^2s therefore the approximation

$$\tau_{1,2}\simeq\tau_{1,1}(m^2s) \qquad \ldots\ldots (9a)$$

can be used. Provided that $\theta<30^\circ$ it gives sufficient accuracy within the range of the approximation for I_2 (see below). The correction terms in (9) only converge slowly unless $m-1$ is small, so that when exact values are needed for larger values of θ it is simpler to calculate $\tau_{1,2}$ from (8).

For computing ΔE_1 the correction terms in (9) are not necessary, since the cumulative error between 30° and 45° is too small to cause appreciable error in ΔE. ΔE_1 is obtained from (5), (7), and (9 *a*), by which

$$\Delta E_1(\theta_0)=\int_{\theta=0}^{\theta_0}\tfrac{1}{2}(\tau_{1,1}+\tau_{1,2})\frac{1}{4\pi}2\pi\sin\theta d\theta$$

$$=\tfrac{1}{4}\int_{\theta=0}^{\theta_0}[\tau_{1,1}(s)+\tau_{1,1}(m^2s)]\sin\theta d\theta.$$

Putting $m^2s=u$ in the expression for $T_{1,2}$ we get

$$\Delta E_1\simeq(m^2-1)\left[\int s\tau_{1,1}(s)ds+m^{-4}\int u\tau_{1,1}(u)du\right]$$

$$=(m^2-1)[f(s)+m^{-4}f(m^2s)] \qquad \ldots\ldots (10)$$

where

$$f(s)=\tfrac{1}{2}s^2+2s^4+\tfrac{4}{3}s^6-\tfrac{4}{3}s^3(1+s^2)^{3/2}; \qquad \ldots\ldots (11)$$

$f(s)$ is plotted in figure 3, from which ΔE_1 may be derived.

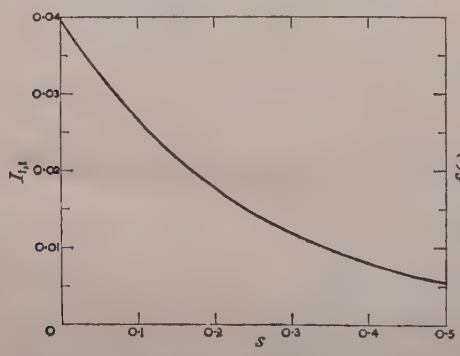

Figure 2. Intensity of light externally reflected, polarization 1 ($m>1$).

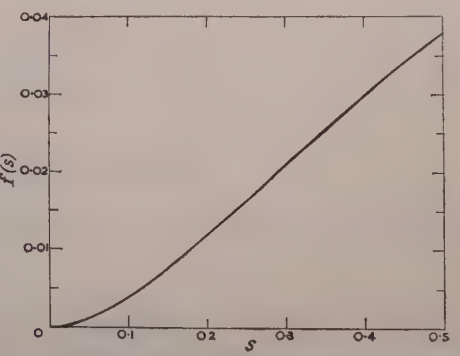

Figure 3. $1/(m^2-1)\times$ flux externally reflected within cone of angle polarization $1(m>1)$.

§ 4. Component 2: Light passing through Sphere without Internal Reflection

4.1. *Exact Expression for Intensity at Angle θ*

For component 2 $\theta=\theta_2=2(i-r)$ (see equation (2)), and since $\sin i=m\sin r$ i may be expressed in terms of θ as follows:

$$2r=2i-\theta$$

$$\sin r=(1/m)\sin i$$

$$=-\sin\tfrac{1}{2}\theta\cos i+\cos\tfrac{1}{2}\theta\sin i$$

$$\sin i[1-m\cos\tfrac{1}{2}\theta]=-m\cos i\sin\tfrac{1}{2}\theta$$

and hence

$$\sin i = \frac{m \sin \frac{1}{2}\theta}{[m^2+1-2m\cos\frac{1}{2}\theta]^{1/2}} \qquad \ldots\ldots (12\,a)$$

and

$$\cos i = \frac{m\cos\frac{1}{2}\theta - 1}{[m^2+1-2m\cos\frac{1}{2}\theta]^{1/2}}. \qquad \ldots\ldots (12\,b)$$

From these may be derived

$$\frac{\sin 2i}{\sin\theta} = \frac{m}{\cos\frac{1}{2}\theta}\cdot\frac{m\cos\frac{1}{2}\theta - 1}{m^2+1-2m\cos\frac{1}{2}\theta} \qquad \ldots\ldots (13)$$

and by differentiating $(12\,a)$

$$\cos i\,.\,di = \frac{(m/2)\cos\frac{1}{2}\theta[m^2+1-2m\cos\frac{1}{2}\theta] - (m^2/2)\sin^2\frac{1}{2}\theta}{[m^2+1-2m\cos\frac{1}{2}\theta]^{3/2}}\,d\theta$$

so that

$$\frac{di}{d\theta} = \frac{m}{2}\cdot\frac{m-\cos\frac{1}{2}\theta}{[m^2+1-2m\cos\frac{1}{2}\theta]}. \qquad \ldots\ldots (14)$$

The transmission coefficients $\tau_{2,1}$ and $\tau_{2,2}$ are $\tau_{2,1}=(1-\rho_1{}^2)^2$ and $\tau_{2,2}=(1-\rho_2{}^2)^2$ (see $(3\,a)$, and $(6\,a)$ and $(6\,b)$). Inserting the values of $\sin i$ and $\cos i$, and putting

$$\sin r = \sin\tfrac{1}{2}\theta/[m^2+1-2m\cos\tfrac{1}{2}\theta]^{1/2}$$

and

$$\cos r = [m-\cos\tfrac{1}{2}\theta]/[m^2+1-2m\cos\tfrac{1}{2}\theta]^{1/2}$$

we get

$$\rho_1 = \frac{2m\cos\frac{1}{2}\theta - m^2 - 1}{m^2-1}$$

and

$$\rho_2 = \frac{(m^2+1)\cos\frac{1}{2}\theta - 2m}{(m^2-1)\cos\frac{1}{2}\theta}.$$

Hence

$$(1-\rho_1{}^2)^2 = \left\{\frac{4m[m\cos\frac{1}{2}\theta-1][m-\cos\frac{1}{2}\theta]}{(m^2-1)^2}\right\}^2 = \tau_{2,1} \qquad \ldots\ldots (14\,a)$$

and

$$(1-\rho_2{}^2)^2 = \left\{\frac{4m[m\cos\frac{1}{2}\theta-1][m-\cos\frac{1}{2}\theta]}{[(m^2-1)\cos\frac{1}{2}\theta]^2}\right\}^2 = \tau_{2,2} \qquad \ldots\ldots (14\,b)$$

From this it follows that $\tau_{2,2}=\tau_{2,1}\sec^4\frac{1}{2}\theta$.

Putting these values into (3) we can express $I_2(\theta)$ in terms of m and θ only:

$$I_2(\theta) = \frac{2}{\pi}\left[\frac{m}{m^2-1}\right]^4 \frac{[m\cos\frac{1}{2}\theta-1]^3[m-\cos\frac{1}{2}\theta]^3}{\cos\frac{1}{2}\theta[m^2+1-2m\cos\frac{1}{2}\theta]^2}\,[1+\sec^4\tfrac{1}{2}\theta] \qquad \ldots\ldots (15)$$

where $I_2(\theta)$ is the sum of the intensities of the beams polarized in two planes perpendicular to one another, the incident light being unpolarized. This may be put alternatively in the form

$$\frac{I_2(\theta)}{(_2(0)} = \frac{[m\cos\frac{1}{2}\theta-1]^3[m-\cos\frac{1}{2}\theta]^3[1+\sec^4\frac{1}{2}\theta]}{2\cos\frac{1}{2}\theta[m^2+1-2m\cos\frac{1}{2}\theta]^2(m-1)^2} = B \qquad \ldots\ldots (15\,a)$$

It is not difficult to show that $B(m,\theta)=B(1/m,\theta)$, and that $I_2(m,\theta)=m^2I_2(1/m,\theta)$, so that only $m>1$ will be considered below.

Equations (15) and $(15\,a)$ greatly simplify the computation of (3) for $n=2$ but they remain formidable obstacles to exact calculations. Similarly, if (15)

is inserted in (5) the integral for ΔE_2 can be evaluated exactly, but the expression obtained is so difficult to compute, involving small differences between relatively large quantities, that it is useless. For many purposes however the light scattered near $\theta = 0$ is that of principal interest; for this, approximations to both I_2 and ΔE_2 are possible.

4.2. *Approximation to* $I_2(\theta)$

The expansion of the right-hand side of (15 *a*) in ascending powers of θ gives an expression containing terms in which θ appears in the combination $\theta/(m-1)$. This greatly restricts its usefulness since in general $\theta \simeq m-1$ when $B \simeq 0{\cdot}5$, and an approximation extending to very much lower values of B is required. Consequently purely empirically a function Θ of m and θ was found such that on plotting B against Θ for various m the curves were as nearly coincident as possible. From the common curve B could be read off for $1{\cdot}02 \leqslant m \leqslant 1{\cdot}65$ and for a range of angles including a large part of the scattered flux. If $m > 1{\cdot}65$ the range over which I can be approximated is limited by I_4 rather than by I_2 (see below) so that as m increases above this value the range of B for which an approximation is required diminishes.

Such an approximation is a compromise between simplicity, accuracy and range of applicability, and the blend of these which is chosen is purely personal. The ranges of both m and θ are involved and if the approximation is to be applied to the sizing of small particles the useful ranges of these are linked through the conditions under which Bricard's method can be used. These may be shown to lead to a useful range of about $\theta = m-1$, but since the approximation derived may be required for other purposes the range was extended to considerably wider angles than this. The aim has therefore been to obtain a curve giving B within 1% for spheres for which $1{\cdot}02 \leqslant m \leqslant 2{\cdot}0$, and for $1{\cdot}02 \leqslant m \leqslant 1{\cdot}65$ to extend the range of application to as high values of $\theta/(m-1)$ as possible. Any approximation doing the latter gives satisfactory agreement for $1{\cdot}65 \leqslant m \leqslant 2{\cdot}0$ up to the maximum angles to which I_4 can be estimated (see below). In fact the range of application extends to higher values of $\theta/(m-1)$ if $m-1$ is small: this is an advantage since (i) if $m-1 \ll 1$ the angle corresponding to $\theta = m-1$ is too small to be of much practical use, and (ii) a smaller proportion of the incident flux is scattered within the cone of semi-angle $k(m-1)$ if m is small.

In order to obtain the required curve (15 *a*) was used to calculate nine to twelve values of B for each of the refractive indices 1·02, 1/0·98, 1·16, 1·33, 4/3, 1·55, and 2·0, θ being chosen in each case so that most of the values of B lay between 1·0 and 0·1. B was then plotted against $m^2\theta/(m-1)(m+1)^2$. The parameter $m\theta/(m-1) = \theta\, di/d\theta$ which seems the obvious one, was not very helpful, and $m^2\theta/(m-1)(m+1)^2$ was chosen instead because $I_2(0)$ is proportional to $\{m^2/(m-1)(m+1)^2\}^2$. The flux scattered in component 2 does not vary very greatly with m, and it seemed plausible that the angular scale was correspondingly contracted.

The plotted points lay fairly well on a curve, and their displacements from it were used to find a more suitable parameter for the abscissae. This process was repeated until an acceptable parameter was found: this was

$$[m^{3/2}(m+10{\cdot}5)\tan\tfrac{1}{2}\theta]/[(m-1)(m+1)^2] = \Theta.$$

B was then calculated for a number of other values of m and θ to see whether they also fitted the curve found. The agreement was surprisingly good, and

figure 4 shows the curve and most of the calculated values of B; where the points crowd too closely upon one another some have been omitted. The scale at the top shows for various m the maximum Θ for which the approximation is valid to within about 1%; in general, computed values of B corresponding to Θ greater than this are not shown, but to illustrate how B behaves over a wider range all the calculated values for $m = 1{\cdot}55$, $1{\cdot}33$ and $1{\cdot}10$, and the curves through them, are given.

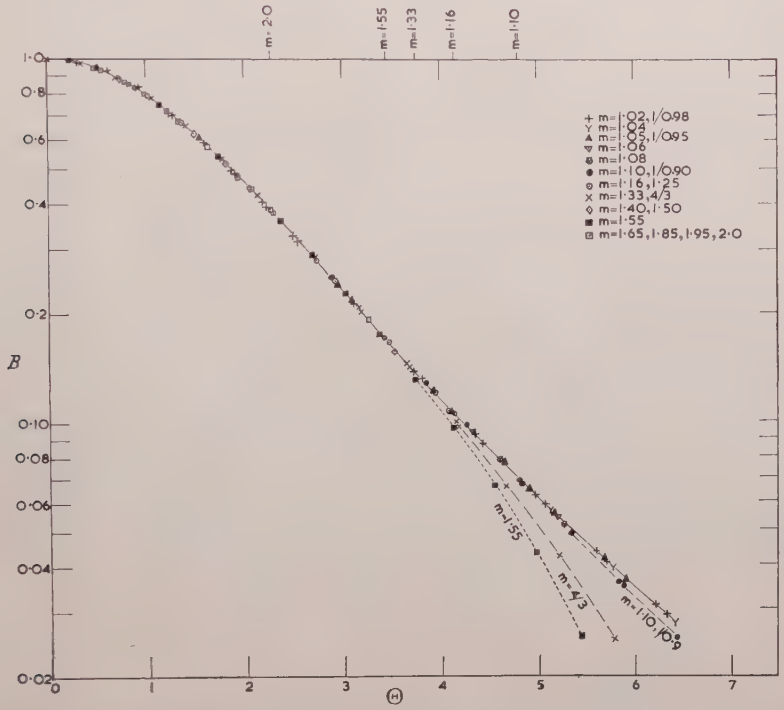

Figure 4. $I_2(\theta)/I_2(0) = B$ as a function of $\Theta = [Q \tan \frac{1}{2}\theta]/(m-1)$. The scale at the top shows, for the values of m marked, the maximum values of Θ for which the curve gives a satisfactory approximation.

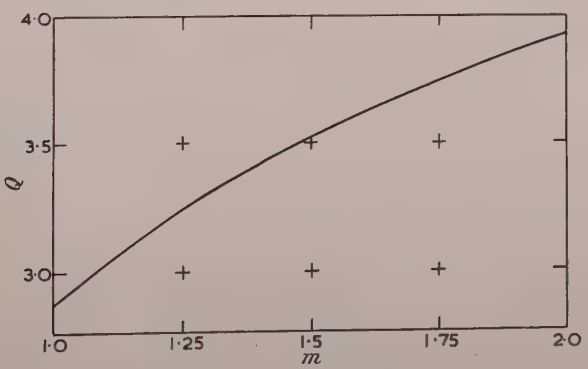

Figure 5. Variation of Q with m.

To simplify the use of figure 4 $m^{3/2}(m+10{\cdot}5)/(m+1)^2 = Q$ is plotted against m in figure 5. If $m > 1$, then to obtain $I_2(\theta)$ Q is read off figure 5 and multiplied by $[\tan \frac{1}{2}\theta]/(m-1)$ to give Θ. B is then read off figure 4, and $I_2(\theta)$ calculated

from it by multiplying by $I_2(0)=(4/\pi)m^4/[(m-1)^2(m+1)^4]$. If $m<1$, $I_2(1/m,\theta)$ is obtained as above and $I_2(m,\theta)$ derived from it by the relation

$$I_2(m,\theta)=m^2 I_2(1/m,\theta)$$

(see above).

4.3. *Approximation to* $\Delta E_2(\theta)$

ΔE_2 is derived from $I_2(\theta)$ by means of (5). As shown in figure 4 however B, and hence $I_2(\theta)$, is a function of Θ, and if this is put in (5) the integrand is a function of m as well as of θ; consequently a solution valid for all m cannot be derived from it.

Instead therefore $B\sin\theta$ was plotted against $m^2\theta/[(m-1)(m+1)^2]$. This is the same parameter as was used in the initial plotting of B and the reason for its selection was the same. The fit of the various points to a common curve was then progressively improved in a similar way to that used for B. In the present case however the fit of individual points is unimportant, but for any m the area under the curve up to a given θ must agree with the corresponding area under the 'average' line to within acceptable limits of error, in this case 1% of the total area under the curve. Since the integral required is with respect to θ the scale of the abscissae must be of the form $f(m)\times\theta$.

The curve chosen is shown in figure 6, in which $C\times B\sin\theta$ is plotted against $\{[m^{3/2}(1-m/4)]/[(m-1)(m+1)^2]\}\theta=K\theta$, θ being measured in degrees; $C=[m^{2/3}(1+|m-1{\cdot}4|/40)]/(m-1)$. The area under this curve, H (obtained graphically), is plotted against $K\theta$ in figure 7. If $m>1$, then to get ΔE_2 $\theta/(m-1)$ (θ in degrees) is multiplied by $(m-1)K$, which is plotted against m in figure 8: H is then read off figure 7, and ΔE_2 obtained from the relation

$$\begin{aligned}\Delta E_2&=2\pi I_2(0)\times(\pi/180)\times(H/CK)\\&=LH.\end{aligned}$$

L is plotted against m in figure 9. If $m<1$ $I_2(\theta)$ is smaller by a factor m^2, so that $\Delta E_2=m^2L(1/m)H(1/m,\theta)$.

§ 5. Light Internally Reflected: $n>2$

When $n>2$ no exact expression for $I_n(\theta)$ in terms of m and θ only was obtained, but a number of generalizations are possible. If n is large, and in particular if m is small and n large, θ varies over a wide range, and for most values of i it varies rapidly with i. Since moreover T_n is a product of n terms each less than unity its mean value diminishes as n increases. Consequently, the overall contributions of I_n and ΔE_n to I and ΔE are normally small. Near $\theta=0$ and $\theta=\pi$ and near the rainbows however they may not be negligible.

For components 1 and 2, θ increases monotonically with increasing i, and to a given value of θ there is only one i even if θ and $-\theta$ are regarded as equivalent. If $n>3$ however neither of these conditions necessarily holds. For a given n, (i) θ may vary over an angular range greater than π, so that $\sin\theta=0$ when $\sin 2i\neq 0$ as well as when $i=0$, and (ii) θ may have a minimum, so that $di/d\theta\to\infty$. In each case therefore the intensity becomes high near the corresponding angle, the former corresponding to coronae and anticoronae and the latter corresponding to the rainbows. Moreover, since θ and $-\theta$, and also $2k\pi+\theta$ and $2k\pi-\theta$, are all equivalent to one another there may be two or more i_n corresponding to a given θ_n. This is indicated in figures 10 (*a*) and 10 (*b*), in which the hatched

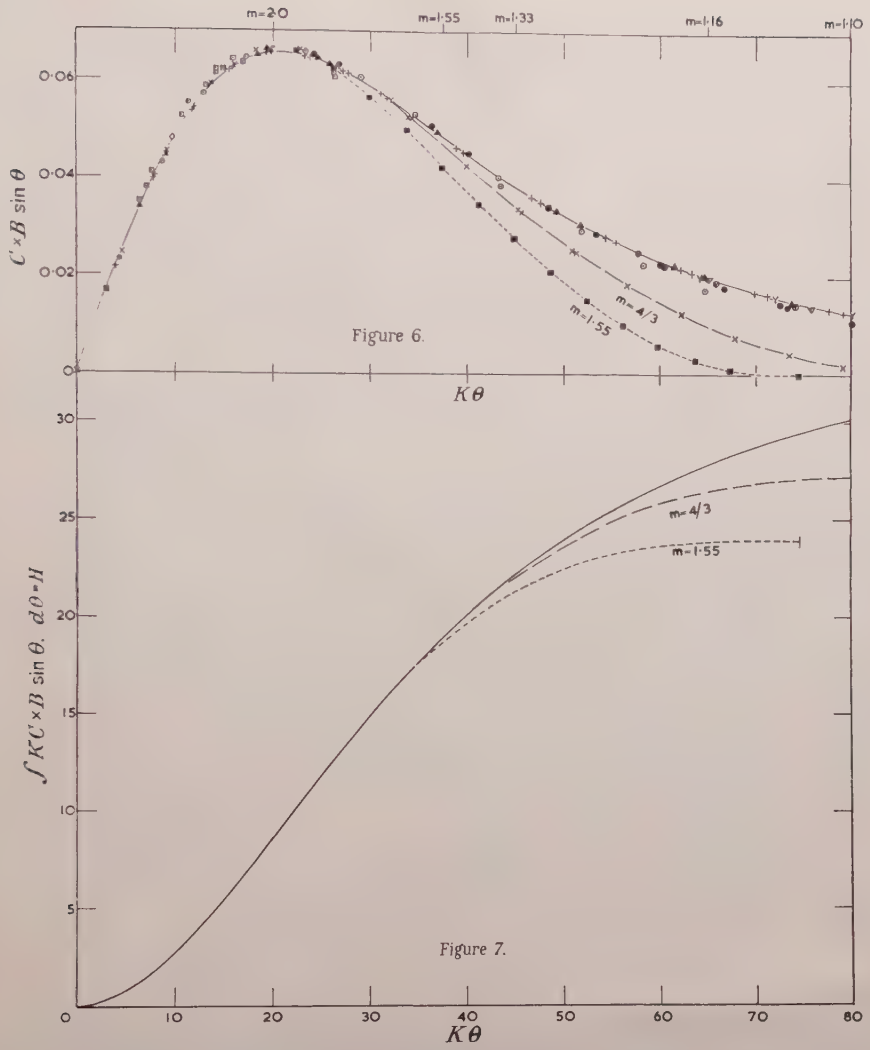

Figure 6. Constant $\times B \sin\theta$ plotted against $K\theta$ for various m and θ. The symbols used for marking individual points are the same as in figure 4.

Figure 7. $\int KC \times B \sin\theta \, d\theta = H$ plotted against $K\theta$. The scale at the top shows, for the values of m marked, the maximum value of $K\theta$ for which the curve giving H is a satisfactory approximation.

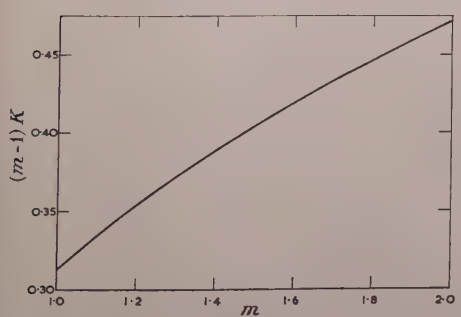

Figure 8. $(m-1)K$ plotted against m.

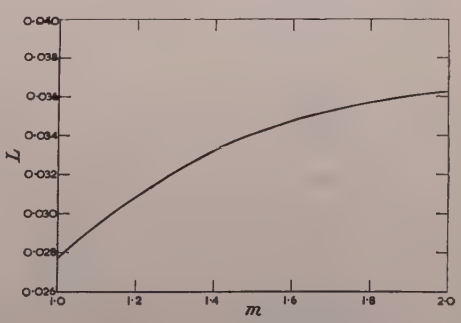

Figure 9. L plotted against m.

areas indicate the angles at which light can be scattered after one and two internal reflections respectively and the density of hatching indicates the number of possible values of i_n corresponding to a given θ_n. These diagrams only deal with $m > 1$. If $m < 1$ there are no rainbows, but there are $(n+1)/2$ values of i_n for which $\theta_n = 0$ if n is odd, and $n/2$ if n is even; if $m > 1$ the number of such values is at least one less.

For $n > 4$ figures such as 10 (*a*) and 10 (*b*) become too complicated to be very helpful. Figure 11 indicates the positions of the rainbows for $n = 5$, 6 and 7.

To bring order into this disorderly array of detail it is considered in three parts: (1) scattering near $\theta = 0$ for which i is small and $n = 4, 6, \ldots$; (2) scattering for which $\sin\theta \to 0$ and $\sin 2i \neq 0$; and (3) scattering near the rainbows.

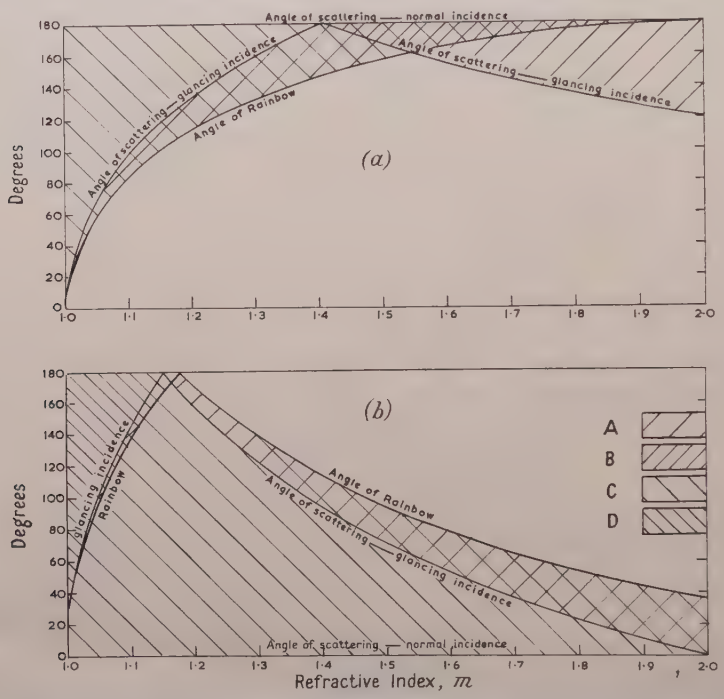

Figure 10. Angles to which light can be scattered (*a*) after one internal reflection, (*b*) after two internal reflections, $1 < m < 2$. A, $i > i_R$, and only one such i_R possible; B, $i > i_R$, and only two such i_R possible; C, $i < i_R$, and only one such i possible; D, $i < i_R$, and only two such i possible.

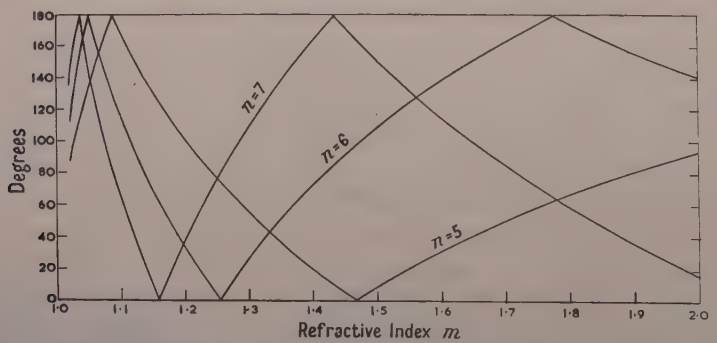

Figure 11. Position of rainbows for $n = 5$, $n = 6$ and $n = 7$.

5.1. *θ and i both small*

When $i=0$, $\theta_n=(n-2)\pi$ and if n is even the scattering is therefore forward. For small i the factors T_n, $\sin 2i/\sin\theta$ and $di/d\theta_n$ in (3) may be expanded in ascending powers of θ giving

$$T_n(\theta)=T_n(0)\times(1+\text{ terms in }\theta^1\text{ and higher powers})$$

$$\sin 2i/\sin\theta_n=\lim_{\theta\to 0}(\sin 2i/\sin\theta_n)\times(1+\text{ terms in }\theta^2\text{ and higher powers})$$

$$di/d\theta_n=(di/d\theta_n)_{\theta=0}\times(1+\text{ terms in }\theta^2\text{ and higher powers})$$

$$T_n(0)=16m^2(m-1)^{2n-4}/(m+1)^{2n},\quad \lim_{\theta\to 0}(\sin 2i/\sin\theta_n)=m/(m-n+1)$$

and

$$(di/d\theta_n)_{\theta=0}=m/2(m-n+1)$$

so by (3)

$$I_n(\theta)=[4m^4(m-1)^{2n-4}/\pi(m+1)^{2n}(m-n+1)^2]\times(1+\text{ terms in }\theta^2\text{ and higher powers}). \qquad \ldots\ldots(16)$$

If $n=6, 8, \ldots$, the terms in $(m-1)^{2n-4}/(m+1)^{2n}$ and $m^2/(m-n+1)^2$ become so small that I_n may be neglected. I_4 must however be considered. For $m<1{\cdot}5$ $I_2(0)\gg I_4(0)$ since $T_4(0)$ is small, but as m increases I_2 diminishes and I_4 increases so that at $m=1{\cdot}75$ $I_4(0)/I_2(0)\simeq 0{\cdot}002$ and at $m=2$ $I_4(0)/I_2(0)=0{\cdot}012$. Although these ratios are small the latter is not negligible. However, since (*a*) I_4 does not contain a term in θ, and (*b*) the rainbow is at fairly wide angles unless m approaches 2, I_4 may be regarded as constant for small θ. If $m<1{\cdot}75$ it may be neglected. If $m>1{\cdot}75$ however the rainbow approaches the forward direction so that I_4 rapidly increases as θ increases. I_4 can then be calculated by means of the expansion in (16), but this unusual case is not further considered. Consequently the angular range over which the approximation may be used diminishes as m approaches 2.

In the range for which I_4 is constant, its contribution to ΔE is derived from (5) and is

$$\Delta E_4(\theta_0)=2\pi(1-\cos\theta_0)I_4(0). \qquad \ldots\ldots(17)$$

5.2. *sin θ→0, sin 2i≠0*

With these θ and i, I_n calculated by (3) is infinite. If $n>4$ and $m>1$, then T_n and $di/d\theta_n$ are so small that only if $\sin\theta$ is very small indeed is I_n appreciable, and this case has been neglected. If $n=3$ $(m>1)$ scattering at $\theta=0$ cannot occur, although if $\sqrt{2}<m<2$ light may be scattered at $\theta=\pi$ when $\sin 2i\neq 0$ (see figure 10 (*a*)). Figure 10 (*b*) likewise shows that for $n=4$ and if $1<m<2$ forward scattering only takes place if $i=0$, but if $m=2$ light incident at $\pi/2$ is scattered at $\theta=0$, and it is clear from the trend of the curve that if $m>2$ light incident near $\pi/2$ will be scattered at $\theta=0$; the case of $2-m$ and $\pi/2-i$ simultaneously small will therefore be considered here.

At $i=\frac{1}{2}\pi$, $di/d\theta=\frac{1}{2}$ (all $n, m>1$), and hence $d(\sin 2i)=-2di=-d\theta$. Therefore if $\theta=\theta_M$ at $i=\frac{1}{2}\pi$ then $\frac{1}{2}\pi-i=(\theta-\theta_M)/2$ and $\sin 2i/\sin\theta=(\theta-\theta_M)/\theta$ approximately if $\frac{1}{2}\pi-i$, θ, and θ_M are all small. T_n may be obtained from the approximations for ${\rho_1}^2$ and ${\rho_2}^2$ near glancing incidence; ${\rho_1}^2=1-4(\frac{1}{2}\pi-i)/(m^2-1)^{1/2}$ and ${\rho_2}^2=1-4m^2(\frac{1}{2}\pi-i)/(m^2-1)^{1/2}$, which are equivalent to the first two terms of the expansions of equations (7) and (8) respectively. Hence

$$I_4=\frac{1}{2\pi}\cdot\frac{\theta-\theta_M}{2\theta}\cdot\frac{1}{2}\cdot\frac{16(\theta-\theta_M)^2}{4(m^2-1)}\left[\left\{1-\frac{2(\theta-\theta_M)^2}{(m^2-1)^{1/2}}\right\}+m^2\left\{1-\frac{2m^2(\theta-\theta_M)^2}{(m^2-1)^{1/2}}\right\}\right]. \qquad \ldots\ldots(18)$$

This increases very rapidly with $\theta-\theta_M$ at first, but since T_4 cannot exceed 1/16 the maximum value of I_4 is $(1/2\pi)(\theta-\theta_M)/32\theta$; even if $m=2$, $\theta_M=0$, this is only about 2% of $I_2(0)$ so the errors are small relative to I. The approximation is clearly only valid if $2m^2(\theta-\theta_M)/(m^2-1)^{1/2}\ll 1$, that is, if $\theta-\theta_M<7\frac{1}{2}^\circ$ for $m=2$ and if $\theta-\theta_M<15^\circ$ if $m=1{\cdot}75$. Within this range of angles ΔE_4 is negligible, for

$$\begin{aligned}\Delta E_4&=\int_{\theta=\theta_M}^{\theta_0} I_4\,.\,2\pi\sin\theta d\theta\\&=\int_{\theta_M}^{\theta_0}[\tfrac{1}{2}(\theta-\theta_M)/\theta]T_4\sin\theta d\theta\qquad\text{(by (3))}\\&<\int_{\theta_M}^{\theta_0}(1/32)(\theta-\theta_M)d\theta=(1/64)(\theta_0-\theta_M)^2\end{aligned}$$

since $T_4\leqslant 1/16$; even if $\theta-\theta_M=\frac{1}{3}$ radian this is less than 0·002.

If $m<1$, then for $n=3$ and $n=4$ as well as for higher n there are values of i near $\sin^{-1}m$ for which $\theta=0$, $\sin 2i\neq 0$. Since near this angle ρ_1 and ρ_2 are high, T may likewise be high and the corresponding I_3 and I_4 cannot be neglected. By (2), if $n=3$ light is scattered directly forward if $i+\frac{1}{2}\pi=2r$.

Hence

$$\begin{aligned}\cos(i+\tfrac{1}{2}\pi)&=\cos 2r\\-\sin i&=1-(2/m^2)\sin^2 i\end{aligned}$$

so that $$i=\sin^{-1}\{(m^2/4)[(1+8/m^2)^{1/2}+1]\}.$$

Similarly, if $n=4$ the angle of incidence for which $\theta=0$ may be shown to be $\sin^{-1}[\frac{1}{2}m^{3/2}(1+3/m)]$.

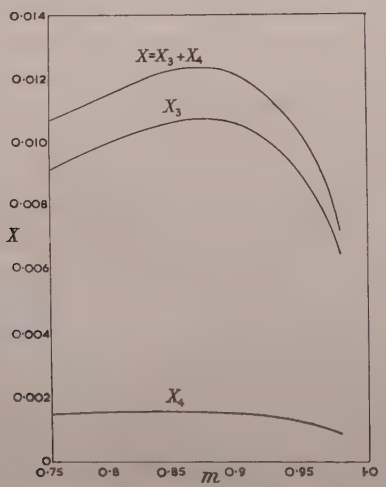

Figure 12. Light internally reflected and scattered near $\theta=0$ ($m<1$). $X_3=\lim_{\theta\to 0}[I_3(\theta)\times\sin\theta]$, $X_4=\lim_{\theta\to 0}[I_4(\theta)\times\sin\theta]$, and $X=X_3+X_4$.

Using these values $X_3=\sin 2i(di/d\theta)T_3$ and $X_4=\sin 2i(di/d\theta)T_4$ were calculated, and hence I_3 and I_4 for small θ may be obtained. In the sum giving I both I_3 and I_4 occur twice, at $+\theta$ and $-\theta$, so the appropriate multiplier is $1/\pi\sin\theta$. X_3 and X_4, and also $X=X_3+X_4$, are shown in figure 12. In practice only the sum is required, since each is multiplied by the same factor and they are then added, but they are shown separately to illustrate the rapid diminution of X_n as n increases; $X_5, X_6, \ldots\ldots$ and $I_5, I_6, \ldots\ldots$ have been neglected.

The values of I_3 and I_4 obtained are strictly speaking only applicable in the limit as $\theta \to 0$; at other angles terms in θ, θ^2, . . ., should be taken into account. In practice however only the sum $I(+\theta)+I(-\theta)$ is used, so that terms in θ and θ^3 cancel out. The term in θ^2 is negligible whenever the approximation to I_2 can be applied.

The contribution to ΔE_n is $2\times\int_{\theta=0}^{\theta_0}(1/2\pi\sin\theta)X_n 2\pi\sin\theta\,.\,d\theta = 2X_n\theta_0$.

5.3. *Scattering near the Rainbows*

Rainbows appear at angles of minimum deviation θ_R, and for any θ near $\theta_R(\theta>\theta_R)$ there are therefore two paths possible within the sphere. Interference between rays following these two paths can take place and consequently the derivation of intensities on the basis of geometrical optics breaks down. The nature of this breakdown was first realized by Thomas Young (1804), and was put on an exact basis by Airy (1838). Since their explanation is based on interference, and I is therefore size-dependent near θ_R, it is not considered here. It is important to know however what fraction of ΔE is scattered near θ_R since it may be appreciable; geometrical optics should indicate its magnitude approximately as long as $a \gg \lambda$.

For $\theta=\theta_R$, $i=i_R=\sin^{-1}[\{(n-1)^2-m^2\}/\{(n-1)^2-1\}]^{1/2}$ from which T_R and $(d^2\theta/di^2)_R$ may be calculated. The angles of incidence of light scattered at $\theta_R+\delta\theta$ may be derived by means of Taylor's theorem, and are

$$i_R+\left[\frac{2\delta\theta}{(d^2\theta/di^2)_R}\right]^{1/2} \quad \text{and} \quad i_R-\left[\frac{2\delta\theta}{(d^2\theta/di^2)_R}\right]^{1/2}$$

approximately. δE, the fraction of the incident light of the same component scattered between θ_R and $\theta_R+\delta\theta$ is therefore

$$\delta E = 2\sin i_R\cos i_R\left[\frac{2\delta\theta}{(d^2\theta/di^2)_R}\right]^{1/2} T_R$$

which can be calculated. Near $\theta=0$ there are rainbows if $n=4$ and $m=2$, if $n=5$ and $m=1{\cdot}5$, and if $n=6$ and $m=1{\cdot}25$; taking $\delta\theta=6°$, then in the first of these cases $\delta E \simeq 0{\cdot}01$ and in each of the other two $\delta E < 0{\cdot}002$.

§ 6. Angular Range of Application of Approximation

For spheres I can in principle be calculated to any required degree of accuracy, and the range of application of an approximation depends only on the error which is acceptable. Since $I=\Sigma_n I_n$ and in this paper each I_n is obtained from an approximation of limited range of validity the overall range is that common to all components; in this paper the aim has been to reduce the overall error to about 1% of I, or to 0·01 in ΔE. The range is shown in figure 13, for both I and ΔE, plotted against m. In each case the boundaries are labelled with the factors limiting the approximation. The lower boundary, near $\theta=0$, is drawn purely arbitrarily as a caveat against applying the approximations too near $\theta=0$; in practice I cannot be measured at very small θ. This restriction does not apply to ΔE, since the flux within the small cone forward is negligible. Otherwise the range for ΔE is broadly similar to that for I.

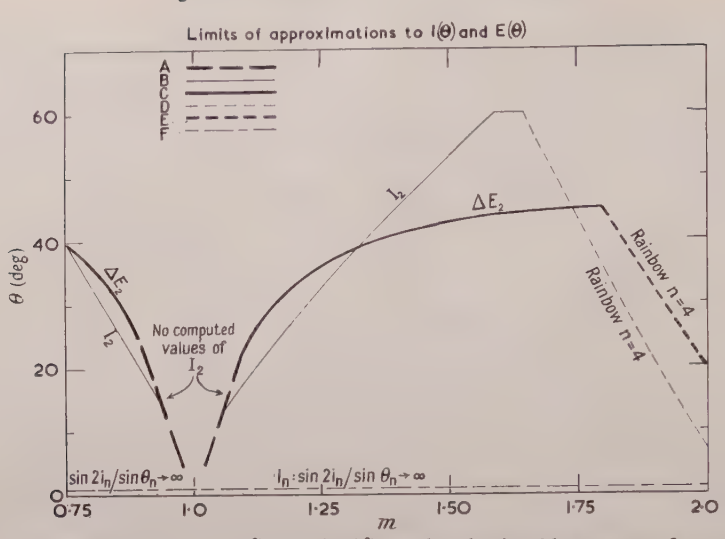

Figure 13. Ranges over which $I(\theta)$ and $\Delta E(\theta)$ can be obtained by means of approximations. Each boundary is marked with the main factor contributing to error on it. Factors limiting ranges of application : A, lack of computed values of I_2 and ΔE_2; B, error of approximation to I_2; C, error of approximation to ΔE_2; D, proximity of rainbow: error in I_4; E, proximity of rainbow: error in ΔE_4; F, I_n not negligible, $n>4$; $\sin 2i_n/\sin\theta_n\to\infty$

§ 7. Polarization of Scattered Light

If $m>1$ the scattered light is only slightly polarized at small θ and polarization is not normally of interest. If required it can be calculated from that of components, 1, 2, and 4. $I_{1,1}$ and $I_{1,2}$ are given separately above,

$$I_{2,1}=I_2/[1+\sec^4\tfrac{1}{2}\theta] \text{ and } I_{2,2}=I_2\sec^4\tfrac{1}{2}\theta/[1+\sec^4\tfrac{1}{2}\theta]$$

(from equations 14 (*a*) and 14 (*b*) above), and I_4 is virtually unpolarized since near $\theta=0$ i is small (if $m>1{\cdot}75$ and $n=4$ rays for which $i\simeq\frac{1}{2}\pi$ also scatter near $\theta=0$; for these the polarization can be derived from (18)).

If $m<1$, and in particular if $m<0{\cdot}9$, that part of components 3 and 4 which is included in the term $X/\sin\theta$ is strongly polarized. This only becomes important at very small θ and is not further considered.

§ 8. Weakly absorbing Particles

If the sphere is weakly absorbing ($m=\nu-i\nu'$, ν' small), ρ_1^2, ρ_2^2, and the angular relationships are unaffected. I_1 will therefore be unaltered and $I_2, I_3, \ldots,$ will each be reduced by a factor $\exp(-4\pi\nu' l/\lambda)$ where $l=$ length of path of ray in sphere $=2a(n-1)\cos r$. If $n=2$, $\cos r=[m-\cos\frac{1}{2}\theta]/[m^2+1-2m\cos\frac{1}{2}\theta]^{1/2}$. Unless $\exp(-8\pi\nu' a/\lambda)<I_1(\nu,0)/I_2(\nu,0)$, I_2 remains the largest contributor to I for small θ, and since l diminishes as θ increases the reduction in I will be greatest near the forward direction. If θ is small, $\cos r$ may be expanded in the form

$$\cos r=1-[\sin^2\tfrac{1}{2}\theta]/2(m-1)^2+[(m+\tfrac{1}{4})\sin^4\tfrac{1}{2}\theta]/2(m-1)^4$$

and then

$$\exp(-4\pi\nu' l/\lambda)=\exp\{-(2\pi a/\lambda)4\nu'\}\times\exp\{[(2\pi a/\lambda)2\nu'\sin^2\tfrac{1}{2}\theta]/(m-1)^2\}\times\ldots$$
$$=\exp(-4\nu' x)\{1+[2\nu' x\sin^2\tfrac{1}{2}\theta]/(m-1)^2-\ldots.\}$$

Table 1. Computation of $I(\theta)$

n	m	Parameter	Quantity Obtained	Multiplier	$I_n(\theta)$ $m<1$	$1<m<1{\cdot}75$	$m>1{\cdot}75$
1	>1	$s=[\sin\frac{1}{2}\theta]/(m^2-1)^{1/2}$	$I_{1,1}(s)=I_{1,1}$ from figure 2	1	—	$I_{1,1}$	$I_{1,1}$
		$m^2 s$	$I_{1,1}(m^2 s)=I_{1,2}$ from figure 2†	1	—	$I_{1,2}$	$I_{1,2}$
	<1		$I_{1,1}=I_{1,2}=1/8\pi$		$1/4\pi$	—	—
2	>1	$Q\tan\frac{1}{2}\theta/(m-1)$ Q from figure 5	$I_2(\theta)/I_2(0)=B$ from figure 4	$I_2(0)=4m^4/[\pi(m-1)^2(m+1)^4]$	—	$BI_2(0)$	$BI_2(0)$
	<1	$Q\left(\frac{1}{m}\right)\tan\frac{1}{2}\theta\Big/\left(\frac{1}{m}-1\right)$	$I_2(\theta)/I_2(0)=B$ from figure 4	$I_2(0)=m^2 I_2\left(\frac{1}{m},0\right)$	$BI_2(0)$	—	—
		$Q\left(\frac{1}{m}\right)$ from figure 5					
3	>1	—	—	—	—	0	0
3+4	<1 $\sin i\to m$	m	$X=X_3+X_4$ from figure 12	$1/\pi\sin\theta$	$X/\pi\sin\theta$	—	—
4	$>1{\cdot}75$		I_4 from (16)+(18)		—	—	I_4
	$<1{\cdot}75$ $\sin i\to 0$				$\simeq 0$	$\simeq 0$	—

† If $\theta>30°$ $I_{1,2}$ should be calculated by means of (8).

Use of table 1 for computing I; I is the sum of a number of terms I_n, and columns 6, 7, and 8 show, for the appropriate ranges of m, those $I_n(n\leqslant 4)$ which enter into the sum. The steps in the calculation of the individual I_n are shown in the corresponding horizontal row.

Table 2. Computation of $\Delta E(\theta)$

n	m	Parameter	Quantity Obtained	Multiplier	$\Delta E_n(\theta)$ $m<1$	$1<m<1{\cdot}75$	$m>1{\cdot}75$
1	>1	$s=[\sin\frac{1}{2}\theta]/(m^2-1)^{1/2}$ m^2s	$F=f(s)$ from figure 3 $G=f(m^2s)$ from figure 3	$M=(m^2-1)$ $N=(m^2-1)/m^4$	— —	MF NG	MF NG
	<1	—	—	—	$(1-\cos\theta)/2$	—	—
2	>1	$K(m)\times\theta:(m-1)\,K(m)$ from figure 8	H from figure 7	$L(m)$ from figure 9	—	LH	LH
	<1	$K\left(\frac{1}{m}\right)\times\theta:\left(\frac{1}{m}-1\right)K\left(\frac{1}{m}\right)$ from figure 8	H from figure 7	$m^2L\left(\frac{1}{m}\right):L\left(\frac{1}{m}\right)$ from figure 9	$m^2L\left(\frac{1}{m}\right)H$	—	—
3	>1	—	—	—	—	0	0
3+4 sin $i\to m$	<1	m	$X=X_3+X_4$ from figure 12	2θ	$2X\theta$	—	—
4 sin $i\leftarrow 0$	$>1{\cdot}75$	—	$I_4(0)$ from (16)	$2\pi(1-\cos\theta)=R$	—	—	$RI_4(0)$
	$<1{\cdot}75$	—	—	—	$\simeq 0$	$\simeq 0$	—
				Sum=	$\Delta E(\theta)$	$\Delta E(\theta)$	$\Delta E(\theta)$

Table 2 is used for computing ΔE in the same way as is table 1 for obtaining I.

Consequently as long as the term in $[\sin^4 \frac{1}{2}\theta]/(m-1)^4$ is sufficiently small,

$$I_2(\nu - i\nu', \theta) = I_2(\nu, \theta) \times \exp(-4\nu' x) \times \{1 + [2\nu' x \sin^2 \tfrac{1}{2}\theta]/(m-1)^2\}.$$

Terms for which $n=3$ do not arise if $m>1$, and for $n=4$

$$\exp(-4\pi\nu' l/\lambda) \simeq \exp(-12\nu' x)$$

for all values of θ accessible to approximation to I_2.

Similarly $\Delta E_2(\nu - i\nu', \theta) \simeq \Delta E_2(\nu, \theta) \times \exp(-4\nu' x)$ as long as

$$\Delta E_2(\nu, \theta) \times \exp(-4\nu' x) \times 2\nu' x[\sin^2 \tfrac{1}{2}\theta]/(m-1)^2 < 0{\cdot}01,$$

and $\Delta E_4(\nu - i\nu', \theta) = \Delta E_4(\nu, \theta) \times \exp(-12\nu' x)$ to within close limits for all values of θ accessible to the approximation to ΔE_2.

§ 9. Summary

The procedures for calculating I and ΔE are summarized in tables 1 and 2 respectively. The approximations given can only be applied near the forward direction, and their angular range of validity depends on m; this is shown in figure 13.

If $0{\cdot}75 < m < 2{\cdot}0$ the forward scattered light is dominated by that transmitted through the drop without internal reflection (component 2): for this component an exact expression in terms of m and θ only is given. This is easily computed, and if used in conjunction with the approximate expressions for the other components a fairly high degree of overall accuracy can be attained.

Acknowledgments

The authors are very grateful to Dr. T. Bedford, Dr. C. N. Davies and Dr. J. C. E. Jennings for their advice and comments on this paper, to Mr. E. J. Ward, who prepared the figures, and to the referees, whose helpful suggestions led to substantial improvements in the paper.

References

Airy, G. B., 1838, *Trans. Camb. Phil. Soc.*, **6**, 379.
Bricard, J., 1946, *Ann. Géophys.*, **2**, 231.
Davis, G. E., 1955, *J. Opt. Soc. Amer.*, **45**, 572.
Ellison, J. McK., 1954, *Ph. D. Thesis*, University of London.
—— 1957, *Proc. Phys. Soc.* B, **70**, 102.
Gumprecht, R. O., Sung, Neng-Lun, Chin, Jin H., and Sliepcevich, C. M., 1952, *J. Opt. Soc. Amer.*, **42**, 226.
van de Hulst, H. C., 1946, *Rech. Astr. Obs. Utrecht*, XI, pt. 1.
—— 1957, *Light Scattering by Small Particles* (New York: John Wiley; London: Chapman and Hall).
Jenkins, F. A., and White, H. E., 1957, *Fundamentals of Optics* (New York, Toronto, London: McGraw-Hill).
Mecke, R., 1920, *Ann. Phys., Lpz.*, **62**, 623.
Mie, G., 1908, *Ann. Phys., Lpz.*, **25**, 377.
Ptolemaeus, C., 1885, *L'Ottica di Claudio Tolomeo* (pubblicata da G. Govi Turin, G. B. Paravia).
Sarton, G., 1947, *Introduction to the History of Science*, **3**, pt. 1 (Baltimore: Williams and Wilkins Co.).
Wiener, C., 1907, *Nova Acta Leop. Carol.*, **73**, 1.
—— 1909, *Ibid.*, **91**, 81.
Young, T., 1804, *Phil. Trans. Roy. Soc.*, **94**, 1.

The Spin of the Neutral Pion

By J. D. PRENTICE†, E. H. BELLAMY and W. S. C. WILLIAMS
Department of Natural Philosophy, The University, Glasgow

MS. received 16*th February* 1959, *in final form* 17*th March* 1959

Abstract. An attempt has been made to detect effects due to non-zero pi-meson spin. The distribution of photons from the decay of neutral pi-mesons was measured and from the results it is concluded either that the spin is zero or that the pi-mesons observed were not appreciably polarized.

§ 1. Introduction

The observation of an anisotropy in the angular distribution of μ-mesons produced in the decay of positive π-mesons (Lattes 1957, Hulubei, Auslander, Baale, Friedlander and Titeica 1957, 1958), raised doubts as to the correctness of the belief that all three types of π-meson have zero spin. The arguments for this belief are based on a detailed balance study of the cross sections observed for the reactions:

$$p + p \rightleftharpoons \pi^+ + d,$$

and on the consistency of the phenomenological analysis of meson phenomena based on the assumption that all the π-mesons have zero spin. Assuming no polarization of the π-meson beam in the above reaction, detailed balancing gives zero spin (Durbins, Loar and Steinberger 1951), but even if the spin is not zero 75% polarization of the π-meson beam employed would give an apparent result of zero spin. This degree of polarization was considered unlikely (Clark 1951) and the π-meson spin was taken to be zero. However, the remaining uncertainties make it worth attempting to detect effects due to non-zero pion spin. This paper reports an attempt made to detect such effects in the decay of the neutral π-meson : the method used was suggested by Kinoshita and Peierls (1957).

A beam of π^0 mesons is produced by an interaction which almost certainly conserves parity : if the π^0 meson has spin, it is possible for the beam to be polarized with a net spin angular momentum directed perpendicularly to the π-meson momentum. Each meson will decay to give two photons moving in a plane having a probability distribution which will be in general anisotropic in the azimuthal angle around the direction of the π^0 momentum. This decay distribution will depend on the meson spin and parity, and on the polarization of the meson beam. The observation of an anisotropy would indicate that the π^0 meson has spin; the observation of an isotropic distribution would indicate either that the spin is zero or that there is no polarization.

A search for such an anisotropy has been reported by Leiss and Schrack (1958): these workers concluded that there was no anisotropy but their observations suffer from large statistical errors, a non-uniform background subtraction,

† Now at the Department of Physics, The University of Toronto.

and a correction for the effects for angular distribution based on a dubious model of photoproduction. A measurement on the charged pi-meson decay, which is similar in principle, has been reported by Crewe, Kruse, Miller and Pondron, (1957): the decay was isotropic within the standard error of about 5%. These results appear to be contradicted by the photographic plate work of Lattes (1957) and of Hulubei *et al.* (1957, 1958). However, the effects of distortion and observer's bias which are involved in such work were carefully examined by Lattes and by several other groups, and reported in 1957 (Venice 1957): it appears that all the asymmetries were instrumental although the exact source is not known. The work reported in this paper was undertaken in the hope of helping to resolve the doubts about the π-meson spin.

§ 2. Experimental Method

The π^0 mesons were produced in a graphite target lying in a 240 MeV bremsstrahlung beam produced by the Glasgow University electron-synchrotron. The decay photons produced by the π^0 mesons were detected in lead fluoride total absorption counters (Williams and Caplan 1957) (C_1 and C_2 in figure 1). Each counter was shielded with lead and had an aperture defined by a 7·5 cm long, 7·5 cm diameter hole in a lead collimator. The hole was filled with a Perspex plug which attenuated the low energy radiation from the target. The axis of the collimator defined the axis of the counter. Two such counters were placed so that they faced the target with their axes at 90° and intersecting at the centre of the target (figure 1).

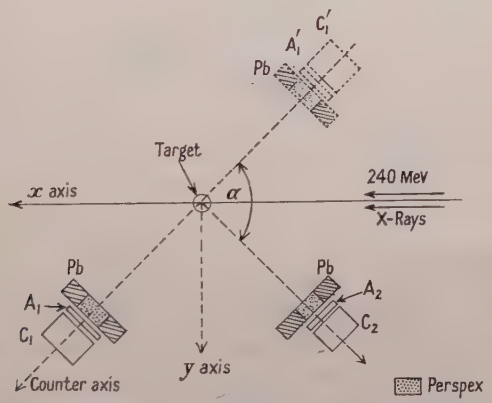

Figure 1. The experimental apparatus : a vertical section for $\theta = 90°$.

A set of cartesian coordinates is set up which clarifies the discussion of the experimental arrangement (figures 2 and 3). This coordinate system has its origin at the centre of the target, its x axis coaxial with the horizontal bremsstrahlung beam, its y axis vertically downwards from the target, its z axis horizontal and projecting to the right from the target when looking along the direction of the beam.

The coincidence of pulses from the photomultipliers of the two counters indicates the simultaneous detection of the two photons from a π^0 meson which has been produced and decayed in the target. Such a coincidence turned out to be a necessary and sufficient condition to indicate a π^0 decay. To be detected in this way, the π^0 meson must have been moving in a direction confined to a

solid angle which is defined by the geometry of the counters and the kinematics of the π^0 meson decay. This solid angle has its axis of symmetry coincident with the bisector of the axes of the counters (figure 2): this solid angle is called the 'solid angle for detection' and its shape is indicated in figure 2. Not all the mesons moving in this solid angle were detected but any meson moving outside the solid angle could not be detected.

If there is a π^0 meson beam directed along the y axis in figure 2 having a polarization which defines a direction perpendicular to the y axis, then the decay rate will depend on the angle between this direction and the plane which contains the decay photon momenta. Consequently, the detection rate will vary with the angle between the plane containing the counter axes and the polarization direction: thus the experiment is reduced to measurement of the detection rate as the counter plane was rotated around the y axis. In fact, the target was an extended source of π^0 mesons, and the definition of the meson direction was limited by the finite solid angle for detection described above.

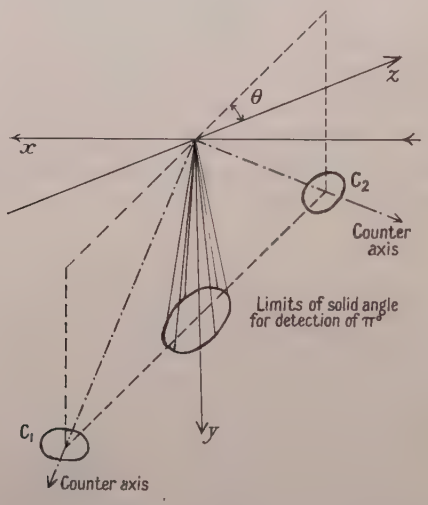

Figure 2. The experimental geometry.

The two counters were set so that their axes were coplanar with the y axis as in figure 2. The angle between this plane and the z axis is called θ and it was with respect to this angle that the decay distribution was observed. Figure 1 shows the section through the experimental apparatus for $\theta = 90°$. The counters were mounted on 45° ramps fixed to the top of a rotating table and arranged so that the counter axes and axis of rotation met at a point which was at the height of the centre of the bremsstrahlung beam. To set the table in the experimental position, the centre of the beam was found by x-ray photography and the table moved until its axis intersected the centre of the beam. When this procedure was complete, the maximum possible distance between the axis of rotation and the centre of the beam was 0·15 cm and the maximum distance from that intersection to either counter axis was 0·30 cm. The errors in setting angles between axes are not important and did not exceed 3°. The target was placed with its centre at the intersection of the beam and the rotation axis (maximum error 0·20 cm). The beam diameter was 5·6 cm. Two targets were tried : the first was a sphere 5·0 cm in diameter, the second was a vertical cylinder 5·0 cm high, 5·0 cm

diameter. No difference in decay distribution, attributable to these differing target shapes, was observed.

The coincidence circuits had a resolving time of about 30 mμsec : two such circuits were used, one to detect prompt coincidences C_1 C_2, and a second to detect random coincidences by delaying one signal by 60 mμsec. The coincident outputs were filtered through a 100 msec gate which enclosed the synchrotron beam pulse and were counted on scalers. The gains of the photomultipliers and the subsequent amplifiers were set high enough to ensure that pulses from the lowest energy photons expected would operate the coincidence circuits. Under these conditions the counters were almost 100% efficient: losses were due to low energy photons entering the lead fluoride crystal close to the edge and producing showers which were inadequately contained in the crystal. These losses would have been constant if the energy spectrum of observed mesons was independent of the angle θ; although this was not so, the effect was negligible.

The coincident count for a constant value of the integrated beam intensity was measured at intervals of $22\frac{1}{2}^\circ$ in θ, starting at 0° and finishing at a complete revolution. The symmetry of the experiment permits the results for a complete revolution to be folded into one quadrant to give counts for $\theta = 0^\circ$, $22\frac{1}{2}^\circ$, 45°, $67\frac{1}{2}^\circ$ and 90°. In all, 14 revolutions were completed. At the end of three revolutions it was clear that there was a marked anisotropy and the experiment was carefully examined for systematic errors; the following points were considered :

(i) The magnetic fields in the region of the apparatus would have an effect on the operation of the photomultipliers which could depend on θ. Adequate screening had been provided but it was extended and improved as an added precaution. There was no change in the observed anisotropy.

(ii) Large angle pair production was not expected to contribute sufficiently to cause an anisotropy of the magnitude observed, but an experimental facility was incorporated into the apparatus to check this conclusion. Plastic scintillation counters $\frac{1}{4}$ in. thick were placed between each Perspex plug and its total absorption counter, A_1 and A_2 in figure 1; the outputs from these counters were added and put into threefold coincidence with the counters C_1 and C_2. The appearance of such a coincidence C_1C_2 (A_1 or A_2) indicated that the C_1C_2 coincidence was due to particles of which at least one was charged on entering the total absorption counter. The distribution of this rate would be more markedly affected by any pair production anisotropy than the C_1C_2 coincidence rate. As expected, this threefold rate showed the same fractional anisotropy and was of a magnitude expected from photon materialization in the target and the Perspex plugs: hence, large angle pair production was not the source of the observed anisotropy.

(iii) The shape of the solid angle for detection (§ 2) encloses a range of π^0 production angles which is a function of θ; if there is a non-linear variation of production cross section in any part of the maximum range covered, then the counting rate will be a function of θ, apart from any decay anisotropy. It is necessary to correct for this effect of the π^0 production angular distribution.

The results of Barringer, Meunier and Osborne (1956) indicated that over the region covered by this solid angle the angular distribution was almost uniform and no effect was expected on the present observed decay distribution. However, Barringer, Meunier and Osborne used a detection efficiency which was peaked

near 100 MeV for neutral pions whereas in the present work the maximum efficiency occurred at 65 MeV. The production angular distribution was therefore determined for the mean pion energies 48, 65 and 84 MeV. For the 65 MeV pions the angular distribution was found to vary rapidly through the production angles 45° to 135° and results in a correction to the observed decay distribution: the determination of the angular distribution and the correction are described in the next section.

The observed decay distribution, uncorrected for this effect, is shown in figure 3: the experimental points are shown with the standard errors which are due to counting statistics alone. The anisotropy is revealed by the deviation of the points from the straight line drawn at the mean.

§ 3. The Angular Distribution Correction

The production angular distribution of pions was determined with the same apparatus, modified so that one total absorption counter was placed above the other in its normal position (see figure 1). With this arrangement, observation of the coincidence rate as the table is rotated about the y axis yields the required angular distribution: this was done for production angles of 45°, 67½°, 90°, 112½° and 135°. As this distribution was required over a considerable energy range it was measured for three values of the angle between the counter axes (α in figure 1); these were 80°, 90° and 100°.

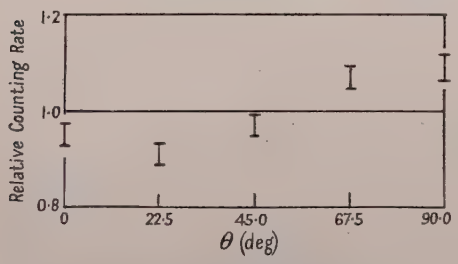

Figure 3. The uncorrected decay distribution.

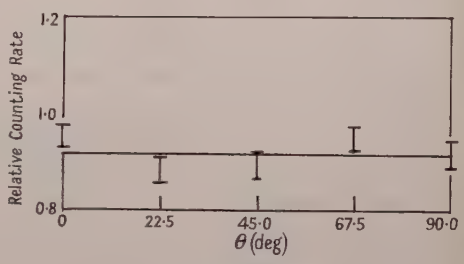

Figure 7. The corrected decay distribution.

The effective solid angle subtended by the counters as a function of pi-meson energy and the angle α was computed and is displayed in figure 4. These curves are cut off at 100 MeV as this is the greatest kinetic energy which can be given to a

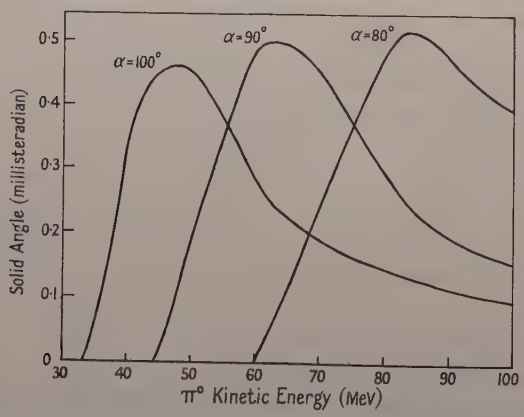

Figure 4. The effective solid angle of the counter for meson detection at three values of α.

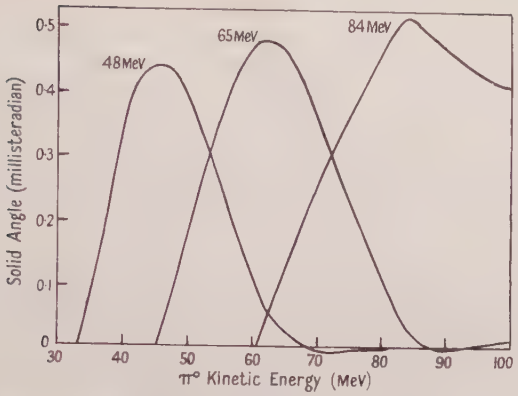

Figure 5. The adjusted solid angles for detection of π° mesons; the curves for meson mean energies 48 and 65 MeV are those for $\alpha = 100^\circ$ and 90° (figure 4) adjusted by subtracting fractions of the curves for $\alpha = 90^\circ$ and 80° respectively.

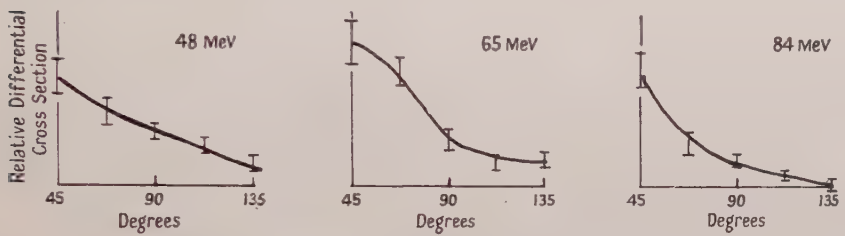

Figure 6. The angular distribution of π^0 mesons of mean energies 48, 65 and 84 MeV.

pi-meson produced by the 240 MeV bremsstrahlung beam. By subtracting a fraction of the yield for one angle α from the yield for another angle α it is possible to calculate cross sections for the energy resolution curves shown in figure 5. This allows the relative differential cross sections for the mean pion energies 48, 65 and 84 MeV to be computed: the results are plotted in figure 6.

These cross sections are used to calculate how the decay distribution is distorted by the varying sample of the production angular distribution. The factors by which the yields have to be reduced are as follows.

θ (deg.)	0	$22\frac{1}{2}$	45	$67\frac{1}{2}$	90
Reduction factor	1·0	1·03	1·08	1·10	1·19

The final corrected decay distribution is given in figure 7.

§ 4. Results and Discussion

The final corrected decay distribution shown in figure 7 is clearly consistent with isotropy and any non-isotropic component is obviously small.

The first non-zero spin angular momentum that can be attributed to the neutral pion is $2\hbar$ (Yang 1950). It is only possible to predict the form of the decay distribution if some assumptions are made (Kinoshita and Peierls 1957). Let P_{sz} represent the probability that a neutral pion with spin component along the z axis of s_z will decay into two photons moving in the plane containing the y and z axes and at equal angles to the y axis. Suppose that the π^0 production interaction contains a factor

$$1 + g \frac{(\mathbf{p}_\pi \times \mathbf{p}_\gamma) \cdot \mathbf{s}_\pi}{|\mathbf{p}_\pi||\mathbf{p}_\gamma|}$$

where $\mathbf{p}_\pi$, $\mathbf{p}_\gamma$ are the pi-meson and incident photon momenta and $\mathbf{s}_\pi$ is the spin of the pi-meson in units of $\hbar$.

This yields the following decay distributions for various assumptions about P_{gz}:

(i) $P_2=P_{-2}=P_0$ $\quad 1+3g^2\cos^2\theta/(5g^2+3)$

(ii) $P_2=P_{-2}=0$ $\quad 1+3g^2\sin^2\theta$

(iii) $P_0=0$ $\quad 1+3g^2\cos^2\theta/(1+g^2)$.

If the meson has odd parity only assumption (ii) is allowed (Yang 1950).

The decay distribution was fitted with a curve of the form $1+a\cos^2\theta$. The result is

$$a=-(0{\cdot}010\pm 0{\cdot}045).$$

This gives values of g^2 as it occurs above :

(i) $g^2=-0{\cdot}010\pm 0{\cdot}045$.

(ii) $g^2=+0{\cdot}003\pm 0{\cdot}015$.

(iii) $g^2=-0{\cdot}003\pm 0{\cdot}015$.

Although the results do not exclude a value for g as great as 0·2, it is obviously over-straining the data to do anything but conclude that the spin of the neutral pion is zero or that the mesons are not produced strongly polarized in the conditions of this experiment.

Acknowledgments

The authors are indebted to Dr. W. McFarlane and to the synchrotron crew for providing many hours of synchrotron beam, to Professor R. V. Jones and Dr. D. A. Jones of Aberdeen University for the gift of the lead fluoride crystals, and to H. S. Caplan for valuable assistance in testing the total absorption counters.

References

Barringer, R., Meunier, R., and Osborne, L. S., 1956, *C.E.R.N. Symposium on Accelerators and Pion Physics*, Vol. 2, p. 282.

Clark, D. L., Roberts, A., and Wilson, R., 1951, *Phys. Rev.*, **83**, 649.

Crewe, A. V., Kruse, U. E., Miller, R. H., and Pondrom, L. G., 1957, *Phys. Rev.*, **108**, 1531.

Durbins, R., Loar, M., and Steinberger, J., 1951, *Phys. Rev.*, **84**, 581.

Hulubei, H., Auslander, J., Balea, E., Friedlander, E., and Titeica, A., 1957, *C.R. Acad. Sci., Paris*, **245**, 1037;

—— 1958, *Ibid.*, **246**, 2197.

Kinoshita, T., and Peierls, R. F., 1957, *Phys. Rev.*, **108**, 161.

Lattes, C. M. G., 1957, *Report of the Varenna Conference on Cosmic Rays*, 1957.

Leiss, J. E., and Schrack, R. A., 1958, *Phys. Rev.*, **109**, 1326.

Williams, W. S. C., and Caplan, H. S., 1957, *Nature, Lond.*, **179**, 1185.

Venice, 1957, *International Conference on Mesons and Recently Discovered Particles*, Padua-Venice, 1957, Session 4.

Yang, C. N., 1950, *Phys. Rev.*, **77**, 242.

RESEARCH NOTES

Determination of the Effective Electron Mass in GaAs by the Infra-Red Faraday Effect

By T. S. MOSS and A. K. WALTON
Radio Department, Royal Aircraft Establishment, Farnborough, Hants.

MS. received 13*th April* 1959, *in final form* 1*st May* 1959

The preferred ways of measuring effective mass are all magneto-optic methods, namely (i) cyclotron resonance at either infra-red or radio wavelengths, (ii) oscillatory magneto-absorption and (iii) infra-red Faraday effect. So far none of these techniques has been applied to GaAs, although this material is now of great fundamental and technological interest. We have used the free carrier Faraday rotation, which essentially determines the dispersion due to cyclotron resonance absorption (Moss 1959), to determine the effective mass in n-type material.

It is shown by use of classical dispersion theory (Mitchell 1955, Moss 1959) that the mass is given by

$$m^* = \lambda\left\{\frac{BNe^3}{8\pi^2c^3\epsilon_0 n\theta}\right\}^{1/2} \qquad \ldots\ldots(1)$$

where θ is the Faraday rotation per unit length at the wavelength λ, N the carrier density, n the refractive index and B the magnetic induction. A more detailed treatment of the effect by Stephen and Lidiard (1959), starting from the Boltzmann transport equation, yields an identical expression, where the interpretation of m^* depends on the band structure. For the complex conduction band of Ge for example, it corresponds to a weighted average of the longitudinal and transverse masses—as has now been verified experimentally (Walton and Moss 1959). For GaAs however where there is theoretical and experimental evidence (Callaway 1957, Glicksman 1959) that the lowest conduction level has a spherical energy surface, equation (1) will give the isotropic effective mass.

Measurements were made on three n-type single crystal specimens over the wavelength range 8–19μ, using a double monochromator with KBr prisms. The techniques involved have been described by Moss, Smith and Taylor (1959) and Smith, Moss and Taylor (1959). The Faraday rotation and Hall constant were measured on the same area of each specimen.

The crystals were ground to rectangular bars approximately $8 \times 3 \times 0{\cdot}5$ mm^3 with plane parallel faces. Low resistance end contacts were applied by various methods: (i) 'electrodeless' Ni plating (as used for Si by Sullivan and Eigler 1957), (ii) Ag electroplating with subsequent electroforming, (iii) soldering with tin using citric acid as flux. The Hall probes were gold wires whose contact resistances were reduced to approximately 1000 Ω by discharging a 1 μF condenser through each contact in the back direction. Hall voltages were taken with both signs of current and field and were very reproducible. Measurements at different points on the specimens showed little spread, and it is concluded that the Hall constants were accurate to $\pm 3\%$. When interpreting

these data, using the relation $R = A/Ne$, there is some uncertainty about the constant A. For intrinsic material, where lattice scattering predominates, $A = 3\pi/8$. With increasing impurity this parameter falls to a broad minimum with $A \sim 1$ and then rises again for very impure material. It seems likely that all our specimens would lie around this minimum region, so we have taken A to be unity. It is possible however that A could be as much as 1·1, so that our carrier concentrations could be too small by this amount.

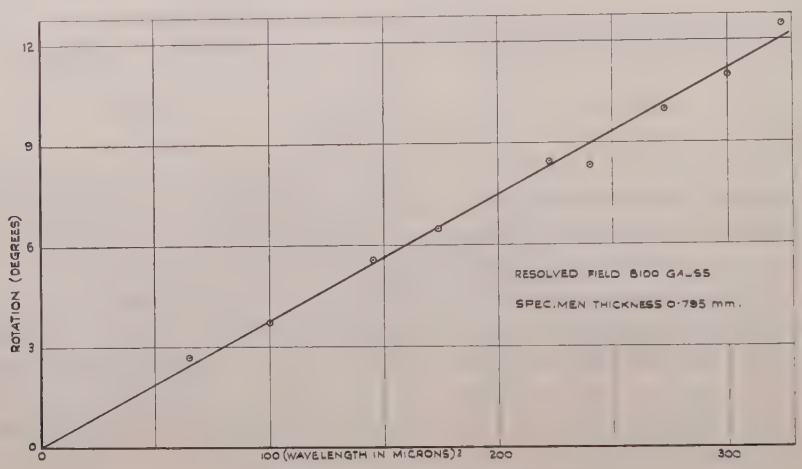

Faraday rotation in gallium arsenide.

The end contact regions were cut off the Hall specimens which were then lightly ground and polished, and used for the Faraday measurements. The measured rotation for one specimen is plotted against λ^2 in the diagram. The expected proportionality is seen to be confirmed. The slope of the straight line (drawn to give a least squares fit) gives θ/λ^2 with a precision near 1%.

The refractive index is taken to be $n = 3{\cdot}3 \pm 3\%$ (Oswald and Schade 1954). It is readily shown that the free carrier dispersion, for the carrier concentrations involved, has a negligible effect on this value.

The component of the magnetic induction resolved along the direction of the radiation was 0·81 W/m^2 for specimen 1, and 0·83 W/m^2 for specimens 2 and 3. The uncertainty in the field is estimated as $\pm 5\%$, mainly due to the uncertainty in the angle between the field and the radiation.

Substituting the above values in equation (1) we find the effective masses given in the table.

N (cm^{-3})	$7{\cdot}4 \times 10^{16}$	$5{\cdot}3 \times 10^{16}$	$3{\cdot}5 \times 10^{16}$
m^*	0·075 m_0	0·068 m_0	0·073 m_0

Average $m^* = 0{\cdot}072\ m_0$

In assessing the overall accuracy of this result it should be noted that equation (1) shows that the only observable proportional to m^* is λ, which can be measured with quite negligible inaccuracy. The parameters, B, n, N and θ give only a square root dependence, so that the overall measuring tolerance in the effective mass is $\pm 6\%$. In addition there is an uncertainty of -0 $+5\%$ arising from the interpretation of the Hall constant giving $m^*/m_0 = 0{\cdot}072(+0{\cdot}008, -0{\cdot}005)$. In view of the fact that three sets of measurements were carried out on different specimens the final errors might be less than those quoted.

The result obtained is consistent with the most recent analysis of electrical properties by Weisberg, Woolston and Glicksman (1958). It is, however, considerably greater than the value of 0·043 given by Barcus, Perlmutter and Callaway (1958) from a study of the infra-red dispersion of GaAs. This latter method of finding effective mass is fundamentally sound, but is inferior to the Faraday effect method because the mass found depends directly on the carrier concentration rather than on its square root. As these workers used polycrystalline material errors in N could be particularly serious. Unfortunately no details of the Hall measurements are given and it is not known if the Hall effect was measured on the same area of material as was studied optically. Also the particular method used by Barcus, Perlmutter and Callaway (1958) to determine the dispersion (that of Simon 1951 a) is generally regarded as unreliable, depending as it does on a study of surface reflection of polarized radiation. For example Simon (1951 b) found for both Si and Ge that *n increased* drastically with increasing wavelength between 4 and 14μ (the indices almost doubled), whereas the index actually *decreases* steadily throughout this range.

Acknowledgments

We wish to thank Drs. O. Simpson and J. T. Edmond, of Services Electronic Research Laboratories, Baldock, for providing the gallium arsenide and advising on silver plating techniques.

References

Barcus, L. C., Perlmutter, A., and Callaway, J., 1958, *Phys. Rev.*, **111**, 167.
Callaway, J., 1957, *J. Electronics*, **2**, 330.
Glicksman, M., 1959, *J. Phys. Chem. Solids*, **8**, 511.
Mitchell, E. J. W., 1955, *Proc. Phys. Soc.* B, **68**, 973.
Moss, T. S., 1959, *Optical Properties of Semiconductors* (London: Butterworths Scientific Publications; New York: Academic Press).
Moss, T. S., Smith, S. D., and Taylor, K. W., 1959, *J. Phys. Chem. Solids*, **8**, 323.
Oswald, F., and Schade, R., 1954, *Z. Naturf.*, **9 a**, 611.
Simon, I., 1951 a, b, *J. Opt. Soc. Amer.*, **41**, 336, 730.
Smith, S. D., Moss, T. S., and Taylor, K. W., 1959, *J. Phys. Chem. Solids*, in the press.
Stephen, M. J., and Lidiard, A. B., 1959, *J. Phys. Chem. Solids*, **9**, 43.
Sullivan, M. V., and Eigler, J. H., 1957, *Trans. Electrochem. Soc.*, **104**, 226.
Walton, A. K., and Moss, T. S., 1959, *J. Appl. Phys.*, **30**, 951.
Weisberg, L. R., Woolston, J. R., and Glicksman, M., 1958, *J. Appl. Phys.*, **29**, 1514.

On *r*-centroids of Molecular Transitions, Equilibrium Internuclear Separations and Oscillator Turning Points

By R. W. Nicholls and W. R. Jarmain
Department of Physics, University of Western Ontario

MS. received 2nd March 1959

The *r*-centroid concept proposed a number of years ago by Fraser (1954 a) has been very useful for the interpretation of molecular band intensities in terms of (*a*) the variation of electronic transition moments of band systems with internuclear separations r, and thereby in terms of (*b*) arrays of smoothed relative vibrational transition probabilities (Turner and Nicholls 1954 a, b,

Wallace and Nicholls 1955, Nicholls 1956 a, b, 1958 a, b, Dixon and Nicholls 1958, Robinson and Nicholls 1958).

The r-centroid of the $v' \rightarrow v''$ band is defined in terms of vibrational wave functions $\psi_{v'}$, $\psi_{v''}$ as

$$r_{v'v''} = \int \psi_{v'} r \psi_{v''} dr \Big/ \int \psi_{v'} \psi_{v''} dr \qquad \ldots\ldots (1)$$

and a number of its properties, methods by which r-centroid arrays can be computed, and the arrays, have been given elsewhere (Nicholls and Jarmain 1955, 1956, Nicholls, Robinson, Parkinson and Jarmain 1956, Nicholls 1958 a).

It is important to relate $\bar{r}_{v'v''}$ to other familiar internuclear separations of diatomic molecules. Thus it is the purpose of this note to derive the relation among the r-centroid $\bar{r}_{v'v''}$, the equilibrium internuclear separations r_e', r_e'' of the two potentials involved, and the turning points r_1', r_2' (or $r'_{1,2}$); r_1'', r_2'' (or $r_{1,2}''$) of the molecular oscillators in the v' and v'' levels respectively.

It has been shown (Nicholls and Jarmain 1956) that if $U'(r)$ and $U''(r)$ are the two molecular potentials concerned and $E_{v'}$ and $E_{v''}$ are the energies of the vibrational levels v' and v'' that

$$U'(\bar{r}_{v'v''}) - U''(\bar{r}_{v'v''}) = E_{v'} - E_{v''}. \qquad \ldots\ldots (2)$$

Further, by definition, the turning points of the classical oscillators for v' and v'' are given by

$$U'(r'_{1,2}) = E_{v'} \quad \ldots\ldots (3\,a); \qquad U''(r''_{1,2}) = E_{v''}. \qquad \ldots\ldots (3\,b)$$

Thus from equations (2), (3 *a*, *b*)

$$U'(r'_{1,2}) - U'(\bar{r}_{v'v''}) = U''(r'_{1,2}) - U''(\bar{r}_{v'v''}). \qquad \ldots\ldots (4)$$

This equation contains the intrinsic relation among $\bar{r}_{v'v''}$, $r'_{1,2}$, $r''_{1,2}$, r_e', r_e'', and particular cases can be worked out analytically for particular forms of molecular potential $U(r)$.

Two specific forms of potential, simple harmonic and Morse, are considered here.

For simple harmonic oscillator potentials

$$U'(r) = k\omega_e'^2 (r - r_e')^2 \quad \ldots\ldots (5\,a); \qquad U''(r) = k\omega_e''^2 (r - r_e'')^2 \ldots\ldots (5\,b)$$

where k is a constant and the symbols are conventional (Herzberg 1950). Thus equation (4) becomes

$$\omega_e'^2 [(r'_{1,2} - r_e')^2 - (\bar{r}_{v'v''} - r_e')^2] = \omega_e''^2 [(r''_{1,2} - r_e'')^2 - (\bar{r}_{v'v''} - r_e'')^2] \qquad \ldots\ldots (6)$$

which may be recast as

$$\frac{(W-1)^2}{W} \left[\frac{\bar{r} - (W r_e' - r_e'')/(W-1)}{r_e' - r_e''} \right]^2 - (W-1) \left[\frac{r'_{1,2} - r_e'}{r_e' - r_e''} \right]^2 + \frac{W-1}{W} \left[\frac{r''_{1,2} - r_e''}{r_e' - r_e''} \right]^2 = 1 \qquad \ldots\ldots (7)$$

where

$$W = (\omega_e'/\omega_e'')^2. \qquad \ldots\ldots (8)$$

Equation (7) is an hyperboloid of one sheet. The independent variables of the hyperboloid are the quantities in the large brackets.

For Morse oscillator potentials

$$U'(r) = D[1 - \exp\{-\alpha'(r - r_e')\}]^2 \qquad \ldots\ldots (9\,a)$$

$$U''(r) = D[1 - \exp\{-\alpha''(r - r_e'')\}]^2 \qquad \ldots\ldots (9\,b)$$

Application of the Fraser–Jarmain approximation (Fraser and Jarmain 1953, Jarmain and Fraser 1953, Fraser 1954*b*) introduced for the calculation of Franck–Condon factor arrays for band systems of 'Morse' molecules, leads to replacing equations (9*a*) and (9*b*) by

$$U'(r)=\mathscr{D}[1-\exp\{-\alpha(r-r_e')\}]^2 \quad \ldots\ldots(10a)$$

$$U''(r)=\mathscr{D}[1-\exp\{-\alpha(r-r_e'')\}]^2 \quad \ldots\ldots(10b)$$

where α is a mean, often the arithmetic mean, of α' and α'' and $\mathscr{D}'$, $\mathscr{D}''$ are the adjusted values of the α-dependent dissociation energies D', D''. Full details of the approximation may be found in the above references.

Substitution of equations (10 *a*, *b*) into equation (4) leads to

$$\frac{\mathscr{D}'}{R_e'^2}\left[(\bar{R}_{v'v''}-R_e')^2-(R'_{1,2}-R_e')^2\right]=\frac{\mathscr{D}''}{R_e''^2}\left[(\bar{R}_{v'v''}-R_e'')^2-(R''_{1,2}-R_e'')^2\right] \quad \ldots\ldots(11)$$

where

$$R_e'=\exp(-\alpha r_e') \quad \ldots\ldots(12a)$$

$$R_e''=\exp(-\alpha r_e'') \quad \ldots\ldots(12b)$$

$$R'_{1,2}=\exp(-\alpha r_{1,2}') \quad \ldots\ldots(12c)$$

$$R''_{1,2}=\exp(-\alpha r_{1,2}'') \quad \ldots\ldots(12d)$$

$$\bar{R}_{v'v''}=\exp(-\alpha\bar{r}_{v'v''}) \quad \ldots\ldots(12e)$$

For any one band system the *variables* are clearly $\bar{R}_{v'v''}$, $R'_{1,2}$, $R''_{1,2}$.

Equation 11, which is of similar form to equation 6, may be recast as:

$$\frac{(V-1)^2}{V}\left[\frac{\bar{R}_{v'v''}-(VR_e'-R_e'')/(V-1)}{R_e'-R_e''}\right]^2-(V-1)\left[\frac{R'_{1,2}-R_e'}{R_e'-R_e''}\right]^2+\frac{V-1}{V}\left[\frac{R''_{1,2}-R_e''}{R_e'-R_e''}\right]^2=1, \quad \ldots\ldots(13)$$

which is also an hyperboloid of one sheet in the variables inside the large brackets where

$$V=\mathscr{D}'R_e''^2/\mathscr{D}''R_e'^2. \quad \ldots\ldots(14)$$

Equation (13) has been confirmed graphically by plotting the cross section curves (hyperbolae and ellipses) of the hyperboloid surface using numerical values of $\bar{r}_{v'v''}$ arrays which have been calculated (Nicholls, Robinson, Parkinson and Jarmain 1956, Nicholls, Ebisuzaki, Van der Laan and Jarmain to be published). Small deviations from the predicted sections were noted particularly at high quantum numbers in cases where the approximation was not completely valid. These were also noted in some cases where the $\bar{r}_{v'v''}$-values had been obtained by graphical solution of equation 2 (using α' and α'' in the U's) rather than by the analytical method (Nicholls and Jarmain 1956) which also involves the use of the Fraser–Jarmain approximation. Even in these cases the general form of the r-centroid surface was very similar to an hyperboloid of one sheet.

Acknowledgments

We should like to acknowledge valuable discussions with Dr. P. A. Fraser and also the numerical and graphical work of Mr. H. Van der Laan in the comparisons mentioned above. The work was supported in part by Contracts AF 19(604)–1718, AF 19(604)–4560 with the Air Force Cambridge Research Center, and by Research grants from The Defence Research Board and National Research Council of Canada.

References

Dixon, R. N., and Nicholls, R. W., 1958, *Canad. J. Phys.*, **36**, 127.
Fraser, P. A., 1954 a, *Canad. J. Phys.*, **32**, 515.
—— 1954 b, *Proc. Phys. Soc. A*, **67**, 939.
Fraser, P. A., and Jarmain, W. R., 1953, *Proc. Phys. Soc.* A, **66**, 1145.
Herzberg, G., 1950, *The Spectra of Diatomic Molecules* (New York: Van Nostrand).
Jarmain, W. R., and Fraser, P. A., 1953, *Proc. Phys. Soc.* A, **66**, 1153.
Nicholls, R. W., 1956 a, *Proc. Phys. Soc.* A, **69**, 741.
—— 1956 b, *The Airglow and Aurorae*, edited by A. Dalgarno and E. B. Armstrong (London: Pergamon Press), p. 302.
—— 1958 a, *Ann. Géophys.*, **14**, 208.
—— 1958 b, *J. Atmos. Terr. Phys.*, **12**, 211.
Nicholls, R. W., and Jarmain, W. R., 1955, *J. Chem. Phys.*, **23**, 1561.
—— 1956, *Proc. Phys. Soc.* A, **69**, 253.
Nicholls, R. W., Robinson, D., Parkinson, W. H., and Jarmain, W. R., 1956, *Proc. Phys. Soc.* A, **69**, 713.
Robinson, D., and Nicholls, R. W., 1958, *Proc. Phys. Soc.*, **71**, 957.
Turner, R. G., and Nicholls, R. W., 1954 a, *Canad. J. Phys.*, **32**, 468.
—— 1954 b, *Ibid.*, **32**, 475.
Wallace, L. V., and Nicholls, R. W., 1955, *J. Atmos. Terr. Phys.*, **7**, 101.

Use of Fractional Parentage Coefficients in the Calculation of Photoelectric Cross Sections

By B. H. ARMSTRONG

Lockheed Aircraft Corporation, Missile Systems Division, Palo Alto, California

Communicated by D. R. Bates; MS. received 22nd January 1959

THE standard quantal formula for the photoelectric cross section

$$k_\nu = \frac{32\pi^4 m^2 e^2}{3h^3 c}\frac{1}{\omega_1}\sum_{\text{initial states}}\sum_{\text{final states}}(\nu v)\left|\int \Psi^{*i}(\Sigma \mathbf{r})\Psi^f d\tau\right|^2 \qquad \ldots\ldots(1)$$

may readily be reduced to

$$k_\nu = \frac{32\pi^4 m^2 e^2}{3h^3 c}(\nu v)\left\{4\pi\zeta_p\left(C_{l+1}\left|\int_0^\infty R^i_{nl}R^f_{\epsilon,l+1}r^3dr\right|^2 + C_{l-1}\left|\int_0^\infty R^i_{nl}R^f_{\epsilon,l-1}r^3dr\right|^2\right)\right\} \qquad \ldots\ldots(2)$$

(cf. Bates 1946) in which ζ_p is the product of the integrals

$$\left|\int_0^\infty R^i_{nl}R^f_{nl}r^2dr\right|^2$$

for the passive electrons, and the factors $C_{l\pm1}$ are constants that arise from the integration over the angular coordinates of the active electron. Bates (1946) has tabulated values of the $C_{l\pm1}$ for some important cases which he calculated from first principles, but refrained from stating their analytical form because of its cumbersomeness. By making use of the formalism of fractional parentage coefficients (Edmonds 1957), a very simple analytical form can be obtained for these factors. A large variety of fractional parentage coefficients have been tabulated (Menzel and Goldberg 1936) and explicit formulae for them have been devised (Edmonds 1957). We shall describe the method briefly.

The atomic wave function for the initial state can be factored into products of single electron wave functions and $n-1$ electron wave functions where n is the number of electrons in the configuration. The result is a linear combination of the various allowed terms of the $n-1$ electron configuration:

$$\Psi^{i}(nSL)=\sum_{S'L'}F_{SL}(nS'L')\Psi[(l^{n-1}S'L')lSL]. \qquad \ldots\ldots(3)$$

In this notation (S, L) define the term to which the initial state belongs, $\Psi[(l^{n-1}S'L')lSL]$ denotes the wave function for a state in which $n-1$ electrons couple together to (S', L') and the remaining electron couples to this total to yield the final coupling (S, L). (S', L') then is the coupling of an allowed term of the $n-1$ electron configuration. These terms are called the parents of the term (S, L), and the coefficients $F_{SL}(nS'L')$ in the expansion (3) are called fractional parentage coefficients. We take them to be normalized such that

$$\sum_{S'L'}\{F_{SL}(nS'L')\}^2=n. \qquad \ldots\ldots(4)$$

The wave functions on the right-hand side of (3) are now in the appropriate form for insertion into the matrix element of equation (1). The $(l^{n-1}S'L')$ wave functions become factors of ζ_{p}, while the l wave function becomes a factor of the single electron dipole integral. The radial factor from this single electron function yields the radial integrals appearing in (2), while the angular factor and fractional parentage coefficients become factors of the $C_{l\pm1}$. The integration over the angular coordinates of the active electron can now be performed along with the average over initial states and sum over final states. Except for the factor $F(nS'L')$ this can be done as in the simple one electron case, following the method described by Bethe and Salpeter (1957) giving $l+1/(2l+1)$ and $l/(2l+1)$ for the transitions to $l+1$ and $l-1$ respectively. Multiplying the fractional parentage coefficient into these yields

$$C_{l\pm1}(SL\rightarrow S'L')=\{F_{SL}(nS'L')\}^2\frac{(l+\frac{1}{2})\pm\frac{1}{2}}{2l+1}. \qquad \ldots\ldots(5)$$

The fractional parentage coefficients needed for the $C_{l\pm1}$ tabulated by Bates (1946) are among the many given by Menzel and Goldberg (1936). For example, for the initial term $(\mathrm{p}^4)^3\mathrm{P}$ and the final term $(\mathrm{p}^3)^2\mathrm{D}$, they give the square of the fractional parentage coefficient as 5/3 so that

$$C_{l\pm1}(^3\mathrm{P}\rightarrow{}^2\mathrm{D})=(5/3)\frac{(l+\frac{1}{2})\pm\frac{1}{2}}{2l+1}=10/9,\ 5/9. \qquad \ldots\ldots(6)$$

These are the values obtained by Bates for this case.

Acknowledgment

This work was supported by the Air Force Special Weapons Center, Kirtland Air Force Base, New Mexico.

References

Bates, D. R., 1946, *Mon. Not. R. Astr. Soc.*, **106,** 432.

Bethe, H. A., and Salpeter, E. E., 1957, *Quantum Mechanics of One- and Two-Electron Systems* (New York: Academic Press), p. 254.

Edmonds, A. R., 1957, *Angular Momentum in Quantum Mechanics* (Princeton, N.J.: Princeton Univ. Press), p. 138.

Menzel, D. H., and Goldberg, L., 1936, *Astrophys. J.*, **84,** 1.

LETTERS TO THE EDITOR

The Reflection Spectrum of CdS

The reflection spectrum of CdS single crystals has been recently obtained by Dutton (1958). At liquid nitrogen temperature using light polarized either parallel or perpendicular to the c axis a different type of structure is obtained. The mid points between reflectance maxima and minima correspond to absorption lines. These are located at 4874 Å and 4844 Å for light polarized perpendicular to c. For light polarized parallel to c, only the shorter wavelength line appears.

Experimental and theoretical work carried out in this laboratory in connection with the polarization of fluorescence in CdS (Lempicki 1959, Birman 1959 a) has led to a model for the valence band in this material. Birman (1959 a, b) has shown that at $k = 000$ the valence band consists of three levels with symmetries Γ_9, Γ_7 and Γ_7. The first two are split by spin orbit coupling. The conduction band has Γ_7 symmetry. If optical absorption corresponds to direct transition from the three valence bands to the single conduction band, then one would expect three rather than two absorption lines.

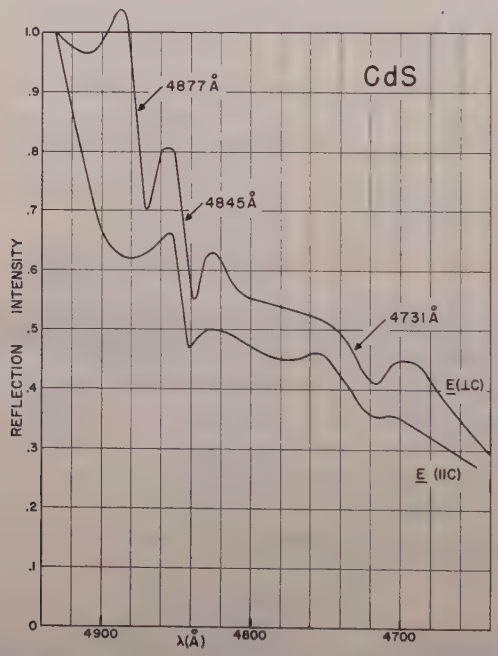

Reflection spectrum of a CdS crystal with polarized light.

The optical selection rules obtained by Birman state that one should observe three lines for $E(\perp c)$ only two of which would be present for $E(\parallel c)$.

We have performed reflectance measurement on a CdS plate containing the c axis in its plane. A Hilger double monochromator with a resolution of about 5 Å was used. The spectra were recorded automatically. The figure gives the reflection intensity (normalized per unit incident intensity and at 4930 Å) at liquid nitrogen temperature. We see that a third line at 4731 Å is

present for both polarizations. The result is thus consistent with the selection rules.

Transition†	E	λ (Å)	Δ Energy (ev)
$\Gamma_{9v}-\Gamma_{7c}$	$\perp$	4877	
			0·0167
$\Gamma_{7v}-\Gamma_{7c}$	$\perp$, $\parallel$	4845	
			0·0616
$\Gamma_{7v}-\Gamma_{7c}$	$\perp$, $\parallel$	4731	

† The symbols v and c refer to valence and conduction bands.

The table gives the tentative assignment of transitions. A theoretical discussion of the selection rules and splittings is given by Birman (1959 b).

Gross, Kapliansky and Novikov (1956) have found additional absorption lines at liquid helium temperatures which they assign to excitons. A more detailed theoretical analysis of selection rules for formation of excitons, spin orbit and crystal field splittings and experiments with polarized light down to liquid helium temperatures are obviously needed for a better understanding of the reflection–absorption structure.

The author is indebted to Dr. J. L. Birman for the theory, and to Dr. I. Broser for the CdS crystal.

Sylvania Research Laboratories,
A Division of Sylvania Electric Products Inc.
Bayside, New York. A. Lempicki.
9th April 1959.

Birman, J. L., 1959 a, *Phys. Rev. Let.*, **2**, 157.
—— 1959 b, *Phys. Rev.*, in the press.
Dutton, D., 1958, *Phys. Rev.*, **112**, 785.
Gross, E. F., Kapliansky, A. A., and Novikov, B. V., 1956, *Dokl. Akad. Nauk U.S.S.R.*, **110**, 761.
Lempicki, A., 1959, *Phys. Rev. Let.*, **2**, 155.

CORRIGENDUM

Diffraction by an Opaque Strip, by R. S. Longhurst (*Proc. Phys. Soc.*, 1958, **72,** 901.

In the above note it was stated (p. 904, line 17, and p. 905, line 33) that the Rubinowicz integral (p. 903, line 35) breaks down at the shadow boundary, and this also seems to be implied in an earlier paper (Martin, L. C., *Proc. Phys. Soc.* B, 1949, **62,** 713, § 2). It is therefore desirable to draw attention to the fact that such a breakdown does not, in fact, occur. A. Rubinowicz (*Ann. Phys., Lpz.*, 1924, **73,** 339) has himself shown how, by a direct application of the method of stationary phase, one may obtain an approximation that is valid in regions removed from the shadow boundary. In effect, the formula given for the visibility of the opaque strip fringes derives from an application of this approximation. Rubinowicz has also obtained an approximation that remains valid at the shadow boundary and gives results that are substantially in agreement with the Sommerfeld theory. However, the first approximation does yield a simple result for the visibility of the opaque strip fringes that is valid near the centre of the pattern where the fringes are usually observed.

NOTICE TO AUTHORS

Authors of papers on experimental measurements are advised to include information concerning the purity and structure (grain size, homogeneity, degree of working phases present, etc.) of materials used. This should be as complete as the nature of the measurements being made requires and should include the source of the material and method of preparation.

REVIEWS OF BOOKS

Handbuch der Physik, Vol. XXVI, *Light and Matter* II, edited by S. FLÜGGE. Pp. vii+965. (Berlin: Springer, 1958.) DM 168.

By far the largest part of the present volume is concerned with infra-red spectroscopy: indeed the bulk of the volume is taken up by a very long article by J. Lecompte on this subject, supplemented by much shorter articles by Z. Mizushima on Raman spectra and by G. A. W. Rutgers on temperature radiation from solids. The article by Lecompte forms a book on its own, taking up 695 of the 937 pages of the text (apart from index); this certainly unbalances the volume, and one wonders whether such a major work should not have appeared as in independent book. The article itself consists of a very lengthy section giving a detailed description of the infra-red absorption spectra of a wide variety of molecules. A number of excellent collections of similar data are, of course, already available, but the discussion of the data by one who has himself contributed so widely in this field of investigation is of considerable value. A much shorter section is devoted to a discussion of absorption spectra of solids in the form of various minerals including oxides, sulphides, selenides etc. The article opens with a brief review of modern spectroscopic techniques including a discussion of detectors, optical components and spectroscopes. This field has recently been covered by other writers and, with such a rapidly growing subject, the present account can hardly be expected to be completely up-to-date. The section on spectrometers is, however, particularly valuable. The article concludes with a brief discussion of observational methods and of current data on dispersion.

The article by Mizushima on the Raman Effect gives a concise account (71 pages) of the various types of Raman Spectra and of the theory used in discussing their origin; techniques for their observation are also briefly discussed. Only a limited amount of mathematics is used, and the complex analysis frequently associated with discussions of Raman spectra is avoided. This is a fairly typical review article dealing with the background and present position.

The first article in this volume is on an entirely different subject—luminescence. It is in many ways complementary to an article by the author, G. F. J. Garlick, in a previous volume of this series (Vol. XIX), on Photoconductivity. It is in the form of a fairly extensive review article (128 pages) and helps to bring up to date the author's well-known book on the subject. The article, as would be expected from one who has himself contributed so much to this field of research is authoritative and collects together a lot of new material which is critically discussed. Electroluminescence, a subject which has recently become of considerable importance is discussed in addition to the more conventional phenomena associated with excitation of luminescence by radiation and by electron bombardment.

The volume is liberally illustrated throughout and the presentation and production maintain the high standard of the whole series. R. A. SMITH.

Handbuch der Physik, Vol. VII/2, *Kristallphysik II*, edited by S. FLÜGGE. Pp. iv+273. (Berlin, Göttingen, Heidelberg: Springer 1958). DM 76.

The first 210 pages of this volume comprise the article on Crystal Plasticity by A. Seeger, essentially the sequel to the same author's article on Lattice Defects.

It concentrates on the glide process, with only brief mention of twinning and kinking. Within this restriction, it provides a very thorough and comprehensive presentation of the complex experimental material, well illustrated by experimental curves and metallographic pictures. A general comprehension of this subject has not been made easier by the optimistic tendency of authors in the past to attempt a complete new theory of the work-hardening curve (or the creep laws) on the basis of each new idea about dislocation behaviour. Seeger has previously been no exception to this, and he is to be congratulated for the fact that in this article he has been able to use theory to give form to his presentation, while keeping the theory and the facts distinct. It seems probable that a great deal of the theory of this subject is now settled, but in any case this will remain an article of permanent value. Literature up to the middle of 1956 is substantially covered. Direct electron-microscopic observations of individual moving dislocations came too late for photographic reproduction, and receive only a short discussion.

The remaining 42 pages of the volume are occupied by an article by U. Dehlinger on Transformations and Precipitations in the Crystalline State. The space is meagre for so large a subject, and though an interesting essay on some subjects comprised within its title, this is a far from comprehensive guide to the subject as a whole, or even to the literature of the portions dealt with.

Both articles are in German. F. C. F.

Quantum Mechanics (*Non-relativistic Theory*), by L. D. Landau and E. M. Lifshitz. Translated from the Russian by J. B. Sykes and J. S. Bell. Pp. xii +515. (London : Pergamon Press, 1958.) 80*s*.

Those who in recent years have been impressed by the versatility and thoroughness of modern Russian theoretical physicists will know that this has been due in part to the excellent text books available in Russian for the teaching of the subject. All those concerned with the training of theoretical physicists in English-speaking countries will be grateful to Pergamon Press for making available English translations of the monumental *Course of Theoretical Physics* which Landau and Lifshitz are writing in nine volumes.

The present volume on non-relativistic quantum mechanics can only be described as masterly. The basic ideas of quantum mechanics are profound and not easy to grasp. But here they are presented with consummate skill and artistry, with clarity and conciseness of expression in which difficulties of conception are clearly distinguished from complexities of formalism.

The choice of subject matter reflects the wide experience and maturity of judgment of the authors. As they state in their preface they have tried to avoid discussion of complicated applications of the theory or of topics which would have needed a detailed account of experimental results. This criterion has led them to give, for example, a fuller discussion of applications of quantum theory in atomic and molecular physics than in nuclear physics.

The first two chapters deal with the bases of quantum mechanics, uncertainty principle, superposition, operators, matrices and the theory of measurement. After a chapter on the Schrödinger equation and simple applications of it they go on to discuss the quantum theory of angular momentum, addition of angular momenta, parity and the problem of motion in a central field. Chapters on

perturbation theory and the relation to classical mechanics follow. In the latter part of the book there are three very clearly written chapters on the difficult topics of spin, identity of particles and group theory. Other chapters deal with atomic and molecular physics, collision theory and problems of motion in a magnetic field.

It concludes with a number of useful mathematical appendices presenting material on functions of mathematical physics that are often needed in applications of quantum mechanics.

The value of the book for teaching purposes is enhanced by the numerous questions of considerable physical interest which are introduced as problems, the broad lines of the solution of which are given, but the details left to be filled in by the student.

A tribute should also be paid to the exceptionally high quality of the English translation in which the clarity of the argument is fully retained. There seems little doubt that this work is destined to play a major part in the future education of theoretical physicists in Britain as well. E. H. S. BURHOP.

Einführung in die Atomphysik, by W. FINKELNBURG. Pp. xi+537. (Berlin, Göttingen, Heidelberg: Springer, 1958.) DM. 45.

This book covers atomic physics in the widest sense from elementary particles to the solid state. Its level corresponds roughly to the requirement of the third year in a four years honours course in one of our Universities.

The problem of atomic spectra is covered with great thoroughness. I was glad to see that the old interpretation of quantum numbers in terms of the diameter and eccentricities of orbits is only mentioned in passing. Its place is taken very usefully by their identification with the nodal surfaces of wave functions. Wave mechanics is taken as far as the solution of the Schrödinger equation for the hydrogen atom. The calculation of transition probabilities is outlined but not treated in detail.

This chapter is followed by one on nuclear physics and elementary particles which gives the impression that the author is not on quite the same sure ground as in the rest of the book. Mesons are classed as leptons although a clear distinction is made between π and μ mesons where their properties are discussed. The chapter finishes with a discussion of fundamental constants which leaves the solid ground of nature more than seems justified for a book of this kind. This chapter also contains the only glaring printing error, extending from page 243 to 244 where whole lines have been put in the wrong order.

The section on molecules returns to its task with the same thoroughness as the earlier parts of the book, dealing with molecular spectra and molecular forces.

The last 100 pages are devoted to the solid state. This section forms a very interesting introduction to a branch of physics that is becoming increasingly important.

There are no references to original papers but each chapter ends with a list of specialized books which are relevant to it. This is a very suitable arrangement for the readers that the author is aiming at.

With the exceptions already mentioned the book is well written and well produced and gives useful insight into atomic physics. S. G. F. FRANK.

Preparation of Single Crystals, by W. D. Lawson and S. Nielsen. Pp. viii + 255. (London: Butterworths Scientific Publications, 1958.) 45*s*.

The work of the Royal Radar Establishment on the growth of semiconductor crystals is well known, and two of the workers principally concerned are the authors of this book. Since it is the first of a series of monographs on semiconductors, the book is mainly concerned with those methods of preparation and purification of materials, and with those methods of growth, that are most suitable for semiconductors. Its general value is enhanced by the inclusion of information regarding other materials such as the alkali halides, but it is most valuable when the authors are writing of their own field—in which they probably have more experience than anyone else in Britain.

While there is much for the specialist, the book could be used as an introduction for research students, since it starts from an elementary level. In this connection, the book could well have taken for granted such items as rotary pumps and Macleod gauges, and given rather more space to more advanced details of techniques.

The authors very properly focus attention on the need for the highest purity, and they give useful surveys of purification methods, and of analytical methods for establishing the chemical composition of the prepared material. One of the potentially most interesting chapters for the specialist could have been that on the preparation and crystallization of compounds, for the authors' experience in this field must be almost unique. Perhaps in the interests of generality, however, they modestly content themselves with examples, when many readers would have appreciated much more detail. Some clue to the depth of this detail is to be found in the interesting section on stoichiometry.

The book includes a survey of defects in crystals and their interactions, and there are some very useful tables of such properties as melting points and energy gaps.

R. V. JONES.

Méthodes Mathématiques de la Mécanique Statistique, by A. Blanc-Lapierre, P. Casal and A. Tortrat. Pp. 180. (Paris: Masson, 1959.) Fr. 3800.

This monograph, written by three professors at the Algerian University, of whom one is a physicist and the other two mathematicians, discusses in great detail the mathematical foundations of statistical mechanics. It is written in the best traditions of the French mathematical literature. It will appeal to those theoretical physicists who are interested in ergodic theory and who are not afraid of detailed mathematical considerations. It must thus be compared with Khinchin's monograph, *The Mathematical Foundations of Statistical Mechanics*. In many ways it is an improvement on that classical exposition, partly because it treats in more detail some of the difficulties connected with the concept of (quasi-) ergodic systems, and partly because it also covers quantum statistics, even though the peculiarities of ergodicity in the quantum case are hardly touched upon; classical ergodic theory, on the other hand, is dealt with in detail.

D. TER HAAR.

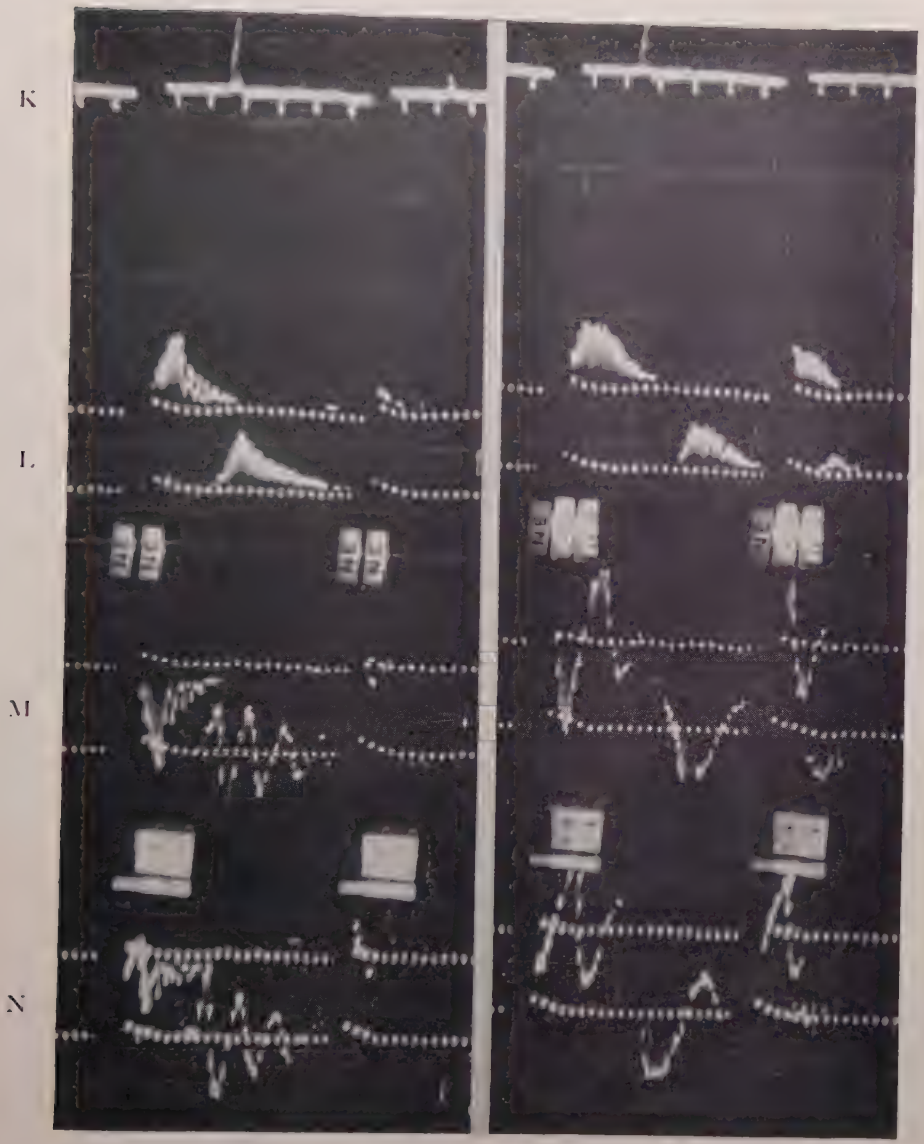

Figure 2. Film records showing measurements of wind velocity at two points along meteor trail.

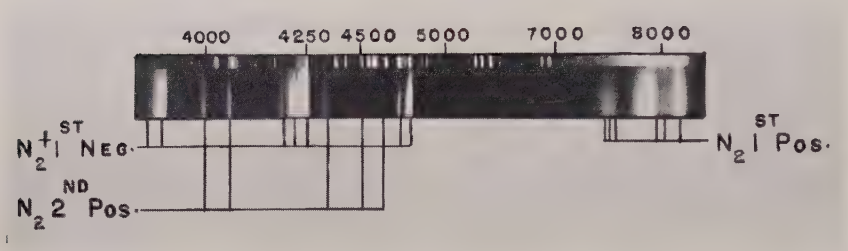

Figure 1. Spectrum arising from the 1 MeV proton bombardment of N_2 at a pressure of 150 μ Hg.

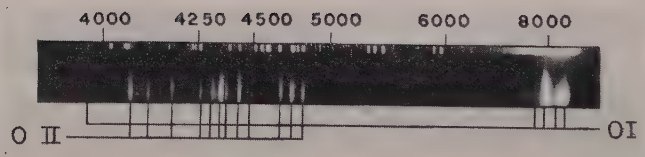

Figure 2. Spectrum arising from 1 MeV proton bombardment of O_2 at atmospheric pressure.

The Low Pressure Plane Symmetric Discharge

By E. R. HARRISON and W. B. THOMPSON
Atomic Energy Research Establishment, Harwell, Berks.

MS. received 5th March 1959

Abstract. It is shown that the low pressure plane symmetric plasma equation, using the collision-free model of Tonks and Langmuir, can be solved analytically. Simple expressions are obtained for the mean velocity and the mean square velocity of the ions, and for the wall potential with respect to the plasma. The conditions for the formation of a stable plasma-sheath boundary are briefly examined and a general criterion is obtained without considering any specific mechanism of ion transport. No assumptions are made regarding the energy distribution of the ions, and the result is therefore a refinement on Bohm's original criterion which was derived by assuming a monoenergetic ion flux. With the aid of the criterion developed in the present treatment conclusions are then drawn in the case of the collision-free model regarding conditions applying at the plasma boundary. The experimental results are found to be consistent with these theoretical conditions.

§ 1. Introduction

In the positive column of the low pressure discharge the mean free path of the ions is large, and in most cases when the magnetic field is zero we may regard the positive ions as falling freely through the plasma from their points of origin. Provided the ions have negligible velocities when formed, their individual speeds are then governed simply by the electric potentials through which they fall. On the basis of this model Tonks and Langmuir (1929) in a classic paper on the general theory of the plasma were able for plane, cylindrical, and spherical symmetries to express the positive ion distribution function $f(v)$ in terms of the potential distribution within the plasma. On equating the electron and ion densities they obtained an integral equation referred to as the 'plasma equation'. Assumptions were then made regarding the rate at which the ions were generated per unit volume and the plasma equation was solved by expressing the various functions as power series in terms of a dimensionless variable. In the case of the low pressure discharge only solutions for plane and cylindrical symmetry were given; the solution for a spherically symmetric plasma has been calculated in a similar manner and is given elsewhere (Harrison 1958).

Using the collision-free model of Tonks and Langmuir it is shown that in the case of plane symmetry the plasma equation can be solved analytically. In addition the conditions for the formation of a stable plasma-sheath boundary are examined and Bohm's (1949) original criterion is reconstructed to include the effect of an energy distribution in the ion flux. This criterion is then used to estimate the maximum range of variation for the electric potential at the plasma boundary. The results of some experimental work are found to be in approximate agreement with the theory.

§ 2. General Theory

2.1. *The Positive Ion Distribution Function*

In this section the treatment of the plane symmetric discharge follows closely the work of Tonks and Langmuir, with the modification that the results are derived analytically. The discharge is assumed to consist of electrons and positive ions, with neutral gas molecules of a sufficiently low density to leave unimpeded the ion motions in a plane transverse to the positive column.

In a low pressure discharge of this kind the positive ions are accelerated towards the walls by an electric field which establishes quasi-neutrality in the plasma and also secures an equality of electron and ion fluxes to the walls. In a plane perpendicular to the plasma column the electric potential is a function of a single coordinate, z. Thus, an ion formed at a point $\zeta \leqslant z$ has a velocity of

$$v_z = (2e/M)^{1/2}(\phi_\zeta - \phi_z)^{1/2}, \qquad \ldots\ldots (1)$$

where e and M are the charge and mass of the ion, and ϕ_ζ and ϕ_z are the electric potentials at the points ζ and z. It is assumed that the initial thermal velocity of the ion is negligibly small.

Suppose now the ions are generated at a rate of $g(z)$ per unit volume. If $f(v_z)\,dv$ is the number of ions at z having velocities in the range v_z to $v_z + dv$, it follows that

$$f(v_z)\,dv = g(\zeta) v_z^{-1}\,d\zeta, \qquad \ldots\ldots (2)$$

where $g(\zeta)\,d\zeta$ is the number of ions formed per second between ζ and $\zeta + d\zeta$. Therefore, from equations (1) and (2), the distribution function at a point $z \geqslant \zeta$ is given by

$$f(v)\,dv = (M/2kT)^{1/2} g(\eta_\zeta)(\eta - \eta_\zeta)^{-1/2}(d\zeta/d\eta)\,d\eta \qquad \ldots\ldots (3)$$

where the suffix z is dropped and $\eta = -e\phi/kT$ is now the variable; T is the electron temperature.

If ψ is any suitable property of the ion motion, it has a mean value

$$\begin{aligned}\langle \psi \rangle &= (n_+)^{-1} \int \psi f(v)\,dv \\ &= (n_+)^{-1}(M/2kT)^{1/2} \int_0^\eta g(\eta_\zeta)(\eta - \eta_\zeta)^{-1/2} \psi_\zeta'\,d\eta \qquad \ldots\ldots (4)\end{aligned}$$

at η, where n_+ is the ion density and primes denote differentiation with respect to η_ζ.

2.2. *Plasma Equation*

The number density of the electrons, assuming that they are in thermal equilibrium, is

$$n_- = n_0\, e^{-\eta} \qquad \ldots\ldots (5)$$

where n_0 is the density at the plane of symmetry at which $\eta = 0$. Taking $n_+ = n_-$ as a condition characteristic of the plasma, the 'plasma equation' is

$$\int f(v)\,dv - n_0\, e^{-\eta} = 0$$

or, using equation (3) and changing the variables to $\eta = x^2$, $\eta_\zeta = x^2 \sin^2\theta$

$$n_0\, e^{-\eta} = (M/2kT)^{1/2} \int_0^{\pi/2} g(x^2 \sin^2\theta)\{d\zeta/d(x^2 \sin^2\theta)\}\,d\theta. \qquad \ldots\ldots (6)$$

Given an integral equation of the form

$$f(x)=(2/\pi)\int_0^{\pi/2} h(x\sin\theta)\,d\theta,$$

then using Schlömilch's transformation (Whittaker and Watson 1950)

$$h(x)=f(0)+\int_0^{\pi/2} f'(x\sin\theta)\,d\theta.$$

Thus, equation (6) can be transformed and integrated to give

$$\pi(M/2kT)^{1/2}g(\eta)\eta^{1/2}(dz/d\eta)=n_0\{1-2\eta^{1/2}\,e^{-\eta}\,D(\eta^{1/2})\} \quad \ldots\ldots(7)$$

where $D(x)$ is the Dawson function:

$$D(x)=\int_0^x \exp t^2\,dt$$

tabulated by Terrill and Sweeny (1944) and Jahnke and Emde (1945).

One notices in equation (7) that at a certain value of η, say η_0, given by

$$1-2\eta_0^{1/2}\exp(-\eta_0)\,D(\eta_0^{1/2})=0, \quad \ldots\ldots(8)$$

that $dz/d\eta=0$, and that therefore the electric field is infinitely large. Thus, η_0 corresponds to the extreme limit of validity for the plasma equation, and is the Tonks–Langmuir plasma boundary value of η. It is interesting to notice that the value of η_0 is independent of the generation function $g(\eta)$ which so far has not been specified. Similarly, using equations (4) and (7), the mean value $\langle\psi\rangle$ of any property of the ion motion is identical in all low pressure plane symmetric plasmas at the Tonks–Langmuir boundary, since $\langle\psi\rangle$ is a function only of η.

The function $D(x)\exp(-x^2)$tabulated by Miller and Gordon (1931) and Lohmander and Rittsten (1958), has its maximum value at $1/2x$ given by $x_0=0{\cdot}9241$. The solution of equation (8) is therefore $\eta_0=x_0^2=0{\cdot}8539$.

Let us now assume that in the plasma the generation function is of the form

$$g(\eta)=\lambda n_0\,e^{-\gamma\eta} \quad \ldots\ldots(9)$$

where λ and γ are constants. When $\gamma=0$ the rate of generation of ions per unit volume is uniform. When $\gamma=1$ the rate of generation is proportional to the electron density. In general, values of γ greater than unity correspond to those cases where ion generation is a multiple stage process dependent upon the electron density. When, however, the density of the neutral gas is appreciably less at the centre of the plasma, γ may have negative values.

Changing to $s=\lambda z(M/2kT)^{1/2}$, the 'transformed plasma equation' (7) can be integrated to give, for $\gamma>0$,

$$s=\frac{2}{\pi(\gamma-1)}\{\gamma^{1/2}D(\gamma\eta)^{1/2}-e^{\eta(\gamma-1)}\,D(\eta^{1/2})\} \quad \ldots\ldots(10)$$

except for $\gamma=1$ (that is, ions are generated at a rate proportional to the electron density), when

$$s=\frac{2}{\pi}\left\{D(\eta^{1/2})-\int_0^\eta D(\eta^{1/2})\,d\eta\right\}$$
$$=\frac{2}{\pi}\eta^{1/2}\left(1-\frac{1}{3}\eta-\frac{1}{30}\eta^2-\frac{1}{210}\eta^3-\frac{1}{1512}\eta^4\ldots\right). \quad \ldots\ldots(11)$$

In this case, when $\eta=\eta_0$, then $s_0=0{\cdot}405$. Also, when $\gamma=0$ (that is, ions are generated at a uniform rate)

$$s=\frac{2}{\pi}e^{-\eta}D(\eta^{1/2}). \qquad \ldots\ldots(12)$$

In this particular case at the Tonks-Langmuir boundary $s_0=1/\pi\eta_0^{1/2}=0{\cdot}344$. Finally, when $\gamma<0$

$$s=-\frac{2}{\pi(\gamma-1)}\left\{\left(-\frac{\pi}{4}\gamma\right)^{1/2}\operatorname{erf}(-\gamma\eta)^{1/2}+e^{\eta(\gamma-1)}D(\eta^{1/2})\right\}. \qquad \ldots\ldots(13)$$

The value of η_0 was calculated by Tonks and Langmuir in the two cases $\gamma=0$ and $\gamma=1$ and was found to be 0·9244 and 0·8540, respectively, as compared with 0·8539 given by equation (8). The first value, for $\gamma=0$, is in error, and it would appear that $\eta_0^{1/2}$ has been given by mistake. In figure 1 η is plotted against s/s_0 for $\gamma=-4,\ -2,\ -1,\ 0,\ 1,\ 2$ and 4.

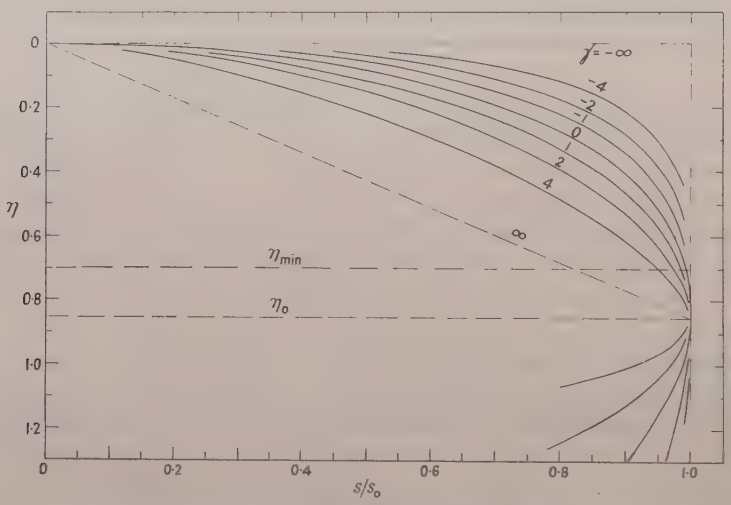

Figure 1. Curves showing the variation of η against s/s_0 for different values of γ. The extreme limits for the plasma boundary potential in terms of η are shown as $\eta_{\min}$ and η_0.

2.3. *Ion Current and the Wall Potential*

The mean speed $\langle v\rangle$ of the positive ions is found by putting

$$\psi=(2kT/M)^{1/2}(\eta-\eta_\zeta)^{1/2}$$

in equation (4). Using the transformed plasma equation (7), one obtains

$$\langle v\rangle=\frac{2}{\pi}\left(\frac{2kT}{M}\right)^{1/2}D(\eta^{1/2}) \qquad \ldots\ldots(14)$$

and expressed in this way as a function of η the mean speed is independent of the spatial variation in the rate of ion generation. At the Tonks–Langmuir plasma boundary $D(\eta_0^{1/2})=1{\cdot}271$, and the mean ion speed is

$$\langle v\rangle_0=1{\cdot}144\,(kT/M)^{1/2}. \qquad \ldots\ldots(15)$$

The positive ion current crossing the plasma boundary is

$$I_+=(2kT/M)^{1/2}n_0e/\pi\eta_0^{1/2}c. \qquad \ldots\ldots(16)$$

If for simplicity it is supposed that there is no secondary emission of electrons at the walls, then on equating the electron and ion fluxes, one obtains

$$\eta_w = \ln\{\pi\eta_0^{1/2}(M/4m)^{1/2}\} \qquad \ldots\ldots(17)$$

where $\eta_w = -e\phi_w/kT$, and ϕ_w is the wall potential with respect to the centre of the plasma. In this derivation it is assumed that the ions generated in the sheath region are of negligible effect.

2.4. *The Mean Square Ion Speed*

The mean square speed of the positive ions in the plasma is found by setting $\psi = (2kT)M)(\eta - \eta_\zeta)$ in equation (4) and integrating with respect to η. Thus

$$\langle v^2\rangle = \frac{kT}{M}(e^\eta - 1) \qquad \ldots\ldots(18)$$

a result which has been obtained elsewhere (Harrison, unpublished A.E.R.E. report). At the Tonks–Langmuir plasma boundary

$$\langle v^2\rangle = 1{\cdot}349\,kT/M. \qquad \ldots\ldots(19)$$

Close to the plane of symmetry in the centre of the plasma, $\eta \ll 1$, and expanding equation (18) one has to first order

$$\tfrac{1}{2}M\langle v^2\rangle + \tfrac{1}{2}e\phi = 0$$

and the mean kinetic energy of the ions is half that of the maximum possible energy.

§ 3. The Plasma Boundary

The transformed plasma equation provides an extreme limit for the plasma boundary, identified by η_0 and s_0. However, in the actual discharge the value of η at the plasma boundary given by η_b, say, is such that $\eta_b < \eta_0$ and the precise value will depend in part on the nature of $g(\eta)$.

It has been shown by Bohm (1949) that for the formation of a stable plasma boundary, in a discharge having plane symmetry, the ions must have a minimum kinetic energy of $\frac{1}{2}kT$. A similar result has been obtained by Allen and Thonemann (1954) without Bohm's original assumption of a zero electric field at the boundary. In both cases it has been assumed that the rate of ion generation is virtually zero in the sheath and, less realistically, that the ions arriving at the plasma boundary are monoenergetic.

A more general result may be obtained in the following manner. Let $f(v_b)$ be the distribution function for the positive ion velocities v_b at the plasma boundary; then provided ion generation can be neglected, the distribution function at any point in the sheath becomes $f(v_b)v_b/\{v_b + [(2kT/M)(\eta_b - \eta_0)]^{1/2}\}$. Using this form of distribution function in Poisson's equation

$$\left(\frac{kT}{4\pi e^2}\right)\frac{\partial^2\eta}{\partial z^2} = \int f(v)\,dv - n_0 e^{-\eta}$$

and expanding $\eta_b - \eta_0$ as a power series in $\Delta\eta$, one obtains

$$\left(\frac{kT}{4\pi e^2}\right)\frac{\partial^2\Delta\eta}{\partial z^2} = \Delta\eta\left\{n_- - n_+\frac{kT}{M}\left\langle\frac{1}{v^2}\right\rangle\right\} \qquad \ldots\ldots(20)$$

to a first order. The condition for a non-oscillatory solution at the sheath edge, where $n_- \simeq n_+$, is therefore

$$M\langle v^{-2}\rangle^{-1} \geqslant kT \qquad \ldots\ldots(21)$$

which is the criterion for the formation of a stable plasma boundary. This result is quite general, and has been obtained without considering any specific mechanism of ion transport in the plasma.

In the sheath the ions are accelerated and the product $\langle v^2\rangle\langle v^{-2}\rangle$ tends towards unity as their energy is increased. In general, however, one can say that $\langle v^2\rangle\langle v^{-2}\rangle > 1$ in the sheath, and therefore at the plasma boundary it follows from relation (21)

$$M\langle v^2\rangle > kT \qquad \ldots\ldots (22)$$

which is the original Bohm criterion for a stable plasma boundary with the exception that $\geqslant$ replaces the inequality sign. Clearly, when ions have a mean kinetic energy of $\frac{1}{2}kT$, a sheath does not form except in the extreme case when the ions are monoenergetic; for all other distributions this value of the mean kinetic energy is attained before the sheath edge is reached.

On integrating Poisson's equation, using the distribution function in equation (3) for the collision-free model, one finds

$$\left(\frac{kT}{8\pi e^2}\right)\left(\frac{\partial\eta}{\partial z}\right)^2 = \eta_+\left(\frac{M}{kT}\right)\langle v^2\rangle + n_- - n_0 \qquad \ldots\ldots (23)$$

for both the plasma and sheath regions. Since the left hand side of this equation is positive, it follows from (22) that at the plasma boundary $n_0 > 2n_b$, or $\eta_b > \ln 2$. Thus, the extreme limits of η_b are given by

$$\eta_{\min} < \eta_b < \eta_0 \qquad \ldots\ldots (24)$$

where $\eta_{\min} = \ln 2 = 0{\cdot}6931$, and $\eta_0 = 0{\cdot}8539$ is the Tonks–Langmuir value. The value of $\eta_{\min}$ is shown in figure 1 and it can be seen that in most instances s/s_0 changes by a small amount in the range given by (24). In the two cases $\gamma = 0$ and $\gamma = 1$ one finds that $(s_0 - s_{\min})/s_0$ amounts to 0·7% and 1·5%, respectively, and for most purposes the range of η_b given by (24) defines the position of the plasma boundary.

§ 4. Experimental Results

Probe measurements were made in a plane symmetric positive column of an argon discharge. The discharge was 90 cm long and had a rectangular cross section of 8 cm by 2·5 cm. Two fine wire probes were used, one was situated at the plane of symmetry and the other was located parallel to and 1·0 mm from the wall, as shown in figure 2. The position of the second probe ensured that for most conditions it was on the plasma side of the plasma-sheath boundary.

A number of dual probe characteristics of the probe potentials and the logarithm of the currents were then plotted. Since both branches of the curve tend to be identical the potential difference ϕ_b can be found with reasonable accuracy. The value of η_b was then obtained by determining the temperature from the slope of the straight section of the curve. From 10 runs the experimental value of η_b was found to be $\eta_b = 0{\cdot}74 \pm 0{\cdot}03$ in the pressure range of 0·8 to 4 microns of mercury, and for discharge currents between 0·2 and 0·4 ampere.

It is interesting to notice that in the positive, cylindrical column of a low pressure mercury arc Langmuir and Mott-Smith (1924) found that the ratio of the random electron current densities (and therefore the electron number

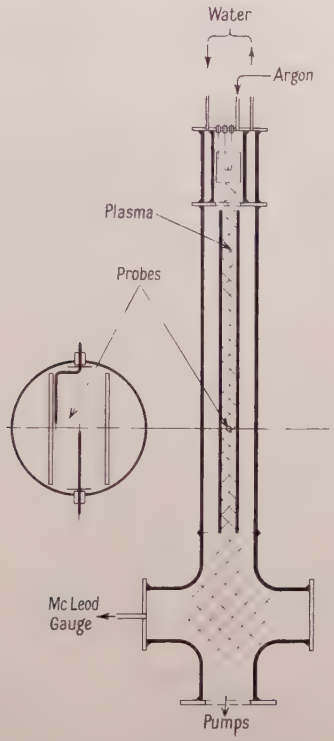

Figure 2. Apparatus used for producing a plane symmetric positive column in argon, showing the position of the probes.

densities) measured on the axis and close to the wall, had a mean value of $n_0/n_b \simeq 2{\cdot}0$ for low pressures in the region of 1 micron of mercury, and hence $\eta_b \simeq 0{\cdot}69$. Killian (1930) observed that $\eta_b \simeq 0{\cdot}7$ in a similar positive column at an even lower pressure of 0·2 microns of mercury. For higher pressures Langmuir and Mott-Smith found that n_0/n_b increased and had a value of approximately 4·0 at 30 microns of mercury. This suggests that at low pressures the neutral gas density close to the tube axis was reduced due to ionization processes, in a manner similar to that suggestd by Allen and Thonemann (1954) in the case of current limitation in the low pressure arc, thus giving a decreased rate of ion generation in this region. The cylindrical plasma may thus tend at low pressures to have the same properties, in so far as they have been discussed in this paper, as the plane symmetric plasma.

Acknowledgment

The authors are indebted to Mr. I. H. Hurdle for experimental assistance.

References

Allen, J. E., and Thonemann, P. C., 1954, *Proc. Phys. Soc.* B, **67**, 768.
Bohm, D., 1949, *The Characteristics of Electrical Discharges in Magnetic Fields*, ch. 3, edited by Guthrie, A., and Wakerling, R. K. (New York: McGraw-Hill).
Harrison, E. R., 1958, *J. of Electronics and Control*, **5**, 319.
Jahnke, E. and Emde, F., 1945, *Tables of Functions* (New York: Dover).
Killian, T. J., 1930, *Phys. Rev.*, **35**, 1238.
Langmuir, I., and Mott-Smith, H., 1924, *Gen. Elect. Rev.*, **27**, 449, 538, 616, 762 and 810.
Lohmander, B., and Rittsten, S., 1958, *K. Fysiogr. Sällsk. Lund. Forh.*, **28** (No. 6), 45.
Miller, W. L., and Gordon, A. R., 1931, *J. Phys. Chem.*, **35**, 2785.
Terrill, H. M., and Sweeny, L., 1944, *J. Franklin Inst.*, **237**, 495, **238**, 220.
Tonks, L., and Langmuir, I., 1929, *Phys. Rev.*, **34**, 876.
Whittaker, E. T., and Watson, G. N., 1950, *A Course on Modern Analysis*, 4th edn (Cambridge: University Press), p. 229.

Susceptibility of Superconducting Spheres

By R. M. MAY and the late M. R. SCHAFROTH
The F.B.S. Falkiner Nuclear Research and Adolph Basser Computing Laboratories, School of Physics†, The University of Sydney, N.S.W.

Communicated by H. Messel; MS. received 25th March 1959

Abstract. We derive an expression for the magnetic susceptibility of a sphere in a homogeneous applied field, assuming a quite general linear relation between the magnetization **M** and induction **B** inside the sphere.

This expression is of interest in analysing experimental results on fine-grained colloidal suspensions of superconductors.

§ 1. Introduction

In this paper we derive an expression for the magnetic susceptibility ‡ κ of a sphere in an applied homogeneous field, when the ratio of the magnetization **M** and the magnetic induction **B** of the material inside the sphere is given (in Fourier space) by some function $K(q)$:

$$\mathbf{M}(\mathbf{q}) = K(q)\mathbf{B}(\mathbf{q}). \qquad \ldots\ldots (1.1)$$

Our treatment is for the so-called 'case of specular reflection' (Bardeen 1956) at the boundary: the 'case of diffuse reflection' has so far been defined only for plane surfaces.

A general expression for the susceptibility of a sphere is of interest in making an analysis of experimental results for the susceptibility of fine-grained colloidal suspensions of superconductors (Shoenberg 1940, Whitehead 1957). This analysis proceeds as follows (cf. Shoenberg 1952): At low frequencies the experimentally measured 'penetration depth' d, which characterizes the depth of penetration of a magnetic field into the material, is defined for specimens of size $R \gg d$ by

$$\left.\begin{aligned} \kappa/\kappa_0 &= 1 - d/R, \quad \text{for a plate of thickness } 2R \\ &= 1 - 2d/R, \quad \text{for a wire of radius } R \\ &= 1 - 3d/R, \quad \text{for a sphere of radius } R \end{aligned}\right\} \qquad \ldots\ldots (1.2)$$

(where κ_0, the bulk susceptibility, is that for a specimen with no penetration at all). On the other hand, in order to interpret, in terms of d, experiments on specimens of size less than or of order of d, it is necessary first to make some assumption as to the nature of the function $K(q)$. One then writes the susceptibility in terms of parameters involved in $K(q)$, and next uses the asymptotic form of this relation in the limit of large R together with (1.2) to get d in terms of such parameters. Finally, these results are combined to obtained an equation which gives the susceptibility of small specimens as some function of d. A comparison between theoretical predictions and experimental results then provides a method of deciding between alternative theories as to the nature of $K(q)$.

† Also supported by the Nuclear Research Foundation within the University of Sydney.

‡ The susceptibility κ is defined as the ratio of the *total* magnetic moment per unit volume to the applied field.

The general expression for the susceptibility of a sphere is derived in § 2; in § 3 we particularize to the London kernel $K_1(q)$ (London and London 1935, London 1950), and to a kernel $K_2(q)$ which has the general form of those suggested on phenomenological grounds by Pippard (1953) and subsequently derived from the microscopic theories of Bardeen, Cooper and Schreiffer (1958) and Bogoljubov (Blatt and Matsubara 1958, May and Schafroth 1959, Bogoljubov 1959†). The analysis outlined above is carried out for these two kernels in § 4. Whitehead's results indicate $K_2(q)$ as the correct one.

§ 2. Susceptibility of a Sphere

To study the penetration law in any definite volume V (bounded by a surface Σ), we begin by introducing a complete orthonormal set $\{\mathbf{u}_k(\mathbf{r})\}$ of vector eigenfunctions for divergence-free fields. These functions are defined by

$$\text{curl curl } \mathbf{u}_k = q_k^2 \mathbf{u}_k \qquad \ldots\ldots (2.1)$$

$$\text{div } \mathbf{u}_k = 0 \qquad \ldots\ldots (2.2)$$

$$(\mathbf{u}_k)_n = 0 \text{ on } \Sigma \qquad \ldots\ldots (2.3)$$

$$\int \mathbf{u}_k \cdot \mathbf{u}_{k'} dV = \delta_{kk'}. \qquad \ldots\ldots (2.4)$$

(For non-zero q_k equation (2.2) is a consequence of (2.1): (2.2) is inserted explicitly to exclude the possibility of $q_k = 0$.) Since **B**, **H** and **M** are divergence-free fields, we may expand them in terms of $\mathbf{u}_k$:

$$\mathbf{H}(\mathbf{r}) = \sum_k H_k \mathbf{u}_k(\mathbf{r}) \qquad \ldots\ldots (2.5)$$

with analogous expressions for B_k and M_k. For an arbitrary kernel function, $K(q_k)$, the following relations hold‡:

$$M_k = K(q_k) B_k \qquad \ldots\ldots (2.6)$$

$$B_k = H_k + 4\pi M_k \qquad \ldots\ldots (2.7)$$

from which we get

$$B_k = \frac{1}{1 - 4\pi K(q_k)} H_k \qquad \ldots\ldots (2.8)$$

$$M_k = \frac{K(q_k)}{1 - 4\pi K(q_k)} H_k. \qquad \ldots\ldots (2.9)$$

We now particularize to the case of a sphere situated in a homogeneous magnetic field.

To construct the relevant set of functions $\mathbf{u}_k$, given by equations (2.1)–(2.4), we first observe that the symmetry of the problem allows us to restrict ourselves to functions of the form (in spherical polar coordinates, with the polar axis parallel to the applied field)

$$\left.\begin{aligned} (\mathbf{u}_k)_r &= u_1(r) \cos\theta \\ (\mathbf{u}_k)_\theta &= u_2(r) \sin\theta \\ (\mathbf{u}_k)_\phi &= 0. \end{aligned}\right\} \qquad \ldots\ldots (2.10)$$

† "*On the principle of compensation and the method of the self-consistent field*" (in Russian), preprint. We are indebted to Prof. Bogoljubov for a copy of this work.

‡ The most general relation between **M** and **B** is $M_k = K_{kk'} B_{k'}$. The implicit assumption made in (2.6), that $K_{kk'}$ is diagonal, is equivalent to assuming specular reflection at the boundary.

Equation (2.1) then requires that

$$\left.\begin{aligned}\frac{2}{r^2}\{u_1+(ru_2)'\}&=q^2u_1\\ \frac{1}{r}\frac{\partial}{\partial r}\{u_1+(ru_2)'\}&=q^2u_2\end{aligned}\right\} \qquad \ldots\ldots(2.11)$$

(the prime indicates differentation with respect to r). The solution of (2.11) which is regular at $r=0$ is

$$u_1(r)=\frac{AJ_{3/2}(qr)}{(qr)^{3/2}}=A\left(\frac{2}{\pi}\right)^{1/2}\frac{\sin(qr)-qr\cos(qr)}{(qr)^3} \qquad \ldots\ldots(2.12)$$

$$u_2(r)=\frac{A}{2}\left\{\frac{J_{3/2}(qr)}{(qr)^{3/2}}-\frac{J_{1/2}(qr)}{(qr)^{1/2}}\right\}=\frac{A}{2}\left(\frac{2}{\pi}\right)^{1/2}\frac{\{1-(qr)^2\}\sin(qr)-qr\cos(qr)}{(qr)^3}. \qquad \ldots\ldots(2.13)$$

The boundary condition (2.3) on the surface of the sphere requires

$$u_2(R)=0. \qquad \ldots\ldots(2.14)$$

This fixes the eigenvalues $q=q_k$: if we call z_k the kth positive root of the equation

$$F(z)\equiv\frac{J_{3/2}(z)}{z^{3/2}}-\frac{J_{1/2}(z)}{z^{1/2}}=0 \qquad \ldots\ldots(2.15a)$$

or

$$\tan z=\frac{z}{1-z^2}\quad(z\neq 0) \qquad \ldots\ldots(2.15b)$$

then these eigenvalues are

$$q_k=z_{k/R}. \qquad \ldots\ldots(2.16)$$

Inserting this into (2.12) and (2.13), we get the components $u_1{}^k$, $u_2{}^k$ of the kth eigenfunctions: the constant A_k is determined by the normalization condition (2.14), i.e.

$$\int_{\text{sphere}} d^3x|\mathbf{u}_k(\mathbf{r})|^2=\frac{4\pi}{3}\int_0^R r^2dr(u_1{}^2+2u_2{}^2)=1. \qquad \ldots\ldots(2.17)$$

Substituting for u_1 and u_2, and making the change of variables $t=qr$, this becomes

$$\frac{8}{3}\frac{A^2}{q^3}\int_0^{qR=z}dt\left[\frac{3}{2}\frac{\sin^2 t}{t^4}-\frac{3\sin t\cos t}{t^3}-\frac{\sin^2 t}{t^2}+\frac{3}{2}\frac{\cos^2 t}{t^2}+\frac{\sin t\cos t}{t}+\frac{1}{2}\sin^2 t\right]=1. \qquad \ldots\ldots(2.18)$$

This integral may be evaluated by a series of partial integrations, commencing with the term to the extreme left in the brackets: the ensuing expression is simplified by use of (2.15b), to get

$$A_k=\left(\frac{3}{4R^3}\right)^{1/2}\frac{z_k}{\sin z_k}\left[\frac{z_k{}^2}{2}-1\right]^{-1/2}. \qquad \ldots\ldots(2.19)$$

This completes the evaluation of the set $\{\mathbf{u}_k\}$ for this problem.

One expects that the field in the outside region can be described by the superposition of the applied field $\mathbf{H}_0$ and the field of a magnetic dipole (of strength a) parallel to $\mathbf{H}_0$. If we do this, the outside field $\mathbf{B}'=\mathbf{H}'$ is given by

$$\left.\begin{aligned}(\mathbf{B}')_r&=H_0\left(1-\frac{2aR^3}{r^3}\right)\cos\theta\\ (\mathbf{B}')_\theta&=H_0\left(1+\frac{aR^3}{r^3}\right)\sin\theta\\ (\mathbf{B}')_\phi&=0.\end{aligned}\right\} \qquad \ldots\ldots(2.20)$$

Inside the sphere, we have to determine fields $\mathbf{H}''$, $\mathbf{B}''$ and $\mathbf{M}''$ which satisfy Maxwell's equations, equation (2.6), and the appropriate boundary conditions. $\mathbf{H}''$ is easily found, since it satisfies

$$\text{div } \mathbf{H}'' = 0 \text{ and curl } \mathbf{H}'' = 0 \qquad \ldots\ldots (2.21)$$

throughout the sphere, and has to have continuous tangential component with $\mathbf{H}'$ outside. $\mathbf{H}''$ is thus homogeneous, proportional to $\mathbf{H}_0$:

$$\mathbf{H}'' = (1+a)\mathbf{H}_0. \qquad \ldots\ldots (2.22)$$

We now employ the set $\{\mathbf{u}_k\}$ to expand $\mathbf{H}''$ according to equation (2.5): the coefficients H_k'' are obtained from the orthogonality properties of these eigenvectors.

$$H_k'' = \int_{\text{sphere}} d^3x\, \mathbf{H}'' \cdot \mathbf{u}_k = (1+a)H_0 \int d^3x [u_1 \cos^2\theta - u_2 \sin^2\theta] \qquad \ldots\ldots (2.23)$$

$$= (1+a)H_0 A_k \left(\frac{2}{\pi}\right)^{1/2} \frac{4\pi}{3} \int_0^R r^2 dr \frac{\sin q_k r}{q_k r} \qquad \ldots\ldots (2.24)$$

i.e.

$$H_k'' = \frac{4\pi}{3} R^3 u_1{}^k(R)(1+a)H_0. \qquad \ldots\ldots (2.25)$$

Use of this expression for H_k'' in conjunction with equations (2.6) and (2.7) gives B_k'' and M_k'', and hence $\mathbf{B}''$ and $\mathbf{M}''$.

The parameter a (the dipole strength) can now be determined in two different ways; the requirements that these two expressions for a be identical provides a check on the original trial solution (2.20).

Firstly, a is fixed by the requirement that $\mathbf{B}$ should have a continuous normal component on the surface of the sphere. This condition together with equations (2.8), (2.10) and (2.20) leads to

$$\frac{1-2a}{1+a} = \sum_k \frac{1}{1-4\pi K(q_k)} \left[\frac{H_k''}{(1+a)H_0}\right] u_1{}^k(R). \qquad \ldots\ldots (2.26)$$

Secondly, by its definition, a is related to the total dipole moment of the sphere $\mathcal{M}$ by

$$\mathcal{M} = -aH_0R^3 \qquad \ldots\ldots (2.27)$$

where also

$$\mathcal{M} = \int d^3x\, \mathbf{M} \cdot \left(\frac{\mathbf{H}_0}{H_0}\right). \qquad \ldots\ldots (2.28)$$

With the help of equations (2.9), (2.22) and (2.23), this reduces to

$$-\frac{aR^3}{1+a} = \sum_k \frac{K(q_k)}{1-4\pi K(q_k)} \left[\frac{H_k''}{(1+a)H_0}\right]^2. \qquad \ldots\ldots (2.29)$$

By making use of the relation (2.25) for H_k'', it is readily seen that these two expressions for a are identical, which provides the required consistency test. Substituting for $u_1{}^k(R)$ from (2.12), (2.16) and (2.19), we have

$$\frac{a}{1+a} = \frac{4}{3} \sum_{k=1}^{\infty} \frac{1}{z_k{}^2 - 2} \left[\frac{-4\pi K(z_k/R)}{1-4\pi K(z_k/R)}\right] \qquad \ldots\ldots (2.30)$$

the summation running over all positive roots of equation (2.15).

We now have an expression for the susceptibility κ of a sphere of material with a general kernel function $K(q)$, in a homogeneous field:

$$V\kappa \equiv \mathcal{M}/H_0 \qquad \ldots\ldots (2.31)$$

$$= -aR^3 \qquad \ldots\ldots (2.32)$$

with a given by (2.30).

§ 3. Some Particular Forms of $K(q)$

In this section we calculate κ for various particular forms of the function $K(q)$ which are of interest with regard to superconductors.

3.1. *The Kernel* $K(q) = -\infty$

This kernel function corresponds to no field penetration: that is to say it gives us the bulk susceptibility κ_0, as defined in § 1. Thus, writing $V\kappa_0 = -a_0R^3$, we get

$$\frac{3}{4}\frac{a_0}{1+a_0} = \sum_{k=1}^{\infty}\frac{1}{z_k^2-2}. \qquad \ldots\ldots (3.1)$$

We consider in detail the evaluation of the above sum, because it provides an example of a technique which may be applied in the case of more complicated functions $K(q)$.

Defining the function $F(z)$ of the complex variable z according to equation (2.15a), we observe that in the right-hand half of the complex z plane the function $F'(z)/F(z)$ has poles, with residues $+1$, at the points z_k along the real axis. We next consider

$$I \equiv (2\pi i)^{-1}\int_C \frac{1}{(z^2-2)}\frac{F'(z)}{F(z)}dz \qquad \ldots\ldots (3.2)$$

where the contour C runs around a large semi-circle in the right-hand half of the z plane, and down the imaginary axis $z = iy$. The contribution from the semi-circle vanishes as the radius becomes very large and the integral over the imaginary axis vanishes because the integrand is odd in y—hence the sum of the residues of the integrand in the right-hand half-plane is zero. That is

$$\sum_{k=1}^{\infty}\frac{1}{z_k^2-2} + \frac{1}{2\sqrt{2}}\frac{F'(\sqrt{2})}{F(\sqrt{2})} = 0 \qquad \ldots\ldots (3.3)$$

i.e.

$$\frac{3}{4}\frac{a_0}{1+a_0} = \frac{1}{4} \qquad \ldots\ldots (3.4)$$

whence we get the bulk susceptibility as

$$V\kappa_0 = -\tfrac{1}{2}R^3. \qquad \ldots\ldots (3.5)$$

3.2. *The London Kernel*

The first account of the phenomenology of superconductors was made on the basis of the London kernel $K_1(q)$:

$$K_1(q) = -\frac{1}{4\pi\lambda_L^2 q^2}. \qquad \ldots\ldots (3.6)$$

Substituting this into equation (2.30) we get a_1:

$$\frac{3}{4}\frac{a_1}{1+a_1} = \sum_{k=1}^{\infty}\frac{1}{z_k^2-2}\frac{1}{(\lambda_L z_k/R)^2+1}. \qquad \ldots\ldots (3.7)$$

The procedure outlined above in § 3.1 may be used to find a_1; the essential difference is that here we must take into account two extra poles in the complex z plane, at $z = \pm iR/\lambda_L$, due to the kernel function. One finds (cf. London 1950)

$$a_1 = \frac{1}{2} - \frac{3}{2}\frac{\lambda_L}{R}\frac{\cosh R/\lambda_L}{\sinh R/\lambda_L} + \frac{3}{2}\left(\frac{\lambda_L}{R}\right)^2. \qquad \ldots\ldots (3.8)$$

The susceptibility κ_1 has the limiting forms

$$V\kappa_1 = -\frac{R^3}{2}\left(1 - \frac{3\lambda_L}{R} + 3\left(\frac{\lambda_L}{R}\right)^2 + \ldots\ldots\right) \text{ for } R > \lambda_L \qquad \ldots\ldots (3.9)$$

$$= -\frac{R^5}{30\lambda_L^2}\left(1 - \frac{2}{21}\left(\frac{R}{\lambda_L}\right)^2 + \ldots\ldots\right) \text{ for } R < \lambda_L. \qquad \ldots\ldots (3.10)$$

3.3. *The Kernel Function* $K_2(q)$

We now consider a model kernel defined by

$$K_2(q) = -\frac{1}{4\pi\lambda^2 q^2}, \quad q < \mu$$

$$K_2(q) = -\frac{\mu}{4\pi\lambda^2 q^3}, \quad q > \mu \qquad \ldots\ldots (3.11)$$

with $\mu\lambda < 1$.

This kernel has the same limiting forms as that proposed by Pippard (μ^{-1} is Pippard's 'coherence length'); it also agrees in the limits of small and large q with kernel functions derived from the Bardeen, Cooper and Schreiffer and Bogoljubov theories for the system of electrons in a metal. In the limit of zero temperature, the Bogoljubov treatment gives λ and μ as

$$\lambda = \left(\frac{4\pi n e^2}{mc^2}\right)^{-1/2} \qquad \ldots\ldots (3.12)$$

$$\mu = \frac{9\pi^2}{16}\left(\frac{kT_c}{1{\cdot}13E_F}\right)k_F \qquad \ldots\ldots (3.13)$$

where n is the number density of electrons, k_F and E_F the Fermi wave number and energy, and T_c the superconducting transition temperature; similar expressions hold for the Bardeen, Cooper and Schreiffer theory.

For this kernel it is not possible to obtain an analytic solution such as (3.8) for a, so we evaluate a as a power series expansion in the regions (i) $R < z_1\delta$, (ii) $R > z_1\delta$, where z_1 is the first zero of $F(z)$, $z_1 = 2{\cdot}746$. The length δ has been introduced for formal convenience as $\delta = \lambda(\mu\lambda)^{-1/3}$.

3.3.1. *Small spheres,* $R < z_1\delta$.

Here we may write

$$\frac{3}{4}\frac{a}{1+a} = \sum_k \frac{1}{z_k^2 - 2}\frac{1}{(\delta z_k/R)^3 + 1} \qquad \ldots\ldots (3.14)$$

and since $\delta z_k/R > 1$ for all z_k, this may be expanded in a power series. We find

$$\frac{a}{1+a} = \frac{4}{3}\alpha\left(\frac{R}{\delta}\right)^3\left[1 - \left(\frac{\beta}{\alpha}\right)\left(\frac{R}{\delta}\right)^3 + \left(\frac{\gamma}{\alpha}\right)\left(\frac{R}{\delta}\right)^6 \ldots\ldots\right] \qquad \ldots\ldots (3.15)$$

with

$$\left.\begin{aligned}\alpha &\equiv \sum_k \frac{1}{(z_k^2-2)z_k^3} = 0{\cdot}00886\\ \beta &\equiv \sum_k \frac{1}{(z_k^2-2)z_k^6} = \frac{107}{2^5.5^3.63} = 0{\cdot}00042\\ \gamma &\equiv \sum_k \frac{1}{(z_k^2-2)z_k^9} = 0{\cdot}00002.\end{aligned}\right\} \quad \ldots\ldots (3.16)$$

Thence, for small spheres,

$$V\kappa_2 = -0{\cdot}0118\frac{R^6}{\delta^3}\left[1-0{\cdot}036\left(\frac{R}{\delta}\right)^3+0{\cdot}001\left(\frac{R}{\delta}\right)^6-\ldots.\right]. \quad \ldots\ldots (3.17)$$

3.3.2. *Large spheres, $R>z_1\delta$.*

In this case we first use equation (3.3) to rewrite (2.30) as

$$\frac{3}{4}\frac{a}{1+a} = \frac{1}{4} - \sum_k \frac{1}{z_k^2-2}\left[\frac{1}{1-4\pi K(z_k/R)}\right]. \quad \ldots\ldots (3.18)$$

Then, noting that for large k the zeros z_k are spaced a distance π apart along the real axis, the above sum is found from Euler's summation formula

$$X \equiv 2\sum_{k=1}^{\infty}\frac{1}{z_k^2-2}\left[\frac{1}{1-4\pi K(z_k/R)}\right] = \frac{2}{\pi}\int_{z_1}^{\infty}\frac{dz}{z^2-2}\left[\frac{1}{1-4\pi K(z/R)}\right] - \left[\frac{1}{(z_1^2-2)\{1-4\pi K(z_1/R)\}}\right]+\ldots. \quad \ldots\ldots (3.19)$$

On substitution of the kernel $K_2(q)$ into this, the integral may be performed in a straightforward manner to get

$$\left.\begin{aligned}X &= \frac{4}{3\sqrt{3}}\frac{\delta}{R}\left[1+O\left(\frac{\delta}{R}\right)^2\right] \text{ for } R<\mu^{-1}\\ &= \frac{4}{3\sqrt{3}}\frac{\delta}{R}\left[1+\frac{3\sqrt{3}}{4\pi}(\mu\delta)^2+O\left(\frac{\mu\delta^2}{R}\right)+O(\mu\delta)^5\right] \text{ for } R>\mu^{-1}.\end{aligned}\right\} \quad \ldots\ldots (3.20)$$

Using equation (3.18), a and thence κ_2 may be written as a power series in this quantity X:

$$V\kappa_2 = -\tfrac{1}{2}R^3(1-3X+3X^2+\ldots.). \quad \ldots\ldots (3.21)$$

§ 4. Conclusion

By comparing equations (1.2) and (3.9), we find that for the London kernel the experimental penetration depth d is given in terms of the quantity λ_L occurring in $K_1(q)$ by

$$d = \lambda_L.\dagger \quad \ldots\ldots (4.1)$$

† By use of plausibility arguments, London wrote λ_L as

$$\lambda_L = \left(\frac{4\pi e^2 n_s}{mc^2}\right)^{-1/2} \quad \ldots\ldots (4.2)$$

where n_s is the " number of superconducting electrons " in the metal. Then the experimental result that the penetration depth at zero temperature d_0 is

$$d_0 \simeq 2\times\lambda \quad \ldots\ldots (4.3)$$

(λ defined by (3.12)) is used to infer the fraction of superconducting electrons at absolute zero

$$n_{s0}/n \simeq 0{\cdot}3. \quad \ldots\ldots (4.4)$$

For the model kernel $K_2(q)$, equations (1.2), (3.20) and (3.21) give the expression for d:

$$d = \frac{4}{3\sqrt{3}} \frac{\lambda}{(\mu\lambda)^{1/3}} \left[1 + \frac{3\sqrt{3}}{4\pi} (\mu\lambda)^{4/3} + \dots \right]. \dagger \qquad \dots\dots (4.5)$$

Now, for a small sphere, equations (3.10) and (4.1) express the susceptibility in terms of d, for the London theory:

$$V\kappa_1 = -\frac{1}{30} \frac{R^5}{d^2} \left(1 - \frac{2}{21} \left(\frac{R}{d} \right)^2 + \dots \right). \qquad \dots\dots (4.6)$$

Thus for a measurement of the magnetic susceptibility of a very fine-grained colloidal suspension, the London theory anticipates

$$\frac{\kappa_1}{\kappa_0} = \frac{1}{15d^2} \frac{\int R^5 \rho(R) dR}{\int R^3 \rho(R) dR} \equiv \frac{1}{15} \frac{\langle R^5 \rangle}{d^2 \langle R^3 \rangle} \qquad \dots\dots (4.7)$$

where $\rho(R)dR$ is the number of (spherical) particles per unit volume with radius between R and $R+dR$.

On the other hand, the kernel $K_2(q)$ gives a qualitatively different result; combining equations (3.17) and (4.5) leads to

$$\frac{\kappa_2}{\kappa_0} = 0{\cdot}0108 \frac{\langle R^6 \rangle}{d^3 \langle R^3 \rangle} \left\{ 1 - 0{\cdot}016 \frac{\langle R^9 \rangle}{d^3 \langle R^6 \rangle} + \dots \right\} \left\{ 1 + \frac{243\sqrt{3}}{64\pi} (\mu d)^2 + \dots \right\}. \qquad \dots\dots (4.8)$$

Whitehead's experimental results for κ/κ_0 are more consistent with the $(R/d)^3$ dependence implied by $K_2(q)$ than with the $(R/d)^2$ London result. As has been pointed out, this then suggests that d varies like $[1-(T/T_c)^4]^{-1\,3}$, in contradiction to experiments on macroscopic specimens which imply a $[1-(T/T_c)^4]^{-1/2}$ variation.

Acknowledgments

We wish to express our appreciation to Professor H. Messel for his constant interest; one of us (R.M.M.) is also indebted to General Motors Holden Ltd. for a Research Fellowship.

References

Bardeen, J., 1956, *Handbuch der Physik*, XV (Berlin : Springer), p. 315.
Bardeen, J., Cooper, L. N., and Schreiffer, J. R., 1958, *Phys. Rev.*, **108**, 1175.
Blatt, J. M., and Matsubara, T., 1958, *Prog. Theor. Phys.*, **20**, 781.
London, F., 1950, *Superfluids*, Vol. I (New York: Wiley).
London, F., and London, H., 1935, *Physica*, **2**, 341.
May, R. M., and Schafroth, M. R., 1959, *Phys. Rev.*, in the press.
Pippard, A. B., 1953, *Proc. Roy. Soc.* A, **216**, 547.
Shoenberg, D., 1940, *Proc. Roy. Soc.* A, **175**, 49.
—— 1952, *Superconductivity* (Cambridge : University Press).
Whitehead, C. S., 1957, *Proc. Roy. Soc.* A, **238**, 175.

† Although this differs from the form anticipated by London, substitution of numerical values for the various constants on the right-hand side of equations (3.12) and (3.13) leads to a value of d_0 in excellent agreement with the experimental result (4.3).

The β-Decay of ^{239}Np

By R. D. CONNOR† and I. L. FAIRWEATHER†

Department of Natural Philosophy, The University, Edinburgh

Communicated by N. Feather; MS. received 2nd February 1959

Abstract. The β-spectrum of ^{239}Np has been examined using a prolate spheroidal magnetic spectrometer of resolution 2% and tranmission 5%, and partial spectra observed having the following end-point energies and intensities: 713 kev (6·5%), 654 kev (4%), 437 kev (48%), 393 kev (13·5%), 332 kev (28%). The half life is found to be $2{\cdot}34 \pm 0{\cdot}02$ days and the total disintegration energy $Q_{\beta-} = 724 \pm 3$ kev. The observations confirm the level scheme proposed by Hollander, and the possibility of a β-transition of end-point energy less than 100 kev as proposed by Baranov and Shlyagin is examined. The $\log_{10} ft$ values of the partial spectra and the nature of the γ-transitions are discussed in the light of the asymptotic selection rules.

§ 1. Introduction

The β-disintegration spectrum of ^{239}Np has recently been studied by several workers using magnetic spectrometers (Tomlinson, Fulbright and Howland 1951, Graham and Bell 1951, Freedman, Wagner, Engelkemeir, Huizenga and Magnusson 1953, Baranov and Shlyagin 1956), while the conversion electron spectrum has been studied using permanent magnet photographic spectrographs (Hollander, Smith and Mihelich 1956).

The energy levels of ^{239}Pu may also be populated by the α-decay of ^{243}Cm, which has been studied by Asaro, Thompson and Perlman (1953) and by the electron capture decay of ^{239}Am of which the conversion electrons have been observed by Smith, Gibson and Hollander (1957). The γ-rays produced in ^{243}Cm decay have been studied by Newton, Rose and Milsted (1956). The γ-rays emitted after Coulomb excitation of ^{239}Pu have been studied by Newton (1957).

There is at present considerable interest in the level scheme of ^{239}Pu and the purpose of the present paper is to present an account of our study of the β-decay of ^{239}Np in this connection.

Twenty γ-rays have been observed and several level schemes have been proposed (Engelkemeir and Magnusson 1955, Baranov and Shlyagin 1956, Newton, Rose and Milsted 1956, Hollander, Smith and Mihelich 1956, Hollander 1957). The presently accepted scheme is that proposed independently by Newton and by Hollander in which all the previously determined levels were raised by 8 kev. The partial β-spectrum previously considered to populate the ground state is now described as populating the first excited state at 8 kev. In this way the spins and energies of the levels of ^{239}Pu can be brought into agreement with the expected values for the rotational bands of an odd A isotope having quantum number $\Omega = \frac{1}{2}$ (Bohr and Mottelson 1953, 1955). Here Ω is the

† Now at the Physics Department, University of Manitoba, Winnipeg, Canada.

component of the total particle angular momentum along the symmetry axis. The initial level spacing under these conditions ($K=1/2$) should be 'anomalous', followed by a 'normal' ($K=5/2$) spacing, K being the component of I (the total angular momentum) along the axis of symmetry of the nucleus. For the lowest rotational band $\Omega=K$. Further, with an 8 kev level available, the level at 57 kev could be de-excited by both 49 and 57 kev γ-rays, and it had been shown that the 49 kev γ-ray is not strong enough to accomplish this unaided.

When the present investigation was started the ground state spin of ^{239}Np had been measured optically (Conway and McLaughlin 1954, Abraham, Jeffries, Kedzie and Wallmann 1957) and found to be $\frac{1}{2}$.† The measured spin of ^{239}Pu (Bleaney, Llewellyn, Pryce and Hall 1954, confirmed by later workers) is $\frac{1}{2}$. Ordinarily, for the ground state of an odd A nucleus $I=K=\Omega$ and the energies of levels forming a rotational band follow

$$E=\frac{\hbar^2}{2J}I(I+1)$$

where J is the moment of inertia. When $\Omega=\frac{1}{2}$, the rotational spectrum is anomalous having

$$E=\frac{\hbar^2}{2J}[I(I+1)+a(-1)^{I+\frac{1}{2}}(I+\tfrac{1}{2})]$$

where

$$a=\sum_j(-1)^{j-\frac{1}{2}}(j+\tfrac{1}{2})|c_j|^2.$$

$|c_j|^2$ is the probability that the last odd particle has an angular momentum j. The current level scheme (figure 2) having energies 0, 8, 57, 76 kev with spins 1/2, 3/2, 5/2, and 7/2, respectively (Strominger, Hollander and Seaborg 1958), fits this latter spectrum with an empirically determined value of a equal to $-0{\cdot}58$. The results of the present investigation are in accord with this level scheme.

§ 2. Experimental

The beta decay of ^{239}Np was examined using the prolate spheroidal field spectrometer designed by Richardson (1952). This instrument has a collecting power of 5% at a resolution of 2% and is calibrated using the accurately known conversion lines of the Th (B + C) spectrum. The beta particles were detected by means of an anthracene crystal, light guide and EMI 6097 photomultiplier, the latter being mounted outside the main magnetic field of the instrument. Corrections for loss of efficiency in the detector for beta particles of energy less than 100 kev were made relative to the spectrum of ^{35}S on the assumption that its Fermi plot is linear (Connor and Fairweather 1957).

The active material was prepared by Atomic Weapons Research Establishment, Aldermaston, by ion exchange following the neutron irradiation of ^{238}U and was of high specific activity. Sources were prepared by evaporating to dryness a 100 μc drop of 2 mm diameter on a supporting film of V.Y.N.S. resin of thickness 2 μg cm^{-2} onto which a conducting gold film of thickness 5 μg cm^{-2} had earlier been evaporated (Pate and Yaffe 1955). The active regions of these sources were barely visible against the supporting film. The radiochemical purity of the source was confirmed by following the decay of each supply of

† But very recently a value of 5/2 has been obtained (Hubbs and Marrus 1958).

material for seven half-value periods. The result obtained for this period was $2{\cdot}34 \pm 0{\cdot}02$ days in good agreement with that obtained (2·35 days) during the pioneer investigations of Feather (1941, 1947) and the recent determination of 2·346 days by Wish (1956).

§ 3. β-particle Spectra End Points

Several runs were made of the lower energy part of the spectrum containing all the observable conversion electron lines. Two runs were also made on the higher energy part of the spectrum above 290 kev using a 3 mm diameter 200 μc source, the slight loss in resolution being of little importance in the absence of

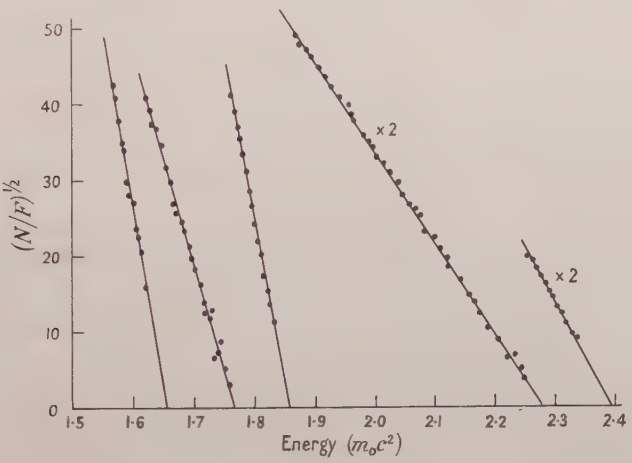

Figure 1.

conversion lines. The Fermi plots resulting from the analysis of the data are shown in figure 1. Any error in the analysis of the relatively weak high energy components will not seriously affect the succeeding analysis. If for the moment any possible components of end-point energy less than 110 kev are ignored, no less than five partial spectra can be clearly resolved. The mean values of the end points of the partial spectra are shown in table 1 together with their relative intensities and $\log_{10} ft$ values calculated from the graphs of Feenberg and Trigg (1950).

Table 1

End-point energy (kev)	Relative intensity (%)	$\log_{10} ft$
713 ± 2	6·5	8·4 ± 1
654 ± 1	4	8·4 ± 0·5
437 ± 1	48	6·8 ± 2
393 ± 2	13·5	7·2 ± 2
332 ± 2	28	6·7 ± 3

An analysis of the runs on the lower energy portion of the spectrum was also made on the basis of the above energy end points. Because of the many conversion lines which were present it was not possible, with the resolution available, to determine with certainty the position of the continuum over much of this

region, but no other component could be observed with energy greater than 110 kev. Baranov and Shlyagin, using a magnetic spectrometer of good resolution report the possibility of a partial beta spectrum with an end point at 70 kev and intensity as great as 22% of the total beta spectrum. In consequence the region below 100 kev was examined closely. There were only three points in this region which appeared to be clear of conversion lines. On the basis of Fermi analysis they could be interpreted as corresponding to a 90 kev β-component of intensity 20% of the total β-spectrum. Such a partial spectrum would have a $\log_{10} ft$ value of about 5·0. Further examination of this region suggested, however, that the overlapping of conversion and Auger lines was so great that the points taken for Fermi analysis were not on the continuum. We were therefore unable to confirm the presence of a β-transition of end-point energy less than 100 kev. This view was strengthened by the fact that we were unable to find, and there is no report in the literature of, γ-rays or conversion lines which such a low-energy disintegration mode would require.

§ 4. Conversion Lines

The energies of the conversion lines of the neptunium spectrum were in good agreement with those found by other workers (Hollander, Smith and Mihelich 1956, Baranov and Shlyagin 1956).

The absolute intensities of those strong conversion lines with electron energies greater than 70 kev were measured and are given in table 2. The lines were not completely resolved and the errors quoted in the table arise from the uncertainty in splitting up those lines which overlap. In the case of the 228 L and 210 M + N conversion lines, which are coincident, the ratio of the intensity of the M + N component to that of the L component of the same transition was taken to be 0·3, as found for the 278 kev transition and as suggested by Newton (1957). It should also be noted that the weaker 226 and 273 kev lines are included in the intensities of the 228 and 278 kev lines respectively.

Table 2

Assignment of conversion line		
Transition energy (kev)	Conversion shell	Absolute intensity (%)
278	M+N	1·3 ± 0·2
278	L	4·4 ± 0·3
228	M+N	1·8 ± 0·3
228	L	5·1 calc. } 5·9 ± 0·6
210	M+N	0·8 calc. }
210	L	2·4 ± 0·3
278	K	16·8 ± 0·2
228	K	17·3 ± 2
106	M+N	2·4 ± 2
210	K	7·5 ± 2
106	L	4·8 ± 2

No conversion lines were found above 300 kev and any such lines must have an absolute intensity of less than 0·1%. This result is in agreement with the observation that the 316 and 335 γ-transitions are very weak. The region below

70 kev contains intense conversion lines many of which are superimposed and it was not possible to separate them.

The K/L ratios of the 278, 228 and 210 kev conversion lines were calculated from the experimental results and are shown in table 3 together with the total conversion electron intensities obtained from table 2. Also shown are Rose's values of the total conversion coefficients for M1 transitions. The tabulation used here is that most recently made available and corrects for the finite size of the nucleus where appropriate (Rose 1958).

Table 3

(1)	(2)	(3)	(4)	(5)
210	$3{\cdot}1 \pm 1$	$10{\cdot}7 \pm 2{\cdot}6$	3·76	$13{\cdot}5 \pm 3$
228	$3{\cdot}4 \pm 0{\cdot}6$	$24{\cdot}2 \pm 2{\cdot}6$	2·92	$32{\cdot}5 \pm 4$
278	$3{\cdot}8 \pm 0{\cdot}3$	$22{\cdot}5 \pm 0{\cdot}7$	1·69	$35{\cdot}8 \pm 1$

(1) Transition energy (kev); (2) K/L ratio (expt.); (3) Total electron intensity $N_e(\%)$; (4) Total conversion coefficient K + L + M (M1); (5) Total transition intensity $N_e + N_\gamma(\%)$.

The K/L ratios, with the measured lifetime of the common initial state (Graham and Bell 1951) of $1{\cdot}1 \times 10^{-9}$ sec indicate that the 210, 228 and 278 kev transitions are M1 with E2 admixtures of $30 \pm 25\%$, $23 \pm 15\%$, and $13 \pm 8\%$ respectively.

The internal conversion coefficients of these three gamma rays have recently been studied in detail with a momentum resolution of 0·35% (Ewan, Knowles and MacKenzie 1957), and it is concluded that a limit of 10% should be placed on the E2 admixture for these radiations. The larger admixtures found here are no doubt due to the inaccuracies in separating the overlapping conversion lines.

Taking these transistions to be pure M1, table 3 also shows the total transition intensities. The presence of E2 admixture would increase the transition intensities. It will be observed that these three transitions, with intensities as given in table 3 and the two highest energy beta-partial spectra (table 1) would populate the ground state rotational band of ^{239}Pu with an intensity of $92 \pm 8\%$ of all beta disintegrations of ^{239}Np. This figure is satisfactorily accommodated in the decay scheme of figure 3.

§ 5. Discussion

5.1. *The β-Transitions*

In table 4 the β-particle end points as determined from Fermi analysis are shown, together with the results from other recent investigations. All the partial spectra are consistent with the allowed shape (figure 1). All intensities in table 4, except those obtained by Hollander, on the basis of γ-ray intensities, were obtained by Fermi analysis of the β-spectrum. There is some agreement

Table 4. ^{239}Np β End Points

705 (7%)	435 (46%)		301 (47%)		Graham and Bell 1951
15 654	440		330 (38%)		Tomlinson *et al.* 1951
15 (4·8%) 655 (1·7%)	441 (31%)	380 (10%)	329 (52%)		Freedman *et al.* 1953
23 (7%) 655	439 (21%)	382 (27%)	327 (45%)		Baranov and Shlyagin 1956
≃650 (5%)	440 (45%)		330 (45%)	212 (5%)	Hollander *et al.* 1956–57
13 (6·5%) 654 (4%)	437 (48%)	393 (13·5%)	332 (28%)		Present work

on end-point energies but the relative intensities vary considerably as between different observers. There is general agreement that about 90% of the transitions have end points in the range 330–440 kev but disagreement as to whether two or three partial spectra are involved. Figure 2 shows the presently accepted disintegration scheme; that suggested by the present work is given in figure 3.

The partial spectra postulated by Hollander include one of end-point energy 212 kev which has not been directly observed in any examination of the β-particles so far reported, but not the 393 kev component. This latter would appear to

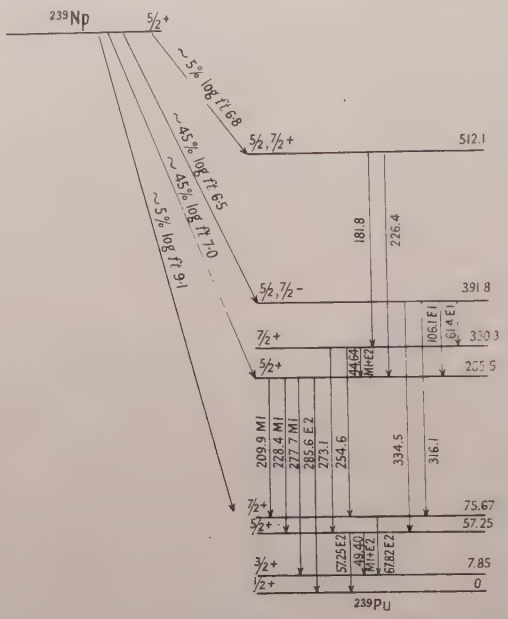

Figure 2.

be definitely established from the present work, but it is possible that we have missed the 212 kev spectrum if its intensity is less than 5%. From the intensities of the γ-rays de-exciting the 512 and 392 kev levels in ^{239}Pu, it is expected that the population of the former is one-tenth that of the latter. If the measured intensity of the 332 kev transition is correct (28%), this would mean a partial β-spectrum of intensity about 3% feeding the 512 kev level. Such a disintegration mode would have a $\log_{10} ft$ value of about 7·1. It should be remarked in this connection that Engelkemeir and Magnusson (1955), from coincidence studies, evaluated the intensity of β-population of the 392 level as 20%.

The spin of the ground state of ^{239}Np presented a problem until very recently. It had twice been measured by different methods, and found to be $\frac{1}{2}$. This value, however, was unacceptable for the purposes of a level scheme for the ^{239}Np β-decay. Each attempt to incorporate it created as many difficulties as it removed. Now, a new determination by another method of high precision has given the value 5/2, and a possible explanation has been advanced for the previous value (Hubbs 1958, private communication). The situation appears at last to be satisfactory, and for present purposes the new value can be accepted. This being done, a β-transition to the $5/2^+$ level at 57 kev is to be expected. In our experiments transitions to the 57 kev and 76 kev levels could not be resolved,

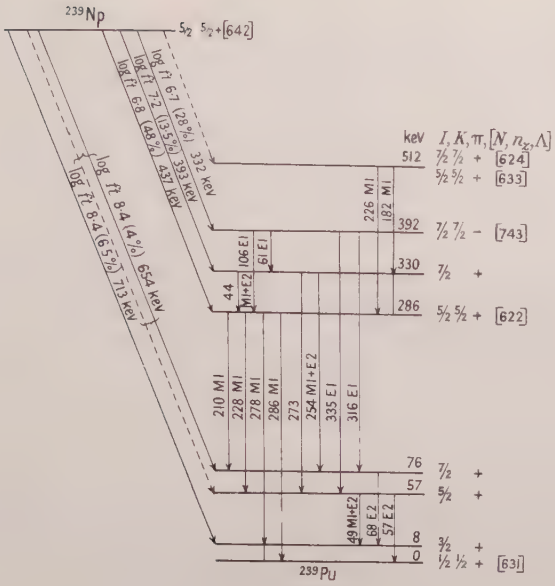

Figure 3.

so the former is shown as a broken line in figure 3. It will be seen, however, that our end-point energy of 654 kev, which was carefully determined, is consistent with the view that two partial spectra are present.

The experimentally determined end points and their associated energy levels in the product nucleus yield a value for the total disintegration energy in the β-decay of ^{239}Np of $Q_{\beta-} = 724 \pm 3$ kev. Our knowledge of the energy differences between the levels of the ^{239}Pu nucleus is chiefly due to the work of Hollander and his associates. The present work is in close agreement with their values (figures 2, 3).

5.2. *The Level Scheme*

It has already been pointed out (Hollander 1957) that the $\log_{10} ft$ values found in the β-decay of ^{239}Np differ somewhat from those expected from the normal selection rules, and that considerable progress can be made by invoking the 'asymptotic' selection rules (Alaga 1955) and the Nilsson diagram (Nilsson 1955). We shall comment briefly on the quantum number assignment of the levels in the light of the Nilsson diagram the relevant portion of which was published by Hollander (1957). The order of the symbols for the levels on figure 3 is $I\ K\ \pi\ [N, n_z, \Lambda]$ where I and K have the usual meaning, π is the parity, N is the principal quantum number of the oscillator and n_z and Λ are, respectively, the components of N and of the particle's orbital angular momentum (l), along the symmetry axis.

Counting up from the 82-proton shell, with two particles per level, gives a probable 5/2 5/2 + [642] configuration for the ground state of ^{239}Np. The state 5/2 5/2 − [523] must be a neighbouring state, but, from the $\log_{10} ft$ values of the β-transitions to the ground state rotational band in ^{239}Pu, it is less likely to represent the ^{239}Np ground state, as is indicated below.

The ^{239}Pu ground state is very likely 1/2 1/2 + [631]. The first four levels form a good example of an anomalous $K = 1/2$ rotational band. β-transitions to the levels of spin 3/2, 5/2, and 7/2 would all be allowed, hindered and K-forbidden,

with $\Delta n_z \neq 0$, $\Delta\Lambda \neq 0$, and $\Delta K > \Delta I$. For allowed, hindered transitions in which the asymptotic rules hold we expect $6{\cdot}0 < \log_{10} ft < 7{\cdot}5$ (Mottelson and Nilsson 1959). The fact that the transition is also K-forbidden could well retard it by a factor of 20–30, and thus accommodate the measured value of 8·4. Had the ground state of ^{239}Np been identified by the negative parity configuration mentioned above these β-transitions would have been first-forbidden, hindered and K-forbidden, and we would have expected $\log_{10} ft \gtrsim 9{\cdot}0$.

The fifth and sixth levels of this ground state rotational band would have spins 9/2 and 11/2 and even parity. They are therefore not populated in the decay of ^{239}Np for the same reason that there is no transition between the ground states. These higher levels would have energies of about 164 and 192 kev respectively and there is evidence of weak excitation of them in the α-decay of ^{243}Cm (Asaro, Stephens and Perlman 1957 unpublished, Strominger, Hollander and Seaborg 1958).

The next intrinsic level occurs at 286 kev (K = 5/2) which has a measured lifetime of $1{\cdot}1 \times 10^{-9}$ sec (Graham and Bell 1951). The M1 transitions which principally de-excite this level are therefore slow, an effect which can be accounted for by the fact that they are K-forbidden and violate the selection rules for electromagnetic transitions. A conveniently situated state, 5/2 5/2 + [622] on the Nilsson diagram is probably to be identified with this level. The second member of the normal rotational band is the $7/2^+$ level at 330 kev. The β-transitions to these levels violate the asymptotic rules and their $\log_{10} ft$ values of 6·8 and 7·2 are in good agreement with the expected values for allowed, hindered transitions. The third $9/2^+$ level would appear at 388 kev, but it is only populated by the α-decay of ^{243}Cm; this state would however, have been populated if the ^{239}Np ground state is represented by the alternative negative parity assignment.

The next intrinsic level occurs at 392 kev. Its measured lifetime is $1{\cdot}93 \times 10^{-7}$ sec (Engelkemeir and Magnusson 1955) which implies heavy retardation of the four E1 γ-transitions which de-populate it. A similar retardation in the case of E1 transitions in ^{237}Np has been discussed by Strominger and Rasmussen (1957). The spin of the level is 5/2 or 7/2. States 5/2 5/2 − [752] and 7/2 7/2 − [743] are available, though rather lower on the Nilsson diagram than expected. The 106 and 61 kev E1 transitions to the 5/2 5/2 + [622] state are not K-forbidden but violate the asymptotic rules. The evidence from the α-decay of ^{243}Cm indicates another rotational band based in this level with $K = 7/2$, of which the other members would occur at 434 and 483 kev. We therefore prefer the assignment 7/2 7/2 − [743] for the 392 kev level. The $\log_{10} ft$ value of the β-transition to this level is consistent with the description, first-forbidden unhindered.

The fourth intrinsic level is at 512 kev. The parity is even and a spin of 5/2 or 7/2 is possible. The states 5/2 5/2 + [633] and 7/2 7/2 + [624] are available. If this level is β-populated the expected $\log_{10} ft$ value of 7·1 would suggest an allowed hindered transition, and both these assignments are consistent with this. The decay of ^{239}Am to this level with a $\log_{10} ft$ of about 6·0 indicates a first-forbidden unhindered transition which is again consistent with both. There is thus little on which to base a preference.

Acknowledgments

We would like to thank Dr. Monk of Atomic Weapons Research Establishment, Aldermaston, for preparing the active material, Dr. L. G. Elliott of Atomic

Energy of Canada, Limited, Chalk River, Canada and Mr. J. Kyles of the University of Edinburgh for their helpful advice and criticism and Professor N. Feather for his continuing interest in the progress of this work.

References

Abraham, M., Jeffries, C. D., Kedzie, R. W., and Wallmann, J. C., 1957, *Phys. Rev.* **106,** 1357.
Alaga, G., 1955, *Phys. Rev.*, **100,** 432.
Asaro, F., Thompson, S. G., and Perlman, I., 1953, *Phys. Rev.*, **92,** 694.
Baranov, S. A., and Shlyagin, K. N., 1956, *J. Nucl. Energy II*, **3,** 132.
Bleaney, B., Llewellyn, P. M., Pryce, M. H. L., and Hall, F. R., 1954, *Phil. Mag.*, **45,** 773, 991.
Bohr, A., and Mottelson, B. R., 1953, *K. Danske Vidensk. Selsk. Mat. Fys. Medd.*, **27,** No. 16.
—— 1955, *β- and γ-ray Spectroscopy*, Ed. K. Siegbahn (Amsterdam: North-Holland), p. 468.
Connor, R. D., and Fairweather, I. L., 1957, *Proc. Phys. Soc.* A, **70,** 769.
Conway, J. D., and McLaughlin, R. D., 1954, *Phys. Rev.*, **96,** 541.
Engelkemeir, D., and Magnusson, L. B., 1955, *Phys. Rev.*, **99,** 135.
Ewan, G. T., Knowles, J. W., and MacKenzie, D. R., 1957, *Phys. Rev.*, **108,** 1308.
Feather, N., 1941, British Atomic Energy Report Br. 46.
—— 1947, *Nature, Lond.*, **160,** 749.
Feenberg, E., and Trigg, G., 1950, *Rev. Mod. Phys.*, **22,** 399.
Freedman, M. S., Wagner, F., Engelkemeir, D. W., Huizenga, J. R., and Magnusson, L. B., 1953, quoted by Hollander, Perlman, and Seaborg, 1953, *Rev. Mod. Phys.*, **25,** 469.
Graham, R. L., and Bell, R. E., 1951, *Phys. Rev.*, **83,** 222.
Hollander, J. M., 1957, *Phys. Rev.*, **105,** 1518.
Hollander, J. M., Smith, W. G., and Mihelich, J. W., 1956, *Phys. Rev.*, **102,** 740.
Hubbs, J. C., and Marrus, R., 1958, *Phys. Rev.*, **110,** 287.
Mottelson, B. R. and Nilsson, S. B., 1959, *K. Danske Vidensk. Selsk. Mat. Fys. Medd.*, in the press.
Newton, J. O., 1957, *Nucl. Phys.*, **3,** 345.
Newton, J. O., Rose, B., and Milsted, J., 1956, *Phil. Mag.*, **1,** 981.
Nilsson, S. G., 1955, *K. Danske Vidensk. Selsk. Mat. Fys. Medd.*, **29,** No 16.
Pate, B. O., and Yaffe, L., 1955, *Canad. J. Chem.*, **33,** 15.
Richardson, H. O. W., 1952, *J. Sci. Instrum.*, **29,** 93.
Rose, M. E., 1958, *Internal Conversion Coefficients* (Amsterdam: North-Holland).
Smith, W. G., Gibson, W. M., and Hollander, J. M., 1957, *Phys. Rev.*, **105,** 1514.
Strominger, D., Hollander, J. M., and Seaborg, G. T., 1958, *Rev. Mod. Phys.*, **30,** 828.
Strominger, D., and Rasmussen, J. O., 1957. *Nucl. Phys*, **3,** 197.
Tomlinson, E. P., Fulbright, H. W., and Howland, J. J., 1951, *Phys. Rev.*, **83,** 223.
Wish, L., 1956, *Nucleonics*, **14,** 102.

Direct Measurement of Domain Wall Energy

By L. F. BATES and P. F. DAVIS†
Department of Physics, University of Nottingham

MS. received 16*th October* 1958, in *final form* 25*th March* 1959

Abstract. Attempts have been made to measure the energy of a Bloch domain wall in a Perminvar ring by a modification of a method suggested by Williams and Goertz based on the fact that a cylindrical domain wall within a ring tends to shrink in order to reduce the total energy of the wall.

§ 1. Introduction

Williams and Goertz (1952) produced a cylindrical domain wall within a ring specimen of magnetically annealed polycrystalline perminvar and they suggested a simple method by which the wall energy might be measured. A modified form of this method has been adopted in the measurements described below.

A circular Bloch wall tends to contract in order to reduce its energy. The magnetic field H required to maintain a wall of radius r in equilibrium with this tendency is given by Williams and Goertz as

$$H=\gamma/2I_0r \qquad \ldots\ldots(1)$$

where γ is the energy of unit area of the wall and I_0 is the intensity of spontaneous magnetization of a domain in the material. Thus, in their specimen, with an impedance to wall motion of about 0·02 Oe and assuming the wall energy to be about 1 erg cm^{-2}, Williams and Goertz calculated that a wall of radius less than 0·2 mm would exert a pressure sufficient to overcome the impedance and thus shrink of its own accord.

§ 2. Method of Measurement of Wall Energy

In a material which exhibits wall impedance, due to the presence of dislocations, inclusions, strains, etc., an additional term $g(r)$ must be included in the equation for H to account for the wall impedance:

$$H=\frac{\gamma}{2I_0r}+g(r). \qquad \ldots\ldots(2)$$

When a small Perminvar ring is magnetized by a current i e.m.u. in a wire passing through the middle of the ring, the field at a radius r in the ring is given by $H=2i/r$ and the wall is in equilibrium when

$$2i=\frac{\gamma}{2I_0}+rg(r). \qquad \ldots\ldots(3)$$

As r tends to zero the term $rg(r)$ tends to zero, provided $g(r)$ remains finite, so that for $r=0$

$$2i=\frac{\gamma}{2I_0}, \qquad \ldots\ldots(4)$$

that is, the wall energy γ is given by $4iI_0$.

† Now at English Electric Co. Ltd., Whetstone.

In practice it is not possible to obtain equilibrium for $r=0$, since the current i must be carried by a wire passing through the middle of the ring. In the present experiments the second term on the right in equation (3) was not negligible, even though the central hole in the perminvar rings was very small, and therefore a process of taking minor hysteresis loops was used in order to reduce the impedance term as much as possible.

Impedance to motion is present whether the wall radius is increasing or decreasing, but the tendency to reduction in wall area always assists a decrease in radius. Provided that on the average the peak values of the impedance to wall motion are independent of whether the wall radius is increasing or decreasing, there will be on the average a difference Δi in the value of the field currents necessary to cause enlargement or contraction of a wall given by

$$\Delta i=\gamma/2I_0. \qquad \ldots\ldots(5)$$

Thus, by describing minor hysteresis loops from chosen points on a main cycle, one may make measurements from which the effect of wall impedance may be eliminated, provided that the latter is independent of the direction of motion of the wall. The effect which we wish to measure should cause the centre of each minor hysteresis loop to be shifted along the field axis by an amount corresponding to $\frac{1}{2}\Delta i$, whatever the radius of the wall, whereas unwanted effects should decrease relatively with decrease in radius.

With their comparatively large perminvar rings, Williams and Goertz found that on reversal of the direction of motion of a wall, the wall impedance was nearly the same as before, although a smaller value of the field started a reversal of motion than was required to continue the motion. This result is in accord with modern theories of coercivity which attribute wall impedance to the anchoring effects of inclusions etc. The difference in field observed by Williams and Goertz in their large perminvar rings was, however, too great to be identified with the Δi of equation (5) above. It could be accounted for by deformation and subsequent springing back of the domain wall, as suggested by them. The latter effect should be reduced by using a very thin specimen, since a domain wall may readily deform about an axis parallel to a direction of easy magnetization, in this case the direction of the magnetic field in the specimen during its thermal treatment, but not as readily about an axis perpendicular thereto.

§ 3. Experimental Procedure

Each specimen was a thin, flat, magnetically annealed, Perminvar ring of small external and very small internal diameter. It was magnetized by means of a wire passing through the middle of the ring. It was not necessary for the wire to be very long and straight as equation (3) holds however the current i is linked with the specimen.

Changes in magnetization of a ring were detected by a search coil, usually wound directly upon the ring. In the case of an exceptionally thin ring, the coil was wound on a Perspex case enclosing the specimen. The search coil output was measured by a galvanometer amplifier system. Visual observations of domain boundaries by the Bitter figure technique were not possible, partly because it was difficult to preserve a perfectly clean surface on a specimen. But the movement of a domain boundary was later followed, using polarized light and a photomultiplier detector, by Dr. E. W. Lee and Mr. D. R. Callaby in this Department.

The specimen under investigation was first saturated in one direction by a field which was then reduced to zero. Upon reversal of the field, hardly any change in magnetization was observed until a critical field strength was reached when much of the magnetization was reversed. This critical field strength was taken to be that necessary to nucleate a domain wall within the specimen; and, when once formed, this wall moved a considerable distance under the action of the field. Now, in order to study the behaviour of a domain wall when its direction of motion is reversed, it is necessary to be able to reverse the motion of the wall with a smaller current than is required to nucleate a new wall. The technique adopted was to nucleate a new wall by sending a sudden discharge from a condenser through the magnetizing wire in series with a small carbon resistance. Thus the wall was left close to the inner edge of the specimen, if the discharge lasted for a very short time, and could be moved outwards and then inwards by means of quite small steady currents, as the fields produced by the currents were greatest near the inner edge.

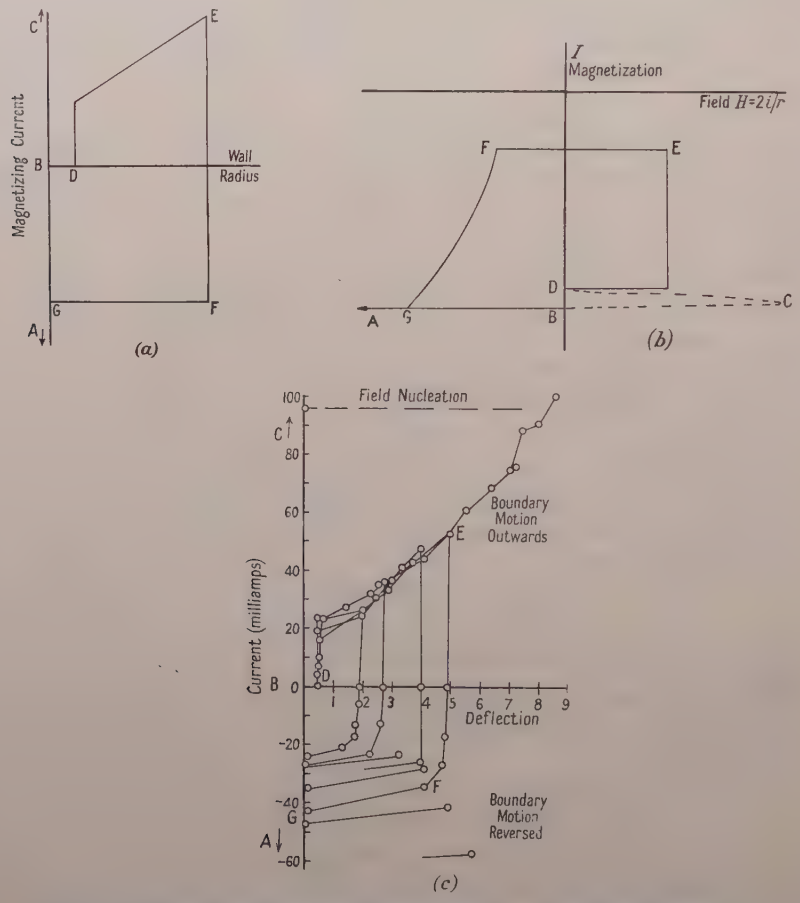

Figure 1. (*a*) and (*b*), explanatory diagrams of sequence of measurements recorded in figure 1 (*c*); (*c*) some minor hysteresis loop measurements for specimen No. 1.

The sequence followed to obtain experimental points may now be described with reference to figures 1(*a*), 1(*b*) and 1(*c*); (*a*) and (*b*) are diagrammatic, (*c*)

shows a set of experimental results. We begin with the specimen in a saturated state represented by the point A off the figures. Removal of the saturation field current takes the specimen to the remanence point represented by B. The passage of the condenser discharge takes the specimen via a point C (off figures 1(*a*) and 1(*c*) to a point D. A steady magnetizing current is now applied and the point E is reached. Then the current is switched off and a smaller current is switched on in the reverse direction and gradually increased until, at the point F, the wall suddenly jumps to the interior edge of the specimen, from F to G. The reason for the large jump is that once the wall moves inwards it proceeds to regions of ever increasing field strength. We thus have readings corresponding to the points E and F for the positions of the wall and the fields at which it moves forward and backward, respectively. The process may then be repeated.

The Perminvar was of normal composition: 45 Ni, 30 Fe and 25 Co. The small rings were cut by a spark cutting technique, each ring being only 0·35 mm in internal diameter. The rings were magnetically annealed. (Since the specimens were so small, we could not make an electronic system for the automatic recording of the re-entrant hysteresis loops with sufficiently rapid response.)

Three specimens were used. Specimen No. 1 had an external diameter of 4 mm and was 150 μ thick; a search coil of 5 turns of No 46 s.w.g. insulated wire was wound directly upon it. Specimen No. 2 had an external diameter of 2 mm and was 200 μ thick; a search coil of 6 turns was wound on it. Specimen No. 3 had an external diameter of 1·4 mm and was only 30 μ thick; it was enclosed in a Perspex case and a search coil of 18 turns of No. 50 s.w.g. wire was wound

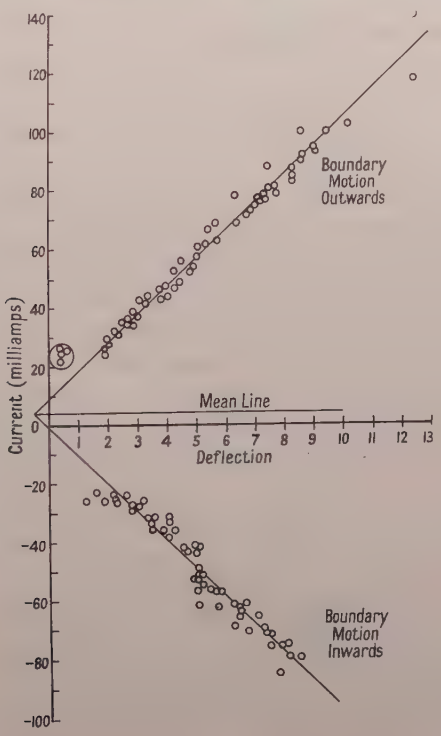

Figure 2. Experimental results for wall movement in specimen No. 1.

thereon; correction for the fact that the coil was not directly wound on the specimen was negligible.

In the accompanying figures, as explained above, the magnetizing field current is plotted against galvanometer amplifier deflection. The latter is proportional to the displacement of the wall. Figure 1(*c*) shows some of the minor hysteresis loop readings obtained with specimen No. 1 as described. Each loop starts from the deflection at which the wall is nucleated, after which the wall moves outwards and then inwards towards the centre of the ring. The field current was changed in small steps in the cases of specimens No. 1 and No. 2, and in figure 1(*c*) the spacing between the points corresponds to the changes in current. Since it was necessary to make a finite change in current to cause the wall to move even when it was just about to jump back to the inner edge of the ring, a mean current at which each jump took place was recorded and plotted in figure 2.

It is seen from figure 1(*c*) that each loop does not initially follow the same path, possibly because of wall deformation, which may give rise to a marked scatter in the readings in addition to any peculiar to the method of measurement. Many readings were therefore taken. Each minor hysteresis loop provided one point in the lower half of figure 2, and one or more points in the upper half, because it is easier to move a wall forwards. Within the limits of experimental error the graphs of current against deflection can be represented by two straight lines, as found by the method of least squares, corresponding to the two directions of motion of the wall. The formulae used for calculating the line $y=mx+c$ from a set of n points (x_i, y_i) where y_i is the deflection and x_i is the magnetizing current are

$$m=\frac{n(\sum x_i y_i)-\sum x_i \sum y_i}{n\sum x_i^2-(\sum x_i)^2}$$

and

$$c=\frac{\sum x_i^2 \sum y_i-\sum x_i \sum x_i y_i}{\sum x_i^2-(\sum x_i)^2}.$$

The small group of readings, surrounded by a large circle in figure 2, which stand apart from the others, are thought to be due to a domain which, although enlarged by the application of a field pulse, did not form a complete circular wall within the specimen until it was further enlarged; these readings were not included in the least squares calculation. The mean of the two lines is almost horizontal and indicates an effect which can be interpreted as a wall pressure inversely proportional to the wall radius and corresponding to an energy of 2·0 erg cm^{-2}; however, the probable error in this result was calculated to be 2·4 erg cm^{-2}, so that it cannot be claimed that the result is significantly different from zero.

The formulae used for calculating the probable errors a_m and a_c in m and c, respectively, were

$$a_m=0{\cdot}6745\left\{\frac{n(\sum \delta_i^2)}{(n-2)[n(\sum x_i^2)-(\sum x_i)^2]}\right\}^{1/2}$$

$$a_c=0{\cdot}6745\left\{\frac{(\sum \delta_i)^2\times(\sum x_i)}{(n-2)[n(\sum x_i^2)-(\sum x_i)^2]}\right\}^{1/2}$$

where $\delta_i=mx_i+c-y_i$ (see Champion and Davy 1943, p. 267).

The formula for calculating the probable error a_γ in γ (see Champion and Davy 1943, p. 268) is

$$a_\gamma^2 = \left(\frac{\partial\gamma}{\partial m_1}\right)^2 a_{m_1}^2 + \left(\frac{\partial\gamma}{\partial m_2}\right)^2 a_{m_2}^2 + \left(\frac{\partial\gamma}{\partial c_1}\right)^2 a_{c_1}^2 + \left(\frac{\partial\gamma}{\partial c_2}\right) a_{c_2}^2$$

where m_1, c_1, and m_2, c_2 are the constants of the two lines from which the value of γ is estimated.

Figure 3 shows results obtained with specimen No. 2. An enlarged scale is used, because the nucleation field corresponded to a very small magnetizing current so that, unfortunately, experiments could not be made over as wide a

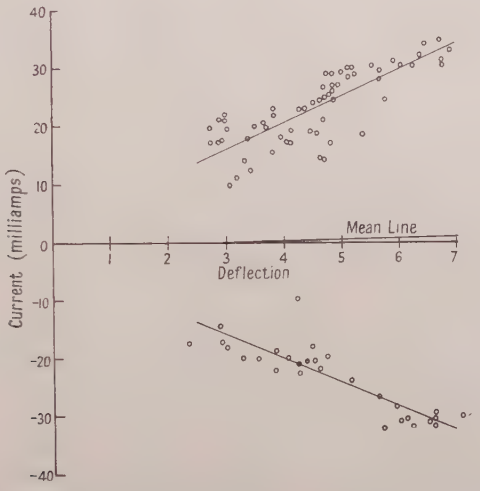

Figure 3. Experimental results for wall movement in specimen No. 2.

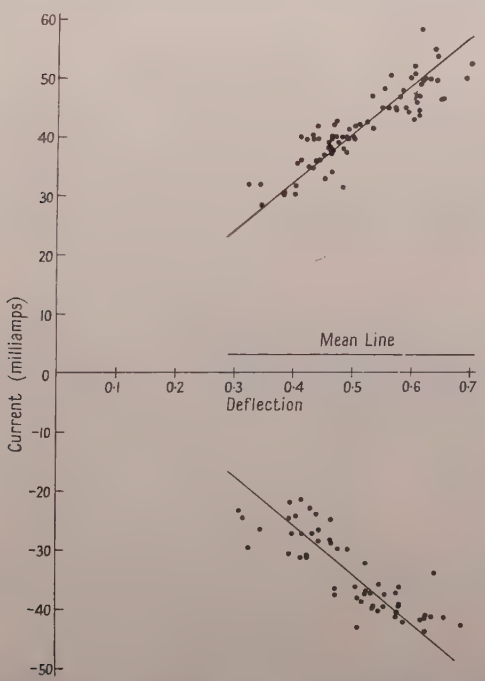

Figure 4. Experimental results for wall movement in specimen No. 3.

range as with specimen No. 1. There is again a discontinuity near the origin and the investigations do not extend to it. The mean of the two graphs gives an effect of 0·2 erg cm^{-2} in the middle of the range of investigations, with a probable error of 0·73 erg cm^{-2}.

Figure 4 gives the results obtained with specimen No. 3 and for the range of wall position investigated, it gives a mean value of 1·6 erg cm^{-2} for the wall energy, with a probable error of 0·9 erg cm^{-2}.

§ 4. Discussion

The experimental results cannot be compared with any reliable theoretical value as the relevant data for magnetically annealed Perminvar have not been published, as far as is known. Williams and Goertz suggested a value of about 1 erg cm^{-2} for their specimen. The inconsistencies in the above values for the three specimens can be attributed to experimental error.

Our technique of taking measurements with a wide range of wall radii should have minimized the effects of chance variations in the difference between the values of the wall impedance for forward and backward motion and should have eliminated wall deformation effects, since at very small radius only the effect sought should predominate. There remains, however, the possibility that radial strain may be present in a specimen and may be important.

Our small specimens behaved very similarly to the larger specimens investigated by Williams and Goertz in that the nucleation field was greater than the wall impedance, and that impedance to a wall moving in one direction was nearly the same as that when the direction of motion was reversed. The wall impedance in our specimens was much higher than that observed by Williams and Goertz. Although consistent values for the wall energy were not obtained, an average value of 1 erg cm^{-2} was indicated.

Acknowledgments

We are grateful to the Electrical and Allied Industries Research Association for financial support which made this work possible and for permission to publish. The numerical calculations were carried out on the Deuce computer of the Nelson Research Laboratories, English Electric Co. Ltd., Stafford, and we are grateful to Mr. C. Robinson for his very kind assistance.

References

Champion, F. C., and Davy, N., 1943, *Properties of Matter* (London : Blackie).
Williams, H. J., and Goertz, M., 1952, *J. Appl. Phys.*, **23**, 316.
Williams, H. J., and Shockley, W., 1949, *Phys. Rev.*, **75**, 179.

Trajectory Plotting in Electron Guns

By G. D. ARCHARD
A.E.I. Research Laboratory, Aldermaston, Berks.

MS. received 26th February 1959

Abstract. A method of representing space charge on a resistance network analogue by means of leak resistances is described and applied to the determination of trajectories in several conventional and unconventional electron guns

§ 1. Introduction

Trajectory plotting in electron guns requires first a knowledge of the potential distribution. This obeys Poisson's equation

$$\nabla^2 V = -4\pi\rho \qquad \ldots\ldots(1)$$

inside the beam, and Laplace's equation

$$\nabla^2 V = 0 \qquad \ldots\ldots(2)$$

outside the beam (V = potential, ρ = space charge density). In addition, the continuity equation

$$\mathrm{div} J = 0 \qquad \ldots\ldots(3)$$

must be satisfied ($J = \rho\sqrt{(2\eta V)}$, $\eta = e/m$) while, for space charge limited emission, the field at the cathode must vanish, i.e.

$$(\partial V/\partial n)_c = 0 \qquad \ldots\ldots(4)$$

(n = normal).

The potential distribution may be determined on a resistance network analogue (Liebmann 1950), provided that currents proportional to ρ are allowed to leak out at each mesh point, the distribution of ρ being governed by equations (3) and (4).

§ 2. Conditions at the Cathode

Equipotentials close to the cathode ordinarily run nearly parallel to it. The space between the cathode and an adjacent equipotential may, therefore, be treated approximately as a plane diode, the current density at any point on the cathode being related to the voltage at a perpendicular distance x away by Langmuir's (1921) expression

$$J_c = \{\sqrt{(2\eta)}/9\pi\}\, V^{3/2}/x^2. \qquad \ldots\ldots(5)$$

The space charge density at a point x away from the cathode will then be

$$\rho = J_c/\sqrt{(2\eta V)} = V/9\pi x^2. \qquad \ldots\ldots(6)$$

Network theory states that the current I which must be allowed to leak out from any mesh point is proportional to ρ; hence from equation (6) it is proportional to

V. Thus it is only necessary to connect each mesh point neighbouring the cathode to earth through a suitable resistance for equation (4) to be fulfilled. Application of Liebmann's (1950) network theory for rotationally symmetric systems leads to the values

$$R = \frac{9}{4}\frac{h}{r}\left(\frac{x}{h}\right)^2 R_0 \qquad \ldots\ldots (7)$$

for the leak resistances, where h is the mesh length, r the radial coordinate, and R_0 the characteristic resistance of the network.

§ 3. Conditions in the Beam

For points other than those neighbouring the cathode, equation (7) must be modified to allow for the fact that in general the local current density differs from J_c. For example, in the case of a spherical diode

$$J = \{\sqrt{(2\eta)}/9\pi\} V^{3/2}/(\alpha\bar{r})^2 \qquad \ldots\ldots (8)$$

where $\bar{r}$ is the radius of the equipotential V, and α is a function of $\bar{r}_0/\bar{r}$ tabulated by Langmuir and Blodgett (1924), $\bar{r}_0$ being the radius of the cathode. The leak resistances for the spherical diode are thus

$$R = \frac{9}{4}\frac{h}{r}\left(\frac{x}{h}\right)^2 h_0 f \qquad \ldots\ldots (9)$$

where $f = (\alpha\bar{r}/x)^2$ and $x = \bar{r}_0 - \bar{r}$.

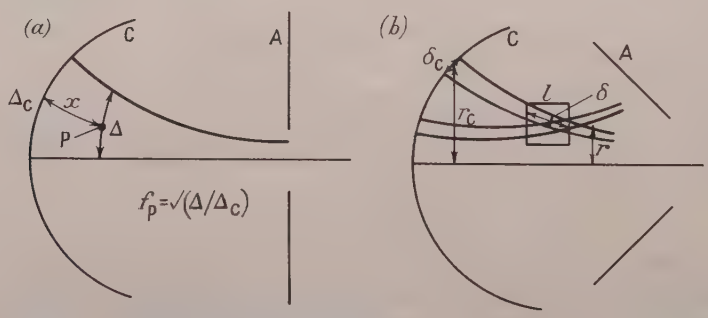

Figure 1. (*a*) Uniformly compressed beam; (*b*) crossing trajectories.

Langmuir's tables show that to a fair approximation $f = \sqrt{(\bar{r}/\bar{r}_0)}$, so that equation (9) fits not only the spherical diode but the plane diode (for which $f = 1$) as well. It is, therefore, reasonable to expect that it will hold, at least approximately, for more general shapes, such as that shown in figure 1 (*a*), where now

$$f = \sqrt{\left(\frac{\text{breadth of beam corresponding to point in question}}{\text{breadth of beam at cathode}}\right)} \qquad \ldots\ldots (10)$$

'breadth' being measured along an arc orthogonal to the trajectories, and x now being the distance of the point in question from the cathode, measured along the beam.

More strictly, the current density J at any point is related to that at a corresponding point on the cathode (figure 1 (*b*)) by the equation

$$Jr\delta = J_c r_c \delta_c \qquad \ldots\ldots (11)$$

where δ, δ_c represent the separation of adjacent tracks near the point in question and at the cathode respectively; for uniform compression $\delta/\delta_c = r/r_c$. This is

another form of the continuity equation (3) and gives leak resistances

$$R=\frac{9}{4}\frac{h}{r}\left(\frac{x}{h}\right)^2 R_0\frac{V^{3/2}/x^2}{(V^{3/2}/x^2)_c}\frac{r\delta}{r_c\delta_c}. \qquad \ldots\ldots(12)$$

Unfortunately in this form V, r and δ enter explicitly, and until some trajectories have been plotted these are not known. The following iterative procedure is therefore indicated : (i) guess the beam shape and work out leak resistances from equations (9) and (10); (ii) read off voltages and plot tracks (either by means of a trajectory plotter or by one of the well-known graphical methods); (iii) work out values of

$$\frac{(V^{3/2}/x^2)}{(V^{3/2}/x^2)_c}\frac{r\delta}{r_c\delta_c}\frac{1}{f}$$

(for uniform compression $r\delta/r_c\delta_c\simeq f$[1]) and multiply the earlier values of R by these; (iv) set up the new R's and repeat. The values of the factors in (iii) were found in several practical examples to lie within $\pm 10\%$ of unity, so that iteration beyond stage (iv) was unnecessary.

§ 4. Crossing Trajectories

Frequently in high perveance guns the compression is anything but uniform, and there is considerable crossing of tracks. According to equation (11), crossing tracks imply infinite current density, corresponding to zero leak resistances. Current density, however, is only an intermediate concept, the actual quantity required for determining R values being the mean space charge density in the neighbourhood of a mesh point (i.e. from the network's point of view, within half a mesh length each way of a mesh point).

The amount of charge brought into a square mesh (figure 1 (*b*)) by a current sheath δ thick is

$$q=2\pi r\delta Jl/\sqrt{(2\eta V)} \qquad \ldots\ldots(13)$$

where l is the length of sheath cut off by the square. If the total current crossing the square is made up of a number of sheaths which may or may not cross each other, the approximate charge per unit volume is

$$\rho=\frac{\sum r\delta Jl}{h^2r\sqrt{(2\eta V)}}=\frac{\sum r_c\delta_c J_c l}{h^2r\sqrt{(2\eta V)}}. \qquad \ldots\ldots(14)$$

This gives leak values

$$R=\frac{9}{4}\left(\frac{x}{h}\right)^2 R_0\frac{V^{3/2}/x^2}{\sum[(V^{3/2}/x^2)_c r_c\delta_c l]}. \qquad \ldots\ldots(15)$$

As a check, if this is applied to a uniformly convergent beam in which the sheaths are equally spaced, the summation becomes

$$(V^{3/2}/x^2)_c r_c\delta_c\sum(l\delta)/\delta$$

and $\Sigma(l\delta)$ simply gives the unit square, so that equation (12) is restored.

§ 5. Applications

The plotting procedure was first tested on a simple Pierce gun shape and found to yield the expected parallel beam. No iteration was needed, as the boundaries of the region requiring leaks could be fairly assigned from the start.

Two slightly less simple shapes (figure 2) were then examined. Trajectories neglecting space charge were first plotted and the beam shapes guessed from these. Leak resistances given by equation (9) were set up and new trajectories plotted. These fell fairly close to the guessed beam boundaries, and only one further iteration was required. It is noticeable that Gun I showed considerable variation in the density of current emitted from various parts of the cathode, while in Gun II density was almost uniform. No crossing of tracks occurred in Gun I, so that equation (15) was not needed. There was slight crossing in Gun II, but not enough to invalidate the simpler equation (9).

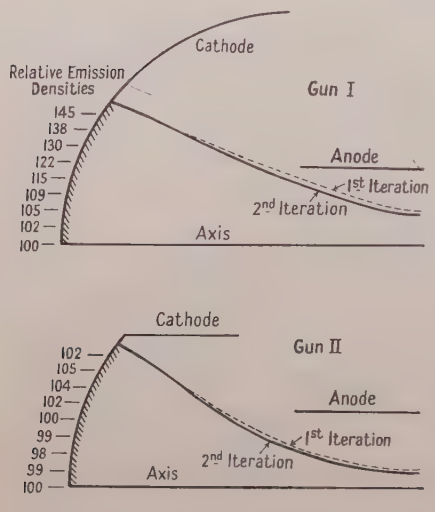

Figure 2. Two types of spherical cathode gun.

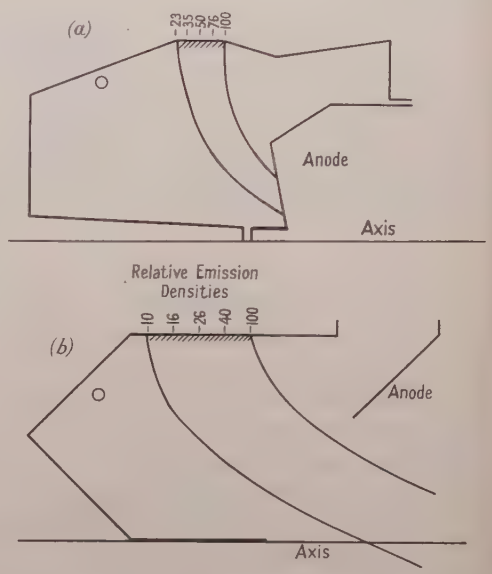

Figure 3. Cylindrical cathode guns.

The microperveance of the guns could be estimated from the formula

$$\text{microperveance} = 2{\cdot}33 \int \left[\frac{(V/V_A)^{3/2}}{x^2} \right]_c dS$$

where V_A = anode voltage and the integration is taken over the area S of the cathode (this follows from Langmuir's expression for the plane diode with units duly adjusted). Guns I and II gave respectively 0·5 and 0·4 microperv, values too small to bring them into the 'high perveance' class required, for example, in travelling wave tubes.

It was found that when points very close to the cathode were used to obtain values of $V^{3/2}/x^2$ these were abnormally high. That this was due to a truncation error was confirmed by setting up a spherical diode on the network, measuring the voltage distribution and comparing with the known analytical solution. The simplest way of avoiding this difficulty is to reject voltages measured at points less than one mesh distant from the cathode, though it is possible also to use a correction curve based on the spherical diode results.

A novel gun shape recently proposed by Kirstein (1958) and promising to fall into the high perveance hollow beam class (figure 3 (*a*)) also required only two

iterations, one using equation (9) and the next, after measurement of voltages, using equation (12). The beam shape agreed with that predicted analytically by Kirstein. There were no crossing trajectories, but the emission varied over the cathode by a factor of 4. The microperveance was estimated at 1·2 micropervs. A simpler version of the same general shape but having tracks actually crossing the axis is shown in figure 3 (*b*). The microperveance was estimated at 1·8 micropervs but the convergence was less satisfactory. It may here be noted that equation (15) covers the case of electrons crossing the axis, although for approximate purposes this can be represented by supplying infinite leaks to the axial points in question (by earthing them).

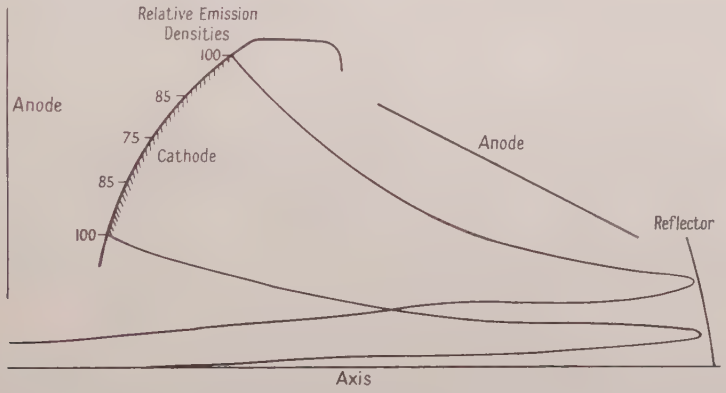

Figure 4. Backward firing gun (' Peashooter 2 ').

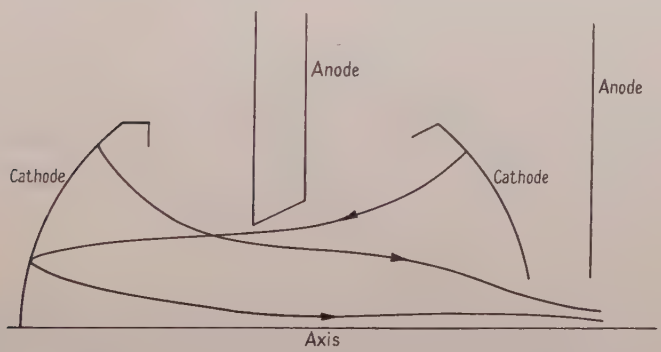

Figure 5. Gun with two cathodes (' Eggwhisk 2 ').

In the case of the guns in figure 3, check plots were made by the graphical parabola method and found to agree quite well with those given by an electronic trajectory plotter. In general the graphical approach may well form a useful first step for guns of awkward shapes.

Another gun of unconventional form appears in figure 4. This resembles Hechtel's (1953) design with the central part of the cathode removed and with the addition of a reflecting electrode and a second electrode at anode potential. It can be seen in a general way that the electrons in the beam moving from left to right repel those in the reverse beam so as to tend to compress it. Thus space charge is in this gun not altogether a hindrance. Also, in Hechtel's gun the emission varied by a factor of 3 over the cathode (the rim of the cathode being nearer to the anode than

its centre). In the present gun, equipotentials from the space to the left of the cathode creep around the edge of the central hole and make up for the local fall-off in the influence of the right-hand anode. The result is relatively uniform emission over the cathode surface. The calculated perveance is a little higher than Hechtel's (4·3 micropervs compared with 3·7) and the smallest cross section of the beam is about 1/100 of the cathode area (Hechtel's compression being 1/45).

Figure 5 shows a further modification in which conventional and backward firing cathodes work in unison. It is essential to make the central anode asymmetrical so that electrons leaving the right-hand cathode reach the reflector before crossing the axis; otherwise they will undergo wide scattering and be lost. The calculated perveance is 6·4 micropervs and the beam is compressed into 1/100 of the left-hand cathode area. Developments of this gun are being investigated.

§ 6. Conclusions

The principle of using leak resistances to represent space charge on a resistance network is applicable to a wide range of electron guns, including those of high perveance and those involving crossing tracks. The principle of driving electrons back through the cathode from which they have come offers hope of increased perveance and greater compression.

Acknowledgments

The author wishes to thank Mr. D. P. R. Petrie for helpful comment, Messrs. R. K. Taylor and R. T. Taylor for the plotting of trajectories, and Dr. T. E. Allibone, Director of the Research Laboratory, Associated Electrical Industries, for permission to publish this paper.

References

Hechtel, R., 1953, *Telefunkenröhre*, 233.
Kirstein, P. T., 1958, *Stanford University M.L. Report* No. 440.
Langmuir, I., 1921, *Phys. Rev.*, **21**, 419.
Langmuir, I., and Blodgett, K., 1924, *Phys. Rev.*, **24**, 49.
Liebmann, G., 1950, *Brit. J. Appl. Phys.*, **1**, 92.

Application of the Mayer Method to the Melting Problem

By H. N. V. TEMPERLEY
Atomic Weapons Research Establishment, Aldermaston, Berks.

MS. received 11*th December* 1958, *in revised form* 24*th February* 1959

Abstract. The antiferromagnetic Ising model can also describe a gas with purely repulsive intermolecular forces, and a comparison of the two is made, the transition of such a 'gas' to a solid-like structure being the analogue of the appearance of an antiferromagnetic structure. Three simple lemmas enable the asymptotic behaviour of the Mayer cluster sums to be related to other combinatorial problems on the lattice, such as that studied by Hammersley and Broadbent (1957). Some information on these problems is already available, but a detailed discussion is reserved to another paper.

The Mayer formalism can be generalized to deal with the antiferromagnetic problem, with the conclusion that the transition is probably first-order and associated with a singularity of the Mayer b-series on the positive real axis of the z variable, but that there is a closer one on the negative real axis. The Mayer β-series can probably be extended beyond the transition and corresponds to a metastable liquid. Its divergence probably represents the absolute limit of the metastable state. The symmetry of the particular model used implies a second transition at a still higher density which may be likened to a change of crystal structure. (The gas of completely rigid molecules is a limiting case, and has only one transition, the transition curve then being a linear relation between P and T.)

These considerations agree well with other work on the antiferromagnetic Ising model. A 'solid–gas' critical temperature seems most unlikely for any realistic interaction, though it could occur for a sufficiently 'soft' one.

§ 1. Introduction

A fundamental question in the theory of changes of phase is the relationship between the intermolecular interaction and the thermodynamic nature of the associated transitions. Until very recently it has been tacitly assumed that these transitions are always associated with an interaction that itself increases in importance as the transition progresses, the classic example being the a/V^2 term in the van der Waals equation. Such terms lead to 'land-slides' hence the name 'co-operative phenomenon'. Theories of sharp transitions have always begun by looking for an interaction with such a property. (The perfect Bose–Einstein gas may seem to be an exception to this sweeping generalization, but it is possible to exhibit its transition as a consequence of 'statistical attraction' between atoms in the same quantum state.)

Machine calculations have shown (Alder and Wainwright 1957, Wood and Jacobson 1957) that a gas of non-attracting rigid spheres would show a transition if compressed to a certain density. It had previously been shown (Temperley

1957) that existing approximate theories give an incorrect radius of convergence for the virial series for one-dimensional models, and therefore give no reliable criterion for the occurrence of a transition. Temperley (1958 a) has also shown that an assembly of non-attracting spheres with a certain 'soft' repulsion probably does *not* show a transition, but that the transition probably would appear if the repulsion were made 'harder'.

The present investigation has the object of finding analytic reasons for transitions in assemblies with purely repulsive interactions. The model used is the Ising nearest-neighbour model with repulsive interactions already studied by Ziman (1951) and Brooks and Domb (1951). This model has been applied to the 'rigid square' and 'rigid cube' problem by Burley; some results of his calculations were reported by Domb (1958). In the limiting case of infinitely strong repulsions between neighbours the two-dimensional model becomes a gas of 'oriented rigid squares', the centres of two squares being prohibited from occupying neighbouring lattice sites. This model is probably the simplest one that can show an 'excluded volume' effect and we shall show that it has a transition.

The method used is based on the Mayer cluster series. Besides studying its early terms, we shall show that it is possible to draw some definite conclusions about the behaviour of the high-order ones. The Ising problem is, as one might expect, found to be closely related to the problem of enumerating single closed domains of points on the lattice, about which some information is available independently (Temperley 1956, 1958 b). Another closely related problem is the enumeration of the number of ways in which a connected array can be formed by using a given number of *links* of the lattice. This has been studied by Hammersley and Broadbent (1957) and has many physical applications of its own. Any study of the series expansions of a partition function which attempts to draw conclusions about the later terms of a series solely from a study of trends of the earlier ones is always a little suspect. Temperley (1958 a) found quite a number of instances of 'small number effects' which persist through distressingly large numbers of the terms of such a series expansion.

The investigation has also thrown light on the relationships between the transition and the divergences of the two Mayer series. Many of Mayer's conclusions (1940) will be substantiated, but the model is probably too simple to possess two critical temperatures of the kind suggested by Mayer. We believe that the actual phase transition is associated with a singularity of the z-series, as Mayer suggested. The virial series can probably be extended beyond the transition, and its divergence seems to correspond, not to a second critical temperature, but to the limit of a metastable state. The Mayer series cannot itself be expected to describe the 'solid-like' phase, since it contains no parameter describing the unequal distribution of atoms over sub-lattices, i.e. the occurrence of an ordered state. We shall show how the cluster-series approach can be modified to allow for this, and a few terms of the more general series can be written down by inspection of the corresponding terms of the ordinary series in the light of our lemmas.

§ 2. Existing Knowledge about the Antiferromagnetic Ising Model

We recall that, with appropriate transcriptions, the same model can describe antiferromagnetism, order–disorder in alloys, and similar effects in adsorbed films with localized sites (Brooks and Domb 1951). To this list we now add the

'lattice gas' with purely repulsive interactions. The corresponding model with attractive interactions was studied by Yang and Lee (1952) who showed that it could give a very satisfactory picture of the formation of a liquid, liquefaction corresponding to the formation of large domains. They showed that the transition could only occur for the case corresponding to vanishing magnetic field, that is to a density of the gas of just half the maximum possible. Their theorem does not hold in the antiferromagnetic case.

It follows rigorously from Onsager's work (1944) that for zero field there is a transition at a value of the interaction given by $\exp(2J/\boldsymbol{k}T) = 1 + \sqrt{2}$, the energy of a like pair of neighbours being taken as $+J$ and that of an unlike pair as $-J$, the antiferromagnetic case thus corresponding to positive J. In discussing the lattice gas, we shall follow Yang and Lee (1952) and identify negative magnets with sites occupied by a molecule and positive magnets with empty sites. An isolated molecule has four neighbouring sites. If we bring two isolated molecules together we gain *two* like–like interactions, resulting in a total energy change of $4J$, since increasing the $- -$ neighbours necessarily results in increasing the $+ +$ neighbours by a like number, if the total number of negatives is held fixed. It is natural to take a completely empty vessel, corresponding to all positive magnets, as having energy zero. In the magnetic case the Boltzmann factor associated with the introduction of one negative magnet leaving all its neighbours positive is $\exp(-2\mu H/\boldsymbol{k}T)\exp(8J/\boldsymbol{k}T)$, since four pairs of neighbours have changed from like to unlike. In this way, we can determine the transcriptions to be used, which are summarized in table 1 for convenience.

Table 1. Corresponding Quantities in Lattice Gas and Magnetic Models

Quantity	Symbol	Corresponding magnetic quantity
Fugacity	z	$x^{-4}\exp(-2\mu H/\boldsymbol{k}T)$
Energy per pair of neighbouring molecules	$4J$	$4J$
Density	$1/v$	$(1+M)/2$
Mayer interaction function	f	x^2-1

In the above table $x = \exp(-2J/\boldsymbol{k}T)$.

There is no transition if $J/\boldsymbol{k}T$ is smaller than Onsager's value, but if it becomes larger, an antiferromagnetic structure can exist for a finite magnetic field. (The actual existence of such a structure in the magnetic case has now been established experimentally for quite a number of magnetic salts, see, for example, Garrett (1951), Gorter (1951) and many later papers.) The analogue of the antiferromagnetic region is the existence of a solid-like ordered state of the lattice gas, the case of completely rigid molecules corresponding to J/T becoming very large. We are thus particularly interested in the shape of the antiferromagnetic region near $T=0$. Simple considerations of energy show that at $T=0$ the antiferromagnetic state becomes unstable, relative to a parallel one, at a positive magnetic field given by $\mu H = 4J$, which, using table 1, seems to suggest that the transition in the lattice gas should take place at $z=1$. Assuming this Brooks and Domb (1951) obtain a figure of 0·226, which, in the present context, is the predicted limiting density of the lattice gas at the transition (a density of unity corresponding to all sites being filled).

However, it does not follow that the limiting value of z is unity. (In fact, it is probably less.) Suppose it approaches a value z_0 at $T=0$. Then the shape of the antiferromagnetic region near $T=0$ is given by

$$\mu H = 4J - \tfrac{1}{2}\boldsymbol{k}T\log z_0$$

that is, that the boundary in the H–T plane has a *finite outward slope* at $T=0$. In fact, Ziman (1951) found exactly such a result, but until it is confirmed it must be regarded as suspect because it was derived using Bethe's approximation, which cannot always be trusted to describe details properly. The outward 'bulge' in the antiferromagnetic region found by Ziman seems 'odd' physically, but no convincing argument against it is known to the author, and an inward slope is also quite possible physically.

§ 3. The Partition Function of the Lattice Gas

We consider a plane square lattice of L sites occupied by N molecules, so that L/N represent the 'volume per molecule' v. For completely rigid molecules v can never be less than 2, but in all other cases a completely filled lattice is possible. Following Mayer and Mayer (1940) we write down the partition function as

$$\sum \prod_{i,j} (1+f_{ij}) \qquad \ldots\ldots(1)$$

where $1+f_{ij}$ is the Boltzmann factor for the interaction between the molecules i and j, and the summation sign means that the product is to be evaluated for each of the N molecules occupying all the L sites in turn. As Mayer shows, (1) can be expressed as

$$\text{Coefficient of } z^N \text{ in } \exp\left(L\sum_l b_l z^l\right) \qquad \ldots\ldots(2)$$

where $L\,b_l$ stands for the result of taking the sum of all possible 'connected f-products' associated with l molecules (e.g. for three molecules the sum is $f_{12}f_{23}+f_{12}f_{13}+f_{13}f_{23}+f_{12}f_{13}f_{23}$), letting each of the l molecules range over all of the L sites, evaluating the sum in all such cases, adding up and finally dividing by $l!$. All this is quite general, the b_l's being the Mayer cluster sums. For our special model we must write

$$f_{ij} = -1 \text{ for } i \text{ and } j \text{ on the same site} \qquad \ldots\ldots(3)$$

$$f_{ij} = f = \mathrm{e}^{-4J/\boldsymbol{k}T} - 1 \text{ for } i \text{ and } j \text{ on neighbouring sites} \qquad \ldots\ldots(4)$$

f_{ij} being zero in all other cases. Thus any configuration of l molecules on the lattice sites which can be joined up into a connected whole by factors of the type (3) or (4) contributes to b_l.

3.1. *Definitions*

We shall refer to a factor of type (3) as a 'pin' and to one of type (4) as a 'link'.

The generating function (2) is, in fact, the grand partition function for L sites. Since the b_l's are not of uniform sign, we cannot safely use standard theory involving steepest descents, though Mayer shows (1940) that the formal results that it suggests are, in fact, correct. We have, for example,

$$\frac{\overline{N}}{L} = \frac{1}{v} = \sum_l l\,b_l z^l \qquad \ldots\ldots(5)$$

$$P = \boldsymbol{k}T\sum_l b_l z^l \qquad \ldots\ldots(6)$$

whenever the series on the right-hand sides are convergent. We can also use Yang and Lee's device (1952) of turning the above expressions 'inside out' and so obtaining expansions in inverse powers of z. We begin with the lattice completely filled, which corresponds to an energy of $4LJ$, since there are $2L$ pairs of sites and a completely empty lattice has zero energy. As we have pointed out already, the symmetry between positive and negative magnets in the magnetic case implies a symmetry between molecules and vacancies. For a fixed N, if we increase the number of nearest neighbour molecule pairs we increase that of nearest neighbour vacancy pairs by a like number, so that we can, if we wish, start with a completely full lattice and progressively 'add vacancies' to it, introducing a factor $\exp(-4J/\boldsymbol{k}T)$ for each pair of neighbouring vacancies, while the addition of an isolated vacancy would, in the magnetic case, introduce a Boltzmann factor, $\exp(2\mu H/\boldsymbol{k}T)\exp(4J/\boldsymbol{k}T)$ the second factor being required because the signs of four nearest-neighbour interactions are reversed if we remove one molecule (negative magnet). Thus we may replace (2) by

$$\text{Coeff. of } z^N \text{ in } z^L \exp\left(\frac{-4LJ}{\boldsymbol{k}T} + L\sum_l b_l z^{-l} x^{-8l}\right) \qquad \ldots\ldots (7)$$

using table 1 for the relation between z and H, the b_l's being exactly the same quantities as before. For a finite L expressions (2) and (7) are finite polynomials in z and can be obtained from one another simply by reversing the order of the terms, but the cluster series are always infinite, and expressions such as (5) and (6) can only be used within their region of convergence, similarly the corresponding series in inverse powers of z can only be so used.

Yang and Lee (1952) found that, in the 'ferromagnetic' case, both types of series converge right up to the point $z=x^4$, corresponding to no magnetic field. The behaviour in the 'antiferromagnetic' case is quite different, a singularity of the series corresponding, almost certainly, to the boundaries of the antiferromagnetic region. On reflection, one sees that this difference is to be expected. In the antiferromagnetic, region one of the interlacing sub-lattices tends to be occupied preferentially by negative magnets (molecules), and this pattern persists over domains comparable with the whole lattice in size. Neither of the above forms of Mayer series contains any parameter that can describe this ordering process, so their breakdown is not surprising. (In the ferromagnetic case, the ordering process consists of the formation of large domains of neighbouring molecules or vacancies, a process that does not lead to any asymmetry in the occupation of sublattices, and can be followed by the Mayer formalism as it stands.)

It is easy to modify the cluster series to allow for a possible asymmetrical occupation of sub-lattices, it being only necessary to replace z by a pair of selector variables z_1 and z_2. In any given configuration that contributes to a cluster sum, the indices of these two variables are to correspond to the numbers of atoms on each of the two sub-lattices. For example, the term $b_2 z^2 = z^2(-\frac{1}{2}+2f)$ is to be replaced by

$$-\tfrac{1}{4}z_1^2 - \tfrac{1}{4}z_2^2 + 2f z_1 z_2 \qquad \ldots\ldots (8)$$

the first term corresponding to two molecules on a site in sub-lattice 1, the second to two molecules on a site in sub-lattice 2, while the third corresponds to pairs of neighbours, one on each sub-lattice. We shall consider this series further below. The determination of its early terms is greatly simplified by the use of three

lemmas, which also throw considerable light on the analytic form of the higher terms in all these series.

As in Yang and Lee's ferromagnetic case (1952) the comparison of the magnetic and lattice gas models has proved very illuminating. Before going further, it is helpful to summarize the physical interpretation of the antiferromagnetic Ising model in its new guise.

If the interaction is too 'soft', or the temperature too high, we have a continuous isotherm with no anomalies. (This may be the explanation of the absence of a transition in the model considered by Temperley (1958 a). *Numerical* comparison between a continuous model in three dimensions and a lattice model in two dimensions is not possible.) If we compress a gas with a 'hard' enough interaction, we get a transition, corresponding to the appearance of an ordered structure, while there is also the possibility of a metastable state, corresponding to the continuous extension of the gas-like isotherm into the 'solid' region.

A further consequence of the symmetry of the magnetic model is that, in its new interpretation, it predicts a second transition. In the magnetic case this is trivial and simply corresponds to the fact that the antiferromagnetic structure can be destroyed by a magnetic field of either sign, but in the lattice gas it leads to a very interesting consequence, on account of the asymmetry between expressions (2) and (7). Physically, it is evident that we can destroy the antiferromagnetic domains (molecules preferentially sited on one or the other sub-lattice) *either* by making the density so low that the molecules can avoid one another without forming an ordered structure, *or* else by crowding so many molecules into the vessel that nearly all the sites are required; the remaining small number of 'vacancies' can then gain entropy by being distributed over both the sublattices instead of one, the energy loss through some of them becoming neighbours being negligible if the total number of vacancies is a small fraction of L. From (7) this transition will occur about when $z = x^8 z_0^{-1}$, z_0 being the appropriate singularity of (2). This second transition may be likened to the changes in crystal structure of the solid phase that sometimes occur quite near the melting line, and is an extremely interesting consequence of this very simple model. (It does not occur for completely rigid molecules.)

§ 4. Simplifications of the Mayer Series

Lemma 1.

Mayer diagrams in which two or more molecules on one site are each connected (solely by links) directly or indirectly with any one molecule on another site make no total contribution to the cluster sums. The proof is almost obvious. Consider the simplest case of molecule 1 being directly linked to molecules 2 and 3, both on the same neighbouring site. Then, no matter what other molecules are attached to this group, we can always add, or omit, a pin between molecules 2 and 3 without affecting the connectivity of the diagram. Since a pin always corresponds to a factor -1, diagrams containing such groups cancel in pairs. The same thing applies however long the two paths 1–2 and 1–3 may be, as long as they are formed solely from links.

We define a *network* as a set of simply occupied lattice sites connected solely by links. From lemma 1, it is easy to convince oneself that we need only consider those Mayer diagrams that are made up by joining together single molecules, single

links (between pairs of molecules) and more complicated networks by means of 'pins' inserted at the sites at which the networks overlap.

Lemma 2.

If two networks overlap at more than one site, it is sufficient to consider pins at any one of these sites (which can be chosen arbitrarily from the set).

Let there be n such sites. The number of ways of pinning together the two networks is $\binom{n}{r}$ if r pins are used. Since each pin introduces a factor -1, total contribution is

$$\sum_{1}^{n}\binom{n}{r}(-1)^r=-1,$$

which is exactly what we should get if we allowed pinning at one site only. (r cannot be zero, because the two networks would be disconnected.)

Lemma 3.

The expression (2) can also be written in the form

$$\exp\left[L\sum b_l z^l\right]=(1+z)^L\exp\left[L\sum c_m\left[z/(1+z)\right]^m\right] \quad \ldots\ldots (9)$$

where c_m is the contribution to the cluster sum obtained by pinning together networks containing a total of m sites but omitting single molecules from explicit consideration.

This includes the well-known result that if we confine ourselves to contributions to the cluster sums involving molecules on only one site, we get the factor $1+z$ per site. This can be proved directly if we think of an assembly containing only one site. Its partition function is $1+z$ and the generating function for its cluster sums is consequently $\log(1+z)$. To prove the rest of the lemma, consider the contribution to (2) arising from the presence of up to (say) three labelled molecules, a, b, and c. For the present, we give each molecule its own selector variable. The contribution to the partition function is to be obtained from the expression

$$\begin{aligned}&1+z_a+z_b+z_c+z_a z_b(1+f_{ab})+z_b z_c(1+f_{bc})\\&+z_a z_c(1+f_{ac})+z_a z_b z_c(1+f_{ab})(1+f_{ac})(1+f_{bc}) \quad \ldots\ldots (10)\end{aligned}$$

where the presence or absence of z_a implies the presence or absence of the molecule a in the assembly. This expression has to be summed over all possible configurations of the three molecules within the assembly (*excluding* overlapping configurations with more than one molecule on the same site).

Dividing out by $(1+z_a)(1+z_b)(1+z_c)$ we get

$$1+\frac{f_{ab}z_a z_b}{(1+z_a)(1+z_b)}+\ldots\ldots\frac{f_{ab}f_{bc}z_a z_b z_c}{(1+z_a)(1+z_b)(1+z_c)}+\ldots\ldots \quad \ldots\ldots (11)$$

In evaluating the partition function as a whole (in contrast to individual cluster sums) we exclude configurations in which molecules are on the same site. For other configurations f_{ab} vanishes unless a and b are nearest neighbours, in which case it is equal to f.

Inspection of expression (11) shows that it contains precisely the same products of f-factors as do (1) and (10), only the terms independent of the f's, corresponding to isolated molecules, having been removed. A similar result is easily

seen to be true however many molecules are present. Mayer's analysis (1940) of these products of the f-factors into connected products, each of which gives rise to a cluster sum, can be applied quite as well to (11) as to (10). The further property of expression (11), that, for example, z_a only appears in the form $z_a/(1+z_a)$ can also be shown, by induction, to be true generally. Giving all the molecules the same selector variable z justifies the form (9), similar to a result found empirically by Domb (1949).

These three simple lemmas enable us to sort out various contributions to the cluster series according to the powers of f and $z/(1+z)$ that are involved. Consider first the contribution arising from the simplest possible network, one link between two neighbouring sites. There are $2L$ such links in the lattice, and at least two molecules involved, so we expect a factor $2Lfz^2$ and, by what we have just said, the total contribution to the cluster sum is expected to be $2Lfz^2/(1+z)^2$, the additional factor arising from the possibility of 'pinning' more molecules to either of the two sites. We shall now verify this result explicitly. Let there be a total of r labelled molecules on site A and s on site B. They can be distributed between the two sites in $\binom{r+s}{r}$ ways. This having been done, the one pair that is to be connected by the link can be chosen in rs ways. The net number of ways in which the r atoms all on site A can be connected up by pins, diagrams with odd numbers of pins being reckoned negatively, is known to be $(-1)^{r-1}\ (r-1)!$, with an analogous factor for site B. Multiplying all these factors up and dividing by $(r+s)!$, we conclude that the function of z involved is

$$\sum_1^\infty \sum_1^\infty (-1)^{r+s} z^{r+s} = z^2/(1+z)^2$$

as stated above. If we wish to distinguish between two sub-lattices, we need only notice that the neighbouring sites A and B are necessarily on different sub-lattices, so that the above expression is to be replaced by $z_1 z_2/(1+z_1)(1+z_2)$. For brevity, we shall write w_1 for $z_1/(1+z_1)$ etc.

We can verify in exactly the same way that networks involving two links and at least three molecules lead to the contribution $3Lf^2(w_1^2 w_2 + w_1 w_2^2)$ because such a network necessarily contains two sites on one sub-lattice and one on the other. Inspection of expression (11), and the corresponding expressions for larger numbers of molecules, shows that one factor w is lost whenever an added link has an end in common with one or more links already present. Expressed differently, a single network gives rise to terms in the cluster series in which the power of f corresponds to the number of links, while the power of w corresponds to the number of lattice sites connected up by them.

This work is fairly easily extended to the case of two or more networks overlapping and being pinned together. By lemma 2, we get nothing fresh by pinning together the same pair of networks at more than one point, but if r networks all overlap one another, the pinning introduces the same factor that occurs if we take account of all ways of pinning together single molecules on a site, that is $(-1)^{r-1}(r-1)!$ It is then only necessary to count up the number of distinguishable ways in which any given pattern, made up of single links and networks pinned together, can be disposed on the lattice (which may require care, as many of the patterns have some degree of symmetry). The appropriate powers of f and z are then introduced, according to the totals of links and sites continued in the

networks. Finally, z is changed to w to allow for the isolated atoms being pinned to the same lattice sites.

The cluster sums up to b_8 have been calculated by Katsura (1958) using Domb and Sykes' (1956) result. By the above process, it was easy to verify the terms in the cluster series up to w^5, and to generalize them to deal with the case of unequal occupation of the two sublattices.

§ 5. Study of the Early Terms of the Mayer Series

Katsura's results are summarized below, in powers of the Mayer function f, omitting the well-known terms independent of f corresponding to the coefficients in the expansion of $\log(1+z)$.

Table 2. Cluster Sums up to b_8

	f	f^2	f^3	f^4	f^5	f^6	f^7	f^8	f^9	f^{10}
b_1	0									
b_2	2	0								
b_3	−4	6	0							
b_4	6	−25	22	1	0					
b_5	−8	64	−148	83	8	0				
b_6	10	−130	1676/3	−831	312	54	2	0		
b_7	−12	230	−1572	4299	−4492	1082	312	22	0	
b_8	14	−371	3682	−31685/2	30434	−23263	3114	3341/2	194	6

Table 3. Mayer Cluster Series expressed in terms of the Variables f and w

$\Sigma\, bl\, z^l = \log(1+z) +$	f	f^2	f^3	f^4	f^5	f^6	f^7	f^8	f^9	f^{10}
w^2	2									
w^3		6								
w^4		−7	22	1						
w^5			−60	87	8					
w^6			116/3	−406	352	54	2			
w^7				578	−2500	1406	324	22		
w^8				−521/2	6832	−14545	5340	3649/2	194	6

In the light of the work in the last section, we are led to try the effect of expressing the b_1 series in terms of f and w. This has been done, and the results are given in table 3.

The advantage of this representation is that it exhibits directly the contributions to the cluster sum according to the numbers of links in the networks that make it up, for example, the terms involving powers of fw^2 represent the result of 'pinning' together single links (a term involving f^2w can only arise from an extremely large domain whose perimeter is negligible compared with its area). Unfortunately this segregation of terms according to the number of links makes it difficult to say anything about probable radii of convergence of the resulting sub-series from a study of the early terms; for example, we have only four terms of the power series in fw^2. We can, however, get a great deal of information about the asymptotic behaviour of the various types of term by using known results on the enumeration of domains and connected patterns of links, but we defer this to a later paper. Meanwhile, we note that the largest terms occur when the indices of f and w are roughly

equal, so that we may expect the radius of convergence of the whole series to be determined by Mayer diagrams with the corresponding property.

The above results have been verified, by direct counting of diagrams, as far as $f^5 w^5$. Inspection of these diagrams enables one to determine the modifications to be made in the corresponding terms of the cluster series when we distinguish between the two interlacing sublattices, variables z_1, z_2 or w_1, w_2 referring to sites on each sub-lattice. There are more terms in the generalized cluster sum than there are in table 4, because of the existence of certain 'odd' types of network, for example, for five sites, the 'Greek cross' contains four sites from one sub-lattice and only one from the other, the distribution for all other networks being 3–2. We quote the result below

$$\begin{aligned}\tfrac{1}{2}\log\{(1+z_1)(1+z_2)\} &+ 2f w_1 w_2 + 3f^2 w_1 w_2 (w_1+w_2) - 7f^2 {w_1}^2 {w_2}^2 \\ &+ 18f^3 {w_1}^2 {w_2}^2 + 2f^3 ({w_1}^3 w_2 + w_1 {w_2}^3) + f^4 {w_1}^2 {w_2}^2 \\ &+ ({w_1}^3 {w_2}^2 + {w_1}^2 {w_2}^3)(-30f^3 + 43f^4 + 4f^5) \\ &+ \tfrac{1}{2}({w_1}^4 w_2 + {w_2}^4 w_1) f^4 + \ldots\ldots \qquad \ldots\ldots (12)\end{aligned}$$

This series must be used with care. For example, it is tempting to break it off after a finite number of terms, to put z_1 and z_2 equal to $z\,e^{\theta}$ and $z\,e^{-\theta}$, so that θ is a parameter measuring the asymmetry of the occupation of the two sub-lattices, and then to look for evidence of an anomaly in the partition function as a function of θ. We already *seem* to get a result of the kind sought if we stop at the second term of the series. We seem to obtain a typical second-order transition of Ehrenfest type if f is positive and greater than unity, the first derivative of the partition function with respect to θ always vanishing at $\theta = 0$, while the second derivative changes sign if $4f = (1+z)^2$, so we might expect a finite equilibrium value of θ for larger values of z. In fact, this conclusion is completely false, first because positive f corresponds to ferromagnetic interaction between neighbours, whereas it clearly needs an anti-ferromagnetic interaction to cause segregation on to one sub-lattice, secondly, because it is easy to convince oneself that the second derivative of any actual partition function with respect to θ can never vanish at all. Consider, for example, the completely 'rigid' case in which nearest neighbour pairs are forbidden altogether ($f = -1$). In a 2×2 assembly the partition function is easily seen to be $1 + 4z \cosh\theta + 2z^2 \cosh 2\theta$ the second derivative of which with respect to θ is quite certainly always positive when $\theta = 0$ and a similar result holds for any larger lattice.

The expected result is that the model should show 'spontaneous antiferromagnetism', that is that the equilibrium value of the parameter θ should be finite within a certain domain of values of the parameters f and z. We already know one boundary point of this domain from Onsager's work (1944), which corresponds to $f = 2 - 2\sqrt{2}$, $z = x^{-4} = (\sqrt{2}+1)^4$. At this point the equilibrium value of θ after the transition is zero, but, as we travel up the transition curve in the direction of increasing numerical values of f (i.e. towards the completely rigid case), we expect the transition to involve jumps in the value of θ to progressively higher values, this conjectured behaviour of θ being quite similar to that of the spontaneous magnetization in the ferromagnetic case. If it is correct, it would almost certainly imply a jump in the interaction energy, and therefore a first-order transition everywhere except at the Onsager point, just as in Yang and Lee's discussion of the gas–liquid (ferromagnetic) case (1952).

One possible approach to the problem would be on the lines of Domb's (1949) treatment of the ferromagnetic problem. We should begin with a completely ordered antiferromagnetic distribution, and describe departures from it by means of an ascending series in e^{θ} or $e^{-\theta}$. Such a series has not yet been found, the difficulty being that an ordered antiferromagnetic distribution can be uniquely defined only when the lattice is exactly half filled. A second approach is suggested by the so-called 'high-temperature series' in the ferromagnetic problem. This series gives equal weight to positively and negatively magnetized configurations but the appearance of spontaneous magnetization is indicated by the first derivative with respect to magnetic field taking an indeterminate value (of the type $0 \times \infty$) at zero field. We are thus led to look for corresponding behaviour of series (12) when differentiated with respect to θ, θ afterwards being put equal to zero. The situation is more complicated than it is in the ferromagnetic case. Tables 2 and 3 seem to show that whether we work with z or w as an expansion variable, the signs of successive terms in the Mayer series alternate. This means that, for positive z, the sum of the series is finite at its limit of convergence, so that it should be possible to continue it analytically to larger values of z.

The radius of convergence of a series such as (12) does not, therefore, determine the transition, whether we work with the variable z or w. What is required if the above conjecture about the 'spontaneous antiferromagnetism' is correct is that, when we differentiate (12) with respect to θ, the coefficient of $\sinh\theta$ 'diverges to infinity', which is only possible if it has a singularity on the *positive* real axis of z or w. (Negative or complex singularities give finite contributions for positive w and can be 'subtracted out'.)

It is obvious from (12) that terms involving equal powers of z_1 and z_2 contribute nothing when differentiated with respect to θ, so that the existence of 'spontaneous antiferromagnetism' must be attributed to one or both of two possible causes : (*a*) The existence of highly asymmetric domains (it is possible to draw large connected domains containing as many as three times as many sites from one sublattice as from the other). (*b*) The existence of terms in the cluster sum corresponding to symmetric domains unevenly occupied. If we differentiate terms like $w_1^{k} w_2^{k}$ and $w_1^{k} w_2^{k+1} w_1^{k+1} w_2^{k}$ with respect to θ, we find that the alternation of signs between terms involving even and odd numbers of sites is unaffected, and we can establish a similar result for the asymmetric domains, the differentiations introducing various functions of m, but not affecting the positions of the singularities of (12). It will be shown in a later paper that (12) *in fact* also has singularities on the *positive* real axis of z and, further, that the most important such singularity probably arises from cause (*b*) above, the asymmetric domains turning out to be relatively scarce, this more than counterbalancing the larger factors introduced by differentiation with respect to θ.

Study of the virial series for the gas-like region is inconclusive since for $f = -1$ its coefficients are very small residues arising from the subtraction of much larger sums of even and odd powers of f. For example, for $7\beta_7$ we find 130648–129953, β_1 to β_3 inclusive being negative, while β_4 to β_7 are positive. (Thus we have a clear example of a 'rigid molecule' model in which the virial coefficients are not all positive.) Burley (private communication) has found that β_8 and β_9 are negative. Thus it is difficult to say anything definite about the convergence of the virial series from a study of its early terms.

Brooks and Domb (1951), working with a formula equivalent to Mayer's result

$$z = \frac{1}{v} \exp\left(- \sum_k \beta_k v^{-k} \right) \qquad \ldots\ldots (13)$$

obtain a 'smooth' series, all the terms up to v^{-8} being positive (though Burley (private communication) has found that the terms v^{-9} and v^{-10} are negative), which appears not to diverge until $1/v = \frac{1}{2}$, and to join up smoothly with an alternative series valid in the immediate neighbourhood of $v = 2$. Brooks and Domb (1951) suggest that this extension describes a metastable state. (There is evidence that some properties of metastable liquids, e.g. density and viscosity, *can* be joined up *smoothly* with those of the stable liquid.)

§ 6. Discussion

If we refer back to lemma 2 we see that it has the effect of introducing a factor -1 whenever two networks have one or more sites in common. If we take the exponential of the transformed cluster series, this result implies that the original Ising problem has been replaced by that of forming links into connected networks, and then disposing them on the lattice in such a way that no two networks overlap. In the new problem each link is assigned a factor f and each site uses a factor w. However, this is not the only way in which the Ising problem of disposing *points* on the lattice is related to the Hammersley and Broadbent (1957) problem of disposing *links* on the lattice. Various writers have pointed out that, if we write down the partition function in the well-known form

$$f = \sum_{ij} \prod (\cosh H + \mu_i \mu_j \sinh H)(\cosh K + \mu_i \sinh K)$$

(the summation sign implying summation over $\mu_i = \pm 1$), only terms containing even powers of all the μ's after the product is multiplied out contribute anything. It is readily verified that there is a 1–1 correspondence between such a term and a diagram drawn on the lattice according to the following rule :

The link ij is inserted whenever the factor $\mu_i \mu_j \sinh H$ is present in the product and, when all the links have been put in, each site intersected by an even number of links is assigned the factor $\cosh K$, while each site intersected by an odd number of links gets the factor $\mu_i \sinh K$.

Thus, the Ising problem is also equivalent to the problem of laying down links on the lattice, assigning a factor $\tanh H$ to each link and $\tanh K$ to each site intersected by an odd number of links, see, for example, Katsura (1958). In a later paper it will be shown that these two transformations of the two types of problem into one another are particular cases of a much more general result (there is in fact a continuous range of such transformations). Since information about the 'link' type of problem is available independently of the work on the Ising problem, a detailed comparison is profitable.

In particular, it has been possible to get information about the analytic behaviour of the Mayer b-series expressed as a function of z or w. The alternation of signs is certainly to be expected for a 'rigid molecule' model, since the way that the Mayer series is built up implies that successive terms correspond to the progressive subtracting away of configurations involving more and more overlaps. (In fact, the alternation probably persists throughout the antiferromagnetic range of interactions.) Study of the 'link' problem definitely shows that b_l should behave like $C_1(-A)^l + C_2 B^l$ with $A > B$, so that the series *has* a singularity on the

positive real axis, as anticipated earlier in this paper, but that allowance has to be made for the fact that this is not the nearest singularity to the origin.

Acknowledgments

I wish to thank Professor C. Domb, Drs. M. F. Sykes and M. E. Fisher and Mr. D. M. Burley for helpful discussions and correspondence, also the Director of the Atomic Weapons Research Establishment for permission to publish this paper.

References

Alder, B. J., and Wainwright, T. E., 1957, *J. Chem. Phys.*, **27**, 1208.
Brooks, J. E., and Domb, C., 1951, *Proc. Roy. Soc.* A, **207**, 343.
Domb, C., 1949, *Proc. Roy. Soc.* A, **199**, 199.
—— 1958, *Nuovo Cim. Suppl.*, **9**, 9.
Domb, C., and Potts, R. B., 1951, *Proc. Roy. Soc.* A, **210**, 125.
Domb, C., and Sykes, M. F., 1956, *Proc. Roy. Soc.* A, **235**, 247.
Garrett, C. C. B., 1951, *Proc. Roy. Soc.* A, **206**, 242.
Gorter, C. J., 1951, *J. Phys. Radium*, **12**, 281.
Hammersley, J. M., and Broadbent, S. R., 1957, *Proc. Camb. Phil. Soc.*, **53**, 629, 642.
Katsura, I. S., 1958, *Progr. Theor. Phys.*, **20**, 192.
Kihara, T., and Kaneko, S., 1957, *J. Phys. Soc. Japan*, **12**, 994.
Mayer, J. E., and Mayer, M. G., 1940, *Statistical Mechanics* (New York : Wiley).
Onsager, L., 1944, *Phys. Rev.*, **65**, 117.
Temperley, H. N. V., 1956, *Phys. Rev.*, **103**, 1.
—— 1957, *Proc. Phys. Soc.* B, **70**, 536.
—— 1958 a, *Proc. Phys. Soc.*, **71**, 238.
—— 1958 b, *Disc. Faraday Soc.*, **25**, 92.
Wood, W. W., and Jacobson, J. D., 1958, *J. Chem. Phys.*, **27**, 1207.
Yang, C. N., and Lee, T. D., 1952, *Phys. Rev.*, **87**, 404.
Ziman, J. M., 1951, *Proc. Phys. Soc.* A, **64**, 1108.

An Investigation of the Protons, Deuterons and Tritons from the Bombardment of ^{9}Be with 5·7 MeV ^{3}He

By S. HINDS and R. MIDDLETON

Atomic Weapons Research Establishment, Aldermaston, Berks.

Communicated by K. W. Allen; *MS. received* 25*th February* 1959, *in final form* 3*rd April* 1959

Abstract. A thin beryllium target has been bombarded by 5·7 MeV ^{3}He particles and the charged reaction products analysed with a high precision broad-range magnetic spectrograph. Angular distributions of nine proton groups, four deuteron groups and a single triton group have been measured. Most angular distributions exhibit strong forward maxima suggesting that the reactions, at least in part, proceed via a direct process.

§ 1. Introduction

It has long been realized that the investigation of ^{3}He induced nuclear reactions might prove to be a particularly fruitful source of nuclear data. In general, Q-values are favourable and frequently it is possible to excite nuclei which hitherto have proved difficult to investigate. Little is yet known about the relative importance of the various possible reaction mechanisms, but there are reasons for believing that direct processes may play an important role at certain energies (Butler 1957). If this is the case then it may be possible to extract useful data from angular distribution measurements in a similar way as for deuteron stripping reactions.

Few detailed investigations of ^{3}He reactions have yet been reported and the majority of the work which has appeared has been concerned with (^{3}He, p) reactions at low incident energies. At such energies it is likely that the fraction of the reaction proceeding via a direct process is small and may well be masked by Coulomb effects. Holmgren, Bullock and Kunz (1956) have measured the angular distributions of the four highest energy proton groups from the reaction ^{9}Be(^{3}He, p)^{11}B at an incident energy of 2 MeV. They conclude that their results are not inconsistent with compound nucleus formation. More extensive measurements have been made by Schiffer, Bonner, Davies and Prosser (1956) on several proton groups from ^{6}Li, ^{11}B and ^{12}C at energies up to 4·7 MeV. Resonances were observed in the excitation functions and, although no strong forward peaks were observed in the angular distributions, neither was symmetry observed about 90°. Thus, at energies below 4·7 MeV there would appear to be little evidence in favour of (^{3}He, p) reactions proceeding predominantly via a direct process.

A more likely ^{3}He reaction to proceed via a direct process is (^{3}He, d). In this case stripping may occur since it is necessary only to strip off a single nucleon as opposed to two in the case of a (^{3}He, p) reaction. Favouring this mechanism are the results of angular distribution measurements made on the inverse processes, namely (d, t) and (d, ^{3}He). Holt and Marsham (1953) and El-Bedewi (1951) report strongly peaked triton angular distributions from ^{6}Li and ^{9}Be respectively. These results have been successfully fitted with theoretical curves calculated by Newns (1952) for a pick-up process.

In this communication measurements are reported of the angular distributions of eight proton groups from the reaction $^{9}Be(^{3}He, p)^{11}B$, four deuteron groups from the $^{9}Be(^{3}He, d)^{10}B$ reaction and also one triton group from the $^{9}Be(^{3}He, t)$ reaction leading to the ground state of ^{9}B. The results suggest that a direct reaction mechanism is important at the bombarding energy of 5·7 MeV employed in this experiment, but further work at higher bombarding energies is required before this can be established with certainty.

§ 2. Experimental Procedure

Singly charged ^{3}He ions have been accelerated in the Aldermaston 6 MeV Van de Graaff generator to an energy of about 5·7 MeV. The emergent beam was deflected through 90° by a 60 cm radius magnet and was collimated by a slit system immediately prior to entering the target chamber. This slit, which was 2 mm wide by 0·25 mm high, served the dual purposes of defining the object for the spectrograph and limiting the energy spread of the incident beam. After collimation the beam current was reduced to about 0·5 μA, which proved to be the maximum current the target would stand before breaking. No direct measurement was made of the energy spread, but measurements made with the spectrograph indicate it to be less than 2 kev.

The beryllium target was prepared by evaporation and consisted of a 15 $\mu g\,cm^{-2}$ layer supported on a 8 $\mu g\,cm^{-2}$ film of carbon. It was not possible to make a self-supporting target of this thickness and considerable difficulty was experienced in choosing a satisfactory backing material. Formvar, which has proved satisfactory when using a deuteron beam, ruptured almost immediately under ^{3}He bombardment. Gold films of about 100 to 150 $\mu g\,cm^{-2}$ thickness were also tried, and although they withstood bombardment, they gave rise to a troublesome background of elastically scattered ^{3}He particles. Eventually carbon films were tried and found to be very satisfactory.

The charged reaction products from the target were analysed by a high precision broad-range magnetic spectrograph. This instrument is similar to that described by Browne and Buechner (1956) and utilizes the focusing properties of a homogeneous magnetic field of 50 cm radius. After deflection through a mean angle of 90° the particles are recorded on a 30 inch nuclear plate. Provision has been made for transverse motion of the plate and it is possible to make four exposures on the one plate without breaking the vacuum. The magnet is mounted on a carriage which can be rotated about the target permitting exposures to be made at angles ranging from 0° to 135°. Monitoring of relative exposure strengths is accomplished by integrating the total beam current passing through the target and entering a Faraday cup.

The spectrograph was energy calibrated some time previously using α-particles from ^{210}Po and cross-checked with the more energetic α-particles from ^{212}Po and ^{212}Bi. The position of a group along the plate is determined by measuring its distance from the nearest of five index lines which are photographed on the plate while still in the plateholder. Due to the finite width of a group its position is defined by extrapolating the maximum slope of its high energy edge to the base line. Using the values of $H\rho$ reported by Briggs (1954) for the ^{212}Po, ^{210}Po and ^{212}Bi α-particles, tables have been compiled relating distance from the various index lines with trajectory radius. Thus to determine the energy of a group it is necessary (*a*) to measure its distance from an index line, (*b*) to determine from

the calibration tables its radius of curvature ρ, (*c*) to obtain $H\rho$, knowing the field strength as determined by a nuclear resonance method, and (*d*) to convert this to energy in the $H\rho$ tables prepared by Enge (1954).

The Q-value of the reaction is then calculated using a relativistic equation. More recently the spectrograph calibration has been transferred on to magnetic tape for use with the Aldermaston I.B.M. 704 computer which has been programmed for the computation of Q-values.

In the case of beryllium, twelve exposures were made at angles ranging from $7\frac{1}{2}°$ to 90°. The angular acceptance of the instrument was fixed at $\pm 2\frac{1}{2}°$ and the average exposure strength was about 1000 micro-coulombs. It may be noted that the latter figure refers to the incident singly ionized ^{3}He and not to the doubly ionized beam which enters the Faraday cup. The target was inclined at angle of 60° with respect to the incident beam for all except the exposures made at 80° and 90° when it was reorientated to 45°. Since at one field setting particles differing in energy by a factor of only 2·5 are simultaneously recorded on the plate, and as beryllium is a very light target nucleus, it was necessary to adjust the spectrograph field at the various exposure angles. Fields were primarily chosen to record the deuterons from the reaction ^{9}Be(^{3}He, d)^{10}B; due to the diversity of Q-values of the other reactions, some proton and triton groups were not recorded. Thus, the ground state proton group from the reaction ^{9}Be(^{3}He, p)^{11}B was not observed and the first excited state group was only observed up to 40°.

§ 3. Results

3.1. $^9Be(^3He, p)^{11}B$

A proton energy spectrum from this reaction obtained at an angle of observation of 15° is shown in figure 1 where the proton groups identified as corresponding to states in ^{11}B are labelled numerically, 1 referring to the first excited state, etc. Several groups due to the principal target impurities of carbon and oxygen were observed. These groups were identified by their rate of change of energy with angle and are labelled by the symbols of the residual nuclei. It will be noticed that group 8 is shown cut-off in figure 1; this is because it was almost completely obscured by a strong deuteron group. Also group 12, which arises from a transition to a broad virtual state of ^{11}B, is coincident with the group leading to the fifth excited state of ^{18}F.

It was not possible to determine the absolute Q-value since the exposures were primarily made to measure angular distributions and no precise determination was made of the beam energy. However, it was possible to determine the energy levels since these depend only on the difference between Q-values. It should be noted that since the ground state proton group was not observed, the energy levels have been normalized to be consistent with the value of 4·459 Mev reported for the second excited state by Van Patter, Buechner and Sperduto (1951). This particular state was chosen since it was the lowest level whose corresponding group was observed at all angles of observation. The energy levels thus obtained are shown in table 1 together with the previously reported values. In general, the differences are small and within the limit of experimental errors.

The excited states above 8·667 Mev are virtual and may decay by α-particle emission. The state at 9·87 Mev has previously been observed by Li and Sherr (1954) who observed resonances in the ^{7}Li (α, $\alpha'\gamma$) reaction. They report a

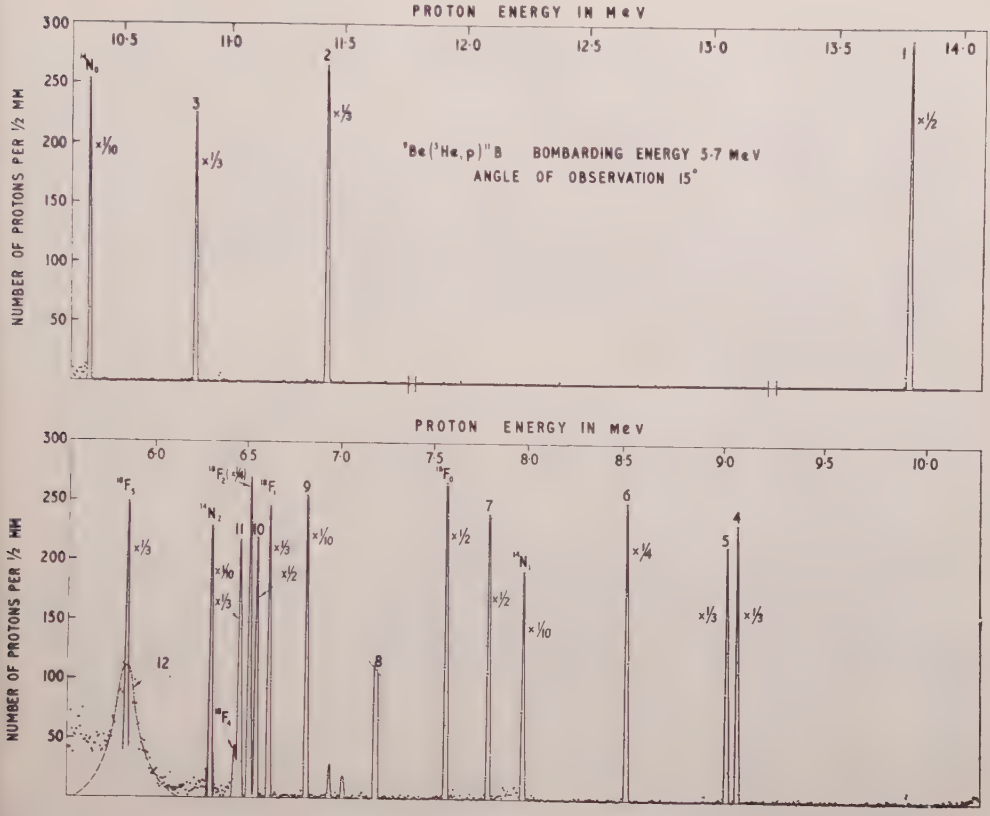
PROTON ENERGY IN MeV
NUMBER OF PROTONS PER ½ MM
$^{9}Be(^{3}He, p)^{11}B$ BOMBARDING ENERGY 5·7 MeV
ANGLE OF OBSERVATION 15°
PROTON ENERGY IN MeV
NUMBER OF PROTONS PER ½ MM

Figure 1. A proton energy spectrum measured at an angle of observation of 15° from the bombardment of a thin target of beryllium with 5·7 MeV ^{3}He.

Table 1. $^{9}Be(^{3}He, p)^{11}B$

Group	Level Energy (MeV) (1)	Level Energy (MeV) (2)	L	Spin and Parity (3)	Spin and Parity (4)	Spin and Parity (5)
0	—	0	—	—	$3/2^-$	$3/2$ to $9/2^-$
1	$2{\cdot}144 \pm 0{\cdot}010$	$2{\cdot}138 \pm 0{\cdot}014$	—	—	$3/2^-$	$3/2$ to $9/2^-$
2	4·459†	$4{\cdot}459 \pm 0{\cdot}014$	0+2	$1/2$ to $5/2^-$	$5/2^-$	$3/2$ to $9/2^-$
3	$5{\cdot}037 \pm 0{\cdot}010$	$5{\cdot}034 \pm 0{\cdot}014$	0+2	$1/2$ to $5/2^-$	$((3/2^-))$	$3/2$ to $9/2^-$
4	$6{\cdot}753 \pm 0{\cdot}010$	$6{\cdot}758 \pm 0{\cdot}013$	(2)	$(1/2^-$ to $9/2^-)$	$(7/2^-)$	$3/2$ to $9/2^-$
5	$6{\cdot}805 \pm 0{\cdot}010$	$6{\cdot}808 \pm 0{\cdot}013$	1+3	$1/2$ to $7/2^+$	$(3/2^+)$	$1/2$ to $11/2^+$
6	$7{\cdot}299 \pm 0{\cdot}010$	$7{\cdot}298 \pm 0{\cdot}012$	1+3	$1/2$ to $7/2^+$	$((5/2^-))$	$1/2$ to $13/2^-$
7	$7{\cdot}989 \pm 0{\cdot}010$	$7{\cdot}987 + 0{\cdot}014$	1+3	$1/2$ to $7/2^+$		$3/2$ to $9/2^-$
8	$8{\cdot}567 \pm 0{\cdot}010$	$8{\cdot}568 \pm 0{\cdot}012$	0	$1/2$ to $5/2^-$		
9	$8{\cdot}923 \pm 0{\cdot}010$	$8{\cdot}927 \pm 0{\cdot}012$	0	$1/2$ to $5/2^-$	$3/2^-, 5/2^-$	$5/2,\ 7/2^+$
10	$9{\cdot}189 \pm 0{\cdot}010$	$9{\cdot}191 \pm 0{\cdot}012$				
11	$9{\cdot}278 \pm 0{\cdot}010$	$9{\cdot}276 \pm 0{\cdot}012$				
12	$9{\cdot}87 \pm 0{\cdot}020$	—				

(1) present investigation; (2) Van Patter *et al.* (1951) and Elkind (1953), from the $^{10}B(d, p)^{11}B$ reaction; (3) spin and parity prediction from double stripping; (4) spins and parities reported by Ferguson *et al.* (1958) and Groshev *et al.* (1958); (5) spins and parities reported by Evans and Parkinson (1954), Sjögren (1957) and Bilaniuk and Hensel (1958) from deuteron stripping.

† The present results were normalized to this value as determined by Van Patter et *al.*

level at 9·86 MeV excitation with a width of 125 ± 10 kev. The latter figure is not inconsistent with an estimated total width of 150 kev made directly from our spectrum but which includes an overall instrumental width of about 20 kev.

The proton angular distributions are shown in the centre-of-mass system in figure 2. The arbitrary unit of intensity, which is the same for all angular distributions reported in this communication, is very roughly equal to 50 μbn sterad^{-1}. The curves shown have been calculated from an approximate expression describing a double stripping process which is discussed in more detail in § 4.1. It may be noted that for the 8·92 MeV state better agreement was obtained by adding a small isotropic background to the theoretical curve.

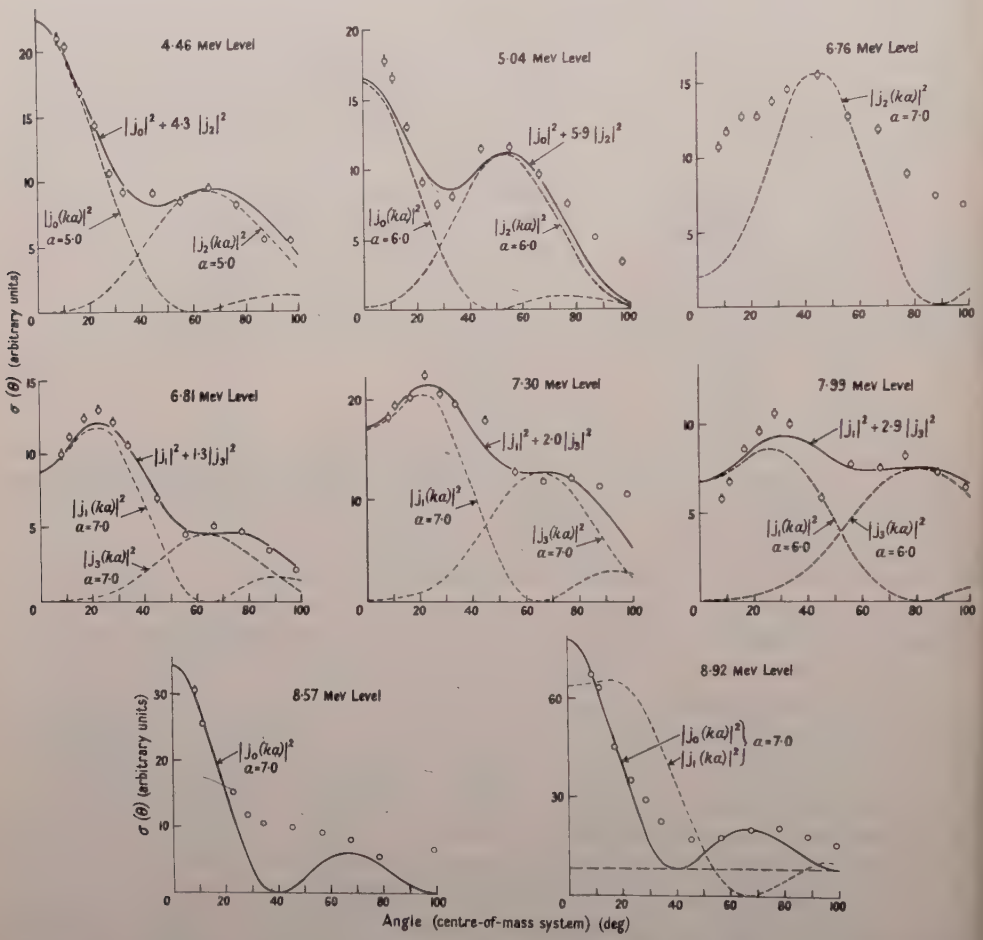

Figure 2. Angular distribution of the proton groups from the ^{9}Be(^{3}He, p)^{11}B reaction. The curves shown were calculated from an approximate form of an expression derived by Newns (to be published) for a double stripping process.

3.2. $^{9}Be(^{3}He, d)^{10}B$

A deuteron energy spectrum, measured from the same nuclear plate used to obtain the proton spectrum of figure 1 is shown in figure 3. All the groups in the figure arise from the ^{9}Be(^{3}He, d)^{10}B reaction except for a small group at an energy of about 5·3 MeV which is from the reaction ^{13}C(^{3}He, d)^{14}N and corresponds to the formation of ^{14}N in its first excited state. No groups were observed

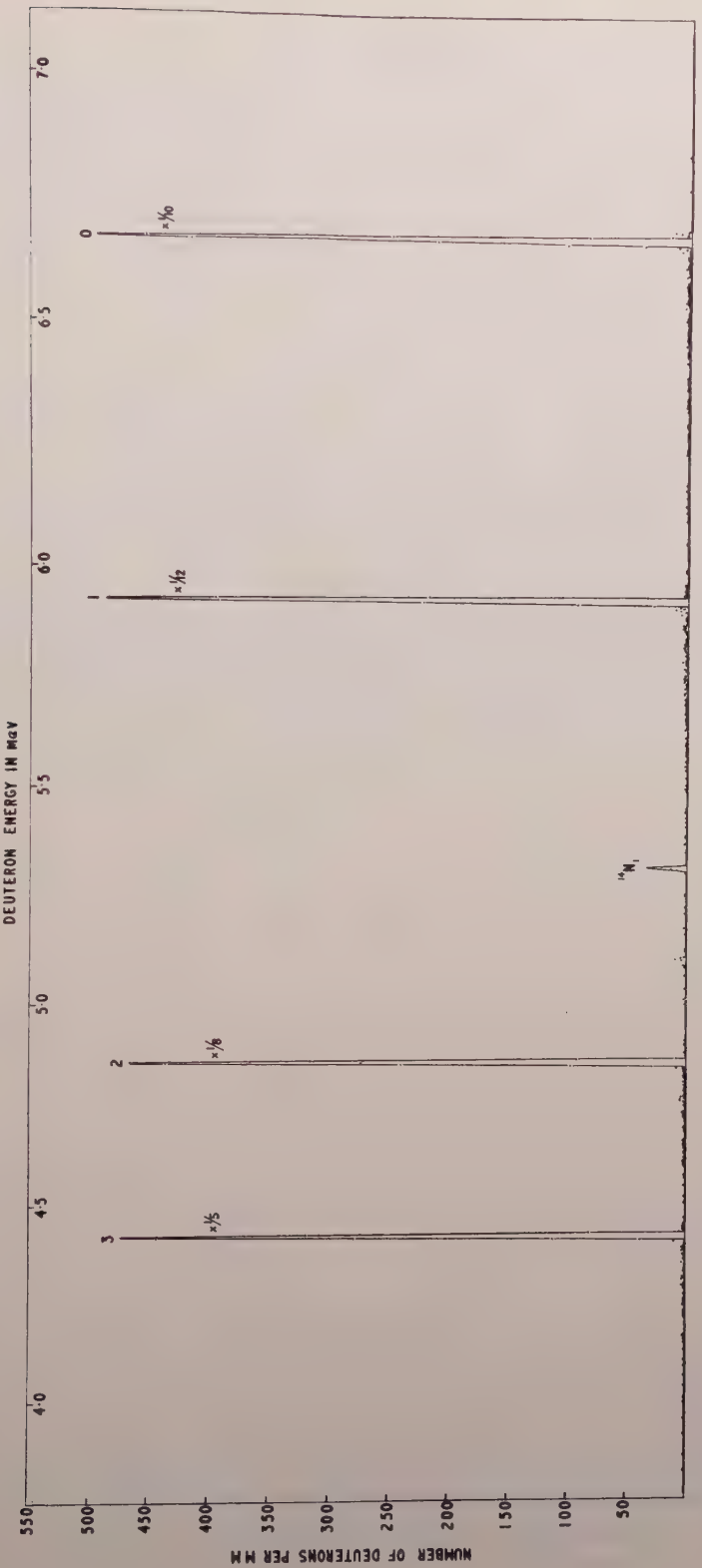

Figure 3. Deuteron spectrum from the $^{9}Be(^{3}He, d)^{10}B$ reaction measured at an angle of observation of 15°.

from the more abundant target impurities of ^{12}C and ^{16}O, since in both cases the (^3He, d) reactions have large negative Q-values.

The energy levels of ^{10}B have been calculated and the mean values of several determinations at various angles are listed in table 2. These are in agreement, within the experimental errors, with the levels reported by Bockelman, Browne, Buechner and Sperduto (1953) from a study of the inelastic scattering of protons and deuterons from ^{10}B. The latter values are also listed in the table.

Table 2. $^9Be(^3He, d)^{10}B$

Group	Level Energy (MeV)		l_p	J_f	T	Ω_1	γ_1^2
	(1)	(2)					
0	0	0	1	3+	0	4	2
1	0·717 ± 0·010	0·727 ± 0·005	1	1+	0	8	4
2	1·744 ± 0·010	1·739 ± 0·005	1	0+	1	15	8
3	2·156 ± 0·010	2·152 ± 0·005	1	1+	0	3	3

(1) present investigation; (2) Bockelman *et al.* (1953) from the $^{10}B(p, p')$ and $^{10}B(d, d')$ reactions; Ω_1 and γ_1^2 in relative units.

Angular distributions of the deuteron groups leading to the ground and first three excited states of ^{10}B have been measured. These are shown in the centre-of-mass system in figure 4. Born approximation stripping curves have been calculated from the theory of Newns (1952). To obtain good agreement it was

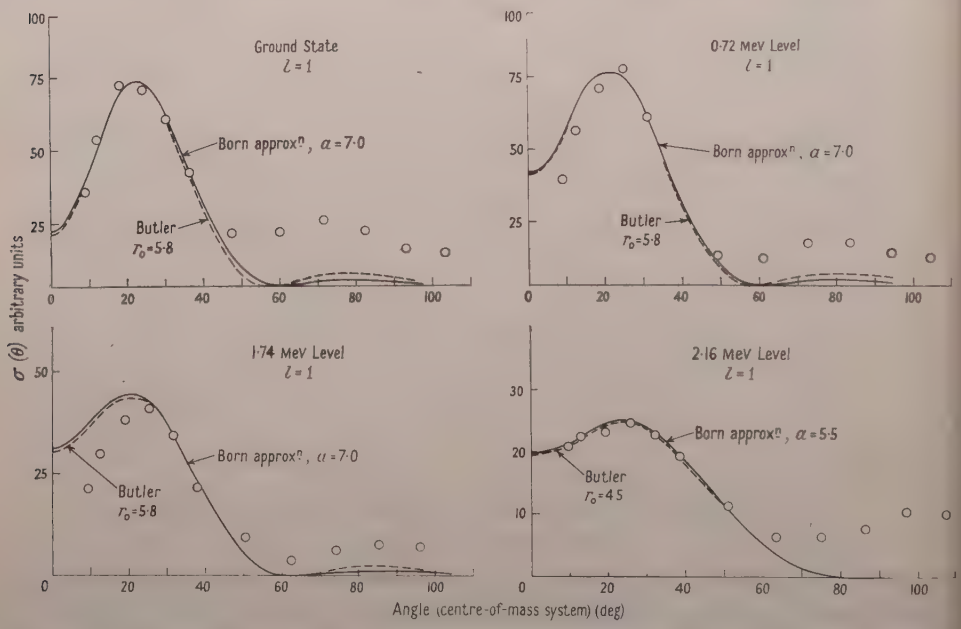

Figure 4. Deuteron angular distributions measured from the $^9Be(^3He, d)^{10}B$ reaction.

necessary to use a radius of interaction equal to 7·0 fermi for the groups leading to the ground and first two excited states and 5·5 fermi for the fourth group. These radii are large compared with the Gamow radius (4·2 fermi) but it is usual to use a value equal at least to the Gamow radius plus one fermi in deuteron stripping when using Born approximation theory, i.e. $a = (1{\cdot}7 + 1{\cdot}22A^{1/3})$ fermi.

Similar curves have also been calculated from the Butler form of the theory (Newns 1952). These are shown in the figure by the broken line. As in the Born approximation case, good agreement was obtained using the same radius for the first three groups and a smaller value for the fourth group. The radii found most satisfactory were 5·8 and 4·5 fermi respectively. The l-values are listed in table 2 together with the known spins, parities and isotopic spins (Ajzenberg and Lauritsen 1955). Also tabulated are the relative proton capture probabilities Ω_1, calculated from the Born approximation theory, and the relative reduced width γ_1^2, derived from the Butler theory.

3.3. $^9Be(^3He, t)^9B$

A strong triton group was observed while measuring the energy spectra of the alpha particles from the ^{9}Be(^{3}He, α)^{8}Be reaction (to be published at a later date). Tritons and alpha particles were simultaneously counted since it is difficult to distinguish between them. The triton group was identified by its rapid rate of change of position with angle and by its large width. Both these factors arise because the dispersion of the instrument is three times as great for tritons as for α-particles and protons. This assignment was also checked by detailed range measurements made with a higher power objective than is usually used for counting. The Q-value was calculated on the assumption that the group was due to the reaction ^{9}Be(^{3}He, t) leading to the ground state of ^{9}B. A Q-value of $-1{\cdot}077$ MeV was obtained which agrees well with the value of $-1{\cdot}087$ MeV expected from the mass defects.

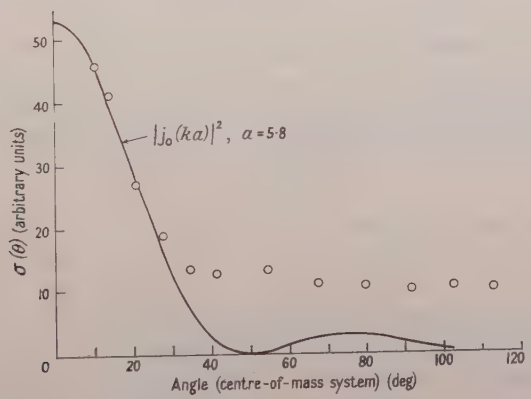

Figure 5. Angular distribution of tritons from the ^{9}Be(^{3}He, t) reaction leading to the ground state of ^{9}B.

The angular distribution of this group has been measured and is shown plotted in the centre-of-mass system in figure 5. There are as yet no specific theories for the (^{3}He, t) reaction but from the strong forward peak observed in the angular distribution it seems likely that the reaction is at least in part proceeding by a direct process. The general form for an angular distribution resulting from a direct reaction is approximately $|j_l(ka)|^2$, where in this case k is the difference in the ^{3}He and triton wave numbers, i.e. the momentum transferred during the interaction. The curve shows was computed for $l=0$ and $a=5{\cdot}8$ fermi.

§ 4. Discussion

Many of the (^{3}He, p), (^{3}He, d) and (^{3}He, t) angular distributions presented in this communication strongly suggest that a direct process is playing an appreciable role in the reaction mechanism. This is rather surprising, since the results of other investigations, admittedly at lower incident energies, show little evidence in favour of this. In particular the work of Schiffer *et al.* (1956) on a number of (^{3}He, p) reactions at an incident energy of 4·7 MeV, as compared with our 5·7 MeV, is inconclusive as to the nature of the reaction mechanism.

A comparison of the peak differential cross sections of the various reactions indicates that the (^{3}He, d) reaction is strongest. This would be a surprising result if the reaction mechanism was due only to compound nucleus formation, since it is hardly likely that deuterons would be emitted with greater probability than protons.

4.1. $^9Be(^3He, p)^{11}B$

Since in a (^{3}He, p) reaction two particles are transferred to the target nucleus as compared with one in a (^{3}He, d) reaction, stripping might be thought to be a less likely reaction mechanism. Also the fraction of the reaction proceeding via compound nuclear formation and decay may be larger than for a (^{3}He, d) or (^{3}He, α) reaction, thus partially masking any stripping contribution. However, the majority of (^{3}He, p) angular distributions measured in the present investigation exhibit fairly strong forward peaks similar to those observed in deuteron stripping. It was therefore considered worth while attempting to explain them on the assumption of a double stripping process. The predicted spins and parities could then be compared with the known values as a check on the stripping assumption.

In a double stripping process a neutron and a proton are captured by the target nucleus with angular momentum l_n and l_p respectively. The resulting angular distribution is then characterized by $\mathbf{L}$, where

$$\mathbf{L}=\mathbf{l}_n+\mathbf{l}_p \qquad \ldots\ldots(1)$$

the spin of the final state $\mathbf{J}_f$ is given by

$$\mathbf{J}_f=\mathbf{J}_i+\mathbf{L}+\tfrac{1}{2}+\tfrac{1}{2} \qquad \ldots\ldots(2)$$

and there is a parity charge only if L is odd. For the formation of a particular state l_n and l_p are determined by the shell model, but unless l_n or l_p is zero, equation (1) allows a multiplicity of L-values. Thus, in general, in a double stripping process, unlike deuteron stripping, the angular distribution is characterized by more than one Bessel function.

An expression for the angular distribution expected from a double stripping process has been derived by Newns (to be published). This is difficult to evaluate and an approximate form has been used to fit the experimental observations in figure 2, viz.

$$\sigma(\theta)\propto\sum_L|A(L).\mathrm{j}_L(ka)|^2$$

where $\mathrm{j}_L(ka)$ is a spherical Bessel function and $A(L)$ is a constant analogous to the capture probability occurring in the Born approximation deuteron stripping theory. For a particular transition, e.g. $L=0+2$, the ratio $A(2)/A(0)$ is solely dependent on the nuclear properties of the state formed and can be determined by fitting the theoretical curve to the experimental points.

To check the validity of the approximation, the exact expression was evaluated for $L=0$ with $l_n=l_p=0$, for $L=1$ with $l_n=1$, $l_p=2$, and for $L=0+2$ with $l_n=l_p=1$. The first two cases applied to the 8·92 MeV state and the third to the 4·46 MeV state. For all cases the curve calculated from the exact expression closely resembled that obtained from the approximate expression. In figure 6 are shown the approximate and exact expressions computed for the 4·46 MeV state with $L=0+2$ and $l_n=l_p=1$. For both curves a radius of interaction of 5·0 fermi was used, and the ratios $A(2)/A(0)$ adjusted to obtain best agreement.

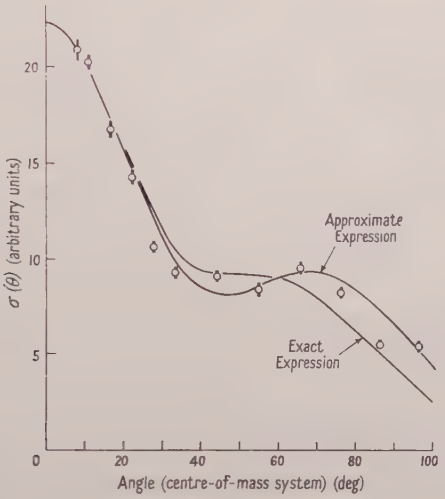

Figure 6. Angular distribution of the protons from the $^{9}Be(^{3}He, p)^{11}B$ reaction corresponding to the state at 4·46 MeV.

It may be noticed that for most of the curves shown in figure 2 it was necessary to use a radius larger than is normally required in deuteron stripping. However, there is some justification for this since in the latter process ^{9}Be is a special case requiring a large radius (Huby 1953).

In table 1 are listed the L-values giving best agreement, and in column (3) are the predicted spins and parities. For comparison in column (4) are listed the spins and parities determined by Ferguson, Gove, Kuehner, Litherland and Bromley (1958) and by Groshev, Demidov, Lutsenko and Pelekhov (1958) from γ-ray investigations, and in column (5) are those determined from deuteron stripping by Evans and Parkinson (1954), Sjögren (1957) and Bilaniuk and Hensel (1958). The L-value assignments are consistent with these data except for the states at 7·299 MeV and 7·989 MeV. The predicted parities for these states disagree with those of Sjögren from 800 kev deuteron stripping. Also for the 7·299 MeV state there is a disagreement with the very tentative parity assignment of Ferguson *et al.* It may be noted that the parity assignment of Bilaniuk and Hensel for the 8·923 MeV state disagrees with that reported by Groshev *et al.* (1958), the latter result being consistent with the present L-value.

The above parity discrepancies may be ascribed to distortions of the angular distributions produced by Coulomb effects. Distortion due to resonances in the compound nucleus is unlikely since the excitation of the latter is about 30 MeV. The present results suggest that double stripping may be the predominant process at a bombarding energy of 5·7 MeV, although the parity discrepancies are

disturbing. However, it is clear that further tests should be made, preferably at higher bombarding energies, before this technique can be used as a tool in nuclear spectroscopy.

4.2. $^{9}Be(^{3}He, d)^{10}B$

A probable mechanism for a (^{3}He, d) reaction is stripping. The inverse process has been theoretically treated by Newns and more recently Butler (1957) has discussed in detail the mechanism of (^{3}He, d) stripping. The good agreement between theoretical stripping curves and the experimental observation shown in figure 4 provides strong evidence in favour of this mechanism. In all cases the l-values are consistent with the known spins and parities of the state of ^{10}B but it is unfortunate that all four curves are of the $l=1$ type.

It may be noticed that in two of the angular distributions shown in the figure, the experimental points fall below the theoretical curves at small angles. This is a familiar phenomenon in deuteron stripping (Dalton, Hinds and Parry 1957) and is probably due to the neglect of Coulomb forces in the stripping theory. It is surprising that the effect is not greater due to the increased charge of a ^{3}He particle but this may have been minimized by adjustment of the radius.

The values of the relative reduced widths, γ_l^2, deduced from observations on some (d, t) and (d, ^{3}He) reactions have been discussed by French and Fujii (1957). These authors conclude, from the available data, that they are not as reliable as those extracted from deuteron stripping reactions. This presumably will also apply to (^{3}He, d) reactions, but, since in the present case the l-values are the same for all groups, and the deuteron energies differ by only 2·3 MeV, the relative reduced widths shown in table 2 may be more meaningful than those discussed by French and Fujii.

4.3. $^{9}Be(^{3}He, t)^{9}B$

The triton angular distribution for the ground state transition has been fitted with an $l=0$ curve calculated for a general type of direct interaction. The measure of agreement obtained confirms that a substantial part of the reaction proceeds via some type of direct process. There are various possibilities for the latter, one of which simply involves a proton–neutron exchange between the ^{3}He projectile and the target nucleus. In detail this may be visualized by considering the ^{3}He particle as consisting of a neutron–proton pair and an odd proton. The latter causes a (p, n) direct surface interaction and the emitted neutron is then captured by the neutron–proton pair which has remained outside the range of nuclear forces throughout the reaction. This mechanism is similar to that proposed by Fairbairn (1957) for the inelastic scattering of deuterons.

The $l=0$ assignment is in agreement with the known spin and parity of the ground state of ^{9}B. It is of interest to note that in a (^{3}He, t) direct reaction between mirror states an $l=0$ transition should always be observed.

Acknowledgments

We would like to thank Dr. K. W. Allen for his continued interest and for much useful discussion and advice. We are grateful to Dr. H. C. Newns for communicating the results of his work on the double stripping process prior to publication, and also to Mr. D. A. Proctor and Mr. H. Marchant for assistance

in making the exposures. Our thanks are also due to the Van de Graaff operating staff, the microscopists for scanning our plates, and to Mr. F. A. Howe for preparing the targets.

References

Ajzenberg, F., and Lauritsen, T., 1955, *Rev. Mod. Phys.*, **27**, 77.
Bilaniuk, O. M., and Hensel, J. C., 1958, *Bull. Amer. Phys. Soc.*, Series II, **3**, 188.
Bockelman, C. K., Browne, C. P., Buechner, W. W., and Sperduto, A., 1953, *Phys. Rev.*, **92**, 665.
Briggs, C. H., 1954, *Rev. Mod. Phys.*, **26**, 1, 472.
Browne, C. P., and Buechner, W. W., 1956, *Rev. Sci. Instrum.*, **27**, 899.
Butler, S. T., 1957, *Nuclear Stripping Reactions* (London : Pitman).
Dalton, A. W., Hinds, S., and Parry, G., 1957, *Proc. Phys. Soc.* A, **70**, 586.
El-Bedewi, F. A., 1951, *Proc. Phys. Soc.* A, **64**, 947.
Elkind, M. M., 1953, *Phys. Rev.*, **92**, 127.
Enge, H. A., 1954, *University of Bergen, Naturvitenskapeleg rekke*, No. 1.
Evans, N. T. S., and Parkinson, W. C., 1954, *Proc. Phys. Soc.* A, **67**, 684.
Fairbairn, W. M., 1957, *Proc. Roy. Soc.* A, **239**, 448.
Ferguson, A. J., Gove, H. E., Kuehner, J. A., Litherland, A. E., and Bromley, D. A., 1958, *Phys. Rev. Letters*, **1**, 414.
French, J. B., and Fujii, A., 1957, *Phys. Rev.*, **105**, 652.
Groshev, L. V., Demidov, A. M., Lutsenko, V. N., and Pelekhov, V. I., 1958, *Atlas of the γ-ray Spectra from Thermal Neutron Capture* (Moscow : Chief Authority for the Utilization of Atomic Energy (G.V.I.A.E.) for the Council of Ministers of the U.S.S.R.).
Holmgren, H. D., Bullock, M. L., and Kunz, W. E., 1956, *Phys. Rev.*, **104**, 1066.
Holt, J. R., and Marsham, T. N., 1953, *Proc. Phys. Soc.* A, **66**, 1032.
Huby, R., 1953, *Progr. Nucl. Phys.*, **3**, 177.
Li, C. W., and Sherr, R., 1954, *Phys. Rev.*, **96**, 389.
Newns, H. C., 1952, *Proc. Phys. Soc.* A, **65**, 916.
Schiffer, J. P., Bonner, T. W., Davies, R. H., and Prosser, Jr., F. W., 1956, *Phys. Rev.*, **104**, 1064.
Sjögren, B., 1957, *Ark. Fys.*, **12**, 537.
Van Patter, D. H., Buechner, W. W., and Sperduto, A., 1951, *Phys. Rev.*, **82**, 248.

The Thermal Conductivity of Monatomic Dielectric Liquids

By R. EISENSCHITZ and A. R. BOOT
Department of Physics, Queen Mary College, University of London

MS. received 30*th January* 1959

Abstract. In thermal equilibrium the relative coordinates of a pair of molecules are statistically independent of the coordinates of their centre of mass. This independence persists in viscous flow and was supposed to persist in presence of a gradient of temperature. This assumption leads, however, to difficulties if the heat flow is to be expressed in terms of molecular interaction. A new distribution function for molecular doublets is deduced which is appropriate to non-uniform temperature and involves the coordinates of the centre of mass and the relative coordinates. This distribution function is superior to those put forward previously as it takes account of the uniformity of pressure and the vanishing of flow in a steady gradient of temperature. By means of this distribution function an expression for the coefficient of thermal conductivity is obtained which differs from similar expressions as put forward by previous authors.

§ 1. Introduction

The conduction of heat in liquefied rare gases and similar fluids is almost entirely due to the transmission of energy by the intermolecular forces. A quantitative relation between the heat flow and the forces was established by Born and Green (1947) and by Green (1952); they obtained an expression for the divergence of the heat flow from the principles of molecular dynamics. A similar deduction by Irving and Kirkwood (1950) gave a result which agrees neither with Born and Green's nor with an expression previously suggested by Kirkwood (1946). By generalizing the virial theorem Eisenschitz (1955) obtained an expression for the heat flow, as distinct from its divergence, which does not agree with any of the above authors' results.

In the present paper the discrepancies between these results are resolved and the validity of the ' virial ' expression is established. This result necessitates a revision of the previous theories of the thermal conductivity of liquids (Eisenschitz 1949, Zwanzig, Kirkwood, Oppenheim and Alder 1954) which depended on the validity of the older expression for the heat flow. The coefficient of thermal conductivity has previously been derived from the distribution function of the relative positions of pairs of molecules without taking account of the distribution of their centre of mass. This is no longer admissible if the new expression for the heat flow is employed.

In the present paper the complete distribution in coordinates for a pair of molecules is derived for the first time in such a way that the gradient of temperature is taken into account. It is found that there are specific statistical correlations between the movement of the mass centre and the relative movement. These correlations do not appear either in thermal equilibrium or in viscous flow. The

resulting expression for the coefficient of thermal conductivity differs sufficiently from previous results to affect any comparison with experiment.

§ 2. The Heat Flow

Consider a pair of molecules labelled h and i. Let m be the mass, $\mathbf{r}_h$ and $\mathbf{r}_i$ their positions and $\mathbf{p}_h$ and $\mathbf{p}_i$ their momenta. It is convenient to employ the variables

$$\left.\begin{aligned} \mathbf{R}_{hi} &= \tfrac{1}{2}(\mathbf{r}_h + \mathbf{r}_i) & \mathbf{r}_{hi} &= \tfrac{1}{2}(\mathbf{r}_h - \mathbf{r}_i) \\ \mathbf{P}_{hi} &= \mathbf{p}_h + \mathbf{p}_i & \mathbf{p}_{hi} &= \mathbf{p}_h - \mathbf{p}_i \end{aligned}\right\} \quad \ldots\ldots (2.1)$$

Intermolecular forces are derived from a potential energy ψ_{hi} which is assumed to be given as a function of the distance apart of the molecules which is equal to $2r_{hi}$. Further, let $f_{hi}^{(2)}$ be the normalized probability distribution in the momenta and coordinates of a pair of molecules. Flow vectors are then defined by

$$\left.\begin{aligned} \mathbf{J}_{hi} &= (1/16m)\int \mathbf{P}_{hi} f_{hi}^{(2)}\, d\mathbf{P}_{hi}\, d\mathbf{p}_{hi} & \mathbf{j}_h &= \tfrac{1}{2}(\mathbf{J}_{hi} + \mathbf{j}_{hi}) \\ \mathbf{j}_{hi} &= (1/16m)\int \mathbf{p}_{hi} f_{hi}^{(2)}\, d\mathbf{P}_{hi}\, d\mathbf{p}_{hi} & \mathbf{j}_i &= \tfrac{1}{2}(\mathbf{J}_{hi} - \mathbf{j}_{hi}) \end{aligned}\right\} \quad \ldots\ldots (2.2)$$

which are, in general, functions of the coordinates.

In this notation the macroscopic flow of heat is equal to (Eisenschitz 1955):

$$\mathbf{Q} = \frac{4N^2}{V}\int \boldsymbol{\chi}(\mathbf{r}_{hi}) \cdot \mathbf{J}_{hi}\, d\mathbf{R}_{hi}\, d\mathbf{r}_{hi} \qquad \ldots\ldots (2.3)$$

where N is the number of molecules, V is the volume $\mathbf{I}$ is the unit tensor and the tensor $\boldsymbol{\chi}$ is defined as

$$\boldsymbol{\chi}(\mathbf{r}_{hi}) = \psi_{hi}(2r_{hi})\mathbf{I} - \mathbf{r}_{hi}\left(\frac{\partial \psi_{hi}}{\partial \mathbf{r}_{hi}}\right). \qquad \ldots\ldots (2.4)$$

The expression given by Born and Green (eqn 4.15 of these authors) differs from (2.3) by omitting that term in (2.4) which is proportional to ψ, apparently assuming that this term vanishes on the average. Equation (2.3) should accordingly be compatible with theory of Born and Green whether or not their assumption is right.

The formula given by Irving and Kirkwood differs from (2.3) by substituting $\frac{1}{2}(\mathbf{J} + \mathbf{j})$ for $\mathbf{J}$, thus admitting a finite value of the heat flow when $\mathbf{J} = 0$. This was indeed implied in the previous theories of thermal conduction but is strictly ruled out if (2.3) is correct.

It can be shown that this result of Irving and Kirkwood is due to a minor error. Equation (6.22) of these authors can be written in the form

$$\mathbf{Q} = \frac{2}{V}\sum_h \sum_i \int (\mathbf{j}_h + \mathbf{j}_i) \cdot \boldsymbol{\chi}(\mathbf{r}_{hi})\, d\mathbf{r}_{hi}\, d\mathbf{R}_{hi} \qquad \ldots\ldots (2.5)$$

which is in accordance with our equation (2.3). The significant term in (2.5) is rearranged by the use of delta functions as

$$\int d\mathbf{r}_{ih}\, d\mathbf{R}_{ih}\Big[\mathbf{j}_i(\mathbf{r}_{ih}, \mathbf{R}_{ih})\int \boldsymbol{\chi}(\mathbf{r}')\,\delta(\mathbf{r}_{ih} - \mathbf{r}')\, d\mathbf{r}' + \mathbf{j}_h(\mathbf{r}_{ih}, \mathbf{R}_{ih})\int \boldsymbol{\chi}(\mathbf{r}')\,\delta(\mathbf{r}_{hi} - \mathbf{r}')\, d\mathbf{r}'\Big] \qquad \ldots\ldots (2.6)$$

where $\mathbf{r}'$ is half the distance vector of two points in three-dimensional space. Subsequently Irving and Kirkwood commute the order of integrations in (2.6). By

doing so they inadvertently change the sign of $\mathbf{r}_{ih}$ in $\mathbf{j}_h$. A permutation of i and h transforms $\mathbf{r}_{ih}$ into $-\mathbf{r}_{ih}$ and $\mathbf{j}_h(-\mathbf{r}_{ih}, \mathbf{R}_{ih})$ into $\mathbf{j}_i(\mathbf{r}_{ih}, \mathbf{R}_{ih})$, leaving χ invariant. By applying this permutation to equations (2.2) it is found that

$$\mathbf{j}_h(-\mathbf{r}_{ih}, \mathbf{R}_{ih}) = \mathbf{j}_i(\mathbf{r}_{ih}, \mathbf{R}_{ih}).$$

Hence the commutation of the integrations does not leave (2.6) invariant but replaces $\mathbf{j}_h$ by $\mathbf{j}_i$ and $\mathbf{j}_i + \mathbf{j}_h$ by $2\mathbf{j}_i$. In this way the result of Irving and Kirkwood's investigation (equation 6.24) is arrived at. Since it is in contradiction to their equation 6.22 it may be regarded as erroneous.

The theory of thermal conduction in liquids should accordingly be based on equation (2.3). If the distribution functions as given by previous authors are inserted into (2.3) the resulting heat flow vanishes. The deduction of the distribution functions appropriate to non-uniform temperature is accordingly due for reconsideration. It will have to be shown that they involve not only the relative positions of molecular doublets but also the positions of their centre of mass.

§ 3. Doublet Distributions in Phase Space

The deductions of this and the following section follow largely a familiar pattern (Kirkwood 1946, Eisenschitz 1952) but involve points of detail which have not yet been clarified.

The normalized distribution in full phase space $f^{(N)}$ satisfies the Liouville equation

$$\left\{\frac{\partial}{\partial t} + \sum_i \left(\frac{\mathbf{p}_i}{m} \cdot \frac{\partial}{\partial \mathbf{r}_i} + \mathbf{F}_i \cdot \frac{\partial}{\partial \mathbf{p}_i}\right)\right\} f^{(N)} = 0 \qquad \ldots\ldots (3.1)$$

where $\mathbf{F}_i$ is the total force acting on the molecule i. Doublet distributions are defined as

$$f_{hi}^{(2)} = \int f^{(N)} d\mathbf{B}_{hi}$$

where the differential applies to positions and momenta of all molecules except h and i. By integrating equation (3.1) with respect to $d\mathbf{B}_{hi}$ a reduced equation is obtained:

$$\left(\frac{\partial}{\partial t} + \frac{\mathbf{p}_h}{m} \cdot \frac{\partial}{\partial \mathbf{r}_h} + \frac{\mathbf{p}_i}{m} \cdot \frac{\partial}{\partial \mathbf{r}_i}\right) f_{hi}^{(2)} = -\int \left(\mathbf{F}_h \cdot \frac{\partial}{\partial \mathbf{p}_h} + \mathbf{F}_i \cdot \frac{\partial}{\partial \mathbf{p}_i}\right) f^{(N)} d\mathbf{B}_{hi}. \qquad \ldots\ldots (3.2)$$

Let the average of some function ξ with respect to momenta and positions of $N-2$ molecules be denoted as

$$\langle \xi \rangle_{hi} = \int \xi f^{(N)} d\mathbf{B}_{hi} \Big/ \int f^{(N)} d\mathbf{B}_{hi}.$$

Averages of this kind are to be added to either side of equation (3.2) so that they vanish in thermal equilibrium and are small if deviations from equilibrium are small. Add accordingly

$$\left(\langle \mathbf{F}_h \rangle_{hi} \cdot \frac{\partial}{\partial \mathbf{p}_h} + \langle \mathbf{F}_i \rangle_{hi} \cdot \frac{\partial}{\partial \mathbf{p}_i}\right) f_{hi}^{(2)}.$$

Equation (3.2) is integrated with respect to the time between $-\tau$ and 0:

$$\tau\left(\frac{\partial}{\partial t}+\frac{\mathbf{p}_h}{m}\cdot\frac{\partial}{\partial \mathbf{r}_h}+\langle\mathbf{F}_h\rangle_{hi}\cdot\frac{\partial}{\partial \mathbf{p}_h}+\frac{\mathbf{p}_i}{m}\cdot\frac{\partial}{\partial \mathbf{r}_i}+\langle\mathbf{F}_i\rangle_{hi}\cdot\frac{\partial}{\partial \mathbf{p}_i}\right)f_{hi}^{(2)}$$
$$=-f_{hi}^{(2)}+\int f_{hi}^{(2)}(\mathbf{p}_h-\Delta\mathbf{p}_h,\mathbf{p}_i-\Delta\mathbf{p}_i)\,W\,d(\Delta\mathbf{p}_h)\,d(\Delta\mathbf{p}_i)$$
$$+\int_{-\tau}^{0}\left(\langle\mathbf{F}_h\rangle_{hi}\cdot\frac{\partial}{\partial \mathbf{p}_h}+\langle\mathbf{F}_i\rangle_{hi}\cdot\frac{\partial}{\partial \mathbf{p}_l}\right)f_{hi}^{(2)}\,dt \qquad \ldots\ldots(3.3)$$

where

$$\Delta\mathbf{p}_h=\int_{-\tau}^{0}\mathbf{F}_h\,dt$$

and

$$W=\int_{\Delta\mathbf{p}_h\ \Delta\mathbf{p}_i\ \text{const.}}\left[\frac{f^{(N)}}{f_{hi}^{(2)}}\right]d\mathbf{B}_{hi} \qquad \ldots\ldots(3.4)$$

can be regarded as a probability distribution in $\Delta\mathbf{p}_h$ and $\Delta\mathbf{p}_i$ which is almost independent of the time. In liquids the increments in momentum are regarded as small so that the right-hand side of (3.3) simplifies:

$$\sum_{l=h,i}\left\{-\frac{\partial}{\partial \mathbf{p}_l}\cdot\left(\langle\Delta\mathbf{p}_l\rangle_{hi}+\tfrac{1}{2}\sum_{n=h,i}(\partial/\partial\mathbf{p}_n)\cdot\langle\Delta\mathbf{p}_l\Delta\mathbf{p}_n\rangle_{hi}\right)\right\}f_{hi}^{(2)}+O\left((\Delta p)^3\right).$$

In this expression the mean values can be expressed in terms of the correlation functions of the intermolecular forces. In this procedure attention has to be given to the difference in temperature at the positions of the molecules. The assumption of local thermal equilibrium is made so that the 'temperature of a molecule' agrees with the experimental temperature recorded in its immediate vicinity. Denoting the gradient by $\mathbf{b}$ the temperature of the molecule i is equal to $T_{ii}=T+\mathbf{b}\,.\,\mathbf{r}_i$, T being the average temperature.

The mean value of $\Delta\mathbf{p}_i$, its square and of $\mathbf{F}_i$ are accordingly derived at the temperature T_{ii}, whereby the $N-2$ molecules differing from h and i are assumed to be at the temperature T. Mean products, such as $\Delta\mathbf{p}_h\,\Delta\mathbf{p}_i$, which are in any case of minor importance, are to be taken at some intermediate temperature

$$T_{hi}=2(T_h^{-1}+T_i^{-1})^{-1}.$$

In evaluating the mean values in equation (3.3) it is assumed that the integrand of (3.4) corresponds to thermal equilibrium at the time $t=0$ but depending upon the increments of momenta:

$$[f_{hi}^{(2)}]^{-1}=\exp\left[-\frac{|\ _i+\Delta\mathbf{p}_i|^2}{2mkT_{ii}}-\frac{|\mathbf{p}_h+\Delta\mathbf{p}_h|^2}{2mkT_{hh}}\right] \qquad \ldots\ldots(3.5)$$

where k is Boltzmann's constant.

Friction tensors are now defined in terms of the temporal correlation functions of the forces

$$\boldsymbol{\beta}_{hi}=(mkT_{hi})\int_{-\tau}^{0}\langle\mathbf{F}_h(t+t')\mathbf{F}_i(t)\rangle_{hi}dt'. \qquad \ldots\ldots(3.6)$$

It is assumed that these quantities are insensitive towards the precise value of τ and have a positive diagonal sum. Reasons for this assumption were advanced by Turner (1958). It follows that

$$\left.\begin{aligned}\langle\Delta\mathbf{p}_i\rangle_{hi}&=-(\boldsymbol{\beta}_{ii}\cdot\mathbf{p}_i+\boldsymbol{\beta}_{ih}\cdot\mathbf{p}_h)+\int_{-\tau}^{0}\langle\mathbf{F}_i\rangle_{hi}dt\\ \langle\Delta\mathbf{p}_h\Delta\mathbf{p}_i\rangle&=2mkT_{hi}\boldsymbol{\beta}_{hi}.\end{aligned}\right\} \qquad \ldots\ldots(3.7)$$

Equation (3.3) is now transformed into

$$\left\{\frac{\partial}{\partial t}+\sum_{l=\mathrm{h,i}}\left[\frac{\mathbf{p}_l}{m}\cdot\frac{\partial}{\partial \mathbf{r}_l}+\langle \mathbf{F}_l\rangle_{\mathrm{hi}}\cdot\frac{\partial}{\partial \mathbf{p}_l}\right]\right\}f_{\mathrm{hi}}^{(2)}=\sum_{l=\mathrm{h,i}}\sum_{n=\mathrm{h,i}}\left\{\frac{\partial}{\partial \mathbf{p}_l}\cdot\boldsymbol{\beta}_{ln}\cdot\mathbf{p}_n f_{\mathrm{hi}}^{(2)}\right)$$
$$+\frac{\partial^2}{\partial \mathbf{p}_l\partial \mathbf{p}_n}:(mkT_{ln}\boldsymbol{\beta}_{ln}f_{\mathrm{hi}}^{(2)})\}+\frac{1}{\tau}\sum_{l=\mathrm{h,i}}\left\{\int_{-\tau}^{0}\langle \mathbf{F}_l\rangle_{\mathrm{hi}}\cdot\frac{\partial f_{\mathrm{hi}}^{(2)}}{\partial \mathbf{p}_l}\,dt\right.$$
$$\left.-\frac{\partial}{\partial \mathbf{p}_l}\cdot\left[f_{\mathrm{hi}}^{(2)}\int_{-\tau}^{0}\langle \mathbf{F}_l\rangle_{\mathrm{hi}}\,dt\right]\right\}. \qquad \ldots\ldots(3.8)$$

It will be shown that the last two terms in this equation may be ignored. If, in addition, the friction tensors with $\mathrm{i}\neq\mathrm{h}$ are neglected, equation (3.8), which is of the type of the Fokker–Planck equation, agrees essentially with an equation put forward by Kirkwood (1946) without deduction and applicable to uniform temperature. Equations of this type are, at present, the only practicable means for describing transport processes in liquids, either by the method employed in this paper or an alternative approach due to M. S. Green (1954). For further calculations the friction tensors $\boldsymbol{\beta}_{\mathrm{ii}}$ are replaced by a scalar constant β and it is assumed that the temperature gradient is constant.

§ 4. Doublet Distribution in Coordinates

In the following the subscripts by which the molecules are labelled will be dropped, since this does not lead to any ambiguity. It should, however, be remembered that the doublet distributions refer to a pair of specified molecules.

Averaging equation (3.8) with respect to the momenta yields

$$\frac{\partial g^{(2)}}{\partial t}+\frac{\partial}{\partial \mathbf{R}}\cdot\mathbf{J}+\frac{\partial}{\partial \mathbf{r}}\cdot\mathbf{j}=0 \qquad \ldots\ldots(4.1)$$

where

$$g^{(2)}(\mathbf{R},\mathbf{r},t)=\tfrac{1}{8}\int f^{(2)}\,d\mathbf{P}\,d\mathbf{p}. \qquad \ldots\ldots(4.2)$$

In this procedure the two last terms of equation (3.8) vanish; this follows from the fact that $f^{(2)}$ can be regarded as a function of the time and the initial momenta so that the time integrations commute with the differentiations and integrations with respect to the momenta.

Multiplying (3.8) in succession by $\mathbf{p}_\mathrm{h}$ and $\mathbf{p}_\mathrm{i}$ and averaging with respect to the momenta results in

$$\left.\begin{aligned}\mathbf{J}&=\frac{1}{m\beta}\left[\langle \mathbf{F}^{+}\rangle-\tfrac{1}{2}k\frac{\partial}{\partial \mathbf{R}}(T+\mathbf{b}\,.\,\mathbf{R})-\tfrac{1}{2}k\frac{\partial}{\partial \mathbf{r}}(\mathbf{b}\,.\,\mathbf{r})\right]g^{(2)}\\ \mathbf{j}&=\frac{1}{m\beta}\left[\langle \mathbf{F}^{-}\rangle-\tfrac{1}{2}k\frac{\partial}{\partial \mathbf{r}}(T+\mathbf{b}\,.\,\mathbf{R})-\tfrac{1}{2}k\frac{\partial}{\partial \mathbf{R}}(\mathbf{b}\,.\,\mathbf{r})\right]g^{(2)}\end{aligned}\right\} \qquad \ldots\ldots(4.3)$$

where $\mathbf{F}^{+}=\tfrac{1}{2}(\mathbf{F}_\mathrm{h}+\mathbf{F}_\mathrm{i})$ and $\mathbf{F}^{-}=\tfrac{1}{2}(\mathbf{F}_\mathrm{h}-\mathbf{F}_\mathrm{i})$. These expressions depend partly upon averages of the squares and products of the momenta which are replaced by their values in thermal equilibrium.

By inserting (4.3) into (4.1) an equation for the function $g^{(2)}$ is obtained. This function is written in the form

$$g^{(2)}=\gamma(\mathbf{R})\exp\left(\frac{-\Phi}{kT}\right)[1+\mathbf{b}\,.\,\mathbf{w}]. \qquad \ldots\ldots(4.4)$$

Here $N^2\gamma$ is the product of the local number densities at two points in the liquid in local thermal equilibrium corresponding to the positions of the two specified

molecules. Φ is the 'effective' potential energy which is related to the forces in thermal equilibrium by (Kirkwood 1935):

$$\langle \mathbf{F}^- \rangle = -\tfrac{1}{2}\left(\frac{\partial \Phi}{\partial \mathbf{r}}\right). \qquad \ldots\ldots (4.5)$$

The unknown function $\mathbf{w}(\mathbf{R}, \mathbf{r}, t)$ specifying the distortion of the local thermal equilibrium distribution is derived from a differential equation which is obtained by inserting (4.4) into (4.1) and neglecting terms of the order b^2.

Φ is, in principle, determined by the radial distribution function in thermal equilibrium. The dependence of γ on $\mathbf{R}$ is derived from the variation of density ρ with the temperature at constant pressure:

$$\nabla \rho + \alpha \mathbf{b} \rho = 0 \qquad \ldots\ldots (4.6)$$

α being the coefficient of thermal expansion.

The force $\langle \mathbf{F}^+ \rangle$ vanishes in thermal equilibrium; its value in presence of a temperature gradient is difficult to assess but its contribution to the coefficient of thermal conductivity should be negligible.

The equation determining the distortion function $\mathbf{w}$ has the form

$$\left[\frac{\partial}{\partial \mathbf{R}}\cdot\frac{\partial}{\partial \mathbf{R}} + \frac{\partial}{\partial \mathbf{r}}\cdot\frac{\partial}{\partial \mathbf{r}} - \frac{1}{kT}\frac{\partial \Phi}{\partial \mathbf{r}}\cdot\frac{\partial}{\partial \mathbf{r}}\right](\mathbf{b}\,.\,\mathbf{w}) = \left[\frac{\partial}{\partial \mathbf{r}}\cdot\frac{\partial}{\partial \mathbf{r}} - \frac{1}{kT}\left(\frac{d\Phi}{dr}\right)^2\right]\frac{\mathbf{b}\,.\,\mathbf{R}}{kT^2}. \qquad \ldots\ldots (4.7)$$

A particular solution is readily found:

$$\mathbf{w} = \mathbf{R}\,u(r) \qquad \ldots\ldots (4.8)$$

where u is a scalar function of a scalar variable and must comply with the equation

$$\frac{d^2u}{dr^2} + \left[\frac{2}{r} - \frac{d\Phi}{kT\,dr}\right]\frac{du}{dr} = \frac{d^2\Phi}{kT^2\,dr^2} - \left[\left(\frac{d\Phi}{dr}\right)^2\frac{1}{k^2T^3}\right]. \qquad \ldots\ldots (4.9)$$

The general solution of equation (4.9) is expressed in terms of two constants of integration C and D as

$$u(r) = D + \int_r^\infty \left[dq\,\frac{1}{q^2}\exp\left(\frac{\Phi(q)}{kT}\right)\left\{-C + \frac{1}{kT^2}\int_q^\infty ds s^2 \exp\left(-\frac{\Phi(s)}{kT}\right)\right.\right.$$
$$\left.\left.\times\left[\frac{d^2\Phi(s)}{ds^2} - \frac{1}{kT}\left(\frac{d\Phi(s)}{ds}\right)^2\right]\right\}\right]. \qquad \ldots\ldots (4.10)$$

Hence, defining

$$v(r) = u(r) - D \qquad \ldots\ldots (4.11)$$

the function (4.4) takes the form

$$g_c^{(2)} = \gamma(R)\exp\left(-\frac{\Phi}{kT}\right)\{1 + \mathbf{b}\,.\,\mathbf{R}[v(r) + D]\}. \qquad \ldots\ldots (4.12)$$

To this can be added any solution of the homogeneous equation corresponding to (4.7) such as

$$g_a^{(2)} = \gamma(R)\exp\left(-\frac{\Phi}{kT}\right)\left[1 + \frac{\Phi}{kT^2}\mathbf{b}\,.\,\mathbf{R}\right]. \qquad \ldots\ldots (4.13)$$

This contribution takes account of the fact that the radial distribution function must vary from point to point when the temperature is not uniform. The complete distribution function is then written in the form

$$g^{(2)} = (1 - A)g_c^{(2)} + Ag_a^{(2)} \qquad \ldots\ldots (4.14)$$

where A is a constant of integration. By (4.14) and (4.3) the following expressions for the flow are obtained:

$$\left.\begin{aligned}\mathbf{J} &= \frac{kT}{2m\beta V^2}\exp\left(-\frac{\Phi}{kT}\right)\left[2\mathbf{b}(\alpha-T^{-1})+\frac{1}{kT^2}\mathbf{b}\,.\,\mathbf{r}\,\frac{\partial\phi}{\partial\mathbf{r}}\right.\\ &\quad\left.-\mathbf{b}\frac{A\Phi}{kT^2}-(1-A)\,\frac{\partial}{\partial\mathbf{R}}\mathbf{b}\,.\,\mathbf{w}\right]\\ \mathbf{j} &= (1-A)\frac{kT}{2m\beta V^2}\exp\left(-\frac{\Phi}{kT}\right)\left[\frac{1}{kT^2}\mathbf{b}\,.\,\mathbf{r}\,\frac{\partial\Phi}{\partial\mathbf{r}}\right.\\ &\quad\left.-\frac{\partial}{\partial\mathbf{r}}\mathbf{b}\,.\,\mathbf{w}\right].\end{aligned}\right\}\quad\ldots\ldots(4.15)$$

In order to specify the distribution function and, hence, the coefficient of thermal conductivity in full, it remains to determine the values of the constants of integration.

§ 5. The Coefficient of Thermal Conductivity

The constants A,C,D are to be determined in such a way that the pressure is uniform and that the flow of matter (in three dimensions) vanishes; the flow of heat should, however, be finite.

The condition of vanishing flow of matter may be expressed in one of the following equations

$$\int(\mathbf{J}_{\mathrm{hi}}+\mathbf{j}_{\mathrm{hi}})d\mathbf{r}_{\mathrm{i}}=0\qquad\int(\mathbf{J}_{\mathrm{hi}}-\mathbf{j}_{\mathrm{hi}})d\mathbf{r}_{\mathrm{h}}=0\,.\qquad\ldots\ldots(5.1)$$

If the distribution (4.14) is employed the two integrals are equal to each other, whatever the value of the constants of integration. This can be shown by separating the integrands into an even and an odd part and showing that the even part enters with equal sign and the odd part with opposite sign into the two expressions.

The first integral is evaluated so that it is a function of $\mathbf{r}_{\mathrm{h}}$. In performing the integration it is admissible to replace $\mathbf{r}_{\mathrm{i}}$ by $\mathbf{r}$ without changing the limits. Cartesian coordinates are employed and the z component of the integral is evaluated. It follows that

$$\left.\begin{aligned}D&=2(\alpha-T^{-1})(1-A)^{-1}-8A(S_3+S_4)[kT^2V(1-A)]^{-1}\\ &\quad-8(S_1+S_2)V^{-1}\\ C&=0\end{aligned}\right\}\quad\ldots\ldots(5.2)$$

where

$$\left.\begin{aligned}S_1&=4\pi\int\exp\left(-\frac{\Phi}{kT}\right)v(r)r^2dr\\ S_2&=\frac{4\pi}{3}\int\exp\left(-\frac{\Phi}{kT}\right)\frac{dv}{dr}r^3dr\\ S_3&=4\pi\int\exp\left(-\frac{\Phi}{kT}\right)\Phi r^2dr\\ S_4&=\frac{4\pi}{3}\int\exp\left(-\frac{\Phi}{kT}\right)\frac{d\Phi}{dr}r^3dr.\end{aligned}\right\}\quad\ldots\ldots(5.3)$$

It can be verified that these values for C and D are suited to satisfy all components of equation (5.1).

The constant A is determined by the condition that the pressure should be uniform. Using an expression for the pressure given by H. S. Green (1947) the condition says that

$$P - \frac{NkT}{V} = \frac{2\pi N^2}{3} \int g^{(2)} \frac{d\phi}{dr} r^3 dr \qquad \ldots\ldots (5.4)$$

should be independent of the coordinates. Writing the function $g^{(2)}$, as determined by equation (4.14), in the form

$$g^{(2)} = \gamma \exp\left(-\frac{\Phi}{kT}\right)[1 + b\Omega] \qquad \ldots\ldots (5.5)$$

the condition becomes

$$\int \frac{d\psi}{dr} \exp\left(-\frac{\Phi}{kT}\right) \Omega r^3 dr = 0. \qquad \ldots\ldots (5.6)$$

Hence:

$$A = \frac{kT[2V - 8T(S_1 + S_2)]S_6 - TVS_5}{8S_6[kT^2(S_1 + S_2) - (S_3 + S_4)] + VS_7 - kT^2VS_5} \qquad \ldots\ldots (5.7)$$

where

$$\left.\begin{aligned} S_5 &= 4\pi \int \exp\left(-\frac{\Phi}{kT}\right) \frac{d\psi}{dr} vr^3 dr \\ S_6 &= 4\pi \int \exp\left(-\frac{\Phi}{kT}\right) r^3 \frac{d\psi}{dr}\, dr \\ S_7 &= 4\pi \int \exp\left(-\frac{\Phi}{kT}\right) \frac{d\psi}{dr} \Phi r^3 dr \end{aligned}\right\}. \qquad \ldots\ldots (5.8)$$

By entering with (5.7), (5.2) and (4.15) into (2.3) the coefficient of thermal conductivity is obtained:

$$\kappa = 2^{3/2}\pi \left(\frac{N}{V}\right)^2 \frac{kT}{\beta m} \int \exp\left(-\frac{\Phi}{kT}\right) \left\{ \psi \left[\frac{r\, d\Phi}{3kT^2 dr} - \frac{A\Phi}{kT^2} - (1 - A)v + E \right] \right.$$
$$\left. + \frac{r\, d\psi}{3\, dr} \left[\frac{r\, d\Phi}{kT^2 dr} - \frac{A\Phi}{kT^2} - (1 - A)v + E \right] \right\} r^2 dr \qquad \ldots\ldots (5.9)$$

where

$$E = \frac{8}{V}\left[(1 - A)(S_1 + S_2) + \frac{A}{kT^2}(S_3 + S_4) \right]$$

and A is given by (5.7).

This expression is the result of the deductions of the last three sections. Before discussing its significance a subsidiary result should be pointed out. By integrating the function $Ng^{(2)}$ with respect to the coordinates of a molecule (for instance $\mathbf{r}_h$) an expression for the local density is obtained. It does not agree with the local density as derived from the assumption of local thermal equilibrium and the use of the experimental coefficient of thermal expansion but provides for an excess in the expansion coefficient equal to

$$2(\alpha - T^{-1}) - 8\left[(1 - A)\frac{S_2}{V} - \frac{AS_4}{kT^2V} \right].$$

§ 6. Discussion

Expression (5.9) for the coefficient of thermal conductivity† differs appreciably from the result of previous deductions. This is a consequence of the revised expression for the flow of energy. The new distribution function depends upon the relative coordinates and the position of the mass centre of molecular doublets, angles entering exclusively by the way of the latter. In contrast the previous distribution functions depended on the orientation of the distance vector. All known or proposed distribution functions are derived from equation (4.1) or an equation of similar form. Previously solutions of this equation were obtained subject to the restriction that deviations from equilibrium were independent of the position of the mass centre. This restriction is abandoned in the present paper and its place is taken by the condition of uniform pressure.

Important aspects of the theory are, however, not affected by the new approach. In particular the previous conclusions concerning the temperature effect (Eisenschitz 1949) remain valid since the new as well as the old distribution function remains continuous at $r=0$. It also remains true that the only quantity specific for transport theory which enters into the coefficient of thermal conductivity is the friction constant β.

Acknowledgment

One of us (A.R.B.) would like to thank the Department of Scientific and Industrial Research for a maintenance award held during the period of this research.

References

Born, M., and Green, H. S., 1947, *Proc. Roy. Soc.* A, **190**, 455.
Eisenschitz, R., 1949, *Proc. Phys. Soc.* A, **62**, 41.
—— 1952, *Proc. Roy. Soc.* A, **215**, 29.
—— 1955, *Phys. Rev.*, **99**, 1059.
Green, H. S., 1947, *Proc. Roy. Soc.* A, **189**, 103.
—— 1952, *Molecular Theory of Fluids* (Amsterdam : North-Holland), Ch. V.
Green, M. S., 1954, *J. Chem. Phys.*, **22**, 398.
Irving, J. H., and Kirkwood, J. G., 1950, *J. Chem. Phys.*, **22**, 817.
Kirkwood, J. G., 1935, *J. Chem. Phys.*, **3**, 300.
—— 1946, *Ibid.*, **14**, 180.
Turner, R. E., 1958, *J. Chem. Phys.*, **29**, 856.
Zwanzig, R. W., Kirkwood, J. G., Oppenheim, I., and Alder, B. J., 1954, *J. Chem. Phys.*, **22**, 783.

† Whereas here a closed expression for κ is obtained there was, so far, no similar expression known for the viscosity since the differential equation corresponding to (4.9) had to be solved numerically. We have now found a solution of this equation in closed form by the use of a Green's function

$$K(\mathbf{r}, \mathbf{r}') = \int_{|\mathbf{r}-\mathbf{r}'|}^{\infty} \exp\left(\frac{\phi(t)}{kT}\right) t^{-2}\, dt$$

which yields the coefficient of viscosity in a form similar to (5.9).

RESEARCH NOTES

On the Thickness of Helium Films

By B. K. AGARWAL
Physics Department, Allahabad University, Allahabad, India

MS. received 13*th April* 1959

Jackson and Grimes (1957, 1958) have recently measured the thickness of liquid helium films for the height range 1–7 cm. Between 1–1·6 cm the (experimental height, thickness) curve can be represented within the probable experimental error by the formula proposed by Atkins (1954),

$$H=\left(\frac{a}{d}\right)^3+\left(\frac{b}{d}\right)^2 \qquad \ldots\ldots(1)$$

where d is the film thickness, H the film height, and a and b are adjustable constants. For curves at the different temperatures the value of b has to be changed. Franchetti (1957) has suggested an expression

$$H=\frac{a}{d^3}+\frac{b}{d^2}+\frac{C(T)}{d^2}, \qquad \ldots\ldots(2)$$

which is expected to hold good for a much wider range, but the final figures are not yet available.

The purpose of this note is to point out that for a sufficiently wide range the variation of film thickness with height can be represented by the simple relation

$$d=Ae^{-H/10}. \qquad \ldots\ldots(3)$$

The value of A and the ranges for which the equation (3) holds good within the experimental error are as follows:

T (°K)	1·62	1·83	2·04
$10^5\times A$ (cm)	$e^{-1\cdot22}$	$e^{-1\cdot19}$	$e^{-1\cdot14}$
Range H (cm)	2–6	2–5	2–5

It is possible to extend the validity of equation (3) for the range 1–5 cm by adding another factor on the right hand side to read

$$d=Ae^{-H/10}+\frac{B}{H^3} \qquad \ldots\ldots(4)$$

where $B=40\times10^{-8}$ cm is another constant. The values of A for equation (4) for the range 1–5 cm are:

T (°K)	1·62	1·83	2·04
$10^5\times A$ (cm)	$e^{-1\cdot24}$	$e^{-1\cdot20}$	$e^{-1\cdot16}$

Above 5 cm height the calculated curves for different temperatures according to equation (4) are consistently lower than the corresponding experimental curves and come closer to each other while the experimental curves appear to diverge in this region. One should expect that at sufficiently great height the film thickness will acquire some minimum value for all temperatures.

ACKNOWLEDGMENT

The author is grateful to Dr. L. C. Jackson for sending an enlarged diagram of the (height, thickness) curves for helium and details about the experimental error.

REFERENCES

ATKINS, K. R., 1954, *Canad. J. Phys.*, **32**, 347.
FRANCHETTI, S., 1957, *Nuovo Cim.*, **5**, 183, 1266.
JACKSON, L. C., and GRIMES, L. G., 1957, reported at Low Temperature Conference, Madison: to be published in *Phil. Mag.*
—— 1958, *Advanc. Phys.*, **7**, 435.

NOTICE TO AUTHORS

Authors of papers on experimental measurements are advised to include information concerning the purity and structure (grain size, homogeneity, degree of working phases present, etc.) of materials used. This should be as complete as the nature of the measurements being made requires and should include the source of the material and method of preparation.

REVIEWS OF BOOKS

Handbuch der Physik, Vol. 38/1, *External Properties of Atomic Nuclei*, edited by S. Flügge. Pp. vi+471. (Berlin, Göttingen, Heidelberg: Springer, 1958.) DM 135.

Probably the most important job for a reviewer of a volume of the *Handbuch der Physik* is to give a list of contents, which is as follows for this volume:

Atomic masses of nuclides, by A. H. Wapstra, 37 pp.

With table of binding energy and mass excess, a discussion of trends and magic number effects, alpha and beta decay systematics.

Determination of atomic masses by microwave methods, by S. Geschwind, 21 pp.

Revised from the article by the same author, Gunther–Mohr and Townes in *Rev. Mod. Phys.*, 1955, **26**, 444.

Determination of nuclear spins and magnetic moments by spectroscopic methods, by F. M. Kelly, 37 pp.

Atomic spectra (optical) and atomic beams; statistics in molecular spectra.

Isotope shifts, by Lawrence Wilets, 24 pp.

Nuclear mass, field, deformation and compressibility effects.

Nuclear magnetic resonance, by G. Laukien, 257 pp.

Theory, practice and results of nuclear magnetic resonance, with table of nuclear magnetic moments and spins.

Determination of nuclear quadrupole moments, by C. H. Townes, 77 pp.

A thorough discussion of nuclear electric quadrupole effects in atoms, molecules and solids, with table of quadrupole moments.

The most striking feature of this volume is that the one article in German (the rest are in English) is an order of magnitude longer than any of the others. Containing such details as circuit diagrams, scale drawings of permanent magnets and magnetic induction heads, Dr. Laukien's article is a good-sized monograph on nuclear magnetic resonance and might perhaps have better been issued as such. It now occupies rather more than half a volume costing DM. 135, and at this price is not likely to be found on the tables of many research students in nuclear magnetic resonance. B. BLEANEY.

Solid State Physics, by A. J. Dekker. Pp. xiv+540. London: Macmillan, 1958). 45*s*.

The transition from the study of the 'properties of matter', as defined in many an examination syllabus, to a real understanding of the properties of solids has now reached a stage when several good undergraduate textbooks have become available. Dekker's *Solid State Physics* is one of the best of these. Messrs Macmillan are to be congratulated on bringing out this edition at so reasonable a price. It is to be hoped that the book will achieve a success that will encourage the production of similar editions of other useful but expensive American texts.

The book opens with an account of the properties of crystals, which moves rapidly from a consideration of crystal lattice types to lattice vibrations, lattice defects and dislocations. There follow chapters on the dielectric and

conduction properties of non-metals, on the electron theory of metals, and on the properties of semiconductors. The remainder of the book discusses special topics, the longest section dealing with magnetic properties. The treatment is generally elementary, with mathematical proofs kept to a minimum. This policy enables the author to cover an immense range of topics without taking the student out of his depth, but some of the omissions are surprising; for example, in the chapters on the electron theory of metals the formula for the free electron specific heat is simply quoted with a reference to Seitz, though a later chapter gives a proof of Bloch's theorem and a discussion of the Kronig–Penney model.

The book succeeds in its object of presenting an overall picture of an important and rapidly growing section of physics. It is well printed and produced, and can be recommended as a very useful text for students in their final undergraduate or first graduate year. A. H. COOKE.

Colloque National de Magnétisme (commémoratif de l'oeuvre de PIERRE WEISS). Pp. x+338. (Paris: Centre National de la Recherche Scientifique, 1958.)

The place and subject of this conference reminds one of the 1939 Strasbourg Conference on Magnetism and one is tempted to compare the two. This would be unfair to the book under review. The 1939 Conference was an international meeting covering all aspects of magnetism. Its proceedings, containing authoritative and meaty reviews of all aspects of magnetism with a seasoning of fully reported discussions, provided a unique picture of the status of magnetism at the outbreak of World War II. This 1957 Conference was modest in scope, and national in character, with only two contributions from outside France. It was organized to celebrate the 50th anniversary of the publication of Pierre Weiss' paper which postulated the ' molecular field ' and thus laid the foundation of modern theories of ferromagnetism.

L. Néel, in a masterly review, traces the development of Weiss' ideas and shows how the replacement of the ' mean ' molecular field by a ' local ' molecular field has finally led to an understanding of antiferromagnetism and to the concept of ferrimagnetism. The other general review in the proceedings is by C. Guillaud and R. Vautier on ferromagnetic domains. It describes, in simple terms, domain theory and the mechanisms of magnetization and is particularly notable for the large number of excellent photographs of Bitter patterns. There is no doubt that if this book fell into the hands of fabric designers or interior decorators we should soon have the ' méandres arborescents ' of the domains of Ni-ferrite greeting us from walls, curtains and—why not—ladies' dresses.

The remaining 24 more specialized contributions cover a variety of topics. There are two comprehensive papers on rare earth metals and oxides (by Trombe and by Mlle. Blanchetais), a brief theoretical discussion by Friedel and de Gennes of the effect of spin disorder on electrical resistivity, several papers on ferrites and garnets, and a paper by Weil on the behaviour of single domain particles (' paramagnétisme apparent ', or ' superparamagnetism ' in American nomenclature). Other subjects include metamagnetism, antiferromagnetism and magnetic resonance and relaxation. On the whole this is a useful book which gives a good idea of the problems and preoccupations of modern magnetism.

N. KURTI.

Principles of Modern Physics, by A. P. FRENCH. Pp. viii+355. (New York: Wiley; London: Chapman and Hall, 1959.) 54*s*.

This is an excellent book about atoms, electrons, radiations and nuclei; its method and style are those of the lecture-room and the tutorial class rather than those of the textbook writer's study. It is suitable for students who are familiar with classical physics as taught in the earlier years of most university courses and who have some preliminary knowledge of the atomic structure of matter, the nuclear structure of atoms and the facts of quantum physics.

Professor French achieves a well-judged balance between the historical approach and the more economical but less educative plan of dealing only with currently accepted facts and theories. He mentions some of the historical blind alleys, without going far up them; and when giving examples of experimental results he chooses sometimes the earliest and sometimes the best measurements. Thus, while the logical framework of his book is the growth of physical concepts, Professor French has managed to include a substantial amount of information, giving much more than a commentary if something less than a full account of the subjects.

The order in which topics are taken is crucial, and those which come early get the best showing. The first two chapters deal with molecules in gases and with electromagnetic theory, the next two with the atomicity of electricity and the quantization of energy. There follows a chapter on quanta and atoms which reviews the main phenomena of atomic physics in terms of the Bohr–Sommerfeld quantum theory; the emphasis on dynamics as opposed to basic structure is illustrated by the small prominence given to Rutherford's discovery of the nucleus. Relativity and de Broglie–Schrödinger quantum mechanics lead to a final chapter in which selected nuclear phenomena are reviewed.

It is easy to criticize the selection of individual topics (for example, the impact of Bohr's theory of nuclear reactions is blunted by the introduction of alpha-ray resonances in place of the more spectacular and historically significant neutron resonances) but it would not be easy to make a generally better selection from the riches of atomic and nuclear physics. P. B. MOON.

Physics, by L. S. POWELL. Vol. I, *Mechanics, Heat and Sound*. Pp. xvi+488. 21*s*. Vol. II, *Electricity and Magnetism*. Pp. xvi+543. 30*s*. Vol. III, *Light*. Pp. xvi+252. 25*s*. (London: Pitman, 1958.)

These volumes are written for students attending National Certificate courses in technical colleges and the complete work is, no doubt, thoroughly adequate for this purpose. The needs of the readers for whom the work is intended are reflected in the distribution of emphasis and the methods of presentation, both of which differ from those in books on pure physics of a comparable standard of attainment, namely G.C.E. advanced and scholarship levels. The emphasis on applied physics is most noticeable in the section on Heat in volume I and in Electricity and Magnetism, volume II.

On the whole, the author makes a praiseworthy attempt to induce his readers to follow and appreciate fairly rigorous presentations of physical principles. Occasionally the attempt is half-hearted, however. For example (although this is perhaps excusable) the idea of mass is only vaguely presented, and the treatment and diagrams of a Fletcher's-trolley type of system may well mislead

students into thinking that the tension in a string supporting a vertically accelerating mass is equal to the weight of the mass. It is questionable, too, whether a cornering cyclist should be treated as a case of equilibrium. The section on the formation of drops (p. 387, volume I) is quite erroneous and appears to lead nowhere.

It is understandable that the author should use the m.k.s. system of units in volume II. In a major work of this kind, however, in which the logical development of the subject is elsewhere by no means ignored, the failure of the m.k.s. method of presentation to exhibit the step-by-step growth of electrical theory is only too obvious. To Mr. Powell's credit it must be said, however, that immediately after stating the m.k.s. definition of the ampere he gives a qualitative account of the action of various current-measuring instruments. This partially bridges the gap (often left wide open in m.k.s. textbooks) between the infinitely long straight wires of the definition and the somewhat more compact instrument labelled ' amperes ' which the student finds on the laboratory bench. Volume II contains a substantial amount of alternating-current theory and of electronics, both of which are well done.

Volume III, on Light, differs very little from an advanced level textbook and is very satisfactory indeed, despite one or two ray diagrams which ought to be re-drawn in the next edition (for example, rays passing through the centre of a lens in figure 81 appear to suffer deviation).

Mr. Powell has made a substantial and, on the whole, a very sound contribution to the collection of physics textbooks for engineers. R. C. BROWN.

Introduction à la Théorie des Gaz Ionisés, by J. L. DELCROIX. Pp. xi + 170. (Paris: Dunod, 1959.) 1100 *fr.*

The theoretical study of ionized gases can be undertaken from two complementary standpoints. One approach is to consider the microscopic description of the state of the gas, determine the velocity distribution functions, taking into account applied forces and collision phenomena, and then apply the methods of the kinetic theory of gases. The other method is to consider the macroscopic description and the hydrodynamics of the ionized gas, which is a more complicated treatment than that for the case of ordinary fluids because an ionized gas is a mixture of several interacting constituents—electrons, ions and neutral molecules. For the reason that the neglect of the microscopic method can, in some circumstances, lead to serious error, the author of this excellent monograph has based his treatment of the fundamentals of ionized gases on the microscopic approach.

There are four useful introductory chapters on the elastic collisions of particles, explaining how the law of scattering is calculated from the law of force between the particles. Chapter V deals with the theory of a free electron gas and considers the effects of an alternating electromagnetic field and the phenomenon of gyromagnetic resonance. In the next two chapters Boltzmann's equation is used to calculate the electrical conductivity and velocity distribution in a weakly ionized gas acted on by a magnetic field and an alternating electric field. In the next two chapters the macroscopic equations applicable to a component of a gaseous mixture are derived and applied to a feebly ionized gas, and in Chapter X the elementary theory of a collective phenomena is given and applied to the oscillations of a plasma. In the final two chapters the microscopic

and macroscopic properties of a strongly ionized gas are treated and the expression for the electrical conductivity is derived.

The treatment is very clear and simple throughout and can be recommended to the Honours undergraduate student and research physicist alike.

F. LL. J.

Liquid Helium, by K. R. Atkins. Pp. x+312. (Cambridge: University Press, 1959.) 60*s*.

In this, the first book devoted entirely to the properties of liquid helium. Professor Atkins has given a wide survey of the work done to date. Experimental methods and observations are quite fully discussed together with accounts of current theories, which now go a long way to explain the behaviour of this strange liquid.

Most of the book, naturally, deals with the properties of helium II, but there are chapters on liquid helium 3 and on liquid mixtures of helium 3 and helium 4. There is a useful introductory chapter in which the chief characteristics of helium II are briefly but clearly described. The author's well-known interests are reflected in two comprehensive chapters on first and second sound and on helium films. One or two topics (especially thermal conductivity) are divided somewhat between several chapters, but can be located with the help of the index.

There are about 500 references which give a pretty complete, although not entirely comprehensive, summary of the literature. All in all, this is a very useful book which will be prescribed reading for workers entering this field and a valuable source of reference for everyone else. J. WILKS.

Le Bruit de Fond, by P. Grivet and A. Blaquiere. Pp. xi+496. (Paris: Masson, 1958.) 6.500 *fr*.

Le Bruit de Fond is the fourth in a series of textbooks on various aspects of electronics written under the direction of Professor Grivet. In general the book is well written although somewhat chaotically organized. It should prove easy to read by students with an elementary knowledge of both French and mathematics. The book is rich in both numerical examples and supplementary references and contains an admirable collection of formulae pertaining to the origins of noise in various electrical systems: transistors, photoelectric cells, ionization chambers, thermocouples, as well as more conventional circuit elements. The last two chapters deal with noise filtered through non-linear networks and noise from the point of view of information theory.

In contrast to the modern content of the sections which deal with the origins of noise in electronic systems, the treatment of the mathematical theory of filtered noise, i.e. the structure of noise, is regrettably old fashioned. At the outset (p. 122) the authors refuse to deal with what in Brownian motion is called the Langevin equation, and statisticians call an auto-regressive scheme. On the one hand it is asserted that such schemes are physically unjustifiable (a debatable point), but on the other they resort to the even more questionable procedure of Fourier analysis of a single noise record. Although the statistical foundation of the time series is acknowledged, the authors only mention the distribution of amplitudes and make no mention of the existence of a transition

probability connecting one amplitude to the next, thereby losing the distinction between a process and an uncorrelated collection of numbers.

For this reason, it would seem advisable for the student to read this book in conjunction with a more theoretical treatment. M. N. MOORE.

Sampled-Data Control Systems, by E. I. JURY. Pp. xv+453. (New York: John Wiley; London: Chapman and Hall, 1958.) 128*s*.

This well-produced book is concerned almost entirely with the mathematical analysis of sampled-data systems, and does not discuss their practical problems. But within the mathematical field the book is comprehensive, and gathers together a great deal of work previously available only in papers and theses. The author, assisted by his research students at the Electronics Research Laboratory of the University of California at Berkeley, has himself made a considerable original contribution to this field of work, and clearly writes with authority. The fact that in some control systems the data are available only as samples—an example of this, of growing importance, is the use of digital computers in a control system—allied with the advantages of sampling even when continuous information is available, e.g. time-sharing, makes the subject one which is certain to grow in importance. It would appear therefore that this book is likely to become a basis for much technical advance.

The main process used in the book is the z-transform method of analysis. (The z-transform is the Laplace transform of a sampled signal.) The mathematical level is high, and the book will be usable only by postgraduate students with a mathematical leaning and research engineers and physicists of the more academic type. To these the book can be recommended. D. G. TUCKER.

The Neutrino, by JAMES S. ALLEN. (Investigations in Physics, Vol. 5.) Pp. viii+168. (Princeton, New Jersey: Princeton University Press; Oxford: University Press, 1958.) 36*s*.

The neutrino was invented in 1933. When it was discovered is difficult to define, but somehow in the past quarter-century it has risen to the status of a fully established elementary particle. This is so in spite of the remarkable paucity of observable properties that can be ascribed to it. In the very recent past, in connection with the discovery of parity violation our knowledge of its characteristics has become much more precise and, in addition, the entirely new fact has been established that the neutrino possesses a screw sense. Unless big surprises are in store our picture of the neutrino now seems to be pretty definitive.

The book under review represents the first attempt to give a survey of the entire field of neutrino physics. Though relevant theory is not omitted, the emphasis is experimental. Chapter by chapter, the book gives an excellent account of how the various attributes of the neutrino have been established. Since work up to March 1958 is included the account is up to date in its main features, though unfortunately some of the most conclusive experiments reported in the past year could not be included. Even so the book can be warmly recommended to both experimental and theoretical workers in the field. It may be hoped that a new, definitive edition will soon appear. N. KEMMER.

Elasticity and Plasticity (Surveys in Applied Mathematics, Vol. I), by J. N. Goodier and P. G. Hodge, Jr. Pp. ix+152. (New York: John Wiley; London: Chapman and Hall, 1958.) 50*s*.

It was an ambitious project to summarize the developments in elasticity and plasticity during the last twelve years within the compass of 120 pages; the coverage can scarcely be adequate, and the condensation must be excessive.

It is odd to find the theory of plates and shells excluded from the theory of elasticity, but by such selection the author is able in 42 pages to mention most of the other main branches of the subject, although no more than a sketch is attempted. Moreover, the exposition is based mainly on the Russian school and on Green and Zerna's book, and the further concentration on the less accessible references makes it difficult for the reader to supplement the author's account from other readier sources. The 77 pages on plasticity prove easier to read but no less difficult to master, because the lucid exposition of the flow theory and the illustrations of kinematic, isotropic and slip hardening by means of the Prager yield stress frame need to be thoroughly understood before the capabilities as well as the limitations of the easier deformation theory can be appreciated. For these reasons neither essay is suitable for students except under expert guidance.

The chapters on plasticity are in the main simply informative; the mathematical tools are laid out in good order, and the reader will find the display useful in selecting the tool for this particular job; and whichever tool he chooses, even if it be the deformation theory, he should be better able to use it to advantage. Far otherwise with the chapters on elasticity, which starting with the complex variable too quickly advance into the realm of purely mathematical analysis, epitomized by the passing reference to singular integral equations. This is a valuable and entrancing study, but it is not the only one, and the subsequent short paragraphs on other branches serve only to heighten the emphasis on boundary, and particularly mixed boundary, problems.

Each paper is in effect a descriptive guide to the mathematical literature, and the gain to the reader will depend on how much more reading he is prepared to undertake.

The printing and proof reading are excellent, the layout not so good.

H. L. Cox.

Liquid Scintillation Counting, edited by C. G. Bell and F. N. Hayes. Pp. xi+292. (London, New York, Paris, Los Angeles: Pergamon Press, 1958.) 70*s*.

This book consists of papers presented at a three-day conference on liquid scintillation counting held at Northwestern University, U.S.A. in August 1957.

It is largely concerned with the use of liquid scintillators in routine counting of ^{14}C and ^{3}H in a wide variety of tracer studies. In view of the widely different interests of the participants, most papers take little for granted and there is consequently a certain amount of duplication in the descriptions.

A large number of the problems encountered in the use of liquid scintillators are however described, surmounted in a variety of ways or merely endured.

Somewhat naturally there tends to be an insufficient discussion of the reasons for using liquid scintillators in particular applications. However, this notably does not apply to the paper on carbon dating by J. R. Arnold. A description of the Los Alamos human counter by E. C. Anderson is of considerable interest.

Of interest to physicists, there are papers by Kallman and Furst on ' The basic processes occurring in the liquid scintillator '; Swank on ' The limits of sensitivity of liquid scintillation counters '; Harrison on ' Liquid scintillation counters and their application to physics ' and Brooks' short paper on ' Scintillation counters with pulse shape selection to distinguish neutrons from γ-rays '. Finally, perhaps most interesting of all, Reines on ' Giant liquid scintillation detectors and their applications '.

In the absence of a textbook devoted to liquid scintillation counters this book constitutes a useful substitute in addition to being a well-produced account of the proceedings of a conference. D. WEST.

Nuclear Spectroscopy Tables, by G. J. NIJGH, A. H. WAPSTRA and R. VAN LIESHOUT. Pp. vii + 135. (Amsterdam: North-Holland Publishing Co., 1958.) 60*s*.

The title of this book is, perhaps, misleading. The book contains very little factual information about nuclear spectra (although there is quite a good deal about *atomic* spectra), as distinct from information relevant to the study of nuclear spectra. The title " Tables for Nuclear Spectroscopists " would have been more accurate.

The book is a compilation of numerous diagrams, tables and nomograms giving such information as: mass and abundances of stable isotopes; range, energy and magnetic rigidity tables for electrons, protons, etc.; absorption and scattering of γ-rays; functions relating to allowed and forbidden β-spectra; x-rays and Auger electrons; angular correlation formula and tables for the simpler types of process. In addition, there is a chapter on nuclear models, which rather surprisingly includes the data on measured nuclear spins and tables of Clebsch–Gordan coefficients, as well as some of the chief results of the ' shell ' and ' collective ' models.

Workers in the field of nuclear spectroscopy will certainly find compilations such as the present one useful, but no two of them would agree about what should or should not be included. Nevertheless, it would seem hard to justify the devotion of much space to such things as logarithmic tables and the theory and practice of errors, whilst at the same time omitting such information as nuclear magnetic and electric moments, Coulomb-excitation cross sections, internal conversion coefficients, and even a table of the known radioactive nuclei. S. DEVONS.

The Green Flash and Other Low Sun Phenomena, edited by D. J. K. O'CONNELL. Pp. 192. (Amsterdam: North-Holland Publishing Co., 1958.) 45*s*.

This book is attractively produced, with 80 photographs in colour, by C. Treusch, chiefly devoted to recording and explaining the causes of an interesting meteorological phenomenon infrequently observed in this country. It is to be seen at early sunrise and late sunset; sunrise in Egypt is propitious. Explanations have been given calling on physiology, sea-wave refraction, anomalous dispersion or selective absorption in the atmosphere, Rayleigh scattering, and absorption and scattering by dust. The author considers that all except the first two are concerned. When the upper rim of the sun is almost on the horizon, most of the orange and yellow is absorbed, the red has already ' set ', and the green and shorter wavelengths are left. If, in addition, the blue and

violet are scattered, green remains. The author has made experiments in the laboratory to simulate these conditions. A. C. MENZIES.

Quantum Particle Dynamics, by J. McConnell. Pp. xii + 252. (Amsterdam: North-Holland Publishing Co., 1958.) 40*s*.

In the introduction, Professor McConnell states that the purpose of this book is to introduce the uninitiated student to (1) the special theory of relativity, (2) quantum mechanics, (3) quantum electrodynamics and (4) their application to meson and elementary particle physics. The book is 245 pages long and the above four topics occupy 23, 120, 62 and 40 pages respectively.

To expound all these ideas satisfactorily in 245 pages has proved impossible. Although the exposition is clear, it suffers from over-condensation, omission of important topics and a lack of applications, so essential for gaining an understanding. These criticisms apply particularly to the 87 pages devoted to non-relativistic quantum mechanics. In the chapters on quantum electrodynamics there are helpful applications to Compton scattering, etc. The non-covariant formalism is used which is probably justifiable in an elementary introduction. Such important topics as the quantization of the Dirac field are omitted.

The two concluding chapters, on mesons, antinucleons and strange particles, could do no more than whet the reader's appetite. Unfortunately, much of the material presented is out of date and misleading. To give one example: rather than repeat the Compton scattering perturbation calculation for meson–nucleon scattering, it would have been better to discuss the $(\frac{3}{2}, \frac{3}{2})$-resonance which dominates pion physics. F. MANDL.

Vacancies and Other Point Defects in Metals and Alloys (Monograph and Report Series No. 23). Pp. iv + 238. (London: The Institute of Metals, 1958.) 40*s*.

In December 1957 the Institute of Metals held a very well attended symposium at Harwell at which the six review articles which are now published were presented. The papers are: Point defects and the mechanical properties of metals and alloys at low temperatures, by A. H. Cottrell; The effect of lattice defects on some physical properties of metals, by T. Broom and R. K. Ham; Point defects and diffusion in metals and alloys, by W. M. Lomer; Point defects and mechanical properties of ionic crystals, by P. L. Pratt; Point defects near the surface of a metal, by E. C. Williams and P. C. S. Hayfield; and Point defects and the mechanical properties of metals and alloys at high temperatures, by D. McLean.

Amongst the many topics which are dealt with are the effect of irradiation on the mechanical properties, resistivity measurements after quenching, irradiation and annealing and their interpretation, creep and the mechanism of oxide film formation. Whilst the papers show how the concept of point defects has enabled us to interpret phenomena in many different fields, they also emphasize that we are still a long way from fully understanding the details of the mechanisms which are involved.

The book includes the discussion of the papers and extensive bibliographies. It should prove a most useful reference to all who are interested in the physics of metals. H. M. ROSENBERG.

Planning of Experiments, by D. R. Cox. Pp. vii + 308. (New York: John Wiley; London: Chapman and Hall, 1958.) 60*s*.

In contriving their experiments most physicists make little use of statistical design methods because their experimental objects are simple compared with biological material and they are able to secure a comparatively large degree of isolation between their experiments and the outside world. Physicists working on the fringes of, say, biology or meteorology, or concerned with experiments on a production scale in industry must, however, know that the efficiency of experiments and the best use of data may depend critically on the proper appreciation of random factors. The book under notice is an admirable elementary account of the techniques of randomization. Its approach is reasonable rather than mathematical; there are a great many examples, taken mainly from agricultural, medical and industrial experiments, which indicate the kinds of error which can be reduced by proper experimental design. Each chapter contains a useful summary of its scope, and is well provided with references.

The analysis of variance, the mathematical treatment of results to assess their significance, is specifically excluded, so that other statistical help will usually be required. The ideas underlying some of this analysis are however presented particularly clearly. H. J. J. BRADDICK.

The Magneto-ionic Theory and its Applications to the Ionosphere, by J. A. Ratcliffe. Pp. x + 206. (Cambridge: University Press, 1959.) 40*s*.

The magneto-ionic theory has found its main applications in radio studies of the earth's ionosphere and since Appleton first published the basic equations in 1927 and 1932, there have been many papers dealing with the interpretation of various aspects of the equations. In this monograph Mr. J. A. Ratcliffe provides a most comprehensive and excellent account of the whole subject. Any consideration of the problem of electromagnetic wave propagation in an ionized medium with an imposed magnetic field, inevitably involves some complicated mathematical formulae and in this book all the relevant mathematics will be found, but the general approach is essentially that of a physicist and at every stage the author has been concerned to present a clear and detailed description of the basic physical processes. The result is a very lucid and satisfying presentation of this complex problem.

In Part I of the book the equations governing the dispersion and the absorption of the waves are each derived from ' macroscopic ' and ' microscopic ' standpoints. Most published work has been based on a macroscopic approach and much of the ' fine-structure ' type of analysis now given, especially the treatment of the absorption process, represents an original (and instructive) approach.

In the six chapters which form Part II, a thorough survey is made of the implications of all the various aspects of the equations and the important features are presented in graphical form. The calculations of the refractive indices and absorption coefficients from the basic equations, for any specified set of conditions, is extremely tedious and in this connection there is a valuable chapter outlining a method whereby the essential features of the curves can be obtained fairly quickly.

The application of the equations to the terrestrial ionosphere is described in Part III and here again attention is given to the physics of the phenomena and an interesting chapter included in which numerical estimates are made of the movements of electrons in the ionosphere under the influence of a wave from a high-power radio sender.

In the concluding section various miscellaneous topics are discussed. These include a consideration of the Lorentz term controversy, of waves in electron–ion mixtures, of propagation in inhomogeneous media and of the relationship between magneto-ionic propagation and the optics of crystalline media.

An adequate bibliography is included with brief notes on the contents of the more important papers.

Unfortunately there has been, until recently, no commonly agreed nomenclature for this subject, but in 1954 a Committee of the International Scientific Radio Union (U.R.S.I.) prepared a comprehensive list of symbols for use in magneto-ionic theory and it is gratifying to note that these have been used in the present volume. It is to be hoped that all future contributors to the subject will now adopt this set of symbols.

The production of the book is fully in keeping with the high standards of the publishers and the monograph will be indispensable to all workers in this field.

W. J. G. BEYNON.

The Electrical and Magnetic Properties of Solids, by N. CUSACK. Pp. xiv + 428. (London: Longmans, Green and Co., 1958.) 45*s*.

While there are excellent books dealing with solid state physics either as a whole, or in specialized applications, there has been a lack of textbooks treating the subject at a level suitable for undergraduate or immediate post graduate students. The present book is therefore very welcome since it provides an introduction at a suitable level to a wide range of phenomena which are of interest both theoretically and experimentally.

The scheme of treatment adopted is to discuss in the first chapter the free electron model and in the next five chapters investigate how far this approximation provides an explanation of observations on contact potential, electrical resistivity, thermoelectric effects and so on. The essential correctness, as well as the inadequacies, of the simple theory are thus demonstrated and the reader is guided to think of the effect of the crystal lattice on the electrons. Chapter 7 introduces the band theory which is used wherever necessary in the following chapters. This method of approach has much to commend it to those readers for whom the book is intended and the treatment of the different topics will enable them to progress to the more specialized articles and books referred to in the text without being overwhelmed at the outset by mathematical complexities. A book of this character, although wisely restricted to deal only with electrical and magnetic phenomena, is still necessarily selective even in this field and the emphasis will almost certainly differ from what is required in some undergraduate courses. However, the arrangement of material is such that supplementary matter may easily be introduced in lecture courses.

The author is to be congratulated on producing a book which admirably fulfils his intentions. The price, clear type and easy opening of the book will contribute to its success.

F. E. HOARE.

Annual Review of Nuclear Science, Vol. 8 (1958), edited by E. SEGRÈ. Pp. vii + 417. (Palo Alto, California: Annual Reviews Inc., 1958.) $7.50.

The eighth volume of this well-known series maintains the tradition of speedy publication established by its predecessors. Many of the articles were completed as little as 8 months before the volume became available for review; as usual they primarily survey developments of the last few years in their subjects, but several give a more extensive general account. Among the latter are the articles by G. C. Wick on ' Invariance principles of nuclear physics ' and by H. Feshbach on ' The optical model and its justification '. Many readers will welcome a statement on the optical model by one of its founders which brings together both the high and low energy aspects of this useful concept.

W. F. Fry gives a short descriptive summary of knowledge on ' Hyper-fragments ' and E. Segrè, in a mainly experimental article of exceptional clarity and interest, relates the story of 'Antinucleons '. Another experimental article, by J. W. M. DuMond, gives an account of the techniques and the extremely precise results of ' Gamma-ray spectroscopy by direct crystal diffraction '. There follows ' Conceptual advances in accelerators ', by D. L. Judd, a stimulating article dedicated to the " almost explosive growth of accelerator construction in the range above 500 MeV in the past 4 years ", and giving impressive testimony to the genius of the late E. O. Lawrence. The evolution of this subject into a major field of theoretical and experimental research is well outlined.

There are four articles, not unrelated, on affairs of the cosmos. H. V. Neher reviews ' The primary cosmic radiation ', H. E. Suess gives a sober, timely account of the ' Radioactivity of the atmosphere and hydrosphere ', L. T. Aldrich and G. W. Wetherill discuss both old and new methods of establishing ' Geochronology by radioactive decay ' and A. G. W. Cameron reports on the whole fascinating story of stellar evolution from condensation to supernova in his article ' Nuclear astrophysics '.

The volume concludes with a useful statement by B. J. Moyer on ' Practical control of radiation hazards in physics research ', a review of radiation damage from the biological point of view (' Cellular radiobiology ' by T. H. Wood) and an article by H. Quastler on ' Information theory in radiobiology '.

W. E. BURCHAM.

The Logic of Scientific Discovery, by K. POPPER. Pp. 480. (London: Hutchinson, 1959.) 50*s*.

This English translation of Professor Popper's *Logik der Forschung*, brought up to date by 150 pages of new appendices, will be welcomed by all those who are interested in the philosophy of science. Professor Popper's widely known main thesis is that the question of ' falsifiability ' and not ' verifiability ' must furnish the basic criterion as to whether or not a theory has a real scientific content (as opposed to being empty of such content, e.g. ' metaphysical '). In this book, the author develops a systematic presentation of his point of view. Along with a cogent criticism of the familiar positivist doctrines concerning the ' meaninglessness ' of any statement that is not verifiable in experience, he presents an answer to many of the obvious objections to his own point of view, which must arise even on a cursory inspection of the problem. For example, the same line of argument which shows that no conceivable set of experiments can ever definitely verify a theory shows equally well that no such set can

definitely falsify a theory either. In order to deal with this and other similar difficulties, Professor Popper has given a set of further criteria, which serve to define what he calls the empirical content of a theory. These criteria include the notion of theories that are sub-classes of broader theories, theories that are of a different ' dimensionality ' with regard to the empirical data and theories that are ' simpler ' than others. In doing this, he has, in fact, begun to develop at least the nucleus of what may be called a theory of the role of theories in scientific research.

Professor Popper does not ignore the basic difficulty that even with the aid of the criteria described above no probability theory can, strictly speaking, be made either falsifiable or verifiable. He proposes to solve this problem by regarding probability statements as ' existential ' (i.e. as statements of particular facts rather than as universal laws). The reviewer must admit that he was not convinced that the problem can satisfactorily be solved in this way. Nevertheless, many of the arguments are well worth further study, especially those involving the suggestion of defining the property of randomness in terms of absence of correlations in recurrent sequences approaching infinite length.

Without a doubt, Professor Popper has successfully answered many of the objections that can be raised against his notion of the fundamental role of falsifiability in scientific theories. The reviewer feels, however, that a number of important questions have not adequately been faced, especially some of those connected with the theory of probability. In addition, he cannot accept the proposal to identify the empirical content of a theory completely with its falsifiability. For example, it is evidently true, as Professor Popper points out, that any theory that is a special or limiting case of a broader one is easier to falsify, and therefore, has in a certain sense, a greater empirical content. Yet, the broader theory may have another kind of content; namely the prediction of new qualities, which are not falsifiable at the time when the theory is first proposed (as the relativity theory, although containing Newtonian mechanics as a special case, also predicted new qualities, such as the transformation of mass into energy, which were capable of being tested only some time after the theory was originally developed). Moreover, it practically never happens that a broader theory does not predict new qualities. Professor Popper's analysis evidently does not provide any clear way of deciding the relative degree of falsifiability of theories standing in the above described relationship, and therefore does not really help guide us in the choice between such theories.

Without wishing to detract from the importance of the idea of falsifiability, the reviewer would like to suggest that there is another question that must be considered seriously first, if this idea is to be placed in its proper setting, namely that of how and why it has been possible for scientific theories *quite systematically* to comprehend new phenomena very different from those that gave rise to them. To answer this question, one may well have to go outside the narrow domain of the problems of verification and falsification, to consider once again the relationship between our theories and the reality about which they are somehow able to give us genuinely new kinds of knowledge.

Finally, with regard to Professor Popper's discussions on quantum mechanics, it seems to the reviewer that they suffer from the fact that he has not taken Niels Bohr's point of view seriously enough. For even those who disagree with Bohr's conclusions must admit that his arguments are coherent, and that in some parts, they furnish very important insights into the meaning of the quantum

theory. Indeed, it seems doubtful that Bohr's interpretation of the theory can be refuted, except by presenting from the outset a very different interpretation. But Professor Popper can perhaps be pardoned for not fully appreciating Bohr's point of view, because the latter has, unfortunately, not anywhere been given a clear systematic, and up to date expression.

There is no question that this translation, with its new appendices, will fulfil a real need, to help make clear the foundations of Professor Popper's notions of falsifiability, which by now have become almost part of the unconscious mental equipment of those who try to think about the meaning of scientific research. The reviewer hopes that the publication of this translation will also serve as a stimulus to all of us, and not least of all, to Professor Popper himself, to think about the many further questions that grow out of the problems that he has treated in this book. DAVID BOHM.

Handbuch der Physik, Vol. LI, *Astrophysics* II: *Stellar Structure*, edited by S. FLÜGGE. Pp. viii+831. (Berlin, Göttingen, Heidelberg: Springer, 1958.) DM 175.

It must be an extremely difficult problem for the editor of an encyclopaedia to decide how much material can go in without allowing the volume to grow beyond reasonable bounds. In the present case it appears that the availability of books has been an important factor in deciding the length of the various contributions. Thus the existence of Schwarzschild's new book on stellar structure has made it possible to have a relatively brief first section (by Marshal H. Wrubel) on stellar interiors and a similarly brief survey (by Halton C. Arp) of the observational situation concerning the Hertzsprung–Russell diagram.

These two useful surveys are followed by a magnificent and lengthy chapter on stellar evolution by E. M. and G. Burbidge. The whole diffuse field is described in detail, with none of the awkward questions and problems glossed over or overlooked. In spite of the rapid developments in this field, the subject of this major article will remain valuable for many years to come.

Next come brief but thorough surveys of the abundances of the elements, by Aller, Suess and Urey, followed by chapters on variable stars and stellar stability by Ledoux and Walraven. These two chapters make up a substantial fraction of the entire volume and give the first connected account of the theory of the subject since Rosseland's book, over ten years ago. The thorough discussion will be of value not only to the specialists, but to anybody who is interested in developments in higher dynamics. This part of the book, together with the brilliant article on stellar evolution already referred to, make up the core of the book and its most permanent contribution to the subject.

The theory of white dwarfs is discussed concisely and comprehensively by Schatzman, and very useful surveys of the subjects of magnetic fields of stars, novae and supernovae are given by Deutsch, C. Payne-Gaposchkin and Zwicky. The comprehensive lists given in these surveys will be of advantage to all students of the subject.

The volume is particularly valuable therefore because it contains surveys of theoretical and observational fields which are not brought together anywhere else in the literature. Its completeness is marred slightly by the brevity of the first chapter, and here and there one is a little disturbed by lack of reference to work done in this country. But these are minor blemishes in a fine book.

H. BONDI.

Fluctuations of Photon Beams: The Distribution of the Photo-Electrons

By L. MANDEL
Department of Physics, Instrument Technology, Imperial College, London, S.W.7

MS. received 16*th October* 1958, *in revised form* 1*st April* 1959

Abstract. The probability distribution $p(n, T)$ of the number of counts n from a photoelectric detector illuminated by coherent light for a time T is studied, by associating photons stochastically with Gaussian random waves. The cumulants of the distribution are derived and it is shown to be of the expected form for a boson assembly in a limited volume of phase space. The distribution depends strongly on the degeneracy of the light beam. It approaches the Poisson form for classical particles at low degeneracies and the distribution characteristic of classical waves at high degeneracies. The analysis leads, incidentally, to an expression for the extent of the unit cell of phase space in the direction of the beam. It is argued that this should be adopted as the measure of coherence length.

§ 1. Introduction

Purcell (1956) has shown that the fluctuations of the number of photons n detected in a light beam can be calculated by associating the photons stochastically with Gaussian random waves of the appropriate spectral distribution. The validity of this approach has been questioned by Fellgett (1957), but it leads to results which are confirmed by experiment (Hanbury Brown and Twiss 1957) and consistent with Bose–Einstein statistics (Mandel 1958).

While the analysis in the last paper was, with one exception, confined to the calculation of the second moments of the fluctuations, here it is proposed to use the same approach to investigate the probability distribution of n. With the help of an approximation it will be shown that the distribution is of the form to be expected for a boson assembly in a finite volume of phase space. The results show that the form of the distribution is largely determined by the degree of degeneracy of the light beam and give a picture of the transition from the classical particle to the classical wave statistics.

In anticipation of some later considerations, it will be useful first to digress briefly, in order to derive generally the probability $p_s(n)$ of finding a state in which n bosons are distributed among s equal cells of phase space. We shall have occasion to refer to it later.

§ 2. The Probability $p_s(n)$ of finding n Bosons distributed among s Equal Cells of Phase Space

Let there be n_i particles in the ith cell, where $i = 1, 2, \ldots, s$, so that

$$n = \sum_{i=1}^{s} n_i \qquad \ldots\ldots(1)$$

and

$$\bar{n} = s\bar{n}_i, \qquad \ldots\ldots(2)$$

since it is assumed that $\bar{n}_1 = \bar{n}_2 = \bar{n}_3$ etc.

If $p'(n_i)$ is the probability distribution of the n_i then it is well known (e.g. Fürth 1928) that

$$p'(n_i) = \frac{1}{(1+\bar{n}_i)(1+1/\bar{n}_i)^{n_i}} \text{ for } n_i \geqslant 0 \text{ and, using (2),}$$

$$= \frac{1}{(1+\bar{n}/s)(1+s/\bar{n})^{n_i}}. \qquad \ldots\ldots (3)$$

The probability of realizing any particular distribution of the n particles, i.e. any microstate, is therefore

$$\prod_{i=1}^{s} p'(n_i) = \frac{1}{(1+\bar{n}/s)^s(1+s/\bar{n})^n}. \qquad \ldots\ldots (4)$$

Since this is independent of the n_i's all distributions are equally likely. $p_s(n)$ is therefore obtained from the above by multiplying by the number of different realizable distributions, which is given by the well-known combinatorial expression

$$\frac{(s+n-1)!}{n!\,(s-1)!}.$$

The required probability $p_s(n)$ is then

$$\left.\begin{aligned} p_s(n) &= \frac{1}{(1+\bar{n}/s)^s(1+s/\bar{n})^n}\,\frac{(s+n-1)!}{n!\,(s-1)!} \\ &= \frac{(\bar{n}/s)^n}{(1+\bar{n}/s)^{n+s}}\,\frac{1}{(s-1)B(n+1,s-1)}, \end{aligned}\right\} \qquad \ldots\ldots (5)$$

where $B(a, b)$ is the beta-function defined by

$$B(a,b) = \int_0^\infty \frac{x^{a-1}}{(1+x)^{a+b}}\,dx = \frac{\Gamma(a)\Gamma(b)}{\Gamma(a+b)}.$$

When $s=1$ the product $(s-1)\,B\,(n+1, s-1)$ is to be interpreted as the limit $s\to 1$. By writing (5) in the form

$$p_s(n) = \frac{1}{(1+\bar{n}/s)^s(1+s/\bar{n})^n}\,\frac{(s-1)(s)(s+1)\ldots(s+n-1)}{(s-1)n!} \qquad \ldots\ldots (6)$$

we can immediately confirm that

$$\sum_{n=0}^{\infty} p_s(n) = \frac{1}{(1+\bar{n}/s)^s}\left[1-\frac{1}{1+s/\bar{n}}\right]^{-s}$$

$$= 1, \text{ as required.}$$

We shall later have occasion to refer to these results, which are quite general. But we now return to consider the special case of a light beam falling on a photo-electric detector.

§ 3. The Probability Distribution of the Photo-Electrons

As before (Mandel 1958) we shall represent the narrow, coherent, plane polarized beam of light by a real Gaussian random variate $y(t)$ with normalized spectral density $\phi(\nu)$ and assume that the r.m.s. spectral width $\Delta\nu$ of $\phi(\nu)$ is small compared with the mean frequency ν_0. When this beam falls on the photoelectric surface, the probability that a photo-electron is ejected in the short interval between t and $t+dt$ will be $\alpha P(t)dt$, where α is a constant representing the quantum

sensitivity of the photo-cathode and $P(t)$ is the classical beam intensity, i.e. $P(t)$ is the local average of $y^2(t)$ defined by

$$P(t) \equiv \langle y^2(t) \rangle \equiv \frac{\nu_0}{r} \int_{t-r/2\nu_0}^{t+r/2\nu_0} y^2(t')\, dt' \; ;$$

r is a small integer.

Now let $p(n, t, T)$ denote the probability that n photo-electrons are detected in the interval between t and $t+T$. From the stochastic association of the photons with the classical wave intensity, we can write

$$p(1, t, dt) = \alpha P(t)\, dt. \qquad \ldots\ldots (7)$$

It then follows from first principles that the expectation value of n in the interval t and $t+T$ is

$$\alpha \int_t^{t+T} P(t')\, dt'$$

and that $p(n, t, T)$ is a Poisson distribution in n:

$$p(n, t, T) = \frac{1}{n!}\left[\alpha \int_t^{t+T} P(t')dt'\right]^n \exp\left[-\alpha \int_t^{t+T} P(t')\, dt'\right]. \qquad \ldots\ldots (8)$$

However, as has already been pointed out (Mandel 1958) this distribution is not observable and only the time average $\overline{p(n, t, T)} \equiv p(n, T)$ has any physical significance. But, if $y(t)$ is a stationary random process, we may regard $p(n, t, T)$ as a function of

$$\int_t^{t+T} P(t')\, dt' \equiv E$$

and average over the ensemble of E.

Unfortunately, the exact probability distribution $\mathscr{P}(E)\, dE$ of E—which is related to that of

$$\int_t^{t+T} y^2(t')\, dt' \equiv F$$

(cf. Mandel, 1959†)—is not, in general, expressible explicitly (cf. Rice 1945, Kac and Siegert 1947, Siegert 1954). Rice (1945) has suggested a simple approximation to the distribution of F, which we shall take up later. But first we shall examine some properties of $p(n, t)$ that follow directly and quite generally from (8).

The moment generating function $M_p(x)$ of $p(n, T)$ is

$$M_p(x) = \sum_{n=0}^{\infty} \exp(xn)\, \overline{p(n, t, T)}.$$

By using the well-known properties of the Poisson distribution this can be written:

$$\begin{aligned} M_p(x) &= \overline{\exp\left[\alpha E(e^x - 1)\right]} \\ &= M_{\mathscr{P}}[\alpha(e^x - 1)], \qquad \ldots\ldots (9) \end{aligned}$$

where the bar now denotes the ensemble average over E and $M_{\mathscr{P}}(x)$ is the moment generating function of the distribution $\mathscr{P}(E)\, dE$. The corresponding expression for the cumulant generating functions $C_p(x)$ and $C_{\mathscr{P}}(x)$ is therefore

$$\begin{aligned} C_p(x) &= C_{\mathscr{P}}[\alpha(e^x - 1)] \\ &= \sum_{i=1}^{\infty} \frac{\alpha^i (e^x - 1)^i}{i!} \kappa_i \\ &= \sum_{i=1}^{\infty} \sum_{j=1}^{\infty} \frac{\alpha^i x^{ij}}{i!\overline{(j!)^i}} \kappa_i \qquad \ldots\ldots (10\,a) \end{aligned}$$

† Paper read at Physical Society conference on Fluctuation Phenomena and Stochastic Processes, March 1959, to be published.

where κ_i is the ith cumulant of the distribution $\mathscr{P}(E)\,dE$. If K_i is the corresponding cumulant of the required distribution $p(n, T)$, we have, by comparing coefficients of powers of x in (10a):

$$\left.\begin{aligned} K_1 &= \alpha\kappa_1 \\ K_2 &= \alpha\kappa_1 + \alpha^2\kappa_2 \\ K_3 &= \alpha\kappa_1 + \alpha^3\kappa_3 \\ K_4 &= \alpha\kappa_1 + 3\alpha^2\kappa_2 + \alpha^4\kappa_4 \\ K_5 &= \alpha\kappa_1 + \alpha^5\kappa_5 \\ &\text{etc.} \end{aligned}\right\} \quad \ldots\ldots (10b)$$

Now the cumulants κ_i of the distribution $\mathscr{P}(F)\,dF$ of F—which is similar to the distribution $P(E)\,dE$ of E when $T \gg 1/\nu_0$ or when $T = r/\nu_0$, where r is a small integer (cf. Mandel 1959)—have been obtained by Slepian (1958). From his results it follows that, for a stationary Gaussian random process $y(t)$, κ_i is expressible as a multiple convolution integral in terms of the normalized autocorrelation function

$$\gamma(\tau) \equiv \overline{y(t+\tau)y(t)}/\bar{P} \text{ of } y(t).$$

Thus:

$$\kappa_i = 2^{i-1}(i-1)!\,\bar{P}^i \int\int_{-T/2}^{+T/2} \gamma(t_1-t_2)\gamma(t_2-t_3)\ldots\gamma(t_i-t_1)\,dt_1\,dt_2\ldots dt_i$$

$$\text{for } i \geqslant 2. \quad \ldots\ldots (11)$$

With the help of (11), the cumulants K_i of $p(n, T)$ then follow directly from (10). In principle, the distribution $p(n, T)$ is therefore determined.

Two limiting cases of $p(n, T)$ are of particular interest: (a) the mean intensity $\bar{P}$ is very small, corresponding to a non-degenerate photon beam; (b) the mean intensity $\bar{P}$ is very great, corresponding to a highly degenerate photon beam (cf. Mandel 1958).

Since $P(t)$ in (8) always occurs in conjunction with α, it is mathematically convenient to explore these two limiting cases by allowing $\alpha \to 0$ under (a) and $\alpha \to \infty$ under (b).

When $\alpha \to 0$, it follows at once from (10) that

$$K_i \to \alpha\kappa_1 = \alpha\bar{E} = \alpha\bar{P}T = \bar{n}, \quad \ldots\ldots (12)$$

so that $p(n, T)$ is a Poisson distribution in n with mean $\bar{n}$. Thus, a weak, non-degenerate photon beam behaves like a beam of classical particles.

In the second case, when $\alpha \to \infty$, we see from (10) that

$$K_i \to \alpha^i\kappa_i, \quad \ldots\ldots (13)$$

so that the distribution of n tends to become identical with that of αE. Now n is the quantal measure of the total energy absorbed in time T, while αE is the classical measure. It follows that the quantal and classical fluctuations of highly degenerate beams become identical. This result is, of course, to be expected from the correspondence principle.,

We see therefore that, as we pass from very weak to very intense light beams we move from the statistics of classical particles to the statistics of classical waves. But it is unfortunately true that the absence of an explicit expression for the distribution $p(n, T)$ prevents us from gaining very much insight into the nature of this transition. For this reason it is useful to explore the form of $p(n, T)$ with

the aid of an explicit approximation to the distribution $\mathscr{P}(E)\,dE$, which arises from a suggestion first made by Rice (1945).

§ 4. The Approximate Form of the Probability Distribution $p(n, T)$

Rice appears to have been the first to investigate the distribution of F and to calculate some of the low order moments. He found (Rice 1945) that

$$\left.\begin{aligned} \bar{F} &= \bar{P}T \\ \overline{\Delta^2 F} &= \overline{F^2} - \bar{F}^2 \\ &= 4\bar{P}^2 \int_0^T (T-\tau)\gamma^2(\tau)\,d\tau. \end{aligned}\right\} \quad \text{and} \quad \ldots\ldots(14\,a)$$

It is readily shown that the corresponding expressions for E are

$$\left.\begin{aligned} \bar{E} &= \bar{P}T \\ \overline{\Delta^2 E} &= 4\bar{P}^2 \int_0^T (T-\tau)\langle \gamma^2(\tau)\rangle\,d\tau \\ &= \bar{P}^2 T\xi. \end{aligned}\right\} \quad \text{and} \quad \ldots\ldots(14\,b)$$

The latter integral was already encountered in the calculation of $\overline{\Delta^2 n}$ and denoted by $\frac{1}{4}T\xi$ (Mandel 1958), where ξ has the dimension of time and $\xi \gg T$. We shall continue to use this notation.

Rice now suggests that, as a first approximation, (aF) is a gamma-variate with parameter k, i.e.

$$P(F)\,dF \simeq \frac{(aF)^{k-1}\exp(-aF)}{\Gamma(k)}\,d(F). \qquad \ldots\ldots(15\,a)$$

where a and k are to be determined so as to satisfy (14 a). We shall now make the assumption that E approximately obeys a similar distribution, namely

$$P(E)\,dE \simeq \frac{(aE)^{k-1}\exp(-aE)}{\Gamma(k)}\,d(aE), \qquad \ldots\ldots(15\,b)$$

in which a and k are determined to satisfy (14 b). How this distribution can arise and some of the approximations involved in the derivation have already been discussed (Mandel 1959). Loosely speaking, (15 b) arises when the wave $y(t)$ is pictured as a serial superposition of a certain number of wave packets. The following properties of the distribution should be noted:

(1) By definition, it gives the first two moments of E correctly, whence it follows from (10 b), that the first two moments of n will also be correct (cf. Mandel 1958).

(2) It is correct for short time intervals $T \ll 1/\Delta\nu$.

(3) It is correct for time intervals $T \gg 1/\Delta\nu$ when the spectral distribution $\phi(\nu)$ is rectangular. This is shown in the Appendix, where it is proved that the rth cumulant of the distribution of E will, in general, be in error by the factor

$$\left[\int_{-\infty}^{\infty} \phi^2(\nu)\,d\nu\right]^{r-1} \Big/ \int_{-\infty}^{\infty} \phi^r(\nu)\,d\nu.$$

(4) It tends to the correct limit as the time interval $T \to \infty$.

From equations (14 b) and the properties of the gamma-distribution (15 b) we

have $\bar{E}=\bar{P}T=k/a$

and $\overline{\Delta^2 E}=\bar{P}^2 T\xi=k/a^2$, } .....(16)

so that $a=1/\bar{P}\xi$

and $k=T/\xi$. } .....(17)

We can now evaluate $p(n, T)$ by averaging (8) over the ensemble of E. Thus

$$p(n,T)=\frac{1}{n!\,\Gamma(T/\xi)}\int_0^\infty(\alpha E)^n\left(\frac{E}{\bar{P}\xi}\right)^{T/\xi-1}\exp\left[-E\left(\alpha+\frac{1}{\bar{P}\xi}\right)\right]d\left(\frac{E}{\bar{P}\xi}\right)$$
$$=\frac{(\alpha\bar{P}\xi)^n}{(1+\alpha\bar{P}\xi)^{n+T/\xi}}\frac{\Gamma(n+T/\xi)}{n!\,\Gamma(T/\xi)}.$$

Since $\alpha\bar{P}T=\bar{n}$, this can be written in the form

$$\left.\begin{aligned}p(n,T)&=\frac{1}{(1+\bar{n}\xi/T)^{T/\xi}(1+T/\bar{n}\xi)^n}\frac{\Gamma(n+T/\xi)}{n!\,\Gamma(T/\xi)}\\&=\frac{(\bar{n}\xi/T)^n}{(1+\bar{n}\xi/T)^{n+T/\xi}}\frac{1}{(T/\xi-1)B(n+1,T/\xi-1)}.\end{aligned}\right\}\quad.....(18)$$

This is the observable probability distribution of the number of counts in an interval T. If we now compare the distributions (18) and (5) it will be seen that they are identical if T/ξ is integral and equal to s. In other words, $p(n, T)$ is the distribution of a boson assembly in a phase space of T/ξ cells.

Of course, while $p_s(n)$ in (5) was defined only for integral values of s, $p(n, T)$ is a continuous function of T/ξ. It can be regarded as a generalization, when one of the cells is not necessarily fully populated on the average. The distinction disappears for long intervals T, when T/ξ becomes a large number. Since $\xi\leqslant T$, we see that the number of cells $T/\xi\geqslant 1$ and the shortest interval T defines one cell. This is in accordance with the interpretation of T/ξ.

As has been shown (Mandel 1958), ξ becomes constant and independent of T for intervals long compared with $1/\Delta\nu$. The asymptotic value ξ_∞ is, by Parseval's theorem,

$$\xi_\infty=4\int_0^\infty\gamma^2(\tau)\,d\tau=4\int_0^\infty\phi^2(\nu)\,d\nu.\qquad.....(19)$$

It is therefore reasonable to regard $1/\xi_\infty$ as the average number of cells per unit time interval, or $c\xi_\infty$ as the average length of a cell associated with the light beam in the direction of motion. Since $c\xi_\infty$ is also the path difference within which interference effects can be observed, there are good reasons for calling ξ_∞ the coherence time of the light. As has been shown (Mandel 1958), ξ_∞ is of the order $1/\Delta\nu$.

We shall return to a discussion of these points. But first we must examine some properties of the distribution (18).

§ 5. Some Properties of the Distribution (18)

Inspection of equation (18) shows that the parameter $(\bar{n}\xi/T)$—the average number of particles per unit cell, or the degeneracy—plays a key role in determining the form of the distribution. If we regard $p(n, T)\equiv p(n, T, \bar{n}\xi/T)$ as a continuous function of the degeneracy parameter $\bar{n}\xi/T$ (with ξ/T constant) which may range from zero to infinity, then $(T/\xi-1)p(n, T, \bar{n}\xi/T)$ is a beta-prime distribution (cf. Kenney and Keeping 1951) of $\bar{n}\xi/T$ with parameters $n+1$ and $T/\xi-1$. The case $T/\xi=1$ must be regarded as a limiting case.

When the degeneracy is very small, $p(n, T)$ simplifies very considerably. By writing (18) in the form (6) it can be seen at once that, for $T/\xi \gg \bar{n}$,

$$p(n, T) \simeq \frac{\exp(-\bar{n})}{(T/\bar{n}\xi)^n} \frac{(T/\xi)^n}{n!} = \frac{\bar{n}^n}{n!} \exp(-\bar{n}), \qquad \ldots\ldots (20)$$

which is the classical Poisson distribution. This confirms the result obtained more generally in § 3.

This situation will generally apply when stellar sources are being studied. The light from these sources is always so weak that $\bar{n}\xi/T \ll 1$ and the degeneracy is unlikely to be detected in measurements on a single beam. The situation is, of course, improved when correlation measurements are undertaken on two or more coherent beams (Hanbury Brown and Twiss 1956), since these measurements single out the degenerate photons (Mandel 1958). Even so it is unlikely that any faint stars could be studied in this way.

When the degeneracy is very great, $p(n, T)$ approaches another limit. If $\bar{n}$ and n are large we can expand $n!$ and $\Gamma(n + T/\xi)$ in (18) by Stirling's theorem and so obtain

$$p(n, T) \simeq \left(\frac{T}{\bar{n}\xi}\right)^{T/\xi} \frac{\exp(-nT/\bar{n}\xi) n^{T/\xi - 1}}{\Gamma(T/\xi)}.$$

By introducing the almost continuous variate $z = n/\bar{n}$ we can express this in the form

$$p(z, T)\, dz = \frac{(zT/\xi)^{T/\xi - 1} \exp(-zT/\xi)}{\Gamma(T/\xi)} d(zT/\xi). \qquad \ldots\ldots (21)$$

Thus, for highly degenerate beams, zT/ξ becomes a gamma variate with parameter T/ξ and behaves like the variate $kE/\bar{E}$ of equation (15 *b*).

This result was, of course, to be expected from the more general considerations of § 3 and directly from the correspondence principle. In the limit of high degeneracy $n/\bar{n} \simeq E/\bar{E}$, since we are dealing with light of limited spectral extent and the distribution of z must tend to that of $E/\bar{E}$. Some examples of the function $p(z, T)$ are shown in the figure for different values of the parameter T/ξ. It should be stressed that the point $z = 0$ does not satisfy the condition $n \gg 1$.

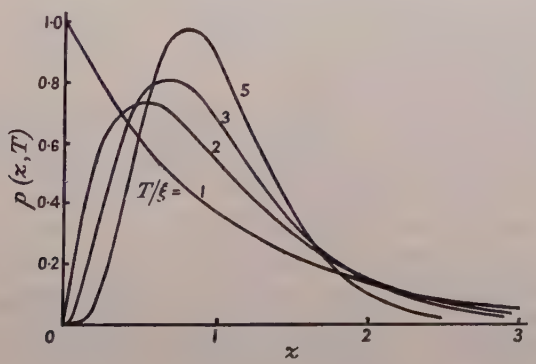

The probability distribution for the highly degenerate case.

Thus, as $(\bar{n}\xi/T)$ ranges from small to large values, we pass from the statistics of classical particles to the statistics of classical waves. Although the forms of the distributions (20) and (21) are generally quite different, they have a common limit. Thus, it is well known that the Poisson distribution for large $\bar{n}$ and the gamma

distribution for large parameter T/ξ, both tend to the Gaussian form. However the similarity of these two limits disappears if we examine the variances.

The moment generating function $M(x, T)$ of $p(n, T)$ is easily found by writing (18) in the form (6). Thus

$$M(x,T) = \sum_{n=0}^{\infty} p(n,T)\exp(xn)$$
$$= \frac{1}{(1+\bar{n}\xi/T)^{T/\xi}}\left[1-\frac{\exp x}{1+T/\bar{n}\xi}\right]^{-T/\xi}$$
$$= [1+(\bar{n}\xi/T)(1-\exp x)]^{-T/\xi}. \qquad \ldots\ldots (22)$$

From this we can immediately obtain the second moment :

$$\overline{n^2} = \bar{n} + \bar{n}^2(1+\xi/T)$$

and

$$\overline{\Delta^2 n} = \bar{n}(1+\bar{n}\xi/T), \qquad \ldots\ldots (23)$$

which is the result found previously (Purcell, 1956, Mandel 1958). Thus for non-degenerate beams $\overline{\Delta^2 n} = \bar{n}$ and for highly degenerate beams $\overline{\Delta^2 n} = \bar{n}^2\xi/T$. The two variances therefore differ by the degeneracy factor, even though the distributions may be of similar form.

§ 6. Coherence Time and Degrees of Freedom

As has been shown in § 4, there are good reasons for adopting the quantity ξ_∞ defined by equation (19) as the measure of coherence time. This definition makes the coherence length in space and the size of the unit cell in phase space complementary concepts in the wave and particle descriptions of the beam. Since ξ_∞ is the interval within which the photons are intrinsically indistinguishable, we see that the idea of coherence, in general, implies a phase relationship in terms of classical waves and intrinsic indistinguishability in terms of photons.

Our definition ξ_∞ is based on the same distribution, viz. $\gamma^2(\tau)$, as the measure of coherence time $\Delta\tau_w$ recently proposed by Wolf (1958) where :

$$(\Delta\tau_w)^2 = \int_0^\infty \tau^2\gamma^2(\tau)\,d\tau \Big/ \int_0^\infty \gamma^2(\tau)\,d\tau. \qquad \ldots\ldots (24)$$

ξ_∞ and $\Delta\tau_w$ are both measures of the width of the $\gamma^2(\tau)$ distribution, but, whereas $\Delta\tau_w$ is chosen a little arbitrarily so as to satisfy an inequality, ξ_∞ arises naturally from consideration of the fluctuations.

It is useful to have some idea of the relation between them. If the spectral density for positive ν has the form of a narrow Gaussian distribution with mean ν_0 and r.m.s. width $\Delta\nu$, then $\gamma(\tau) = \cos(2\pi\nu_0\tau)\exp(-2\pi^2\Delta\nu^2\tau^2)$. It follows that

$$\xi_\infty = 1/(2\sqrt{\pi}\Delta\nu)$$

and

$$\Delta\tau_w = 1/(2\sqrt{2\pi}\Delta\nu),$$

so that $\xi_\infty/\Delta\tau_w = \sqrt{(2\pi)}$ in this case. Since the spectral distributions encountered in practice are often nearly Gaussian, the order of magnitude relation

$$(\xi_\infty\Delta\nu)^2 \simeq 1/4\pi \qquad \ldots\ldots (25)$$

will usually hold.

We have seen that, for long intervals, T/ξ gives the mean number of independent cells of phase space contained within T and hence the number of independent data or statistical degrees of freedom of the energy distribution within T. This number should be compared with the upper limit fT given by the sampling

theorem (Gabor 1946, Shannon 1949) for the intensity of a wave whose normalized spectral density $\phi(\nu)$ vanishes outside a frequency interval f. We find that, for any shape of the narrow distribution $\phi(\nu)$, $\xi_\infty \geqslant 1/f$, so that $T/\xi_\infty \leqslant fT$. The number of independent data determined by the coherence time ξ_∞ therefore has an upper bound given by the sampling theorem. These independent data describing the energy distribution of the beam within T are just the quantum numbers $n_i (i = 1 \text{ to } T/\xi_\infty)$ which were used to define the state of the radiation field in § 2 (cf. also Gabor 1950)†. In general, T/ξ_∞ will be of the order $\Delta\nu T$. For example, for the Gaussian spectral density, $T/\xi_\infty = 2\sqrt{\pi}\Delta\nu T$.

Although the definition of ξ_∞ is based on $\gamma^2(\tau)$, it is clear from (16) that ξ_∞/T is simply the percentage variance of the classical energy E in a long wave train and we can write

$$\lim_{T\to\infty} (\xi_\infty/T) = \overline{\Delta^2 E}/\bar{E}^2. \qquad \ldots\ldots (26)$$

This equation also follows from (23) by the correspondence principle, since $n \propto E$ for highly degenerate beams.

It is interesting to note that (26) is the relation to be expected if the long wave train of duration T is pictured as a random assembly of similar elementary wave packets of duration ξ_∞. Since $P(t)$ varies only slowly within the interval ξ_∞ (Mandel 1958), the picture is not altogether unsound. These wave packets in real space must not be confused with the wave packets in phase space which are occasionally used as representations of photons (cf. Sillito 1957). In the first case the number of wave packets within the interval T is quite independent of the intensity. Thus ξ_∞ can be defined and interpreted in purely classical, as well as quantum statistical terms.

We have seen that the quantity $\bar{n}\xi/T$, the mean number of photons per unit cell or the degeneracy, plays a crucial role in determining the statistical behaviour of n. When $\bar{n}\xi/T$ is large, the distribution of n or of energy tends to the classical form for Gaussian waves. Conversely, when $\bar{n}\xi/T$ is small $p(n, T)$ tends to the classical distribution for particles. Although most of the phase cells are then empty, the classical waves associated with the beam do not change their general form and, on the average, consist of just as many wave packets as before. If we interpret the variate $y(t)$ as the magnitude of the electric vector associated with the light beam, then the continuing rapid fluctuations of $y(t)$, even when few photons are present, can be regarded as a consequence of the uncertainty relations connecting the electric field strength and the number of photons. For the operators representing the field strength and the photon number do not commute (cf. Heitler 1954) and the product of the uncertainties in the field strength and in number is therefore finite. As the degeneracy gets less and less, the classical representation of the beam therefore becomes increasingly inaccurate.

† In a recent paper on beam fluctuations, Kahn (1958) used the sampling theorem to expand the classical wave amplitude in a series of sinc functions centred at the sampling points. The degrees of freedom or ' modes ' are the expansion coefficients.

References

Fellgett, P. B., 1957, *Nature, Lond.*, **179**, 956.
Fürth, R., 1928, *Z. Phys.*, **48**, 323.
Gabor, D., 1946, *J. Instn Elect. Engrs*, **93**, Pt. IV, 429.
—— 1950, *Phil. Mag.*, **41**, 1161.

Hanbury Brown, R., and Twiss, R. Q., 1956, *Nature, Lond.*, **178**, 1046.
—— 1957, *Proc. Roy. Soc.* A, **243**, 291.
Heitler, W., 1954, *The Quantum Theory of Radiation*, 3rd Edn (Oxford : Clarendon Press).
Kac, M., and Siegert, A. J. F., 1947, *J. Appl. Phys.* **18**, 383.
Kahn, F. D., 1958, *Opt. Acta*, **5**, 93.
Kenney, J. F., and Keeping, E. S., 1951, *Mathematics of Statistics II*, 2nd Edn (Amsterdam: Van Nostrand).
Mandel, L., 1958, *Proc. Phys. Soc.*, **72**, 1037.
—— 1959, see footnote in § 3.
Purcell, E. M., 1956, *Nature, Lond.*, **178**, 1449.
Rice, S. O., 1945, *Bell Syst. Tech. J.*, **24**, 46.
Shannon, C. E., 1949, *Proc. Inst. Rad. Engrs*, **37**, 10.
Siegert, A. J. F., 1954, *Trans. Inst. Rad. Engrs, PGIT*-3, 4.
Sillito, R. M., 1957, *Nature, Lond.*, **179**, 1127.
Slepian, D., 1958, *Bell. Syst. Tech. J.*, **37**, 163.
Wolf, E., 1958. *Proc. Phys. Soc.*, **71**, 257.

APPENDIX

The Cumulants of E when $T \gg 1/\Delta\nu$

It is well known that, for a narrow band process, $\gamma(\tau)$ is expressible in the form

$$\gamma(\tau) = V(\tau)\exp(2\pi i\nu_0\tau) + V^*(\tau)\exp(-2\pi i\nu_0\tau),$$

where $V(\tau)$ is a slowly varying, decreasing function, which becomes very small for $\tau \gg 1/\Delta\nu$ (cf. Mandel 1958). It follows that the integrand in (11) will be greatest when $t_1 \simeq t_2 \simeq \ldots \simeq t_r$ etc. and very small when $t_1 - t_2 \gg 1/\Delta\nu$, etc. If $T \gg 1/\Delta\nu$ and if we introduce the substitutions

$$\begin{aligned} t_r - t_1 &= x_r \\ t_{r-1} - t_r &= x_{r-1} \\ &\cdots\cdots\cdots \\ t_2 - t_3 &= x_2 \end{aligned}$$

into the multiple integral (11), we can write

$$\kappa_r \simeq 2^{r-1}(r-1)!\,\bar{P}^r \int_{-T/2}^{T/2} dt_1 \int\int_{-\infty}^{\infty} \ldots \int \gamma(x_2 + x_3 + \ldots x_r) \times \gamma(x_2)\gamma(x_3)\ldots\gamma(x_r)\,dx_2\,dx_3\ldots dx_r. \qquad \ldots\ldots (A\,1)$$

Now, from the Wiener–Khintchine theorem,

$$\int_{-\infty}^{\infty} \gamma(x_2 + x_3 + \ldots x_r)\gamma(x_2)\,dx_2 = \int_{-\infty}^{\infty} \phi^2(\nu)\exp[2\pi i\nu(x_3 + x_4 + \ldots x_r)]\,d\nu, \qquad \ldots\ldots (A\,2)$$

since $\phi(\nu)$ is the Fourier transform of $\gamma(\tau)$. When (A 2) is introduced into (A 1), all the remaining variables become separable and we obtain

$$\kappa_r \simeq 2^{r-1}(r-1)!\,\bar{P}^r T \int_{-\infty}^{\infty} \phi^r(\nu)\,d\nu. \qquad \ldots\ldots (A\,3)$$

Next consider the approximate distribution (15 *b*) with a and k given by (17). From the properties of the γ-variate the rth cumulant is given by

$$\kappa_r = (r-1)!\,\bar{P}^r T \xi^{r-1} \qquad \ldots\ldots (A\,4)$$

But, as has been shown (Mandel 1958), for $T \gg 1/\Delta\nu$,

$$\xi \simeq 2\int_{-\infty}^{\infty} \phi^2(\nu)\,d\nu,$$

so that (A 4) becomes

$$\kappa_r \simeq 2^{r-1}(r-1)!\,\bar{P}^r T\left[\int_{-\infty}^{\infty} \phi^2(\nu)\,d\nu\right]^{r-1}. \qquad \ldots\ldots (A\,5)$$

Comparison of (A 3) and (A 5) shows that the second cumulant is always correct, but that the higher ones are in error by the factor

$$\left[\int_{-\infty}^{\infty} \phi^2(\nu)\,d\nu\right]^{r-1} \Big/ \int_{-\infty}^{\infty} \phi^r(\nu)\,d\nu.$$

This factor is unity for a rectangular spectrum of the form

$$\phi(\nu) = 1/2\Delta\nu \quad \text{for} \quad \nu_0 - \tfrac{1}{2}\Delta\nu < \nu < \nu_0 + \tfrac{1}{2}\Delta\nu,$$

$$= 0, \quad \text{for any other } \nu \geqslant 0,$$

and $\qquad \phi(-\nu) = \phi(\nu).$

If we transform the variable E to the standard form

$$(E - \bar{E})/(\overline{\Delta^2 E})^{1/2} = (E - \bar{P}T)/\bar{P}(T\xi)^{1/2},$$

the first cumulant of the new distribution is zero and the higher cumulants are multiplied by $[\bar{P}(T\xi)^{1/2}]^{-r}$. Inspection of (A 3) and (A 5) now shows that, as $T \to \infty$, the cumulants of higher order than the second tend to zero. Since the second cumulants given by (A 3) and (A 5) are, in any case, equal it follows that the limit of the approximate distribution (15 *b*) is Gaussian with the correct mean and variance.

Optical Energy Gap Variation in the GaSb–InSb System

By J. C. WOOLLEY, J. A. EVANS and C. M. GILLETT

Department of Physics, University of Nottingham

Communicated by L. F. Bates; MS. received 18th March 1959, in final form 29th April 1959

Abstract. The production of specimens of alloys in the GaSb–InSb system suitable for electrical and optical work is first discussed. X-ray data are given to show the variation in composition and the degree of homogeneity of specimen sections cut from long rod ingots produced by very slow directional freezing techniques. The results of measurements of infra-red transmission on such specimens are presented together with a graph of the variation of wavelength for onset of transmission, interpreted as optical energy gap, as a function of composition. The form of this graph is briefly discussed.

§ 1. Introduction

Recent work has shown that in many alloy systems involving two $A^{III}B^{V}$ compounds, solid solution occurs throughout the whole range of composition (Folberth 1955, Weiss 1956, Goryunova and Fedorova 1955, Woolley and Smith 1958, to be referred to as I). The results already obtained for the germanium–silicon system (Herman, Glicksman and Parmenter 1957), where solid solution also occurs at all compositions, show that the values of such semiconductor parameters as energy gap and mobility vary continuously with composition from the germanium values at one end to the silicon values at the other. By analogy, a similar variation of parameter values might be expected to occur in the ranges of solid solution between compounds. Up to the present, few of the systems involving compounds have been investigated to any extent, the main data available being the optical and electrical results for the InAs–InP and GaAs–GaP systems (Folberth 1955, Weiss 1956). In addition, some optical work has been carried out on similar alloy systems involving $A_2^{III}B_3^{VI}$ compounds (Goryunova and Grigor'eva 1957), and $A^{II}B^{VI}$ compounds (Goryunova, Grigor'eva, Konovalenko and Ryvkin 1955, Kolomiets and Malkova 1958, Lawson, Nielsen, Putley and Young 1959). The present work reports an investigation of the variation of optical energy gap in the GaSb–InSb system by means of infra-red absorption methods.

§ 2. Preparation of Alloys

Each of the two compounds concerned was first prepared separately, by melting together under vacuum the appropriate amounts of the elements. The elements used were all of 99·999% purity, and in the case of InSb the compound was further purified by normal zone refining methods.

As has been indicated previously (I), the preparation of solid ingot alloys in the GaSb–InSb system is somewhat difficult because of the very low diffusion rates in the materials. One method by which such alloys may be produced is by very slow directional freezing of an ingot of suitable mean composition. In I it

was shown that for an ingot of length 14 cm, frozen so that the freezing surface required 14 days to move from one end of the ingot to the other, there was a smooth variation of composition along the length of the ingot, but that in each cross section there was an inhomogeneity in composition of approximately ± 4 mol%. In the present work in order to obtain better homogeneity in the section of an ingot, the same directional freezing techniques were used, but the rate of cooling was reduced so that freezing of the whole ingot required 5 weeks. It was shown in I that for an ingot of initial mean composition 50 mol% GaSb 50 mol% InSb, the resulting range of composition was from 85 mol% GaSb 15 mol% InSb to 6 mol% GaSb 94 mol% InSb. In the present work in order to obtain specimens representing the whole range of composition in the system, two different ingots were prepared, of initial mean compositions 30 mol% GaSb 70 mol% InSb (ingot A) and 70 mol% GaSb 30 mol% InSb (ingot B) respectively.

Several sections were cut from each ingot perpendicular to its length, and parts of each section were powdered and x-rayed using a 9 cm powder camera and Cu Kα radiation. This x-ray photograph was then used to find the composition of the material of the particular section, from a determination of the lattice parameter. For this purpose, reference was made to the results showing variation of lattice parameter with composition given in I. As these results were effectively the standard of reference as far as the directionally frozen specimens were concerned, representative specimens, annealed to good equilibrium condition in powder form, were first x-rayed and then sent to Messrs. Johnson Matthey for chemical analysis. The results of the analysis and the estimated compositions were found to agree within ± 1 mol%.

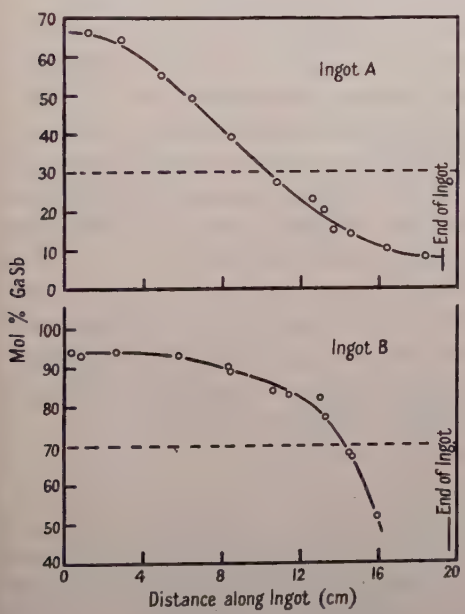

Figure 1. Variation of composition as a function of position along a directionally frozen ingot. Ingot A, mean composition 30 mol % GaSb 70 mol % InSb, ingot B, mean composition 70 mol % GaSb 30 mol % InSb.

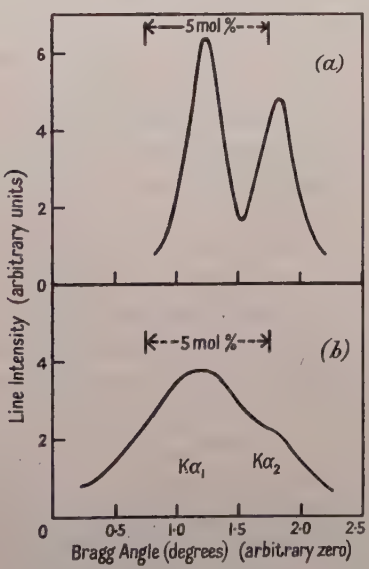

Figure 2. Profile of 731 line of typical specimens used for infra-red transmission measurements.

From the x-ray measurements on sections of the ingots, the variation of composition with position along the ingot was determined for each ingot and these results are shown in figure 1.

For investigation at compositions close to GaSb, alloys containing less than 5 mol% InSb were made in ingot form by melting appropriate amounts of GaSb and InSb together and then annealing the resulting ingot until a reasonable homogeneity was obtained. For these particular compositions, it was found that annealing for 4 weeks at 520°c gave a satisfactory material.

Sections were cut both from the directionally frozen ingots and also from the annealed ingots, and prepared for the infra-red measurements as indicated below. After the infra-red measurements had been made, each specimen was powdered and x-rayed. The resulting x-ray photograph was used to determine both the composition of the sample and its homogeneity. The homogeneity was found to vary to some extent with position on the ingot, and the degree of homogeneity obtained is illustrated by the curves in figure 2. These show the measured profile of a suitable high angle x-ray line (the 731 line) for two different specimens, the intensity of line being plotted as a function of Bragg angle. For this high angle line, the Cu Kα doublet is easily resolved with a 9 cm camera, and figure 2 (*a*) shows the profile obtained with a specimen of good homogeneity the Kα_1 and Kα_2 components being resolved. A number of the specimens used for the infra-red work showed this degree of homogeneity, which is little worse than the results for the separate compounds. Many of the samples had a degree of homogeneity illustrated by figure 2 (*b*) where the two peaks are considerably broadened and the occurrence of the Kα_2 peak can only just be observed. The change in Bragg angle corresponding to a change in composition of 5 mol% is also shown in figure 2, so that the inhomogeneity in composition corresponding to the curve in figure 2 (*b*) can be estimated. Specimens which to any great extent were less homogeneous than that illustrated by figure 2 (*b*) were rejected, because although an infra-red absorption edge could be observed, it was not possible to determine with reasonable accuracy the composition to which this edge corresponded. Preliminary results for infra-red work on this system given by the authors at the Brussels International Conference (Woolley, Smith and Evans 1959) are modified to some extent by the present work, because of the use initially of less homogeneous specimens.

Preliminary electrical measurements, including conductivity and Hall effect, have been made on specimens cut from ingot A. All such specimens were found to be p-type in the impurity range. With specimens taken from adjacent sections to those used in the infra-red work, the effective number of impurity carriers was found in all cases to be in the range from 1×10^{17} to 5×10^{17} per cm^3.

§ 3. Optical Measurements

Measurements were made of the percentage transmission through the various specimens as a function of wavelength. For this purpose, sections cut from the ingots, as described above, were each ground to a parallel sided plate some 200 μ thick, and were then polished with diamond paste, giving specimens which had thicknesses somewhere in the range 70–120 μ. These were then used for normal transmission measurements with a converted Halle spectrometer using a single beam and a calcium fluoride prism. The detector was a Schwarz thermocouple, the output from which was amplified by a Barr and Stroud thermocouple amplifier,

the incident beam to the specimen being chopped at 5 c/s to give the necessary modulation.

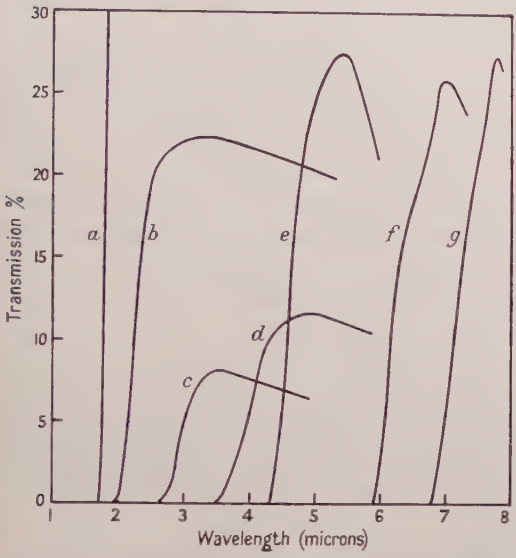

Figure 3. Variation of percentage transmission as a function of wavelength, (*a*) GaSb, (*b*) 90 mol % GaSb 10 mol % InSb, (*c*) 68 mol % GaSb 32 mol % InSb, (*d*) 48 mol % GaSb 52 mol % InSb, (*e*) 36 mol % GaSb 64 mol % InSb (approx.), (*f*) 20 mol % GaSb 80 mol % InSb, (*g*) 8 mol % GaSb 92 mol % InSb.

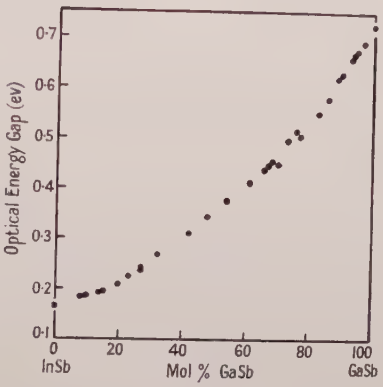

Figure 4. Variation of optical energy gap as a function of composition.

Figure 3 shows graphs of percentage transmission as a function of wavelength for various typical specimens. For each specimen, the wavelength corresponding to apparent onset of transmission has been estimated, and this wavelength converted into an energy value which has been taken as the optical energy gap E_g. The resulting values of E_g for specimens of various composition are shown in figure 4.

§ 4. Conclusions

In the case of the germanium–silicon alloys, the graph of optical energy gap against composition shows two sections (Johnson and Christian 1954, Braunstein, Moore and Herman 1958) with a definite discontinuity at 15 at. % Si. Herman and his co-workers have suggested (Herman, Glicksman and Parmenter 1957) that in the Ge–Si case, the alloys between pure silicon and the discontinuity have a band structure similar to that of silicon with the conduction band minima in the 100 directions, while those between the discontinuity and pure germanium have the germanium type of band structure with the conduction band minima in the 111 direction. Each band structure is continuously modified by change in composition, and there is a change in the effective conduction band minima at the composition corresponding to the point of discontinuity. It is also suggested that at compositions around the point of discontinuity interband scattering should occur, and this is observed experimentally in an extra reduction in the value of carrier mobility at these compositions (Glicksman 1958).

It is of interest to see whether similar effects occur in the GaSb–InSb alloy system. It is possible that the values of E_g shown in figure 4 show two discontinuities, one at 20 and one at 73 mol% GaSb. The method of estimating E_g from transmission data however does not allow a sufficiently accurate determination of E_g to state this with complete certainty. The problem is also complicated by the fact that at the moment little information is available concerning the band structure of the compounds, particularly GaSb. More detailed measurements of optical effects are to be made for various compositions close to the values at which discontinuities are suggested. Additional data will be obtained from electrical measurements. Also, to increase the accuracy of these later measurements it is hoped to improve the methods of producing the alloys, so as to obtain more homogeneous specimens.

Acknowledgments

The authors are indebted to Professor L. F. Bates for the facilities of his laboratory. The work described forms part of an investigation carried out for the Admiralty, and acknowledgment is made to Dr. O. Simpson, Dr. C. Hilsum, and Mr. J. T. Edmond of the Services Electronics Research Laboratory, Baldock, for helpful discussions.

References

Braunstein, R., Moore, A. R., and Herman, F., 1958, *Phys. Rev.*, **109,** 695.
Folberth, O. G., 1955, *Z. Naturf.*, **10a,** 502.
Glicksman, M., 1958, *Phys. Rev.*, **111,** 125.
Goryunova, N. A., and Fedorova, N. N., 1955, *J. Tech. Phys., Moscow,* **24,** 1339.
Goryunova, N. A., and Grigor'eva, V. S., 1957, *Sov. Phys.-Tech. Phys.*, **1,** 2094.
Goryunova, N. A., Grigor'eva, V. S., Konovalenko, B. M., and Ryvkin, S. M., 1955, *J. Tech. Phys., Moscow,* **25,** 1675.
Herman, F., Glicksman, M., and Parmenter, R. H., 1957, *Progress in Semiconductors,* **2,** 1 (London : Heywood).
Johnson, E. R., and Christian, S. M., 1954, *Phys. Rev.*, **95,** 560.
Kolomiets, B. T., and Malkova, A. A., 1958, *J. Tech. Phys., Moscow,* **28,** 1662.
Lawson, W. D., Nielsen, S., Putley, E. H., and Young, A. S., 1959, *J. Phys. Chem. Solids,* **9,** 325.
Weiss, H., 1956, *Z. Naturf.*, **11a,** 430.
Woolley, J. C., and Smith, B. A., 1958, *Proc. Phys. Soc.*, **72,** 214.
Woolley, J. C., Smith, B. A., and Evans, J. A., 1959, *Proceedings of Solid State Physics Conference, Brussels* (London : Academic Press).

Electron Spin Resonance of Gd^{3+} in Lanthanum Fluoride

By D. A. JONES†, J. M. BAKER‡ and D. F. D. POPE‡§

† Department of Natural Philosophy, Marischal College, Aberdeen
‡ The Clarendon Laboratory, Oxford

MS. received 11*th March* 1959

Abstract. Electron spin resonance in a single crystal of LaF_3 containing 0·01% Gd^{3+} shows three magnetically distinguishable ions per unit cell in a rhombic crystalline electric field which is consistent with a hexamolecular unit cell of symmetry C6/mcm. This is in disagreement with recent crystallographic measurements, but in agreement with the interpretation of the Faraday rotation given by Van Vleck and Hebb. The parameters of the spin Hamiltonian are given in table 1. The crystal field splitting in zero magnetic field is of the order of 0·3 cm^{-1} which makes this a possible salt for maser operation in low magnetic field.

§ 1. Introduction

There is interest in the investigation of new lanthanon salts, particularly those without water of crystallization, as some of them may be suitable for use in solid state masers. From a theoretical point of view it is of additional interest to study a homologous series of salts so that the changes in crystalline electric field parameters can be traced from ion to ion throughout a large part of the lanthanon series. Some work has been started on the anhydrous lanthanon trifluorides; this paper discusses the results of electron spin resonance of Gd^{3+} in a single crystal of LaF_3.

The anhydrous lanthanon trifluorides do not form an isomorphous series. Those lanthanons with larger ionic radius form fluorides isomorphous with hexagonal Tysonite (LaF_3) and the others are isomorphous with orthorhombic YF_3. However, some of the smaller ions such as Ho^{3+} and Tm^{3+} appear to crystallize in both forms, and it is probable that small quantities of any of the lanthanons could be substituted in the lattice of LaF_3.

There has been some doubt until recently about the crystal structure of LaF_3; it was not known whether the unit cell is bimolecular with C6/mmc symmetry or hexamolecular with C6/mcm symmetry (see Wyckoff 1951), though recent crystallographic evidence favours the smaller unit cell (Schlyter 1952). A paramagnetic ion replacing either of the La^{3+} ions in the smaller unit cell would experience the same crystalline electric field, and hence its electron spin resonance spectrum in either site would be the same, giving only one effective magnetic ion per unit cell. In the larger unit cell the principal axes of the crystalline electric field could be different at all six sites; or, if one of the principal axes lies along the crystal hexad axis (afterwards called the crystal axis), then the six sites are magnetically equivalent in pairs leaving three effective magnetic ions per unit cell. The latter symmetry was suggested by Van Vleck and Hebb (1934) to explain the

§ Now with the Operational Research Dept., Richard Thomas and Baldwins Ltd., Ebbw Vale, Mon.

Faraday rotation in single crystals of CeF_3, which is isomorphous with LaF_3. They supposed that the three ions are situated in electric fields of rhomic symmetry which are identical except for a 120° rotation about the crystal axis between each of them; one of the principal axes of the rhombic field is parallel to the crystal axis. These authors pointed out that this was the simplest model which fitted the experimental data, but that more complicated models, such as one where the principal axes of the crystal fields are tipped away from the crystal axis, could not be excluded. One cannot distinguish between these models because the Faraday rotation is an average effect of all ions.

Electron spin resonance is a technique ideally suited to investigate this problem further as ions in different crystal fields give different resolved spectra. We have not been able to observe resonance in LaF_3 containing Ce^{3+} at temperatures above 15°K, but it is expected that the Gd^{3+} ion, in which resonance has been observed, has the same symmetry†.

§ 2. Crystal Preparation and Structure

The specimens were made by crystallization from the melt, using lanthanum fluoride, specially prepared by Thorium Ltd. The method of crystallization was that normally used for the growth of crystals of fluorides, in which a crucible containing the melt was lowered through a sharp temperature gradient. A vacuum furnace was used, and its construction was substantially the same as that previously described by Stockbarger (1949). The crystals were grown in graphite crucibles and in an atmosphere of dry oxygen-free nitrogen at a pressure of 20 microns of mercury.

Some purification of the lanthanum fluoride powder was required before satisfactory crystals could be grown. This was done by 'scavenging' the material with lead fluoride. The procedure was to mix about 5% PbF_2 with the LaF_3 powder before loading into the crucible. The furnace chamber was then evacuated and when the pressure had dropped to about 1μ, the temperature of the furnace was raised to about 70°C and left to dry out for twenty-four hours. At the end of this period the temperature was slowly raised to the melting point of LaF_3, taking care that at no time the pressure exceeded 5μ. When the temperature was about 100°C below the melting point of LaF_3, nitrogen was introduced into the furnace to bring the pressure to 20μ. This was necessary to avoid loss of material by evaporation. The melting point has not been measured accurately but was between 1400 and 1450°C. When the salt was completely molten, the crucible was lowered in the furnace at a rate of 2 mm per hr.

The first crystallization produced a polycrystalline mass about 70% of which was clear optically. These clear pieces were picked out and recrystallized again, using 5% PbF_2 as scavenger. The resulting material was colourless and of very good optical quality.

Gadolinium was introduced into the lanthanum fluoride crystal by mixing the appropriate percentage of GdF_3 with LaF_3 which had been purified by the above method. This mixture was again crystallized by the method described.

The figure shows the immediate neighbours of a trivalent ion in projection on a plane perpendicular to the crystal axis. Figure (*a*) shows the bimolecular unit

† *Note added in proof :* Mr. R. S. Rubins at the Clarendon Laboratory has observed resonance at 20°K in specimens of LaF_3 containing Ce^{3+} since this paper was submitted for publication. The analysis of these results is not yet complete, and there may be 3 or 6 ions in the unit cell.

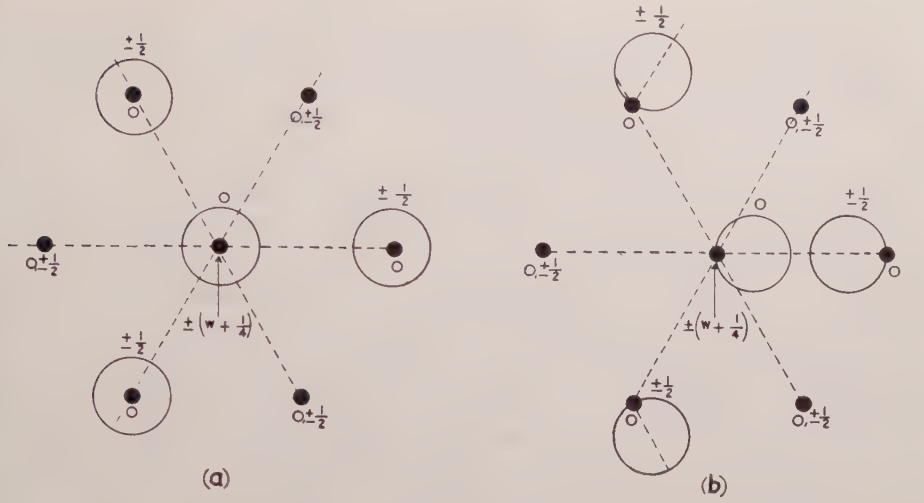

The environment of a trivalent ion shown in projection on a plane perpendicular to the crystal axis; (*a*) for the bimolecular unit cell C6/mmc, (*b*) for the hexamolecular unit cell C6/mcm. The unshaded circles represent trivalent ions and the shaded ones represent fluorine ions; distances above and below the plane are given as fractions of the lattice parameter, those for trivalent ions being written above the circle, those for fluorine below the circle.

cell and figure(*b*) the hexamolecular unit cell with the distortion from the simpler symmetry somewhat exaggerated.

The crystals were found to cleave in a plane perpendicular to the crystal axis, which facilitated the mounting of the crystals in the resonance cavity.

§ 3. Experimental Results

Resonance was observed at 90°K and above at both X band ($\sim 0{\cdot}3\,\mathrm{cm}^{-1}$) and K band ($\sim 0{\cdot}8\,\mathrm{cm}^{-1}$) in a single crystal grown from a melt containing 0·01% molar concentration of gadolinium. The measurements show that there are three ions per unit cell each being in a site with rhombic symmetry and related to one another by 120° rotations about the crystal axis. One of the principal axes of the rhombic crystal field, the x axis, for all ions lies along the crystal axis. The spectrum of each ion is described by the following spin Hamiltonian:

$$\mathscr{H} = g\beta \mathbf{H} \,.\, \mathbf{S} + B_2^0 O_2^0 + B_4^0 O_4^0 + B_6^0 O_6^0 + B_2^2 O_2^2 + B_4^2 O_4^2 + B_6^2 O_6^2 + B_4^4 O_4^4 + B_6^4 O_6^4 + B_6^6 O_6^6.$$

Here the B_n^m form a set of empirical coefficients which can be calculated from the experimental results and the O_n^m are spin operators, which have been described by Stevens (1952) and whose explicit form is given in table 3 of the Appendix.

When the external field is in the z direction the off-diagonal terms in the energy matrix are small. This gives rise to a spectrum which is almost symmetrically disposed about the $\frac{1}{2} \longleftrightarrow -\frac{1}{2}$ transition, and which is described essentially by the first four terms only of the spin Hamiltonian.

When the external field is in the x or y directions the Hamiltonian may be written in a form diagonal in the Zeeman term by transforming the spin operators in a way described in the Appendix. This gives the following form, where only

those terms which give diagonal and appreciable off-diagonal elements have been retained (the upper sign is for the x direction and the lower for the y direction):

$$\mathcal{H} = g\beta \mathbf{H} \cdot \mathbf{S} + \{-\tfrac{1}{2}B_2^0 \pm \tfrac{1}{2}B_2^2\}O_2^0 + \{\tfrac{3}{8}B_4^0 \mp \tfrac{1}{8}B_4^2 + \tfrac{1}{8}B_4^4\}O_4^0$$
$$+ \{-\tfrac{5}{16}B_6^0 \pm \tfrac{1}{16}B_6^2 - \tfrac{1}{16}B_6^4 \pm \tfrac{1}{16}B_6^6\}O_6^0 + \{-\tfrac{3}{2}B_2^0 \mp \tfrac{1}{2}B_2^2\}O_2^2$$
$$+ \{\tfrac{5}{2}B_4^0 \mp \tfrac{1}{2}B_4^2 - \tfrac{1}{2}B_4^4\}O_4^2.$$

In these directions the off-diagonal elements cannot be regarded as small compared with the Zeeman splitting and second and third order effects are appreciable.

From measurements at one frequency in the three principal directions it should be possible to evaluate all of the crystal field parameters and, as B_6^2 and B_6^6 cannot be separated, there is one more equation available than unknowns to be found so that a check of self-consistency should be obtained. Measurements in intermediate directions in the xy plane would enable B_6^2 and B_6^6 to be separated but as

Table 1. Parameters of the Spin Hamiltonian for Gd^{3+} in LaF_3 at 90°K

$b_2^0 = 3B_2^0 =$	$+239 \pm 1$
$b_2^2 = 3B_2^2 =$	-5 ± 2
$b_4^0 = 60B_4^0 =$	$-5{\cdot}6 \pm 0{\cdot}2$
$b_4^2 = 60B_4^2 =$	$+27 \pm 3$
$b_4^4 = 60B_4^4 =$	-43 ± 3
$b_6^0 = 1260B_6^0 =$	$+0{\cdot}14 \pm 0{\cdot}2$
$b_6^2 + b_6^6 = 1260\,(B_6^2 + B_6^6) =$	$+8{\cdot}5 \pm 3$
$b_6^4 = 1260B_6^4 =$	-1 ± 5
$g =$	$1{\cdot}990 \pm 0{\cdot}001$

The crystal field parameters are given in units of 10^{-4} cm^{-1}, and the signs are only relative.

Table 2. Measured line positions (gauss) and those calculated from the parameters in table 1. The remaining discrepancy in the x and y directions may be partially due to a small contribution of the O_6^2 term

Measurements at X band

H parallel to z		H parallel to x		H parallel to y	
Measured	Calculated	Measured	Calculated	Measured	Calculated
1691	1691	——*	2881	——*	2712
2379	2378	2733	2725	2744	2749
2906	2904	2906	2908	2996	3019
3340	3340	3266	3266	3293	3293
3776	3776	3653	3658	3584	3585
4301	4302	3921	3926	3864	3870
4986	4989	——*	3922	4068	4073

Measurements at K band

H parallel to x		H parallel to y	
Measured	Calculated	Measured	Calculated
7765	7768	——	7504
7659	7656	7561	7576
7852	7840	7842	7841
8230	8230	8147	8149
8630	8634	8463	8453
8867	8862	8718	8718
8809	8810	——	8872

* Lines which may be unresolved from a neighbouring line.

these terms proved to be small and the spectrum analysis would be complex, this was not attempted. In fact we were not able to find all of the transitions in the principal directions at either of the two frequencies used but just enough data were available at X band to calculate all of the crystal field parameters; the K band data provided a check. The values of the parameters are listed in table 1, while the observed line positions and those calculated using the parameters are compared in table 2. From this table it can be seen that some of the lines are almost coincident with others in the spectrum. This at least partially explained the initially puzzling fact that the spectrum appeared to consist of too few lines; for all of the missing lines at X band their predicted position is such that they could be obscured by another line.

The line width increases appreciably on going from the $\frac{1}{2} \leftrightarrow -\frac{1}{2}$ transition to the $\pm 7/2 \leftrightarrow \pm 5/2$ transitions, presumably due to a random distribution of values of the crystal field parameters. With the external field parallel to the z axis the full width at half intensity of the central line is 10 gauss and that of the outer lines is 40 gauss. In the x and y directions the width of the outer lines is slightly greater and that of the central line is 16 gauss (y direction) and 20 gauss (x direction). The large linewidth of the $\pm 7/2 \leftrightarrow \pm 5/2$ transitions prevents their being observed in some directions even when they should be resolved from other transitions; whenever they are observed their intensity is correspondingly small.

As the resonance saturated at 20°K it was not possible to measure the absolute signs of the crystal field parameters in the usual way. Hence the signs given in table 1 are only relative to one another.

§ 4. Conclusions

The positions of the paramagnetic resonance transitions of the Gd^{3+} ion in LaF_3 are adequately described by the usual type of spin Hamiltonian. Of the crystal field parameters B_2^0 is by far the largest, as is usually found to be the case in other gadolinium salts (see Bowers and Owen 1955). Thus the strongest term in the part of the spin Hamiltonian arising from crystal fields effects is an axial one about an axis perpendicular to the crystal axis. This is very different from the six-fold symmetry about the crystal axis which each ion would have if the crystal structure were of the simpler form.

Our results are completely consistent with the larger hexamolecular unit cell. The symmetry of the crystal field is precisely that which this structure would give, as can be seen from the figure (*b*). It should be said, however, that the existence of three magnetically distinct ions in the unit cell with a symmetry which is consistent with the larger of the proposed unit cells does not conclusively prove that this is the crystal structure which is appropriate to pure lanthanum fluoride. It is possible that the distortion of the axial symmetry of the La^{3+} site in the smaller unit cell is caused by a misfit in the lattice of the larger gadolinium ion. It is also possible that the distortions necessary to produce the crystal field observed are too small to be detected in the crystallographic measurements (in this connection it is unfortunate that the theory of the crystalline Stark effect in S-state ions is too rudimentary to enable one to calculate the size of distortion required to give the observed crystal field parameters). The discovery of three magnetically distinct ions in the unit cell with staggered rhombic fields does, however, add confirmation to the theory of Hebb and Van Vleck explaining the

Faraday rotation in Tysonite. As the Faraday rotation measurements were made in pure CeF_3 this evidence strongly favours the larger hexamolecular unit cell for the lattice which is undistorted by impurity ions.

The fact that there are three magnetically distinct ions per unit cell is a distinct disadvantage of the crystals examined considered as the element of a solid state maser. However, the crystals are mechanically robust and insoluble in water, and the large crystal field splitting, which is about 0·3 cm^{-1} in zero magnetic field, may make the substance useful for maser applications in this frequency range as only a small magnetic field would be required.

Acknowledgments

The authors wish to express their gratitude to Professor B. Bleaney for stimulating an interest in LaF_3 and for many valuable discussions, and to Mrs. B. Bleaney and Mr. F. I. B. Williams for assistance in checking the transformation properties of spin operators and the values of their matrix elements. They are also grateful to Professor R. V. Jones for the crystal growing facilities. The authors are also indebted to the Board of Admiralty and to the United States Air Force for financial support.

APPENDIX

The spin Hamiltonian used in this paper to describe the spectrum of Gd^{3+} in LaF_3 has non-zero values for the coefficients of all possible even terms in the expansion of the crystalline Stark effects in terms of spin operators O_n^m. The form of these spin operators is given in table 3. The matrix elements of those which have not previously been tabulated (Stevens 1952, Elliott and Stevens 1953, Judd 1955, Baker, Bleaney and Hayes 1958) are given in table 4.

Table 3. Form of Operators O_n^m

$$O_2^0 = 3S_z^2 - S(S+1)$$
$$O_2^2 = \tfrac{1}{2}(S_+^2 + S_-^2)$$
$$O_4^0 = 35S_z^4 - \{30S(S+1) - 25\}S_z^2 - 6S(S+1) + 3S^2(S+1)^2$$
$$O_4^2 = \tfrac{1}{4}[\{7S_z^2 - S(S+1) - 5\}(S_+^2 + S_-^2) + (S_+^2 + S_-^2)\{7S_z^2 - S(S+1) - 5\}]$$
$$O_4^4 = \tfrac{1}{2}(S_+^4 + S_-^4)$$
$$O_6^0 = 231S_z^6 - 105\{3S(S+1) - 7\}S_z^4 + \{105S^2(S+1)^2 - 525S(S+1) + 294\}S_z^2 - 5S^3(S+1)^3 + 40S^2(S+1)^2 - 60S(S+1)$$
$$O_6^2 = \tfrac{1}{4}[\{33S_z^4 - [18S(S+1) + 123]S_z^2 + S^2(S+1)^2 + 10S(S+1) + 102\}(S_+^2 + S_-^2) + (S_+^2 + S_-^2)\{33S_z^4 - \text{etc.}\}]$$
$$O_6^4 = \tfrac{1}{4}[\{11S_z^2 - S(S+1) - 38\}(S_+^4 + S_-^4) + (S_+^4 + S_-^4)\{11S_z^2 - S(S+1) - 38\}]$$
$$O_6^6 = \tfrac{1}{2}(S_+^6 + S_-^6)$$

In order to calculate the position of the resonance transitions when the external field is not parallel to the z axis it is convenient to use states such that the Zeeman terms, which are usually the biggest, are on the diagonal of the energy matrix. One therefore has to consider what happens to the operator equivalents O_n^m on rotation. The operator O_n^m is written for $O_n^{+m} + O_n^{-m}$ because the symmetry of the crystal field is such that they occur added in this way. However, as O_n^{+m} and O_n^{-m} do not transform in the same way upon rotation, arbitrary direction of the external field it is necessary to consider all of the components O_n^{+m} and O_n^{-m} separately and they do not have equal coefficients after rotation. When the external field is in the plane perpendicular to the z direction

$$O_2^2 = \tfrac{1}{2}(S_+^2 + S_-^2)$$

S	$\langle \pm 1 \| \mp 1 \rangle$	$\langle \pm 2 \| 0 \rangle$	$\langle \pm 3 \| \pm 1 \rangle$	$\langle \pm 4 \| \pm 2 \rangle$	$\langle \pm 5 \| \pm 3 \rangle$	$\langle \pm 6 \| \pm 4 \rangle$	$\langle \pm 7 \| \pm 5 \rangle$	$\langle \pm 8 \| \pm 6 \rangle$
1	1							
2	3	$\sqrt{6}$						
3	6	$\sqrt{30}$	$\sqrt{15}$					
4	10	$3\sqrt{10}$	$3\sqrt{7}$	$2\sqrt{7}$				
5	15	$\sqrt{210}$	$2\sqrt{42}$	$6\sqrt{3}$	$3\sqrt{5}$			
6	21	$2\sqrt{105}$	$6\sqrt{10}$	$3\sqrt{30}$	$\sqrt{165}$	$\sqrt{66}$		
7	28	$6\sqrt{21}$	$15\sqrt{3}$	$5\sqrt{22}$	$6\sqrt{11}$	$3\sqrt{26}$	$\sqrt{91}$	
8	36	$6\sqrt{35}$	$\sqrt{1155}$	$3\sqrt{110}$	$2\sqrt{195}$	$\sqrt{546}$	$3\sqrt{35}$	$2\sqrt{30}$

	$\langle \pm \frac{3}{2} \| \mp \frac{1}{2} \rangle$	$\langle \pm \frac{5}{2} \| \pm \frac{1}{2} \rangle$	$\langle \pm \frac{7}{2} \| \pm \frac{3}{2} \rangle$	$\langle \pm \frac{9}{2} \| \pm \frac{5}{2} \rangle$	$\langle \pm \frac{11}{2} \| \pm \frac{7}{2} \rangle$	$\langle \pm \frac{13}{2} \| \pm \frac{9}{2} \rangle$	$\langle \pm \frac{15}{2} \| \pm \frac{11}{2} \rangle$
/2	$\sqrt{3}$						
/2	$3\sqrt{2}$	$\sqrt{10}$					
/2	$2\sqrt{15}$	$3\sqrt{5}$	$\sqrt{21}$				
/2	$5\sqrt{6}$	$3\sqrt{14}$	$2\sqrt{21}$	6			
/2	$3\sqrt{35}$	$2\sqrt{70}$	$6\sqrt{6}$	$3\sqrt{15}$	$\sqrt{55}$		
/2	$14\sqrt{3}$	$6\sqrt{15}$	$15\sqrt{2}$	$\sqrt{330}$	$3\sqrt{22}$	$\sqrt{78}$	
/2	$12\sqrt{7}$	$3\sqrt{105}$	$5\sqrt{33}$	$2\sqrt{165}$	$6\sqrt{13}$	$\sqrt{273}$	$\sqrt{105}$

$$O_4^2 = \tfrac{1}{4}[\{7S_z^2 - S(S+1) - 5\}(S_+^2 + S_-^2) + (S_+^2 + S_-^2)\{7S_z^2 - S(S+1) - 5\}]$$

F	$\langle \pm 1 \| \mp 1 \rangle$	$\langle \pm 2 \| 0 \rangle$	$\langle \pm 3 \| \pm 1 \rangle$	$\langle \pm 4 \| \pm 2 \rangle$	$\langle \pm 5 \| \pm 3 \rangle$	$\langle \pm 6 \| \pm 4 \rangle$	$\langle \pm 7 \| \pm 5 \rangle$	$\langle \pm 8 \| \pm 6 \rangle$
3	-4	$\sqrt{6}$						
3	-20	$-\sqrt{30}$	$6\sqrt{15}$					
3	-60	$-11\sqrt{10}$	$10\sqrt{7}$	$30\sqrt{7}$				
21	-20	$-\sqrt{210}$	0	$10\sqrt{3}$	$12\sqrt{5}$			
3	-280	$-22\sqrt{105}$	$-24\sqrt{10}$	$23\sqrt{30}$	$24\sqrt{165}$	$45\sqrt{66}$		
3	-504	$-94\sqrt{21}$	$-130\sqrt{3}$	$15\sqrt{22}$	$116\sqrt{11}$	$121\sqrt{26}$	$66\sqrt{91}$	
7	-360	$-54\sqrt{35}$	$-6\sqrt{1155}$	$-3\sqrt{110}$	$12\sqrt{195}$	$15\sqrt{546}$	$78\sqrt{35}$	$78\sqrt{30}$

S	F	$\langle \pm \frac{3}{2} \| \mp \frac{1}{2} \rangle$	$\langle \pm \frac{5}{2} \| \pm \frac{1}{2} \rangle$	$\langle \pm \frac{7}{2} \| \pm \frac{3}{2} \rangle$	$\langle \pm \frac{9}{2} \| \pm \frac{5}{2} \rangle$	$\langle \pm \frac{11}{2} \| \pm \frac{7}{2} \rangle$	$\langle \pm \frac{13}{2} \| \pm \frac{9}{2} \rangle$	$\langle \pm \frac{15}{2} \| \pm \frac{11}{2} \rangle$
/2	3	$-5\sqrt{2}$	$3\sqrt{10}$					
/2	6	$-4\sqrt{15}$	$\sqrt{5}$	$5\sqrt{21}$				
/2	21	$-5\sqrt{6}$	$-\sqrt{14}$	$2\sqrt{21}$	18			
/2	12	$-8\sqrt{35}$	$-3\sqrt{70}$	$5\sqrt{6}$	$13\sqrt{15}$	$9\sqrt{55}$		
/2	3	$-210\sqrt{3}$	$-62\sqrt{15}$	$-15\sqrt{2}$	$13\sqrt{330}$	$95\sqrt{22}$	$55\sqrt{78}$	
/2	6	$-120\sqrt{7}$	$-23\sqrt{105}$	$-15\sqrt{33}$	$8\sqrt{165}$	$80\sqrt{13}$	$25\sqrt{273}$	$36\sqrt{105}$

$$O_6^2 = \tfrac{1}{4}[\{33S_z^4 - 18S_z^2\,S(S+1) - 123\,S_z^2 + S^2(S+1)^2 + 10S(S+1) + 102\}(S_+^2 + S^2)$$
$$+ (S_+^2 + S_-^2)\{33S_z^4 - 18S_z^2 S(S+1) - 123S_z^2 + S^2(S+1)^2 + 10S(S+1) + 102\}]$$

F	$\langle \pm 1 \| \mp 1 \rangle$	$\langle \pm 2 \| 0 \rangle$	$\langle \pm 3 \| \pm 1 \rangle$	$\langle \pm 4 \| \pm 2 \rangle$	$\langle \pm 5 \| \pm 3 \rangle$	$\langle \pm 6 \| \pm 4 \rangle$	$\langle \pm 7 \| \pm 5 \rangle$	$\langle \pm 8 \| \pm 6 \rangle$
24	15	$-2\sqrt{30}$	$\sqrt{15}$					
30	83	0	$-36\sqrt{7}$	$24\sqrt{7}$				
360	28	$2\sqrt{210}$	$-11\sqrt{42}$	$-14\sqrt{3}$	$-14\sqrt{5}$			
72	420	$22\sqrt{105}$	$-63\sqrt{10}$	$-84\sqrt{30}$	$-14\sqrt{165}$	$70\sqrt{66}$		
1080	70	$10\sqrt{21}$	$-7\sqrt{3}$	$-14\sqrt{22}$	$-21\sqrt{11}$	0	$11\sqrt{91}$	
264	315	$78\sqrt{35}$	$\sqrt{1155}$	$-42\sqrt{110}$	$-49\sqrt{195}$	$-20\sqrt{546}$	$13\sqrt{315}$	$182\sqrt{30}$

S	F	$\langle \pm \frac{3}{2} \| \mp \frac{1}{2} \rangle$	$\langle \pm \frac{5}{2} \| \pm \frac{1}{2} \rangle$	$\langle \pm \frac{7}{2} \| \pm \frac{3}{2} \rangle$	$\langle \pm \frac{9}{2} \| \pm \frac{5}{2} \rangle$	$\langle \pm \frac{11}{2} \| \pm \frac{7}{2} \rangle$	$\langle \pm \frac{13}{2} \| \pm \frac{9}{2} \rangle$	$\langle \pm \frac{15}{2} \| \pm \frac{11}{2} \rangle$
/2	24	$7\sqrt{15}$	$-21\sqrt{5}$	$5\sqrt{21}$				
/2	240	$7\sqrt{6}$	$-3\sqrt{14}$	$-5\sqrt{21}$	21			
/2	216	$12\sqrt{35}$	$-\sqrt{70}$	$-35\sqrt{6}$	$-14\sqrt{15}$	$14\sqrt{55}$		
/2	720	$35\sqrt{3}$	$-3\sqrt{15}$	$-36\sqrt{2}$	$-4\sqrt{330}$	$-3\sqrt{22}$	$11\sqrt{78}$	
/2	1320	$30\sqrt{7}$	$3\sqrt{105}$	$-7\sqrt{33}$	$-7\sqrt{165}$	$-21\sqrt{13}$	$\sqrt{273}$	$13\sqrt{105}$

The numbers in column F are multiplying factors common to all the elements in the row.

this complication does not arise provided that either the x' or y' axes of the new system of coordinates in which the rotated operator equivalents are described is allowed to coincide with the initial z axis. Under these circumstances the operator equivalents transform as shown in table 5 when the external field, and therefore the z' axis, makes an angle ϕ with the initial x axis.

It is seen that when the external field is parallel to either of the initial principal directions (x or y) of the crystal field, the terms O_n^m where m is odd drop out and the expression becomes fairly simple. It is in these directions that the measurements previously described were made. For this reason the form of the odd operator equivalent has not been calculated. However, in order to obtain the expressions in table 5 it has been assumed, in accordance with past practice, that

Table 5. Transformation of spin operators on rotation of the z axis into the perpendicular plane xy so that z' makes and angle ϕ with x and y' is parallel to z

$$O_2^0 \rightarrow -\frac{1}{2}O_2^0-\frac{3}{2}O_2^2$$

$$O_2^2 \rightarrow \left(\frac{1}{2}O_2^0-\frac{1}{2}O_2^2\right)\cos 2\phi-2iO_2^1\sin 2\phi$$

$$O_4^0 \rightarrow \frac{3}{8}O_4^0+\frac{5}{2}O_4^2+\frac{35}{8}O_4^4$$

$$O_4^2 \rightarrow \left(-\frac{1}{8}O_4^0-\frac{1}{2}O_4^2+\frac{7}{8}O_4^4\right)\cos 2\phi+i\left(\frac{1}{2}O_4^1+\frac{7}{2}O_4^3\right)\sin 2\phi$$

$$O_4^4 \rightarrow \left(\frac{1}{8}O_4^0-\frac{1}{2}O_4^2+\frac{1}{8}O_4^4\right)\cos 4\phi-i(O_4^1-iO_4^3)\sin 4\phi$$

$$O_6^0 \rightarrow -\frac{5}{16}O_6^0-\frac{105}{32}O_6^2-\frac{63}{16}O_6^4-\frac{231}{32}O_6^6$$

$$O_6^2 \rightarrow \left(\frac{1}{16}O_6^0+\frac{17}{32}O_6^2+\frac{3}{16}O_6^4-\frac{33}{32}O_6^6\right)\cos 2\phi-i\left(\frac{1}{4}O_6^1+\frac{9}{8}O_6^3+\frac{33}{8}O_6^5\right)\sin 2\phi$$

$$O_6^4 \rightarrow \left(-\frac{1}{16}O_6^0-\frac{5}{32}O_6^2+\frac{13}{16}O_6^4-\frac{11}{32}O_6^6\right)\cos 4\phi+i\left(\frac{1}{2}O_6^1+\frac{5}{4}O_6^3-\frac{11}{4}O_6^5\right)\sin 4\phi$$

$$O_6^6 \rightarrow \left(\frac{1}{16}O_6^0-\frac{15}{32}O_6^2+\frac{3}{16}O_6^4-\frac{1}{32}O_6^6\right)\cos 6\phi-i\left(\frac{3}{4}O_6^1-\frac{5}{8}O_6^3+\frac{3}{8}O_6^5\right)\sin 6\phi$$

the spin operator is derived from that part of the cartesian form of the appropriate spherical harmonic Y_n^m which is left after any common numerical factor has been taken out. The rules for proceeding from the cartesian to operator form have been given by Stevens (1952).

References

Baker, J. M., Bleaney, B., and Hayes, W., 1958, *Proc. Roy. Soc.* A, **247**, 141.
Bowers, K. D., and Owen, J., 1955, *Rep. Progr. Phys.*, **18**, 304 (London : Physical Society).
Elliott, R. J., and Stevens, K. W. H., 1953, *Proc. Roy. Soc.* A, **218**, 553.
Judd, B. R., 1955, *Proc. Roy. Soc.* A, **227**, 552.
Schlyter, K., 1952, *Ark. Kemi*, **5**, 73.
Stevens, K. W. H., 1952, *Proc. Phys. Soc.* A, **65**, 209.
Stockbarger, K. D., 1949, *J. Opt. Soc. Amer.*, **39**, 731.
Van Vleck, J. H., and Hebb, H. M., 1934, *Phys. Rev.*, **46**, 17.
Wyckoff, R. W. G., 1951, *Crystal Structures*, Vol. II (New York: Interscience Publishers).

The Scattering of Fast Charged Particles: V
Multiple Scattering of Fast Electrons and Positrons in Xenon

By K. PHILLIPS and K. R. ALLEN
Research Department, Metropolitan-Vickers Electrical Company Ltd., Manchester

MS. received 12*th January* 1959, *in final form* 24*th March* 1959

Abstract. The multiple scattering of fast electrons and positrons within the energy range of 7 to 17 MeV in xenon has been measured using a cloud chamber. A study has been made of the errors involved and also the use of the technique of overlapping intervals. At the higher energies the multiple scattering agrees, within the experimental errors, with the theoretical values predicted by Molière but at energies of less than 10 MeV the experimental values tend to be lower. The measured scattering for the mean energy values agree with the predicted values of Molière but are higher than the values given by the theory of Williams. There is no significant difference between the multiple scattering of electrons and positrons.

§ 1. Introduction

After traversing a layer of matter the distribution of the angular deflections of scattered electrons is given by

$$F(\theta)=G(\theta)+S(\theta) \qquad \ldots\ldots(1)$$

where $G(\theta)=(2\pi\sigma^2)^{-1/2}\exp(-\theta^2/2\sigma^2)$ is the Gaussian distribution and $S(\theta)$, the single scattering contribution which only becomes important at large angles. The factor describing the shape of the normal distribution is the variance σ^2 and it is this quantity, or its square root, which is often studied in any experimental investigation of the multiple scattering of fast particles.

One of the earliest theories of multiple scattering was due to Williams (1939) who based his work on the fact that after traversing a layer of matter the distribution of the angular deflections is Gaussian. The variance of the normal distribution according to Williams is given by

$$\sigma^2=8\pi N\frac{Z^2}{A}r_0{}^2\frac{\mu^2}{p^2\beta^2}\,dx\ln\frac{\theta_{\max}}{\theta_{\min}} \qquad \ldots\ldots(2)$$

where N, Z and A are the number of scattering centres per cubic centimetre of the material, its atomic number and atomic weight respectively, r_0 and $\mu(=m_0c^2)$ are the classical electronic radius ($2{\cdot}81\times10^{-13}$ cm) and the rest mass of the electron with energy $p\beta$, dx is the path length of matter traversed by the particles in g cm^{-2}. The angles $\theta_{\max}$ and $\theta_{\min}$ are the limits of the deflections which have to be introduced in order to keep the variance finite, and $\theta_{\max}/\theta_{\min}$ may be taken as $(181Z^{-1/3})^2$.

The single scattering term $S(\theta)$ in equation (1) can be expressed approximately as π/θ^3 with a suitable cut-off at smaller angles. A later theory by Goudsmit and Saunderson (1940) was developed from the idea that the probability that an electron is scattered between angles θ and $\theta+d\theta$ can be expressed as a

series of Legendre polynomials. The coefficients in the series depend upon two parameters which are proportional to the path lengths and to the screening of the nucleus by the orbital electrons. This makes the theory valid for all angles. For a Thomas–Fermi atomic model, the log term of equation (2) becomes $\ln 219(p/mc)Z^{-1/3}$ where p is the momentum of the particle.

The theory of Molière (1947, 1948) is similar to that of Goudsmit and Saunderson, namely, that both theories depend upon a single scattering parameter but the derivation of the results is different. Molière's method consists of determining separately the contributions to the scattering of particles which are scattered one, two..... i times and then summing these contributions to obtain the total angular scattering distribution. This theory also predicts an approximately normal distribution with the variance defined as the product of the two quantities B and D which are related by the expression

$$e^B = 1{\cdot}31B^{1/2}D^{1/2}/\theta_{\min}$$

where $\theta_{\min}$ is a minimum angle due to the screening such that

$$\theta_{\min} = 1{\cdot}142(mcZ^{1/3}/181p)[1{\cdot}13 + (1{\cdot}94Z/137\beta)^2]^{1/2}.$$

Another theory by Snyder and Scott (1949) which gives results closely related to those of Molière, is based on the solution of the diffusion equation. None of these theories however considers the spin-orbital coupling and consequently all give the same results for positrons and electrons. The differences have been estimated by Mohr (1954) based on the extrapolated values of the single scattering of electrons and positrons below 30° for energies of 1, 4 and 13 Mev and for a range of values of $Z/137$.

In recent years there have been many experiments on the multiple scattering of electrons in foils. One of the most notable of these experiments was carried out with a range of elements varying in atomic number from 3 to 82 and was reported by Kultchitsky and Latyshev (1942) and later by Andrievsky, Kultchitsky and Latyshev (1943). These investigators used electrons with an energy of 2·25 Mev and they found reasonable agreement with the theory of Williams, and Goudsmit and Saunderson, provided that the width of the distribution calculated for nuclear collisions was multiplied by $(1+1/Z)^{1/2}$, to account for electron–electron scattering in the light nuclei. For heavy nuclei, however, the experimental results gave a distribution which was approximately 10% narrower than the theoretical values.

A later paper by Hanson, Lanzl, Lyman and Scott (1951) described the results of scattering of 15·7 Mev electrons in thin beryllium and gold foils. The e^{-1} widths of the angular distribution of the electrons agreed well with the theory of Molière. However Spencer and Blanchard (1954) have improved this theory by introducing a more accurate single scattering expression for larger angles. This modified Molière distribution still differed from the results of Hanson *et al.* which indicate an excess of scatters at larger angles.

Other investigators have used nuclear emulsions to study multiple scattering, in particular Gottstein, Menon, Mulvey, O'Ceallaigh and Rochat (1951) of the Bristol group, and the method has been established to such an extent that multiple scattering measurements are now frequently used to estimate both the energy and mass of fast particles. Some disagreement between experiment and theory has been found notably by Voyvodic and Pickup (1952) and Hisdal(1952). Corson (1950, 1951) however, found satisfactory agreement with Molière for

20 MeV positrons and electrons in nuclear emulsions. More recently Heymann and Williams (1956) measured the mutiple scattering of electrons and positrons in nuclear emulsions in the energy range 1 to 3 MeV, and found larger differences than predicted by Mohr.

Multiple scattering in gases has been studied with cloud chambers by Rüling and Gheri (1949), Groetzinger, Berger and Ribe (1950) and Groetzinger, Humphrey and Ribe (1952). The former studied the scattering of electrons in air at energies from 4 to 10 MeV and found quite large discrepancies with theory. Groetzinger *et al.* examined the scattering of β-particles from ^{32}P source (up to 1·7 MeV) and positrons and electrons from ^{52}Mn (up to 2·6 MeV) and ^{106}Rh (up to 3·55 MeV) in a cloud chamber containing argon and found a difference of about 10% between the scattering of electrons and positrons. Furthermore the variation of the r.m.s. scattering angle with energy indicated that the theoretical results were too high at the lower energies and decreased too rapidly with increasing energy. Cusack and Stott (1955 a) carried out an elegant experiment to investigate the mutiple scattering of positrons and electrons with energies of about 0·4 MeV, and found no significant difference in the behaviour of positrons and electrons.

Another interesting experiment on the multiple scattering of protons in nuclear emulsions in the energy range 1 to 5 MeV has been reported by Bird and Hines (1954). The shape of the curve showing the variation of the r.m.s. scattering angle with proton energy is very similar to the one given by Groetzinger, Berger and Ribe. In general it may be said that some of the experimental work is in accord with the theoretical results but there are still some outstanding experimental results which are difficult to explain and in particular the variation of the scattering with energy. Altogether there are only a few reports on multiple scattering measurements of high energy electrons using the cloud chamber and there have been no direct comparisons of positron and electron scattering at higher energies. One of the fundamental advantages of the cloud chamber method is that by using a magnetic field the energy of individual particles in the scattering gas can be measured. In their concluding remarks Bird and Hines suggest that the energy dependence of scattering should be investigated at higher energies and it is the purpose of this work to measure this for positrons and electrons with energies in the 10 MeV region. The single scattering of positrons and electrons has already been studied for angles greater than 5° (see Allen *et al.* 1956, 1957) and the present paper describes an extension of the work to smaller angles.

§ 2. Experimental Arrangement and the Method of Measuring Multiple Scattering

The source of high energy electrons was a 20 MeV betatron. It is possible to extract the beam of electrons from the betatron with a magnetic shunt, but a sufficient number of electrons was obtained by scattering in the target within the betatron toroid. The high energy photons were absorbed in a lead wall and the electrons collimated into a magnetic channel which directed them into the cloud chamber through a 0·020 inch thick aluminium window. Positrons were formed by pair production in a 0·020 inch thick lead foil, and were deflected into the chamber through a magnetic channel. The electrons were directed into a lead wall.

The cloud chamber was 28 cm diameter mounted horizontally between a Helmholtz coil system, consisting of two groups of three-layer pancake coils wound with $\frac{1}{2}$ inch wide copper strip. The coils produced a field of 1200 gauss and fluxmeter measurements of the uniformity of the field in the median plane of the chamber indicated a reduction of only 2% in the field strength at a distance of 12 cm from the centre. Illumination was provided by two type LSD.14 flash tubes, the light being focused into a well-defined parallel beam with cylindrical lenses. The chamber was filled to a pressure of 96 cm mercury, the gas mixture consisting of 20% xenon, and 80% helium. The gas mixture was analysed by means of a mass spectrometer which yielded an accuracy to better than 1%.

Two methods of measuring the multiple scattering were investigated. Initially the photographs were reprojected through the same optical system used for taking the photographs. The image was projected full size on a screen, and the angle between successive inch long chords along the track was measured. This method was rejected as being too inaccurate. The second method which was finally adopted was to measure the film directly with a travelling microscope (Cambridge universal measuring machine). Angles were measured with a protractor eye-piece. This method was more tedious and slower than the first but yielded more accurate results. The position of the film was adjusted so that the zero point on the graticule in the microscope eye-piece coincided with the point A at the beginning of the track, the protractor eye-piece being positioned so that the graticule lay along the line AB. The film was then moved along the x and y axes, so that the ends of the graticule crossed the tracks at points B and C. The difference between the two protractor readings gave the angle between the adjacent chords. By carrying out this procedure for successive chords CD, DE, EF, etc. the multiple scattering along the track length was measured. Lattimore (1948) has shown that the scattering measured by determining the angles α_i between chords is equivalent to measuring the angles between the tangents. The distribution of these angles is approximately normal with a sample variance of

$$(\alpha^2)_{\mathrm{av}} = \frac{1}{n-1}\sum_{i=1}^{n}(\alpha_i - m)^2 \quad \text{where} \quad m = \frac{1}{n}\sum_{i=1}^{n}\alpha_i.$$

As n increases the experimental value of $(\alpha^2)_{\mathrm{av}}$ approaches $\frac{2}{3}\sigma^2$ where σ^2 is the theoretical mean square scattering deflection, see Groetzinger *et al.*

The maximum amount of information on the scattering of a track could be obtained by measuring the angles between the lines joining adjacent droplets but this is almost physically impossible. On the other hand in order to compare the experimental results with Molière's theory it is necessary to use a cell length greater than a certain value. This arises in connection with the single scattering terms in the Molière expression; these terms converge slowly for small cell lengths. From these considerations a chord length of 2·54 cm was used for these measurements.

In an attempt to obtain a more accurate estimate of the mean value of the scattering angles for a given track, overlapping measurements were made on a group of tracks. This was done by dividing the primary cell length into four equal parts. After the angles between chords had been measured once, the measurements were started from a point one-quarter of the primary cell length from the beginning of the track. Further sets of scattering measurements were

obtained starting from points one-half and three-quarters the length of the prime cell length from the beginning. This increased the number of angles per track by almost a factor of four and is similar to the overlapping method used for nuclear emulsions with one exception. Thus when the gas pressure in the cloud chamber is approximately 76 cm of mercury, the number of angles per track is small since the cell length is normally only about an order of magnitude less than the total track length. Furthermore, the minimum cell length is governed by the minimum permissible number of scatters per cell length. Obviously in the limiting case, when a very small cell length with only one scatter occurs, angular deflections could hardly be considered to be due to multiple scattering. Normally in photographic plates it is nearly always possible to obtain up to 30 second differences per track but the average number of angles for multiple scattering measurements in the cloud chamber is rarely greater than seven and if corrections due to distortion near the chamber walls are made this number may be reduced. The sets of overlapping readings are dependent and although the amount of labour involved in measuring the tracks may be increased several fold it does not necessarily imply that the increased accuracy in determining m has warranted this increased effort. In order to examine this question of accuracy, the multiple scattering of 24 electron tracks was measured with a primary cell length of 2·54 cm and three additional sets of $\frac{1}{4}$, $\frac{1}{2}$ and $\frac{3}{4}$ times the primary cell length overlapping the readings were taken. The value of m was calculated for all sets of readings giving a total of 4 values for each of the 24 tracks. The correlation between these sets of results can be examined by measuring the intra-class correlation coefficient ρ which was given by Kendall (1945) as

$$\rho = \frac{1}{k-1}\left(\frac{kv_m}{v} - 1\right)$$

where k is the number of overlaps, v is the variance of the means and v_m is the variance of the mean of each track about the total mean of the individual means.

The value of ρ for the four separate populations was found to be $+0{\cdot}29$ indicating quite a significant correlation. The question is then if this value of ρ arises by chance from populations which are uncorrelated. Kendall has shown that the sampling distributions of ρ for a normal population is

$$\frac{\Gamma(r-\frac{1}{2})}{\Gamma(r-1)}(2\pi)^{1/2}\operatorname{sech}^{r-1/2}(z-\zeta)\exp -\tfrac{1}{2}(z-\zeta)$$

where

$$z = \tfrac{1}{2}\ln\frac{1+l}{1-l} \qquad \text{and} \qquad \zeta = \ln\frac{1+\lambda}{1-\lambda};$$

r is the number of tracks, l is the sample intra-class coefficient and

$$\lambda = \frac{1}{k-1}\left[\frac{k\sigma_2^2}{(k-1)\sigma_1^2+\sigma_2^2} - 1\right]$$

where σ_1^2 is the population value of $v - v_m$ and that of v_m is $\sigma_2^2/(k-1)$.

If we test the hypothesis that the intra-class correlation is zero, then $z = 0{\cdot}36$ and $\zeta = 0$.

Now the variance of $z - \zeta$ is approximately equal to

$$\frac{1}{r-1}\left(1 + \frac{1}{2r+1}\right) = 0{\cdot}04$$

for the present case. The deviation $z-\zeta$ is then nine times greater than the variance. This is very improbable and therefore the observed correlation is not likely to be purely accidental.

Another check on the correlation between the overlapping angular measurements may be obtained by examining their distribution for different amounts of overlap. The distribution of the mean

$$m=\frac{1}{n}\sum_{i=1}^{n}\alpha_i$$

of the 24 tracks is shown in figure 1 (*a*), whilst figure 1 (*b*) gives the distribution of the means of angles used in (*a*) together with the first set of overlapping readings.

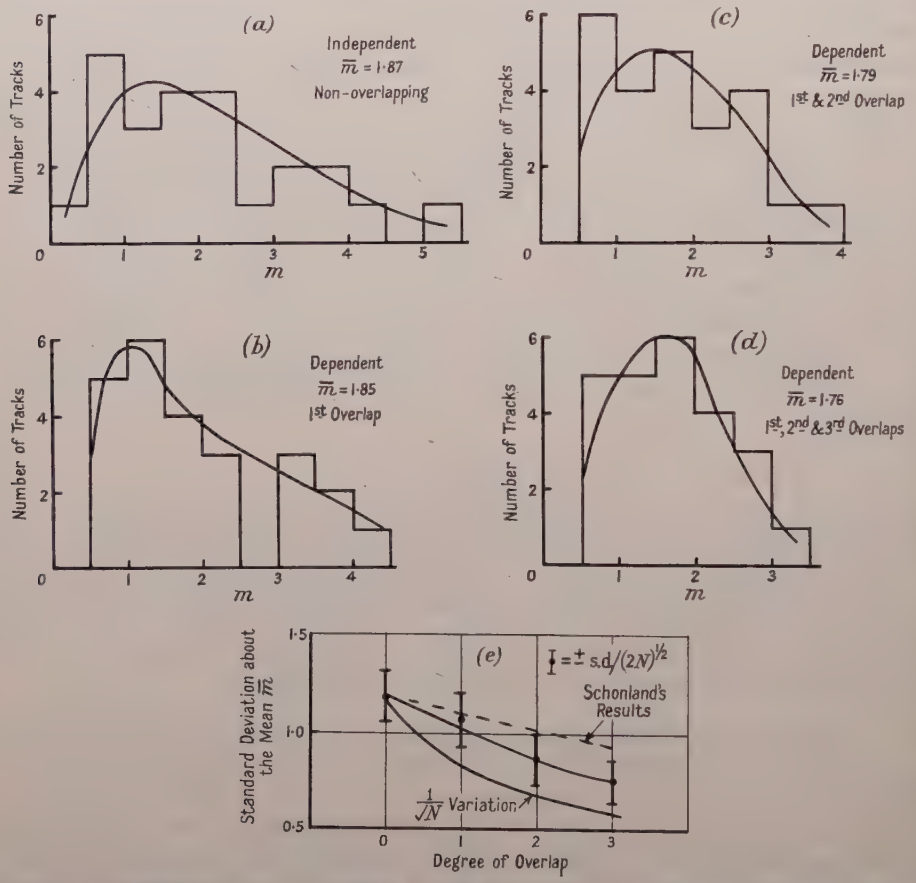

Figure 1. Histograms of overlapping values for different degrees of overlap, (*a*) non-overlapping, n angles, (*b*) non-overlapping and 1st set of overlapping readings, $\sim 2n$ angles, (*c*) non-overlapping with 1st and 2nd set of overlapping readings, $\sim 3n$ angles, (*d*) non-overlapping with 1st, 2nd and 3rd set of overlapping readings, $\sim 4n$ angles, (*e*) comparison of the relative standard deviation for different degrees of overlap.

Figures 1 (*c*) and 1 (*d*) include the second and third set of overlapping readings respectively. From the shape of these distributions it is easy to see that the effect of using the additional angles obtained from the overlapping readings is to yield a narrower distribution of m. The standard deviation about the mean $\overline{m}$ for the four distributions has been calculated and is plotted in figure 1 (*e*) against

the degree of overlap. The error limits are taken as plus and minus the standard deviation of the standard deviation which for a normal population N is given by the s.d./$(2N)^{1/2}$. The reduction of the standard deviation with overlap is quite significant but it is not as large as one would like. For instance in the third overlap there are almost four times as many second differences than if the readings were completely independent. The use of overlapping intervals in multiple scattering measurements for the coordinate method has been studied theoretically by Schonland (1955). He showed that the minimum value of the relative errors were only reduced by about 12% by using doubly overlapping intervals and by a further 4% when triply overlapping measurements were made. These results have also been plotted in figure 1 (*e*) for the purpose of comparison and tend to show a smaller reduction than the present values indicate. It may not be strictly permissible to compare Schonland's values here since the overlapping techniques are somewhat different and furthermore the present results are only for a few angular deflections per track. Even so the measurements substantiate Schonland's idea that the decrease in the error is not commensurate with the additional work involved.

§ 3. Estimation of Errors

The angle between successive chords of an electron track in a cloud chamber, i.e. for any cloud chamber track divided into sections, may be taken as a measure of the radius of the track in the magnetic field, and the multiple scattering of the track. These measurements are modified by the observer errors and any distortion of the track due to turbulence of the gas in the cloud chamber. As the validity of an experiment of this sort depends so much on the estimation and elimination of such errors, a careful study of the various sources of error was made.

Although each track was measured twice it was felt that a true estimate of the errors could not be effectively made once the observer had carried out a series of measurements and had access to the results during the repeat run. This method may help to eliminate any large errors such as taking the wrong scale reading, but there may be a tendency for the observer to keep to the initial set of readings. In an attempt to estimate the observer errors, successive measurements of the angles were made on one track and repeated at an interval of several days, the observer not being allowed access to the previous measurements. This precaution was taken in an effort to eliminate any bias and not only gave an accurate estimate of the error but also an idea of the long term consistency of the results. A total of ten separate measurements was made on the same track, giving ten readings for the angle between the first and second chord, second and third chord, etc. The means of these sets of readings were calculated and the variances were found to be 0·057 for the electrons and 0·051 for the positrons.

Another likely source of error is due to the motion of the gas in the chamber. Cusack and Stott (1955 b) have shown by a double flash technique that only when the first photographic flash occurred at a time interval greater than 100 milliseconds after the expansion of the chamber, and when the time interval between the first and second flashes was more than 150 milliseconds was it possible to detect track doubling. They also point out that the distortion nearly always occurs at the edge of the chamber. In an attempt to avoid distortion in the present experiment the time interval between expansion and the light flash was kept as small as possible. Not all of the distortion due to gas turbulence is time dependent, and

in the course of the scanning, it was noticed that some of the tracks had small single scatters near the edge of the chamber. This effect was possibly due to the motion of the gas, caused by temperature gradients or irregularities at the chamber's edge, and was examined in greater detail by comparing the angular deflections of the first and last measurements with the other angles along the rest of the track. An analysis of the variance of these two groups of measurements was carried out from a sample of 67 electron tracks.

The variance ratio between tracks and the remainder was 3·68 whilst the variance ratio between groups and the remainder was 180. The theoretical F value for these degrees of freedom are approximately 1·5 and 9·8 respectively, thus indicating that the distortion in the end cell was highly significant and on the basis of this result, portions of tracks included in a ring 2·5 cm wide around the edge of the chamber were ignored. Distortion also arises when an electron track. approached an area of intense ionization such as may be produced by heavily ionizing particles. In order to avoid this, photographs which showed any form of α-particle contamination were discarded.

In the determination of particle energy the obvious question arises as to how the multiple scattering of the electron affects the measured energy of the particle. Williams pointed out that multiple scattering introduced a spurious curvature of a track in a magnetic field. Bethe (1946) gave an expression for the mean scattering curvature of the form $\bar{\rho}/\rho = \bar{\beta}/\beta_0$ where $\beta_0\, c$ is the critical particle velocity, below which major contribution to the curvature arises from scattering, with

$$\beta_0 = 16{\cdot}5 \frac{Z}{H}\left(\frac{BP}{x}\right)^{1/2}$$

where H is the magnetic field in oersteds, Z is the atomic number, P is the number of nuclei per molecule, $B = 1 + 0{\cdot}444 \log (p\phi_{\max})/(mcZ^{1/2})$, x and p are the path length and momentum of the electron respectively, $\phi_{\max}$ is the maximum angle which can be readily recognized as a single scatter = 0·1 radian.

Under the conditions of the present experiment these expressions indicate that the error in the radius due to multiple scattering is only about 1% for a track of 40 cm radius. Normally the radius of curvature of a reprojected electron track is measured by comparing the track with circular arcs inscribed on a thin Perspex sheet. This method works very well on a track which is not scattered. For instance it was found that the radii of test circles could be measured to within ± 0·5 cm. For a track which had a certain amount of scattering, particularly small single scatters of about 15°, errors in the radius were as large as ± 20%, if the observer did not take into account the scattering. A better method of estimating the radius of the track was obtained from the angular deflections of successive chords. The radius is given by chord length/(2 sin $\frac{1}{2}m$). By this method small single scatters can be detected and eliminated.

Due to the curvature of the track in the magnetic field the chord length does not exactly correspond to the length of the track. For instance for a track of 40 cm radius the chord length is less than the true length of the track by about 4%. Since, however, the mean scattering angle is proportional to the square root of the chord length the error will only be about 2%.

§ 4. Results and Comparison with Theory

About 200 positron and 200 electron tracks were measured and after end measurements had been eliminated in an attempt to avoid distortion, about

1000 second differences remained. The mean energy of the tracks which were distributed in the energy range 7 to 17 MeV was 13·5 MeV for the electrons and 10·9 MeV for the positrons. The distribution of the angular deflections for both electrons and positrons is plotted on arithmetical probability paper in figures 2 (*a*) and 2 (*b*) together with the normal part of the distribution for Molière's and Williams' theory. The theoretical values have been adjusted to take into account the errors in measurement and a correction was also made to the actual path length due to the curvature of the track. The value of the experimental standard deviation for electrons with a mean energy of 13·5 MeV was found to be $0{\cdot}98 \pm 0{\cdot}045$ and the theoretical value given by Molière was 1·04. For the positrons with a mean energy of 10·9 MeV the experimental standard deviation was $1{\cdot}32 \pm 0{\cdot}044$ and the theoretical value was 1·36. The error limits on the experimental values are taken as plus and minus the standard error/$(2N)^{1/2}$. From these results it can be seen that there is reasonable agreement between the experimental results and

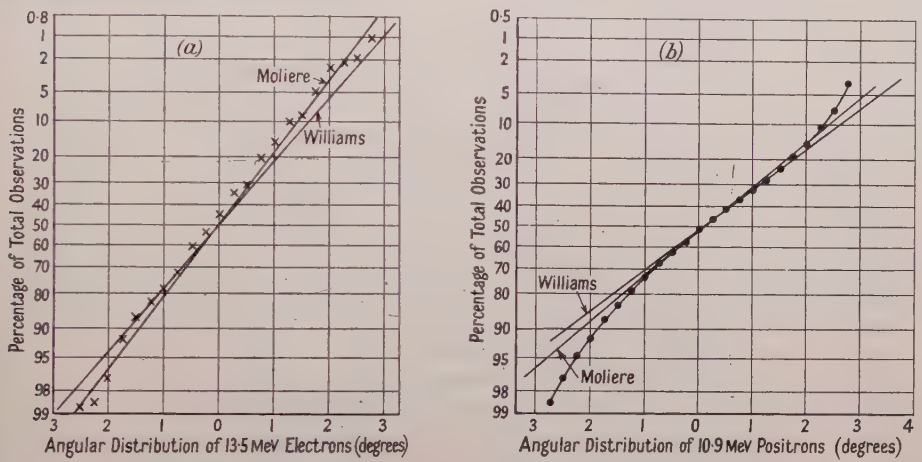

Figure 2. (*a*) Experimental angular distribution of electrons compared with the normal part of the distribution for the theories of Molière and Williams. (*b*) Experimental angular distribution of positrons compared with the normal part of the distribution for the theories of Molière and Williams.

values given by Molière's theory. The theoretical values given by the Williams theory, equation (1), are about 10% higher than these values. There are slight discrepancies in the angular distribution between the experimental results and the theory of Molière for electrons particularly in the larger angles. The differences are relatively small and cannot be considered significant.

In order to investigate the variation of scattering with energy, the total population of electrons and positrons was divided into 1 MeV groups and the r.m.s. multiple scattering deflection of each group was calculated. These results are shown in figures 3 (*a*) and 3 (*b*) together with the theoretical curves of Molière and Williams. In general there is reasonable agreement with the theory but it is not possible to differentiate between the two theories due to the magnitude of the statistical errors in the experimental results. There is however a tendency for the experimental variation of the multiple scattering with energy to be flatter than the theoretical curves for both electrons and positrons, i.e. the values are lower than the theory for energies less than 10 MeV. The shapes of these curves shown in

figures 3 (*a*) and 3 (*b*) are very similar to the results of Bird and Hines for the multiple scattering of protons up to 5 MeV and Groetzinger *et al.* for electrons up to 2 MeV. In both cases the experimental results were too low at the lower energies and do not fall off rapidly enough with increase in energy. Even so it does not seem reasonable to compare the present results with the results of these investigations as they were carried out in different energy ranges. Since there is good agreement with theory for the mean value of the energy, averaged out over the whole range, it seems necessary to look for another explanation of this effect. If there were large errors in determining the energy of the individual tracks it is likely that the mean value of the energy of the total population is accurate but the errors in the energy determinations would re-distribute some low energy tracks in the higher energy region and vice versa. This argument may be applied to the results of all cloud chamber experiments but it cannot be applied to the results of Bird and Hines who chose accurately known Q-values and energy spectra which made it possible to determine the energy of the protons accurately. It does seem

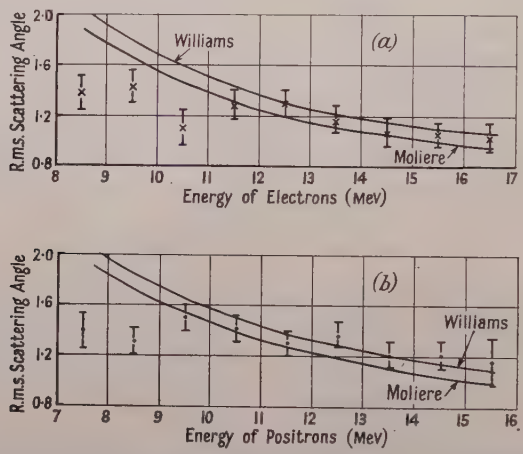

Figure 3. (*a*) Variation of the experimental value of the r.m.s. scattering angle with energy for electrons compared with the theories of Molière and Williams. (*b*) Variation of the experimental value of the r.m.s. scattering angle with energy for positrons compared with the theories of Molière and Williams.

however that the multiple scattering of electrons at low energies (approximately 0·5 MeV) is less than that predicted by Molière theory. Hisdal who measured the scattering in nuclear emulsions found that the ratio of the observed mean angle of scattering to the theoretical value was 0·62. The work of Cusack and Stott for scattering in argon tends to confirm these results. In the present work unless there is an error in the energy determination it is difficult to see how any other experimental error can possibly reduce the multiple scattering. Experimental errors which were larger than estimated would only widen the distribution with a consequent increase in the r.m.s. scattering. If the present results are extrapolated to lower energies they will give similar discrepancies to those found by other workers. At the higher energies the results agree reasonably well with theory and confirm the measurements of Corson (1950, 1951) for the scattering of 20 MeV positrons and electrons in nuclear emulsions and also with Hanson *et al.* for 15·7 MeV electrons. Since the majority of experimental results tend to be low at lower energies it is of interest to enquire into the reason for this. It is difficult to see

that the differences are due to the statistical theory of multiple scattering but they may be attributed to the approximation made in the Thomas–Fermi field. Some doubt has already been thrown on this field representation by Lenz (1954) who was able to find better agreement with the results of the small angle scattering by Biberman, Sushkin and Fabrikant (1949).

§ 5. Conclusions

The following conclusions may be drawn from the results of the present work: (i) Good agreement is found between the theory of Moliere for the multiple scattering of electrons and positrons with mean energies of 13·5 and 10·9 Mev respectively. (ii) The experimental r.m.s. scattering angles indicate a slightly smaller value at energies less than 10 Mev but agree reasonably well with theory at higher energies. This tends to confirm the results of previous workers that the scattering at lower energies may be smaller than predicted by theory. (iii) There is no significant difference between the multiple scattering of electrons and positrons. This is in agreement with the calculations of Mohr who indicates that the differences were only likely to be of the order of 1%. This differs from the findings of Heymann and Williams. (iv) Overlapping measurements of the multiple scattering indicate that there is little advantage to be gained by this technique.

Acknowledgments

The authors wish to acknowledge the help given to them by Mrs. I. Johnson, and to thank Sir Willis Jackson, Director of Research and Education, Metropolitan-Vickers Electrical Co. Ltd., for permission to publish.

References

Allen, K. R., Finlay, E. A., Lipsicas, M. M., Major, D., and Phillips, K., 1957, *Proc. Phys. Soc.* A, **70**, 355.
Allen, K. R., Lipsicas, M. M., Major, D., and Phillips, K., 1956, *Proc. Phys. Soc.* A, **69**, 141.
Allen, K. R., Phillips, K., and Whittaker, F., 1957, *Proc. Phys. Soc.* A, **70**, 536.
Andrievsky, A. I., Kulchitsky, L. A., and Latyshev, G. D., 1943, *J. Phys. Moscow*, **6**, 279.
Bethe, H. A., 1946, *Phys. Rev.*, **70**, 821.
Biberman, L., Sushkin, N., and Fabrikant, N., 1949, *Dokl. Akad. Nauk. S.S.S.R.*, **66**, 185.
Bird, J. R., and Hines, K. C., 1954, *Aust. J. Phys.*, **7**, 586.
Corson, D. R., 1950, *Phys. Rev.*, **80**, 303;
—— 1951, *Ibid.*, **84**, 605.
Cusack, N., and Stott, P., 1955 a, *J. Sci. Instrum.*, **32**, 34.
—— 1955 b, *Phil. Mag.*, **46**, 632.
Gottstein, K., Menon, M. G. K., Mulvey, J. H., O'Ceallaigh, C., and Rochat, O., 1951, *Phil. Mag.*, **42**, 708.
Goudsmit, S., and Saunderson, J. L., 1940, *Phys. Rev.*, **57**, 24;
—— 1940, *Ibid.*, **58**, 36.
Groetzinger, G., Berger, M. J., and Ribe, F. L., 1950, *Phys. Rev.*, **77**, 584.
Groetzinger, G., Humphrey, W., and Ribe, F. L., 1952, *Phys. Rev.*, **85**, 78.
Hanson, A. O., Lanzl, L. H., Lyman, E. M., and Scott, M. B., 1951, *Phys. Rev.*, **84**, 634.
Heymann, F. F., and Williams, W. F., 1956, *Phil. Mag.*, **1**, 212.
Hisdal, E., 1952, *Phil. Mag.*, **43**, 790.
Kendall, M. G., 1945, *The Advanced Theory of Statistics* (London: Griffin).

Kulchitsky, L. A., and Latyshev, G. D., 1942, *Phys. Rev.*, **61,** 254.
Lattimore, S., 1948, *Nature, Lond.*, **161,** 518.
Lenz, F., 1954, *Z. Naturf.*, **9a,** 195.
Mohr, C. B. O., 1954, *Proc. Phys. Soc.* A, **67,** 730.
Molière, G., 1947, *Z. Naturf.*, **2a,** 133;
—— 1948, *Ibid.*, **3a,** 78.
Rüling, J., and Gheri, H., 1949, *Acta Phys. Austr.*, **2,** 335.
Schonland, D. S., 1955, *Proc. Phys. Soc.* A, **68,** 447.
Snyder, H. S., and Scott, W. T., 1949, *Phys. Rev.*, **76,** 220.
Spencer, L. V., and Blanchard, C. H., 1954, *Phys. Rev.*, **93,** 114.
Voyvodic, L., and Pickup, E., 1952, *Phys. Rev.*, **85,** 91.
Williams, E. J., 1939, *Proc. Roy. Soc.* A, **169,** 531;
—— 1940, *Phys. Rev.*, **58,** 292.

A Scalar Representation of Electromagnetic Fields: II†

By E. WOLF ‡
Department of Theoretical Physics, University of Manchester

Communicated by B. H. Flowers; MS. received 9th January 1959, in final form 19th March 1959

Abstract. It is shown that the scalar representation of electromagnetic fields introduced in an earlier paper leads to a new model for energy transport. The energy may be considered to be carried by two mutually incoherent scalar waves, each of which arises from contributions of circularly polarized components of the same helicity. In a monochromatic field the energy density and the energy flow of each of these two partial waves are time-independent and the energy flow is at every point of the field in the direction of the normal to the surface of constant phase of the wave. Mathematically, the two partial waves are represented by 'analytic signals' (containing spectral components of only positive or negative frequencies) into which the complex potential of the field may be decomposed.

As an immediate consequence of these results, a new representation of an unpolarized quasi-monochromatic electromagnetic field is obtained and it is shown that, under usual conditions, the 'complex disturbance' of the classical scalar diffraction theory of optics may be identified with the complex potential of this representation.

§ 1. Introduction

In an earlier paper (Green and Wolf 1953, to be referred to as I) a new representation of electromagnetic fields in a vacuum was introduced. The field was represented by a (generally complex) scalar potential, in terms of which the energy density and the energy flow were defined by expressions similar to the quantum mechanical expressions for the probability density and the probability current. Such a representation was obtained by utilizing, in an appropriate manner, the subsidiary (Lorentz) condition of electromagnetic theory. The analysis was extended to regions which include charges and currents by Roman (1955), and the method was used by him and also by Nagy (1955) in quantum mechanical investigations. Focke (1957) employed the theory in the analysis of an optical diffraction problem for which the usual optical scalar theory is inadequate. Recently Roman (1959) has investigated the transformation properties of the complex potential and derived the associate energy–momentum tensor.

In the present paper some further aspects of this new representation are discussed. In particular it is shown that the representation leads to an interesting new model for energy transport: The energy may be considered to be carried by two mutually incoherent scalar waves, each of which contains contributions

† The research described in this paper was sponsored by the Air Force Cambridge Research Center of the Air Research and Development Command, United States Air Force, through its European Office, under Contract No. AF 61(052)—169.

‡ Now at the Institute of Optics, University of Rochester, N.Y., U.S.A.

from circularly polarized plane wave components of definite helicity (right- or left-handed). Mathematically these two waves are represented by two 'analytic signals' (containing spectral components of only positive or negative frequencies) into which the complex potential of the field may be decomposed. In a monochromatic field, the energy density and the energy flow vector of each of the two waves are time-independent and the energy flow of each is along the normal to its surface of constant phase.

As an immediate consequence of these results a new representation of an unpolarized quasi-monochromatic electromagnetic field is obtained, and it is shown, that under usual conditions the (usually undefined) 'complex disturbance' of the classical scalar diffraction theory of optics may be identified with the complex potential of this representation. This analysis places the optical scalar theory on a rigorous foundation and the theory is found to have a much wider range of validity than is usually believed to be the case.

§ 2. Transition to the Scalar Theory

It will be useful to begin by briefly summarizing the main results obtained in I. At the same time some of the formulae will be recast into forms which are somewhat more convenient for the purpose of the present discussion.

As is well known an electromagnetic field in vacuum is completely specified by a real vector potential $\mathbf{A}(\mathbf{x}, t)$, which satisfies the subsidiary condition

$$\operatorname{div} \mathbf{A} = 0. \qquad \ldots\ldots (2.1)$$

We assume that $\mathbf{A}$ may be represented in the form of a Fourier integral

$$\mathbf{A}(\mathbf{x}, t) = \int_{K^+} \{\mathbf{a}(\mathbf{k}, t) \cos(\mathbf{k}.\mathbf{x}) + \mathbf{b}(\mathbf{k}, t) \sin(\mathbf{k}.\mathbf{x})\}\, d\mathbf{k}, \quad \ldots\ldots (2.2)$$

where, since $\mathbf{A}$ is real, the integration is taken over half of $\mathbf{k}$-space. We chose the half-space (denoted by K^+) for which the z-component k_z of $\mathbf{k}$, with respect to some fixed system of Cartesian rectangular axes is non-negative.

The condition (2.1) implies that for each $\mathbf{k}$ (except perhaps for a set of measure zero which is of no physical interest)

$$\mathbf{k}.\mathbf{a}(\mathbf{k}, t) = \mathbf{k}.\mathbf{b}(\mathbf{k}, t) = 0. \qquad \ldots\ldots (2.3)$$

To utilize fully these conditions we associate with each $\mathbf{k}$ two real, mutually orthogonal unit vectors $\mathbf{l}_1(\mathbf{k})$ and $\mathbf{l}_2(\mathbf{k})$, both at right angles to $\mathbf{k}$:

$$\mathbf{l}_1(\mathbf{k}) = \frac{\mathbf{n} \wedge \mathbf{k}}{|\mathbf{n} \wedge \mathbf{k}|}, \quad \mathbf{l}_2(\mathbf{k}) = \frac{\mathbf{k} \wedge \mathbf{l}_1}{|\mathbf{k} \wedge \mathbf{l}_1|}, \qquad \ldots\ldots (2.4)$$

where $\mathbf{n}$ is a (real) arbitrary but fixed vector. According to (2.3) the vectors $\mathbf{a}$ and $\mathbf{b}$ lie in the plane of $\mathbf{l}_1$ and $\mathbf{l}_2$ and hence may be expressed in the form

$$\left.\begin{aligned} \mathbf{a}(\mathbf{k}, t) &= a_1\mathbf{l}_1 + a_2\mathbf{l}_2 \equiv (\mathbf{a}.\mathbf{l}_1)\mathbf{l}_1 + (\mathbf{a}.\mathbf{l}_2)\mathbf{l}_2, \\ \mathbf{b}(\mathbf{k}, t) &= b_1\mathbf{l}_1 + b_2\mathbf{l}_2 \equiv (\mathbf{b}.\mathbf{l}_1)\mathbf{l}_1 + (\mathbf{b}.\mathbf{l}_2)\mathbf{l}_2. \end{aligned}\right\} \qquad \ldots\ldots (2.5)$$

Next we form the complex combinations

$$\left.\begin{aligned} \alpha(\mathbf{k}, t) &= a_1 + ia_2, \\ \beta(\mathbf{k}, t) &= b_1 + ib_2, \end{aligned}\right\} \qquad \ldots\ldots (2.6)$$

and regard α and β as Fourier coefficients of a new function V, called the *complex potential* of the field:

$$V(\mathbf{x}, t) = \int_{K^+} \{\alpha(\mathbf{k}, t) \cos(\mathbf{k}.\mathbf{x}) + \beta(\mathbf{k}, t) \sin(\mathbf{k}.\mathbf{x})\}\, d\mathbf{k}. \quad \ldots\ldots (2.7)$$

Once the constant vector $\mathbf{n}$ which enters the expressions (2.4) for the base vectors has been chosen, the complex potential V is uniquely specified by the Fourier components $\mathbf{a}$ and $\mathbf{b}$ of the vector potential $\mathbf{A}$ and hence by $\mathbf{A}$ itself; conversely it is easily seen by using the Fourier inversion formula that the vector potential $\mathbf{A}$ is uniquely specified by the complex potential V.

We shall now express the relation between $\mathbf{A}$ and V in a more compact form. For this purpose it is convenient to begin from a Fourier representation of $\mathbf{A}$ which involves the exponential rather than trigonometric functions, i.e we write

$$\mathbf{A}(\mathbf{x},t)=\int_{\mathrm{K}}\mathbf{c}(\mathbf{k},t)\exp(i\mathbf{k}.\mathbf{x})\,d\mathbf{k}, \qquad \ldots\ldots(2.8)$$

where the integration is now taken over the whole $\mathbf{k}$-space (denoted by K). In place of (2.3) one now has, as a consequence of (2.1)

$$\mathbf{k}.\mathbf{c}(\mathbf{k},t)=0, \qquad \ldots\ldots(2.9)$$

for every $\mathbf{k}$. Moreover, since $\mathbf{A}$ is real,

$$\mathbf{c}(-\mathbf{k},t)=\mathbf{c}^*(\mathbf{k},t), \qquad \ldots\ldots(2.10)$$

where the asterisk denotes the complex conjugate.

Next we introduce a set of complex base vectors $\mathbf{L}$, defined in terms of $\mathbf{l}_1$ and $\mathbf{l}_2$ of equation (2.4) by

$$\mathbf{L}(\mathbf{k})=\mathbf{l}_1(\mathbf{k})+i\mathbf{l}_2(\mathbf{k}) \quad (k_z\geqslant 0), \qquad \ldots\ldots(2.11a)$$

$$\mathbf{L}(-\mathbf{k})=\mathbf{L}(\mathbf{k}), \qquad \ldots\ldots(2.11b)$$

and define the quantities

$$\gamma(\mathbf{k},t)=\mathbf{L}(\mathbf{k}).\mathbf{c}(\mathbf{k},t). \qquad \ldots\ldots(2.12)$$

Then the complex potential V is given by†

$$V(\mathbf{x},t)=\int_{\mathrm{K}}\gamma(\mathbf{k},t)\exp(i\mathbf{k}.\mathbf{x})\,d\mathbf{k}. \qquad \ldots\ldots(2.13)$$

Now from (2.12), using the Fourier inverse of (2.13),

$$\gamma(\mathbf{k},t)=\frac{1}{(2\pi)^3}\mathbf{L}(\mathbf{k}).\int\mathbf{A}(\mathbf{x}',t)\exp(-i\mathbf{k}'.\mathbf{x}')\,d\mathbf{x}', \qquad \ldots\ldots(2.14)$$

the integration being taken over the whole $\mathbf{x}'$-space. Substitution from (2.14) into (2.13) leads finally to the formula

$$V(\mathbf{x},t)=\int\mathbf{A}(\mathbf{x}',t).\mathbf{M}(\mathbf{x}'-\mathbf{x})\,d\mathbf{x}', \qquad \ldots\ldots(2.15)$$

where

$$\mathbf{M}(\mathbf{x})=\frac{1}{(2\pi)^3}\int_{\mathrm{K}}\mathbf{L}(\mathbf{k})\exp(-i\mathbf{k}.\mathbf{x})\,d\mathbf{k}. \qquad \ldots\ldots(2.16)$$

† Between the quantities $\mathbf{a}$, $\mathbf{b}$ and $\mathbf{c}$, and between α, β and γ the following relations hold:

$$\mathbf{ck}(t)=\begin{cases}\frac{1}{2}[\mathbf{a}(\mathbf{k},t)-i\mathbf{b}(\mathbf{k},t)] & k_z\geqslant 0,\\ \frac{1}{2}[\mathbf{a}(-\mathbf{k},t)+i\mathbf{b}(-\mathbf{k},t)], & k_z<0,\end{cases}$$

$$\gamma(\mathbf{k},t)=\begin{cases}\frac{1}{2}[\alpha(\mathbf{k},t)-i\beta(\mathbf{k},t)] & k_z\geqslant 0,\\ \frac{1}{2}[\alpha(-\mathbf{k},t)+i\beta(-\mathbf{k},t)]. & k_z<0.\end{cases}$$

These relations, as well as the equivalence of the formulae (2.13) and (2.7) are easily established by direct comparison, expressing the right-hand sides of (2.8) and (2.13) as sums of two integrals, each over one half of the $\mathbf{k}$-space and on using the fact that $\mathbf{A}$ is real.

The formula (2.15) expresses the complex potential V as a linear transform of the real vector potential $\mathbf{A}$, the kernel $\mathbf{M}$ of this transformation being the Fourier transform of the set of the complex base vectors $\mathbf{L}(\mathbf{k})$.

The inverse transition from the complex potential V to the vector potential $\mathbf{A}$ may also be expressed as a linear transform. One finds from (2.12), with the help of (2.11) and (2.10) that

$$\mathbf{c}(\mathbf{k},t)=\tfrac{1}{2}[\gamma(\mathbf{k},t)\mathbf{L}^*(\mathbf{k})+\gamma^*(-\mathbf{k},t)\mathbf{L}(\mathbf{k})]. \qquad \ldots\ldots (2.17)$$

On substituting on the right of (2.17) from the Fourier inverse of (2.13) it follows that

$$\mathbf{c}(\mathbf{k},t)=\frac{1}{2}\frac{1}{(2\pi)^3}\left[\mathbf{L}^*(\mathbf{k})\int V(\mathbf{x}',t)\exp\left(-i\mathbf{k}\,.\,\mathbf{x}'\right)d\mathbf{x}'+\mathbf{L}(\mathbf{k})\int V^*(\mathbf{x}',t)\right.$$
$$\left.\times\exp\left(-i\mathbf{k}\,.\,\mathbf{x}'\right)d\mathbf{x}'\right]. \qquad \ldots\ldots (2.18)$$

On substituting from (2.18) into (2.8), and using the relation $\mathbf{M}(-\mathbf{x})=\mathbf{M}(\mathbf{x})$ which follows from (2.16) and (2.11 *b*), we obtain the required formula:

$$\mathbf{A}(\mathbf{x},t)=\mathscr{R}\int V(\mathbf{x}',t)\mathbf{M}^*(\mathbf{x}'-\mathbf{x})\,d\mathbf{x}', \qquad \ldots\ldots (2.19)$$

$\mathscr{R}$ denoting the real part.

It was shown in I, that because $\mathbf{A}$ satisfies the vector wave equation

$$\nabla^2\mathbf{A}=\frac{1}{c^2}\ddot{\mathbf{A}}, \qquad \ldots\ldots (2.20)$$

the complex potential V satisfies the scalar wave equation

$$\nabla^2 V=\frac{1}{c^2}\ddot{V}, \qquad \ldots\ldots (2.21)$$

a result which may also readily be verified with the help of (2.15).

For the purpose of later discussion, the following results are also needed: In terms of V, the energy density w of the field may be expressed in the form

$$w=\frac{1}{8\pi}\left(\frac{1}{c^2}\dot{V}\dot{V}^*+\nabla V\,.\,\nabla V^*\right), \qquad \ldots\ldots (2.22)$$

and the energy flow vector $\mathbf{S}$ is given by

$$\mathbf{S}=-\frac{1}{8\pi}\left(\dot{V}^*\nabla V+\dot{V}\nabla V^*\right). \qquad \ldots\ldots (2.23)$$

These expressions, which satisfy the usual conservation law

$$\frac{dw}{dt}+\operatorname{div}\mathbf{S}=0, \qquad \ldots\ldots (2.24)$$

are formally identical with the quantum mechanical expressions for the probability density and the probability current. A justification of the expressions (2.22) and (2.23) was given in I. A more complete discussion of this point will be found in a paper by Roman (1959).

§ 3. A New Model for Energy Transport

Let us represent the complex potential V as a Fourier integral with respect to the time variable t:

$$V(\mathbf{x},t)=\int_{-\infty}^{\infty} v(\mathbf{x},\omega)\exp\left(-i\omega t\right)d\omega. \qquad \ldots\ldots (3.1)$$

We divide the range of integration into two parts corresponding to negative and positive frequencies and write

$$V(\mathbf{x},t)=V_+(\mathbf{x},t)+V_-(\mathbf{x},t), \qquad \ldots\ldots (3.2)$$

where

$$\left.\begin{aligned} V_+(\mathbf{x},t)&=\int_{-\infty}^{0} v(\mathbf{x},\omega)\exp(-i\omega t)\,d\omega=\int_0^{\infty} v(\mathbf{x},-\omega)\exp(i\omega t)\,d\omega,\\ V_-(\mathbf{x},t)&=\int_0^{\infty} v(\mathbf{x},\omega)\exp(-i\omega t)\,d\omega. \end{aligned}\right\} \qquad (3.3)$$

Since V is in general complex, V_+ and V_- are *not*, in general, complex conjugates of each other. Because V satisfies the wave equation each Fourier component $v(\mathbf{x},\omega)$ of V, and hence also each Fourier component of V_+ and V_- satisfies the Helmholtz equation. This implies that V_+ and V_- satisfy the wave equation, i.e.

$$\nabla^2 V_+=\frac{1}{c^2}\ddot{V}_+, \qquad \nabla^2 V_-=\frac{1}{c^2}\ddot{V}_-. \qquad \ldots\ldots (3.4)$$

We shall refer to V_+ and V_- as *partial waves.*

Consider the energy density w of the field. If we substitute (3.2) into (2.22) we obtain

$$w=w_++w_-+w', \qquad \ldots\ldots (3.5)$$

where

$$\left.\begin{aligned} w_+&=\frac{1}{8\pi}\left(\frac{1}{c^2}\dot{V}_+\dot{V}_+^*\nabla+\nabla V_+.\nabla V_+^*\right),\\ w_-&=\frac{1}{8\pi}\left(\frac{1}{c^2}\dot{V}_-\dot{V}_-^*+\nabla V_-.\nabla V_-^*\right) \end{aligned}\right\} \qquad \ldots\ldots (3.6)$$

are the energy densities of the two partial waves and

$$w'=\frac{1}{8\pi}\left[\frac{1}{c^2}(\dot{V}_+\dot{V}_-^*+\dot{V}_+^*\dot{V}_-)+(\nabla V_+.\nabla V_-^*+\nabla V_+^*.\nabla V_-)\right] \qquad \ldots\ldots (3.7)$$

is the contribution to the total energy density arising from the interference of the two partial waves.

Similarly, according to (3.2) and (2.23), the energy flow vector $\mathbf{S}$ of the field may be expressed in the form

$$\mathbf{S}=\mathbf{S}_++\mathbf{S}_-+\mathbf{S}', \qquad \ldots\ldots (3.8)$$

where

$$\left.\begin{aligned} \mathbf{S}_+&=-\frac{1}{8\pi}(\dot{V}_+^*\nabla V_++\dot{V}_+\nabla V_+^*),\\ \mathbf{S}_-&=-\frac{1}{8\pi}(\dot{V}_-^*\nabla V_-+\dot{V}_-\nabla V_-^*) \end{aligned}\right\} \qquad \ldots\ldots (3.9)$$

are the energy flow vectors of the two partial waves and

$$\mathbf{S}'=-\frac{1}{8\pi}(\dot{V}_+^*\nabla V_-+\dot{V}_+\nabla V_-^*+\dot{V}_-^*\nabla V_++\dot{V}_-\nabla V_+^*) \qquad \ldots\ldots (3.10)$$

is the contribution to the total flow vector arising from the interference of the two partial waves.

We shall now evaluate the time averages of w and $\mathbf{S}$. For this purpose consider a typical term on the right of (3.7). Using (3.3) it may be expressed in terms of the spectrum v of V as follows:

$$\dot{V}_+\dot{V}_-^* = -\int_0^\infty\int_0^\infty \omega\omega' v(\mathbf{x}, -\omega)v^*(\mathbf{x}, \omega')\exp[i(\omega+\omega')t]\,d\omega\,d\omega'.$$

Hence the time average (denoted by angular brackets) of this quantity is

$$\begin{aligned}\langle \dot{V}_+\dot{V}_-^*\rangle &= -\lim_{T\to\infty}\frac{1}{2T}\int_{-T}^{T} dt\int_0^\infty\int_0^\infty \omega\omega' v(\mathbf{x}, -\omega)v^*(\mathbf{x}, \omega')\exp[i(\omega+\omega')t]\,d\omega\,d\omega' \\ &= -\int_0^\infty\int_0^\infty \omega\omega' v(\mathbf{x}, -\omega)v^*(\mathbf{x}, \omega')\left\{\lim_{T\to\infty}\left(\frac{\sin[(\omega+\omega')T]}{(\omega+\omega')T}\right)\right\}d\omega\,d\omega' \\ &= 0. \qquad \ldots\ldots (3.11)\end{aligned}$$

In the same way the time average of each of the other three terms in (3.7) may be shown to vanish, so that

$$\langle w'\rangle = 0. \qquad \ldots\ldots (3.12)$$

In a similar manner it follows that

$$\langle \mathbf{S}'\rangle = 0. \qquad \ldots\ldots (3.13)$$

Thus on the time average, the two partial waves do not give rise to interference effects, the time averaged energy density and the time averaged energy flow vector of the field being equal to the sum of the time averaged energy densities and the time averaged energy flow vectors respectively, of the two partial waves:

$$\left.\begin{aligned}\langle w\rangle &= \langle w_+\rangle + \langle w_-\rangle, \\ \langle \mathbf{S}\rangle &= \langle \mathbf{S}_+\rangle + \langle \mathbf{S}_-\rangle.\end{aligned}\right\} \qquad \ldots\ldots (3.14)$$

We may say that *the two partial waves are mutually incoherent.*

Since according to (3.3) each of the partial waves has spectral components which belong to one half of the frequency range only, the wave functions V_+ and V_- each represent what in communication theory is known as an *analytic signal*†. This name derives from the fact that under fairly general conditions such a function, when considered as function of complex t is analytic in one half of the complex plane, V_+ being analytic in the lower, and V_- in the upper half of this plane. The real and imaginary parts of such a function are related by Hilbert's reciprocity relations. Thus if superscripts r and i refer to real and imaginary parts, i.e. if we write

$$V_+ = V_+^{(r)} + iV_+^{(i)}, \quad V_- = V_-^{(r)} + iV_-^{(i)}, \qquad \ldots\ldots (3.15)$$

where $V_+^{(r)}$, $V_+^{(i)}$, $V_-^{(r)}$ and $V_-^{(i)}$ are all real, then

$$\left.\begin{aligned}V_+^{(i)}(\mathbf{x}, t) &= -\frac{P}{\pi}\int_{-\infty}^{+\infty}\frac{V_+^{(r)}(\mathbf{x}, t')}{t'-t}\,dt', \quad V_+^{(r)}(\mathbf{x}, t) = \frac{P}{\pi}\int_{-\infty}^{+\infty}\frac{V_+^{(i)}(\mathbf{x}, t')}{t'-t}\,dt', \\ \text{and} \\ V_-^{(i)}(\mathbf{x}, t) &= \frac{P}{\pi}\int_{-\infty}^{+\infty}\frac{V_-^{(r)}(\mathbf{x}, t')}{t'-t'}\,dt', \quad V_-^{(r)}(\mathbf{x}, t) = -\frac{P}{\pi}\int_{-\infty}^{+\infty}\frac{V_-^{(i)}(\mathbf{x}, t')}{t'-t}\,dt',\end{aligned}\right\} \qquad \ldots\ldots (3.16)$$

and P denotes Cauchy's principal value at $t'=t$.

† The concept of an analytic signal is due to Gabor (1946). The properties of such 'signals' have been extensively studied (cf. Ville 1948, 1950, Oswald 1956). Analytic signals also play an important role in some branches of optics (cf. Born and Wolf 1959, chap. X).

Before discussing the physical significance of the two partial waves it will be shown that the decomposition into these waves has some interesting consequences for a monochromatic field, i.e. when $\mathbf{A}$ is of the form

$$\mathbf{A}(\mathbf{x},t)=\mathbf{F}(\mathbf{x})\exp(-i\omega t)+\mathbf{F}^*(\mathbf{x})\exp(i\omega t), \qquad \ldots\ldots(3.17)$$

where $\mathbf{F}$ is a (generally complex) vector function of position. If we apply to (3.17) the transformation (2.15), we obtain

$$V(\mathbf{x},t)=V_-(\mathbf{x},t)+V_+(\mathbf{x},t), \qquad \ldots\ldots(3.18)$$

where

$$V_-(\mathbf{x},t)=U_-(\mathbf{x})\exp(-i\omega t), \quad V_+(\mathbf{x},t)=U_+(\mathbf{x})\exp(i\omega t), \qquad \ldots\ldots(3.19)$$

and

$$\left.\begin{aligned} U_-(\mathbf{x})&=\int \mathbf{F}(\mathbf{x}')\,.\,\mathbf{M}(\mathbf{x}'-\mathbf{x})\,d\mathbf{x}',\\ U_+(\mathbf{x})&=\int \mathbf{F}^*(\mathbf{x}')\,.\,\mathbf{M}(\mathbf{x}'-\mathbf{x})\,d\mathbf{x}'. \end{aligned}\right\} \qquad \ldots\ldots(3.20)$$

On substituting from (3.19) into (3.6) and (3.9) the following expressions are obtained for the energy densities and energy flow vectors of the two partial waves:

$$\left.\begin{aligned} w_-&=\frac{1}{8\pi}\left(\frac{\omega^2}{c^2}U_-U_-^*+\nabla U_-.\nabla U_-^*\right),\\ w_+&=\frac{1}{8\pi}\left(\frac{\omega^2}{c^2}U_+U_+^*+\nabla U_+.\nabla U_+^*\right), \end{aligned}\right\} \qquad \ldots\ldots(3.21)$$

$$\left.\begin{aligned} \mathbf{S}_-&=-\frac{i\omega}{8\pi}(U_-^*\nabla U_- - U_-\nabla U_-^*),\\ \mathbf{S}_+&=\frac{i\omega}{8\pi}(U_+^*\nabla U_+ - U_+\nabla U_+^*). \end{aligned}\right\} \qquad \ldots\ldots(3.22)$$

The formulae (3.21) and (3.22) show that *the energy density and the energy flow vector of each of the two partial waves associated with a monochromatic field are time-independent.*

Let a_- and a_+ be the amplitudes, and ϕ_- and ϕ_+ the phases of U_- and U_+ respectively, i.e. let

$$U_-=a_-\exp(i\phi_-), \quad U_+=a_+\exp(i\phi_+), \qquad \ldots\ldots(3.23)$$

where the a's and the ϕ's are real. On substituting from (3.23) into (3.22) it follows that

$$\mathbf{S}_-=\frac{\omega}{4\pi}a_-^2\nabla\phi_-, \quad \mathbf{S}_+=-\frac{\omega}{4\pi}a_+^2\nabla\phi_+, \qquad \ldots\ldots(3.24)$$

i.e. *the energy flow of each of the two partial waves associated with a monochromatic field is at every point in the direction of the normal to the surface of constant phase of the wave.*

In the usual representation the orthogonality between the energy flow and the surface of constant phase is, in general, valid only in the limit of the geometrical optics approximation, i.e. in the high frequency limit $\omega\to\infty$ (cf. Born and Wolf 1959, pp. 112-113). In the present representation this orthogonality is seen to hold rigorously for each of the two partial waves of a monochromatic field, irrespective of the frequency.

§ 4. The Physical Significance of the two Partial Waves

In order to appreciate the physical significance of the two partial waves it will be sufficient, as will be seen shortly, to consider a monochromatic field. Thus we consider a vector potential of the form (3.17):

$$\mathbf{A}(\mathbf{x},t)=\mathbf{F}(\mathbf{x})\exp(-i\omega t)+\mathbf{F}^*(\mathbf{x})\exp(i\omega t). \qquad \ldots\ldots(4.1)$$

We represent $\mathbf{F}$ in the form of an angular spectrum of plane waves, i.e. in the form†

$$\mathbf{F}(\mathbf{x})=\int_{-\infty}^{+\infty}\int_{-\infty}^{+\infty}\exp\{i(k_x x+k_y y)\}[\mathbf{P}(k_x,k_y)\exp(ik_z z)+\mathbf{Q}(k_x,k_y)\exp(-ik_z z)]\times dk_x\,dk_y, \qquad \ldots\ldots(4.2)$$

where‡

$$k_z=+\left[\left(\frac{\omega}{c}\right)^2-k_x{}^2-k_y{}^2\right]^{1/2}. \qquad \ldots\ldots(4.3)$$

On substituting from (4.2) into (3.20) and using the inverse of (2.16) one finds that

$$\left.\begin{aligned}U_-(\mathbf{x})&=\int_{-\infty}^{+\infty}\int_{-\infty}^{+\infty}\{\mathbf{L}(\mathbf{k}^{(+)}).\mathbf{P}(k_x,k_y)\exp(i\mathbf{k}^{(+)}.\mathbf{x})\\&\qquad+\mathbf{L}(\mathbf{k}^{(-)}).\mathbf{Q}(k_x,k_y)\exp(i\mathbf{k}^{(-)}.\mathbf{x})\}\,dk_x\,dk_y,\\U_+(\mathbf{x})&=\int_{-\infty}^{+\infty}\int_{-\infty}^{+\infty}\{\mathbf{L}(\mathbf{k}^{(+)}).\mathbf{P}^*(k_x,k_y)\exp(-i\mathbf{k}^{(+)}.\mathbf{x})\\&\qquad+\mathbf{L}(\mathbf{k}^{(-)}).\mathbf{Q}^*(k_x,k_y)\exp(-i\mathbf{k}^{(-)}.\mathbf{x})\}dk_x\,dk_y.\end{aligned}\right\}$$

where $\qquad \ldots\ldots(4.4)$

$$\mathbf{k}^{(+)}\equiv k_x,k_y,+\left[\left(\frac{\omega}{c}\right)^2-k_x{}^2-k_y{}^2\right]^{1/2},\quad \mathbf{k}^{(-)}\equiv k_x,k_y,-\left[\left(\frac{\omega}{c}\right)^2-k_x{}^2-k_y{}^2\right]^{1/2}. \qquad \ldots\ldots(4.5)$$

It is seen that for each pair of values k_x, k_y, there are two monochromatic plane scalar waves which contribute to V_- viz.

$$\left.\begin{aligned}\mathscr{V}_-{}^{(+)}(\mathbf{x},t)&=\mathscr{U}_-{}^{(+)}(\mathbf{x})\exp(-i\omega t)\\&=\mathbf{L}(\mathbf{k}^{(+)}).\mathbf{P}(k_x,k_y)\exp[i(\mathbf{k}^{(+)}.\mathbf{x}-\omega t)],\\\mathscr{V}_-{}^{(-)}(\mathbf{x},t)&=\mathscr{U}_-{}^{(-)}(\mathbf{x})\exp(-i\omega t)\\&=\mathbf{L}(\mathbf{k}^{(-)}).\mathbf{Q}(k_x,k_y)\exp[i(\mathbf{k}^{(-)}.\mathbf{x}-\omega t)].\end{aligned}\right\} \qquad \ldots\ldots(4.6)$$

These wave functions represent waves propagated in the direction specified by the vectors $\mathbf{k}^{(+)}$ and $\mathbf{k}^{(-)}$ respectively.

There are two similar contributions to the other partial wave V_+, namely

$$\left.\begin{aligned}\mathscr{V}_+{}^{(+)}(\mathbf{x},t)&=\mathscr{U}_+{}^{(+)}(\mathbf{x})\exp(i\omega t)\\&=\mathbf{L}(\mathbf{k}^{(+)}).\mathbf{P}^*(k_x,k_y)\exp[-i(\mathbf{k}^{(+)}.\mathbf{x}-\omega t)]\\\mathscr{V}_+{}^{(-)}(\mathbf{x},t)&=\mathscr{U}_+{}^{(-)}(\mathbf{x})\exp(i\omega t)\\&=\mathbf{L}(\mathbf{k}^{(-)}).\mathbf{Q}^*(k_x,k_y)\exp[-i(\mathbf{k}^{(-)}.\mathbf{x}-\omega t)].\end{aligned}\right\} \qquad \ldots\ldots(4.7)$$

† That such a representation is possible is shown in the Appendix. If, as is often the case in practice, the field obeys Sommerfeld's radiation condition in the half-space $z>0$, then $\mathbf{Q}(k_x,k_y)\equiv 0$.

‡ When $k_x{}^2+k_y{}^2>\omega^2/c^2$, k_z is complex and equal to $i[k_x{}^2+k_y{}^2-(\omega/c)^2]^{1/2}$. The corresponding terms in (4.2) then represent evanescent (damped) waves.

To find what kind of vector potential corresponds to these waves we apply the transformation (2.19). Let $\mathfrak{A}^{(+)}$ denote the vector potential corresponding to $\mathscr{V}^{(+)}$, $\mathfrak{A}^{(-)}$ the vector potential corresponding to $\mathscr{V}^{(-)}$ etc. Then, if the inverse of (2.16) and the relation (2.11 *b*) are also used one finds that

$$\mathfrak{A}_{-}^{(+)}(\mathbf{x},t)=\mathscr{R}[\mathbf{L}(\mathbf{k}^{(+)}).\mathbf{P}(k_x,k_y)]\mathbf{L}^*(\mathbf{k}^{(+)})\exp[i(\mathbf{k}^{(+)}.\mathbf{x}-\omega t)], \quad \ldots\ldots(4.8)$$

$$\mathfrak{A}_{+}^{(+)}(\mathbf{x},t)=\mathscr{R}[\mathbf{L}(\mathbf{k}^{(+)}).\mathbf{P}^*(k_x,k_y)]\mathbf{L}^*(\mathbf{k}^{(+)})\exp[-i(\mathbf{k}^{(+)}.\mathbf{x}-\omega t)]. \quad \ldots\ldots(4.9)$$

The vector potential $\mathfrak{A}_{-}^{(-)}$ may be formally obtained from (4.8) by replacing $\mathbf{P}$ by $\mathbf{Q}$ and $\mathbf{k}^{(+)}$ by $\mathbf{k}^{(-)}$, and the vector potential $\mathfrak{A}_{+}^{(-)}$ by making the same substitution in (4.9). Next we set

$$\left.\begin{aligned}\mathbf{L}(\mathbf{k}^{(+)}).\mathbf{P}(k_x,k_y)&=g\exp(i\psi),\\ \mathbf{L}(\mathbf{k}^{(+)}).\mathbf{P}^*(k_x,k_y)&=h\exp(i\chi),\end{aligned}\right\} \quad \ldots\ldots(4.10)$$

where g, h, ψ and χ are real. Remembering that $\mathbf{L}^*=\mathbf{l}_1-i\mathbf{l}_2$, (4.8) and (4.9) become

$$\mathfrak{A}_{-}^{(+)}=g\{\mathbf{l}_1^{(+)}\cos[\psi+\mathbf{k}^{(+)}.\mathbf{x}-\omega t]+\mathbf{l}_2^{(+)}\sin[\psi+\mathbf{k}^{(+)}.\mathbf{x}-\omega t]\}, \quad \ldots\ldots(4.11)$$

$$\mathfrak{A}_{+}^{(+)}=h\{\mathbf{l}_1^{(+)}\cos[\chi+\mathbf{k}^{(+)}.\mathbf{x}-\omega t]-\mathbf{l}_2^{(+)}\sin[\chi+\mathbf{k}^{(+)}.\mathbf{x}-\omega t]\}, \quad \ldots\ldots(4.12)$$

where $\mathbf{l}_1^{(+)}$ is written in short for $\mathbf{l}_1(\mathbf{k}^{(+)})$ etc. Since $\mathbf{l}_1$ and $\mathbf{l}_2$ are mutually orthogonal unit vectors at right angles to the propagation vector, it follows that $\mathfrak{A}_{-}^{(+)}$ and $\mathfrak{A}_{+}^{(+)}$ each represents a *circularly polarized plane monochromatic wave*, one of these waves being *left-handed*, the other *right-handed*. There is a similar interpretation for $\mathfrak{A}_{-}^{(-)}$ and $\mathfrak{A}_{+}^{(-)}$. The following theorem is now evident:

If the vector potential of an electromagnetic field is decomposed into monochromatic plane waves of all possible frequencies and directions of propagation, and if, further, each plane wave is decomposed into two circularly polarized components, one left-handed the other right-handed, then the partial wave V_- is the complex potential formed by all the circularly polarized components of one kind, and the partial wave V_+ is formed by all the circularly polarized components of the other kind.†

Now each circularly polarized monochromatic plane vector wave may be specified by: (1) its propagation vector $\mathbf{k}$, (2) the radius a of it polarization circle, (3) a phase angle θ and (4) the sense in which the polarization circle is described (helicity). The corresponding contribution of such a wave to the appropriate partial wave of our scalar theory is $a\exp\{i[\theta\pm(\mathbf{k}.\mathbf{x}-\omega t)]\}$ the choice of the sign in the exponent depending on the helicity.

§ 5. A Representation of an Unpolarized Quasi-monochromatic Field

It will now be shown that the preceding analysis leads to a very simple representation of an unpolarized, quasi-monochromatic field.

Let us consider such a field and let the associated complex potential be decomposed into the two partial waves,

$$V(\mathbf{x},t)=V_-(\mathbf{x},t)+V_+(\mathbf{x},t). \quad \ldots\ldots(5.1)$$

† The superposition of circularly polarized plane waves of the same frequency but of different directions of propagation does not, in general, give rise to a wave which itself is circularly polarized. Hence the suggestion made in the last sentence of the footnote on p. 1134 of I, relating to the significance of a partial wave is incorrect.

On physical grounds it is obvious that on the time average the two partial waves (5.1) have now the same energy density and also the same energy flow; for if this were not so, there would be an asymmetry in the physical situation which is inconsistent with our conception of an unpolarized field. Hence

$$\langle w_- \rangle = \langle w_+ \rangle, \quad \langle \mathbf{S}_- \rangle = \langle \mathbf{S}_+ \rangle$$

and from (3.14) one sees that

$$\left.\begin{aligned} \langle w \rangle &= 2\langle w_- \rangle = 2\langle w_+ \rangle, \\ \langle \mathbf{S} \rangle &= 2\langle \mathbf{S}_- \rangle = 2\langle \mathbf{S}_+ \rangle. \end{aligned}\right\} \qquad \ldots\ldots (5.2)$$

It follows that *the (time averaged) energy density and energy flow vector of an unpolarized field may be derived from a single complex scalar wave function which is an analytic signal, i.e. which contains only negative, or only positive, frequency components.*

Consider now a stationary quasi-monochromatic field, which for simplicity is assumed to exist only for a finite but long time interval† $-T \leqslant t \leqslant T$. Then it follows by a straight forward calculation similar to that made in connection with (3.11), that

$$\langle w \rangle \sim \frac{1}{2T}\int_0^\infty w_\omega \, d\omega, \qquad \langle \mathbf{S} \rangle \sim \frac{1}{2T}\int_0^\infty \mathbf{S}_\omega \, d\omega, \qquad \ldots\ldots (5.3)$$

the approximation arising from the replacement of the integral

$$\int_{-T}^{T} \exp\{-i(\omega-\omega')t\}\, dt$$

by $\delta(\omega-\omega')$, δ being the Dirac delta function. In (5.3) w_ω is the energy density and $\mathbf{S}_\omega$ the energy flow vector associated with a typical monochromatic (Fourier) component $v(\mathbf{x}, \mp\omega)\exp(\pm i\omega t)$, of the complex wave function‡. If $a_\omega(\mathbf{x})$ denotes the amplitude and $\phi_\omega(\mathbf{x})$ the phase of v, i.e. if one writes

$$v(\mathbf{x}, \pm\omega) = a_\omega(\mathbf{x}) \exp\{i\phi\ (\mathbf{x})\}, \qquad \ldots\ldots (5.4)$$

where a_ω and ϕ_ω are real, then

$$\begin{aligned} w_\omega &= \frac{1}{4\pi}\left\{\left(\frac{\omega}{c}\right)^2 vv^* + \nabla v \,.\, \nabla v^*\right\} \\ &= \frac{1}{4\pi}\left\{\left[\left(\frac{\omega}{c}\right)^2 + (\nabla\phi_\omega)^2\right] a_\omega^{\,2} + (\nabla a_\omega)^2\right\}, \qquad \ldots\ldots (5.5) \\ \mathbf{S}_\omega &= \pm\frac{i\omega}{4\pi}\left\{v^*\nabla v - v\nabla v^*\right\} \\ &= \mp\frac{\omega}{2\pi} a_\omega^{\,2}\nabla\phi_\omega. \qquad \ldots\ldots (5.6) \end{aligned}$$

According to (5.3) the time averaged energy density $\langle w \rangle$ of the field is proportional to the integral of the energy densities w_ω associated with all the spectral

† By ' long ' we mean here that $T \gg 1/\Delta\omega$, where $\Delta\omega$ is the effective spectral range. The restriction to a finite time interval is imposed here to avoid a lengthy mathematical refinement which, whilst necessary in rigorous treatment of stationary random processes, adds little to the physical significance of our results.

‡ The upper or lower signs are taken here and also on the right hand side of (5.6) according to whether V_+ or V_- is chosen to represent the unpolarized wave.

components (incoherent superposition); and the time averaged energy flow vector $\mathbf{S}$ of the field is proportional to the integral of the flow vectors $\mathbf{S}_\omega$. If the spectral range is sufficiently small† and centered on a mean frequency $\bar{\omega}$, one can take the energy density $w_{\bar{\omega}}$ and the energy flow $\mathbf{S}_{\bar{\omega}}$ which correspond to this mean frequency as being representative of the spectral distribution of $\langle w \rangle$ and $\langle \mathbf{S} \rangle$ themselves.

These results have an interesting bearing on the question of validity of the scalar diffraction theory used frequently in optics, in the study of diffraction effects of apertures and in the analysis of optical images. In such investigations a single monochromatic scalar wave function is usually used to represent the 'complex disturbance' (or the 'light disturbance'); and the intensity $I(\mathbf{x})$ of the light is determined from the time independent part $v(\mathbf{x}) = a(\mathbf{x}) \exp\{i\phi(\mathbf{x})\}$ of this wave function by means of the formula

$$I(\mathbf{x}) = Cvv^*, \qquad \ldots\ldots (5.7)$$

where C is a constant. As is well known, this procedure, which, from the theoretical point of view is usually regarded as a crude approximation, is in excellent agreement with experiment. However, the meaning of the 'complex disturbance' is obscure.

It is tempting to try to identify the complex disturbance with the complex potential of our theory. If the optical intensity is interpreted as the absolute value of the time averaged flow vector $\mathbf{S}$, such an identification is, according to (5.6), justified as long as in the region under consideration the absolute value of the gradient of the phase function varies slowly from point to point in comparison with the variation of the squared amplitude $a^2 = vv^*$. This later requirement is usually satisfied. In the limiting case of very high frequency (the geometrical optics limit), one may in fact assume that $|\nabla\phi| = \omega/c = \text{constant}$‡. But even under conditions where the geometrical optics approximation is not valid, the identification may be justified. Consider, for example, the region of focus. Here the diffraction effects are very prominent, but it was shown recently (Linfoot and Wolf 1956, Farnell 1957, 1958) that in the immediate neighbourhood of focus the surfaces of constant phase are effectively plane and uniformly spaced, so that the gradient of the phase function is nearly constant. In this case, one again has, by (5.6), a proportionality between $|\langle \mathbf{S} \rangle|$ and vv^*.

If the optical intensity is identified with the time averaged electric energy density the situation is somewhat less clear. However, if the first term on the right of the first relation in (5.5) is assumed to represent the electric energy density and the second term the magnetic energy density as seems plausible from the discussion given in I, then the intensity is strictly proportional to vv^*.

In any case we may conclude that our present representation is completely adequate to answer all questions relating to the time averaged energy density and the time averaged energy flow in an unpolarized quasi-monochromatic field.

† An estimate of the permissible spectral range must be made separately in every particular case (cf. Theimer, Wassermann and Wolf (1952), p. 435).

‡ This result follows in the usual way by setting $\phi = \omega\mathscr{S}(\mathbf{x})/c$, then substituting

$$v = a \exp\{i\omega\mathscr{S}(\mathbf{x})/c\}$$

into the Helmholtz' equation and retaining the terms of highest power in ω only; one then obtains the eikonal equation $(\nabla\mathscr{S})^2 = 1$ and this is equivalent to the relation $|\nabla\phi| = \omega/c$.

APPENDIX

In this Appendix the formula (4.2) will be established. According to this formula the time independent part $\mathbf{F}(\mathbf{x})$ of a monochromatic wave function may be represented in the form

$$\mathbf{F}(\mathbf{x})=\int_{-\infty}^{\infty}\int_{-\infty}^{\infty}\exp\{i(k_x x+k_y y)\}[\mathbf{P}(k_x,k_y)\exp(ik_z z)+\mathbf{Q}(k_x,k_y)\exp(-ik_z z)]\,dk_x\,dk_y, \quad \ldots\ldots(A1)$$

where $k_z=+[(\omega/c)^2-k_x{}^2-k_y{}^2]^{1/2}$.

It will be assumed that $\mathbf{F}(\mathbf{x})\equiv\mathbf{F}(x,y,z)$ has a Fourier integral representation with respect to the variables x and y, i.e. that $\mathbf{F}$ may be represented in the form

$$\mathbf{F}(\mathbf{x})=\int_{-\infty}^{\infty}\int_{-\infty}^{\infty}\mathbf{f}(k_x,k_y,z)\exp\{i(k_x+k_y y)\}\,dk_x\,dk_y. \quad \ldots\ldots(A2)$$

Since $\mathbf{F}$ satisfies Helmholtz' equation, one has from (A 2), on using the Fourier inversion formula,

$$\frac{d^2\mathbf{f}(k_x,k_y,z)}{dz^2}=-\mu^2\mathbf{f}(k_x,k_y,z), \quad \ldots\ldots(A3)$$

where

$$\mu^2=\left(\frac{\omega}{c}\right)^2-k_x{}^2-k_y{}^2. \quad \ldots\ldots(A4)$$

The general solution of (A 3) is

$$\mathbf{f}(k_x,k_y,z)=\mathbf{P}(k_x,k_y)\exp(i\mu z)+\mathbf{Q}(k_x,k_y)\exp(-i\mu z), \quad \ldots.(A5)$$

where $\mathbf{P}$ and $\mathbf{Q}$ are arbitrary functions of k_x and k_y. On substituting from (*A* 5) into (A 2) and writing k_z in place of that value of μ which is given by the positive square root on the right-hand side of (A 4), the formulae (A 1) follows.

References

Born, M., and Wolf, E., 1959, *Principles of Optics* (London: Pergamon Press).
Farnell, G. W., 1957, *Canad. J. Phys.*, **35**, 777.
—— 1958, *Ibid.*, **36**, 935.
Focke, J., 1957, *Optica Acta*, **4**, 124.
Gabor, D., 1946, *J. Instn Elect. Engrs*, **93**, 429.
Green, H. S., and Wolf, E., 1953, *Proc. Phys. Soc.* A, **66**, 1129.
Linfoot, E. H., and Wolf, E., 1956, *Proc. Phys. Soc.* B, **69**, 823.
Nagy, K., 1955, *Acta Phys. Hung.*, **4**, 327.
Oswald, J. R. V., 1956, *Instn Radio Engrs Trans.*, CT-3, 244.
Roman, P., 1955, *Acta Phys. Hung.*, **4**, 209.
—— 1959, *Proc. Phys. Soc.*, **74**, 281.
Theimer, O., Wassermann, G. D., and Wolf, E., 1952, *Proc. Roy. Soc.* A, **212**, 426.
Ville, J., 1948, *Câbles et Transm.*, **2**, 61.
—— 1950, *Ibid.*, **4**, 9.

A Scalar Representation of Electromagnetic Fields: III†

By P. ROMAN
Department of Theoretical Physics, University of Manchester

Communicated by B. H. Flowers; MS. received 9th January 1959, in revised form 26th March 1959

Abstract. The transformation properties of the single complex quantity, introduced by Green and Wolf to describe the electromagnetic field, are investigated and the physical energy–momentum tensor of this field is derived in terms of the scalar theory. In particular, it is found that the energy density, as defined in the previous paper, is identical with that given by the physical energy–momentum tensor; and that the energy flow density differs from the one given by this tensor only by a divergence-free vector.

§ 1. Introduction

Some years ago Green and Wolf (1953) succeeded in describing the free electromagnetic radiation field in terms of a single complex 'scalar' potential. The formalism has been extended by the present author to the case where charges and currents are also present (Roman 1955). In this paper it was also shown that Green and Wolf's theory describes properly the spin of the electromagnetic field. Further, the quantization of the general field was performed successfully. Recently, Wolf (1959) derived further properties of the formalism.

A 'scalar' theory of electromagnetism is indeed very useful when dealing for instance with diffraction phenomena. Green and Wolf's theory utilizes, in essentials, the fact that in a proper gauging all electromagnetic quantities can be expressed by two (transversal) components of the vector potential. These are then rearranged in such a way that, as we shall see later, they form in a certain sense a two-component quantity: The field has definite transformation properties, if one uses always a proper gauge. However, before applying the formalism to actual optical problems, there is still a question to be settled, namely that of the proper form of the energy- and momentum-density of the field.

In their original paper, Green and Wolf (1953) derived expressions for these quantities such that their integrals over the whole space give indeed the total energy and momentum of the electromagnetic field. We shall see later that their expressions agree with those obtained from the canonical energy–momentum tensor. In the case of the energy density, this fact has already been used by Roman (1955). But it is well known that the canonical energy–momentum tensor, which is derived from invariance under the operations of space and time translations alone, is generally not the same as the 'physical' energy–momentum tensor, which was defined by Hilbert (1915) as the source of the gravitational

† The work reported in this paper has been partially sponsored by the Air Force Cambridge Research Center of the Air Research and Development Command, U.S. Air Force, through its European Office, under Contract No. AF61(052)-169.

field. In our special case, the problem has another aspect, too. The scalar theory is completely equivalent to the usual vector theory. As pointed out, for example by Hill (1951), it therefore follows that the Lagrangians of the two theories can differ only by a four-divergence. Then, although the *total* energy, for example, will be the same in the two theories, the density of any dynamical quantity may be a different function in the two theories. Conditions for the identity of the densities were recently investigated in general by the present author (Roman 1958). In particular, it was shown that the canonical energy- and momentum-densities in two equivalent theories agree if, and only if, the two Lagrangians differ by a four-divergence which does not depend explicitly on the coordinates. Since in the present case the transition from the vector theory to the scalar theory is accomplished by an essentially non-local transformation, this criterion cannot be fulfilled. One may try to proceed in the straightforward way, expressing the original Lagrangian in terms of the scalar potential alone and finding in this way the difference between the two Lagrangians explicitly. One would then construct from this the terms which must be added to the canonical densities. Due to the non-locality of the transformation, however, the mathematical expressions become unwieldy and it does not seem possible to obtain useful results in this way.

The only solution to the problem seems then to accept the view that every theory has a *unique* physical energy–momentum tensor as defined by Hilbert.† We have therefore to calculate Hilbert's physical tensor in the scalar theory and then, knowing that the scalar theory is equivalent to the vector theory, we can be sure that this will be the proper physical energy–momentum tensor for electromagnetism.

Now the Hilbert tensor is given for theories with a first-order Lagrangian by

$$T^{ik}=2\frac{\partial L}{\partial g^{ik}}-g^{ik}L,$$

where g^{ik} are the components of the metric fundamental tensor. Therefore we ought to know the general covariance properties of the fields. At this point one usually runs into difficulties, as for instance in the present case. Hilbert's physical energy–momentum tensor, however, can also be calculated in the framework of special relativity. In fact, Belinfante (1939, 1940) has developed an *ad hoc* method to calculate a symmetrical energy–momentum tensor. This starts with the canonical tensor and gives a prescription for calculating some terms which have to be added. Rosenfeld (1940) has shown that the Belinfante tensor is identical with the physical tensor of Hilbert. A simpler and more general proof of the identity, which applies also for higher-order fields and for fields in interaction with external sources, was given by Marx and Roman (1956) (see also Marx 1952). It should be pointed out that the canonical tensor itself does not necessarily agree with the physical Hilbert tensor even if it happens to be already symmetric. Thus, when working in the framework of special relativity, one has always to make sure that the additional terms of Belinfante vanish. An example to the contrary is furnished by the Lagrangian of the electromagnetic field used by Schwinger (1948), and this was treated by Marx and Roman (1956). Another instance is given, as we shall see, by the scalar theory of electromagnetism which we are considering here.

† We are indebted to Professor D. Bohm (Bristol) for this enlightening remark.

The applicability of Belinfante's method depends on the Lorentz-covariance of the theory. Green and Wolf's scalar theory of electromagnetism, however, is not covariant in the usual sense: the 'scalar' field function V has Fourier coefficients which are linear combinations of the first and second components of a vector. Nevertheless, the formalism that we shall derive is covariant under a combined Lorentz and gauge transformation. Although the physical implications of such transformations are somewhat less obvious than those of pure Lorentz transformations, the result is a self-consistent scheme readily applicable to practical problems for which the scalar theory was intended.

In § 2 we shall investigate the transformation properties of the field and in § 3 deduce the physical energy–momentum tensor.

§ 2. Transformation Properties and Covariance

The 'scalar' field function in Green and Wolf's (1953) theory may be defined by†

$$V(\mathbf{x}, t)=\int \gamma(\mathbf{k}, t)\exp(i\,\mathbf{kx})d\,\mathbf{k} \qquad \ldots\ldots(2.1)$$

where

$$\gamma(\mathbf{k}, t)=\gamma_1(\mathbf{k}, t)+i\gamma_2(\mathbf{k}, t), \qquad \ldots\ldots(2.2)$$

with

$$\gamma_1=\mathbf{c}.\mathbf{l}_1, \qquad \gamma_2=\mathbf{c}.\mathbf{l}_2. \qquad \ldots\ldots(2.3)$$

Here $\mathbf{c}$ is the Fourier component of the electromagnetic vector potential $\mathbf{A}$ of the usual theory, and this is resolved into three components according to‡

$$\mathbf{c}(\mathbf{k}, t)=\gamma_1\mathbf{l}_1(\mathbf{k})+\gamma_2\mathbf{l}_2(\mathbf{k})+\gamma_3\mathbf{l}_3(\mathbf{k}), \qquad \ldots\ldots(2.4)$$

where $\mathbf{l}_3=\mathbf{k}/|\mathbf{k}|$, and $\mathbf{l}_1$, $\mathbf{l}_2$, $\mathbf{l}_3$ are the unit vectors of a right-handed coordinate system in half of the Fourier space, e.g. where $k_z\geqslant 0$. We agree further to associate with $-\mathbf{k}$ a left-handed system, so that

$$\mathbf{l}_1(-\mathbf{k})=\mathbf{l}_1(\mathbf{k}), \qquad \mathbf{l}_2(-\mathbf{k})=\mathbf{l}_2(\mathbf{k});$$

and therefore we have the reality conditions

$$\left.\begin{aligned}\gamma_1(-\mathbf{k}, t)&=\gamma_1^*(\mathbf{k}, t),\\ \gamma_2(-\mathbf{k}, t)&=\gamma_2^*(\mathbf{k}, t).\end{aligned}\right\} \qquad \ldots\ldots(2.5)$$

γ is a complex quantity, and we have

$$V^*(\mathbf{x}, t)=\int \gamma^*(\mathbf{k}, t)\exp(-i\mathbf{kx})d\mathbf{k}. \qquad \ldots\ldots(2.6)$$

Now it follows (using the Lorentz condition) that V and V^* satisfy the field equations

$$\Box V=0, \qquad \Box V^*=0. \qquad \ldots\ldots(2.7)$$

These can be derived from the action integral

$$W=-\frac{1}{8\pi ic}\int \partial_i V\partial_i V^*dx\equiv\frac{1}{ic}\int L dx \qquad \ldots\ldots(2.8)$$

† We use here complex Fourier representation, as in Roman (1955), but a Fourier integral rather than a series. The field function we denote by V, as was done in Green and Wolf (1953), and the Fourier coefficients of V by γ.

‡ In the paper of Green and Wolf the gauge was chosen from the outset so that $\gamma_3\equiv 0$.

($i=1, 2, 3, 4$; $x_4=ict$, $\partial_i=\partial/\partial x_i$, $dx=dx_1dx_2dx_3dx_4$; and summation over dummy indices i from 1 to 4 is throughout understood).

The transformation properties of V can be inferred, if one realises that according to (2.4) the quantities γ_1, γ_2 are the first and the second components of a vector, and therefore the Fourier coefficients $\gamma(\mathbf{k})$ of V, given by (2.2), are linear combinations of these vector-components.

Let us now perform a coordinate transformation of the Fourier-space frame $\mathbf{l}_1$, $\mathbf{l}_2$, $\mathbf{l}_3=\mathbf{k}/|\mathbf{k}|$, for each Fourier component separately. We can easily find the corresponding changes in γ_1 and γ_2 and thus in $\gamma(\mathbf{k}, t)$.

In particular, consider first an infinitesimal rotation in k-space with an angle ϵ around the axis $\mathbf{l}_3=\mathbf{k}/|\mathbf{k}|$. Then

$$\gamma_1\rightarrow\gamma_1'=\gamma_1+\epsilon\gamma_2,$$
$$\gamma_2\rightarrow\gamma_2'=-\epsilon\gamma_1+\gamma_2,$$

so that, by (2.2),

$$\left.\begin{aligned}\gamma\rightarrow\gamma'&=\gamma-i\epsilon\gamma,\\ \gamma^*\rightarrow\gamma^{*\prime}&=\gamma^*+i\epsilon\gamma^*.\end{aligned}\right\} \qquad \ldots\ldots(2.9)$$

Next we show that this rotation, if performed separately in each Fourier component, amounts to a definite rotation around the third axis of an overall coordinate system. Such a coordinate system can be constructed by a suitable averaging over the individual wave vectors $\mathbf{k}$. In fact, consider the three mutually orthogonal vectors

$$\left.\begin{aligned}\mathbf{A}(\mathbf{k})&=\mathscr{R}\gamma(\mathbf{k})\mathbf{l}_1(\mathbf{k})-\mathscr{I}\gamma(\mathbf{k})\mathbf{l}_2(\mathbf{k}),\\ \mathbf{B}(\mathbf{k})&=\mathscr{I}\gamma(\mathbf{k})\mathbf{l}_1(\mathbf{k})+\mathscr{R}\gamma(\mathbf{k})\mathbf{l}_2(\mathbf{k}),\\ \mathbf{C}(\mathbf{k})&=|\gamma(\mathbf{k})|\mathbf{l}_3(\mathbf{k}).\end{aligned}\right\} \qquad \ldots\ldots(2.10)$$

Using (2.9) we find that when performing the transformation in the individual Fourier components, the result is

$$\mathbf{A}\rightarrow\mathbf{A}+\epsilon\mathbf{B}, \qquad \mathbf{B}\rightarrow-\epsilon\mathbf{A}+\mathbf{B}, \qquad \mathbf{C}\rightarrow\mathbf{C}.$$

We can at this point choose a coordinate system in x-space, adapted to the radiation field. This may be done in an arbitrary manner, but we shall choose to take the vectors

$$\mathbf{X}=\mathbf{A}(\mathbf{P}), \qquad \mathbf{Y}=\mathbf{B}(\mathbf{P}), \qquad \mathbf{Z}=\mathbf{C}(\mathbf{P}) \qquad \ldots\ldots(2.10\,a)$$

as a system of orthogonal axes. Here $\mathbf{P}$ is some suitably chosen average over the wave vectors, for example the total field momentum.

It now follows that under (2.9) $\mathbf{X}\rightarrow\mathbf{X}+\epsilon\mathbf{Y}$, $\mathbf{Y}\rightarrow-\epsilon\mathbf{X}+\mathbf{Y}$, $\mathbf{Z}\rightarrow\mathbf{Z}$, i.e. the transformation (2.9) amounts to a rotation by an angle ϵ around the third axis of the coordinate system in x-space specified by $\mathbf{X}$, $\mathbf{Y}$, $\mathbf{Z}$. Thus, our procedure of performing the rotation on the individual Fourier components is indeed meaningful as a coordinate transformation in the usual sense and therefore, substituting the transformed values (2.9) of γ into (2.1) and (2.6), we obtain the transformation formulae in x-space

$$\left.\begin{aligned}V\rightarrow V'&=V-i\epsilon V,\\ V^*\rightarrow V^{*\prime}&=V^*+i\epsilon V^*.\end{aligned}\right\} \qquad \ldots\ldots(2.11)$$

These describe the behaviour of V and V^*, if a rotation with the infinitesimal angle ϵ is performed around the third axis of the overall coordinate system specified by the vectors $\mathbf{X}$, $\mathbf{Y}$, $\mathbf{Z}$.

Equations (2.11) show that it is useful to join V and V^* in a two-component quantity

$$\psi = \begin{bmatrix} \psi_1 \\ \psi_2 \end{bmatrix} = \begin{bmatrix} V \\ V^* \end{bmatrix}, \qquad \ldots\ldots (2.12)$$

so that the infinitesimal transformation in x-space can be written

$$\psi \to \psi' = (1 + \epsilon I_{12})\psi.$$

Here I_{12} is the infinitesimal operator for the rotation around the third axis and has the matrix elements

$$I_{12}^{11} = -i, \qquad I_{12}^{22} = +i, \qquad I_{12}^{12} = I_{12}^{21} = 0. \qquad \ldots\ldots (2.13)$$

We can now proceed similarly with other rotations and special Lorentz transformations. We shall find, however, that those matrix elements of all other infinitesimal operators I_{rk} which act on ψ_1 and ψ_2 (i.e. V and V^*), vanish identically. In fact, a rotation around, say, the $\mathbf{l}_1$ axis in k-space gives

$$\gamma_1 \to \gamma_1' = \gamma_1,$$
$$\gamma_2 \to \gamma_2' = \gamma_2 + \epsilon\gamma_3;$$

thus

$$\gamma \to \gamma' = \gamma + \epsilon\gamma_3,$$

where γ_3 is the Fourier component of the 'longitudinal' part of the potential. On the other hand, a rotation around the $\mathbf{l}_1$ (or $\mathbf{l}_2$) directions of each Fourier component is again equivalent to an overall rotation about the axis **X** (or **Y**) in the x-space.

An analogous result is obtained if we apply a special Lorentz transformation. Then the scalar potential enters.

In both cases it thus appears that the coordinate transformation leads one out of the framework furnished by the ψ-description of the electromagnetic field. The situation can, however, be remedied if we amend the coordinate transformation by suitable gauge transformations. To see this, let us write for the complete electromagnetic field

$$\chi = \begin{bmatrix} \psi \\ A \end{bmatrix},$$

where both ψ and A have two components; ψ is given by (2.12) and A contains the longitudinal and scalar part of the field. Apply now a gauge transformation Q_1 such that

$$Q_1\chi = \begin{bmatrix} \psi \\ 0 \end{bmatrix} \equiv \bar{\chi}.$$

Apply now to $\bar{\chi}$ a general Lorentz transformation Λ. This can be represented by

$$\Lambda = \begin{bmatrix} R & S \\ T & U \end{bmatrix},$$

where R, S, T, U are 2×2 matrices. We obtain

$$\bar{\chi} \to \Lambda\bar{\chi} = \begin{bmatrix} R\psi \\ T\psi \end{bmatrix} \equiv \bar{\chi}'.$$

Let us now apply a second gauge transformation Q_2, such that

$$Q_2\bar{\chi}' = \begin{bmatrix} R\psi \\ 0 \end{bmatrix} \equiv \bar{\bar{\chi}}.$$

The net result of the three transformations can be written as

$$\chi \to \chi' \equiv \bar{\bar{\chi}} = Q_2 \Lambda Q_1 \chi \equiv \Lambda' \chi,$$

where

$$\Lambda' = \begin{pmatrix} R & 0 \\ 0 & 0 \end{pmatrix}.$$

This then shows that for the Λ' transformations the ψ-field will provide a covariant representation space, in the sense that

$$\psi \to \psi' = R\psi.$$

However, gauge transformations commute with Lorentz transformations and the product of two gauge transformations is again a gauge transformation. Therefore we may write

$$\Lambda' = Q\Lambda.$$

Further, all physical observables of the theory are gauge invariant; therefore the physical effect of Λ' will be the same as that of a pure Lorentz transformation Λ.

For an infinitesimal transformation, in particular, we may put

$$R = 1 + \tfrac{1}{2}\epsilon_{rk} I_{rk},$$

where $\epsilon_{rk} = -\epsilon_{kr}$ are the infinitesimal parameters of the coordinate transformation and I_{rk} are the corresponding infinitesimal operators. From the above digressions it follows that their relevant matrix elements are

$$I_{rk}^{\alpha\beta} = 0 \text{ for } (r, k) \neq (1, 2), \qquad \ldots\ldots (2.14)$$

while for $(r, k) = (1, 2)$ they are given by (2.13).

Now we proceed to show that the theory is covariant under the Λ'-group. The general criterion for covariance is clearly

$$\delta L = \frac{\partial L}{\partial \psi}\delta\psi + \frac{\partial L}{\partial \partial_r \psi}\delta\partial_r\psi = 0. \qquad \ldots\ldots (2.15)$$

Here $\delta\psi$ and $\delta\partial_r\psi$ are the infinitesimal variations of the field functions and their derivatives under a Λ'-transformation. In particular

$$\delta\partial_r\psi = \epsilon_{ri}\partial_i\psi + \tfrac{1}{2}\epsilon_{ik} I_{ik}\partial_r\psi; \qquad \ldots\ldots (2.16)$$

and ψ represents in (2.15) the totality of the field functions and summation over these must be understood.

In order to apply the criterion (2.15), it is useful to rewrite the Lagrangian in (2.8) in terms of the two-component field function introduced in (2.12). We have clearly

$$L = -\frac{1}{16\pi}\partial_i\psi^*\partial_i\psi. \qquad \ldots\ldots (2.17)$$

Since

$$\left.\begin{aligned} \frac{\partial L}{\partial \psi} &= 0, \\ \frac{\partial L}{\partial \partial_r \psi} &= -\frac{1}{16\pi}\partial_r\psi^*, \end{aligned}\right\} \qquad \ldots\ldots (2.18)$$

the left-hand side of criterion (2.15) gives, using (2.16),

$$-16\pi\delta L = \epsilon_{ri}\partial_r\psi^*\partial_i\psi + \tfrac{1}{2}\epsilon_{ik}\partial_r\psi^* I_{ik}\partial_r\psi + \text{c.c.}$$

The first term vanishes by symmetry. Due to (2.14) only one term survives from the second half, and this vanishes in the end as well:

$$-16\pi\delta L=\epsilon_{12}\partial_r\psi^* I_{12}\partial_r\psi+\text{c.c.}=\epsilon_{12}\partial_r|V^*V|\begin{pmatrix}-i & 0\\ 0 & i\end{pmatrix}\partial_r\left[\frac{V}{V^*}\right]+\text{c.c.}=0.$$

Thus (2.15) is indeed fulfilled for the Λ'-transformation group defined above.

§ 3. The Energy–Momentum Tensor

Belinfante's method starts off by calculating first the canonical energy–momentum tensor θ_{ik} according to the well-known prescription

$$\theta_{ik}=L\delta_{ik}-\frac{\partial L}{\partial\partial_k\psi}\partial_i\psi-\frac{\partial L}{\partial\partial_k\psi^*}\partial_i\psi^*. \qquad \ldots\ldots (3.1)$$

Then the physical energy–momentum tensor is

$$T_{ik}=\theta_{ik}+T_{ik}', \qquad \ldots\ldots (3.2)$$

where

$$T_{ik}'=\partial_r B_{rki}, \qquad \ldots\ldots (3.3)$$

with

$$B_{rki}=-\tfrac{1}{2}(S_{rki}-S_{kir}-S_{irk}). \qquad \ldots\ldots (3.4)$$

Here

$$S_{rki}=-\frac{\partial L}{\partial\partial_i\psi}I_{rk}\psi-\frac{\partial L}{\partial\partial_i\psi^*}I_{rk}{}^*\psi^*. \qquad \ldots\ldots (3.5)$$

Due to the antisymmetry of the infinitesimal operators I_{rk}, the quantity S_{rki} is antisymmetric in its first two indices, and the same holds for B_{rki}.

The operators I_{rk} in (3.5) denote the infinitesimal operators of the Lorentz group. We have proved that the 'scalar theory' is invariant under the Λ'-group, and that the infinitesimal operators of this group reduce to the relevant part of the infinitesimal operators of the Lorentz group if we eliminate consistently the longitudinal and scalar field by suitable gauge transformations. Thus we are now prepared to use (3.5) for constructing the physical energy–momentum tensor. The significant matrix elements of I_{rk} are given by (2.14).

Using the Lagrangian (2.17) we obtain the canonical tensor from (3.1):

$$\theta_{ik}=-\delta_{ik}\frac{1}{16\pi}\partial_r\psi^*\partial_r\psi+\frac{1}{16\pi}\partial_k\psi^*\partial_i\psi+\frac{1}{16\pi}\partial_k\psi\partial_i\psi^*. \qquad \ldots\ldots (3.6)$$

In particular, for the energy density $w=-\theta_{44}$ we obtain

$$\begin{aligned} w&=\frac{1}{8\pi}\partial_r V^*\partial_r V-\frac{1}{4\pi}\partial_4 V^*\partial_4 V\\ &=\frac{1}{8\pi}\left(\operatorname{grad}V^*\operatorname{grad}V+\frac{1}{c^2}\dot{V}^*\dot{V}\right), \qquad \ldots\ldots (3.6\,a)\end{aligned}$$

and for the energy flow density $g_i=-i\theta_{i4}$ $(i\neq 4)$:

$$\begin{aligned} g_i&=-\frac{i}{8\pi}(\partial_4 V^*\partial_i V+\partial_4 V\partial_i V^*)\\ &=-\frac{1}{8\pi c}(\dot{V}^*\partial_i V+\dot{V}\partial_i V^*). \qquad \ldots\ldots (3.6\,b)\end{aligned}$$

These are just the expressions derived in Green and Wolf's (1953) paper.

Now we proceed to construct the quantities S_{rki}, as defined by (3.5). Remembering (2.14), only four of them will be different from zero, and we have for these

$$S_{12i} = -S_{21i} = \frac{1}{16\pi}[\partial_i\psi^* I_{12}\psi + \partial_i\psi I_{12}{}^*\psi^*]$$

$$= \frac{i}{8\pi}(V^*\partial_i V - V\partial_i V^*), \quad (i=1, 2, 3, 4). \qquad \ldots\ldots (3.7)$$

Therefore, the only (independent) non-vanishing elements of B_{rki} are, according to (3.4),

$$\left.\begin{aligned} B_{12i} &= -\tfrac{1}{2}S_{12i} \qquad (i=1, 2, 3, 4)\\ B_{231} &= \tfrac{1}{2}S_{123}\\ B_{312} &= \tfrac{1}{2}S_{123}\\ B_{142} &= -\tfrac{1}{2}S_{124}\\ B_{241} &= \tfrac{1}{2}S_{124}. \end{aligned}\right\} \qquad \ldots\ldots (3.8)$$

We can now calculate the 'correction terms' T_{ik}' to θ_{ik}, as given by (3.3). According to (3.8), there is no B_{r44} different from zero so that

$$T_{44}' = 0. \qquad \ldots\ldots (3.9)$$

Then

$$T_{14}' = \partial_2 B_{241} = \tfrac{1}{2}\partial_2 S_{124} = \frac{i}{16\pi}\partial_2(V^*\partial_4 V - V\partial_4 V^*)$$

$$= \frac{1}{16\pi c}\partial_2(V^*\dot{V} - V\dot{V}^*). \qquad \ldots\ldots (3.10\,a)$$

Similarly

$$T_{24}' = -\frac{1}{16\pi c}\partial_1(V^*\dot{V} - V\dot{V}^*), \qquad \ldots\ldots (3.10\,b)$$

but

$$T_{34}' = 0. \qquad \ldots\ldots (3.10\,c)$$

It follows from the manner of derivation that these correction terms are valid in the coordinate system defined by the vectors **X**, **Y** and **Z** which were introduced in (2.10 *a*). Hence the asymmetry of T_{i4}'.

Putting

$$F = V^*\dot{V} - V\dot{V}^*,$$

we notice that the correction terms to the energy flow density are (apart from a constant) the components of the curl of the vector

$$\mathbf{M} = (0, 0, F).$$

Therefore, in applications where integration over a surface is involved, as is usually the case in optics, one can use the original canonical energy flow density as well. The energy density, moreover, is in any case equal to the canonical one.

We notice that the energy–momentum tensor, as derived above, has no 'obvious' transformation properties. Nevertheless, it is the physically meaningful quantity which can be used consistently in the framework of the 'scalar' theory.

ACKNOWLEDGMENT

The author is indebted to Dr. E. Wolf for calling his attention to the problem and for many delightful clarifying discussions.

References

Belinfante, F., 1939, *Physica*, **6**, 884.
—— 1940, *Ibid.*, **7**, 449.
Green, H. S., and Wolf, E., 1953, *Proc. Phys. Soc.* A, **66**, 1129.
Hilbert, D., 1915, *Göttinger Nachrichtungen*, 395.
Hill, E. L., 1951, *Rev. Mod. Phys.*, **23**, 253.
Marx, G., 1952, *Acta Phys. Hung.*, **1**, 209.
Marx, G., and Roman, P., 1956, *Magyar Tud. Akademia, III. Oszt. Közl.*, **6**, 269.
Roman, P., 1955, *Acta Phys. Hung.*, **4**, 209.
—— 1958, *Nuovo Cim.*, **10**, 546.
Rosenfeld, L., 1940, *Mém. Acad. R. Méd. Belg.*, **8**, No. 6.
Schwinger, J., 1948, *Phys. Rev.*, **74**, 1439.
Wolf, E., 1959, *Proc. Phys. Soc.*, **74**, 269.

Magnetic Susceptibilities of Iron–Chromium Alloys

By M. M. NEWMANN and K. W. H. STEVENS
Department of Physics, University of Nottingham

Communicated by L. F. Bates; MS. received 13th January 1959, in final form 23rd March 1959

Abstract. Measurements are reported on the magnetic and other properties of alloys of chromium with small quantities of iron. The results show, as expected, that each iron atom carries a moment of 2β, but it is surprising to find that the moments are freely orientable in a matrix of chromium, which is presumably antiferromagnetic. The implications of this are discussed and further experiments are suggested.

§ 1. Introduction

The metals of the first transition series range from scandium to nickel, and are a group of elements in which, in the free atoms, the energies of the electrons in 3d and 4s states are not very different. The tendency is for the 4s shell to contain only one or two electrons while the number in the 3d shell increases from one for scandium to eight for nickel. It is to the partially filled d-shell that the magnetic properties of the transition metals are mainly attributed.

In the solid, metallic, state the concept of electrons in 3d and 4s orbits is less satisfactory and many attempts have been made to formulate more suitable schemes. One such theory is due to Mott and Stevens (1957), and it was with this in mind that the present experiments were begun. From a survey of the experimental results obtained with iron and its alloys it is suggested that metallic iron can be regarded as composed of a sea of conduction electrons together with, on each iron atom, two localized electrons with parallel spins. The moment of approximately two Bohr magnetons from each pair of localized (non-conducting) electrons accounts for most of the moment of ferromagnetic iron, and it is supposed that in the ferromagnetic state these localized moments are parallel. Above the Curie temperature the localized moments still exist but there is no ordering. While it is not certain how the coupling between the localized moments takes place it is probably due to the existence of the conduction electrons, which are slightly polarized.

Metallic chromium has two less electrons per atom than iron, and has the same crystal structure and almost the same lattice constant. It is not, however, ferromagnetic. This suggests that chromium may differ from iron in that it does not have the two localized electrons per atom. The clouds of conduction electrons may, however, be similar in the two metals. One difficulty is that chromium is known to be weakly antiferromagnetic, and it is not clear whether antiferromagnetism arises from the conduction cloud or whether it is due to partial populations of the localized orbits by electrons.

It seemed that some light might be thrown on these problems by studying the magnetic and other properties of iron atoms dispersed in chromium metal. For this purpose we obtained a chromium specimen and alloys no. 1, 2, 3 and 4,

containing 1·05, 2·06, 5·76 and 16·88% of iron in chromium respectively, and investigated their susceptibilities, electrical resistances and thermal expansion.

§ 2. Experimental Details

2.1. *Preparation and Treatment of Specimens*

The specimens were prepared from spectroscopically standardized iron and chromium supplied by Johnson, Matthey and Co. The chromium contained dissolved oxygen. All the specimens, which were prepared in an argon arc furnace at the Atomic Energy Research Establishment, Harwell, were sealed in evacuated quartz tubes and annealed at about 1200°K for a month. This temperature was chosen because it is approximately the highest temperature at which no excessive volatilization of the chromium occurs. The alloys were then water quenched, ensuring that they remained in the body-centred cubic α-phase. The anneal served to homogenize the specimens. It is not clear what happens to the oxygen. It may remain dissolved or it may form chromic oxide, but in either case it will have little effect on the magnetic properties, particularly as all measurements were made relative to the chromium. A trial experiment with alloy 3 showed that a further anneal and quench had no effect upon the susceptibility. X-ray powder photographs taken after the quench showed only lines corresponding to the body-centred cubic structure, indicating that no other phases were present.

The alloys were analysed by Johnson, Matthey and Co., who also conducted a micrographic analysis to see if any 'coring' had occurred. There was no sign of this in any of the alloys. The specimen of chromium was given the same heat treatment as the alloys.

Finally, the specimens were machined into the form of 2 cm long rods of varying diameters, such that they would fit the specimen holder of the Gouy apparatus used to measure the low temperature susceptibilities.

2.2. *Magnetic Measurements*

The temperature dependence of the susceptibilities was investigated over the range 90° to 700°K. From 90° to 293°K the Gouy method was used (Bates 1951). Various magnetic fields were used throughout the temperature run and in no case was ferromagnetic impurity detected, although, as will be seen later, the susceptibility of alloy 3 showed a field dependence at low temperatures. The homogeneity of the specimens was checked at room temperature by reversing the specimen in its holder. Above room temperature the susceptibility was measured in an apparatus based on the Curie method (Leach 1955, Newmann 1958). Each apparatus was calibrated using pure tantalum as a standard (Hoare and Walling 1951).

2.3. *Resistance Measurements*

The resistivities of the specimens were measured for temperatures ranging from 90°K up to temperatures between 293° and 393°K. The potential differences across the specimen and across a standard resistance in series with it were measured on a potentiometer (Loasby 1957).

2.4. *Expansion Measurements*

The linear expansions of alloys 1, 2 and 3 were measured over the ranges 90° to 340°K, 293°K and 393°K respectively, using a simple extensometer, the specimens being the 2 cm rods used in the previous measurements.

§ 3. Experimental Results

3.1. *Susceptibility Measurements*

The susceptibility of the chromium specimen is shown as a function of temperature in figure 1 and the reciprocal susceptibility $1/\chi_a$ of the alloys in figures 2, 3, and 4. The susceptibility of the chromium is almost independent of temperature, rising from $3{\cdot}52 \times 10^{-6}$ e.m.u. g^{-1} at 90°K to $3{\cdot}61 \times 10^{-6}$ at room temperature. Above this it remains constant up to the highest temperatures

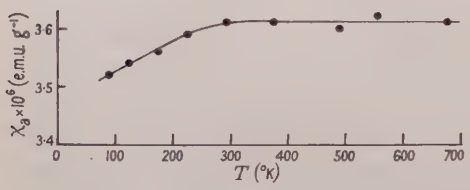

Figure 1. Temperature variation of susceptibility for chromium.

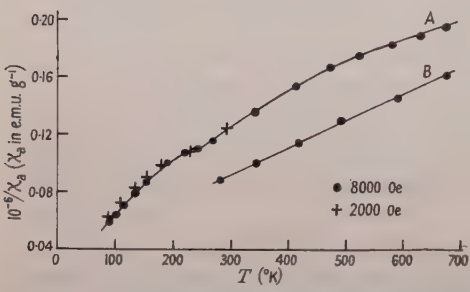

Figure 3. Temperature variation of $1/\chi_a$ for alloy 3 (5·76%Fe): A, specimen annealed at 1200°K and quenched; B, specimen aged by cold-working and annealing at 700°K.

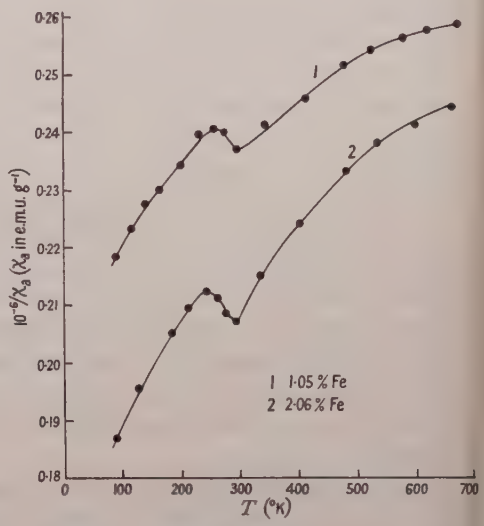

Figure 2. Temperature variation of $1/\chi_a$ for alloys 1 and 2.

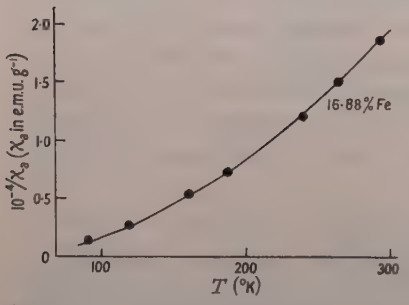

Figure 4. Temperature variation of $1/\chi_a$ for alloy 4.

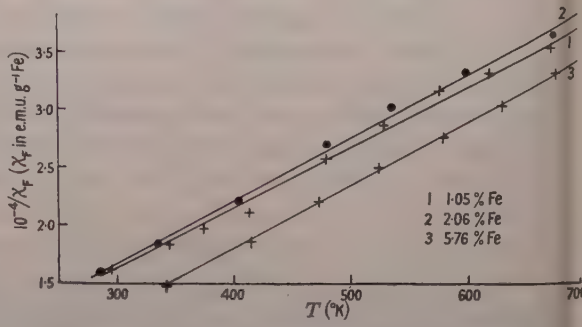

Figure 5. Temperature variation of $1/\chi_F$ for alloys 1, 2 and 3.

obtained. The behaviour of the alloys is significantly different, for they all show marked temperature dependence. This is emphasized in figure 5 which has been obtained as follows. We assume that the chromium matrix in the alloys has the same susceptibility as pure chromium and that the net susceptibility of an alloy

is the sum of the chromium and iron susceptibilities. Then the susceptibility per gramme of iron is given by

$$\chi_F = \frac{\chi_a - (1-g)\chi_c}{g}$$

where χ_c is the measured susceptibility per gramme of chromium and χ_a is the measured susceptibility per gramme of an alloy containing a fraction g by weight of iron. Linear $(1/\chi_F, T)$ curves, above the temperature of the kink, were then obtained for alloys 1, 2 and 3, from which estimates of the effective magneton number, p_{eff}, per iron atom, could be made with fair accuracy. The results obtained were:

Alloy	%Fe	p_{eff}
1	1·05	2·87
2	2·06	2·85
3	5·76	2·90

Referring again to figures 2, 3 and 4 it will be noticed that, with the exception of alloy 4, the $(1/\chi_a, T)$ curves shows a kink, representing a susceptibility increase with increase of temperature of about 0·2, 0·2 and $0{\cdot}5 \times 10^{-6}$ e.m.u. g^{-1} for alloys 1, 2 and 3 respectively. For alloy 3 the susceptibility at temperatures below the anomaly is slightly field dependent, but in the wrong direction for ferromagnetic impurities. In figure 3 two $(1/\chi_a, T)$ curves are shown for alloy 3 above room temperature. Curve A represents the results for the specimen after the 1200°K anneal and quench, while curve B represents the results after ageing the specimen by cold-working and annealing at 700°K for three days. It is apparent that an increase in the susceptibility has occurred as a result of the latter treatment, and subsequent x-ray analysis showed lines other than those belonging to the body centred cubic phase, indicating the presence of a second phase. It is likely that this is σ-phase iron–chromium, which is known to precipitate in more concentrated alloys. No use has been made of this susceptibility curve for estimating p_{eff}.

In interpreting these results we assume that all the iron has entered the chromium lattice. We have been conscious that this does not necessarily happen and that there is the alternative that particles of free iron may exist in our alloys. The long anneals were carried out in an attempt to dissolve any such particles. That we were successful is indicated because if there were appreciable amounts of free iron present the susceptibilities would be much greater, since χ is proportional to $\overline{M^2}$, the average value of the squares of the moments of the particles. For example, the susceptibility of n ferromagnetically coupled iron atoms is approximately n times as great as that of n independent ions.

3.2. *Resistance Measurements*

Figure 6 shows the resistivities of chromium and the alloys plotted against temperature. The curve for each alloy (except that of 4) shows a marked decrease in resistivity at about the same temperature as that at which the susceptibility anomaly occurs. The magnitude of the change increases with iron content, while the temperature at which it occurs decreases almost linearly with increase in iron content. It is apparent that if alloy 4 shows an anomaly it will be below the lowest temperature used. As all the samples contained some oxygen the absolute values of the resistivities are probably not representative of the pure alloys, but the temperature variations should be reliable.

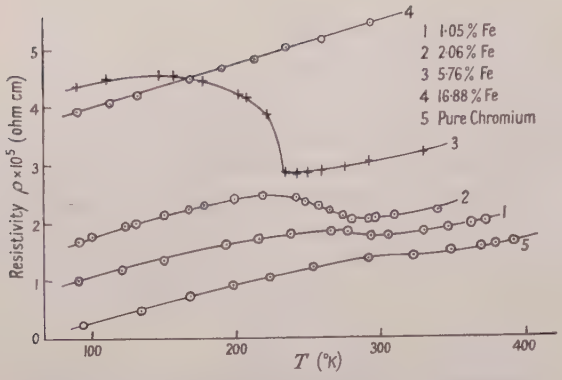

Figure 6. Temperature variation of resistivity for chromium and chromium–iron alloys.

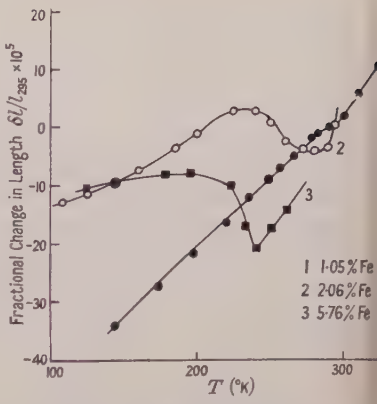

Figure 7. Thermal expansion of alloys 1, 2 and 3.

3.3. *Expansion Measurements*

The fractional change in length of alloys 1, 2 and 3 with temperature is shown in figure 7. The main importance of these results is that they show that there is a sharp drop in the expansion coefficient, and in some cases an actual contraction, at about the same temperature as there are anomalies in the resistivities and susceptibilities.

3.4. *Discussion*

The observation that the addition of iron to chromium gives a temperature dependent contribution to the susceptibility, with p_{eff} approximately equal to 2·87, strongly suggests that the iron atoms have localized moments corresponding to unit spin. For, neglecting orbital contributions, the theoretical p_{eff} should then be 2·83. This conclusion is in good agreement with the ideas put forward by Mott and Stevens (1957), and we may suppose that the unit spin results because the two extra electrons on each iron atom are in non-conducting orbitals, of which there are two per iron atom. The fact that the susceptibility of the separated iron atoms follows a Curie–Weiss law with a small Curie–Weiss constant then leads to the result that the iron atoms, which are fairly well separated from one another, cannot be interacting strongly either with themselves or with the chromium atoms. It is not easy to understand why. The difficulty arises because chromium is reported to be antiferromagnetic (Shull and Wilkinson 1953). While this conclusion has been questioned, and if it were in error we would have a simple explanation of the weak interactions between the iron atoms, we prefer to assume that the chromium atoms do carry moments, which are antiferromagnetically aligned in our temperature range, and to look for another explanation. We therefore suppose that the chromium matrix in which the iron atoms are placed is antiferromagnetic below 473 °K, the Néel temperature of pure chromium. Without inquiring too deeply into the origin of the antiferromagnetism we suppose that each chromium moment is aligned by coupling to its neighbours. If we now substitute iron atoms for some of the chromium atoms, and allow that these iron atoms also have unpaired electrons, how is it that the moments of the iron atoms are not also aligned? It can be argued that the interaction between an iron atom

and its neighbouring chromium atom is much weaker than that between two chromium atoms. We know that, in ferromagnetic iron, there are strong ferromagnetic couplings between neighbouring iron atoms and it is just possible that the iron–chromium interaction is a mean of the iron–iron and chromium–chromium interactions, in which case it would be small. Even if this is so there remains the problem of the anomaly in the physical properties of all the alloys and of pure chromium. Although this is the last point which we shall discuss we believe that its understanding is the key to the whole problem.

It has been suggested that the anomaly in the susceptibility of chromium at about room temperature is due to the presence of chromic oxide, which has an antiferromagnetic Curie point in this region. We do not believe this is the full explanation because: (i) the presence of dissolved oxygen is not necessarily the same as having free chromic oxide, (ii) the anomaly occurs in all the physical properties of chromium, and is most pronounced in those properties which would seem least likely to be affected by the change in magnetic phase of the oxide (e.g. electrical resistance) and (iii) the addition of a small amount of iron depresses the transition temperature by a disproportionate amount. We would like to put forward the following consideration. The neutron diffraction work on chromium, while showing that it is antiferromagnetic, has not been used to determine the superlattice structure. Now in a body-centred cubic structure at least two different superlattices are possible. One would consist of two interpenetrating simple cubic sub-lattices with each simple cubic lattice having ferromagnetic alignment, but with the moments of the two sub-lattices balancing. The second would have interpenetrating simple cubic lattices each of which is itself antiferromagnetic. We suggest that the anomaly at room temperature in pure chromium is due to a change from one antiferromagnetic structure to another. Suppose now that a chromium atom is replaced by an iron atom. There is then the possibility that, in the neighbourhood of the iron atom, one of these antiferromagnetic structures is preferentially stabilized. We suppose that it is the high temperature structure. As the temperature is lowered the chromium matrix will want to change its magnetic phase at about room temperature, but the presence of the iron will tend to prevent it happening. That is, it will stabilize the high temperature sub-lattice structure to lower temperatures, giving a qualitative explanation of the depression of the anomaly by addition of iron. If also the high temperature structure is the second of the two we have described, then each iron atom is surrounded by a magnetically balanced array of chromium atoms, and it may indeed be very weakly coupled to them. Such a model seems capable of explaining qualitatively all the observations, but in view of its tentative nature we shall not pursue it further.

§ 4. Conclusion

This work was started because it offered the possibility of testing some of the ideas of Mott and Stevens. In particular we wanted to see, by separating iron atoms in a matrix which, as far as the conduction electrons are concerned, is probably very similar to iron, whether the iron atoms would show a spin of unity. This proved to be so, though, because of the inherent antiferromagnetism of chromium, the investigation seems to have raised more problems than it has solved. We have regarded it as of value to discuss these at some length and to put forward certain suggestions, but undoubtedly more experiments are required.

The results of Lingelbach (1958) and Wei, Cheng and Beck (1959) suggest directions in which further study will be of value.

Acknowledgments

We would like to thank Professor L. F. Bates for his encouragement and help at all stages of this work. The alloys used were prepared by Miss J. R. Murrey, Atomic Energy Research Establishment, and we greatly appreciate her assistance and advice.

References

Bates, L. F., 1951 *Modern Magnetism* (Cambridge : University Press).
Hoare, F. E., and Walling, J. C., 1951, *Proc. Phys. Soc.* B, **64**, 337.
Leach, S. J., 1955, *Thesis*, University of Nottingham.
Lingelbach, R., 1958. *Z. phys. Chem.*, **14**, 1.
Loasby, R. G., 1957, *Thesis*, University of Nottingham.
Mott, N., and Stevens, K. W. H., 1957, *Phil. Mag.*, **2**, 1364.
Newmann, M. M., 1958, *Thesis*, University of Nottingham.
Shull, C. G., and Wilkinson, M. K., 1953, *Rev. Mod. Phys.*, **25**, 100.
Wei, C. T., Cheng, C. H., and Beck, P. A., 1959, *Phys. Rev. Let.*, **2**, 95.

Electron Attachment Coefficients in Oxygen, Dry Air, Humid Air and Water Vapour

By E. KUFFEL
Research Department, Metropolitan-Vickers Electrical Co. Ltd., Manchester

MS. received 23rd December 1958, in final form 7th April 1959

Abstract. Electron attachment coefficients were measured in oxygen, dry air, air saturated with water vapour at room temperature and in water vapour. An electron filter type apparatus was used. The results have been compared with those of other workers. An approximate evaluation has been made of the influence of humidity on the breakdown voltage of air gaps in a uniform field using the present results and the known ionization coefficient data.

§ 1. Introduction

It has long been known that the breakdown voltage of the gap between two spherical or plane electrodes was slightly higher in moist air than in dry air at atmospheric pressure. Earlier experiments of Ritz (1932) showed that the breakdown voltage of a 1 cm gap with a uniform field at atmospheric pressure increased by about 2% when the water vapour pressure was increased from 10 to 25 mm Hg. With a 2 cm gap the change was 3% when the water vapour pressure rose from 5 to 15 mm Hg.

Recently Köhrmann (1956) measured the increase of breakdown voltage in air at a total pressure of 760 mm Hg when the water vapour pressure was changed from zero to 10 mm Hg. He found that the percentage difference increased slightly with gap length; it was 2·4% for a 0·5 mm gap and 3·2% for a 2·0 cm gap.

It is possible that this increase of breakdown voltage with moisture content could be explained in terms of electron attachment. It is well known that the formation of negative ions by electron capture modifies the Townsend equation for the pre-breakdown current and this phenomenon changes the breakdown voltage. The effect is most pronounced in electronegative gases and in recent years the problem has been studied in connection with the insulation properties of these gases (Harrison and Geballe 1953, Howard 1957).

The attachment of electrons in dry air has been investigated earlier by Bradbury (1933) and more recently by Harrison and Geballe (1953) and the author (Kuffel 1958). A considerable discrepancy was observed between the earlier results of Bradbury and the present results but the latter are in reasonable agreement with the more recent results of Harrison and Geballe (1953).

This paper describes data obtained for electron attachment in dry air, in a mixture of air and water vapour corresponding to saturated air at atmospheric temperature and pressure, and in water vapour.

In addition measurements were made of the attachment coefficients in oxygen. These were made primarily for comparative purposes and for checking the apparatus. The results are in good agreement with those of other workers.

§ 2. Apparatus

The method employed was similar to that used by Bradbury (1933); the chamber was considerably larger than Bradbury's and to some extent this avoided the early onset of corona discharges. Consequently the present method was applicable at slightly higher mean electron energies.

Provision was made for varying the relative distance between the grids and the emitting plate.

The essential parts of the apparatus are shown in figure 1. A beam of ultra-violet light from a mercury arc was focused at the centre of a polished copper plate P where it generated photo-electrons. The electrons then proceeded in

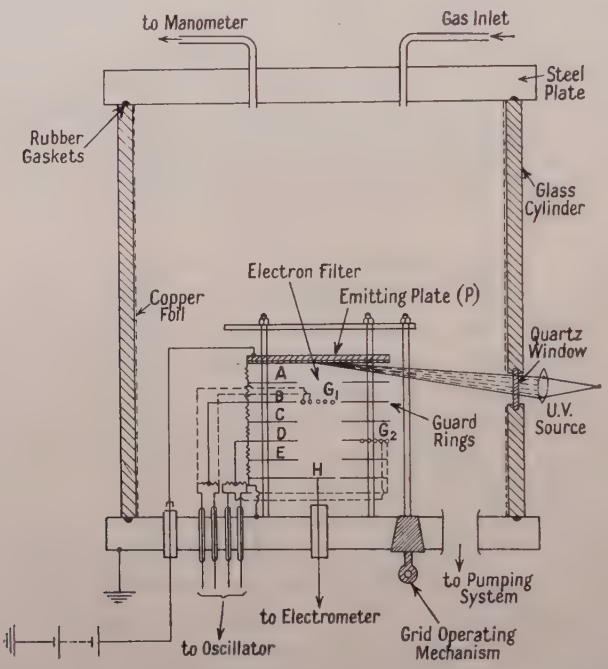

Figure 1. Cross section of the electron filter apparatus.

the field towards a collector H which was connected to an electrometer. The field was maintained uniform between P and H by means of a potential divider chain and the guard rings A, B, C, D, E. Each ring consisted of a brass disc of 8 cm outside diameter and 4 cm inside diameter and they were spaced at intervals of 1 cm. The beam of electrons was limited to the central part of the channel by covering most of the emitting plate with a layer of graphite. The graphite was deposited by painting the plate with an aqueous suspension of graphite and subsequently it was baked in an oven at a temperature of 200°C for several hours. Only the central part of about 1 cm diameter was exposed to the ultra-violet illumination.

Two identical grids G_1 and G_2 each consisting of co-planar parallel copper wires 0·10 mm diameter 1 mm apart were employed for separating electrons from negative ions. The wires were cemented with an araldite resin on to a flat mica ring and they were so arranged that a high-frequency alternating field could be applied between each pair of adjacent wires.

Grids consisting of 0·05 mm diameter wires spaced 0·5 mm apart were also tried with the hope of extending the method to higher pressures. However a difficulty was encountered with the onset of corona discharges at rather low values of E/p and consequently the finer grids were abandoned.

A suitable choice of field strength and frequency of the alternating field between grid wires will cause the electrons to be collected by the grid. The mobility of the negative ions is lower by a factor of 1000 or more, so that if the grid field frequency is high enough the ions will continue to flow towards the collector H with very little transverse disturbance of their motion. The oscillator supplying the high frequency alternating field was a modified Hartley type. The frequency of the ouput voltage could be varied between 2 and 16 Mc/s and the output voltage could be varied between 0 and 100 volts (r.m.s.).

The grids were maintained at a mean potential equal to that of the adjacent guard ring and consequently they did not distort the main field appreciably.

The distance between the grids was measured with a travelling microscope and for most of the work the grids were set 2·0 cm apart. When the attachment values were high (e.g. in oxygen and water vapour) the spacing was reduced to 1·0 cm. In the study of dry air for which the attachment value was relatively small the grid spacing was increased to 3·0 cm. Whenever it was decided to change the spacing between the grids, comparable readings were taken with both spacings and good agreement was obtained.

The whole assembly was enclosed in a glass cylinder 12 in. in diameter and 12 in. high. The grids could be moved into the central region or they could be retracted by a mechanical arrangement which was operated from outside the chamber. The chamber could be evacuated down to about 10^{-5} mm Hg. Leakage increased the pressure overnight to a value not greater than 10^{-4} mm Hg. The gas pressure was measured with a manometer containing Apiezon oil B for which the vapour pressure at room temperature was approximately 10^{-7} mm Hg.

§ 3. Experimental Procedure and Results

3.1. *General*

The attachment coefficients were determined from measurements of the surviving electronic currents at the grids G_1 and G_2. When the alternating potential between the grid wires of G_1 was zero, and G_2 was retracted, the electrometer measured the total ionic and electronic current reaching the collector H. On applying a suitable voltage V_g and frequency f between each pair of adjacent wires of the grid G_1 the electrons in the vicinity of G_1 would be collected by the grid. Then the electrometer registered only the ionic current which was formed in the space between the plate P and grid G_1. The procedure was repeated with G_2 in the central position and G_1 retracted. If we denote the current registered by the electrometer when $V_{g1,2}=0$ by i_0 and the values when $V_{g1}=V$ and $V_{g2}=V$ by i_1 and i_2 respectively, then the ratio of the surviving electronic currents I_1 and I_2 at G_1 and G_2 respectively will be

$$\frac{I_1}{I_2}=\frac{i_0-i_1}{i_0-i_2}. \qquad \ldots\ldots(1)$$

Also, the ratio of the electronic currents at two points distant x_1 and x_2 from plate P will be given by

$$\frac{I_2}{I_1}=\exp\{-\eta(x_2-x_1)\} \qquad \ldots\ldots(2)$$

where η is the attachment coefficient which is defined by analogy with Townsend's ionization coefficient as the mean fraction of the electrons which form negative ions by attachment per centimetre of their drift in the field direction.

Hence from equation (2)

$$\eta = \frac{1}{x_2 - x_1} \ln \frac{I_1}{I_2}. \qquad \ldots\ldots (3)$$

Equation (3) gives the attachment coefficient directly in terms of the measured current ratio.

It remained to determine suitable values for the grid voltages and frequencies but the problem has been fully discussed by Loeb (1955). A plateau of a nearly constant value of ion current can be observed over a considerable range of V_g. A typical curve for oxygen is shown in figure 2. Thus it was necessary to deter-

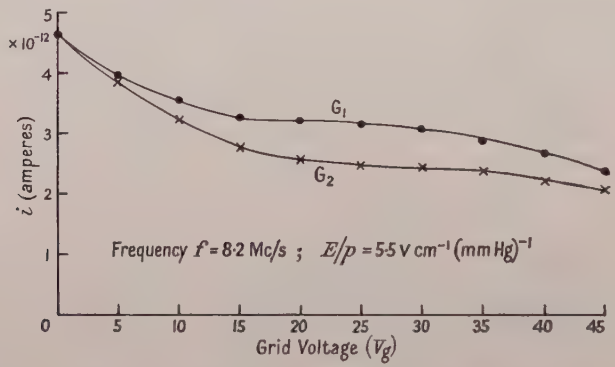

Figure 2. Variation of electrometer current with grid voltage in oxygen.

mine the optimum values of f and V_g for each particular field strength E and pressure p. Most of the present work was done at gas pressures between 6·8 and 10·0 mm Hg.

3.2. *Results on Oxygen*

The attachment coefficients in oxygen have been studied by various workers and the oxygen data are generally accepted as the most reliable. The present apparatus was checked by measuring the attachment coefficients in oxygen. Furthermore, whenever the apparatus was modified the method was re-checked with oxygen. Medical grade oxygen over 99·5% pure was used. (The typical impurities quoted by the suppliers were $A < 0{\cdot}5\%$, $H_2O = 0{\cdot}02\%$, N_2 possibly a trace, $CO_2 < 10$ parts per million, H_2 and CO nil.) Measurements were made with samples from three separate cylinders and the results in each case were the same within the limits of experimental error. A typical curve for oxygen is shown in figure 3 which also shows the comparable results of other investigators (Bradbury 1933, Healy and Reed 1941, Herreng 1952, Doehring 1952). The present results generally fall within the range of variation of the other results and this criterion was taken as an indication that the apparatus was operating correctly.

3.3. *Results on Humid and Dry Air*

The results obtained during the study of dry and humid air are shown in figure 4. The investigations were carried out over a period of 3 months, but the

temperature remained within the limits 23 ± 1°c. Air was dried by storing it for several hours (usually overnight) in a flask containing P_2O_5. Subsequently the air was passed slowly through a trap cooled by liquid nitrogen and then into a subsidiary flask containing P_2O_5 from which it was admitted into the experimental chamber. The introduction of a drying agent (P_2O_5) into the chamber had no influence on the results.

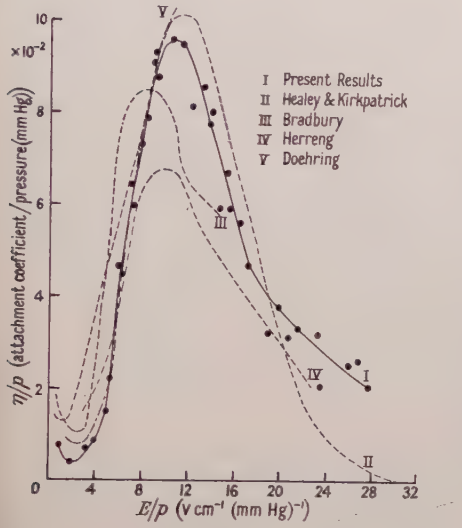

Figure 3. Variation of attachment coefficient with E/p in oxygen.

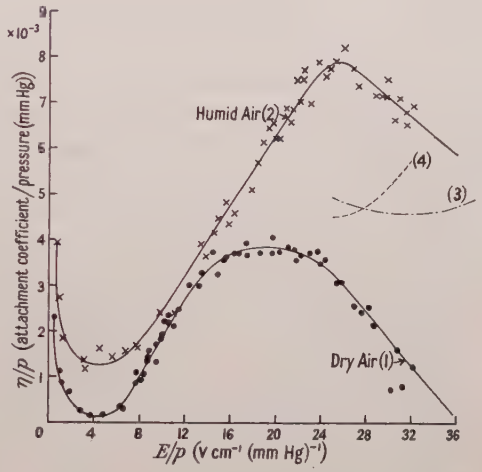

Figure 4. Variation of attachment coefficient with E/p in air: curve 3, Harrison and Geballe's curve for dry air, curve 4, curve 1 corrected for ionization.

In the humid air experiments two methods were employed for obtaining the required mixtures of air and water vapour. In one case the air was stored in a large flask which also contained water at room temperature. The air–water vapour mixture was then introduced into the evacuated chamber so that the partial pressures were in the same ratio as in saturated air at atmospheric temperature and pressure. In the second method the chamber was evacuated and a predetermined amount of water vapour was introduced by measuring the vapour pressure carefully. Dry air at room temperature was then allowed into the chamber until the total pressure was reached at which the proportions of the constituents corresponded to those of saturated air at atmospheric temperature and pressure. The attachment values in the two cases agreed well and either method was employed during the subsequent investigations.

The difference in the measured attachment coefficients for wet and dry air was checked by making successive measurements in dry air and in wet air and vice versa. Each set of results was found to be reproducible within the experimental error.

In all the experiments the air was freed from dust particles and from other condensation nuclei by passing it through a cotton-wool filter.

3.4. *Results for Water Vapour*

The formation of negative ions in water vapour has been studied by Bailey and Duncanson (1930) and also by Bradbury (1934). The attachment curve obtained by Bailey and Duncanson increased very rapidly above $E/p = 13$ and flattened off at about $E/p = 20$ v cm^{-1}(mm Hg)$^{-1}$. The value for the attachment coefficient in terms of η/p on the flat part was 0·25. At lower values of E/p Bradbury reported a pressure dependence of the attachment coefficient which he explained as due to the presence of a large number of aggregates of molecules which may be very effective in forming negative ions. The problem was further investigated in the present work and the results were similar to those of Bradbury (see figure 5). At higher values of E/p a difficulty was found in appointing the correct grid voltage V_g and frequency f. The plateau part on the current–grid voltage curves did not appear unless the pressure exceeded 2·5 mm Hg. Examples of the current–grid voltage curves which were obtained at 2·5 and 6·8 mm Hg pressures are given in figure 6. With the lower pressures the curves

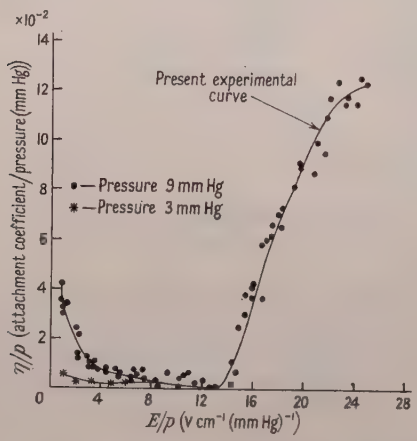

Figure 5. Variation of attachment coefficient with E/p for water vapour.

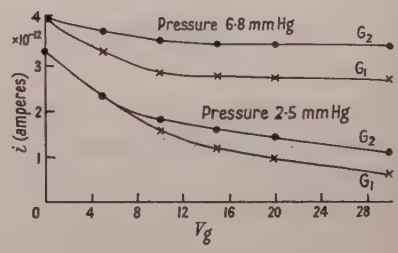

Figure 6. Variation of electrometer current with grid voltage in water vapour.

were found to decrease continuously with increasing grid voltages and no plateau was observed. On the other hand the flat part at 6·8 mm Hg pressure extended over a wide range of V_g without an appreciable change in the current (see figure 6). Experiments at 15 mm Hg pressure showed that after the initial drop the (current, V_g) curves remained flat over the full range of the available grid voltage (up to 100 volts).

The pressures used in the water vapour experiments varied generally between 6·8 and 10·0 mm Hg but for most of the work the pressure remained at 9·0 mm Hg. The variation of the attachment coefficient η/p with E/p is shown in figure 5.

§ 4. Discussion of Results

4.1. *Oxygen Results*

The results for oxygen shown in figure 3 fall between Healy and Kirkpatrick's and Bradbury's results. The rising part of the present curve runs along the recent Doehring's curve (1952). Formerly the sharp increase and the peak in the attachment curve were believed to be due to the excitation of oxygen at 1·62 ev

by a process of electron capture giving O_2^- at nearly zero energy with a collision stabilization (Bradbury 1933, Massey 1950). Recently Craggs, Tozer and Thorburn (1957) obtained results in a discharge experiment showing that the peak can be explained in terms of a resonance capture which starts with electron energies of 4·6 ev. The resonance capture is shown to be due to the process $O_2 + e \rightarrow O(^3P) + O^-(^2P^0)$.

4.2. *Dry Air*

Figure 4 gives the experimental values of the attachment coefficients for dry air and wet air; the curve for dry air, as previously reported (Kuffel 1958), when corrected for ionization meets the lower end of a comparable curve which was obtained by Harrison and Geballe (1953) by a totally different method. At higher values of E/p (e.g. 30) the two curves diverge from each other (see curves 3 and 4 of figure 4). The corrections for ionization in this region will exceed the values of the apparent attachment coefficients measured by the present method. To compute the true attachment coefficients accurate values of the ionization coefficients and accurate apparent attachment coefficients would be required. Thus the corrected curve 4 of figure 4 may be in considerable error due to the rapid increase of ionization by collision as the field strength is increased. However, the results may be used for comparing the effects with dry and wet air.

4.3. *Humid Air*

There are no published data with which to compare the attachment coefficients of wet air (shown in figure 4). The increase in the attachment coefficient for humid air was quite pronounced. Curve 2 of figure 4 refers to an air and water vapour mixture in the same proportions as would be obtained with saturated air at atmospheric pressure and a temperature of 23 °c (i.e. 21 mm Hg at a total pressure of 760 mm Hg). The maximum value of the attachment coefficient was about double the corresponding value for dry air and it occurred at a rather higher value of E/p. The increase in the coefficients for both dry and wet air was approximately at the same rate for values of E/p above 6 or 8. However, the wet air coefficient continued to increase approximately linearly with E/p into the region of $E/p = 20$ to 26 where the ionization effects were shown previously to have an important influence on the apparent attachment coefficient in dry air (see curves 1 and 3 of figure 4). The continued increase indicates that the increase of the attachment coefficient in water vapour was greater than the increase of the ionization coefficient in this latter region of E/p.

4.4. *Water Vapour*

The continuous current decrease with V_g (see figure 6) observed for lower pressures of water vapour is not fully understood. A possible explanation may be as follows. At low pressures the ions will consist of a mixture of H^-, O^- and OH^-. These have widely different mobilities. Recently Muschlitz and Bailey (1956) showed by mass spectrometer studies that the proportions of the three types of ions vary with pressure. At pressures below 0·5 mm Hg H^- was most abundant and OH^- was barely detectable. Beyond 2 mm Hg pressure OH^- became more common than O^- and at still higher pressure OH^- became the most abundant. At that stage the proportion of OH^- to H^- increased very rapidly with pressure. It would be expected that with a mixture of H^- and OH^- a flat part on the current–V_g curve would be unlikely at the lower pressures.

At higher pressures with the predominance of ions of one type a distinct plateau would be observed.

The relatively high attachment near zero electron energies is thought to be due to the electrons attaching themselves to large clusters of molecules. Such clusters are numerous at higher pressures.

The observed increase in attachment above $E/p = 13$ (see figure 5) appears less rapid than was previously reported (Bailey and Duncanson 1930). The present values in the region of E/p of about 25 or more may be reduced appreciably as a result of ionization by collision. No correction for ionization can be made at this stage since there are no available data for ionization coefficients in water vapour below $E/p = 31$. Earlier workers (von Engel and Steenbeck 1932) quote values for the ionization coefficient (α) in water vapour above $E/p = 31$, and in the region of E/p between 31 and 50 their values fall between those for hydrogen and air.

The sharp increase in attachment above $E/p = 13$ was formerly believed to be due to dissociative attachment represented by the reaction (Bradbury 1934)

$$H_2O + e + 5{\cdot}11 \text{ volts} \rightarrow OH^- + H$$

or possibly

$$H_2O + e + \text{energy} \rightarrow H_2 + O^-.$$

Muschlitz and Bailey's (1956) investigations indicate that the OH^- ion originates from an ion-molecule reaction of the form

$$H^- + H_2O \rightarrow OH^- + H_2$$

or

$$O^- + H_2O \rightarrow OH^- + OH$$

where H^- and O^- ions are formed in single collisions of electrons with water molecules.

4.5. *Estimated Influence of Humidity on the Breakdown Voltage of an Air Gap*

A knowledge of the values of the ionization and attachment coefficients for dry and humid air could be used to estimate the breakdown voltages of uniform field gaps in humid air. The principles are outlined in the Appendix and the method determines the increase in the breakdown voltage above the accepted values for dry air.

The experimental values of attachment given in figure 4 do not extend to sufficiently high values of E/p for spark gaps in air at atmospheric pressure. Accordingly, the curves have been extrapolated to an E/p value of about 40 which is the approximate region for the breakdown of a 1·0 cm gap in air. For the present purposes it has been assumed that the difference between the values of the attachment coefficients for wet and dry air remains nearly constant over the range of E/p under consideration.

The table gives the estimated changes in the breakdown voltages of 0·5 to 2·0 cm uniform field gaps for dry and humid air at atmospheric pressure. The humid air was approximately saturated with water vapour at a temperature of 23 °C; the water vapour pressure was 21 mm Hg.

The breakdown voltages for dry air in the table were measured in this laboratory. They were in good agreement with those of Köhrmann (1958). The attachment coefficients were measured at 23 °C and for comparison purposes the measured breakdown voltages were reduced to 23 °C. The corresponding

ionization and attachment coefficients α_d and η_d were taken from Harrison and Geballe (1953).

The ratios of the measured breakdown voltage (table) were also determined from measurements at 23°c during the present experiments.

There are no published data for the ionization coefficients in moist air and for the present purpose it was assumed that the increase of humidity did not change the value of the ionization coefficient α_w; the values shown in the table are those corresponding to dry air at the increased breakdown voltage. The attachment coefficients for humid air were obtained by correcting the dry air attachments coefficient. The correction was made by adding to the known attachment coefficients in dry air Harrison and Geballe (1953) at the increased breakdown voltage the difference between the extrapolated curves 1 and 2 of figure 4.

Dry Air						Saturated air at 23°c				
(1)	(2)	(3)	(4)	(5)	(6)	(4)	(5)	(6)	(7)	(8)
0·5	16·45	16·29	42·8	20·2	4·31	44·77	25·15	9·79	1·046	1·042
1·0	30·1	29·79	39·2	12·85	3·93	41·55	17·63	9·04	1·060	1·050
1·5	43·2	42·85	37·6	9·97	3·78	40·12	14·65	8·79	1·067	1·059
2·0	56·0	55·44	36·48	8·23	36·9	39·22	12·90	8·60	1·075	1·062

(1) Gap length (cm); (2) breakdown voltage (kv) at 20°c; (3) breakdown voltage (kv) at 23°c; (4) E/p at 23°c; (5) ionization coefficient at 23°c; (6) attachment coefficient at 23°c; (7) estimated V_w/V_d; (8) observed V_w/V_d (V = breakdown voltage).

The predicted increase in the breakdown voltage for saturated air was greater than the measured increase (see table). Nevertheless, the agreement between the two sets of results was considered satisfactory in the circumstances. However, in view of the various assumptions which were made, and because of the lack of experimental data for the various ionization coefficients, the general agreement between the predicted and observed results may be fortuitous. Further measurements of attachment and ionization coefficients in the appropriate region of E/p are required before it can be concluded that the increase in breakdown voltage in wet air is due primarily to the increase of the attachment coefficient, which was assumed in the present considerations.

§ 5. Conclusions

The present paper provides some information on the electron attachment coefficients in oxygen, dry air, humid air and water vapour. It includes new information on the influence of humidity on the attachment of electrons in air.

The electron attachment coefficients which were obtained for oxygen were in reasonably good agreement with the results of other workers (Bradbury 1933, Healy and Reed 1941, Herreng 1952). In dry air there was a discrepancy between the present results and the early results obtained by a similar method. However, the present results are in reasonable agreement with more recent data obtained with a different method (Harrison and Geballe 1953). The matter has been discussed earlier (Kuffel 1958). In the case of humid air there is no available information with which to compare the present results. The latter showed that the attachment coefficient was approximately twice the corresponding value for dry air at certain conditions of E/p.

In water vapour the attachment coefficient at first decreased as E/p was increased from zero. Then it increased rapidly for $E/p = 13$ and higher which is

in agreement with the earlier investigations (Bailey and Duncanson 1930, Bradbury 1934). However, the present values were considerably lower than the results of earlier workers.

At low values of E/p the attachment coefficient was found to be pressure dependent in agreement with Bradbury's observations (1934). At higher values of E/p difficulty was experienced in separating the electrons from the negative ions unless the pressure was higher than 2·5 mm Hg. This was due probably to the presence of ions with widely different mobilities.

The results for humid air together with the existing ionization and attachment data were used to make an approximate estimation of the increase in the breakdown voltage of uniform field gaps when the air humidity is increased. The estimation was made on the assumption that the higher attachment value for humid air was the factor responsible for the increase in breakdown voltage. In addition it was assumed that the primary ionization coefficient η and the secondary ionization γ remained the same for humid air as for dry air. The estimated change in breakdown voltage with humidity was in general agreement with the experimental results.

Further measurements are required before the suggested method of estimation could be applied with confidence. In particular more precise information is required on the values of the ionization coefficient α in humid air and of the secondary coefficient γ in dry and humid air.

Acknowledgments

The author wishes to thank Mr. A. S. Husbands for many helpful suggestions, Mr. K. J. Cornick for the design and construction of the oscillator and for his invaluable assistance in some measurements, and Mr. F. S. Edwards for his interest and support of the programme.

The author thanks Sir Willis Jackson, Director of Research and Education, Metropolitan Vickers Electrical Co. Ltd., for permission to publish this paper.

References

Bailey, V. A., and Duncanson, W. E., 1930, *Phil. Mag.*, **10**, 145.
Bradbury, N. E., 1933, *Phys. Rev.*, **4**, 883.
—— 1934, *J. Chem. Phys.*, **2**, 835.
Craggs, J. D., Thorburn, R., and Tozer, B. A., 1957, *Proc. Roy. Soc.* A, **240**, 471.
Doehring, A., 1952, *Z. Naturf.*, **7a**, 253.
Druyvesteyn, M. J., and Penning, F. M., 1940, *Rev. Mod. Phys.*, **12**, 112.
von Engel, A., and Steenbeck, M., 1932, *Electrische Gasentladungen* (Berlin : Springer), p. 105.
Geballe, R., and Reeves, M. L., 1953, *Phys. Rev.*, **92**, 867.
Harrison, M. A., and Geballe, R., 1953, *Phys. Rev.*, **91**, 1.
Healy, R. H., and Reed, J. W., 1941, *The Behaviour of Slow Electrons in Gases* (Sydney Amalgamated Wireless, Ltd.), p. 94.
Herreng, P., 1952, *Cah. Phys.*, **38**, 7.
Howard, P. R., 1957, *J. Instn Elect. Engrs*, Pt. A, **104**, 139.
Kuffel, E., 1958, *Proc. Phys. Soc.*, **71**, 516.
Köhrmann, W., 1956, *Ann. Phys., Lpz.*, **18**, 379.
Loeb, L. B., 1955, *Basic Processes of Gaseous Electronics* (University of California Press), p. 401.
Massey, H. S. W., 1950, *Negative Ions* (Cambridge : University Press).
Muschlitz, E. E., and Bailey, T. L., 1956, *J. Phys. Chem.*, **60**, 681.
Ritz, H., 1932, *Arch. Elektrotech.*, **26**, 219.

APPENDIX

Uniform Field Breakdown in Dry and Humid Air Gaps

In the case of electron-attaching gases the equation for the current flowing in a uniform field gap is given by (Geballe and Reeves 1953)

$$i = i_0 \frac{\left[\frac{\alpha}{\alpha-\eta}\right] e^{(\alpha-\eta)d} - \frac{\eta}{\alpha-\eta}}{1-\gamma\frac{\alpha}{\alpha-\eta}\left[e^{(\alpha-\eta)d}-1\right]} \qquad \ldots\ldots(A1)$$

where α is Townsend's primary ionization coefficient, η the attachment coefficient, γ the secondary ionization coefficient, d the gap length and i_0 the background current. The critical conditions for the formation of a spark is that the denominator equals zero,

i.e. $$\gamma_s \frac{\alpha_s}{\alpha_s-\eta_s}\left[\exp\{(\alpha_s-\eta_s)d\}-1\right]=1$$

or, approximately, since $\exp\{(\alpha_s-\eta_s)d\} \gg 1$,

$$\gamma_s \frac{\alpha_s}{\alpha_s-\eta_s}\exp\{(\alpha_s-\eta_s)d\}=1 \qquad \ldots\ldots(A2)$$

where α_s, η_s and γ_s are the corresponding values of α, η and γ at the sparking condition.

The terminology used by Druyvesteyn and Penning (1940) for non-attaching gases may be extended to attaching gases. Let $\epsilon_s=(\alpha_s-\eta_s)/E_s$ where $E_s=V_s/d$, V_s being the breakdown voltage. Then equation (A2) becomes

$$\gamma_s \frac{\alpha_s}{\alpha_s-\eta_s} e^{\epsilon_s V_s}=1. \qquad \ldots\ldots(A3)$$

Using subscripts d and w at the sparking condition for dry and humid air respectively and assuming that γ_s remains the same in dry or humid air then equation (A3) for the two cases becomes

$$\gamma_s \frac{\alpha_w}{\alpha_w-\eta_w} e^{\epsilon_w V_w}=1, \qquad \ldots\ldots(A4)$$

$$\gamma_s \frac{\alpha_d}{\alpha_d-\eta_d} e^{\epsilon_d V_d}=1. \qquad \ldots\ldots(A5)$$

Dividing equation (A4) by equation (A5) and re-arranging gives

$$\epsilon_w V_w-\epsilon_d V_d=\ln\frac{\alpha_w-\eta_w}{\alpha_w}-\ln\frac{\alpha_d-\eta_d}{\alpha_d}. \qquad \ldots\ldots(A6)$$

The breakdown voltage in dry air V_d is known and the values of α_d and η_d are available (Harrison and Geballe 1953).

If the values of α_w and η_w were known for the appropriate range of E/p then V_w could be determined from equation (A6) by a process of trial and error. In the present estimation it will be assumed that α_w equals α_d at the increased breakdown voltage due to the presence of water vapour. In addition, it is assumed that η_w equals η_d at the increased breakdown voltage plus the difference between curves 1 and 2 of figure 4. (The latter curves have to be extrapolated to cover the required range of E/p.)

For convenience re-write equation (A6) as

$$(\alpha_w - \eta_w)d - (\alpha_d - \eta_d)d = \ln \frac{\alpha_w - \eta_w}{\alpha_w} - \ln \frac{\alpha_d - \eta_d}{\alpha_d}. \quad \ldots\ldots (A7)$$

Consider as an example the case of a 1·0 cm gap in air at atmospheric pressure and 23 °c. The breakdown voltage for dry air is 29·8 kv and this gives the breakdown field strength per mm Hg pressure as $E/p = 39{\cdot}2$. The corresponding values of α/p and η/p taken from Harrison and Geballe (1953) are 16·9 and 5·17 respectively. This gives $\alpha_d = 12{\cdot}85$ and $\eta_d = 3{\cdot}93$. Take V_w (the breakdown voltage in air saturated with water vapour at 23 °c) arbitrarily as 5·8% higher than V_d, then $E/p = 41{\cdot}48$. The corresponding dry air values for α and η are 17·48 and 4·32 respectively. When the attachment coefficient is corrected for the presence of water vapour this gives $\alpha_w = 17{\cdot}48$ and $\eta_w = 9{\cdot}04$. Substitute these values into equation (A7) to obtain

$$\text{left-hand side} = (17{\cdot}48 - 9{\cdot}04) - (12{\cdot}85 - 3{\cdot}93) = -0{\cdot}48,$$

$$\text{right-hand side} = 2{\cdot}3 \left\{ \log \frac{8{\cdot}44}{17{\cdot}48} - \log \frac{8{\cdot}92}{12{\cdot}85} \right\} = -0{\cdot}36.$$

The agreement is inexact and a higher value of V_w is required. Take V_w 6·2% higher than V_d so that $E/p = 41{\cdot}63$. This gives $\alpha_w = 17{\cdot}77$ and $\eta_w = 9{\cdot}06$. Substituting into equation (A7) gives:

$$\text{left-hand side} = -0{\cdot}22, \quad \text{right-hand side} = -0{\cdot}345.$$

The correct value of V_w to give solution of equation (A7) lies between 5·8% and 6·2% above the breakdown value for dry air. The corresponding experimental value is 5·0%.

The Early Stages of Spark Channel Expansion

By J. M. SOMERVILLE and J. F. WILLIAMS
The University of New England, N.S.W., Australia

MS. received 25*th February* 1959

Abstract. Investigations are reported, based on a study of the mark left on the anode by a spark in air, which give information about the distribution of conductivity across a spark channel during the first microsecond after initiation. These indicate (*a*) that the spark channel becomes 'hollow' after a few tens of millimicroseconds, with maximum conductivity towards its periphery, (*b*) that the diameters of the conducting channel, of the mark left on the anode, and of the shock front generated by the spark are approximately coincident for about one hundred millimicroseconds, and (*c*) that the energy which generated the shock is all supplied to the channel during the first few tens of millimicroseconds.

§ 1. Introduction

In previous publications (Somerville and Grainger 1956a, b) a technique has been described which makes visible the areas of the anode surface through which the current of a spark discharge flows. In air at atmospheric pressure, using spark discharges carrying currents of some tens of amperes in rectangular pulses of varying duration, it was shown (Somerville and Grainger 1956b) that, after the first microsecond or two, the current leaves the anode through a ring-shaped area, indicating that the spark channel is 'hollow' at the anode, its conductivity being greater at its periphery than at the centre. Such a state of affairs appears to persist for times of the order of 10 μsec or more.

In those experiments, the ring structure at the anode was found to be already established by the end of the duration of the shortest current pulse used, namely 2 μsec. The first part of this article describes an extension of this work, using shorter current pulses, down to 20 mμsec duration, for the purpose of studying the development of the anode mark prior to the establishment of the ring structure.

§ 2. Experimental Procedures and Results

2.1. *Single Current-Pulse Method*

Figure 1 shows schematically the apparatus used for generating a spark in which the current passes as a single rectangular pulse and for obtaining the mark left on the anode by the spark. The pulse is formed by discharging the effectively open-ended coaxial line L, of variable length, through its characteristic impedance R_0 (50Ω) in series with the spark gap. This gap is enclosed in a spark chamber S, which is joined to the coaxial line by a conical matching section. (A second similar chamber is capable of evacuation.) The hemispherically ended tungsten cathode C (radius 1·7 mm) may be inserted in one of several holes, at varying distances from the axis of the system, in the small metal strip B mounted on the polystyrene disc D. The plane circular anode A may be moved axially and also rotated by means of the knob K, so that several concentric rings of anode

marks may be obtained on a single anode. The coaxial line is charged to a negative potential between 1 and 5 kv through the large resistance R (60 MΩ). The spark is initiated by slowly moving the anode towards the cathode until breakdown takes place.

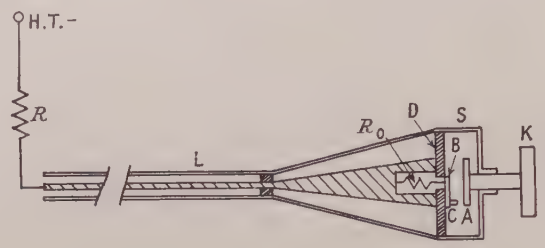

Figure 1. Spark gap and pulse forming line used for generating millimicrosecond current pulses.

The anode was polished palladium covered with a film of barium stearate a few hundred ångströms thick, as previously described. Results similar to those described in this article were also obtained by using both a copper anode covered with a copper oxide film and an aluminium anode covered with an electrolytically formed film, so that the phenomena are not specific to either the material of the anode or the film.

Figure 2 (Plate I) shows a typical series of anode marks left by current pulses of durations from 20 mμsec to approximately 500 mμsec. It will be seen that the area over which the individual spots forming the anode mark are spread increases during the first 100 mμsec or so, but that thereafter no significant further increase in this area takes place. Instead, the outer spots begin to grow in size. This is shown graphically in the histograms of figure 3.

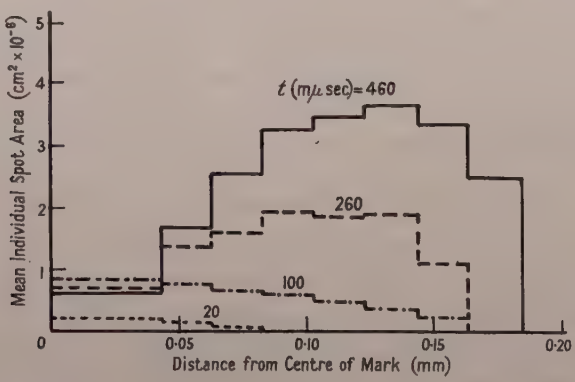

Figure 3. Histograms showing the mean area of the individual spots constituting anode marks like those of figure 2, as a function of the distance of the spots from the centre of the mark. The time t is the duration of the spark forming the mark.

The obvious physical interpretation of these observations is that initially current flows from the anode through the central spots, but quickly transfers to an outer ring of spots which increase in area with time, due to melting, as energy

continues to be supplied to them. The fact that the central spots do not increase in area indicates that after some tens of millimicroseconds no further energy is supplied to them, i.e. current ceases to flow through them.

One may seek to identify the expansion of the anode mark in the early stages with the expansion of the conducting spark channel itself. However, in a situation in which current flows from the anode continuously during the life of the spark channel, there is the possibility that the development of the anode mark may be substantially influenced or even determined by specifically *anode* processes rather than by the expansion of the spark channel.

2.2. *Double Current-Pulse Method*

In order to eliminate to a large extent the role played by anode processes, a second technique was used. The spark channel was initiated by a 30 mμsec current pulse, and was then allowed to expand freely without any current through it for a variable time, after which a second, probing pulse was passed through the channel. Anode marks caused by the initiating pulse alone and by the initiating pulse followed by the probing pulse were obtained and studied. The apparatus used for generating these pairs of pulses, having, perhaps, applications other than the specific one for which it was designed, is described elsewhere (Somerville 1959).

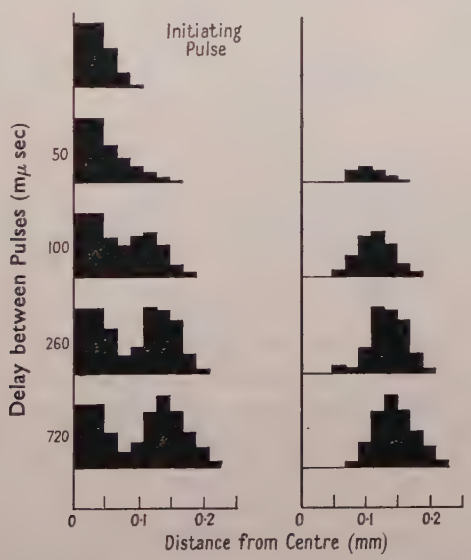

Figure 5. Histograms showing the number of individual spots of an anode mark as a function of distance from the centre of the mark. The left-hand set of histograms shows the distribution of all spots formed by a 30A 30 mμsec initiating pulse followed by a similar probing pulse after a delay as indicated. The right-hand set of histograms shows the result of subtracting the distribution for the initiating pulse alone from the total distribution.

Figure 4 (*a*) (Plate II) shows the mark left on the anode by a 30 mμsec 30 A initiating pulse and figure 4 (*b*) that left by a similar initiating pulse followed by a probing pulse 720 mμsec later. It is readily seen that the probing pulse current passes from the anode through a distinct outer ring of spots. Figure 5 shows histograms giving the radial distribution of individual spots in the anode mark

for various values of the delay between the initiating and probing pulses. From the set of histograms on the left it is clear that the central spots are properly attributable to the initiating pulse, and the right-hand set is the result of subtracting the distribution attributable to the initiating pulse from the whole, thus obtaining the distribution of the additional spots formed by the probing pulse. For the longer delays, the double-peaked nature of the total distribution suggests strongly that the probing pulse current passes only through the outer ring of spots. An interesting transition case occurs at a delay of 50 mμsec, when some of the inner spots can be seen to be unusually large, indicating that they have been used both by the initiating and the probing pulses.

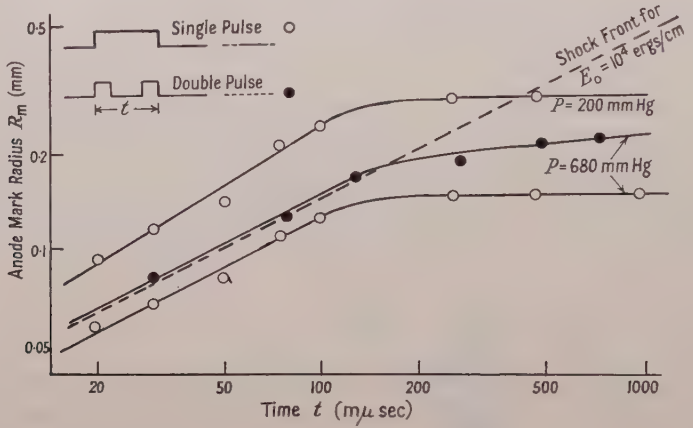

Figure 6. Graphs showing the radius R_m of the mark left on a coated palladium anode by both single and double current-pulses as a function of the time t as defined in the figure. The peak value of the current in each case was 30A and the duration of the individual pulses of the double pulse was 30 mμsec. The sparks were in air at the pressures indicated.

Figure 6 shows a double logarithmic plot of the radius of the anode mark R_m (the radius of the smallest circle which will enclose all the individual spots forming the mark) as a function of t where t is the duration of a single pulse, or the time between the beginning of an initiating pulse and the end of a probing pulse, as the case may be.

§ 3. Discussion

The anode marks left by single and by double pulses are consistent with the view that within a few tens of millimicroseconds the conducting spark channel has a hollow structure with most of the plasma conductivity near the periphery. In the double pulse method, when the electric field of the probing pulse is applied, electrons are deposited on the thin insulating anode layer which breaks down and allows the passage of current. The role of the coated anode under these circumstances is that of an indicator of the distribution of plasma conductivity. In the case of a single sustained pulse, the current initially flows through the central spots, but, as the region of maximum plasma conductivity moves outwards, these spots become untenable and other spots form in an outer ring or rings and the current transfers to them. Figure 6 shows that, for the first

100 mμsec, there is no great difference in the radii of marks formed by single and double pulses with corresponding values of t.

Experimental investigations (Abramson and Gegechkori 1951, Vanyukov, Isaenko and Khazov 1955) have shown that, for a time after the initiation of a spark, the boundary of the luminous conducting channel substantially coincides with the shock front generated by the release of energy in the spark. Subsequently, the shock front leaves the luminous channel, which continues to expand more slowly. It is consequently of interest to compare the rate of expansion of the anode mark with the rate of expansion of a cylindrical shock front such as the spark might generate.

Drabkina (1951) has shown that if the energy per unit length supplied to the axis of the spark up to time t is $E(t)$ erg cm^{-1}, then the radius $R(t)$ cm of the resulting cylindrical shock front is given by

$$R(t)=\left(\frac{\alpha}{\rho_0}\right)^{1/4}\left[\int_0^t \{E(t)\}^{1/2}dt\right]^{1/2} \qquad \ldots\ldots(1)$$

where ρ_0 (g cm^{-3}) is the initial gas density and α is a dimensionless constant whose value for air is 0·55. The radius of the shock front thus depends not only on the total energy supplied but also on the way in which it is supplied in time. If we take two special cases, one in which the energy E_0 is all supplied instantaneously at time $t=0$, and another in which the energy is supplied uniformly, so that $E(t)=Wt$ where W is a constant, we get

Instantaneous release: $R(t)=(\alpha/\rho_0)^{1/4}E_0^{1/4}t^{1/2}$ $\ldots\ldots(1\,a)$

Uniform release: $R(t)=(\alpha/\rho_0)^{1/4}(\frac{2}{3})^{1/2}W^{1/4}t^{3/4}$. $\ldots\ldots(1\,b)$

In figure 6 the initial parts of the (log R_m, log t) curves are approximately linear, with a slope close to 0·5, so that comparison with (1 a) and (1 b) shows that the variation with time of R_m is of the same type as that of a cylindrical shock front caused by an instantaneous energy release. This is consistent with the fact, previously noted, that the radius of the mark left by a spark in which the current flows continuously for a time t is no greater (actually slightly less) than that of the mark left by two 30 mμsec pulses spanning the same time t. Clearly, the energy supplied after the first 30 mμsec contributes little or nothing to the expansion of the channel. If the spark channel expands in the same way irrespective of whether the current is single or double pulsed, one might well expect the mark left by a single pulse to be somewhat smaller than that left by a double pulse. This would be so, because, with current flowing continuously from the anode, the channel boundary must advance somewhat before existing spots are abandoned and new ones formed, thus introducing a lag between mark radius and channel radius.

The energy supplied in the initial stages to the channel is given substantially to the electrons, and the time taken to generate the shock will depend on the time required for the transfer of energy from the electrons to the molecules in the form of kinetic energy. In air at atmospheric pressure, an electron with a few volts energy makes about 2×10^{12} collisions per second, and the fraction of its energy passed on at collision to a molecule in kinetic form is of the order of 3×10^{-5}, so that the characteristic time for such energy transfer between electrons and molecules is of the order of 2×10^{-8} sec, which is consistent with the conclusions of the previous paragraph. It is of interest to note, moreover, that the curve of figure 6 corresponding to an air pressure of 200 mm Hg has a slope of

0·6, which is consistent with the fact that at the lower pressure the time for generation of the shock is increased and the supply of energy no longer effectively instantaneous with respect to time of the order of 10^{-7} sec, over which the major part of the expansion takes place.

It would be an advantage to be able to make an absolute comparison between equation (1 *a*) and the observed rate of growth of the anode mark. This requires a knowledge of E_0, the energy input per unit length to the channel. In the brief times involved, estimates of power input from voltage and current measurements are not very satisfactory and we have attempted to estimate E_0 by collecting and measuring the energy which is not dissipated in the spark and subtracting this from the energy originally stored. This gives little better than an order of magnitude estimate, but the value of E_0 under the conditions prevailing for those curves of figure 6 appropriate to atmospheric pressure is probably 10^4 erg cm^{-1} to within a factor of two. The broken line in figure 6 shows the radius of a cylindrical shock front generated by this amount of energy instantaneously released and it is seen that it is approximately the same as the observed radius of the anode mark. The rate of expansion of the shock wave is, according to equation (1 *a*), very insensitive to E_0, depending on its fourth root, so that, in spite of the uncertainty in E_0, we may say that the rate of expansion of the anode mark is roughly equal to that of the shock wave during the first 100 mμsec. Thereafter, in the case of a sustained current, the current appears to anchor completely at the outer spots. The mark left by the pair of pulses, on the other hand, continues to expand, but very slowly, much more slowly, in fact, than the rate of expansion of the conducting channel predicted by Drabkina (1951) subsequent to the separation of the channel from the shock front.

3.1. *The Influence of Initial Gas Density*

Figure 7 shows the influence of the initial gas density ρ_0 (which is proportional to the gas pressure P) on the size of the anode mark for various single current-pulse durations. This influence is seen to be quite marked and, to within the

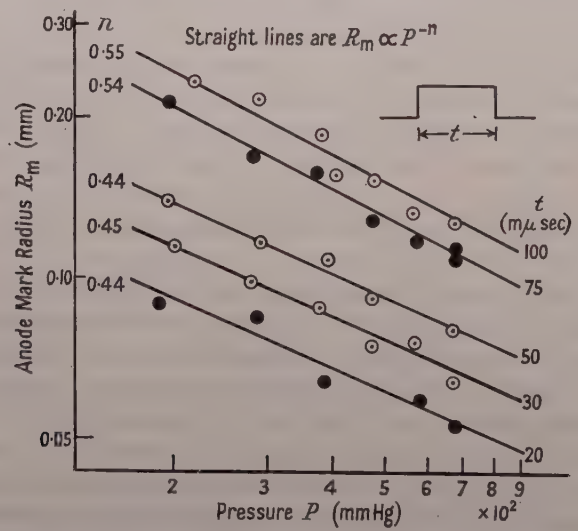

Figure 7. The radius R_m of the mark left on a coated palladium anode by 30 A sparks of varying duration t in air as a function of the air pressure P.

accuracy of the measurements, the variation of R_m with ρ_0 may be represented by a relationship of the form $R_m \propto \rho_0^{-n}$ where n lies between 0·44 and 0·55. *If E_0 or W were independent of ρ_0* equations (1 *a*) and (1 *b*) would both predict a variation in which $n = 0{\cdot}25$. If we are correct in substantially identifying the early expansion of the anode mark with that of the shock front, then it would follow that, under the conditions of the experiment, i.e. static breakdown of the gap, the energy per unit length going into the shock increases as the pressure is lowered.

§ 4. Acknowledgments

We wish to acknowledge the help of Dr. K. Landecker in making estimates of the energy dissipation in the spark. One of us (J. M. S.) wishes to acknowledge the benefit of discussions with Professor L. Goldstein of the University of Illinois and Professor R. G. Fowler of the University of Oklahoma.

References

Abramson, I. S., and Gegechkori, N. M., 1951, *J. Exp. Theor. Phys. U.S.S.R.*, **21**, 484.
Drabkina, S. I., 1951, *J. Exp. Theor. Phys., U.S.S.R.*, **21**, 473.
Somerville, J. M., 1959, *Proc. Phys. Soc.*, **74**, 378.
Somerville, J. M., and Grainger, C. T., 1956 a, *Brit. J. Appl. Phys.*, **7**, 109.
—— 1956 b, *Ibid.*, **7**, 400.
Vanyukov, M. P., Isaenko, V. I., and Khazov, L. D., 1955, *J. Tech. Phys., U.S.S.R.*, **25**, 1248.

Lens Designing by Electronic Digital Computer: II

By M. NUNN and C. G. WYNNE
Wray (Optical Works) Ltd., Bromley, Kent

MS. received 24th October 1958, in revised form 25th March 1959

Abstract. The method of Successive Linear Approximation at Maximum Steps, described in the previous paper, has been applied to automatic lens designing on an electronic digital computer. A description is given of the form of programme used and the results of applying the method to three design problems are quoted.

§ 1. Introduction

The work described in this paper has been carried out using the Ferranti Mark 1* electronic digital computer at the Armaments Research and Development Establishment of the Ministry of Supply, Fort Halstead.

The aim of this work has been to find a method of programming the machine to alter the design parameters of a given form of lens system so as to give the highest attainable optical performance, in terms of some criterion supplied to the machine. No attempt has so far been made to programme the machine to initiate new lens forms, for example by adding further components.

The problem of optimizing the performance of a given lens form is one of considerable complexity. The aberrations of a system are determined by the tracing of a number of sampling rays passing through appropriate points in the aperture and object field; for practically useful systems from 25 to 50 such aberrations may be required to give an adequate description of the lens performance. These aberrations are highly non-linear functions of the design parameters, which in typical systems may be from 20 to 50 in number.

The method we have adopted is that of Successive Linear Approximation at Maximum Steps (SLAMS) described by Wynne (1959). Our initial purpose was to explore the effectiveness of this method for automatic lens designing and to find the best way to apply it. The first machine programme was, therefore, restricted in the number and type of variables available to the machine for the automatic correction process, and also in the degree to which the machine programme was fully automatic, manual intervention and control being either necessary or possible at various stages. As experience of the method has confirmed its efficacy and thrown light on the type of controls required, the scope of the programme is being extended.

The main initial limitations have been:

(*a*) The machine has so far been programmed only to deal with spherical surfaces and with changes in surface curvatures and separations, i.e. the available continuous variables, the problem of automatic design with the discontinuous and mutually related refractive indices and dispersions of available optical materials having been deferred to a later stage.

(*b*) The SLAMS method requires that a least squares solution be found to a number of simultaneous equations, the number of equations being equal to the

sum of the number of design parameters being used and the number of aberrations being corrected, and the number of variables being equal to the number of design parameters. Our initial programme was restricted to a maximum of 32 equations in 20 variables. This has since been extended to 48 equations in 20 variables and further extension is being undertaken.

(*c*) A number of rays are traced through the initial optical system and through subsequent variants of it, it being important for effective lens designing that these rays should pass through the most significant sampling points in the aperture and object. No attempt has been made to programme the machine to select these sampling points automatically: suitable points have been found by previous ray-tracing for each initial system and the automatic design programme has continued to use these for subsequent variants. This has so far proved satisfactory, presumably because we have used the automatic design methods on initial systems either already having a first-order correction of their aberrations, or being not very far from such correction, so that no fundamental changes have been effected in the lens form by the process of improvement. However, if all stages of optical design were to be programmed for an automatic machine method, the selection of appropriate sampling points would be a necessary part of this. A discussion of the problem is given as an Appendix to this paper.

§ 2. The Programme

The general structure of the programme of automatic design will be described first in this section, certain necessary complications to it being discussed thereafter.

(*a*) The first operation of the machine is to trace the specified set of rays through the initial optical system and to compute its aberrations. The ray-tracing method used is an algebraic one based on that first given by T. Smith (1915, 1918) for skew rays, a simplified scheme of the same type being used for rays in a meridian plane. A manual control can cause the results to be printed out at this stage or at any subsequent stage of ray-tracing. Two alternative ray-tracing programmes are available, the second, which is only called into operation occasionally, giving the coordinates of the intersection of each ray with each surface in addition to the aberrations of the system. For principal rays the distortion and the departure of the sagittal and tangential foci from the paraxial focal plane are calculated and for other rays the distance of the ray-intersection point on this plane from the principal ray intersection point. In addition the optical path length of each ray in each dispersive medium is calculated and the chromatic aberration is computed from these as a wave-front aberration. At this, and subsequent complete ray traces on new systems, more aberrations may be calculated, and therefore available for inspection, than are subject to the process of automatic improvement.

(*b*) Next the system is subjected to a systematic set of changes of each of the available design parameters (curvatures and separations), the set of rays giving the aberrations to be automatically controlled is traced through each of these systems, and the change in each aberration for each change is stored in the machine; if desired these can also be printed. In changing the design parameters, a method is used which avoids changes in the equivalent focal length of the system. Each curvature is changed, proceeding serially from the front, by a fixed amount; for each such curvature change the next following air–glass or glass–air surface

is adjusted to restore the paraxial ray convergence in the following space, and the remainder of the curvatures are scaled to conserve the paraxial ray angles of incidence; similarly each separation is changed, one by one, and the following curvatures are again scaled to conserve paraxial angles. A matrix of numbers a_{ij} is thus calculated giving the change of each aberration A_i with each of the design parameter changes Δ_j, the parameter changes themselves not being simple ones, but between them comprising all the available curvature and separation changes in the complete lens and being of such a nature that the compounding of given multiples of each of the changes into a new lens design can be performed by the machine. Some latitude exists in the choice of the basic parameter changes; they must be large enough for the aberration changes they produce to be substantially larger than the cumulative rounding-off errors of the ray-tracing, but small enough to be within the range of approximate linearity of the aberrations with parameter changes; for maximum efficiency of the SLAMS method the basic change of each parameter should be chosen to have the same range of linearity.

For the first cycle, matrix elements a_{ij} will generally be calculated for changes of every curvature and separation, though this is not always the case. For example, the register glass in a lens for aerial photography may be of some specified thickness, so that this is not an available parameter; or again, in the type of wide-angle lens using large divergent front lenses to increase the relative illumination at large field angles by introducing coma of the entrance pupil (Slussareff 1941), the requirement of maximum pupil coma for a given power defines the shape and distance from the stop of these front negative lenses, so that these are not available design parameters for the correction of other aberrations. Controls are available to restrict the range of variables used by the machine in such cases and subsequently the range is restricted automatically in cases which are discussed below.

(*c*) Having computed the matrix of differentials a_{ij}, the machine proceeds to set up the equations used in the SLAMS method,

$$\left.\begin{aligned}[a_{ij}]x_{(j} + A_{(i} &= 0 \\ Px_{(j} &= 0\end{aligned}\right\} \qquad \ldots\ldots (1)$$

the first set of these equations giving the proportion x_j of each basic design parameter change Δ_j which would be required to reduce each of the aberrations A_i to zero if the aberrations changed linearly with the design parameters, and the second set of equations (1) having the effect, when P is suitably chosen, of restricting the size of the parameter changes to the largest size for which the assumption of linearity is approximately valid, as described in the previous paper (Wynne 1959). Having set up equations (1), the machine forms the normalized equations corresponding to a least squares solution of these and solves for $x_{(j}$ using the method of pivotal condensation. Before this can be done, the size of the weighting factor P must be specified and also the metric of the various aberrations A_i and of the corresponding matrix elements a_{ij}.

Considering first the metric of the aberrations, it will be immediately obvious that the aberrations calculated are not directly comparable, since they are of a variety of essentially different kinds—wave-front aberrations for the chromatic terms, longitudinal ray-aberrations for the sagittal and tangential foci, and transverse ray-aberrations for the remainder. Making reasonable approximations, the aberrations that are not transverse ray ones may be converted to this

form by multiplying by the appropriate function of the aperture angle, for example the transverse axial chromatic aberration of a marginal ray would be obtained by dividing the wave-front aberration by half the aperture angle. A second factor affecting the appropriate metric for the various aberrations is that, when these are all converted to the same form, they are not generally of equal importance in the final correction; for example, the degree of correction of distortion required is often less than that of aberrations affecting resolution of the image; again the lens performance at the extreme field angle may be of less importance than that at smaller angles. A suitable metric for each aberration A_i, which takes the form of an appropriate weighting factor multiplier for each A_i in the first set of equations (1), must therefore be supplied to the machine. Reasonable first trial values for these weighting factors, to meet the requirements mentioned above, can be estimated after some experience of the method, and these can be adjusted in the light of the results of one or more cycles of automatic improvements by the machine, more weight being given to aberrations which are being corrected rather slowly, and less to aberrations whose correction is particularly good. Once suitable values are found, these can be used satisfactorily for a series of cycles.

The weighting factor P is also chosen initially in the light of previous experience with the method and adjusted if necessary after the first cycle of the programme. A first check on the suitability of the P value is available when the machine has carried out the least squares solution of equations (1), the values of x_j so found being printed out. These are inspected and, with the size of basic change of the design parameters we are using, if the largest x_j is not in excess of 2 or 3, nor less than unity, the value of P is retained and the machine is allowed to proceed to the next stage. If the largest x_j is much less than unity, a smaller value of P is used in equations (1) and the process is repeated, giving a solution with larger values of x_j; similarly if the largest x_j is too large, P is increased.

(*d*) When, by an appropriate choice of P, a set of values of x_j of the required range of magnitude has been obtained, the machine sets up a new lens design derived from the original one by taking x_j times the basic change of the jth design parameter for all the parameters; the data for this new lens may be printed if desired. The complete set of rays is traced through the new lens, and the aberrations printed, together with values of the aberrations predicted assuming that they change linearly with the design parameters, these predicted values being simply the residuals of the first set of equations (1), reduced by the corresponding weighting factor, for the x_j values used. The aberrations calculated by actual ray-tracing can then be compared with those predicted and if the difference is large compared with the improvement effected from the initital lens, the machine can return to a solution of equations (1) with a larger value of P, giving smaller x_j values and therefore a closer approximation to the linear prediction. The choice of P from the earlier criterion is however generally found to be satisfactory, and a suitable value of P found at the first cycle is found to be so for subsequent cycles.

This concludes one cycle of the basic machine programme. At this stage the machine has produced a new design of lens with improved aberrations, the improvement being the maximum which is possible, within the range of linearity of the aberration changes with design parameters, for the value of Σx_j^2

which has been determined, by the choice of P, to be as large as the range of approximate linearity allows. The machine returns to the first stage, using the improved lens design as its starting point, and repeats the cycle as often as is required.

In the description of the basic programme above, it has been assumed that the design parameters are infinitely variable. This is not in fact the case, in particular the range of lens thicknesses for physically realizable systems must be restricted. All separations between surfaces must be positive both along the axis and at the full aperture that is being used; for divergent lenses the centre thickness must be sufficient for manufacture to be possible, and for convergent lenses the thickness must be sufficient to allow a diameter rather larger than that required to pass the full cone of light, so that the lenses can be held in a mount. Provision is made in the programme to ensure that these conditions are met. A minimum value can be set, independent of changes of curvatures of surfaces, for axial separations between lenses and for axial thicknesses of divergent lenses; these are supplied to the machine inititally. When the least squares solution of equations (1) has been found and the new lens set up corresponding to the solution, the machine tests these separations to see whether the conditions have been violated. If any thicknesses or separations have been reduced below their minimum values, these design parameters are removed from the set of design parameters available to the machine and a new set of equations (1) set up and solved excluding these variables. In addition, since it has been found from experience that similar changes of the design parameters are generally made in successive cycles of the SLAMS method, the exclusion of the variables which have violated the minimum conditions at one cycle is automatically maintained for the two following cycles, by which time a lens form will have been evolved so different from the previous one that its aberration characteristics will often no longer tend to produce further reduction of these separations. For the requirement of positive edge-separations between surfaces, the position is rather more complicated, since the edge-separation depends both on the axial separation and on the curvatures, which are being changed in the design process. A limit to the centre thickness of a convergent lens or a divergent air space can be given to the machine exactly as for the cases above and, where the curvatures bounding the space concerned are changing slowly, this is an appropriate procedure. Alternatively, no limit may be set to such separations at this stage and the machine proceeds, having solved the equations for x_j, to trace the complete set of rays for the corresponding new system. At this stage it computes the path length between successive surfaces and if, for the ray passing between them at the greatest distance from the axis, this length is less than some positive value previously specified to the machine, it again reverts to equations (1) with the offending variable removed for this and two succeeding cycles.

A further safeguard, this time against machine faults, is that at intervals throughout the programme, the whole state of the calculation at that point is stored, so that in the event of a machine fault developing, the machine can be switched to revert to the previous safeguard point and repeat the calculation from there.

§ 3. Applications of the Method

It is axiomatic that no computing programme can give a solution to an insoluble problem. The present state of knowledge of aberration theory is

inadequate to determine in general what forms of lens are capable of yielding a high degree of aberration correction, but for simple forms of two or three lenses the presence of inherent limitations to correction are demonstrable. For a satisfactory test of the ability of the methods described in this paper to yield highly corrected lens designs, lens forms of at least a moderate degree of complexity must, therefore, be chosen. On the other hand, the limited number of variables with which the present programme can operate has excluded very complicated systems, leaving only a restricted range of problems that could be usefully undertaken. By choosing optical systems of moderate complexity and restricting the automatic correction to the monochromatic aberrations, it has however been possible to demonstrate the potentialities of the method with the limited matrix size of the initial programme. The systems chosen were ones in which the mean refractive indices of some of the components were ones for which glasses are available having a variety of different dispersions, so that the correction of the chromatic aberrations, omitted by the machine, could be carried out as a separate operation, either simply by an appropriate choice of dispersions, or by inserting cemented surfaces, without disturbing the monochromatic correction.

Since these problems were the first to which the method was applied, the application has involved considerable experimental work on the effect of different weighting factors on the aberrations and of different step-sizes, so that the course of the machines work has not been as direct as will be possible in future applications of the method, and the times taken on the machine cannot generally be given. This is, however, done in one case below in section (*c*) where the results of a single direct machine run are quoted.

Example (*a*). The automatic design programme was first applied to an attempt to improve the performance of a wide-angle lens of 5 glass double-Gauss form, having the type of construction described by Wynne (1953) which had already been brought to a high degree of correction for this type of lens using traditional methods of lens designing. In this form of lens, a general improvement to the aberrations can be effected by reducing the thickness of any of the components, so that in the initial design these were already reduced to the minimum values attainable in production, and the number of variables at the machine's disposal was thereby automatically limited. In this lens, a number of the aberrations have both their first and second orders balanced against their third orders, so that for example the graphs of sagittal and tangential field curvature and of distortion against field angle had the form shown in figure 1, curve (*a*). By increasing the weight attached to any one of these aberrations so that the machine paid more attention to the correcting of this rather than of the other aberrations, the curve could be automatically flattened at each lobe, curve (*b*), showing an automatic correction simultaneously of three orders of aberration, but this could only be achieved at the expense of a deterioration of other aberrations. No general improvement of the performance of this particular lens appeared to be possible with the variables available to the machine.

Example (*b*). A lens of symmetrical double-Gauss form, having a very high degree of correction at unit magnification over a moderate aperture and field angle (f/3·9 $\pm$ 17·3° field) was taken, and the machine was given the problem of redesigning this to be corrected for an object at infinity. The design of a symmetrical lens at unit magnification is simpler than for any other conjugates, since symmetry ensures the complete correction of all orders of coma and distortion.

This problem was chosen since it seemed plausible that a form of lens having a high degree of correction at one magnification might have the potentiality of a high correctibility for other magnifications; this proved to be true in this case.

Figure 1.

The results of the process of automatic design are shown graphically in figure 2. The upper curves show the longitudinal aberration from the paraxial focal plane, as a fraction of the equivalent focal length, as abscissa against aperture as ordinate for object points on axis and at field angles 12·3° and 17·3° off axis; curves (*a*) show the aberrations of the original lens at unit magnification, curves (*b*) the aberrations of the same lens, before correction, with an object at infinity, and curves (*c*) those of the corrected design produced by the machine. The points marked on the curves indicate the rays actually traced, sixteen different aberrations having been used by the machine in the automatic correction process. The distance of the zero aperture point from the origin in the curves for oblique imagery represent the tangential field curvature, and the isolated points on axis marked S denote the position of the sagittal foci. In order to make the upper curves of figure 2, relating to lenses at different magnifications, more readily comparable, curves (*a*) have been drawn with an aberration scale one quarter that of curves (*c*), so that curves (*a*) as drawn, if taken to be on the same scale as curves (*c*), would represent the longitudinal aberrations of a lens corrected for an object at infinity having the same wave-front aberrations as those existing in the original 1:1 lens; in this sense the upper curves (*a*) and (*c*) are directly comparable. The curves (*b*) are on one tenth the scale of curves (*c*). The lower curves show the percentage distortion as abscissa against field angle off axis as ordinate. For the original symmetrical lens at unit magnification the distortion is, by symmetry, zero at all field angles.

It is clear from curves (*b*) that the effect of transferring the object of the 1:1 lens to infinity is to introduce heavy aberrations, mainly primary but also some higher order ones, all of which the machine, in redesigning the lens, has reduced to very small values indeed. We do not know of any lens of comparable aperture and field having such a high degree of correction as this final design.

Example (*c*). A third type of lens on which the automatic design process has been used is a wide-angle one of the form in which large front divergent lenses are used to give increased illumination at the outer part of the field, by introducing

coma of the entrance pupil. The shape and position relative to the stop of this front part of the lens system are fixed by the requirement that the pupil coma shall be a maximum, so that these variable were not made available to the machine in the design process. Behind this divergent front part, the lens system had

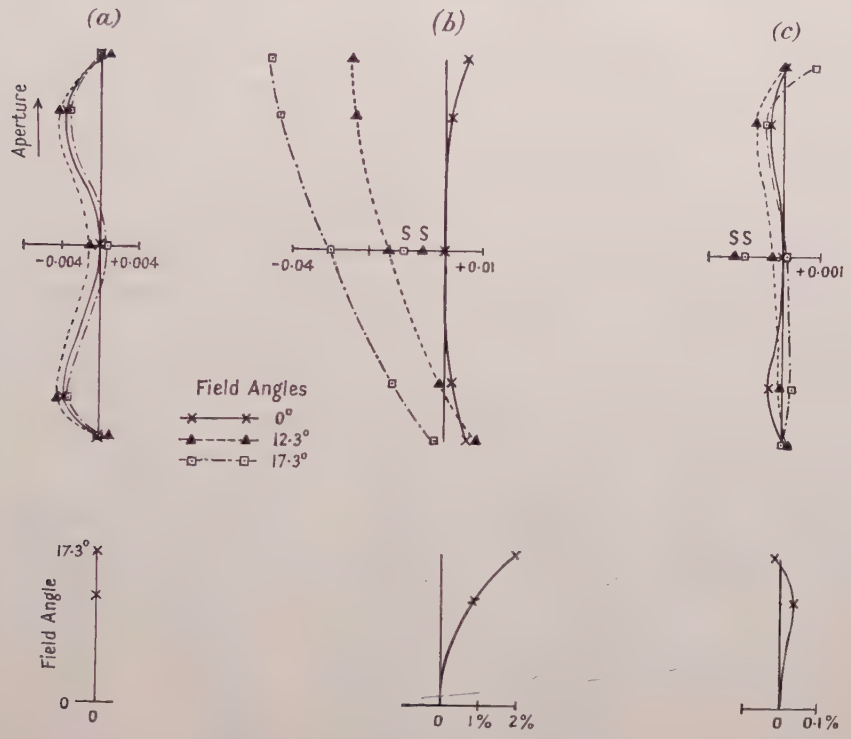

Figure 2. The upper curves show the longitudinal aberration as a fraction of the focal length at three field angles, 0°, 12·3° and 17·3°, (*a*) being for the original lens at unit magnification, (*b*) for the same lens with the object at infinity, and (*c*) for the corrected lens with object at infinity. The lower curves show the percentage distortion in the three cases.

five additional lens components. The front divergent component, besides introducing the desired pupil coma, also has the effect of reducing the obliquity in the rest of the system of the wide-angle pencils in the object space, and in consequence fewer orders of aberration of oblique imagery are significant than in the double-Gauss form of wide-angle lens discussed under (*a*) above, and an adequate account of the lens performance can be derived from rays traced from only two off-axis sampling points in the object.

The initial design given to the machine was one on which one of us (C. G. W.) had worked using traditional methods for a considerable time. Its longitudinal aberrations, on axis at f/5·8 and for substantially unvignetted pencils both in the meridian plane and in the secondary planes, at 30° and 45·3° off axis, and its distortion are shown in figure 3(*a*). Considerable higher order coma, astigmatism and distortion are present, with appropriate primary aberrations to balance these, a second order overcorrect oblique spherical aberration in the meridian plane in evidence at 30° is balanced against a still higher order undercorrection

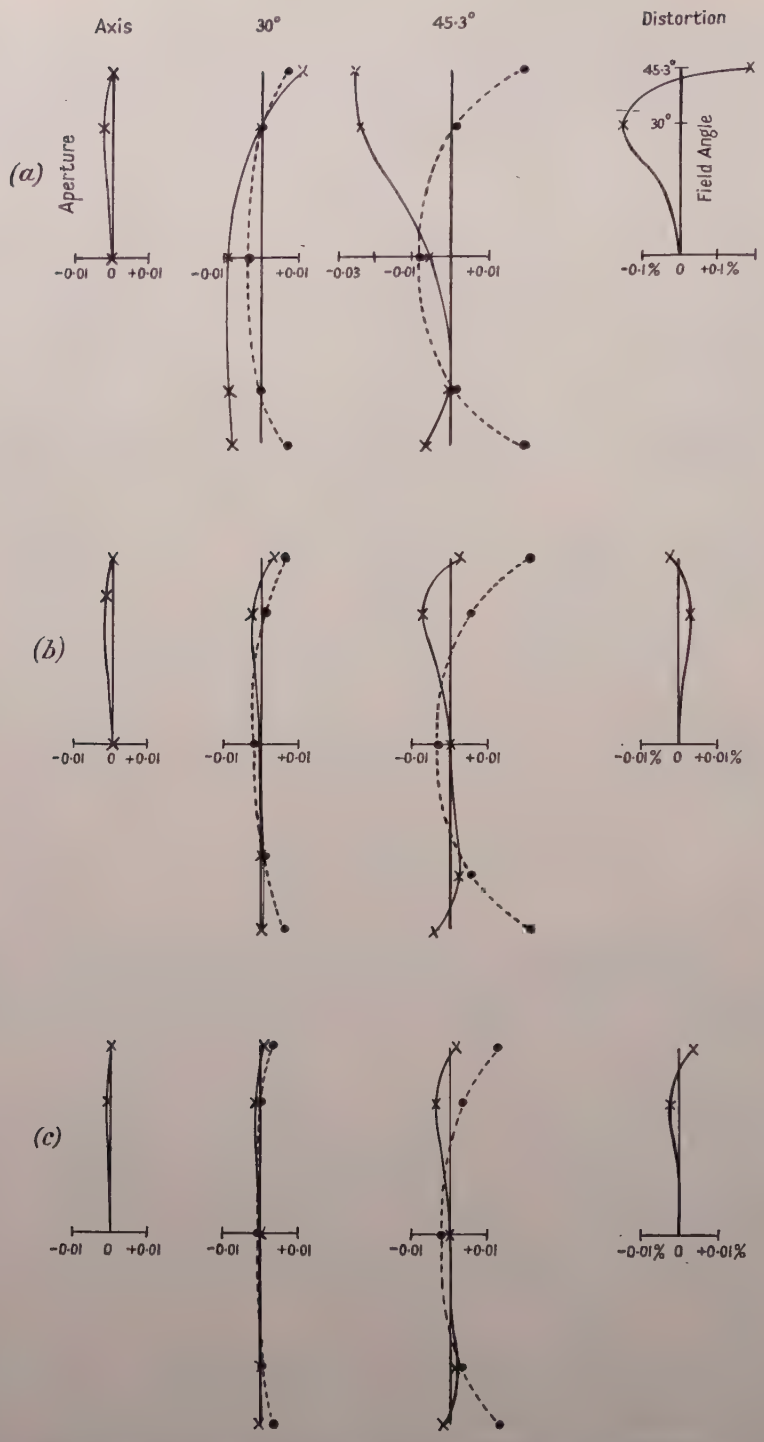

Figure 3. The sets of curves (*a*), (*b*) and (*c*) show the aberrations of the original *f*/5·8 wide-angle lens, and of two successive improved designs derived from it. The first three graphs in each set show the longitudinal aberration, as a fraction of the focal length, on axis and at field angles of 30° and 45·3° off-axis, the full line showing the aberration in a meridian plane and the dotted line the aberration in the secondary plane. The right-hand curve in each set gives the variation of distortion with field angle, that for lens (*a*) being on one-tenth the scale of (*b*) and (*c*).

at 45·3°, and in the secondary plane (the dotted curves in figure 3) a higher order overcorrect oblique spherical aberration of oblique imagery is present, the sagittal field curvature having been left undercorrect to reduce the effect of this.

After a continuous run of 4½ hours of the automatic design process, involving six iterations, the machine had arrived at the design whose aberrations are shown in figure 3(*b*), in which the distortion curve is drawn on a scale ten times that of the corresponding curve in 3(*a*). Very considerable reduction is evident in the higher order aberrations in the meridian plane, the first order ones being reduced accordingly; the higher order overcorrect oblique spherical aberrations in the secondary planes from the sagittal focus has been slightly reduced, and the sagittal field curvature reduced correspondingly.

The table gives the constructional data of the original lens design, lens 1, whose aberrations are shown in figure 3(*a*), and of the design whose aberrations are given in figure 3(*b*) (lens 2). The radii, separations and glass constants are given serially from the front, a positive radius being one which is convex toward the front, a negative one concave. Both designs are given for an equivalent length of unity.

Lens 1		Lens 2			
Radii	Axial separations	Radii	Axial separations	n_d	ν
1·51712		1·51712			
	0·03408		0·03408	1·700	56·2
0·79484		0·79484			
	0·81275		0·82732	1	
0·41764		0·41838			
	0·20318		0·10247	1·613	59·3
1·21430		1·32849			
	0·03216		0·11965	1	
0·27141		0·29030			
	0·02130		0·03077	1·748	27·9
0·21875		0·23754			
	0·23346		0·23059	1	
−0·21875		−0·20770			
	0·02130		0·02130	1·748	27·9
−0·26565		−0·26307			
	0·00102		0·00350	1	
−1·29659		−1·30014			
	0·21553		0·21553	1·651	58·6
−0·41553		−0·40854			
	0·80937		0·76947	1	
−0·76831		−0·75128			
	0·03408		0·03408	1·748	27·9
−1·49349		−1·49148			

Entrance pupil 0·8627 behind front surface.

Beyond this point, no significant improvement could be effected by the machine with the variables available to it, i.e. the curvatures and separations alone, with the types of glass fixed. Since the automatic process does not yet embody changes of glass constants, manual intervention was employed in changing some of the glass types, in ways suggested by general experience of lens designing.

Various changes were tried; the effect of glass changes made in this way is, of course, to give a lens whose aberrations are at first uncorrected, the lens being then subjected to the automatic design process to give the best performance possible with the new glasses. The best form of lens so far produced by this process has aberrations shown in figure 3(*c*). A further considerable improvement over figure 3(*b*) is evident, including a halving of the aberrations in the secondary plane. The degree of aberration correction in this final lens design is very high and we believe this to be the first published example of a systematic reduction of the aberrations of skew rays.

§ 4. Conclusion

The results given above, although limited in scope by the size of the initital programme capacity, demonstrate the power of the method. Apart from the gain in speed from an electronic digital computer, the simultaneous variation of up to twenty variables to give the greatest possible reduction of up to twenty aberrations within a limited range of approximate linearity is a task beyond the scope of traditional methods and in the examples (*b*) and (*c*) above, a higher degree of correction has in fact been achieved by the machine than was possible hitherto. It appears to be possible to accommodate within the capacity of the machine an extended programme, using the same basic method, allowing the correction of a greater number of aberrations and providing for the automatic choice of the refractive indices and dispersions of lens components as well as of curvatures and separations. With such an extension, the advantage over traditional methods should be still greater; work to this end is proceeding.

Acknowledgments

We gratefully acknowledge the advice and assistance given by Mr. H. J. Gawlick, Head of the Computer Branch, Armaments Research and Development Establishment, Fort Halstead, and his staff, especially the initial instruction in the methods of programming and operating the computer.

APPENDIX

Sampling Points for Ray Tracing

In order to obtain reasonably complete information about the aberrations of an optical system by the tracing of a finite number of rays, the sampling points in the object and pupil through which these rays are traced must be suitably chosen. For well corrected systems this choice of the most significant rays is a matter of some complexity, depending on (*a*) the form of the aberration curves, (*b*) the aberrations of the entrance pupil, which is the image of the physical stop, and (*c*) when oblique pencils of light are vignetted, on the degree and type of this vignetting, the best choice of which again depends on the form of the oblique aberrations. The complications involved in a choice of sampling rays are well known to lens designers, but little attention seems to have been paid to the problem in the optical literature.

(*a*) *The form of the aberration curves.*

The aberrations of a lens system are a function of ρ, σ and ϕ where σ is the distance off-axis of an object point and ρ, ϕ are polar coordinates of a ray inter-

section point in the pupil plane, the angle ϕ being measured from the meridian plane containing the object point. One aspect of the choice of sampling points in the aperture and field (i.e. of values of ρ, σ and ϕ for which rays are to be traced) can be considered in terms of a set of curves showing the variation of the aberration with one of these variables at a time, for constant values of the other two. For example, curves may be considered showing the change of longitudinal aberration with aperture ρ, for different values of σ and ϕ, and the variation of distortion with σ, as was done in figures 2 and 3; similarly the tangential and sagittal field curvature ($\rho=0$, $\phi=0$ and $\pi/2$) could be shown as a function of the field size σ, and so on. For a system whose aberrations are uncorrected, each of these curves will be of the form shown in figure 4(a), the aberration increasing progressively with aperture ρ or field size σ. For such a system the obviously necessary sampling points are at zero and the maximum values of the varying parameters: that is to say one would trace a paraxial ray, a principal ray, with its associated astigmatism calculation, at the maximum field size σ, and full aperture rays through the axial object point and at the maximum field size. When, in the first stage of optical design, suitable amounts of the primary aberrations are introduced to balance the higher order aberrations present, the various aberration curves will take the form of figure 4(b). At this stage a reasonably full description

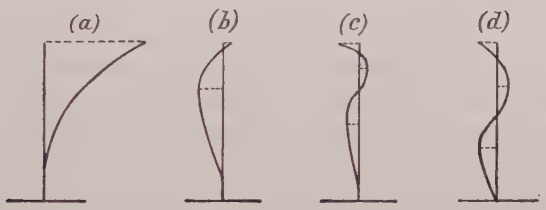

Figure 4.

of the aberrations of the system will require the tracing of rays not only at zero and the extreme values of the aperture and field, but also at intermediate ones, corresponding to the maximum bulge in figure 4(b); that is to say rays will be required at zero, full and an appropriate intermediate aperture both at zero, full, and an intermediate field size; in some systems, where no possibility exists of correcting the skew aberrations, rays will be traced only in a meridian plane ($\phi=0$); in more highly corrected systems a corresponding set will be traced in secondary planes ($\phi=\pi/2$). For systems more highly corrected still, rays would be necessary for further values of ϕ.

In systems for which a reduction of the higher order aberrations is possible, the first stages of this reduction generally lead to a flattening of curve 4(b) without change of its form, but in some cases it is possible to reduce to zero at any rate some of the aberrations for the full and the chosen intermediate value of the parameter, the curve then generally taking the form of figure 4(c). To determine the form of the aberration in this case, rays at new sampling points corresponding to values of the varying parameter near the two bulges are required. In highly corrected lenses a correction of this form is sometimes attainable for a number of the aberration curves; it can often be achieved for axial spherical aberration and in lenses of large field angle this form of correction may be obtained for both

sagittal and tangential field curvature, distortion and coma. A further complication is that the curves for different aberrations may have maxima at significantly different values of a parameter; for example, in a wide-angle lens with sagittal and tangential field curvatures of the form of figure 1(*c*), the effective distortion curve, which is not normal to the axis of abscissae at the origin, may have the form of curve 4(*d*), requiring additional sampling values of σ to determine its maxima.

For the designer using traditional methods, information is obtained of the state of correction at successive stages of the design, the change in form of the aberration curves is generally obvious, and the ray sampling points are adjusted accordingly. For a completely automatic machine process of design starting from an uncorrected form the necessary programming to determine the most significant sampling points would appear to present considerable problems if the number of rays traced at each stage is not to be very large.

(*b*) *Pupil aberrations.*

The entrance pupil of an optical system, which is the image of the physical stop formed by the part of the lens between this stop and the object, is itself subject to aberrations; these are normally not corrected and they may be large, being sometimes deliberately made so, for example to increase marginal illumination. The normal procedure in lens designing is initially to assume the entrance pupil to be aberration-free; a ray at the full aperture required from an axial object point is then traced, together with rays at each of the required field angles through the centre and at the full aperture of the Gaussian image of the physical stop. Such a set of rays is indicated in figure 5, M being a full aperture axial ray and A_1 P_1 Z_1 A_2 P_2 Z_2 rays at two obliquities, the entrance pupil being shown

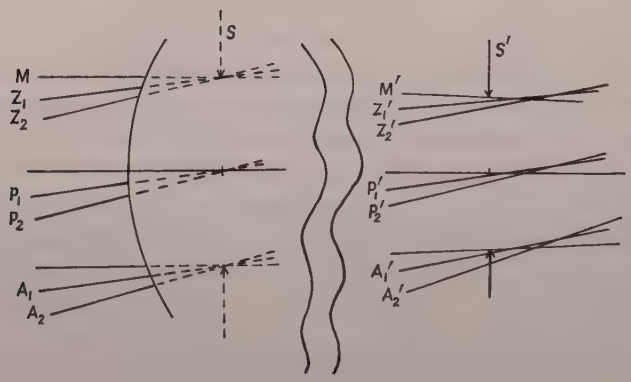

Figure 5.

by the dotted lines S. In general when these rays are traced to the space containing the physical stop S′, where the rays are indicated as P_1', P_2' etc., P_1' and P_2' will not pass through the centre, nor A_1', Z_1', A_2', Z_2' through the edge of the physical stop. From the pupil aberrations found by the ray-tracing new incident ray coordinates are calculated, a Gaussian approximation usually being sufficient, to give incident ray pencils which pass appropriately through the stop. For a fully automatic design programme on a computer making very considerable

changes to the lens form, this procedure would have to be programmed and repeated at intervals in the design process.

(*c*) *Vignetting.*

The discussion hitherto has assumed that the lenses permit the passage at each field angle of the full cone of light passed by the main aperture stop. In many lenses this is not the case, pencils at the larger field angles being restricted by the diameter of lens mountings or by vignetting apertures before and behind the axial aperture stop. For most common forms of lens this is necessary to secure an adequate performance, the full aperture pencils at the larger field angles being very heavily aberrated. For some relatively simple forms of lens the large aperture oblique correction may be so bad as to make it desirable to secure the maximum degree of vignetting attainable by restricting the diameter of both the front and the back lens to the minimum required to transmit the full aperture axial pencil; in this case the problem of specifying ray coordinates is fairly simple. But for better corrected lenses the determination of the best form of vignetting is of considerable complexity; a discussion of some of the problems, ignoring the effects of stop aberrations, was given by Wynne (1944). In general, if for a pencil at a particular field angle some determined degree of vignetting is required to give adequate performance, this may be achieved by vignetting stops of suitable diameter located over a range of positions before and behind the main stop; the effect of choosing these vignetting apertures nearer to the main stop is that the degree of vignetting at smaller field angles is increased, while that at larger angles is reduced, and vice versa for vignetting apertures further from the main stop. The determination of the optimum vignetting aperture positions and sizes therefore requires a consideration of the whole aberration characteristics of the lens; and for any choice of vignetting apertures the effective entrance-pupil through which the incident rays must be appropriately directed is formed by the superposition in the object space of the images of at least three physical stops, each having different aberrations. Once again a completely automatic machine programme to deal with the problem would present considerable difficulties.

References

Slussareff, G., 1941, *J. Phys., Moscow*, **4**, 537.
Smith, T., 1915, *Proc. Phys. Soc., Lond.*, **27**, 502.
—— 1918, *Ibid.*, **30**, 221.
Wynne, C. G., 1944, *Proc. Phys. Soc.*, **56**, 366.
—— 1953, *British Patent Specification* No. 689, 916.
—— 1959, *Proc. Phys. Soc.*, **73**, 777.

The Matrix Elements of Tensor Operators for the Electronic Configurations f^n

By B. R. JUDD†
The Clarendon Laboratory, University of Oxford

MS. received 20*th March* 1959

Abstract. It is shown that many simple relations exist between various reduced matrix elements of the form $(f^n\, WUSL \,||\, U^k \,||f^n\, W'U'SL')$, where $W=(w_1w_2w_3)$ and $U=(u_1u_2)$ are irreducible representations of R_7 and G_2 respectively. This is done by using the fact that for $k=2$, 4 and 6, the components $U_q{}^k$ of the tensor operators $\mathbf{U}^k$, when multiplied by $\sqrt{(2k+1)}$, transform among themselves as the irreducible representations (200) of R_7 and (20) of G_2. The number of linearly independent sets of matrix elements for a given W and W' is equal to the number of times the identity representation (000) of R_7 occurs in the reduction of the product $(w_1w_2w_3)\times(200)\times(w_1'w_2'w_3')$; similarly, the number of times the identity representation (00) of G_2 occurs in the reduction of the product $(u_1u_2)\times(20)\times(u_1'u_2')$ determines the number of linearly independent sets of matrix elements that can exist with $U=(u_1u_2)$ and $U'=(u_1'u_2')$. These two numbers, which are denoted by $c(WW'(200))$ and $c(UU'(20))$, are tabulated for all W, W', U and U' which occur in f^n, and the use of the tables in calculating the splittings induced in the levels of rare earth ions by the surrounding crystal lattice is illustrated with a number of examples.

§ 1. Introduction

An extremely common problem in quantum mechanics is the evaluation of matrix elements of the type $(A_i\,|\,H_j\,|\,B_k)$. Sometimes it is known how A_i, H_j and B_k transform under the operations of a group $\mathcal{G}$. For simplicity, we shall restrict our attention to those cases where the states $A_i\,(1\leqslant i\leqslant a)$ and $B_k\,(1\leqslant k\leqslant b)$ span the respective irreducible representations Γ_A and Γ_B of dimensions a and b, and where the operator components H_j $(1\leqslant j\leqslant h)$ transform like the h-dimensional irreducible representation Γ_H. Other matrix elements $(A_i^{(n)}\,|\,H_j^{(n)}\,|\,B_k^{(n)})$ can often be constructed with states $A_i^{(n)}$ and $B_k^{(n)}$ which also span the same irreducible representations Γ_A and Γ_B of $\mathcal{G}$, and with operator components $H_j^{(n)}$ which transform like Γ_H. We shall suppose that a one-to-one correspondence exists between the quantities A_i, H_j, B_k and $A_i^{(n)}$, $H_j^{(n)}$, $B_k^{(n)}$; for example, the matrices describing how the states A_i transform among themselves under the operations of $\mathcal{G}$ are identical to the matrices for the states $A_i^{(n)}$. The following theorem is central to the present paper: if the identity representation Γ_1 occurs x times in the reduction of the product $\Gamma_A\times\Gamma_H\times\Gamma_B$, it is not possible to construct $x+1$ sets of matrix elements $(A_i^{(n)}\,|\,H_j^{(n)}\,|\,B_k^{(n)})$, each set comprising *ahb* matrix elements, such that every set is linearly independent of every other set. In other words, any set of matrix elements can be expressed as a linear combination

† Now at the Radiation Laboratory, University of California, Berkeley 4.

of x independent sets, i.e. constants g_n can always be found such that

$$(A_i|H_j|B_k)=\sum_{n=1}^{x} g_n\,(A_i^{(n)}|H_j^{(n)}|B_k^{(n)}) \qquad \ldots\ldots(1)$$

for all i, j and k. This result may be proved for finite groups by first constructing the various functions involved in evaluating the matrix elements, and then setting up the linear combinations of these functions which transform as the irreducible representations contained in the reduction of $\Gamma_A \times \Gamma_H \times \Gamma_B$. The coefficients of the functions are determined by group-theoretical considerations alone. When we integrate over all space, only those linear combinations which transform like Γ_1 are non-zero; hence we obtain $ahb - x$ equations relating the matrix elements of a set to one another, and the x degrees of freedom left are expressed in an equivalent way by (1). The theorem is equally true for continuous groups; see, for example, Weyl (1928, p. 158, or 1931, p. 177).

Before applying the theorem to obtain relations between the matrix elements of tensor operators, it might clarify matters to discuss a simple case which has recently arisen in the theory of paramagnetic resonance (Bleaney 1959a, b). When a paramagnetic ion is situated in a cubic lattice, it sometimes happens that the ground state is a quadruplet. In Bethe's (1929) notation, the four states form a basis for the irreducible representation Γ_8 of the cubic group. The question arises as to whether the matrix elements of the term $\beta\mathbf{H}.\Sigma_i(\mathbf{l}_i+2\mathbf{s}_i)$ in the Hamiltonian can be reproduced by an operator between states with an effective spin $S=\frac{3}{2}$. (In this expression, $\mathbf{H}$ stands for the magnetic field.) These states also form a basis for Γ_8, so one requirement is satisfied. Now $\Sigma(\mathbf{l}_i+2\mathbf{s}_i)$ is a vector, and transforms like Γ_4; in addition it can be shown that Γ_1 occurs twice in the reduction of $\Gamma_8\times\Gamma_4\times\Gamma_8$, so we have a case of $x=2$. The three components S_x^p, S_y^p and S_z^p transform like Γ_4 when p is an odd integer; hence the matrix elements of $\beta\mathbf{H}.\Sigma(\mathbf{l}_i+2\mathbf{s}_i)$ between the various states of the quadruplet can be reproduced by the expression

$$\beta H_x(gS_x^p+fS_x^q)+\beta H_y(gS_y^p+fS_y^q)+\beta H_z(gS_z^p+fS_z^q)$$

between states of effective spin $\frac{3}{2}$, provided p and q are odd (and unequal) and g and f are suitably chosen. In selecting $p=1$ and $q=3$, Bleaney (1959*a*, *b*) puts the 'spin-Hamiltonian' in its most convenient form.

§ 2. Irreducible Tensor Operators

The irreducible tensor operator $\mathbf{T}^k$ is defined as a set of $2k+1$ operators T_q^k, where $q=k, k-1, \ldots, -k$, which transform like the spherical harmonics Y_k^q. Tensor operators are of fundamental importance, for many interactions which arise in atomic and nuclear physics can be expressed in terms of them. Our present interest in them derives from a desire to calculate the splittings induced in the levels of a rare earth ion when the ion is situated in a crystal lattice; for it is convenient to expand the electric potential in which the 4f-electrons of the rare earth ion move in a series of spherical harmonics. The problem is therefore to calculate matrix elements of the form

$$(f^n\tau SLJJ_z|U_q^k|f^n\tau' SL'J'J_z'),$$

where S, L, J and J_z have their usual meanings, τ stands for additional quantum numbers which may be necessary to specify a state, and where the tensor operator

$\mathbf{U}^k$ is the sum of the n single particle operators $\mathbf{u}^k$ for which

$$(f\,||\,u^k\,||\,f)=1.$$

Racah (1949) has shown that by classifying the states according to the irreducible representations W and U of the groups R_7 and G_2 respectively, an immense simplification is achieved. In fact, for terms of the highest and next-to-highest multiplicities in the configurations f^n, the quantum numbers $f^n\,WUSLJJ_z$ uniquely specify a state.

From Elliott, Judd and Runciman (1957), with a slight change of notation,

$$(f^n\,\tau\,SLJJ_z\,|\,U_q^k\,|f^n\,\tau'\,S'L'J'J_z')$$
$$=\delta(S,S')(-1)^{J-J_z}\begin{pmatrix} J & k & J' \\ -J_z & q & J_z' \end{pmatrix}(f^n\,\tau\,SLJ\,||\,U^k\,||f^n\,\tau'\,SL'J'), \qquad \ldots\ldots(2)$$

where

$$(f^n\,\tau\,SLJ\,||\,U^k\,||f^n\,\tau'\,SL'J')$$
$$=(-1)^{S+k+J+L'}[(2J+1)(2J'+1)]^{1/2}\begin{Bmatrix} L & J & S \\ J' & L' & k \end{Bmatrix}(\psi\,||\,U^k\,||\psi'), \qquad \ldots\ldots(3)$$

and

$$(\psi\,||\,U^k\,||\psi')$$
$$=n\sum_{\bar{\psi}}(\psi\{|\bar{\psi})(\psi'\{|\bar{\psi})(-1)^{L+k+3+L}[(2L+1)(2L'+1)]^{1/2}\begin{Bmatrix} 3 & L & \bar{L} \\ L' & 3 & k \end{Bmatrix}. \qquad \ldots\ldots(4)$$

The symbol ψ stands for the set of quantum numbers τSL. The only difficult step in this procedure is the last. The fractional parentage coefficients $(\psi\{|\bar{\psi})$ must be constructed from the table of Racah (1949), and the sum over the parent states can be very tedious. It is the purpose of the present paper to show that extremely simple relations hold between many of the reduced matrix elements $(\psi\,||\,U^k\,||\,\psi')$ of different configurations, so that the summation in (4) can often be avoided.

§ 3. Representations

In order to apply the theorem expressed by (1), we must examine the transformation properties of the states and the operators U_q^k. Under rotations in three-dimensional space, the $2J+1$ states $|J,\,J_z\rangle$ transform as the irreducible representation $\mathfrak{D}_J$ of R_3, while the components of $\mathbf{U}^k$ transform like $\mathfrak{D}_k$. In evaluating $(f^n\,\tau\,SLJJ_z\,|\,U_q^k\,|f^n\,\tau'\,SL'J'J_z')$, we therefore investigate $\mathfrak{D}_J\times\mathfrak{D}_k\times\mathfrak{D}_{J'}$. The identity representation $\mathfrak{D}_0$ occurs once only in the reduction of this product, but this knowledge is not of any value to us since it merely gives a group-theoretical reason for the existence of equation (2). However, we obtain non-trivial results when we examine how the states and operators transform under rotations in the seven-dimensional space spanned by the states $l_z=3,\,2,\,\ldots,\,-3$ of a single f-electron. The irreducible representations of R_7 are described by three integral numbers $W=(w_1\,w_2\,w_3)$ satisfying

$$w_1\geqslant w_2\geqslant w_3\geqslant 0. \qquad \ldots\ldots(5)$$

Racah (1949) has observed that under rotations in R_7 the quantities $\sqrt{(2k+1)}\,U_q^k$

for $k=2, 4, 6$ and all permissible values of q transform according to the irreducible representation (200) of R_7. This simple result is of great use, since it is precisely these values of k which are required in applications of the theory (see Judd 1957, 1959 b). On performing the reduction $R_7 \rightarrow G_2$, an irreducible representation of R_7 breaks up into a number of irreducible representations of G_2. The latter are described by two integers $U=(u_1 u_2)$ satisfying

$$u_1 \geqslant u_2 \geqslant 0. \qquad \ldots\ldots (6)$$

It is particularly fortunate that (200) breaks up into the single irreducible representation (20) of G_2, for we can now consider the three tensors $\mathbf{U}^2$, $\mathbf{U}^4$ and $\mathbf{U}^6$ as transforming like either (200) or (20) as we please.

The first problem is to determine how many times the identity representation (000) of R_7 occurs in the reduction of

$$(w_1 w_2 w_3) \times (200) \times (w_1' w_2' w_3').$$

This number, which is obviously the same as the number of times $(w_1' w_2' w_3')$ occurs in the reduction of $(w_1 w_2 w_3) \times (200)$, will be denoted by $c(WW'(200))$. We may proceed in either of two ways :

(i) A rather indirect, but sometimes very rapid, method is to form the product of the Young tableaux $[w_1 w_2 w_3]$ and [2] after the manner described by Littlewood (1950, p. 94). In the present case this consists of adding two cells to the tableau $[w_1 w_2 w_3]$ in every way possible such that the final tableau is standard and the two additional cells are not in the same vertical column. For example,

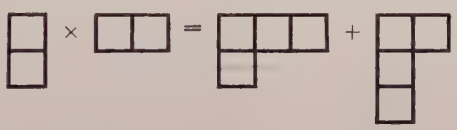

In symbols:

$$[11] \times [2] = [31] + [211].$$

We can apply a dimension check by using table 3 of Flowers (1952):

$$21 \times 28 = 378 + 210.$$

The Young tableaux describe irreducible representations of the unitary group in seven dimensions U_7, and the branching rules for $U_7 \rightarrow R_7$ may be obtained either from Littlewood (1950, p. 240) or from table 6 of Flowers (1952). Thus, for the present example,

$$(110) \times \{(200) + (000)\} = (310) + (200) + (110) + (211) + (110).$$

But

$$(110) \times (000) = (110),$$

and by subtraction,

$$(110) \times (200) = (310) + (200) + (110) + (211). \qquad \ldots\ldots (7)$$

We can immediately apply a dimension check with the aid of table 4 of Flowers (1952):

$$21 \times 27 = 330 + 27 + 21 + 189.$$

(ii) Weyl (1926, p. 389) has given a general formula for the characters of a semi-simple group, and it may be adapted to deal with the present case. We use a theorem due to the same writer (Weyl 1946, p. 229) to obtain the final result

$$(w_1w_2w_3)\times(200)=2(w_1w_2w_3)+\sum(w_1+x,\ w_2+y,\ w_3+z). \quad \ldots\ldots(8)$$

The sum runs over all integral values of x, y and z satisfying

$$|x|+|y|+|z|\leqslant 2.$$

Because negative values of x, y and z are allowed, irreducible representations of R_7 sometimes occur in the sum which do not satisfy (5). In these cases the following equivalences may be used :

$$\left.\begin{aligned}(w_1w_2w_3)&=-(w_2-1,w_1+1,w_3)=-(w_1,w_3-1,w_2+1),\\(w_1,w_2,-1)&=-(w_1,w_2,0),\\(w_1,w_2,-2)&=-(w_1,w_2,1).\end{aligned}\right\}\quad\ldots\ldots(9)$$

We observe that $(w_1,\ w_1+1,\ w_3)$, $(w_1,\ w_2,\ w_2+1)$ and $(w_1,\ w_2,\ w_1+2)$ are null representations. The required numbers $c(WW'(200))$ are set out in table 1 for all irreducible representations occurring in the configuration f^n.

Table 1. The Numbers $c(WW'(200))$

	(000)	(100)	(110)	(200)	(111)	(210)	(211)	(220)	(221)	(222)
(000)	–	–	–	1	–	–	–	–	–	–
(100)	–	1	–	–	–	1	–	–	–	–
(110)	–	–	1	1	–	–	1	–	–	–
(200)	1	–	1	1	–	–	–	1	–	–
(111)	–	–	–	–	1	1	1	–	–	–
(210)	–	1	–	–	1	2	–	–	1	–
(211)	–	–	1	–	1	–	2	1	1	–
(220)	–	–	–	1	–	–	1	1	–	1
(221)	–	–	–	–	–	1	1	–	2	1
(222)	–	–	–	–	–	–	–	1	1	1

§ 4. The Group G_2

We have now to carry out an analogous treatment for G_2. The number of times (00) occurs in the reduction of the product

$$(u_1u_2)\times(20)\times(u_1'u_2')$$

will be denoted by $c(UU'(20))$. The method corresponding to (i) involves knowing the branching rules for $R_7\rightarrow G_2$. The special cases which have been given (Racah 1949) are not complete enough for the present purpose, and the following general rule was therefore derived:

$$(w_1w_2w_3)\rightarrow\sum[(i-k,j+k)+(j-k-1,i-j)],$$

where the sum extends over all integral values of i, j and k satisfying

$$w_1\geqslant i\geqslant w_2,\qquad w_2\geqslant j\geqslant w_3,\qquad w_3\geqslant k\geqslant -w_3.$$

Equations analogous to (9) are required when representations appear which are

not consistent with (6). They are

$$\left.\begin{aligned}(u_1u_2) &= -(u_2-1, u_1+1),\\ (u_1, -1) &= 0,\\ (u_1, -2) &= -(u_1-1, 0).\end{aligned}\right\} \qquad \ldots\ldots (10)$$

The dimension of (u_1u_2) may be obtained by using the general formula of Weyl (1926, p. 389). The result is

$$(u_1+2)(u_2+1)(u_1-u_2+1)(u_1+u_2+3)(u_1+2u_2+4)(2u_1+u_2+5)/120.$$

Equations (10) are consistent with this expression. The general method will be illustrated by an example. From (7),

$$\{(10)+(11)\}\times(20) = (31)+(30)+(21)+(20)+(10)+(11)$$
$$+(30)+(21)+(20)+(11)+(10).$$

By subtracting

$$(10)\times(20) = (30)+(21)+(20)+(11)+(10),$$

which itself can be obtained by considering $(100)\times(200)$, we obtain

$$(11)\times(20) = (31)+(30)+(21)+(20)+(10)+(11).$$

The dimension check is

$$14\times 27 = 189+77+64+27+7+14.$$

For irreducible representations of G_2 of high dimensionality, this process becomes lengthy, and it is more convenient to use the analogue of (8). It can be found by a similar method and is

$$(u_1u_2)\times(20) = (u_1u_2) + \sum(u_1+x, u_2+y).$$

The summation runs over all integral values of x and y which satisfy

$$|x|\leqslant 2, \qquad |y|\leqslant 2, \qquad |x+y|\leqslant 2,$$

with the additional proviso that the terms in the sum for which

$$|x|\leqslant 1, \qquad |y|\leqslant 1, \qquad |x+y|\leqslant 1$$

occur twice. The numbers $c(UU'(20))$ are collected in table 2. Both tables 1 and 2 must obviously be symmetrical, and since they have been constructed row by row, all off-diagonal numbers are automatically checked.

Table 2. The Numbers $c(UU'(20))$

	(00)	(10)	(11)	(20)	(21)	(30)	(22)	(31)	(40)
(00)	–	–	–	1	–	–	–	–	–
(10)	–	1	1	1	1	1	–	–	–
(11)	–	1	1	1	1	1	–	1	–
(20)	1	1	1	2	2	1	1	1	1
(21)	–	1	1	2	2	2	1	2	1
(30)	–	1	1	1	2	2	1	2	1
(22)	–	–	–	1	1	1	1	1	1
(31)	–	–	1	1	2	2	1	3	2
(40)	–	–	–	1	1	1	1	2	2

§ 5. Application of the Tables

The general technique can probably best be described by means of examples. From table 1, we see that (200) occurs once only in the reduction of $(111)\times(111)$. Hence (000) occurs only once in the reduction of $(111)\times(200)\times(111)$. The terms of maximum multiplicity of f^3, namely ^4S, ^4D, ^4F, ^4G and ^4I belong to (111). This result can be obtained from the tables of Racah (1949), of Flowers (1952), or of Elliott *et al.* (1957). Hence a constant Ω exists such that

$$(f^n(111)U^{2S+1}L||U^k||f^n(111)U'^{2S+1}L') = \Omega(f^3(111)U^4L||U^k||f^3(111)U'^4L') \quad \ldots\ldots(11)$$

for all U, U', L and L' consistent with the existence of the states in question and for $k=2$, 4 and 6. The reduced matrix elements on the right-hand side of (11) have been tabulated by Judd (1959 a). Suppose we wish to investigate the crystal splittings of the terms of maximum multiplicity of $Pm^{3+}4f^4$. We set $n=4$, $S=2$ in (11) and use (4) once to find Ω. In fact $\Omega=-1$ for this case. (It might be mentioned in passing that the equation $\Omega^2=1$ could be obtained by finding the eigenvalues of an operator formed by subtracting Casimir's operator for R_7 from an analogous operator for U_7. This operator is given explicitly in equation (15) of Judd (1959 a).) The summation in (4) is thus completely avoided for the remaining $3\times5^2-1=74$ reduced matrix elements. (The saving of labour is not quite as great as this figure implies, for a number of matrix elements are obviously zero when the triangular conditions for the non-vanishing of the 6-j symbols in (4) are not satisfied.) Again, for $n=6$, $S=2$, we find $\Omega=-\frac{1}{3}$. This result would be required in an investigation of the excited states of Eu^{3+} or Am^{3+}.

Table 2 can lead to equally powerful results. For example, (00) occurs once only in the reduction of $(10)\times(20)\times(21)$, and therefore a constant Ω' exists such that

$$(f^nW(10)^{2S+1}\mathrm{F}||U^k||f^nW'(21)^{2S+1}L') = \Omega'(f^3(100)(10)^2\mathrm{F}||U^k||f^3(210)(21)^2L')$$

for all allowed values of L', and for $k=2$, 4 and 6. The symbol F denotes a state with $L=3$. When $n=6$, $S=2$, $W=(111)$ and $W'=(210)$, we find $\Omega'=\sqrt{\frac{1}{2}}$. Again, the equation

$$(f^6(210)(20)^5L||U^k||f^6(210)(20)^5L') = \tfrac{2}{3}(f^3(111)(20)^4L||U^k||f^3(111)(20)^4L') + \tfrac{2}{3}(f^3(210)(20)^2L||U^k||f^3(210)(20)^2L')$$

for k, L, $L'=2$, 4 or 6 (in any combination) exists in virtue of the fact that (00) occurs twice in the reduction of $(20)\times(20)\times(20)$.

Certain simple results for the configurations f and f^2 make themselves felt in more complex configurations. Since

$$(f(100)(10)^2\mathrm{F}||U^k||f(100)(10)^2\mathrm{F})=1,$$

and since (00) occurs once only in the reduction of $(10)\times(20)\times(10)$, the reduced matrix elements

$$(f^nW(10)^{2S+1}\mathrm{F}||U^k||f^nW'(10)^{2S+1}\mathrm{F})$$

will always be independent of k (provided k is even).

Since all the fractional parentage coefficients $(f^2\{|f)$ are unity, we obtain from (4)

$$(f^2(200)(20)^1L||(2k+1)^{1/2}U^k||f^2(200)(20)^1L')$$
$$=2[(2L+1)(2k+1)(2L'+1)]^{1/2}\begin{Bmatrix} L & k & L' \\ 3 & 3 & 3 \end{Bmatrix}. \qquad \ldots\ldots(12)$$

The right-hand side is symmetrical with respect to any interchange of L, k or L'. It is sufficient to remark that

$$(f^3(111)(20)^4L||(2k+1)^{1/2}U^k||f^3(111)(20)^4L')$$

shares the same property and that (00) occurs twice in the reduction of $(20)\times(20)\times(20)$ to prove in general that

$$(f^nW(20)^{2S+1}L||(2k+1)^{1/2}U^k||f^nW'(20)^{2S+1}L')$$
$$=(f^nW(20)^{2S+1}k||(2L+1)^{1/2}U^L||f^nW'(20)^{2S+1}L')$$

for $k=2$, 4 or 6.

We shall conclude this discussion by giving an example which can be expressed directly in terms of experimental observations. Consider the levels $^6P_{3/2}$ and $^6F_{3/2}$ of $Dy^{3+}4f^9$. To discover how these levels split up when a dysprosium ion is situated in a crystal lattice, we set up the two 4×4 matrices spanned by the states $J_z=\frac{3}{2}$, $\frac{1}{2}$, $-\frac{1}{2}$, $-\frac{3}{2}$. The perturbation can be represented by $\sum A_k{}^qU_q{}^k$, where the constants $A_k{}^q$ depend on the particular environment of the ion. Because all the relevant matrix elements are between states of the same parity, terms in the summation for odd k can be discarded. The term $k=0$ may also be dropped, since it does not affect the splittings of the levels. The 3-j symbol in (2) vanishes unless J, k and J' form a triangle; hence we need only concern ourselves with $k=2$. From (2) it is apparent that every element of the matrix for $^6F_{3/2}$ stands to the corresponding element of the matrix for $^6P_{3/2}$ as $(f^9\tau^6F_{3/2}||U^2||f^9\tau^6F_{3/2})$ stands to $(f^9\tau'^6P_{3/2}||U^2||f^9\tau'^6P_{3/2})$, since the factors

$$\begin{pmatrix} \frac{3}{2} & 2 & \frac{3}{2} \\ -J_z & q & J_z' \end{pmatrix}A_2{}^q$$

multiplying the reduced matrix elements will occur in both matrices. A theorem of Kramers (1930) assures us that the 4×4 secular determinants formed from these matrices will give a pair of doubly degenerate levels; and from what has already been said we see that the ratio of the splittings of $^6F_{3/2}$ and $^6P_{3/2}$ is

$$R=\frac{(f^9(110)(10)^6F_{3/2}||U^2||f^9(110)(10)^6F_{3/2})}{(f^9(110)(11)^6P_{3/2}||U^2||f^9(110)(11)^6P_{3/2})},$$

where the symbols τ and τ' have been replaced by the appropriate WU classifications. From (3),

$$R=\frac{\begin{Bmatrix} 3 & \frac{3}{2} & \frac{5}{2} \\ \frac{3}{2} & 3 & 2 \end{Bmatrix}(f^9(110)(10)^6F||U^2||f^9(110)(10)^6F)}{\begin{Bmatrix} 1 & \frac{3}{2} & \frac{5}{2} \\ \frac{3}{2} & 1 & 2 \end{Bmatrix}(f^9(110)(11)^6P||U^2||f^9(110)(11)^6P)}.$$

Now (000) occurs once only in the reduction of $(110)\times(200)\times(110)$, and hence

$$R=\frac{\begin{Bmatrix}3 & \frac{3}{2} & \frac{5}{2}\\ \frac{3}{2} & 3 & 2\end{Bmatrix}(f^2(110)(10)^3\mathrm{F}\|U^2\|f^2(110)(10)^3\mathrm{F})}{\begin{Bmatrix}1 & \frac{3}{2} & \frac{5}{2}\\ \frac{3}{2} & 1 & 2\end{Bmatrix}(f^2(110)(11)^3\mathrm{P}\|U^2\|f^2(110)(11)^3\mathrm{P})}$$

$$=\begin{Bmatrix}3 & \frac{3}{2} & \frac{5}{2}\\ \frac{3}{2} & 1 & 2\end{Bmatrix}7\begin{Bmatrix}3 & 2 & 3\\ 3 & 3 & 3\end{Bmatrix}\Big/\begin{Bmatrix}1 & \frac{3}{2} & \frac{5}{2}\\ \frac{3}{2} & 1 & 2\end{Bmatrix}3\begin{Bmatrix}1 & 2 & 1\\ 3 & 3 & 3\end{Bmatrix}.$$

The last step can be easily made, since the reduced matrix elements for f^2 may be immediately written down in the same manner as (12). Using the tables of Biedenharn (1952) to evaluate the 6-j symbols, we find

$$R=-\tfrac{1}{3}.$$

To first-order in perturbation theory we therefore conclude that the separation between the two doublets of $^6\mathrm{P}_{3/2}$ is three times the corresponding separation for $^6\mathrm{F}_{3/2}$, and that either level is inverted with respect to the other. This result is independent of the nature of the crystal lattice. Dieke and Singh (1956) have carried out an investigation of the absorption and fluorescence spectra of $\mathrm{DyCl_3}.6\mathrm{H_2O}$. They claim to have observed the level $^6\mathrm{P}_{3/2}$, but the present writer considers that it is much more likely to be $^6\mathrm{F}_{3/2}$ from its position in the spectrum. It would be out of place here to discuss the problem of identifying levels in a complex spectrum; the point of the above analysis is to illustrate the theory for a simple case and show how it has a direct bearing on actual observations. When experiments on other dysprosium crystals have been performed it might be possible to test the value of R; at any rate it should be of service in distinguishing the levels $^6\mathrm{P}_{3/2}$ and $^6\mathrm{F}_{3/2}$.

§ 6. Conclusion

If we wish to examine the splittings induced by a crystalline electric field in the levels of a rare earth or actinide ion, the procedure is first to discover whether states of the same W or U occur in f, f^2, or f^3. If they do, then we examine tables 1 and 2 to see how we can make the best use of the results for these fairly simple configurations. But even if they do not, we might nevertheless find it easier to perform the summations (4) for configurations where the terms corresponding to the ones we are interested in have fewer parents. The question as to whether closed expressions exist for (4) has not yet been answered, though several comments on the problem have been made by Judd (1959 a). It is clear that the general technique could be extended to the configurations d^n, since in the five-dimensional space spanned by the states $l_z=-2,\ -1,\ 0,\ 1$ and 2 of a single d-electron, $\sqrt{5}\,\mathbf{U}^2$ and $3\,\mathbf{U}^4$ transform like the irreducible representation (20) of R_5. An extension in another direction would be an investigation of the tensor operators of odd rank. This would be of considerable mathematical interest, since these operators form a complete set of operators for the group R_7.

References

Bethe, H., 1929, *Ann. Phys., Lpz.*, **3**, 133.
Biedenharn, L. C., 1952, *Tables of the Racah Coefficients*, ORNL 1098.
Bleaney, B., 1959 a, *Proc. Phys. Soc.*, **73**, 937.
—— 1959 b, *Ibid.*, **73**, 939.
Dieke, G. H., and Singh, S., 1956, *J. Opt. Soc. Amer.*, **46**, 495.
Elliott, J. P., Judd, B. R., and Runciman, W. A., 1957, *Proc. Roy. Soc.* A, **240**, 509.
Flowers, B. H., 1952, *Proc. Roy. Soc.* A, **210**, 497.
Judd, B. R., 1957, *Proc. Roy. Soc.* A, **241**, 414.
—— 1959 a, *Ibid*, **250**, 562.
—— 1959 b, *Ibid*, **251**, 134.
Kramers, H. A., 1930, *Proc. Acad. Sci. Amst.*, **33**, 959.
Littlewood, D. E., 1950, *The Theory of Group Characters* (Oxford : University Press).
Racah, G., 1949, *Phys. Rev.*, **76**, 1352.
Weyl, H., 1926, *Math. Z.*, **24**, 377.
—— 1928, 1931, *Gruppentheorie und Quantenmechanik* (Leipzig: Hirzel Verlag).
—— 1946, *The Classical Groups* (Princeton : University Press).

The Meissner Effect, Gauge Invariance and Electron Correlations

By G. L. SEWELL
Mathematical Institute, The University, Liverpool

Communicated by H. Fröhlich; *MS received* 18*th March* 1959

Abstract. A perturbative method, which is gauge invariant in infinite order, is employed to investigate whether the Bardeen, Cooper and Schrieffer–Bogoliubov treatment of the theory of superconductivity leads to the Meissner effect. It is found that the theory does not reveal, in any finite order of perturbation, the long range correlations between the electronic momenta that are necessary for the Meissner effect.

§ 1. Introduction and Summary

The experimental discovery of the isotope effect has led to the belief that the basic properties of the superconducting state should be derivable from a suitable theoretical treatment of Fröhlich's phonon–electron model (1952). The recent approaches to a microscopic theory of superconductivity, due to Bardeen, Cooper and Schrieffer (1957, to be referred to as BCS) and Bogoliubov (1958), have both been based on methods in which Fröhlich's Hamiltonian H is split into two parts:

$$H = H_0 + H'. \qquad \ldots\ldots (1.1)$$

In these treatments it was attempted to interpret the main properties of the superconducting state in terms of H_0, the other part H' being regarded as a small correction. This procedure led to a satisfactory theory of the thermal properties of superconductors.

On the other hand, this same treatment has led to difficulties in connection with the theory of the Meissner effect. Here one is concerned with the response of the system to an applied magnetic field. The Hamiltonian for Fröhlich's model in the presence of such a field may be written as

$$H + H_{\mathfrak{f}}, \qquad \ldots\ldots (1.2)$$

the part $H_{\mathfrak{f}}$ being due to the field. The derivations of the Meissner effect by Rickayzen (1958), who used Bogoliubov's method, and by BCS, were based on the replacement of H by H_0 in (1.2). Thus, the magnetic properties of the model were investigated on the basis of the Hamiltonian

$$H_0 + H_{\mathfrak{f}}. \qquad \ldots\ldots (1.3)$$

In addition, the applied field was represented by a transversely gauged vector potential. It is the replacement of (1.2) by (1.3) which renders these derivations doubtful. The reason for this is that, while the former Hamiltonian is gauge invariant, the latter one is not (cf. Schafroth 1958).

Apart from this criticism, the above approaches are unsatisfactory in so far as they fail to come to grips with the very feature of the superconducting state which can be regarded as being responsible for the Meissner effect—namely, the long range of the correlations between the electronic momenta. This can be seen if,

following Schafroth (1951), we express the relationship between the applied magnetic field, given by the vector potential $\mathbf{A}(\mathbf{x})$, and the resultant equilibrium current $\mathbf{J}(\mathbf{x})$ in the form

$$\mathbf{J}(\mathbf{x}) = \int \mathbf{K}(\mathbf{x}-\mathbf{x}').\mathbf{A}(\mathbf{x}')\,d\mathbf{x}'. \qquad \ldots\ldots(1.4)$$

The tensor $\mathbf{K}$ may be expressed in the form (cf. Nakajima 1956)

$$\mathbf{K}(\mathbf{x}) = -\frac{N_0 e^2}{mc}\delta(x) + \frac{1}{c}\mathbf{C}(\mathbf{x}), \qquad \ldots\ldots(1.5)$$

where N_0 is the number of electrons per unit volume, and $\mathbf{C}$ is a tensor which represents the space-correlation between the electronic momenta. It is given by

$$\mathbf{C}(\mathbf{x}-\mathbf{x}') = \int_0^\beta \mathrm{Av}\,[\exp(\lambda H)\,\mathbf{j}(\mathbf{x}')\exp(-\lambda H)\,\mathbf{j}(\mathbf{x})]\,d\lambda, \qquad \ldots\ldots(1.6)$$

where

$$\beta = (\kappa T)^{-1}, \qquad \ldots\ldots(1.7)$$

where H, $\mathbf{j}$ denote the Hamiltonian and current density operator, respectively, for the model *in the absence of any applied field*, and Av denotes the thermal average at temperature T. Thus the magnetic properties of a model are given in terms of the space-correlation function $\mathbf{C}$, which is specified by the state of the system in the absence of the applied field.

These properties can be analysed in terms of the Fourier transforms of $\mathbf{K}(\mathbf{x})$, $\mathbf{C}(\mathbf{x})$, namely

$$\left.\begin{aligned} \mathbf{K}(\mathbf{p}) &= \int \mathbf{K}(\mathbf{x})\exp(-i\mathbf{p}.\mathbf{x})\,d\mathbf{x} \\ \text{and}\qquad \mathbf{C}(\mathbf{p}) &= \int \mathbf{C}(\mathbf{x})\exp(-i\mathbf{p}.\mathbf{x})\,d\mathbf{x}. \end{aligned}\right\} \qquad \ldots\ldots(1.8)$$

The requirements of isotropy and gauge invariance lead respectively to

$$\mathbf{K}(p^2) = p^2 f_1(p^2) - \mathbf{pp} f_2(p^2) \qquad \ldots\ldots(1.9)$$

and

$$f_1(p^2) = f_2(p^2) = f(p^2), \text{ say,} \qquad \ldots\ldots(1.10)$$

the f's being scalar functions of p^2. A simple criterion for the Meissner effect is that

$$\left.\begin{aligned} f(p^2) &= \frac{\alpha}{p^2} + f_r(p^2), \text{ for Meissner effect,} \\ \text{and}\qquad f(p^2) &= f_r(p^2), \quad \text{for no Meissner effect.} \end{aligned}\right\} \qquad \ldots\ldots(1.11)$$

Here α is a positive constant and f_r is a regular function of p^2. It now follows from (1.5), (1.8)–(1.11) that

$$\left.\begin{aligned} \mathbf{C}(\mathbf{p}) &= -c\alpha\hat{\mathbf{p}}\hat{\mathbf{p}} + \left(\alpha + \frac{N_0 e^2}{mc}\right) + c(p^2 - \mathbf{pp}) f_r(p^2) \\ \text{with}\qquad \hat{\mathbf{p}} &= \mathbf{p}/p \end{aligned}\right\} \qquad \ldots\ldots(1.12)$$

if the Meissner effect is to be exhibited. Only in this case does $\mathbf{C}(\mathbf{p})$ contain a term $\hat{\mathbf{p}}\hat{\mathbf{p}}$. This term is proportional to the Fourier transform of $\nabla\nabla(1/|\mathbf{x}|)$, a non-local function, whereas the remaining terms on the right-hand side of (1.12) are transforms of localized functions (e.g. $\delta(\mathbf{x})$). We may therefore regard the non-local nature of the electronic momenta correlations, as manifested by the term $\hat{\mathbf{p}}\hat{\mathbf{p}}$, as being the essential physical property responsible for the Meissner effect.

This property is necessarily overlooked in any non-gauge invariant theory in which a transverse gauge ($\mathbf{p}.\mathbf{A}(\mathbf{p})=0$ in Fourier representation) is used. For, in such a theory, it follows, by (1.9), that the current–field equation will still be given by (1.4), but with $\mathbf{K}(\mathbf{p})$ replaced by $p^2 f_1(p^2)$, the term $\mathbf{p}\mathbf{p} f_2(p^2)$ being irrelevant. It is only this latter term, however, which could possibly lead to a term $\hat{\mathbf{p}}\hat{\mathbf{p}}$, and one cannot obtain its form from that of f_1 in a non-gauge invariant theory, because of the violation of (1.10).

In the present paper we investigate the magnetic properties of the model, as treated by Bogoliubov, by means of a method which takes the part H' of the Hamiltonian into account and thereby restores gauge invariance. The essence of our method is that we use equations (1.1), (1.6) and (1.8) to express $\mathbf{C}(\mathbf{p})$ in terms of a perturbative expansion in H', i.e.

$$\mathbf{C}(\mathbf{p})=\sum_s \mathbf{C}_s(\mathbf{p}). \qquad \ldots\ldots (1.13)$$

This expansion renders our treatment exact in infinite order, and thus retrieves the gauge invariance of the model.

After performing the expansion (1.13), we examine the formulae for the $\mathbf{C}_s$'s to determine whether any of them possess a term $\hat{\mathbf{p}}\hat{\mathbf{p}}$. It is found that none of them do so, each term tending, as $p\to 0$, to a limit which is independent of the direction of $\mathbf{p}$. Hence we conclude that the method does not reveal the long range correlations, required for the Meissner effect, in any finite order of perturbation.

We have now two alternatives. Either (*a*) the series (1.13) is uniformly convergent or (*b*) it is not. If (*a*) is the correct alternative, then $\mathbf{C}(\mathbf{p})$ cannot possess a term $\hat{\mathbf{p}}\hat{\mathbf{p}}$, and the Bogoliubov treatment will not lead to a Meissner effect. This would mean that the apparent Meissner effect which appears in Rickayzen's treatment would be cancelled by perturbative effects when gauge invariance is restored.

If (*b*) is the correct alternative, then it is conceivable that $\mathbf{C}(\mathbf{p})$ possesses a term $\hat{\mathbf{p}}\hat{\mathbf{p}}$ even though the $\mathbf{C}_s$'s do not. Even in this case, however, the Bogoliubov theory could not be said to lead to a Meissner effect in a satisfactory manner, since a comprehensible theory of that effect must surely be one in which the required long range correlations could be seen to arise in zero or low order perturbation—i.e. could be seen to arise as a result of the properties of H_0, on which the theory of the superconducting state is based.

§ 2. The Model

In this section we shall summarize the relevant features of Fröhlich's phonon–electron model, as treated by Bogoliubov. The Hamiltonian for the model is

$$\mathscr{H}=\sum_{\mathbf{k},\sigma}\epsilon(\mathbf{k})\alpha^+_{\mathbf{k}\sigma}\alpha_{\mathbf{k}\sigma}+\sum_{\mathbf{q}}\omega(\mathbf{q})b^+_{\mathbf{q}}b_{\mathbf{q}} + \sum_{\mathbf{k}'=\mathbf{k}+\mathbf{q}} g\left(\frac{\omega(\mathbf{q})}{2V}\right)^{1/2}(\alpha^+_{\mathbf{k}\sigma}\alpha_{\mathbf{k}'\sigma}b^+_{\mathbf{q}}+\text{c.c.}). \qquad \ldots\ldots (2.1)$$

Here, $b^+_{\mathbf{q}}$, $\omega(\mathbf{q})$ represent the creation operator and energy for a free phonon of wave-vector $\mathbf{q}$; $\alpha^+_{\mathbf{k}\sigma}$, $\epsilon(\mathbf{k})$ represent the corresponding quantities for a free electron of wave-vector $\mathbf{k}$ and spin σ; g is an interaction constant and V is the volume of the body. The operators representing the total number of electrons and the current density are

$$N=\sum_{\mathbf{k},\sigma}\alpha^+_{\mathbf{k}\sigma}\alpha_{\mathbf{k}\sigma} \qquad \ldots\ldots (2.2)$$

and $$\mathbf{j}(\mathbf{x}) = V^{-1/2} \sum_{\mathbf{p}} \mathbf{j}(\mathbf{p}) \exp(i\mathbf{p}.\mathbf{x}) \quad \ldots\ldots (2.3)$$

respectively, where $$\mathbf{j}(\mathbf{p}) = \frac{e\hbar}{mV^{1/2}} \sum_{\mathbf{k},\sigma} \alpha^{+}_{\mathbf{k}\sigma}\alpha_{\mathbf{k}+\mathbf{p},\sigma}(\mathbf{k}+\tfrac{1}{2}\mathbf{p}). \quad \ldots\ldots (2.4)$$

In Bogoliubov's treatment, the constancy of N is not enforced. Instead, a chemical potential ζ is introduced, and the properties of the system are derived from the Hamiltonian

$$H = \mathscr{H} - \zeta N. \quad \ldots\ldots (2.5)$$

ζ is specified by the requirement that the expectation value of N is equal to the total number of electrons present. It is found to differ by very little from the Fermi energy for the free electron system.

The properties of the system are analysed by means of the transformation

$$\left.\begin{aligned} a_{\mathbf{k}0} &= u_{\mathbf{k}}\alpha_{\mathbf{k}\uparrow} \quad - v_{\mathbf{k}}\alpha^{+}_{-\mathbf{k}\downarrow} \\ a_{\mathbf{k}1} &= u_{\mathbf{k}}\alpha_{-\mathbf{k}\downarrow} \quad + v_{\mathbf{k}}\alpha^{+}_{\mathbf{k}\uparrow} \end{aligned}\right\} \quad \ldots\ldots (2.6)$$

where u, v are real numbers satisfying

$$u^2 + v^2 = 1.$$

The operators a^{+} represent creation operators for quasi-particles, and satisfy the Fermi anticommutation rules. The quantities u, v, which are temperature-dependent, were calculated by Bogoliubov according to his principle of internal compensation of critical graphs (i.e. graphs which lead to divergencies). This calculation led to two sets of values for u, v, one set corresponding to the normal state, the other to the superconducting state. It is only with the latter state that we shall be concerned.

In view of (2.1), (2.2) and (2.6), we may rewrite (2.5) in the form (1.1) with

$$H_0 = \sum_{\mathbf{k}} E(\mathbf{k})(a^{+}_{\mathbf{k}0}a_{\mathbf{k}0} + a^{+}_{\mathbf{k}1}a_{\mathbf{k}1}) + \sum_{\mathbf{q}} \omega(\mathbf{q}) b^{+}_{\mathbf{q}} b_{\mathbf{q}} \quad \ldots\ldots (2.7)$$

and
$$\begin{aligned} H' = \sum_{\mathbf{k}'=\mathbf{k}+\mathbf{q}} g\left(\frac{\omega(\mathbf{q})}{2V}\right)^{1/2} & [\{(u_{\mathbf{k}}v_{\mathbf{k}'} + u_{\mathbf{k}'}v_{\mathbf{k}})(a^{+}_{\mathbf{k}0}a^{+}_{\mathbf{k}'1} + a_{\mathbf{k}1}a_{\mathbf{k}'0}) \\ & + (u_{\mathbf{k}}u_{\mathbf{k}'} - v_{\mathbf{k}}v_{\mathbf{k}'})(a^{+}_{\mathbf{k}0}a_{\mathbf{k}'0} + a^{+}_{\mathbf{k}1}a_{\mathbf{k}'1})\} b^{+}_{\mathbf{q}} \\ & + \text{complex conj.}] \\ + \sum_{\mathbf{k}} & 2(\epsilon(\mathbf{k}) - \zeta) u_{\mathbf{k}}v_{\mathbf{k}}(a^{+}_{\mathbf{k}0}a^{+}_{\mathbf{k}1} + a_{\mathbf{k}1}a_{\mathbf{k}0}) \\ + \sum_{\mathbf{k}} & [(\epsilon(\mathbf{k}) - \zeta)(u_{\mathbf{k}}^2 - v_{\mathbf{k}}^2) - E(\mathbf{k})](a^{+}_{\mathbf{k}0}a_{\mathbf{k}0} + a^{+}_{\mathbf{k}1}a_{\mathbf{k}1}) \\ + \sum_{\mathbf{k}} & 2(\epsilon(\mathbf{k}) - \zeta) v_{\mathbf{k}}^2. \end{aligned} \quad \ldots\ldots (2.8)$$

The quantity $E(\mathbf{k})$ is the energy required to create a single quasi-particle $a^{+}_{\mathbf{k}0}$ or $a^{+}_{\mathbf{k}1}$ from the vacuum. Its least value, which occurs when $\mathbf{k}$ is on the Fermi surface, is positive and represents the energy gap in a one-particle picture of the superconducting state.

Similarly, it follows from (2.4) and (2.6) that

$$\begin{aligned} \mathbf{j}(\mathbf{p}) = \frac{e\hbar}{2mV^{1/2}} \sum_{\mathbf{k}'=\mathbf{k}+\mathbf{p}} & (\mathbf{k}+\mathbf{k}')[(u_{\mathbf{k}}u_{\mathbf{k}'} + v_{\mathbf{k}}v_{\mathbf{k}'})(a^{+}_{\mathbf{k}0}a^{+}_{\mathbf{k}'0} - a^{+}_{\mathbf{k}1}a_{\mathbf{k}'1}) \\ & + (u_{\mathbf{k}}v_{\mathbf{k}'} - v_{\mathbf{k}}u_{\mathbf{k}'})(a^{+}_{\mathbf{k}1}a^{+}_{\mathbf{k}'0} - a_{\mathbf{k}0}a_{\mathbf{k}'1})]. \end{aligned} \quad \ldots\ldots (2.9)$$

The formulae for H and $\mathbf{j}$, given by (2.7)–(2.9), are exact, whatever the values of u, v, E. It is only in the calculations of these latter quantities that approximations are made.

The property of u, v and E that concerns us is that these quantities are all continuous functions of $\mathbf{k}$. It was this property, together with the fact that E has a positive lower bound, which in Rickayzen's treatment led to a Meissner effect.

§ 3. Calculational Aids

In this section we shall note some very general properties of the model which we shall require when formulating the correlation function.

Ignoring the last sum in (2.8) (a constant c-number), we see from that equation that H' is a sum of terms, each one of which is of the form $\gamma\theta$, where θ is a product of creation and destruction operators and γ is a c-number. Thus, we may write

$$H' = \sum_P \gamma(P)\theta(P), \qquad \ldots\ldots (3.1)$$

where P is a well-defined process, involving the creation and (or) destruction of specified quanta. In order to illustrate our definition of the θ's, we remark that one θ corresponding to a term in the first sum in (2.8) is $a^+_{\mathbf{k}0}a^+_{\mathbf{k}'1}b^+_{\mathbf{q}}$, and its coefficient γ is $g\{\omega(\mathbf{q})/2V\}^{1/2}(u_{\mathbf{k}}v_{\mathbf{k}'}+u_{\mathbf{k}'}v_{\mathbf{k}})$. The process P represented by this θ is the creation of a phonon $\mathbf{q}$, and two fermions, $(\mathbf{k},0)$ and $(\mathbf{k}',1)$.

Similarly, we may rewrite (2.9) as

$$\mathbf{j}(p) = \sum_Q \mathbf{d}(Q)\theta(Q), \qquad \ldots\ldots (3.2)$$

where $\theta(Q)$ is a product of creation and destruction operators for the process Q.

Every process P (or Q) involves the creations and destructions of specified quanta. The energy of each quantum is well defined, $E(\mathbf{k})$ or $\omega(\mathbf{q})$, and hence the energy increase in H_0 due to the process P is specified completely by the form of $\theta(P)$. In fact, this energy increase is

$$e(P) = e_+(P) - e_-(P),$$

where e_+ and e_- denote the total energies of the quanta associated with the creation and destruction operators, respectively, which form the product $\theta(P)$. (For example, if $\theta(P) = a^+_{\mathbf{k}0}a_{\mathbf{k}'1}b^+_{\mathbf{q}}$, then $e(P) = E(\mathbf{k}) + \omega(\mathbf{q}) - E(\mathbf{k}')$.)

On comparing (2.8), (2.9) with (3.1), (3.2) we see that $\gamma(P)$ and $\mathbf{d}(Q)$ are continuous functions of the wave-vectors $(\mathbf{k},\mathbf{q})$ involved in the processes P and Q. The energies $e(P)$ and $e(Q)$ are likewise continuous in these wave vectors, in view of the continuity of $\omega(\mathbf{q})$, $E(\mathbf{k})$.

In our perturbative calculations, we shall use the interaction representation

$$\tilde{\xi}(\lambda) = \exp(\lambda H_0)\xi \exp(-\lambda H_0) \qquad \ldots\ldots (3.3)$$

for various operators ξ. It now follows from our definitions of e, θ that (cf. Schweber *et al.* 1954, p. 170)

$$\tilde{\theta}(P,\lambda) = \theta(P)\exp(\lambda e(P)).$$

Hence, by (3.1)–(3.3),

$$\tilde{H}'(\lambda) = \sum_P \gamma(P)\exp(\lambda e(P))\theta(P) \qquad \ldots\ldots (3.4)$$

and

$$\tilde{\mathbf{j}}(\mathbf{p},\lambda) = \sum_Q \mathbf{d}(Q)\exp(\lambda e(Q))\theta(Q). \qquad \ldots\ldots (3.5)$$

§ 4. The Correlation Function

In this section we shall employ a perturbative expansion to analyse the properties of the correlation function. By (1.6), (1.8) and (2.3),

$$\mathbf{C}(\mathbf{p}) = \exp(\beta F) \int_0^\beta \mathrm{Sp}[\mathbf{j}(\mathbf{p}) \exp(-\lambda H) \mathbf{j}^+(\mathbf{p}) \exp\{-(\beta-\lambda)H\}]\, d\lambda, \quad \ldots\ldots (4.1)$$

where F is the free energy of the system at temperature T. We shall concern ourselves with cases where T is non-zero, i.e. where β is finite. It is convenient to write

$$F = F_0 + F', \quad \ldots\ldots (4.2)$$

where F_0 is the free energy for the system H_0, so that F' may be regarded as a perturbation. Thus, we may rewrite (4.1) as

$$\mathbf{C}(\mathbf{p}) = \exp(\beta F') \int_0^\beta \mathrm{Av}_0[\exp(\lambda H_0)\mathbf{j}(\mathbf{p}) \exp(-\lambda H)\mathbf{j}^+(\mathbf{p}) \exp(-(\beta-\lambda)H) \times \exp(\beta-\lambda)H_0]\, d\lambda,$$

where $\mathrm{Av}_0(\xi)$ denotes the thermal average of ξ for the system H_0.

Consequently, using (3.3),

$$\mathbf{C}(\mathbf{p}) = \exp(\beta F') \int_0^\beta \mathrm{Av}_0[\tilde{\mathbf{j}}(\mathbf{p}, \lambda) S(\lambda) \mathbf{j}^+(\mathbf{p}) S^+(\beta-\lambda)]\, d\lambda, \quad \ldots\ldots (4.3)$$

where

$$S(\lambda) = \exp(\lambda H_0) \exp(-\lambda H). \quad \ldots\ldots (4.4)$$

Expanding $\exp(-\lambda H)$ perturbatively in powers of H' (cf. Nakajima 1955) (4.4) becomes

$$S(\lambda) = 1 - \int_0^\lambda \tilde{H}'(\lambda_1)\, d\lambda_1 + \int_0^\lambda d\lambda_1 \int_0^{\lambda_1} \tilde{H}'(\lambda_1)\tilde{H}'(\lambda_2)\, d\lambda_2 + (-1)^s \int_0^\lambda d\lambda_1 \int_0^{\lambda_1} d\lambda_2 \ldots \int_0^{\lambda_{s-1}} \tilde{H}'(\lambda_1)\tilde{H}'(\lambda_2)\ldots\tilde{H}'(\lambda_s)\, d\lambda_s + \ldots \quad \ldots\ldots (4.5)$$

Hence, by (3.4), (3.5), (4.3) and (4.5), we may write

$$\mathbf{C}(\mathbf{p}) = \exp(\beta F') \sum \mathbf{\Gamma} \mathrm{Av}_0(\Theta), \quad \ldots\ldots (4.6)$$

where

$$\Theta = \theta(Q)\theta(P_1)\theta(P_2)\ldots\theta(P_s)\theta^+(Q')\theta^+(P_t')\theta^+(P_{t-1}')\ldots\theta^+(P_1') \quad \ldots\ldots (4.7)$$

and

$$\mathbf{\Gamma} = (-1)^{s+t} \mathbf{d}(Q)\mathbf{d}(Q') \prod_{j=1}^{s} \gamma(P_j) \prod_{k=1}^{t} \gamma(P_k') \times \int_0^\beta \left[\exp(\lambda e(Q)) \left\{ \int_0^\lambda d\lambda_1 \int_0^{\lambda_1} d\lambda_2 \ldots \int_0^{\lambda_{s-1}} \exp\left(\sum_{j=1}^{s} \lambda_j e(P_j) \right) d\lambda_s \right\} \times \left\{ \int_0^{\beta-\lambda} d\lambda_1' \int_0^{\lambda_1'} d\lambda_2' \ldots \int_0^{\lambda_{t-1}'} \exp\left(\sum_{k=1}^{t} \lambda_k' e(P_k') \right) d\lambda_t' \right\} \right] d\lambda. \quad \ldots\ldots (4.8)$$

It is to be understood that the summation in (4.6) is taken over all processes P, P', Q, Q', and over all integers s, $t \geqslant 0$.

It follows from (4.7) and our definition of the θ's in § 3 that each Θ is a product formed from creation and destruction operators, e.g.

$$\Theta = a_1 b_2^+ a_3 b_2 a_3^+ a_1^+.$$

The creation and destruction operators in the product for Θ may always be re-arranged, using the appropriate commutation rules, so that Θ may be re-expressed in the form

$$\Theta = O_1(\tau_1)O_2(\tau_2)\dots O_m(\tau_m), \qquad \dots\dots(4.9)$$

where each τ represents a 'particle' (phonon or fermion), and O_s is an operator formed from the creation and destruction operators representing τ_s. As we are concerned only with operations for which $\mathrm{Av}_0(\Theta) \neq 0$, it follows that each O_s must be a product containing equal numbers of creation and destruction operators. From this it follows that O_s may be expressed as a polynomial function of the number operator n_s representing τ_s

$$(\text{e.g. } a^+a = n,\ a^+aaa^+ = n\,(1-n),\ \text{etc.})$$

In view of this, we may rewrite (4.9) as

$$\left.\begin{aligned} &\Theta = \prod_{s=1}^{m} g_s(n_s) \\ &\text{where } n_s = a^+a \text{ (fermions) or } b^+b \text{ (phonons),} \end{aligned}\right\} \qquad \dots\dots(4.10)$$

and where g_s is a polynomial function of n_s.

Moreover, it may easily be verified that $\mathrm{Av}_0(n^l)$ (l an integer) is a polynomial of degree l in $\bar{n}$ ($=\mathrm{Av}_0(n)$) (e.g. for bosons $\mathrm{Av}_0(n^2) = \bar{n}^2 + \bar{n} - 1$). Hence, by (4.10),

$$\mathrm{Av}_0(\Theta) = \Phi(\bar{n}_1, \bar{n}_2, \dots, \bar{n}_m), \qquad \dots\dots(4.11)$$

where Φ is a polynomial function of the $\bar{n}$'s. It is now convenient to introduce $\mathbf{K}_s$ ($=\mathbf{k}$ or $\mathbf{q}$) as the wave vector for the 'particle' τ_s. Thus, we may write

$$\bar{n}_s = \bar{n}(\mathbf{K}_s), \qquad \dots\dots(4.12)$$

where

$$\left.\begin{aligned} &\bar{n}(\mathbf{k}) = [\exp(\beta E(\mathbf{k})) + 1]^{-1} \\ \text{and} \quad &\bar{n}(\mathbf{q}) = [\exp(\beta\omega(\mathbf{q})) - 1]^{-1}. \end{aligned}\right\} \qquad \dots\dots(4.13)$$

From (4.11) and (4.12) it follows that Φ is a well-defined function of the $\mathbf{K}$'s.

Similarly, the tensor $\boldsymbol{\Gamma}$ is a function of the wave-vectors of the 'particles' participating in the operation Θ, i.e.

$$\boldsymbol{\Gamma} = \boldsymbol{\Psi}(\mathbf{K}_1, \dots, \mathbf{K}_m). \qquad \dots\dots(4.14)$$

It follows from (4.8) that, for finite β, $\boldsymbol{\Psi}$ is a regular function of the relevant γ's, $\mathbf{d}$'s and e's. Therefore since, as was shown in § 3, these latter quantities are all continuous in the $\mathbf{K}$'s, it follows that $\boldsymbol{\Psi}$ is a continuous function of the $\mathbf{K}$'s.

It follows from (4.11), (4.12) and (4.14) that the contribution to the sum in (4.6) due to the process Θ is

$$\mathbf{T}(\mathbf{K}_1, \dots, \mathbf{K}_m) \equiv \Phi(\bar{n}(\mathbf{K}_1), \dots, \bar{n}(\mathbf{K}_m))\,\boldsymbol{\Psi}(\mathbf{K}_1, \dots, \mathbf{K}_m). \qquad \dots\dots(4.15)$$

The precise form of $\mathbf{T}$ depends on the nature of the process Θ. Corresponding to each form for $\mathbf{T}$, i.e. corresponding to each Feynman graph G, the total contribution to the sum in (4.6) is

$$\mathbf{C}_G(\mathbf{p}) = \sum_{\mathbf{K}_1, \dots, \mathbf{K}_m} \mathbf{T}(\mathbf{K}_1, \dots, \mathbf{K}_m); \qquad \dots\dots(4.16)$$

and equation (4.6) may now be rewritten as

$$\mathbf{C}(\mathbf{p}) = \exp(\beta F') \sum_G \mathbf{C}_G(\mathbf{p}), \qquad \dots\dots(4.17)$$

the summation to be taken over all graphs.

We shall now show that $\mathbf{T}$ is a continuous function of the $\mathbf{K}$'s. For this purpose we first note that, as shown above, Ψ is continuous in those vectors. The function Φ, on the other hand, is a polynomial function of the $\bar{n}$'s. As may be seen from (4.13), $\bar{n}(\mathbf{k})$ is a regular function of $\mathbf{k}$, but $\bar{n}(\mathbf{q})$ is irregular in $\mathbf{q}$, tending to infinity as $\omega(\mathbf{q})\to 0$. The function Φ is therefore regular in the $\mathbf{k}$'s, but has singularities in the $\mathbf{q}$'s. Nevertheless, the function $\mathbf{T}=\Phi\Psi$ does not have any such singularities, for the folowing reason.

It may be seen on comparing (2.8), (2.9) with (3.1), (3.2) that whenever a process θ has $b_{\mathbf{q}}$ or $b_{\mathbf{q}}{}^{+}$ as a factor, then its coefficient γ has $(\omega(\mathrm{q}))^{1/2}$ as a factor. Therefore, by (4.7), (4.8), for every $n(\mathbf{q})$ in Θ, there is a factor $\omega(\mathbf{q})$ in Γ. Hence, by (4.11), (4.14) for every $\bar{n}(q)$ in Φ, there is an $\omega(\mathbf{q})$ in Ψ. The quantity $\omega(\mathbf{q})\,\bar{n}(\mathbf{q})$ is continuous in $\mathbf{q}$, as may be seen from (4.13). Hence it follows from (4.15) that $\mathbf{T}$ is continuous in all the $\mathbf{K}$'s, i.e. in the $\mathbf{q}$'s as well as the $\mathbf{k}$'s.

In order to ascertain the nature of the dependence of $\mathbf{C}_G$ on $\mathbf{p}$, we note that, by (4.7), there are exactly two Q-processes, namely $\theta(Q)$ and $\theta^{+}(Q')$, in each process Θ; and, by (2.9) and (3.2), the quanta involved in each Q-process are a pair of fermions whose wave-vectors differ by $\mathbf{p}$. It follows that four of the $\mathbf{K}$'s in the summand in (4.16) must be fermion wave-vectors $\mathbf{k}_1, \mathbf{k}_1+\mathbf{p}$; $\mathbf{k}_2, \mathbf{k}_2+\mathbf{p}$. If now we denote the wave-vectors of the phonons and of the remaining fermions participating in the operation Θ as $\mathbf{q}_1, \ldots, \mathbf{q}_l$; $\mathbf{k}_3, \ldots, \mathbf{k}_n$, respectively, we may write

$$\mathbf{T}=\mathbf{T}(\mathbf{k}_1, \mathbf{k}_1+\mathbf{p};\ \mathbf{k}_2, \mathbf{k}_2+\mathbf{p};\ \mathbf{k}_3, \ldots, \mathbf{k}_n;\ \mathbf{q}_1, \ldots, \mathbf{q}_l). \qquad \ldots\ldots (4.18)$$

Moreover, by (2.8) and (2.9), any $\mathbf{q}$ appearing in an operator θ is always the difference between two fermion wave-vectors appearing in that operator. Hence, we may express a relation between the $\mathbf{q}$'s and $\mathbf{k}$'s appearing in (4.18), i.e.

$$\mathbf{q}_s=\mathbf{k}_i-\mathbf{k}_j+r\mathbf{p};\ r=0,\ 1 \text{ or } -1. \qquad \ldots\ldots (4.19)$$

The actual values of i, j, r corresponding to any $\mathbf{q}_s$ will depend on the form of the graph G.

Since $\mathbf{T}$ is continuous in the $\mathbf{k}$'s and $\mathbf{q}$'s, it follows that, on substituting (4.19) into (4.18), we may re-express $\mathbf{T}$ as

$$\mathbf{T}=\mathbf{U}(\mathbf{k}_1, \ldots, \mathbf{k}_n;\ \mathbf{p}), \qquad \ldots\ldots (4.20)$$

where $\mathbf{U}$ is continuous both in $\mathbf{p}$ and the $\mathbf{k}$'s. Thus, equation (4.16) may now be rewritten as

$$\mathbf{C}_G(\mathbf{p})=\sum_{\mathbf{k}_1, \ldots, \mathbf{k}_n} \mathbf{U}(\mathbf{k}_1, \ldots, \mathbf{k}_n;\ \mathbf{p}). \qquad \ldots\ldots (4.21)$$

This sum may be converted to an integral, proportional to

$$\int \mathbf{U}(\mathbf{k}_1, \ldots, \mathbf{k}_n;\ \mathbf{p})\, d\mathbf{k}_1 \ldots d\mathbf{k}_n. \qquad \ldots\ldots (4.22)$$

In view of the continuity of $\mathbf{U}$ with respect to $\mathbf{p}$, the integral (4.22) will tend, as $p\to 0$, to a limit independent of the direction of $\mathbf{p}$. Hence, $\mathbf{C}_G$ likewise tends to such a limit, and cannot therefore contain a term $\hat{\mathbf{p}}\hat{\mathbf{p}}$. Thus, by (4.17), we have established the contention made in § 1, namely that the model does not reveal the long range order required for the Meissner effect, in any finite order perturbative development from the Bogoliubov theory.

It is important to point out that the reason for the continuity of each $\mathbf{C}_G$, as given in our theory, is not due to the finiteness of the volume of the system. For this finiteness means only that $\mathbf{p}$ can never be zero, and not that the *function* $\mathbf{C}_G(\mathbf{p})$ does not tend to a definite limit as $\mathbf{p}\to 0$.

In any case we can avoid all difficulties due to the finiteness of the system by replacing (4.17) by a linked cluster expansion for $\mathbf{C}$ (cf. Goldstone 1957, Hubbard 1957). Thus, using linked cluster theory, we may rewrite (4.17) as

$$\mathbf{C}(\mathbf{p}) = \sum_G{}' \mathbf{C}_G(\mathbf{p}), \qquad \ldots\ldots (4.23)$$

the prime over the Σ denoting summation over linked diagrams only. The exponential term of (4.17) is omitted from (4.23) since it deviates from unity due to volume-dependent terms which, according to linked cluster theory, are cancelled by contributions to $\Sigma \mathbf{C}_G$ that arise from unlinked diagrams.

If we now reapply our earlier arguments to (4.23) instead of (4.17), it follows without further difficulty that the perturbative expansion will not, in any finite order, lead to the required long range correlations.

§ 5. Conclusion

It is now of interest to consider the possibility of deriving the Meissner effect by a perturbative method which is based on a different treatment of Fröhlich's Hamiltonian. As was pointed out in § 1, it would be desirable that the method should reveal the required long range correlations in a low order of perturbation.

Thus we shall consider treatments in which H is split up as in (1.1), with H_0 the part of the Hamiltonian on which the theory is based. Moreover we shall restrict ourselves to formulations in which H_0 is diagonal in the number operators representing the various quanta in terms of which the theory is described. (These quanta would not necessarily be the same as in the Bogoliubov theory.)

We can therefore apply the analysis of §§ 3 and 4, and the correlation function will again be given by the equations (4.15), (4.16) and (4.23). Our aim in discussing these equations will be to try to determine which basic properties H_0 should possess if the treatment is to reveal the long range correlations in a finite order of perturbation, i.e. if for some linked graph G, $\mathbf{C}_G$ possesses a term $\hat{\mathbf{p}}\hat{\mathbf{p}}$.

On re-applying the theory of § 4 to equation (4.16), it may be seen that $\mathbf{C}_G$ can possess a term $\hat{\mathbf{p}}\hat{\mathbf{p}}$ (having no direction-independent limit as $\mathbf{p}\to 0$) only if $\mathbf{T}$ is singular in at least one of the $\mathbf{K}$'s. (It is not sufficient for $\mathbf{T}$ to have a finite discontinuity across some surface in $\mathbf{K}$-space, since this would be removed on integration.) In other words, the term $\hat{\mathbf{p}}\hat{\mathbf{p}}$ cannot arise in $\mathbf{C}_G$ unless either Φ or Ψ possesses a singularity.

The function Φ is a polynomial in the $\bar{n}(\mathbf{K})$'s. These latter quantities are regular functions of $\mathbf{K}$ for fermions, but are singular (as energy tends to zero) for bosons. Hence, it follows that the required singularity can occur in Φ only if the basic Hamiltonian, H_0, contains bosons.

On the other hand, it may be seen from (4.8) and (4.14) that a singularity could arise in Ψ only as a result of a singularity in a coefficient γ or $\mathbf{d}$. Such a singularity would render the perturbative expansion extremely doubtful.

It therefore appears that a perturbative treatment can lead to the Meissner effect in a satisfactory manner only if the basic approximation H_0 represents a system which contains low energy bosons. (It is also important that the

singularities in Φ, arising from these 'particles', are not cancelled by zeroes in the expansion coefficients, as was the case with the phonons in Bogoliubov's treatment.) Thus, it might be that suitable low energy bosons could arise from some collective oscillations of the fermions in the system, as has been suggested by Blatt and Matsubara (1958).

Acknowledgments

The author would like to express his indebtedness to Professor H. Fröhlich and to Dr. S. Doniach for a number of valuable discussions.

References

Bardeen, J., Cooper, L. N., and Schrieffer, J. R., 1957, *Phys. Rev.*, **108**, 1175.
Blatt, J. M., and Matsubara, T., 1958, *Progr. Theor. Phys., Japan*, **20**, 781.
Bogoliubov, N. N., 1958, *Nuovo Cim.*, **7**, 794.
Fröhlich, H., 1952, *Proc. Roy. Soc.* A, **215**, 291.
Goldstone, J., 1957, *Proc. Roy. Soc.* A, **239**, 267.
Hubbard, J., 1957, *Proc. Roy. Soc.* A, **240**, 539.
Nakajima, S., 1955, *Adv. Phys.*, **4**, 363.
—— 1956, *Proc. Phys. Soc.* A, **69**, 441.
Rickayzen, G., 1958, *Phys. Rev.*, **111**, 817.
Schafroth, M. R., 1951, *Helv. Phys. Acta*, **24**, 645.
—— 1958, *Phys. Rev.*, **111**, 72.
Schweber, S. S., Bethe, H. A., and de Hoffmann, F., 1954, *Mesons and Fields*, Vol. 1 (Evanston, Illinois: Row, Peterson and Co.).

On the Electron Coincidence Spectrum in Double Beta Decay†

By S. P. ROSEN
Department of Physics, Washington University, Missouri, U.S.A.

MS. received 10*th February* 1959, *in final form* 30*th March* 1959

Abstract. Though simple qualitative arguments imply that the electron coincidence spectra for two-neutrino, and for no-neutrino double β-decay are broadly peaked at $\frac{1}{2}E_0$ and infinitely sharply peaked at E_0 respectively (E_0 is the energy release), a recent calculation has shown that in some circumstances the two-neutrino case spectrum may also be broadly peaked in the region of E_0. A simple model, in which only one state of the intermediate nucleus gives a non-zero contribution to the matrix element, is used to recalculate these spectra. Two extreme approximations are considered: the energy of the intermediate state is equal to, or much greater than, that of the initial state. In both cases, the qualitative result is confirmed, and the recent calculation mentioned above is regarded as incorrect. The model is applied to the double β-decays of ^{96}Zr and ^{48}Ca. The relation between the conservation of lepton 'charge' and the shape of the spectrum is also considered in some detail.

§ 1. Introduction

The general nucleon–lepton interaction Hamiltonian (Pauli 1957, Enz 1957, Luders 1958, Pursey 1957, Primakoff and Rosen 1959).

$$H=\sum_{\lambda}(\psi_{\mathrm{p}}{}^{+}\mathrm{O}_{\lambda}\psi_{\mathrm{n}})\{C_{\lambda}(\psi_{\mathrm{e}}{}^{+}\mathrm{O}_{\lambda}(1+\delta_{\lambda}\gamma_5)\psi_{\nu})+D_{\lambda}(\psi_{\mathrm{e}}{}^{+}\mathrm{O}_{\lambda}(1+\eta_{\lambda}\gamma_5)\psi_{\bar{\nu}})\}$$

$$+\mathrm{h.c.}=\{C+D\}+\mathrm{h.c.} \qquad \ldots\ldots(1)$$

engenders two types of double β-decay: in the first, two neutrinos are emitted simultaneously with two electrons,

$$\mathrm{n}_1+\mathrm{n}_2 \xrightarrow{\text{via } C} \mathrm{n}_1+\mathrm{p}_2+\mathrm{e}_2+\bar{\nu}_2 \qquad \ldots\ldots(2)$$

then

$$\xrightarrow{\text{via } C} \mathrm{p}_1+\mathrm{e}_1+\bar{\nu}_1+\mathrm{p}_2+\mathrm{e}_2+\bar{\nu}_2$$

and in the second there are no neutrinos

$$\mathrm{n}_1+\mathrm{n}_2 \xrightarrow{\text{via } C} \mathrm{n}_1+\mathrm{p}_2+\mathrm{e}_2+\bar{\nu}_2 \qquad \ldots\ldots(3)$$

then

$$\xrightarrow{\text{via } D} \mathrm{p}_1+\mathrm{e}_1+\mathrm{p}_2+\mathrm{e}_2.$$

The coincidence spectrum for the sum of the energies of the two electrons emitted simultaneously (referred to as the electron coincidence spectrum) in the two-neutrino decay (2), will be continuous; and since it is reasonable to assume that

† This research was supported in part by the United States Air Force through the Air Force Office of Scientific Research of the Air Research and Development Command, under contract No. AF 18(603)-108.

the electron and neutrino pairs have roughly the same average energy, the peak of this spectrum should occur at about $\frac{1}{2}E_0$, where E_0 is the energy release of the decay. For the no-neutrino decay (3), however, the sum of electron energies is always E_0.

The two-neutrino decay (2) is possible whatever the choice of coupling constants in (1), but, if either of the following conditions is satisfied, then no-neutrino double β-decay cannot occur:

$$D_\lambda = 0 \quad (\text{all } \lambda) \qquad \ldots\ldots (4)$$

or

$$\delta_\lambda = \eta_\lambda = \pm 1 \quad (\text{all } \lambda). \qquad \ldots\ldots (5)$$

When the conditions (4), (5) do not hold the lifetime of (3) will in general be shorter than that of (2) by a factor 10^5–10^6 (see Primakoff and Rosen 1959 to be referred to as I, for a full discussion of these points). However, if (4), (5) are satisfied only approximately, then these lifetimes may become comparable (for example, if $D_\lambda \simeq C_\lambda$ and $\delta_\lambda = \eta_\lambda = 0{\cdot}997$, they are roughly equal), and the electron coincidence spectrum should show two peaks, a fairly broad one at $\frac{1}{2}E_0$ and an infinitely sharp one at E_0. So far, this qualitative analysis imples that a sufficiently accurate experimental determination of the electron coincidence spectrum would lead to a clear cut decision regarding the nature of double β-decay (i.e. whether it is no-neutrino in whole or in part). However, there is quoted in a recent review article (I) the result of an earlier calculation (Rosen 1957) which showed that, in one special case, the electron coincidence spectrum for two-neutrino double β-decay is broadly peaked near the energy E_0. If this surprising result (it implies that, on the average, the electrons carry off much more energy than the neutrinos) is true in general, then the electron coincidence spectrum, observed under moderate resolution, would always appear to be peaked in the region of E_0 regardless of the nature of double β-decay, and extremely high resolution would be required to decide whether the double β-decay is in fact two-neutrino or no-neutrino.

Since the completion of the review article, this spectrum has been re-examined in great detail, and its behaviour is now more clearly understood. In the following sections, the calculations and the spectra obtained are discussed at length. Applications to the double β-decays of ^{96}Zr and ^{48}Ca are also described, by means of a simple nuclear model.

§ 2. The Calculation

There are numerous choices for the coupling constants in (1), all of which describe the main features of single β-decay, and all of which give the same probabilities for two-neutrino double β-decay; for convenience, we take

$$\left.\begin{aligned} &C_{\mathrm{V}} = D_{\mathrm{V}} = \frac{1}{\sqrt{2}} F_{\mathrm{V}} : \delta_{\mathrm{V}} = \eta_{\mathrm{V}} = 1 \\ &C_{\mathrm{A}} = D_{\mathrm{A}} = \frac{1}{\sqrt{2}} F_{\mathrm{A}} : \delta_{\mathrm{A}} = \eta_{\mathrm{A}} = 1 \\ &C_\lambda = D_\lambda = 0 \qquad (\lambda = \text{S. T. P.}) \\ &|F_{\mathrm{V}}| \simeq |F_{\mathrm{A}}| = F. \end{aligned}\right\} \qquad \ldots\ldots (6)$$

The probability distribution $P(E)$ for pairs of electrons emitted simultaneously in two-neutrino double β-decay (2), with energy mc^2E (m is the electron rest mass), is given by

$$P(E)=\text{constant}\times\int P(E_1,E_2;k_1,k_2)\mathscr{F}(Z,E_1)\mathscr{F}(Z,E_2)$$
$$\times\delta(E_0-E_1-E_2-k_1-k_2)\delta(E-E_1-E_2)$$
$$\times p_1E_1\,dE_1p_2E_2\,dE_2k_1^2\,dk_1k_2^2\,dk_2 \qquad \ldots\ldots(7)$$

where mc^2E_0 is the energy release of the decay; mc^2E_i are the energies of the electrons, and mcp_i their momenta ($p_i^2=E_i^2-1$; $i=1,2$) mc^2k_i are the neutrino energies; $\mathscr{F}(Z,E)$ is the Fermi function, allowing for the Coulomb effect of the nucleus. Approximately

$$\mathscr{F}(Z,E)\simeq\left[\frac{2\pi Z}{137}\right]\left[\frac{E}{p}\right]\left[1-\exp\left(-\frac{2\pi Z}{137}\frac{E}{p}\right)\right]^{-1}. \qquad \ldots\ldots(8)$$

From (7) and (8), it follows that

$$P(E)=\text{const.}\times\left(\frac{2\pi Z}{137}\right)^2\times\int P(E_1,E_2;k_1,k_2)\left[1-\exp\left(-\frac{2\pi Z}{137}\frac{E_1}{p_1}\right)\right]^{-1}$$
$$\times\left[1-\exp\left(-\frac{2\pi Z}{137}\frac{E_2}{p_2}\right)\right]^{-1}\delta(E_0-E_1-E_2-k_1-k_2)$$
$$\times\delta(E-E_1-E_2)E_1^2\,dE_1E_2^2\,dE_2k_1^2\,dk_1k_2^2\,dk_2. \qquad \ldots\ldots(9)$$

To calculate $P(E_1,E_2;k_1,k_2)$ consider a transition from the ground state $|i\rangle$ of nucleus (A,Z) via states $|m\rangle$ of nucleus $(A,Z+1)$ to the ground state $|f\rangle$ of $(A,Z+2)$. In all cases of experimental interest, (A,Z) and $(A,Z+2)$ are even–even nuclei, and so it will be assumed that both $|i\rangle$ and $|f\rangle$ have zero spin and even parity (0^+). The states $|m\rangle$ must then have either zero spin, or unit spin, and even parity (0^+ or 1^+). The transitions $|i\rangle\rightarrow|m\rangle$, $|m\rangle\rightarrow|f\rangle$ are both engendered by the Fermi interaction (i.e. vector) if $|m\rangle$ is 0^+ and by the Gamow–Teller interaction (axial vector) if $|m\rangle$ is 1^+. Assume that there is only *one* state $|m\rangle$, via which the transition proceeds: then

$$P(E_1,E_2;k_1,k_2)=2^4|F|^4\{[K^2+L^2-KL]|\langle f|\textstyle\sum\tau^+|m\rangle\langle m|\sum\tau^+|i\rangle|^2$$
$$+3[K^2+L^2+KL]|\tfrac{1}{3}\langle f|\textstyle\sum\tau^+\boldsymbol{\sigma}|m\rangle\,.\,\langle m|\sum\tau^+\boldsymbol{\sigma}|i\rangle|^2$$
$$-6KL\times\mathscr{R}(\langle f|\textstyle\sum\tau^+|m\rangle\langle m|\sum\tau^+|i\rangle$$
$$\times\tfrac{1}{3}\langle f|\textstyle\sum\tau^+\boldsymbol{\sigma}|m\rangle^\times\langle m|\sum\tau^+\boldsymbol{\sigma}|i\rangle^\times)\} \qquad \ldots\ldots(10)$$

where

$$K=\frac{1}{W_{mi}+E_1+k_1}+\frac{1}{W_{mi}+E_2+k_2}$$
$$L=\frac{1}{W_{mi}+E_1+k_2}+\frac{1}{W_{mi}+E_2+k_1} \qquad \ldots\ldots(11)$$

and mc^2W_{mi} is the energy difference between states $|m\rangle$ and $|i\rangle$. $\sum\tau^+$ represents the sum over single nucleon isotopic spin operators τ^+, which transform neutrons to protons. $\boldsymbol{\sigma}$ is the usual Pauli spin matrix.

If $|m\rangle$ is 0^+, then

$$\langle f|\sum\tau^+\boldsymbol{\sigma}|m\rangle\,.\,\langle m|\sum\tau^+\boldsymbol{\sigma}|i\rangle \text{ vanishes while } \langle f|\sum\tau^+|m\rangle\langle m|\sum\tau^+|i\rangle$$

is non-zero; and vice versa for the case $|m\rangle$ is 1^+. Should there exist two possible intermediate states, $|m\rangle$ and $|m'\rangle$, such that one, $|m\rangle$, is 0^+ and the other, $|m'\rangle$, is 1^+, and also such that their energy difference is negligible, then none of the terms of (10) vanish (provided that $|m\rangle$ is replaced by $|m'\rangle$ in the appropriate matrix element). W_{mi} will then be an average energy difference between $|m\rangle$, $|m'\rangle$ and $|i\rangle$. (The above formulae are taken from I, § 3.5.)

The chief aim of the calculation is to discover how the behaviour of $P(E)$ depends on the quantity W_{mi} appearing in K, L (equations 10, 11): in particular, if E_p is the energy at which the broad peak of the spectrum occurs, how does E_p vary as a function of W_{mi}? [The recent calculation mentioned above implied that as W_{mi} decreases from large values to zero, E_p moves from $\frac{1}{2}E_0$ to E_0.] Two extreme cases are considered:

$$\text{(i)}\ W_{mi}=0$$
$$\text{(ii)}\ W_{mi}\gg E_i+k_j. \qquad \ldots\ldots (12)$$

The functions $\left[1-\exp\left(-\frac{2\pi Z}{137}\frac{E_i}{p_i}\right)\right]^{-1}$

(see (9)) will be treated as constant $=[1-\exp(-2\pi Z/137)]^{-1}$ and it will be shown later that they do not affect the shape of the spectrum very seriously (§ 2.3). We also take $E_0=8$, since this is roughly the energy release of ^{96}Zr.

2.1. *Approximation* $W_{mi}=0$

Treating the exponentials as constants, the integrals to be evaluated are, from (9) and (10),

$$A(E)=\int E_1^2E_2^2k_1^2k_2^2[K^2+L^2]\delta(E_0-E_1-E_2-k_1-k_2)$$
$$\times\delta(E-E_1-E_2)\,dE_1\,dE_2\,dk_1\,dk_2 \qquad \ldots\ldots (13)$$

and

$$B(E)=\int E_1^2E_2^2k_1^2k_2^2[KL]\delta(E_0-E_1-E_2-k_1-k_2)$$
$$\times\delta(E-E_1-E_2)\,dE_1\,dE_2\,dk_1\,dk_2. \qquad \ldots\ldots (14)$$

From (11) and (12, (i)) we have, after integration over k_1 and k_2,

$$A(E)=A_1(E)-A_2(E) \qquad \ldots\ldots (15)$$

where

$$A_1(E)=2\int E_1^2E_2^2(E_0-E)[E_0^2+E_0E-2E_1E_2]\delta(E-E_1-E_2)\,dE_1\,dE_2$$

$$A_2(E)=\frac{4}{E_0}\int E_1^2E_2^2\Big\{E_1(E_0-E_2)[E_0^2-E_2(E_0-E_1)]\log\frac{E_0-E_2}{E_1}$$
$$+E_2(E_0-E_1)[E_0^2-E_1(E_0-E_2)]\log\frac{E_0-E_1}{E_2}\Big\}$$
$$\times\delta(E-E_1-E_2)\,dE_1\,dE_2. \qquad \ldots\ldots (16)$$

Likewise

$$B(E)=B_1(E)-B_2(E) \qquad \ldots\ldots(17)$$

where

$$B_1(E)=E_0^2\int E_1^2E_2^2(E_0-E)\delta(E-E_1-E_2)\,dE_1\,dE_2$$

$$B_2(E)=2E_0\int E_1^2E_2^2\left\{\frac{E_1^2(E_0-E_2)^2}{(E_1-E_2)(E_0+E_1-E_2)}\log\frac{E_0-E_2}{E_1}\right.$$
$$\left.+\frac{E_2^2(E_0-E_1)^2}{(E_2-E_1)(E_0+E_2-E_1)}\log\frac{E_0-E_1}{E_2}\right\}\delta(E-E_1-E_2)\,dE_1\,dE_2. \qquad \ldots\ldots(18)$$

These functions vanish identically for $E=2$ and $E=E_0$. For other values of E they have been calculated to six figures and (with $E_0=8$) their values are shown in the table. The integrals of terms like $(E_2-E_1)^{-1}\log(E_0-E_1)$ are special cases of Euler's Dilogarithm (see Bateman Manuscript Project)

$$\mathscr{L}_2(x)=-\int_0^x\frac{\log(1-t)}{t}\,dt=\sum_{u=1}^{\infty}\frac{x^n}{n^2} \qquad (|x|\leqslant 1)$$

and do not become infinite.

The shapes of $A_1(E)$, $A_2(E)$ are very similar, both being strongly peaked for some E between 6·5 and 7; the difference between them, $A(E)$, is small (in fact, as the table indicates, it is necessary to go to six figures to obtain $A(E)$ accurately). Moreover, the shape of $A(E)$ is markedly different from that of $A_1(E)$, $A_2(E)$: it rises sharply to a maximum at $E\simeq 4{\cdot}3$ and then falls rapidly, with a pronounced tail in the region $7\leqslant E\leqslant 8$ (see figure 1). Similarly for $B_1(E)$, $B_2(E)$ and $B(E)$: $B_1(E)$ and $B_2(E)$ have large peaks in the region $6{\cdot}5\leqslant E\leqslant 7$, their differences, $B(E)$ is small and behaves exactly like $A(E)$.

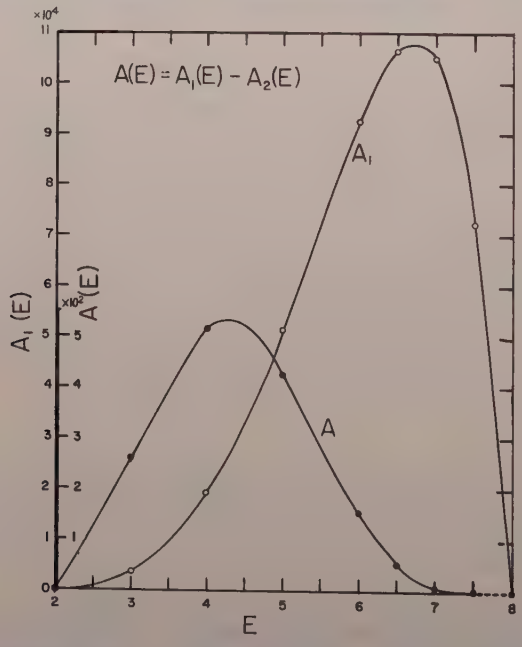

Figure 1. Approximation $W_{mi}=0$. On the above scale the difference between $A_1(E)$ and $A_2(E)$ would hardly be noticeable. $A_1(E)$ is shown together with $A(E)$, which is magnified by a factor of 100. The curves for $B_1(E)$ and $B(E)$ are similar.

E	3	4	5	6	6·5	7	7·5
$A_1(E)$	3932	19179	51221	92446	106462	105148	75549
$A_2(E)$	3669	18663	50796	92294	106405	105136	75548
$A(E)$	262	516	425	153	57	12	1
$B_1(E)$	1504	6929	17683	30822	35011	34187	24340
$B_2(E)$	1363	6668	17471	30746	34983	34181	24340
$B(E)$	141	261	212	76	28	6	~ 0

From (9), (10), (13) and (14), the coincidence spectra are given by

(*a*) $|m\rangle$ is 0^+

$$P_{\mathrm{V}}(E;\ W_{mi}=0)=A(E)-B(E) \qquad \ldots\ldots(19)$$

(*b*) $|m\rangle$ is 1^+

$$P_{\mathrm{A}}(E;\ W_{mi}=0)=3\{A(E)+B(E)\} \qquad \ldots\ldots(20)$$

(*c*) $|m\rangle$ is 0^+, $|m'\rangle$ is 1^+

$$P_{\mathrm{V-A}}(E;\ W_{mi}=0)=4\{A(E)-B(E)\} \qquad \ldots\ldots(21)$$

(assuming $\langle f|\sum\tau^+|m\rangle\langle m|\sum\tau^+|i\rangle\simeq\frac{1}{3}\langle f|\sum\tau^+\boldsymbol{\sigma}|m\rangle\,.\,\langle m|\sum\tau^+\boldsymbol{\sigma}|i\rangle$).

The factors $2^4|F|^4$ and the nuclear matrix elements are merely scale factors, and have therefore been ignored. Since $A(E)$ is greater than $B(E)$ and (19), (20), (21) are linear combinations of these two, the shapes of the spectra

$$P_X(E;\ W_{mi}=0) \quad (X=\mathrm{V},\mathrm{A},\mathrm{V}-\mathrm{A})$$

will be similar to the shapes of $A(E)$, $B(E)$ (see figure 2).

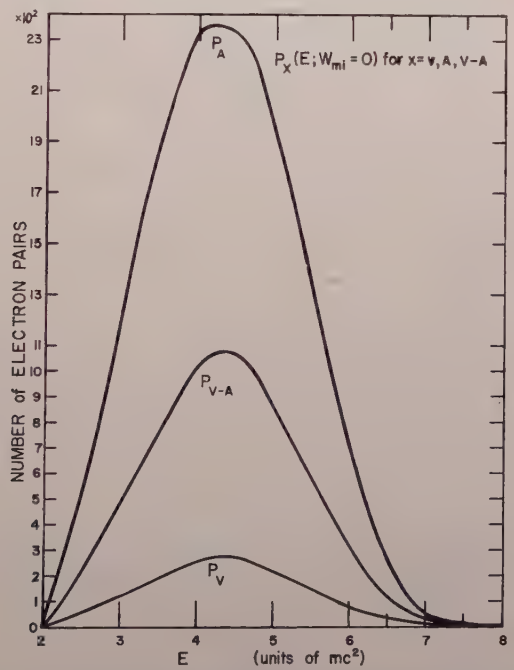

Figure 2. Approximation $W_{mi}=0$. The electron coincidence spectra $P_X(E;\ W_{mi}=0)$ are shown for $X=\mathrm{V}$, A and V−A.

2.2. *Approximation* $W_{mi} \gg E_i + k_j$

In this approximation, the denominators $W_{mi} + E_i + k_j$ (see equation (11)) are replaced by some average W (see Konopinski 1955, Primakoff and Rosen 1959). Then

$$K = L = \frac{2}{W} \qquad \ldots\ldots (22)$$

and neither K nor L depends on E_i, k_j. From equations (9), (10), (11) and (22), the coincidence spectra are determined by the integral

$$C(E) = \int E_1^2 E_2^2 k_1^2 k_2^2 \delta(E - E_1 - E_2)\delta(E_0 - E - k_1 - k_2)\, dE_1\, dE_2\, dk_1\, dk_2$$

$$= \frac{1}{(30)^2}(E_0 - E)^5(E^5 - 20E^2 + 30E - 12) \qquad \ldots\ldots (23)$$

and are given by (ignoring the same scale factors as before):

$$\left.\begin{aligned} &(a) \quad P_{\mathrm{V}}(E;\ W_{mi} \gg E + k) = \frac{4}{W^2} C(E) \\ &(b) \quad P_{\mathrm{A}}(E;\ W_{mi} \gg E + k) = \frac{36}{W^2} C(E) \\ &(c) \quad P_{\mathrm{V-A}}(E;\ W_{mi} \gg E + k) = \frac{16}{W^2} C(E) \end{aligned}\right\} \qquad \ldots\ldots (24)$$

The shape of $C(E)$, and hence of spectra (24), is very much like that of $A(E)$, $B(E)$: strongly peaked at $E \simeq 4{\cdot}3$, with a long tail in the region $6{\cdot}5 \leqslant E \leqslant 8$ (see figure 3): this $C(E)$ is identical with the $P''(\epsilon)$ given in I, eqn (79) with $\epsilon = E - 2$.

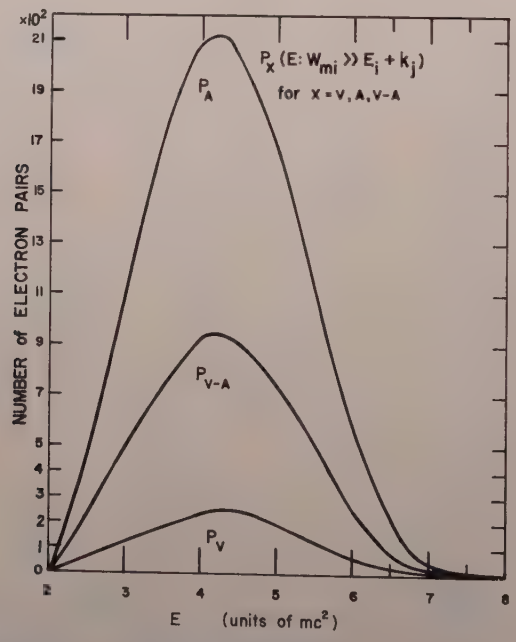

Figure 3. Approximation $W_{mi} \gg E_i + k_j$: the electron coincidence spectra $P_X(E;\ W_{mi} \gg E + k)$ for $X = \mathrm{V}$, A and V − A. The scale is the same as in figure 2; areas under corresponding curves for the two approximations are roughly equal.

The strong similarity of $C(E)$ to $A(E)$, $B(E)$ suggests that the above calculations may be looked at from a different point of view. Consider the case $W_{mi}=0$: then, to obtain the spectra $P_X(E, W_{mi}=0)(X=\mathrm{V}, \mathrm{A}, \mathrm{V}-\mathrm{A})$, we may either treat the energy denominators in K, L, exactly, as in § 2.1; or, alternatively, we may replace the energy denominators by a constant $W'=\langle E_j+k_i\rangle_{\mathrm{av}}$. In the first case the spectra are given by (19), (20) and (21) and in the second, by (24) with W replaced by W':

$$\left.\begin{aligned} &(a) \qquad P_{\mathrm{V}}(E;\ W_{mi}=0)\simeq \frac{4}{(W')^2}C(E)\\ &(b) \qquad P_{\mathrm{A}}(E;\ W_{mi}=0)\simeq \frac{36}{(W')^2}C(E)\\ &(c) \qquad P_{\mathrm{V-A}}(E;\ W_{mi}=0)\simeq \frac{16}{(W')^2}C(E)\end{aligned}\right\} \qquad \ldots\ldots (24')$$

As shown above (see figures 2 and 3), both methods lead to the same shapes for the spectra. Now, in each of the cases (a), (b), (c), the area under the coincidence spectrum must represent the same total probability, regardless of whether we have used the exact results of (19), (20), (21), or the approximate ones of (24′). Therefore W' must be chosen so that areas under corresponding curves are equal: from this condition it is found that

$$W'\simeq 4=\tfrac{1}{2}E_0. \qquad \ldots\ldots (25)$$

Equation (25) suggests that in the case $W_{mi}\neq 0$, the spectra may be obtained either by an exact calculation, similar to that of § 2.1, or by an approximate calculation, in which the energy denominators $W_{mi}+k_j+E_i$ of K, L are replaced by a constant W, where

$$W\simeq W_{mi}+\tfrac{1}{2}E_0. \qquad \ldots\ldots (25')$$

§ 2.3. *Coulomb Correction*

The function

$$y(E)=\left[1-\exp\left(-\frac{2\pi Z}{137}\frac{E}{p}\right)\right]^{-1} \qquad \ldots\ldots (26)$$

is shown in figure 4 for the case

$$\frac{2\pi Z}{137}\simeq 1 \quad (\text{i.e. } Z\simeq 20).$$

It rises rapidly from 1 at $E=1$ to 1·46 at $E=2$, and then tends asymptotically to 1·58 as E increases further. It does not seem possible to calculate $P(E)$ using the explicit form of $y(E)$, and so the following step function is used as a crude approximation (see figure 4)

$$\begin{aligned} y(E)&=1{\cdot}58 \quad (E\geqslant 2)\\ &=1{\cdot}20 \quad (1\leqslant E\leqslant 2) \end{aligned} \qquad \ldots\ldots (27)$$

In the approximation $W_{mi}\gg E_i+k_j$ the integral $C(E)$ of equation (23) is replaced by $C'(E)$, where

$$C'(E)=\frac{1}{30}(E_0-E)^5\int E_1^2E_2^2y(E_1)y(E_2)\delta(E-E_1-E_2)\,dE_1\,dE_2. \qquad \ldots\ldots (28)$$

Calculations using (27) and (28) show that the shape of $C'(E)$ is not very different from that of $C(E)$: the peak is shifted from 4·3 to $E\simeq 4{\cdot}5$. (This may

be expected, as $y(E)$ of (27) does not enhance $C'(E)$ (relative to $C(E)$) as much for low energies as it does for high energies.) The ratio of the area of $C'(E)$ to that of $C(E)$ gives a constant $y^2_{\text{effective}}$ ($\simeq 2{\cdot}2$) which can be used as a rough estimate for $y(E_1)y(E_2)$ in (28).

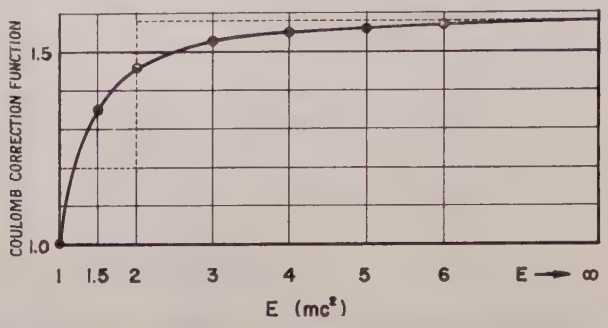

Figure 4. The Coulomb correction function $y(E)$ of equation (26). Also shown is the step function used as a crude approximation (broken line).

It seems reasonable to suppose that the functions $y(E)$ of (26) and (27) both have the same general effect on the shape of $C'(E)$, and, as shown above, this effect is not important. Moreover, it is quite likely that the modification to $A(E)$ and $B(E)$ due to $y(E_1)y(E_2)$ is also unimportant. Thus it can be concluded that, for $E_0 \simeq 8$ $y(E_1)y(E_2)$ has no serious effect on the shapes of the coincidence spectra, whichever of the approximations (12(i), or 12(ii)) is used, and that it may be treated as a constant (see § 2).

From the shape of $y(E)$ (figure 4), it is obvious that the larger E_0, the more accurate the above conclusion; but, if E_0 were smaller than 8, say 4, then (27) is much too crude an approximation, and the effect of $y(E_1)y(E_2)$ may become important. However, for small E_0, the lifetime for the decay is so long (see I) as to make it unamenable to experiment.

Finally, it is worth noting that the only dependence of $P(E)$ on Z, apart from the multiplicative factor $(2\pi Z/137)^2$, comes from $y(E_1)\,y(E_2)$. As Z increases $y(E)$ approaches unity: therefore any small effect that it has for $Z \simeq 20$, will become even less important for larger Z.

2.4. *Discussion of Spectra*

The preceding calculations show that the electron coincidence spectrum for two-neutrino double β-decay has the same general properties irrespective of the approximation used for W_{mi} (see 12(i), 12(ii)): in other words, the position E_p, of the peak (see § 2) is roughly independent of W_{mi}. This result, together with the behaviour of the functions occurring in §§ 2.1, 2.2, 2.3 can be understood in the following way.

Consider $A_1(E)$, $A_2(E)$ (equation (16)) and $B_1(E)$, $B_2(E)$ (equation (18)): after integration over E_2 the integration over E_1 is performed between the limits 1 and $E-1$. Obviously when $E=2$ these limits are equal, and all the integrals vanish. Since $A_1(E)$, $B_1(E)$ have a factor $E_0-E_1-E_2=E_0-E$, they vanish for $E_0=E$. In accordance with the δ-function, the factors $\log\{(E_0-E_1)/E_2\}$ and $\log\{(E_0-E_2)/E_1\}$ of $A_2(E)$, $B_2(E)$ are equal to $\log\{(E_0-E_1)/(E-E_1)\}$ and $\log\{(E_0-E+E_1)/E_1\}$ respectively: therefore $A_2(E)$, $B_2(E)$ vanish when $E_0=E$.

For large E, $A_1(E)$ and $A_2(E)$ are roughly proportional to $(E_0-E)E^7$ (since $\log\frac{E_0-E+E_1}{E_1}\simeq\frac{E_0-E}{E_1}$) and $B_1(E)$, $B_2(E)$ to $(E_0-E)E^5$. These functions have maxima at $E=\frac{7}{8}E_0$ and $E=\frac{5}{6}E_0$ respectively, and therefore the peaks of $A_i(E)$, $B_i(E)$ occur fairly close to E_0.

Since the integrands of equations (15), (17) are positive definite, $A(E)$, $B(E)$ are always positive: therefore $A_1(E)>A_2(E)$ and $B_1(E)>B_2(E)$. However, $A_1(E)$ is roughly of the same order of magnitude as $A_2(E)$ and similarly $B_1(E)\simeq B_2(E)$. Therefore the differences $A_1(E)-A_2(E)$ and $B_1(E)-B_2(E)$ (equal to $A(E)$, $B(E)$ respectively) will be small.

From (23), it is clear the $C(E)$ vanishes when $E=2$ and when $E_0=E$. For $2\leqslant E\leqslant E_0$, $C(E)$ is roughly proportional to $E^5(E_0-E)^5$ and since the maximum of this function occurs at $E=\frac{1}{2}E_0$, the peak of $C(E)$ will occur at $E\simeq\frac{1}{2}E_0$.

There are good reasons for believing that the curves for $A(E)$, $B(E)$, $C(E)$ all behave alike. From (11), (13), (14) and (23), it can be seen that each has the form

$$Q(E)=\int Q(E_1,E_2;\ k_1,k_2)\delta(E-E_1-E_2)\delta(E_0-E-k_1-k_2)\times dE_1\,dE_2\,dk_1\,dk_2 \quad \ldots\ldots(29)$$

where

$$\left.\begin{aligned}Q(E_1,E_2;\ k_1,k_2)&=Q(E_i,E_j;\ k_r,k_s)\\&=Q(k_r,k_s;\ E_i,E_j)\end{aligned}\right\} \quad \ldots\ldots(30)$$

(i,j) and (r,s) are any permutations of $(1,2)$. (Note that (30) is true for all values of W_{mi}). From (29),

$$Q(E)=\int_1^{E-1}dE_1\int_0^{E_0-E}dk_1Q(E_1,E-E_1;\ k_1,E_0-E-k_1) \quad \ldots\ldots(31)$$

(E_i includes the rest energy of the electron). When $E=2$ the limits for E_1 are equal, and when $E=E_0$, the limits for k_1 are equal. Therefore

$$Q(2)=Q(E_0)=0.$$

Since $Q(E_1,E_2;\ k_1,k_2)$ is symmetrical under the interchange of E_1,E_2 with k_1,k_2 the average energy of the electron pair $\bar{E}$ will be roughly equal to that of the neutrino pair, $\bar{k}$(i.e. $\bar{E}\simeq\bar{k}\simeq\frac{1}{2}E_0$). But because E_i includes the electron rest energy, $\bar{E}$ will be slightly greater than $\frac{1}{2}E_0$:

$$\bar{E}=\tfrac{1}{2}E_0+\epsilon \quad \ldots\ldots(32)$$

where ϵ is small and positive and tends to 0 as $E_0\to\infty$. (Though a general proof for (32) has not been found, it has been verified in a few special cases. In single β-decay the result analogous to (32) can be proved for any $Q(E,k)=Q(k,E)$.) The peak of $Q(E)$ occurs in the region of $\bar{E}$ and so from (32), it must be at some E_p slightly greater than $\frac{1}{2}E_0$.

$A(E)$, $B(E)$, $C(E)$ all approach zero asymptotically as $E\to E_0$ (i.e. they have 'tails') because their first, and perhaps higher, derivatives vanish at $E=E_0$. This may be seen from (11), (13) and (14), where integration over neutrino energies is roughly

$$\int_0^{E_0-E}k_1(E_0-E-k_1)\,dk_1\sim(E_0-E)^3$$

and from (23).

One last point: these similarities between $A(E)$, $B(E)$ and $C(E)$, combined with equations (25), (25′) show that for any W_{mi} a good approximation to the spectrum is given by replacing the energy denominators of (11) by a constant $W \simeq W_{mi} + \frac{1}{2}E_0$ (Konopinski 1955, Primakoff and Rosen 1959, eqn (75)). Such an approximation greatly reduces the labour of calculation.

§ 3. The Double β-decays of ^{96}Zr and ^{48}Ca

Throughout § 2 it is assumed that the double β-decay of the 0^+ ground state $|i\rangle$ of (A, Z) to the 0^+ ground state $|f\rangle$ of $(A, Z+2)$ proceeds either via

one state $|m\rangle$ (0^+ or 1^+) of intermediate nucleus $(A, Z+1)$ (assumption (i))

or via

two states, $|m\rangle$ (0^+) and $|m'\rangle$ (1^+) whose energy difference is negligible (assumption (ii)).

Though such assumptions appear to be arbitrary, at least one of them does, in fact, apply to two of the double β-decays most amenable to experiment.

^{96}Zr has 40 protons and 56 neutrons, it decays via ^{96}Nb (41p, 55n) to ^{96}Mo (42p, 54n). On a simple shell model, the ground state of ^{96}Zr has 40 protons in a closed shell, and the lowest available level for the next proton is $1g_{9/2}$. Fifty neutrons form a closed shell, and it seems reasonable to assume (see for example Mayer and Jensen 1955, p. 136) that, in ground state configurations odd neutrons just above $N=50$ prefer the $2d_{5/2}$ level, but pairs (which always couple to zero angular momentum) the $1g_{7/2}$ level. Thus the ground state configuration of nucleons outside closed shell can be written, for ^{96}Zr, as $(n:\ 1g_{7/2})^6{}_{0^+}$. By similar arguments the ground state of ^{96}Nb is

$$[(n:1g_{7/2})^4{}_{0^+}\,(n:2d_{5/2})(p:1g_{9/2})]$$

and that of ^{96}Mo is

$$[(n:\ 1g_{7/2})^4{}_{0^+}\ \ (p:\ 1g_{9/2})^2{}_{0^+}]_{0^+}.$$

In the decay of $|i\rangle$ to $|f\rangle$, two $1g_{7/2}$ neutrons change into two $1g_{9/2}$ protons. The only possible way for this to occur is by means of the axial vector interaction according to the scheme

$$(n:1g_{7/2})^6{}_{0^+} \rightarrow [(n:1g_{7/2})^5\,(p:1g_{9/2})]_{1^+} \rightarrow [(n:1g_{7/2})^4{}_{0^+}\,(p:1g_{9/2})^2{}_{0^+}]_{0^+} \qquad \ldots\ldots(33)$$

At the present time there seems to be no data available for the separation between the $2d_{5/2}$ and $1g_{7/2}$ neutron levels in ^{96}Nb. However, Goldhaber and Hill (1952) give such a separation in ^{97}Mo as 0·665 Mev. If, as seems reasonable, the extra proton has little effect on this separation, then it may be taken as roughly the same in both cases. Then, from the data given in I, $E_0 = 8{\cdot}6$ and $W_{mi} = +0{\cdot}05$ (in units of mc^2) for the double β-decay of ^{96}Zr.

Similar considerations show that there are two possible decay schemes for ^{48}Ca.

$$(n:1f_{7/2})^8{}_{0^+} \begin{cases} \nearrow [(p:1f_{7/2})(n:1f_{7/2})^7]_{0^+} \\ \searrow [(p:1f_{7/2})(n:1f_{7/2})^7]_{1^+} \end{cases} \begin{cases} \searrow \\ \nearrow \end{cases} [(p:1f_{7/2})^2{}_{0^+}\,(n:1f_{7/2})^6{}_{0^+}]_{0^+} \qquad \ldots\ldots(34)$$

The outer configurations represent the ground states of ^{48}Ca and ^{48}Ti respectively, and the two middle ones are two excited states of ^{48}Sc, the ground state being $[(p:1f_{7/2})(n:1f_{7/2})^7]_{6+}$. The separation between these isomeric levels of ^{48}Sc is small (300→400 kev) compared with the separation between ^{48}Ca and ^{48}Ti (5·3 Mev), and so $W_{mi} \simeq W_{m'i} = (-1{\cdot}0) \rightarrow (-0{\cdot}8)$ and $E_0 = 10{\cdot}6$.

This simple model shows that assumption (i) applies to the double β-decay of ^{96}Zr, and it would appear that assumption (ii) holds for ^{48}Ca. However, it can be shown from considerations of an isobaric spin selection rule (see I) that in the case of ^{48}Ca

$$\langle f|\sum\tau^+|m\rangle\langle m|\sum\tau^+|i\rangle \simeq 0;$$

therefore in this case also there is effectively only one intermediate state via which the decay proceeds. (Much of the above discussion is taken from Rosen 1957.)

§ 4. Conclusions

The electron coincidence spectrum for two-neutrino double β-decay has been shown to have two general properties which contradict the earlier calculation mentioned in § 1 (Rosen 1957). They are (i) the broad peak occurs at an energy E_p equal to $\frac{1}{2}E_0 + \epsilon$, where ϵ is small (E_0 is the energy release), (ii) a definite 'tail' as E approaches E_0 (see figures 2 and 3). The calculations of § 2 have been very carefully checked, and, since they are in agreement with the qualitative arguments of § 2·4, it is now believed that the earlier calculation, which gave $E_p \simeq E_0$, is incorrect.

It is interesting to apply these results to the double β-decay of ^{96}Zr and of ^{48}Ca. Consider the Hamiltonian (1), and the conditions (4) and (5) for the non-occurrence of no-neutrino double β-decay: the latest data on single β-decay show that (5) is true to within 10%. If it turns out that (5) is exact, then the measured coincidence spectra will have both properties (i) and (ii). But suppose (5) is only approximate, say

$$\delta_\lambda = \eta_\lambda = 0{\cdot}997. \qquad \ldots\ldots (5')$$

The value of D_λ cannot be learned from single β-decay alone. However, the likeliest possibilities are either (lepton 'charge' conserved)

$$D_\lambda = 0 \quad (\text{all } \lambda) \qquad \ldots\ldots (4)$$

in which case the probability for no-neutrino double β-decay is zero, or (lepton 'charge' not conserved)

$$D_\lambda \simeq C_\lambda \,(\text{all } \lambda). \qquad \ldots\ldots (4')$$

With (4′) and (5′) for the coupling constants, two-neutrino and no-neutrino double β-decay have roughly the same probabilities, and the coincidence spectrum will have not only a broad peak at $\frac{1}{2}E_0$, but also an infinitely sharp peak at E_0 (apart from instrumental broadening). This latter peak will appear taller than that at $\frac{1}{2}E_0$, because the areas under the peaks represent the relative probabilities of the two processes, and the one at $\frac{1}{2}E_0$ will certainly be the broader of the two. Thus in the event that (5) is only approximate, i.e. in the event that parity violation is non-maximal, careful study of the double β-decay electron coincidence spectrum offers a test for lepton 'charge' conservation.

In conclusion, it may be again stated that the simple qualitative picture of § 1, relating the nature of double β-decay to the shape of the electron coincidence spectrum, has been proved correct.

Acknowledgments

The author would like to thank Dr. R. J. Blin-Stoyle and Professor H. Primakoff for their continued helpful interest in this work, and also Professor R. E. Peierls for a useful suggestion (transmitted via Dr. Blin-Stoyle). He is also grateful to Professor Primakoff for reading the manuscript.

References

Bateman Manuscript Project : *Higher Transcendental Functions*. A. Erdelui, editor (McGraw-Hill, 1953).

Enz, C. D., 1957, *Nuovo Cim.*, **6**, 250.

Goldhaber, M., and Hill, R., 1952, *Rev. Mod. Phys.*, **24**, 179.

Konopinski, E. J., 1955, *Los Alamos Reports*, L.A.M.S.—1949.

Luders, G., 1958, *Nuovo Cim.*, **7**, 171.

Mayer, M. G., and Jensen, J. H. D., 1955, *Elementary Theory of Nuclear Shell Structure* (New York : John Wiley).

Pauli, W., 1957, *Nuovo Cim.*, **6**, 204.

Primakoff, H., and Rosen, S. P., 1959, *Rep. Progr. Phys.*, **22**, 121 (London : Physical Society).

Pursey, D. L., 1957, *Nouvo Cim.*, **6**, 266.

Rosen, S. P., 1957, *D. Phil. Thesis*, University of Oxford.

Hall Coefficient and Magnetoresistance in Semiconducting Diamond†

By R. T. BATE and R. K. WILLARDSON
Battelle Memorial Institute, Columbus, Ohio

MS. received 9th March 1959

Abstract. The Hall coefficient and transverse magnetoresistance of two type II-b semiconducting diamonds (p-type) were measured as a function of magnetic field from 500 gauss to 20 000 gauss at fixed temperatures between 0°c and 100°c. These diamonds have $R\sigma$ values of about 1000 $cm^2 v^{-1} sec^{-1}$ at room temperature. The Hall coefficient increases monotonically with increasing field, the total variation being about 10 per cent. This behaviour is similar to that which has been reported for p-type silicon at liquid nitrogen temperature, and it suggests a warped valence band. The transverse magnetoresistance is proportional to H^2 at low fields, but deviates from this behaviour at fields above 4000 gauss. The magnetoresistance is larger than would be expected for a spherical band but can be explained if a warped valence band is assumed. A warped band is also suggested by the longitudinal magnetoresistance which is about one-third the transverse value.

§ 1. Introduction

The analysis of galvanomagnetic effects has been quite helpful in elucidating the band structures of the Group IV semiconductors, germanium (Willardson, Harman and Beer 1954), and silicon (Beer and Willardson 1958). A similar analysis of diamond, the first member of the group, should aid in correlating the properties of these three elemental semiconductors.

The principal difficulty in experimental investigations of diamonds is the lack of control of composition. Natural semiconducting diamonds (the so-called 'type II-b' diamonds) (Custers 1952) are usually rather impure compared with available germanium and silicon, and the impurity distributions are usually more or less inhomogeneous. Thus, galvanomagnetic analysis of natural diamonds can probably yield information of only a general nature.

§ 2. Experimental Details

The two diamonds used in this investigation were rectangular parallelepipeds approximately 4 mm × 2 mm × 2 mm. Contacts were made with silver paint after the polished surface was first roughened by spreading No. 600 Carborundum powder on the surface and rubbing with a needle at the point where contact was to be made. Contacts made in this way were ohmic and of very low resistance. Spring-loaded probes were used to contact the silver paint dots on the diamonds.

Very precise temperature control was required for some of the measurements (particularly where the Hall coefficient was determined as a function of magnetic field) because of the strong temperature dependence of the carrier concentration. This was accomplished by circulating water from a constant-temperature bath

† This research was supported by the U. S. Air Force through the Office of Scientific Research of the Air Research and Development Command.

through a jacket surrounding the sample. The water temperature was regulated by using a simple thermistor controller to control heaters in the bath. This arrangement kept the temperature of the diamond constant to within $\pm 0{\cdot}05\,^{\circ}\mathrm{C}$.

§ 3. Results and Discussion

Figure 1 shows a plot of the Hall coefficient R which is positive for both diamonds, as a function of temperature. In the case of sample S the Hall voltage was found to vary considerably depending on the placement of the Hall probes, probably indicating that the impurity distribution is inhomogeneous. The plot shown here is for a particular placement of the Hall contacts. In sample L the effect of moving the Hall probes was negligible so that in this case the plot may be considered approximately characteristic of the entire diamond.

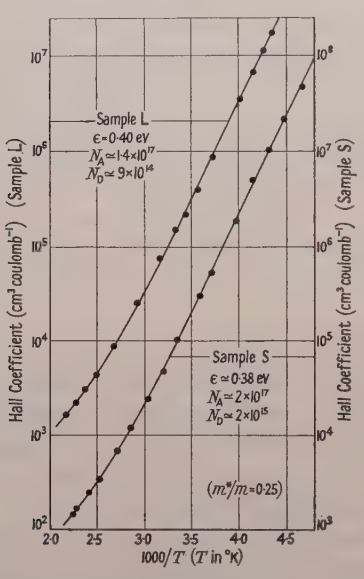

Figure 1. Temperature dependence of the Hall coefficient of type II-b semiconducting diamond.

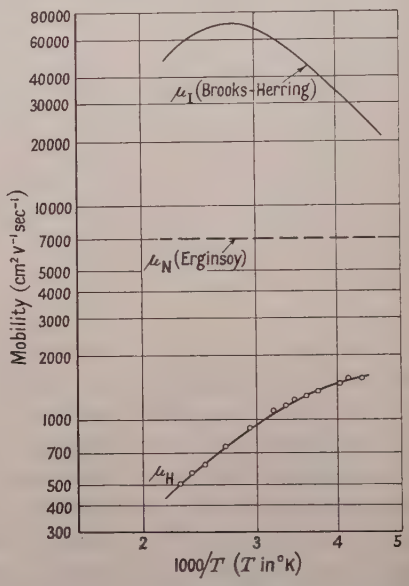

Figure 2. Temperature dependence of Hall mobility of semiconducting diamond.

Assuming that the impurities consist of one type of ionized donor and a large concentration of one type of acceptor, and that these impurities are not multiply ionized, the hole concentration p is given by (Shockley 1950):

$$p(p+N_D)/(N_A-N_D-p)=(2\pi m^* kT/h^2)^{3/2}\exp(-\epsilon/kT). \quad \ldots\ldots(1)$$

Making use of the strong field relation†

$$p=1/Re, \quad \ldots\ldots(2)$$

the values of acceptor activation energy ϵ and the donor and acceptor concentrations N_D and N_A which make equation (1) fit the data, have been determined. These values are noted in figure 1. (The impurity concentrations noted for the inhomogeneous sample S have only order of magnitude significance.) An effective mass ratio of 0·25, which is suggested by the work of Wedepohl (1957), ha

† The magnetic-field dependence of the Hall coefficient indicates that this assumption is probably accurate within 10% or so when the Hall coefficient is measured at 10 000 oersted (see figure 3).

been used in this calculation. It was, of course, not possible to obtain mobility values on sample S but figure 2 shows the temperature dependence of the Hall mobility $\mu_H = R/\rho$ for sample L (the bottom curve). An interesting fact about this plot is that the mobility curve seems to bend over at low temperatures, which suggests that impurity scattering is important at temperatures as high as room temperature. It is of interest to calculate the mobility which would be expected if only impurity scattering were important. Considering first *ionized* impurity scattering, the mobility is calculated from the Brooks–Herring relation (see discussion by Debye and Conwell (1954), Dingle (1955) and Brooks (1955)):

$$\mu_I = (8\sqrt{2}/\pi\sqrt{\pi})\{K^2(\boldsymbol{k}T)^{3/2}/\boldsymbol{e}^3 m^{*1/2} N_I\}/[\mathrm{Log}\,(1+b) - b/1+b]$$
$$b = 6Km^*(\boldsymbol{k}T)^2/\pi p\hbar^2\boldsymbol{e}^2, \qquad \ldots\ldots (3)$$

where N_I is the ionized-impurity concentration and K is the static dielectric constant, which is taken as 5·7 for diamond. N_I is just $p + 2N_D$ where p is given by equation (1) or (2). Since p is very temperature dependent, the screening effect of the carriers will be also, and the variation of b with temperature must be taken into account. The top curve in figure 2 is a plot of μ_I as given by equation (3). The mobility decreases at high temperatures because of thermal ionization of acceptors. This predicted mobility is obviously too large to explain the low-temperature data.

Erginsoy (1950) has considered scattering by *neutral* impurities at low temperatures. His results yield the following relation for the mobility due to neutral-impurity scattering :

$$\mu_N = 2\pi^3 m^* \boldsymbol{e}^3/5KN_N h^3, \qquad \ldots\ldots (4)$$

where N_N is the neutral-impurity concentration given by

$$N_N = N_D + N_A - N_I = N_A - N_D - p$$

for the model postulated above. Inspection of the data shows that $N_N \simeq N_A$ over the temperature range covered by the measuremnts, so that mobility predicted by equation (4) is temperature independent (middle curve in figure 2). The use of the Erginsoy relationship at such high temperatures is probably not justified, but it should indicate the order of magnitude of the neutral-impurity contribution. This calculation suggests that neutral-impurity scattering is more important than ionized-impurity scattering in the temperature range covered. Of course, if multiple ionization of impurities occurs, the analysis would require modification.

Figure 3 shows the magnetic-field dependence of the Hall coefficient of the two diamonds at two different temperatures. We have normalized to the 1000-oersted value to facilitate comparison. The scatter in the experimental points is due to temperature variations within the limit of control.

There are two interesting features about these plots: first, the Hall coefficient increases with increasing magnetic field, and second, the Hall coefficient is field dependent even at weak magnetic fields. The increase with increasing magnetic field is similar to the behaviour observed in p-type silicon (Beer and Willardson 1958) and is usually associated with a warped band. The field dependence at weak fields does not seem consistent with the measured mobility values as long as one assumes that only one type of carrier contributes to conduction. However, the presence of a warped light-mass band and associated high-mobility holes might explain the variation.

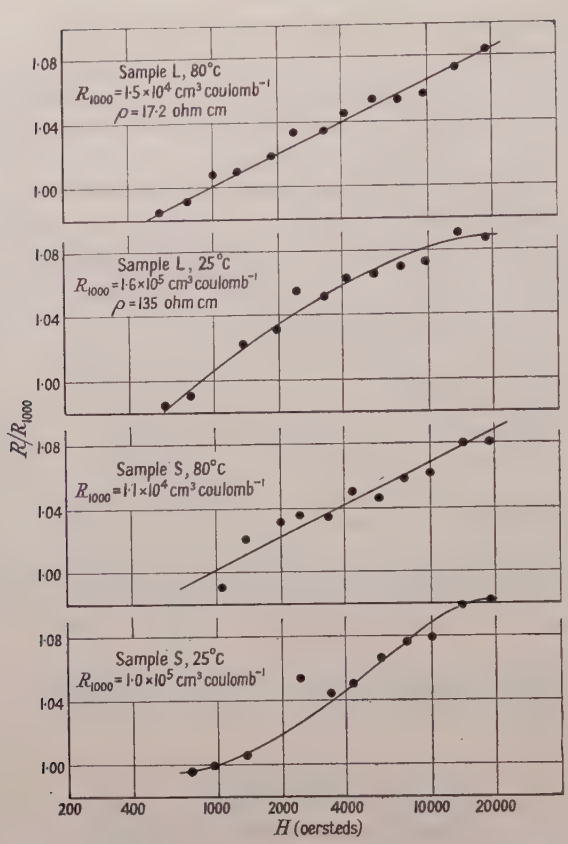

Figure 3. Magnetic-field dependence of the Hall coefficient of semiconducting diamond.

Figure 4 shows the corresponding plot of magnetoresistance as a function of magnetic field. Note that the magnetoresistance is approximately proportional to H^2 at low fields but definitely deviates from this behaviour at higher fields. The magnitude of the magnetoresistance is much greater than we would expect for a single spherical band, unless the relaxation time is extremely energy dependent, but could be easily explained if the valence band were suitably warped or degenerate. Additional evidence for a warped valence band in diamond is provided by the longitudinal magnetoresistance measurements of Mitchell and Wedepohl (1957), who find a longitudinal magnetoresistance effect about one-third as large as the transverse effect.

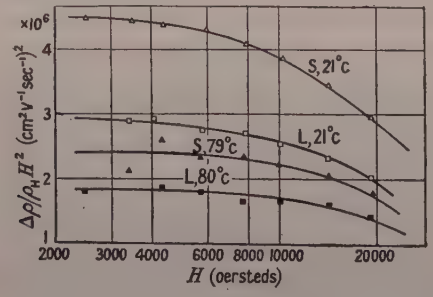

Figure 4. Magnetoresistance of semiconducting diamond.

Since the galvanomagnetic effects are very sensitive to different scattering mechanisms, and in view of the uncertainty about the scattering mechanisms involved, it does not seem worth while at present to attempt a more detailed analysis of the data.

Acknowledgments

The authors are indebted by Dr. J. F. H. Custers and the Diamond Research Laboratory, Industrial Distributors (1946) Ltd., Johannesburg, for the loan of the diamonds used in this research, to Dr. P. T. Wedepohl for his advice on contacting methods, and to Dr. A. C. Beer for his suggestions and review of the manuscript.

References

Beer, A. C., and Willardson, R. K., 1958, *Phys. Rev.*, **110,** 1286.
Brooks, H., 1955, *Advances in Electron Physics* (New York : Academic Press), pp. 157–58.
Custers, J. F. H., 1952, *Physica*, **18,** 489.
Debye, P. P., and Conwell, E. M., 1954, *Phys. Rev.*, **93,** 693.
Dingle, R. B., 1955, *Phil. Mag.*, **46,** 831.
Erginsoy, C., 1950, *Phys. Rev.*, **79,** 1013.
Mitchell, E. W. J., and Wedepohl, P. T., 1957, *Proc. Phys. Soc.* B, **70,** 527.
Shockley, W., 1950, *Electrons and Holes in Semiconductors* (New York : Van Nostrand), pp. 248–49.
Wedepohl, P. T., 1957, *Proc. Phys. Soc.* B, **70,** 177.
Willardson, R. K., Harman, T. C., and Beer, A. C., 1954, *Phys. Rev.*, **96,** 1512.

The Equilibrium of a Double Layer

By R. CADE
University College of the West Indies, Jamaica

Communicated by R. Fürth; MS. received 27th January 1959

Abstract. Generally, a body immersed in a fluid is surrounded by an electric double layer at least part of which resides in the fluid. In a previous paper (which contains an error corrected in the present paper), it was found that the double layer must satisfy certain conditions of macroscopic theory in order to be in equilibrium. In this paper it is shown that the conditions can be simultaneously satisfied, but not uniquely so, so that they do not determine the structure of the double layer, although in certain circumstances, they determine it partially.

A discussion is given of the relationship of the present theory to the microscopic theory, and its role in relation to that theory.

§ 1. Introduction

In a previous paper (Cade 1954, to be referred to as I) an amendment was made to the general theory of electrostatic forces developed independently by Slepian (1950) and Brown (1951), to take into account the effect of a double layer surrounding an immersed body. A result of the theory was a set of conditions that a double layer, or the part of it in fluid, must satisfy in order to be in a state of stationary equilibrium. The object here is to investigate the possibility of simultaneously satisfying the conditions, and the extent to which they determine the structure of the double layer.

In the case of a double layer consisting of fixed dipoles, it is found that all of the conditions are identically satisfied except one, which simply requires that the polarization vector be effectively normal to the surface. Otherwise, the conditions do not restrict or determine the structure in any way and are therefore of little interest. However, the case itself is probably of minor physical importance. In general a double layer consists of fixed dipoles and free charges, and the other extreme occurs when it consists entirely of free charges. The position is now reversed; the condition which previously was not identically satisfied, now is, while the others are not. This is probably the case of major physical importance, and the conditions are not satisfied in any obvious manner. Accordingly, this is the case with which the paper is essentially concerned. It is shown that the conditions can be satisfied, but not uniquely, so that again the structure of the double layer is not determined by them. However, we now find that if there is no external field, the structure is partially determined by them in a certain sense.

The conditions appeared as a by-product of the theory of I, and while the purpose of this paper is to develop this aspect, it also provides an opportunity to correct an error which affects the main conclusions. A basic assumption of I

was, in the notation of that paper, that a function in the boundary layer can be expressed in the form

$$\mathrm{f}\left\{\frac{x^0-c_s}{a}, x^1, x^2, a\right\} \qquad \ldots\ldots(1)$$

and can be expanded into a power series in a. If the lowest power is the nth, the function is said to be of order a^n. The quantity a is a small parameter which we call the thickness of the boundary layer. There is, of course, no 'thickness' in the strict geometrical sense; the most that can be said is that there is a distance of the same order as a from the boundary outside which double layer effects are negligible, and by the boundary layer we simply mean the fluid within this distance. It was argued in I that the acceleration in the boundary layer is of order a^{-1} when Cartesian coordinates are used, although it is known to be of order a^0 in terms of the curvilinear coordinates (x^0, x^1, x^2). This argument is evidently without foundation and, in fact, the order is a^0 irrespective of the choice of coordinates. It follows that the force of inertia of the boundary layer is of order a and not a^0 as previously stated. It is therefore very small and, as a result, although the electrostatic stresses may become modified in the boundary layer, giving rise to electrokinetic motion and to a modification of the stresses acting upon the immersed body, there can be no appreciable modification of the total force on the body, obtained by integrating the stresses. A similar argument applies to the torque.

The validity of the conditions found to be imposed upon the double layer is unaffected. A further feature of the methods used was the assumption that a is to some extent arbitrary. Thus when, in an equation, functions were expressed as power series in a, factors of the same powers of a could be equated, and in this way one equation provided several equations corresponding to the various powers of a. For example, the equations expressing the conditions upon the double layer contain various physical and geometrical quantities, and it is understood that really only the factors of the lowest powers of a are involved. Consequently, our discovery that the total force on the immersed body due to the layer is zero to one power higher in a than was first thought, leads to an additional set of conditions corresponding to this higher power. However, in this paper we shall abandon the assumption that a is arbitrary. The consequence of this is that if we have an equation like,

$$(A-B)a+(C-D)a^2=0, \qquad \ldots\ldots(2)$$

where A, B, C and D are numbers of the same order, we cannot infer that $A=B$, $C=D$. However, given that a is very small, we can infer that $A=B$ approximately, but we can say nothing about C and D. We therefore see that, with this different assumption, the conditions upon the double layer that we already have hold *approximately*—very closely in fact since the error involves higher powers of the very small number a—but we cannot assert any higher-order conditions.

The new assumption seems more reasonable on physical grounds, as all the evidence is to the effect that a or some similar parameter is a characteristic of two materials which are in contact. However, without invoking such evidence, one could argue on logical grounds that the assumption is more general since it leads to less restrictions.

In the notation of I, the conditions upon the double layer are

$$[P_\mu \mathbf{a}_\mu, \mathbf{a}_0]=0 \quad (\mu=0, 1, 2), \qquad \ldots\ldots(3)$$

$$\int_S \left\{ -\mathbf{a}_0 \tfrac{1}{2} E_0 D^0 \frac{\partial}{\partial x^0} \log (g_{11} g_{22}) + \mathbf{a}_1 \left[\tfrac{1}{2} g^{00} \frac{\partial g_{00}}{\partial x^1} E_0 D^0 + \frac{\partial}{\partial x^1} (E_0 D^0) \right] \right.$$
$$\left. + \mathbf{a}_2 \left[\tfrac{1}{2} g^{00} \frac{\partial g_{00}}{\partial x^2} E_0 D^0 + \frac{\partial}{\partial x^2} (E_0 D^0) \right] \right\} dS_0 = 0, \quad \ldots\ldots (4)$$

$$\int_S \left\{ [\mathbf{a}_0, \mathbf{r}] \tfrac{1}{2} E_0 D^0 \frac{\partial}{\partial x^0} \log (g_{11} g_{22}) + [\mathbf{r}, \mathbf{a}_1] \left[\tfrac{1}{2} g^{00} \frac{\partial g_{00}}{\partial x^1} E_0 D^0 + \frac{\partial}{\partial x^1} (E_0 D^0) \right] \right.$$
$$\left. + [\mathbf{r}, \mathbf{a}_2] \left[\tfrac{1}{2} g^{00} \frac{\partial g_{00}}{\partial x^2} E_0 D^0 + \frac{\partial}{\partial x^2} (E_0 D^0) \right] \right\} dS_0 = 0, \quad \ldots\ldots (5)$$

$$\frac{\partial D^{*0}}{\partial x^\alpha} E_0^* - \frac{\partial D^{*0}}{\partial x^0} E_\alpha^* + \tfrac{1}{2} g^{00} \frac{\partial g_{00}}{\partial x^\alpha} D^{*0} E_0^* = 0 \quad (\alpha = 1, 2). \quad \ldots\ldots (6)$$

Formula (3) is a summary of the discussion following (36) of I, while (4)—(6) are identical with (40)—(42) of I except that we no longer use the upper suffix [2]. The reason is that this suffix meant the term of the lowest power in a in the expansion of the associated quantity, and in accordance with what has been said above, such considerations no longer enter; symbols now refer to whole quantities. Conditions (3)—(5) are of hydrodynamical origin and they hold quite generally, while (6) is of thermodynamical origin and holds only when there is no external field. It will be recalled that the asterisks in (6) imply the values of field quantities in the boundary layer when there is no external field.

The significance of (3) is simply that the polarization vector P_μ is effectively normal to the solid boundary, and this condition needs no further examination. A double layer consisting of fixed dipoles is such that P_μ is the only effective source of the electrokinetic potential Φ. In this case, Poisson's equation,

$$\frac{1}{\sqrt{g}} \frac{\partial}{\partial x^\mu} (D^\mu \sqrt{g}) = 4\pi\rho, \quad \ldots\ldots (7)$$

is such that $\rho = 0$ to the relevant order in a, and the solution corresponding to this order is

$$D^0 = 0, \quad \ldots\ldots (8)$$

whence the conditions (4) and (5) are satisfied identically, as also is (6) if there is no external field, that is, $D^\mu = D^{*\mu}$. However, according to formulae obtained in I, there can be no appreciable electrokinetic flow if D^0 is zero to this order. Physically, this phenomenon is well known and is one of the most important observable effects associated with a double layer. We must infer that a double layer which exhibits it consists at least partly of free charges. We shall assume that the double layer consists entirely of free charges as regards the order in a which contributes effectively to Φ, and we therefore put

$$D_\mu = E_\mu. \quad \ldots\ldots (9)$$

The existence of electrokinetic flow when there is an external field means that one can in general only speak of equilibrium in the sense of stationary equilibrium, that is, the velocity, regarded as a vector field, is time-independent. Stationary equilibrium includes static equilibrium as the special condition of no electrokinetic flow.

Demonstration that the conditions upon the double layer can be satisfied is clearly necessary for the internal consistency of the macroscopic electrical theory

In particular, we shall find that the conditions are satisfied by a double layer for which Φ is constant over the surface. This property has generally been assumed. In this case we obtain no information on the form of the potential ϕ within the boundary layer, but in other cases, if we take a general form and assume that the dependence upon x^1 and x^2 is known, it appears that the dependence upon x^0 is determined by (6).

The structure of a double layer is determined by microscopic theory, and the present theory is therefore relatively impotent for the purpose. The matter will be discussed at greater length later, and it will be found that the real value of the present theory lies in a certain complementary role to the microscopic theory.

§ 2. Mathematical Simplification of the Conditions

The curvilinear coordinates (x^0, x^1, x^2) are assumed to be orthogonal and such that one of the surfaces $x^0 = \text{const.}$, $\bar{S}$ say, coincides with the surface of the solid. The possibility of this is assured, and the conditions (4)—(6) can be expressed much more simply, if the coordinates are defined according to a general prescription of differential geometry. Accordingly, the surfaces $x^1 = \text{const.}$, $x^2 = \text{const.}$ are developables generated by the normals to the lines of curvature on $\bar{S}$, and those for $x^0 = \text{const.}$ are such that each member S is parallel to $\bar{S}$, $\bar{S}$ itself being given by $x^0 = 0$.

The essentials of the theory of this coordinate system are given in tensor notation by Eisenhart (1947). The complete theory is given by Weatherburn (1947), but in long notation. It is evidently a system of immense value for problems of the boundary-layer kind in mathematical physics. It has previously been used, in long notation, by Howarth (1951) and his followers.

We shall use the suffices μ, ν, taking the values 0, 1, 2, to denote tensors in space, and the suffices α, β, taking the values 1, 2, to denote tensors on one of the surfaces S. Bars will be used to denote quantities on $\bar{S}$ corresponding to those on S. We proceed to summarize some useful properties of the new coordinate system:

(i) The fundamental tensor of space, $g_{\mu\nu}$, is such that $g_{\mu\nu} = 0$ $(\mu \neq \nu)$ and $g_{00} = g^{00} = 1$.

(ii) The first fundamental tensor of S, $g_{\alpha\beta}$, is such that $g_{\alpha\beta} = 0$ $(\alpha \neq \beta)$, and g_{11} and g_{22} are equal, respectively, to the components g_{11} and g_{22} of $g_{\mu\nu}$.

(iii) The second fundamental tensor of S, $d_{\alpha\beta}$, and the first fundamental tensor of the spherical image, $h_{\alpha\beta}$, are such that $d_{\alpha\beta} = h_{\alpha\beta} = 0$ $(\alpha \neq \beta)$.

(iv) With a proper choice of the mutual coordinate directions, the tensors $g_{\alpha\beta}$, $d_{\alpha\beta}$ and $h_{\alpha\beta}$ are related to the corresponding quantities on $\bar{S}$ by

$$\left.\begin{aligned} g_{\alpha\beta} &= \bar{g}_{\alpha\beta} - 2x^0\bar{d}_{\alpha\beta} + (x^0)^2\bar{h}_{\alpha\beta}, \\ d_{\alpha\beta} &= \bar{d}_{\alpha\beta} - x^0\bar{h}_{\alpha\beta}, \\ h_{\alpha\beta} &= \bar{h}_{\alpha\beta}. \end{aligned}\right\} \qquad \ldots\ldots (10)$$

(v) The mean curvature K_{m} and the Gaussian curvature K of S are given by

$$K_{\mathrm{m}} = \frac{d_{11}}{g_{11}} + \frac{d_{22}}{g_{22}}, \qquad \ldots\ldots (11)$$

$$K = \frac{d_{11}d_{22}}{g_{11}g_{22}}. \qquad \ldots\ldots (12)$$

(vi) The unitary vectors $\mathbf{a}_\mu$, defined by Wills (1931), are related to the unit vectors $\mathbf{n}, \mathbf{s}, \mathbf{t}$ in the respective x^0, x^1 and x^2 directions by $\mathbf{a}_0 = \mathbf{n}$, $\mathbf{a}_1 = \sqrt{g_{11}}\mathbf{s}$, $\mathbf{a}_2 = \sqrt{g_{22}}\mathbf{t}$. The unit normal $\mathbf{n}$ is the same at corresponding points of all the surfaces S.

(vii) The quantity dS_0, the 0-component of the covariant surface-element vector, is numerically equal to the element of area dS, so that

$$dS_0 = \pm dS = \pm \sqrt{(g_{11}g_{22})}dx^1dx^2. \qquad \ldots\ldots(13)$$

The sign depends upon the mutual orientation of the coordinate directions; this ambiguity is unimportant in the applications here.

By virtue of (i) and equation (9), condition (4) reduces at once to the pair of differential equations

$$\frac{\partial E_0^*}{\partial x^\alpha} E_0^* - \frac{\partial E_0^*}{\partial x^0} E_\alpha^* = 0. \qquad \ldots\ldots(14)$$

The application of (i) and (9) provides the first major reduction in conditions (5) and (6). The next is to get rid of the terms containing $\mathbf{a}_1$ and $\mathbf{a}_2$. This can be done with the use of (vi) and (vii) and the application of Green's theorem in the forms

$$\int \nabla U d\tau = \int U\mathbf{n}dS, \quad \int [\mathbf{r}, \nabla]U d\tau = \int [\mathbf{r}, \mathbf{n}]UdS, \qquad \ldots\ldots(15)$$

to the space between an arbitrary pair of surfaces S, where U is a function equal to E_0^2 in the present case, and $d\tau$ is a volume-element. Finally, with the use of (10) and (11), the quantity $(\partial/\partial x^0)\log(g_{11}g_{22})$ is found to be equal to $-2K_m$.

The result is that conditions (5) and (6) are reduced to

$$\int K_m E_0^2 \mathbf{n} dS = 0, \qquad \ldots\ldots(16)$$

$$\int K_m E_0^2 [\mathbf{r}, \mathbf{n}] dS = 0. \qquad \ldots\ldots(17)$$

§ 3. Solution of the Conditions

The potential ϕ, having the value ϕ^* under conditions of no external field, is related to E^μ by

$$E_\mu = \frac{\partial \phi}{\partial x^\mu}. \qquad \ldots\ldots(18)$$

The general solution of the equations (14) is

$$\phi^* = \mathbf{f}\{x^0 + \psi(x^1, x^2)\}, \qquad \ldots\ldots(19)$$

where ψ is an arbitrary function. This solution can be verified by substitution. It can be deduced by putting $E_\alpha^* = u_\alpha E_0^*$ and using (18), whence the equations become replaced by linear differential equations for ϕ^* which are solvable by separation of variables. The details are given in the Appendix.

To obtain solutions of (16) and (17) we make use of the following identities:

$$\int \mathbf{n} dS = 0, \quad \int [\mathbf{r}, \mathbf{n}] dS = 0, \qquad \ldots\ldots(20)$$

$$\int K_m \mathbf{n} dS = 0, \quad \int K_m [\mathbf{r}, \mathbf{n}] dS = 0, \qquad \ldots\ldots(21)$$

$$\int K\mathbf{n}dS = 0, \quad \int K[\mathbf{r}, \mathbf{n}]dS = 0. \qquad \ldots\ldots(22)$$

The first two follow from (15) when $U=1$. The other pairs are derivable from this pair by substituting for dS from (13), differentiating twice successively with respect to x^0 under the integral sign and using (10)—(12). Comparing (21) with (16) and (17), we find immediately that (16) and (17) are satisfied if ϕ is a function of x^0 alone. In particular, if there is no external field,

$$\phi^* = F(x^0), \qquad \ldots\ldots (23)$$

and this is consistent with (19) if ψ is a constant.

The double layer described by this solution is the one usually contemplated; for a given distance x^0 from $\bar{S}$, it is uniform with respect to x^1 and x^2, and the electrokinetic potential Φ (a *potential difference* corresponding to two prescribed values of x^0) is a constant.

In the case of surfaces for which K_m has always the same sign, we get another solution of (16) and (17) from (20):

$$E_0^2 = \xi(x^0)/K_m. \qquad \ldots\ldots (24)$$

In this equation we can replace K_m by $\bar{K}_m$ because the difference between the two is of order a, which is three orders higher in a than E_0^2 and so well within the intrinsic margin of uncertainty. Therefore,

$$\phi = \frac{\eta(x^0)}{\sqrt{|\bar{K}_m|}}, \quad \eta = \pm \int |\xi|^{1/2} dx^0. \qquad \ldots\ldots (25)$$

This has to be consistent with (19) if there is no external field, which is possible only if

$$\phi = \phi^* = \frac{A}{\sqrt{|\bar{K}_m|}} \exp(kx^0), \qquad \ldots\ldots (26)$$

where A and k are constants. The function ψ is given by

$$\psi = B - \frac{1}{2k} \log |\bar{K}_m|, \qquad \ldots\ldots (27)$$

where B is another constant.

Yet another solution is supplied by (22) provided that now K/K_m has always the same sign on the surface. We find by the same argument as above,

$$\phi^* = A\sqrt{|\bar{K}/\bar{K}_m|} \exp(kx^0), \qquad \ldots\ldots (28)$$

with

$$\psi = B - \frac{1}{2k} \log |\bar{K}_m/\bar{K}|. \qquad \ldots\ldots (29)$$

Other solutions, of a more general character, are obtainable by considering the identities formed by the addition of (20)–(22).

The finding of other solutions demonstrates the lack of uniqueness. The extent of the non-uniqueness is indeed very large, as we can show by reference to a special surface, the sphere $r=r_0$, in terms of spherical polar coordinates (r, θ, ω). If the sphere is surrounded by a double layer such that

$$\phi^* = p(x^1, x^2) \exp(kx^0) = p(\theta, \omega) \exp\{k(r-r_0)\}, \quad p(\theta, \omega) = p(\theta) = p(\pi - \theta),$$

then all the conditions are satisfied. It is equally easy to form the function p so that the conditions are not satisfied, but the significant thing is that the number of functions which satisfy the conditions is evidently an infinity of the same order as the number of functions which do not.

While the conditions do not determine the structure of the double layer, it will be noticed that so far, except in the case of the solution (23), the dependence of ϕ^* upon x^0 has always been exponential. This is because each solution of (16) and (17) has been of the form

$$\phi^* = p(x^1, x^2)q(x^0), \qquad \ldots\ldots (30)$$

and for any solution of this form, except that in which $p(x^1, x^2)$ is constant, corresponding to (23), (19) fixes $q(x^0)$ as an exponential function, so that

$$\phi^* = p(x^1, x^2) \exp(kx^0). \qquad \ldots\ldots (31)$$

It is likely that if we had solutions of (16) and (17) of forms other than (30), assuming that this is possible, (19) would again fix the dependence upon x^0, but the general question of this is one of considerable mathematical difficulty. However, it is evident, if only from the fact that (31) follows from (30), that if we assume a special form and know the dependence upon x^1 and x^2, the conditions may fix the dependence upon x^0, and in this sense, the conditions can be said partially to determine the structure. It is noteworthy, though, that in the case of the specially important solution (23), mentioned above, we obtain no information of this kind. This is perhaps understandable as (23), while a special case of (30), is also a special case of many other forms, in each of which, no doubt, the dependence upon x^0 is different when ϕ^* is non-constant with respect to x^1 and x^2.

§ 4. Discussion

The object of the foregoing study has been twofold, to establish that the macroscopic conditions upon a double layer can be simultaneously satisfied, and to investigate the extent to which they determine the structure. The latter was relatively sterile, but the former is quite successful in that ways in which the conditions can be satisfied correspond quite well with established views.

As already stated, it has been generally assumed that Φ is constant, and the possibility of this is guaranteed by our solution (23). Secondly, the early views of the 'diffuse' double layer were that the dependence upon x^0 is exponential. This corresponds to solutions of the form (31).

Theoretical studies of the double layer have hitherto always been in terms of microscopic statistical mechanics, and this approach is very powerful in that it allows the complete determination of the structure. However, statistical mechanics has difficulties of its own, and different treatments have led to different results. For example, according to the Chapman–Gouy theory (cited by Bockris 1954), the solution for x^0 is a hyperbolic function. However, a recent deduction by Morris (1958) indicates that the dependence should always be exponential †, in accordance with the earlier views.

It is therefore evident that the real practical value of the present theory is in providing general criteria which must be conformed to by the results of a theory, in this case statistical mechanics, which, if more powerful to produce specific results, is more subject to controversy. In order to obtain a precise understanding

† Morris finds that

$$\phi^* = \frac{A}{\sigma_0} \exp(kx^0),$$

where σ_0 is the surface density of charge on either sheet of the double layer. This provides an interesting comparison with our solution (26), as it suggests a dependence of surface charge density upon curvature such as one finds elsewhere in electrostatics.

of how the macroscopic and microscopic theories are complementary in this way, we shall examine why the macroscopic theory does not determine the structure completely, and yet, at the same time, why it determines it at all when this is also done by a microscopic theory using different concepts and methods.

It has emerged that the integral conditions (16) and (17) do not really contribute to the determination of the structure, and that such determination as is possible is by the differential equations (14). The basis of our macroscopic approach is, as set out in I, generalized Navier–Stokes equations of motion and an equation of continuity. These are four equations in which the four unknowns are the components of velocity and the pressure. Many other quantities are present, but these must be regarded as the data, and they include the electrical quantities. It is not therefore to be expected that the equations determine the electrical quantities. However, it is a common mathematical phenomenon for restrictions upon the data of a set of differential equations to be necessary in order that the equations be simultaneously solvable. The integral conditions are simply restrictions of this type.

Now the reason that, in general, the structure is partially determined by the differential equations (14) is that these equations are obtained by equating the three components of velocity to zero, so that one can regard the three components of electric field strength as replacing them as unknowns in the original equations of motion. The fact that the structure is only partially determined is due to the fact that we have no boundary conditions.

The fact that the macroscopic differential equations (14) can do in part what the microscopic theory can do completely is evidently because these equations are of thermodynamical origin. It is well known that thermodynamical equations are expressions of the results of applying the laws of mechanics on the atomic scale. Generally, however, not every feature of a microscopic theory is reproduced in this way, and presumably this corresponds in the present case to the absence of boundary conditions in the differential equations.

What is somewhat surprising is that the thermodynamical argument should fail in one particularly important special case, namely that of a double layer of uniform electrokinetic potential. Quite clearly the difficulty is mathematical rather than physical. If one imagines a succession of double layers approximating closer and closer to one of uniform electrokinetic potential, one would not assume any discontinuity in the physical behaviour in this limit, although mathematical discontinuities might be possible.

In conclusion then, regarding our macroscopic conditions as criteria which must be satisfied by the results of microscopic theory, we note that this is a common role for thermodynamical conditions, in which we classify equations (14), and we assert that the integral conditions (16) and (17) are the more important as they do not correspond to anything in microscopic theory. They are obtained by the solution of the macroscopic equations of motion. In microscopic theory, the equations of motion cannot be solved. The thermodynamical conditions represent, as we have pointed out, the statement of certain statistical generalities in macroscopic language, and we would therefore expect them to be satisfied by the results of any microscopic theory which is correct within the framework of its postulates. The integral conditions, though, having no microscopic counterpart, represent a distinct addition to the theory as a whole; correctness of the microscopic theory is not alone sufficient to ensure that they will be satisfied.

Acknowledgments

I am indebted to Dr. R. Fürth of Birkbeck College, University of London, for his deep analysis and criticisms of earlier versions of this paper, and for making known to me the results of unpublished work of his research group in the field. I am also grateful to Dr. G. M. Bell of the University of Manchester, for valuable discussions.

References

Bockris, J. O'M., 1954, *Modern Aspects of Electrochemistry* (London: Butterworths Scientific Publications).
Brown, W. F., Jr., 1951, *Amer. J. Phys.*, **19**, 290, 333.
Cade, R., 1954, *Proc. Phys. Soc.* B, **67**, 689.
Eisenhart, L. P., 1947, *Differential Geometry* (Princeton: University Press).
Howarth, L., 1951, *Phil. Mag.*, **42**, 239.
Morris, E., 1958, *Ph.D. Thesis*, University of London.
Slepian, J., 1950, *Proc. Nat. Acad. Sci., Wash.*, **36**, 485.
Weatherburn, C. E., 1947, *Differential Geometry* (Cambridge: University Press).
Wills, A. P., 1931, *Vector and Tensor Analysis* (New York: Prentice Hall).

APPENDIX

Solution of the Differential Equations

The pair of differential equations

$$\frac{\partial E_0^*}{\partial x^\alpha} E_0^* - \frac{\partial E_0^*}{\partial x^0} E_\alpha^* = 0, \qquad \ldots\ldots (A1)$$

can be solved with the help of the substitution

$$E_\alpha^* = u_\alpha E_0^*. \qquad \ldots\ldots (A2)$$

Since E_μ^* is the gradient of a potential, we have

$$\frac{\partial E_2^*}{\partial x^1} - \frac{\partial E_1^*}{\partial x^2} = 0, \qquad \ldots\ldots (A3)$$

$$\frac{\partial E_0^*}{\partial x^\alpha} - \frac{\partial E_\alpha^*}{\partial x^0} = 0. \qquad \ldots\ldots (A4)$$

Substituting (A2) and (A4) into (A1), and then (A2) into (A3), we obtain

$$\frac{\partial u_\alpha}{\partial x^0} = 0, \qquad \ldots\ldots (A5)$$

$$\frac{\partial u_2}{\partial x^1} - \frac{\partial u_1}{\partial x^2} = 0. \qquad \ldots\ldots (A6)$$

These equations show that u_α, a covariant vector with respect to transformations on S, is the gradient of a function $\psi(x^1, x^2)$.

The problem is now resolved to that of solving the equations (A2) using the knowledge gained about u_α. In terms of the potential ϕ^*, these equations are the differential equations

$$\frac{\partial \phi^*}{\partial x^0} = \frac{1}{u_\alpha(x^1, x^2)} \frac{\partial \phi^*}{\partial x^\alpha} \quad (\alpha \text{ not summed}), \qquad \ldots\ldots (A7)$$

and if we put $\phi^* = L(x^0)M(x^1, x^2)$, we easily find by separation of variables that a solution is

$$\phi^* = A \exp \gamma(x^0 + \psi), \qquad \ldots\ldots (A8)$$

where γ is the separation constant, which may be complex, and A a constant of integration. The most general solution obtainable by this method is an infinite series of solutions of the type (A8) for different values of γ and A. If we restrict the values of γ to positive and negative integer multiples of an appropriate imaginary constant, the fact that ϕ^* is real shows that the series is just the Fourier series of an arbitrary function. The general solution is therefore

$$\phi^* = \mathrm{f}(x^0 + \psi). \qquad \ldots\ldots (A9)$$

RESEARCH NOTES

A Method of Generating Pairs of Millimicrosecond Current Pulses separated by a Variable Interval

By J. M. SOMERVILLE
The University of New England, Armidale, N.S.W., Australia

MS. received 25th February 1959

In connection with an investigation of the properties of spark channels (Somerville and Williams 1959) it became necessary to generate pairs of current pulses of 30 mμsec duration which could be passed through the channel with a variable interval of up to 1 μsec between them. The apparatus used for this purpose is shown in the figure. The first rectangular pulse is formed by the discharge of the effectively open-ended coaxial line L through the spark gap into a piece of identical line L_1 of variable length. The pulse travels down L_1 and is reflected at the short-circuited end, returning and passing through the spark gap, which is still conducting, with current flowing in the same direction as before. The interval between the first and second passages through the gap is, of course, determined by the length of L_1. If the clipping valve shown in the figure were absent, the pulse would be reflected at the open end of L and would traverse the gap again with current flowing in the reverse direction as shown in (*a*) of the figure. There would then be a further reflection at the end of L_1, and so on. To prevent this, the clipping valve is used to clip the pulse as soon as it is about to change sign by reflection at the end of L. This leaves only the two unidirectional current pulses as shown in (*b*).

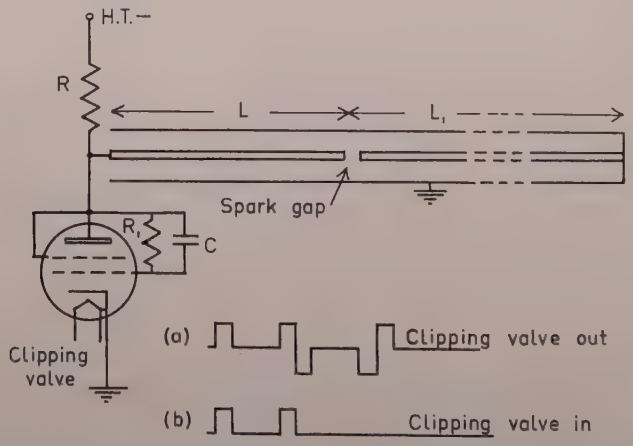

Detail of double pulse forming circuit. ($R = 20$ MΩ, $R_1 = 100$ kΩ, $C = 20$ pF. Clipping valve : Raytheon 715 B ; h.t. variable between -1 and -5 kv). (*a*) and (*b*) show idealized waveforms of the current through the spark gap.

The valve acts in a manner similar to that of a conventional clipping diode, with one modification, designed to secure as good a match as possible between the line L and the average effective impedance of the valve, while it is conducting.

If the valve is connected as a simple diode, with plate, screen and grid tied together, its effective impedance is lower than that of the line L(50 Ω). The effective impedance may be raised in several ways: a resistance may be placed in series with the valve, but this has the disadvantage of loading the line with a resistive component of impedance even while the valve is non-conducting; the valve heater voltage may be lowered; or the circuit shown in the figure may be used. This circuit operates as follows. The resistance R_1 keeps the grid at the same voltage as the plate and screen for all but very rapid variations. When the voltage at the end of L does rise very suddenly to a value V however, the grid voltage rises momentarily to a value less than V, determined by the ratio of C to the grid-to-ground capacity of the valve. Varying C can thus vary the current drawn through the valve, and hence its effective impedance. This method has the advantage of making the capacity across the end of L less than it would be with the valve connected as a diode.

Although this device was designed for the study of spark channels and uses a spark gap as a switch, there does not appear to be any reason why other types of switch such as thyratrons should not be used, nor why the device should not be operated at very much lower voltages than those (several kv) which we have used. It is possible to obtain pairs of voltage pulses of either the same or opposite direction. The current through the gap or switch is in the same direction during both conducting periods so that the voltage across any small resistance in series with the switch will consist of two pulses in the same direction. On the other hand, the voltage between the switch end of the internal conductor of the line L_1 and ground consists of two pulses in opposite directions.

Acknowledgments

I wish to acknowledge the assistance of Dr. K. Landecker and Mr. J. F. Williams in connection with the development of this equipment.

Reference

Somerville, J. M., and Williams, J. F., 1959, *Proc. Phys. Soc.*, **74**, 309.

NOTICE TO AUTHORS

Authors of papers on experimental measurements are advised to include information concerning the purity and structure (grain size, homogeneity, degree of working phases present, etc.) of materials used. This should be as complete as the nature of the measurements being made requires and should include the source of the material and method of preparation.

REVIEWS OF BOOKS

The Physics of Rubber Elasticity, by L. R. G. Treloar. 2nd Edition. Pp. vii+342. (Oxford : University Press, 1958.) 40*s*.

The appearance of a second edition of this interesting book is very welcome. The first edition, which appeared in 1949, fulfilled a useful purpose in giving a connected account of the development of the statistical-thermodynamic theory of rubber elasticity and other related topics. The subject continues to grow in a lively manner, and to do justice to the new experimental evidence and to the more detailed applications of the basic concepts, the author has found it necessary to expand the text by one-third and to rearrange some of the material. The rearrangement has improved the general design of the book; a chapter on large elastic deformations, which appeared at the end of the first edition and seemed like an after-thought (it was stop-press news at the time) now appears in a more logical place in the middle of the book, following the main story of the development of elasticity theory. The book now proceeds in a satisfying way from a preliminary account of the general physical properties and general thermodynamics to its main theme, the statistical-thermodynamic theory of chain molecules and networks (there are two new chapters here, on swelling phenomena and on the estimation of the degree of cross-linking respectively), and thence to the photo-elastic properties which, linked to the statistical theory, are yielding important suggestions on the more detailed molecular interpretation; it then deals with crystallization phenomena and their effects on mechanical properties, and ends with two chapters on the non-equilibrium phenomena of stress relaxation, creep and flow, and behaviour under transient or cyclic stresses.

The book is beautifully written, in more than one sense: it is not only very readable by virtue of the detailed structure of its sentences, but it also leads the reader on by a natural sequence of ideas; moreover, it takes great care to make clear just what assumptions and approximations are made at each stage of development of the basic concepts. This, I said to myself more than once while I was reading it, is how a monograph or a textbook *ought* to be written.

There are inevitably places where the reader would like to argue a point with the author, or suggest the inclusion of discussions of other aspects of the subject. For instance, the differences of molecular flexibility between rubber, gutta-percha and polythene, which are so strongly suggested by the photo-elastic properties, deserve some discussion on a stereochemical basis, and some correlation with other properties, such as melting points; in the chapter on dynamic mechanical properties, I should like to see more about the dependence of the dynamic Young's modulus and loss factor on temperature and frequency in different rubber-like materials; and I do not agree that there are no serious packing difficulties in Nyburg's crystal structure of natural rubber which contains left- and right-handed molecules at random. But such things do not affect the dominant impression that this is a book which everyone interested in polymer properties (not only rubber elasticity) would find interesting and stimulating.

One of the results of reading a book like this is that the reader is led to take stock of the subject and ask " what next ?". The statistical theory accounts in a general way for the form of the force-deformation relations, but gives an absolute

value for the modulus which is considerably lower than the experimental value. This, as the author says, is not really surprising : the " important consideration is that the degree of agreement is as close as it is, when it is remembered that we are concerned with the prediction of the absolute magnitude of a physical property of a material from a very general mathematical basis ". One defect of the theory in its present form is that it treats the molecules, or rather the segments of them between cross-linked points of the network, as if they were free to behave as if in isolation; in actual fact they are crowded together, and the attractions between them would be expected to modify their configurations and their movements. Is the next step to be an attempt to take into account the fact that rubber is a condensed phase, not a cross-linked gas ? C. W. BUNN.

Fast Reactions in Solids, by F. P. Bowden and A. D. Yoffe. Pp. ix + 164. (London: Butterworths Scientific Publications, 1958.) 40*s*.

This book is about explosions, of course. It is a sequel to the same authors' book *The Initiation and Growth of Explosion in Liquids and Solids* (Cambridge, 1952). The choice of synonym for title implies that the main emphasis is on the physical chemistry of the process of explosion, as well as being concentrated on the solid explosives. Not much attention is paid to the hydrodynamic aspects of the subject—to these authors the insensitiveness of the hydrodynamic theory of detonation to what happens in the detonation front is its weakness rather than its strength. Attention is principally directed to the initial stages of causation of an explosion by heat, light, shock or nuclear radiation (though the latter hardly ever causes one). The book is above all an account of experiments, with just enough theory to elucidate the experiments when they *can* be elucidated, which is by no means always the case. When it is not, the experimental facts are presented with considerable care. Anyone who feels challenged to understand the behaviour of matter may find here a number of problems worthy of his thought (explosions are too much fun to be left entirely to the military men). He will find here, in addition to the experimental facts and a valuable guide to the literature, a useful compilation in the appendices of some of the fundamental data on explosives which are otherwise hard to come by. F. C. F.

Leitfaden zur Berechnung von Schallvorgängen, by O. Brosze. Pp. ii + 168. (Berlin: Springer, 1958.) 31.50 DM.

This book by O. Brosze, which is in German, is the revised second edition of an earlier volume on the same subject written by Dr. H. Stenzel and published in 1939. It deals with the pattern of the sound fields of various simple types of source configurations, and collects together information which up to now is largely scattered in many different journals.

The book is divided into three main sections, the first being devoted to the consideration of the sound field more distant from the radiator, the second with the near sound field, and the third with the sound fields of spherical radiators and with the scattering effect of rigid spheres and infinite rigid cylinders placed in a sound field.

After developing the fundamental ideas and formulae, the author applies them to a number of straightforward practical problems. Numerous graphs and

tables, expressed in terms of the appropriate parameters, are included in the text and at the end of the book. A useful list of books for general reading and of references to original papers dealing with specific acoustic wave problems are added in an Appendix. This book will undoubtedly prove a useful aid to research workers and industrial designers who are concerned with knowing how the acoustic energy is distributed in the sound fields of their sources and with similar problems. R. W. B. STEPHENS

Experimental Techniques in Low Temperature Physics, by G. K. WHITE. Pp. viii + 328. (London : Oxford University Press, 1959.) 45*s*.

In the thirties low temperature research was still confined to a few laboratories and cryogenic techniques, often of a rather individual nature, were developed in these. Since the war, and particularly since the Collins helium liquefier has become commercially available, work in the region near absolute zero has become very widespread. A manual on experimental techniques of the low temperature field is long overdue.

Dr. White's book goes a long way towards filling this need. Accounts of gas liquefaction and storage are followed by a most useful chapter on heat exchangers and one on temperature measurement down to the helium range. While some of this information can also be gathered—with some difficulty—from existing summary articles or original papers, it is the second section of the book which is especially valuable. This deals with the lay-out of experimental technique, the choice of cryogenic approach and the construction of the different types of cryostat. Here, the author has made a critical selection of existing techniques and, more important, has found a way of giving sound advice to those who enter the cryogenic field. He discusses the limitations set by heat influx and temperature control and also devotes some space to the kind of ' useful hints ' which very often make all the difference between success and failure of a piece of research. Here, too, production and measurement of magnetic temperatures are discussed. A short final section deals with some physical data, for a full and satisfactory presentation of which a book of this kind offers, however, not sufficient scope.

Even in the first two sections Dr. White had to limit his account severely and, on the whole, his selection has been highly judicious. Nevertheless, one regrets that important experimental difficulties such as vapour oscillations, lambda-leaks and the helium film had to be relegated to asides. A more serious omission is the complete lack of information on ^{3}He as a cryogenic and thermometric substance. The failure to deal with this important topic is explained by the date of the preface (July 1957) which is a sad reflection on the fact that in these days of technical progress, it often takes longer to print a book than to write it. This is a great pity when, as here, an excellent book is concerned which deserves strong recommendation. K. MENDELSSOHN.

The Physical Theory of Neutron Chain Reactors, by A. M. WEINBERG and E. P. WIGNER. Pp. xii + 801. (Chicago : University of Chicago Press, 1958.) £5 12*s*. 6*d*.

This is a masterly exposition of the theory of nuclear reactors, quite outstanding in its conception and execution, by two distinguished authors, both of whom have themselves made substantial contributions to the subject.

Nuclear reactor theory is one of the sections of what is often loosely called nuclear engineering, which has already reached an advanced stage of development and several books have already been written on different aspects of the subject. However, none so far has attempted such a comprehensive survey. The aim of the authors has been to write a book, or as they prefer to call it, a monograph, on the theory of nuclear chain reactions where the fundamental approach is from the physics of the problem. They believe, quite rightly, that a full and complete understanding of the theory can only follow from a deep and proper understanding of the physics of the problem. The result is a book which firmly lays down the basis of nuclear reactor theory. Again the authors have not allowed themselves to be sidetracked into giving two detailed expositions of particular branches of the subject. The broad field of reactor theory is covered and yet at the same time they have been able to keep much of the mathematical theory relatively simple. In addition, they have shown how the theory links up with practice, so that the reader is not simply presented with a textbook (as so often happens with books in theoretical physics) which does not tell him how successful the different methods which are presented are in solving his particular problem.

In pursuance of their stated principles, the first of the four sections of the book is devoted to nuclear physics and this section occupies more than one fifth of the whole volume. A very full description is given of the physics necessary for an understanding of all the physical processes which take place in a reactor. This section particularly deals with nuclear reaction, cross sections, resonance reactions, the fission process and the shell structure of nuclei and the different nuclear models.

The next section deals with the problems of the transport of neutrons and is introduced by an elementary discussion of chain reactions. This leads naturally to a consideration of, first, elementary diffusion theory, and then transport theory, both for the case of monoenergetic neutrons. Having dealt with the theory of monoenergetic neutrons the discussions then turn to the consideration of problems where the neutrons have ranging velocity. In particular the phenomenon of neutron slowing down is dealt with coupled with the calculation of resonance capture and the energy spectrum of the neutrons in the slowing down process.

The necessary information has now been assembled to consider the calculation of the critical size of a reactor along with its behaviour. This forms the main subject matter of the third section. The simpler problems of a bare homogeneous uniform reactor is first considered and specific reactor systems are considered in detail with theory and experiment compared. Special aspects of these systems are considered such as their conversion ratio and the temperature effects on their parameters.

In general, reactors are not uniform and also have reflectors and the theory of such reactors is next considered, different methods of dealing with such systems being given and again these are compared with actual measurements.

The very important application of perturbation theory is next dealt with, particularly as applied to the one, two and multi group methods of critical size calculations, and the first chapter of this section is on reactors in the non-steady state.

The final section largely deals with practical calculations. Many reactors are heterogeneous and so special methods are needed for calculating their parameters. The factors of the multiplication constant are taken in turn and methods of calculating them are discussed and compared with experimental results. In addition the diffusion and slowing down lengths are calculated and the section ends with a chapter on the calculation of the effect of control rods.

This description of the contents of the volume shows its scope and extent and it will be clearly recognized that such a comprehensive study has not been previously attempted. It can be said without question that this is the most important book on general reactor theory so far written and will unquestionably remain a standard work for many years to come. J. F. HILL.

The Structure and Evolution of the Universe, by G. J. WHITROW. Pp. xi + 212. (London : Hutchinson, 1959.) 21*s*.

A feature of science today is the extreme interest in astronomy, no doubt primarily because of the stimulation which the subject has received from the development of new observational techniques. In fact the developments during the last ten years have been such that Dr. Whitrow has had to rewrite his original book *The Structure of the Universe* which appeared in 1949, and as befits its new title the book is far more than a new edition of the original. Anyone with an interest in astronomy and cosmology will profit from a reading of this book. Dr. Whitrow does not attempt to over-simplify the complexities of the contemporary views of space and time, of the cosmological aspect of relativity, or of the various theoretical models of the universe which are extant today. However, he writes with clarity and insight and no student of physics or mathematics should have any difficulty in following the argument. The parts of the book which describe the features of the universe as observed out to the present day observational limits are also excellently done. The book is quite up to date as evidenced by the inclusion of some of the latest contributions of radio astronomy, particularly the new opportunities which are now presented for applying an observational test to the conflict between the evolutionary and steady state theories of the universe. A. C. B. LOVELL.

Theoretical Physics, by GEORG JOOS. Third edition. Pp. xxiii + 885. (London, Glasgow: Blackie, 1958.) 70*s*.

Joos' *Theoretical Physics* is too well known to need detailed description or survey. It is planned to cover the whole field of theoretical physics at honours level.

In the third edition there are two additional chapters: (1) Phenomenological theory of superconductivity, (2) Theory of elastomers; and the chapter on Nuclear physics is considerably modified. A section on Fundamentals of the matrix calculus has been added to the first chapter and one on The role of lattice defects in dielectric crystals to chapter XLI. The Table of Physical Constants has also been revised. A. C. S.

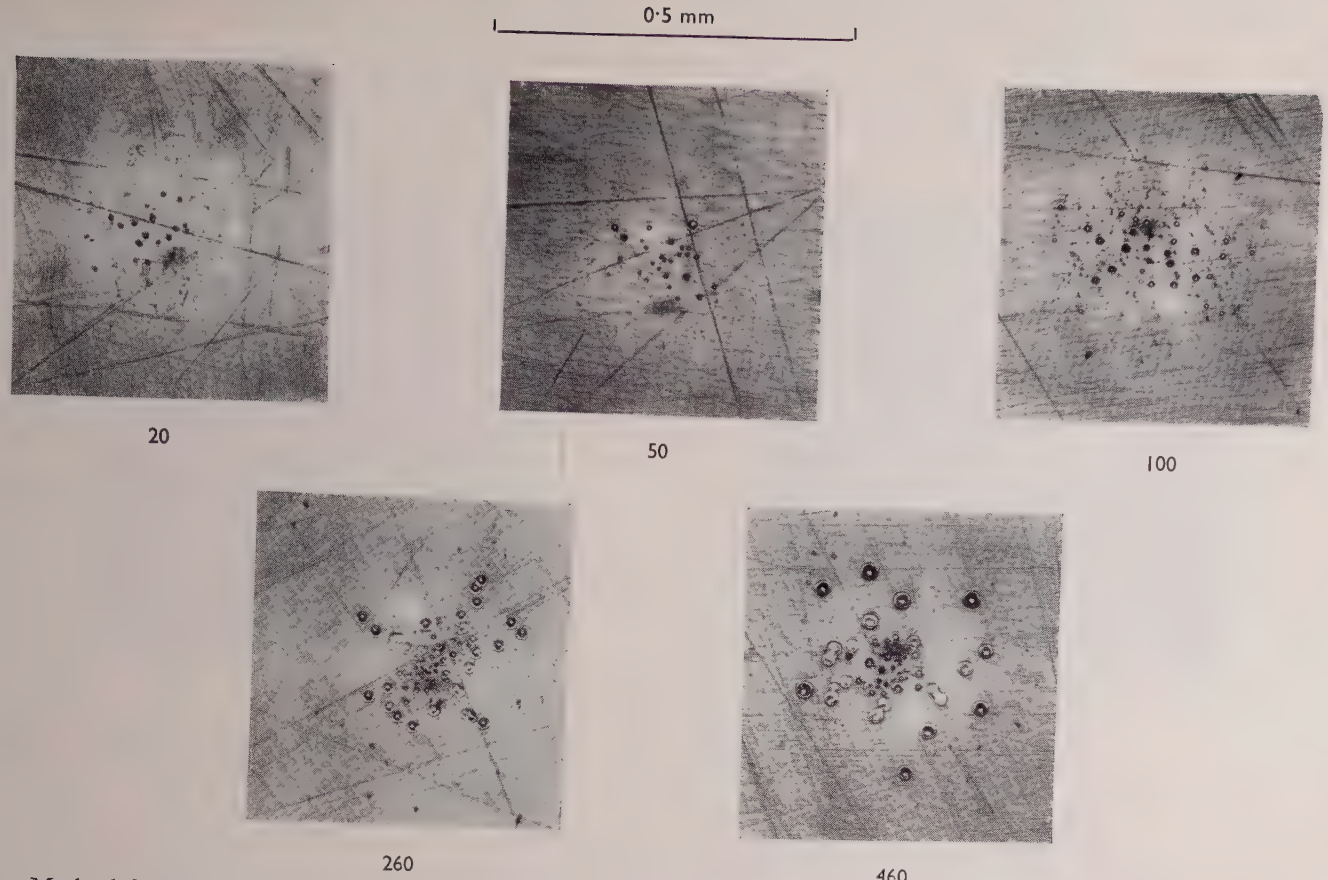

Figure 2. Marks left on a coated palladium anode by 30 A sparks of different durations in air at atmospheric pressure. Each photograph shows the mark, consisting of numerous individual spots, left on the anode by a single spark. The duration (in mμsec) of each spark is indicated beneath the corresponding mark.

PLATE I

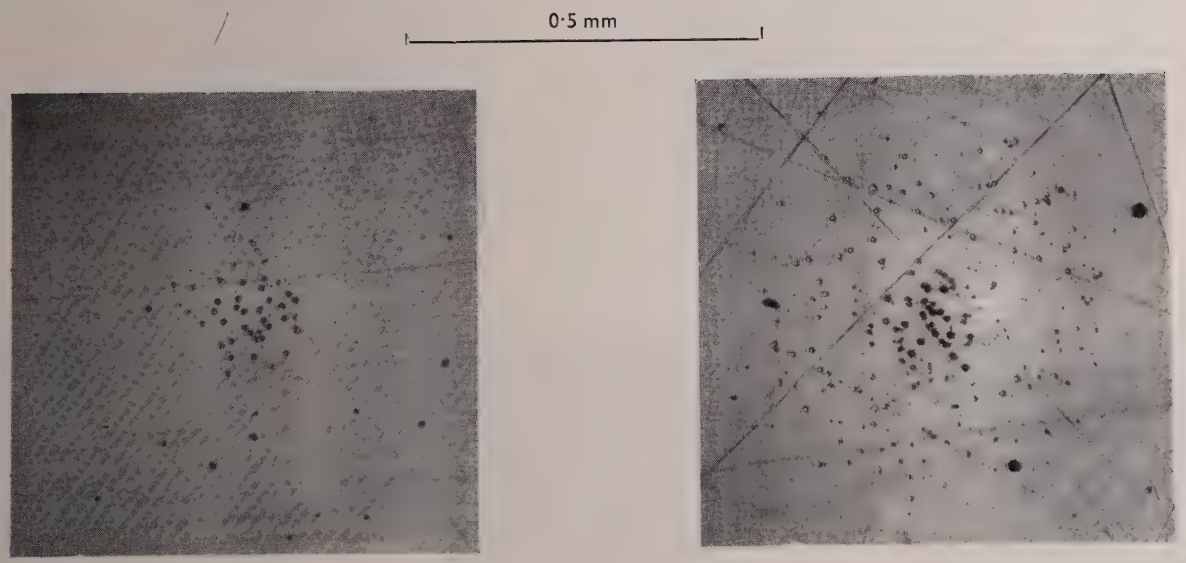

(*a*) (*b*)

Figure 4. Marks left on a coated palladium anode (*a*) by a single initiating 30 A current pulse of 30 mμsec duration, and (*b*) by a 30 A 30 mμsec initiating pulse followed by a similar probing pulse after a delay of 720 mμsec.

PLATE II

A Self-consistent Calculation of the Graphite π Band

By T. E. PEACOCK† and R. McWEENY‡
University College of North Staffordshire
† Department of Chemistry
‡ Departments of Mathematics, Physics and Chemistry

MS. received 17*th April* 1959

Abstract. The approximate self-consistent field theory, recently developed in calculations of molecular wave functions, is applied to a two-dimensional crystal—the graphite layer. The crystal orbitals for the π electrons are constructed from atomic orbitals, as in the usual tight binding approximation, but the methods of *many*-electron theory are used in setting up the self-consistent field. Matrix elements of the one-electron Hartree–Fock Hamiltonian (which in the usual tight binding model are identified empirically) are expressed in terms of the π-electron density matrix, whose elements may be evaluated by integration over the occupied region of **k** space, and are systematically adjusted until Hamiltonian and charge density are self-consistent.

The results, besides being of intrinsic interest, suggest that with the further development of automatic computation similar calculations on three-dimensional crystals will become feasible.

§ 1. Introduction

The electronic structure of graphite has recently received considerable attention. In first approximation each layer in the graphite lattice may be considered individually as a two-dimensional crystal and this results in an unusual simplification in theoretical analysis. In the approach most commonly used, the electrons occupy the 'crystal' orbitals of a one-determinant wave function; and when these are built up out of atomic orbitals the resultant 'tight binding' approximation is the crystal counterpart of the LCAO MO§ approximation of molecular theory. The crystal orbitals would ideally be solutions of a Hartree–Fock problem. But in the tight binding method they are rough approximations of LCAO form, found by solving a restricted secular problem in which the matrix elements of the Hartree–Fock Hamiltonian are given plausible values chosen to fit empirical and other data (see for example Slater and Koster 1954). The calculations reported by Coulson (1947), Bradburn, Coulson and Rushbrooke (1947–48), Wallace (1947), Barriol and Metzger (1950), and Coulson and Taylor (1952), are all of this type. In addition, they confine attention to the most loosely bound electrons (the so-called π electrons), which occupy orbitals having a node in the plane of the nuclei: they are in fact a limiting case of Hückel-type calculations on polycyclic aromatic hydrocarbons (Hückel 1931) and contain identical basic parameters—the 'Coulomb' and 'resonance' integrals, α and β. Later work has been concerned with the inclusion of resonance integrals for more distant neighbours, the description of the more tightly bound σ electrons, the inclusion of inter-layer effects, and the calculation of conductivity and other

§ Linear-combination-of-atomic-orbitals molecular orbital.

properties (see, for example, Brennan 1951, Lomer 1955, Johnston 1955, 1956, Yamazaki 1957, Slonczewski and Weiss 1958). Corbato (1956) has made an *ab initio* calculation, on a one-electron model, considering both σ and π electrons.

All these calculations are unfortunately marred by the difficulty of properly defining the Hartree–Fock Hamiltonian and of introducing self-consistency. In order to develop a true self-consistent field (SCF) method, comparable with that used in atomic theory, it would be necessary to relate the one-electron Hamiltonian to the charge density function and to systematically adjust both in order to achieve self-consistency. In recent years, however, considerable progress has been made in *molecular* SCF theory, using the LCAO approximation (see, for example, Roothaan 1951, McWeeny 1956a, b), particularly in the theory of aromatic hydrocarbons whose natural limit is the graphite layer. This encourages the belief that similar methods can be extended to solid state theory and that the difficulties of specifying a true Hartree–Fock Hamiltonian will eventually be overcome. The present paper represents a preliminary step in this direction. The graphite layer was chosen for test calculations partly because it is two-dimensional, and therefore relatively simple, and partly in order to utilize a large body of experience in the field of aromatic hydrocarbons. For simplicity, attention is confined to the π band, the more tightly bound σ electrons being represented by a 'framework field', as in molecular π-electron theory. Matrix elements involving the framework field are then identified empirically; but this does not preclude the proper definition of a π-electron SCF Hamiltonian, related to the π-electron density, and the achievement of limited self-consistency using a variant of the standard Hartree–Fock method.

§ 2. Formulation of the Problem

Let us take as unit cell the parallelogram in figure 1, containing two carbon atoms A and B. Translationally equivalent atoms throughout the lattice then fall into two sets, A atoms and B atoms, and the following Bloch orbitals may be defined:

$$\left.\begin{aligned}\psi_{\mathrm{A},\mathbf{k}}(\mathbf{r}) &= \frac{1}{G}\sum_m \exp\{i\mathbf{k}\,.\,(\mathbf{r}_\mathrm{A}+\mathbf{R}_m)\}\phi_{\mathrm{A},\mathbf{R}_m}(\mathbf{r}), \qquad \mathbf{r}_\mathrm{A} = \tfrac{1}{3}\mathbf{a}_1 + \tfrac{1}{3}\mathbf{a}_2 \\ \psi_{\mathrm{B},\mathbf{k}}(\mathbf{r}) &= \frac{1}{G}\sum_n \exp\{i\mathbf{k}\,.\,(\mathbf{r}_\mathrm{B}+\mathbf{R}_n)\}\phi_{\mathrm{B},\mathbf{R}_n}(\mathbf{r}), \qquad \mathbf{r}_\mathrm{B} = \tfrac{2}{3}\mathbf{a}_1 + \tfrac{2}{3}\mathbf{a}_2.\end{aligned}\right\} \quad \ldots\ldots (2.1)$$

Here, for instance, $\phi_{\mathrm{A},\mathbf{R}_m}(\mathbf{r})$ is an (orthonormalized) atomic orbital on the A atom of the unit cell indicated by lattice vector $\mathbf{R}_m = m_1\mathbf{a}_1 + m_2\mathbf{a}_2$ and may therefore be written alternatively as $\phi(\mathbf{r}-(\mathbf{r}_\mathrm{A}+\mathbf{R}_m))$ where $\phi(\mathbf{r}))$ is a similar function for an atom at the origin. By using orthogonalized atomic orbitals (see, for example, Löwdin 1950, McWeeny 1955a, 1956b) we ensure that the Bloch orbitals are normalized over the periodic region which extends G unit cells in each of the directions $\mathbf{a}_1$ and $\mathbf{a}_2$. The wave vector $\mathbf{k}$ is defined by

$$\mathbf{k} = k_1(2\pi\mathbf{b}_1) + k_2(2\pi\mathbf{b}_2), \quad k_1, k_2 = 0, \quad 1/G, \ldots (G-1)/G$$

where $\mathbf{b}_1$ and $\mathbf{b}_2$ are vectors of the reciprocal lattice and there are thus G^2 Bloch orbitals of each type. These may be indicated by points within a parallelogram in $\mathbf{k}$ space or by the translationally equivalent set contained in the central hexagonal zone (figure 2).

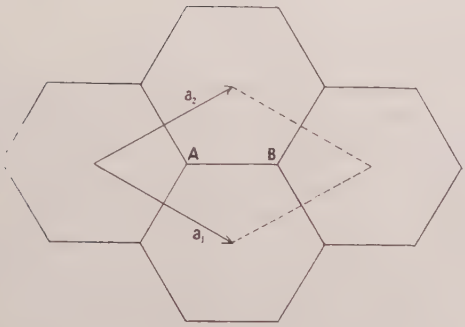

Figure 1. Basis vectors and unit cell in graphite layer.

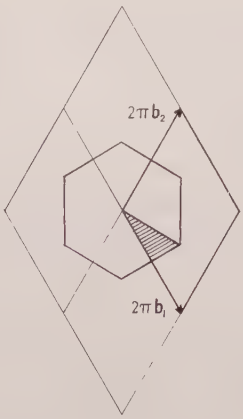

Figure 2. Basis vectors, unit cells and hexagonal central zone in **k** space showing one-twelfth hexagon over which integrals are evaluated.

Since only functions of the same translational symmetry combine, the approximate crystal orbitals occur as linear combinations of two Bloch orbitals of given **k**. The coefficients are determined, for each separate **k** vector, by solving the equation

$$\begin{vmatrix} h_{AA}(\mathbf{k})-\epsilon & h_{AB}(\mathbf{k}) \\ h_{BA}(\mathbf{k}) & h_{BB}(\mathbf{k})-\epsilon \end{vmatrix} = 0 \qquad \ldots\ldots (2.2)$$

where

$$h_{AA}(\mathbf{k}) = h_{BB}(\mathbf{k}) = \int \psi_{A,\mathbf{k}}^{*}(\mathbf{r}) \mathfrak{h} \psi_{A,\mathbf{k}}(\mathbf{r})\, d\mathbf{r},$$

$$h_{AB}(\mathbf{k}) = h_{BA}(\mathbf{k})^{*} = \int \psi_{A,\mathbf{k}}^{*}(\mathbf{r}) \mathfrak{h} \psi_{B,\mathbf{k}}(\mathbf{r})\, d\mathbf{r} \qquad \ldots\ldots (2.3)$$

and $\mathfrak{h}$ is the one-electron Hartree–Fock Hamiltonian. Now $\mathfrak{h}$ depends not only upon the field of the framework, which remains when the π electrons are removed, but also upon the whole π-electron distribution. This is recognized by writing $\mathfrak{h} = \mathfrak{f} + \mathfrak{G}$, where $\mathfrak{f}$ is a bare-framework Hamiltonian and $\mathfrak{G}$ is an electron interaction operator which takes account of the mean (Coulomb–exchange) interaction between a single π electron and the total π-electron distribution, in the usual Hartree–Fock sense. Matrix elements of the operator $\mathfrak{f}$ will be regarded as empirically determinable parameters, but those of $\mathfrak{G}$ depend explicitly upon the π-electron density matrix and must be revised iteratively until self-consistency is achieved. Briefly, solution of (2.2) using the simple nearest-neighbour approximation (cf. Coulson and Taylor 1952) allows a calculation of the π-electron density; the matrix elements (2.3) of the Hartree–Fock Hamiltonian may then be calculated, using well-established methods from molecular theory, and (2.2) may be revised: solution then leads to a revision of the π-electron density; and this cycle may be repeated until no further changes in density occur. It is true, of course, that at certain symmetry points in **k** space the solutions of (2.2)

are completely determined by symmetry and have no flexibility; but elsewhere $\psi_{A,\mathbf{k}}$ and $\psi_{B,\mathbf{k}}$ are combined with $\mathbf{k}$-dependent phase factors and this flexibility is sufficient to permit considerable variation in the π-electron density.

§ 3. Matrix Elements and Charge Density

In this section we use the density matrix formalism developed elsewhere (see Löwdin 1955, McWeeny 1955 b, c, 1956 a, b). The n doubly occupied orbitals of a one-determinant wave function may be collected into a row matrix

$$\boldsymbol{\psi} = (\psi_1 \ldots \psi_l \ldots \psi_n)$$

and expressed in terms of a row matrix of basis functions, $\boldsymbol{\varphi} = (\phi_1 \ldots \phi_i \ldots \phi_m)$ by

$$\boldsymbol{\psi} = \boldsymbol{\varphi}\mathbf{T} \qquad \ldots\ldots (3.1)$$

where $\mathbf{T}$ is an $m \times n$ matrix whose columns represent the occupied orbitals. The system is completely described, in this approximation, by the idempotent matrix $\mathbf{R} = \mathbf{T}\mathbf{T}^\dagger$: the one-electron (spinless) density matrix is

$$\mathbf{P} = 2\mathbf{R} = 2\mathbf{T}\mathbf{T}^\dagger \qquad \ldots\ldots (3.2)$$

and the electron density function itself is

$$P(\mathbf{r}) = \sum_{i,j} \phi_i(\mathbf{r}) P_{ij} \phi_j^*(\mathbf{r}). \qquad \ldots\ldots (3.3)$$

Explicitly,

$$P_{ij} = 2\sum_l T_{il} T^\dagger_{lj} = 2\sum_l T_{il} T^*_{jl}. \qquad \ldots\ldots (3.4)$$

In the present case, i refers to an atom in the lattice and will be specified more completely by (A, $\mathbf{R}_n$) or (B, $\mathbf{R}_n$), according to type and unit cell, while l becomes the $\mathbf{k}$ vector of an occupied orbital and the summation is over the occupied region of $\mathbf{k}$ space.

In terms of the elements of $\mathbf{P}$ the matrix elements of the Hartree–Fock Hamiltonian for graphite are formally identical with those for a polycyclic hydrocarbon. The use of orthonormalized atomic orbitals then leads to very simple expressions, since all electron repulsion integrals except those of Coulomb type are in this case exceedingly small (McWeeny 1955 a, p. 299). In fact the matrix elements of $\mathfrak{h}$ between two such orbitals are related to the prevailing charge distribution by (e.g. McWeeny 1956 b)

$$\left.\begin{aligned} h_{ii} &= \omega_i + \tfrac{1}{2}P_{ii}(ii|g|ii) + \sum_{j(\neq i)} (P_{jj} - 1)(ij|g|ij) \\ h_{ij} &= \beta_{ij} - \tfrac{1}{2}P_{ij}(ij|g|ij). \end{aligned}\right\} \qquad \ldots\ldots (3.5)$$

Here ω_i measures the energy of an electron in orbital ϕ_i on that part of the bare framework associated with atom i, and is independent of the π-electron distribution, while β_{ij} is the usual 'resonance' integral (also for an electron in the field of the bare framework) and is small except when i and j are nearest neighbours. The two-electron integrals are, as usual,

$$(ij|g|ij) = e^2 \int \phi_i^*(\mathbf{r}_1)\phi_j^*(\mathbf{r}_2) \frac{1}{r_{12}} \phi_i(\mathbf{r}_1)\phi_j(\mathbf{r}_2)\, d\mathbf{r}_1\, d\mathbf{r}_2.$$

The numerical values of all such quantities may be taken over from molecular theory; we adopt the values used by McWeeny and Peacock (1957). The expressions (3.5) are further simplified if we anticipate one important result. The system considered is essentially a large 'alternant' molecule in that its atoms fall into two sets (in this case A and B), no atom having a neighbour in

the same set; and a general property of such systems, assuming $\beta_{ij} \neq 0$ for nearest neighbours only, is that $P_{ii} = 1$ while $P_{ij} = 0$ $(i \neq j)$ for all atoms i, j *in the same set* (Coulson and Rushbrooke 1945, Pople 1953). Thus, putting $\omega_i + \frac{1}{2}(ii|g|ii) = \alpha$,

$$\left.\begin{aligned} h_{ii} &= \alpha \\ h_{ij} &= \beta_{ij} - \tfrac{1}{2}P_{ij}(ij|g|ij). \end{aligned}\right\} \qquad \ldots\ldots (3.6)$$

It is now seen that although β_{ij} is assumed negligible except for nearest neighbours h_{ij} may fall off quite slowly with increasing separation of i and j, for $(ij|g|ij)$ varies roughly as the inverse distance. Consequently, the off-diagonal elements of $\mathfrak{h}$ will depend strongly upon the prevailing charge density.

It remains to obtain the P_{ij} for as many neighbours as may prove necessary, using the occupied orbitals which arise from (2.2). The matrix elements in (2.2) reduce as follows:

$$h_{\mathrm{AA}} = \frac{1}{G^2}\sum_{\mathbf{R}_n}\int \phi^*_{\mathrm{A},\mathbf{R}_n}(\mathbf{r})\mathfrak{h}\phi_{\mathrm{A},\mathbf{R}_n}(\mathbf{r})\,d\mathbf{r} = \int \phi^*_{\mathrm{A},0}(\mathbf{r})\mathfrak{h}\phi_{\mathrm{A},0}(\mathbf{r})\,d\mathbf{r} = \alpha$$

(**k**-independent) $\qquad \ldots\ldots (3.7)$

since P_{ij}, and hence h_{ij}, is zero for all i, j in the same set, and

$$h_{\mathrm{AB}}(\mathbf{k}) = \frac{1}{G^2}\sum_{\mathbf{R}_m,\mathbf{R}_n}\exp\left[i\mathbf{k}\,.\,\{(\mathbf{r}_{\mathrm{B}}+\mathbf{R}_n)-(\mathbf{r}_{\mathrm{A}}+\mathbf{R}_m)\}\right]\int \phi^*_{\mathrm{A},\mathbf{R}_m}(\mathbf{r})\mathfrak{h}\,\phi_{\mathrm{B},\mathbf{R}_n}(\mathbf{r})\,d\mathbf{r}.$$

If we introduce $h(\rho_n)$ to denote the matrix element of $\mathfrak{h}$ between atomic orbitals separated by a vector $\boldsymbol{\rho}_n = \mathbf{R}_n + \mathbf{r}_{\mathrm{B}} - \mathbf{r}_{\mathrm{A}}$, where $\mathbf{R}_n$ is any lattice vector,

$$h_{\mathrm{AB}}(\mathbf{k}) = \sum_n \exp(i\mathbf{k}\,.\,\boldsymbol{\rho}_n)\,h(\rho_n), \quad h(\rho_n) = \int \phi^*_{\mathrm{A},0}(\mathbf{r})\mathfrak{h}\phi_{\mathrm{B},\mathbf{R}_n}(\mathbf{r})\,d\mathbf{r}. \qquad \ldots\ldots (3.8)$$

The summation in (3.8) is thus over all B-neighbours of any A atom: this may conveniently be broken into parts arising from different orders of neighbourhood (ascending values of $|\boldsymbol{\rho}_n|$) to give

$$h_{\mathrm{AB}}(\mathbf{k}) = h_1\sigma_1(\mathbf{k}) + h_2\sigma_2(\mathbf{k}) + \ldots = h_1\left[\sigma_1(\mathbf{k}) + \frac{h_2}{h_1}\sigma_2(\mathbf{k})\ldots\right] = h_1\omega(\mathbf{k})$$

$\qquad \ldots\ldots (3.9)$

where $\sigma_p(\mathbf{k}) = \sum_{(p)}\exp(i\mathbf{k}\,.\,\boldsymbol{\rho}_n)$ and $h_p = h(\rho_p)$, are defined for the neighbourhood in which $|\boldsymbol{\rho}_n| = \rho_p$. It should be remembered that neighbours here belong to the different sets (A and B), so that 'second' neighbours in this sense are atoms at opposite vertices of a hexagon. The evaluation of these 'structure sums' leads to rather complicated trigonometric expressions which need not be reproduced (cf. Lomer 1955); but they depend only upon the nature of the lattice and are therefore carried unchanged throughout the self-consistent field calculation.

The equation (2.2) may now be written

$$\begin{vmatrix} \alpha-\epsilon & h_1\omega(\mathbf{k}) \\ h_1\omega(\mathbf{k}) & \alpha-\epsilon \end{vmatrix} = 0 \qquad \ldots\ldots (3.10)$$

and has solutions

$$\epsilon(\mathbf{k}) = \alpha \pm h_1|\omega(\mathbf{k})|. \qquad \ldots\ldots (3.11)$$

Since h_1 is negative, the states of lowest energy are obtained by taking the upper sign. There are G^2 such states holding the $2G^2$ available π electrons and filling the first Brillouin zone (figure 2). At low temperatures, to which our calculations

relate, this zone will be occupied throughout the calculation. The corresponding crystal orbitals are

$$\psi_{\mathbf{k}}(\mathbf{r}) = \frac{1}{\sqrt{2}}\left[\psi_{\mathrm{A},\mathbf{k}}(\mathbf{r}) + \left(\frac{\omega^*(\mathbf{k})}{\omega(\mathbf{k})}\right)^{1/2}\psi_{\mathrm{B},\mathbf{k}}(\mathbf{r})\right]$$

$$\text{i.e. } \psi_{\mathbf{k}}(\mathbf{r}) = \frac{1}{G\sqrt{2}}\sum_m \exp\{i\mathbf{k}\,.\,(\mathbf{r}_{\mathrm{A}}+\mathbf{R}_m)\}\phi_{\mathrm{A},\mathbf{R}_m}(\mathbf{r}) + \frac{1}{G\sqrt{2}}\left(\frac{\omega^*(\mathbf{k})}{\omega(\mathbf{k})}\right)^{1/2}\sum_r \exp\{i\mathbf{k}\,.\,(\mathbf{r}_{\mathrm{B}}+\mathbf{R}_n)\}\phi_{\mathrm{B},\mathbf{k}}(\mathbf{r}). \quad \ldots\ldots (3.12)$$

The elements of $\mathbf{P}$ are of two types, which will be dealt with in turn:

(i) From (3.4), using $T_{\mathrm{A},\mathbf{R}_m}(\mathbf{k})$ to denote the coefficient of $\phi_{\mathrm{A},\mathbf{R}_m}(\mathbf{r})$ in $\psi_{\mathbf{k}}(\mathbf{r})$ etc., we obtain

$$P_{\mathrm{A},\mathbf{R}_m;\,\mathrm{A},\mathbf{R}_n} = 2\sum_{\mathbf{k}} T_{\mathrm{A},\mathbf{R}_m}(\mathbf{k})T_{\mathrm{A},\mathbf{R}_n}(\mathbf{k})^* = 2\frac{1}{2G^2}\sum_{\mathbf{k}}\exp\{i\mathbf{k}\,.\,(\mathbf{R}_m-\mathbf{R}_n)\}.$$

Since there are G^2 occupied states and hence G^2 terms in the sum it follows immediately that

$$P_{\mathrm{A},\mathbf{R}_m;\,\mathrm{A},\mathbf{R}_n} = 1 \text{ for } m=n$$
$$= 0 \text{ for } m\neq n. \quad \ldots\ldots (3.13)$$

(ii) Again from (3.4) and (3.12)

$$P_{\mathrm{A},\mathbf{R}_m;\,\mathrm{B},\mathbf{R}_n} = \frac{1}{G^2}\sum_{\mathbf{k}}\{\exp(i\mathbf{k}\,.\,\boldsymbol{\rho})\}\left(\frac{\omega^*(\mathbf{k})}{\omega(\mathbf{k})}\right)^{1/2}$$

where $\boldsymbol{\rho} = (\mathbf{r}_{\mathrm{A}}+\mathbf{R}_m)-(\mathbf{r}_{\mathrm{B}}+\mathbf{R}_n)$ is the separation of the atoms in question. Since the summation extends over a centro-symmetric zone in $\mathbf{k}$ space, each term will be accompanied by its complex conjugate to give a real result. Moreover, the identical results for all the equivalent neighbours of an atom may be summed to give a more symmetrical expression. If an atom has n_p equivalent pth neighbours with $|\boldsymbol{\rho}| = \rho_p$, the corresponding element of $\mathbf{P}$ is given by

$$n_p P(\rho_p) = \frac{1}{G^2}\sum_{\mathbf{k}}\sum_{(p)}\exp(i\mathbf{k}\,.\,\boldsymbol{\rho})\left(\frac{\omega^*(\mathbf{k})}{\omega(\mathbf{k})}\right)^{1/2}.$$

If $|2\pi\mathbf{b}_1|$ is taken as the unit of length in $\mathbf{k}$ space, the hexagonal zone has an area of $\sqrt{3}/2$ and contains G^2 states. The expression may then be converted to an integral, taking the final form

$$P_p = P(\rho_p) = \frac{2}{n_p\sqrt{3}}\int \sigma_p(\mathbf{k})\left(\frac{\omega^*(\mathbf{k})}{\omega(\mathbf{k})}\right)^{1/2} d\mathbf{k}. \quad \ldots\ldots (3.14)$$

The evaluation of the integrals (3.14) is considered in an Appendix. From any assumed set of occupied crystal orbitals it is then possible to calculate the charge density and to revise the Hartree–Fock Hamiltonian accordingly; with an obvious notation, (3.6) becomes

$$h_p = \beta_p - P_p\gamma_p. \quad \ldots\ldots (3.15)$$

§ 4. Results

The simplest approximation (see, for example, Coulson and Taylor 1952) arises on putting $h_p = \beta$ when $p=1$ (i.e. for nearest neighbours) and $h_p = 0$ when $p>1$. This provides a convenient initial approximation for the SCF calculation. $P(\rho_p)$ is then the zero order term in (A3) (see Appendix) and for $p=1$

is the 'mobile bond order' of the C–C link. This latter quantity has already been evaluated by Coulson and Taylor (and indirectly by Bradburn, Coulson and Rushbrooke 1947–48) and is found to have the value $P_1 = 0{\cdot}527$. This may be compared with bond orders, calculated with the same approximations, of 1·0 for ethylene, 2/3 for benzene, the values in these two instances being completely determined by symmetry. In general, however, bond orders in molecules are often considerably affected when self-consistency is introduced. The bond orders calculated using the starting approximation are summarized below, along with the revised set of matrix elements which they indicate:

p	1	2	3	
P_p	0·5267	−0·2140	−0·0502	
h_p	$0{\cdot}896h_{\text{benz}}$	$-0{\cdot}112h_{\text{benz}}$	$-0{\cdot}020h_{\text{benz}}$	$(h_{\text{benz}} = -4{\cdot}79\,\text{ev})$

ρ_4 is associated with atoms 5 bond lengths apart and h_4 has a value of approximately $0{\cdot}005h_{\text{benz}}$. Rough estimates show that the inclusion of matrix elements of this order would not significantly affect the final results and they are therefore omitted.

The iterative process itself (using (3.15)) and (A4) is trivial, seven cycles leading to density matrix elements which are self-consistent to three places of decimals:

p	1	2	3
P_p	0·525	−0·223	−0·037
h_p	$0{\cdot}895h_{\text{benz}}$	$-0{\cdot}116h_{\text{benz}}$	$-0{\cdot}015h_{\text{benz}}$

The surprisingly small change in the C–C bond order is immediately accounted for by (A3), for in the case $p = 1$ the first order terms vanish identically.

From the final results it is a simple matter to obtain $\epsilon(\mathbf{k})$ from (3.11) and to plot the energy contours in $\mathbf{k}$ space. The results appear in figure 3 and are compared with those obtained using the initial approximation in figure 4. The

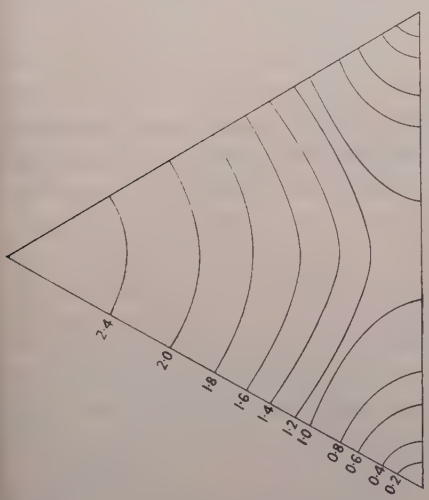

Figure 3. Energy contours within the occupied zone of the $\mathbf{k}$ space (one sixth of the full hexagon).

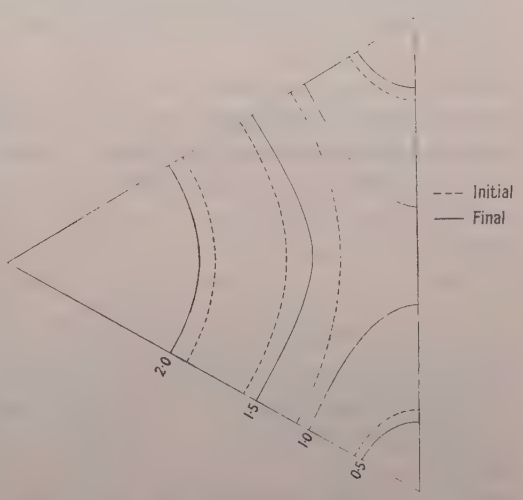

Figure 4. Comparison of initial and final contours, showing effect of introducing distant-neighbour interactions and self-consistency.

considerable shifts which occur are due to (i) the inclusion of electron interaction and (ii) the iterative introduction of self-consistency. In this case, largely owing to the insensitivity of the nearest-neighbour bond order, the first of these effects is dominant. It is, in fact, almost immaterial whether the Hartree–Fock Hamiltonian is estimated from the initial approximation or from the final self-consistent orbitals. The most important single factor is the inclusion of the resonance integral h_2 for atoms at opposite vertices of a hexagon. It should be noted that this quantity arises entirely from electron interaction effects (in fact from an exchange correlation) and that it has the opposite sign from that usually adopted in more empirical approaches.

It is possible, without further calculation, to make only one direct comparison with experiment. Since, by Koopmann's theorem, the orbital energy is numerically equal to the energy of ionization from the orbital, we obtain an immediate estimate of the work function of graphite. The energy at the surface of the first Brillouin zone is, from (3.11), simply $\epsilon(\mathbf{k})=\alpha$. With the parameter values adopted in molecular theory (McWeeny and Peacock 1957) this gives $I=4{\cdot}0$ ev which compares satisfactorily with the experimental estimate of 4·3 ev.

However, since the present approach is firmly based upon a *many*-electron wave function, it is also possible to make an immediate estimate of the *total* π-electron energy (including both Coulomb and exchange electron interactions). In terms of the matrix $\mathbf{P}$ (McWeeny 1956 a) and the bare-framework matrix $\mathbf{f}$ (given on putting $\mathbf{P}=0$ in (3.5)),

$$E=\tfrac{1}{2}\operatorname{tr}\mathbf{Pf}+\tfrac{1}{2}\operatorname{tr}\mathbf{Ph}=\tfrac{1}{2}\sum_{i,j}P_{ij}(f_{ji}+h_{ji})$$

where the summation is over all pairs of atoms in the periodic region and therefore gives

$$E=G^2\sum_p n_p P_p(f_p+h_p). \qquad \ldots\ldots (4.1)$$

The resultant π-electron energy is 222·7 kcal mol^{-1} of carbon atoms, compared with 188·9 kcal in ethylene and 205·8 kcal in benzene; this shows the usual trend, binding energy per atom increasing with delocalization. Unfortunately, the π-electron energy is somewhat difficult to evaluate experimentally since the heat of atomization gives information only about the *total* binding energy. Rough estimates, based on various current values of C—C (single) bond energies and of the carbon valence state energy, fall on either side of the theoretical figure, but are too unreliable to be of much value. A satisfactory comparison must await a detailed treatment of the σ electrons.

§ 5. Conclusion

The approximate self-consistent field method of molecular theory has been successfully applied to a two-dimensional crystal. Although the results are not without intrinsic interest, it is clear that the significance of these calculations is primarily methodological. There is evidently no insuperable difficulty in the application to crystals of an approximate SCF theory based on tight binding wave functions. The main obstacles to be overcome are (i) the evaluation of one- and two-electron integrals over (orthonormalized) atomic orbitals, (ii) the evaluation of structure sums, and (iii) the evaluation of integrals over $\mathbf{k}$ space. With the rapid development of automatic computation it seems likely that considerable progress in this direction can be made.

APPENDIX

Only the real part of the integrand in (3.14) need be considered since integration over the centro-symmetric zone in **k** space must lead to a real result. We may therefore use the alternative form

$$P_p = \frac{2}{n_p\sqrt{3}} \int \frac{\mathscr{R}(\sigma_p \omega^*)}{|\omega|}\, d\mathbf{k}. \qquad \ldots\ldots (A1)$$

On writing ω of (3.9) as

$$\omega = \sigma_1 + \sum_{p>1} h_p' \sigma_p \qquad (h_p' = h_p/h_1)$$

the denominator in (A1) may readily be expanded in ascending powers of the h_p' (which fall off rapidly with increasing p). Neglecting terms of third and higher degree, the integrand becomes

$$\begin{aligned}
\frac{\mathscr{R}(\sigma_p\omega^*)}{|\omega|} &= \frac{1}{|\sigma_1|}\mathscr{R}(\sigma_p\sigma_1^*) && \text{(zero order)}\\
&+ \frac{1}{|\sigma_1|}\sum_{r>1} h_r'\left[\mathscr{R}(\sigma_p\sigma_r^*) - \frac{1}{|\sigma_1|^2}\mathscr{R}(\sigma_p\sigma_1^*)\mathscr{R}(\sigma_1\sigma_r^*)\right] && \text{(first order)}\\
&+ \frac{1}{4|\sigma_1|}\sum_{r>1} h_r'^2\left[3\mathscr{R}(\sigma_p\sigma_1^*)\mathscr{R}\left(\frac{\sigma_r^2}{\sigma_1^2}\right) + \frac{|\sigma_r|^2\mathscr{R}(\sigma_p\sigma_1^*) - 4\mathscr{R}(\sigma_p\sigma_r^*)\mathscr{R}(\sigma_1\sigma_r^*)}{|\sigma_1|^2}\right]\\
&+ \frac{1}{2|\sigma_1|}\sum_{\substack{r<s\\(s>1)}} h_r'h_s'\left[3\mathscr{R}(\sigma_p\sigma_1^*)\mathscr{R}\left(\frac{\sigma_r\sigma_s}{\sigma_1^2}\right)\right.\\
&\qquad \left. + \frac{\mathscr{R}(\sigma_r^*\sigma_s)\mathscr{R}(\sigma_p\sigma_1^*) - 4\mathscr{R}(\sigma_p\sigma_s^*)\mathscr{R}(\sigma_1\sigma_r^*)}{|\sigma_1|^2}\right]\\
&\qquad\qquad \text{(second order)} \qquad \ldots\ldots (A2)
\end{aligned}$$

All the terms in (A2) are complicated trigonometric expressions and the double integration over **k** space must be performed numerically. The method employed was the two-dimensional analogue of Simpson's rule (see, for example, Willers 1948). The area over which the integral is to be evaluated is covered by a rectangular mesh and the contribution from an elementary rectangle, with sides of length $2h$ and $2k$, is given by

$$\tfrac{2}{3}hk(2z_{00} + z_{10} + z_{-10} + z_{01} + z_{0-1}) \qquad \ldots\ldots (A3)$$

where z_{00} is the value of the integrand at the centre and the other values refer to the corners. Owing to symmetry, the integration need only be extended over one twelfth of the occupied zone (figure 2). The boundaries of this area form a right-angled triangle and some approximation to the contribution from the boundary elements must therefore be made; on choosing $h = \sqrt{3}k$ the boundary rectangles are bisected by the diagonal and the contribution from each triangular element is, in good approximation, just half that given by (A3).

In the preliminary calculations (Peacock 1958) the pertinent integrals in (A2) were evaluated, with a mesh of 200 points, using a desk calculator. The calculations have since been refined by programming the most important integrals for the Ferranti 'Mercury' computer at the University of Manchester, using a mesh of 10 000 points. Substitution of the final results into (A1) then yields the following equations

$$\left.\begin{aligned}
P_1 &= 0{\cdot}5268 - 0{\cdot}0748h_2'^2\\
P_2 &= -0{\cdot}2140 + 0{\cdot}1498h_2' - 0{\cdot}3170h_3' + 0{\cdot}3052h_2'^2\\
P_3 &= -0{\cdot}0502 - 0{\cdot}1586h_2' + 0{\cdot}3140h_3' - 0{\cdot}1538h_2'^2
\end{aligned}\right\} \qquad \ldots\ldots (A4)$$

the terms in $h_3'^2$ and $h_2'h_3'$ being negligible. These equations provide the basis for the iterative process.

Acknowledgments

The work reported in this paper forms part of a research programme supported partly by the Department of Scientific and Industrial Research and partly by the U.S. Department of the Army, through its European Office.

The authors are grateful for the facilities provided by the Manchester University Computing Laboratory and wish to thank the staff (and particularly Mr. R. A. Brooker) for their encouragement and assistance. One of the authors (T. E. P.) wishes to acknowledge the award of a Ramsay Memorial Fellowship, during the tenure of which this research was carried out.

References

Barriol, J., and Metzger, J., 1950, *J. Chim. Phys.*, **47,** 432.
Bradburn, M., Coulson, C. A., and Rushbrooke, G. S., 1947–48, *Proc. Roy. Soc. Edin.* A, **62,** 336.
Brennan, R. O., 1951, *J. Chem. Phys.*, **20,** 40.
Corbato, F. J., 1956, *Q. Prog. Rep.* No. 21, Solid State & Molecular Theory Group (Massachusetts Institute of Technology).
Coulson, C. A., 1947, *Nature, Lond.*, **159,** 265.
Coulson, C. A., and Rushbrooke, G. S., 1945, *Proc. Camb. Phil. Soc.*, **36,** 193.
Coulson, C. A., and Taylor, R., 1952, *Proc. Phys. Soc.* A, **65,** 815.
Hückel, E. P., 1931, *Z. Phys.*, **72,** 310.
Johnston, D. F., 1955, *Proc. Roy. Soc.* A, **227,** 349.
—— 1956, *Ibid.*, **237,** 48.
Lomer, W. M., 1955, *Proc. Roy. Soc.* A, **227,** 349.
Löwdin, P.-O., 1950, *J. Chem. Phys.*, **18,** 365.
—— 1955, *Phys. Rev.*, **97,** 1474.
McWeeny, R., 1955 a, *Proc. Roy. Soc.* A, **227,** 288.
—— 1955 b, *Tech. Rep.* No. 7, Solid State & Molecular Theory Group (Massachusetts Institute of Technology).
—— 1955 c, *Proc. Roy. Soc.* A, **232,** 114.
—— 1956 a, *Ibid.*, A, **235,** 496.
—— 1956 b, *Ibid.*, **237,** 355.
McWeeny, R., and Peacock, T. E., 1957, *Proc. Phys. Soc.* A, **70,** 41.
Peacock, T. E., 1958, *Ph.D. Thesis*, University of Durham.
Pople, J. A., 1953, *Trans. Farad. Soc.*, **49,** 1375.
Roothaan, C. C. J., 1951, *Rev. Mod. Phys.*, **23,** 69.
Slater, J. C., and Koster, G. F., 1954, *Phys. Rev.*, **94,** 1498.
Slonczewski, J. C., and Weiss, P. R., 1958, *Phys. Rev.*, **109,** 272.
Wallace, P. R., 1947, *Phys. Rev.*, **71,** 622.
Willers, F. A., 1948, *Practical Analysis* (New York: Dover).
Yamazaki, M., 1957, *J. Chem. Phys.*, **26,** 930.

Recombination Relaxation Effects in Germanium Surfaces

By D. H. LINDLEY and P. C. BANBURY
Department of Physics, University of Reading

Communicated by R. W. Ditchburn; *MS. received* 17*th April* 1959

Abstract. The conductance of a thin single crystal slab of germanium has been modulated by a small electric field of variable frequency capacitively applied to the large face. The resulting dispersion which is related to the generation and recombination of minority carriers at the surface has been studied as a function of surface potential by using different ambient gases. The results show some agreement with the single energy level model analysed by Garrett and indicate in addition that the etched surfaces investigated were non-uniform.

§ 1. Introduction

There exists strong experimental evidence that two types of surface state are present on single crystal etched germanium surfaces. The two types are defined by their characteristic time constants for relaxation of their electron occupancy with changes of carrier concentrations in the bands. The time constants associated with the slow states are of the orders of seconds, while those of the fast states are believed to lie in the range 10^{-8} second or shorter at room temperature.

The present paper is concerned with the fast state properties connected with the screening of charge induced in the surface and with the recombination at the surface of excess carriers injected into the bulk. We have based our experiment on the modulation of conductance of a thin flat germanium slab arising from the application of a small a.c. electric field capacitively applied to a large face. Montgomery (1957) demonstrated that under variation of the frequency of the field the conductance changes showed a dispersion in the range 10^3–10^5 c/s and possibly an additional one around 5×10^7 c/s. Garrett (1957) has proposed a model based on a single trapping level at the surface in the forbidden gap. The predictions from the model are qualitatively in agreement with Montgomery's results. We have made more detailed measurements in the range 10^2–10^5 c/s and have derived characteristic surface state parameters by comparison with Garrett's expressions.

§ 2. Theory

The field effect can be described in terms of a field effect mobility μ_{fe} which is defined by Schrieffer (1955) as

$$\mu_{fe} = \frac{\Delta G_s}{\Delta \sigma}$$

where ΔG_s is the change in surface conductance resulting from an applied charge $\Delta\sigma$ per unit area.

Garrett (1957) derived the variation of μ_{fe} with frequency of a sinusoidal induced charge on an extrinsic specimen within the imposed limitation on $\Delta\sigma$ that disturbances of hole and electron concentrations were small in comparison with equilibrium values. The surface state model used was a single level whose

occupancy changes were characterized by Shockley–Read (1952) statistics. μ_{fe} was found to undergo a dispersion with characteristic time constant τ_d related to rates at which holes and electrons recombine and are generated in the filament. The further dispersion predicted at higher frequencies is outside our experimental range of frequencies and we shall not be concerned with it here. Under certain conditions τ_d can be equated to the filament lifetime for minority carriers as defined by Shockley (1950). In particular, if bulk recombination is negligible and the two large surfaces of the slab are assumed to have identical properties, τ_d may be written $\tau_d = T/2s$. Here T is the thickness of the slab and s is a function of the trap parameters and the surface potential and is identical with the expression obtained by Stevenson and Keyes (1954) and Many and Gerlich (1957) for the recombination velocity s of injected carriers at a surface. From measurement of τ_d against the surface potential u_s it is therefore possible to obtain similar information to that derived from direct measurement of s. Details of interpretation giving trap energy and capture cross sections are given in the above papers.

μ_{fe} as a function of frequency is found to be given by the real part of

$$\mu_{fe} = \mu_{dc} + \mu_{hf}\left(\frac{\omega\tau_d(\omega\tau_d + i)}{1+\omega^2\tau_d^2}\right).$$

μ_{dc} is the field effect mobility under conditions of equilibrium between the fast states and the bands and has been studied as a function of surface potential by many workers (Montgomery and Brown 1956, Garrett and Brattain 1956).

μ_{hf} is the amplitude of the dispersion and for an n-type extrinsic sample is of the form

$$\mu_{hf} = (\mu_n + \mu_p)\left[\frac{-\partial\Gamma_p/\partial u_s + C_p f_0 p_s/\Omega}{N_t f_0(1-f_0) - (\partial/\partial u_s)(\Gamma_p - \Gamma_n)}\right]$$

where $\Omega = C_p(p_s + p_1) + C_n(n_s + n_1)/N_t$, μ_n, μ_p are the electron and hole mobilities, Γ_n, Γ_p the excess electron, hole densities per unit area in the barrier, u_s the surface potential in units of $\boldsymbol{kT}$, p_s, n_s hole, electron concentrations at the surface, f_0 the Fermi occupancy factor at the trap energy, C_p, C_n the electron and hole capture cross sections, N_t the trap density, n_1, p_1 the electron and hole concentrations when the Fermi level is at the trap energy. μ_{hf} can be shown to become trivial beyond a value of surface potential determined solely by the bulk properties of the germanium. Physically this can be seen to be acceptable. Following Garrett (1957) it can be said that any small charge induced at the surface is taken up in the barrier as a certain number of holes and electrons depending on the value of surface potential. For example, in a strong inversion layer on n-type material the charge appears completely as holes. Any minority carriers required at the surface are assumed to be taken from the bulk where, after an appropriate time, they are replaced by generation. This time is the dispersion time τ_d. Thus at values of u_s where no holes are needed there is no disturbance in the bulk and hence no dispersion.

The theory could readily be extended to cover more than one state provided the additional levels were of such cross sections as to exclude their being recombination centres. Experimental evidence however suggests this to be of small usefulness.

The above discussion indicates that the dispersion for small signal electric fields should be measured at various surface potentials to evaluate the three quantities τ_d, μ_{dc} and μ_{hf} as a function of u_s.

§ 3. Experimental Technique

The filaments of dimensions 2 cm × 0·5 cm × 0·02 cm were etched in C.P.4 and mounted on polished brass electrodes with a mica spacer. The filament ends extended beyond the electrode and were sandblasted around the soldered end contacts to reduce injection effects. The surface potential was held at various values by enclosing the specimen in a glass system and using ambient gases as described by Brattain and Bardeen (1953), and Wang and Wallis (1957). The surface potential u_s was determined by measurement of conductance changes caused by the application of a large 50 c/s electric field which moved the barrier through the minimum of conductance in the manner of Bardeen *et al.* (1956). The resistance of the specimen was measured by Wheatstone bridge.

The small signal conductance change was studied as a function of frequency by using a modification of Low's (1955) circuit shown in figure 1. With B_1 and B_2 in opposition (i.e. no sweeping current flowing) the signal in the oscilloscope O was entirely due to charging current in R_1, R_2, C_1 and C_2. By adjustment of R_1 and C_1 this could be reduced to zero. On reversal of either B_1 or B_2 the signal in O was proportional to ΔR, the modulation of the specimen resistance by the field. The oscilloscope trace showed the variation of ΔR with field applied. The arrangement was satisfactory up to about 10^5 c/s when non-linear effects made initial balance impossible.

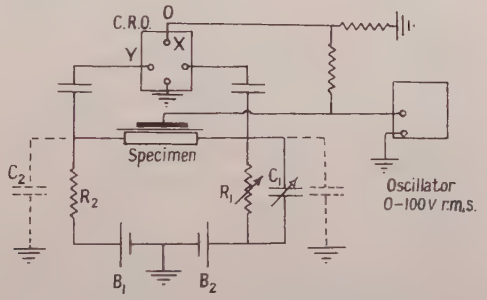

Figure 1. Circuit diagram.

§ 4. Discussion of Results

4.1. *Surface Recombination Velocity*

The specimens were all n-type, of resistivity from 16 Ω cm to 31 Ω cm and bulk lifetime greater than 350μsec. A typical plot of μ_{fe} against frequency is shown in figure 2. This can be represented by a dispersion with a single characteristic time constant. The values of μ_{fe} around $f_d(=1/2\pi\tau_d)$ are in the in-phase component. From the inflection point the dispersive frequency and hence τ_d can be found. A plot of $T/2\tau_d(=s)$ against u_s is shown in figure 3. The theoretical curve is drawn for a recombination centre of energy, as measured from the centre of the gap, of either $E_t - E_i = 4{\cdot}7\boldsymbol{k}T$ or $-1{\cdot}5\boldsymbol{k}T$ (Many and Gerlich 1957). The maximum value of s and its corresponding u_s give capture cross sections C_p and C_n. When $u_s \leqslant -2$ the experimental points deviate from the theory. This is common to all our results and is similar to the variation found by Garrett and Brattain (1956) measuring photoconductance. There are three possible explanations: a reversible variation of surface structure with ambient, an additional recombination centre or an inhomogeneous surface. The first possibility although suggested by the results of Many and Gerlich (1957) is

thought unlikely since similar curves have been found by measuring s by injection under constant ambient and using an electric field to swing the barrier (J. Holt, private communication). The evidence is considered to favour the last possibility although the second is not excluded. Additional data suggesting an inhomogeneous surface will be presented below.

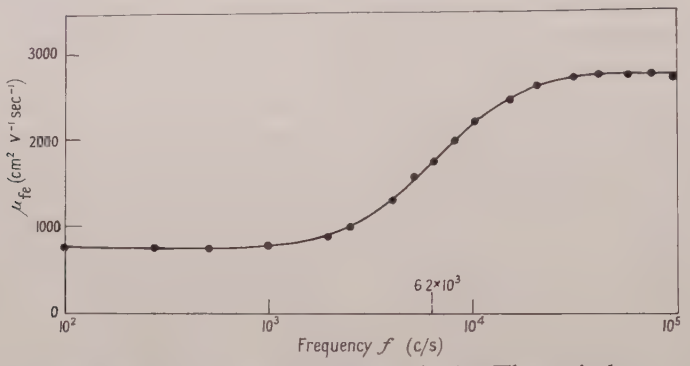

Figure 2. μ_{fe} plotted against frequency of applied field. Theoretical curve drawn for a dispersion of time constant 25·6 μsec ($f_d = 6{\cdot}2 \times 10^3$ c/s).

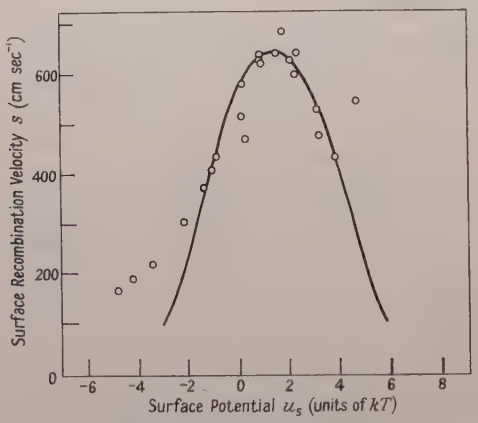

Figure 3. Variation of s with surface potential u_s. Theoretical curve drawn for $E_t - E_i = 4{\cdot}7\ kT$ and $C_p/C_n = 20$.

The s curves were not obtained immediately after etching but after days or even weeks. Initially the surface was unstable and points were not reproducible. Even after the stable configuration had been achieved changes were observed to occur with time. These however indicated a change in trap density only, other parameters remaining constant as found by Wang and Wallis (1957). The scatter of the points is larger than expected and would appear to arise from ambient induced structure changes or undetected drifts in values of u_s during measurement.

The interpretation of the τ_d data demands the resolution of the ambiguous trap energy. We have selected the value in the upper half of the gap. If the trap were at the centre of the gap, i.e. $E_t - E_i \simeq -1\,kT$ the trapping frequency would lie in the range $10^5 \simeq 10^6$ c/s. Since no such effect has been observed either by Montgomery (1957) or in the present work where this has been studied over a range of u_s at frequencies up to 4×10^5 c/s, it seems unlikely, as pointed out

by Garrett, that there are traps near the centre of the gap. Measurements of the temperature variation of s by Many and Gerlich (1957) also indicated the higher value.

Using the theoretical fits for ten such curves we find the mean results at room temperature

$$E_t - E_i = (4{\cdot}8 \pm 0{\cdot}5)\boldsymbol{k}T$$
$$C_p/C_n = 15\text{–}80$$
$$C_p/N_t = 2\text{–}7 \times 10^{-7}\ \mathrm{cm^3\,sec^{-1}}.$$

The trap density N_t was obtained from the (μ_{dc}, u_s) curve in a manner similar to that of Many and Gerlich (1957).

4.2. μ_{hf}

A typical plot of μ_{hf} against u_s for two specimens is shown in figure 4. The theoretical curve is obtained with a trap having the mean parameters found in the s measurements. Since $E_t - E_i \simeq 5\boldsymbol{k}T$ the trap is empty for most of the range

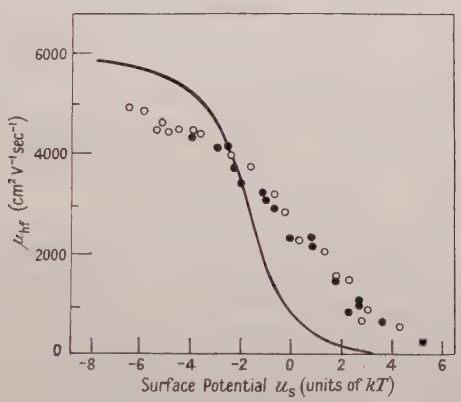

Figure 4. High frequency field effect mobility μ_{hf} plotted against u_s for two specimens. Theoretical curve drawn for a surface state of energy $E_t - E_i = 5\ \boldsymbol{k}T$ and density $7 \times 10^{10}\ \mathrm{cm^{-2}}$, for position of bulk Fermi level defined by $u_B = 1{\cdot}5$.

of this curve shown, i.e. it is not operative as a trapping level. Thus the curve is characteristic of a surface with no surface states. In principle additional states could be taken in the range shown and the μ_{hf} curve fitted to experiment. These states could have arbitrarily small capture cross sections for *one* carrier and hence would not be significant recombination centres. As mentioned in § 2 the theoretical plot indicates that μ_{hf} is small at $u_s = 1$ independently of surface state structure. From the experimental points it can be seen that μ_{hf} is about 2×10^3 at $u_s = 1$ and is still greater than $0{\cdot}5 \times 10^3$ at 4. This variation at large u_s is a common property of all the surfaces investigated. It was thought to be due to injection of minority carriers through the end contact but experiments with controlled injection through a p–n dot junction on the back surface showed a decrease in μ_{hf} rather than in increase with injected carriers.

It could alternatively be argued that this might be an ambient-induced effect. However, pulsed field measurements at constant ambient, varying u_s by electric field, have shown qualitatively similar results. Low (1955) observed similar effects using large pulses to swing his barrier under constant ambient. The explanation proposed is that this anomalous dispersion is directly a result of a

patchy surface. This implies that a measured surface conductance is that of a barrier not of uniform height but rather with a range of heights. Thus although the conductance change from minimum to a given value would indicate on a uniform surface that minority carriers no longer contribute to the incremental surface conductance, in fact the range would include values of u_s where this is not true. A patchy surface would in principle not yield a single time constant dispersion curve. Considerations of the magnitudes involved show however that changes in the shape of the dispersion would lie near the limit of experimental detection. If this proposed modification to the model is correct then there is little point in postulating additional surface states and fitting their energy and density to the experimental points. The effect of a patchy surface will be largest in the region of the minimum of conductance and hence our results are of least interest in the range $-5 \leqslant u_s \leqslant 1$. For this reason we have not fitted the results.

4.3. μ_{dc}

The μ_{dc} variation with u_s was similar to that found by Many and Gerlich (1957) and Bardeen *et al.* (1956). It could be fitted with two sets of traps in the range $u_s = -3$ to $u_s = 6$ as were the results of Many and Gerlich, one set being the recombination level. These fits, for reasons given above, are considered of little interest however: they serve to show that our results are similar to those of other workers. The second set of traps would of course have to fit both the μ_{dc} and the μ_{hf} data.

§ 5. Conclusions

The results of the experiment are in accord with Garrett's model and have given surface recombination data in agreement within experimental error with other data derived by different techniques. They have also indicated that our surfaces are inhomogeneous since in effect the dispersion is a detector of minority carriers in the barrier. As pointed out by Garrett (1957) this patch effect might account for the apparent screening observed in field effect measurements in regions of u_s near the centre of the gap where high frequency measurements indicate the absence of surface states.

Acknowledgments

Thanks are due to Professor R. W. Ditchburn for the provision of research facilities, and to the Admiralty for support and permission to publish.

References

Bardeen, J., Coovert, R. E., Morrison, S. R., Schrieffer, J. R., and Sun, R., 1956, *Phys. Rev.*, **104**, 47.
Brattain, W. H., and Bardeen, J., 1953, *Bell Syst. Tech. J.*, **32**, 1.
Garrett, C. G. B., 1957, *Phys. Rev.*, **107**, 478.
Garrett, C. G. B., and Brattain, W. H., 1956, *Bell. Syst. Tech. J.*, **35**, 1019.
Low, G. G. E., 1955, *Proc. Phys. Soc.* B, **68**, 10.
Many, A., and Gerlich, D., 1957, *Phys. Rev.*, **107**, 404.
Montgomery, H. C., 1957, *Phys. Rev.*, **106**, 441.
Montgomery, H. C., and Brown, W. L., 1956, *Phys. Rev.*, **103**, 865.
Schrieffer, J. R., 1955, *Phys. Rev.*, **97**, 641.
Shockley, W., 1950, *Electrons and Holes in Semiconductors* (New York: Van Nostrand), p. 318.
Shockley, W., and Read, W. T., 1952, *Phys. Rev.*, **87**, 835.
Stevenson, D. T., and Keyes, R. J., 1954, *Physica*, **20**, 1041.
Wang, S., and Wallis, G., 1957, *Phys. Rev.*, **105**, 1459, **107**, 947.

Absorption of Microwaves in Ethyl Chloride

By G. P. SRIVASTAVA
Department of Physics, University of Gorakhpur, Gorakhpur, India

MS. received 11*th March* 1959

Abstract. Pressure variation of the microwave absorption coefficient of ethyl chloride in the vapour state has been studied at frequencies of $0{\cdot}29\,cm^{-1}$ and $1{\cdot}14\,cm^{-1}$. It has been found that Van Vleck and Weisskopf's theory of absorption due to pressure broadened lines can explain approximately the pressure variation up to one atmosphere pressure in this case. The allowed rotational frequencies of the Q and R branches have been computed from the rotational constants of ethyl chloride. The intensities of various transitions have been calculated with the help of tables of Cross, King and Hainer. The absorption due to these transitions have been calculated at $0{\cdot}29\,cm^{-1}$, $0{\cdot}8\,cm^{-1}$ and $1{\cdot}14\,cm^{-1}$. The absorption at $0{\cdot}29\,cm^{-1}$ is found to be entirely due to Q branch transitions which are nearly at zero wave number. At $0{\cdot}8\,cm^{-1}$ the absorption due to R branch transitions has to be taken into account. At $1{\cdot}14\,cm^{-1}$ the calculated value is about 37·5% lower than the experimental value if the absorption due to only Q and R branches transitions is taken into account. An attempt is made to explain this discrepancy.

§ 1. Introduction

Hershberger (1946) measured the absorption coefficient of a few organic molecules at frequencies of $0{\cdot}29\,cm^{-1}$ and $0{\cdot}8\,cm^{-1}$. They tried to explain the observed absorption on the basis of Van Vleck and Weisskopf's (1945) relation. Qualitatively their results agreed with the predictions of Van Vleck and Weisskopf's theory. They also attempted to explain the results quantitatively. They partially succeeded in the case of ammonia and other symmetrical top molecules such as methyl halides. The results were later explained in the case of symmetrical top molecules by Bleaney and Loubser (1950), but no attempt was made to reach a quantitative agreement in the case of asymmetric molecules such as ethyl halides.

The total microwave absorption at a given frequency is the sum of resonant and non-resonant absorption. Van Vleck and Weisskopf's theory has the distinction of being able to explain both. Ethyl chloride is one of the simplest asymmetric top molecules and its rotational lines are distributed throughout the microwave region. The absorption at any frequency is the sum of resonant absorption due to transitions at that frequency and the transitions at other frequencies the effect of which is observed as the result of broadening of every line due to collision. Rotational constants and the asymmetry parameter of ethyl chloride are known (see Wagner and Dailey 1954). Ethyl chloride is a prolate molecule whose asymmetry parameter is $-0{\cdot}96$; its dipole moment is chiefly along the a axis. Therefore transitions involving μ_a have high probability. The majority of Q branch transitions occur at zero wave number. Their effects are observed at high frequencies because of collision broadening giving rise to Debye type (non-resonant) absorption. As all these things are known in the case of ethyl chloride an attempt is made to explain the observed absorption theoretically.

§ 2. Experimental Results and Technique

The details of the arrangement used for measuring the absorption coefficient of ethyl chloride at frequencies of $0{\cdot}29\,\mathrm{cm}^{-1}$ and $1{\cdot}14\,\mathrm{cm}^{-1}$ are given elsewhere (Krishnaji and Srivastava 1957). At $0{\cdot}29\,\mathrm{cm}^{-1}$ they use a klystron 2K39 as the source and a crystal 1N23 as the detector. Microwave power is measured when the experimental waveguide is filled with ethyl chloride vapour and when it is evacuated. The absorption coefficient is calculated by means of the relation

$$\alpha = \frac{1}{L}\log\left\{\frac{\theta}{\theta-\Delta\theta}\right\}\left\{1-\left(\frac{\lambda}{2b}\right)^2\right\}^{1/2}\mathrm{cm}^{-1}$$

where θ is the output galvanometer deflection when the cell is evacuated, $\Delta\theta$ is the reduction in the deflection of the galvanometer when the gas is admitted to the cell, L is the length of the absorption cell, λ the wavelength of the radiation, and b the larger dimension of the waveguide.

At $1{\cdot}14\,\mathrm{cm}^{-1}$ a klystron Qk292 was used to generate the power.

The values of the absorption coefficient at various pressures up to one atmosphere and at wave numbers $0{\cdot}25\,\mathrm{cm}^{-1}$, $0{\cdot}29\,\mathrm{cm}^{-1}$, $0{\cdot}80\,\mathrm{cm}^{-1}$ and $1{\cdot}14\,\mathrm{cm}^{-1}$ are as follows.

Wave number	Pressure (cm Hg)							
(cm^{-1})	10	20	30	40	50	60	70	76
0·25	0·05	0·20	0·40	1·00	1·80	3·10	4·80	5·70
0·29	0·20	0·55	1·05	1·80	3·00	4·40	6·30	7·10
0·80	0·50	1·25	2·40	4·40	6·10	8·50	12·10	14·50
1·14	1·75	4·20	7·80	11·60	18·50	24·70	30·20	32·10

The values at $0{\cdot}80\,\mathrm{cm}^{-1}$ are computed from the data of Walter and Hershberger (1946), the other values given here are the average of ten readings for each pressure.

§ 3. Discussion

The absorption coefficient due to a line is

$$\frac{\alpha}{\nu^2} = \frac{8\pi^2 N}{3kT} f_v f_{J_\tau} |\mu_{ij}|^2 \left[\frac{\Delta\nu}{\Delta\nu^2+(\nu-\nu_{ij})^2} + \frac{\Delta\nu}{\Delta\nu^2+(\nu+\nu_{ij})^2}\right]$$

where f_v is the fraction of the molecule in the vibrational states concerned, f_{J_τ} the fraction of the molecule in the lower rotational state, $|\mu_{ij}|$ is the dipole matrix element, $\nu(\mathrm{cm}^{-1})$ the frequency of observation, $\nu_{ij}(\mathrm{cm}^{-1})$ the frequency associated with the transition, and $\Delta\nu(\mathrm{cm}^{-1})$ the half width parameter.

Since the measurements are made at high frequencies the effect on absorption due to fine structure is negligible. Hence the value of f_v is taken as unity. The value of f_{J_τ} in the case of asymmetrical molecule ethyl chloride is (Townes and Schawlow 1955)

$$f_{J_\tau} = \frac{(2J+1)\exp(-W_{ij}/kT)}{\left\{\frac{\pi}{ABC}\left(\frac{kT}{h}\right)^3\right\}^{1/2}}$$

where A, B and C are the rotational constants of ethyl chloride in cycles per second. Therefore the relation for the absorption coefficient is

$$\frac{\alpha}{\nu^2} = \frac{8\pi^2 N}{3kT}\frac{(2J+1)|\mu_{ij}|^2\exp(-W_{ij}/kT)}{\left\{\frac{\pi}{ABC}\left(\frac{kT}{h}\right)^3\right\}^{1/2}F(\nu,\nu_{ij})}$$

where $F(\nu, \nu_{ij})$ is the shape factor and is equal to

$$F(\nu, \nu_{ij}) = \left[\frac{\Delta\nu}{\Delta\nu^2 + (\nu - \nu_{ij})^2} + \frac{\Delta\nu}{\Delta\nu^2 + (\nu + \nu_{ij})^2} \right].$$

For an asymmetric molecule $(2J+1)|\mu_{ij}|^2$ is just $\mu_x{}^2 {}^xs_{ij}$ where ${}^xs_{ij}$ is the transition strength calculated by Cross, Hainer and King (1944), μ_x is the component of the dipole moment (Debye units) μ_a, μ_b and μ_c whichever is responsible for the the transition. Wagner and Dailey (1954) have indicated that in the case of ethyl chloride μ_c is practically zero and that the transitions involving μ_a are four times stronger than those involving μ_b. Therefore only transitions involving μ_a have been considered, and for μ the value of μ_a has been substituted ($\mu_a{}^2 = \frac{4}{5}\mu^2$). The value of $\Delta\nu$ has been taken as $0{\cdot}25\ \text{cm}^{-1}$ atm which gives the best fit. Trial was made with three or four values of $\Delta\nu$.

The values of the rotational constants of ethyl chloride are $B = 5493{\cdot}76$ Mc/s, $A = 30\,124$ Mc/s and $C = 4962{\cdot}24$ Mc/s (Wagner and Dailey 1954). The frequencies of all the transitions have been calculated with the help of the expression

$$\nu = \tfrac{1}{2}(A+C)J(J+1) + \tfrac{1}{2}(A-C)\epsilon_\tau$$

and have been reported in an earlier paper (Krishnaji and Srivastava 1958). There are very few P branch lines which are allowed and moreover their contribution to absorption is almost negligible. Therefore the calculations are limited to Q and R branch transitions.

Calculations for $J > 12$ has been carried out approximately.

Table 1 shows the calculated microwave absorption at $\nu = 0{\cdot}29\ \text{cm}^{-1}$, $0{\cdot}80\ \text{cm}^{-1}$ and $1{\cdot}14\ \text{cm}^{-1}$ at two pressures, $\frac{1}{4}$ atm and 1 atm, due to all allowed rigid rotor transitions of R branch involving the dipole moment μ_a. Table 2 shows the calculated absorption at the same frequencies due to Q branch transitions.

At $\nu = 0{\cdot}29\ \text{cm}^{-1}$, the absorption it appears is almost due to Q branch transitions, the majority of which are at zero wave number. The absorption can therefore be considered as due to a zero frequency line of intensity $22{\cdot}84 \times 10^{-4}$ per atmosphere, and $\Delta\nu = 0{\cdot}25\ \text{cm}^{-1}$ per atmosphere. The figure shows such a curve in which α/ν^2 is plotted against ν. The points at $0{\cdot}25\ \text{cm}^{-1}$ and $0{\cdot}29\ \text{cm}^{-1}$ are seen to fit in very well in the curve, for higher frequencies the contribution due to Q branch transitions can be seen to be almost constant.

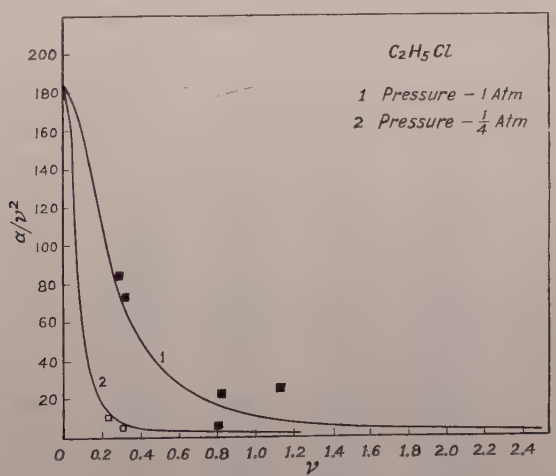

Theoretically calculated α/ν^2 plotted against ν in cm^{-1}.

Table 3 gives a comparison of the observed and calculated values of the absorption coefficient.

Table 1. Contribution of R Branch Transitions to the Absorption Coefficient

No.	Transitions	ν_{ij}	$\alpha \times 10^4$ at 1·14 cm^{-1}		at 0·80 cm^{-1} pressure (p)		at 0·29 cm^{-1}	
			$\frac{1}{4}$ atm	1 atm	$\frac{1}{4}$ atm	1 atm	$\frac{1}{4}$ atm	1 atm
1.	$0_{0,0} \rightarrow 1_{0,1}$	0·3476	0·001	0·012	0·001	0·013	0·004	0·007
2.	$1_{0,1} \rightarrow 2_{0,2}$	0·6949	0·004	0·054	0·025	0·085	0·000	0·004
3.	$1_{1,1} \rightarrow 2_{1,2}$	0·6784	0·003	0·036	0·015	0·062	0·000	0·003
4.	$1_{1,0} \rightarrow 2_{1,1}$	0·7119	0·003	0·040	0·024	0·066	0·000	0·003
5.	$2_{0,1} \rightarrow 3_{0,3}$	1·0418	0·082	0·256	0·009	0·077	0·000	0·003
6.	$2_{1,2} \rightarrow 3_{1,3}$	1·0175	0·066	0·214	0·010	0·075	0·000	0·003
7.	$2_{1,1} \rightarrow 3_{1,2}$	1·0678	0·115	0·261	0·007	0·062	0·000	0·002
8.	$2_{2,1} \rightarrow 3_{2,2}$	1·0428	0·045	0·140	0·005	0·042	0·000	0·001
9.	$2_{2,0} \rightarrow 3_{2,1}$	1·0438	0·045	0·140	0·005	0·042	0·000	0·001
10.	$3_{0,3} \rightarrow 4_{0,4}$	1·3878	0·023	0·197	0·002	0·032	0·000	0·002
11.	$3_{1,3} \rightarrow 4_{1,4}$	1·3567	0·027	0·208	0·002	0·032	0·000	0·002
12.	$3_{1,2} \rightarrow 4_{1,3}$	1·4234	0·017	0·164	0·002	0·027	0·000	0·002
13.	$3_{2,2} \rightarrow 4_{2,3}$	1·3902	0·017	0·146	0·002	0·023	0·000	0·001
14.	$3_{2,1} \rightarrow 4_{2,2}$	1·3927	0·017	0·146	0·002	0·023	0·000	0·001
15.	$3_{3,1} \rightarrow 3_{3,2}$	1·3909	0·010	0·084	0·001	0·013	0·000	0·001
16.	$3_{3,0} \rightarrow 4_{3,1}$	1·3909	0·010	0·084	0·001	0·013	0·000	0·001
17.	$4 \rightarrow 5$	9 lines	0·036	0·514	0·007	0·122	0·000	0·007
18.	$5 \rightarrow 6$	11 lines	0·020	0·301	0·007	0·086	0·000	0·009
19.	$6 \rightarrow 7$	13 lines	0·016	0·245	0·006	0·087	0·000	0·009
20.	$7 \rightarrow 8$	15 lines	0·011	0·202	0·001	0·074		
21.	$8 \rightarrow 9$	17 lines	0·013	0·179	0·001	0·071		
22.	$9 \rightarrow 10$	19 lines	0·011	0·158	0·000	0·067		
23.	$10 \rightarrow 11$	21 lines	0·011	0·147	0·000	0·062		
24.	$11 \rightarrow 12$	23 lines	0·009	0·136	0·000	0·060		
Contribution of higher transitions (calculated approximately)			0·250	2·545	0·000	0·721	0·000	0·000
Total			0·889	6·602	0·148	2·036	0·006	0·064

Table 2 Contribution of Q Branch Transitions to the Absorption Coefficient

No.	Transitions	ν_{ij}	$\alpha \times 10^4$ at 1·14 cm^{-1}		at 0·80 cm^{-1} pressure (p)		at 0·29 cm^{-1}	
			$\frac{1}{4}$ atm	1 atm	$\frac{1}{4}$ atm	1 atm	$\frac{1}{4}$ atm	1 atm
1.	$1_{1,0} \rightarrow 1_{1,1}$	0·0168	0·001	0·014	0·001	0·013	0·001	0·008
	$2_{2,0} \rightarrow 2_{2,1}$	0·0002	0·002	0·029	0·002	0·028	0·002	0·013
	$3_{3,0} \rightarrow 3_{3,1}$	0·0000	0·003	0·045	0·003	0·043	0·003	0·027
	$4_{4,0} \rightarrow 4_{4,1}$	0·0000	0·004	0·060	0·004	0·057	0·004	0·036
	$5_{5,0} \rightarrow 5_{5,1}$	0·0000	0·005	0·072	0·005	0·069	0·004	0·044
	$6_{6,0} \rightarrow 6_{6,1}$	0·0000	0·005	0·083	0·005	0·079	0·005	0·050
	$7_{7,0} \rightarrow 7_{7,1}$	0·0000	0·006	0·091	0·006	0·087	0·006	0·055
	$8_{8,0} \rightarrow 8_{8,1}$	0·0000	0·006	0·097	0·006	0·093	0·006	0·059
	$9_{9,0} \rightarrow 9_{9,1}$	0·0000	0·007	0·101	9·007	0·096	0·006	0·061
	$10_{10,0} \rightarrow 10_{10,1}$	0·0000	0·007	0·106	0·007	0·102	0·007	0·064
	$11_{11,0} \rightarrow 11_{11,1}$	0·0000	0·007	0·113	0·007	0·097	0·006	0·061
	$12_{12,0} \rightarrow 12_{12,1}$	0·0000	0·006	0·098	0·006	0·094	0·006	0·066

No.	Transitions	ν_{ij}	$\alpha \times 10^4$ at 1·14 cm^{-1}		at 0·80 cm^{-1}		at 0·29 cm^{-1}	
			pressure (p)					
			$\frac{1}{4}$ atm	1 atm	$\frac{1}{4}$ atm	1 atm	$\frac{1}{4}$ atm	1 atm
2.	$2_{1,1} \rightarrow 2_{1,2}$							
	$3_{2,1} \rightarrow 3_{2,2}$							
	$4_{3,1} \rightarrow 4_{3,2}$		0·044	0·677	0·044	0·648	0·042	0·411
	. .							
	. .							
	$12_{11,1} \rightarrow 12_{11,2}$							
3.	$3_{1,2} \rightarrow 3_{1,3}$							
	$4_{2,2} \rightarrow 4_{2,3}$		0·033	0·508	0·033	0·487	0·032	0·306
	. .							
	. .							
	$12_{10,2} \rightarrow 12_{10,3}$							
4.	$4_{1,3} \rightarrow 4_{1,4}$							
	. .		0·085	0·375	0·025	0·359	0·025	0·229
	. .							
	$12_{9,3} \rightarrow 12_{9,4}$							
5.	$5_{1,4} \rightarrow 5_{1,5}$							
	. .		0·018	0·267	0·018	0·254	0·016	0·162
	. .							
	$12_{8,4} \rightarrow 12_{8,5}$							
6.	$6_{1,5} \rightarrow 6_{1,6}$							
	. .		0·012	0·183	0·012	0·176	0·013	0·110
	. .							
	$12_{7,5} \rightarrow 12_{7,6}$							
7.	$7_{1,6} \rightarrow 7_{1,7}$							
	. .		0·008	0·121	0·009	0·112	0·006	0·067
	. .							
	$12_{6,6} \rightarrow 12_{6,7}$							
8.	$8_{1,7} \rightarrow 8_{1,8}$							
	. .		0·004	0·080	0·005	0·081	0·005	0·047
	. .							
	$12_{5,7} \rightarrow 12_{5,8}$							
9.	$9_{1,8} \rightarrow 9_{1,9}$							
	. .		0·002	0·042	0·008	0·045	0·003	0·022
	. .							
	$12_{4,8} \rightarrow 12_{4,9}$							
10.	$10_{1,9} \rightarrow 10_{1,10}$							
	. .		0·001	0·027	0·004	0·023	0·002	0·011
	. .							
	$12_{3,9} \rightarrow 12_{3,10}$							
11.	$11_{1,10} \rightarrow 11_{1,11}$		0·011	0·021	0·000	0·008	0·000	0·004
	$12_{2,10} \rightarrow 12_{2,11}$							
12.	$12_{1,11} \rightarrow 12_{1,12}$		0·002	0·011	0·000	0·016	0·000	0·000
	$J > 12$							
1.	$J_{k-1,0} \rightarrow J_{k-1,1}$	0·0000	0·045	0·692	0·045	0·661	0·017	0·419
2.	$J_{k-1,1} \rightarrow J_{k-1,2}$	0·0000	0·047	0·723	0·047	0·691	0·018	0·438
3.	$J_{k-1,2} \rightarrow J_{k-1,3}$	0·0000	0·049	0·745	0·048	0·711	0·019	0·451
4.	$J_{k-1,3} \rightarrow J_{k-1,4}$	0·0000	0·048	0·737	0·048	0·703	0·018	0·446
5.	$J_{k-1,4} \rightarrow J_{k-1,5}$	0·0000	0·048	0·736	0·048	0·700	0·018	0·444
6.	$J_{k-1,5} \rightarrow J_{k-1,6}$	0·0000	0·044	0·676	0·044	0·645	0·017	0·410
7.	$J_{k-1,6} \rightarrow J_{k-1,7}$	0·0000	0·043	0·653	0·042	0·624	0·016	0·396
8.	$J_{k-1,7} \rightarrow J_{k-1,8}$	0·0000	0·040	0·607	0·039	0·579	0·015	0·368
9.	$J_{k-1,8} \rightarrow J_{k-1,9}$	0·0000	0·035	0·535	0·035	0·511	0·013	0·324
Higher transitions			0·201	3·528	0·196	3·187	0·037	1·267
TOTAL			0·829	12·85	0·800	12·175	0·412	6·892

Table 3. Comparison of the Observed and the Calculated Values of the Absorption Coefficient

	Absorption Coefficient (cm^{-1})					
	$\nu = 0{\cdot}29\ cm^{-1}$		$\nu = 0{\cdot}80\ cm$		$\nu = 1{\cdot}14\ cm^{-1}$	
	$p\ \frac{1}{4}$ atm	p 1 atm	$p\ \frac{1}{4}$ atm	$p^{-1}1$ atm	$p\ \frac{1}{4}$ atm	p 1 atm
Author	0·55	7·10	—	—	4·20	32·10
Hershberger†	—	7·60	1·25	15·00	—	—
Theoretical:						
due to Q branch transitions	0·41	6·89	0·80	12·17	0·83	12·85
due to R branch transitions	0·01	0·06	0·15	2·04	0·89	6·60
Total theoretical value	0·42	6·95	0·95	14·21	1·72	19·42

† Hershberger's data are at $\nu = 0{\cdot}31\ cm^{-1}$.

It is clear from the above analysis that the experimental and the thoeretical values agree very closely at $\nu = 0{\cdot}29\,cm^{-1}$ and $\nu = 0{\cdot}80\,cm^{-1}$. At $\nu = 1{\cdot}14\,cm^{-1}$ the theoretical value is about 37·5% lower than the experimental value.

It is estimated that the difference can be accounted for to a large extent if we consider the following points: (i) contribution of transitions involving the dipole moment μ_b, (ii) since ethyl chloride is a asymmetric top molecule many other transitions which are weak may occur at higher pressures, (iii) R branch transitions become comparatively more important and therefore a small error in the value of $\Delta\nu$ will appreciably affect the contribution due to R branch lines, (iv) Pressure variation of $\Delta\nu$ may be non-linear, (v) ν_{ij} shifts towards lower frequencies with increasing pressure and therefore alters the contribution to absorption due to various transitions, (vi) line width may be different for different transitions.

In view of the good agreement between the experimental and the theoretical values of the absorption coefficient at $0{\cdot}29\,cm^{-1}$ and $0{\cdot}80\,cm^{-1}$ and reasonable explanation of the difference at $1{\cdot}14\,cm^{-1}$, it can be concluded that the assumed mechanism of the microwave absorption in the molecule is correct. The assumed value of $\Delta\nu$ is also fairly close to the correct value. Further work for the experimental determination of $\Delta\nu$ for individual lines is being undertaken in the laboratory.

Acknowledgments

The author expresses his deep sense of gratitude to Professor Krishnaji of the Department of Physics, University of Allahabad, under whose supervision the present investigations were carried out at the J.K. Institute of Applied Physics, University of Allahabad. The author is also indebted to Professor D. Sharma, Head of the Physics Department, University of Gorakhpur, for his interest in the work, and to Shri B. N. Jha, Vice-Chancellor, University of Gorakhpur, for providing facilities and encouragement towards establishing a Microwave Laboratory at the University of Gorakhpur and carrying out the present investigations.

References

Bleaney, B., and Loubser, J. H. N., 1950, *Proc. Phys. Soc.*, A, **63,** 483.
Cross, P. C., Hainer, H. M., and King, G. W., 1943, *J. Chem. Phys.*, **11,** 27.
—— 1944, *Ibid.*, **12,** 210.
Hershberger, W. D., 1946, *J. Appl. Phys.*, **17,** 495.
Krishnaji, and Srivastava, G. P., 1951, *J. Sci. Industr. Res.*, **16a,** 289.
—— 1958, *Z. Phys.*, **152,** 116.
Srivastava, G. P., 1957, *D.Phil. Thesis*, University of Allahabad.
Townes, H., and Schawlow, A. L., 1955, *Microwave Spectroscopy* (New York: McGraw-Hill).
Van Vleck, J. H., and Weisskopf, V. H., 1945, *Rev. Mod. Phys.*, **17,** 225.
Wagner, R. S., and Dailey, B. P., 1954, *J. Chem. Phys.*, **22,** 1458.
Walter, J. E., and Hershberger, W. D., 1946, *J. Appl. Phys.*, **17,** 814.

Proton Magnetic Resonance in Liquid *Iso*-Butyl Bromide

By K. LUSZCZYNSKI and J. G. POWLES
Physics Department, Queen Mary College, London, E.1

MS. received 24*th March* 1959

Abstract. Proton magnetic resonance relaxation times T_1 and T_2 in liquid *iso*-butyl bromide [$(CH_3)_2CHCH_2Br$] have been measured at $21{\cdot}5 \times 10^6$ c/s over the temperature range 110°K to 330°K. The results, together with others for T_2 down to 90°K, are interpreted in terms of molecular motion of the molecule as a whole and of the methyl groups in it. This extremely wide temperature range without phase transitions allows a severe test of the validity of theories of nuclear relaxation in molecular substances. The correlation frequency as a function of temperature which ranges from 10^2 c/s to 10^{11} c/s is deduced and a remarkably good correlation with dielectric loss measurements is found. A distribution of correlation frequencies of molecular reorientation at low temperatures is confirmed and the effect of the more rapid reorientation of one methyl group is found. This is a case in which the nuclear resonance parameters are controlled principally by the motion of the molecule as a whole but are modified by an internal molecular motion which is considerably faster.

§ 1. Introduction, Experimental Arrangement and Results

The proton magnetic resonance relaxation times have been measured for *iso*-butyl bromide as a liquid and as a supercooled liquid in the temperature range 110°K to 330°K by transient methods. The melting point of the crystal is 154·5°K and the boiling point of the liquid is 364·5°K.

The spin–lattice relaxation time T_1 was measured by the application of a short (about 20×10^{-6} sec) intense pulse of radio-frequency field ($21{\cdot}5 \times 10^6$ c/s) so as to turn the nuclear magnetization through 180° (this is called a 180° pulse) followed at time τ later by a 90° pulse. T_1 is determined from the nuclear signal following the 90° pulse as a function of τ (Carr and Purcell 1954).

The spin–spin relaxation time T_2 was measured when it was less than 200×10^{-6} sec, from the decay of the nuclear signal following a single 90° pulse. Values of T_2 greater than 200×10^{-6} sec were measured from the amplitude of the nuclear 'echo' signal at 2τ, following a 90°, τ, 180° pulse sequence, as a function of τ (Hahn 1950, Carr and Purcell 1954). Alternatively a 90°, τ, 180°, 2τ, 180° etc. pulse sequence was used giving echoes at 2τ, 4τ, etc. from which T_2 was determined and by means of which the effects of self diffusion were reduced (Carr and Purcell 1954). Details of the apparatus and method of measurement are given by Luszczynski and Powles (1959).

The samples of *iso*-butyl bromide were prepared from 'analar' material which was fractionally distilled and deoxygenated by the freeze–pump–thaw method and sealed in spherical bulbs varying from 3 to 10 mm in diameter. The atmospheric oxygen must be removed because of its effect in shortening the nuclear resonance relaxation times to an appreciable extent when the true

relaxation times are longer than about one second. The freeze pump-thaw procedure was applied about ten times and was found to be more efficient than other methods such as bubbling nitrogen through the liquid. More recently we have found that if the liquid is passed slowly through a sintered glass plate under reduced pressure the oxygen is removed as effectively and rather more quickly.

Since liquid *iso*-butyl bromide supercools very readily and forms a glass, values of T_1 and T_2 are obtained over a very wide range of temperature without phase changes. The nuclear resonance phenomena in *iso*-butyl bromide as a crystal and as a glass have been discussed elsewhere (Powles and Kail 1959, to be referred to as PK) and these results will be used in the interpretation of the present ones.

The values of T_1 and T_2 are interpreted in terms of the thermal motions occurring in the liquid. The results are correlated with information concerning molecular motion derived from dielectric loss measurements.

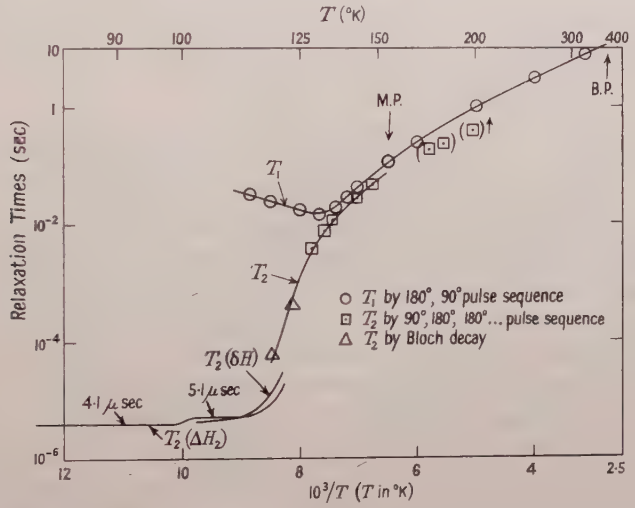

Figure 1. Relaxation times in liquid *iso*-butyl bromide. Also shows T_2 deduced from measurements of line width δH and root mean square line width ΔH_2 (*from* Powles and Kail 1959). B.P. boiling point; M.P. melting point of the crystalline form.

The measured values of T_1 and T_2 are given in figure 1. The measurements indicated simple exponential decay of both longitudinal and transverse magnetization at all temperatures. On the same figure are shown some results for T_2 deduced from line width δH and second moment ΔH_2^2 in gauss^2 given by PK. We have used the relations

$$T_2 = \alpha/2\gamma\Delta H_2 \ldots . (1a) \quad \text{and} \quad T_2 = \alpha/\gamma\delta H \ldots . (1b)$$

where γ is the proton gyromagnetic ratio. α is a constant of order unity to allow for the fact that T_2 is only strictly defined for a Lorentzian shaped line. If the line is Lorentzian the α in (1*b*) is $2/\sqrt{3}$. The curves for T_2 obtained by the two methods should join continuously; however in the region of T_2 of about 50×10^{-6} sec (line width of about one half gauss for protons) both experimental arrangements were subject to the greatest inaccuracy being at the limits of their range. Work is in hand to achieve a satisfactory overlap of the two pieces of apparatus. An important change in T_2 occurs in the region of 100°K which is rather obscured by the plot in figure 1 (see fig. 2 of PK).

Again the values of T_2 above about 150°K are low owing to the onset of self-diffusion effects which could not be entirely eliminated by use of the 90°, 180°, 180° etc. pulse sequence. We shall assume that the values of T_1 and T_2 do not in fact differ greatly in this temperature range. Further, the measurement of T_2 above 200°K was complicated by the appearance of echo amplitude modulation (Hahn and Maxwell 1952) due to indirect spin–spin coupling J between the chemically shifted, δ, protons in the molecule. This effect becomes observable when the direct dipole–dipole interaction between protons has been sufficiently reduced by increasingly rapid thermal motion. The echo amplitude modulation corresponded to $\delta \simeq 53$ c/s at 21·5 Mc/s and $J \simeq 6{\cdot}3$ c/s in reasonable agreement with reported preliminary measurements on this and similar molecules (Crawford and Foster 1956).

§ 2. Interpretation of the Results

2.1. *General Interpretation*

The theory of Bloembergen, Purcell and Pound (1948, to be referred to as BPP) leads to the following formulae for T_2 and T_1:

$$\frac{1}{T_2^2} = \frac{1}{T_{2r}^2}\frac{2}{\pi}\tan^{-1}\left(\frac{\alpha\xi}{2\pi\nu_c T_2}\right) \qquad \ldots\ldots(2)$$

$$\frac{1}{T_1} = \frac{1}{T_{2r}^2}\frac{\alpha\xi}{3\pi^2\nu_r}\left(\frac{\nu_r/\nu_c}{1+(\nu_r/\nu_c)^2} + \frac{\beta 2\nu_r/\nu_c}{1+(2\nu_r/\nu_c)^2}\right). \qquad \ldots\ldots(3)$$

$\beta = 1$ and ξ is a constant of order unity and covers an uncertainty in the theory; T_{2r} is the 'rigid lattice' transverse relaxation time i.e. when $\nu_c \to 0$; ν_c is the correlation frequency of the motion and is used for convenience in place of the more usual correlation time τ_c and $2\pi\nu_c\tau_c = 1$. ν_r is the resonant frequency which in our experiments is 21·5 Mc/s. We shall assume for simplicity that $\alpha = 2/\sqrt{3}$ and $\xi = 1$. This will not affect our interpretation substantially. More recent modification of the theory (Kubo and Tomita 1954, to be referred to as KT, Solomon 1955) change the expressions (2) and (3) to some extent and in particular mean that in equation (3), $\beta = 2$ and in equation (2) the function is not $\tan^{-1}$ but a rather similar one. In fact these changes make little difference to our interpretation and we shall retain the BPP form but quote the values for the KT theory where of interest.

The results in figure 1 are generally in agreement with the equations (2) and (3) if ν_c increases with temperature. Equation (3) shows that there is a minimum of T_1 when $\nu_c = \sqrt{2}\nu_r$ (when $\nu_c = 1{\cdot}69\nu_r$ for KT if $\nu_r \gg 1/2\pi T_{2r}$) and $T_{1\min} = (9\sqrt{3}/4\sqrt{2})\pi^2\nu_r T_{2r}^2 = 27{\cdot}1\nu_r T_{2r}^2$. Using the experimental result that the minimum of T_1 is $14{\cdot}1 \times 10^{-3}$ sec at 131°K we deduce $T_{2r} = 4{\cdot}9 \times 10^{-6}$ sec and this compares well with the observed rigid lattice value of $T_2 = 5{\cdot}1 \times 10^{-6}$ sec (figure 1) which is obtained from $\Delta H_{2r}^2 = 18$ gauss^2 (PK). The further fall in T_2 to $4{\cdot}1 \times 10^{-6}$ sec at even lower temperatures is discussed later.

Again the equations (2) and (3) predict that T_1/T_2 at the minimum of T_1 (131°K) is 2·25 (1·56 for KT) and the observed value is 2·2. We therefore proceed to apply the BPP theory in detail and deduce from the observed values of T_1 and T_2 the value of ν_c as a function of temperature. At temperatures below the minimum of T_1 the values of T_1 and T_2 cannot be made consistent if we use the formulae (2) and (3) with a constant value of T_{2r} of $4{\cdot}9 \times 10^{-6}$ sec independent of temperature, as is strongly suggested by the preliminary discussion above. If T_1 and T_2 are consistent with equations (2) and (3), at for instance 120°K, we

would have $\nu_c = 2{\cdot}2 \times 10^6$ c/s and $T_{2r} = 2{\cdot}4 \times 10^{-6}$ sec and both these figures are most unlikely. We therefore give in figure 2 the values of ν_c derived from equations (2) and (3) independently, and call them $\nu_c(T_1)_s$ and $\nu_c(T_2)_s$. We also include values of ν_c denoted by $\nu_c(\Delta H_2)_s$ which are derived from the values of ΔH_2 given by PK using equations (1) and (2).

Also in figure 2, we have plotted values of ν_{cD} which is the frequency corresponding to the maximum of the (dielectric loss, frequency) curve (Hennelly, Heston and Smyth 1948, Baker and Smyth 1939, Denney 1957). In the BPP theory the relation $\nu_c = 3\nu_{cD}$ holds if the same motion is referred to because of the different angle functions involved. Evidently the motions for the two frequencies ν_c and ν_{cD} may in general be different since the former refers to the variation of the interaction of the protons with time and the latter to the reorientation of the dipolar part of the molecule (-C(CH$_3$)$_2$-Br).

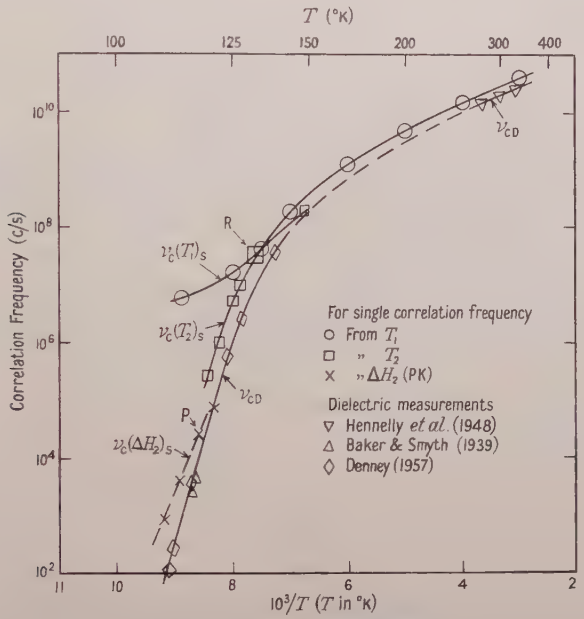

Figure 2. Correlation frequencies in liquid *iso*-butyl bromide as a function of temperature obtained as indicated.

The agreement in figure 2 between the values of ν_c deduced from the nuclear resonance results and the values of ν_{cD} in the room temperature microwave region (Hennelly, Heston and Smyth 1948) is striking. The actual ratio ν_c/ν_{cD} in this region is 1·5 which is sufficiently close to 3 in view of the reservations already mentioned. The results using the KT theory are almost identical. This matter is considered further in § 3. The slopes of the curves of ν_c and ν_{cD} correspond to 1·9 kcal mol^{-1} and 1·7 kcal mol^{-1} respectively. We conclude therefore that in this temperature region and indeed down to the minimum of T_1 (131°K) the theory is adequate with a constant value of T_{2r} which is deduced from the minimum of T_1. In fact T_{2r} may be expected to rise slightly with increasing temperature as a result of the thermal expansion of the liquid. However this effect is probably smaller than other imperfections in the theory. The effect would be to give deduced values of ν_c not more than a few tens per cent

higher in the higher temperature region which will still leave substantial agreement with the dielectric loss measurements.

We note in passing that the dielectric measurements in the microwave region indicate that there is a single correlation frequency ν_{cD} and that the same assumption has been made in the nuclear relaxation theory.

2.2. *A Distribution of Correlation Frequencies*

The divergence of $\nu_c(T_1)_s$ and $\nu_c(T_2)_s$ below 130°K and the difference in slope of the (ν_c, temperature) curve deduced from ΔH_2 and that of ν_{cD} obtained from dielectric measurements (Baker and Smyth 1939, Denney 1957) are, we believe due to a distribution of correlation frequencies at the lower temperatures. The general effect of more than one correlation frequency, or motion, can be seen by generalizing equations (2) and (3) to two correlation frequencies when we obtain (Powles and Luszczynski 1959)

$$\frac{1}{T_2^2} = \frac{2}{\pi}\left[\frac{1}{T_{2r1}^2}\tan^{-1}\left(\frac{1}{\sqrt{3\pi\nu_{c1}T_2}}\right) + \frac{1}{T_{2r2}^2}\tan^{-1}\left(\frac{1}{\sqrt{3\pi\nu_{c2}T_2}}\right)\right] \quad \ldots\ldots(4)$$

$$\frac{1}{T_1} = \frac{2}{3\sqrt{3\pi^2\nu_r}}\left[\frac{1}{T_{2r1}^2}g\left(\frac{\nu_r}{\nu_{c1}}\right) + \frac{1}{T_{2r2}^2}g\left(\frac{\nu_r}{\nu_{c2}}\right)\right] \quad \ldots\ldots(5)$$

where $g(x) = x/(1+x^2) + 2x/(1+4x^2)$. We define also for convenience the geometric mean frequency $\nu_g = (\nu_{c1}\nu_{c2})^{1/2}$ and a distribution parameter a where $a^2 = \nu_{c2}/\nu_{c1}$, i.e. $\nu_g = a\nu_{c1} = \nu_{c2}/a$.

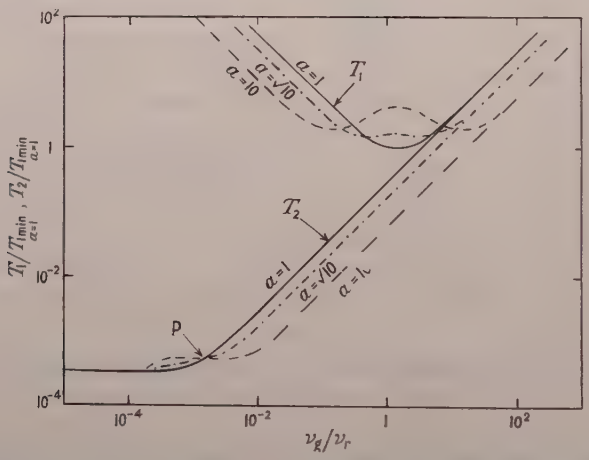

Figure 3. Effect on the nuclear resonance relaxation times of a double correlation frequency spectrum with equal intensities (eqns (4) and (5)). If the two frequencies are ν_{c1} and ν_{c2}, then $\nu_g = (\nu_{c1}\nu_{c2})^{1/2}$ and $a^2 = \nu_{c2}/\nu_{c1}$. Note the invariant point P and that the double minimum of T_1 is not resolved for $a \lesssim \sqrt{10}$.

The general effect on T_1 and T_2 as a function of ν_g for $a = \sqrt{10}$ and $a = 10$ is shown in figure 3 for $T_{2r1} = T_{2r2}$. For $a = \sqrt{10}$ the two processes are not well resolved either in T_1 or T_2 and might be taken to be single correlation frequency curves. If there is in fact a distribution but the equations (2) and (3) are used nevertheless to deduce values of ν_c from T_2 or ΔH_2 in the broad line region (as in figure 2) the variation of ν_c with temperature will be slower than that of ν_g which should be compared with ν_{cD}. Since the dielectric measurements at low temperature show a distribution of correlation frequencies (Baker and Smyth 1939,

Denney 1957) and the value plotted in figure 2 is the geometric mean value (or more precisely the value for maximum dielectric loss) it seems reasonable to explain the difference between $\nu_c(\Delta H_2)_s$ and ν_{cD} in this region as due to the distribution. It is readily shown that the middle of the line width transition region gives the true geometric mean value, ν_g, of ν_c independent of the distribution if this is symmetric on a logarithmic scale (Powles and Luszczynski 1959). This is the point P on figures 3 and 4. Baker and Smyth (1939) find a symmetric distribution but Denney's (1957) later and possibly more accurate results show a somewhat asymmetric distribution. Consequently $\nu_c(\Delta H_2)_s$ should agree substantially with ν_{cD} at this particular temperature apart from the factor 3 already mentioned. This point is the point P on figure 2 and after correction by a factor $3(=\nu_c/\nu_{cD})$ it would fall nicely on the ν_{cD} curve. The effect of a distribution on T_1 is discussed in § 2.3.

We can also generalize equation (2) for a continuous distribution as follows.

$$\frac{1}{T_2^2} = \frac{1}{T_{2r}^2}\frac{2}{\pi}\int_{-\infty}^{\infty} I(\ln \nu_c)\tan^{-1}\left(\frac{1}{\sqrt{3}\pi\nu_c T_2}\right)d(\ln \nu_c). \qquad \ldots\ldots(6)$$

Since the dielectric loss measurements suggest that the distribution of correlation frequencies for dipolar reorientation is not far from symmetric on a logarithmic scale we shall assume for simplicity a 'rectangular' distribution,

$$\begin{aligned} I(\ln \nu_c) &= 1/(2\ln b) \quad \text{for} \quad \nu_g/b < \nu_c < b\nu_g \\ &= 0 \qquad\quad\ \ \text{for} \quad \nu_g/b > \nu_c \ \text{and} \ \nu_c > b\nu_g. \end{aligned} \qquad \ldots\ldots(7)$$

The effect of this on T_1 and T_2 is shown in figure 4. The dielectric measurements analysed in a similar manner indicate that b is of order 10 for the dipolar

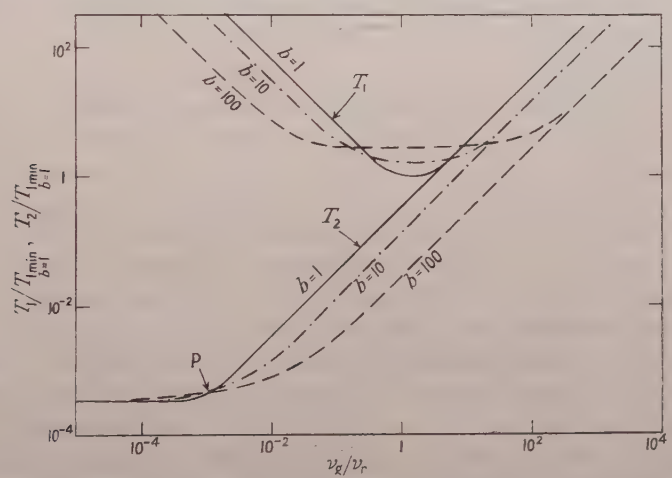

Figure 4. As figure 3 but for a continuous distribution of correlation frequencies of extent b which is defined in equation (7).

reorientation at 115°K. Using this value of b in equation (6), which can be solved numerically for given b, and taking $T_{2r}=5{\cdot}1\times10^{-6}$ sec we have deduced new values of $\nu_c(\Delta H_2)$ which are shown in figure 5. These agree well with ν_{cD} after allowing for the factor of approximately 3. Again the distribution is expected to fall with temperature ($b\to1$) and the fact that $\nu_c(T_1)_s$ and $\nu_c(T_2)_s$ agree at the minimum of T_1 means that there is no distribution ($b=1$) at this

temperature. It seems likely from the nuclear resonance measurements that b is practically unity down to about 125°K. A more detailed analysis would require measurements at other resonant frequencies.

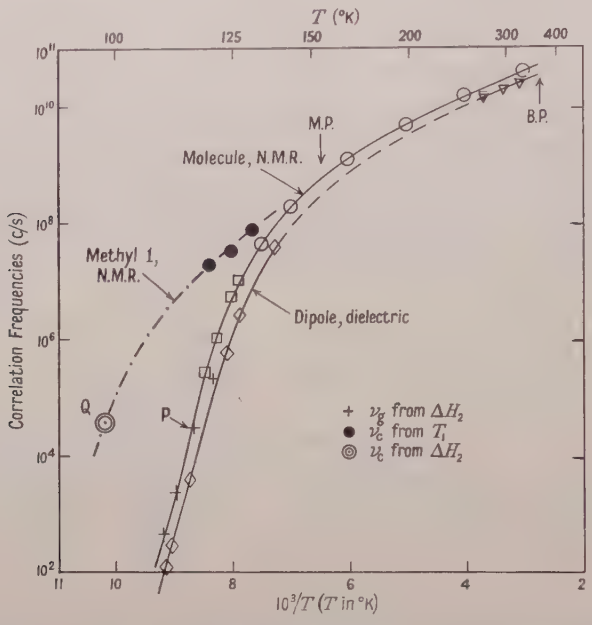

Figure 5. As figure 2 but with the final interpretation of the proton magnetic resonance measurement. The points which are not described in figure 2 are indicated. Note the excellent agreement between ν_c for the molecular motion deduced in this paper and ν_{cD} from the dielectric measurements, bearing in mind that $\nu_c/\nu_{cD} \simeq 3$ if the motions are the same.

The corresponding correction to equation (3) cannot explain the value of T_1 at temperatures just below the minimum of T_1 as is shown in the following section.

2.3. *The Effect of Two Motions with very Different Frequencies*

We now consider the discrepancy between $\nu_c(T_1)_s$ and $\nu_c(T_2)_s$ in the region 110°K to 131°K. This cannot be explained by a continuous distribution of any width unless unlikely values of T_{2r} are admitted. This is because the observed T_1 is shorter than that expected from the simple theory and as we see from figure 4 the introduction of a distribution of ν_c, with the same T_{2r}, makes T_1 longer near the minimum. Further, the curve $\nu_c(T_2)_s$ below 131°K seems to be in excellent agreement with the ν_{cD} curve. We have therefore considered the possibility that in this temperature region T_1 is controlled mainly by one motion and T_2 by another as has already been suggested for a certain temperature region in poly-*iso*-butylene (Powles and Luszczynski 1959) although the situation there is a little different. That is to say we use equations (4) and (5) but suppose that ν_{c1} and ν_{c2} differ considerably as shown for example in figure 3 for $a = 10$. The fact that two motional processes are present is already suggested by the broad line measurements where there is a fall in second moment of 10 gauss² centred at 98°K and then another of 18 gauss² centred at 116°K (PK). The corresponding changes in T_2 can be seen on figure 1. The fall at 98°K has been interpreted as

due to rapid reorientation of one methyl group per molecule (PK). Using equation (4) with $T_{2r1} = 2{\cdot}2 \times 10^{-6}$ sec and $T_{2r2} = 5{\cdot}1 \times 10^{-6}$ sec we obtain from the centre of this line width transition the point Q on figure 5, similar in nature to P which corresponds to reorientation of the whole molecule. If we now use the same constants in equation (5) for T_1 and also ν_{c1} as deduced from the values of T_2 (i.e. in effect using equation (4) and noting that the term due to ν_{c2} is negligible in this temperature region) we can calculate ν_{c2} in the range where T_1 has been measured. The result of doing this is shown in figure 5. It seems not unreasonable then to draw in tentatively the variation of ν_{c2} marked Methyl 1, N.M.R. in this figure. We now see that although two distinct rises in T_2 are observed (figure 1), two distinct minima of T_1 will not be because at the higher temperature at which the minimum of T_1 occurs the ratio ν_{c2}/ν_{c1} has fallen to about 25 instead of 1000 or more. Thus in the region just below the minimum of T_1 $a \simeq 5$ and the double minimum of T_1 is barely resolved (figure 3). Moreover each of these two processes still has in addition a slight distribution (figure 4) and so we get finally the observed rather flat asymmetric minimum of T_1 shown in figure 1.

§ 3. Conclusions

We have found that the proton magnetic resonance interactions in *iso*-butyl bromide at low temperatures are affected by two motions. A fast one which is the reorientation of the molecule as a whole whose correlation frequency agrees with the dielectric loss correlation frequency. The dielectric loss has a distribution of correlation frequencies at low temperatures and this is confirmed by the nuclear resonance results. The second motion is that of one methyl group which probably has a distribution also but measurements of T_1 at lower temperatures would be required to confirm this. As the temperature rises the distributions of each motion get smaller ($b \to 1$) and they become more comparable in frequency ($a \to 1$). They are apparently indistinguishable at temperatures above about 135°K. Above the minimum of T_1 both T_1 and T_2 depend mainly on the slowest of any multiple motions (see figures 3 and 4) i.e. in this case they depend mainly on that of the molecule as a whole. This is of course also true up to temperatures of 300°K and above and the agreement of ν_c from nuclear resonance and ν_{cD} from dielectric loss measurements is quite clear.

The fact that the nuclear resonance results agree so well with the dielectric ones shows that the motion of the dipolar part of the molecule and the molecule as a whole are very similar. The nuclear resonance results mean that all molecules move and therefore that the dielectric behaviour is not due to a fraction of molecules in special sites.

At higher temperatures the self diffusion could be the 'slowest' motion. However in this case T_{2r}^2 in equation (3) would be reduced by a factor of about ten which would make the deduced value of ν_c ten times *smaller*, i.e. poorer agreement with the dielectric results. This therefore suggests that molecular reorientation and interactions between protons internal to the molecule are still the most important processes. The reverse situation may hold in molecular solids (Andrew 1955) in some temperature regions.

Finally we predict that dielectric measurements in the temperature range between 138°K and 278°K, which are not at present available, will have a correlation frequency as a function of temperature which will follow rather closely

the dashed curve shown in figure 5. Further, the distribution of correlation frequencies will fall with increasing temperature and will probably not be readily observable at temperatures greater than about 138°K.

The interpretation of the variation of the correlation frequency with temperature is a problem in itself in the theory of liquids. We merely point out here that the present measurements have provided values of this parameter over a range of $10^9:1$ for one substance.

Acknowledgments

Part of the apparatus was provided by the Central Research Fund of the University of London and by Imperial Chemical Industries Ltd. It is a pleasure to acknowledge the generous support given to us by Professor G. O. Jones.

References

Andrew, E. R., 1955, *Defects in Crystalline Solids* (London: Physical Society), p. 60.
Baker, W. O., and Smyth, C. P., 1939, *J. Amer. Chem. Soc.*, **61**, 2063.
Bloembergen, N., Purcell, E. M., and Pound, R. V., 1948, *Phys. Rev.*, **73**, 679.
Carr, H. Y., and Purcell, E. M., 1954, *Phys. Rev.*, **94**, 630.
Crawford, G. J. B., and Foster, J. S., 1956, *Canad. J. Phys.*, **34**, 663.
Denney, D. J., 1957, *J. Chem. Phys.*, **27**, 259.
Hahn, E. L., 1950, *Phys. Rev.*, **80**, 580.
Hahn, E. L., and Maxwell, D. E., 1952, *Phys. Rev.*, **88**, 1070.
Hennelly, E. J., Heston, W. M., and Smyth, C. P., 1948, *J. Amer. Chem. Soc.*, **70**, 4102.
Kubo, R., and Tomita, K., 1954, *J. Phys. Soc. Japan*, **9**, 888.
Luszczynski, K., and Powles, J. G., 1959, *J. Sci. Instrum.*, **36**, 57.
Powles, J. G., and Kail, J. A. E., 1959, *Proc. Phys. Soc.*, **73**, 833.
Powles, J. G., and Luszczynski, K., 1959, *Physica*, **25**, 455.
Solomon, I., 1955, *Phys. Rev.*, **99**, 559.

The Electronic Specific Heats of Some Nickel–Cobalt Alloys

By J. C. WALLING and P. B. BUNN
Mullard Research Laboratories, Salfords, nr. Redhill, Surrey

MS. received 29th April 1959

Abstract. Low temperature specific heat measurements on nickel, cobalt and four alloys of nickel and cobalt are described. It is shown, as a result of these measurements, that the 3d band is unlikely to be parabolic, as has frequently been assumed, at the Fermi limit in nickel. Assuming that the relative magnetization is unity for nickel and the alloys the shape of the 3d band is calculated from the measured values of γ, the coefficient of electronic heat capacity, the resultant curve being in good agreement with the theoretical curve obtained by Fletcher in 1952 at the nickel rich end.

§ 1. Introduction

The ferromagnetic elements nickel and cobalt form a continuous series of solid solutions. In view of its great interest from the magnetic point of view and of its simplicity the alloy system has been extensively investigated (see Wohlfarth 1949 for a bibliography). However, although the electronic heat capacities of both nickel and cobalt have been previously determined (Ni: Keesom and Clark (1935) and Rayne and Kemp (1956); Co: Duyckaerts (1939) and Heer and Erickson (1947)) those of the alloys have not. Since some information regarding the shape of the 3d band in the first transition series can be obtained from such measurements the present work was undertaken.

§ 2. Preparation of Specimens

The specimens of nickel, cobalt and the nickel–cobalt alloys used in this investigation were prepared from nickel and cobalt sponge by Johnson, Matthey and Co. Ltd., the purity of these materials being at least 99·95%. After being pressed into rods to facilitate handling the specimens were melted in recrystallized alumina crucibles using an induction heater, the actual melting being carried out in an atmosphere of hydrogen. Prior to solidification the hydrogen was pumped out of the furnace and the specimens were maintained *in vacuo* at a temperature just below the melting point to remove any dissolved hydrogen. After being reduced to size the specimens were homogenized by annealing for several hours at 1200°c in an atmosphere of argon. Subsequent chemical and metallurgical examination of the alloys indicated that they were homogeneous. The proportions of the constituent elements of the specimens as determined by chemical analysis were always in close agreement with proportions of the original powder mixture. In what follows each alloy is specified in terms of its approximate cobalt content, i.e. NiCo 20 refers to an alloy with 20 atomic per cent cobalt; the exact proportions

of each alloy as determined by chemical analysis are given in table 1 together with the weight of each specimen.

Table 1

Specimen	Ni	NiCo 10	NiCo 20	NiCo 50	NiCo 70	Co
At. % Co	0·0	10·0	20·0	52·8	67·8	100·0
Weight (g)	33·11	38·24	37·65	37·17	42·41	32·46

§ 3. Apparatus

The specific heat measurements were made using the conventional vacuum calorimeter sketched in figure 1. The silver calorimeter shell C carried the heating coil, the carbon resistance thermometer and also a vapour pressure thermometer bulb into which a small quantity of helium could be condensed for thermometer calibration purposes.

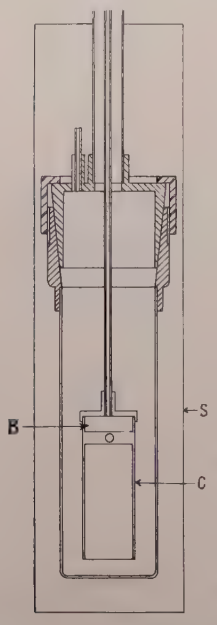

Figure 1. The calorimeter.

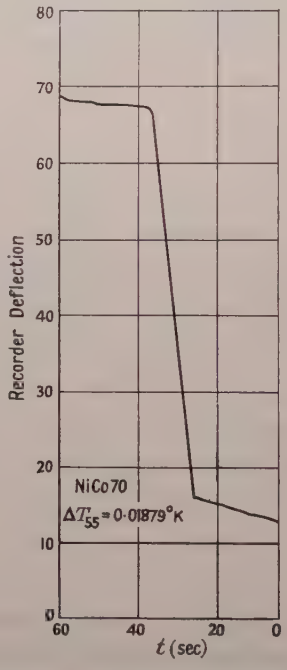

Figure 2. Typical heating curve.

The cylindrical specimen was secured in the calorimeter by means of a small copper spigot and good thermal contact between the specimen and the calorimeter was obtained by coating the specimen with a thin film of a silicone grease (Type MS4). The specimen fitted tightly in the calorimeter and it was felt that the heat capacity of the silicone grease would be negligible. The quality of the thermal contact obtained by this technique may be judged from the typical heating curve reproduced in figure 2, there being no evidence of any over-heating of the calorimeter.

The ground joint in the outer can of the calorimeter greatly facilitated specimen changing and when coated with silicone grease proved vacuum tight even when immersed in liquid helium at a temperature below the λ-point.

During initial experiments it was noticed that the heat leak into calorimeter and specimens was excessively large; this was found to be due to hysteresis heating of the ferromagnetic specimens caused by stray 50 c/s magnetic fields and was completely eliminated by surrounding the whole calorimeter assembly by a mumetal shield S.

The heater and thermometer leads were made from constantan, and the current in, and the potential drop across, the 600 ohm constantan heater were determined potentiometrically during each heating period, the duration of which was measured by means of a stop clock; the clock and the calorimeter heating current being controlled by the same switch.

§ 4. Thermometry

The resistance thermometer element used in this work consisted of a $\frac{1}{4}$ watt 56 ohm Allen Bradley carbon resistor, which had the outer layer of insulant removed and was permanently secured in the calorimeter by means of Bakelite varnish. The thermometer was calibrated by measuring the vapour pressure of a small amount of liquid helium contained in the bulb B and simultaneously determining the thermometer resistance. The temperature being determined using the agreed 1955 liquid helium vapour pressure–temperature scale (Clement *et al.* 1955). It was found that the resistance temperature relation was of the form

$$\frac{1}{T_R} = \frac{a^2}{\log_{10} R} + b^2 \log_{10} R + 2ab$$

and throughout this work the temperatures T_R were calculated from the thermometer resistance R using

$$\frac{1}{T_R} = \frac{0{\cdot}81008}{\log_{10} R} + 0{\cdot}31626 \log_{10} R - 1{\cdot}01232. \qquad \ldots\ldots (1)$$

Immediately prior to each heat capacity experiment a thermometer calibration was made and a deviation curve, $T_R - T_{55}$ against T_R, was plotted. It was found that the shape of this deviation curve (figure 3) remained substantially constant

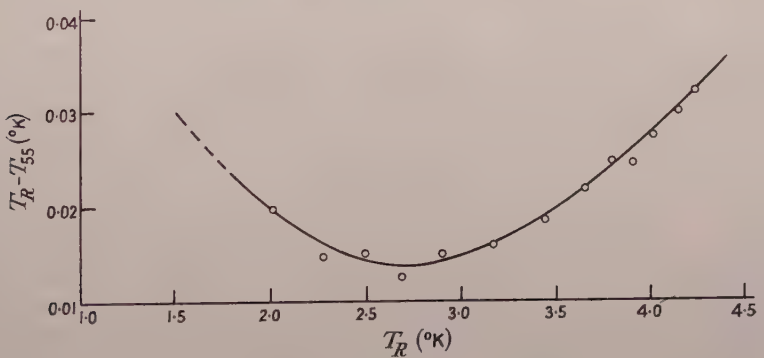

Figure 3. Resistance thermometer deviation plot.

from one experiment to the next but that there was a tendency for $T_R - T_{55}$ at a given T_R to increase with successive coolings. This increase, of course, did not affect the accuracy of the thermometry, and in any case the total shift of the deviation plot over the period during which the experiments were made was less than 0·02°K.

It was found convenient to use a 5-dial Tinsley Diesselhorst potentiometer for the resistance thermometer measurements. During a heat capacity measurement the out-of-balance voltage was taken through a d.c. amplifier of the type used in the Philips valve voltmeter type GM6010 and having input impedance of about 1 megohm, and then through a simple potential divider to a Sunvic recording potentiometer. In this way the heating curves were recorded automatically, a typical curve being shown in figure 2.

The corrected temperature rise was found from the heating curves by extrapolating the fore and after periods (almost invariably found to be linear) to the centre of the heating period, determining the thermometer resistance at these points and hence, using (1), the initial and final temperatures of the calorimeter on the resistance thermometer scale. The temperature rise could thus be accurately determined in terms of the resistance thermometer scale. The temperature rise on the 1955 scale could then be determined from the deviation plot using

$$\Delta T_{55} = \Delta T_R \left(1 - \frac{d\delta}{dT_R}\right) \qquad \ldots\ldots (2)$$

where

$$\delta = T_R - T_{55}. \qquad \ldots\ldots (3)$$

In practice

$$0{\cdot}98 < 1 - \frac{d\delta}{dT_R} < 1{\cdot}02.$$

§ 5. Results

Measurements were made over the temperature range 1·9–4·2°K on the empty calorimeter and on specimens of nickel, NiCo 10, NiCo 20, NiCo 50 and NiCo 70. Measurements were also made on pure cobalt but were not extended to temperatures lower than 2·2°K.

It was assumed for each specimen that the specific heat followed a law of the usual form:

$$C_v = \gamma T + bT^3$$

where γ is the coefficient of the electronic heat capacity and the term bT^3 is taken to represent the heat capacity of the lattice.

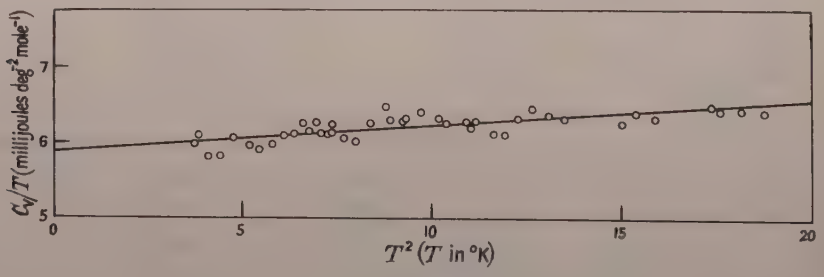

Figure 4. C_v/T plotted against T^2 for NiCo 10.

Following conventional practice the results were plotted as C_v/T against T^2 and using the method of least squares the most probable values of γ and b were determined for each case. The (C_v/T, T^2) plot for NiCo 10 is given in figure 4. The scatter of the experimental points obtained for each of the specimens is similar

to that for NiCo 10 and the root mean square deviation of all points from the mean square straight lines is 2%. The results of the work are summarized in table 2.

Table 2

Specimen	γ (millijoules deg^{-2} $mole^{-1}$)	θ_D (°K)
Ni	$6{\cdot}70 \pm 0{\cdot}05$	348 ± 15
NiCo 10	$5{\cdot}88 \pm 0{\cdot}04$	382 ± 15
NiCo 20	$5{\cdot}39 \pm 0{\cdot}04$	370 ± 15
NiCo 50	$4{\cdot}75 \pm 0{\cdot}04$	337 ± 15
NiCo 70	$4{\cdot}52 \pm 0{\cdot}05$	370 ± 15
Co	$4{\cdot}44 \pm 0{\cdot}05$	416 ± 20

The errors quoted in table 2 are Gaussian probable errors obtained from the least squares data in the standard manner. It seems probable that the accuracy obtained might have been considerably improved had larger specimens been used.

The low temperature specific heat of cobalt contains in addition to the electronic and lattice contributions a contribution due to the interaction of the ^{59}Co nuclear moment with the 3d electrons, known as the hyperfine coupling term. This term has been measured by Heer and Erickson (1957) and prior to the least squares analysis of the present results for cobalt the hyperfine coupling term was subtracted from the measured specific heats. The term is very small in the temperature range covered by the present work but it does have a significant effect on the

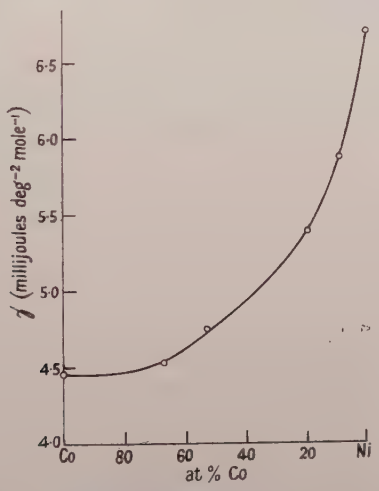

Figure 5. γ plotted against cobalt concentration.

apparent value of θ_D obtained by least squares analysis. This method was adopted since the present results do not extend to sufficiently low temperatures to allow unambiguous separation of the lattice, nuclear and electronic contributions to the specific heat.

In view of the large uncertainty in the values of θ_D obtained from specific heat measurements in the liquid helium region alone (a Gaussian probable error of 15° corresponds to a maximum error of 75°), the fact that the present value of θ_D for nickel is somewhat lower than has been observed previously is not of great significance.

The variation of the electronic term γ with concentration is plotted in figure 5.

§ 6. Discussion

According to the band theory of metals the contribution to the specific heat made by a single isolated band in the absence of ferromagnetism is

$$C_e = \tfrac{2}{3}\pi^2 k^2 \nu(\epsilon_0) T$$

$\nu(\epsilon_0)$ being the number of states per unit energy range for one direction of spin at the Fermi limit.

For a ferromagnetic the positive and negative sub-bands are shifted in energy relative to each other and are thus filled to different extents. The ratio of this population difference to the sum of electrons (or holes) in both bands is known as the relative magnetization ζ_0.

Clearly for a ferromagnetic in which $\zeta_0 = 1$ only one sub-band is populated and contributes to the electronic specific heat. For this case there is a simple relation between the electronic heat and the density of states at the Fermi limit

$$C_e = \tfrac{1}{3}\pi^2 k^2 \nu(\epsilon_0) T.$$

Assuming that the shape of the 3d band is unaltered on alloying and that the distribution of states is parabolic, Wohlfarth (1949) has shown that $\zeta_0 = 1$ for all nickel–cobalt alloys. Electronic heat measurements then should give a direct measure of the density of states at the Fermi limit and these results taken in conjunction with experimental data on the saturation magnetization of the alloys (directly proportional to the number of holes in the 3d band) should enable the shape of the 3d band to be determined.

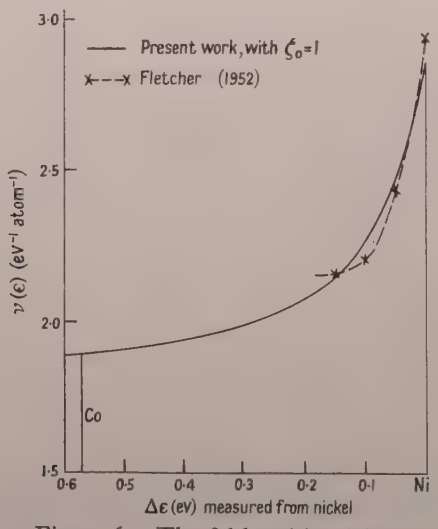

Figure 6. The 3d band in nickel.

It is apparent from the present results, however, that the 3d band in nickel is unlikely to be parabolic at the Fermi limit. In fact, if we retain the condition $\zeta_0 = 1$, we find that, close to the Fermi limit for nickel $\nu(\epsilon) \propto \epsilon^{-2/5}$ rather than $\nu(\epsilon) \propto \epsilon^{1/2}$ as assumed by Wohlfarth.

The correct values of ζ_0 for the nickel–cobalt alloys are then unknown and therefore the shape of the 3d band cannot be properly determined from the present results except possibly by a ' self-consistent band ' method which would be exceedingly laborious.

It is probable, however, that ζ_0 is not particularly sensitive to band form for these alloys (Wohlfarth, private communication) and if we take $\zeta_0 = 1$ the shape of the 3d band can be determined. It follows from the saturation magnetization data quoted by Wohlfarth (1949) for NiCo alloys that the number of holes in the d-band varies linearly with cobalt concentration and is given by

$$(n_d)_c = 0{\cdot}605\,(1 + 1{\cdot}973c)$$

where c is the fractional cobalt concentration. Using this result together with the γ values given in this paper and following the procedure outlined by Hoare *et al.* (1953) the energy density of states can be calculated as a function of energy measured downwards from the Fermi limit in pure nickel.

The band shape calculated in this way is given in figure 6 together with the theoretical result of Fletcher (1952). The close similarity between Fletcher's curve and that derived from the present results is interesting but it must be emphasized that it is only correct to treat the experimental results in this way if $\zeta_0 = 1$, which as we have pointed out, is not necessarily true.

It is clear, however, that the results of the present work support Fletcher's conclusions regarding the shape of the 3d band close to the Fermi limit in nickel although further experimental work particularly on nickel rich nickel–cobalt and nickel–copper alloys would be desirable. If Fletcher's picture is correct then the electronic heat of nickel rich nickel–copper alloys should increase, initially, with increasing copper concentrations.

Acknowledgments

The authors are indebted to the Directors of Mullard Limited for permission to publish this paper and for allowing the use of the low temperature facilities of these Laboratories for this work.

Acknowledgment is also due to Dr. E. P. Wohlfarth who suggested the problem.

References

Clement, J. R., Logan, J. K., and Gaffney, J., 1955, *Phys. Rev.*, **100,** 743 (see note added in proof).

Duyckaerts, G., 1939, *Physica*, **6,** 817.

Fletcher, G. C., 1952, *Proc. Phys. Soc.* A, **65,** 192.

Heer, C. V., and Erickson, R. A., 1957, *Phys. Rev.*, **108,** 896.

Hoare, F. E., Matthews, J. C., and Walling, J. C., 1953, *Proc. Roy. Soc.* A, **216,** 502.

Keesom, W. H., and Clark, C. W., 1935, *Physica*, **2,** 513.

Rayne, J., and Kemp, W., 1956, *Phil. Mag.* [8], **1,** 918.

Wohlfarth, E. P., 1949, *Phil. Mag.* (7), **40,** 1095.

Interpretation of Isotope Shifts in the Rare Gases

By A. P. STONE
Union Christian College, Alwaye, South India

MS. received 5*th March* 1959, *in final form* 4*th May* 1959

Abstract. A successful qualitative interpretation of observed isotope shifts in Ne, A, Kr, Xe is obtained by considering the specific mass effect in intermediate coupling.

§ 1. Introduction

Isotope shifts in atomic spectra arise from two causes, the nuclear mass effect (Hughes and Eckart 1930) and the nuclear field effect (Reiner 1955 and references therein). The mass effect is divided into two parts, the normal mass effect, which is the effect of the reduced mass of the electron, and the specific mass effect. The mass effect predominates in light elements and the field effect predominates in heavy elements.

In their derivation of the effect of the reduced mass of the electron, Hughes and Eckart (1930) neglected the spin–orbit interaction. In the rare gas sequence Ne–Xe the spin–orbit interaction is an increasingly large fraction of the term value and must be taken into account. Unpublished work by the author shows that when relativistic terms are included in the Hamiltonian a term from the electron–proton Breit operator (Breit 1930, 1932) combines with the spin–orbit interaction to make its effect on the isotope shift generally negligible. In Xe, where the spin–orbit interaction is large, the effect is just negligible at the accuracy obtained experimentally.

Isotope shifts in the rare gas sequence Ne–Xe have been measured by various observers (Nagaoka and Mishima 1930, 1934, Ritschl and Schober 1937, Kopfermann and Krüger 1937, Meyer 1953, Rasmussen and Middelboe 1955, Koch and Rasmussen 1950). The only calculations which have been made are those of Bartlett and Gibbons (1933) for Ne, under the assumption of LS coupling. Even in Ne the degree of intermediate coupling turns out to have an appreciable effect on the isotope shift and the effect is larger in the other rare gases, which progressively approach the jj coupling limit. In § 3 the influence of intermediate coupling on the specific shift is determined for the relevant configuration, p^5s, by applying a general procedure derived in § 2. The nuclear field shift is shown to be independent of the coupling. The linear relation obtained in this way is applied to Ne, A, Kr, Xe in §§ 4–7 respectively, with general qualitative agreement.

Because of the smallness of the residual shifts in the $1s_3$, $1s_4$, $1s_5$ states of A and Kr when the normal shifts are subtracted the observers did not feel justified in attributing any specific shifts to those states, having assumed the nuclear field shifts to be negligible (Kopfermann and Krüger 1937, Meyer, 1935, Rasmussen and Middelboe 1955). They also introduced uncertainties by estimating term shifts from the measured line shifts. In the present work the observed line shifts

are compared directly with the theory and without the use of term shifts as intermediate quantities. The smallness of certain residual shifts is given a natural explanation.

The Paschen and spectroscopic notations for levels are both employed. Isotope shifts are expressed in units of $10^{-3}\,\mathrm{cm}^{-1}$ (millikaysers, mK).

§ 2. Connection between Specific Shifts and the Coulomb Interaction

The specific mass effect comes from the term

$$(1/M)\sum_{k>l}\mathbf{p}_k\cdot\mathbf{p}_l \qquad \ldots\ldots(1)$$

in the electronic Hamiltonian, where M is the nuclear mass and the summation is over pairs of electrons (Hughes and Eckart 1930). It is customary to treat the specific effect in configuration space, but in momentum space the operator (1) is analogous to the second term in the expansion of the Coulomb interaction of the electrons:

$$\sum_{k>l}\frac{e^2}{r_{kl}}=\sum_{k>l}\frac{e^2}{r_>}+\sum_{k>l}\frac{e^2}{r_>^3}\,\mathbf{r}_k\cdot\mathbf{r}_l+\ldots.$$

This analogy yields a connection between the energies of the specific effect and the Coulomb interaction.

Since the one-electron wave functions in the central field approximation have the same angular dependence in momentum space as in configuration space (Duncanson and Coulson 1948), the specific effect may be included by the substitution

$$R^1(ab,cd)\to R^1(ab,cd)+(m/M)P(ab,cd),$$

where $R^1(ab,cd)$ is a generalized Slater integral (Condon and Shortley 1935, 8^6) and

$$mP(ab,cd)=\int_0^\infty P_aP_cp^3\,dp\int_0^\infty P_bP_dp^3\,dp,$$

P_a being the radial part of the one-electron wave function in momentum space with quantum numbers a.

Within a configuration the only change is

$$G^1(a,b)\to G^1(a,b)+(m/M)P(a,b), \qquad \ldots\ldots(2)$$

$G^1(a,b)$ being the Slater integral $R^1(ab,ba)$ and

$$P(a,b)=P(b,a)\equiv P(ab,ba)>0.$$

Comparison with the result given by Condon and Shortley (1935, 9^6) for a closed shell shows that the contribution to the diagonal matrix element of the operator (1) from a closed shell $\{n'l'\}$ and any nl electron is

$$-\tfrac{1}{2}(2l'+1)C_{rl1}(m/M)P(n'l',nl).$$

For $l'=l\pm1$ the contributions are

$$\{n'l+1\}nl:\ -\frac{l+1}{2l+1}\frac{m}{M}P(n'l+1,nl), \qquad \ldots\ldots(3\,a)$$

$$\{n'l-1\}nl:\ -\frac{l}{2l+1}\frac{m}{M}P(n'l-1,nl). \qquad \ldots\ldots(3\,b)$$

Matrix elements found by Bartlett and Gibbons (1933) show that $P(nl, n'l-1)$ is given in terms of the radial parts of the one-electron wave functions in configuration space by

$$mP(nl, n'l-1)=\left[\int_0^\infty r^2 R_{nl}\left(\frac{d}{dr}-\frac{l-1}{r}\right)R_{n'l-1}\,dr\right]^2.$$

The quantity G_1 (Condon and Shortley 1935, 8^6) is related to G^1 by

$$G'(nl, n'l-1)=(2l+1)(2l-1)G_1(nl, n'l-1).$$

In terms of G_1 the substitution (2) becomes

$$G_1(nl, n'l-1)\to G_1(nl, n'l-1) + (m/M)P(nl, n'l-1)/[(2l+1)(2l-1)]. \quad \ldots\ldots(4)$$

§ 3. Intermediate Coupling in the Rare Gases

In this section a general formula is derived for the isotope shifts of the lines p^5p-p^5s in the rare gases. The variation of energy within the configuration np^5n_1s is given by

$$\left.\begin{aligned} {}^1P_1'\colon\ s_2 \\ {}^3P_1'\colon\ s_4 \end{aligned}\right\} = \pm[(G_1-\tfrac{1}{4}\zeta)^2+\tfrac{1}{2}\zeta^2]^{1/2}+\tfrac{1}{4}\zeta,$$
$$\left.\begin{aligned} {}^3P_0\colon\ s_3 &= -G_1+\zeta, \\ {}^3P_2\colon\ s_5 &= -G_1-\tfrac{1}{2}\zeta, \end{aligned}\right\} \quad \ldots\ldots(5)$$

(Condon and Shortley 1935, 5^{13}). The substitution (4) with $l=1$ gives the variation of the specific shift, to which must be added the constant part $-\frac{2}{3}(m/M)P(np, n_1s)$ found by the diagonal sum rule in LS coupling. The other contributions to the specific shift come from closed shells and are found from (3).

The nuclear field effect on the n_1s electron gives an energy shift

$$V=C(\pi a_0^3/Z)|\psi(0)|^2,$$

where C is the isotope constant for the two isotopes concerned (Brix and Kopfermann 1949). In general, C is different for each pair of isotopes. The n_1s electron density at the origin, $|\psi(0)|^2$, is the same for each level of the configuration after averaging over M_J. Thus the nuclear field shift V is the same for each level.

If the observed shift is given in the same direction as the normal shift and $\delta(m/M)$ and V are positive, the final result for the shift of a line $np^5n_2p-np^5n_1s$ is that the residual shift $\Delta\nu$ (i.e. the observed shift minus the normal shift) is given by

$$\left.\begin{aligned} \Delta\nu &= A-BX, \\ A &= A_1+A_2-V, \\ A_1 &= \delta\frac{m}{M}\left[\tfrac{1}{3}\sum_{n'}P'(n_2p, n's)-\sum_{n'}P(n'p, n_1s)\right], \\ A_2 &= \frac{5}{3}\delta\frac{m}{M}\sum_{n'}[P'(np, n's)-P(np, n's)] \\ &\quad +2\delta\frac{m}{M}\sum_{n', n''}[P'(n'p, n''s)-P(n'p, n''s)], \end{aligned}\right\} \quad \ldots\ldots(6)$$

where the summation is over closed shells and the integrals P' refer to the n_2p state;

$$B=\delta(m/M)P(n\mathrm{p},n_1\mathrm{s}),$$
$$X=1 \text{ for } \mathrm{s}_3,\ \mathrm{s}_5,$$
$$=\tfrac{2}{3}\mp\tfrac{1}{3}x(x^2+\tfrac{1}{2})^{-1/2} \text{ for } \begin{cases}\mathrm{s}_2,\\ \mathrm{s}_4\end{cases}$$

where $x=G_1/\zeta-\frac{1}{4}$.

For any given pair of isotopes, B is determined when P is known. The values of B used in the calculations may be found from the values of $P(n\mathrm{p},n_1\mathrm{s})$ given in table 2. For the states considered in this paper the value of n runs from 2–5 for Ne–Xe and $n_1=n+1$.

The factor X may be expressed in other ways. If $T_2,\ldots$ represent the term values of $\mathrm{p}^5\mathrm{s}$,

$$x(x^2+\tfrac{1}{2})^{-1/2}=[\tfrac{2}{3}(2T_3+T_5)-(T_4+T_2)]/(T_4-T_2),$$
$$=\left[1-\frac{8}{9}\left(\frac{T_5-T_3}{T_4-T_2}\right)^2\right]^{1/2}.$$

The sign of the square root is the same as the sign of the first expression. A comparison of the two values gives a measure of the relative accuracy with which the measured term intervals fit the theoretical formulae (5). For a state given by

$$\psi=a\psi(^1\mathrm{P}_1)+b\psi(^3\mathrm{P}_1),$$
$$X=\tfrac{1}{3}(b^2-a^2+2).$$

The values of X in LS coupling are s_3, s_4, s_5: 1; s_2: $\frac{1}{3}$ and in jj coupling, s_3, s_5: 1; s_2: 7/9; s_4: 5/9. The values of X for Ne, A, Kr, Xe are given in table 1.

If primed quantities refer to a second pair of isotopes,

$$A\delta'\frac{m}{M}-A'\delta\frac{m}{M}=V'\delta\frac{m}{M}-V\delta'\frac{m}{M}. \qquad \ldots\ldots(7)$$

Table 1. Values of X

State	Ne	A	Kr	Xe
$1\mathrm{s}_2$	0·380	0·469	0·68	0·71
$1\mathrm{s}_4$	0·953	0·865	0·65	0·63

The experimental values of $\Delta\nu$ given in tables 3–6 have been averaged over the initial p states.

§ 4. Neon

Isotope shifts of the lines 1s–2p of Ne were measured by Nagaoka and Mishima (1930, 1934). Bartlett and Gibbons (1933) calculated the specific shifts on the assumption of LS coupling using orthogonalized Hartree functions without exchange. Treanor (1954) has remarked that the calculated shifts are all too small by about 30 mK.

Bartlett and Gibbons assumed that $P(1\mathrm{s},2\mathrm{p})$, $P(2\mathrm{s},2\mathrm{p})$ do not change on going from $2\mathrm{p}^5 3\mathrm{p}$ to $2\mathrm{p}^5 3\mathrm{s}$. Their calculations correspond to $A_1=13{\cdot}6$ mK, $A_2=0$, $B=29{\cdot}3$ mK. V is negligible in Ne. The residual shifts calculated by equation (6) with the same value of B and $A=44{\cdot}7$ mK are given in the third column of table 3 (parameters are given in table 2). The experimental shifts

in the second column of table 3 were obtained from the final values of Nagaoka and Mishima (1934), taking into account the additional shifts given by Ritschl and Schober (1937). The calculated and experimental residual shifts in table 3 agree to within 0·3 mK.

Table 2. Values of Parameters

Element	Isotope pair	$P(np, n_1s)$ (cm^{-1})	$A(2p)$ (mK)	$A(3p)$ (mK)
Ne	20–22	11750	44·7	
A	36–38	19450	14·0	13·5
	36–40		26·6	25·6
Kr	82–84	24900	4·60	4·24
	84–86	25700	4·65	4·34
Xe	132–134	38700	−0·6	
	134–136		−2·1	

Table 3. Residual Shifts $\Delta\nu$ in Ne (mK)

Lines	Expt	Calc
$1s_2$–2p	33·7 ± 3·0	33·6
$1s_4$–2p	16·5 ± 3·0	16·8
$1s_3$–2p	15·5 ± 3·0	15·4
$1s_5$–2p	15·6 ± 3·0	15·4

Bartlett and Gibbons' value of B agrees with experiment. Their value of A is too small by 31 mK. A_1 depends only on $P'(3p, 1s) + P'(3p, 2s)$ and A_2 depends only on the change in $P(2p, 1s) + P(2p, 2s)$ on going from $2p^5 3p$ to $2p^5 3s$. Inclusion of exchange for the $2p^3 3p$, $2p^3 3s$ states of O I (Nicklas and Treanor 1958) gave a 10% increase in the value of $P'(3p, 1s) + P'(3p, 2s)$ over the value without exchange and the change in $P(2p, 1s) + P(2p, 2s)$ for the two configurations was of the same order of magnitude as the other contributions to the specific shift. Since the configurations in Ne are similar to those of O I the calculated value of A for Ne may be expected to improve with the use of more accurate wave functions.

§ 5. Argon

Isotope shifts of some 1s − 2p, 1s − 3p lines of A were measured by Kopfermann and Krüger (1937) and by Meyer (1953). Meyer also measured some individual lines belonging to other series.

The $^{36}A - ^{38}A$ shifts obey equation (6) to within 0·3 mK with the parameter values of table 2, as illustrated by figure 1 for the 1s − 2p lines. The calculated and experimental residual shifts are given in table 4. The ^{36}A–^{40}A shifts in table 4 were calculated with the same value of $P(3p, 4s)$ as before and values of $A(2p)$, $A(3p)$ derived from the previous values by means of equation (7) on the assumption that the nuclear field shifts are zero. These parameters are given in table 2. The experimental residual shifts obey equation (6) within the limits of experimental error; the divergence for $1s_4$–3p may be accounted for by the fact that only one line shift was measured. Thus all the shifts are fitted with three parameters.

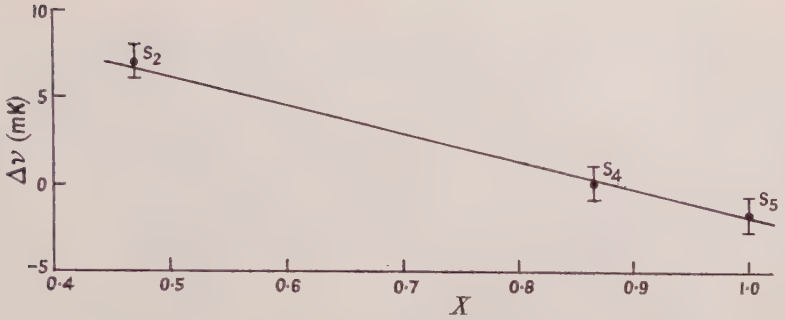

Figure 1. Residual shifts $\Delta\nu$ of 1s–2p for ^{36}A–^{38}A.

Table 4. Residual Shifts $\Delta\nu$ in A (mK)

Lines	36–38 Expt (M)	36–38 Calc	36–40 Expt (M)	36–40 Expt (K)	36–40 Calc
$1s_2$–2p	7·0 ± 1·0	6·7	13·0 ± 1·5	13·2 ± 2·0	12·7
$1s_4$–2p	0·2 ± 1·0	0·5	−0·3 ± 1·0	1·4 ± 1·5	1·0
$1s_5$–2p	−1·5 ± 1·0	−1·6	−3·6 ± 1·0		−3·0
$1s_3$–3p	6·0 ± 1·0	6·2	12·7 ± 1·5	13·2 ± 4·5	11·7
$1s_4$–3p	−0·1 ± 1·0	0	2·1 ± 1·5		0
$1s_3$–3p				−2 ± 3	−4·0
$1s_5$–3p	−1·8 ± 1·0	−2·1	−4·2 ± 1·5		−4·0

M = Meyer (1953), K = Kopfermann and Krüger (1937).

§ 6. Krypton

Rasmussen and Middelboe (1955) measured isotope shifts of the lines 1s – 2p, 1s – 3p with separated Kr isotopes. No difference was found between the ^{82}Kr–^{84}Kr and ^{84}Kr–^{86}Kr shifts.

The degree of intermediate coupling in Kr 1s is such that x is just negative when the term intervals are given as closely as possible by equations (5). Thus the $1s_2$ shifts should be just less than the $1s_4$ shifts, whereas the reverse was found experimentally although the linear relation (6) is still obeyed at the limits of experimental error (see figure 2 for the 1s – 2p shifts for ^{82}Kr – ^{84}Kr). Deviations from equations (5) can arise from spin–spin, spin–other orbit and other small interactions as well as from perturbations. A more comprehensive theory would modify the theoretical form of X and alter its values.

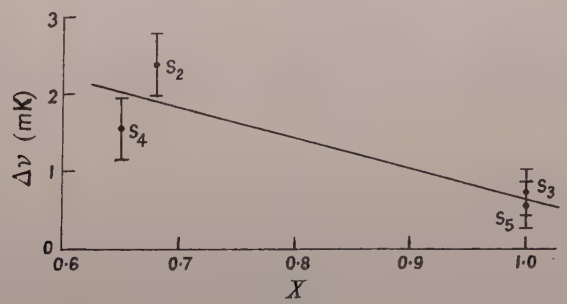

Figure 2. Residual shifts $\Delta\nu$ of 1s–2p for ^{82}Kr–^{84}Kr.

With the parameters given in table 2 the calculated and experimental residual shifts agree at the limits of experimental error, as shown in table 5. The shifts of the two pairs of isotopes determine two slightly different values for $P(4p, 5s)$. The values of A are not determined sufficiently accurately by the experiments to make the left-hand side of equation (7) significantly different from zero. Consequently the experiments do not reveal a nuclear field shift in Kr.

Table 5. Residual shifts $\Delta\nu$ in Kr (mK)

	82–84		84–86	
Lines	Expt	Calc	Expt	Calc
$1s_4$–2p	$1{\cdot}56 \pm 0{\cdot}4$	2·02	$1{\cdot}64 \pm 0{\cdot}4$	2·11
$1s_2$–2p	$2{\cdot}37 \pm 0{\cdot}4$	1·90	$2{\cdot}47 \pm 0{\cdot}4$	1·99
$1s_3$–2p	$0{\cdot}70 \pm 0{\cdot}3$	0·64	$0{\cdot}80 \pm 0{\cdot}3$	0·74
$1s_5$–2p	$0{\cdot}57 \pm 0{\cdot}3$	0·64	$0{\cdot}68 \pm 0{\cdot}3$	0·74
$1s_4$–3p	$1{\cdot}27 \pm 0{\cdot}5$	1·66	$1{\cdot}42 \pm 0{\cdot}5$	1·80
$1s_5$–3p	$0{\cdot}67 \pm 0{\cdot}4$	0·28	$0{\cdot}80 \pm 0{\cdot}4$	0·43

§ 7. Xenon

Isotope shifts of three Xe lines 1s – 2p were measured by Koch and Rasmussen (1950) for ^{132}Xe–^{134}Xe and ^{134}Xe–^{136}Xe.

The spin–spin and other small interactions may be expected to be important in Xe and perturbations are also present (Bohr, Koch and Rasmussen 1952). Thus equation (6) may not be completely adequate but there are not sufficient experimental values to test this.

Table 6. Residual Shifts $\Delta\nu$ in Xe (mK)

	132–134		134–136	
Lines	Expt	Calc	Expt	Calc
$1s_5$–2p	−3·2	−3·0	−4·2	−4·4
$1s_4$–2p	−1·9	−2·1	−3·8	−3·6

The nuclear field effect predominates but the experimental shifts indicate that the specific mass effect is appreciable. The calculated and experimental residual shifts given in table 6 agree to within 0·2 mK. The parameters used in the calculations are given in table 2. The value of $P(5p, 6s)$ is in good agreement with the slow increase in the value of the corresponding P integrals given in table 2 for Ne–Kr.

For Ne, A, Kr the parameter A may be taken to be equal to $A_1 + A_2$. The gradual decrease in the value of $A(2p)$ from Ne to Kr for a difference of two neutrons, shown in table 2, indicates that the value of $A_1 + A_2$ required in Xe may be 1–2 mK. According to the definition of A (equation (6)) the nuclear field shifts V would then be about 2–3 mK for ^{132}Xe–^{134}Xe and about 3–4 mK for ^{134}Xe–^{136}Xe.

§ 8. Conclusions

Isotope shifts in the rare gases Ne–Xe can be understood on the basis of intermediate coupling. Most of the integrals have not been calculated directly so that the agreement is qualitative. In Ne the value of A calculated by Bartlett and Gibbons (1933) is 31 mK too small.

The nuclear field effect is negligible in Ne and A and small in Kr. In Xe accurate values for the field effect cannot be obtained without accurately calculated values of A_1+A_2 and experimental results for several lines.

The calculations for Xe may have to take account of small terms such as the spin-spin interaction and also perturbations by neighbouring states. Similar difficulties may arise in Kr.

The effect of intermediate coupling on specific shifts in other elements should be considered. Even if the deviation from *LS* or *jj* coupling be small the effect should at least be estimated.

References

Bartlett, J. H., and Gibbons, J. J., 1933, *Phys. Rev.*, **44,** 538.
Bohr, A., Koch, J., and Rasmussen, E., 1952, *Ark. Fys.*, **4,** 455.
Breit, G., 1930, *Phys. Rev.*, **36,** 383.
—— 1932, *Ibid.*, **39,** 616.
Brix, P., and Kopfermann, H., 1949, *Z. Phys.*, **126,** 344.
Condon, E. U., and Shortley, G. H., 1935, *The Theory of Atomic Spectra* (Cambridge: University Press).
Duncanson, W. E., and Coulson, C. A., 1948, *Proc. Phys. Soc.*, **60,** 175.
Hughes, D. S., and Eckart, C., 1930, *Phys. Rev.*, **36,** 694.
Koch, J., and Rasmussen, E., 1950, *Phys. Rev.*, **77,** 722.
Kopfermann, H., and Krüger, H., 1937, *Z. Phys.*, **105,** 389.
Meyer, H., 1953, *Helv. Phys. Acta*, **26,** 811.
Nagaoka, H., and Mishima, T., 1930, *Sci. Pap. Inst. Phys. Chem. Res., Tokyo,* **13,** 293.
—— 1934, *Ibid.*, **25,** 223.
Nicklas, J. P., and Treanor, C. E., 1958, *Phys. Rev.*, **110,** 370.
Rasmussen, E., and Middelboe, V., 1955, *K. Danske Vidensk. Selsk. mat.-fys. Medd.*, **30,** no. 13.
Reiner, A. S., 1955, *Physica*, **21,** 783.
Ritschl, R., and Schober, H., 1937, *Phys. Z.*, **38,** 6.
Treanor, C. E., 1954, *Phys. Rev.*, **95,** 1472.

On the Asymptotic Behaviour of the Mayer Cluster Series in the Antiferromagnetic Problem

By H. N. V. TEMPERLEY
Atomic Weapons Research Establishment, Aldermaston, Berks.

MS. received 6th April 1959

Abstract. In continuation of the work of a former paper, it is shown that the Mayer series for the antiferromagnetic problem can be related in various ways to the placing of *links* on the lattice. The two such transformations found in the former paper are shown to be special cases of a general theory, which can also be used to relate many other problems of physical interest with the Onsager–Ising problem. The Mayer series is analysed into sub-series, the behaviour of some of which can be determined from known results on the 'link' problem, while that of others can, in principle, be obtained from the general transformation theory just mentioned. The conclusion of the former paper, that the Mayer z-series has a positive singularity determining the transition but a negative singularity nearer the origin determining its radius of convergence, is confirmed, as are most of the conclusions from the earlier work. The results appear to be reliable in the interesting region near $T=0$ but break down as we approach $H=0$ on the transition curve.

§ 1. Introduction

In a previous paper (Temperley 1959, to be referred to as I) we have examined the application of the Onsager–Ising antiferromagnetic model to the problem of solidification of a gas with purely repulsive interactions. It was shown that the Onsager–Ising problem of disposing *points* on the lattice could be related to certain problems of disposing *links* on the same lattice and that this could always be done in at least two distinct ways. We shall now show that there exists a continuous range of such transformations. This fact not only helps us to draw definite conclusions about the asymptotic behaviour of the Mayer cluster sums in the antiferromagnetic problem, but also enables us to relate the solutions of a large number of other problems of physical interest (e.g. the packing of linear and branched polymers on a lattice, cross-linking, gel formation, etc.) to that of the Ising model. (The numerical properties of the latter are obtainable from series expansions except in the neighbourhood of the transition regions.)

Apart altogether from this transformation, information quite independent of the Ising model is available about the 'link' problem (e.g. Hammersley and Broadbent 1957, Temperley 1958). This problem is of considerable physical interest in its own right, for instance in circuit and switching theory, imperfect conductors, flow in porous media, etc. In this paper we shall show that information about it can be made to throw light on the asymptotic behaviour of the Mayer cluster sums in the antiferromagnetic (solidification) problem. These

two quite distinct approaches point to the same conclusion, namely that the asymptotic behaviour of the Mayer b_l's is of the form

$$A(-B)^l + CD^l \qquad \ldots\ldots (1)$$

where A, B, C, D are slowly varying functions of l and $B > D$. In other words, the nearest singularity of the z-series is on the negative real axis. In I we concluded that this was reasonable but that the transition to the antiferromagnetic (ordered) state seemed to call for a singularity on the positive real axis also. We shall now indicate how the Mayer z-series can be analysed into sub-series and shall bring forward evidence that at least some of these do behave in the way suggested by (1). (There are also complex singularities in the antiferromagnetic case. Their existence in the ferromagnetic case is of course well known from the work of Yang and Lee (1952). Expression (1) is to be understood to mean that the behaviour of the terms is dominated by the negative singularity.)

§ 2. An Application of the 'Decoration' Transformation

This transformation is applicable to any lattice, but the results rapidly become less useful as the order of the nodes of the lattice increases. Accordingly, we consider here the plane honeycomb lattice. The 'decoration' process consists of introducing extra nodes on the mid-points of the links (figure 1). A generalization of this process, with useful applications, had been given by Fisher (to be published). The nodes on the hexagon sides are numbered, while those on the hexagon corners are lettered. Each lettered magnet interacts with three neighbouring numbered magnets, while each numbered magnet interacts with its two lettered neighbours. We can write down an expression for the partition function for the decorated lattice in a magnetic field

$$\sum_{\substack{\mu_A = \pm 1 \\ \mu_1}} \exp\left(D_1 \sum \mu_A + D_2 \sum \mu_A \mu_1 + D_3 \sum \mu_1\right) \qquad \ldots\ldots (2)$$

where D_2 describes the interaction, and D_1 and D_3 are proportional to the magnetic moments of the lettered and numbered magnets respectively. Plainly if there

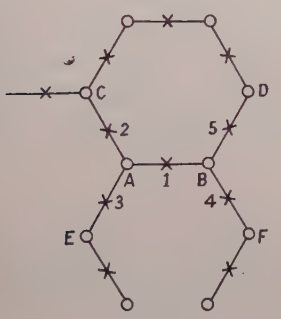

Figure 1. Portion of the decorated honeycomb lattice.

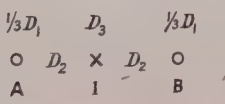

Figure 2. Portion of the decorated lattice appropriate for summation over μ_1.

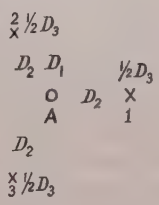

Figure 3. Portion of the decorated lattice appropiate for summation over μ_A.

are L hexagon corners there are $3L/2$ sides and $3L$ interactions. We first carry out the summations called for by (2) with respect to the numbered μ's, figure 2

showing the portion of the lattice appropriate to one such magnet. Thus we have to evaluate

$$\sum_{\mu_1=\pm 1} \exp\left[\tfrac{1}{3}D_1(\mu_A+\mu_B)+D_2(\mu_A\mu_1+\mu_B\mu_1)+D_3\mu_1\right]$$

which is equivalent to $P\exp\left[\tfrac{1}{3}H_1(\mu_A+\mu_B)+H_2\mu_A\mu_B\right]$ .....(3)

where $$\exp(4H_1)=\exp(4D_1)\frac{\cosh^3(2D_2+D_3)}{\cosh^3(2D_2-D_3)} \quad .....(4)$$

$$\exp(4H_2)=1+\frac{\sinh^2 2D_2}{\cosh^2 D_3} \quad .....(5)$$

$$16P^4=\cosh^2 D_3\cosh(2D_2+D_3)\cosh(2D_2-D_3). \quad .....(6)$$

We can also sum first over the lettered magnets. As is well known, the numbered magnets by themselves form the 'basket' or Kagomé lattice, and Naya (1954) showed that, if we put $D_1=0$, this 'star-triangle' summation enables us to relate the partition functions of the hexagonal and Kagomé lattices with magnetic field. The appropriate portion of the lattice is shown in figure 3. We have to evaluate

$$\sum_{\mu_A=\pm 1} \exp\left[\tfrac{1}{2}D_3(\mu_1+\mu_2+\mu_3)+D_2(\mu_1\mu_A+\mu_2\mu_A+\mu_3\mu_A)+D_1\mu_A\right] \quad .....(7)$$

At first sight, our more general case does not seem to lead to anything very useful, since it involves the unphysical interaction between three magnets at a time (through the product $\mu_1\mu_2\mu_3$). However, instead of comparing (7) with the Kagomé lattice, we compare it with the expression

$$\begin{aligned}&\tfrac{1}{8}x_0(1-\mu_1)(1-\mu_2)(1-\mu_3)\\&\quad+\tfrac{1}{8}x_1[(1-\mu_1)(1-\mu_2)(1+\mu_3)+(1-\mu_1)(1+\mu_2)(1-\mu_3)\\&\quad+(1+\mu_1)(1-\mu_2)(1-\mu_3)]\\&+\tfrac{1}{8}x_2[(1-\mu_1)(1+\mu_2)(1+\mu_3)+\text{two similar expressions}]\\&\quad+\tfrac{1}{8}x_3(1+\mu_1)(1+\mu_2)(1+\mu_3)\end{aligned} \quad .....(8)$$

expression (8) being equal to x_0 when all three magnets are negative, to x_1 when exactly one of the three is positive, and so on. Since each numbered magnet corresponds to just one *link* on the non-decorated honeycomb lattice, the product of $3L/2$ factors of type (8) enumerates all the ways of disposing links on this lattice, each term corresponding to one such arrangement, the index of x_0 *counting the number of nodes* that are not intersected by any link, that of x_1 the number intersected by exactly one link, and so on. Only the ratios of the x's are of interest, and (7) contains three disposable parameters, so that a very wide range of problems concerned with the disposition of links on a lattice can be reduced to the corresponding Ising problem with the help of expressions (3) to (8). We find

$$\begin{aligned}x_0:x_1:x_2:x_3::&\cosh(D_1-3D_2)\exp(-\tfrac{3}{2}D_3):\cosh(D_1-D_2)\exp(-\tfrac{1}{2}D_3):\\&\cosh(D_1+D_2)\exp(\tfrac{1}{2}D_3):\cosh(D_1+3D_2)\exp(\tfrac{3}{2}D_3)\end{aligned} \quad .....(9)$$

which can readily be solved for the D's and H's in terms of the x's. The following simple relation for H_2 should be noted:

$$\exp(4H_2)=\frac{(x_0x_3-x_1x_2)^2-4(x_1x_3-x_2^2)(x_0x_2-x_1^2)}{(x_0x_2+x_1x_3-x_1^2-x_2^2)^2}+1. \quad .....(10)$$

The general expression for H_1 seems to be very complicated and no compact expression in terms of the x's has been found, though simple ones exist in particular cases. The two ways of connecting the 'points' and 'links' problems found in I correspond to the following particular choices of the x's:

$$x_0 : x_1 : x_2 : x_3 : : 1 : f^{1/2}w : fw : f^{3/2}w \quad \ldots\ldots (11)$$

$$x_0 : x_1 : x_2 : x_3 : : 1 : s^{1/2}t : s : s^{3/2}t \quad \ldots\ldots (12)$$

where $1+f=\exp(4H_2)$, $w=z/(1+z)$, $s=\tanh H_2$, $t=\tanh H_1$; z is Mayer's variable, which, for the honeycomb lattice, takes the value $z=\exp(-2H_1-6H_2)$. It can be verified without difficulty that (11) and (12) are special cases of the above general theory. The generating function obtained from factors of type (8) can be evaluated, in terms of the Onsager–Ising partition function, for any assigned values of the ratios of the x's, as can its differential coefficients. This, by the ordinary formalism of statistical mechanics and the use of the method of steepest descents, enables us to determine the number of arrangements of links on the lattices corresponding to specified numbers of the four types of node. As examples of particular cases of physical interest, we may mention the following:

$x_3=0$. This implies that at most two links go through any lattice point. In other words, we have the problem of packing flexible linear chains on to the lattice, the mean length of the chains being fixed by the relative values of x_1 and x_2, while the total number of unoccupied nodes depends on the ratios of these quantities to x_0. Thus, we have a model describing linear polymers on a lattice or in solution. By letting x_3 increase gradually from zero we can study such problems as cross-linking and gelation.

x_2 and x_3 small compared with x_1. This describes the solution of 'dimers' (molecules occupying two lattice sites) which repel one another, but sharing of one site is not absolutely prohibited.

x_1 and x_2 small compared with x_3. This describes the formation of domains of a given average area fixed by the ratio of x_3 to x_1 and x_2, their density on the lattice depending on the ratio of x_3 to x_0. This problem is of direct interest in studying the antiferromagnetic problem and has, moreover, a bearing on the more general 'rigid molecule' problem. We recall that the rigid molecule problem with continuous coordinates is the limiting case of the corresponding 'lattice' problem when each molecule 'covers' a very large number of points on the lattice. Discussion of the other problems is deferred, as their application to the antiferromagnetic problem is less direct.

§ 3. The Early Terms of the Mayer Series

Returning to the plane square lattice, we find from I, table 2, that this series can be written as follows, in terms of f, the Mayer function, and $w=z/(1+z)$

$$\begin{aligned}\sum b_l z^l = \log(1+z) &+ 2fw^2 - 7f^2w^4 + \frac{116}{3}f^3w^6 - \frac{521}{2}f^4w^8 \\ &+ 6f^2w^3 - 406f^4w^6 + \ldots. \\ &+ 22f^3w^4 - 14545f^6w^8 + \ldots. \\ &- 60f^3w^5 \\ &+ f^4w^4 + (3649/2)f^8w^8 + \ldots.\end{aligned} \quad \ldots\ldots (13)$$

where we have grouped together terms involving f and w in the same ratios of powers. Study of these ratios at once tells us the type of networks of links that

must be involved. Thus, fw^2 can only describe one link connecting two nodes, and the higher powers should correspond to such 'dimers' overlapping at one or both sites (figure 4). In other words, we expect the top line of expression (13) to be the cluster series for the 'dimer' problem, two dimers being prohibited from sharing a site. (This has been confirmed by taking the Lth power of the exponential and verifying that it does, in fact, enumerate arrangements of non-overlapping dimers.) Similarly, we can interpret a term like f^2w^3 as describing

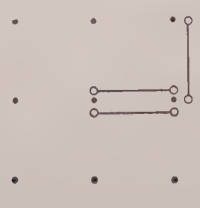

Figure 4. One contribution to the term in f^3w^6. Overlap of 'dimers'.

Figure 5. One contribution to the term in f^3w^5. Overlap of a 'dimer' and a 'trimer'.

networks of two links connecting three points and we expect the cluster series to contain higher powers of this variable, corresponding to the 'subtracting out' of overlapping configurations of such networks. We also expect to find in (13) cross terms that prevent the overlap of different types of network. The first such term is $-60f^3w^5$, which cannot correspond to any single network (since we cannot connect five points with only three links) and is interpreted as arising from the overlapping of a 'dimer' (factor fw^2) and a 'trimer' (factor f^2w^3) (figure 5). (By Lemma 2 of I it does not matter whether they have one or two sites in common: a factor -1 appears in either case.)

We are thus led to compare the cluster series expressed in terms of f and w with the results we would expect if we distributed on the lattice, without overlap, networks of a fixed average size. Inspection of the available terms in table 2 of I suggests that the series is, in fact, dominated by terms in which the indices of f and w are nearly equal, but this gives us no real indication of the size of the most 'important' networks (and this size may itself vary with f and w). We therefore try to estimate the contribution of networks of various sizes. In the first instance we distinguish between networks involving only a few lattice sites, where the singularities in the corresponding cluster sub-series arise because these networks are prevented from overlapping, and networks containing numbers of sites comparable with L, for which singularities also arise because of the large number of ways in which one such network can be made up. We first discuss very small networks, which lead to problems very similar to the 'rigid molecule' one from which we started. For networks of intermediate size the transformation theory of the last section is applicable while, for the very large networks, we may use various results concerned with a single connected domain (Hammersley and Broadbent 1957, Temperley 1956, 1958).

A. *The dimer and trimer problems.*

We have seen that the top line of expression (13) represents the beginning of a series describing the placing of single *links* on the lattice in such a way as to have no sites in common. Each link has a site in common with six others, so placing one on the lattice excludes the possibility of any of these six being also present

This is therefore a problem of the same type as our original problem, in which one molecule is placed on a lattice point and 'covers' its four nearest neighbours. We may therefore expect it to lead to a cluster series of the same type as did the original problem in the limiting case of $f=-1$. Analysis of the known terms of the original series from the ratio b_l/b_{l-1} and extrapolating to infinity leads to a radius of convergence of about 0·13 and we find similar figures if we write down the partition functions of small assemblies containing up to 4×4 lattice points. For the dimer problem we expect a somewhat shorter radius of convergence because of the larger number of 'neighbours', that is, the main singularity should occur at about $Z=-0{\cdot}1$, where Z is the selector variable for the dimer problem. In the present application Z is replaced by fw^2 and this means that for $f=-1$ we expect singularities at $w=\pm 0{\cdot}3$ approx. In other words, the dimer terms in (13) by themselves imply the postulated behaviour of the z series—a dominant negative singularity, together with a positive one somewhat further away. If, as seems almost certain, the dimer series also has complex singularities, they exist in the original problem also. The discussion for trimers is very similar. If the cluster series behaves in the same way and has a dominant negative singularity, and subsidiary positive and complex singularities, then so has the original series. (The difference arises because the trimer terms in (13) involve f^2 rather than f.)

B. *Networks of moderate size.*

We have already pointed out above that the general transformation theory given in the last section should be applicable. We illustrate the possibilities from the plane honeycomb lattice. (Discussion of the plane square lattice by this method is more difficult, since we cannot vary the x variables all independently and thus meet with complications in applying the process of steepest descents.) Inspection of (10) shows that the transformation always leads to a real value of H_2 for real values of the x's, which is an advantage, since this case is much better understood than is the imaginary or complex one. It is known from the work of Yang and Lee (1952) that a singularity in the ferromagnetic partition function itself occurs only for $H_1=0$ and $\sinh^2 2H_2>3$, but singularities also occur if, for example, the denominator of (10) vanishes. Calculations have been made in a few representative cases for the hexagonal lattice, for example $x_0=x_1=x_2=x_3$ leads to $\bar{M}_0=\bar{M}_3=L/8$, $\bar{M}_1=\bar{M}_3=3L/8$, which corresponds to a term $\simeq 2^{3L/2}w^{7L/8}f^{3L/4}$ which is not unreasonable, but a proper estimate of the radius of convergence for a definite choice of ratios of powers of w and f would be extremely lengthy, since it calls for choosing a large number of ratios of the x's, calculating the $\bar{M}$'s and then interpolating. We can, however, look at the situation slightly differently. Suppose we give, for example, x_0, x_1, x_2 fixed values and let x_3 increase steadily from zero. We always run into a singularity on the positive real axis (arising from the transformation laws between the x's and H's or from the partition function itself) which means that we can always arrive at a positive singularity if we group our terms properly. Again, a very extensive computing programme would be required to locate the positive singularity closest to the origin.

C. *Very large networks.*

We now consider the contributions to the partition function and cluster series due to very large networks. The main problem here is the number of such networks involving specified numbers of links and lattice points. The

inclusion in the cluster series of terms preventing the overlap of such networks is unlikely to change our qualitative conclusions. (It could, moreover, be handled as a particular case of the transformation theory outlined above. A large network will contain a high proportion of nodes intersected by two, three or four links. The corresponding problem in the plane hexagonal lattice occurs when x_2/x_1 and x_3/x_1 are becoming large.)

A very large network may contain nearly twice as many links as points if it is nearly rectangular and all the possible links are used. We are, however, not compelled to use all the links, it being still possible to form a connected network if N points are connected by $N-1$ links. Such networks are devoid of closed cycles and are known as 'trees'. Thus, the contribution of *large* networks to the cluster series can range from terms involving f^2w to terms involving fw. We shall now give reasons for thinking that terms of nearly the latter type will be by far the most frequent even if we consider the contribution of large networks only. The actual numbers will be further swelled by the fact that such terms can also arise from the contribution of small networks containing as few as four lattice points. Inspection of table 2 of I shows, very strikingly, the dominance of terms involving about equal powers of f and w. One might expect the maximum contribution to come from a certain size of network, but this size has not yet been located and the maximum is probably rather flat.

We now consider the enumeration of large connected networks on the plane square lattice. Various forms of this problem have been studied by Hammersley and Broadbent (1957) who conclude that, if links are distributed at random on the lattice, the probability of forming a large connected network first becomes appreciable when the number of links is about half the total of $2L$ available. This 'critical probability' has, in fact, been shown to lie between 0·5 and 0·647 (Hammersley, private communication). From this we can deduce that, at all events for this particular lattice, the most frequent types of connected network do not differ greatly from trees, the dominant terms in the generating function being of the form fw^t where t lies between 1 and 1·29. We can, therefore, hope that the enumeration of trees leads to a useful first approximation to the enumeration of connected networks in general, and this conclusion will be confirmed by the data in the Appendix.

A further simplifying circumstance is the following. If points are selected at random, subject only to the constraint that they must form a connected domain on the lattice, the most likely result is a domain where perimeter and area are numerically comparable, that is, it must be expected to be 'long and thin'.

Temperley (1956) considered the problem of enumerating domains as a function of their area or perimeter. For the former problem he found an exact enumerating generating function for all domains of a particular type:

$$G(p, q) = \frac{pq(1-q)^3}{(1-q)^4 - p(q-q^2-q^3+q^4) - p^2q^3} \qquad \ldots\ldots (14)$$

where the index of q counts the number of sites in the domain, and that of p the total numbers of rows involved. From (14) we can conclude that the number of domains containing N sites is of the order of $A \times 3{\cdot}0^N$ where A is the order of unity. A would be altered (and might become a function of N) if *all* domains could be included, but the factor 3·0 per site is unlikely to be increased significantly. By a study of (14) as a function of p it is also possible to deduce the

expected number of rows in a 'random' domain of N sites. This is estimated to be $0{\cdot}45N$, that is, the average number of sites in a row is between 2 and 3, i.e. the 'random' domain is 'long and thin'. The number of domains of a total perimeter S has been shown by Fisher (1958) to be about $(2.64)^S$ and this agrees well with the value $(2{\cdot}67)^S$ deduced from the machine computations of Wall, Hiller and Atchison (1955). Comparing the methods of enumerating domains implies that the perimeter S of a random domain is about $1{\cdot}2\,N$, which agrees well with the above conclusion that domains are long and thin if the sites are put together at random.

The enumeration of the number of trees that can be made, using all the sites in an $M \times N$ rectangle, that is the *complexity* of the rectangle of sites, can be solved analytically. From the theory given by Temperley (1958) it can be shown that, for M and N both large, the complexity is proportional to $(3{\cdot}21)^{MN}$. For very narrow rectangles the factor per site falls off, as one might expect (see Appendix). We can now estimate the number of networks that can be made from domains of various shapes, in the light of Hammersley and Broadbent's (1957) results which indicate that the most common type of network probably resembles a tree. (Apart from this the enumeration of trees certainly gives us a useful lower limit on the number of networks.) Some numerical results on particular types of domain are given in the Appendix. If we start from a 'random' domain, containing N sites, we know that it will have a mean breadth of about three lattice sites, and that there are about 3^N such domains. The figures suggest that, by omitting some of the links, each such domain can then give rise to about $1{\cdot}4^N$ different networks. We might also begin with a 'compact' domain, by which we mean one whose length and breadth are comparable. Such domains are relatively scarce. The perimeter of such a domain is of the order of $4N^{1/2}$, which implies that their number goes up only as a power of $N^{1/2}$. This means that the number of trees that correspond to compact domains is thus effectively proportional to $3{\cdot}2^N$, for this is the number of trees that can be formed from one such domain. From the Appendix we conclude that the total number of networks that can be so formed goes up with a somewhat higher power of N.

Thus we can sort out the terms in table 2 of I into categories according to the relative powers of f and w. This sorting has been carried out in expression (13). Our conclusion is that, if we confined ourselves to domains with a specified number of sites, we could expect them to contribute to the cluster sum a dominant singularity on the negative real axis of w, a subsidiary positive singularity, and complex singularities, though in particular cases, one or both of the latter can be absent. We now list these contributions:

(i) Variable w^2f. (Extreme left of table. Top line in expression (13).) This series is the solution of the 'rigid dimer' problem, and the convergence condition and positive singularity are both estimated to be given by $|w^2f| \simeq 0{\cdot}1$.

(ii) Variable wf^2. (None actually appear in the table, but would come on its extreme right.) These terms only arise from compact domains with all their links preserved. The number of such domains is always negligibly small, exactly L if N is a perfect square, and of the order of $L \times 2^{N^{1/2}}$ otherwise. The convergence condition and positive singularity are both given by $|wf^2| = 1$.

(iii) Variable near to wf. (Middle of table.) We have seen that these terms can arise in three distinct ways: (*a*) From trees and similar networks formed from

large compact domains. The number of such domains is negligible, but we have seen that, from such a domain containing N sites, about $3{\cdot}2^N$ trees can be formed. This leads to a convergence condition $|wf| \leqslant 0{\cdot}31$ but apparently not to a positive singularity. (*b*) From trees and similar networks formed from large random domains. The number of such domains is of the order of 3^N, and the number of networks that can be formed from each one is about $1{\cdot}4^N$, leading to a convergence condition $|wf| \leqslant 0{\cdot}24$. In this case the positive singularity is somewhat further out from the origin of w, at $|wf| \sim 0{\cdot}3$ say. (*c*) From the overlapping of medium sized networks. Numerical values are not yet available, but could be obtained from the transformation theory outlined above.

There is some independent evidence that the relationship $|wf^a| = c$, where a is near to unity, is correct, at all events for the portion of the transition curve near zero temperature ($f = -1$), for this assumption leads to the following equation for the transition curve

$$2\mu H = 8J - kT \log c + kT \log [(1 - e^{-4J/kT})^a - c] \qquad \ldots\ldots (15)$$

which is of exactly the type found in Ziman's (1951) approximate calculation, permitting the finite outward slope and 'bulge' in the curve near $T = 0$. There is almost certainly some cancellation of singularities as we approach the Onsager point ($H = 0$), since the known position of the singularity $w \simeq 1, f = -0{\cdot}83$ is definitely further out than any of the above criteria suggest. Such effects are familiar in conditionally convergent series, but we can still be fairly confident about the estimates of the cluster sums in the neighbourhood of $f = -1$ which is the case of greatest interest. An attempt to apply these processes to the ferromagnetic case would be completely fallacious, since considerable cancellation of the large terms in the b_l's occurs, in fact Katsura (1958) has shown that the higher cluster sums vanish very rapidly once we are a little above the Curie temperature. In any case, it is known from the work of Yang and Lee (1952) that the only singularities occur for $H = 0$, so such an investigation is superfluous.

§ 4. Conclusions

The preliminary study of the asymptotic form of the Mayer series leads to conclusions agreeing with those that result from a study of the early terms and those which were implicit in earlier work on the antiferromagnetic problem. We summarize them here:

(i) A gas with purely repulsive interactions has under compression a transition to a solid-like state with long range order, provided only that the repulsion is sufficiently 'hard'. If the repulsion is too 'soft', there is no transition. (We are not yet able to give a precise numerical criterion of 'hardness'.)

(ii) The transition point is the nearest positive singularity of the Mayer z-series and corresponds to the abrupt appearance of long-range order. (A more suitable variable than z for this expansion probably exists.)

(iii) An accompanying anomaly of some kind is possible in the virial series, but it can be extended continuously through the transition point and represents a metastable disordered state. Its singularity almost certainly marks the limit of the metastable state, rather than a second critical temperature.

(iv) The model used automatically predicts a second transition at still higher density, which corresponds to a change of crystal structure in the 'solid' region.

(v) Comparison of the present work with that of Yang and Lee (1952) suggests that condensation is a consequence of attractive forces, but that solidification is an 'excluded volume' effect which can, in principle, occur as the result of external compression alone. It therefore seems well worth examining the Ising model with attraction between second nearest neighbours and repulsion between neighbours to see if it exhibits two transitions. We reserve this for another paper.

(vi) The alternation in sign of the b_l's seems to be a characteristic property of antiferromagnetic interactions.

Acknowledgments

The author wishes to thank Professor C. Domb, Drs. M. F. Sykes and M. E. Fisher and Mr. D. M. Burley for helpful discussions and correspondence, also the Director, Atomic Weapons Research Establishment, for permission to publish this paper.

APPENDIX

Some Numerical Data on the Numbers of 'Networks' obtained from various shapes of Domain

It is possible, by a matrix method, to enumerate not only trees but all types of connected network for large domains of any given specification. Consider, as an example, the $2 \times N$ domain. Suppose, as in the Onsager–Ising problem, that we build up this domain row by row. We need only distinguish between two 'configurations' of the two points last added to the domain. They may be connected, by either a direct link or an indirect chain of links, or they may be disconnected so that the incomplete network falls into two parts. One row of the enumerating matrix corresponds to each of these two configurations. We now add the next pair of points and consider the effect of adding one or more of the three links that can be added with them. Not all ways of adding them are permissible, as some of them would leave one or both points in the lower pair isolated, so that they could never be connected into the network. A permissible selection of the links will lead to each lower point being connected to at least one upper point, and to the upper pair of points being either connected or disconnected in the sense defined above, and we distinguish between these two possibilities by the use of the two columns of our matrix. If we introduce a factor f for each of the three links and enter up all the relevant possibilities in the appropriate cell of our matrix, the result is as follows:

$$\begin{array}{c|cc} & C & D \\ C & f^3+3f^2, & 2f \\ D & f^3 \quad , & f^2 \end{array} \qquad \ldots\ldots (A1)$$

which has the following eigenvalue equation

$$\lambda^2-\lambda(f^3+4f^2)+f^5+f^4=0 \qquad \ldots\ldots (A2)$$

and the generating function for networks obtained from a domain of N rows will be given, in the usual way, by $A\lambda_l^N$ where A is a constant of the order of unity, and λ_l is the numerically largest eigenvalue of (A1).

This method is perfectly general and can be applied to domains with longer rows or with rows of unequal lengths, but the numbers of possible 'configurations'

of each row, and of permissible ways of connecting up the sites added in each row, increase extremely rapidly with the breadth of the domain. Fortunately we are interested mainly in domains of small breadth, 'long and thin', since, as we have seen above, these are the most common. (Domains that may contain up to three sites per row are, in fact, very nearly as numerous as completely 'random' ones.) For domains other than rectangular ones we are interested in the factor introduced per added *site* rather than per added row and we can readily allow for this by multiplying every matrix element in the row corresponding to a given 'configuration' by w^n, where n is the number of sites involved in that configuration. Then, if T is a matrix such as (A1), we can obtain the generating function for a domain of r rows from the matrix T^{r-1} or, if the number of rows is not of direct interest, we can sum over all r, and $(1-T)^{-1}$ will then enumerate all networks obtainable from domains of the given specification. Our problem thus reduces effectively to that of factorizing $\det(1-T)$, considered as a function of w, since the coefficient of w^N counts the networks containing N sites, and we can then reduce any element of $(1-T)^{-1}$ to the form

$$\frac{A}{w_1-w}+\frac{B}{w_2-w}+\ldots.$$

Four types of result are of particular interest:

(*a*) The total number of networks that can be made from domains of N sites. For this we put $f=1$ in a matrix such as (A1).

(*b*) The net number of networks, when we reckon negatively these containing an odd number of links, that can be made from such domains. (This corresponds to the 'rigid' case $f=-1$.)

(*c*) The number of 'trees', i.e. connected networks without cycles, that can be made from such domains. For this we omit those terms from the matrix element that lead to the formation of closed cycles (e.g. the term f^3 in the C–C cell of (A1)) afterwards putting $f=1$.

(*d*) In cases where the numerically smallest root of $\det(1-T)$ is negative, we are interested also in the smallest positive root.

We give below some data for rectangular domains and also for 'random' domains of the special type considered by Temperley (1956), for which all the sites in any one row are contiguous. The results in all cases are expressed as a *factor per site added* to the network. If this factor is negative, as always seems to be the case for $f=-1$, this implies that the corresponding type of domain leads to a contribution to the cluster sum alternating in sign with the number of sites involved. If, however, there is also a positive root of $\det(1-T)$ there are further

Data for Domains of Various Sizes

(1)		(2)	(3)	(4)	(5)
Rectangular	$2\times N$	2·1	−1·7	1·9	1
	$3\times N$	2·6	−2·1	2·3	1
	$4\times N$			2·5	1
	$N\times N$			3·2	1
Random up to 2 sites per row		3·0	−2·7 (+1·9)	2·9	2·3
up to 3 sites per row			−3·5 (+2·3)		2·9
row unrestricted					3·0

(1) Type of domain; (2) total number of networks; (3) net number of networks; (4) number of trees; (5) number of domains.

terms, smaller in numerical magnitude, but of constant sign, and these imply that the cluster series has a singularity on the positive real axis. The positive factors are given in brackets in the table and it is interesting that they seem to exist for the random domains but not the rectangular ones.

The blank spaces in the table have not yet been computed as they involve matrices of high order. The order can be reduced appreciably for the 'net number' problem while the tree problem can be solved analytically for any rectangle (Temperley 1958).

However, the results so far do confirm the validity of the assumptions made in the text, namely that even for the extreme case $f = -1$ the mutual cancellation of networks is not catastrophic, and that the number of trees gives a reasonable first approximation to the total and net numbers of networks.

References

Fisher, M. E., 1958, *Disc. Faraday Soc.*, No. 25, 200.
Hammersley, J. M., and Broadbent, S. R., 1957, *Proc. Camb. Phil. Soc.*, **53**, 629, 642.
Katsura, S., 1958, *Progr. Theor. Phys., Japan*, **20**, 192.
Mayer, J. E., and M. G., 1940, *Statistical Mechanics* (New York: Wiley).
Naya, S., 1954, *Progr. Theor. Phys., Japan*, **11**, 53.
Onsager, L., 1944, *Phys. Rev.*, **65**, 117.
Temperley, H. N. V., 1956, *Phys. Rev.*, **103**, 1.
—— 1958, *Disc. Faraday Soc.*, No. 25, 92.
—— 1959, *Proc. Phys. Soc.*, **74**, 183.
Wall, F. T., Hiller, L. A., and Atchison, W. F., 1955, *J. Chem. Phys.*, **23**, 913.
Yang, C. N., and Lee, T. D., 1952, *Phys. Rev.*, **87**, 404.
Ziman, J. M., 1951, *Proc. Phys. Soc.* A, **64**, 1108.

Can the 'Lattice' Model of a Gas describe both Liquefaction and Solidification?

By H. N. V. TEMPERLEY
Atomic Weapons Research Establishment, Aldermaston, Berks.

MS. received 11*th December* 1958, *in revised form* 14*th May* 1959

Abstract. A preliminary study is made of a two-dimensional model of an imperfect gas of 'attracting rigid squares' which is a limiting case of the two-dimensional Ising model with second-nearest neighbour interactions studied by Domb and Potts. The qualitative behaviour of the high order Mayer cluster-sums is determined by a method used by Temperley. It is found that at high temperatures these sums alternate in sign, which is what would be expected if the approaching transition were the formation of an ordered structure. As we lower the temperature, the analytic behaviour of the cluster-sums progressively changes to what was found by Yang and Lee when the approaching transition involves the formation of large domains, analogous to liquefaction.

It is tenatively concluded that this version of the Ising model may show two transitions below a certain critical temperature, just like a real imperfect gas.

§ 1. Introduction

In two previous papers Temperley (1959a, b, referred to as I and II) has considered the nearest neighbour plane square Ising model with repulsive interactions. The appearance of antiferromagnetism can, by appropriate transcriptions, also give a description of solidification under pressure, the ordering process being a preferential occupation of one of the two interlacing sublattices. Yang and Lee (1952) had previously shown that the same model with attractive interactions describes liquefaction as the analogue of the formation of large domains in a ferromagnetic. Temperley (1954) showed that the Weiss model, with long-range attractions, also gives a description of liquefaction, but that difficulties arise when we go to the limit of a large assembly. See also Katsura (1955) for a more detailed discussion of this model.

We know that real molecules exert attractive forces at long distances and repulsive forces at short distances and it has long been realized that liquefaction and solidification should be explicable on such a basis without having to introduce elaborations such as directional effects or three-body forces. An approximate treatment of a simple lattice model, leading to such a result, has been given by Morita (1957) following up some similar work by Kikuchi (1951). It is therefore of great interest to ask whether an Ising model, in which nearest neighbours repel but second nearest neighbours attract, is capable of describing both transitions. A preliminary study of this model by Domb and Potts (1951) did not envisage the possibility of two transitions ever occurring. (They were guided by the analogy with the plane triangular lattice, which is equivalent to the square lattice with interactions along one set of diagonals only and which is known to have no more

than one transition.) Apart altogether from the present application, the two models, triangular and second-nearest neighbour, do differ in several respects, which may make it dangerous to push the analogy too far: (*a*) The triangular lattice has a dual, but the second-nearest neighbour one has not. (*b*) The problem of the second-nearest neighbour lattice has been translated into operator form by Temperley (1956). By turning the whole assembly through a right angle, we interchange the diagonal interactions described by, for example, the operators $e^{H}+e^{-H}C_2$ and $\exp(HS_1S_3)$, while leaving the nearest-neighbour interactions unaltered. This means that we can relate the partition function of a lattice with diagonal interaction H to that of one with a diagonal interaction $H^*=\frac{1}{2}\log(\coth H)$ (cf. Onsager 1944). This strongly suggests that the diagonal interactions can, in certain circumstances, give rise to a second transition temperature, given by Onsager's relation $\sinh 2H=1$. (*c*) The effect of attractive forces is equivalent to a Weiss type field to a first approximation. If we take the one-dimensional Ising model with repulsion between nearest neighbours and then introduce such a field, it can be shown rigorously that we obtain either two transition temperatures or none at all.

§ 2. The Effect of Second-nearest Neighbour Attractions

The rather elaborate investigations of I and II led to the conclusion that an assembly of hard squares is qualitatively described by an equation of the type

$$\frac{1}{v}=\sum_l lb_l z^l \simeq z+\frac{rz^2}{(1+sz)^t} \qquad \ldots\ldots(1)$$

as long as we are outside the 'solid' region. (At least one more parameter is required to describe the situation in the 'solid' region.) By reverting (1) we can obtain z as a function of v, and hence the approximate virial series. The singularity (if any) of the latter probably corresponds not to the transition but to the limit of the metastable gas-like state.

Working with the rigid-sphere model, Kihara and Kaneko (1957) noticed that the introduction of a *long-range* attraction could be rigorously represented by a modification of the *one* irreducible cluster sum β_1, at all events as long as we are in the gaseous region. This is equivalent to the introduction of a van der Waals term of the type $-a/v^2kT$ into the virial series, which in turn would lead to a 'van der Waals loop' below the critical temperature. Temperley (1954) showed that this difficulty arises because we have neglected the fact that the other cluster sums are also changed by infinitesimal amounts, and gave reasons for thinking that the required flat isotherm would be obtained if this could be properly allowed for.

When we go over to an interaction of short-range type, we find that its effect can also be represented to a first approximation as a change in β_1, but that the other β_l's are now also changed by finite amounts. We again expect a transition with a critical temperature, below which an isotherm may have a horizontal portion. In the light of Yang and Lee's work (1952), we anticipate that the Mayer b_l series will become useless in the 'liquid' region, because its singularities are now indefinitely close to the positive real axis.

We shall study the version of the Ising model in which there is completely 'rigid' repulsion between nearest neighbours, so that the Mayer function $f=-1$, but there is a finite attraction between second-nearest neighbours. We denote

the corresponding Mayer function ($=\exp(-E_2/kT)-1$, where E_2 is the energy associated with a second-nearest neighbour pair of molecules) by g, which quantity may take any positive value. For fixed E_2, g becomes very small at high temperatures, but f remains equal to -1, so that our model then reduces to that studied in the previous paper. For this case, we obtained evidence that the b_l's alternate in sign, so that the dominant singularity is on the negative real axis, and the Mayer z-series can accordingly be analytically continued up to the 'solidification' curve which is probably associated with a singularity on the *positive* real axis of z. As the temperature falls, g increases, and we anticipate that, as in Yang and Lee's model (1952), the dominant singularities of the z-series should become first complex and then real and positive as we approach the vapour–liquid critical temperature. We shall now show that some of the work of II can be extended to deal with the second-nearest neighbour model, and shall obtain semi-quantitative confirmation that the b_l's indeed behave in the way anticipated. As in the former paper, our knowledge of the 'network generating function' is insufficiently precise to permit of firm predictions of the transition points, but the 'order of magnitude' results are in reasonable agreement with the other evidence.

§ 3. The 'Network Generating Function'

The three lemmas used in I apply to *any* lattice model in which no more than one molecule may be on a site. In the nomenclature of that paper, a 'pin' connecting two molecules on the same site in a Mayer diagram introduces a factor -1, and as in I, we conclude that the problem of enumerating cluster-sums is closely related to that of enumerating connected 'networks' consisting of sets of lattice sites connected by links. The present problem differs from the former one in that the networks may now contain second-neighbour links (factor g), as well as nearest-neighbour links (factor f).

In II we studied a number of types of network and in all cases the qualitative behaviour was the same, namely that the total number of networks containing N sites was proportional to AB^N, and that a similar law, with slightly different values of B, could be used also to enumerate (a) trees and (b) net numbers of networks when those with an odd number of links are reckoned negatively. In the last case, the net number alternates in sign with even and odd numbers of sites in the domain, and this behaviour was revealed by the dominant pole (i.e. the one nearest to the origin) of the network generating function being negative. It was inferred that such behaviour is characteristic not only of the extreme case $f=-1$, but of the whole region of f negative, and that it would give rise to a similar alternation of signs of the Mayer b_l's in the antiferromagnetic case.

For our typical domain we consider one that may contain in each row either one lattice site or two contiguous sites. As before, we can set up a matrix corresponding to the addition of one new row of sites to a network, and we must always keep enough links to ensure that the network is completely connected when the final row of sites is added. We distinguish three possible ways of adding a fresh row.

S, a single site. This must be connected to at least one site in the previous row. C, a row of two connected sites. The connection may be either via a nearest-neighbour link or else be indirect via links with one or more sites already added. D, a row of two unconnected sites. Each of them may, but need not, be connected to one or more other sites already added, but they are not connected directly or

indirectly with one another. If we distinguish the 'configurations' of each successive row in this way, it is then easy to enumerate the possible ways of adding a fresh row to a network if the configuration of the last row is known. The following simple rules will be found to be necessary and sufficient to ensure connectivity of the final network: (*a*) There must be at least one link between each successive pair of rows. (*b*) If any row is D, each of the sites in it must be connected to at least one site in the immediately following row (in particular, the final row must not be D).

We can, as usual in this type of problem, set up a matrix associated with the process of adding another row to the network, the rows of the matrix corresponding to the possible configurations of the row added to the network, while the columns correspond to the configurations of the previous row. For example, the element SC corresponds to adding a single site to a pair of connected sites. The single site must be a second neighbour of one of the pair (two possibilities) or a nearest neighbour of one of the pair and a second neighbour of the other (again two possibilities). In the first case, we have available just one g-link, in the second case one g-link and one f-link, so that the total matrix element, enumerating all possibilities complying with rule (*a*) above, must be $2g+2fg+2f+2g$. The other elements can be derived by analogous arguments and in fact we find, for the case $f=-1$,

	S	C	D	
S	$w(2g-1)$	$w(2g-2)$	$-2wg$	
C	$w^2(2-4g)$	$w^2(4-4g)$	$w^2(-1+4g-3g^2)$	$=T$..... (2)
D	$w^2(4g-2)$	$w^2(4g-4)$	$w^2(1-4g+3g^2)$	

There is no difficulty in extending this work to larger domains and other values of f, but the work becomes extremely cumbersome. The experience in II indicates that this particular domain may be regarded as fairly 'typical'. The powers of w introduced into the matrix elements of (2) enable one to keep count of the total number of sites involved. The generating function for such networks involving n rows is obtained by adding up all the elements in the S and C rows of the matrix T^{n-1}. (We must not include the D rows since the last row of the domain may not be D.) If we want networks with all possible numbers of rows we must sum over all positive n, so that our problem becomes practically the same as that of calculating $(1-T)^{-1}$. If we do this, all the elements contain the following expression in the denominator

$$\det(1-T)=1+w(1-2g)-w^2(5-8g+3g^2)-w^3(1-2g+3g^2-6g^3). \quad \ldots\ldots (3)$$

The coefficient of w^m enumerates networks containing m sites. As in II there is a corresponding contribution to the Mayer b_l series, w having the same significance as in that paper, $(=z/(1+z))$, in that it allows for clusters involving multiple occupation of sites. Thus, we may expect the expansion of the reciprocal of expression (3) to behave qualitatively like the Mayer series itself.

The behaviour of the dominant zero, i.e. the one nearest the origin, of expression (3) has been studied numerically. It is found to be negative when g is negative. This we might expect, since the model is now a wholly repulsive one and should behave qualitatively like the model discussed in I and II for which $g=0$ and f is negative. The dominant root remains negative until g reaches a value of about 0·8 and for higher values of g it is complex, asymptotically

approaching the value $2/g$ when g becomes large. This is exactly the type of behaviour we might have expected as a result of comparing II with Yang and Lee's work (1952). It will be remembered that they found that, as the strength of the attractive forces between nearest neighbours was increased, the singularities of the b_l series gradually 'spread around' the unit circle, starting from the negative real axis of z, first touching the positive real axis at the critical temperature, then 'piling up' there as the interaction was increased still further.

This shows that at high temperatures we may expect a solid–gas transition, the model becoming equivalent to that discussed in I and II. At lower temperatures the b_l series is behaving in the way that we would expect if a liquid–gas transition were approaching, though the above argument is not yet able to predict the critical temperature, even roughly. Since our model is of the same qualitative type as Yang and Lee's (1952) (attracting molecules with a rigid core) we can infer that it also has a critical temperature. From the argument in § 1(*b*) we expect the corresponding value of g to be near to $4+2\sqrt{2}$, and we deduce a value of the same order of magnitude if we take account of the effect of the attractive forces on β_1 alone and treat the resulting virial equation exactly like that of van der Waals.

§ 4. Conclusion

We have still not decided whether there are one or two transitions, but we have shown that at all temperatures a transition will occur at an appropriate density and have obtained evidence that the nature of this transition changes as the temperature falls. It does remain possible, though unlikely in view of § 1(*c*) above, that there is only one transition curve, relating temperature to density, and we cannot expect to settle this question by a study of the b_l series alone. It will be remembered that Yang and Lee (1952) had to change their expansion variable in order to get a series suitable for the 'liquid' region, and a similar step seems to be required in the present case.

References

Domb, C., and Potts, R. B., 1951, *Proc. Roy. Soc.* A, **210**, 125.
Katsura, S., 1955, *Progr. Theor. Phys., Japan*, **13**, 571.
Kihara, T., and Kaneko, S., 1957, *J. Phys. Soc. Japan*, **12**, 994.
Kikuchi, R., 1951, *J. Chem. Phys.*, **19**, 1230.
Morita, T., 1957, *J. Phys. Soc. Japan*, **12**, 1195.
Onsager, L., 1944, *Phys. Rev.*, **65**, 117.
Temperley, H. N. V., 1954, *Proc. Phys. Soc.* A, **67**, 233.
—— 1956, *Changes of State* (London: Cleaver-Hume), p. 167.
—— 1959 a, *Proc. Phys. Soc.*, **74**, 183. Referred to as I.
—— 1959 b, *Ibid.*, **74**, 432. Referred to as II.
Yang, C. N., and Lee, T. D., 1952, *Phys. Rev.*, **87**, 404.

The Decay of ^{144}Ce

By N. J. FREEMAN†
Bedford College, London

Communicated by H. O. W. Richardson; MS. received 26th March 1959

Abstract. The beta, gamma and internal conversion electron spectra of ^{144}Ce have been studied with a magnetic spectrometer, scintillation counter and coincidence techniques. The internal conversion coefficients of the 80 kev and 133 kev γ-rays were measured. Four partial beta spectra were observed and new evidence has been found for a level at 166 kev in the ^{144}Pr nucleus. No evidence was found for the 95 kev and 145 kev γ-rays in the decay.

§ 1. Introduction

The fission product ^{144}Ce of half life 285 days decays by the emission of low energy β-rays and γ-rays to the ground state of ^{144}Pr which further decays to ^{144}Nd (half-life 17·5 min) by emitting high energy β-rays and γ-rays of low intensity but high energy. A number of inconsistencies are evident in recent attempts to elucidate the decay scheme. The highest excited level in ^{144}Pr has been variously placed at 134 kev by Porter and Cook (1952), Pullman and Axel (1956) and Hickok, McKinley and Fultz (1958), at 175 kev by Emmerich, Auth and Kurbatov (1954) and Parfenova, Forafontov and Shpinel (1957) and at 225 kev by Cork, Brice and Schmid (1954). The ordering of the lower intensity transitions is controversial and these authors further disagree about the existence of some γ-rays in the decay. In addition to measurements of conversion lines and beta spectra, electron–gamma and beta–gamma coincidence experiments have been made in the present work in an attempt to resolve the apparent contradictions.

§ 2. Experimental Technique

A 5 mm diameter disc source was prepared by vacuum distillation of cerium oxide on to a 250 μg cm^{-2} aluminium backing strengthened by a 50 μg cm^{-2} nylon film. The beta spectra were recorded with the large iron shrouded prolate spheroidal magnetic field spectrometer (Evans *et al.* 1958) and the γ-rays were analysed with a NaI (Tl) scintillation counter. The coincidence counting techniques have been previously described (Freeman 1959). During the coincidence measurements delay line adjustments were made to correct for the variations in the transit time of electrons through the spectrometer.

§ 3. Beta Spectra

The total β-spectrum was recorded with the spectrometer adjusted to give a resolution of 1·3% and a transmission of 2·6% of 4π. The statistical error of each point was always less than 1%. After subtracting the tail of the high energy β-rays from ^{144}Pr an allowed Fermi–Kurie analysis (figure 1) of the residual spectrum yielded the four components β_0, β_1, β_2 and β_3 in table 1. The calculated log ft values suggest that all the transitions are first forbidden. This would require an

† Now at Atomic Weapons Research Establishment, Aldermaston, Berks.

odd parity assignment to the beta excited levels in ^{144}Pr since the ground state spin of the even–even parent ^{144}Ce must be 0^+.

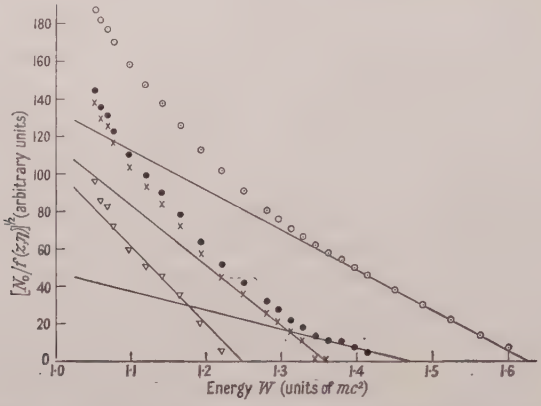

Figure 1. The allowed Fermi analysis of the singles β-spectrum of ^{144}Ce.

The β-rays in coincidence with each of the three peaks in the gamma counter pulse height spectrum (figure 3) were measured to verify the end-point energies found above, and to determine the excited levels from which these γ-rays are emitted. Figure 2 shows the allowed Fermi plots of the recorded spectra while the end-point energies and intensities are presented in table 1.

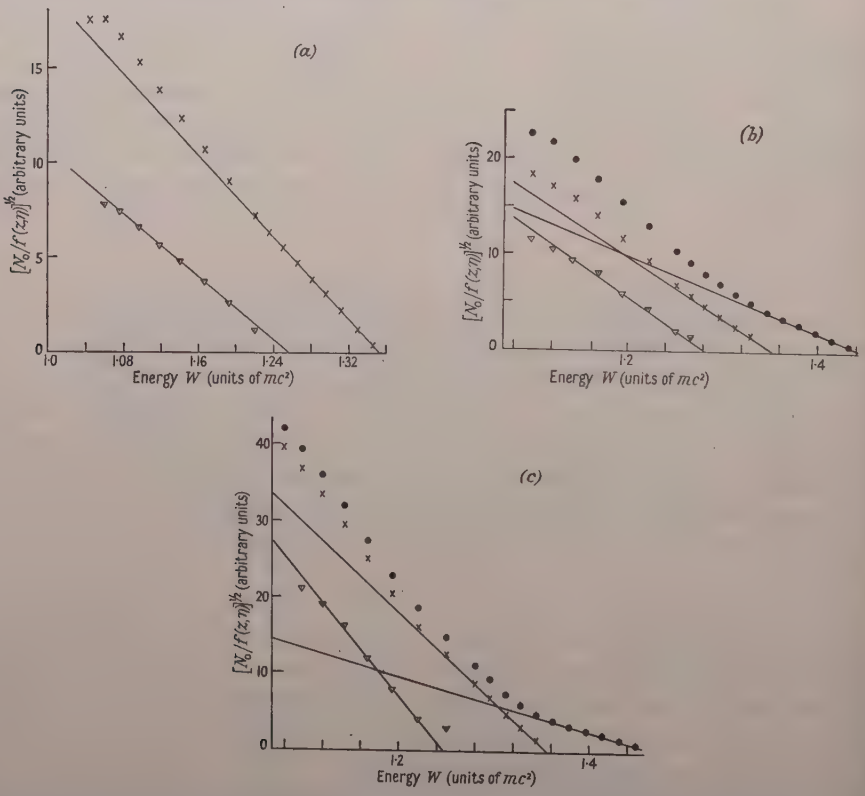

Figure 2. The allowed Fermi analysis of the β-spectra in coincidence with the (*a*) 133 keV γ-ray, (*b*) 80 keV γ-ray, (*c*) X-rays.

Table 1. The end point energies E(kev), intensities I(%), and log ft values of the four partial beta spectra (β)

	Single Spectrum			Coincidences					
				133 kev		80 kev		X-ray	
β	E(kev)	I%	log ft	E(kev)	I%	E(kev)	I%†	E(kev)	I%
β_0	319 ± 5	60	7·5						
β_1	240 ± 10	5	8·2			230	44	240	13
β_2	185 ± 5	23	7·2	180	83	181	32	182	56
β_3	128 ± 15	12	6·9	130	17	143	24	126	31

† The intensities of the components in coincidence with the 80 kev γ-ray have been corrected for the background pulses due to the 133 kev γ-ray (see figure 3).

Two further measurements of the β–γ (133) coincidences with a source mounted on a 3·5 mg cm^{-2} backing yielded an energy difference $\beta_2 - \beta_3$ of 47 kev and 66 kev.

Assuming the ground state transition to be 60% abundant the intensity of the other β-ray components was calculated from the coincidence data : β_1 (7·5%), β_2 (22·5%), β_3 (10%), in fair agreement with the estimates from the total spectrum analysis. This second value of the β_1 intensity gives a log ft value of 8·0 (compared with 8·2 for a 5% intensity).

The existence of β_3 provides strong evidence for an energy level in ^{144}Pr above 133 kev. No evidence was found for a 95 kev β-ray component as required by the Cork *et al.* decay scheme. Parfenova *et al.* employing a similar technique have reported four partial spectra β_0 310 kev (61%), β_1 230 kev (6%), β_2 175 kev (26%), and β_3 130 kev (7%), in excellent agreement with the above data. However, a recent note by Geiger, Graham and Ewan (1959) on internal conversion line measurements at high resolution places the upper excited level at 133 kev.

§ 4. The Gamma Spectrum

The gamma spectrum as recorded by the NaI(Tl) scintillation counter is shown in figure 3 uncorrected for absorption. The background extending to high energy is due to the ^{144}Pr γ-rays. The main peaks are attributed to the 133 kev

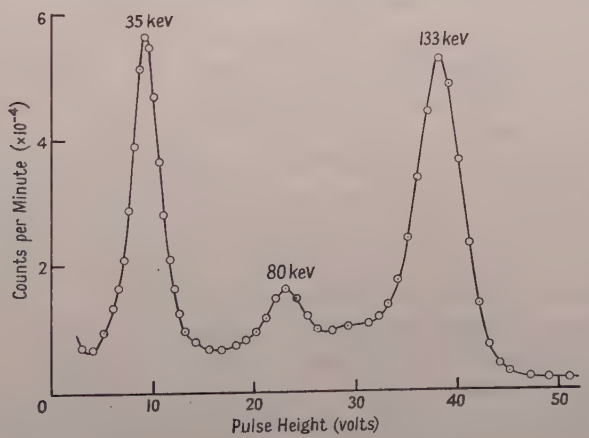

Figure 3. The low energy γ-ray spectrum of the ^{144}Ce–^{144}Pr–^{144}Nd decay.

and 80 kev γ-rays together with a predominantly x-ray peak at 35 kev. By com paring the peak shapes with the spectrum of ^{141}Ce (145 kev γ-ray and 35 kev x-ray and with the 70 kev x-ray of ^{203}Hg, the residual spectrum yielded additional peak at 55 kev and 100 kev. The ratios of the γ-ray intensities were estimated to be 133 kev : 80 kev : 35 kev = $100(\pm 10) : 24(\pm 5) : 90 \pm 10$ in agreement wit earlier work. The intensities of the 55 kev and 100 kev peaks were $\leqslant 10\%$ an $\leqslant 5\%$ respectively of the 133 kev γ-ray intensity.

The x-ray peak was noticeably wider (by a factor 1·4) than the pure x-ra peak of ^{141}Ce. This strongly suggests the presence of γ-radiation of this energ (possibly the 33 kev and 40 kev γ-rays).

From a β–γ delayed coincidence curve (resolving time $2\tau = 8 \times 10^{-9}$ sec) a upper limit of 5×10^{-10} sec was placed on the half life of the 133 kev gamm transition. This would be in accord with an M1 assignment to the transition.

§ 5. Internal Conversion Coefficients

The K and L conversion coefficients of the 133 kev and 80 kev γ-rays wer calculated from the ratio of the conversion line intensities to the β-rays in coinci dence with the corresponding γ-ray. The estimated values were :

$$\alpha_K(133) = 0{\cdot}45\,(\pm 0{\cdot}07), \quad \alpha_L(133) = 0{\cdot}06\,(\pm 0{\cdot}01); \quad \alpha_K(80) = 1{\cdot}4(\pm 0{\cdot}3),$$
$$\alpha_L(80) = 0{\cdot}2\,(\pm 0{\cdot}05).$$

Assuming the value of $\alpha_K(133)$ a second value of $\alpha_K(80) = 1{\cdot}13(\pm 0{\cdot}2)$ wa found from the intensity ratios for the γ-rays and the conversion lines. Th tables of theoretical K conversion coefficients of Sliv and Band (1956) and th L coefficients of Rose (1958) give $\alpha_K(133) = 0{\cdot}48$, $\alpha_L(133) = 0{\cdot}065$; $\alpha_K(80) = 2{\cdot}($ $\alpha_L(80) = 0{\cdot}29$ for pure M1 transitions. The measured conversion coefficient combined with the K/L ratios of table 2 suggest that both transitions are M1 The spins of the excited levels are therefore 1^- since present evidence (Freema 1959) favours a spin of 0^- for the ^{144}Pr ground state. The log *ft* values of th partial β-spectra feeding these levels agree with this assignment.

§ 6. Internal Conversion Lines

The conversion lines were measured with a transmission of 1·3% of 4π and resolution of 0·9% as recorded for the 91 kev conversion line with the 5 mm diameter source. Below 50 kev the resolving power falls off owing to source scattering. Figure 4 shows the spectrum above 15 kev while table 2 summarize the energies and intensities ($\propto$ area of each line) relative to a value of 1000 assigne to the 91 kev line.

The interpretation of some of the weaker lines is tentative since the possibili of source contamination was not excluded by following the decay period of th lines. The existence of a line at 11·2 kev, due to K conversion electrons of th 53 kev γ-ray, was confirmed by measurements with a lens spectrometer which had high detection efficiency for low energy electrons.

Measurements were made of coincidences between the γ-rays and the mo intense conversion lines. The statistics of this time absorbing experiment we rather poor but some qualitative information may be derived from figure 5 whi was recorded with a spectrometer resolution and transmission set at 1·3% a 2·7% of 4π respectively.

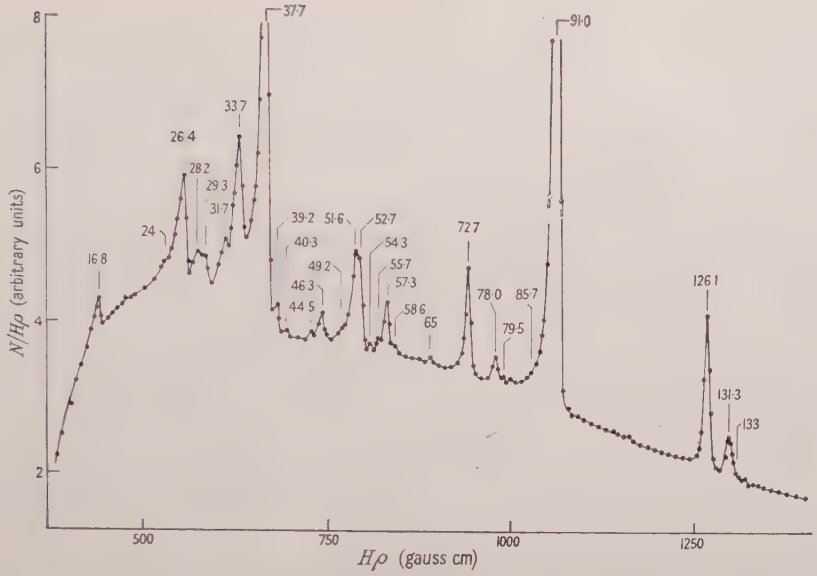

Figure 4. The internal conversion line spectrum of the ^{144}Pr γ-rays (the line energies are given in kev).

Table 2. A summary of the energy E, interpretation A, relative intensity I and the K/L, L/M ratios of the Internal Conversion Lines

E(kev)	A	I	Ratio	E(kev)	A	I	Ratio
11·2	K53·1	~30	K/L < 1·5	54·3		5	
16·8	K58·8	29	K/L 0·22	55·7		7	
24	K66	~14	K/L ~2	57·3	M58·7 }	39	
26·4	L33·2	140	L/M 2·4	57·3	K99·3 }		
28·2 }	KLL Auger	30		58·6	L66	6	L/M ~1·5
29·3 }		30		65	M66	4	
31·7	M33·2	57		72·7	L79·5	80	L/M 4·5
33·7	KLM Auger	~25		78·0	M79·5	18	
33·7	L40·5	183	L/M 6·5	79·5	N79·5 }	4	
37·7	K79·7	600	K/L 7·5	79·5	L86·5 }		
39·2	M40·5	28		85·7	M86·5	3	
40·3	N40·5	5		91·0	K133	1000	K/L 6·9
44·5	K86·5	5		97·5	M99	3	
46·3	L53·1	28	L/M 2·5	126·1	L133	146	L/M 4·3
49·2		12		131·3	M133	34	
51·6	M53·1	11		133·0	N133	4	
51·6	L_I 58·5	68	L/M > 3·4				
52·7	L_{III} 58·7	66					

We deduce that : (i) the 133 kev γ-ray is in coincidence with the 26·4 kev line (L of 33·2 kev γ-ray), (ii) the 80 kev γ-ray is in coincidence with the 26·4 kev line and with the L and M lines of the 53 kev γ-ray. From the measured L/M ratio of 2·5 we calculate the intensity of the unresolved M line in the singles spectrum to be 11 (see table 2), (iii) the x-ray peak is in coincidence with the 26·4 kev line, the L and M lines of the 53 kev γ-ray and with the line at 57·3 kev.

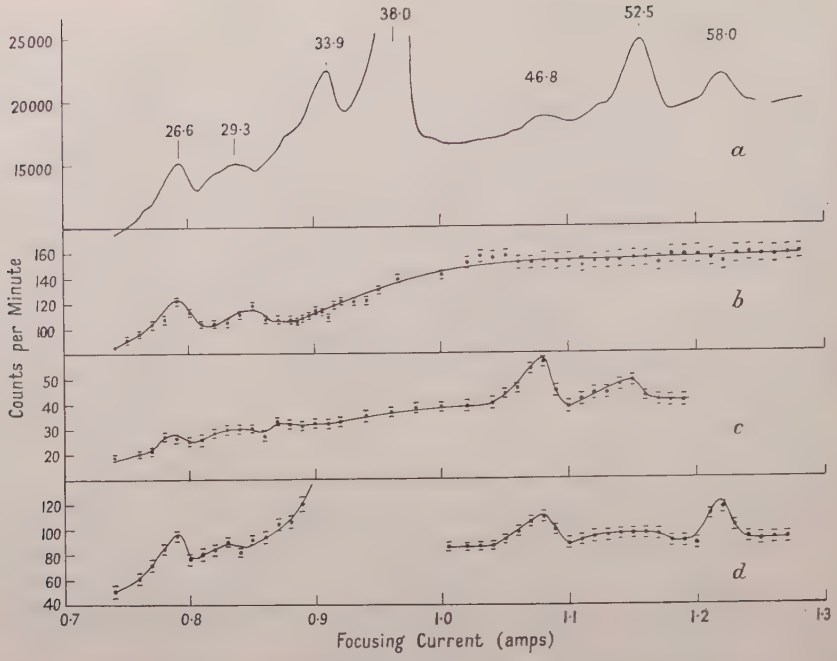

Figure 5. The internal conversion lines recorded with a 1·3% resolution. *a*, singles spectrum; *b*, coincident with 133 kev γ-ray; *c*, coincident with 80 kev γ-ray; *d*, coincident with x-rays.

§ 7. Discussion

In agreement with previous analyses the positions of the 53 kev, 80 kev and 133 kev γ-rays in the ^{144}Pr level scheme are well established. Some difficulties appear when trying to decide the positions of other levels.

The conversion line at 52 kev is interpreted as mainly an L_I–L_{III} doublet of a 58·7 kev γ-ray with ratios $K/L \sim 0{\cdot}2$ and $L_I/L_{III} \sim 1$. This evidence shows that the transition is probably M3 with a long lifetime of the order of 100 seconds. As no coincidences were detected between its conversion electrons and other gamma radiation we assume it is a transition to the ground state. Cork *et al.*, however, attributed most of the L_{III} line at 52·7 kev to K conversion electrons of a 95 kev γ-ray between levels at 175 kev and 80 kev. We find no evidence for coincidences between this line and the 80 kev γ-ray + x-rays and the K conversion electron intensity is estimated as less than 0·05% per disintegration.

Cork *et al.* assigned the line at 57·3 kev to the M conversion of the 58·7 kev γ-ray. The observed coincidences between the x-rays and this line, together with the absence of coincidences with the L lines of the 58·7 kev γ-ray shows that part of this line must be attributed to K conversion electrons of a 99·3 kev γ-ray.

No coincidences were recorded between γ-rays + x-rays and the conversion lines of the 40·5 kev γ-ray. If this is a short half life transition (Geiger *et al.* favour an M1 assignment) this γ-ray cannot originate from a level at 175 kev as required by the decay schemes of Emmerich *et al.*, Cork *et al.* and Parfenova *et al.* The lack of evidence for a 95 kev γ-ray further conflicts with this level assignment.

A search for conversion lines of a 145 kev γ-ray found by Cork *et al.* gave a negative result and we estimate an upper limit of 0·03% per disintegration for the intensity of any line due to this γ-ray.

An energy analysis shows that the 99·3 kev γ-ray could represent a crossover transition for the 40·5 kev and 58·7 kev γ-rays. The 99·3 kev level would then be fed by the 66 kev γ-ray together with possible unresolved β-rays to account for the intensity of the transitions from this level.

From the measurement of concidences between the 133 kev γ-ray and the 26·4 kev line we deduce that the 33·2 kev γ-ray is a transition from a 166 kev level. In view of the rather poor resolution in this low energy region and taking into account the good agreement between the 133 kev energy and the summation (99·3 + 33·2) kev, the 26·4 kev line might represent L conversion electrons of two gamma rays of approximately 33·2 kev energy. The second γ-ray would then be placed between the 133 kev and 99·3 kev levels as Geiger *et al.* suggest.

It appears difficult to identify the average energy difference of 50 kev between β_2 and β_3 in table 1, with the quantum energy of the 33 kev γ-ray without assuming a back-scatter distortion of the β-spectra. However, the results with a thicker source mount do not appear to support this assumption. Pullman and Axel have found evidence for a 12 kev γ-ray which might be placed in coincidence with the 33·2 kev γ-ray to account for the discrepancy.

§ 8. Conclusion

A decay scheme including most of the recorded data is tentatively suggested in figure 6. It does not include gamma transitions which might be assigned to some of the weaker conversion lines in table 2. The important feature of these results is the evidence for an excited level above 133 kev together with the placing of a 33·2 kev gamma transition above this level in disagreement with the recent work of Geiger *et al.* We find no evidence for 95 kev and 145 kev γ-rays in the decay.

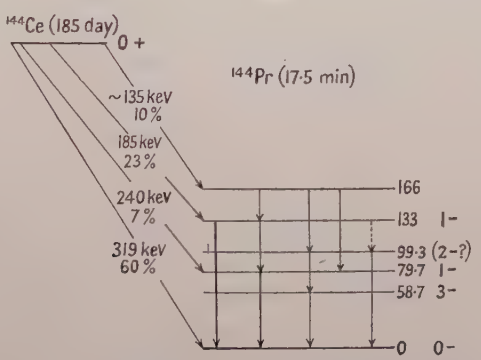

Figure 6. The proposed decay scheme of ^{144}Ce.

There is an obvious need for more accurate data on the low intensity conversion lines and for further measurements of coincidences with the conversion lines. In particular, e^-–e^- coincidence experiments would be invaluable in resolving the uncertainties in the decay scheme.

Acknowledgments

It is a pleasure to thank Professor H. O. W. Richardson for his constant encouragement and stimulating discussions. My sincere thanks are due to Dr. D. K. Butt of Birkbeck College, London, for his interest and for the use of a lens spectrometer, and to Exeter University and Bedford College for Research Scholarships which enabled me to carry out this work.

References

Cork, J. M., Brice, M. K., and Schmid, L. C., 1954, *Phys. Rev.*, **96,** 1295.
Emmerich, W. S., Auth, W. J., and Kurbatov, J. D., 1954, *Phys. Rev.*, **94,** 110.
Evans, P. R., Freeman, N. J., McGinty, G. K., Armitage, B. H., and Richardson, H. O. W., 1958, *Proc. Phys. Soc.*, **72,** 949.
Freeman, N. J., 1959, *Proc. Phys. Soc.*, **73,** 600.
Geiger, J. S., Graham, R. L., and Ewan, G. T., 1959, *Bull. Amer. Phys. Soc.*, **4,** 57.
Hickok, R. L., McKinley, W. A., and Fultz, S. C., 1958, *Phys. Rev.*, **109,** 113.
Parfenova, V. I., Forafontov, N. V., and Shpinel, V. S., 1957, *Izv. Akad. Nauk S.S.S.R., Ser. Phys.*, **21,** 1601 (in Russian).
Porter, F. T., and Cook, C. S., 1952, *Phys. Rev.*, **87,** 464.
Pullman, I., and Axel, P., 1956, *Phys. Rev.*, **102,** 1366.
Rose, M. E., 1958, *Internal Conversion Coefficients* (Amsterdam: North Holland Publishing Co.).
Sliv, L. A., and Band, I. M., 1956, *Leningrad Physico-Technical Institute Report* (translation : Report 57ICCK1) (Physics Dept., Univ. of Illinois).

Double Charge Transfer and the Mobility of He^{2+} Ions in Helium

By A. F. FERGUSON and B. L. MOISEIWITSCH
Department of Applied Mathematics, The Queen's University of Belfast

MS. received 21*st April* 1959

Abstract. The interaction energies between a He^{2+} ion and a He atom are calculated for a wide range of internuclear distances. These energies are used to determine the cross section for double charge transfer between He^{2+} ions and He atoms as well as the diffusion cross section and mobility of these ions in helium gas.

§ 1. Introduction

Just as the resonance single charge transfer process

$$He^+ + He \rightarrow He + He^+ \qquad \ldots\ldots (1)$$

considered in two previous papers (Moiseiwitsch 1956, Lynn and Moiseiwitsch 1957) is an important factor in determining the passage of He^+ ions through helium, the resonance double charge transfer process

$$He^{2+} + He \rightarrow He + He^{2+} \qquad \ldots\ldots (2)$$

is an important factor in determining the passage of He^{2+} ions through helium for a wide range of impact energies.

The present paper is concerned with a theoretical investigation of process (2) using the method of impact parameters. This process has already been the subject of exploratory calculations by Betts and Jackson (1955), but these are only accurate to within a factor of about two or so.

§ 2. Theoretical Discussion

If we let $V^+(R)$ and $V^-(R)$ be the interaction energies between a He^{2+} ion and a He atom corresponding to states of even and odd symmetry respectively, the theory of slow collisions between heavy particles given by Bates, Massey and Stewart (1953) results in the equations

$$\frac{d^2 g_l^{\pm}}{dR^2} + \left\{ k^2 - \frac{2M}{\hbar^2} V^{\pm}(R) - \frac{l(l+1)}{R^2} \right\} g_l^{\pm}(R) = 0 \qquad \ldots\ldots (3)$$

where $g_l^{\pm}(R)$ is zero at the origin and for large internuclear distances R has the asymptotic form

$$g_l^{\pm} \sim k^{-1} \sin\left(kR - \tfrac{1}{2} l\pi + \eta_l^{\pm}\right), \qquad \ldots\ldots (4)$$

M being the reduced mass of the system, k being the wave number of the initial relative motion and $\eta_l^{\pm}$ being the phase shifts for the lth order partial wave. The cross section for resonance charge transfer in which both electrons are exchanged between the He^{2+} ion and the He atom is given by

$$Q_T = \frac{\pi}{k^2} \sum_{l=0}^{\infty} (2l+1) \sin^2(\eta_l^+ - \eta_l^-) \qquad \ldots\ldots (5)$$

and the diffusion cross section by

$$Q_D = \frac{4\pi}{k^2} \sum_{l=0}^{\infty} (l+1) \sin^2 (\eta_l - \eta_{l+1}) \qquad \ldots\ldots (6)$$

where $\eta_{2r} = \eta_{2r}^{+}$ and $\eta_{2r+1} = \eta_{2r+1}^{-}$, the nuclei being assumed to obey Bose–Einstein statistics.

The mobility can then be written in the form

$$\mu = eD/\boldsymbol{k}T \qquad \ldots\ldots (7)$$

where the coefficient of diffusion D is given by (cf. Chapman and Cowling 1941)

$$D = \frac{3\pi^{1/2}}{16n} \frac{1}{P} \left(\frac{2\boldsymbol{k}T}{M} \right)^{7/2} (1-\epsilon_0)^{-1} \qquad \ldots\ldots (8)$$

and

$$P = \int_0^{\infty} v^5 Q_D(v) \exp (-Mv^2/2\boldsymbol{k}T)\, dv, \qquad \ldots\ldots (9)$$

e being the ionic charge, $\boldsymbol{k}$ being Boltzmann's constant, T being the absolute temperature, n being the number density of helium atoms, v being the velocity of relative motion and ϵ_0 being a very small term which can be neglected.

Using Jeffrey's approximation for the phase shifts, Bates, Massey and Stewart (1953) have shown that

$$Q_T = 2\pi \int_0^{\infty} p \sin^2 \Gamma \, dp \qquad \ldots\ldots (10)$$

where

$$\Gamma(p) = \frac{1}{\hbar v(\infty)} \int_p^{\infty} \frac{R(V^+ - V^-)}{(R^2 - p^2)^{1/2}} \, dR, \qquad \ldots\ldots (11)$$

$v(\infty)$ being the initial velocity of relative motion and $p = (l+\frac{1}{2})/k$ being the impact parameter.

If p^* is the largest value of p for which $\Gamma(p) \gtrsim \frac{1}{2}\pi$ then $\sin^2 \Gamma$ oscillates rapidly for $0 \leqslant p \leqslant p^*$ and may be replaced by its average value $\frac{1}{2}$. It follows that we may write

$$Q_T = \tfrac{1}{2}\pi p^{*2} + 2\pi \int_{p^*}^{\infty} p \sin^2 \Gamma \, dp. \qquad \ldots\ldots (12)$$

Further, putting $\zeta^{\pm}(p) = \eta_l^{\pm} - \eta_{l+1}^{\mp}$ and replacing the summation over l in equation (6) by an integration over p we obtain (cf. Dalgarno 1958)

$$Q_D = 2\pi \int_0^{\infty} p(\sin^2 \zeta^+ + \sin^2 \zeta^-)\, dp. \qquad \ldots\ldots (13)$$

For sufficiently large values of p, Massey and Mohr (1934) have shown that

$$\eta^{\pm}(p) = -\frac{1}{\hbar v(\infty)} \int_p^{\infty} \frac{RV^{\pm}(R)}{(R^2 - p^2)^{1/2}} \, dR \qquad \ldots\ldots (14)$$

and so if p^* can be chosen such that this approximation is valid for $p > p^*$ and such that $\sin^2 \zeta^{\pm}$ is a rapidly oscillating function for $p < p^*$ we get

$$Q_D = \pi p^{*2} + 2\pi \int_{p^*}^{\infty} p(\sin^2 \zeta^+ + \sin^2 \zeta^-)\, dp \qquad \ldots\ldots (15)$$

with

$$\zeta^{\pm}(p) = \mp \Gamma(p) + \beta(p) \qquad \ldots\ldots (16)$$

where

$$\beta(p)=\frac{1}{4\mathscr{E}}\frac{\partial}{\partial p}\int_p^\infty \frac{R(V^+ + V^-)}{(R^2-p^2)^{1/2}}\,dR, \qquad \ldots\ldots(17)$$

$\mathscr{E}$ being the energy of relative motion.

§ 3. Interaction Energies

We see from the preceding analysis that in order to calculate the charge transfer cross section Q_T, the diffusion cross section Q_D and the mobility μ we require the $He^{2+}-He$ interaction energies V^+ and V^- corresponding to the states of even and odd symmetry respectively. Approximate values for these as a function of the distance R between the helium nuclei A and B can be obtained by employing the variational principle. For the state of odd symmetry we adopt as approximate wave function†

$$\psi_t^- = \phi(r_{A1}, r_{A2}) - \phi(r_{B1}, r_{B2}) \qquad \ldots\ldots(18)$$

where

$$\phi(r_1, r_2) = \exp(-\alpha r_1 - \beta r_2) + \exp(-\alpha r_2 - \beta r_1) \qquad \ldots\ldots(19)$$

with $\alpha = 2{\cdot}19$ and $\beta = 1{\cdot}18$, is the two-parameter helium atom wave function which was found to be satisfactory in the investigation of the passage of He^+ ions through He gas (Moiseiwitsch 1956, Lynn and Moiseiwitsch 1957).

In the case of the state of even symmetry it is necessary to take account of the presence of a lower singlet state of the same symmetry associated with the two He^+ ions in their ground states. We therefore adopt as the trial wave function for the state of even symmetry

$$\psi_t^+ = c_1\chi_1^+ + c_2\chi_2^+ \qquad \ldots\ldots(20)$$

where

$$\chi_1^+ = \phi(r_{A1}, r_{A2}) + \phi(r_{B1}, r_{B2}) \qquad \ldots\ldots(21)$$

and

$$\chi_2^+ = \exp\{-2(r_{A1}+r_{B2})\} + \exp\{-2(r_{B1}+r_{A2})\}, \qquad \ldots\ldots(22)$$

c_1 and c_2 being adjustable parameters.

At infinite nuclear separation the χ_2^+ term represents two He^+ ions in their ground 1s states. Its presence in the trial function ψ_t^+ has a considerable effect as can be seen by referring to table 1 where the interaction energies V^+ and V_0^+ calculated with and without this term included are tabulated. Whereas V_0^+ is negative for $R \gtrsim 2{\cdot}0a_0$, V^+ is positive and in fact is greater than V^- for all R.

Table 1. Interaction Energies between a He^{2+} Ion and a He Atom

R (a_0 units)	V_0^+ (Ryd)	V^+ (Ryd)	V^- (Ryd)
1·0	$0{\cdot}63 \times 10^{-1}$	$0{\cdot}459 \times 10$	$0{\cdot}307 \times 10$
1·5	$-0{\cdot}342$	$0{\cdot}182 \times 10$	0·991
2·0	$-0{\cdot}198$	0·621	0·332
2·5	$-0{\cdot}808 \times 10^{-1}$	0·188	0·110
3·0	$-0{\cdot}286 \times 10^{-1}$	$0{\cdot}540 \times 10^{-1}$	$0{\cdot}357 \times 10^{-1}$
4·0	$-0{\cdot}303 \times 10^{-2}$	$0{\cdot}462 \times 10^{-2}$	$0{\cdot}357 \times 10^{-2}$
5·0	$-0{\cdot}300 \times 10^{-3}$	$0{\cdot}426 \times 10^{-3}$	$0{\cdot}347 \times 10^{-3}$
6·0	$-0{\cdot}30 \times 10^{-4}$	$0{\cdot}41 \times 10^{-4}$	$0{\cdot}34 \times 10^{-4}$
7·0	$-0{\cdot}3 \times 10^{-5}$	$0{\cdot}4 \times 10^{-5}$	$0{\cdot}3 \times 10^{-5}$

† We employ Hartree units hereafter.

In these calculations the polarization of the helium atom by the ion has not been included. To a good approximation the effect of polarization is to add the term $-4\alpha/R^4$, where $\alpha = 1{\cdot}39$ is the polarizability of a helium atom, to both V^+ and V^- so that $V^+ - V^-$ is not affected by polarization except at small values of R.

§ 4. Double Charge Transfer Cross Sections

An analytical expression for $\Gamma(p)$ can be obtained if $V^+ - V^-$ is fitted to a sum of exponential terms having the form $AR^n e^{-\gamma R}$ by using the basic integral

$$K_0(p\gamma) = \int_p^\infty \frac{e^{-\gamma R}}{(R^2 - p^2)^{1/2}} dR \qquad \ldots\ldots (23)$$

where K_0 is a modified Bessel function. The remaining integrals which are required can be found by differentiating with respect to γ.

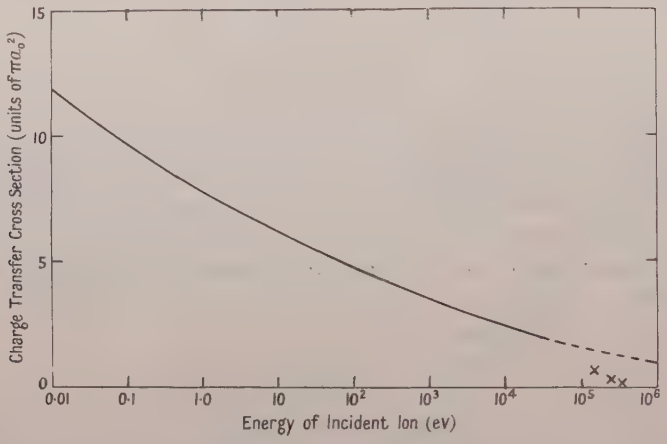

Figure 1. Cross section Q_T for double charge transfer between He^{2+} ions and He atoms. The crosses refer to the experimental points obtained by Allison. The broken curve was obtained by extrapolating the calculated cross section.

The charge transfer cross sections can then be calculated by using expression (12), the relevant integral being evaluated numerically. The results of the calculation are given in figure 1 where the cross section for double charge transfer between He^{2+} ions and He atoms is displayed as a function of the incident energy E of the He^{2+} ion on a log scale. The upper limit to the range of energies covered was 40 kev. At higher impact energies reliable charge transfer cross sections cannot be obtained until a more accurate knowledge of V^+ and V^- at very small values of R becomes available. However, if the calculated cross sections are extrapolated to higher energies a comparison can be made with the experimental double charge transfer cross sections obtained by Allison (1958). At 150 kev Allison obtains a cross section of $0{\cdot}65\pi a_0^2$ which is rather smaller than the extrapolated theoretical value of $1{\cdot}4\pi a_0^2$ at the same impact energy. Furthermore, the experimental cross sections decrease by a factor of about 5 between 150 and 350 kev which is a much more rapid fall off with energy than is shown by the extrapolation of the calculated cross sections. This behaviour of the experimental cross sections is due to momentum transfer which becomes important when E is greater than an energy of the order of 10–100 kev. The effect of momentum transfer has been neglected in the calculations presented here.

The single charge transfer cross sections for process (1) are about 3 to 4 times larger than the double charge transfer cross sections for process (2) at the same value of E for the entire range of impact energies investigated.

§ 5. Diffusion Cross Sections and Mobility

Using equations (15) and (16) we have for the diffusion cross section

$$Q_D = \pi p^{*2} + 4\pi \int_{p^*}^{\infty} p\,(\sin^2\Gamma + \sin^2\beta - 2\sin^2\Gamma\sin^2\beta)\,dp. \quad \ldots\ldots (24)$$

For large R the major contribution to the interaction energies between a He^{2+} ion and a helium atom arises from the polarization of the atom and so we may put

$$V^+ = V^- = -\frac{4\alpha}{R^4}. \quad \ldots\ldots (25)$$

It follows from (17) that for large p we have

$$\beta(p) = \frac{3\pi\alpha}{2\mathscr{E}p^4}. \quad \ldots\ldots (26)$$

For energies of relative motion $\mathscr{E} \lesssim 0{\cdot}1$ ev the terms involving Γ give a negligible contribution to Q_D and so

$$Q_D = \pi p^{*2} + 4\pi \int_{p^*}^{\infty} p \sin^2\beta\,dp \quad \ldots\ldots (27)$$

where β may be taken to be given by expression (26).

When $\mathscr{E} \gtrsim 2$ ev the terms involving β give a negligible contribution to Q_D and then we have

$$Q_D = 2Q_T. \quad \ldots\ldots (28)$$

If the energy of relative motion lies between about 0·1 ev and 2 ev all the terms in (24) need to be taken into account. The results of the calculation of the momentum transfer (or diffusion) cross section Q_D are given in figure 2.

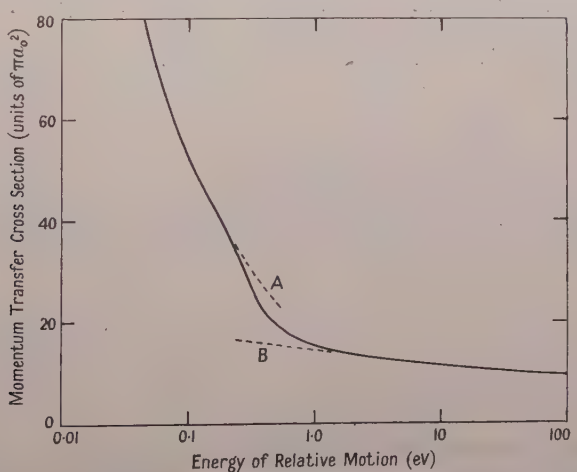

Figure 2. Momentum transfer cross section Q_D for He^{2+} ions in helium. Curves A and B have been obtained by using respectively equations (27) and (28) of the text.

Substituting into the integral expression (9) for P the diffusion coefficient D may be readily calculated and hence the mobility μ for He^{2+} ions in helium obtained. This is displayed as a function of the temperature T in table 2.

Table 2. Mobility of a He^{2+} Ion in Helium

T(°K)	100	200	300	400	500	1000	2000	5000	8000
μ ($cm^2\,v^{-1}\,sec^{-1}$)	24	25	25	25	25	26	27	26	23

At temperatures below about 200°K expression (27) for the diffusion cross section may be used for the determination of the mobility. Dalgarno, McDowell and Williams (1958) have shown that the mobility is then given by

$$\mu = A/(\alpha M)^{1/2}\,cm^2\,v^{-1}\,sec^{-1}, \qquad \ldots\ldots (29)$$

where the constant A depends without much sensitivity on the particular value of p^* used in (27) and the reduced mass M is in units of the proton mass.

If the mobility corresponds to a constant gas density of $2{\cdot}69 \times 10^{19}\,cm^{-3}$, the value of A used in the present paper is 40, giving rise to a constant mobility at low temperatures of $24\,cm^2\,v^{-1}\,sec^{-1}$. Due to the use of the Massey and Mohr approximation (14) this is about 10% larger than the classical value obtained by using the theory of Langevin (1905) and Hassé (1926).

As the temperature rises the mobility is found to increase to a maximum value of $27\,cm^2\,v^{-1}\,sec^{-1}$ at 2000°K and then begins to fall as still higher temperatures are attained and the effect of charge transfer becomes important.

Acknowledgments

We are very grateful to Professor D. R. Bates and Dr. A. Dalgarno for valuable discussions.

References

Allison, S. K., 1958, *Phys. Rev.*, **109**, 76.
Bates, D. R., Massey, H. S. W., and Stewart, A. L., 1953, *Proc. Roy. Soc.* A, **216**, 437.
Betts, D. D., and Jackson, J. D., 1955, *Phys. Rev.*, **98**, 1149.
Chapman, S., and Cowling, T. G., 1941, *Mathematical Theory of Non-Uniform Gases*, 2nd Edn (Cambridge: University Press).
Dalgarno, A., 1958, *Phil. Trans. Roy. Soc.* A, **250**, 426.
Dalgarno, A., McDowell, M. R. C., and Williams, A., 1958, *Phil. Trans. Roy. Soc.* A, **250**, 411.
Hassé, H. R., 1926, *Phil. Mag.*, **1**, 139.
Langevin, P., 1905, *Ann. Chim.* (*Phys.*), **8**, 245.
Lynn, N., and Moiseiwitsch, B. L., 1957, *Proc. Phys. Soc.* A, **70**, 474.
Massey, H. S. W., and Mohr, C. B. O., 1934, *Proc. Roy. Soc.* A, **144**, 188.
Moiseiwitsch, B. L., 1956, *Proc. Phys. Soc.* A, **69**, 653.

Electron Loss from Fast Negative Ions of Atomic Hydrogen passing through Atomic Hydrogen

By M. R. C. McDOWELL† and G. PEACH
Department of Mathematics, Royal Holloway College, Englefield Green, Surrey

MS. received 22nd January 1959, in revised form 7th May 1959

Abstract. Born's approximation is used to calculate the cross sections of the processes

$$H(1s)+H^-(1s^2)\rightarrow H(1s \text{ or } 2p)+H(1s \text{ or } 2p)+e$$

at impact energies between 2·5 kev and 10 Mev. The sensitivity of the cross section of the process

$$H(1s)+H^-(1s^2)\rightarrow H(1s)+H(2p)+e$$

to the choice of bound and free H^- wave function is examined, as is that of the process

$$H(1s)+H^-(1s^2)\rightarrow H(2p)+H(1s)+e$$

to the choice of free H^- wave function. The electron loss cross section $\sigma_{-1,0}$ is approximated by a sum rule, for the simplest choice of wave function. The results are compared with those of Allison for H^- electron loss in H_2. The energy distribution of ejected electrons at high impact energies is also given.

§ 1. Introduction

In recent years a detailed theoretical study of fast collision processes involving hydrogen and helium atoms and positive ions, has been carried out by Bates and his colleagues using Born's approximation (see Bates and Dalgarno 1956 for a brief summary of this work up to that date, Boyd, Moiseiwitsch and Stewart 1957, Bates and Williams 1957).

Considerable interest is attached to comparable studies of processes involving the negative ion of atomic hydrogen H^-. Electron loss cross sections for fast H^- in He to Born's approximation have been published by Sida (1955). In this paper we investigate the simplest of such processes, single electron loss from fast H^- in H. Since the negative ion is a much more diffuse system than the corresponding neutral atom, one would expect the cross sections for these processes to be more sensitive to choice of atomic wave functions than the atom–atom and atom–positive ion collisions previously studied. We therefore employ a variety of wave functions in some of the calculations, to investigate this sensitivity.

There are no available experimental data in the magnitude of the electron loss cross section, though measurements are now being undertaken elsewhere. However, Allison (1958) has recently reviewed the results for H^- electron loss in molecular hydrogen. Preliminary data on the atomic case (Branscomb and Fite 1959, private communication) suggest that the cross sections are closely similar, near their maximum.

† Now at Georgia Institute of Technology, Atlanta, Georgia.

§ 2. Theory

We consider a collision between a fast H^- ion and a hydrogen atom. Both systems are initially in their ground states; an electron is ejected from the negative ion only and each of the residual atoms may be left in any discrete state. Born's approximation is employed, exchange being neglected. The electron loss cross section $\sigma_{-1,0}$ may be expressed as

$$\sigma_{-1,0}=\sum_{n'l'}{}' \sum_{nl}{}' Q(1s;1s^2\rightarrow n'l';nl,\mathrm{C}) \qquad \ldots\ldots(1)$$

the dashes on the summations indicating that only discrete terms are to be included. Here $Q(1s;1s^2\rightarrow n'l';nl,\mathrm{C})$ is the cross section for the process

$$H(1s)+H^-(1s^2)\rightarrow H(n'l')+H(nl)+e. \qquad \ldots\ldots(2)$$

This cross section is given by (Mott and Massey 1949)

$$Q(1s;1s^2\rightarrow n'l';nl,\mathrm{C})=\frac{8\pi^3\mu^2e^4}{h^4k_i^2}\int\int_0^{\kappa_{\max}}\int_{\kappa_{\min}}^{\kappa_{\max}}|L(n'l';\ nl,\mathrm{C})|^2KdKd\kappa d\omega \qquad \ldots\ldots(3)$$

the ejected electron having momentum $\hbar\boldsymbol{\varkappa}$, lying in the solid angle $d\omega$ about the direction (χ,ψ). The momentum of relative motion is $\hbar\mathbf{K}$,

$$\mathbf{K}=\mathbf{k}_i-\mathbf{k}_f;\ \mathbf{k}_i=\frac{\mu\mathbf{v}_i}{\hbar};\ \mathbf{k}_f=\frac{\mu\mathbf{v}_f}{\hbar} \qquad \ldots\ldots(4)$$

where μ is the reduced mass of the system, $\mathbf{v}_i$ and $\mathbf{v}_f$ are the initial and final relative velocities and the z axis is taken along $\mathbf{K}$.

The matrix element $L(n'l';\ nl,\mathrm{C})$ is

$$L(n'l';\ nl,\mathrm{C})=\int\int\int\int\Psi_i^*(\boldsymbol{\rho}_1,\mathbf{r}_2,\mathbf{r}_3)\,\Psi_f(\boldsymbol{\rho}_1,\mathbf{r}_2,\mathbf{r}_3)\exp\{i\mathbf{K}.\mathbf{R}\}\times V(\mathbf{R},\boldsymbol{\rho}_1,\mathbf{r}_2,\mathbf{r}_3)d\boldsymbol{\rho}_1d\mathbf{r}_2d\mathbf{r}_3d\mathbf{R}, \qquad \ldots\ldots(5)$$

in which Ψ_i and Ψ_f are the initial and final wave functions of the whole system, $\mathbf{R}$ is the internuclear separation, $\boldsymbol{\rho}_1$ is the position vector of the target particles' electron with respect to its nucleus; $\mathbf{r}_2$ and $\mathbf{r}_3$ are the position vectors of the H^- electrons with respect to the nucleus of the ion; and $V(\mathbf{R},\boldsymbol{\rho}_1,\mathbf{r}_2,\mathbf{r}_3)$ is the interaction potential, which may be written in the form

$$V(\mathbf{R},\boldsymbol{\rho}_1,\mathbf{r}_2,\mathbf{r}_3)=\frac{1}{R}-\frac{1}{|\mathbf{R}-\boldsymbol{\rho}_1|}-\frac{1}{|\mathbf{R}+\mathbf{r}_2|}-\frac{1}{|\mathbf{R}+\mathbf{r}_3|}+\frac{1}{|\mathbf{R}+\mathbf{r}_2-\boldsymbol{\rho}_1|}+\frac{1}{|\mathbf{R}+\mathbf{r}_3-\boldsymbol{\rho}_1|}. \qquad \ldots\ldots(6)$$

Integration over $\mathbf{R}$-space yields

$$Q(1s;1s^2\rightarrow n'l';\ nl,\mathrm{C})=\frac{2}{\mathscr{S}_i^2}\int\int_0^{\kappa_{\max}}\int_{\kappa_{\min}}^{\kappa_{\max}}\times\mathscr{I}(1s^2\rightarrow nl,\mathrm{C})|^2|G(1s\rightarrow n'l')|^2K^{-3}dKd\kappa d\omega, \qquad \ldots\ldots(7)$$

all quantities being in atomic units. The integral $\mathscr{I}(1s^2\rightarrow nl,\mathrm{C})$ depends only on the initial and final states of the H^- ion; similarly the integral $G(1s\rightarrow n'l')$ depends only on those of the target H atom. Both may be evaluated analytically by elementary methods.

The unit of energy is defined by

$$\mathscr{S}_i^2=mv_i^2/2I_H \qquad \ldots\ldots(8)$$

where I_H is the ionization potential of atomic hydrogen and m is the electronic mass.

§ 3. Sensitivity of the Cross Sections to choice of Wave Functions

The wave functions are written as products of atom and ion wave functions, a valid approximation at large **R**. We put

$$\Psi_{\mathrm{i,f}} = \psi(n'l'\,;\boldsymbol{\rho}_1)\psi_{\mathrm{i,f}}(\mathrm{H}^-) \qquad \ldots\ldots(9)$$

where $\psi(n'l', \boldsymbol{\rho}_1)$ is the wave function of a hydrogen atom in the $n'l'$ state, and

$$\left.\begin{aligned}\psi_{\mathrm{i}}(\mathrm{H}^-) &= N_{\mathrm{i}}\{\psi(\alpha, \mathbf{r}_2)\psi(\beta, \mathbf{r}_3) + \psi(\alpha, \mathbf{r}_3)\psi(\beta, \mathbf{r}_2)\}\\ \psi_{\mathrm{f}}(\mathrm{H}^-) &= N_{\mathrm{f}}\{\psi(nl, \mathbf{r}_2)\psi_\kappa(\mathbf{r}_3) + \psi(nl, \mathbf{r}_3)\psi_\kappa(\mathbf{r}_2)\}.\end{aligned}\right\} \qquad \ldots\ldots(10)$$

Consider first the initial H^- wave function. Studies of the binding energy, attachment energy, and other properties of H^- (cf. Bethe and Salpeter 1957) suggest that a good wave function must take explicit account of the electrons mutual repulsion. This leads to great analytical complexity and was not adopted. If $\psi(\alpha, \mathbf{r})$ and $\psi(\beta, \mathbf{r})$ are taken to be hydrogenic 1s orbitals with effective nuclear charges α and β, then a variational calculation of the binding energy yields $\alpha = 1{\cdot}04$, $\beta = 0{\cdot}2808$ and gives a close approximation to the attachment energy (Chandrasekhar 1944). This wave function has also been used in calculations of the photo detachment cross section (Chandrasekhar and Breen 1946) and of symmetric (H^-, H) charge transfer (Dalgarno and McDowell 1956, Branscomb, Fite, Stebbings and Hummer 1959, to be published) and gives good agreement with the experimental data in both cases. We have used it to calculate the cross section of the process

$$\mathrm{H(1s)} + \mathrm{H}^-(1s^2) \rightarrow \mathrm{H(1s)} + \mathrm{H(2p)} + \mathrm{e} \qquad \ldots\ldots(11)$$

in which the matrix element is greatly simplified by orthogonality of the atomic orbitals. Its use with any but the simplest free electron wave function, or in other processes, led to prohibitively lengthy calculations. We therefore adopted the simple hydrogenic wave function with $\alpha = \beta = 0{\cdot}6875$ for the remainder of our work, using (11) as a scaling process. It should be remarked that the success of a wave function in predicting the binding energy implies only that it is accurate in regions near the nucleus, and is in itself no criterion of its value in collision problems, in which the electron density distribution over a wide range of radial distances may be important.

The ejected electron moves in the field of a hydrogen atom in the *nl* state. Since this field falls off exponentially it would appear a reasonable first approximation to represent the free electron by a plane wave

$$\psi_1(\boldsymbol{\kappa}) = \frac{\kappa}{(2\pi)^{3/2}}\, \mathrm{e}^{i\boldsymbol{\kappa}\cdot\mathbf{r}} \qquad \ldots\ldots(12)$$

where we have normalized $\psi(\boldsymbol{\kappa})$ according to

$$\int d\omega \int \psi(\boldsymbol{\kappa})\psi(\boldsymbol{\kappa}')d\boldsymbol{\kappa} = \delta(\kappa' - \kappa). \qquad \ldots\ldots(13)$$

It should be noted that the resulting H^- wave function is not orthogonal to the ground state wave function. A better approximation would be to use the one-body approximation (Mott and Massey 1949), that is, to solve the Schrödinger equation for an electron in the static field of a hydrogen atom in the *nl* state,

$$\psi_2(\boldsymbol{\kappa}) = \frac{\kappa^{1/2} g_0(r)}{(2\pi)^{3/2} Cr} \qquad \ldots\ldots(14)$$

where $g_0(r)$ is the solution bounded at the origin and having asymptotic form

$$g_0(r) \sim \frac{\sin \kappa r}{\kappa^{1/2}} \qquad \ldots\ldots (15)$$

of the equation

$$\left\{ \frac{d^2}{dr^2} + \kappa^2 - 2V_0(r) \right\} g_0(r) = 0 \qquad \ldots\ldots (16)$$

in which

$$V_0(r) = \int |\psi(nl)|^2 \left\{ \frac{1}{r_2} - \frac{1}{|\mathbf{r}_2 - \mathbf{r}_3|} \right\} d\mathbf{r}_2, \qquad \ldots\ldots (17)$$

the normalization of $g_0(r)$ being carried out by the method of Strömgren (cf. Bates and Seaton 1949). The resulting wave function represents the s-wave of the continuum only.

We considered the two sets of processes

$$\mathrm{H(1s) + H^-(1s^2) \rightarrow H}(n'l') + \mathrm{H(1s) + e} \qquad \ldots\ldots (18)$$

and

$$\mathrm{H(1s) + H^-(1s^2) \rightarrow H}(n'l') + \mathrm{H(2p) + e.} \qquad \ldots\ldots (19)$$

For the second of these, process (19), only the s-wave of the continuum contributes, so the use of (14) is no limitation. A more refined variational wave function for an electron in the field of H(2p) has been developed by Khashaba and Massey (1958). It may be written in the form

$$\psi_3(\boldsymbol{\varkappa}) = \frac{\kappa}{(2\pi)^{3/2}} \left\{ \frac{\sin \kappa r}{\kappa r} (1 + d\mathrm{e}^{-r}) + c(1 - \mathrm{e}^{-r}) \frac{\cos \kappa r}{\kappa r} \right\}, \qquad \ldots\ldots (20)$$

where c and d are variationally determined parameters. These parameters vary rapidly with κ and are only tabulated at four points. They were interpolated graphically for other values of κ. The results obtained cannot therefore be regarded as very accurate.

We have calculated the cross section for (19) taking $n'l' = 1\mathrm{s}$ with each of $\psi_1(\boldsymbol{\varkappa})$, $\psi_2(\boldsymbol{\varkappa})$ and $\psi_3(\boldsymbol{\varkappa})$ and with $\psi_1(\boldsymbol{\varkappa})$ used both a one parameter and a two parameter bound wave function. The results are displayed in figure 1. As might be expected the two parameter bound wave function, which portrays the ion as a very diffuse system, yields a cross section an order of magnitude larger than does the one parameter approximation. Almost all of the effect arises from small values of κ; the term in the integration over κ involving $\beta = 0{\cdot}2808$ is much larger for $\kappa < 1{\cdot}0$ than is the corresponding term in the one parameter approximation involving $\alpha = 0{\cdot}6875$, even when allowance is made for the much smaller normalizing factor. The result of improving the free electron wave function is surprising in that the one body approximation compares quite favourably with that of Khashaba and Massey. Both reduce the cross section considerably, the latter by an order of magnitude, and this is true at all impact energies considered.† (It might have been supposed that distortion would only be important at low impact energies, since at high energies more of the contribution to the cross section comes from large values of κ for which the plane wave representation should be valid.) The energy variation of the cross section is not, of course, sensitive to the choice of wave function. The corrections to its magnitude occasioned by

† The behaviour is controlled by the normalizing factor which is very small in the region of κ of interest, since the s-wave phase shift becomes quite large. Cancellation is also significant.

improvements in the bound wave function are opposite in sense but, perhaps fortuitously, of the same magnitude as are those due to improvement of the free electron wave function. It is clear that the behaviour shown in figure 1 is typical of all processes of type (19), since the term in the matrix element involving $n'l'$ acts primarily as a scale factor. The remaining calculations on these processes may therefore be greatly simplified by adopting $\psi_1(\kappa)$ and the one parameter bound wave function. The relative magnitudes of the cross sections for the processes considered should be quite accurate, and their absolute values should not be greatly in error.

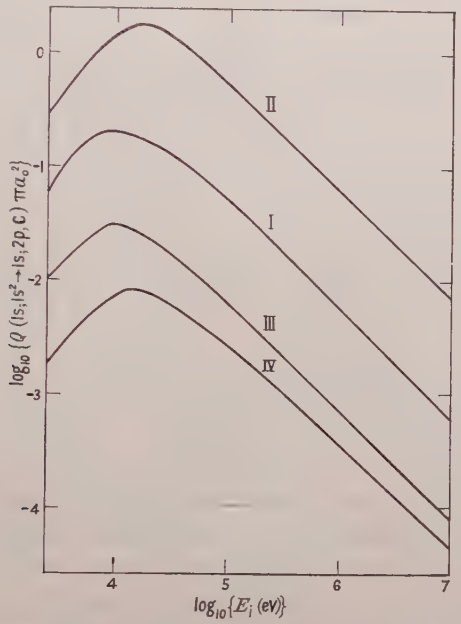

Figure 1. Cross section $Q(1s;\ 1s^2\rightarrow 1s;\ 2p, C)$ computed on Born's approximation.
I. One parameter bound, plane wave free electron.
II. Two parameter bound, plane wave free electron.
III. One parameter bound, one-body free electron.
IV. One parameter bound, Khashaba–Massey free electron.

We consider now processes of type (18), and again employ $\psi_1(\kappa)$ as a first approximation, together with the simple one parameter bound wave function. In the absence of a closed form for the total cross section we restrict ourselves to a consideration of the s and p waves of the continuum. The neglect of higher partial waves is unlikely to be serious at the low values of κ which are of importance.

Much effort has been spent on obtaining improved s-waves for an electron outside a hydrogen atom in the ground state (cf. Bransden, Dalgarno, John and Seaton 1958, hereafter referred to as BDJS) and recently the above authors have obtained a variationally determined p-wave. Their results seem in better agreement with the experimental evidence on slow elastic scattering than do any others (Brackmann, Fite and Neynaber 1958). We have therefore adopted their wave functions for the symmetric exchange case,

$$\psi_4(\boldsymbol{\varkappa}\,;\mathrm{s})=\frac{1}{(2\pi)^{3/2}r}\left\{\sin\kappa r+a_0{}^{+(i)}\{1-\mathrm{e}^{-2r}\}\cos\kappa r+b\kappa r\,\mathrm{e}^{-r}\right\} \quad \ldots\ldots(21)$$

in which $\eta_0^+ = \tan a_0^{+(l)}$ is the s-wave phase shift and b is a variational parameter. For the p-wave BDJS adopt

$$\psi_4(\boldsymbol{\kappa}, \mathrm{p}) = \frac{1}{(2\pi)^{3/2} r} \{ j_1(\kappa r) - a_1^{(l)}[1 - e^{-2\kappa r}]^3 y_1(\kappa r) + b_1(\kappa r)^2 e^{-3\kappa r} \} \quad \ldots\ldots (22)$$

where

$$j_1(x) = \left(\frac{\pi x}{2}\right)^{1/2} J_{3/2}(x); \quad y_1(x) = \left(\frac{\pi x}{2}\right)^{1/2} J_{-3/2}(x) \quad \ldots\ldots (23)$$

while $a_1^{(l)}$ and b_1 are variational parameters.

The s-wave function (21) was used for $\kappa = 0{\cdot}1(0{\cdot}1)0{\cdot}4$ to calculate $|\mathscr{I}(1s^2 \rightarrow 1s, C)|^2$ and the results compared with those obtained using the s-component of the plane wave. The general behaviour of the matrix element, as a function of K and κ was but little changed; however, it is multiplied by a

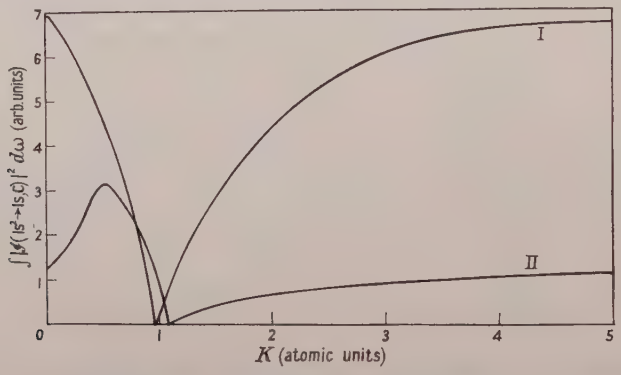

Figure 2. The s and p wave contribution to $\int |\mathscr{I}(1s^2 \rightarrow 1s, C)|^2 \, d\omega$ for $\kappa = 0{\cdot}5$.
I. Plane wave. II. BDJS wave function.

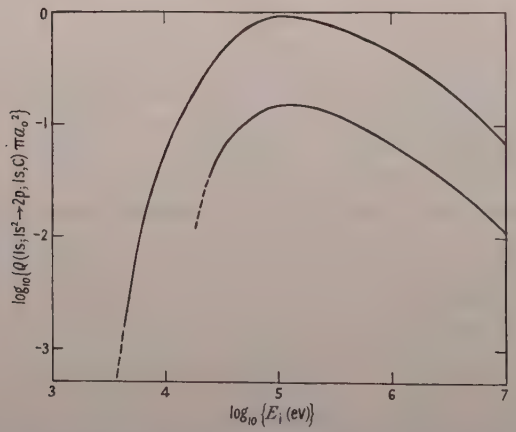

Figure 3. Cross section $Q(1s;\ 1s^2 \rightarrow 2p;\ 1s, C)$: upper curve, plane wave for free electron; lower curve, BDJS wave function.

normalizing factor of $1/[1 + a_0^{+(l)^2}]$. In the region of interest η_0^+ passes through $\pi/2$ and $a_0^{+(l)}$ becomes very large. Thus over the whole range of κ considered, the s-wave contribution to the matrix element is decreased by about a factor of seven. The results were extrapolated to $\kappa = 0{\cdot}5$ in order to compare them with the p-wave contribution, which was evaluated for $\kappa = 0{\cdot}5$ and $\kappa = 1{\cdot}0$. The general behaviour is the same in both cases, the modified p-wave being about

10% less than the p component of the plane wave. The p-wave contribution is but a small fraction of the s-wave contribution in the plane wave case, except in the region near $K=1{\cdot}0$ where they both have a zero and here it is always smaller than the s-wave. However, in the BDJS case the s-wave contribution is greatly reduced while that of the p-wave is scarcely altered and hence dominates at small K, giving a sharp maximum in the matrix element near $K=0{\cdot}5$ (cf. figure 2). The total cross section was then calculated on the assumption that the matrix element was decreased in the same ratio (for a given K) for $\kappa>0{\cdot}5$ as for $\kappa=0{\cdot}5$. Errors in this assumption are unlikely to be serious since there is only a small contribution to Q from large κ. The results are shown in figure 3 for $n'l'=2\text{p}$.

§ 5. Electron Loss Cross Sections

It is unlikely that the effect of improving the bound wave function for processes of type (18) will be significantly different from that in processes of type (19); that is, they will be slightly larger but of opposite sign to the corrections obtained by modifying the free wave function. Hence the cross sections calculated for processes of type (18) using the one parameter bound and plane wave free wave functions should be correct, relative to each other and to the similar results for processes of type (19), and their absolute magnitudes should be fairly good, perhaps to within a factor of five.

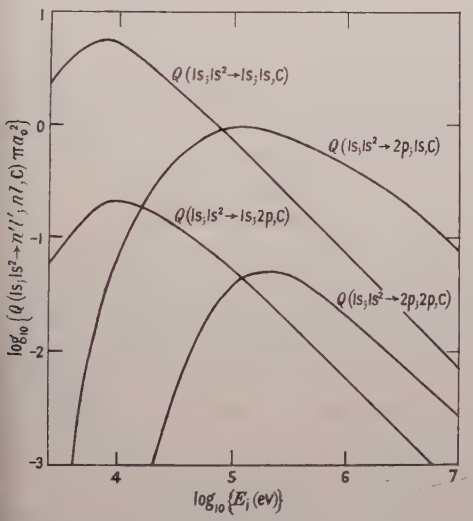

Figure 4. Born approximation cross sections for the processes $H(1s)+H^-(1s^2)\rightarrow H(1s \text{ or } 2p)+H(1s \text{ or } 2p)+e$ computed using a one parameter bound wave function and a plane wave for the free electron.

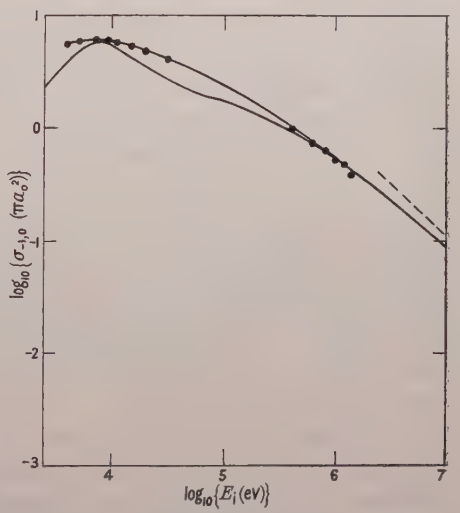

Figure 5. Electron loss cross section $\sigma_{-1,0}$ for H^- ions in H. The upper curve is drawn through the experimental points (cf. Allison 1958). The lower curve gives the computed values. The broken line to the right represents the approximate asymptotic result. The experimental results of Whittier (1954) lie some 20% higher at 4 kev.

These cross sections, for $nl=1\text{s}$ and 2p, are shown in figure 4. The cross sections for which the target particle is unexcited have their maxima at much lower energies than do those in which it is left in a 2p state. This results in a much slower fall off of $\sigma_{-1,0}$ with increasing impact energy than would otherwise be

expected. Further, for any given $n'l'$ the major contribution comes from single transitions of the H^- ion, that is, from electron loss without excitation of the residual atom.

The cross sections shown in figure 4 should make the most significant contribution to $\sigma_{-1,0}$ at all energies. Previous work on $H^{+,0}$ collisions with H and He (cf. Bates and Dalgarno 1956) indicates that at any given energy the Born approximation cross sections for any given l or l' fall off rapidly with increasing n or n'; and conversely for any given n or n' and Δl or $\Delta l' \neq \pm 1$, they fall off rapidly with increasing l or l'. The sum of the cross sections for processes (18) and (19) with $n'l' = 1s$ or $2p$ is displayed as $\sigma_{-1,0}$ in figure 5. It is possible to get an approximate asymptotic representation of $\sigma_{-1,0}$ by ignoring the contribution (which should be small) from processes in which the target atom is left in states other than 1s or 2p; that is

$$\sigma_{-1,0} \simeq \sum_{nl} \{Q(1s; 1s^2 \rightarrow 1s; nl, C) + Q(1s; 1s^2 \rightarrow 2p; nl, C)\}. \quad \ldots\ldots (24)$$

(This summation includes an integration over the continuum and so takes account of double electron loss $\sigma_{-1,+1}$.) Using a sum rule technique this can be evaluated to yield

$$\sigma_{-1,0} \sim \frac{42{\cdot}16}{\mathscr{I}_1^2} (\pi a_0^2). \quad \ldots\ldots (25)$$

There are no direct experimental data on $\sigma_{-1,0}$. Several authors have however presented results on $\sigma_{-1,0}$ for H^- ions in H_2 (Whittier 1954, Stier and Barnett 1956, Rose, Connor and Bastide 1958) which have been reviewed by Allison (1958). While there are sound theoretical reasons for supposing that H_2 is equivalent to two hydrogen atoms for collisions with H^+, this is not so for collisions with H^-, and indeed Gerjuoy (1958) has argued the contrary. However in the absence of direct experimental data the comparison is made in figure 5. The agreement is surprisingly good, in view of the approximations made. The theoretical results should not be in error by more than a factor of five at high energies. They are much less trustworthy, through the failure of Born's approximation, near the maximum cross section, where they should considerably over-estimate. Preliminary data obtained with atomic hydrogen by Branscomb and Fite indicate a cross section of between 5·0 and 10·0 πa_0^2 at 5000 ev remaining steady to much lower energies. This may imply that our results at high energies are too small; which would in turn imply that the use of a bound wave function taking explicit account of the electronic interaction would increase the cross sections even more than does the replacement of the one parameter by the two parameter approximation. Further discussion must await the detailed experimental results.

The energy distribution of the ejected electrons is of interest in connection with secondary processes. In figure 6 we show the variation of

$$\log_{10}\{Q(1s; 1s^2 \rightarrow 2p; 1s, C|\kappa^2, E_i)\}$$

as a function of κ for some selected incident particle energies. This is such that $Q(1s; 1s^2 \rightarrow 2p; 1s, C|\kappa^2, E_i)d\kappa^2$ is the cross section for the process in which $n'l' \rightarrow 2p; nl \rightarrow 1s$ and an electron is ejected with energy between κ^2 and $\kappa^2 + d\kappa^2$ times I_H, by an incident particle of energy E_i. These curves show the same general behaviour as do those presented for

$$H^+ + H(1s) \rightarrow H^+ + H^+ + e \quad \ldots\ldots (26)$$

by Bates and Griffing (1953), but a very much faster fall off at any given energy. That is, there are relatively few high energy electrons ejected: this picture is substantiated by the data on $\mathcal{F}(\kappa^2|E_i)$, the fraction of electrons ejected with energy greater than $\kappa^2 I_H$ at incident energy E_i, which are displayed in figure 7. Only

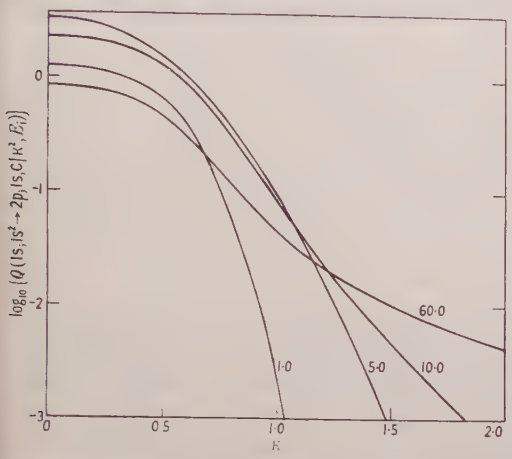

Figure 6. The energy distribution of the ejected electrons. The numbers on the curves give the energy of the incident particle in units of $\mathscr{S}_i^2$.

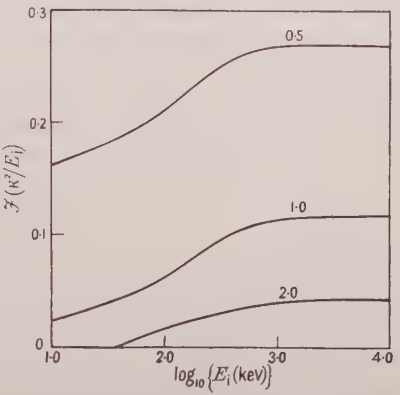

Figure 7. The fraction of ejected electrons which have energy greater than $\kappa^2 I_H$. The numbers on the curves give the relevant values of κ^2.

25% of the electrons have energies greater than $0{\cdot}5 I_H$ and only 10% have energies exceeding one I_H, even at the highest impact energies. While figures 6 and 7 only refer to the $n'l' = 2p$, $nl = 1s$ case, this is dominant at the high energies of interest in auroral studies.

Acknowledgments

We should like to thank Dr. A. Dalgarno and a referee for their helpful comments on an earlier version of this paper. Drs. Branscomb and Fite have kindly allowed us to quote their results before publication. One of us (G. P.) would like to thank the Department of Scientific and Industrial Research for a studentship.

References

Allison, S. K., 1958, *Rev. Mod. Phys.*, **30**, 1137.

Bates, D. R., and Dalgarno, A., 1956, *The Airglow and the Aurorae* (Ed. Armstrong, E. B., and Dalgarno, A., London: Pergamon Press), p. 328.

Bates, D. R., and Griffing, G., 1953, *Proc. Phys. Soc.* A, **66**, 961.

Bates, D. R., and Seaton, M. J., 1949, *Mon. Not. R. Astr. Soc.*, **109**, 698.

Bates, D. R., and Williams, A., 1957, *Proc. Phys. Soc.* A, **70**, 306.

Bethe, H. A., and Salpeter, E. E., 1957, *Handb. der Physik*, **35**, 88 (Berlin: Springer-Verlag).

Boyd, T. J. M., Moiseiwitsch, B. L., and Stewart, A. L., 1957, *Proc. Phys. Soc.* A, **70**, 110.

Brackmann, R. T., Fite, W. L., and Neynaber, R. H., 1958, *Phys. Rev.*, **112**, 1157.

Bransden, B. H., Dalgarno, A., John, T. L., and Seaton, M. J., 1958, *Proc. Phys. Soc.*, **71**, 877.

Chandrasekhar, S., 1944, *Astrophys. J.*, **100**, 176.

Chandrasekhar, S., and Breen, F. H., 1946, *Astrophys. J.*, **104**, 432.

Dalgarno, A., and McDowell, M. R. C., 1956, *Proc. Phys. Soc.* A, **69**, 615.

Gerjuoy, E., 1958, *Proc. Gatlinburg Conference, Section I* (University of Chicago: Enric Fermi Institute).
Khashaba, S., and Massey, H. S. W., 1958, *Proc. Phys. Soc.*, **71,** 574.
Mott, N. F., and Massey, H. S. W., 1949, *Theory of Atomic Collisions*, 2nd Edn (Oxford Clarendon Press).
Rose, P. H., Connor, R. J., and Bastide, R. P., 1958, *Bull. Amer. Phys. Soc.* II, **3,** 40.
Sida, D. W., 1955, *Proc. Phys. Soc.* A, **68,** 240.
Stier, P. M., and Barnett, C. F., 1956, *Phys. Rev.*, **103,** 896.
Whittier, A. C., 1954, *Canad. J. Phys.*, **32,** 275.

Electron Collision Cross Sections in Helium

By D. T. STEWART† and E. GABATHULER†
Physics Department, Queen's University, Belfast

Communicated by K. G. Emeleus; *MS. received 28th April* 1959

Abstract. Electron collision cross sections in helium have been measured by an optical method, using a photoelectric spectrophotometer. The results are in general agreement with those of previous workers. Some values for the cross sections for collisions of the second kind in helium are also given.

In the course of an investigation of the excitation functions of the atmospheric gases, some measurements were made of the electron collision cross sections of helium, to test the experimental techniques. These cross sections had been previously measured by Lees (1932) and Thieme (1932). There are, however, differences between their results. In view of this it was felt that our results, obtained by new photoelectric techniques, and covering more of the spectrum, might be of interest.

The basic experimental arrangement has been described in previous communications (Stewart 1956, Stewart and Gabathuler 1958). The electron gun, which had been designed to provide an intense well-collimated beam of electrons for the investigation of weak bands, did not prove suitable for the study of the initial portions of the excitation functions of the helium lines. Electrical measurements on the electron energy distribution in the beam at pressures less than 10^{-2} mm Hg showed that 95% of the electrons lay within a 2-volt range of the applied accelerating voltage. Nevertheless, in helium, it proved difficult to maintain a collimated beam below about 27 v over a sufficiently wide range of gas pressure and beam current to check that the light from the source was only produced by single electron impact and to be certain of the absence of space charge effects. Above this voltage the beam was well behaved, possibly due to the increasing concentration of positive ions, and the usual tests could be applied to determine the optimum source conditions for the measurement of electron collision cross sections.

The dependence of intensity of the lines on beam current was first investigated over a wide range of conditions; it was found that the intensities of all the lines studied (table 1) were directly proportional to current, indicating that cumulative excitation was absent.

The variation of intensity with pressure was next investigated. It was found that the intensities of the lines of the 2^1P–n^1S, the 2^3S–n^3P and the 2^3P–n^3S series were all directly proportional to pressure, indicating that the n^1S, n^3P and n^3S levels were being mainly populated by single electron impact with the helium atom in the ground state. The lines of the 2^1S–n^1P, 2^1P–n^1D and 2^3P–n^3D series did however exhibit a non-linear variation of intensity with pressure; typical results are shown in figure 1. No measurements were made at pressures greater than 2×10^{-2} mm Hg, as the increasing concentration of slow electrons in the beam tends to become important at higher pressures and makes analysis of results less

† Now at Department of Natural Philosophy, The University, Glasgow.

certain. The anomalous variation of intensity with pressure for the 2^1S–n^1P series is due to the population of the n^1P levels by absorption of 1^1S–n^1P radiation emitted from the beam (Lees and Skinner 1932). In agreement with Lees (1932), we found that much of the light emitted in transitions from the n^1P levels came from regions outside the beam. In fact, at pressures above 1×10^{-2} mm Hg a green halo due to the 2^1S–3^1P line at 5016 Å could be observed around the beam. The explanation of the non-linear variation of intensity with pressure in the case of the 2^1P–n^1D and 2^2P–n^3D series is more complex and requires consideration of the excitation functions for analysis.

Table 1. Electron Collision Cross Sections $Q_{jk(\max)}$ of the Lines measured at the Electron Energy $E_{\max}$ of the Maximum Probability of Excitation

Transition	Line (Å)	$Q_{jk(\max)} \times 10^{-20}$ cm^2 ($E_{(\max)}$) Lees	Thieme	Stewart and Gabathuler
2^1S–3^1P	5016	100 (100)	84 (100)	94·6 (100)
2^1S–4^1P	3965	34 (100)	29 (100)	23·5 (100)
2^1S–5^1P	3613	5·7 (100)	—	2·8 (100)
2^1S–6^1P	3447	—	—	1·3 (100)
2^1P–4^1S	5047	—	16·5 (40)	16·3 (36)
2^1P–5^1S	4437	2·8 (36)	8·1 (37)	4·9 (36)
2^1P–6^1S	4169	1·2 (36)	4 (35)	2·6 (36)
2^1P–4^1D	4922	11·0 (74)	23 (50)	17·4 (45)
2^1P–5^1D	4388	6·0 (74)	12 (50)	7·9 (45)
2^1P–6^1D	4143	—	6 (50)	4·2 (45)
2^1P–7^1D	4009	—	2·5 (50)	2·1 (45)
2^1P–8^1D	3926	—	—	1·4 (45)
2^3S–3^3P	3889	72 (32)	1700 (30)	95 (32)
2^3S–4^3P	3188	—	—	10·3 (32)
2^3P–4^3S	4713	21 (30)	38 (30)	21·9 (30)
2^3P–5^3S	4121	4·1 (30)	19 (30)	8·2 (30)
2^3P–6^3S	3867	—	9 (30)	3·2 (30)
2^3P–7^3S	3732	—	—	1·4 (30)
2^3P–3^3D	5875	—	42 (30)	44·9 (35)
2^3P–4^3D	4472	12 (34)	18 (30)	14 (35)
2^3P–5^3D	4026	—	—	5·1 (35)
2^3P–6^3D	3820	—	—	2·7 (35)
2^3P–7^3D	3705	—	—	2·2 (35)
2^3P–8^3D	3634	—	—	1·16 (35)
2^3P–9^3D	3578	—	—	0·5 (35)

The numbers in brackets are the voltages for maximum cross sections.

There is good general agreement between the forms of the excitation functions of the various series found in the present investigation (Gabathuler 1957) and by Lees and Thieme, the only serious disagreement being for the 2^1P–n^1D lines. Typical excitation functions of this series at different pressures are shown in figure 2. At a pressure of 3×10^{-3} mm Hg figure 1 shows that the 4^1D level is mainly populated by direct electron impact, and therefore curve A in figure 2, which is

similar to that found by Thieme, gives nearly the true electron excitation function. However, at 8×10^{-3} mm Hg (curve B) where the n^1D levels are evidently being partly populated by some secondary process, the apparent excitation function exhibits a secondary maximum centred around 100 volts, of which there is in fact a

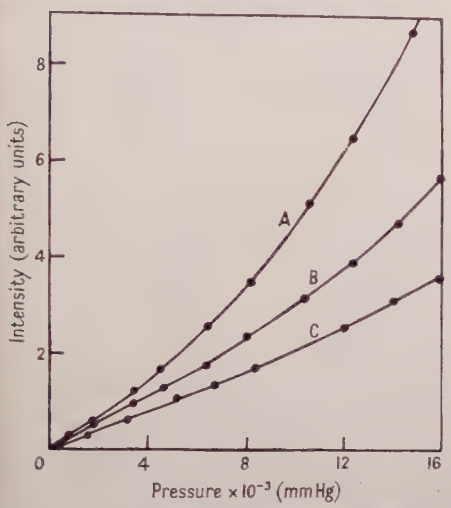

Figure 1. Intensity plotted against pressure at an electron energy of 100 v for:
A, (2^1S–3^1P) line at 5016 Å
B, (2^1P–4^1D) line at 4922 Å
C, (2^3P–4^3D) line at 4472 Å

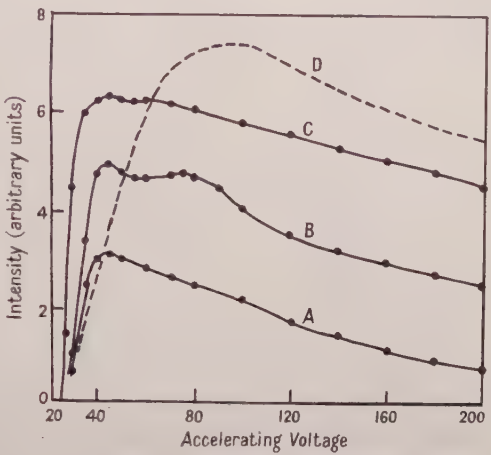

Figure 2. Relative excitation functions of the 2^1P–4^1D line at a pressure of:
A, 3×10^{-3} mm Hg
B, 8×10^{-3} mm Hg
C, $1{\cdot}5 \times 10^{-2}$ mm Hg
Curve D illustrates the relative excitation function of the 2^1S–3^1P line.

small trace in A. Curve C obtained at $1{\cdot}5 \times 10^{-2}$ mm Hg resembles that found by Lees. As the only levels in helium which have a maximum probability of excitation greater than 50 v are the n^1P levels, this, together with work by Wolf and Maurer (1940), suggests that the n^1D levels can be populated via n^1P levels by the process

$$\mathrm{He}(n^1\mathrm{P}) + \mathrm{He}(1^1\mathrm{S}) \rightarrow \mathrm{He}(1^1\mathrm{S}) + \mathrm{He}(n^1\mathrm{D}).$$

The energy defect between the ^1P levels and the ^1D levels of the same n, of the order of a few millivolts, can be supplied by the thermal kinetic energies of the colliding atoms. A similar process (Lees and Skinner 1932) can account for the indirect population of n^3D levels:

$$\mathrm{He}(n^1\mathrm{P}) + \mathrm{He}(1^1\mathrm{S}) \rightarrow \mathrm{He}(1^1\mathrm{S}) + \mathrm{He}(n^3\mathrm{D}).$$

The maximum values of the cross sections Q_{jk} for electron excitation of the lines are given in table 1, together with the values found by Lees and Thieme. The observed values of electron energy for maximum probability of excitation are also given in each case. Where comparison is possible (neglecting the value of Thieme for the 2^3S–3^3P line which is obviously in error) it can be seen that in general our values lie between those of Lees and Thieme.

The cross sections at maximum probability of excitation of the upper levels of these lines, derived from our measurements and using calculated values of transition probability (Hylleraas 1937, Goldberg 1939, Bates and Damgaard 1950, Dalgarno and Lynn 1958, private communication) are shown in table 2.

Table 2. Cross Sections $Q_{j(\max)}$ for Excitation of the Helium Levels derived from the Cross Sections $Q_{jk(\max)}$ given in table 1

Level	$Q_{j(\max)} \times 10^{-20}$ cm^2	Level	$Q_{j(\max)} \times 10^{-20}$ cm^2
3^1P	4477	3^3P	106·6
4^1P	942	4^3P	12
5^1P	103		
6^1P	43·3	4^3S	37·1
		5^3S	18·9
4^1S	26	6^3S	6·2
5^1S	10·4		
6^1S	6·2	3^3D	44·9
		4^3D	17·8
4^1D	23·8	5^3D	7·3
5^1D	12·2	6^3D	4·0
6^1D	6·4	7^3D	3·2
7^1D	3·3	8^3D	1·7
8^1D	2·2	9^3D	0·75

Recently, Frost and Phelps (1958) have analysed all available experimental data for the rates of excitation to the principal levels in helium. Cross sections derived from this analysis are in good agreement with the values reported here, apart from those for the n^1P levels. In this case an analysis of the effects of the imprisonment of the 1^1S–n^1P radiation (Phelps 1958) suggests that our values of cross sections of these levels are too large by a factor of approximately ten. Although figure 1 does indicate that there is little indirect population of the n^1P levels at pressures less than 5×10^{-3} mm Hg, the lower values are in better agreement with calculations based on the Born approximation (Massey 1957).

Since the dependence of intensity on pressure for the 2^1P–n^1D and 2^3P–n^3D lines was linear at low pressures, an estimate can be made of the rates of population of the n^1D and n^3D levels, due to the transfer reactions, from the departure from linearity at higher pressures. The cross sections for these collisions of the second kind can then be found, as the populations of the parent n^1P levels can be calculated from known excitation cross sections and transition probabilities (Gabathuler 1957). The transfer cross sections are given in table 3, together with the values measured by Wolf and Maurer (1940) using a basically similar method.

Table 3. Cross Sections for Transfer Reactions in Helium

(1)	(2)	(3)	(4)
4^1P–4^1D	0·006	67	12·3
4^1P–4^3D	0·006	15	2·6
5^1P–5^1D	0·003	51	76·0
5^1P–5^3D	0·003	27	11·9

(1) Reaction; (2) resonance discrepancy (ev); (3), (4) cross section (10^{-15} cm^2): (3) Wolf and Maurer, (4) present experiment.

It can be seen that the Wigner spin rule is partially obeyed, the ratio between cross sections for transfer to triplet and singlet levels of the same n being 1 to 5 or 6. These transfer reactions occur in a two body collision and should be strongly resonant near zero energy difference. This is borne out by the results, as a

reduction by a factor of two in the energy discrepancy gives approximately a six-fold increase in the cross sections in both cases.

Acknowledgments

We would like to express our gratitude to Professor K. G. Emeleus for guidance and encouragement. Our thanks are also due to Dr. A. Dalgarno and Dr. A. V. Phelps for stimulating discussions on this work.

References

Bates, D. R., and Damgaard, A., 1950, *Phil. Trans. Roy. Soc.* A, **242,** 101.
Frost, L. S., and Phelps, A. V., 1958, Westinghouse Research Report.
Gabathuler, E., 1957, *M.Sc. Thesis*, Queen's University, Belfast.
Goldberg, L., 1939, *Astrophys. J.*, **90.** 414.
Hylleraas, E. A., 1937, *Z. Phys.*, **106,** 395.
Lees, J. H., 1932, *Proc. Roy. Soc.* A, **137,** 173.
Lees, J. H., and Skinner, H. W. B., 1932, *Proc. Roy. Soc.* A, **137,** 186.
Massey, H. S. W., 1957, *Handbuch der Physik*, Vol. 36 (Berlin: Springer).
Phelps, A. V., 1958, *Phys. Rev.*, **110,** 1363.
Stewart, D. T., 1956, *Proc. Phys. Soc.* A, **69,** 437.
Stewart, D. T., and Gabathuler, E., 1958, *Proc. Phys. Soc.*, **72,** 287.
Thieme, O., 1932, *Z. Phys.*, **78,** 412.
Wolf, R., and Maurer, W., 1940, *Z. Phys.*, **115,** 410.

RESEARCH NOTES

The Decay of ^{147}Pm

By R. JAKEWAYS and W. G. V. ROSSER
Physics Department, The University, Exeter

MS. received 11*th May* 1959

It is known that ^{147}Pm is practically a pure β-emitter decaying to ^{147}Sm with a maximum energy of 226 kev and a half-life of 2·65 years. Accompanying the β-decay there is a continuous spectrum of γ-rays due to internal and external bremsstrahlung. During an investigation of internal bremsstrahlung Lederer and Langevin-Joliot (1956) observed several discrete γ-rays accompanying the continuous γ-spectrum from ^{147}Pm obtained from fission fragments. Most of these were removed by paper chromatography and were identified as cerium and europium impurities. However a γ-ray of energy 121 kev having an intensity of $(3{\cdot}0 \pm 0{\cdot}5) \times 10^{-5}$ photons per β-decay remained. The half-life of this activity was found to be comparable with that of the β-activity. A similar γ-ray having the same intensity was reported by Starfelt and Cederlund (1957). In the 'Table of Isotopes' (Strominger, Hollander and Seaborg 1958) it was left as a query whether or not some of the β decays of ^{147}Pm go via an excited level at 121 kev in ^{147}Sm. The purpose of the present work was to investigate this possibility using β–γ coincidence techniques.

A sample of ^{147}Pm was obtained from the Radiochemical Centre, Amersham, in the form of a solution in 1N HCl. A source was prepared by evaporating a few drops of this solution on to a thin mica disc. The source was covered with a collodion film. The β-rays were observed with a $1\frac{1}{4}$ in. $\times \frac{1}{8}$ in. NE 102 phosphor and the γ-rays with a $1\frac{1}{2}$ in. $\times$ 2 in. NaI(Tl) crystal used in conjunction with EMI type 9514B photomultipliers. A resolving time of 3×10^{-8} second was used and a 30-channel kicksorter was available to measure energy spectra.

Observations of the single γ-ray spectrum showed that the 121 kev γ-ray was present in the same proportion in our sample as reported by Lederer and Langevin-Joliot (1956) and by Starfelt and Cederlund (1957). If this γ-ray arose via β-decay to an excited level at 121 kev in ^{147}Sm the end point of the energy spectrum of β-rays in coincidence with γ-rays of 121 kev should be about 100 kev. The end point of the β-spectrum in coincidence with internal bremsstrahlung of the same energy should also be about 100 kev. The energy spectrum of β-rays in coincidence with γ-rays in the region 110–130 kev showed in addition to a spectrum with an end point below 200 kev, a high energy spectrum with an end point of $2{\cdot}0 \pm 0{\cdot}2$ Mev. This suggested that the 121 kev γ-rays were in coincidence with high energy β-rays.

To check this, the spectrum of γ-rays in coincidence with all β-rays was observed, different thicknesses of aluminium absorbers being placed between the source and the β-counter. Typical results are shown in the figure. The intensity of the 121 kev peak is hardly reduced with use of an absorber of 45 mg cm^{-2}, which is sufficient to absorb all β-rays below 200 kev, whereas the

continuous spectrum due to bremsstrahlung has disappeared. It is reasonable to conclude that all the 121 kev γ-rays are in coincidence with β-rays of maximum energy about 2 Mev, and so cannot arise from the decay of ^{147}Pm.

It can be seen from the figure that in addition to the 121 kev γ-ray there are peaks at approximately 80 kev and 40 kev, the latter being possibly an x-ray, the intensity of which would indicate that the conversion coefficient of the121kev γ-ray is not large. Some γ-rays were observed above 150 kev in the coincidence spectrum using an integral discriminator but the intensity was too low to make any detailed measurements.

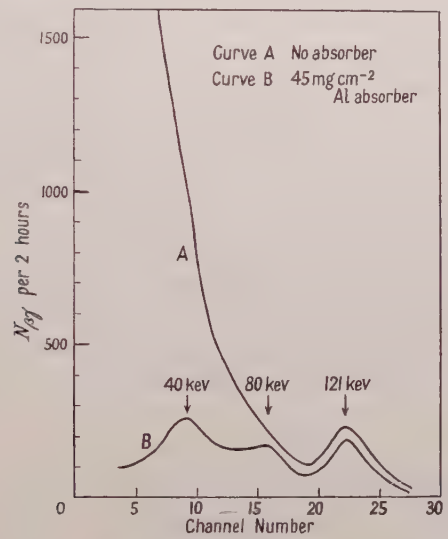

The high energy β-spectrum was observed by counting single β-particles, the end point of this spectrum was also in the region of 2 Mev. The intensity was comparable with that in coincidence with the 121 kev γ-ray suggesting that a substantial proportion of the β-decays of the unidentified nucleus were in coincidence with this γ-ray.

From energy considerations the 121 kev γ-ray cannot arise during the β-decay of ^{147}Pm to ^{147}Sm. The only reported β^- unstable promethium isotope with a comparable lifetime is ^{146}Pm. Little is known of its decay scheme although the results reported by Kistiakowsky (1952) and Long, Pool and Kundu (1952) suggest that the end point of its β-spectrum is around 0·7 Mev. No conclusion can be made of the origin of the 121 kev γ-ray other than that it does not arise from the decay of ^{147}Pm.

References

Kistiakowsky, V., 1952, *Phys. Rev.*, **87**, 859.
Lederer, J., and Langevin-Joliot, H., 1956, *J. Phys. Radium*, **17**, 497.
Long, J. K., Pool, M. L., and Kundu, D. N., 1952, *Phys. Rev.*, **88**, 171(A).
Starfelt, N., and Cederlund, J., 1957, *Phys. Rev.*, **105**, 241.
Strominger, D., Hollander, J. M., and Seaborg, G. T., 1958, *Rev. Mod. Phys.*, **30**, 585.

Vacuum Polarization due to Charged Bosons

By J. G. GILSON
Chelsea College of Science and Technology, London

MS. received 24*th March* 1959, *in final form* 27*th May* 1959

§ 1. Introduction

Euwema and Wheeler (1956) have calculated the vacuum polarization effect of the electron positron field using a dispersion relation. In their paper they remark on the simplicity of the method. This paper is similar in principle to their paper and much simpler. Here we calculate the boson field polarization effect. The more complicated interaction Hamiltonian for the boson case does not complicate the procedure. This is partly due to the choice of a particularly simple external electric field. That the choice of the external field is at our disposal is because the vacuum polarization constant is independent of the external field amplitude in the first approximation. The other point of difference is that by renormalizing the complex dielectric constant as a whole and not just its real component, we find that the convergence factor introduced in the Euwema–Wheeler paper is unnecessary. This last simplification can also be used in the fermion case.

§ 2. Discussion

The interaction Hamiltonian for a boson in an external electromagnetic field is (Wentzel 1949)

$$H' = -ieA_1\left(\frac{\partial\phi^*}{\partial x}\phi - \frac{\partial\phi}{\partial x}\phi^*\right) + e^2\phi^*\phi A_1{}^2,$$

if we use the one component field

$$A_1 = (E/\omega)\sin\omega t, \quad A_2 = A_3 = A_4 = 0.$$

Expanding $\phi(x)$ in terms of boson destruction and anti-boson creation operators, we can write

$$\phi(x) = (2\pi)^{-3/2}\int (2p_0)^{-1/2}\, d^3p\{a(p)\,e^{ipx} + b^*(p)e^{-ipx}\}. \qquad \ldots\ldots(1)$$

Now

$$\int H'\,d^4x = -ie\int A_1\left(\frac{\partial\phi^*}{\partial x}\phi - \frac{\partial\phi}{\partial x}\phi^*\right)d^4x, \qquad \ldots\ldots(2)$$

where the term in e^2 has been neglected because we require the probability correct only to the second order in e. Hence substituting 1 into 2 we find the total coefficient of a^*b^* and b^*a^* to be

$$\frac{\pi eE}{\omega}\int(-ip_1)(p_0p_0')^{-1/2}\,\delta^4(p+p'-\omega)\,d^3p\,d^3p'.$$

The integrand here is the amplitude for the production of a pair in the range $d^3p\,d^3p'$. Since we are taking no account of vacuum to vacuum effects the total number of pairs produced over the whole of space time is

$$\left(\frac{\pi eE}{\omega}\right)^2\int p_1{}^2(p_0p_0')^{-1}\,[\delta^4(p+p'-\omega)]^2\,d^3p\,d^3p'. \qquad \ldots\ldots(3)$$

After carrying out the integrations in (3), using the fact that the particles are on the mass shell, and dividing out the interaction four-volume, we obtain for the number of pairs produced per unit space–time volume

$$[(eE)^2/48\pi]\,\omega^{-3}\,(\omega^2-4m^2)^{3/2}\,\theta\,(|\omega|-2m).$$

The step function arises from the dp_0 integration. Each pair production event transfers an amount of energy $2p_0=\omega$ from the electric field to the boson field. Therefore the total energy transformed is

$$[(eE)^2/48\pi]\,\omega^{-2}\,(\omega^2-4m^2)^{3/2}\,\theta\,(|\omega|-2m),$$

which by the theory of dielectrics (Fröhlich 1958) is equal to $(E^2/8\pi)\,\epsilon_2(\omega)\omega$ since $E(t)=(\partial/\partial t)\,A(t)=E\cos\omega t$. Hence

$$\epsilon_2(\omega)=\tfrac{1}{6}e^2\,\omega^{-3}\,(\omega^2-4m^2)^{3/2}\,\theta\,(|\omega|-2m). \qquad \ldots\ldots(4)$$

Now for causality (Toll 1956) to hold $\epsilon(\omega)$, the complex dielectric constant, must be analytic in the upper complex ω plane. Therefore if we take a contour C indented at the point ω on the real axis and composed of the real axis and a large semicircle in the upper complex u plane, Cauchy's formula gives

$$\epsilon(\omega)=(\pi i)^{-1}\mathscr{P}\int_C\frac{\epsilon(u)\,du}{u-\omega}.$$

We renormalize at this stage, by subtracting the constant $\epsilon(0)$. That is

$$\epsilon(\omega)-\epsilon(0)=(\pi i)^{-1}\mathscr{P}\int_C\frac{\epsilon(u)\,\omega du}{u(u-\omega)}.$$

Taking the real part of this, we obtain

$$\epsilon_1(\omega)-\epsilon_1(0)=\pi^{-1}\mathscr{P}\int_{-\infty}^{+\infty}\frac{\epsilon_2(u)\,\omega du}{u(u-\omega)}, \qquad \ldots\ldots(5)$$

where we have assumed for the moment that $\epsilon(u)$ is not more divergent than $\log u$ so that the contribution of the large semicircle is zero. Substituting (4) into (5) we obtain

$$\epsilon_1(\omega)-\epsilon_1(0)=(e\omega)^2\,(3\pi)^{-1}\int_{2m}^{\infty}\frac{(u^2-4m^2)^{3/2}\,du}{u^4\,(u^2-\omega^2)}.$$

This is easily evaluated by means of the substitution $u=2m\,(1-T^2)^{-1/2}$, the final result being

$$\epsilon_1(\omega)-\epsilon_1(0)=e^2(3\pi)^{-1}\left[\frac{4}{3}-4m^2\omega^{-2}+\frac{1}{2}\,(1-4m^2\omega^{-2})^{3/2}\log\left|\frac{1-(1-4m^2\omega^{-2})^{1/2}}{1+(1-4m^2\omega^{-2})^{1/2}}\right|\right]. \qquad \ldots\ldots(6)$$

We now see from (4) and (6) that the assumption that $\epsilon(u)$ is not more divergent than $\log u$ is indeed justified.

Acknowledgment

The author wishes to thank Dr. S. Zienau for valuable discussions.

References

Euwema, R. W., and Wheeler, J. A., 1956, *Phys. Rev.*, **103**, 803.

Fröhlich, H., 1958, *Theory of Dielectrics* (Oxford: Clarendon Press), p. 14.

Toll, J. S., 1956, *Phys. Rev.*, **104**, 1760.

Wentzel, G., 1949, *Quantum Theory of Fields* (New York: Interscience Publishers), p. 69.

A Measurement of the Spin Correlation Coefficient C_{nn} in p–p Scattering at 320 MeV, for 90° Centre of Mass Scattering Angle

By J. V. ALLABY, A. ASHMORE, A. N. DIDDENS and J. EADES
Nuclear Physics Research Laboratory, University of Liverpool

MS. received 25th May 1959

Spin correlation measurements in p–p scattering at 382 MeV for 90° centre-of-mass scattering angle have been made of the coefficients C_{nn} (Ashmore, Diddens, Huxtable and Skarsvåg 1958) and C_{KP} (Ashmore, Diddens and Huxtable 1959). Owing to the uncertainty of the variation of the coefficients with energy these results cannot be used to distinguish between sets 1 and 2 of the modified phase shift analysis at 310 MeV (Cziffra, MacGregor, Moravcsik and Stapp 1958). The measurement of C_{nn} at 320 MeV was undertaken to make a more direct comparison with the predictions of these sets of phase shifts.

The energy of the external proton beam from the synchrocyclotron was reduced by means of a polyethylene absorber placed close to the cyclotron tank. Scattering in the absorber reduced by a factor of the order of 10 the intensity of the beam collected by the bending magnet and focused in the experimental area. Also the focused spot was considerably larger than for the full energy beam and the background was higher. By modifications to the beam collimators and the introduction of extra shielding, satisfactory running conditions were established for a proton energy of 320 MeV using the full circulating beam in the cyclotron.

The experimental arrangement and procedure were almost the same as in the previous measurements. For the measurement of the analysing powers of the second scatterings from carbon a polarized beam was produced by scattering at an angle of 20·2° from carbon. This angle was chosen on the basis of data from Uppsala and Harwell, and the polarization estimated to be $0{\cdot}93 \pm 0{\cdot}03$ after correcting for angular resolution and inelastic scattering. The observed asymmetries for the two analysers, corrected for the intensity distribution across the second targets, were $0{\cdot}411 \pm 0{\cdot}012$ and $0{\cdot}426 \pm 0{\cdot}012$. Dividing by the initial polarization and correcting for the different contribution from inelastic scattering in the measurement of C_{nn}, the analysing powers were found to be $P_1 = 0{\cdot}427 \pm 0{\cdot}020$ and $P_2 = 0{\cdot}442 \pm 0{\cdot}020$. These are rather lower than would have been expected from Harwell data.

For the measurement of C_{nn} a beam of about $0{\cdot}8 \times 10^9$ protons per second was used in a spot about 1 in. square at the 1 in. diameter hydrogen target. As in the measurement of C_{nn} at 382 MeV the first scintillators were 2 in. high, but their width was increased to 0·75 in. The energy resolution was 7·2 MeV, and the angular resolutions in the first and second scatterings 1·0° and 3·3°. All these figures are standard deviations. In about 185 hours running a total of 4929 coincidence counts was obtained of which 355 were estimated to be random coincidences. The genuine coincidences were divided between the four positions as follows.

LL	1330 ± 40	LR	924 ± 32
RR	1331 ± 40	RL	989 ± 35

These give an asymmetry $\dfrac{\mathrm{LL}+\mathrm{RR}-\mathrm{LR}-\mathrm{RL}}{\mathrm{LL}+\mathrm{RR}+\mathrm{LR}+\mathrm{RL}} = +0{\cdot}163 \pm 0{\cdot}016.$

The correction arising from the geometry of the first scattering was estimated to be $-0{\cdot}021 \pm 0{\cdot}005$, giving a corrected asymmetry $e = +0{\cdot}142 \pm 0{\cdot}017$. Then from $C_{nn} = e/P_1P_2$, $C_{nn} = +0{\cdot}75 \pm 0{\cdot}11$.

The values predicted for C_{nn} at 310 MeV from the modified phase shift analysis of Cziffra, MacGregor, Moravcsik and Stapp (1958) are

Set 1	$+0{\cdot}38 \pm 0{\cdot}08$
Set 2	$+0{\cdot}61 \pm 0{\cdot}06$

Thus from the present measurement alone set 2 is preferred. But when this result is combined with the other experimental data in the phase shift analysis both sets will give goodness of fit parameters just within the range of 50% probability.

Acknowledgments

The authors wish to thank Professor H. W. B. Skinner and Professor J. M. Cassels for their interest and encouragement, and the cyclotron crew for their helpful co-operation; A.N.D. is indebted to CERN for the provision of a fellowship; J.V.A. and J.E. are indebted to the Department of Scientific and Industrial Research for the provision of maintenance grants.

References

Ashmore, A., Diddens, A. N., and Huxtable, G. B., 1959, *Proc. Phys. Soc.*, **73**, 957.

Ashmore, A., Diddens, A. N., Huxtable, G. B., and Skarsvåg, K., 1958, *Proc. Phys. Soc.*, **72**, 289.

Cziffra, P., MacGregor, M. H., Moravcsik, M. J., and Stapp, H. P., 1958, *University of California Radiation Laboratories Report* No. 8510.

The Response of Plastic Scintillators to Protons

By H. C. Evans and E. H. Bellamy

Natural Philosophy Department, University of Glasgow

MS. received 11*th May* 1959

The fluorescent response of organic scintillators to heavily ionizing particles is known to be non-linear. Birks (1951, 1953) has expressed the specific fluorescence dS/dr in organic crystals as a function of specific energy loss dE/dr as

$$\frac{dS}{dr} = \frac{A\,dE/dr}{1 + kB\,dE/dr} \qquad \ldots\ldots(1)$$

A and kB being constants for a given scintillator.

Birks interprets the scintillation phenomena in organic crystals in terms of primary emission by ion recombinations and molecular de-excitation processes. The non-linear dependence of dS/dr on dE/dr is due to quenching of the primary emission in the ionization column. $A\,dE/dr$ represents the number of ionized or excited molecules per unit path length capable of primary emission, and $kB\,dE/dr$ represents the probability of quenching relative to the probability of primary emission.

In organic solution phosphors or phosphor-plastic mixtures, the primary emission is by the solvent or base, and the values of A and kB would be expected to depend upon the nature of the base and the fluorescent material and its concentration. The variation of these constants with concentration has been investigated by Harrison (1952) for liquid solutions of p-terphenyl.

The response of a plastic scintillator has been investigated by Boreli and Grimeland (1955) who assumed equation (1) to be true and made use of the two limiting cases, $kB\,dE/dr \ll 1$ applicable to electrons giving $S = AE$, and $kB\,dE/dr \gg 1$ applicable to slow α-particles giving $S = rA/kB$. They obtained a value of $kB = 10{\cdot}5$ cm air equivalent per MeV (equivalent to $1{\cdot}1 \times 10^{-2}$ g cm^{-2} MeV^{-1} if the air equivalent range is defined at 15°C and 760 mm Hg). The scintillator used (of French manufacture) was tetraphenyl 1, 1, 4, 4, butadiene 1, 3 in polystyrene.

Since plastic scintillators are often used to detect and measure the energies of nuclear particles, and in many applications the energy determination depends upon an extrapolation from a calibration using the response to electrons or nuclear particles of known energy, it was decided to check the applicability of formula (1) and to determine, if formula (1) was found to be obeyed by the plastic scintillators, the value of kB for a commercially available plastic. These latter more commonly use a polyvinyltoluene base rather than the polystyrene base of the scintillator used by Boreli and Grimeland.

Protons of initial energy 14·8 MeV were obtained from the reaction $d + {}^3He \rightarrow p + {}^4He$ using deuterons accelerated in a Cockcroft–Walton high-voltage machine. The ^{3}He was present as a decay product in a tritium target. To reduce the background due to knock-on protons from the high flux of neutrons present, the protons were detected in a coincidence counter telescope. The front counter was a thin proportional counter, which gated the output of the scintillation counter, the latter being displayed on a 100 channel kicksorter. The energy of the protons entering the plastic scintillator was varied by interposing aluminium absorbers between the two counters. The pulse height distributions for protons at nine energies between $14{\cdot}0 \pm 0{\cdot}4$ MeV and $3{\cdot}08 \pm 0{\cdot}18$ MeV were determined in this way. The pulse height distribution for protons of energy $1{\cdot}2 \pm 0{\cdot}1$ MeV was obtained using protons from the reaction, $^{12}C + d \rightarrow {}^{13}C + p$.

The response of the scintillator to protons was normalized to the electron response using the Compton edges from the 2·62 MeV thorium γ-rays and the 1·28 MeV ^{22}Na γ-rays.

The range energy tables of Atkinson and Willis (1957) were used to determine the residual energy of the protons entering the scintillator.

The experimental points for NE.102 plastic scintillator (Nuclear Enterprises G.B. Ltd.), of which a sample 2 in. in diameter and $\frac{1}{2}$ in. thick was used, are shown in the figure. A 2 in. long Perspex light guide was interposed between the scintillator and an RCA type 6810 photomultiplier.

The pulse height scale has been normalized using the γ-ray data, so that the pulse height from a 1 MeV electron is unity.

The solid and broken curves in the figure have been calculated from equation (1) using the values of kB indicated in the figure. The range–energy relationship in the plastic was taken as that for CH given by the tables of Rich and Madey (1954). For NE.102 the best fit is seen to be for a value of $kB = 1{\cdot}0 \times 10^{-2}$ g cm^{-2} MeV^{-1}.

The response of a second sample of plastic scintillator of 3 in. diameter and 2 in. thick, also having a polyvinyltoluene base, but manufactured by Messrs. Nash

and Thompson Ltd. (originally purchased in 1956 and not current stock) was best fitted with $kB = 1{\cdot}1 \times 10^{-2}$ g cm^{-2} MeV^{-1}.

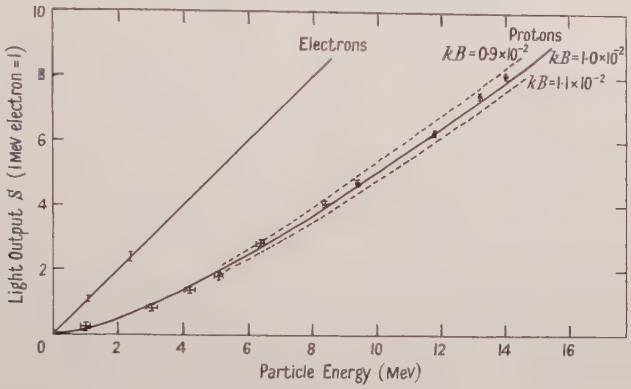

Response of plastic scintillator NE.102 to electrons and protons.

It is seen from the figure that equation (1) quite accurately gives the response of the plastic scintillator, and it may be noted that the values of kB obtained for the two samples used, and also that used by Boreli and Grimeland, differ only slightly. Since the concentration of fluorescent material used by the manufacturers is generally chosen to optimize the light output, and since samples using both polystyrene and polyvinyltoluene bases behave similarly, it is plausible that similar values of kB would apply to all such plastic scintillators. Uncertainties in the value of kB of about 10% lead to small inaccuracies in proton energy measurement using electron calibration as can be seen from the table.

Electron Equivalent Pulse Height from Protons

E_p (MeV)	1	5	10	20	50	100
$S(kB = 1{\cdot}1 \times 10^{-2})$	0·19	1·81	4·82	12·06	37·26	82·70
$S(kB = 1{\cdot}0 \times 10^{-2})$	0·20	1·91	5·03	12·45	37·96	83·70

The error due to such uncertainty in kB for high-energy protons is even further reduced if protons of energy about 10 MeV for example are used for calibration. Such a calibration together with an electron calibration would readily check on the value of kB for any given scintillator.

Acknowledgment

We are grateful to Mr. W. Jack who kindly provided both the tritium target and the deuteron beam. One of us (H.C.E.) is indebted to the National Research Council of Canada for grants held.

References

Atkinson, J. H., Jr., and Willis, B. H., 1957, *High Energy Particle Data*, Vol. II, URCL. 2426 (U.S. Atomic Energy Commission).

Birks, J. B., 1951, *Proc. Phys. Soc.* A, **64**, 874.

—— 1953, *Scintillation Counters* (London: Pergamon Press).

Boreli, F., and Grimeland, B., 1955, *Nuovo Cim.*, **2**, 336.

Harrison, F. B., 1952, *Nucleonics*, **10**, No. 6, 40.

Rich, M., and Madey, R., 1954, *Range Energy Tables*, URCL. 2301 (U.S. Atomic Energy Commission).

The Entropy of a Non-Equilibrium Ideal Quantum Gas

By P. T. LANDSBERG
Department of Natural Philosophy, Marischal College, Aberdeen

MS. received 20*th April* 1959, *in revised form* 28*th May* 1959

It is usual to write for the entropy of an ideal Fermi gas

$$S = -\boldsymbol{k}\sum_j [(1-n_j)\ln(1-n_j)+n_j \ln n_j] \qquad \ldots\ldots (1)$$

where $\boldsymbol{k}$ is Boltzmann's constant, n_j the mean occupation number of the jth quantum state, and the summation is over all single particle quantum states. This result is valid in equilibrium. In the presence of interactions between the particles, and in non-equilibrium situations, it has often been assumed to remain valid, provided the departure from the case of an ideal gas in equilibrium is not too great. In such theories equation (1) is sometimes fundamental, and it is therefore worth while to examine its range of validity. We shall show that in fact (1) follows very simply for equilibrium and for certain non-equilibrium situations from the entropy concept as developed in information theory.

One can derive (1) from the grand canonical distribution, by the observation that, in a usual notation,

$$TS = U-\mu N+pV = \sum_j \left\{ \frac{e_j-\mu}{t_j^{-1}+1} + \boldsymbol{k}T\ln(1+t_j) \right\}. \qquad \ldots\ldots (2)$$

Here e_j is the energy of the jth single particle quantum state, $t_j \equiv \exp(\mu-e_j)/\boldsymbol{k}T$, and μ is the chemical potential. We have here used the connection between pV and the grand partition function. Use of

$$n_j = 1/(t_j^{-1}+1) \qquad \ldots\ldots (3)$$

in (2) yields (1). This derivation, though exact, is confined to equilibrium. In the absence of equilibrium it is usual (see, for instance Landau and Lifshitz 1958) to group a large number G_j of quantum states together, and to assume that N_j particles are in this group. The number of distinct ways of achieving this is $W_j \equiv G_j!/N_j!\,(G_j-N_j)!$. Assuming that the different groups can be occupied independently, the total number of states compatible with the given specification is $W = \Pi_j W_j$. If each of these states has the same *a priori* probability, one can write $S = \boldsymbol{k}\ln W$, assume $G_j - N_j \gg 1$, $N_j \gg 1$, use Stirling's approximation, and one then arrives at (1) if $n_j \equiv N_j/G_j$. The assumption of equal *a priori* probabilities is not self evident away from equilibrium, and there are other reasons why the procedure is not altogether satisfying (Landsberg 1954).

Instead, we assume here the properties of the entropy which are normally adopted when proving the uniqueness theorem of information theory (see, for instance, Khinchin 1957). These are that, given a set of probabilities $P_1, P_2, \ldots, P_n$, there exists a function $S(P_1, \ldots, P_n)$ called entropy. It has the properties

$$S(P_1, \ldots, P_n) \leqslant S(n^{-1}, \ldots, n^{-1}), \qquad \ldots\ldots (4)$$

$$\underbrace{S(P_1, \ldots, P_n, 0)}_{n+1 \text{ states}} = \underbrace{S(P_1, \ldots, P_n)}_{n \text{ states}}. \qquad \ldots\ldots (5)$$

Condition (4) asserts that the entropy is a maximum when the accessible states are equally likely. This corresponds to an equilibrium state of an isolated system. Condition (5) implies that the inaccessible states do not affect the entropy. There is a third assumption which implies, among other things, that if two probability schemes $P_1, \ldots, P_n$; $Q_1, \ldots, Q_m$ are independent, then for the compound scheme in which both types of events can occur, the entropy is simply the sum of the two entropies. From these three assumptions one finds for any probability scheme $P_1, P_2, \ldots, P_n$,

$$S = -k \sum_i P_i \ln P_i \qquad \ldots\ldots (6)$$

which is unique, apart from the choice of a constant k greater than zero. The idea that entropy is a concept which applies to a probability distribution will now be utilized. It will be assumed that this entropy is consistent with the entropy of thermodynamics, and k will be identified as Boltzmann's constant $\boldsymbol{k}$.

Let P_i in (6) be interpreted as the probability $P(N_1, N_2, \ldots)$ of finding N_1 particles in the single particle quantum state 1, N_2 in state 2, etc., so that the summation in (6) is over all admissible sets of numbers $N_1, N_2, \ldots$. If the probability distributions $p_j(N_j)$ of finding N_j particles in the jth quantum state are independent,

$$P(N_1, N_2, \ldots) = p_1(N_1) p_2(N_2) \ldots \qquad \ldots\ldots (7)$$

and (6) becomes

$$S = -\boldsymbol{k} \sum_j \sum_{N_j=0} p_j(N_j) \ln p_j(N_j), \quad \text{where} \sum_{N_j=0} p_j(N_j) = 1 \text{ for all } j. \qquad \ldots\ldots (8)$$

The summations are over all permitted occupation numbers. The assumption (7) implies that the system is in contact with an energy and a particle reservoir.

In the case of fermions $N_j = 0$ or 1, and $p_j(1)$ is the mean occupation number, whence (8) yields immediately (1) which, assuming (7) and the uniqueness theorem, is an *exact* result. The equi-probability of states in the non-equilibrium situation has not been assumed, nor has a restriction been made to small departures from equilibrium. Note, incidentally, that maximization of (1), subject to a given mean total number of particles and a given mean energy, yields the usual equilibrium Fermi distribution. The distribution laws for ensembles, Stirling's approximation, or the grouping of quantum states are not required for this deduction. The approach to equilibrium is regarded as a process in which the mean occupation numbers for different quantum states come into equilibrium with each other.

In the Bose case the argument is not quite as elegant. One has to assume that the probability of an *additional* particle occupying a state is independent of the number already in this state:

$$p_j(N_j) \propto q_j{}^{N_j}, \quad 0 \leqslant q_j \leqslant 1, \qquad \ldots\ldots (9)$$

where q_j is fixed for a given quantum state. Normalization leads to the identification $1 - q_j$ for the proportionality constant, and hence

$$n_j = q_j/(1 - q_j). \qquad \ldots\ldots (10)$$

Equations (8)–(10) yield after some calculation the usual result

$$S = \boldsymbol{k} \sum [(1 + n_j) \ln (1 + n_j) - n_j \ln n_j], \qquad \ldots\ldots (11)$$

which is exact for non-equilibrium situations, provided assumptions (7) and (9) and the uniqueness theorem are valid. The usual equilibrium Bose distribution can be derived from (11) on the same assumptions.

Only trivial changes are required in order to pass from (1) or (11) to expressions for the entropy in terms of the mean number of particles in groups of equally probable states. This corresponds to a transition from a fine grained to a coarse grained entropy.

If, instead of expressing (6) in terms of mean occupation numbers, one maximizes this expression subject to appropriate subsidiary conditions (expressing a given mean energy and/or a given mean number of particles), one obtains immediately the form of the canonical and grand canonical distributions, together with their more rarely used generalizations. This is an attractive approach to the ensembles of statistical mechanics (see also Jaynes 1957†) which the author has found useful in lectures to honours students.

Acknowledgment

I am indebted to my colleague Dr. C. W. McCombie for a helpful discussion.

References

Jaynes, E. T., 1957, *Phys. Rev.*, **106**, 620.
Khinchin, A. I., 1957, *Mathematical Foundations of Information Theory* (New York: Dover Publications).
Landau, L. D., and Lifshitz, E. M., 1958, *Statistical Physics* (London: Pergamon), p. 154.
Landsberg, P. T., 1954, *Proc. Nat. Acad. Sci.*, **40**, 149.

† I am grateful to Dr. W. K. Burton for drawing my attention to this reference.

LETTERS TO THE EDITOR

Bonding in Cadmium Telluride

The attention of the author has been drawn to a letter by Garlick, Hough and Fatehally (1958) which suggests that bonding in cadmium telluride is homopolar. and that this is in disagreement with views expressed earlier by the author (1955 to be referred to as I). The following points should be noted:

(i) Homopolar (or covalent) bonding is usually understood to describe equal sharing of bonding electrons between bonded atoms. With CdTe this would lead to the formulation $Cd^{2-}Te^{2+}$ (Pauling 1945), and to a very large bond dipole. The evidence of Garlick *et al.* presumably indicates no such charge separation, so that the bonding in CdTe is approximately 'neutral' (see I for further discussion of this concept) and *not* covalent.

(ii) In I it was suggested that bond length and energy gap data can give an indication of relative departures from bond neutrality. While no absolute ionicity scale could be derived it was pointed out that silver iodide must lie near the limit of stability of the zinc blende lattice (which requires an appreciable covalent component of bonding). For AgI the difference between neutral and ionic bonding (Ag^0I^0 and $Ag^{1+}I^{1-}$) is equivalent to the displacement of only a single electronic charge. Accordingly for there to be some covalency the effective charges with AgI must be appreciably less than one unit. Since the data given by the author in I indicated that CdTe is less ionic than AgI, the effective ionic charge with CdTe should be only a fraction of the electronic charge and an experiment of the kind described by Garlick *et al.* (1958) might not detect its presence, though this appears unlikely. However as pointed out by Garlick *et al.* their results were obtained relatively near the main absorption edge where anomalies might occur. It may be significant that the refractive index at the longest wavelength studied ($1{\cdot}1\,\mu$) does indicate a high frequency dielectric constant ($n^2 = 9{\cdot}8$) slightly lower than the low frequency value ($\epsilon = 11{\cdot}0$). Data for longer wavelengths would appear of interest.

(iii) Garlick *et al.* also state that the approach by Goodman "...ignored the electronegativity difference between the constituent atoms...". The concept of an electronegativity difference between constituent atoms was in fact used by the author to derive a parameter indicating relative bond ionicity. The indirect treatment used was necessary because, as was explicitly stated, no existing electronegativity scale could be applied directly to diamond type lattices.

C. H. L. Goodman.

Research Laboratories,
The General Electric Company Limited,
Wembley, England.
5th February 1959.

Addendum. A reststrahlen frequency for CdTe of $150\,cm^{-1}$ can be deduced from a recent note by Mitsuishi *et al.* (1958). This, in conjunction with the high frequency dielectric constant at the longest wavelength studied by Garlick *et al.*, would appear to indicate (using the Born equation) an effective ionic charge of

0·19*e*. Any further fall in refractive index towards longer wavelengths would of course lead to a larger value of charge.

8th April 1959.

GARLICK, G. F. J., HOUGH, J. M., and FATEHALLY, R. A., 1958, *Proc. Phys. Soc.*, **72**, 925.
GOODMAN, C. H. L., 1955, *J. Electronics*, **1**, 115.
MITSUISHI, A., YOSHINAGA, H., and FUJITA, S., 1958, *J. Phys. Soc. Japan*, **13** 1235.
PAULING, L., 1945, *The Nature of the Chemical Bond* (New York: Cornell Univ. Press), p. 178.

The Extent of Ionic Binding in Cadmium Telluride

Recent measurements of the refractive index of cadmium telluride by Garlick, Hough and Fatehally (1958) and of the dielectric constant by de Nobel and Hofman (1956) may be used to obtain an estimate of the effective ionic charge in this compound.

For the refractive index the measured values are 3·47 at 0·903 μ and 3·13 at 1·10 μ. These values may be fitted to a normal dispersion formula of the type

$$\frac{1}{n^2-1} = B - \frac{A}{\lambda^2} \qquad \ldots\ldots (1)$$

where $B = 0{\cdot}162$ and $A = 0{\cdot}0582$.

Hence the undispersed value of the refractive index (i.e. $\lambda \to \infty$) is $n_0 = 2{\cdot}68$ or $n_0^2 = 7{\cdot}2$.

The low-frequency dielectric constant is $\epsilon = 11$, so that on passing through the reststrahlen band there will be a change in dielectric constant of $\Delta\epsilon = 3{\cdot}8$. This change in dielectric constant is related to the effective charge e^* by the Szigeti (1949) formula

$$\Delta\epsilon = \frac{4\pi(n_0^2+2)^2 N e^{*2}}{9M\omega_R^2} \qquad \ldots\ldots (2)$$

where N is the density of atom pairs, M is their reduced mass and $\omega_R/2\pi$ is the reststrahlen frequency.

The reststrahlen wavelength for CdTe has not been measured but may be calculated from the compressibility by use of the second Szigeti (1950) relation

$$\frac{1}{\kappa} = \frac{1}{3} N r^2 \frac{\epsilon+2}{n^2+2} M\omega_R^2 \qquad \ldots\ldots (3)$$

where r, the nearest neighbour distance, is 2·79 Å. According to Bridgman (1931) $\kappa = 2{\cdot}38 \times 10^{-12}$ cm^2 dyn^{-1}, giving $M\omega_R^2 = 7{\cdot}5 \times 10^4$ c.g.s. units, or $\lambda_R = 69\,\mu$. Thus equation (2) gives $e^*/e = 0{\cdot}83$.

An alternative estimate of the effective charge may be obtained from the mobility of either electrons or holes. This will be determined mainly by polar scattering and we may use the expression given by Ehrenreich (1959) for the room temperature mobility:

$$\mu = 2 \times 10^{31} S \left(\frac{e}{e_f}\right)^2 \left(\frac{m}{m^*}\right)^{3/2} \frac{M\omega}{N} \left\{\exp\left(\frac{h\omega}{kT}\right) - 1\right\} \text{cm}^2\text{v}^{-1}\text{sec}^{-1} \qquad \ldots\ldots (4)$$

where $\omega^2/\omega_R{}^2=\epsilon/n^2$, S is a screening parameter with values near unity, and the effective charge used by Ehrenreich is given by $e_f=e^*(n^2+2)/3n^2$.

Using data from Kroger and de Nobel (1955) for effective masses and their highest mobilities, namely

$$\mu_e=680\,\text{cm}^2\text{v}^{-1}\,\text{sec}^{-1} \text{ for } 4{\cdot}4\times10^{16}\,\text{cm}^{-3} \text{ carriers},$$
$$\mu_h=56\,\text{cm}^2\text{v}^{-1}\,\text{sec}^{-1} \text{ for } 5{\cdot}3\times10^{15}\,\text{cm}^{-3} \text{ carriers},$$
$$m_e=0{\cdot}14m \text{ and } m_h=0{\cdot}37m,$$

we obtain effective charges $e^*=0{\cdot}62e$ and $e^*=0{\cdot}95e$.

These values are in reasonable agreement with that deduced above from the optical properties. It is therefore concluded that the effective charge is almost as large as in ZnS (Moss 1959), so that there is a considerable degree of ionicity in this compound.

Royal Aircraft Establishment, T. S. Moss.
Farnborough, Hants.
1st May, 1959.

Bridgman, P. W., 1931, *Proc. Amer. Acad. Arts Sci.*, **66**, 255.
Ehrenreich, H., 1959, *J. Phys. Chem. Solids*, **8**, 130.
Garlick, G. F. J., Hough, J. M., and Fatehally, R. A., 1958, *Proc. Phys. Soc.*, **72**, 925.
Kroger, F. A., and de Nobel, D., 1955, *J. Electron. and Control*, **1**, 190.
Moss, T. S., 1959, *Optical Properties of Semiconductors* (London: Butterworths Scientific Publications).
de Nobel, D., and Hofman, D., 1956, *Physica*, **22**, 252.
Szigeti, B., 1949, *Trans. Faraday Soc.*, **45**, 155.
—— 1950, *Proc. Roy. Soc.* A, **204**, 51.

Electron Spin Resonance Absorption for Polycrystalline Substances

Approximate calculations for line shape of polycrystalline substances with g-value anisotropy have been performed by Bleaney (1950) and Sands (1955). The basis of the calculations is that, with random orientation, the fraction of crystals whose axes lie between the angles θ and $\theta+d\theta$ with the magnetic field is $\frac{1}{2}\sin\theta\,d\theta$. To explain spectra obtained from biological materials, Gordy *et al.* (1958) have suggested that the line shape obtained is due to resonance of bound oxygen, which should have an axially symmetric g-value. We have made exact calculations of the line shape on the basis of the following assumptions:

(i) The shape of the absorption curve of a single crystal is the Lorentzian

$$I=\frac{4\pi AK}{1+\pi^2K^2(x-c)^2}$$

where A is proportional to the total number of spins, and $K=2/\pi\Delta x$, where Δx is the line width. If the absorption is obtained experimentally by sweeping the frequency ν, $x=h\nu/\beta H$ and $c=g$. If the absorption is obtained experimentally by sweeping the field H, $x=\beta H/h\nu$ and $c=1/g$.

(ii) The line width for a single crystal is independent of angle θ.

(iii) c varies with θ according to the equation $c=(c_{\parallel}-c_{\perp})\cos^2\theta+c_{\perp}$. I can then be integrated exactly over all θ.

$$\mathscr{I}=\int_0^{\pi/2}\frac{AK2\pi\sin\theta\,d\theta}{1+\pi^2K^2(x-c)^2}=\int_{c_{\parallel}}^{c_{\perp}}\frac{AK2\pi\sin\theta\,(d\theta/dc)\,dc}{1+\pi^2K^2(x-c)^2}.$$

Therefore

$$\mathscr{I}=\frac{A}{ps}\left[a\left\{\frac{\pi}{2}+\tan^{-1}\left(\frac{p^2-s}{2bp}\right)\right\}+\frac{b}{2}\ln\left(\frac{p^2+2ap+s}{p^2-2ap+s}\right)\right]$$

and

$$\frac{d\mathscr{I}}{dx}=\frac{-A}{2ps^2}\left[\frac{1}{s}\left\{a\alpha\left[\frac{\pi}{2}+\tan^{-1}\left(\frac{p^2-s}{2\,bp}\right)\right]+\frac{b\beta}{2}\ln\left(\frac{p^2+2ap+s}{p^2-2ap+s}\right)\right\}\pm\frac{2pd(2y\mp p^2)}{(p^4\mp 2p^2y+s^2)}\right]$$

where $y=x-c_{\perp}$, $d=\dfrac{1}{\pi K}$, $s=(y^2+d^2)^{1/2}$, $p=|c_{\perp}-c_{\parallel}|^{1/2}$, $a=\{\frac{1}{2}s\pm\frac{1}{2}y\}^{1/2}$,

$b=\{\frac{1}{2}s\mp\frac{1}{2}y\}^{1/2}$, $\alpha=\pm 2y-s$, $\beta=\pm 2y+s$, where the upper sign holds for $c_{\parallel}>c_{\perp}$ and the lower sign for $c_{\parallel}<c_{\perp}$.

These functions can be evaluated numerically, and then $g_{\parallel}$ and $g_{\perp}$ can be determined by comparison with the experimentally measured line shape. Thus as an example the figure shows the derivative calculated for sweeping the field, with a resonant frequency of 23 000 Mc/s, a line width of 1·025 gauss, and

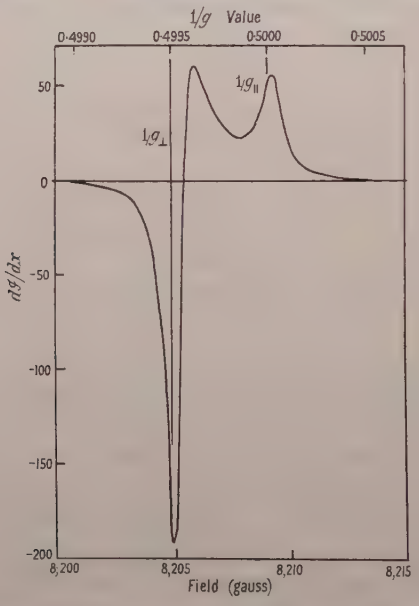

First differential of absorption in polycrystalline substance.

$g_{\parallel}=2{\cdot}000$ and $g_{\perp}=2{\cdot}002$. As can be seen from the figure the first peak of the derivative corresponds closely with $g_{\perp}$ and this was found by numerical investigation to be within 2% of the g-value variation. The third peak corresponds roughly with $g_{\parallel}$ to within 10% of the g-value variation. The shape of the curve is in good agreement with the experimental curves of Gordy *et al.*

Acknowledgments

The numerical evaluation of these curves was performed on Pegasus at the Northampton College, and we wish to express our thanks to the members of the

Computer Section of the Mathematics Department for their ready help. One of us (R. C. S.) acknowledges a grant from the British Empire Cancer Campaign.

Mathematics Department,
Northampton College,
London, E.C.1. J. W. Searl.

Physics Department,
Medical School,
Guy's Hospital,
London, S.E.1. R. C. Smith,
S. J. Wyard.

25th May 1959.

Bleaney, B., 1950, *Proc. Phys. Soc.* A, **63**, 407.
Gordy, W., Miyagawa, I., Watabe, N., and Wilbur, K., 1958, *Proc. Nat. Acad. Sci., Wash.*, **44**, 613.
Sands, R. H., 1955, *Phys. Rev.*, **99**, 1222.

CORRIGENDUM

The Spin Hamiltonian of a Γ_8 *Quartet*, by B. Bleaney (*Proc. Phys. Soc.*, 1959, **73**, 939).

Equation (2) *should read*

$$\mathscr{H} = g\beta H_z S_z + f\beta H_z S_z^3 + \beta[\tfrac{1}{2}g + \tfrac{1}{8}f\{3S(S+1)-2\}](H_+S_- + H_-S_+) - (3f\beta/8)S_z(H_+S_- + H_-S_+)S_z + \tfrac{1}{8}f\beta(H_+S_+^3 + H_-S_-^3). \quad \ldots\ldots (2)$$

P. 941, 9 lines from the bottom. The value of p^2 in the susceptibility *should read*

$$p^2 = \tfrac{3}{4}(5\gamma^2 + 3\delta^2).$$

The author is indebted to Mr. H. Hutchinson of Mullard Research Laboratories for drawing his attention to these errors.

NOTICE TO AUTHORS

Authors of papers on experimental measurements are advised to include information concerning the purity and structure (grain size, homogeneity, degree of working phases present, etc.) of materials used. This should be as complete as the nature of the measurements being made requires and should include the source of the material and method of preparation.

REVIEWS OF BOOKS

Electromagnetic Phenomena in Cosmical Physics: Report of Symposium No. 6 of the International Astronomical Union, edited by B. LEHNERT. Pp. xiii + 545. (Cambridge: University Press, 1958.) 50*s*.

Magneto-hydrodynamics, a branch of physics which is developing rapidly yet frequently remains controversial, provides an excellent subject for scientific conference discussion. Certainly the Stockholm conference of 1956, where the emphasis was on cosmical applications, appears to have been of quite exceptional interest. The conference report is produced with the usual standards of excellence of the Cambridge University Press.

After an opening address by H. Alfvén, van de Hulst gave a survey report on magnetic fields in astrophysics. The remainder of the first session was concerned with recent theoretical and experimental work on magneto-hydrodynamic phenomena. Session II was concerned with solar electrodyanamics, problems of active regions, flares and prominences.

Session III, on stellar magnetism, began with surveys of observational work (H. W. Babcock) and of theory (L. Spitzer). Certain magnetic stars are found to have heavy element abundances which exceed the abundances for normal stars by factors as great as 10^3; these abundance anomalies may be due to nuclear reactions occurring in magnetic star atmospheres (E. M. Burbidge, G. R. Burbidge and W. A. Fowler). The session on stellar magnetism also included an account of Soviet observational work (G. A. Shajn) on interstellar magnetic fields.

Sessions IV and V were concerned with solar magnetic fields and with electromagnetic phenomena in interplanetary space. The interpretation of observational work on photospheric magnetic fields (H. W. Babcock and H. D. Babcock) is disputed by H. Alfvén and his collaborators. The full reports of the conference discussions are here particularly valuable in giving a clear indication of the issues in dispute. The session on solar magnetism included a very interesting paper by J. P. Terletzky on the theory of ionized interstellar gas motion.

Theories of magnetic storms remain controversial; the merits of rival theories were surveyed by V. C. A. Ferraro, L. Block and S. F. Singer.

Cosmic ray observations provide a remarkable method of studying cosmical electromagnetic phenomena. In order to account for variations in cosmic ray intensity one must suppose that some cosmic rays are produced by the sun and also that the observed flux of galactic cosmic rays is modified by variable interplanetary magnetic fields (J. A. Simpson and E. N. Parker).

Session VI, on high current discharges, contains three valuable papers by Soviet scientists, all written in German. The final session contains two papers by I. S. Shklovsky on the optical emission of radio sources due to relativistic electrons and a paper by G. R. Burbidge on magnetic fields in radio sources.

M. J. SEATON.

Fourier Transforms and X-ray Diffraction, by H. LIPSON and C. A. TAYLOR. Pp. vii + 76. (London : G. Bell and Sons, 1958.) 18*s*. 6*d*.

The appearance of this monograph, in which two of the leading workers in the field describe how the theory of x-ray diffraction may be developed in terms of the Fourier transform theory, is to be welcomed.

About half the book is devoted to a lucid sketch of the theory in which a good balance is struck between emphasis on the physical basis of the subject and on the mathematics necessary to exploit it. The authors treat diffraction by a (non-periodic) group of scattering centres before that by a crystal, with which x-ray diffraction began historically and with which most existing books on the subject begin. The value of the present approach is that it is better suited to dealing with systems which are less ordered than a perfect crystal and which are being studied more and more nowadays. The second half deals with a number of applications of the theory and should appeal particularly to research workers who have some prior knowledge of the problems discussed. The book is, however, too short to give more than a glimpse of the possibilities of the method to those readers less well-prepared.

It is a pity that the Abbe theory of image formation is not mentioned, but perhaps this topic will be dealt with in a future publication, promised by the authors, on the details of optical diffraction procedures for crystal structure determination. In the present volume, the authors can be said to have succeeded in their aim of showing the great power of the Fourier transform approach for tackling many problems that arise in x-ray diffraction, and it is to be hoped that the appearance of this book will help influence the teaching of the subject in this direction.

A. KLUG.

Mathematical Aspects of Subsonic and Transonic Gas Dynamics, by L. BERS. Pp. xv+164. (New York: John Wiley; London: Chapman and Hall, 1958.) 62*s*.

This book is devoted entirely to the analytical treatment of problems that arise in two-dimensional flow of a compressible inviscid fluid and to a discussion of various methods which have been evolved for their solution. The basic differential equations of flow are given in Chapter I and the consequences of various modifications and approximations discussed in some detail. Some particular solutions of the hodograph equations are outlined.

Chapter II deals with the mathematical difficulties of subsonic flow theory. The characteristic features of equations of elliptic type are discussed and the use, for instance, of quasi-conformal mappings and of pseudo-analytic functions in their solution are outlined; special emphasis is placed on techniques that have been developed fairly recently. This is followed by a chapter giving some applications to such problems as the determination of subsonic flow around a profile, subsonic flow in a channel and related mapping theorems, and subsonic flow with free boundaries.

The mathematical background of transonic flow theory is given in Chapter IV. Properties of partial differential equations of mixed elliptic–hyperbolic type are described and particular solutions of Tricomi's equation for transonic flow are discussed. Basic questions of uniqueness and existence in relation to problems of mixed flow are given particular attention. The final Chapter discusses regions of local shock-free supersonic flow and regions terminating in a shockwave. Applications of theory to specific problems of practical interest are also included. A brief account of numerical methods is given in an Appendix and the text ends with a list of nearly 400 references, a good many of Russian origin, covering work up to about 1956.

Emphasis is placed throughout on the development of mathematical techniques rather than on physical aspects and attention is drawn to the importance

of aerodynamic research as a source of mathematical problems. This publication should be of great interest to theoretical aerodynamicists and is, in the reviewer's opinion, a most valuable monograph. W. P. JONES.

Nuclear Reactions, edited by P. M. ENDT and M. DEMEUR. Pp. xii + 502. (Amsterdam: North-Holland Publishing Company, 1958.) 86*s*.

It is becoming quite the fashionable thing to publish, more or less verbatim, the proceedings of international conferences in physics. The present writer has often been doubtful of the value of these expensive volumes; for does one really want a permanent record of what was after all of only transitory interest? And who but the most hardy of conference-goers would want his more naive questions (or answers) engraved upon so impressive a tombstone?

However, the present volume (which promises to be the first of two) is different. True, its origins lie in the 1956 Amsterdam Conference on Nuclear Reactions of which this participant, amongst many others, has many pleasant memories (albeit somewhat dimmed by the passage of time). The book is based upon the principal papers presented to the conference, but each chapter is a properly written monograph upon a particular topic dealt with more briefly at that time. The result is therefore a book and not a conference report: a free-standing monument and not a tombstone.

The articles presented here are all by leading authorities in their respective fields: the many-body system is reviewed by R. J. Eden, the shell model by J. P. Elliott, heavy ion reactions by J. H. Fremlin, and angular correlations by L. J. B. Goldfarb. Resonance reactions are dealt with theoretically by E. Vogt, and experimentally by H. E. Grove (in spite of the list of contents which would have it otherwise). K. J. Le Couteur has given a summary of work on the statistical model of nuclear reactions; D. J. Hughes and R. L. Zimmerman a useful survey of the analysis of neutron resonances, while P. C. Gugelot has contributed an article on reactions at medium energies. Finally, A. K. Kerman presents a wealth of information on rotational motion in nuclei. The reader will note that in spite of the title much of this book is devoted to nuclear structure rather than to reactions, a sign that the reaction mechanism, so long disguised by the bulk properties of the nucleus, is at last becoming understood in terms of the particles which constitute it and their motions.

The Editors are to be congratulated on having produced a well-balanced account of much that is important in low-energy nuclear physics, and one that is almost as up to date now as it was during the Amsterdam Conference. One would certainly have liked to have seen articles on photo-reactions and direct interactions as well, but these are promised in a second volume. B. H. FLOWERS.

Les Spectres Electroniques en Chimie Théorique, by C. SANDORFY. Pp. 230. (Paris : Revue d'Optique Théorique et Instrumentale, 1959.) 2000 *fr*.

This book is a survey of all the theoretical work on the ultra-violet absorption of π-electron molecules. After an introductory chapter on selection rules and group theory, the author who is professor of chemistry at the Université de Montreal, reports all the main theoretical calculations in the literature, using both the valence-bond resonance approximation and the molecular-orbital approximation. Relatively little of the material here set out may be found in any other textbook, and the writing is clear. There is an excellent collection of references. C. A. COULSON.

The Mobility of Potassium Ions in Nitrogen and Neon at 294°K

By R. W. Crompton and M. T. Elford†
Physics Department, University of Adelaide

Communicated by L. G. H. Huxley; MS. received 9th March 1959, in revised form 24th April 1959

Abstract. The mobility of potassium ions in nitrogen and neon has been measured by an electrical shutter method of the type developed by Bradbury and Nielsen for measuring electronic drift velocities. The values obtained for the mobility μ_0, 2·54 and 7·42 $cm^2 volt^{-1} sec^{-1}$ for nitrogen and neon respectively, are in good agreement with those listed by Tyndall. The variation of the mobility with E/p_0 is shown to be in qualitative agreement with theoretical considerations while the disagreement between the present results and those of Mitchell and Ridler is discussed.

§ 1. Introduction

Measurements of the mobility of alkali ions in gases afford valuable information concerning the forces of interaction between ions and gas molecules. In particular a knowledge of the variation of the ionic mobility with temperature enables the energy of interaction between an ion and a gas particle to be evaluated. This evaluation has been carried out by Dalgarno, McDowell and Williams (1958) for the experimental data available which are almost wholly those obtained by the group working at Bristol (Tyndall 1938) who used the four-gauze method of Tyndall and Powell. This method involves calibrating the apparatus used by reference to one absolute measurement of the mobility of helium ions in helium made by Tyndall and Powell (1932) and a possible source of error in all subsequent measurements is thus introduced. In addition, as will be shown, the procedure which has been used is not valid for values of E/p_0 such that the mobility μ_0 is not constant, E being the electric field in volt cm^{-1} and p_0 the normalized gas pressure in millimetres of mercury.

In making measurements of the variation of the ionic mobility with temperature an absolute method, with an order of accuracy better than that previously obtained using the four-gauze method, is clearly desirable. Moreover, such an improved accuracy is essential for further investigation of the anomalous 'elbow' in the curve of μ_0 against E/p_0 which Mitchell and Ridler (1934) reported for K^+ ions in nitrogen. Accordingly the method devised by Bradbury and Nielsen (1936) to measure electronic drift velocities was investigated and found to be capable of measuring the drift velocities of positive ions to a high order of accuracy. By careful attention to the accuracy with which the experimental parameters were measured, an accuracy to better than 0·5% has been obtained. The order of accuracy obtained previously with the four-gauze method was to approximately 2%.

† Present address: Division of Pure Physics, National Research Council, Ottawa, Ontario.

In this paper details of the experimental method are given together with the results obtained for mobilities at room temperature. In a later paper the results of mobilities at low temperatures will be presented.

§ 2. Experimental Details

In the method of Bradbury and Nielsen (figure 1) the time taken for the centre of mass of a group of ions to traverse a known distance d between two grids G_1 and G_2 is measured in terms of the frequency of an alternating potential difference. In the present apparatus each grid consists of 0·08 mm diameter nichrome wires stretched parallel and coplanar across an annulus of mica, and spaced 0·52 mm apart. Alternate wires are connected together and, on the application of an alternating voltage between the two sets so formed, ions are transmitted only during the interval when the voltage between alternate wires is small. If the frequency of the alternating voltage is such that the groups of ions formed each half cycle by the first grid traverse the distance between the grids in the time interval corresponding to an integral number of half cycles, the groups will be transmitted by the second grid also, since the voltages applied to both grids are in phase.

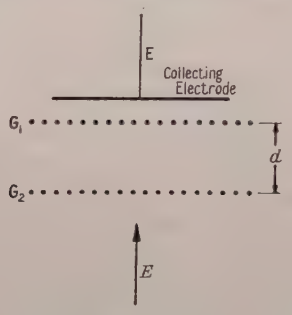

Figure 1. The Bradbury–Nielsen shutter method.

The current received by the collecting electrode E will then be at a maximum. A graph of current as a function of frequency will therefore consist of a series of maxima and minima; furthermore, since successive maxima should occur at integral multiples of the frequency f_0 corresponding to the first maximum, a

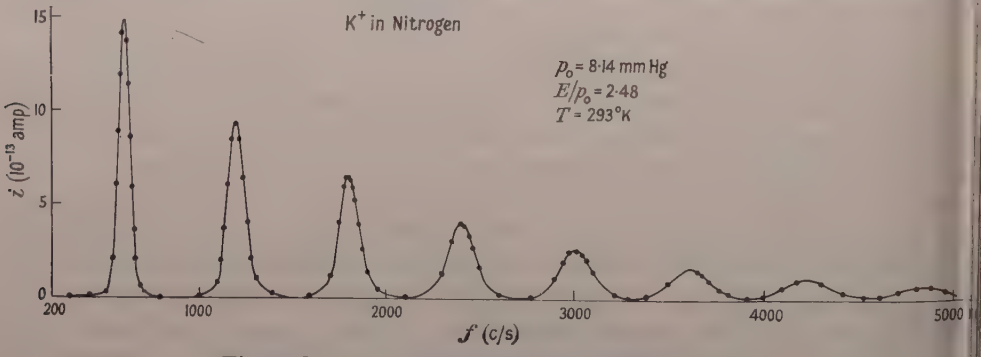

Figure 2. A typical ion current–frequency curve.

valuable internal check on the experimental method is provided. A typical experimental curve is shown in figure 2. The values of f_0 derived from successive maxima are given in table 1. The frequencies at which the first two maxima

Table 1

Peak No.	1	2	3	4	5	6	7	8
Frequency at max. (c/s)	600	1200	1800	2399	3007	3607	4227	4817
f_0 (c/s)	600	600	600	600	601	601	604	602

occurred were measured in all determinations of the ionic drift velocity. The value of f_0 derived from the higher frequency was averaged with the value corresponding to the position of the first maximum to obtain the best estimate of f_0.

The apparatus used is shown in figure 3. The electrode system consists of lapped and polished brass plates maintained in vertical alignment by three brass rods sheathed with glass tubing and separated by accurately ground glass spacers. The upper ends of the rods are extended above the topmost electrode to reduce the possibility of electrical discharge occurring between the earthed rods and the electrode which is held at a high positive potential. Nuts at both ends of the rods enable the whole assembly to be clamped tightly together. The distance of 6 cm from the top electrode to the first grid ensures that no thermal gradients are present in the region between the grids, while as an additional precaution the heat from the source of ions is largely removed by surrounding it with a water jacket.

The uniform electric field E was maintained by means of guard electrodes at potentials appropriate to their position in the electrode system. The leads from the electrodes consist of phosphor bronze springs and are brought out of the envelope by means of tungsten–glass seals of which two only are shown in figure 3.

In the construction of the experimental tube care was taken to maintain a high degree of gas purity by rigorously excluding greases and waxes and by inserting a cold-trap in the vacuum line as close as possible to the envelope. The vacuum system was pumped to a pressure less than 10^{-4} mm Hg (the lower limit of the Pirani gauge on the system) by a two-stage oil diffusion pump and, during shut down tests over twelve hour periods, the gauge failed to detect a rise in pressure.

An apparatus similar to the one described but specifically designed for low temperature experiments was subjected to low temperature baking at 200°C for three periods each of three hours duration. On each occasion the curve of mobility as a function of E/p_0 was obtained before and after baking. On the first two occasions the curves obtained agreed well with the curve shown in figure 4 but, on the third occasion, the values of mobility were 2·8% lower over the entire range of values of E/p_0. Since this behaviour is not that to be expected were the contamination of the gas reduced by the baking process it was concluded that the gas purity without outgassing was adequate and that the change in the measured values of mobility had been caused by a change in length of the apparatus. The results quoted are therefore those obtained with the apparatus not subjected to baking and for which the dimensions are accurately known.

For the experiments in nitrogen the gas was produced by the thermal decomposition of sodium azide while the neon, obtained from a flask supplied by the British Oxygen Company, was stated to be spectroscopically pure. In each case the gas was admitted to the apparatus only after passage through a series of cold-traps.

The source of potassium ions was of the type developed by Blewett and Jones (1936) in which an alumino-silicate of an alkali metal is used. The method of preparation adopted in these experiments is due to Couchet (1953). To avoid self-repulsion in the beam of ions the current employed was of the order of

10^{-12} amp. A valve electrometer was used to measure the current received by the collecting electrode.

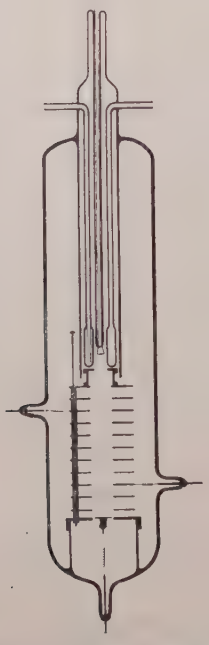

Figure 3. Experimental tube.

Apart from gas purity the reliability of the experimental results depends on the accurate determination of the following four quantities.

(*a*) *The distance between the two grids.*

A cathetometer was used to measure the distance at regular intervals around the circumference of the apparatus. The mean value obtained was $3{\cdot}999 \pm 0{\cdot}005$ cm.

(*b*) *The potential difference between the grids.*

By means of an accurately constructed potential divider the voltage applied between the grids was compared with the e.m.f. of a standard cell using a potentiometer. Since the distance between the grids is known the field E could be calculated with an overall accuracy to better than 0·1%.

(*c*) *The pressure of the gas.*

A precision mechanical gauge employing an evacuated capsule (Crompton and Elford 1957) enabled the gas pressure to be measured with an accuracy to better than 1% at 1 mm Hg and 0·1% at 20 mm Hg.

(*d*) *The frequency of the alternating voltage applied between the two sets of wires of each grid.*

The alternating voltage was derived from a high stability oscillator which was initially calibrated against a frequency standard. The stability of the oscillator enabled determinations of frequency to be made to better than 0·1%.

Experimental accuracy could be affected by local field distortion produced by the alternating voltages applied to the grids. In the course of the experiments the peak voltage between either set of grid wires and the guard electrode upon

which the grid is mounted was approximately one half the voltage between successive guard electrodes. That the effects of such field distortion were negligible can be judged from the agreement between the values of f_0 for the higher orders as shown in table 1 and from the fact that doubling the alternating voltage produced a change in f_0 of less than 0·1%. These experimental results confirmed predictions made from field plots conducted initially by means of an electrolytic tank.

The measurement of the four quantities listed above to the accuracy stated enabled an overall accuracy to better than 0·5% to be achieved.

§ 3. Results

The mobility μ_0 is defined as the ratio of the drift velocity W to the electric field E in a gas whose density is equal to that of a gas at standard density and pressure (i.e. $2{\cdot}69 \times 10^{19}$ atoms cm $^{-3}$). For a gas at pressure p and temperature T the mobility is therefore given by the relation

$$\mu_0 = \frac{W}{760(E/p)} \frac{273}{T}.$$

No correction other than that for gas density is made for the direct influence of the gas temperature on the mobility μ_0. The values obtained for the mobility of K^+ ions in nitrogen and neon (extrapolated to $E/p_0 = 0$) are shown in table 2.

Table 2. Mobility μ_0 (cm^2 v^{-1} sec^{-1})

	N_2	Ne
Present	2·54	7·42
Tyndall	2·53	7·50

The variation of the mobility with E/p_0 (where p_0 is the normalized pressure defined as $p_0 = p \times 273/T$) is shown in figures 4 and 5, all results being taken at 294°K.

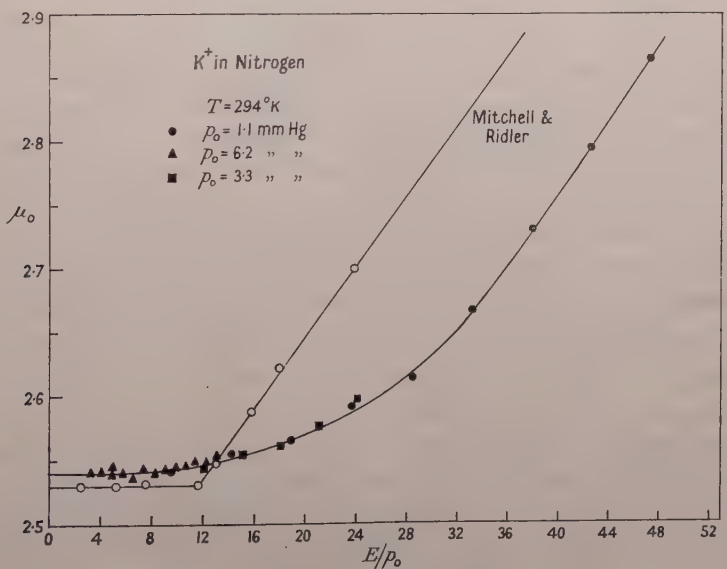

Figure 4. Variation of μ_0 with E/p_0 (K^+ in N_2).

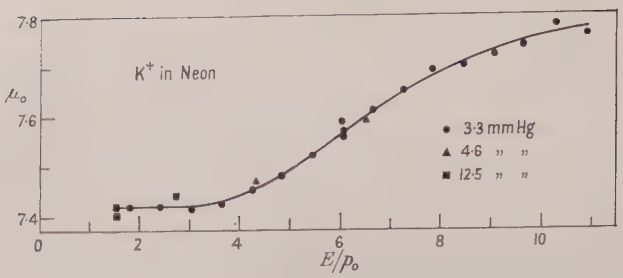

Figure 5. Variation of μ_0 with E/p_0 (K^+ in Ne).

§ 4. Discussion

For each gas the results obtained agree with those listed by Tyndall within the combined limits of experimental error. The excellent agreement confirms the accuracy of the results obtained for low values of E/p_0 by the group working at Bristol. In the earlier work it was necessary to calibrate each apparatus since the correction to be applied to account for end effects introduced by the pairs of grids was unknown. The mobility of helium ions in helium was used for this purpose and was determined in the first instance by Tyndall and Powell using an apparatus in which the length of the drift space could be varied thereby eliminating the need for correction. Since the accuracy of all subsequent work depended on the accuracy of this initial determination the present results confirm the accuracy of this result also. Dalgarno, McDowell and Williams (1958) have suggested that the results of these workers may be subject to a systematic error of 8% which is the discrepancy between their theoretical values and those observed experimentally. However, the excellent agreement of the present results with those obtained previously indicates that no such systematic error is present.

The variation of μ_0 with E/p_0 (figure 4) observed by Mitchell and Ridler for K^+ ions in nitrogen, which suggests that the breakdown in Langevin's law occurs very sharply, is in marked disagreement with the present results. That such a sharp breakdown is unlikely can be seen from a qualitative consideration of the forces of interaction present. At low values of E/p_0 the predominant force of interaction is that of polarization attraction. As the value of E/p_0 increases, the effect of the attractive forces decreases and at very high values of E/p_0 the hard sphere repulsion is the predominant force present. The mobility then varies inversely as the square root of E/p_0. Since the effect of attractive forces decreases smoothly as the value of E/p_0 is increased, at low values of E/p_0 the rise in mobility is expected to be gradual and not discontinuous. The considerable disagreement between the two sets of results at values of E/p_0 greater than that at which Langevin's law breaks down may possibly be attributed to the method of calibration and the subsequent operation of the four-gauze apparatus used by Mitchell and Ridler.

§ 5. A Possible Source of Error in Determinations of Mobility using the Four Gauze Method

The four-gauze method has previously been the only method extensively used to obtain the mobility of alkali ions in gases (Tyndall 1938). Two sets of metal gauzes AB and CD are situated a distance d apart (figure 6). A sinusoidal voltage is applied between the gauzes A and B and between C and D such that a group of ions may be transmitted by each pair once every cycle when the field is in the forward direction. If the frequency of the alternating voltage is continually

increased the current received by the collecting electrode will have a series of maximum and minimum values and, since the voltages applied to both pairs of gauzes are in phase, the drift velocity W will be given by $W=fd$ where f is the frequency at the first maximum. However, as Tyndall and Powell point out, the fields produced by the alternating voltages cause a periodic disturbance of the field E for which no accurate correction can be applied. For a given ion, if the field E and the magnitude of the applied alternating voltages are kept constant, then fp_0 is constant ($W=fd$, $W\propto 1/p_0$). Similarly, assuming the same field distribution, fp_0 is constant for any other ion, the ratio of the constants being the ratio of the mobilities. Thus although the four-gauze method does not directly measure mobilities it does enable relative mobilities to be determined. From Tyndall and Powell's absolute determination of the mobility of helium ions in helium it is possible to calibrate any four-gauze apparatus under known conditions of field and hence use it to determine other ionic mobilities. The conditions for which this experimental procedure is valid are now considered.

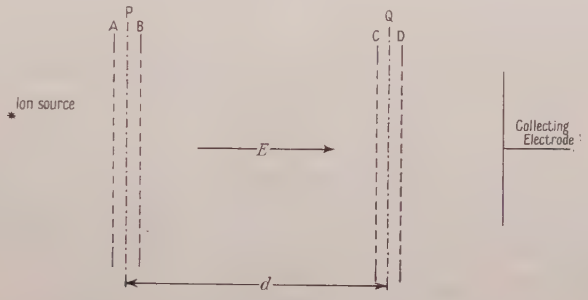

Figure 6. Tyndall–Powell four-gauze method.

In figure 6, P and Q are planes which lie parallel to the YOZ plane midway between the grids A and B and C and D respectively. Let the distance between P and Q be d. At points between the grids B and C and some distance from each the field may be considered uniform and of magnitude E_1. However, the experimental conditions under which the grids are operated to modulate the beam of ions will cause the field in the regions AB and CD to differ from that in the region BC. In addition some field distortion will then exist in this latter region in the neighbourhood of the grids B and C. Let the field at a distance x from the plane P (situated at $x=0$) be $E(x)$ and let $W(x)$ and $\mu_0(x)$ be the values of drift velocity and mobility respectively corresponding to the field $E(x)$.

It is possible to replace the value d by a value d_1 such that the measured time of flight of the ions between P and Q would equal the transit time over the distance d_1 were the field uniform and equal to E_1. If f be the frequency at which the first maximum occurs in the graph of ion current as a function of frequency then

$$\frac{1}{f}=\frac{d_1}{W_1}=\int_0^d \frac{dx}{W(x)}$$

where $W_1=760(E_1/p_0)\mu_{01}$ and W_1 and μ_{01} are the values of W and μ_0 appropriate to the field E_1.

Two cases are considered:

(*a*) When the field $E(x)$ nowhere exceeds the value E_c above which Langevin's law ceases to hold, that is $\mu_0(x)$ is constant and $\mu_0(x)=\mu_{01}=\mu_{00}$ where μ_{00} is the value of μ_0 corresponding to $E/p_0=0$. In this case

$$\frac{d_1}{760(E_1/p_0)\mu_{00}} = \int_0^d \frac{dx}{760[E(x)/p_0]\mu_{00}}$$

that is $d_1 = E_1 \int_0^d \frac{dx}{E(x)}$

and d_1 is a function only of the constants of the apparatus and the potentials applied to the various electrodes.

(*b*) When $\mu_0(x)$ is not constant, that is, when the field in part or all of the region PQ exceeds the value E_c for the particular ion, gas and gas pressure being investigated. Then

$$\frac{d_1}{760[E_1/p_0]\mu_{01}} = \int_0^d \frac{dx}{760[E(x)/p_0]\mu_0(x)}$$

i.e. $d_1 = E_1\mu_{01} \int_0^d \frac{dx}{E(x)\mu_0(x)}$

and d_1 is no longer a constant for a given apparatus and a fixed set of field conditions.

From the foregoing analysis it is apparent that the four-gauze method is liable to error for values of E/p_0 close to and in excess of the value above which Langevin's law ceases to hold. Whether the magnitude of the disagreement between the present results and those of Mitchell and Ridler for K^+ ions in nitrogen can be wholly attributed to this cause is being further investigated.

Acknowledgments

The authors wish to thank Professor L. G. H. Huxley for valuable criticism and advice. They also wish to thank Oliphant Brothers Ltd. and Mr. H. Dickinson for carrying out the necessary glassblowing. One of them (M. T. E.) wishes to acknowledge gratefully the financial assistance afforded by the University of Adelaide and by Philips Electrical Industries Ltd.

References

Blewett, J. P., and Jones, E. J., 1936, *Phys. Rev.*, **50**, 464.
Bradbury, N. E., and Nielsen, R. A., 1936, *Phys. Rev.*, **49**, 388.
Couchet, G., 1953, *C.R. Acad. Sci., Paris*, **236**, 1, 1240.
Crompton, R. W., and Elford, M. T., 1957, *J. Sci. Instrum.*, **34**, 405.
Dalgarno, A., McDowell, M. R. C., and Williams, A., 1958, *Phil. Trans. Roy. Soc.* A, **250**, 411.
Mitchell, J. H., and Ridler, K. E. W., 1934, *Proc. Roy. Soc.* A, **146**, 911.
Tyndall, A. M., 1938, *The Mobility of Positive Ions in Gases* (Cambridge: University Press).
Tyndall, A. M., and Powell, C. F., 1932, *Proc. Roy. Soc.* A, **134**, 125.

The Magnetocrystalline Anisotropy of Cobalt-Substituted Manganese Ferrite

By R. F. PEARSON
Mullard Research Laboratories, Salfords, Surrey

MS. received 1st *April* 1959, *in final form* 30th *May* 1959

Abstract. The first order anisotropy constant K_1 has been measured by torque methods on substituted manganese ferrite crystals containing 1, 2, 4, 6, 8, 10 and 25 mol % cobalt ferrite from 160° to 300°K. The contribution to the anisotropy from the cobalt ions is found to vary linearly with cobalt concentration up to 25%. The extrapolated contributions of the cobalt ions in manganese ferrite lead to K_1 values of $0{\cdot}8 \times 10^6$ ergs cm^{-3} compared with the value of 3×10^6 found for cobalt ferrite and $K_1 = 1{\cdot}5 \times 10^7$ for cobalt substitution in magnetite. The anisotropy contribution is found to vary much faster with temperature for substitution in manganese ferrite than in magnetite.

§ 1. Introduction

It has long been known that the addition of small quantities of cobalt considerably modifies the magnetic properties of ferrites. Cobalt ferrite ($CoFe_2O_4$) is found to have a large positive anisotropy ($K_1 \sim 2$–3×10^6 ergs cm^{-3}) at room temperature compared with the small negative anisotropy ($K_1 \sim 5 \times 10^4$ ergs cm^{-3}) commonly found in other ferrites, and consequently materials of approximately zero anisotropy may be produced by the substitution of small amounts of cobalt in other ferrites. Experimental evidence regarding the magnetocrystalline anisotropy of cobalt-substituted ferrites may be divided into two classes; firstly, direct measurements of the first order anisotropy constant K_1 on single crystals and secondly, indirect evidence from measurements of the initial permeability on polycrystalline samples (Van der Burgt 1957). These measurements indicate that although the anisotropy contribution from the substituted cobalt ions is purely an additive effect at low concentrations, it tends to vary in magnitude in different ferrites. For example, Seavey and Tannenwald (1956) have measured K_1 (by microwave resonance methods) for a single crystal of manganese ferrite containing four mol per cent cobalt ferrite and find that K_1 is still negative at room temperature whereas Bickford (1957) from torque measurements on cobalt-substituted magnetite crystals showed that only one mol per cent of cobalt ferrite was required to change the sign of K_1 at room temperature although the anisotropy of magnetite ($K_1 = -13 \times 10^4$ ergs cm^{-3}) is more negative than that of manganese ferrite ($K_1 = -3{\cdot}8 \times 10^4$ ergs cm^{-3}).

As the behaviour of cobalt ions in substituted magnetite crystals is now well understood (Slonczewski 1958), it seemed desirable to make careful measurements of the anisotropy constants of other cobalt-substituted ferrites, in particular to try to explain why the cobalt ion is less effective in influencing the anisotropy of other ferrites.

In this paper results are presented of anisotropy measurements on substituted single crystals of nominal composition $Co_xMn_{1-x}Fe_2O_4$ where $x=0$, 0·01, 0·02, 0·04, 0·06, 0·08, 0·10, 0·25, over the temperature range 160°K to 300°K.

§ 2. Preparation and Analysis of Crystals

Large single crystals (approximately 4 cm long by 1 cm diameter) of cobalt-substituted manganese ferrite of all the above nominal compositions were grown by Mr. J. L. Page of these Laboratories using the flame fusion method. The chemical analysis of these crystals is shown in table 1. Chemical analysis indicates

Table 1

Nominal composition		Chemical analysis (nearest sample)
$Mn\ Fe_2O_4$	M Mn	$Mn_{0\cdot98}\ Fe_{1\cdot99}O_4$
$Co_{0\cdot01}\ Mn_{0\cdot99}\ Fe_2O_4$	Co (01)	$Co_{0\cdot009}\ Mn_{0\cdot99}\ Fe_{1\cdot98}O_4$
$Co_{0\cdot02}\ Mn_{0\cdot98}\ Fe_2O_4$	Co (02)	$Co_{0\cdot019}\ Mn_{1\cdot03}\ Fe_{1\cdot94}O_4$
$Co_{0\cdot04}\ Mn_{0\cdot96}\ Fe_2O_4$	Co (04)	$Co_{0\cdot038}\ Mn_{0\cdot98}\ Fe_{1\cdot97}O_4$
$Co_{0\cdot06}\ Mn_{0\cdot94}\ Fe_2O_4$	Co (06)	$Co_{0\cdot056}\ Mn_{0\cdot96}\ Fe_{1\cdot97}O_4$
$Co_{0\cdot08}\ Mn_{0\cdot92}\ Fe_2O_4$	Co (08)	$Co_{0\cdot077}\ Mn_{0\cdot92}\ Fe_{1\cdot99}O_4$
$Co_{0\cdot10}\ Mn_{0\cdot90}\ Fe_2O_4$	Co (0·10)	$Co_{0\cdot094}\ Mn_{0\cdot91}\ Fe_{1\cdot97}O_4$
$Co_{0\cdot25}\ Mn_{0\cdot75}\ Fe_2O_4$	Co (0·25)	$Co_{0\cdot245}\ Mn_{0\cdot747}Fe_{1\cdot99}O_4$

a variation in cobalt concentration along the boule and therefore care was taken in selecting the position in the boule of the slice from which the samples were cut. The specimens were shaped into the form of spheres approximately 1·5 mm diameter, using a sphere grinder of the type described by Bond (1951). In cases where it was difficult to make perfect spheres a manual technique mentioned by Bond (1954) was used. Accurate values of the volume of the spheres were deduced from the weight and the x-ray density. Values of the lattice constants (derived from x-ray powder photographs) for the crystals are shown in table 2.

Table 2

Nominal mol % Co in crystal	Lattice constant (Å)	X-ray density
0	8·512 ± 0·005	4·967
1	8·514 ± 0·005	4·964
2	8·509 ± 0·005	4·970
4	8·511 ± 0·005	4·972
6	8·495 ± 0·005	5·002
8	8·505 ± 0·005	4·986
10	8·503 ± 0·005	4·991
25	8·488 ± 0·005	5·031

§ 3. Anisotropy Measurements

The first order anisotropy constant K_1 was measured by the torque method. The single crystal spheres were oriented by x-ray methods and the torque in a (100) crystallographic plane was determined using the automatic recording torque magnetometer mentioned by Pearson (1959) in which the torque curves are directly

plotted on an X–Y recorder. A schematic diagram of the apparatus is shown in figure 1. The measurements were carried out in a field of 12 000 oersteds although at low temperatures where the anisotropy tended to become large ($K_1 \sim 5 \times 10^5$ ergs cm^{-3}) fields of up to 15 000 oersteds could be applied for short periods. With the larger anisotropies it was found necessary to reduce the size of the specimens to less than 1 mm diameter since otherwise the balancing torques become very large (greater than 500 dyn cm) and cause instability in the torque curves as pointed out by Harrison (1956).

The anisotropy energy of cubic crystals is usually expressed in terms of the direction cosines (α_1, α_2, α_3) of the magnetization with respect to the crystallographic axes by the following expression:

$$E = K_1(\alpha_1^2\alpha_2^2 + \alpha_2^2\alpha_3^2 + \alpha_3^2\alpha_1^2) + K_2\alpha_1^2\alpha_2^2\alpha_3^2$$

where K_1, K_2 are the magnetocrystalline anistropy constants. The term containing K_1 is usually more important than higher order terms. Then the torque exerted by the anisotropy forces when a crystal is magnetized to saturation in a particular crystal plane is given by $L = -\partial E/\partial\theta$ where θ is the angle between the magnetization and the reference direction in the plane.

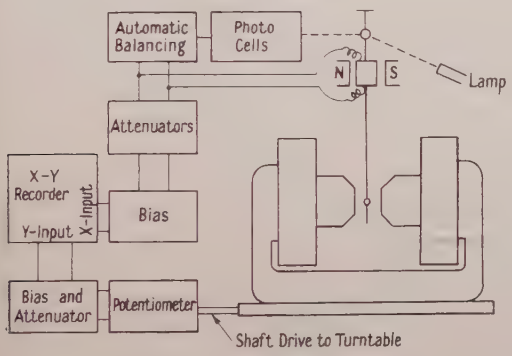

Figure 1. Schematic diagram of automatic recording torque magnetometer.

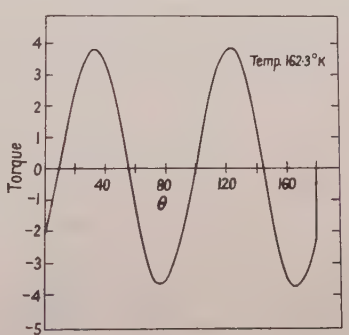

Figure 2. Typical chart record of torque curve: [100] torque curve of $Co_{0\cdot04}Mn_{0\cdot96}Fe_2O_4$.

Torque expressions for the principal crystallographic planes are given by Bozorth (1951), and it is seen that the torque curve in a (100) plane depends solely on K_1, being given by $L = \frac{1}{2} - K_1 \sin 4\theta$ where θ is the angle between the [100] direction and the magnetization. The values of K_1 were simply derived from the peak heights of the plotted curves. A typical chart record is shown in figure 2. Measurements were taken at approximately 10°K intervals over the temperature range 160°K to 300°K.

§ 4. Experimental Results

The experimental values of K_1 for the whole series of cobalt-substituted manganese ferrite crystals are plotted as a function of temperature in figure 3 and are also conveniently tabulated in table 3. All these results were derived from torque measurements in a (100) plane. The values of K_1 are thought to be accurate to within $1{\cdot}5 \times 10^3$ ergs cm^{-3} or 2% whichever is the greater, and difficulties in temperature control and measurement limit the accuracy of the temperature values to 1°K. These data are compared in table 4 with values of K_1 given by

Table 3. Experimental Values of K_1

Temp. (°K)	Values of K_1 (ergs cm^{-3} × 10^{-3}) for cobalt-substituted crystals of manganese ferrite							
	M Mn	Co(01)	Co(02)	Co(04)	Co(06)	Co(08)	Co(10)	Co(25)
300	−37·1	−28·1						
290	−40·7	−31·2	−22·2	−7·0	+6·3	+29·1	+37·3	+171
280	−45·1	−34·2	−23·0	−5·0	+14·0	+41·3	+53·1	+220
270	−51·3	−37·1	−23·2	+0·2	+23·8	+54·9	+72·9	+279
260	−57·8	−39·8	−22·2	+7·7	+36·1	+72·3	+96·8	+351
250	−64·4	−42·1	−20·7	+16·9	+52·1	+94·7	+127·3	+434
240	−71·3	−44·0	−18·0	+27·5	+72·2	+124·5	+163·7	+532
230	−78·4	−45·9	−13·9	+42·3	+95·9	+163·7	+210·0	—
220	−87·1	−47·0	− 8·0	+61·4	+126·0	+210·9	+265	—
210	−95·8	−47·8	0	+83·9	+165·0	—	+327	—
200	−105·0	−46·8	+10·0	+112·2	+210·0	—	+407	—
190	−115·3	−43·9	+23·0	+146·8	—	—	—	—
180	−126·0	−39·2	+39·8	+189·5	—	—	—	—
170	−136·7	−34·1	+60·3	+241·6	—	—	—	—
160	—	—	+91·8	+303	—	—	—	—

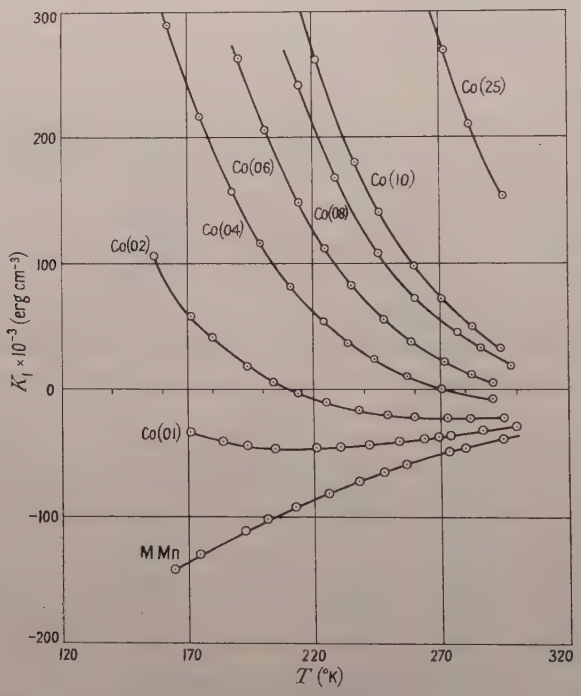

Figure 3. Experimental values of K_1 plotted against temperature for cobalt-substituted crystals.

Seavey and Tannenwald (1957) (assuming $M_s = 400$) at room temperature, 295°K, for crystals containing 0, 4 and 10 mol % substitution of cobalt ferrite. Although our value of K_1 for manganese ferrite is significantly higher, presumably the Seavey and Tannenwald crystal in this case contained more ferrous ferrite which we have found reduces the numerical value of K_1. However, these

Table 4

Cobalt concentration	K_1 (ST)	K_1 (torque method)
0 mol %	−28000	−39000
4 (3·8)	− 8000	− 8000
10 (9·4)	+44000	+30000

The values of the cobalt concentration given in brackets correspond to the chemical analysis of our crystals. The chemical analysis of the crystals used by Seavey and Tannenwald (ST) is not known.

differences will be more fully discussed in a separate report on the intrinsic anisotropy of manganese ferrite, whereas here we are primarily concerned with the effect of the substituted cobalt ions.

§ 5. Discussion of Results

The results shown in figure 3 confirm that the qualitative effect of cobalt on the anisotropy of manganese ferrite is similar to that reported for magnetite by Bickford (1957). The cobalt ions (Co^{2+}) introduce a positive contribution to the first order anisotropy constant K_1 and this contribution increases rapidly as the temperature is reduced. In figure 4, the temperature at which K_1 passes through zero is plotted as a function of cobalt concentration, while on the same graph are

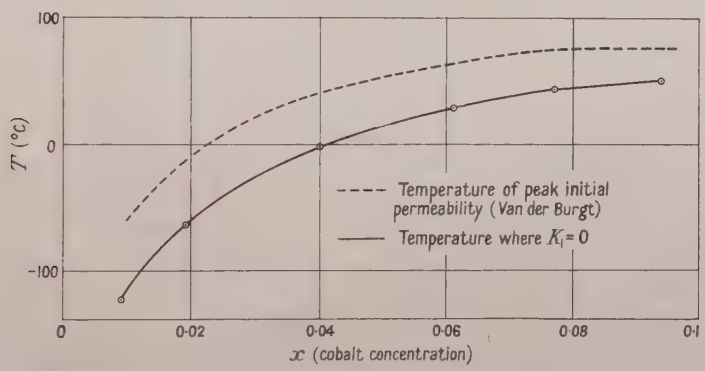

Figure 4. Temperature at which $K_1 = 0$ plotted as a function of cobalt concentration.

plotted results of Van der Burgt (1957) showing the temperatures at which peaks in the initial permeability of cobalt substituted manganese ferrite occur. Although these curves show the same variation with composition, our results indicate that K_1 passes through zero at 0°c for a cobalt substitution of 4 mol % compared with a value of about 2·2 mol % deduced from the results of Van der Burgt. This disagreement may be due to the effect of K_2 the second order anisotropy constant on the permeability, in which case one would not expect the permeability peak to occur exactly at the temperature at which K_1 goes through zero.

If now from the results shown in figure 3 we evaluate the contribution of the Co^{2+} ion to the anisotropy, by subtracting the value of K_1 for manganese ferrite from the value of K_1 for the cobalt-substituted crystal, we find that at a particular temperature this contribution is a linear function of the cobalt concentration x. In figures 5 and 6, these contributions to the anisotropy are plotted for different

temperatures from 290° K to 170° K. If we consider the results plotted for 290°K, we see rather surprisingly that the anisotropy contribution is a linear function of cobalt concentration up to 25% substitution compared to the limit of 10% found in cobalt-substituted magnetite crystals by Bickford (1957). Also if we extend the line to 100% cobalt-substitution a value of $K_1 = 0{\cdot}8 \times 10^6$ ergs cm^{-3} is obtained, whereas the previously reported values of K_1 for cobalt ferrite are about 3×10^6 erg cm^{-3}. Using the notation of Van der Burgt (1957) we may write the anisotropy constant K_x of the substituted ferrite in terms of the K_1 values for the pure ferrite ($x=0$), in our case manganese ferrite, and the K_1 value for cobalt ferrite ($x=1$), i.e. $K_x = (1-x)K_{x=0} + axK_{x=1}$ where the coefficient a describes the activity of the cobalt substitutions and is not necessarily unity and in addition depends on temperature. In figure 7, the value of a is plotted as a function of temperature, for substitutions in magnetite and manganese ferrite. The coefficient a is less than unity for manganese ferrite at room temperature and increases steadily as the temperature is decreased. However, the values of a should be treated with caution as the K_1 values for cobalt ferrite used in the calculation of the results were obtained by Shenker (1956) on a crystal of composition $Co_{1{\cdot}01}Fe_{2{\cdot}0}O_{3{\cdot}62}$ which is obviously non-stoichiometric.

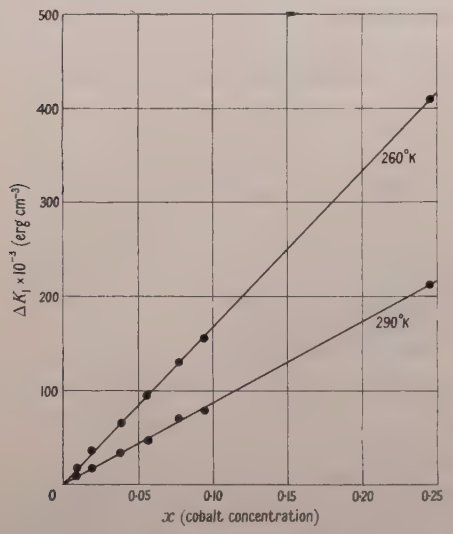

Figure 5. Contribution to K_1 plotted against cobalt concentration at 290°K, 260°K.

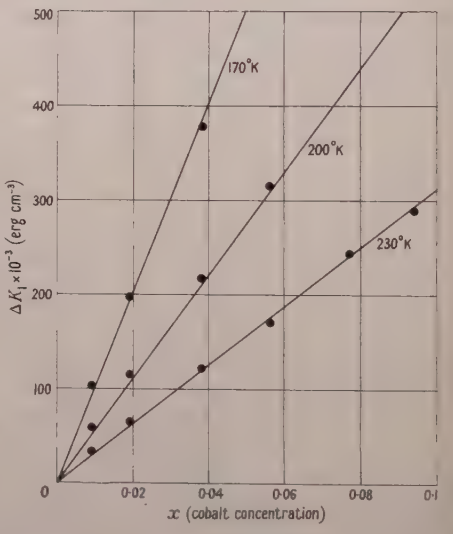

Figure 6. Contribution to K_1 plotted against cobalt concentration at 230°K, 200°K, 170°K.

Finally, in figure 8 we have plotted the contribution to the anisotropy of 1 mol % cobalt-substitution in manganese ferrite as a function of temperature. These values have been derived from the gradients of the lines shown in figures 5 and 6. The graph shows quite clearly, by comparison with results of Bickford (1957) and Shenker (1957), the different variation with temperature of the anisotropy contributions from Co^{2+} ions substituted in manganese ferrite to that in magnetite.

Although the distribution of the magnetic ions (Mn^{2+}, Mn^{3+}, Fe^{2+}, Fe^{3+}) in manganese ferrite is more complex than in magnetite, we have assumed that the contribution to the anisotropy from these ions is small compared with that from the substituted Co^{2+} ions, which are assumed to prefer the octahedral sites of the

spinel lattice. Therefore we might expect that the theory put forward by Slonczewski (1958) to explain the anisotropy of Co^{2+} ions in Fe_3O_4 would be applicable for manganese ferrite. Slonczewski has pointed out that since the lowest orbital level of the Co^{2+} ion on an octahedral site is degenerate, then a small trigonal crystal field will tend to couple the angular momentum to the [111] axis of the lattice. Spin orbit interaction then effectively couples the spin to the lattice producing a resultant magnetocrystalline anisotropy which satisfactorily describes the experimental observed values of K_1. An attempt has been made to fit the theoretical expressions derived by Slonczewski to the present results by adjustment of the atomic parameter $\alpha\lambda$. (Taken to be 132 cm^{-1} for Co^{2+} ions in magnetite.) However, although particular values of K_1 may be fitted to different values of this parameter, no value can be found which gives satisfactory agreement over the whole temperature range.

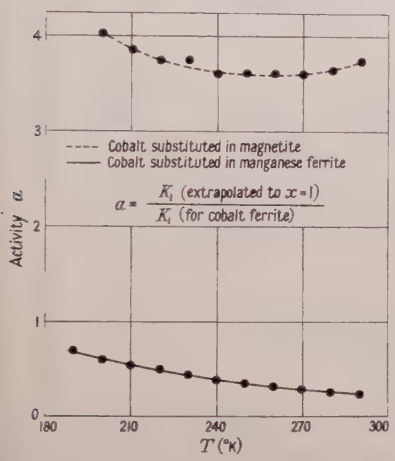

Figure 7. Activity of cobalt substitution as a function of temperature.

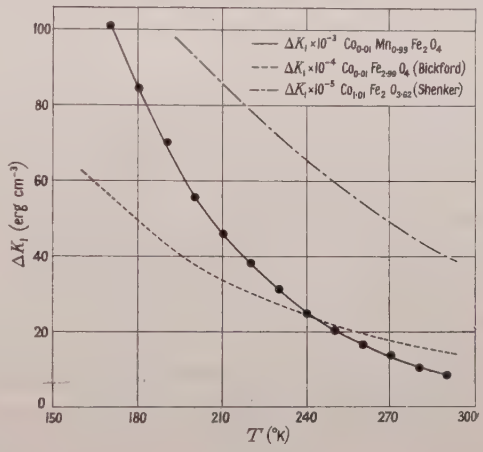

Figure 8. Contribution to anisotropy of Co^{2+} ion in $MnFe_2O_4$ as a function of temperature.

On the other hand it has been suggested by Smit (1958, private communication) and Wolf (1958, private communication) that in manganese ferrite the substituted cobalt ion would not be in a field of trigonal symmetry and the Co^{2+} ion would be effectively in a singlet orbital ground state. It is then possible to apply the theoretical treatment given by Wolf (1957) for ions in S-states. However, it would appear at the moment that this theory would still give rise to a much smaller temperature variation of the anisotropy than is found experimentally.

Bickford (1957) suggested that the effect of cobalt on the anisotropy of magnetite was enhanced by the presence of divalent iron ions and therefore further experimental results of the anisotropy of cobalt substituted manganese ferrous ferrite would be of interest. Preliminary measurements on this system indicate that no simple correlation can be found between the divalent iron content and the activity of substituted cobalt ions. It seems clear at the moment that further experimental work on the anisotropy of cobalt substituted ferrites is necessary before a clear understanding of the behaviour of cobalt ions in spinel ferrites can be gained.

§ 6. Conclusion

Experimental measurements of the anisotropy of cobalt-substituted manganese ferrite crystals have confirmed that cobalt substitutions in this material are much less effective in influencing the anisotropy than for magnetite. The variation with temperature of the contribution to the anisotropy from the substituted cobalt ions has been found to be greater in manganese ferrite than in magnetite. Attempts to interpret these results in terms of theoretical models recently proposed to explain the anisotropy of the cobalt ion have proved unsuccessful.

Acknowledgments

The author wishes to thank Dr. K. Hoselitz, under whose direction this work was carried out, and various members of the Mullard Research Laboratories for their co-operation, particularly Mr. J. L. Page of the Crystal Growing Section, Mr. R. Cooper who made all the experimental measurements and Mr. J. Roberts for the chemical analysis.

References

Bickford, L. R., Jr., Brownlow, M. S., and Penoyer, R. F., 1957, *Proc. Instn Elect. Engrs* B, **104,** Suppl., 238.
Bond, W. L., 1951, *Rev. Sci. Instrum.*, **22,** 344.
—— 1954, *Ibid.*, **25,** 401.
Bozorth, R. M., 1951, *Ferromagnetism* (New York: Van Nostrand), p. 579.
Harrison, F. W., 1956, *J. Sci. Instrum.*, **33,** 5.
Pearson, R. F., 1959, *J. Phys. Radium*, **20,** 409.
Seavey, M. M., and Tannenwald, P. E., 1956, *Proc. Inst. Radio Engrs, N.Y.*, **44,** 1343.
Shenker, H., 1957, *Phys. Rev.*, **107,** 1246.
Slonczewski, J. C., 1958, *Phys. Rev.*, **110,** 1341.
Van der Burgt, C. M., 1957, *Philips Res. Rep.*, **12,** 97.
Wolf, W. P., 1957, *Phys. Rev.*, **108,** 1152.

The Principal g Values of Ytterbium Ions in Yttrium Acetate, a Triclinic Crystal

By J. G. PARK†
Clarendon Laboratory, University of Oxford

MS. received 8th May 1959

Abstract. The principal g values of ytterbium ions in yttrium acetate have been determined by a method which requires that the single crystal specimen can be rotated about a horizontal axis inside the cavity of a paramagnetic resonance apparatus, as well as the more usual requirement that the horizontal magnetic field can be rotated about a vertical axis. By this method the principal g values are measured directly when they are located, whereas in other methods that have been proposed they are calculated from measurements of certain g values and angles.

The orientation of the g tensor was not determined in our experiments, but a method for finding it is outlined here. The results were (choosing x, y, z so that $g_x > g_y > g_z$)

$$g_x = 4{\cdot}583 \pm 0{\cdot}008, \quad g_y = 2{\cdot}117 \pm 0{\cdot}004, \quad g_z = 0{\cdot}71 \pm 0{\cdot}03.$$

§ 1. Introduction

The principal g values of the lowest doublet of Yb^{3+} ions in an yttrium acetate crystal have been determined, using a device for rotating the crystal about a horizontal axis inside a paramagnetic resonance apparatus. The concentration of Yb^{3+} ions was about 1%. Crystals of yttrium acetate, $Y(CH_3COO)_3.4H_2O$, are triclinic and x-ray oscillation photographs have shown that there are two molecules in the unit cell. Only one paramagnetic resonance spectrum has been observed, so that the two types of Yb^{3+} ion must be equivalent magnetically. Furthermore, the spectrum must be due to the lowest doublet, since a crystalline electric field of rhombic or lower symmetry (it must be lower than rhombic in a triclinic crystal) splits the free ion levels into Kramers' doublets, in any of which resonance transitions are allowed. In a magnetic field the splitting of each doublet depends on the direction of the field in relation to the crystal and can be characterized by a g tensor with principal values g_x, g_y and g_z, provided two levels of different doublets do not approach too close to one another. Since only one spectrum is observed it is unlikely that the next doublet is near enough to affect the separation of the lowest doublet levels. The energy levels of the lowest doublet in a magnetic field are then given by the effective spin Hamiltonian (Pryce 1950)

$$\mathscr{H} = \beta \sum_{i=x,\,y,\,z} g_i H_i S_i$$

to which must be added further terms if the ions have a nuclear spin. The axes x, y, z are here the principal axes of the g tensor, the S_i are components of the spin

† Now at H. H. Wills Physics Laboratory, University of Bristol.

operator for spin $\frac{1}{2}$ and β is the Bohr magneton. For a magnetic field H in the direction (l, m, n) the 'g value' is defined by

$$g^2 = g_x^2 l^2 + g_y^2 m^2 + g_z^2 n^2. \qquad \ldots\ldots (1)$$

For ions without nuclear spin the splitting of the doublet is $g\beta H$.

The paramagnetic resonance spectrum of Yb^{3+} ions in yttrium acetate has been observed at 4·2°K and a wavelength of 3 cm (Cooke and Park 1956). At higher temperatures the lines in the spectrum are broadened by spin–lattice relaxation, and at liquid hydrogen temperatures they could not be observed. The spectrum has a hyperfine structure due to the two isotopes ^{171}Yb and ^{173}Yb which have nuclear spin, but there is a single strong line, the 'main line', corresponding to isotopes of even mass which constitute 70% of ytterbium and have no nuclear spin. From the position of the 'main line' at a field H, g can be calculated directly; if the microwave frequency is ν, $g = h\nu/\beta H$.

In the method described here for measuring the principal g values, each of the axes of the g tensor is aligned in turn with the magnetic field by rotating the crystal about a horizontal axis and the corresponding g value can then be measured directly, along with the angle between the tensor axis and the crystal rotation axis. If only the magnitudes of the principal g values are required, no angles need be measured. Other methods that have been proposed do not determine the g tensor so directly (Geusic and Brown 1958, Schonland 1959, Weil and Anderson 1958) but calculate its orientation and principal values from measurements of g values and certain angles in three mutually orthogonal planes in the crystal. These other methods are probably not capable of such precision as ours, but could be used when it is not possible or convenient to rotate a crystal about a horizontal axis from outside the paramagnetic resonance apparatus.

§ 2. Method

The construction of the crystal rotator will only be outlined here. It consists of two concentric tubes. The outside tube supports a Perspex gear wheel which can rotate inside the resonant cavity about a horizontal axis, and to this gear the crystal is attached. A second gear wheel with its axis vertical is fixed to the inside tube, and engages with the first. When the inside tube is turned and the outside tube held still, the crystal rotates.

For each setting of the rotator, the maximum and minimum g values in the horizontal plane, g_+ and g_-, can be measured by rotating the horizontal magnetic field about a vertical axis into the positions for which the 'main line' appears in minimum or maximum field. In 180° rotation of the crystal g_+ and g_- themselves each have a maximum and a minimum. It is clear that the maximum g_+ ($g_+^{\max}$) and the minimum g_- ($g_-^{\min}$) are respectively the largest and smallest of the principal g values, g_x and g_z, say. (Throughout this paper we shall label the axes to make $g_x > g_y > g_z$.) One of the other two extreme values $g_+^{\min}$ and $g_-^{\max}$ is g_r, the g value when the magnetic field lies along the crystal rotator axis; the remaining one is g_y as we show below. Provided the direction of the rotator axis is roughly known, and the angle between it and the g_y axis is not too small, g_y and g_r can be distinguished. Alternatively, they can be distinguished by experiments with different axes of rotation. Either $g_+^{\min}$ or $g_-^{\max}$ will be g_y, and this value common to all the experiments can easily be picked out.

The orientation of the g tensor axes can be determined at the same time since in measuring the principal g values, the g tensor axes and the rotator axis are located by the magnetic field. Thus the angles between each of the tensor axes and the crystal rotation axis can be measured as angles turned through by the magnet.

§ 3. Theory of the Method

Suppose that in the g tensor system of axes x, y, z, fixed in the crystal, the axis of rotation of the crystal rotator is given by the direction cosines (p, q, r). The normal to the horizontal plane, and to (p, q, r) which lies in it, is then (a, b, c), where,

$$a=\sqrt{(1-p^2)}\cos\epsilon,\quad b=-\sqrt{(1-q^2)}\cos(\epsilon+\beta),\quad c=-\sqrt{(1-r^2)}\cos(\epsilon-\gamma). \qquad \ldots\ldots(2)$$

Here $\tan\beta=r/pq$, $\tan\gamma=q/rp$ and ϵ is the angle through which the crystal has been rotated from a position in which the x-axis lies in the vertical plane through (p, q, r).

The most straightforward way of calculating g_+ and g_- is to relate new axes x', y', z' to the tensor axes x, y, z, using Euler angles θ, ϕ, ψ making x' the magnetic field direction and $x'-y'$ the horizontal plane. If varying ψ rotates x' about z' then $g=g_\pm$ when $\partial g/\partial\psi=0$. One thus finds that

$$g_\pm{}^2=\tfrac{1}{2}P\pm\sqrt{(P^2-4Q)} \qquad \ldots\ldots(3)$$

where

$$P=g_x{}^2(1-a^2)+g_y{}^2(1-b^2)+g_z{}^2(1-c^2)$$
$$Q=g_y{}^2g_z{}^2a^2+g_z{}^2g_x{}^2b^2+g_x{}^2g_y{}^2c^2.$$

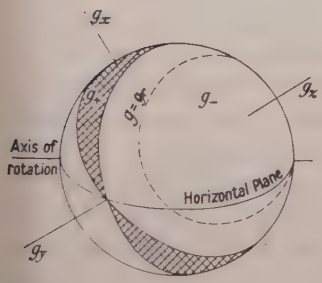

Figure 1.

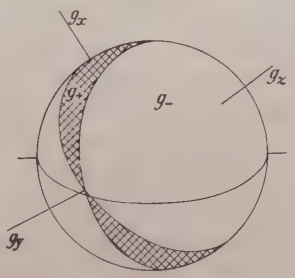

Figure 2.

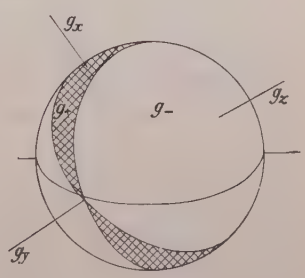

Figure 3.

The figures show, with the aid of the text, that g_y $(g_x>g_y>g_z)$ is $g_+{}^{\min}$, and g_r, the g value along the axis of rotation, is $g_-{}^{\max}$ in the example illustrated. In general g_y and g_r may be either $g_+{}^{\min}$ or $g_-{}^{\max}$ depending on the axis of rotation in relation to the crystal axes.

It can be shown by differentiating (3) with respect to ϵ that three of the four extreme values of g_+ and g_- are g_x, g_y and g_z. Since

$$g_+{}^{\max}=g_x \quad\text{and}\quad g_-{}^{\min}=g_z \quad g_y=g_+{}^{\min} \quad\text{or}\quad g_-{}^{\max}.$$

Presumably it can also be proved using (2) and (3) that g_r is the fourth extreme value but we have been content with the following proof.

Suppose the variation of g with field direction to be represented by a set of contours of constant g on the surface of a sphere; as the crystal rotates, the sphere rotates with it. Then it can be shown that the contours $g=g_y$ $(g_x>g_y>g_z)$ form

two great circles intersecting at the point on the surface corresponding to the g_y axis, as shown in figures 1 to 3, and that these contours separate two regions: in one region $g > g_y$ and in the other $g < g_y$. The region $g > g_y$ is shown shaded in the figures. As long as the horizontal plane does not include the g_y axis, g_- is found in the shaded region and g_+ in the other region, as in figures 2 and 3. In the example shown, the rotator axis lies in the unshaded region and when the horizontal plane does pass through g_y, as in figure 1, $g_y = g_+$. It can be seen from figures 2 and 3 that for small rotations about the rotator axis in either sense away from $g_+ = g_y$, g_- increases. Thus, in this example, g_y is $g_+^{\min}$.

In figure 1, the contour $g = g_r$ is shown by a dotted line. Inside the contour $g < g_r$. Generally the horizontal plane and the contour cut one another and $g_- < g_r$, but in one orientation of the crystal they touch and then $g_r = g_-^{\max}$. If the rotator axis lies in the g_- region then $g_y = g_-^{\max}$ and $g_r = g_-^{\min}$. If it happens to lie in one of the planes $g = g_y$, two extreme values of g_- coincide and

$$g_+^{\min} = g_-^{\max} = g_y = g_r.$$

§ 4. Experimental Results

The principal g values for 1% Yb^{3+} in yttrium acetate were found to be

$$g_x = 4{\cdot}583 \pm 0{\cdot}008$$
$$g_y = 2{\cdot}117 \pm 0{\cdot}004$$
$$g_z = 0{\cdot}71 \pm 0{\cdot}03.$$

The magnetic field was measured by proton resonance. The proton resonance coil was wound on a Perspex former which was itself the proton sample.

No g value less than 1·4 could be measured directly in our apparatus, since it would require a higher magnetic field than we could obtain and g values less than 1·4 had to be found by extrapolation. When the magnetic field makes an angle θ with the direction corresponding to g_+, $g^2 = (g_+^2 - g_-^2)\cos^2\theta + g_-^2$. Thus if g_- was less than 1·4, g values greater than 1·4 were measured for various θ, and g^2 was plotted against $\cos^2\theta$ and extrapolated to $\cos^2\theta = 0$ to determine g_-. This method was used to find the smaller values of g_- in order to determine $g_-^{\min}$ which is g_z.

In these experiments the orientation of the g tensor was not determined.

Acknowledgments

I should like to thank Dr. A. H. Cooke for his help and encouragement in this work, Dr. R. G. Chambers for help in writing this paper and for making the principles of the method described in it clearer to me with the aid of figures 1 to 3, Mrs. J. Kamper for taking the x-ray oscillation photographs, and the Department of Scientific and Industrial Research for a maintenance grant while the work was being carried out.

References

Cooke, A. H., and Park, J. G., 1956, *Proc. Phys. Soc.* A, **69,** 282.
Geusic, J. E., and Brown, L. C., 1958, *Phys. Rev.*, **112,** 64.
Pryce, M. H. L., 1950, *Proc. Phys. Soc.* A, **63,** 25.
Schonland, D. S., 1959, *Proc. Phys. Soc.*, **73,** 788.
Weil, J. A., and Anderson, J. H., 1958, *J. Chem. Phys.*, **28,** 864.

On the Angular Distribution of (d, p) Stripping Reactions

By T. HONDA and M. NAGASAKI†
Department of Physics, Rikkyo University, Tokyo, Japan

MS. received 2nd March 1959, in final form 30th April 1959

Abstract. It is numerically investigated how the angular distributions of some typical (d, p) stripping reactions given by the Butler theory are modified by the supposition that in a simple (d, p) stripping process protons do not penetrate into the nucleus, in contrast to the assumption of the Butler theory that protons move freely even in the nucleus. The result of the calculation shows that the general trend of the angular distributions given by the present model gives a better fit to the experimental data than that given by the Butler theory, though it is not greatly altered in both relative and absolute values in the cases of relatively light nuclei and high incident energies. The best fit nuclear radii determined by the present model are found to be given by the Gamow–Critchfield formula $a=(1{\cdot}22A^{1/3}+1{\cdot}70)\times 10^{-13}$ cm. These nuclear radii are smaller than some of the best fit nuclear radii obtained in the analyses hitherto done by using the Butler theory.

§ 1. Introduction

It is well known that the theory of deuteron stripping reactions developed by Butler (1951) has accounted well for the pronounced structure at small angles in the angular distributions of (d, p) and (d, n) reactions at energies of several million electron volts above the Coulomb barrier. Making use of the Butler formula for the cross section, the spins and parities of many nuclear energy levels have been determined by experiments.

The basic assumption in the Butler theory is that in a deuteron stripping reaction one of the nucleons in the incident deuteron is absorbed into the target nucleus, while the other nucleon merely carries off the balance of energy and momentum without interacting with the nucleus. It is, therefore, assumed that the nucleon to be stripped off moves freely even in the nucleus. Thus, the Butler formula for the cross section includes the contribution from the configuration in which both nucleons of the incident deuteron are simultaneously in the nucleus. For such a configuration, however, it seems more natural to take into account the possibility of forming the compound nucleus.

In a previous paper, one of the present authors (Nagasaki 1956) has given a formula for the cross section for deuteron induced nuclear reactions, in which the interactions between the target and both of the nucleons in the incident deuteron are taken into account. In the cross section for the deuteron stripping reaction derived in that paper only that process has been included in which one of the nucleons in the deuteron is absorbed into the nucleus while the other nucleon emerges without entering into the nucleus. The process in which the whole deuteron penetrates into the nucleus, on the other hand, has been considered to

† Now at Instituo di Fisica, Università Catania, Italy.

cause the formation of the compound nucleus. Nagasaki's formula for the cross section for the stripping reaction is, therefore, somewhat different from that of Butler.

The purpose of the present paper is to investigate numerically the consequence of this modification in the angular distribution of some typical (d, p) stripping reactions.

In § 2 the underlying assumptions are briefly described and the formula for the cross section for the (d, p) stripping reaction is given, and the results of the present numerical calculations are shown and compared with the Butler theory and the experimental data.

In § 3 discussions are given and the conclusion derived from the present analysis is stated.

§ 2. Calculation and Results

2.1. *Calculation*

According to Nagasaki (1956), the differential cross section for the (d, p) stripping reaction is given by the following formula

$$\frac{d\sigma}{d\Omega_{\mathrm{p}}} = \frac{M_{\mathrm{pF}} M_{\mathrm{dI}} k_{\mathrm{p}}}{(2\pi\hbar)^2 k_{\mathrm{d}}} \frac{1}{3(2I+1)} \sum_{\text{spin}} \left| \int_{(\mathrm{ext})} d\tau \exp\left(-i\mathbf{k}_{\mathrm{p}}\mathbf{r}_{\mathrm{p}}'\right) \chi_{\mathrm{f}}^{*}(\mathbf{r}_{\mathrm{n}}, \xi) \right.$$
$$\left. \times (V_{\mathrm{n}\xi} + V_{\mathrm{p}\xi}) \exp\left(i\mathbf{k}_{\mathrm{d}}(\mathbf{r}_{\mathrm{p}} + \mathbf{r}_{\mathrm{n}})/2\right) w_{\mathrm{d}}(\mathbf{r}) \chi_{\mathrm{i}}(\xi) \right|^2. \qquad \ldots\ldots (2.1)$$

Here χ_{i} represents the wave function of the initial nucleus together with the spin functions of the initial system of the deuteron and the nucleus. ξ being the internal coordinates of the initial nucleus and all the spin coordinates of the system. χ_{f} is the product of the wave function of the final nucleus and the spin function of the proton, and w_{d} is the internal wave function of the deuteron. $V_{\mathrm{n}\xi}$ and $V_{\mathrm{p}\xi}$ are the interaction potential of the neutron and the proton with the initial nucleus, respectively. $\hbar\mathbf{k}_{\mathrm{p}}$ and M_{pF} are the momentum and the reduced mass, respectively, of the relative motion between the proton and the final nucleus. $\hbar\mathbf{k}_{\mathrm{d}}$ is the momentum and M_{dI} is the reduced mass of the incident deuteron relative to the initial nucleus. $\mathbf{r}_{\mathrm{p}}$ and $\mathbf{r}_{\mathrm{n}}$ are the vectors connecting the centre of mass of the initial nucleus and the proton and the neutron, respectively, while $\mathbf{r}_{\mathrm{p}}'$ is the separation of the proton from the centre of mass of the final nucleus. I is the spin of the initial nucleus and $\sum_{\text{spin}}$ denotes summation over the directions of the spins of the initial and final nuclei, proton and deuteron. $\int_{(\mathrm{ext})}$ means the integration with respect to all the coordinates of the system over the external region (Nagasaki 1956), including the summation with respect to all the spin variables.

In deriving this formula, exchange effects among nucleons are neglected. Also the Coulomb interaction between the emerging proton and the residual nucleus and that between the incident deuteron and the target nucleus are not taken into account. The actual differential cross section may be affected by the interaction between the stripped proton and the residual nucleus, the compound nucleus formation and by the possibility that deuterons emitted from the compound nucleus or scattered by the target nucleus are stripped again (Nagasaki 1956). All these effects, however, are left out of account here and only the simple stripping process will be considered.

In (2.1), that part of integration which contains $V_{p\xi}$ contributes only through the exponentially damped tail of $\chi_f(\mathbf{r}_n, \xi)$ for $\mathbf{r}_n$ which is beyond the range of the interaction of the neutron with the initial nucleus. This contribution may be neglected if the binding energy of the captured neutron is not too small. Also, if the exponentially decaying tail of $\chi_i(\xi)$ for the proton extends over a long distance $V_{n\xi}+V_{p\xi}$ contributes to the cross section through the extension, and the process which arises from this fact is the so called heavy particle stripping reaction (Owen and Madansky 1957). Assuming the binding energy of protons in the initial nucleus not to be so small, this process will be left out of consideration too. Thus (2.1) reduces to

$$\frac{d\sigma}{d\Omega_p} = \frac{M_{pF}M_{dI}k_p}{(2\pi\hbar)^2 k_d}\frac{1}{3(2I+1)}\sum_{\text{spin}}\left|\int_{r_n<a_0} d\mathbf{r}_n \int_{r_p'>a} d\mathbf{r}_p' \int d\xi \exp(-i\mathbf{k}_p\mathbf{r}_p')\right.$$
$$\left.\times \chi_f^*(\mathbf{r}_n,\xi)V_{n\xi}\exp(\tfrac{1}{2}i\mathbf{k}_d(\mathbf{r}_p+\mathbf{r}_n))w_d(\mathbf{r}_p-\mathbf{r}_n)\chi_i(\xi)\right|^2, \quad \ldots\ldots (2.2)$$

where a_0 is the range of the interaction between the captured neutron and the initial nucleus and a is that between the stripped off proton and the final nucleus. In the following calculation, it will be assumed that $a_0 = a$.

Using the Schrödinger equations that $\exp(-i\mathbf{k}_p\mathbf{r}_p')\chi_f^*(\mathbf{r}_n,\xi)$ and

$$\exp(i\mathbf{k}_d(\mathbf{r}_p+\mathbf{r}_n)/2)w_d(\mathbf{r})\chi_i(\xi)$$

satisfy for $r_n < a$ and $r_p' > a$, and assuming that the kinetic energy of the neutron in the nucleus is large compared with that of the proton outside the nucleus on account of the strong interaction between the neutron and nucleus, (2.2) can be rewritten as

$$\frac{d\sigma}{d\Omega_p} = \frac{M_{pF}M_{dI}k_p}{(4\pi)^2 M_{nI}^2 k_d}\frac{2J+1}{2(2I+1)(2l_n+1)}\left(\frac{8\pi\sqrt{(2\pi\alpha)}a}{K^2+\alpha^2}C_{l_n}\right)^2$$
$$\times\sum_{m_n}\left|A_{l_n}Y_{l_n}m_n^*(\Omega_q) - \sum_l\sum_\lambda B_{l\lambda}^{l_n}(l\lambda m_n 0|\,l\lambda l_n m_n)Y_{lm_n}^*(\Omega_k)\right|^2, \quad \ldots\ldots (2.3)$$

where

$$A_{l_n} = i^{l_n}\{i\beta a h_{l_n}^{(1)\prime}(i\beta a)j_{l_n}(qa) - qa\,j_{l_n}'(qa)h_{l_n}^{(1)}(i\beta a)\} \quad \ldots\ldots (2.3\,a)$$

$$B_l^{l_n} = (\alpha a)i^{l+\lambda}\{(2l+1)/(2l_n+1)\}^{1/2}(2\lambda+1)(l\lambda 00|\,l\lambda l_n 0)$$
$$\times\{Kaj_{l-1}(Ka)j_l(i\alpha a) - i\alpha a j_l(Ka)j_{l-1}(i\alpha a)\}$$
$$\times\{i\beta a h_{l_n}^{(1)\prime}(i\beta a)h_l^{(1)}(i\tilde{\alpha}a)j_\lambda(\tfrac{1}{2}k_d a)$$
$$- i\tilde{\alpha}a h_{l_n}^{(1)}(i\beta a)h_l^{(1)\prime}(i\tilde{\alpha}a)j_\lambda(\tfrac{1}{2}\tilde{k}_d a)$$
$$- \tfrac{1}{2}\tilde{k}_d a h_{l_n}^{(1)}(i\beta a)h_l^{(1)}(i\tilde{\alpha}a)j_\lambda(\tfrac{1}{2}\tilde{k}_d a)\}. \quad \ldots\ldots (2.3\,b)$$

Here

$\mathbf{q} = \mathbf{k}_d - (M_I/M_F)\mathbf{k}_p$, q and Ω_q being the length and direction of $\mathbf{q}$;

$\mathbf{K} = (1/2)\mathbf{k}_d - \mathbf{k}_p$, K and Ω_k being the length and direction of $\mathbf{K}$;

$\tilde{\alpha} = \alpha(M_I/M_F)$, and $\tilde{k}_d = k_d \cdot M/M_{pF}$.

M_{nI} is the reduced mass of the captured neutron relative to the initial nucleus, M_I and M_F are the masses of the initial and the final nucleus respectively and M is the mass of a nucleon.

$j_l(z)$ and $h_l^{(1)}(z)$ are the first kind spherical Bessel and the Hankel functions, respectively, of order l of argument z. Y_{lm} is the normalized spherical harmonic. Primes attached to these functions denote differentiation with respect to their

respective arguments. In the deduction of (2.3) the internal wave function of deuteron $w_d(\mathbf{r})$ is chosen as

$$w_d(\mathbf{r}) = (\alpha/2\pi)^{1/2} e^{-\alpha r}/r,$$

where $\alpha = (M/\hbar)^{1/2} \times$ (binding energy of the deuteron)$^{1/2} = 0{\cdot}23 \times 10^{13}\,\mathrm{cm}^{-1}$. Also the wave function of the neutron captured in the final nucleus $\zeta(\mathbf{r}_n)$ given by

$$\zeta(\mathbf{r}_n) = \int d\xi \chi_1^*(\xi) \chi_f(\mathbf{r}_n, \xi)$$

is assumed to take the form of the shell model wave function

$$\zeta(\mathbf{r}_n) = C_{l_n} h_{l_n}^{(1)}(i\beta r_n) \mathscr{Y}_{\frac{1}{2} l_n}^{j\mu},$$

near the surface of the nucleus, namely for $r_n \geqslant a$. $\hbar^2\beta^2/2M_{nI}$ is the binding energy of the captured neutron, and $\mathscr{Y}$ is the spin angle wave function defined by Blatt and Weisskopf (1952), j and μ are the spin and its z component, respectively, of the captured neutron. λ gives the angular momentum of the neutron due to the motion of the centre of mass of the incident deuteron, while l gives the angular momentum carried by the neutron on account of its motion in the deuteron. m_n denotes the z-component of the orbital angular momentum of the captured neutron, the z axis being taken in the direction of the incident beam.

If all the $B_{l\lambda}^{l_n}$ were zero, (2.3) would give the same results as the Butler theory. The correction terms proportional to the $B_{l\lambda}^{l_n}$ are due to the supposition that the compound nucleus is formed when the proton and neutron enter into the nucleus simultaneously. Thus the wave function of stripped-off proton is no longer a plane wave as is in the Butler theory, but its amplitude vanishes in the nucleus. This, in turn, gives rise to the modification from the plane wave in the wave function of the corresponding captured neutron and results in the correction term mentioned above.

2.2. *Results*

Numerical calculations are carried out for (d, p) stripping reactions in which the target nuclei are comparatively light and the energies of incident deuterons and emerging protons are high, so that the Coulomb force does not affect angular distributions seriously. In order to avoid complexities in angular distributions, only such cases are treated for which neutrons are captured with a definite orbital angular momentum.

Results of the numerical calculation are shown in twelve graphs (figures 1 to 4). Figures 1(*a*) and (*b*) show the case $l_n = 0$; figures 2 (*a*)–(*d*), $l_n = 1$; figures 3(*a*)–(*e*), $l_n = 2$ and figure 4, $l_n = 3$. The ordinates represent the differential cross sections $d\sigma/d\Omega_p$ in arbitrary units, and the abscissae the angles of emerging protons in the centre-of-mass coordinate system in degrees. In each figure the differential cross section obtained from the present calculation is shown by a solid line and that given from the Butler theory by a dotted line, both being normalized to unity at the maxima of the curves.

The meanings of the notations indicated in each graph are as follows:

E_d = energy of incident deuteron in the laboratory system in Mev, $Q = Q$ value of the reaction in Mev, l_n = orbital angular momentum of the captured neutron, a = best fit nuclear radius in 10^{-13} cm, ρ = ratio of the maximum value of the differential cross section obtained from the present calculation to that given by the

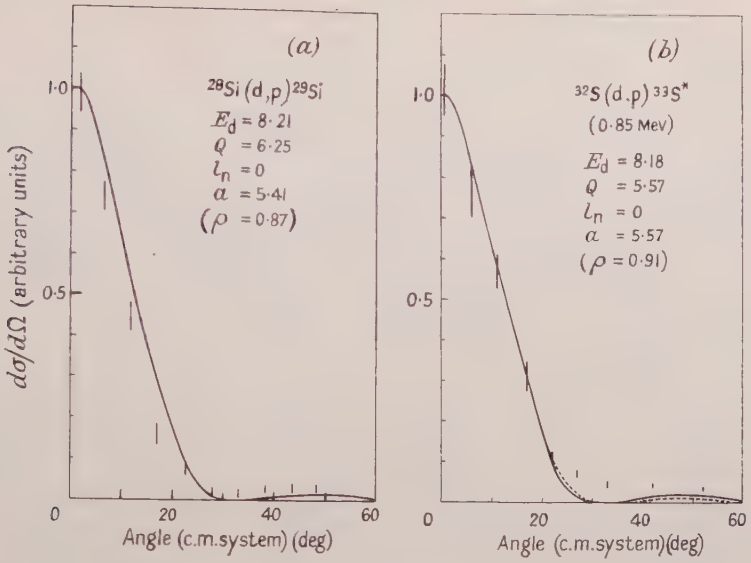

Figure 1. The centre-of-mass angular distributions of (d, p) stripping reactions for $l_n = 0$. The solid lines represent the angular distributions as given by formula (2.3), while the dotted lines represent those given by the Butler theory. The values of parameters used in the calculations, E_d (laboratory energy of deuteron), l_n (orbital angular momentum of captured neutron), Q-value of the reaction, and a (nuclear radius), are indicated in each figure. Also shown in parentheses are the values of ρ, the ratio of the maximum differential cross section obtained from the calculation to that given by the Butler theory.

The experimental data shown by vertical bars are taken from the work of Holt and Marsham (1953 a) for both figures.

Butler theory. The best fit nuclear radii are determined so as to fit the theoretical curves to the experimental data indicated by vertical bars or circles. The angular distributions based on the Butler theory are ones calculated for the nuclear radii so determined.

In these calculations, as is described in § 2.1, the Yukawa type wave function of the deuteron is adopted. It is revealed from several examples, however, that the adoption of the Hulthén type wave function makes little difference from the present calculation in the calculated angular distribution.

§ 3. Conclusion and Discussion

From the figures in § 2 it is seen that the modification of the Butler theory due to the supposition that in simple (d, p) stripping reactions protons do not penetrate into the nucleus does not much alter the numerical results in the calculated (d, p) angular distribution. This is probably due to the fact that the nuclei treated in this paper are relatively light, so that the nuclear radii are not so large compared with the extension of the wave function of the deuteron. For heavier nuclei, the angular distributions given by the Butler theory might be altered more by this modification. For example, in the case of the ^{207}Pb(d, p)^{208}Pb reaction at $E_d = 15{\cdot}1$ Mev for which l_n is taken to be one, ρ is observed to take the value 0·68.

The reduced widths determined from (d, p) reactions using the Butler formula for the cross section are known to be comparatively smaller than those determined

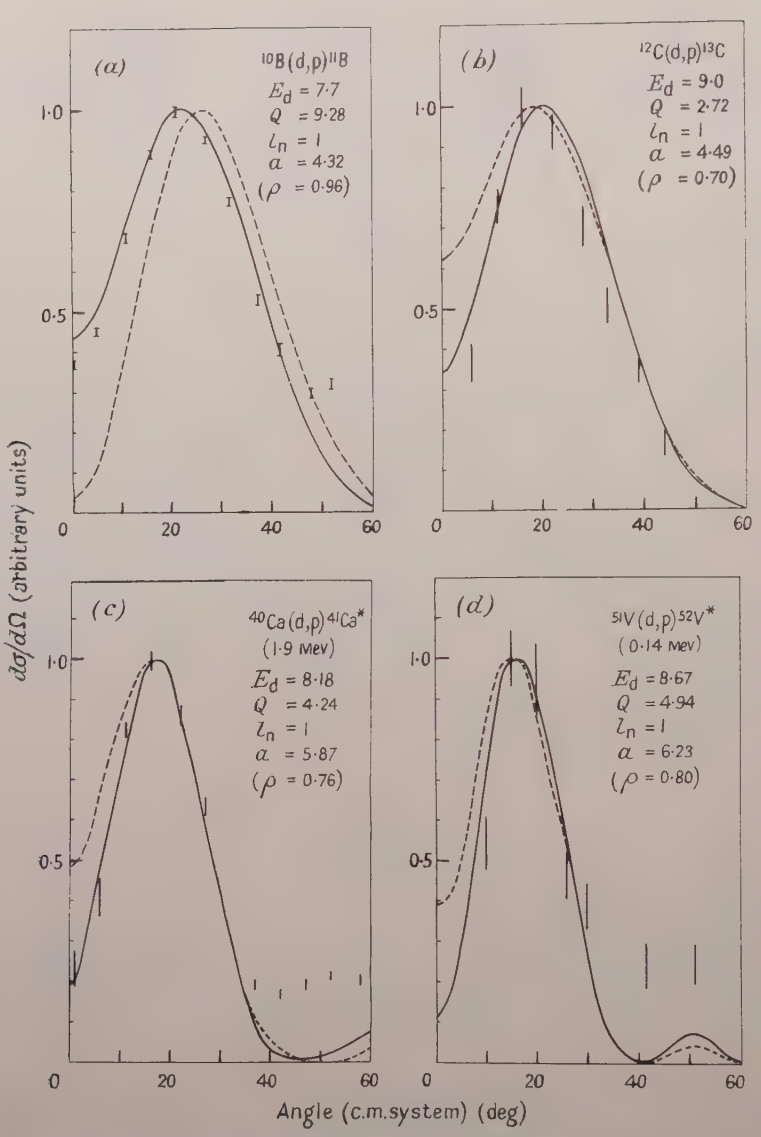

Figure 2. The centre-of-mass angular distributions of (d, p) stripping reactions for $l_n = 1$ (see the caption of figure 1).

The experimental data shown by vertical bars are taken from the work of Evans and Parkinson (1954), Green and Middleton (1956), Holt and Marsham (1953 b) and El-Bedewi and Tadros (1958) for figures 2 (*a*)–(*d*). respectively.

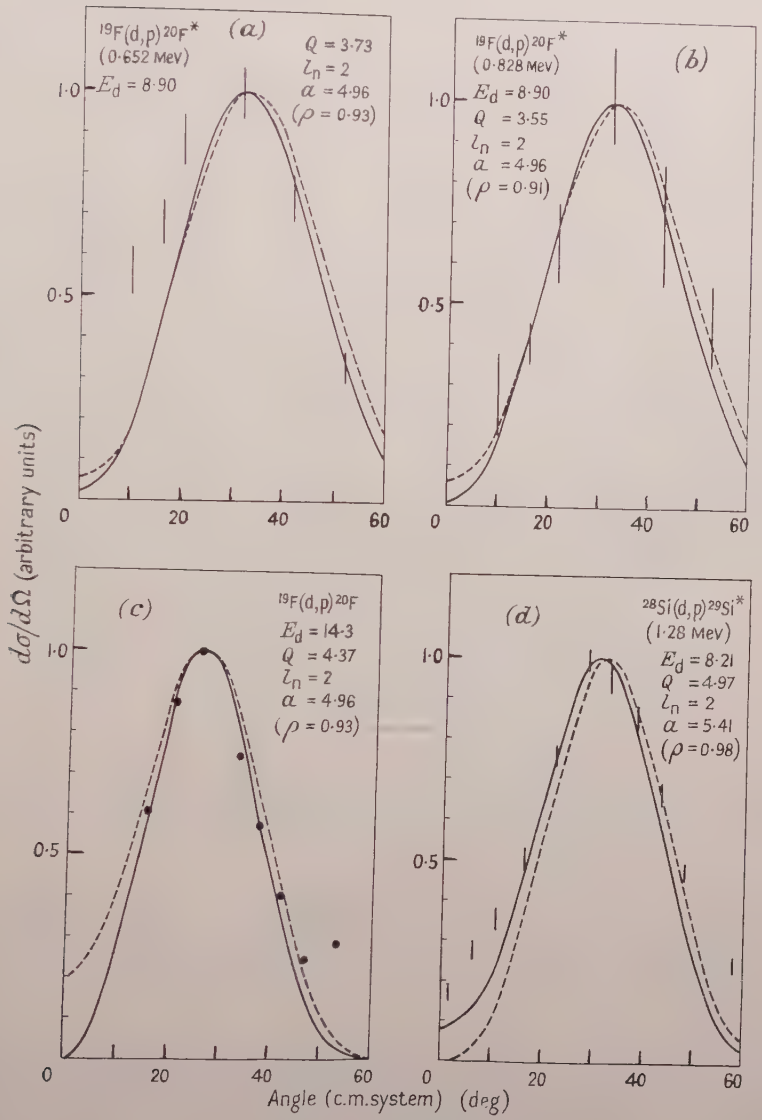

Figure 3. The centre-of-mass angular distributions of (d, p) stripping reactions for $l_n = 2$ (see the caption of figure 1).

The experimental data shown by vertical bars or circles are taken from the work of El-Bedewi (1956), Black (1953) and Holt and Marsham (1953 a) for figures 3 (*a*)–(*b*), (*c*), (*d*)–(*e*) respectively.

from other nuclear reactions (Fujimoto, Kikuchi and Yoshida 1954). This situation is not much improved by the present analysis, since the values of ρ differ from unity by at most about 30%.

It seems interesting to note that the best fit nuclear radii indicated in the figures in § 2 are relatively small. In the analyses hitherto made of experimental data on deuteron stripping reactions using the theory of Butler or Bhatia (1952), there have often been the cases in which the best fit nuclear radii are remarkably large compared with those deduced from other nuclear reactions.

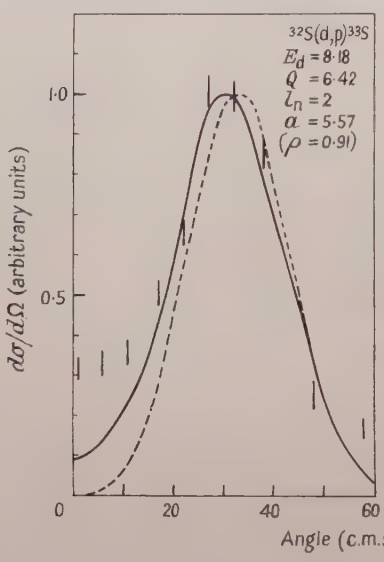

Figure 3 (*e*).

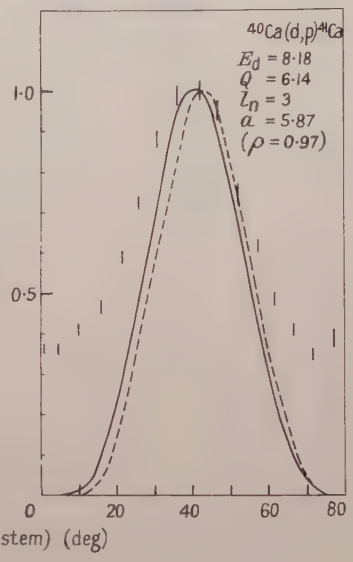

Figure 4.

Figure 4. The centre-of-mass angular distribution of (d, p) stripping reaction for $l_n = 3$ (see the caption of figure 1). The experimental data shown by vertical bars are taken from the work of Holt and Marsham (1953 b).

In the case of the $^{10}B(d, p)^{11}B$ reaction at $E_d = 7{\cdot}7$ MeV for which $l_n = 1$, the nuclear radii of $5{\cdot}32 \times 10^{-13}$ cm and $4{\cdot}32 \times 10^{-13}$ cm must be chosen for the Butler theory and the present model, respectively, in order to fit the position of the maximum of the theoretical angular distribution to the experiments as shown in figure 5(*a*).

If the nuclear radius is chosen in this way, the peak of the angular distribution given by the Butler theory, as is seen from figure 5(*a*), becomes narrower in width than those with smaller nuclear radii, and consequently the fit of the theoretical angular distribution to the experimental one becomes worse than the angular distribution given by the present model.

Figure 5(*b*) shows, as an example for $l_n = 2$, the case of the $^{32}S(d, p)^{33}S$ reaction at $E_d = 8{\cdot}18$ MeV. The nuclear radius determined by fitting the position of the maximum of the angular distribution given by the Butler theory is $6{\cdot}57 \times 10^{-13}$ cm, which is larger than the best fit nuclear radius obtained from the present model by $1{\cdot}00 \times 10^{-13}$ cm.

As in the case of boron, it is seen from the figure that the angular distribution given by the present model fits the experiments much better than that given by the Butler theory.

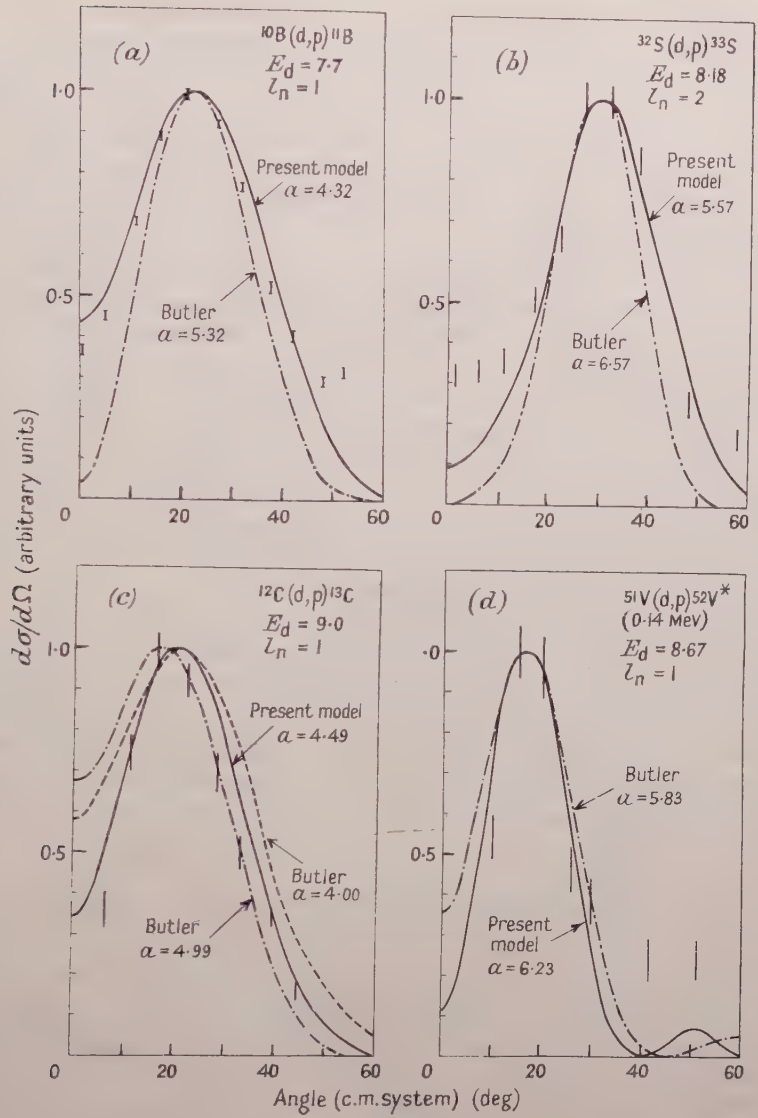

Figure 5. The centre-of-mass angular distributions of (*a*) $^{10}B(d, p)^{11}B$ reaction at $E_d = 7{\cdot}7$ MeV, (*b*) $^{32}S(d, p)^{33}S$ reaction at $E_d = 8{\cdot}18$ MeV, (*c*) $^{12}C(d, p)^{13}C$ reaction at $E_d = 9{\cdot}0$ MeV, and (*d*) $^{51}V(d, p)^{52}V^*$ (0·14 MeV) reaction at $E_d = 8{\cdot}67$ MeV. The solid lines in (*a*), (*b*), (*c*) and (*d*) are the angular distributions given by the present model with the nuclear radii $4{\cdot}32 \times 10^{-13}$ cm, $5{\cdot}57 \times 10^{-13}$ cm, $4{\cdot}49 \times 10^{-13}$ cm, and $6{\cdot}23 \times 10^{-13}$ cm for the cases of ^{10}B, ^{32}S, ^{12}C and ^{51}V, respectively, and are the same ones as the solid lines in figures 2 (*a*), 3 (*e*), 2 (*b*) and 2 (*d*), respectively. The chain lines in (*a*), (*b*), (*c*) and (*d*) are the angular distributions given by the Butler theory with nuclear radii $a = 5{\cdot}32 \times 10^{-13}$ cm, $6{\cdot}57 \times 10^{-13}$ cm, $4{\cdot}99 \times 10^{-13}$ cm and $5{\cdot}83 \times 10^{-13}$ cm for the cases of ^{10}B, ^{32}S, ^{12}C and ^{51}V, respectively. The broken line in (*c*) is the angular distribution given by the Butler theory with the nuclear radius $4{\cdot}00 \times 10^{-13}$ cm for the case of ^{12}C.

The best fit nuclear radii determined by fitting the maximum of the angular distribution given by the Butler theory to the experimental data in the cases of the reactions $^{19}F(d, p)^{20}F^*(0{\cdot}652\,\text{MeV})$ ($E_d = 8{\cdot}90\,\text{MeV}$), $^{19}F(d, p)^{20}F^*(0{\cdot}828\,\text{MeV})$ ($E_d = 8{\cdot}90\,\text{MeV}$) and $^{28}Si(d, p)^{29}Si^*$ ($1{\cdot}28\,\text{MeV}$) ($E_d = 8{\cdot}21\,\text{MeV}$), for which l_n are taken to be 2, are found to be $5{\cdot}06 \times 10^{-13}$ cm, $5{\cdot}26 \times 10^{-13}$ cm, and $5{\cdot}91 \times 10^{-13}$ cm, respectively. These radii are to be compared with the best fit nuclear radii obtained from the present model, $4{\cdot}96 \times 10^{-13}$ cm for the two fluorine cases and $5{\cdot}4 \times 10^{-13}$ cm for the silicon case.

In the case of the $^{19}F(d, p)^{20}F(E_d = 14{\cdot}3\,\text{MeV})$ reaction for which $l_n = 2$, the position of maximum of the angular distribution given by the Butler theory coincides with that given by the present model, both being calculated by using the same nuclear radius of $4{\cdot}96 \times 10^{-13}$ cm. But the latter gives a narower peak of the angular distribution than the former, and fits to the experimental data than the former, as is seen from figure 3(*c*).

In the case of the $^{40}Ca(d, p)^{41}Ca$ reaction at $E_d = 8{\cdot}18\,\text{MeV}$ for which $l_n = 3$, the nuclear radius must be chosen as $6{\cdot}37 \times 10^{-13}$ cm in order to fit the maximum of the Butler's theoretical angular distribution to the experiments. This nuclear radius is larger by $0{\cdot}50 \times 10^{-13}$ cm than the best fit nucelar radius obtained by the present model $a = 5{\cdot}87 \times 10^{-13}$ cm indicated in figure 4.

In the two cases of the $^{12}C(d, p)^{13}C$ reaction at $E_d = 9{\cdot}0\,\text{MeV}$ and the $^{51}V(d, p)^{52}V^*(0{\cdot}14\,\text{MeV})$ reaction at $E_d = 8{\cdot}67\,\text{MeV}$, as seen from figures 2 (*b*) and(*d*), the position of maximum of the angular distribution given by the Butler theory is observed to be smaller in angle than that given by the present model, if the same nuclear radius is used for the two models in each case. It might, therefore, be supposed that for these two cases nuclear radii smaller than those indicated in figures 2 (*b*) and (*d*) could be obtained by fitting the position of maximum of the angular distribution given by the Butler theory to that given by the present model.

Figure 5(*c*) shows the angular distribution given by the Butler theory for the case of carbon obtained by using a nuclear radius of $4{\cdot}00 \times 10^{-13}$ cm, which gives the same position of the maximum of the angular distribution as that of the best fit angular distribution due to the present model with $a = 4{\cdot}49 \times 10^{-13}$ cm shown in figure 2 (*b*). It is clear from this figure that Butler's theoretical angular distribution with $a = 4{\cdot}00 \times 10^{-13}$ cm does not give over-all fit to the experimental data. As to the over all fit to the experimental data, Butler's theoretical angular distribution with $a = 4{\cdot}49 \times 10^{-13}$ cm used in figure 2 (*b*) is seen to give better fit, though it does not give the steep dip at small angles of the experimental angular distribution. This steep dip at small angles has been noted not to be reproduced by the Butler theory (Green and Middleton 1956). Thus, if this feature is disregarded Butler's theoretical angular distribution with the nuclear radius $a = 4{\cdot}99 \times 10^{-13}$ cm used by Green and Middleton (1956) rather seems to give the best fit, as is shown in figure 5(*c*).

Figure 5(*d*) shows the angular distribution given by the Butler theory for the case of vanadium obtained by using a nuclear radius $a = 5{\cdot}83 \times 10^{-13}$ cm which gives the same position of the maximum of the angular distribution as that of the best fit angular distribution due to the present model with $a = 6{\cdot}23 \times 10^{-13}$ cm shown in figure 2(*d*). Butler's theoretical angular distribution obtained by using this smaller nuclear radius $a = 5{\cdot}83 \times 10^{-13}$ cm also, as is seen from this figure, cannot explain the steep dip at small angles observed in the experiments

(El-Bedewi and Tadros 1958) and moreover the fit at larger angles becomes worse. Thus, the nuclear radius $a = 6{\cdot}23 \times 10^{-13}$ cm indicated in figure 2 (*d*) will be adopted as the best fit one for the Butler theory.

In the case of the $^{40}Ca(d, p)^{41}Ca^*$ (1·9 MeV) reaction at $E_d = 8{\cdot}18$ MeV, for which $l_n = 1$ as in the cases of carbon and vanadium discussed above, it has also been noted (Holt and Marsham 1953 b) that the steep dip of the experimental angular distribution at small angles cannot be explained by Butler's theoretical angular distribution with the nuclear radius $a = 5{\cdot}87 \times 10^{-13}$ cm, which gives the same position of maximum of the theoretical angular distribution as that of the experimental one. The theoretical angular distribution given by the present model with the same nuclear radius $a = 5{\cdot}87 \times 10^{-13}$ cm, however, gives much better fit to the experimental angular distribution, as is seen from figure 2 (*c*).

In the table are summarized the best fit nuclear radii for both the Butler theory and the present model determined from the discussions given above. The best fit nuclear radii determined for the present model shown in the table agree with those given by the Gamow–Critchfield formula $a = (1{\cdot}22A^{1/3} + 1{\cdot}70) \times 10^{-13}$ cm.

Reactions	l_n	Best fit nuclear radii	
		Present model	Butler theory
$^{28}Si(d, p)^{29}Si$	0	5·41 (10^{-13} cm)	5·41 (10^{-13} cm)
$^{32}Si(d, p)^{33}S^*$ (0·85 MeV)	0	5·57	5·57
$^{10}B(d, p)^{11}B$	1	4·32	5·32
$^{12}C(d, p)^{13}C$	1	4·49	4·99
$^{40}Ca(d, p)^{41}Ca^*$ (1·9 MeV)	1	5·87	5·87
$^{51}V(d, p)^{52}V^*$ (0·14 MeV)	1	6·23	6·23
$^{19}F(d, p)^{20}F^*$ (0·652 MeV)	2	4·96	5·06
$^{19}F(d, p)^{20}F^*$ (0·828 MeV)	2	4·96	5·26
$^{19}F(d, p)^{20}F$	2	4·96	4·96
$^{28}Si(d, p)^{29}Si^*$ (1·28 MeV)	2	5·41	5·91
$^{32}Si(d, p)^{33}S$	2	5·57	6·57
$^{40}Ca(d, p)^{41}Ca$	3	5·87	6·37

The effect of the Coulomb interaction on the angular distribution, which is not considered in the present calculation, has been investigated by several authors (Butler and Austern 1954, Tobocman and Kalos 1955). Taking into account the Coulomb interaction, the peak of the angular distribution has been observed to move toward larger angles. If the Coulomb interaction is introduced further into the present calculation, it might therefore be expected that the nuclear radii obtained in the present analysis should be enlarged more or less in order to fit the maxima of the theoretical angular distributions to the experimental data. It has been observed, however, that the effect of introducing the nuclear interaction of liberated protons is in general opposite to the Coulomb effect, that is, the peak is displaced toward smaller angles. It has been also observed that when both the Coulomb and nuclear interaction are introduced at sufficiently high energies, these interactions affect the angular distribution in opposite sense and compensate each other at least partly. This compensation is expected to occur also in the present case. Further investigation is needed however in order to know how the best fit nuclear radii obtained in the present analysis may be modified by the introduction of the Coulomb and nuclear interactions.

The reason why the angular distributions for angles larger than 60° are not plotted in the figures of § 2 is that for these large angles where the amplitudes

of the stripping process are small, the angular distribution may not be determined only by the simple stripping process. Processes which are not taken into account in the present calculation, such as the nucleon exchange process, the heavy particle stripping process or a process proceeding through formation of a compound nucleus, may be important. In fact, many of the experimental data analysed in § 2 show deviations from theoretical angular distributions at these large angles, though they are not plotted in the figures of § 2.

Results on (d,n) angular distributions using the present model will be discussed in another paper.

Acknowledgment

One of us (T.H.) was supported by the Yomiuri–Yukawa fellowship.

References

Black, C. F., 1953, *Ph.D. Thesis*, Massachusetts Institute of Technology (unpublished), as quoted in Tobocman and Kalos (1955).

Blatt, J. M., and Weisskopf, V. F., 1952, *Theoretical Nuclear Physics* (New York: John Wiley and Sons), Appendix A.

Bhatia, A. B., Kun Huang, Huby, R., and Newns, H. C., 1952, *Phil. Mag.*, **43**, 485.

Butler, S. T., 1951, *Proc. Roy. Soc.* A, **208**, 559.

Butler, S. T., and Austern, N., 1954, *Phys. Rev.*, **93**, 355.

El-Bedewi, F. A., 1956, *Proc. Phys. Soc.* A, **69**, 221.

El-Bedewi, F. A., and Tadros, S., 1958, *Nucl. Phys.*, **8**, 71.

Evans, N. T. S., and Parkinson, W. C., 1954, *Proc. Phys. Soc.* A, **67**, 684.

Fujimoto. Y., Kikuchi, K., and Yoshida, S., 1954, *Progr. Theor. Phys., Japan*, **11**, 264.

Green, T. S., and Middleton, R., 1956, *Proc. Phys. Soc.* A, **69**, 28.

Holt, J. R., and Marsham, T. N., 1953 a, *Proc. Phys. Soc.* A, **66**, 467.

—— 1953 b, *Ibid.*, **66**, 565.

Nagasaki, M., 1956, *Progr. Theor. Phys., Japan*, **16**, 429.

Owen, G. E., and Madansky, L., 1957, *Phys. Rev.*, **105**, 1766.

Tobocman, W., and Kalos, M. H., 1955, *Phys. Rev.*, **97**, 132.

The Scattering of Alpha Particles by Helium

By A. C. BUTCHER† and J. M. McNAMEE‡

† Mathematics Department, University of Glasgow
‡ Physics Department, University College, London

Communicated by H. S. W. Massey ; *MS. received 6th May* 1959

Abstract. Nuclear phase shifts are calculated for the scattering of two alpha particles, using the method of the resonating group structure, and assuming central Gaussian internucleonic potentials and Gaussian wave functions. It is found that a mixture of two-thirds Serber and one-third MHWB exchange force gives good agreement with the experimentally observed phase shifts.

§ 1. Introduction

In 1927 Rutherford and Chadwick (1927) discovered anomalous scattering of alpha particles in helium; Chadwick (1930) followed this by low energy experiments which verified Mott's law for identical particles (Mott 1930), thus indicating that the alpha particle has spin O and a spherically symmetric force field. In the 1930's experiments at energies up to 7 MeV were performed by Wright (1932), Mohr and Pringle (1937), and Devons (1939) all with radioactive sources. These had large inaccuracies due to spread in energy and angle, and their results analysed in terms of phase shifts by Wheeler (1941) are in conflict with later measurements and with disintegration experiments.

Since 1950 more accurate work has been done using particle accelerators. The range 150 kev–3 MeV was investigated by Heydenberg and Temmer (1956) with a Van de Graaff machine. The range 3·0–6·0 MeV was studied by Russell, Philips and Reich (1956) at the Rice Institute. Their (phase shift, energy) curves fit well on to those of Heydenberg and from the behaviour of δ_2 near to 6 MeV they deduce an $L=2$ excited state of ^{8}Be near 3 MeV as required by disintegration experiments. The range 6–12 MeV has not been investigated at all so far.

The range 12–23 MeV has been studied by two groups: Nilson *et al.* (1956, 1958) at Illinois, and Steigart and Sampson (1953) at Indiana, both using cyclotrons. Both sets of cross sections were analysed in terms of phase shifts on the ILLIAC computer by Nilson. They agree quite well above 15 MeV but differ very considerably below that energy. The Indiana results indicate a resonance at 15 MeV in δ_0 (0^+ 7·5 state of ^{8}Be) but Nilson's do not. Evidence from other reactions favour Nilson's results. Isolated results by Mather (1951) at 20 MeV and Braden *et al.* (1951) at 20·4 agree reasonably well with Nilson's cross sections.

The range 23·1–38·5 MeV has been investigated by Burcham, Gibson *et al.* (1957 and private communication) on the Birmingham (England) cyclotron and phase shifts derived on ILLIAC, and there are also some results reported by Yavin (private communication) between 37·6 and 40 MeV; the phases fit well on to Nilson's curve.

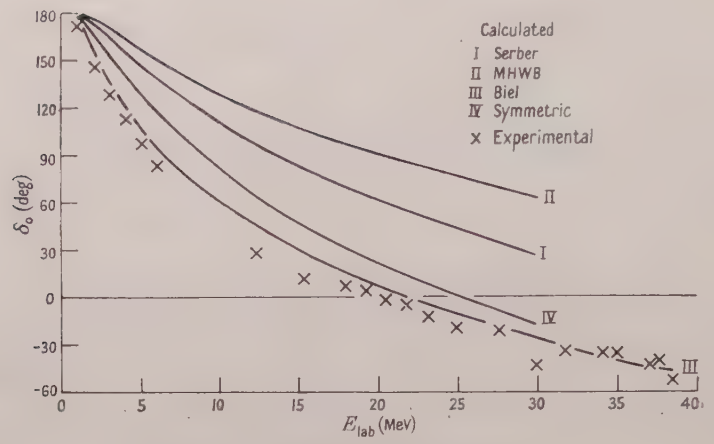

Figure 1. Phase shifts for $L=0$.

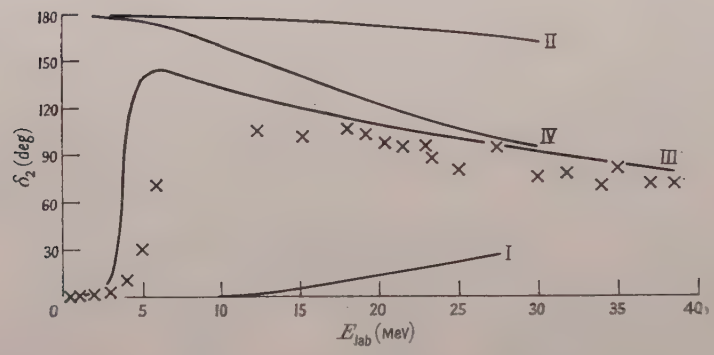

Figure 2. Phase shifts for $L=2$ (key as in figure 1).

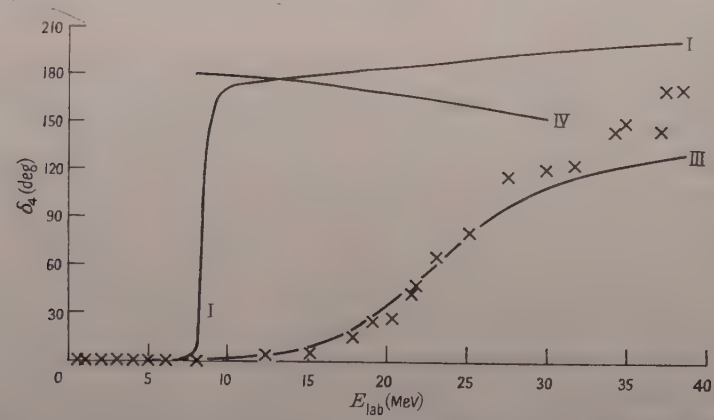

Figure 3. Phase shifts for $L=4$ (key as in figure 1). (Note. For MHWB force δ_4 remained practically zero in whole range.)

The phase shifts deduced from all these experiments are shown in figures 1–3 (In the region 12–22 MeV only the Illinois data are shown.) The behaviour in the uninvestigated range 6–12 MeV can only be conjectured; but since no bound states are suspected in this region it is probably as indicated; a resonance would lead to a shift of 180°.

On the theoretical side several attempts have been made to account for the anomolous scattering in terms of a nuclear potential. Earlier calculations treated each alpha particle as a single particle with a central potential.

Taylor (1931) took a simple square well for the attractive nuclear potential and calculated δ_0, obtaining rough agreement with the low-energy data then available. Margenau (1941) used an infinite repulsive core for $0 < r < r_1$, an attractive square well from r_1 to $4{\cdot}5 \times 10^{-13}$ cm and Coulomb repulsion outside this. He also obtained agreement at low energies for δ_0. Haefner (1951) used

$$V(r) = -D + \frac{q^2\hbar^2}{2\alpha r} \quad (r < r_0) \quad \text{and} \quad V(r) = \frac{4e^2}{r} \quad (r > r_0)$$

giving a strong repulsion at small r, attraction at intermediate range and Coulomb repulsion beyond. His results agree well with experiment up to 6 MeV (the limit of his calculation), but Nilson with the same potential could not get agreement at higher energies, and Humphries (1958) finds agreement possible only by making D depend on L.

Van der Spuy and Pienaar (1958) and Snyder (Burcham *et al.* 1958, private communication) have also tried to fit this type of potential but meet with the same difficulties; Snyder found attempts to explain the phase-shifts by means of dispersion theory not wholly satisfactory.

The present calculation takes into account all the interactions between individual nucleons but regards them as remaining in their alpha-groups. Account is taken of exchange of nucleons between different groups, using the method of Wheeler's resonating group structure (1937). No account is taken of polarization except indirectly. A single central Gaussian potential is assumed for the nuclear force, and also a single Gaussian wave-function for the alpha particles. Several different combinations of the Wigner, Majorana, Bartlett and Heisenberg exchange operators are taken, including Ordinary, Serber and MHWB mixtures. A range of E_{lab} from 0 to 38·5 MeV is studied.

The resonating group model has met with considerable success in explaining light-nuclei scattering and binding energy data. The first application was to neutron–deuteron scattering using central forces (Buckingham and Massey 1941, Buckingham *et al.* 1952, de Borde and Massey 1955, Burke and Robinson 1957). Bransden (1950) included tensor forces at high energies, and Bransden, Smith and Tate (1958) have formulated the problem with tensor forces at low energies. Swan (1953 a, b) and Bransden and Robertson (1956, 1958) have investigated nucleon–triton and nucleon–^{3}He collisions. Neutron–alpha collisions have been studied by Bransden and McKee (1954), Hochberg *et al.* (1954) (with central forces), and also including the spin–orbit coupling (1955), while Sugie *et al.* (1957) considered the effects of tensor forces. Work is in progress (Burke and Laskar 1958) on collisions of deuteron with deuteron and ^{3}He.

Binding energy calculations include those by Irving for the alpha particle (1951, 1953), Edwards (1952) for ^{8}Be and Biel (1957) for ^{8}Be and ^{12}C. These are closely related to the present problem, which is perhaps the severest test so far of

the resonating group model; it is the first collision problem attempted in which both the nuclei contain more than one nucleon. On the other hand the closely bound nature of the alpha particle gave grounds for confidence in this model.

§ 2. General Formulation

The basic spatial wave function for the problem is

$$\phi(12, 13, 14, 23, 24, 34)\,.\,\phi(56, 57, 58, 67, 68, 78) f(\mathbf{r}) G(\mathbf{R})$$

where $\mathbf{R} = (\mathbf{r}, +\ldots\ldots\mathbf{r}_8)/8$; $\mathbf{r} = (\mathbf{r}_1+\mathbf{r}_2+\mathbf{r}_3+\mathbf{r}_4)/4-(\mathbf{r}_5+\mathbf{r}_6+\mathbf{r}_7+\mathbf{r}_8/)4$; (12) means $\mathbf{r}_1-\mathbf{r}_2$. Since the two alpha particles are identical $f(\mathbf{r})=f(-\mathbf{r})$; $f(\mathbf{r})$ expresses the separation of the two particles, $G(\mathbf{R})$ the movement of the overall centre of gravity. Each ϕ is the wave function of a single alpha particle and is symmetrical in the space coordinates of the four constituent nucleons. We can write the function in the form $\psi(1234, 5678)$ where $\psi(A, B)=\psi(B, A)=$ (perm. of A, perm. of B).

The wave function has to be anti-symmetrized according to the Pauli exclusion principle; we take

$$\Psi = A_{1\ldots8}\,\alpha(1)\,\beta(2)\,\alpha(3)\,\beta(4)\,\alpha(5)\,\beta(6)\,\alpha(7)\,\beta(8).$$
$$a(1)\,a(2)\,b(3)\,b(4)\,a(5)\,a(6)\,b(7)\,b(8)\,\psi(1234, 5678)$$

where $\alpha(n)$, $\beta(n)$ represent spin function and $a(n)$, $b(n)$ represent isotopic spin;

$$A_{1\ldots8} = \frac{1}{8!}\sum_{\text{all perms}} \mathscr{E} p_1 \ldots p_8 P\begin{pmatrix} 12\ldots8 \\ p_1 p_2 \ldots p_8 \end{pmatrix}.$$

The Hamiltonian is

$$H = \sum_{i,j}(W + BP_{ij}^{\sigma} - HP_{ij}^{\tau} + MP_{ij}^{r})\,V(r_{ij}) + \sum_{i,j}\tfrac{1}{4}(1+\tau_3^{i})(1+\tau_4^{j})\,\frac{e^2}{r_{ij}}$$
$$-\frac{\hbar^2}{2m}\sum_i \frac{\partial^2}{\partial \mathbf{r}_i^2}$$

where P_{ij}^{σ} interchanges spin coordinates etc. and

$$\frac{\partial^2}{\partial \mathbf{r}_i^2} = \frac{\partial^2}{\partial x_i^2} + \frac{\partial^2}{\partial y_i^2} + \frac{\partial^2}{\partial z_i^2}.$$

Since the function is symmetrical in σ and τ, P_{ij}^{σ} and P_{ij}^{τ} have the same effect and we may replace this by $H' = (W + QP_{ij}^{\sigma} + MP_{ij}^{r}) + \ldots +$ etc., where $Q = B - H$.

To get the equations of motion we use the variational principle

$$\delta\left(\frac{\int\psi^* H'\psi}{\int\psi^*\psi}\right) = 0, \text{ giving } (H'-E)=0,$$

i.e. $\{T + C + \sum WV(r_{ij}) + \sum MP_{ij}^{r}\,V(r_{ij}) - E\}\sum A_{1\ldots8}\,\alpha(1)\ \ \beta(2)\ldots$

$$\psi(1\ldots8) + Q\sum_{(i,j)}^{28} A_{1\ldots8}\,\alpha(1)\,\beta(2)\ldots\,\psi(1\ldots8) = 0$$

with ij spin interchanged, where T = kinetic energy operator, C = Coulomb terms.

Now 1, 3, 5, 7 have the same spin = 'α' and 2, 4, 6, 8, have the same spin = 'β'. Therefore for (i, j) consisting of odd pairs (${}^4C_2 = 6$ cases) or of even the interchange makes no difference. For the mixed pairs only those with the same isotopic spin need be considered. The effect of these is the same as leaving spin unchanged

but altering the space coordinates with a change of sign. Then using the symmetry properties of ψ we get

$$[T+C+W\Sigma V(r_{ij})+M\Sigma P_{ij}{}^{r}V(r_{ij})-E+Q\Theta]. \quad [1-(P_{15}{}^{r}+P_{26}{}^{r}+P_{37}{}^{r}+P_{48}{}^{r}) + (P_{15}{}^{r}P_{26}{}^{r}+P_{15}{}^{r}P_{37}{}^{r}+P_{15}{}^{r}P_{48}{}^{r})]\psi=0$$

where

$$\Theta=V(24)+V(26)+\ldots.+V(13)+V(15)+\ldots-P_{12}{}^{r}V(12)-P_{16}{}^{r}V(16) -P_{34}{}^{r}V(34)-P_{38}{}^{r}V(38)-P_{56}{}^{r}V(56)-P_{52}{}^{r}V(52)-P_{78}{}^{r}V(78)-P_{74}{}^{r}V(74).$$

Premultiply by $\psi^*(12\ldots8)$ and integrate over $\mathbf{r}_1\ldots\mathbf{r}_8$; then using the fact that

$$\int\psi^*V(12)\psi\,d\mathbf{r}_1\ldots d\mathbf{r}_8=\int\psi^*V(13)\psi\,d\mathbf{r}_1\ldots\text{etc.},$$

we get

$$E=\frac{\int\psi^*[T+a-4(T+b)P_{15}{}^{r}+3(T+c)P_{15}{}^{r}P_{26}{}^{r}]\psi\,d\mathbf{r}_1\ldots}{\int\psi^*[1-4P_{15}{}^{r}+3P_{15}{}^{r}P_{26}{}^{r}]\psi\,d\mathbf{r}_1\ldots d\mathbf{r}_8}$$

where

$$a=12(W+M)V(12)+4(4W+2Q-M)V(15)+\frac{2e^2}{r_{12}}+\frac{4e^2}{r_{15}}$$

$$b=6(W+M)V(12)+6(W+M)V(52)+(W+2Q-4M)V(15) +6(W+M)V(23)+3(3W-2M+2Q)V(26) +e^2\left(\frac{1}{r_{12}}+\frac{1}{r_{52}}+\frac{1}{2r_{15}}+\frac{1}{r_{23}}+\frac{5}{2r_{26}}\right)$$

$$c=2(W+M)V(12)+2(W+M)V(56)+8(W+M)V(13)+8(W+M)V(53) +4(2W-3M+2Q)V(15)+e^2\left(\frac{1}{r_{12}}+\frac{1}{3r_{56}}+\frac{4}{3r_{13}}+\frac{4}{3r_{53}}+\frac{8}{3r_{15}}\right).$$

Using the variational principle again we get as our scattering equation:

$$[(T+a-E)-4(T+b-E)P_{15}{}^{r}+3(T+c-E)P_{15}{}^{r}P_{26}{}^{r}]\psi=0.$$

§ 3. Explicit Form

The above contains eight vectors $\mathbf{r}_1\ldots\mathbf{r}_8$. All but two of these can be eliminated as follows. We make the transformation

$$\mathbf{p}_1=\mathbf{r}_1-(\mathbf{r}_2+\mathbf{r}_3+\mathbf{r}_4)/3 \qquad \mathbf{p}_5=\mathbf{r}_5-(\mathbf{r}_6+\mathbf{r}_7+\mathbf{r}_8)/3$$
$$\mathbf{p}_2=\mathbf{r}_2-(\mathbf{r}_3+\mathbf{r}_4)/2 \qquad \mathbf{p}_6=\mathbf{r}_6-(\mathbf{r}_7+\mathbf{r}_8)/2$$
$$\mathbf{p}_3=\mathbf{r}_3-\mathbf{r}_4 \qquad \mathbf{p}_7=\mathbf{r}_7-\mathbf{r}_8$$

$\mathbf{r}$ and $\mathbf{R}$ as before.

Now ϕ has the form $N\exp[-\alpha(r_{12}{}^2+r_{13}{}^2\ldots+r_{34}{}^2)]$; it becomes

$$N\exp\left[-\alpha\left(3p_1{}^2+\frac{8}{3}p_2{}^2+2p_3{}^2\right)\right];$$

T becomes $-\frac{\hbar^2}{2m}[\frac{4}{3}(\nabla_{\mathbf{p}_1}{}^2+\nabla_{\mathbf{p}_5}{}^2)+\frac{3}{2}(\nabla_{\mathbf{p}_2}{}^2+\nabla_{\mathbf{p}_6}{}^2)+2(\nabla_{\mathbf{p}_3}{}^2+\nabla_{\mathbf{p}_7}{}^2)+\frac{1}{2}\nabla_{\mathbf{r}}{}^2 +\frac{1}{8}\nabla_{\mathbf{R}}{}^2]=(\text{say})\,T_0+T_r+T_R.$

We now put $T_RG(R)=E_RG(R)$ and replacing E by $E'=E-E_R$ the equation becomes

$$[(T_0+T_r+a-E')-4(T_0+T_r+b-E')P_{15}{}^{r}+3(T_0+T_r+c-E')P_{15}{}^{r}P_{26}{}^{r}] \times\phi(\mathbf{p}_1\mathbf{p}_2\mathbf{p}_3)\phi(\mathbf{p}_5\mathbf{p}_6\mathbf{p}_7)f(\mathbf{r})=0$$

where P_{15}^{r} refers to $\mathbf{r}_1$ and $\mathbf{r}_5$. Multiplying by $\phi^*(\mathbf{p}_1\mathbf{p}_2\mathbf{p}_3)\,\phi^*(\mathbf{p}_5\mathbf{p}_6\mathbf{p}_7)$ and integrating over $d\mathbf{p}_1 \ldots d\mathbf{p}_7$ we get

$$\int \phi^*(\mathbf{p}_1\mathbf{p}_2\mathbf{p}_3)\,\phi^*(\mathbf{p}_5\mathbf{p}_6\mathbf{p}_7)\,[(T_0+T_r+a-E')\,\phi(\mathbf{p}_1\mathbf{p}_2\mathbf{p}_3)\,\phi(\mathbf{p}_5\mathbf{p}_6\mathbf{p}_7)f(\mathbf{r})$$
$$-4(T_0+T_r+b-E')\,\phi(\mathbf{p}_1'\mathbf{p}_2'\mathbf{p}_3')\,\phi(\mathbf{p}_5'\mathbf{p}_6'\mathbf{p}_7')f(\mathbf{r}')$$
$$+3(T_0+T_r+c-E')\,\phi(\mathbf{p}_1''\mathbf{p}_2''\mathbf{p}_3'')\,\phi(\mathbf{p}_5''\mathbf{p}_6''\mathbf{p}_7'')f(\mathbf{r}'')]\,d\mathbf{p}_1 \ldots d\mathbf{p}_7 = 0$$

where $'$ refers to single exchange (P_{15}^{r}) and $''$ to double exchange ($P_{15}^{r}P_{26}^{r}$) e.g. $\mathbf{p}_1' = \frac{1}{4}\mathbf{p}_1 + \frac{3}{4}\mathbf{p}_5 - \mathbf{r}$ is formed by expressing $\mathbf{p}_1$ in terms of $\mathbf{r}_i$'s, interchanging $\mathbf{r}_1$ and $\mathbf{r}_5$ and re-expressing it in terms of $\mathbf{p}_i$'s.

After several applications of Green's theorem this becomes

$$[\nabla_{\mathbf{r}}^2 + k^2 - W(\mathbf{r})]f(\mathbf{r}) = \int K(\mathbf{r},\mathbf{r}')f(\mathbf{r}')\,d\mathbf{r}' \quad \text{where} \quad k^2 = \frac{2m}{\hbar^2}E_{\text{lab}}$$

$$W(\mathbf{r}) = \int \frac{1}{\lambda}\,[4(4W+2B-2H-M)\,V(|\tfrac{3}{4}\mathbf{p}_1 - \tfrac{3}{4}\mathbf{p}_5 + \mathbf{r}|) + \frac{4e^2}{\lambda}\,|\tfrac{3}{4}\mathbf{p}_1 - \tfrac{3}{4}\mathbf{p}_5 + \mathbf{r}|^{-1}$$
$$\{\phi(\mathbf{p}_1\mathbf{p}_2\mathbf{p}_3)\,\phi(\mathbf{p}_5\mathbf{p}_6\mathbf{p}_7)\}^2]\,d\mathbf{p}_1 \ldots d\mathbf{p}_7$$

where λ is a normalization constant. The left hand side arises from the no-exchange part, the right-hand side from the single and double exchange parts.

$K(\mathbf{r},\mathbf{r}')$ contains three parts.

(1) nuclear potential terms such as

$$\int \phi^*(\mathbf{p}_1\mathbf{p}_2\mathbf{p}_3)\,\phi^*(\mathbf{q}_5\mathbf{p}_6\mathbf{p}_7)\,\phi(\mathbf{q}_1'\mathbf{p}_2\mathbf{p}_3)\,\phi(\mathbf{q}_5'\mathbf{p}_6\mathbf{p}_7)\,6(W+M)\,V(\mathbf{p}_1 - \tfrac{2}{3}\mathbf{p}_2)\,d\mathbf{p}_1$$
$$\times d\mathbf{p}_2 d\mathbf{p}_3 d\mathbf{p}_5 d\mathbf{p}_6 d\mathbf{p}_7,$$

where $\mathbf{q}_5 = \mathbf{p}_1 + \frac{8\mathbf{r}'}{3} - \frac{4\mathbf{r}}{3}$, $\mathbf{q}_1' = \mathbf{p}_1 + 2\mathbf{r}' - 2\mathbf{r}$, $\mathbf{q}_5' = \mathbf{p}_1 + \frac{2\mathbf{r}'}{3} + \frac{2\mathbf{r}}{3}$

(2) Coulomb terms such as $\int \phi(\quad)\ldots\frac{e^2}{|\mathbf{p}_1 - \frac{2}{3}\mathbf{p}_2|}\,d\mathbf{p}_1\ldots$

(3) kinetic energy term such as

$$-\int f(\mathbf{r}')\,\phi^*(\mathbf{p}_1\mathbf{p}_2\mathbf{p}_3)\,\phi^*(\mathbf{p}_5\mathbf{p}_6\mathbf{p}_7)\,\frac{\hbar^2}{4m}\,\nabla_{\mathbf{r}}^2\,\phi(\mathbf{p}_1'\mathbf{p}_2'\mathbf{p}_3')\,\phi(\mathbf{p}_5'\mathbf{p}_6'\mathbf{p}_7')\,d\mathbf{p}_1\ldots.$$

We take $V(r_{ij}) = A\exp(-\beta r_{ij}^2)$.

The integrations over $\mathbf{p}_1 \ldots \mathbf{p}_7$ are performed by first making a transformation which orthogonalizes the exponent in the integrand (i.e. gets rid of terms of the type $\mathbf{p}_1 \cdot \mathbf{p}_2$) and makes the argument of the potential function one of the new variables.

Thus our typical nuclear term becomes

$$\int \exp[-(6\alpha+\beta)\mathbf{s}_1^2 - 8\alpha\mathbf{s}_1\cdot(2\mathbf{r}'-\mathbf{r}) - \frac{16}{3}\mathbf{p}_6^2 - \ldots]\,dx_1\,dy_1\,dz_1\ldots.$$

Using result that

$$\int \exp(-\lambda x^2 + \mu x)dx = \exp(\mu^2/4\lambda)(\pi/\lambda)^{1/2},$$

this gives

$$B\exp\left[\frac{-8}{6\alpha+\beta}\,(10\alpha+2\beta)\mathbf{r}^2 - (16\alpha+4\beta)\mathbf{r}\mathbf{r}' + (10\alpha+3\beta)\mathbf{r}'^2\right]$$

where B is a constant.

The Coulomb terms are of the type

$$\operatorname{erf}\{\tfrac{2}{3}(2\alpha)^{1/2}\,|2\mathbf{r}'-\mathbf{r}|\}\exp\left\{\frac{-8}{3\alpha}\,(5\mathbf{r}^2-8\mathbf{r}\,.\,\mathbf{r}'+5\mathbf{r}'^2)\right\}.$$

The kinetic energy terms require several applications of Green's theorem.

We now analyse the motion into partial waves by putting

$$f(\mathbf{r})=\sum_{n=0}^{\infty}\frac{f_L(r)}{r}P_L(\cos\theta)\quad(L=2n)$$

and

$$K(\mathbf{r},\mathbf{r}')=\frac{1}{4\pi rr'}\sum_{L}(2L+1)\,K_L(r,r')\,P_L\left(\frac{\mathbf{r}\,.\,\mathbf{r}'}{rr'}\right).$$

Note.—Since $f(-\mathbf{r})=f(\mathbf{r})$ only even L appear.

Then equation becomes

$$\left\{\frac{d^2}{dr^2}+k^2-W(r)-\frac{L(L+1)}{r^2}\right\}f_L(r)=\int_0^{\infty}K_L(r,r')f_L(r')\,dr'$$

where

$$K_L(r,r')=2\pi rr'\int_{-1}^{1}K(\mathbf{r},\mathbf{r}')\,P_L(\mu)\,d\mu\quad(\mu=\cos\theta),$$

and $W(r)$ are given in full in the Appendix.

The kernels were evaluated numerically in the form of a 30×30 matrix at intervals $h=0{\cdot}25\times10^{-13}$ cm in r and r', using the DEUCE computer; then the integro-differential equation is converted to a set of simultaneous algebraic equations using the difference relation

$$\frac{d^2}{dr^2}f(r)=\frac{1}{h^2}\{\delta^2f-\frac{1}{12}\delta^4f+\ldots\},$$

and Gregory's formula for the integral (for details see Robertson 1956). These equations are solved to give the values of the wave function $f_L(r)$ at 28 pivotal points $h, 2h, \ldots$. Now for large r, $f_L(r)$ should tend asymptotically to

$$\frac{1}{k}\sin(kr-\tfrac{1}{2}L\pi-\eta\log 2kr+\sigma_L+\delta_L),$$

where $\eta=8me^2/k\hbar$, $\sigma_L=\arg\,\Gamma(L+1+i\eta)$, δ_L is the 'nuclear phase shift'; assuming this is so, we can take the last two values of f and compute δ_L. The phase shifts δ_L so calculated can be compared with those deduced directly from scattering observations by the methods described by Nilson *et al.* (1958).

§ 3. Numerical Values Assumed

Calculations have been carried out for the various types of exchange force shown in the table, based on

$$x=m+w-h-b=0{\cdot}6$$
$$m+w+h+b=1$$

where x is the ratio of singlet to triplet interaction.

Only δ_0, δ_2, δ_4 were calculated as δ_6 is found experimentally to be small in the energy range considered. Numerical values taken (from Hochberg *et al.* 1954) were:

$$\alpha=0{\cdot}0789\times10^{26}\,\text{cm}^{-2}\qquad\beta=0{\cdot}2657\times10^{26}\,\text{cm}^{-2}$$
$$E=-28{\cdot}2\,\text{Mev}=-45{\cdot}1724\times10^{-6}\,\text{erg}$$
$$A=-45\,\text{Mev}\quad=-72{\cdot}0837\times10^{-6}\,\text{erg}.$$

	Ordinary	Serber	Symmetric
w	$\frac{1}{2}(1+x)=0{\cdot}8$	$\frac{1}{4}(1+x)=0{\cdot}4$	0
m	0	$\frac{1}{4}(1+x)=0{\cdot}4$	$\frac{1}{2}(1+x)=0{\cdot}8$
b	$\frac{1}{2}(1-x)=0{\cdot}2$	$\frac{1}{4}(1-x)=0{\cdot}1$	0
h	0	$\frac{1}{4}(1-x)=0{\cdot}1$	$\frac{1}{2}(1-x)=0{\cdot}2$

	MHWB ($m=2b$, $h=2w$)	Biel ($\frac{2}{3}$ Ser + $\frac{1}{3}$ MHWB) (see note (2))	90% Ser. + 10% MHWB
w	$\frac{1}{6}(1-3x)=-0{\cdot}13$	0·222	0·347
m	$\frac{1}{3}(1+3x)=0{\cdot}93$	0·58	0·453
b	$\frac{1}{6}(1+3x)=0{\cdot}47$	0·222	0·137
h	$\frac{1}{3}(1-3x)=-0{\cdot}27$	−0·022	0·063

(1) The values of ' Ordinary ', ' Serber ' and ' Symmetric ' forces are those given by Massey (1953).

(2) This force combination was found by Biel (1957) to give the correct value of the binding energy of ^{8}Be and ^{12}C on the basis of a calculation similar to the present one.

§ 4. Results and Discussion

The calculated and observed phase shifts are plotted as a function of energy in figures 1–3. The best agreement is obtained with Biel's force (see note (2) of table); for a large range of E this gives agreement within or just outside the limits of observational error (estimated at $\pm 8°$ by Nilson *et al.* (1958)). The most serious discrepancy is found in the range 2–6 MeV for δ_2. We find the expected resonance effect but displaced about 2 MeV to the left. This would indicate a level at 2·0 MeV instead of 3 MeV in ^{8}Be. This may be because the effects of polarization (i.e. distortion of wave function), neglected in this calculation, are more important in a region of resonance scattering than elsewhere. It would be interesting to see whether inclusion of polarization removes the discrepancy. The fact that the force combination which gives the correct binding energy for ^{8}Be also gives the correct phase shifts for $L=0$ in alpha–alpha scattering was to be expected; it can be regarded as a check on the numerical calculations in both cases. However, the substantial agreement with $L=2$, 4 phases given by the same force is a definite success for the resonating group model; also it appears that the neglect of tensor forces with use of an equivalent central force gives a good approximation.

The most recent calculations on light nuclei scattering indicate that a different exchange combination is needed for each particular nucleus. Thus for proton–triton and proton–^{3}He Robertson *et al.* (1958, private communication) found Serber force gave best agreement; for nucleon–^{4}He Hochberg *et al.* (1955) used 90% Serber + 10% MHWB to give the correct p phase (although they had to use pure Serber force for S phases (1954); while Biel's binding energy calculations (Biel 1957) on ^{8}Be and ^{12}C together with present work require 70% Serber + 30% MHWB. We see that as the nuclei become larger the percentage of MHWB force required increases. A possible explanation is the following: the 'true' internucleonic interaction is believed to contain a repulsive core at very short range; for a given value of angular momentum and energy of incident nucleus the internuclear ' distance of closest approach ' decreases with increasing mass, and hence *internucleonic* ' distance of closest approach ' decreases still more, so that the hard core becomes more important. Now the hard core has not been explicitly

allowed for in the calculation mentioned, but the Symmetric exchange (MHWB) force has a similar effect of producing short-range repulsion so a greater proportion is needed as nuclei become larger. Work is in progress on the application of a hard core to binding energies of ^{2}H, ^{4}He, ^{8}Be, ^{12}C.

Acknowledgments

Our thanks are due to Professor H. S. W. Massey for suggesting the problem, to the Director of the National Physical Laboratory for permission to use the DEUCE Computer, to the English Electric Co., for the use of their DEUCE, and in particular to Dr. H. H. Robertson and Dr. P. Burke for their advice in preparing programmes.

APPENDIX

The Kernels K(r, r′)

Carrying out the angular integrations, and using $E'=E-\hbar^2k^2/4m$ we get (with $\lambda=\beta/\alpha$)

$$
\begin{aligned}
K_L(r,r') = {} & \frac{m}{\hbar^2}A\left(\frac{\alpha}{\pi}\right)^{1/2}\Bigg[-\frac{(W+2Q-4M)}{8+\lambda}\frac{2^{12}}{\sqrt{3}}\exp\{-\tfrac{4}{3}\alpha(10+3\lambda)(r^2+r'^2)\} \\
& \times \mathscr{I}_{L+1/2}\left\{\frac{8\alpha}{3}(8+3\lambda)rr'\right\} \\
& - \frac{(W+M)3\,.\,2^{12\cdot5}}{(4+\lambda)(6+\lambda)^{1/2}}\exp\left\{-\frac{8\alpha}{6+\lambda}[(10+3\lambda)r^2+(10+2\lambda)r'^2]\right\}\mathscr{I}_{L+1/2} \\
& \times\left\{32\alpha\,.\,\frac{4+\lambda}{6+\lambda}rr'\right\} - \frac{(W+M)\,.\,3\,.\,2^{12\cdot5}}{(4+\lambda)(6+\lambda)^{1/2}}\exp\left\{-\frac{8\alpha}{6+\lambda}[(10+3\lambda)r^2+(10+2\lambda)r'^2]\right\} \\
& \times \mathscr{I}_{L-1/2}\left\{32\alpha\,.\,\frac{4+\lambda}{6+\lambda}rr'\right\} - \frac{(W+M)\,.\,3^{1/2}\,.\,2^{13}}{(4+\lambda)^{3/2}}\exp\left\{-\frac{40\alpha}{3}(r^2+r'^2)\right\}\mathscr{I}_{L+1/2} \\
& \times\left\{\frac{64\alpha}{3}rr'\right\} - \frac{(3W-2M+2Q)\,.\,3\,.\,2^{12\cdot5}}{(8+\lambda)(6+\lambda)^{1/2}}\exp\left\{-\frac{16\alpha}{6+\lambda}(5+\lambda)(r^2+r'^2)\right\}\mathscr{I}_{L+1/2} \\
& \times\left\{16\alpha\,.\,\frac{8+\lambda}{6+\lambda}rr'\right\} + \frac{(2W-3M+2Q)\,.\,3\,.\,2^{12\cdot5}}{(8+\lambda)^{1/2}\lambda}\exp\left\{-16\alpha\frac{(4+\lambda)}{8+\lambda}(r^2+r'^2)\right\} \\
& \times \mathscr{I}_{L-1/2}\left\{\frac{16\beta}{8+\lambda}rr'\right\}\Bigg] + \left(\frac{\alpha}{\pi}\right)^{1/2}\frac{2^{10}}{\sqrt{3}}\exp\left\{-\frac{40\alpha}{3}(r^2+r'^2)\right\}\Bigg[\left\{\frac{m}{\hbar^2}E\alpha-\frac{67}{3}\alpha\right. \\
& \left.+\frac{7\times2^7}{9}\alpha^2(r^2+r'^2)\right\}\mathscr{I}_{L+1/2}\left(\frac{64}{3}\alpha rr'\right) - \frac{13}{9}\,.\,2^7\alpha^2rr'\mathscr{I}_{L+1/2}'\left(\frac{64}{3}\alpha rr'\right)\Bigg] \\
& + k^2\left(\frac{\alpha}{\pi}\right)^{1/2}\frac{2^7}{\sqrt{3}}\exp\left\{-\frac{40\alpha}{3}(r^2+r'^2)\right\}\mathscr{I}_{L+1/2}\left(\frac{64\alpha}{3}rr'\right) \\
& + \frac{m}{\hbar^2}A\left(\frac{\alpha}{\pi}\right)^{1/2}rr'\Bigg[\frac{(W+M)\alpha\,.\,3\,.\,2^{15}}{(4+\lambda)^{3/2}}\exp\{-8\alpha(r^2+r'^2)\} \\
& + \frac{(W+M)\alpha\,.\,3\,.\,2^{19}}{(16+3\lambda)^{3/2}}\exp\left\{-8\alpha\left[\frac{16+5\lambda}{16+3\lambda}r^2+r'^2\right]\right\} \\
& + \frac{(W+M)\,.\,\alpha\,.\,3\,.\,2^{19}}{(16+3\lambda)^{3/2}}\exp\left\{-8\alpha\left[r^2+\frac{16+5\lambda}{16+3\lambda}r'^2\right]\right\}\Bigg] \\
& - \frac{\alpha^{3/2}}{\pi^{1/2}}rr'\,.\,3\,.\,2^{11}\left\{\frac{m}{\hbar^2}E\alpha+32\alpha^2(r^2+r'^2)-27\alpha\exp\{-8\alpha(r^2+r'^2)\}\right\} \\
& - k^2\frac{\alpha^{3/2}}{\pi^{1/2}}rr'\,.\,3\,.\,2^8\exp\{-8\alpha(r^2+r'^2)\}.
\end{aligned}
\qquad \left.\begin{array}{l} \\ \\ \\

The Coulomb kernels are:

$$\frac{m}{\hbar^2}e^2\frac{\alpha^{3/2}}{\pi^{1/2}}\Bigg[-\frac{2^{13}}{\sqrt{3}}\left(\frac{8\alpha}{3}\right)^{1/2}rr'\exp\left\{-\frac{40\alpha}{3}(r^2+r'^2)\right\}\int_{-1}^{1}\frac{\operatorname{erf}\left\{\frac{8\alpha}{3}(4r'^2-4rr'\mu+r^2)\right\}^{1/2}}{\left\{\frac{8\alpha}{3}(4r'^2-4rr'\mu+r^2)\right\}^{1/2}}$$

$$\times\exp\{64\alpha rr'\mu\}P_L(\mu)d\mu-\frac{2^{13}}{\sqrt{3}}\left(\frac{8\alpha}{3}\right)^{1/2}rr'\exp\left\{-\frac{40\alpha}{3}(r^2+r'^2)\right\}$$

$$\times\int_{-1}^{1}\frac{\operatorname{erf}\left\{\frac{8\alpha}{3}(r'^2+4r^2-4rr'\mu)\right\}^{1/2}}{\left\{\frac{8\alpha}{3}(4r^2-4rr'\mu+r'^2)\right\}^{1/2}}\exp\left\{\frac{64\alpha}{3}rr'\mu\right\}P_L(\mu)\,d\mu-\frac{2^{12}}{3\sqrt{3}}rr'$$

$$\times\exp\left\{-\frac{40\alpha}{3}(r^2+r'^2)\right\}\int_{-1}^{1}\frac{\exp\left\{\frac{64\alpha}{3}rr'\mu\right\}}{(r'^2-2r'r\mu+r^2)^{1/2}}P_L(\mu)d\mu-\frac{5.2^{12}}{\sqrt{3}}\left(\frac{8\alpha}{3}\right)^{1/2}rr'$$

$$\times\exp\left\{-\frac{40\alpha}{3}(r^2+r'^2)\right\}\int_{-1}^{1}\frac{\operatorname{erf}\left\{\frac{8\alpha}{3}(r^2+2rr'\mu+r'^2)\right\}^{1/2}}{\left\{\frac{8\alpha}{3}(r^2+2rr'\mu+r'^2)\right\}^{1/2}}\exp\left\{\frac{64\alpha}{3}rr'\mu\right\}P_L(\mu)d\mu$$

$$+2^{12}(8\alpha)^{1/2}rr'\exp\{-8\alpha(r^2+r'^2)\}\int_{-1}^{1}\frac{\operatorname{erf}\{8\alpha(r^2-2rr'\mu+r'^2)\}^{1/2}}{\{8\alpha(r^2-2rr'\mu+r'^2)\}^{1/2}}P_L(\mu)\,d\mu$$

$$-\frac{2^{11}}{\sqrt{3}}\frac{1}{(\alpha\pi)^{1/2}}\exp\left\{-\frac{40\alpha}{3}(r^2+r'^2)\right\}\mathscr{I}_{L+1/2}\left(\frac{64\alpha}{3}rr'\right)$$

$$+\left(\frac{\alpha}{\pi}\right)^{1/2}2^{13}rr'\exp\{-8\alpha(r^2+r'^2)\}$$

$$+2^{12}.4\left(\frac{\alpha}{3}\right)^{1/2}rr'\exp\{-8\alpha(r^2+r'^2)\}\frac{\operatorname{erf}\left\{4\left(\frac{\alpha}{3}\right)^{1/2}r'\right\}}{4\left(\frac{\alpha}{3}\right)^{1/2}r'}$$

$$+2^{12}.4\left(\frac{\alpha}{3}\right)^{1/2}rr'\exp\{-8\alpha(r^2+r'^2)\}\frac{\operatorname{erf}\left\{4\left(\frac{\alpha}{3}\right)^{1/2}r\right\}}{4\left(\frac{\alpha}{3}\right)^{1/2}r}\Bigg]$$

$L=0$ only.

where $\mathscr{I}_{L+1/2}(x)=(-1)^L(\frac{1}{2}\pi x)^{1/2}I_{L+1/2}(x)$ and $I(x)$ is the modified Bessel function as defined by Watson (1922, p. 80).

Also

$$W(r)=\frac{m}{\hbar^2}\Bigg[(4W+2Q-M)\frac{A\alpha^{3/2}}{(16\alpha+3\beta)}.2^{10}\exp\left\{-\frac{16\alpha\beta}{3(16\alpha+3\beta)}r^2+e^2\frac{16}{r}\right.$$

$$\left.\times\operatorname{erf}\left(4\left(\frac{\alpha}{3}\right)^{1/2}r\right)\right\}\Bigg].$$

References

Biel, S. J., 1957, *Proc. Phys. Soc.* A, **70,** 866.
de Borde, A. H., and Massey, H. S. W., 1955, *Proc. Phys. Soc.* A, **68,** 769.
Braden, C. H., Carter, S. M., and Ford, A. G., 1951, *Phys. Rev.*, **84,** 837.
Bransden, B. H., 1950, *Proc. Phys. Soc.* A, **209,** 380.
Bransden, B. H., and McKee, J. S. C., 1954, *Phil. Mag.*, **45,** 869.
Bransden, B. H., and Robertson, H. H., 1956, *Proc. Phys. Soc.* A, **69,** 877.
—— 1958, *Ibid.*, **72,** 779.
Bransden, B. H., Smith, K., and Tate, C., 1958, *Proc. Roy. Soc.* A, **247,** 73.
Buckingham, R. A., and Massey, H. S. W., 1941, *Proc. Roy. Soc.* A, **179,** 123.
Buckingham, R. A., Hubbard, S. J., and Massey, H. S. W., 1952, *Proc. Roy. Soc.* A, **211,** 183.
Burcham, W. E., Gibson, W. M., Prowse, D. J., and Rotblat, J., 1957, *Nucl. Phys.*, **3,** 217.
Burke, P., and Laskar, W., 1958, *C.R. Acad. Sci., Paris,* **246,** 3158.
Burke, P., and Robertson, H. H., 1957, *Proc. Phys. Soc.* A, **70,** 777.
Chadwick, J., 1930, *Proc. Roy. Soc.* A, **128,** 120.
Devons, S., 1939, *Proc. Roy. Soc.* A, **172,** 559.
Edwards, S. F., 1952, *Proc. Camb. Phil. Soc.*, **48,** 652.
Haefner, R., 1951, *Rev. Mod. Phys.*, **3,** 228.
Heydenberg, N. P., and Temmer, G. M., 1956, *Phys. Rev.*, **104,** 123.
Hochberg, S., Massey, H. S. W., and Underhill, L. H., 1954, *Proc. Phys. Soc.* A, **67,** 957.
Hochberg, S., Massey, H. S. W., Robertson, H. H., and Underhill, L. H., 1955, *Proc. Phys. Soc.* A, **68,** 746.
Humphries, G. H., quoted by Nilson *et al.*, I958.
Irving, J., 1951, *Phil. Mag.* (7), **42,** 338.
—— 1953, *Proc. Phys. Soc.* A, **66,** 17.
Margenau, H., 1941, *Phys. Rev.*, **59,** 37.
Mather, K. B., 1951, *Phys. Rev.*, **82,** 126.
Massey, H. S. W., 1953, *Progr. Nucl. Phys.*, **3,** 243.
Mohr, C. B. O., and Pringle, G. E., 1937, *Proc. Roy. Soc.* A, **160,** 190.
Mott, N. F., 1930, *Proc. Roy. Soc.* A, **126,** 259.
Nilson, R., Jentschke, W. K., Briggs ,G. R., Kerman, R. O., and Snyder, J. N., 1958, *Phys. Rev.*, **109,** 850.
Nilson, R., Kerman, R. O., Briggs, G. R., and Jentschke, W. K., 1956, *Phys. Rev.*, **104,** 1673.
Robertson, H. H., 1956, *Proc. Camb. Phil. Soc.*, **52,** 538.
Russell, J. L., Phillips, G. C., and Reich, C. W., 1956, *Phys. Rev.*, **104,** 135.
Rutherford, E., and Chadwick, J., 1927, *Phil. Mag.*, **4,** 605.
Steigart, F. E., and Sampson, M. B., 1953, *Phys. Rev.*, **92,** 660.
Sugie, A., Hodgson, P. E., and Robertson, H. H., 1957, *Proc. Phys. Soc.* A, **70,** 1.
Swan, P., 1953 a, *Proc. Phys. Soc.* A, **66,** 238.
—— 1953 b, *Ibid.*, **66,** 740.
Taylor, H. M., 1931, *Proc. Roy. Soc.* A, **134,** 103.
—— 1932, *Ibid.*, **136,** 605.
Van der Spuy, E., and Pienaar, H. J., 1958, *Nucl. Phys.*, **7,** 397.
Watson, G. N., 1922, *The Theory of Bessel Functions* (Cambridge: University Press), p. 80.
Wheeler, J. A., 1937, *Phys. Rev.*, **52,** 1083.
—— 1941, *Ibid.*, **59,** 16.
Wright, P., 1932, *Proc. Roy. Soc.* A, **134,** 677.

Electron Spin Resonance of Colloid Centres in Lithium Hydride

By W. T. DOYLE†, D. J. E. INGRAM‡ and M. J. A. SMITH
Department of Electronics, University of Southampton

MS. received 12*th May* 1959, *in final form* 24*th July* 1959

Abstract. Lithium hydride becomes additively coloured by exposure to ultra-violet light. An optical absorption band is produced at 6500 Å. From the position and general behaviour of the absorption band it may be assumed that this is due to colloidal particles comparable in size with the wavelength of visible light. It is supposed that the coloration process follows the Gurney–Mott theory of the photographic process. The irradiated specimens also exhibit a symmetrical, temperature-independent electron spin resonance absorption. This resonance is attributed to conduction electrons in colloidal particles which are small compared with the skin depth at 9000 Mc/s.

§ 1. Introduction

Although colour centres have long been known to occur quite generally in ionic crystals, interest has been focused principally on the alkali halides, due to the simplicity of their electronic and lattice structure. It is strange, however, that so little is known about colour centres in the simplest ionic crystal, lithium hydride. The more so since commercial lithium hydride often exhibits coloration to a noticeable degree. In this note preliminary observations on the colorability of lithium hydride by ultra-violet light and some properties of the centres so produced are presented.

One of the earliest observations on the coloration of hydrides was made by Elster and Geitel (1910), who subjected them to electron bombardment while attempting to make improved photoelectric cells. They attributed the coloration and concomitant increase in photoelectric yield to the presence of colloidal alkali metal. A recent analysis of the selective photoelectric effect (Doyle 1959) supports this hypothesis. Additional experimental confirmation of the presence of reduced metal in coloured LiH is presented below.

The most thorough chemical study of lithium hydride is that of Moers (1920). He established that LiH is an ionic salt. In the course of his investigations he also made qualitative observations on the coloration and decomposition of LiH by light and observed that additive coloration could be achieved by solidifying the electrolysed melt. There is little doubt that coloration by electrolysis would proceed just as well below the melting point so the resemblance to the alkali halides is very close.

Bach and Bonhoeffer (1933) measured the ultra-violet absorption spectrum of uncoloured LiH and found that the fundamental absorption of LiH begins at about 1900 Å. They also observed a strong, narrow absorption band at 2512 Å. Rauch (1938), who also measured the fundamental absorption in LiH, attributed this narrow band to F centres, though it did not occur in his specimens. Bach and

† National Science Foundation postdoctoral fellow. On leave from Dartmouth College, Hanover, New Hampshire, U.S.A.

‡ Now at Physics Dept., University College of North Staffs.

Bonhoeffer found that irradiation in the 2512 band (Hg 2537 line) led to photo-decomposition of the salt. They measured the hydrogen gas evolved and determined a quantum yield of 5% and attribute the low measured yield to trapping of H_2 in the lattice.

§ 2. Optical Experiments

We have irradiated commercial LiH obtained from Hopkins and Williams, Ltd., with 2537 Å ultra-violet light from a 25 watt mercury lamp. An exposure of 15 minutes at a distance of 10 cm produces a dark coloration, but detailed optical measurements of the quantum yield have not yet been made. Figure 1 shows an absorption spectrum taken with a very small single crystal, referred to the same crystal before coloration. The crystal appeared greenish blue after irradiation and its appearance did not change appreciably with temperature from 100 to 500°K. The coloration was not bleached by exposure to intense white light provided the sample was kept at room temperature, but was bleached by prolonged heating at about 400°C.

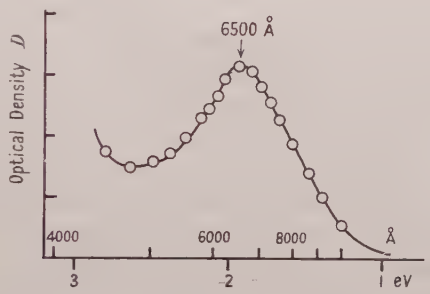

Figure 1. Optical absorption spectrum of irradiated LiH. Optical density is plotted against photon energy in ev.

It is clear from the fact that hydrogen gas was evolved in Bach and Bonhoeffer's (1933) experiment that irradiation leads to additive coloration in LiH. In this respect the hydride is closer to the silver salts than to the alkali halides. A still closer resemblance to the silver salts is indicated by the general appearance and insensitivity of the induced absorption band.

It is of interest to compare the position of the observed absorption band with the positions of the F, R and M bands expected on the basis of Ivey's empirical formula (Ivey 1947). The lattice constant of LiH is 2·08 Å (Zintl and Harder 1931) so the predicted positions of the F, R_1, R_2 and M bands are 2700, 3140, 3400 and 4400 Å respectively, assuming that Ivey's relation may be applied to hydrides. It is concluded that the observed band does not correspond to F or aggregate bands in the halides. The 2512 Å band observed by Bach and Bonhoeffer, on the other hand, does agree with the position of the F band computed by Ivey's rule.

The resistance to optical bleaching and the temperature independence of the band strongly suggest that it is due to colloidal metal. The position of the colloid band may be computed from the index of refraction of the host medium and the Wood–Zener, or plasma, wavelength of the alkali metal (Doyle 1958) if the particle diameter is much less than the wavelength of visible light. The index of refraction of LiH has not been measured. However, Bode (1930) using empirical regularities

has estimated the molar refractivity of LiH to be 4·0. Using this value together with Wood and Lukens' (1938) value for the plasma wavelength of lithium metal the position of the colloid band in LiH is found to be 4200 Å. This is not in agreement with the measured band. Actually, preliminary measurements of the index of refraction of LiH using the Becke method indicate that Bode's estimate for the molar refractivity of LiH is too large. Moreover, the position of the colloid band in LiF (Pringsheim 1954) suggests that the Wood and Luken plasma wavelength may also be too large, in agreement with electron energy loss experiments (Pines 1956). Thus the lack of agreement between the calculated position of the colloid band and the observed band may be even worse than appears. We conclude that the band at 6500 Å in LiH is not due to small colloids.

It is known that the peak of the colloid band shifts to longer wavelength as the size of the particles increase (Savostianowa 1930). The shift is accompanied by increased light scattering. Comparison with Savostianowa's computations for NaCl shows that it is necessary to assume very large particles (> 800 Å diameter) to account for the position of the observed band in this way. The growth of such large particles should be observable as a colour change during irradiation. As the particle size grows the peak should shift from the ultra-violet over to 6500 Å. No colour change has yet been observed. Although the conditions for viewing it were not good, it is surprising that no scattered light was produced. Nevertheless, the possibility that the observed band is due to colloidal particles comparable in size with the wavelength of visible light cannot yet be rejected, for it is conceivable that few nuclei are available for colloid growth so that the particles were already large before the coloration became noticeable. Moreover, the electron spin resonance experiments, to be described below, indicate the presence of a large colloid content in the crystal. Although the final identification of the new band will require further experiments on larger single crystals, it is tentatively assigned to large colloid particles. The coloration probably occurs along the lines of the Gurney–Mott theory of the photographic print out effect (Mott and Gurney 1940).

§ 3. Electron Spin Resonance Experiments

Electron spin resonance of the irradiated LiH has been observed at 9000 Mc/s using a transmission cavity spectrometer with 100 kc/s field modulation and phase sensitive detection. Experiments were performed at room temperature and at liquid oxygen temperature. For calibration purposes and g value measurements runs were made under identical conditions using a standard free-radical sample containing $1{\cdot}4 \times 10^{16}$ spins.

In all irradiated LiH samples a single resonance at $g = 2{\cdot}002 \pm 0{\cdot}001$ with a half width of 0·3 gauss was observed. The material before irradiation was not paramagnetic and gave no absorption signal. The extreme narrowness of the line rules out the possibility that it could be due to any of the usual electron excess centres. Such centres give rise to wide inhomogeneously broadened lines (Portis 1953). Since the single narrow line was thought to be due to the conduction electrons in colloidal particles of lithium, the temperature dependence of the resonance was also carefully studied. To effect this the intensity of the signal from LiH was compared with that from the standard free-radical sample at room temperature and liquid oxygen temperature. The results are shown in figure 2. It will be noted that the magnitude of the free-radical signal is much larger at the lower temperature, while the LiH signal is unchanged. The temperature

independence of the LiH signal is strong evidence that it is due to conduction electrons in colloidal lithium metal. The slight asymmetry and breadth of the lines shown in figure 2 is entirely an instrumental effect. Other curves show that the conduction electron resonance is symmetrical and much narrower than the free-radical resonance. The symmetry of the line shows that the colloid particles are small compared with the microwave skin depth (Dyson 1955).

Previous work on the electron spin resonance of conduction electrons in metals is reviewed by Baggulay and Owen (1957). Lithium has been studied by Feher and Kip (1955) in both bulk metal and in powders, and by Levy (1956) in the form of colloidal lithium metal precipitated from frozen solutions of liquid ammonia. The present observation differs chiefly in the size of the colloidal particles and in the manner of preparation. The manner of preparation via the ultra-violet irradiation as used here is a convenient one and should work for any crystal in which metallic colloids may be produced in suitable concentrations. Such samples are quite stable, and the particles size is small compared with the microwave skin depth.

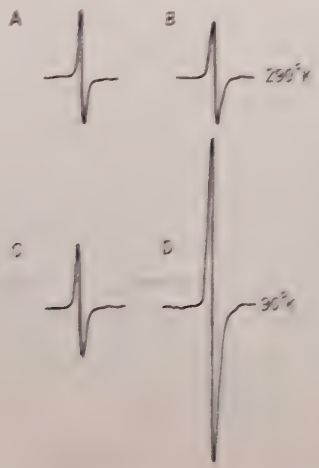

Figure 2. Electron spin resonance in irradiated LiH. Curves A and B show the derivative of the absorption signals obtained from LiH and from a standard free-radical sample respectively, at room temperature. Curves C and D show the corresponding signals at liquid oxygen temperature.

§ 4. Discussion

The width of the conduction electron spin resonance lines is related, by spin–orbit coupling, to the conduction mean free path of the electron in the metal (Elliott 1954). In bulk metal the mean free path is limited by electron–phonon and electron–impurity scattering. Previous measurements (Feher and Kip 1955, Levy 1956) have yielded line widths independent of temperature in lithium. It has been concluded that impurity scattering dominated in the specimens used. Although the line width reported here is also temperature independent and comparable in width with the narrowest lines previously observed in lithium, the very small size of the colloidal particles in LiH may make surface scattering the more important effect. Further experiments are under way to study the effects

of surface scattering on the optical and electron spin resonance spectra with a view to studying the spin–orbit coupling mechanism for surface scattering.

It might also be noted that studies on the thermal and optical decomposition of various azides have yielded narrow electron spin resonance signals. Preliminary measurements indicate that both colour centres and colloids are involved in this case. It is hoped that the work on the lithium hydride will assist in the analysis of these results, and more detailed measurements will be made in the near future.

References

Bach, F., and Bonhoeffer, K., 1933, *Z. phys. Chem.* B, **23,** 256.

Bagguley, D. M. S., and Owen, J., 1957, *Rep. Progr. Phys.* (London: Physical Society), **20,** 304.

Bode, H., 1930, *Z. phys. Chem.* B, **6,** 251.

Doyle, W. T., 1958, *Phys. Rev.*, **111,** 1067.

—— 1959, *Proc. Phys. Soc.*, **74,** 27.

Dyson, F. J., 1955, *Phys. Rev.*, **98,** 349.

Elliott, R. J., 1954, *Phys. Rev.*, **96,** 266.

Elster, J., and Geitel, H., 1910, *Phys. Z.*, **11,** 257.

Feher, G., and Kip, A. F., 1955, *Phys. Rev.*, **98,** 337.

Ivey, H. F., 1947, *Phys. Rev.*, **72,** 341.

Levy, R. A., 1956, *Phys. Rev.*, **102,** 31.

Moers, K., 1920, *Z. anorg. Chem.*, **113,** 179.

Mott, N. F., and Gurney, R. W., 1940, *Electronic Processes in Ionic Crystals* (Oxford: University Press), p. 227.

Pines, D., 1956, *Rev. Mod. Phys.*, **28,** 184.

Portis, A. M., 1953, *Phys. Rev.*, **91,** 1071.

Pringsheim, P., 1954, *Z. Phys.*, **136,** 573.

Rauch, W., 1938, *Z. Phys.*, **111,** 650.

Savostianowa, M., 1930, *Z. Phys.*, **64,** 262.

Wood, R. W., and Lukens, C., 1938, *Phys. Rev.*, **54,** 332.

Zintl, E., and Harder, A., 1931, *Z. phys. Chem.* B, **14,** 265.

Electron Lattice Interaction in Metals

By P. G. HARPER

Commonwealth Scientific and Industrial Research Organization,
Electrical Research Laboratory, University of Electrocommunication, Sydney, N.S.W.

MS. received 9th October 1958, in revised form 22nd May 1959

Abstract. A solution to the electron lattice equations of motion is derived which exactly describes resultant harmonic lattice motion. The solution equations admit two alternative solutions: (1) a simple renormalization of the sound velocity, (2) a renormalization of the sound velocity accompanied by a displacement of the equilibrium positions of the ion cores, the latter being represented by a static component of the plasma amplitudes. These solution equations are solved and their possible application to the superconducting state briefly discussed.

§ 1. Introduction

A basic assumption in the theory of metals is that mutual interaction of the lattice waves, due to anharmonicities of the lattice forces, may be always treated as a perturbation. The Fröhlich electron lattice Hamiltonian formed by adding an electron lattice interaction to an already formed free-phonon plus free-electron energy describes a system whose exact solution goes beyond the normal approximation since it leads to non-harmonic lattice forces. However the resultant (observed) motion is, for many purposes, required only in the harmonic approximation, that is to say, as **non-interacting quantized lattice waves**. It is the purpose of this paper to show that two alternative harmonic lattice states may exist, in one of which the equilibrium lattice ion sites suffer small random displacements of the order of 10^{-10} cm. An application to the superconducting state is briefly discussed.

§ 2. The Electron Lattice Scalar Equations

The electron field $\psi(\mathbf{x})$ is expanded as

$$\psi(\mathbf{x}) = V^{-\frac{1}{2}} \sum_{\mathbf{k}} a_{\mathbf{k}} e^{i\mathbf{k}\cdot\mathbf{x}}$$

where V is the volume of the metal. This gives the free electronic energy as

$$H_e = \sum_{\mathbf{k}} a^{+}_{\mathbf{k}} a_{\mathbf{k}} \varepsilon_{\mathbf{k}} \qquad \ldots\ldots (2.1)$$

where $\varepsilon_{\mathbf{k}} = \hbar^2 k^2 / 2m$. The amplitudes $a_{\mathbf{k}}, a_{\mathbf{k}}^{+}$ satisfy the quantization relations

$$a_{\mathbf{k}} a_{\mathbf{l}}^{+} + a_{\mathbf{l}}^{+} a_{\mathbf{k}} = \delta_{\mathbf{k},\mathbf{l}}$$
$$a_{\mathbf{k}} a_{\mathbf{l}} + a_{\mathbf{l}} a_{\mathbf{k}} = 0. \qquad \ldots\ldots (2.2)$$

The electrons are supposed to interact with the longitudinal lattice oscillatory modes only. Taking a continuum model the lattice displacement at a point $\mathbf{x}$ is denoted by $\mathbf{Q}(\mathbf{x}, t)$, the total lattice energy then being

$$H_L = NM \int \left(\dot{\mathbf{Q}}^2 - c^2 \mathbf{Q}^2 \right) d\tau \qquad \ldots\ldots (2.3)$$

where M is the ionic mass and N the number of ions per unit volume; s' denotes the longitudinal sound velocity in the absence of any interaction with electrons. It is then convenient to expand $\mathbf{Q}$ into plane wave normal modes belonging to (2.3) thus:

$$\mathbf{Q}(\mathbf{x}, t)=i\sum_{\mathbf{w}}\mathbf{v}\left(\frac{\hbar}{NMVs'w}\right)^{1/2}q_{\mathbf{w}}\,e^{i\mathbf{w}\cdot\mathbf{x}} \qquad \ldots\ldots(2.4)$$

where $\mathbf{v}$ denotes a unit wave vector in the $\mathbf{w}$ direction. Since $\mathbf{Q}(\mathbf{x}, t)$ is real, $q_{\mathbf{w}}{}^{+}=q_{-\mathbf{w}}$. The lattice displacement velocity is similarly described by

$$\dot{\mathbf{Q}}(\mathbf{x}, t)=i\sum_{\mathbf{w}}s'w\left(\frac{\hbar}{NMs'w}\right)^{1/2}p_{\mathbf{w}}\,e^{-i\mathbf{w}\cdot\mathbf{x}} \qquad \ldots\ldots(2.5)$$

and again, $p_{\mathbf{w}}{}^{+}=p_{-\mathbf{w}}$. In terms of $q_{\mathbf{w}}$, $p_{\mathbf{w}}$, the lattice energy becomes,

$$H_{\mathrm{L}}=\tfrac{1}{2}\sum_{\mathbf{w}}\hbar s'w(q_{\mathbf{w}}{}^{+}q_{\mathbf{w}}+p_{\mathbf{w}}{}^{+}p_{\mathbf{w}}). \qquad \ldots\ldots(2.6)$$

Quantization of the lattice motion requires that

$$[p_{\mathbf{w}}, p_{\mathbf{w}'}]=[q_{\mathbf{w}}, q_{\mathbf{w}'}]=0, \quad [p_{\mathbf{w}}, q_{\mathbf{w}'}]=i\delta_{\mathbf{w},\mathbf{w}'}. \qquad \ldots\ldots(2.7)$$

Finally, the energy of interaction of electrons and longitudinal lattice vibrations is given by

$$H_{\mathrm{int}}=C\int\rho(\mathbf{x})\,\mathrm{div}\,\mathbf{Q}\,d^3\mathbf{x} \qquad \ldots\ldots(2.8)$$

where $\rho(\mathbf{x})$ denotes the electron density $\psi^{+}\psi$ and C is an empirical interaction constant. From (2.4), (2.8) becomes

$$H_{\mathrm{int}}=\sum_{\mathbf{w},\mathbf{k}}D_{w}q_{\mathbf{w}}a_{\mathbf{k}}{}^{+}a_{\mathbf{k}-\mathbf{w}} \qquad \ldots\ldots(2.9)$$

where

$$D_{w}{}^{2}=\frac{C^2\hbar w}{NMVs'}. \qquad \ldots\ldots(2.10)$$

The total Hamiltonian is given by

$$H=H_{\mathrm{el}}+H_{\mathrm{L}}+H_{\mathrm{int}}$$

and for the equations of motion we have exactly

$$[a_{\mathbf{k}}, H]=\epsilon_{\mathbf{k}}a_{\mathbf{k}}+\sum_{\mathbf{w}}D_{w}q_{\mathbf{w}}a_{\mathbf{k}-\mathbf{w}} \qquad \ldots\ldots(2.11)$$

$$[[q_{\mathbf{w}}, H], H]=(\hbar\omega)^2q_{\mathbf{w}}+\hbar\omega D_{w}\sum_{\mathbf{k}}a^{+}{}_{\mathbf{k}-\mathbf{w}}a_{\mathbf{k}} \qquad \ldots\ldots(2.12)$$

where $\omega=s'w$. For the lattice motion (2.12) we require $a^{+}{}_{\mathbf{k}-\mathbf{w}}a_{\mathbf{k}}$ which, using (2.11) is given by

$$[a^{+}{}_{\mathbf{k}-\mathbf{w}}a_{\mathbf{k}}, H]=\Delta a^{+}{}_{\mathbf{k}-\mathbf{w}}a_{\mathbf{k}}+\sum_{\mathbf{w}'}D_{w'}(a^{+}{}_{\mathbf{k}-\mathbf{w}}a_{\mathbf{k}-\mathbf{w}'}-a^{+}{}_{\mathbf{k}-\mathbf{w}+\mathbf{w}'}a_{\mathbf{k}})q_{\mathbf{w}'} \qquad \ldots\ldots(2.13)$$

where $\Delta=\epsilon_{\mathbf{k}}-\epsilon_{\mathbf{k}-\mathbf{w}}$. The $\mathbf{w}'\neq\mathbf{w}$ terms in (2.13) contribute only anharmonic terms, $q_{\mathbf{w}'}q_{\mathbf{w}-\mathbf{w}'}$, towards the motion of $q_{\mathbf{w}}$. For harmonic motion it is sufficient to retain only $\mathbf{w}'=\mathbf{w}$ terms, when we have

$$[a^{+}{}_{\mathbf{k}-\mathbf{w}}a_{\mathbf{k}}, H]=\Delta a^{+}{}_{\mathbf{k}-\mathbf{w}}a_{\mathbf{k}}+D_{w}q_{\mathbf{w}}(\nu_{\mathbf{k}-\mathbf{w}}-\nu_{\mathbf{k}}) \qquad \ldots\ldots(2.14)$$

where $\nu_{\mathbf{k}}=a_{\mathbf{k}}{}^{+}a_{\mathbf{k}}$. Putting $\mathbf{w}=0$ in (2.13) we have, exactly,

$$[\nu_{\mathbf{k}}, H]=\sum_{\mathbf{w}}D_{w}(q_{\mathbf{w}}a_{\mathbf{k}}{}^{+}a_{\mathbf{k}-\mathbf{w}}-q_{\mathbf{w}}{}^{+}a^{+}{}_{\mathbf{k}-\mathbf{w}}a_{\mathbf{k}}). \qquad \ldots\ldots(2.15)$$

Equations (2.12), (2.14), (2.15) may now be solved in the phonon representation which diagonalizes the total Hamiltonian H, the quantum numbers being $n_{\mathbf{w}}$, the number of excited lattice quanta of wave vector $\mathbf{w}$. The phonon energy is given by

$$H(n_{\mathbf{w}}+1)-H(n_{\mathbf{w}})\equiv\hbar\Omega.$$

In this representation $q_{\mathbf{w}}$ connects only adjacent states but in addition may have diagonal elements, this being the most general harmonic transformation possible. Thus between states differing by one excited phonon $\mathbf{w}$, equation (2.14) becomes

$$-(\hbar\Omega+\Delta)(a^{+}_{\mathbf{k}-\mathbf{w}}a_{\mathbf{k}})_{n+1,n}=D_w\{(q_{\mathbf{w}})_{n+1,n}(\nu_{\mathbf{k}-\mathbf{w}}-\nu_{\mathbf{k}})_{n,n}+\sigma_{\mathbf{w}}(\nu_{\mathbf{k}-\mathbf{w}}-\nu_{\mathbf{k}})_{n+1,n}\}$$

where for convenience $n_{\mathbf{w}}$ is written as n, and $\sigma_{\mathbf{w}}$ denotes the diagonal value of $q_{\mathbf{w}}$. Considering equation (2.15) between the same states, and using the fact that the diagonal values of $[\nu_{\mathbf{k}}, H]$ vanish identically, we further obtain

$$\hbar\Omega(\nu_{\mathbf{k}-\mathbf{w}}-\nu_{\mathbf{k}})_{n+1,n}=2D_w\{\sigma_{\mathbf{w}}(a_{\mathbf{k}}{}^{+}a_{\mathbf{k}-\mathbf{w}})_{n+1,n}-\sigma_{\mathbf{w}}{}^{*}(a^{+}_{\mathbf{k}-\mathbf{w}}a_{\mathbf{k}})_{n+1,n}\}.$$

It is now straightforward to solve these matrix equations for $(\nu_{\mathbf{k}-\mathbf{w}}-\nu_{\mathbf{k}})_{n+1,n}$ which is given by

$$(\nu_{\mathbf{k}-\mathbf{w}}-\nu_{\mathbf{k}})_{n+1,n}=\frac{4D_w{}^2\sigma_{\mathbf{w}}(q_{\mathbf{w}})_{n+1,n}}{(\hbar\Omega)^2-\Delta^2-4D_w{}^2|\sigma_{\mathbf{w}}|^2}(\nu_{\mathbf{k}-\mathbf{w}}-\nu_{\mathbf{k}})_{n,n}.$$

Secondly, $(a^{+}_{\mathbf{k}-\mathbf{w}}a_{\mathbf{k}})_{n+1,n}$ is given by

$$(a^{+}_{\mathbf{k}-\mathbf{w}}a_{\mathbf{k}})_{n+1,n}=-\frac{D_w(\hbar\Omega-\Delta)(q_{\mathbf{w}})_{n+1,n}}{(\hbar\Omega)^2-\Delta^2-4D_w{}^2|\sigma_{\mathbf{w}}|^2}(\nu_{\mathbf{k}-\mathbf{w}}-\nu_{\mathbf{k}})_{n,n}. \qquad \ldots\ldots (2.16)$$

A diagonal value of the electron density component is obtained by taking diagonal values of (2.14):

$$(a^{+}_{\mathbf{k}-\mathbf{w}}a_{\mathbf{k}})_{n,n}=-\frac{D_w}{\Delta}\sigma_{\mathbf{w}}\left\{1-\frac{4D_w{}^2(|(q_{\mathbf{w}})_{n+1,n}|^2+|(q_{\mathbf{w}})_{n,n-1}|^2)}{(\hbar\Omega)^2-\Delta^2-4D_w{}^2|\sigma_{\mathbf{w}}|^2}\right\}(\nu_{\mathbf{k}-\mathbf{w}}-\nu_{\mathbf{k}})_{n,n}. \qquad \ldots\ldots (2.17)$$

Finally, the harmonic secular equations are obtained by inserting into (2.12) the non-diagonal and diagonal values of $(a_{\mathbf{k}-\mathbf{w}}{}^{+}a_{\mathbf{k}})$, thus:

$$\left\{(\hbar\omega)^2-(\hbar\Omega)^2-D_w{}^2\hbar\omega\sum_{\mathbf{k}}\frac{(\hbar\Omega-\Delta)(\nu_{\mathbf{k}-\mathbf{w}}-\nu_{\mathbf{k}})_{n,n}}{\Delta^2+4D_w{}^2|\sigma_{\mathbf{w}}|^2-(\hbar\Omega)^2}\right\}(q_{\mathbf{w}})_{n+1,n}=0. \qquad \ldots\ldots (2.18)$$

$$\left\{\hbar\omega-D_w{}^2\sum_{\mathbf{k}}\frac{(\nu_{\mathbf{k}-\mathbf{w}}-\nu_{\mathbf{k}})_{n,n}}{\Delta}\left(1+\frac{4D_w{}^2(|(q_w)_{n+1,n}|^2+|(q_w)_{n,n-1}|^2)}{\Delta^2+4D_w{}^2|\sigma_{\mathbf{w}}|^2-(\hbar\Omega)^2}\right)\right\}\sigma_{\mathbf{w}}=0. \qquad \ldots\ldots (2.19)$$

This pair of simultaneous equations determines the resultant harmonic motion of the lattice exactly in terms of the two quantities Ω, $\sigma_{\mathbf{w}}$, both functions of $\mathbf{w}$.

It is immediately apparent that there are two alternative solutions, $\sigma_{\mathbf{w}}=0$ and $\sigma_{\mathbf{w}}\neq 0$.

(i) $\sigma_{\mathbf{w}}=0$.

Equation (2.19) vanishes identically, and there remains

$$(\hbar\omega)^2-(\hbar\Omega)^2=D_w{}^2\hbar\omega\sum_{\mathbf{k}}\frac{(\nu_{\mathbf{k}-\mathbf{w}}-\nu_{\mathbf{k}})_{n,n}}{\hbar\Omega+\Delta}. \qquad \ldots\ldots (2.20)$$

This equation for the re-normalized frequency Ω was first described by Fröhlich (1952) and leads to the relation

$$s_0 = (1 - 2\nu F')^{1/2} s', \qquad \ldots\ldots (2.21)$$

where $\Omega = s_0 w$, and the interaction parameter F' is defined as

$$F' = \frac{3}{8} \frac{C^2}{\zeta M s'^2}, \qquad \ldots\ldots (2.22)$$

ζ being the electron Fermi potential.

Chester and Houghton (1959) have considered the modifications to the interaction function D_w brought about by the effects of Coulomb interaction between electrons. Generally it is sufficient to disregard $\hbar\Omega$ in the denominator of the right-hand sum, which is then equivalent to an adiabatic treatment of the lattice motion. However, the resonances of the exact denominator formally indicate that real electron–phonon collisions are permitted in this state.

(ii) $\sigma_{\mathbf{w}} \neq 0$.

Equation (2.19) requires the value of $(q_{\mathbf{w}})_{n+1,n}$ which is obtained from the identity

$$[p_{\mathbf{w}}, q_{\mathbf{w}}] = i$$

as

$$|(q_{\mathbf{w}})_{n+1,n}|^2 = \frac{\omega}{2\Omega}(n_{\mathbf{w}} + 1)$$

i.e. a re-normalization of the 'bare' matrix element. Since (2.18), (2.19) were obtained by treating the lattice displacement field as consisting of a single normal mode, normalization requires that $|(q_{\mathbf{w}})_{n+1,n}|^2$ and $|\sigma_{\mathbf{w}}|^2$ both be corrected by a factor N where N is the number of ions per unit volume.

The value of $(\nu_{\mathbf{k}-\mathbf{w}} - \nu_{\mathbf{k}})_{n,n}$ is not, strictly speaking, that due to an arbitrary electron momentum distribution. In fact, from (2.15) we have, taking the diagonal value,

$$\sum_{\mathbf{w}} \frac{\hbar\omega D_w^2 (\nu_{\mathbf{k}-\mathbf{w}} - \nu_{\mathbf{k}})_{n,n}}{(\hbar\Omega)^2 - \Delta^2 - 4D_w^2 |\sigma_{\mathbf{w}}|^2} = 0 \qquad \ldots\ldots (2.23)$$

which is an integral equation to be satisfied in both the displaced ($\sigma_{\mathbf{w}} \neq 0$) and undisplaced ($\sigma_{\mathbf{w}} = 0$) lattice states. It appears, however, that for $k_0 \gg ms/\hbar$, k_0 the Fermi wave number, the Fermi ground state distribution is sufficiently accurate.

In this displaced state the free electron-pair energy Δ is replaced by $(\Delta^2 + 4D_w^2 |\sigma_{\mathbf{w}}|^2)^{1/2}$ in the denominator. This latter energy is that due to electrons moving in a static sinusoidal potential of wave vector $\mathbf{w}$, amplitude $D_w|\sigma_{\mathbf{w}}|$ which is evidently the potential field due to the rigid sinusoidal displacement of lattice sites. Each lattice mode therefore carries its own static 'inner field' which is maintained in a self-consistent way by the electrons. It will appear later that a real solution of (2.18), (2.19) exists only when $2D_w|\sigma_{\mathbf{w}}| > \hbar\Omega$. Since $2D_w|\sigma_{\mathbf{w}}|$ is the energy gap of the electronic energy spectrum due to the phonon static Bloch potential, it follows that there can be no electron phonon collisions which satisfy energy conservation.

All lattice modes are actually present of course, and the total electronic wave function is then the linear resultant of the above states. This is not the same as a many-particle wave function composed of single electron states of particles moving in the resultant *potential*. The total electronic wave function cannot be presented in terms of single particle states in fact.

§ 3. Approximate Solution of the Secular Equations

The summations over $\mathbf{k}$ in (2.18), (2.19) are conveniently carried out by first keeping $\epsilon_{\mathbf{k}}-\epsilon_{\mathbf{k}-\mathbf{w}}$ constant and summing $\nu_{\mathbf{k}-\mathbf{w}}-\nu_{\mathbf{k}}$ over allowable values of $\mathbf{k}$ such that $\epsilon_{\mathbf{k}}-\epsilon_{\mathbf{k}-\mathbf{w}}=\Delta$ and then secondly summing over pair energies Δ. This last summation is replaced by an integration over $d\Delta$ with a density factor equal to the inverse spacing of Δ values. Thus

$$\sum_{\mathbf{k}}\ldots\rightarrow\left(\frac{L}{2\pi}\right)\frac{m}{\hbar^2 w}\int\ldots\xi(\Delta,w)d\Delta$$

where

$$\xi(\Delta,w)=\sum_{\mathbf{k}}(\nu_{\mathbf{k}-\mathbf{w}}-\nu_{\mathbf{k}})\delta(\epsilon_{\mathbf{k}}-\epsilon_{\mathbf{k}-\mathbf{w}}-\Delta).$$

For the ground state Fermi distribution it is easily shown (Harper 1956) that $\xi(\Delta, w)$ is given as follows:

$w<2k_0$,

$$\xi=\left(\frac{L}{2\pi}\right)^2\frac{2m\pi}{\hbar^2}\begin{cases}\Delta, & \epsilon_+<\zeta\\ \zeta-\epsilon_-, & \epsilon_-<\zeta<\epsilon_+\\ 0, & \zeta<\epsilon_-\end{cases}$$

$w>2k_0$,

$$\xi=\left(\frac{L}{2\pi}\right)^2\frac{2m\pi}{\hbar^2}(\zeta-\epsilon_-)$$

where

$$\epsilon_\pm=\frac{\hbar^2}{2m}\left(\frac{m\Delta}{\hbar^2 w}\pm\frac{1}{2}w\right)^2$$

and L^3 is the volume V. Since ξ is odd in Δ, the contribution proportional to $\hbar\Omega$ in the right-hand sum of (2.18) vanishes. Taking new dimensionless variables defined as $t=w/2k_0$, $z=\Delta/4\zeta$ and defining as dependent variable f by $(4\zeta f)^2=4D_w{}^2|\sigma_{\mathbf{w}}|^2-(\hbar\Omega)^2$ then the secular equations (2.18), (2.19) become for $w<2k_0$, i.e. $t<1$,

$$\left(\frac{s}{s'}\right)^2=1-\frac{2\nu F'}{t}\int_0^{t-t^2}\frac{z^2dz}{z^2+f^2}-\frac{\nu F'}{2t}\int_{t-t^2}^{t+t^2}\left\{1-\left(\frac{z}{t}-t\right)^2\right\}\frac{zdz}{z^2+f^2}$$

$$=1-\nu F'\left\{1-\frac{f}{t}\left(\tan^{-1}\frac{t+t^2}{f}+\tan^{-1}\frac{t-t^2}{f}\right)\right.$$

$$\left.+\frac{1}{4t}\left(1-t^2+\frac{f^2}{t^2}\right)\ln\frac{(t+t^2)^2+f^2}{(t-t^2)^2+f^2}\right\}\qquad\ldots\ldots(3.1)$$

$$\frac{1}{2\nu F'}=\frac{1}{t}\int_0^{t-t^2}\left(1+\frac{4F}{3}\frac{ms}{\hbar K_0}\frac{\bar{n}+\frac{1}{2}}{z^2+f^2}t\right)dz$$

$$+\frac{1}{4t}\int_{t-t^2}^{t+t^2}\left\{1-\left(\frac{z}{t}-t\right)^2\right\}\left(1+\frac{4F}{3}\frac{ms}{\hbar k_0}\frac{\bar{n}+\frac{1}{2}}{z^2+f^2}t\right)dz$$

$$=\frac{1}{2}+\frac{1-t^2}{4t}\ln\frac{1+t}{1-t}+\frac{2F}{3}\frac{ms}{\hbar k_0}\frac{\bar{n}+\frac{1}{2}}{f^2}\left\{f\tan^{-1}\frac{t+t^2}{f}+f\tan^{-1}\frac{t-t^2}{f}\right.$$

$$\left.+\frac{1-t^2}{2}\ln\frac{1+t}{1-t}-\frac{1}{4}\left(1-t^2+\frac{f^2}{t^2}\right)\ln\frac{(t+t^2)^2+f^2}{(t-t^2)^2+f^2}\right\}\qquad\ldots\ldots(3.2)$$

where f^2 has been anticipated to be positive, and ν denotes the number of free electrons per ion. The phonon quantum n has been replaced by a mean value $\bar{n}$ whose determination will be discussed later. The F, s that occur on the right-hand side of (3.2) are the re-normalized values connected with F', s' by $F^2s^2=F'^2s'^2$.

The first two F-independent terms on the right-hand side of (3.2) may be replaced by 1 for t small and $\frac{1}{2}$ for $t \lesssim 1$. From their integral form, the terms proportional to F are seen to remain positive and in order to satisfy (3.2) it is clearly necessary that $2\nu F' < 1$. This condition is sufficient to ensure a real solution for f and at the same time exclude real poles from the $\mathbf{k}$ summations in (2.18), (2.19).

Considering (3.1) when $t \ll 1$, the logarithmic term is very nearly equal to unity, and the inverse tangents very nearly equal. When $t \to 1$ however, the logarithmic term and the second written inverse tangent vanish. We therefore replace (3.1) approximately by

$$\left(\frac{s}{s'}\right)^2 = 1 - 2\nu g F' \left(1 - \frac{f}{t}\tan^{-1}\frac{t}{f}\right) \qquad \ldots\ldots (3.3)$$

where

$$g = 1, \; w \ll 2k_0$$
$$= \tfrac{1}{2}, \; w \gtrsim 2k_0.$$

Similarly, (3.2) is replaced by

$$1 - 2\nu g F' = \frac{8}{3} g \nu F F' \frac{ms}{\hbar k_0} (\bar{n} + \tfrac{1}{2}) \frac{1}{f} \tan^{-1}\frac{t}{f}. \qquad \ldots\ldots (3.4)$$

The equations (3.3), (3.4) for f and s are clearly not capable of exact solution, but we may obtain useful approximate solutions in two extreme cases, one of which proves sufficient for practical purposes.

Consider (i) $t \ll f$. In this case $\tan^{-1}(t/f) \simeq t/f$ and we obtain immediately

$$f^2 \simeq \frac{8}{3} \frac{g\nu F F'}{1 - 2g\nu F'} \frac{ms}{\hbar k_0} (\bar{n} + \tfrac{1}{2}) t \qquad \ldots\ldots (3.5)$$

$$\left(\frac{s}{s'}\right)^2 = 1 - \frac{2}{3} g \nu F' \left(\frac{t}{f}\right)^2 \simeq 1. \qquad \ldots\ldots (3.6)$$

This solution holds whenever $t^2 \ll f^2$ or, retaining only dimensional magnitudes,

$$\hbar s' w \ll ms^2 (\bar{n} + \tfrac{1}{2}).$$

Taking for $\bar{n}$ a thermal average, then for $\boldsymbol{k}T \gg ms^2 \simeq 0{\cdot}1$ deg K $\times$ (Boltzmann's constant), this (very) low frequency solution holds for

$$\hbar s' w \ll (ms^2 \boldsymbol{k} T)^{1/2}. \qquad \ldots\ldots (3.7)$$

(ii) In the opposite extreme, $f \ll t$, $\tan^{-1}(t/f) \simeq \frac{1}{2}\pi$ and the solution becomes

$$f \simeq \frac{8}{3} \frac{g\nu F F'}{1 - 2g\nu F'} \frac{ms}{\hbar k_0} \frac{\pi}{2} (\bar{n} + \tfrac{1}{2}) \qquad \ldots\ldots (3.8)$$

$$\left(\frac{s}{s'}\right)^2 \simeq 1 - 2g\nu F' \left(1 - \frac{\pi f}{2t}\right)$$

or

$$s = s_0 + \frac{8\pi^2}{3} \left(\frac{g\nu F'}{1 - 2\nu g F'}\right)^2 F \frac{ms^2}{\hbar w} (\bar{n} + \tfrac{1}{2}) \qquad \ldots\ldots (3.9)$$

where $s_0 = (1 - 2\nu g F')^{1/2} s'$ is the undisplaced sound velocity (equation (2.21)).

Only the short wave solution, $\hbar s' w \gg (ms . \boldsymbol{k}T)^{1/2}$ is of practical interest, and we note that when $w < 2k_0$ there is an increase of sound velocity relative to the undisplaced state. For the same wavelengths, using (3.8), the magnitude of

$D_w|\sigma_{\mathbf{w}}|$, i.e. the energy gap due to a single mode $\mathbf{w}$, is seen to be nearly independent of w and of magnitude $(ms^2.\zeta)^{1/2}$. The magnitude of $|\sigma_{\mathbf{w}}|^2$ in the region $w \lesssim 2k_0$ is then given by $|\sigma_{2k_0}|^2 \sim ms/\hbar k_0$.

It remains to discuss the solution of (2.18), (2.19) for $w > 2k_0$, i.e. $t > 1$. Using the expression for $\xi(\Delta, w)$ given for $w > 2k_0$, we obtain for equation (2.19)

$$\left\{\frac{1}{2} - \frac{t^2-1}{2t}\ln\frac{t+1}{t-1} + \frac{F}{3}\frac{ms}{\hbar k_0}\frac{\bar{n}+\frac{1}{2}}{t^2}\int_{t^2-t}^{t^2+t}\frac{t^2-(z-t^2)^2}{z^2+f^2}\frac{dz}{z} - \frac{1}{2\nu F'}\right\}\sigma_{\mathbf{w}} = 0. \quad \ldots\ldots (3.10)$$

The first and second terms (independent of F) decrease from $\frac{1}{2}$ at $t=1$ and vanish as t^{-2}, remaining always positive. Supposing $f^2 > 0$ the integral is always positive and has an upper limit independent of f,

$$\int \frac{t^2-(z-t^2)^2}{z(z^2+f^2)}\,dz \leqslant \int \frac{t^2-(z-t^2)^2}{z^3}\,dz = O(t^{-3}) \quad t \gg 1$$

Thus no positive f^2 can satisfy (3.10). Suppose secondly that $f^2 < 0$, say, $= -f'^2$. Then if $f' > t^2 + t$ the integral is negative, and obviously cannot satisfy (3.10). If $f' < t^2 + t$, the integral may have a real pole but again, taking principal parts,

$$\frac{1}{t^2}\int \frac{t^2-(z-t^2)^2}{z^2-f'^2}\frac{dz}{z}$$

has an upper bound independent of f' which decreases to zero, thus failing to provide a real solution.

It is concluded therefore, that when $w > 2k_0$ (3.10) is satisfied only by $\sigma_{\mathbf{w}} = 0$, $s = s_0$. That is to say, the displaced lattice motion is identical with the undisplaced lattice motion when $w > 2k_0$. There is thus a negative discontinuity in the displaced phonon spectrum at $w = 2k_0$ which results in a double degeneracy of phonon states in the energy interval $\hbar\Omega \pm O(ms^2)$. This is illustrated in the figure. The existence of an infinite discontinuity in the gradient of the phonon spectrum at $w = 2k_0$ has recently been suggested by Kohn (1959) in a calculation of the lattice screening due to a periodic perturbation. Though this was intended to describe adiabatically the phonon itself it more closely relates to the static deformation considered here.

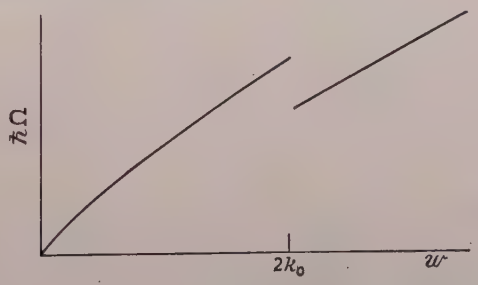

Displaced phonon energy as a function of wave number w.

We complete this brief discussion of the displaced state by considering the mean displacement of the ionic sites. This is generally given by

$$\mathbf{Q}_s(\mathbf{x}) = i\sum_{\mathbf{w}} \mathbf{v}\left(\frac{\hbar}{NMVs'w}\right)^{1/2}\sigma_{\mathbf{w}}\,e^{i\mathbf{w}.\mathbf{x}}.$$

On the average this must vanish since the phase of $\sigma_{\mathbf{w}}$ is arbitrary and random. The mean square $\langle \mathbf{Q}_s^2 \rangle$ however will not vanish and is given by

$$\langle \mathbf{Q}_s^2 \rangle = \frac{V}{(2\pi)^3} \int^{2k_0} \frac{\hbar}{NMVs'} |\sigma_{\mathbf{w}}|^2 w dw.$$

Since the greatest contribution will come from the upper limit, we get dimensionally,

$$\langle \mathbf{Q}_s^2 \rangle \simeq \frac{\hbar}{NMs'} \cdot \frac{ms}{\hbar k_0} \cdot k_0^2$$

$$= \frac{m}{M} \frac{k_0}{N} \sim 10^{-20}\,\mathrm{cm}^2.$$

Thus the root mean square ionic displacement

$$\langle \mathbf{Q}_s^2 \rangle^{1/2} \simeq 10^{-10}\,\mathrm{cm}.$$

If, more generally, we consider the correlation

$$\langle \mathbf{Q}_s \rangle (\mathbf{x}) \mathbf{Q}_s (\mathbf{x} + \mathbf{R})$$

it is found that this quantity is nearly constant and equal to $\langle \mathbf{Q}_s^2 \rangle$ for $\hbar s' R^{-1} \gg (\boldsymbol{kT} . ms^2)^{1/2}$ and thereafter decreases as R^{-1}.

The effect of the static random displacement of ion sites on the reflection of neutrons and x-rays is similar to that produced by thermal agitation. That is to say, there is an enhancement of the normal thermal background scattering. Since at low temperatures the mean thermal amplitude is of order 10^{-10} cm, the displaced state contribution would be of comparable magnitude.

§ 4. Specific Heat of the Displaced State

The phonon energies in the undisplaced state $\hbar\Omega_0$ and in the displaced state, $\hbar\Omega_d$ say, are normal mode eigenvalue differences of the same Hamiltonian, but belonging to alternative lattice states. Moreover, each spectrum separately exhausts all degrees of freedom of the lattice. This is in contrast to the case of non-combining rotational spectra of a molecule, say, where *all* rotational bands due to possible electronic excitations are required to account for the total motion of the molecule. Since the eigenvalues of a Hamiltonian are unique the undisplaced and displaced spectra must be identical. Since the (Ω, w) relation is not perfectly linear, the $\mathbf{w}$ spacing in the displaced state is non-uniform. This is unusual, but since a lattice site displacement implies a non-uniform volume strain it is plausible that $\mathbf{w}$ spacing need no longer be determined by the usual periodic boundary conditions.

The undisplaced and displaced phonon states contribute identical mean thermal energies to the total lattice thermal energy. In the energy region $\hbar\Omega(2k_0) \pm \mathrm{O}(ms^2)$, however, the extra (degenerate) displaced phonons contribute an additional mean energy $\Delta_L(T)$ equal to

$$\Delta_L(T) = \frac{V}{(2\pi)^3} \left[\exp\left(\frac{\hbar\Omega(2k_0)}{\boldsymbol{kT}} \right) - 1 \right]^{-1} 4\pi (2k_0)^2 \hbar\Omega(2k_0) \frac{\gamma ms^2}{\hbar s}$$

where

$$\gamma = \frac{8\pi^2}{3} \left(\frac{\frac{1}{2}\nu F'}{1 - \nu F'} \right)^2 F(\bar{n} + \tfrac{1}{2}) \quad \text{(eqn (3.9))}.$$

For low temperatures $kT \ll 2\hbar s k_0$, $\Delta_L(T)$ has the exponential temperature dependence characteristic of the (electronic) specific heat of many superconductors. The activation energy (energy gap), namely, $2\hbar s k_0$ is however, somewhat high unless the effective electronic density is low, say $k_0 \simeq 10^7\,\mathrm{cm}^{-1}$ It may be noted that the specific heat contribution per electron is proportional to ms^2.

The complete specific heat, and therefore, the possibility of a thermodynamic transition, cannot be discussed without knowing the electronic behaviour about which nothing has been said in this paper. For a second-order transition it would be necessary that the electronic energy in the displaced ground state be lower than the undisplaced electron energy. It then remains to account for the absence of the electronic heat linear in temperature. The following consideration is put forward tentatively. Since in the above solution real electron scattering is completely prohibited there appears to be no thermal contact between the electron gas and the lattice and consequently no necessity for a common temperature. In that case, if the displaced lattice state is reached through a transition temperature T_c then for lattice temperatures $T < T_c$ the electron gas might be expected to remain at T_c thus possessing no specific heat. This would suggest that the mean phonon quantum number $\bar{n}$ in (2.19) should equal the thermal mean at T_c rather than the lattice temperature T.

References

Chester, G. V., and Houghton, A., 1959, *Proc. Phys. Soc.*, **73**, 609.
Fröhlich, H., 1952, *Proc. Roy. Soc.* A, **215**, 291.
Harper, P. G., 1956, *Proc. Phys. Soc.* B, **69**, 1095.
Kohn, W., 1959, *Phys. Rev. Letters*, **2**, 393.

On the Structure of Extensive Cosmic Ray Air Showers: The Penetrating Component

By E. W. KELLERMANN and N. DICKINSON†
Department of Physics, The University of Leeds

MS. received 12*th May* 1959

Abstract. The penetrating components of extensive cosmic-ray air showers of sizes ranging from 4×10^4 to 5×10^5 particles have been examined at distances from 3 to 18 metres from the shower cores. Within these distances the nucleonic particles, of energy 2 Gev or larger, examined here have a lateral distribution not flatter than that of the electrons which is described by a power law $r^{-0.75}$, whereas the muon component decreases as $r^{-0.3}$ with distance from the core. The numbers of nucleonic particles and muons decrease relative to the electron numbers $\mathcal{N}$ with increasing shower size, the number of nucleons being proportional to $\mathcal{N}^{0.6}$.

§ 1. Introduction

Penetrating particles in extensive air showers, at one time regarded as an admixture to the supposed main component of electrons and photons in showers, are now not only recognized as the determining factor of shower development, but may even provide a more reliable means of detection and examination of showers than that afforded by the soft component.

Earlier reports of the air shower work at Leeds, 100 m above sea level, have been concerned with a determination of the core location of showers (Kellermann, Shaw and Dickinson 1957, to be referred to as I) and, based on this, with an examination of the electron–photon component (Kellermann, Shaw and Walker 1958, to be referred to as II). The present paper discusses the penetrating particles, namely the nuclear-active, or N-component, and the muons. Preliminary results comparing the relative distribution of the electron–photon, the nucleonic, and the muon component were given first at the Cosmic Ray Conference at Guanajuato in 1955 (Kellermann 1958). Work by other groups on these problems is summarized in the report of the 1957 International Convention on Cosmic Rays, Varenna (1958).

§ 2. Method

In I a 'core-detecting' apparatus was described and its performance assessed, it being shown that more than 50% of the showers detected in this way had axes falling within 3 m of the centre of the core detector. The units included arrays of unshielded counters which allowed showers of different sizes to be distinguished: four groups (referred to as (3.3), (4.2), (5.1), and (6.0)) corresponding to densities of roughly 25, 40, 90, and 200 particles m^{-2} at about 3 m from the shower-axis were distinguished. These probably correspond to showers of total size 4×10^4, 8×10^4, 2×10^5, and 5×10^5 particles respectively.

† Now at the Nuclear Power Plant Co. Ltd., Knutsford, Cheshire.

The central unit of the core detector consisted essentially of two counter trays within a lead block with full side and bottom shielding. The upper tray lay under 5 cm lead, the lower one under 20 cm, and records of the individual counters were photographed in a hodoscope display. Core detection involved the selection of events applying a specific criterion in the discharge pattern of the central unit. Other selections here are those recognizably associated with the passage of muons through the lead pile or with the products of nuclear interactions taking place in the pile. To a first approximation, a discharge of only one of the ten counters in the lower tray would indicate the presence of a muon, and that of more than one the presence of nuclear-active particles. Corrections made necessary by this simple differentiation will be considered below.

Since two units were in use, and since the separation between them was varied, data were obtained relating the detection of shower cores in one unit with the occurrence of the two kinds of penetrating events in the other, at various distances of separation ranging from 3 to 18 m.

The analysis of the measurements was carried out as follows: the rates of air showers in which penetrating particles were detected were calculated with the help of the expressions used in II and employing only one new parameter, namely the density k of the penetrating component expressed as a fraction of the electron density. Rates were calculated for different values of this parameter, and by fitting of the calculated to the observed rates, a best value for k was found with its standard deviation. Values were computed for the penetrating component as a whole as well as separately for the N- and the μ-component.

It was assumed that within each of the four shower density groups considered k was constant so that in any one group the spectrum of the penetrating particles could be described by a power law with the same exponent $\gamma = 1{\cdot}5$ as that applicable to the electron density spectrum. The assumption is not correct if taken to hold over the whole range of shower densities, but is found to be a sufficiently good approximation within limited density ranges since k is found to vary only slowly with density. The approximation is valid, too, whether one considers the total penetrating component or either of its constituent parts. It was found useful in the representation and the discussion of the results, to express the penetrating particle density at distance r either as a fraction k of the electron density $\varkappa$ at the core detector, or as a fraction k_r of the electron density prevailing at the distance r from the core detector. In II it was shown that the electron density at distance r from the detector was $\varkappa . \alpha(r)$ where $\alpha < 1$, and the lateral dependence of α on r was determined. Hence the $k_r = k/\alpha(r)$ can be tabulated quickly. The values of α used here were taken from smooth curves fitted to the values given in II.

The actual integrals are readily written down: $S_i^c(x)\,dx$ is the spectrum determined in II, describing the showers in density group i for which a core-response is also registered. Penetrating particles, occurring with density kx, falling on the lead pile and leading to the discharge of one or more of the ten counters, each of area A, in the bottom tray can be described by the response

$$R_k(x) = 1 - e^{-10Akx},$$

regarding here the ten counters as one counter of area $10A$ and without differentiating between single and multiple discharges of the individual counters.

The response to a single discharge of one of the ten counters only by which the response to a muon is identified can be written as

$$R_{k_\mu}(x) = \{1 - \exp(-Ak_\mu x)\} \exp(-9Ak_\mu x).$$

As shown in II, the rates of these events would then be $\mathscr{R}_{i,k}$ or $\mathscr{R}_{i,k_\mu}$, where

$$\mathscr{R}_{i,k} \propto \int_0^\infty S_i^c(x) R_k(x)\, dx$$

or

$$\mathscr{R}_{i,k_\mu} \propto 10 \int_0^\infty S_i^c(x) R_{k_\mu}(x)\, dx.$$

The rate of $\mathscr{R}_{i,k_N}$ of multiple events under lead associated with N-particles is then obtained as

$$\mathscr{R}_{i,k_N} = \mathscr{R}_{i,k} - \mathscr{R}_{i,k_\mu}.$$

The density spectrum contains a constant of proportionality, and it is preferable, therefore, to express all rates above as a fraction of the rate of all core-selected showers

$$\mathscr{R}_i \propto \int_0^\infty S_i^c(x)\, dx.$$

If the ratios $\rho_{i,k} = \mathscr{R}_{i,k}/\mathscr{R}_i$,
then

$$\rho_{i,k_N} = \rho_{i,k} - \rho_{i,k_\mu}.$$

All the integrals were evaluated for a series of values of k. The ratios $\rho_{i,k}$ and ρ_{i,k_μ} were fitted to the observed ratios of the total penetrating and of the muon component respectively, as was also their difference to that of the multiple component. The best fit in each case yielded the values of k, k_μ, and k_N with their standard variations.

§ 3. Results

About 3000 showers were observed. Table 1 gives the rate of showers in which a penetrating particle was recorded at various distances from the core,

Table 1. Observed Penetrating Events as percentage of Showers

Density group	Distance of core-detector to penetrating particle detector (m)				
	3	6	10	14	18
(3.3)	$\frac{24}{122} = 19{\cdot}7 \pm 3{\cdot}6$	$\frac{16}{159} = 10{\cdot}1 \pm 2{\cdot}4$	$\frac{12}{118} = 10{\cdot}2 \pm 2{\cdot}8$	$\frac{22}{191} = 11{\cdot}5 \pm 2{\cdot}3$	$\frac{7}{98} = 7{\cdot}1 \pm 2{\cdot}6$
(4.2)	$\frac{37}{154} = 24{\cdot}0 \pm 3{\cdot}4$	$\frac{49}{216} = 22{\cdot}7 \pm 2{\cdot}8$	$\frac{19}{116} = 16{\cdot}4 \pm 3{\cdot}4$	$\frac{41}{295} = 13{\cdot}9 \pm 2{\cdot}0$	$\frac{15}{128} = 11{\cdot}7 \pm 2{\cdot}8$
(5.1)	$\frac{49}{154} = 31{\cdot}8 \pm 3{\cdot}8$	$\frac{59}{196} = 30{\cdot}1 \pm 3{\cdot}3$	$\frac{30}{134} = 22{\cdot}4 \pm 3{\cdot}6$	$\frac{47}{237} = 19{\cdot}8 \pm 2{\cdot}6$	$\frac{12}{94} = 12{\cdot}8 \pm 3{\cdot}4$
(6.0)	$\frac{70}{135} = 51{\cdot}9 \pm 4{\cdot}3$	$\frac{70}{155} = 45{\cdot}1 \pm 4{\cdot}0$	$\frac{28}{68} = 41{\cdot}2 \pm 6{\cdot}0$	$\frac{56}{144} = 38{\cdot}9 \pm 4{\cdot}1$	$\frac{18}{59} = 30{\cdot}5 \pm 6{\cdot}0$

as a percentage of the core-selected showers for each density group. From these observed rates the density of penetrating particles k and k_μ are obtained as outlined in § 2. They are collected in tables 2 and 3. The crude separation of the observed penetrating events into an N- and a muon-component according to the multiple or single discharges caused by them respectively under 20 cm Pb requires certain corrections. μ-events will give rise to more than one discharge

if accompanied by knock-on electrons or if muons arrive in pairs or in even larger numbers simultaneously. The rate of knock-on events was measured and found to be not more than 4% of the rate of single muons, and the rates were corrected accordingly; the multiple muon rate was estimated from an analysis of all events

Table 2. The Density of all Penetrating Particles as percentage k of the Electron Density at the Core-Detector

Density group	Distance of core-detector to penetrating particle detector (m) 3	6	10	14	18
(3.3)	2·03 ± 0·43	0·96 ± 0·25	0·97 ± 0·29	1·10 ± 0·24	0·65 ± 0·25
(4.2)	1·56 ± 0·27	1·46 ± 0·22	1·00 ± 0·24	0·83 ± 0·14	0·68 ± 0·19
(5.1)	1·32 ± 0·20	1·24 ± 0·17	0·86 ± 0·17	0·74 ± 0·12	0·46 ± 0·14
(6.0)	1·29 ± 0·19	1·01 ± 0·15	0·88 ± 0·20	0·80 ± 0·13	0·56 ± 0·15

Table 3. The Densities of all Penetrating Events as percentage k_r of the Electron Density at Distance r from the Core

Density group	Distance of core-detector to penetrating particle detector (m) 3	6	10	14	18
(3.3)	1·90 ± 0·40	1·68 ± 0·44	2·86 ± 0·86	4·66 ± 1·02	3·71 ± 1·43
(4.2)	1·29 ± 0·22	2·40 ± 0·36	2·87 ± 0·69	3·52 ± 0·59	3·98 ± 1·11
(5.1)	1·02 ± 0·15	1·90 ± 0·26	2·31 ± 0·46	2·93 ± 0·47	2·50 ± 0·76
(6.0)	0·87 ± 0·13	1·35 ± 0·20	2·05 ± 0·47	2·75 ± 0·45	2·65 ± 0·71

and was found to be insignificant. The problem of the N-component is more complicated: nucleons of low energy on interaction will normally give no charged secondaries of range sufficient to reach the lower counter tray; very energetic nucleons on the other hand will be expected to give rise to multiple counts. The identification of multiple events with the interaction of nucleons may in a first approximation, therefore, be regarded as defining a lower energy limit of the nucleons under investigation. This limit has been estimated by Froehlich

Table 4. Density of the N-Component as percentage k_N of the Electron Density at the Core

Density group	Distance of core-detector to penetrating particle detector (m) 3	6	10	14	18
(3.3)	1·25 ± 0·38	0·39 ± 0·16	0·32 ± 0·18	0·34 ± 0·12	0·06 ± 0·06
(4.2)	0·57 ± 0·17	0·37 ± 0·10	0·52 ± 0·18	0·20 ± 0·06	0·10 ± 0·07
(5.1)	0·74 ± 0·16	0·61 ± 0·11	0·41 ± 0·12	0·20 ± 0·05	0·15 ± 0·08
(6.0)	0·52 ± 0·09	0·28 ± 0·04	0·46 ± 0·14	0·20 ± 0·10†	0·10 ± 0·04

† Obtained by interpolation.

Table 5. Density of the N-Component as percentage $k_{r,N}$ of the Electron Density r metres from the Core

Density group	Distance of core-detector to penetrating particle detector (m) 3	6	10	14	18
(3.3)	1·17 ± 0·36	0·68 ± 0·28	0·94 ± 0·53	1·44 ± 0·51	0·34 ± 0·34
(4.2)	0·47 ± 0·14	0·61 ± 0·16	1·49 ± 0·52	0·85 ± 0·25	0·58 ± 0·41
(5.1)	0·57 ± 0·12	0·94 ± 0·17	1·10 ± 0·32	0·79 ± 0·20	0·82 ± 0·43
(6.0)	0·35 ± 0·06	0·37 ± 0·05	1·07 ± 0·32	0·68 ± 0·34	0·47 ± 0·19

Table 6. Density of the μ-Component as percentage k_μ of the Electron Density at the Core

Density group	Distance of core-detector to penetrating particle detector (m)				
	3	6	10	14	18
(3.3)	$0{\cdot}87 \pm 0{\cdot}29$	$0{\cdot}59 \pm 0{\cdot}20$	$0{\cdot}68 \pm 0{\cdot}25$	$0{\cdot}80 \pm 0{\cdot}23$	$0{\cdot}60 \pm 0{\cdot}26$
(4.2)	$1{\cdot}00 \pm 0{\cdot}24$	$1{\cdot}10 \pm 0{\cdot}23$	$0{\cdot}52 \pm 0{\cdot}17$	$0{\cdot}67 \pm 0{\cdot}14$	$0{\cdot}61 \pm 0{\cdot}20$
(5.1)	$0{\cdot}61 \pm 0{\cdot}16$	$0{\cdot}64 \pm 0{\cdot}15$	$0{\cdot}45 \pm 0{\cdot}14$	$0{\cdot}55 \pm 0{\cdot}11$	$0{\cdot}32 \pm 0{\cdot}13$
(6.0)	$0{\cdot}49 \pm 0{\cdot}18$	$0{\cdot}57 \pm 0{\cdot}20$	$0{\cdot}29 \pm 0{\cdot}14$	$0{\cdot}66 \pm 0{\cdot}23$	$0{\cdot}42 \pm 0{\cdot}23$

Table 7. Density of the μ-Component as percentage $k_{r,\mu}$ of the Electron Density r metres from the Core

Density group	Distance of core-detector to penetrating particle detector (m)				
	3	6	10	14	18
(3.3)	$0{\cdot}81 \pm 0{\cdot}27$	$1{\cdot}03 \pm 0{\cdot}35$	$2{\cdot}01 \pm 0{\cdot}74$	$3{\cdot}39 \pm 0{\cdot}97$	$3{\cdot}43 \pm 1{\cdot}49$
(4.2)	$0{\cdot}83 \pm 0{\cdot}20$	$1{\cdot}81 \pm 0{\cdot}38$	$1{\cdot}49 \pm 0{\cdot}49$	$2{\cdot}84 \pm 0{\cdot}59$	$3{\cdot}57 \pm 1{\cdot}17$
(5.1)	$0{\cdot}47 \pm 0{\cdot}12$	$0{\cdot}98 \pm 0{\cdot}23$	$1{\cdot}23 \pm 0{\cdot}38$	$2{\cdot}17 \pm 0{\cdot}43$	$1{\cdot}74 \pm 0{\cdot}71$
(6.0)	$0{\cdot}33 \pm 0{\cdot}12$	$0{\cdot}76 \pm 0{\cdot}27$	$0{\cdot}68 \pm 0{\cdot}32$	$2{\cdot}27 \pm 0{\cdot}79$	$1{\cdot}99 \pm 1{\cdot}09$

et al. (1952) (cf. also Camerini *et al.* 1951) as 2 Gev. Further, all energetic nucleons will not interact. Assuming an interaction length of 160 g cm^{-2}, only about 76% will do so; of the remainder about half will be neutrons and completely undetected, the other half will be mistakenly identified as muons. The muon rate has been corrected for this effect. From the corrected rates, the values of k were computed for the two components. They are given in tables 4–7 with their standard errors.

§ 4. Discussion of Results

The results shed light, in the main, on two aspects of shower structure: firstly on the ratios of the various components of a shower of given size, and secondly on the variation of the composition of showers with shower size. Our values refer to distances of 3–18 m from the shower core, and it must not be assumed that they may be extrapolated towards the immediate core region which must be examined by a different kind of experiment.

4.1. *The N-Component*

The relationship of the N-component to the electron component is shown in table 5. The weighted average value of $k_{r,N}$ is $(0{\cdot}56 \pm 0{\cdot}10)\%$, and the whole set of results in this table is consistent with this value, that is to say with the conclusion that the density of N-particles is proportional to that of the electrons both for the lateral range 3–18 m and over the size range 4×10^4–5×10^5 electrons.

While the values of $k_{r,N}$ in table 5 are consistent with a constant value which is independent of shower size, they give some indication that $k_{r,N}$ diminishes with increasing shower size. In this sense they are in agreement with the result of other workers, namely Kasnitz and Sitte (1954), Marsden and Doran (1956), Nikol'skii *et al.* (1956), and Lehane *et al.* (1958). Table 8 shows the weighted averages of $k_{r,N}$ over all distances in each of the four size groups of table 5. The values of β given by Marsden and Doran, corresponding to our $k_{r,N}$, are shown for comparison. The fact that the absolute values of the β are larger than the $k_{r,N}$ suggests that this work includes N-particles of lower energy. a conclusion

Table 8

Size group (particles)	Marsden and Doran $\beta(\%)$	Present work $k_{r,\,N}$ (%)	Nikol'skii $k_{r,\,N}$ (%)
4×10^4	$2{\cdot}3\pm0{\cdot}3$	$0{\cdot}81\pm0{\cdot}18$	0·95
8×10^4	$2{\cdot}2\pm0{\cdot}3$	$0{\cdot}61\pm0{\cdot}10$	0·50
2×10^5	$1{\cdot}7\pm0{\cdot}3$	$0{\cdot}74\pm0{\cdot}09$	0·25
5×10^5	$0{\cdot}9\pm0{\cdot}3$	$0{\cdot}38\pm0{\cdot}07$	0·20

quite in keeping with the respective modes of detection. It is interesting to note that the variation with size of the two quantities is similar. Table 8 also contains the values of $k_{r,\,N}$ which have been obtained from the graphs of Nikol'skii *et al.* The variation of our values of $k_{r,\,N}$ over the size range considered and that of the quantity β used by Marsden and Doran agrees with the assumption of Lehane *et al.* that the number of nuclear particles in this range is proportional to $\mathcal{N}^{0{\cdot}6}$ where $\mathcal{N}$ is the number of electrons; the values given by Kasnitz and Sitte are not directly comparable, since their size groups are defined differently. Nikol'skii *et al.* reach a conclusion which is not easily reconciled with the present work nor with that of Marsden and Doran and of Lehane *et al.*, unless a totally different situation exists at the high altitude (3860 m) at which their experiments were carried out. They find that for $\mathcal{N}<10^5$, $k_{r,\,N}\propto\mathcal{N}^{-0{\cdot}8}$ while for $\mathcal{N}>10^5$ $k_{r,\,N}$ is constant, yielding a general form of variation quite different from that reported here. In view of these differences in the results it is premature to attempt an explanation of the discontinuity at $\mathcal{N}=10^5$ reported by Nikol'skii *et al.*

Regarding the lateral distribution, when the data of table 5 are examined together with the results of other workers there is some indication that the ratio of nuclear particles to electrons decreases slightly with increasing distance from the core. Nikol'skii *et al.* assign an index 1·4 to the variation of the nuclear component with core distance, and so, effectively, an index 0·65 to the lateral variation of $k_{r,\,N}$, since the decrease of the electronic component (cf. II) is best represented by an index 0·75. The values of β tabulated by Marsden and Doran fit best with the assumption that there is a small decrease with increasing radial distance from the shower core.

4.2. *The Muon-Component*

The muon-component (tables 6 and 7) is described by values of $k_{r,\mu}$, which increase with distance from the shower core and which decrease with increasing shower size. These effects are, to the accuracy of the present work, separable. The lateral density distribution (table 6) may be represented for all shower sizes used in our experiment by a power law $r^{-(0{\cdot}3\pm0{\cdot}1)}$, and this value can be compared with the results of other workers for showers of similar size and at comparable distances from the core. Thus Vavilov *et al.* (1957) find a power law $r^{-0{\cdot}58}$, and for a larger average distance from the core Fujioka (1955) finds $r^{-0{\cdot}7}$.

Tables 6 and 7 show, in addition, a general decrease of $k_{r,\,\mu}$ with shower size. Since our results do not go beyond a distance of 18 metres from the shower core they cannot give a proportion of muons in the whole shower. A decrease has, however, been found by Vavilov *et al.* and Lehane *et al.* This generally observed decrease of the proportion of muons with increasing shower size probably reflects

the different absorption properties of the muon-component and of the cascade component of showers rather than any difference in the formation process.

The ratio N/μ is given by corresponding values from tables 4 and 6. There is no significant difference between the four size groups and, plotting the average of N/μ over all sizes against lateral distance from the shower core (see figure)

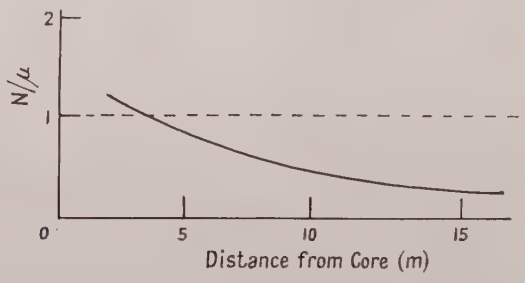

The ratio N/μ averaged over all sizes as a function of distance from the core.

equality of the two penetrating components occurs between three and four metres from the core. A similar value (~ 5 m) was obtained by Lehane *et al.*, but no great significance is to be attached to this figure since comparison with the results of Marsden and Doran suggests that the percentage of detectable nucleons is sensitive to the method of detection.

Acknowledgments

The authors wish to express their thanks to Professor E. C. Stoner for the facilities provided, and to Professor J. G. Wilson for valuable discussions of the manuscript. N. D. wishes to acknowledge a maintenance grant from the Department of Scientific and Industrial Research.

References

Camerini, U., Davies, J. H., Franzenetti, C., Lock, W. O., Perkins, D. H., and Yekutieli, G., 1951, *Phil. Mag.*, **42**, 1261.

Froehlich, F. E., Harth, E. M., and Sitte, K., 1952, *Phys. Rev.*, **87**, 504.

Fujioka, G., 1955, *J. Phys. Soc., Japan*, **10**, 245.

International Convention (1957) on Cosmic Rays, Varenna, 1958, *Nuov. Cim., Suppl.* 2, **8**, Ser. 10, part 4.

Kasnitz, H. L., and Sitte, K., 1954, *Phys. Rev.*, **94**, 977.

Kellermann, E. W., *Report of the Fifth International Congress* (1955) *on Cosmic Radiation, Guanajuato*, 1958, Instituto Nacional De Investigacion Cientifica, pp. 179–181.

Kellermann, E. W., Shaw, T., and Dickinson, N., 1957, *Proc. Phys. Soc.* A, **70**, 452.

Kellermann, E. W., Shaw, T., and Walker, G. O., 1958, *Proc. Phys. Soc.*, **71**, 491.

Lehane, J. A., Millar, D. D., and Rathgeber, M. H., 1958, *Nature, Lond.*, **182**, 1699.

Marsden, P. L., and Doran, G. A., 1956, *Proc. Phys. Soc.* A, **69**, 894.

Nikol'skii, S. N., Vavilov, Y. N., and Batov, V. V., 1956, *Doklady Akad. Nauk S.S.S.R.*, **111**, 71. (English translation, 1957, *Soviet Physics, Doklady*, **1**, 625.)

Vavilov, Y. N., Evstigneev, Y. F., and Nikol'skii, S. I., 1957, *J. Exp. Theor. Phys. (U.S.S.R.)* **32**, 1319. (English translation, 1957, *Soviet Physics, JETP*, **5**, 1078.)

The Coupling of a Spin System to a Cavity Mode

By K. W. H. STEVENS and B. JOSEPHSON, Jr.†
Department of Physics, University of Nottingham

MS. received 23rd *April* 1959, *in final form* 26*th May* 1959

Abstract. The problem of a non-interacting spin system coupled to a damped resonant cavity is formulated wave-mechanically. An exact solution of the Schrödinger equation is found for this system, and the expectation value M_z of the z component of total spin angular momentum S_z is determined in series form from an expansion of the solution. The expectation value is obtained exactly and in closed form only for very small values of the total spin quantum number S. Approximate solutions in closed form are obtained for the initial conditions $M \simeq S$ and $M \simeq -S$. For the former condition, $\langle t|S_z|t\rangle$ exhibits exponential decay for small values of t. The approximations break down for larger values of t, but damped oscillatory behaviour is suggested. The results are discussed in terms of the total number of spins, and a value of at least 10^{18} spins seems necessary for an appreciable exponential change in $\langle t|S_z|t\rangle$ to occur, under typical experimental conditions. Reasons are given why a simple, closed form for $\langle t|S_z|t\rangle$ seems unlikely for the general case of arbitrary S, and some mathematical difficulties are considered in more detail.

§ 1. Introduction

Recent developments in maser technology have brought into prominence a problem in magnetic resonance which has always existed but which has not previously attracted much attention. It is the problem of describing and understanding in detail how a spin system is coupled to a cavity mode. When the coupling is weak, as is usually the case in paramagnetic resonance, a simple discussion can be given. It is only now that much tighter coupling is being used that the necessity arises for a more comprehensive theory.

In setting up any formalism it is necessary to describe the spin system, the cavity mode and the coupling between them. The spin system is most conveniently described wave-mechanically while the cavity mode, which is necessarily damped by the wall losses, is most conveniently described classically. This is an unfortunate mixture and to make progress it seems desirable either to describe both spin system and cavity mode classically or to describe both wave-mechanically. In certain cases, particularly where the Bloch equations can be used, it is possible to describe both systems classically as was done by Bloembergen and Pound (1954) and Bloom (1957). Where the spin system cannot be described classically, as is often the case in masers, the only alternative is to describe the cavity mode wave-mechanically. Whether one chooses to work classically or wave-mechanically some errors are likely to occur (for example, the Bloch equations do not fully describe ferromagnetic resonance), but in the most favourable cases these will be small. In the wave-mechanical treatment of the cavity a first possibility is to try to describe the motions of the electrons in the

† Now at the Rice Institute, Houston, Texas.

cavity walls, taking wall losses into account by considering the coupling of the electrons to the radiation fields in the cavity and to the lattice. This is an extremely complex problem and something simpler is required.

The approximation we use is based on the intuitive belief that, for maser problems, the properties of a cavity mode are adequately described by its field configurations, frequency and Q factor. For example, we do not believe that it matters what the cavity is made from provided that its electrical properties are known. Detailed considerations involving the number of free electrons in the walls and their collision times should be adequately summarized by the bulk properties of the material of the cavity wall, since in microwave masers there is no interest in fluctuations at frequencies comparable with electron collision frequencies. Our theory will need extension, however, if appreciable microwave noise arises from the mixing of these high-frequency fluctuations.

This type of approximation has been considered in detail by one of us (Stevens 1958, hereafter referred to as I) where it was shown that it is possible to quantize a damped harmonic oscillator, using a damped tuned circuit as a model. Our present discussion will use similar arguments for a cavity mode. In addition we shall consider the coupling of such a cavity mode to a spin system and examine the possibility of solving the Schrödinger equation for the coupled system.

In this paper we wish to keep our examples as simple as possible consistent with exhibiting clearly the essential features of our method. For this reason we shall not aim at maximum generality but will, in fact, take advantage of whatever simplifications present themselves. More complicated problems are left for later consideration. By treating a few examples from what is certainly a large class of problems, we hope to demonstrate the value of our technique.

§ 2. Description of the Cavity Mode

Our first problem is to set up the classical Hamiltonian for a damped cavity mode. This can then be quantized as in I. If the cavity damping is due to wall losses a complication arises when Maxwell's equations are applied to describe the fields because there are two distinct regions, inside the cavity and in the walls, in which the equations must be solved. There are also problems connected with matching the solutions on the boundaries. It is within the spirit of our approximation to consider instead a cavity which has perfectly reflecting walls but which is filled with a dielectric of finite conductivity σ. The properties of this new cavity are chosen to give the same resonance frequency and Q as the cavity we are actually interested in. The handling of Maxwell's equations is greatly simplified by this procedure.

Introducing the vector potential $\mathbf{A} = A_1(t) . f(x, y, z)$ and the scalar potential $\phi(t, x, y, z)$ into Maxwell's equations, we can choose a gauge which makes ϕ zero. We have, then,

$$\mathbf{E} = -\frac{\mu}{c}\frac{\partial \mathbf{A}}{\partial t}, \quad \mathbf{H} = \text{curl } \mathbf{A}, \qquad \ldots\ldots (1)$$

where $\mathbf{A}$ satisfies the wave equation

$$\nabla^2 \mathbf{A} - \frac{4\pi\sigma\mu}{c^2}\frac{\partial \mathbf{A}}{\partial t} - \frac{\mu\epsilon}{c^2}\frac{\partial^2 \mathbf{A}}{\partial t^2} = 0. \qquad \ldots\ldots (2)$$

μ and ϵ are the magnetic and electric permeabilities and c is the velocity of light.

It is possible to take **A** in many different ways, according to the problem being tudied. We find it convenient to set

$$\mathbf{A} = A_1(\mathbf{i}k_2 \cos k_1 x \sin k_2 y - \mathbf{j}k_1 \sin k_1 x \cos k_2 y) \sin k_3 z,$$

where **i** and **j** are unit vectors in the x and y directions and A_1 is a function of ime only. Then

$$\mathbf{E} = -\frac{\mu}{c}\frac{dA_1}{dt}(\mathbf{i}k_2 \cos k_1 x \sin k_2 y - \mathbf{j}k_1 \sin k_1 x \cos k_2 y) \sin k_3 z,$$

o that the tangential components of **E** vanish on the planes $x=0, \pi/k_1, 2\pi/k_1 \ldots$; $=0, \pi/k_2, 2\pi/k_2 \ldots$; and $z=0, \pi/k_3, 2\pi/k_3 \ldots$ Thus we shall be considering a node which can exist in any cavity formed by a selection of these planes. Equation (2) then leads to

$$(k_1^2+k_2^2+k_3^2)A_1 + \frac{4\pi\sigma\mu}{c^2}\frac{dA_1}{dt} + \frac{\mu\epsilon}{c^2}\frac{d^2A_1}{dt^2} = 0, \qquad \ldots\ldots (3)$$

which shows that A_1, the time dependent part of the vector potential for this node, satisfies the differential equation of a damped harmonic oscillator.

The problem of quantizing a similar classical equation (for the charge in a esonant circuit) was investigated in I. In order to follow the same formalism t is convenient to make the present notation the same as that used in I. Equation 3) can be multiplied through by a factor α, so that $\alpha(\mu\epsilon/c^2)$ has the dimensions of nductance (α has the dimension of cm^{-1}). Then L, C and R are defined by

$$L = \alpha\left(\frac{\mu\epsilon}{c^2}\right), \quad R = \alpha\left(\frac{4\pi\sigma\mu}{c^2}\right), \quad \frac{1}{C} = \alpha(k_1^2+k_2^2+k_3^2).$$

Setting $A_1 = Q$, equation (3) becomes

$$L\frac{d^2Q}{dt^2} + R\frac{dQ}{dt} + \frac{Q}{C} = 0. \qquad \ldots\ldots (4)$$

From I, the Hamiltonian for this differential equation is

$$\mathscr{H}_c = e^{-Rt/L}\frac{P^2}{2AL} + e^{Rt/L}\frac{AQ^2}{2C} \qquad \ldots\ldots (5)$$

where P is conjugate to Q. It is of some importance to investigate the constant A which appears in $\mathscr{H}_c$; we consider first the undamped case, $R=0$. The Hamiltonian is then just the total energy in the mode, which can be written lternatively as

$$\frac{1}{8\pi}\int(\epsilon\mathbf{E}.\mathbf{E} + \mu\mathbf{H}.\mathbf{H})dV.$$

This integral is readily evaluated, and when compared with (5), leads to

$$A = \mu V(k_1^2+k_2^2)/32\pi\alpha,$$

where V is the volume of the resonator. (In I, A was determined after quantiation. It seems preferable here to use this alternative derivation.) When the avity is damped (i.e. $R \neq 0$) the following argument seems valid. Suppose we easure from time t_0 onwards, If we assume that the damping is switched on at , there seems no reason to suppose that the instantaneous Hamiltonian of quation (5) will be affected. Therefore we take

$$A = \frac{\mu V(k_1^2+k_2^2)}{32\pi\alpha}\exp\left(-\frac{Rt_0}{L}\right).$$

The Hamiltonian for the cavity mode can now be quantized, as in I, by interpreting P and Q as operators which satisfy $QP-PQ=i\hbar$.

§ 3. The Spin System

We suppose that the cavity contains an assembly of spins which are also in an external magnetic field H_0. If they are non-interacting (we also neglect spin-lattice coupling) and have identical g-values the contribution to the total energy is $\mathscr{H}_m=\mu g\beta\mathbf{H}_0\,.\,\mathbf{S}$, where $\mathbf{S}=\Sigma_i\mathbf{s}_i$. There is also an additional energy from their interaction with the radiation field in the cavity. From general considerations (Dirac 1947) we expect this to be

$$\sum_i \mu g\beta(\mathbf{s}_i\,.\,\mathrm{curl}\,\mathbf{A}).$$

Assuming that the spins are so close to one another that the vector potential is constant over the spin system, the interaction energy is

$$\mathscr{H}_i=\mu g\beta Q\left[\begin{array}{c} S_x k_1k_3\sin k_1x\cos k_2y\cos k_3z+S_yk_2k_3\cos k_1x\sin k_2y\cos k_3z \\ -S_z(k_1^2+k_2^2)\cos k_1x\cos k_2y\sin k_3z. \end{array}\right]$$

The Hamiltonian for the system of independent spins in the excited cavity is then the sum of $\mathscr{H}_c$, $\mathscr{H}_m$ and $\mathscr{H}_i$.

§ 4. Solution of the Schrödinger Equation

The problem which now confronts us is that of finding solutions of the Schrödinger equation

$$i\hbar\frac{d}{dt}\,|t\rangle=(\mathscr{H}_c+\mathscr{H}_m+\mathscr{H}_i)|t\rangle=\mathscr{H}|t\rangle$$

and in particular finding how a state $|t_0\rangle$, determined at time t_0, develops with time.

With no loss in generality, some simplification is possible if we assume that the spins are placed in the cavity in a region where the d.c. magnetic field and the oscillating field are mutually perpendicular. For example, if we take H_0 along the z axis the spin system can be placed at a point where $\cos k_2y=\cos k_3z=1$. For this case, the Hamiltonian becomes:

$$\mathscr{H}=\hbar\omega_0S_z+\left(e^{-Rt/L}\frac{P^2}{2AL}+e^{Rt/L}\frac{AQ^2}{2C}\right)+\mu ag\beta QS_x$$

where $a=k_1k_3\sin k_1x$,
and $\hbar\omega_0=\mu g\beta H_0$.

We now set $|t\rangle=\exp\{-i\omega_0S_z(t-t_0)\}|T_1,t\rangle$. Then the transformed ket $|T_1,t\rangle$ satisfies a Schrödinger-type equation

$$i\hbar\frac{d}{dt}\,|T_1,t\rangle=\mathscr{H}_1|T_1,t\rangle$$

with
$$\begin{aligned}\mathscr{H}_1&=\exp\left[i\omega_0S_z(t-t_0)\right]\mathscr{H}\exp\left[-i\omega_0S_z(t-t_0)\right]-\hbar\omega_0S_z\\&=\mathscr{H}_c+\tfrac{1}{2}\mu ag\beta Q\{\exp\left[i\omega_0S_z(t-t_0)\right](S_++S_-)\exp\left[-i\omega_0S_z(t-t_0)\right]\}\end{aligned}$$

where we have written $S_x=\frac{1}{2}(S_++S_-)$ and where $S_\pm=S_x\pm iS_y$. Now $S_\pm S_z=(S_z\mp1)S_\pm$, $S_\pm S_z^2=(S_z\mp1)^2S_\pm$ and therefore

$$\begin{aligned}&S_\pm\exp\left[-i\omega_0S_z(t-t_0)\right]=\exp\left[-i\omega_0(S_z\mp1)(t-t_0)\right]S_\pm\\&\exp\left[i\omega_0S_z(t-t_0)\right]S_\pm\exp\left[-i\omega_0S_z(t-t_0)\right]=\exp\left[\pm i\omega_0(t-t_0)\right]S_\pm.\end{aligned}$$

Thus

$$\mathscr{H}_1 = \left[e^{-Rt/L} \frac{P^2}{2AL} + e^{Rt/L} \frac{AQ^2}{2C} \right] + \frac{\mu a g \beta Q}{2} \{ \exp [i\omega_0(t-t_0)] S_+ + \exp [-i\omega_0(t-t_0)] S_- \}$$

which shows that the Zeeman energy can be eliminated at the expense of complicating the interaction terms.

The terms which describe the cavity mode have been treated in I, where transformations which eliminate these terms are developed. The reader is referred there for a complete account, but we list the results here for completeness. Using the following definitions:

$$2P = (2AL\hbar\omega\, e^{Rt_0/L})^{1/2}(Q_+ + Q_-)$$

$$i2Q = \left(\frac{2C}{A}\hbar\omega\, e^{-Rt_0/L}\right)^{1/2}(Q_+ - Q_-)$$

$$Q_- = i\cosh\theta\, q_+ - \sinh\theta\, q_-$$

$$Q_- = \sinh\theta\, q_+ - i\cosh\theta\, q_-$$

$$\omega = (LC)^{-1/2}$$

$$\tanh 2\theta = -R/2\omega L$$

$$\cosh 2\theta = \omega/\Omega$$

$$\Omega = \left(\frac{1}{LC} - \frac{R^2}{4L^2}\right)^{1/2}$$

where $[Q_-, Q_-] = [q_-, q_-] = 1$ so that q_- and Q_- are creation operators and q_- and Q_- are annihilation operators, the following transformation will eliminate $\mathscr{H}_c$:

$$|T_1, t\rangle = \exp(iS) \exp\{-\tfrac{1}{2}i\Omega(q_+q_- + q_-q_+)(t-t_0)\} |T_2, t\rangle$$

where

$$S = \frac{R(t-t_0)}{4\hbar L}(PQ + QP) = -\frac{R(t-t_0)}{4\hbar L}\left[\frac{R}{2\Omega L}(q_-q_- + q_-q_+) - \frac{i\omega}{\Omega}(q_+^2 - q_-^2)\right].$$

Then $|T_2, t\rangle$ satisfies another Schrödinger-type equation:

$$i\hbar \frac{d}{dt}|T_2, t\rangle = \mathscr{H}_2 |T_2, t\rangle$$

where now

$$\mathscr{H}_2 = \frac{\mu a g \beta}{2}(\exp [i\omega_0(t-t_0)] S_+ + \exp [-i\omega_0(t-t_0)] S_-) \cdot \left(\frac{C}{2A}\hbar\omega\right)^{1/2} \times \exp(-Rt/2L) \{ q_-(\cosh\theta + i\sinh\theta) \exp [i\Omega(t-t_0)] + q_-(\cosh\theta - i\sinh\theta) \times \exp [-i\Omega(t-t_0)] \}.$$

We have found it convenient to introduce a new variable

$$x = \exp [-R(t-t_0)/2L]$$

and new creation and annihilation operators

$$p_\pm = \exp(\pm i\phi) q_\pm$$

where $\exp(-i\phi).(\cosh\theta+i\sinh\theta)=(\cosh 2\theta)^{1/2}$. We also write $\frac{\omega L}{R}=Q_0$, the Q-factor of the cavity mode. Thus

$$i\hbar\frac{d}{dx}|T_2,t\rangle=K(x^{-2iQ_0\omega_0/\omega}S_+ + x^{2iQ_0\omega_0/\omega}S_-).(x^{-2iQ_0\Omega/\omega}p_+ + x^{2iQ_0\Omega/\omega}p_-)|T_2,t\rangle$$

where

$$K=-4ag\beta Q_0\left[\frac{\pi\mu\hbar}{(k_1^2+k_2^2+k_3^2)(k_1^2+k_2^2)V\Omega}\right]^{1/2}.$$

This equation can now be integrated to determine how $|T_2,t\rangle$, and hence $|t\rangle$, develops with time. The result is very complicated and it seems of more value to make certain restrictions and approximations. Therefore, we assume that the external d.c. magnetic field is adjusted so that $\omega_0=\Omega$ i.e. the spins and the cavity are resonant to the same frequency. Terms in $x^{\pm 2iQ_0\Omega/\omega}$ can be neglected. Then

$$i\hbar\frac{d}{dx}|T_2,t\rangle=K(S_+p_-+S_-p_+)|T_2,t\rangle$$

which has the solution

$$|T_2,t\rangle=\exp\left[\frac{-iK}{\hbar}(S_+p_-+S_-p_+)(x-1)\right]|t_0\rangle$$

where $|t_0\rangle$ is just the initial state of the system. The complete wave function, showing how the initial state develops in time, is

$$|t\rangle=\exp\{-i\omega_0S_z(t-t_0)\}\exp(iS)\exp\left\{-\frac{i\Omega}{2}(q_+q_-+q_-q_+)(t-t_0)\right\}$$
$$\times\exp\left\{-\frac{iK}{\hbar}(S_+p_-+S_-p_+)(x-1)\right\}|t_0\rangle.$$

For convenience, we write

$$|t\rangle=\Phi(t-t_0)\,|t_0\rangle. \qquad \ldots\ldots(6)$$

§ 5. Physical Properties of $\langle S_z\rangle$. The Case of $S=\frac{1}{2}$

To obtain results of physical significance it is necessary to study the variation with time of the expectation value of certain operators. Although we have investigated a number of these, we will confine our attention to S_z in this paper. This operator is of considerable importance and gives a good example of the general problem.

The expectation value of S_z at any time t is given by $\langle t|S_z|t\rangle$. Using equation (6), $|t\rangle$ can be written in terms of $|t_0\rangle$, which is independent of time. Only the last transformation does not commute with S_z, and we are left with the problem of evaluating

$$\langle t|S_z|t\rangle=\langle t_0|e^{-iX}S_z\,e^{iX}|t_0\rangle$$

where

$$X=-\frac{K}{\hbar}(S_+p_-+S_-p_+)(x-1).$$

Clearly, S_z and X commute with $S_x^2+S_y^2+S_z^2$, so that the total spin S is a good quantum number. Therefore, if $|t_0\rangle$ is expanded in states of definite total spin,

$$|t_0\rangle=\sum a_r|S=r,\,t_0\rangle$$

we obtain

$$\langle t_0|e^{-iX}S_z\,e^{iX}|t_0\rangle=\sum_r|a_r|^2\langle S=r,\,t_0|\,e^{-iX}S_z\,e^{iX}|S=r,\,t_0\rangle$$

and it is enough to study the properties of $\langle t_0|\,e^{-iX}S_z e^{iX}|t_0\rangle$ where $|t_0\rangle$ is now a state of definite total spin.

We should say at the outset that we have not been able to find a closed, simple form for $e^{-iX}S_z e^{iX}$. Exact expressions for $\langle t|S_z|t\rangle$ can be found for small values of S, but for the general case (arbitrary S) we have had to use approximations. As we shall show, there is good reason to suppose that no striking simplification is possible.

We begin by treating the simplest case, where $|t_0\rangle$ is taken to be an eigenstate of S^2 with $S=\frac{1}{2}$ and $M=\frac{1}{2}$. (The eigenvalues of S_z will be denoted by M.) It is simultaneously an eigenstate of $(p_+p_-+p_-p_+)$ with eigenvalue $2n+1$. Thus $|t_0\rangle=|n,+\rangle$, where the plus sign indicates the state $M=+\frac{1}{2}$.

$$\text{Now}\quad X^2|n,+\rangle=\frac{K^2}{\hbar^2}(x-1)^2p_-p_+S_+S_-|n,+\rangle$$

$$=\frac{K^2}{\hbar^2}(x-1)^2(n+1)|n,+\rangle$$

$$\text{or}\qquad X^2|n,+\rangle=b^2|n,+\rangle,\ \text{where}\ b^2=\frac{K^2}{\hbar^2}(x-1)^2(n+1)$$

$$\text{Hence}\quad e^{iX}|n,+\rangle=\tfrac{1}{2}\{(e^{iX}+e^{-iX})+(e^{iX}-e^{-iX})\}|n,+\rangle$$

$$=\left(\cos b+i\frac{\sin b}{b}X\right)|n,+\rangle$$

$$=\cos b\,|n,+\rangle-i\sin b\,|n+1,-\rangle$$

$$=\cos\left\{\frac{K}{\hbar}(x-1)(n+1)^{1/2}\right\}|n,+\rangle-i\sin\left\{\frac{K}{\hbar}(x-1)(n+1)^{1/2}\right\}|n+1,-\rangle.$$

Similarly, we determine

$$e^{iX}|n,-\rangle=\cos\left\{\frac{K}{\hbar}(x-1)n^{1/2}\right\}|n,-\rangle-i\sin\left\{\frac{K}{\hbar}(x-1)n^{1/2}\right\}|n-1,+\rangle.$$

With these relations it is simple to obtain the time dependence of the expectation value of any operator. In particular,

$$\left.\begin{aligned}&\langle n,+|e^{-iX}S_z e^{iX}|n,+\rangle=\tfrac{1}{2}\cos\left\{\frac{2K}{\hbar}(x-1)(n+1)^{1/2}\right\}\\ \text{and}\qquad&\langle n,-|e^{-iX}S_z e^{iX}|n,-\rangle=-\tfrac{1}{2}\cos\left\{\frac{2K}{\hbar}(x-1)n^{1/2}\right\}.\end{aligned}\right\}\ \ldots\ldots(7)$$

To obtain some physical insight into the meaning of these results we shall consider the simplest way of obtaining $S=\frac{1}{2}$, which is by supposing that the cavity contains just a single spin of $\frac{1}{2}$. The above formulae then show that if the spin is in one orientation at time t_0 there is a chance that subsequently it will be found to have reversed, for the expectation value of S_z in a sinusoidal function of x. It must be remembered, however, that x and t are related by

$$x=\exp\{-R(t-t_0)/2L\},$$

so that as t goes from t_0 to infinity, x goes from 1 to 0. The number of cycles that $\langle S_z\rangle$ goes through as t goes to infinity thus depends on the magnitude of K and n. Suppose that initially the spin has $M=\frac{1}{2}$ and that there is energy in the cavity. The energy is gradually dissipated in wall losses, but while it remains there is always the possibility that the spin will be stimulated to emit, giving its energy to the cavity and moving to the $M=-\frac{1}{2}$ state. After this has occurred there

will still be energy in the cavity and it may happen that the spin will re-absorb some energy and return to $M=\frac{1}{2}$, whereupon the process may repeat itself. Meanwhile the cavity energy is being reduced by wall losses and the probability of the spin making a transition is constantly being reduced. If Q_0 is small the cavity energy is dissipated in the walls before the spin has a chance to make a transition. We shall not deal much further with this example, since one spin in a cavity is a highly academic situation from which no significant, quantitative deductions can be made. Nevertheless, the discussion of this case is of value because of the suggestion that the spin and cavity may exchange energy in a manner analogous to the behaviour of coupled circuits. There is one final point of interest: as t goes to infinity, the formulae of equation (7) do not inevitably lead to $\langle S_z\rangle = -\frac{1}{2}$, a result which might be expected on physical grounds, since this would put the spin ultimately in its lowest state. The reason for this is as follows. In preparing to quantize the cavity mode we were led to equation (4), which is similar to the usual charge equation in lumped circuit theory. However, the corresponding lumped circuit equation is incomplete. The point has been made very clearly to us by Professor M. H. L. Pryce that it is physically unsatisfactory to introduce a damping term into the harmonic oscillator equation without also introducing some means whereby the oscillator can acquire energy from the fluctuations of the dissipative system. To do this classically it is usual to rewrite equation (4) as

$$L\frac{d^2Q}{dt^2}+R\frac{dQ}{dt}+\frac{Q}{C}=V(t)$$

where $V(t)$ represents a noise voltage. In so far as we have omitted a similar term from our mode equation our cavity must be regarded as noise-free. There seems little doubt that if we were to include the noise (which is a problem for future investigation) we would find that $\langle S_z\rangle$ tends to a constant value, determined by the temperature of the cavity, as t becomes infinite. Similar considerations apply to the exclusion of spin relaxation processes from the problem. The conclusion is that the formulae we give are only applicable for times which are less than the spin relaxation time and for cavities which are very cold. It seems likely that these restrictions can be removed by further refining the theory, for it is possible to quantize the mode equation when a noise voltage is included (see I.)

§ 6. Large Values of S

An analysis similar to the above can be given for $S=1$, but the indications are that no method applicable to an arbitrary value of spin can be found (see below). Thus to obtain an exact solution for a large value of spin it seems necessary to evaluate $\langle t_0|\mathrm{e}^{-iX}S_z\mathrm{e}^{iX}|t_0\rangle$ by expansion in powers of iX. This is a straightforward but laborious process, and without giving the full details we shall quote the results for the first few terms. The intial state $|t_0\rangle$ is taken as one which is an eigenstate of S^2, S_z and of $p_-p_+ + p_+p_-$, with eigenvalues $S(S+1)$, M and $2n+1$ respectively. We write

$$\mathrm{e}^{-iX}S_z\mathrm{e}^{iX}=S_z+i\hbar[S_z,iX]+\frac{(i\hbar)^2}{2!}[[S_z,iX],iX]+ \quad \ldots\ldots(8)$$

We use the commutator notation of Dirac, i.e. $(AB-BA)=i\hbar[A,B]$.

With $X=-\frac{K}{\hbar}(x-1)(S_+p_-+S_-p_+)$ we obtain

$$\langle M,n|e^{-iX}S_z e^{iX}|M,n\rangle=\sum\frac{\delta_r}{r!}\left\{\frac{K(x-1)}{\hbar}\right\}^r$$

where $\delta_{2r+1}=0, \quad \delta_0=M$

$$\delta_2=-\{4Mn+2(S+M)(S-M+1)\}$$

$$\delta_4=16\{Mn^2-n[4M^2-M-2S(S+1)]+(S+M)(S-M+1)(1-M)\}$$

$$\delta_6=-16\left[\begin{array}{l}4Mn^3-2n^2(42M^2-3M-16)\\ \quad+2n\{8M^3+26M^2+11M-(S+M)(S-M+1)(52M-32)\}\\ \quad-(S+M)(S-M+1)(34M-8M^2-17)\end{array}\right]$$

Any general features of the variation of $\langle S_z\rangle$ with time are obscured by the complexity of the series, and for this reason we have investigated approximate ways of evaluating

$$\langle M,n|e^{-iX}S_z e^{iX}|M,n\rangle.$$

The case of M approximately equal to S is of considerable interest. To evaluate the commutators of equation (8) for this case, we first introduce the operator U_z, where $S_z=S-U_z$. Then

$$S_+|U_z=1\rangle=[S(S+1)-(S-1)S]^{1/2}|U_z=0\rangle=(2S)^{1/2}|U_z=0\rangle$$

$$S_+|U_z=2\rangle=[S(S+1)-(S-2)(S-1)]^{1/2}|U_z=1\rangle=(4S-2)^{1/2}|U_z=1\rangle$$

$$\vdots \qquad\qquad \vdots \qquad\qquad \vdots$$

$$S_+|U_z=r\rangle=[S(S+1)-(S-r)(S-r+1)]^{1/2}|U_z=r-1\rangle=$$
$$\times[2rS-r(r-1)]^{1/2}|U_z=r-1\rangle$$

so that if $r\ll S$, the matrix elements of S_+ are approximately equal to those of $\sqrt{(2S)}a_-$, where a_- is an annihilation operator. Similarly, $S_-\simeq\sqrt{(2S)}a_+$, a_+ being the corresponding creation operator. Therefore

$$iX=-\frac{iK}{\hbar}(x-1)(S_+p_-+S_-p_+)\simeq-\frac{iK}{\hbar}(x-1)\sqrt{(2S)}(a_-p_-+a_+p_+)$$

and

$$[S_z,iX]=-\frac{K}{\hbar^2}(x-1)(S_+p_--S_-p_+)\simeq-\frac{K}{\hbar^2}(x-1)\sqrt{(2S)}(a_-p_--a_+p_+).$$

We now quickly obtain

$$[[S_z,iX],iX]\simeq\frac{2K^2(x-1)^2}{\hbar^4}.2S.(a_-a_++p_-p_+)$$

$$[[[S_z,iX],iX],iX]\simeq-\frac{4K^2(x-1)^2}{\hbar^4}.2S[S_z,iX]$$

so that each term in the series can be written in terms of

$$[S_z,iX] \text{ and } [[S_z,iX],iX].$$

Substituting into equation (11), we obtain

$$e^{-iX}S_z e^{iX}\simeq S_z+[S_z,iX]\left[(i\hbar)+\frac{(i\hbar)^3}{3!}\left\{\frac{-4K^2(x-1)^2.2S}{\hbar^4}\right\}+\ldots\right]$$

$$+[[S_z,iX],iX]\left[\frac{(i\hbar)^2}{2!}+\frac{(i\hbar)^4}{4!}\left\{\frac{-4K^2(x-1)^2.2S}{\hbar^4}\right\}+\ldots\right].$$

Now

$$\langle M, n|[S_z, iX]|M, n\rangle = 0$$

and

$$\langle M, n|[[S_z, iX], iX]|M, n\rangle = \frac{2K^2(x-1)^2}{\hbar^4}\{2Mn + (S+M)(S-M+1)\}$$

so that

$$\langle M, n|e^{-iX}S_z e^{iX}|M, n\rangle \simeq M + \left\{\frac{2Mn+(S+M)(S-M+1)}{4S}\right\} \times \left\{1-\cosh\frac{2K(x-1)\sqrt{(2S)}}{\hbar}\right\} \quad \ldots\ldots (9)$$

Comparing an expansion of this expression with the exact expansion (in terms of $\delta_2, \delta_4, \ldots$) it is seen that δ_2 is given correctly. The terms in n^2, n^3 etc in δ_4 and higher terms cannot be obtained, but if $M \simeq S$ and S is large compared with n the higher terms agree. We thus conclude that the above approximation is valid provided that n is small, M is large and approximately equal to S, and $(x-1)$ is small. The final requirement ensures that the behaviour of the series is determined by its first few terms and is equivalent to restricting the time interval to be so small that the value of $\langle S_z\rangle$ does not change by enough to invalidate the approximation $M \simeq S$.

As an aid to examining the behaviour of $\langle S_z\rangle$ in more detail we assume that all the spins are aligned parallel at t_0, so that $M = S$, and insert some numerical values. For $M = S$, equation (9) becomes

$$\langle S, n|e^{-iX}S_z e^{iX}|S, n\rangle \simeq S + \tfrac{1}{2}(n+1)\left[1-\cosh\left\{\frac{2K(x-1)\sqrt{(2S)}}{\hbar}\right\}\right] \quad \ldots\ldots (10)$$

The time dependence is contained in the factor $x-1 = \exp[-\omega(t-t_0)/2Q_0]-1$ which goes from 0 to -1 as $t-t_0$ goes from zero to ∞. It is convenient to continue the discussion in terms of the ratio

$$\zeta \equiv \frac{\langle S_z\rangle_{(t-t_0)\to\infty}}{\langle S_z\rangle_{(t-t_0)=0}} = 1 + \left(\frac{n+1}{2S}\right)\left\{1-\cosh\frac{2K\sqrt{(2S)}}{\hbar}\right\} \quad \ldots\ldots (11)$$

where

$$\frac{2K}{\hbar} = -\frac{8ag\beta Q_0}{\hbar}\left\{\frac{\pi\mu\hbar}{(k_1^2+k_2^2+k_3^2)(k_1^2+k_2^2)V\Omega}\right\}^{1/2}.$$

We take $g=2$, $Q_0 = 5\times 10^3$, $k_1 = k_3 = 1$, $k_2 = 0$, $a = k_1 k_3 \sin k_1 x = 1$, $\mu = 1$, $V = \pi^3$ and $\Omega = \omega = 2\pi . 10^{10}$. Inserting these values into the above expressions we obtain $2K/\hbar \simeq -10^{-8}$ and

$$\zeta = 1 + \left(\frac{n+1}{2S}\right)(1-\cosh 10^{-8}\sqrt{(2S)}).$$

First of all we note that $\omega/2Q_0 \simeq 2\pi . 10^6$, so that the value $\langle S_z\rangle_{(t-t_0)\to\infty}$ is effectively reached after a few microseconds. Since $Q_0 \simeq \sqrt{\omega}$, $\langle S_z\rangle_{(t-t_0)\to\infty}$ will be reached in less time as the frequency is raised.

Secondly, for $2S$ less than 10^{18} ζ is effectively unity, but on increasing $2S$ to 10^{20} it decreases to approximately $-(n+1)10^{23}$ because of the term $\cosh 100$. The approximations break down for such a large change in $\langle S_z\rangle$, but the general implication is clear: for $2S$ less than or equal to 10^{18} the change in $\langle S_z\rangle$ is very small, while $\langle S_z\rangle$ changes very rapidly with time if $2S$ is increased to 10^{20}. Therefore, our formalism predicts a threshold below which the spin system

changes relatively slowly, but above which the energy in the spins is rapidly given up to the cavity.

The physical interpretation of this is as follows. If $2S$ is below 10^{18} and the spin system makes a transition (so that $\langle S_z \rangle$ decreases by unity) the energy thereby given to the mode is so rapidly dissipated by the wall losses that there is very little probability that it will induce the spin system to make another transition. However, if $2S$ is increased to 10^{20}, the coupling between the spin moment and the cavity fields is increased sufficiently to ensure that the energy released on a first transition remains long enough to induce a second transition, which more than replaces the energy lost to the walls. A cascade process results, during which there is a rapid build-up in the cavity energy and a corresponding decrease in $\langle S_z \rangle$. This rapid build-up cannot continue indefinitely, for the spin system contains only a limited amount of energy. In fact, as $\langle S_z \rangle \to -S$, the couple on the spin arising from the cavity fields decreases because, although the cavity magnetic field may still be increasing, the component S_x on which it acts is decreasing more rapidly.

For a single spin of $\frac{1}{2}$, we have seen that $\langle S_z \rangle$ can oscillate between $\pm \frac{1}{2}$. We have also calculated exactly what happens for spin 1 and again find oscillatory behaviour, although if the system starts with $\langle S_z \rangle = 1$ it does not go to $\langle S_z \rangle = -1$, but to a value slightly greater. Making a very considerable extrapolation it seems likely that an exact treatment for an arbitrary value of spin would show an initial exponential decrease in $\langle S_z \rangle$ followed by damped oscillatory behaviour. The oscillations arise because, in a sense, the rapid decrease in $\langle S_z \rangle$ over-shoots. When a situation is reached in which there is more energy in the cavity than in the spin system, the spin system begins to re-absorb energy from the cavity mode. Under such circumstances the energy in the cavity should also show a rapid build-up followed by a damped oscillatory behaviour. The similarity between the behaviour of a spin system coupled to a cavity mode and the behaviour of coupled circuits is striking, and may form a useful analogue.

In our example, we have assumed that *all* the spins in the cavity are aligned antiparallel to the field at t_0, i.e., $N = 2S$, where N is the number of spins in the cavity. The quantity $2S$ occurs inside the hyperbolic cosine in equations (10) and (11), showing that the behaviour of N spins in a cavity is not given by multiplying the result for a single spin of $\frac{1}{2}$ by N. In practice it is unlikely that the spin system will be prepared so that at t_0 it is in such an eigenstate of $\mathbf{S}^2$. It is more likely that $\frac{1}{2}(N+2\sigma)$ spins will be in the state $M = \frac{1}{2}$, and $\frac{1}{2}(N-2\sigma)$ spins will be in the state $M = -\frac{1}{2}$. Such a state will contain a superposition of states with total spin quantum numbers ranging from σ to $\frac{1}{2}N$. Thus the initial state can be written

$$|t_0\rangle = \sum_r^{N/2} a_r |S = r,\ M = \sigma\rangle.$$

Therefore if $|t\rangle = \Phi(t-t_0)|t_0\rangle$ then $|t\rangle = \sum_r^{N/2} a_r \Phi(t-t_0)|S = r,\ M = \sigma\rangle$.

We may now ask what our theory predicts for $\langle S_z \rangle$ in the case where the spin system is not in an eigenstate of $\mathbf{S}^2$ at t_0. We have shown previously that each substate can be considered independently, the behaviour of the system as a whole being a linear superposition of the behaviour of the substates. Each substate will radiate at a different rate depending on its value of total spin r; the

larger the value of r (for a given M) the larger the transverse, precessing component of the magnetic moment and the faster the rate of radiation. Therefore, if we assume that $\langle S_z \rangle$ for each substate goes into damped oscillation after its initial exponential decay, it seems likely that the superposition will soon lose its oscillatory character and will show a fairly steady decay because the component oscillations are unrelated in phase. This argument leads to a picture of $\langle S_z \rangle$ for the system as a monotonically decreasing function whose initial decay is exponential, but whose decay rate decreases with time. On the other hand, if $\frac{1}{2}N-\sigma$ is small, (almost complete reversal) it seems likely that, after the initial exponential decay, $\langle S_z \rangle$ will retain some periodic character for a time. Some evidence which may be relevant comes from the observations of Feher *et al.* (1958) and Chester, Wagner and Castle (1958) who report unexpected modulations of the power output of two-level solid-state masers when oscillating, though it must be borne in mind that there may be other explanations. In this connection, it would be instructive to observe the variation of $\langle S_z \rangle$ directly rather than indirectly by monitoring the cavity energy.

Having seen what happens if one starts with $M \simeq S$ it is of interest to see what is predicted if, initially, $M \simeq -S$, still assuming that n is small. For this it is convenient to define a new operator, $V_z = S + S_z$. Then

$$S_-|V_z=1\rangle = [S(S+1)-S(S-1)]^{1/2}|V_z=0\rangle = (2S)^{1/2}|V_z=0\rangle$$

and

$$\begin{aligned} S_-|V_z=r\rangle &= [S(S+1)-(S-r)(S+1-r)]^{1/2}|V_z=r-1\rangle \\ &= [2rS-r(r-1)]^{1/2}|V_z=r-1\rangle. \end{aligned}$$

Thus, for $r \ll S$, the matrix elements of S_- and S_+ are approximately equal to those of $\sqrt{(2S)}b_-$ and $\sqrt{(2S)}b_+$, where b_- and b_+ are annihilation and creation operators. Making the approximation that $S_\pm = \sqrt{(2S)}b_\pm$, we obtain

$$iX \simeq -\frac{iK(x-1)}{\hbar}\sqrt{(2S)}(b_+p_- + b_-p_+).$$

It is convenient to define other creation and annihilation operators which will make X diagonal:

$$\beta_\pm = \frac{1}{\sqrt{2}}(b_\pm + p_\pm), \quad \gamma_\pm = \frac{1}{\sqrt{2}}(b_\pm - p_\pm).$$

The commutation rules for these operators are

$$[\beta_\pm, \gamma_\pm] = [\beta_\pm, \gamma_\mp] = 0$$
$$[\beta_-, \beta_+] = [\gamma_-, \gamma_+] = 1.$$

Therefore

$$iX \simeq -\frac{iK}{2\hbar}(x-1)\sqrt{(2S)}(\beta_+\beta_- + \beta_-\beta_+ - \gamma_+\gamma_- - \gamma_-\gamma_+)$$

and

$$[S_z, iX] = -\frac{K(x-1)}{\hbar^2}(S_+p_- - S_-p_+) \simeq -\frac{K(x-1)}{\hbar^2}\sqrt{(2S)}(\gamma_+\beta_- - \gamma_-\beta_+).$$

Instead of using the direct expansion of $e^{-iX}S_z e^{iX}$, we proceed as follows. Setting $[S_z, iX] = Y$, we find

$$\begin{aligned} [S_z, (iX)^2] &= Y(iX) + (iX)Y \\ [S_z, (iX)^3] &= Y(iX)^2 + (iX)Y(iX) + (iX)^2Y \\ &\vdots \\ [S_z, e^{iX}] &= \text{coefficient of } \lambda \text{ in the expansion of } e^{iX+\lambda Y}. \end{aligned}$$

Following the method of Karplus and Schwinger (1948), we find

$$[S_z, e^{iX}] = e^{iX}\int_0^1 e^{-i\alpha X} Y e^{i\alpha X} d\alpha.$$

so that

$$e^{-iX} S_z e^{iX} = S_z + i\hbar\int_0^1 e^{-i\alpha X} Y e^{i\alpha X} d\alpha.$$

Writing X and Y in terms of $\beta_\pm$ and $\gamma_\pm$, we find that our approximations lead to

$$Y = -\frac{K}{\hbar^2}(x-1)\sqrt{(2S)}(\gamma_+\beta_- - \gamma_-\beta_+)$$

$$\gamma_+\beta_-(i\alpha X) = (i\alpha X + i4\alpha\rho)\gamma_+\beta_- \quad : \quad \gamma_-\beta_+(i\alpha X) = (i\alpha X - i4\alpha\rho)\gamma_-\beta_+$$
$$\gamma_+\beta_-(i\alpha X)^2 = (i\alpha X + i4\alpha\rho)^2\gamma_+\beta_- \quad : \quad \gamma_-\beta_+(i\alpha X)^2 = (i\alpha X - i4\alpha\rho)^2\gamma_-\beta_+$$
$$\vdots \qquad\qquad\qquad\qquad\qquad \vdots$$
$$\gamma_+\beta_- e^{i\alpha X} = e^{i(\alpha X + i4\alpha\rho)}\gamma_+\beta_- \quad : \quad \gamma_-\beta_+ e^{i\alpha X} = e^{i(\alpha X - i4\alpha\rho)}\gamma_-\beta_+$$

where

$$\rho = -\frac{K}{2\hbar}(x-1)\sqrt{(2S)}.$$

Therefore

$$e^{-i\alpha X} Y e^{i\alpha X} = -\frac{2}{\hbar}\rho\{e^{i4\alpha\rho}\gamma_+\beta_- - e^{-i4\alpha\rho}\gamma_-\beta_+\}$$

so that

$$e^{-iX} S_z e^{iX} = S_z - \tfrac{1}{2}[(e^{i4\rho}-1)\gamma_+\beta_- + (e^{-i4\rho}-1)\gamma_-\beta_+]$$
$$= S_z + i\sin\left\{\frac{K(x-1)\sqrt{(2S)}}{\hbar}\right\}\left[\gamma_+\beta_-\exp\left\{-\frac{iK(x-1)\sqrt{(2S)}}{\hbar}\right\}\right.$$
$$\left. -\gamma_-\beta_+\exp\left\{\frac{iK(x-1)\sqrt{(2S)}}{\hbar}\right\}\right].$$

Now

$$\langle M, n|\gamma_+\beta_-|M, n\rangle \simeq \langle M, n|\tfrac{1}{2}\left\{\frac{S_+}{\sqrt{2}} - p_+\right\}\left\{\frac{S_-}{\sqrt{2}} + p_-\right\}|M, n\rangle$$
$$= \tfrac{1}{2}\{S(S+1) - M(M-1) - n\} \simeq \langle M, n|\gamma_-\beta_+|M, n\rangle.$$

Therefore

$$\langle M, n|e^{-iX} S_z e^{iX}|M, n\rangle = M - \{S(S+1) - M(M-1) - n\}\sin^2\left\{\frac{K(x-1)\sqrt{(2S)}}{\hbar}\right\}$$

and, in particular,

$$\langle -S, n|e^{-iX} S_z e^{iX}|-S, n\rangle = -S + n\sin^2\left\{\frac{K(x-1)\sqrt{(2S)}}{\hbar}\right\}.$$

The satisfactory feature of this result is that the variation of $\langle S_z\rangle$ with $x-1$ is now a sinusoidal function, in contrast with the previous case where it was a hyperbolic cosine. It is reasonable to expect a less violent dependence on $x-1$ for, when M changes from $-S$ to $-S+1$, there is absorption from the cavity, so that although $\langle S_x\rangle$ increases there is less energy available to induce a further transition. There is thus reason to expect that no sort of cascade process can occur.

§ 7. More Detailed Examination of e^{tX}

From the above special cases it is clear that an exact treatment of $e^{iX}|t_0\rangle$ is required, and the considerations now to be presented result from a detailed examination of the problems involved in this.

Consider a state which is an eigenstate of S and S_z, with $M = S$. The cavity is, as usual, described by n. We require $e^{iX}|S, n\rangle$ where

$$iX = -\frac{iK}{\hbar}(x-1)(S_+p_- + S_-p_+)$$

Now

$$(S_+p_- + S_-p_+)|S, n\rangle = (2S)^{1/2}(n+1)^{1/2}|S-1, n+1\rangle$$

$$(S_+p_- + S_-p_+)^2|S, n\rangle = 2S(n+1)|S, n\rangle + (2S \cdot 3S)^{1/2}[(n+1)(n+2)]^{1/2}|S-2, n+2\rangle.$$

Continuing to operate successively with $S_+p_- + S_-p_+$ it is seen that $|S-r, n+r\rangle$ can be expressed in terms of powers of $S_+p_- + S_-p_+$ acting on $|S, n\rangle$. The minimum value which M can have is $-S$, which means that as far as operating on $|S, n\rangle$ is concerned, any function of $S_+p_- + S_-p_+$ can be written as a linear combination of powers of $S_+p_- + S_-p_+$ up to $(S_+p_- + S_-p_+)^{2S}$. In particular there is a relation

$$\{u_0 + u_1(S_+p_- + S_-p_+) + u_2(S_+p_- + S_-p_+)^2 + \ldots + u_{2S+1}(S_+p_- + S_-p_+)^{2S+1}\}|S, n\rangle = 0$$

where $u_0, u_1, u_2, \ldots$ etc. depend on S and n. This relation can be regarded as the characteristic equation for the sub-matrix of $S_+p_- + S_-p_+$ formed from the states $|S, n\rangle$, $|S-1, n+1\rangle, \ldots |-S, n+2S\rangle$. By a well-known theorem for matrices (Ferrar 1941) a unitary transformation exists which diagonalizes this submatrix and the elements which appear on the diagonal are real and are the roots of

$$u_0 + u_1\lambda + u_2\lambda^2 + \ldots + u_{2S+1}\lambda^{2S+1} = 0.$$

Denoting them by $\lambda_1, \lambda_2, \ldots \lambda_{2S+1}$ and the corresponding eigenfunctions by $|\lambda_1\rangle, |\lambda_2\rangle, \ldots |\lambda_{2S+1}\rangle$ it follows that

$$e^{iX}|S-r, n+r\rangle = e^{iX}\sum_{m=1}^{2S+1}|\lambda_m\rangle\langle\lambda_m|S-r, n+r\rangle = \sum_{m=1}^{2S+1}\exp\left\{\frac{-iK(x-1)}{\hbar}\lambda_m\right\}\langle\lambda_m|S-r, n+r\rangle.$$

Then

$$\langle S-r, n+r|e^{-iX}S_z e^{iX}|S-r, n+r\rangle = \sum_{\tau=1}^{2S+1}\sum_{m=1}^{2S+1}\exp\left\{-\frac{iK(x-1)}{\hbar}(\lambda_m-\lambda_\tau)\right\}\langle S-r, n+r|\lambda_\tau\rangle\langle\lambda_\tau|S_z|\lambda_m\rangle\langle\lambda_m|S-r, n+r\rangle.$$

The time dependence of $\langle S_z\rangle$ is thus described by a sum of sinusoidal functions of $(x-1)$, the frequencies of which are determined by the differences $\lambda_m - \lambda_\tau$. This is a rigorous result, but it does not take us as far as we could wish, and it is a problem for future consideration to determine the distribution of the differences. It does, however, suggest that, as we remarked earlier, there is no simple expression for $\langle t|S_z|t\rangle$. The initial exponential variation which occurs when $M \simeq S$ and n is small presumably arises from a particular superposition of oscillatory terms, which further supports the assumption that subsequently an oscillatory behaviour ensues. The periodic type of behaviour which arises when we start with $M = -S$ must be a result of an entirely different superposition.

§ 8. General Remarks and Conclusion

In most of the above reasoning the cavity mode at t_0 has been described by the quantum number n. We have assumed, however, that the resistance is switched on at t_0 with no change in energy. Therefore the energy at t_0 is

$$\langle n|\exp\left(-\frac{Rt_0}{L}\right)\frac{P^2}{2AL} + \exp\left(\frac{Rt_0}{L}\right)\frac{AQ^2}{2C}|n\rangle$$

which can be expressed as

$$\tfrac{1}{2}\hbar\omega\langle n|Q_+Q_- + Q_-Q_+|n\rangle$$
$$= \tfrac{1}{2}\hbar\omega\langle n|\{(q_+q_- + q_-q_+)\cosh 2\theta + i(q_+^2 - q_-^2)\sinh 2\theta\}|n\rangle$$
$$= \tfrac{1}{2}(2n+1)\hbar\omega\cosh 2\theta = \frac{(2n+1)(\hbar\omega)^2}{2\hbar\Omega},$$

since $|n\rangle$ is an eigenstate of $(q_+q_- + q_-q_+)$. It will however be noticed that $|n\rangle$ is not an eigenstate of the energy at t_0. It is, in fact, quite complicated to express the eigenstates of the energy at t_0 in terms of the eigenstates of $q_+q_- + q_-q_+$, and we have found it most convenient to work with the $|n\rangle$'s. As an example, let $|N=0\rangle$ be the eigenstate of $Q_+Q_- + Q_-Q_+$ corresponding to

$$(Q_+Q_- + Q_-Q_+)|N\rangle = (2N+1)|N\rangle \text{ with } N=0.$$

Then
$$|N=0\rangle = \sum_{n=0}^{\infty}|n\rangle\langle n|N=0\rangle.$$

Now $0 = Q_-|N=0\rangle = (\sinh\theta\, q_+ - i\cosh\theta\, q_-)\sum|n\rangle\langle n|N=0\rangle$
so that $0 = \sum|n\rangle\{\langle n-1|N=0\rangle\sinh\theta\,.\,\sqrt{n} - \langle n+1|N=0\rangle i\cosh\theta\,.\,\sqrt{(n+1)}\}$ or

$$\langle n+1|N=0\rangle = -i\tanh\theta\frac{\sqrt{n}}{\sqrt{(n+1)}}\langle n-1|N=0\rangle.$$

It now follows, after some manipulation, that

$$|N=0\rangle = (\cosh\theta)^{-1/2}\exp\{-\tfrac{1}{2}i\tanh\theta\, q_+^2\}|n=0\rangle.$$

It is finally of interest to review the achievements of this quite lengthy analysis. The most important result seems to be that the technique developed in I is of value in considering the interactions between spin systems and cavity modes. It is true that we have used about the simplest possible type of spin system, coupled to only one cavity mode but we have obtained results abouts its behaviour which, as far as we are aware, cannot be obtained by any other method. Furthermore, these results appear to be satisfactory, except possibly for the limitation that we cannot follow the whole development with time of $\langle S_z\rangle$. This however is due to our deficiencies in mathematics, not to a failure in the formalism. A good deal remains to be done, and it is particularly desirable to have a theory which takes into account a driving signal in the cavity. Various difficulties are introduced by this, not because of limitations in our description of the cavity, but because it now becomes necessary to include the relaxation processes to which the spin system may be subject. We hope to examine this problem later.

Acknowledgment

One of us (B. J.) gratefully acknowledges a grant from the United States Government under the Fulbright Act.

References

Bloembergen, N., and Pound, R. V., 1954, *Phys. Rev.*, **95,** 8.
Bloom, S., 1957, *J. Appl. Phys.*, **28,** 800.
Chester, P. F., Wagner, P. E., and Castle, J. G., 1958, *Phys. Rev.*, **110,** 281.
Dirac, P. M., 1947, *Quantum Mechanics* (Oxford: University Press).
Feher, G., Gordon, J. P., Buehler, E., Gere, E. A., and Thurmond, C. D., 1958, *Phys. Rev.*, **109,** 221.
Ferrar, W. L., 1941, *Algebra* (Oxford : University Press).
Karplus, R., and Schwinger, J., 1948, *Phys. Rev.*, **73,** 1020.
Stevens, K. W. H., 1958, *Proc. Phys. Soc.*, **72,** 1027.

The Inverse Skin Effect

By M. G. HAINES
Physics Department, Imperial College, London

Communicated by R. Latham; MS. received 24th April 1959, in final form 3rd June 1959

Abstract. The axial current density in an infinite cylindrical conductor is calculated as a function of radius and time. In the problem studied the total axial current is specified as a function of time. The case of a rigid conductor is studied first, and the analysis is extended to the case of a radially expanding or contracting cylinder such as occurs in a linear pinched plasma. The radial velocity is assumed proportional to the radius, while the outside radius of the conductor is a general but specified function of time.

It is shown that the variation of total current with time can give rise to distributions of current density which bear no resemblance to the normal skin effect. In fact, an inverse skin effect or even reversal of current may occur. This latter effect causes a reversed pinch force and perhaps eventual break-up near the surface of a plasma. Some special total current profiles are used to illustrate these features.

§ 1. Introduction

The current density distribution in a conductor is of considerable interest to those working on electrical discharges because this distribution affects the circuit parameters. There is a special interest in the field of discharges in ionized gases such as the linear pinched discharge, because the distribution of current also affects the behaviour of the plasma, including its stability.

In a normal high frequency alternating current case it can be shown that the current is confined to a thin layer at the surface of the conductor due to the skin effect (see e.g. Harnwell 1949). The simple theory shows that the current penetrates to a depth δ of the order of $\sqrt{\{2/(\omega\mu\sigma)\}}$, where ω is the frequency of the applied field, and μ and σ are the permeability and conductivity respectively of the conductor.

However, to assume that the current is confined to the surface of the conductor in all cases where the current changes rapidly with time is incorrect. In general during the initial stages of a discharge, when the total current is increasing rapidly with time, the current first appears at the surface as might be expected, but in a time τ (of the order of $\mu\sigma a^2/15$ for a cylindrical conductor, where a is its radius) it diffuses into the conductor. After the initial stages, when this diffusion has occurred, the concept of a skin might no longer hold. Then if the total current decays with time, it will be shown that an inverse skin effect (that is, the current is a maximum at the centre of the conductor) occurs, and the current may even be reversed at the surface. This is due to an induced back e.m.f. near the surface of the conductor.

Complications also arise in the case of a conducting plasma due to its motion. A simple theoretical example of the effect of motion of a plasma carrying a current is given by Alfvén (1950), and will be discussed later. Experimental measurement by probes of axial current density distributions in a cylindrical conducting plasma

show that the inverse skin effect and the reversed current effect do in fact occur, see, for example, Andrianov, *et al.* (1958), Kurchatov (1956), Burkhardt and Lovberg (1958).

In this paper a general theory is first developed for calculating the axial current density distributions over the radius of a rigid cylindrical conductor, which is assumed to be infinitely long and axially symmetrical. The total axial current $\mathscr{I}(t)$ is assumed to be a specified, though quite general, function of time.

Two special examples of current profile will illustrate the results. The first example is an oscillatory current, when the effect of the transient terms in the solution at the start of the waveform are shown. This is compared with the steady-state solution, which is the well-known skin effect, as given by McLachlan (1949). The second example taken is the current pulse obtained from an overdamped discharge of a condenser through a resistance and inductance. This example will be used to illustrate the normal skin effect in the early stages, and the inverse skin effect and reversed current effect later on.

Finally, the more general problem of a radially expanding or contracting conductor is considered. This is the case found, for example, in the linear pinched discharge when the conducting plasma possesses a radial velocity, and its outside radius changes with time. In order to obtain an analytical solution to the problem, assumptions are made as to the radial dependence of this velocity and the electrical conductivity. However, in this theory the outside radius and the electrical conductivity can be quite general functions of time and, knowing these functions (from experiment) and the variation with time of the total current, current density distributions can in general be calculated. The effect of this radial velocity will be discussed qualitatively but, because of the difficulties involved in calculation, no special example will be given.

Throughout the analysis, rationalized m.k.s. units are used.

§ 2. General Theory for a Rigid Conductor

A rigid cylindrical conductor carrying an axial current is considered. It is assumed to be infinitely long and axially symmetrical.

Employing Maxwell's equations in the form

$$\nabla \times \mathbf{E} = -\frac{\partial \mathbf{B}}{\partial t}$$

$$\nabla \times \mathbf{H} = \mathbf{i} + \frac{\partial \mathbf{D}}{\partial t}$$

$$\nabla . \mathbf{B} = 0$$

$$\nabla . \mathbf{D} = q_v,$$

the relevant components, neglecting displacement currents, are

$$\frac{\partial E_z}{\partial r} = \frac{\partial B_\phi}{\partial t} \qquad \ldots\ldots (1)$$

$$\frac{1}{r}\frac{\partial}{\partial r}(rB_\phi) = \mu i_z \qquad \ldots\ldots (2)$$

where $\mathbf{B} = \mu\mathbf{H}$, μ being the permeability of the conductor.

When the inertial effects of the current carriers and thermal diffusion effects are ignored, Ohm's law is

$$i_z = \sigma E_z \qquad \ldots\ldots (3)$$

where σ is the electrical conductivity, assumed a constant for this case.

Changes with time of the total current always affect the current density distribution at the surface directly. This can be seen by integrating equation (4) below and obtaining

$$\left(\frac{\partial i_z}{\partial r}\right)_{r=a} = \frac{\mu\sigma}{2\pi a}\frac{d\mathscr{I}}{dt}.$$

This equation means that the gradient of the current density at the surface of the conductor is proportional to the rate of change of total current with time: this is also true for the radially moving conductor.

From (1), (2) and (3) the differential equation for current density is derived as follows

$$\frac{1}{r}\frac{\partial}{\partial r}\left(r\frac{\partial i_z}{\partial r}\right) - \mu\sigma\frac{\partial i_z}{\partial t} = 0. \qquad \ldots\ldots (4)$$

Let $x = r/a$ and $y = t/\mu\sigma a^2$, where a is the outside radius of the conductor. Then, in terms of these dimensionless variables x and y, equation (4) becomes

$$\frac{1}{x}\frac{\partial}{\partial x}\left(x\frac{\partial i_z}{\partial x}\right) - \frac{\partial i_z}{\partial y} = 0. \qquad \ldots\ldots (5)$$

This equation is of the same form as the well-known diffusion equation. Equation (5) is required to be solved to obtain $i_z(x, y)$ when the total current $\mathscr{I}(y)$ is a known function of time. The relation between $\mathscr{I}(y)$ and $i_z(x, y)$ is

$$\mathscr{I}(y) = 2\pi a^2 \int_0^1 i_z(x, y) x\, dx. \qquad \ldots\ldots (6)$$

There is a boundary condition that the total current is zero until $y = 0$, and the current density is also zero everywhere until $y = 0$, that is

$$\mathscr{I}(y) = 0, \qquad y \leqslant 0$$
$$i_z(x, y) = 0, \qquad y \leqslant 0, \quad \text{for all } x.$$

To obtain a solution, the Laplace transform is used. Let

$$\bar{i}(x, p) = \int_0^\infty i_z(x, y) e^{-py}\, dy. \qquad \ldots\ldots (7)$$

The transform of equation (5), using the boundary condition, is

$$\frac{\partial^2 \bar{i}}{\partial x^2}(x, p) + \frac{1}{x}\frac{\partial \bar{i}}{\partial x}(x, p) - p\bar{i}(x, p) = 0. \qquad \ldots\ldots (8)$$

The solution to this subsidiary equation in terms of Bessel functions is

$$\bar{i}(x, p) = \Phi(p) I_0(p^{1/2}x) + \Gamma(p) K_0(p^{1/2}x). \qquad \ldots\ldots (9)$$

Since $K_0(p^{1/2}x)$ is infinite at $x = 0$, $\Gamma(p)$ must be put to zero. $\Phi(p)$ is an arbitrary function of p to be determined from equation (6). To do this, the Laplace transform of equation (6) can be taken and compared with the result obtained by multiplying equation (9) by x and integrating with respect to x between the limits 0 and 1. Then it can be seen that

$$\Phi(p) = \frac{p^{1/2}}{2\pi a^2 I_1(p^{1/2})} \int_0^\infty \mathscr{I}(q) e^{-pq}\, dq \qquad \ldots\ldots (10)$$

where q is a dummy variable equivalent to y. On substituting (10) into (9) one obtains

$$\bar{i}(x, p) = \frac{p^{1/2} I_0(p^{1/2}x)}{2\pi a^2 I_1(p^{1/2})} \int_0^\infty \mathscr{I}(q) e^{-pq}\, dq. \qquad \ldots\ldots (11)$$

On taking the appropriate inversion of (11) using the Fourier–Mellin theorem, the general solution for the axial current density distribution becomes

$$i_z(x,y)=\frac{1}{2\pi i}\lim_{\eta\to\infty}\int_{\zeta-i\eta}^{\zeta+i\eta}\frac{e^{yp}\,p^{1/2}\,I_0(p^{1/2}x)}{2\pi a^2\,I_1(p^{1/2})}\int_0^\infty \mathscr{I}(q)e^{-pq}\,dq\,dp. \quad \ldots\ldots(12)$$

This is an open contour integral, and ζ is a constant greater than all the singularities of $\bar{i}(x,p)$.

§ 3. Special Case I: Sinusoidal Current Waveform

The total axial current in this case is given by

$$\left.\begin{aligned}\mathscr{I}(q)&=\sin\omega' t\\&=\sin\omega q\end{aligned}\right\},\qquad t>0,$$
$$=0,\qquad t\leqslant 0,$$

where $q=t/\mu\sigma a^2$ and $\omega'=\omega/\mu\sigma a^2$.

Then the current density distribution is

$$i_z(x,y)=\frac{1}{2\pi i}\lim_{\eta\to\infty}\int_{\zeta-i\eta}^{\zeta+i\eta}\frac{e^{yp}\,p^{1/2}\,I_0(p^{1/2}x)}{2\pi a^2\,I_1(p^{1/2})}\frac{\omega}{\omega^2+p^2}\,dp.$$

On expansion it can be shown that the integrand is a single-valued function of p, with poles of $\bar{i}(x,p)$ occurring at $p=+i\omega$, $p=-i\omega$ and $p=-\gamma_n{}^2$, where γ_n, $n=1,2\ldots$ are the roots of the equation $J_1(\gamma_n)=0$.

From an evaluation of the residues at these poles one obtains

$$\begin{aligned}i_z(x,y)=&\frac{\omega^{1/2}}{2\pi a^2(\mathrm{ber}_0{}'^2\,\omega^{1/2}+\mathrm{bei}_0{}'^2\,\omega^{1/2})}\\&\times[\cos\omega y(\mathrm{ber}_0\,\omega^{1/2}x\ \ \mathrm{ber}_0{}'\,\omega^{1/2}+\mathrm{bei}_0\,\omega^{1/2}x\ \ \mathrm{bei}_0{}'\,\omega^{1/2})\\&+\sin\omega y\,(\mathrm{ber}_0\,\omega^{1/2}x\ \ \mathrm{bei}_0{}'\,\omega^{1/2}-\mathrm{bei}_0\,\omega^{1/2}x\ \ \mathrm{ber}_0{}'\,\omega^{1/2})]\\&-\sum_{n=1,2\ldots}^{\infty}\frac{\exp(-\gamma_n{}^2y)\gamma_n{}^2\,J_0(\gamma_n x)}{\pi a^2\,J_0(\gamma_n)}\frac{\omega}{\omega^2+\gamma_n{}^4}\end{aligned}\qquad\ldots\ldots(13)$$

where the Bessel functions of complex argument are defined by

$$i^nI_n(i^{1/2}z)=J_n(i^{3/2}z)=\mathrm{ber}_n z+i\,\mathrm{bei}_n z.$$

The first term is the steady-state or long-time solution for an oscillatory current. This is in agreement with the results of McLachlan when the imaginary components of his results are used. (This is because he used

$$\mathscr{I}(q)=e^{i\omega q}=\cos\omega q+i\sin\omega q.)$$

The transient terms decay as $\exp(-\gamma_1{}^2y)$ where $\gamma_1=3{\cdot}83$, that is, the characteristic time for decay of these terms is

$$\tau=\mu\sigma a^2/\gamma_1{}^2. \qquad\ldots\ldots(14)$$

As an example of the value of τ, let $\mu=4\pi\times10^{-7}\,\mathrm{H\,m^{-1}}$, $\sigma=5{\cdot}8\times10^7\,\mathrm{ohm^{-1}\,m^{-1}}$ (for copper), $a=10^{-2}\,\mathrm{m}$, then $\tau\simeq5\times10^{-4}\,\mathrm{sec}$.

To illustrate the current density distributions at various times, an arbitrary value of ω equal to 25 was used. For the above example of copper wire, this would correspond to 546 c/s. The total current is plotted against time in figure 1, and at various times q during the first cycle the current density distributions are drawn (full line). It is to be noted that the current is initially confined near the surface, but that, before the total current has completed its first half cycle, i.e. it is still flowing in the positive direction, the current density is reversed at the

surface. On the same diagrams are plotted (broken line) the current density distributions at similar times in the cycle many cycles later on. These distributions are the steady-state distributions as derived before by McLachlan, and can be compared with the first cycle distributions to see the effect of the transient terms.

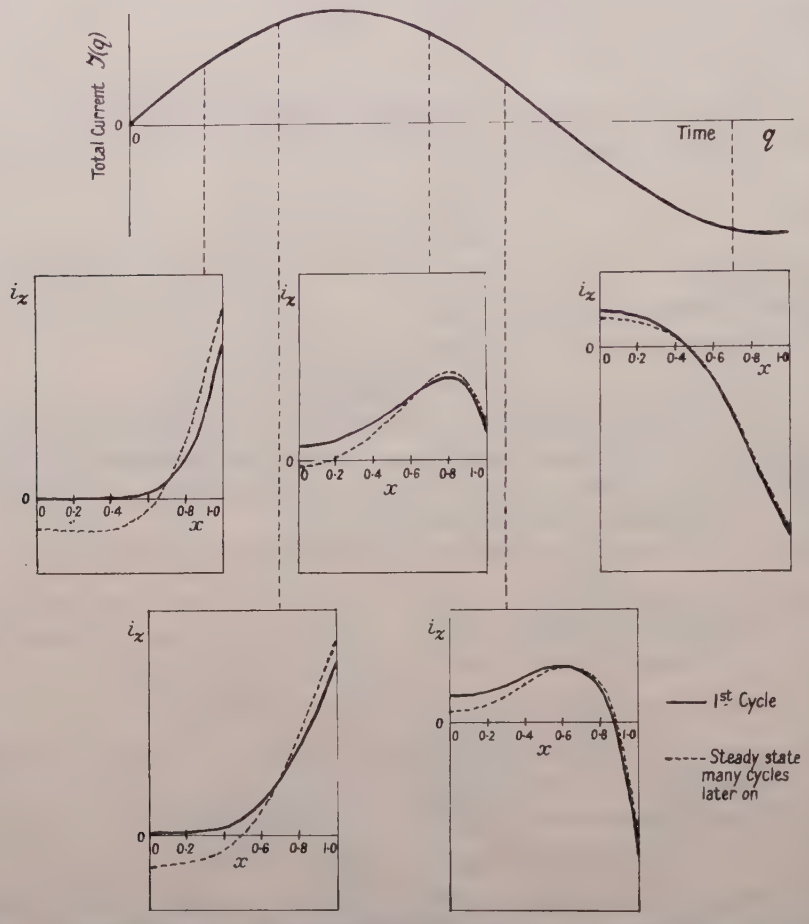

Figure 1. Radial distributions of current density are shown at times on the total current profile $\mathcal{I} = \sin 25\,q$ as indicated by the broken lines.

§ 4. Special Case II: Current Pulse from Overdamped Discharge

The total current waveform produced by an overdamped discharge of a condenser C through an inductance L and a resistance R is of the form

$$\mathcal{I}(t) = \exp(-\alpha' t) - \exp(-\beta' t), \qquad t > 0$$
$$= 0, \qquad t \leqslant 0$$

where

$$\beta' = \frac{R}{2L} + \left[\frac{R^2}{4L^2} - \frac{1}{LC}\right]^{1/2}$$

$$\alpha' = \frac{R}{2L} - \left[\frac{R^2}{4L^2} - \frac{1}{LC}\right]^{1/2}$$

and

$$\beta' > \alpha', \qquad \frac{R^2}{4L^2} > \frac{1}{LC}.$$

$\mathscr{I}(t)$ can be written

$$\mathscr{I}(q)=\exp(-\alpha q)-\exp(-\beta q)$$

where $q=t/\mu\sigma a^2$, $\alpha'=\alpha/\mu\sigma a^2$ and $\beta'=\beta/\mu\sigma a^2$. From equation (13) the current density is given by

$$i_z(x,y)=\frac{1}{2\pi i}\lim_{\eta\to\infty}\int_{\zeta-i\eta}^{\zeta+i\eta}\frac{e^{yp}\,p^{1/2}\,I_0(p^{1/2}x)}{2\pi a^2\,I_1(p^{1/2})}\left(\frac{1}{\alpha+p}-\frac{1}{\beta+p}\right)dp.$$

Again, from an evaluation of the residues at the poles of $\bar{\imath}(x,p)$, one obtains

$$i_z(x,y)=\frac{e^{-\alpha y}\,\alpha^{1/2}\,J_0(\alpha^{1/2}x)}{2\pi a^2\,J_1(\alpha^{1/2})}-\frac{e^{-\beta y}\,\beta^{1/2}\,J_0(\beta^{1/2}x)}{2\pi a^2\,J_1(\beta^{1/2})}$$
$$-\sum_{n=1,2}^{\infty}\frac{\exp(-\gamma_n{}^2y)\,\gamma_n{}^2\,J_0(\gamma_n x)}{\pi a^2\,J_0(\gamma_n)}\left(\frac{1}{\alpha-\gamma_n{}^2}-\frac{1}{\beta-\gamma_n{}^2}\right)\quad\ldots\ldots(15)$$

where γ_n, $n=1, 2\ldots$ are, as before, the roots of the equation $J_1(\gamma_n)=0$.

At the start of the current pulse the transient effects (the infinite summation term) are important, and the current is confined to the surface of the conductor.

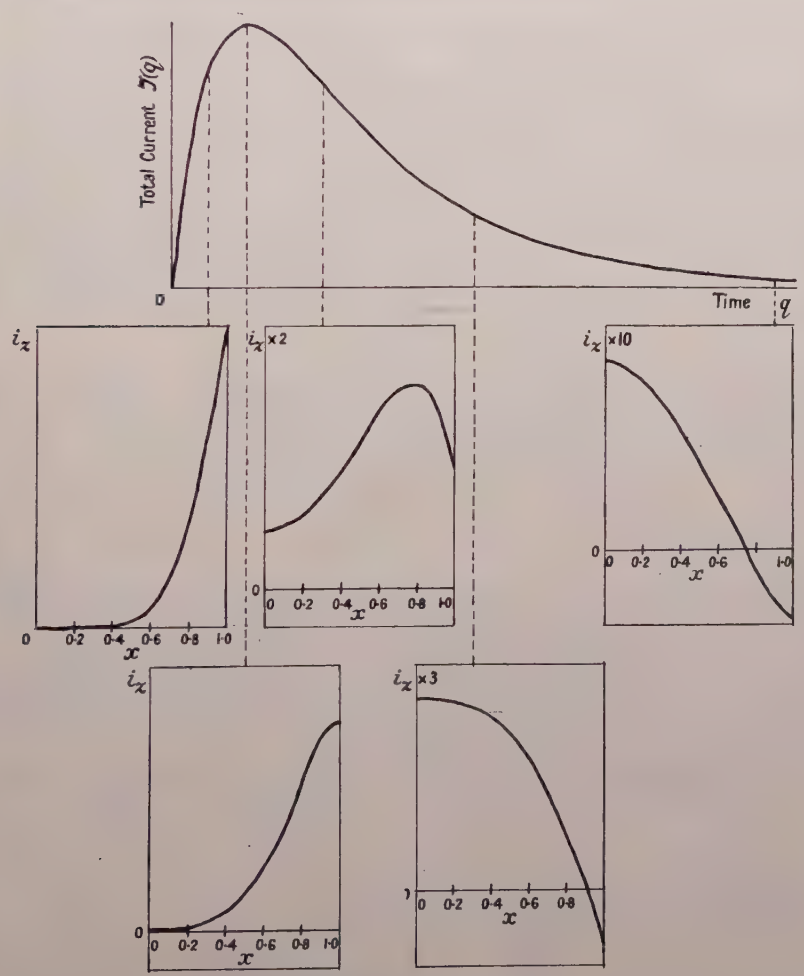

Figure 2. Radial distributions of current density are shown at times on the total current profile $\mathscr{I}=e^{-12\cdot96q}-e^{-36q}$ as indicated by the broken lines.

These transient terms die away as before with a characteristic time τ of the order of $\mu\sigma a^2/\gamma_1^2$.

It can be seen that after sufficient time has elapsed, one of the terms in this expression will be dominant due to the exponential time dependence of each term. If $\alpha<\gamma_1^2$ the term containing $e^{-\alpha y}$ is the dominant one, and if $\alpha>\gamma_1^2$ the term containing $\exp(-\gamma_1^2 y)$ dominates after sufficient time. In both cases, there is an inverse skin effect at this time, i.e. the current density is a maximum at $x=0$ due to the spatial dependence on $J_0(\alpha^{1/2}x)$ or $J_0(\gamma_1 x)$.

If $\alpha^{1/2}>\xi_1$, where $\xi_1=2{\cdot}4048$ and is the first zero of $J_0(\xi_n)$, then, after sufficient time, the current density reverses in sign at a certain radius. This radius is always greater than $x=\xi_1/\gamma_1=0{\cdot}6276$ for this current profile. Outside this radius the current density flows in the opposite direction to the total current. The effect of this reversed current density in the case of a plasma will be discussed in § 6.

A numerical example illustrating the skin effect found early in the pulse, changing to the inverse skin effect and showing a reversed current near the surface, is given in figure 2. α and β are chosen arbitrarily as 12·96 and 36 respectively.

§ 5. General Theory for a Radially-Moving Conductor

Ohm's law for a conductor moving with a velocity $\mathbf{v}$ is modified to

$$\mathbf{i}=\sigma(\mathbf{E}+\mathbf{v}\times\mathbf{B}).$$

The component of this equation which is relevant to the problem is

$$i_z=\sigma(E_z+v_r B_\phi). \qquad \ldots\ldots(16)$$

Equations (1) and (2) remain unaltered. For a plasma the radial velocity v_r and the electrical conductivity σ should be determined from the magneto-hydrodynamic equations. The electrical conductivity of a plasma depends essentially on the temperature. Thus v_r and σ are in general functions of the radius and time.

In order to obtain a tractable solution to the problem, assumptions have to be made as to the radial dependence of v_r and σ. It is assumed in this analysis that the outside radius $a(t)$ of the conducting plasma is a known but quite general function of time, and that the radial velocity is given by

$$v_r(r,t)=\frac{r}{a(t)}\frac{da(t)}{dt}. \qquad \ldots\ldots(17)$$

This linear radial dependence means that the conductor expands and contracts uniformly across its radius. The electrical conductivity σ is assumed to be independent of the radius, and just a general specified function of time. These two conditions are probably only valid for a slowly moving hot plasma, when the temperature is uniform across the radius due to a high thermal conductivity, and when no shock waves are present in the gas.

From equations (1), (2), (16) and (17) the following equation can be derived

$$\frac{1}{r}\frac{\partial}{\partial r}\left[r\frac{\partial i_z}{\partial r}(r,t)\right]=\mu\sigma(t)\left[\frac{\partial i_z}{\partial t}(r,t)+\frac{1}{ra}\frac{da}{dt}\frac{\partial}{\partial r}\{r^2 i_z(r,t)\}\right]. \qquad \ldots\ldots(18)$$

By suitable changes of variables, namely

$$x=\frac{r}{a(t)}, \qquad y=\int_0^t\frac{dt}{\mu\sigma(t)\,a^2(t)} \qquad \ldots\ldots(19)$$

and

$$\psi(x,y)=a^2(t)i_z(x,t) \qquad \ldots\ldots(20)$$

the modified differential equation for current density is

$$\frac{1}{x}\frac{\partial}{\partial x}\left[x\frac{\partial \psi}{\partial x}(x,y)\right]-\frac{\partial \psi}{\partial y}(x,y)=0. \qquad \ldots\ldots(21)$$

This equation is the same as equation (5), and the relation between $\psi(x,y)$ and the known variation of the total axial current with time becomes

$$\mathscr{I}(y)=2\pi\int_0^1 \psi(x,y)x\,dx. \qquad \ldots\ldots(22)$$

The boundary conditions are also similar, namely

$$\mathscr{I}(y)=0, \qquad y\leqslant 0,$$
$$\psi(x,y)=0, \qquad y\leqslant 0, \quad \text{for all } x.$$

Then using the Laplace transformation as before, the solution for the current density distribution is

$$i_z(x,t)=\frac{1}{2\pi i a^2(t)}\lim_{\eta\to\infty}\int_{\zeta-i\eta}^{\zeta+i\eta}\frac{e^{yp}\,p^{1/2}\,I_0(p^{1/2}x)}{2\pi\,I_1(p^{1/2})}\int_0^\infty \mathscr{I}(q)e^{-pq}\,dq\,dp. \qquad \ldots\ldots(23)$$

Thus, knowing the variation with time of the total current, the electrical conductivity, and the outside radius of the conducting cylinder, the current density can be calculated as a function of the radius and time.

No specific example of the effect of the radial velocity is given here owing to the difficulties involved both in computation and also in interpreting the results. Changes with time of the outside radius of the plasma and its conductivity effectively alter only the time scale. A change of total axial current with time has more effect when the surface radius or the conductivity is large than when small. This can be seen from

$$\mu\sigma(t)a^2(t)\frac{d\mathscr{I}}{dt}=\frac{d\mathscr{I}}{dy}$$

because it is the variation of $\mathscr{I}$ with y rather than t which affects the distribution of current density (see equation (23)). Thus, when the plasma possesses an outward radial velocity, changes with time of the total current are increasingly important in affecting the current distribution, and decreasingly important with time for an inward motion. However, it is to be noted that the sign of $d\mathscr{I}/dt$ is the same as the sign of the scaled $d\mathscr{I}/dy$, and it is the magnitude only which is scaled.

Alfvén, using a particular solution of the problem for a plane cartesian case, obtained an inverse skin effect. No boundary to the plasma was introduced, i.e. an infinite conductor was the model used, and its velocity was equal to $-x/\tau_0$. The total current was rising exponentially with time (with no boundary conditions at $t=0$), but because the velocity increased to infinity at the infinitely placed boundaries, this had more effect on the current distribution than the rising current. In fact, in this artificial case a Gaussian distribution of current density was obtained.

§ 6. Effect of Current Density Distributions on a Plasma

The radial force equation which applies to a plasma carrying an axial current can be written as

$$\rho\frac{dv_r}{dt}=-i_z B_\phi-\frac{\partial p}{\partial r} \qquad \ldots\ldots(27)$$

where ρ and p are the plasma density and pressure respectively. In an equilibrium condition the pressure gradient will balance the magnetic pinch force, and $\rho\, dv_r/dt$ will be zero. Now, at the surface of the plasma the density and pressure fall off to zero, i.e. $\partial p/\partial r$ must be a negative quantity at the surface.

For containment, therefore, $i_z B_\phi$ must be a positive quantity, large enough to balance $\partial p/\partial r$. If it exceeds $\partial p/\partial r$, further pinching will occur, i.e. a negative or an inward radial acceleration will be possessed by the plasma.

However, if at the surface the current density is reversed in sign relative to the total axial current, the electromagnetic pinch force will be a negative quantity. (B_ϕ at the surface depends only on the sign and magnitude of the total current.) Then, without the added consideration of an axial magnetic field and azimuthal current, $\rho\, dv_r/dt$ will be a positive quantity at the surface, and containment of the plasma might not occur. With a reversed pinch force, the outer shell of the plasma will be forced to expand radially and perhaps separate from the rest of the gas. Perhaps this would be seen in an experiment on a pinched plasma as a growth of instability at its surface eventually causing a break-up of the ionized column. A more general theory of stability of confined plasmas taking account of possible current density distributions would be desirable.

Acknowledgments

The author is indebted to Professor P. M. S. Blackett for his continued interest and help during this work, to members of the High Temperature Physics group for advice and assistance, and to Professor H. Jones and Dr. O. Penrose of the Mathematics Department for valuable discussions. The work was done while the author was in receipt of a maintenance grant from the Department of Scientific and Industrial Research.

References

Alfvén, H., 1950, *Cosmical Electrodynamics* (Oxford: Clarendon Press).

Andrianov, A. M., *et al.*, 1958, *Proceedings of the Second International Conference on the Peaceful Uses of Atomic Energy*, **31**, 348 (United Nations: Geneva).

Burkhardt, L. C., and Lovberg, R. H., 1958, *Proceedings of the Second International Conference on the Peaceful Uses of Atomic Energy*, **32**, 29 (United Nations: Geneva); 1958, *Nature, Lond.*, **181**, 228.

Harnwell, G. P., 1949, *Principles of Electricity and Electromagnetism* (New York: McGraw-Hill).

Kurchatov, I. V., 1956, *On the Possibility of Producing Thermonuclear Reactions in a Gas Discharge, Atomnaya Energ.*, **1**, 65. (English translation, *J. Nucl. Energy*, 1957, **4**, 1953.)

McLachlan, N. W., 1949, *Bessel Functions for Engineers* (Oxford: University Press).

The Experimental Determination of the Range–Energy Relations for Alpha Particles in Water and Water Vapour, and the Stopping Power of Water and Water Vapour for Alpha Particles at Energies below 8·78 MeV

By R. B. J. PALMER† and H. A. B. SIMONS
Department of Physics, Royal Free Hospital School of Medicine, London, W.C.1

MS. received 13*th March* 1959, *in revised form* 9*th June* 1959

Abstract. A method for measuring the residual energy of alpha particles which have traversed paths of various lengths in water is described, and also a method for determining total alpha-particle range in water, the results being used to deduce a range–energy relation for alpha particles of energy up to 8·78 MeV in liquid water. A method is described for measuring the residual energy of alpha particles which have passed through air and through water vapour, and by means of a scintillation detector the complete alpha-particle range in air and in water vapour is established. From these results range–energy relations are deduced for alpha particles in air and in water vapour. The differential and integral stopping power of water and water vapour at various energies is calculated and the results are discussed.

§ 1. Introduction

The dissipation of energy by alpha particles from naturally radioactive substances on passing through an absorbing medium is considered to be due almost entirely to the ionization and electronic excitation of atoms along their path. It would therefore be expected, as stated by the Bragg rule, that the rate of absorption of energy at any particular alpha-particle energy would depend only upon the nature and density of the atoms in the absorbing medium, and not upon its inter- or intra-molecular structure. Certain experimental determinations of the stopping power of water for alpha particles have not confirmed this (Gray 1944). Experiments by Philipp (1923) and Michl (1914) indicated that the integral stopping power of liquid water was considerably higher than would be predicted by the Bragg rule from a knowledge of the molecular stopping power of hydrogen and oxygen. In a later determination, Appleyard (1951) found the stopping power of water to be about 20% higher than the value predicted by the Bragg rule. Other determinations (Wilkins 1950, unpublished, de Carvalho and Yagoda 1952, Ellis, Rossi and Failla 1955, Aniansson 1955, and McInally 1956) are in much closer agreement with the predicted value, the differences not exceeding 5% in any of these cases.

The results mentioned involve either a determination of the total range in water of alpha particles from naturally radioactive substances, or a measurement of the differential stopping power relative to air of a water layer or film over a limited energy range. It therefore seemed desirable to design an experiment which would give a continuous range–energy relation for alpha particles in water over as wide a range as possible. In addition, since relatively little experimental

† This paper contains material submitted by R. B. J. Palmer to the University of London as part of a thesis for the degree of Ph.D.

information is available regarding the stopping power of water vapour for alpha particles, it was decided to determine the range–energy relation for alpha particles in water vapour in order that the stopping power values for water in the liquid and vapour phases could be directly compared.

In most of the experiments to be described nuclear emulsion techniques have been employed. Alpha particle ranges were obtained from the mean of a number of track lengths in emulsion, and hence mean energy values were found. The alpha-particle path lengths in water and water vapour were derived from the mean track lengths in emulsion, so these will also be mean values. For alpha particles of one particular energy, the distribution of track lengths about the mean value is approximately normal, and the mean value therefore also represents the most probable range for a particle of the energy considered.

§ 2. The Range–Energy Relation for Liquid Water

In order to determine the range–energy relation for alpha particles in liquid water, alpha particles from thorium C (8·78 MeV) were allowed to travel through water layers of various known thicknesses and then to pass into photographic emulsion. From the known range–energy relation for alpha particles in photographic emulsion (Rotblat 1951) the energy of the alpha particles on entering the emulsion could be determined, and hence the loss of energy on passing through a given thickness of water could be found. The total range of the alpha particles in water was also determined, and hence the range–energy relation for the alpha particles in water was deduced.

2.1. *The Relation between Path Lengths traversed and Residual Energy*

An active deposit source of thorium C was collected on a highly polished steel cylinder of radius 9·51 mm and a thin film of polyvinyl formal resin ('Formvar', Messrs. Shawinigan Ltd.), which was equivalent to $\frac{1}{2}\mu$ of C 2 emulsion in stopping power for alpha particles of 8·78 MeV energy, was wrapped round the cylinder. A 100 μ C 2 nuclear research plate was covered with a similar Formvar film, and about $\frac{1}{2}$ cm^3 of distilled water, to which Formvar is impervious, was placed in the centre of the plate and the cylinder was laid on it, thus trapping a quantity of water between the cylinder surface and the emulsion (figure 1 (*a*)). Alpha particles thus passed from the cylinder surface through the water and into the emulsion. The plate was exposed in this way for $1\frac{1}{2}$ minutes. During this time a beam of x-rays was allowed to fall normally on to the plate producing an x-ray shadow of the cylinder from which the line of contact of the cylinder with the plate could later be determined. The plate was processed and tracks in the emulsion were measured, the distance x from the line of contact of the plate and emulsion to the point at which each track entered the emulsion being noted, and also the angle of dip of the track in the emulsion θ ($\angle$BAC) and the angle ϕ ($\angle$CAD) that the projection of the track on a horizontal plane made with a vertical plane in the x direction (figure 1 (*b*)). If the path length of a certain track in the water is denoted by T, and if the projection of T on a vertical plane in the x direction is denoted by p, then

$$T^2 = \frac{p^2}{\sin^2\theta + \cos^2\theta\cos^2\phi}.$$

If the angle between p and the plane of the emulsion ($\angle$EAD) is denoted by ω,

$$\tan\omega = \tan\theta/\cos\phi.$$

Hence ω could be computed from experimental data and, by means of a scale diagram of a right circular section of the cylinder, the distance x being known,

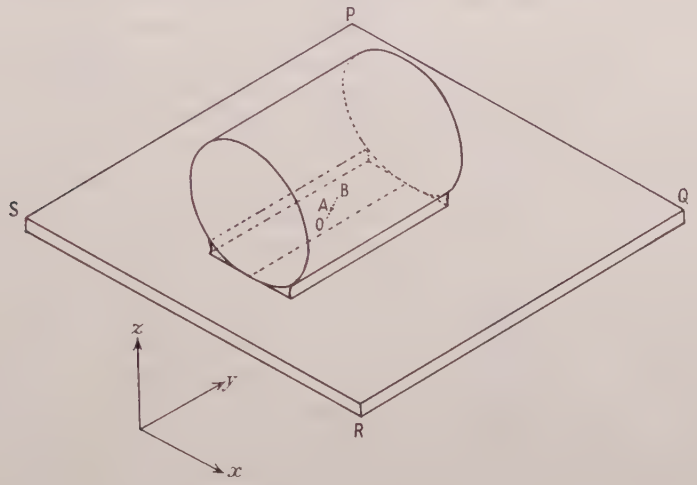

Figure 1 (*a*). Isometric diagram showing arrangement for irradiation of nuclear emulsion through water.

p could be found. From this the path length in water T corresponding to the measured residual track length in the emulsion L could be found. A correction was applied to each residual track length for losses in the Formvar films.

Measurements of between 125 and 280 tracks were carried out on each of six plates and for the purpose of analysis the track measurements were divided

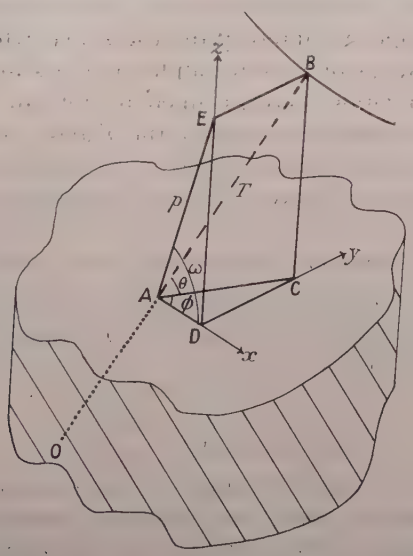

Figure 1 (*b*). Enlargement of typical alpha particle path, shown in figure as BAO.

into groups depending upon the value of T. The mean value of T in each group and the corresponding mean value of L were determined and a graph was plotted of T against L for each plate. Results obtained for values of L smaller than about $15\,\mu$ were found to be unreliable owing to difficulties in measuring θ and ϕ accurately in short tracks. Values of L near the line of contact of the cylinder and plate were low in some cases, possibly due to the wrinkling of the Formvar around the region of contact. Results for one of the plates are shown in figure 2. In each case the graph of T against L was found to be a straight line, and the slope of this was found by the method of weighted means. The six values obtained

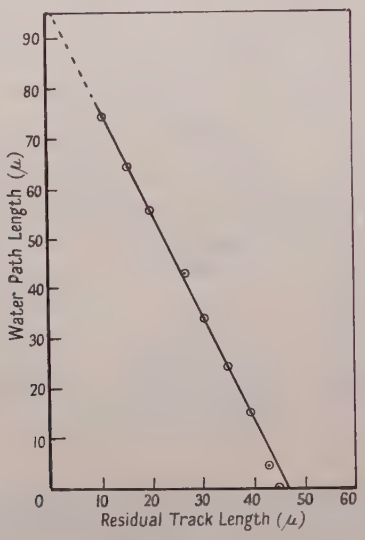

Figure 2.

for the slope were found to be the same within the limits of experimental error ($2{\cdot}09 \pm 0{\cdot}04$), and the mean result of the experiments can therefore be expressed by a line having this slope and intercepting the L axis where $L = 47\,\mu$, this value being assumed for the range of 8·78 Mev alpha particles in C 2 emulsion (Rotblat 1951). If this linear relation were assumed to hold for values of L less than $15\,\mu$, and the line were then extrapolated to the T axis, a value for the total range of 8·78 Mev alpha particles in water of $98{\cdot}2 \pm 1{\cdot}8\,\mu$ would be obtained. This assumption cannot be made, however, without experimental confirmation.

2.2. *Determination of the Total Range of* 8·78 *MeV Alpha Particles in Water*

Assuming that the atomic stopping powers of the constituents of a mixture may be added, it may be shown that the range R_M of an α-particle in a mixture of two components is given by

$$\frac{1}{R_M} = \frac{\rho_1^*}{\rho_1 R_1} + \frac{\rho_2^*}{\rho_2 R_2}$$

where R_1 and R_2 are the respective ranges of the particle in the components of normal densities ρ_1 and ρ_2, which have 'reduced' densities of ρ_1^* and ρ_2^* as they occur in the mixture. The 'reduced' density is defined as the mass of a component per unit volume of mixture.

The range of an α-particle in water may therefore be deduced by measuring the range in wet emulsion if the range in dry emulsion is known.

If a volume v of dry emulsion swells to a volume V when a volume of water W is absorbed, and the ranges of the particle in dry emulsion, wet emulsion and water are L, R and X respectively, then

$$\frac{1}{R} = \frac{v}{VL} + \frac{W}{VX}$$

and hence X may be found.

400 μ C 2 nuclear research plates were used in these experiments. The plates were soaked in water for 2 or 3 days and were then transferred to water containing ThC ions in which they remained for a further 48 hours. Special precautions were taken in preparing the radioactive solution to ensure that there was no change in the quantity of water absorbed by the emulsion when it was transferred to this solution, and this was checked by weighing. It was not assumed in these experiments that the volumes of dry emulsion and water are additive in wet emulsion. In all the plates examined the final volume of the swollen emulsion V was less than the sum of the dry volume of the emulsion v and the volume of water absorbed W. The 'apparent density' of the water when absorbed, which is given by $W\rho/(V-v)$, where ρ is the normal density of water, was found to be $1{\cdot}07 \pm 0{\cdot}01\,\mathrm{g\,cm^{-3}}$. In each case the volume of water absorbed was found by weighing the plate before and after soaking. The volume of the emulsion was determined by measuring its thickness and area. The dry area was found to increase by about 3% after soaking, whereas the thickness increased by a factor of about 4·5. Considerable care was necessary for the accurate measurement of emulsion thickness. Before soaking each plate, the corners were cut off and part of the emulsion was scraped from the glass backing at each corner. The emulsion thickness was then found by focusing in turn on the emulsion surface and on the glass backing, a mean of many estimates being taken. In order to obtain a value for the wet emulsion thickness, the corners were soaked with the rest of the plate and a thin cover-slip was then placed on the emulsion surface, thus trapping water between the cover-slip and the glass backing in the space from which the emulsion had previously been removed. This prevented evaporation and consequent shrinkage of the emulsion during the measurement of the wet emulsion thickness which was carried out as before by differential focusing, due allowance being made, however, for refraction in the water.

Eight plates were examined in this way, and in each case from a mean of 80 to 100 track measurements a value was obtained for the range of 8·78 MeV alpha particles in water. The mean range value obtained from all the plates was $96{\cdot}6 \pm 1{\cdot}7\,\mu$. This result is not significantly different from the extrapolated value indicated by the previous experiments. In the light, however, of the results obtained for water vapour and air which are given later there seems to be no justification by analogy for assuming a linear relation between residual track length and water path length at low energies, so a total range of 96·6 μ has been assumed for 8·78 MeV alpha particles in liquid water at 20°C.

The values of the residual path lengths in emulsion L were converted to residual energy values E and hence the range–energy relation for alpha particles in water was derived (figure 3). The results of previous range measurements are also indicated in figure 3 for comparison purposes.

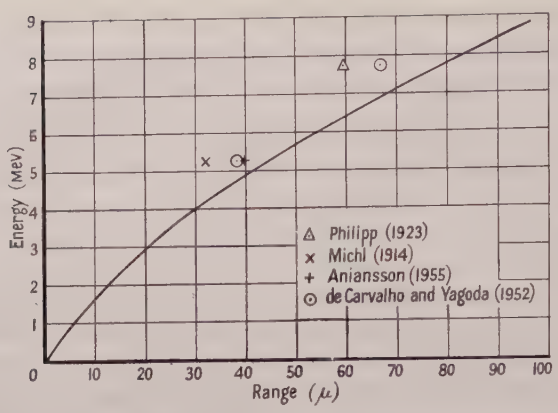

Figure 3. Range–energy relation for alpha particles in water.

§ 3. The Range–Energy Relation for Alpha Particles in Water Vapour and in Air

The determination of the range–energy relation for alpha particles in water vapour was carried out by means of two separate series of experiments. Alpha particles of 8·78 Mev energy were passed through a chamber containing water vapour at various known pressures and the residual particle energy was determined from the lengths of tracks then formed by the particles in nuclear emulsions. From these results a graph was plotted of concentration of water vapour molecules against residual track length for a fixed alpha particle path length in water vapour. The concentration of water vapour molecules required just to stop the alpha particles at the end of the given path length was determined by a second series of experiments in which a scintillation counter was used to detect the alpha particles near the end of their range.

Similar experiments were carried out for air, so that a comparison could be made between the results obtained for air and the present accepted range–energy relation for alpha particles in air (Bethe 1950). In addition, stopping power values for water vapour relative to air could be derived by the direct comparison of experimental results which had been obtained by means of the same technique.

3.1. *Absorption Measurements in Water Vapour and in Air*

The apparatus used in these experiments is shown in figure 4. It was constructed of brass and consisted of a vacuum chamber A, an annular water chamber B, a lid and heater support C, and an outer tube D. The thorium C was deposited on a steel disc of diameter 1 cm which had one face coated with platinum foil, and this disc was held by means of a magnet at E. F was a vacuum-tight rotatable shutter which covered the source except during irradiation of the plates. Alpha particles emitted by the source passed down the tube and through the window at G. The window consisted of a hole of diameter 1·9 cm covered with fine mesh copper gauze supporting two sheets of Formvar which were sealed to the brass by means of a waterproof adhesive. In the vacuum chamber below the window a nuclear research plate rested on the support H which was inclined at an angle of 66° to the horizontal. All alpha particles from the source 78·5 cm above the window were therefore incident on the plate at an angle of $24 \pm 1°$

to the emulsion surface. 'O' ring vacuum seals were fitted to the apparatus at I, J and K, so that any required vapour or air pressure less than atmospheric pressure could be maintained within the apparatus.

The heater assembly consisted of six short threaded cylinders of fireclay L wound with constantan wire and supported at the ends of six long brass rods encased in tubes of bakelized paper. The length of the rods was such that, when the apparatus was assembled and the annular water container was full of water, the heater coils were completely immersed but did not touch the bottom of the container. Connection was made to the heater coils by means of fine copper wires, one of which was wound on an insulated former which fitted over the

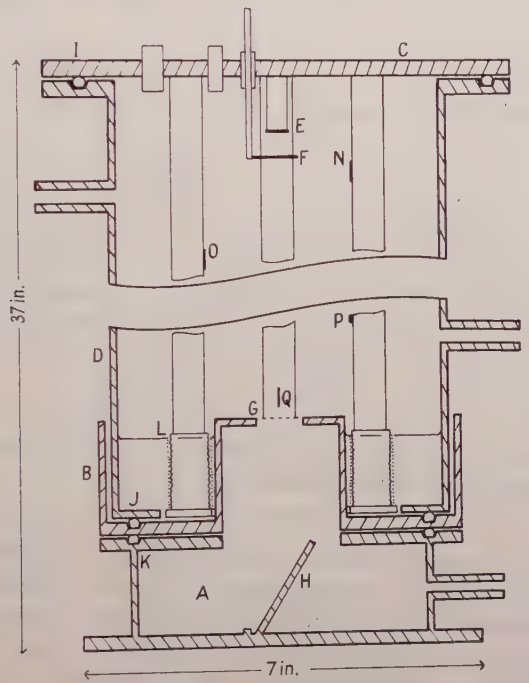

Figure 4. Water vapour and air absorption chamber.

magnet at E, thus keeping the temperature of the magnet and source slightly above that of the immediate surroundings during experiments and preventing the condensation of water on the source. Temperature measurements at four points inside the vapour chamber were made by means of thermistors which were fixed to the vertical rods at N, O, P and Q. When in use the complete apparatus was placed on a brass box filled with ice which kept the vacuum chamber and nuclear plate cool during the experiment.

Before each experiment the absorption chamber was evacuated and the water heated, and when temperature and pressure conditions were constant at the required values the plate was irradiated for about 1 hour. A series of experiments was carried out with vapour pressures varying from 1·35 to 11·37 cm Hg. From the known mean temperature and pressure conditions the concentration n of water vapour molecules in the vapour chamber was found and a graph was plotted of n against residual track length in the emulsion (figure 5). The residual track lengths were corrected for energy loss in the Formvar window.

Similar experiments were carried out with air at room temperature in the absorption chamber, and the resultant graph of molceules per cm^3 against residual track length is also shown in figure 5.

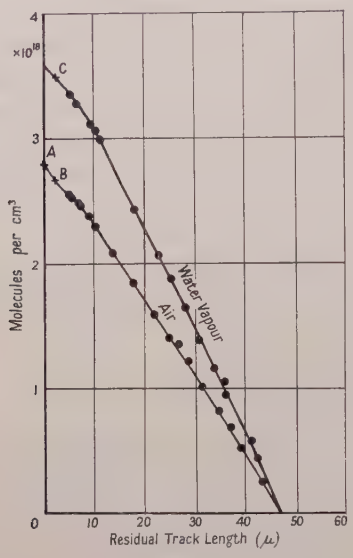

Figure 5.

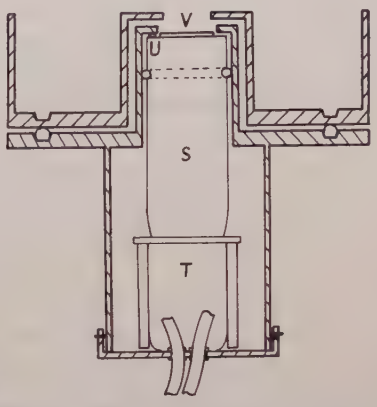

Figure 6. Photomultiplier holder. V, scintillator; U, contact spring; S, photomultiplier; T, dynode assembly.

3.2. *Determination of the Molecular Concentration required for Complete Alpha Particle Absorption in a Fixed Path Length through Air and through Water Vapour*

For these experiments the absorption chamber previously described was used, the vacuum chamber being replaced by a brass holder containing a scintillation counter as shown in figure 6. A plastic scintillator, consisting of polyvinyl toluene plus sensitizers (Naton 11, Messrs. Nash and Thompson) was used as the alpha-particle detector. The scintillator was prepared in the form of a film about 5 μ thick on a small glass plate by evaporation of the Naton 11 from a solution in chloroform. The photomultiplier tube used was an E.M.I. tube type 6260. Different amplifier gains could be used to give a pulse amplification of 40, 50, 170, 500 or 1500 as required, the amplified pulses greater than 5 volts being registered by a scaling unit.

The counting rate was measured for various air pressures and water vapour pressures in the absorption chamber, and typical results are shown in figure 7. In the water vapour experiments counts were taken over half-minute intervals as the temperature and hence the pressure slowly increased, whereas in the air experiments, in which conditions were static, it was possible to measure the counting rate over longer intervals of time. Hence the points on the water vapour graph are more scattered than those on the air graph.

In the experiments described in § 3.1, the mean residual track length represented the most probable energy of the alpha particles after passing through the absorption chamber which contained air or water vapour at a given pressure. In order, therefore, to be consistent in the definition of range used in these experiments, the pressure end-point selected to represent complete alpha particle

absorption was the pressure at which the greatest number of alpha particles were just stopped on reaching the surface of the scintillator, that is, the pressure at which the maximum rate of reduction of counting rate with pressure occurred.

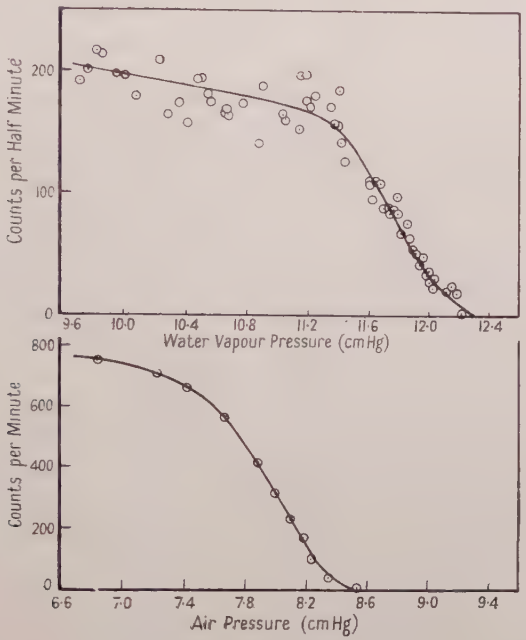

Figure 7. Typical end-point graphs for water vapour and air.

The results of experiments carried out for air showed that the pressure end-point for 8·78 MeV alpha particles was independent of amplifier gain at amplifications of 170 or over, the mean value obtained corresponding to a molecular density of $2{\cdot}80 \pm 0{\cdot}02 \times 10^{18}$ cm^{-3}. At lower amplifications, the value obtained for the pressure end-point decreased, a molecular density of $2{\cdot}68 \pm 0{\cdot}01 \times 10^{18}$ cm^{-3} being found to correspond with the pressure end-point when the pulse amplification was reduced to 40. It was inferred from this that alpha particles at the extreme end of their range could not be detected with amplifications less than 170.

An attempt was made to carry out similar experiments with water vapour as the absorbing medium, using the same range of pulse amplification. It was found, however, that the counting rate increased very rapidly with temperature in the 50 to 60°C range, since thermal electrons emitted from the photocathode were detected when the amplification of the pulses from the photomultiplier was too high. As the pressure end-point was approached, the counting rate rose so steeply, due to the temperature increase, that it masked the fall in counting rate due to the stopping of the alpha particles in the absorption chamber. It was found impracticable to cool the photomultiplier as this caused condensation of water on the scintillator. It was therefore possible to obtain results for water vapour only with a pulse amplification of 40 and a mean value for the molecular density of water vapour required to stop 8·78 MeV alpha particles under these conditions was found to be $3{\cdot}48 \pm 0{\cdot}03 \times 10^{18}$ mol cm^{-3}. The final end-point for water vapour corresponding to zero alpha-particle energy was deduced as

follows. The pressure end-point for air was inserted on the ordinate of the absorption graph, figure 5, at the corresponding molecular density of $2{\cdot}80 \times 10^{18}$ cm^{-3}. The line was extended to this point A, and a point B, at which the molecular density was $2{\cdot}68 \times 10^{18}$ cm^{-3} corresponding to the end-point obtained with a pulse amplification of 40, was inserted on the graph. The residual track length corresponding to this molecular density was $2{\cdot}3\,\mu$, so that, from the range–energy relation for alpha particles in photographic emulsion, it can be seen that the minimum alpha-particle energy detectable by the scintillation counter, using a pulse amplification of 40, was 0·65 MeV.

Since the apparent end-point for water vapour was measured under the same conditions, the end-point value obtained must be the pressure required to reduce the energy of the alpha particles to 0·65 MeV in a 78·5 cm path. A point C was therefore added to the water vapour graph shown in figure 5, having coordinates $3{\cdot}48 \times 10^{18}$ mol cm^{-3} and $2{\cdot}3\,\mu$, which corresponded to the apparent pressure end-point and to the equivalent emulsion path length of the 0·65 MeV alpha particles respectively. The graph was extended to C and extrapolated to the axis, intercepting it at the molecular density value of $3{\cdot}58 \times 10^{18}$ cm^{-3}, and this value has been taken to represent complete absorption of the alpha particles under the given conditions. The extrapolation necessary was small and it would seem unlikely that it would give rise to an error greater than 2%.

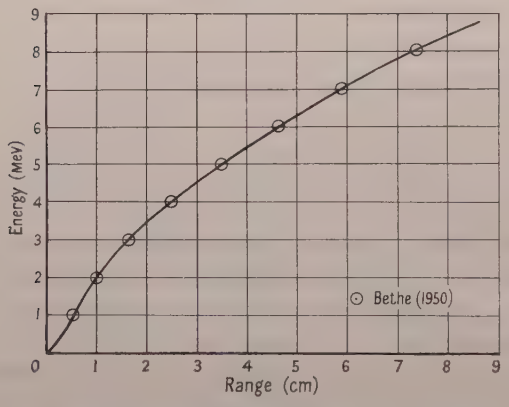

Figure 8. Range–energy relation for alpha particles in air at 15°c and 760 mm Hg pressure.

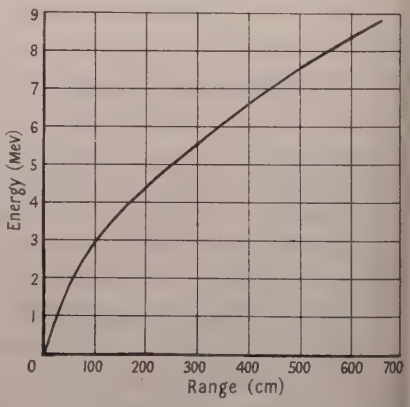

Figure 9. Range–energy relation for alpha particles in water vapour at 15°c and 12·79 mm Hg pressure.

From the results shown in figure 5, graphs were plotted of the molecular density of air and of water vapour against residual energy of the alpha particles after they have traversed a 78·5 cm path. Assuming that at any particular energy the rate of loss of energy by an alpha particle in water vapour is proportional to the molecular density, it follows that a molecular density of n molecules cm^{-3} in a path length of 78·5 cm, will give rise to the same reduction in alpha-particle energy as a molecular density of n' molecules cm^{-3} in a path length p cm, where $pn' = 78{\cdot}5n$. It is possible therefore to convert the information displayed in figure 5 into range–energy relations for alpha particles in air and in water vapour at any required pressure. The range–energy relation obtained for alpha particles in

air at 15°c and 76 cm Hg pressure is displayed in figure 8. The range–energy relation for alpha particles in water vapour under saturation conditions (12·79 mm Hg pressure) at 15°c is shown in figure 9.

§ 4. The Stopping Power of Water and Water Vapour Relative to Air

The differential and integral stopping powers of water s_w and S_w and of water vapour s_{wv} and S_{wv} relative to air at various alpha-particle energies have been deduced from the range–energy curves shown in figures 3, 8 and 9 and these are displayed in table 1. The differential stopping power values are obtained

Table 1. Differential and Integral Stopping Power Values for Water and Water Vapour at Various Alpha-Particle Energies

Energy (MeV)	s_w	s_{wv}	s_P	S_w	S_{wv}	S_P
8	1·48	1·53	1·47	1·33	1·57	1·47
7	1·44	1·54	1·47	1·31	1·59	1·47
6	1·41	1·50	1·48	1·30	1·62	1·47
5	1·38	1·53	1·50	1·29	1·66	1·47
4	1·36	1·52	1·55	1·24	1·76	1·46
$3\frac{1}{2}$	1·37	1·56	1·56	1·22	1·81	1·44
3	1·29	1·61	1·55	1·20	1·89	1·42
$2\frac{1}{2}$	1·18	1·63	1·50	1·20	1·99	1·40
2	1·06	1·66	1·40	1·22	2·08	1·39
$1\frac{1}{2}$	0·98	1·78	1·33	1·30	2·23	1·40

All stopping power values quoted are stopping powers per molecule of water or water vapour relative to that of one ' atom ' of air.

s_w and s_{wv} are the experimental differential stopping powers of water and water vapour respectively. S_w and S_{wv} are the experimental integral stopping powers of water and water vapour respectively. s_P and S_P are the differential and integral stopping power values for water as calculated by Platzman.

from the ratio of the slopes of the water or water vapour and air graphs at corresponding energy values. The errors in the differential stopping power values therefore arise solely from errors in constructing the best line through the experimental points in the initial graphs and in measuring the slopes of the derived range–energy curves at various energies. These errors are estimated not to exceed 2% at energies above 2 MeV, but may be greater at low energy since the differential stopping power is then very dependent upon the accuracy of the total range determinations. The main source of error in the integral stopping power values is considered to be the complete range determination for thorium C alpha particles in water and water vapour. The consequent error in S is estimated not to exceed 3% at an energy of 8 MeV, but increases in inverse proportion to the alpha-particle range. The values of the differential and integral stopping powers s_P and S_P as calculated by Platzman (1950), which are considered to apply to both water and water vapour, are also shown in table 1 for comparison. These values were calculated from atomic data for hydrogen and oxygen by modified application of the Bethe formula and the Bragg rule. It can be seen that the differential stopping power values for water do not agree with the calculated

values except at the highest energy. The calculated values are, however, likely to be in error at the lower energies owing to the lack of theoretical knowledge regarding the behaviour of alpha particles of low energy in an absorbing medium. The effect of capture and loss of electrons has been ignored in these calculations, and no consideration has been given to the possible effect on the stopping power of the polarization of the surrounding medium by the incident alpha particles; this is likely to be of significance in the case of liquid water but not in the case of water vapour.

The range in water of alpha particles of various energies obtained from the range–energy relation of figure 3 is seen to be greater than the range values that have previously been obtained. The differential stopping power value obtained by McInally (1956) is about 4% higher than that obtained from the present experiments over the same energy range. Other differential stopping power values differ more widely from the present experimental results.

The value of $1{\cdot}52 \pm 0{\cdot}03$ for the differential stopping power of water vapour at energies greater than 3·5 MeV would seem to be in agreement with the approximate value predicted by theory in its present form. The increase in stopping power at low alpha-particle energies may be due to increased energy transfer to the rotational and vibrational modes of the molecules. A further complication is added by the capture and loss of electrons which occurs when the velocity of the incident alpha particle is comparable with that of the orbital electrons. In addition, the contribution to the stopping power by the K electrons of oxygen and nitrogen is likely to be reduced appreciably by the screening of the outer electrons in the atoms as the alpha-particle energy decreases. These factors are all liable to produce a change in the stopping power of water vapour relative to air at low alpha-particle energies.

The lower values obtained for the differential stopping power of water in the liquid phase at low energies would appear to be due to polarization of the water by the incident alpha particles. Fermi (1940) states that, for incident alpha particles in the energy region at present under consideration, the decrease in rate of energy loss of the particles with distance travelled in an absorbing medium is given by

$$C_p = (2\pi n Z^2 e^4 \ln \epsilon)/mv^2$$

where m, e and n are the mass, charge and number per unit volume of the electrons in the absorbing medium, Ze is the charge on the alpha particle, v is the velocity of the alpha particle and ϵ is the dielectric constant of the medium concerned. By introducing appropriate values for the constants n, Z, e and m the value of C_p for alpha particles of velocity v in liquid water is given by

$$(4{\cdot}94 \times 10^{14} \ln \epsilon)/v^2 \text{ erg cm}^{-1}.$$

Hence for alpha particles of various energies the required correction to the rate of energy loss with distance C_p may be calculated provided that the appropriate value for the dielectric constant is known. When the action of electromagnetic radiation on water is considered, the appropriate value of ϵ varies with the frequency of the radiation from below 1 at very high frequencies to the static value of 81. The value of ϵ that is applicable to the field produced by a moving charged particle, however, is not immediately obvious, although it would be reasonable to assume that it depends on the velocity of the particle. In table 2 the value of C_p in terms of $\ln \epsilon$ is given for various alpha-particle energies. Values

for the rate of alpha-particle energy loss with distance, dE/dx in erg cm^{-1} obtained from the range–energy relation shown in figure 3, are also tabulated in table 2.

Table 2. Correction to Stopping Power Values for Liquid Water due to the Polarization Effect

(1)	(2)	(3)	(4)	(5)	(6)	(7)
2	0·98	5·1	2·1	24·4	57	10·5
3	1·20	3·4	1·8	19·0	28	4·4
4	1·39	2·56	1·5	17·1	9	1·7
5	1·55	2·05	1·3	15·8	11	2·0
6	1·70	1·71	1·2	14·2	6	1·5
7	1·84	1·46	1·1	13·3	7	1·7
8	1·96	1·28	1·0	12·0	3	1·3

(1) Particle energy (MeV); (2) v (10^9 cm sec^{-1}); (3) $C_p/\ln \epsilon$ (10^{-4} erg cm^{-1}); (4) dE/dx (10^{-3} erg cm^{-1}); (5) $C_p/\ln \epsilon$ as percentage of dE/dx; (6) C_{ex}; (7) ϵ.

Since the polarization correction for alpha particles in water vapour is negligible, the difference in the experimental values obtained for the stopping powers of water and water vapour is likely to be entirely due to the polarization effect in liquid water. The experimental difference in differential stopping power expressed as a percentage of the differential stopping power of water C_{ex} is shown in column (6) of table 2 and may be compared with the calculated correction C_p expressed as a percentage of dE/dx (as determined from figure 3), which is shown in column (5) in the same figure. In column (7) of table 2 the value of ϵ is quoted which, if used in the calculation of C_p, would make C_p equal to C_{ex} at each alpha-particle energy stated.

The required value of ϵ is seen to be $1{\cdot}6 \pm 0{\cdot}4$ for alpha particles of energy 4 MeV and above. At lower energies the value of ϵ rises to $10{\cdot}5 \pm 4{\cdot}0$ at 2 MeV. This may be explained as a dispersion effect, the impulsive action of the alpha particles of various energies being compared with that of electromagnetic waves of certain frequencies in the ultra-violet range. It is convenient to consider this by means of a model. For the present purpose each water molecule can be considered to consist of a number of electronic oscillators of known natural frequencies. An alpha particle passing such a molecule will distort the electronic field in such a way as to reduce the influence of the alpha particle upon neighbouring molecules. The electrons which will be influenced to the greatest extent and hence will make the greatest contribution to the polarization are those which are the most loosely bound in their constituent atoms, and these have a natural period of 3×10^{-16} second (Sternheimer 1952). If a passing alpha particle influences such oscillators for a time greater than $1{\cdot}5 \times 10^{-16}$ second, the resulting polarization will cause an appreciable reduction in the rate of ionization loss of the alpha particle. If the oscillators are influenced for a time less than $1{\cdot}5 \times 10^{-16}$ second, however, the electronic distortion will be diminished and will occur too late to produce an appreciable shielding effect. The time during which an oscillator is influenced by a passing alpha particle will depend upon the velocity v of the alpha particle and the distance x over which the alpha particle can be said to exert an appreciable influence. This time will be $2x/v$ for an oscillator which is close to the alpha-particle path and will diminish to zero for oscillators at a distance x from the alpha-particle path. It is necessary to postulate

a value for x in order to obtain an estimate of the velocity of the alpha particle below which the effect of polarization will become appreciable, and the value suggested is 10 Å. Although excitation probably takes place over a wider range than this, the proportion of the total alpha-particle energy lost by such distant interactions is likely to be small, and the effect of distortion of distant electronic fields upon the ionization loss will be negligible. Using this postulated value for the effective range of influence of an alpha particle it can be shown that the shielding due to polarization will be negligible for alpha-particle velocities greater than $1{\cdot}33 \times 10^9$ cm sec^{-1} (energy 3·3 MeV). For 3 MeV and 2 MeV alpha particles, effective polarization will occur for oscillators which are within 4 Å and 6·6 Å respectively of the alpha-particle path.

§ 5. Conclusion

Range–energy relations have been obtained experimentally for alpha particles at energies below 8·78 MeV in water and water vapour, and from these the stopping power of water and water vapour for alpha particles is shown to be the same at high energies. At low energies, however, the stopping power of water vapour is shown to increase, while that of liquid water decreases. It is suggested that the polarization of water due to the moving field of the alpha particles in the particular energy range considered is complicated by dispersion, and that this accounts for the decrease in stopping power observed at low alpha-particle energies.

References

Aniansson, G., 1955, *Phys. Rev.*, **98,** 300.
Appleyard, R. K., 1951, *Proc. Camb. Phil. Soc.*, **47,** 443.
Bethe, H. A., 1950, *Rev. Mod. Phys.*, **22,** 213.
de Carvalho, H. G., and Yagoda, H., 1952, *Phys. Rev.*, **88,** 273.
Ellis, R. H., Rossi, H. H., and Failla, G., 1955, *Phys. Rev.*, **97,** 1043.
Fermi, E., 1940, *Phys. Rev.*, **57,** 485.
Gray, L. H., 1944, *Proc. Camb. Phil. Soc.*, **40,** 72.
McInally, M., 1956, *Proc. Roy. Soc.* A, **237,** 28.
Michl, W., 1914, *S.B. Akad. Wiss. Wien, Math naturw. Kl. Abt.*, 2A, **123,** 1965.
Philipp, K., 1923, *Z. Phys.*, **17,** 23.
Platzman, R. L., 1950, *Symposium on Radiobiology* (London: Chapman & Hall), p. 153.
Rotblat, J., 1951, *Nature, Lond.*, **167,** 550.
Sternheimer, R. M., 1952, *Phys. Rev.*, **88,** 851.

The Magnetic Susceptibility of Bismuth Telluride

By R. MANSFIELD
Department of Physics, Bedford College, London, N.W.1

MS. received 26th March 1959, in revised form 25th June 1959

Abstract. Measurements of the susceptibility of Bi_2Te_3 over the temperature range 100°K to 600°K, with magnetic field parallel ($\chi_{\parallel}$) and perpendicular ($\chi_{\perp}$) to the c axis, are reported. Bi_2Te_3 is diamagnetic and $\chi_{\parallel}$ has the larger algebraic value.

The contributions to the susceptibility from the core and valence electrons, free carriers and impurities are discussed, and it is suggested that the effect of the impurities is negligible, the free carriers give rise to a paramagnetic contribution and the main contribution is from the core and valence electrons.

§ 1. Introduction

The electrical properties of bismuth telluride have been the subject of many recent papers. The transport phenomena have been measured and attempts have been made to explain the results. In particular magneto-resistance measurements have been used to investigate the band structure of Bi_2Te_3 (Drabble, Groves and Wolfe 1958). For a more complete study, measurements of cyclotron resonance would be very desirable. However, it is doubtful if such measurements on Bi_2Te_3 are possible since it is unlikely that specimens having sufficiently low concentrations of charge carriers can be prepared. In the case of germanium, measurements on the magnetic susceptibility have proved useful in the determination of the parameters of the charge carriers and it was considered that similar measurements on bismuth telluride might yield further information on its band structure.

§ 2. Experimental Procedure

Bismuth telluride is anisotropic having a layer type lattice. It is diamagnetic and the susceptibility is also anisotropic. It is therefore possible to measure the susceptibility using the method developed by Krishnan and Banerjee (1935). If a crystal is placed in a uniform magnetic field with c axis horizontal or cleavage planes vertical a couple G acts on it which is given by the formula

$$G = \tfrac{1}{2}(\chi_{\perp} - \chi_{\parallel}) \sin 2\phi \,.\, H^2 m$$

where ϕ = angle between the cleavage planes and the magnetic field H, m = mass of specimen, and $\chi_{\perp}$ and $\chi_{\parallel}$ are the mass susceptibilities with magnetic field perpendicular and parallel to the c axis.

The couple acting on the crystal is a maximum when $\phi = 45°$ and can be measured by suspending the crystal from a quartz fibre. The procedure is to set the torsion head so that initially $\phi = 0$, that is application of the magnetic field causes no rotation of the crystal. The angle through which the torsion head has to be rotated in order to twist the specimen through an angle of 45° is then

measured for a known magnetic field. This angle can be accurately measured since the specimen becomes unstable and flips round when rotated through 45°. The quartz fibre can be chosen such that the torsion head is rotated through several revolutions.

In order to obtain the individual susceptibilities it is now only necessary to measure the ratio $\chi_\perp/\chi_{\parallel}$. This can be determined by suspending the crystal in a non-uniform magnetic field and measuring the ratio of the forces exerted on the specimen when it is rotated through 90°. The balance described by McGuire and Lane (1949) was used. The magnetic force was balanced by the force between a double coil mounted on the balance arm and a fixed coil, the balance arm being supported by a torsion strip. The electric currents flowing through the coils were measured by a vernier potentiometer and the product of the currents was proportional to the force on the specimen. Four measurements were made by reversing the magnetic field and the currents flowing through the coils. The balance and specimen were contained in a vessel which could be evacuated.

The two methods give $\chi_\perp - \chi_{\parallel}$ and $\chi_\perp/\chi_{\parallel}$ and observations, say, at room temperature enable the individual values of $\chi_\perp$ and $\chi_{\parallel}$ to be calculated. To determine the variation of $\chi_\perp$ and $\chi_{\parallel}$ with temperature it was only necessary to use the balance. However as a check, values of $\chi_\perp - \chi_{\parallel}$ were determined over the temperature range using the quartz fibre method and compared with values of $\chi_\perp - \chi_{\parallel}$ deduced from the other method. The agreement between the two methods was satisfactory.

The magnetic field was produced by an electromagnet designed for experiments on magnetic resonance and consequently had a field which was uniform over a considerable volume. The field was determined using the Hall effect of a specimen of indium antimonide. This specimen had previously been calibrated using the proton resonance method. Temperatures were measured using T_1–T_2 thermocouples. Preliminary measurements of $\chi_\perp - \chi_{\parallel}$ on each specimen for different magnetic fields showed no indication of ferromagnetic impurities. Measurements were made on two p-type specimens R 5 and R 8. The electrical properties of these specimens had been measured and are described by Mansfield and Williams (1958). Measurements were also made on an n-type specimen R 9·1. The properties of material adjacent to this specimen in the original ingot have been measured by Williams (1959).

The error likely in the values of the susceptibility at room temperature depends on the accumulation of errors of both methods and is estimated to be 2%. The susceptibility at different temperatures relative to the room temperature values can, however, be determined more accurately.

§ 3. Discussion

The variation of the susceptibilities $\chi_\perp$ and $\chi_{\parallel}$ with temperature is shown in the figure. Values of the Hall constant for the different specimens at 90°K are also given. For an account of the transport properties of these specimens reference should be made to Mansfield and Williams (1958) and Williams (1959).

Matyas (1958) has recently determined the susceptibilities of several V–VI compounds and finds for a polycrystalline specimen of p-type Bi_2Te_3 a mass susceptibility of $-0{\cdot}402 \times 10^{-6}$ which is independent of the temperature. This value is closer to $\chi_\perp$ than the average susceptibility obtained in this investigation.

Matyas analyses his results assuming these compounds to be essentially ionic and the contribution to the susceptibility of the free carriers and impurity centres to be negligible. He shows that the susceptibility is proportional to the number

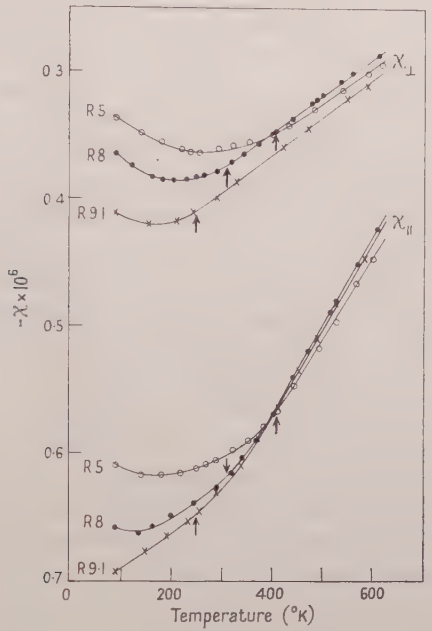

Mass susceptibility of bismuth telluride. Hall coefficients of specimens R 5, R 8 and R 9·1 at 90°K are +0·2, +0·9 and −1·7 cm^3 $coul^{-1}$ respectively.

of electrons per molecule Z (the values of Z for Bi_2Se_3 and Bi_2Te_3 are given incorrectly and should be 268 and 322 respectively). Such an analysis is useful for discussing the order of magnitude of the susceptibility but cannot explain the anisotropy or temperature variation.

It was assumed initially that the anisotropy of the susceptibility was due to the free carriers which take part in the transport phenomena and that their contribution could be calculated using the Landau–Peierls formula, the effective masses of the carriers being anisotropic. The following discussion shows, however, that this is not the case.

The measured susceptibility is composed of a number of contributions, χ_L due to core and valence electrons, χ_C due to free carriers and χ_I due to the impurity centres. Reasons will be given later to show that χ_I is negligible and it is only necessary to consider χ_L and χ_C. Now the concentration of charge carriers, and consequently χ_C, varies both with impurity content and with temperature. At a given low temperature the susceptibility decreases in magnitude as the concentration of carriers increases, indicating that the free carriers give rise to a paramagnetic contribution. Because of this it is suggestive to attribute the high temperature linear decrease of the susceptibility to the free carriers, since their concentration increases due to excitation of electrons from the valence band to the conduction band.

This explanation, however, is not adequate. By analysing the variation of electrical conductivity with temperature, it is possible to determine the

temperature when the concentration of intrinsic carriers is comparable with the extrinsic carriers. Writing the electrical conductivity as $\sigma = \sigma_i + \sigma_s$ with σ_i and σ_s the contributions due to intrinsic and extrinsic carriers, then the temperatures at which σ_i/σ_s is 10% have been determined for each of the specimens and are shown on the figure by arrows. For temperatures below those indicated by the arrows, the concentration of carriers is constant, while above these temperatures the concentration increases. This increase is relatively slow because the energy gap between valence and conduction bands is small. Now a comparison of the results for the two p-type specimens R 5 and R 8 indicates firstly that, over the temperature range where the concentration of carriers is constant, the difference in susceptibilities of R 5 and R 8 decreases, that is the contribution of the free carriers decreases as the temperature increases. Secondly, in the high temperature range where there is an appreciable temperature variation of susceptibility, a large temperature change is required to alter the concentration of carriers by an amount comparable to the difference of concentration of carriers in R 5 and R 8. Thus the concentration of extrinsic holes in specimen R 5 is three times the concentration of extrinsic holes in R 8. In order to increase the concentration of holes in R 8 by a factor three it is necessary to increase the temperature to 500°K. The change in susceptibility of R 8 as the temperature is increased from 300°K to 500°K is several times larger than the difference in susceptibilities of R 5 and R 8 at 300°K. (It is unlikely that this change is due to the contribution of the electrons produced when the temperature is increased.)

It would appear therefore that the linear decrease in susceptibility at high temperatures is not primarily due to a temperature dependent contribution of the carriers, but due to the core and valence contribution χ_L. A temperature dependence of the susceptibility χ_L of germanium has been observed and Krumhansl and Brooks (1956) have attributed this effect to a Van Vleck paramagnetic term. Because of the small energy gap such a term would be considerably larger in Bi_2Te_3 and would be temperature dependent, since the energy gap varies with temperature. However, it must be noted that the rate of variation of susceptibility is much larger in Bi_2Te_3 than in germanium.

The contribution due to the free carriers, given by the difference in susceptibilities of the different specimens at low temperatures, is much larger than the contribution predicted by the Landau–Peierls formula. Thus the maximum paramagnetic effect given by this formula is $n\mu_0^2/\rho \boldsymbol{k} T$ (μ_0 = Bohr magneton, ρ = density, n = concentration of free carriers). The effect of degeneracy and orbital motion of the free carriers would reduce this quantity. Using values of n given by the Hall constant, this expression gives a contribution which is negligibly small compared with the observed difference in susceptibilities of specimens R 5 and R 8.

This qualitative discussion shows that the main diamagnetic contribution to the susceptibility is from the core and valence electrons and indicates that the valence electrons must exhibit a large Langevin type diamagnetism, the electron configuration being anisotropic. Bismuth telluride has a layer type lattice and similar anisotropy of susceptibility has been observed in other materials with this type of lattice.

The reasons for assuming χ_I is negligible must now be considered. This contribution arises from both the ionized and un-ionized impurities; however it is usual to assume that the effect of the ionized impurities is negligible,

especially if they are substitutional impurities. A combination of bismuth and tellurium in the proportion 2 : 3 gives p-type specimens having properties similar to R 5. In order to reduce the concentration of holes or to produce n-type specimens, the starting material is doped with donors, iodine was used in the case of R 8 and R 9·1. The electrical properties show that the concentration of carriers is constant in the extrinsic range, suggesting that the activation energy of the impurity centres is zero or very small. Hence specimen R 5 contains acceptors which are all ionized, R 8 contains donors and acceptors, the former are ionized and a number of acceptors, having the same concentration as donors, are un-ionized. In specimen R 9·1 all the acceptors are compensated and the donors are ionized. It is expected therefore that χ_I will be negligible in the case of specimen R 5, which has all its acceptors ionized, and will be larger for R 8 and R 9·1. The reverse happens in the case of the free carrier contribution χ_C, since the concentration of carriers increases from R 9·1 to R 5. If, therefore, χ_I is responsible for the difference in susceptibility of R 5 and R 8, this contribution must be diamagnetic; if, on the other hand, χ_C is responsible, it must be a paramagnetic contribution. There are two factors which suggest that χ_I is not responsible; firstly, the diamagnetic term for this effect is independent of temperature and one would expect the difference in susceptibilities of the specimens to persist at higher temperatures, whereas the difference decreases until the curves tend to a common intrinsic curve; secondly, the linear dependence of the susceptibility, which appears to be an intrinsic effect, extends to lower temperatures in R 9·1 than R 5, indicating that the impurity contribution is least in R 9·1. This would be the case if the carriers produced by the impurities are responsible for the difference in susceptibilities.

Finally, it should be pointed out that although it has been suggested that the free carriers, in particular the free holes, give rise to a paramagnetic contribution, it is possible that there is a group of electrons having a large diamagnetic effect which is reduced when these electrons are trapped at acceptors or excited to the conduction band to produce the holes.

References

Drabble, J. R., 1958, *Proc. Phys. Soc.*, **72,** 380.
Drabble, J. R., Groves, R. D., and Wolfe, R., 1958, *Proc. Phys. Soc.*, **71,** 430.
Krishnan, K. S., and Banerjee, S., 1935, *Phil. Trans.* A, **234,** 265.
Krumhansl, J. A., and Brooks, H., 1956, *Bull. Amer. Phys. Soc.*, **1,** 117.
McGuire, T. R., and Lane, C. T., 1949, *Rev. Sci. Instrum.*, **20,** 489.
Mansfield, R., and Williams, W., 1958, *Proc. Phys. Soc.*, **72,** 733.
Matyas, M., 1958, *Czech. J. Phys.*, **8,** 309.
Williams, W., 1959, *Proc. Phys. Soc.*, **73,** 739.

An Analysis of the Soft X-ray Emission Spectroscopy of Graphite and an Appropriate Electronic Picture of it†

By A. K. DUTTA
Indian Association for the Cultivation of Science, Calcutta, India

MS. received 7th January 1959, in final form 30th May 1959

Abstract. From an analysis of the soft x-ray emission spectra of graphite, it is deduced that the fundamental Brillouin zone of graphite is bounded by two independent sets of planes, the electrons overlapping one such set into the next zone, and that the total band width is about $24(\pm 3)$ ev. On comparing these results with the properties of the three Brillouin zones which have been suggested for graphite, namely the 1-, 3- and 4-electron zones, the last is found to be the most suitable. It is also shown that the K-value for the vertical bounding planes of the four-electron zone corresponds to the energy difference between the origin and the first peak of the soft x-ray spectra, and that there is sufficient σ–π interaction in the C–C bond formation to make the four-electron zone plausible.

§ 1. Introduction

The Brillouin zone of graphite has been investigated theoretically by many authors (Wilson 1954, Johnston 1955, 1956, Lomer 1955, Nozières 1958, McClure 1957, Slonczewski and Weiss 1958) during the last few years, and it has been found to have the shape of a flat hexagonal prism, the energy surfaces normally overlapping into the next zone across the vertical zone boundaries. It is therefore interesting to see how far the results of the soft x-ray emission spectroscopy (which, as is well known, can furnish reasonable ideas regarding the band structure of a solid) are in conformity with the above theoretical findings, and also to determine the number of electrons per carbon atom which can just be accommodated in the fundamental zone. The present publication gives an account of these discussions.

§ 2. Interpretation of the Soft X-ray Emission Spectra of Graphite and Discussion of a Suitable Brillouin Zone for it

The soft x-ray emission spectrum of graphite has been obtained by Skinner (1940) and others (Siegbahn and Magnusson 1935, Magnusson 1938, Chalklin 1948). Since the work of Skinner is of a more detailed nature than that of the others, we shall utilize his observations only. He has given a curve for graphite showing the variation of the density of states $N(E)$ with energy, obtained from soft x-ray emission spectroscopy, which is reproduced here ($N(E) \propto I(E)/\nu^3$). It will be seen from the diagram that as the energy increases $N(E)$ also increases, reaches a maximum at about 17 ev, then decreases, shows a kink at about 21 ev, rises again, exhibits a peak at about 22 ev and finally diminishes rather sharply, the

† A preliminary account of this has been published in the Report of the Symposium on Magnetism held in 1954 in Calcutta and published by the Indian Association for the Cultivation of Science, Calcutta-32.

absorption edge lying at about 24 ev in the lower part of this steep portion of the falling curve†. Now according to the usual methods of interpreting soft x-ray emission spectra (Skinner 1940, Wilson 1954), the behaviour is identical with that of a semi-metal, the first peak representing the touching by the energy surfaces of one set of bounding planes of the Brillouin zone. In view of the kink observed these boundary planes have evidently been overlapped, while the second peak presumably indicates the contiguity of the energy surfaces to another set of boundary planes and it also determines the maximum energy up to which the levels are normally filled. Thus the total band width of graphite can be taken to be 24 ± 3 ev.

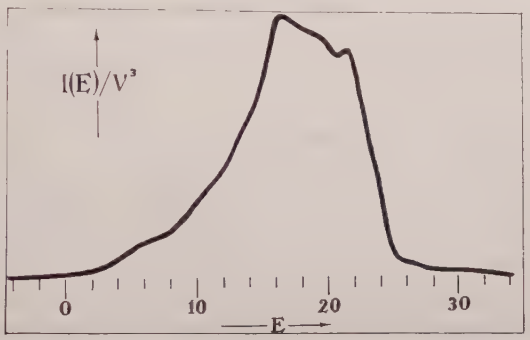

Intensity distribution of the soft x-ray emission spectra of graphite. $I(E)$ = intensity in numbers of quanta per second of radiation in the emitted band in the unit range of quantum energy, ν = absolute energy of transition, E = energy in electron volts (± 3).

From the table, which gives some details of the three Brillouin zones of graphite which have been proposed from time to time (Wilson 1936, Mott and Jones 1936, Ganguli and Krishnan 1941, Wallace 1947, for other references, see § 1), it is evident that the Fermi energy calculated according to the simple Sommerfeld formula taking all the four valency electrons of carbon in graphite into consideration is 22 ev and the total band width as obtained from x-ray emission spectra has

Details of the Different Brillouin Zones suggested for Graphite

(1)	(2)	(3)	(4)	(5)	(6)
One	Flat hexagonal prism	(1 $\bar{1}$ 0, 0) (0 0 0, 2)	1 4	1·47 0·92	8·4
Three	Flat hexagonal prism	(2 $\bar{1}$ $\bar{1}$, 0) (0 0 0, 2)	4 4	2·55 0·92	17·6
Four	Flat hexagonal prism	(2 2 0, 0) (0 0 0, 2)	1 4	2·95 0·92	22

(1) No. of electrons just accommodated in the volumes of the different Brillouin zones in K-space; (2) shape of the Brillouin zone; (3) bounding planes; (4) structure factors for the bounding planes; (5) value of K, the wave vector for the bounding planes (10^8 cm^{-1}); (6) Fermi energy calculated according to the simple Sommerfeld formula (ev).

† The high energy tailing effects have, however, been neglected in these discussions.

nearly the same value (24 ± 3 ev). It is also evident that since the energy discontinuities, which are proportional to the structure factors for the planes, are very low across the $(2\bar{2}0, 0)$ planes—much lower than those across the (000, 2) planes—normal overlapping will probably take place across the former set of planes. Thus we may safely conclude that the four-electron Brillouin zone is the proper one for graphite, the vertical boundary planes, i.e. the $(2\bar{2}0, 0)$ planes, being overlapped, and it is evident that there is a large anisotropy in the energy surfaces. But before finally accepting this conclusion, a few points involved in doing so need careful consideration.

§ 3. Evaluation of K for the Set of Planes Overlapped

According to its definition, $N(E)$, the density of states per unit volume, is given by

$$N(E) = \frac{1}{8\pi^3} \int\int \frac{dS}{|\text{grad } E|}, \qquad \ldots\ldots(1)$$

where the integration is over the entire constant energy surface in K-space. Now in the particular case of graphite, in view of its highly anisotropic structure it will be sufficient to assume that the energy surfaces are approximately cylindrical, and we need only consider the energy distribution in the basal plane. Therefore, instead of considering equi-energy surfaces we have to consider equi-energy curves, which in this case are approximately circular. Now if we assume that the energy distribution is similar in all such parallel basal planes, the density of states per unit volume of the crystal will evidently be the same as the density in any particular plane. In consequence the equation (1) may be represented as

$$N(E) = \frac{1}{8\pi^3} \frac{1}{|dE/dK|} \int dl, \qquad \ldots\ldots(2)$$

where dl is any element of the circular energy contour, the integration being, as before, over the entire constant energy curve, and where grad E is constant for a circle and is equal to $|dE/dK|$.

Now experimentally from a study of the soft x-ray emission spectrum of graphite we obtain for energies ranging from 0 to about 17 ev, i.e. up to the first peak (see figure)†,

$$N(E) = 1{\cdot}4P\,e^{0{\cdot}2E}, \qquad \ldots\ldots(3)$$

where P is some unknown constant of proportionality between the actual $N(E)$ values and the values expressed in some arbitrary units as obtained from the soft x-ray spectra, and where E is the energy in electron volts.

Again, we know that the electronic specific heat C_v is given by the relation (Mott and Jones 1936)

$$C_v = \tfrac{2}{3}\pi^2 k^2 T N(E)_0 A/\rho \qquad \ldots\ldots(4)$$

per gramme atom, where $N(E_0)$ is the energy density per unit volume on the Fermi surface, ρ is the density and A the atomic mass, the other symbols having their usual significance. From a measurement of the specific heat of graphite at very low temperatures, De Sorbo (1955) obtained the electronic component of specific heat as

$$C_v = 1{\cdot}1 \times 10^{-5} T \qquad \ldots\ldots(5)$$

per gramme atom. Therefore, in view of the relations (2) and (4) and the data (3) and (5) and taking as already stated the band width of graphite to be about

† Such an exponential variation has also been indicated by Chalklin (1948).

24 ev, the value of K for the planes overlapped is found to be about $3 \times 10^8\,\mathrm{cm}^{-1}$. From the table above we find that K for $(2\bar{2}0,\ 0)$ planes is $2{\cdot}95 \times 10^8\,\mathrm{cm}^{-1}$. In consequence, it may now be stated that the first peak represents the touching by the Fermi surface of the $(2\bar{2}0,\ 0)$ planes, which have, as already shown, been overlapped. Thus, the result obtained from a simple analysis of the soft x-ray spectra, namely that the four-electron Brillouin zone of graphite is the appropriate one, is further corroborated by this necessary test.

§ 4. Possibility of σ–π Interaction in the C–C Bond Formation in Graphite

The earliest idea regarding the inter-carbon bond formation in graphite was that the 3σ electrons are involved in direct planar bond formation with the three neighbouring carbon atoms. The remaining one electron, namely the π-electron, was supposed to move freely over the entire lattice while remaining completely distinct and separate even though it might be involved in some form of C–C bond formation. Thus the π-electron was considered to be solely responsible for all the electronic properties of graphite, the σ-electrons being considered ineffective for such purposes. In consequence the one-electron Brillouin zone would become inevitable for graphite, which as we have seen appears contradictory to the soft x-ray data. To escape this difficulty the simplest way appears to be to assume some form of admixture and interaction between the electrons, which amounts to the acceptance of a four-electron zone.

Looking at the actual bond formation in graphite, one finds that whatever bonds exist are all located in the basal plane only, and that the bond distance is much shorter than the single bond C–C distance, thereby accounting for the enhanced bond energy and stability of graphite. It is therefore evident that the π-electrons are affecting in some way the bond formation by the σ-electrons. Now it has been shown by Coulson *et al.* (1951, 1952), Altmann (1952) and others (e.g. March 1952) that there is no rigorous division into π- and σ-electrons, and that the one merges into the distribution of the other, possibly with some amount of interaction. Pariser (1953) characterized the assumption of the energy of the σ-electrons remaining constant and independent of the charge distribution of the π-electrons as undoubtedly unrealistic, and he has shown how by considering the effect of the σ-electrons on the π-electron distribution better results could be obtained. Finally, quite recently, Niira (1952), Davies (1955), Haugh and Hirschfelder (1955) have proved the existence of a sufficient amount of σ–π interaction in such cases. Thus the adoption of the four-electron Brillouin zone may safely be said to be well justified from the consideration of the presence of σ–π interaction also.

§ 5. Concluding Remarks

It is thus proved that the four-electron Brillouin zone is the proper one for graphite, and that the peculiar properties of graphite are as already indicated by theoretical workers (see § 1) due to electrons overlapping from this zone across the vertical zone boundaries. That this overlapping is a normal one and not thermally effected is proved theoretically by McClure and others (see § 1) and also by the fact that graphite has a positive temperature coefficient of resistance (Dutta 1953). It must, however, be borne in mind that the possibility of thermal overlapping cannot altogether be ruled out; but if it exists at all it must always be masked by the

more pronounced normal overlapping. It is needless to point out here that although electrons have been held mainly responsible for the various properties of graphite yet the positive holes created in the full zone due to overlapping of electrons, as shown by McClure and others (see § 1), also play an important part.

Acknowledgments

In conclusion, the author wishes to express his sincere thanks to Professor A. Bose for his kind interest in the work and to the referees for helpful suggestions.

References

Altmann, S. L., 1952, *Proc. Roy. Soc.* A, **210**, 327, 343.
Chalklin, F. C., 1948, *Proc. Roy. Soc.* A, **194**, 42.
Coulson, C. A., Higgs, P. W., and March, N. H., 1951, *Nature, Lond.*, **160**, 1039.
Coulson, C. A., Higgs, P. W., and Taylor, R., 1952, *Proc. Phys. Soc.* A, **65**, 815.
Davies, P. L., 1955, Dissertation for doctorate degree, King's College, London. (Quoted in Haugh and Hirschfelder's paper.)
De Sorbo, W., 1955, *J. Chem. Phys.*, **23**, 1970.
Dutta, A. K., 1953, *Phys. Rev.*, **90**, 187.
Ganguli, N., and Krishnan, K. S., 1941, *Proc. Roy. Soc.* A, **177**, 530.
Haugh, E. F., and Hirschfelder, J. O., 1955, *J. Chem. Phys.*, **23**, 1778.
Johnston, D. F., 1955, *Proc. Roy. Soc.* A, **227**, 349.
—— 1956, *Ibid.*, **237**, 48.
Lomer, W. M., 1955, *Proc. Roy. Soc.* A, **227**, 330.
Magnusson, T., *Nova Acta Soc. Sci. Uppsal.*, **11**, No. 3.
March, N. F., 1952, *Acta Cryst., Camb.*, **5**, 187.
McClure, J. W., 1957, *Phys. Rev.*, **108**, 612.
Mott, N. F., and Jones, H., 1936, *The Theory of Properties of Metals and Alloys* (Oxford: University Press), p. 179.
Niira, K., 1952, *J. Chem. Phys.*, **20**, 1498.
Nozières, P. P., 1958, *Phys. Rev.*, **109**, 1510.
Pariser, R., 1953, *J. Chem. Phys.*, **21**, 568.
Pariser, R., and Parr, R. G., 1953, *J. Chem. Phys.*, **21**, 767.
Siegbahn, M., and Magnusson, T., 1935, *Z. Phys.*, **96**, 1.
Skinner, H. W. B., 1940, *Phil. Trans. Roy. Soc.* A, **279**, 95.
Slonczewski, J. C., and Weiss, P. R., 1958, *Phys. Rev.*, **109**, 272.
Wallace, P., 1947, *Phys. Rev.*, **71**, 622.
Wilson, A. H., 1936, *Theory of Metals* (Cambridge: University Press), p. 88.
—— 1954, *Ibid.*, 91.

The Measurement of the Lattice Expansions and Debye Temperatures of Titanium and Silver by X-ray Methods

By J. SPREADBOROUGH† and J. W. CHRISTIAN‡

†Battelle Memorial Institute, Geneva

‡Department of Metallurgy, The University Museum, Oxford

MS. received 7th May 1959, *in final form* 15*th June* 1959

Abstract. A high temperature diffractometer has been used to determine the lattice spacing–temperature relations for both α- and β-titanium. For α-titanium, the mean coefficients of thermal expansion over the temperature range 0–600°C are $9{\cdot}55\times10^{-6}\,\mathrm{deg}^{-1}$ for the a spacing, and $10{\cdot}65\times10^{-6}\,\mathrm{deg}^{-1}$ for the c spacing; for β-titanium, the mean expansion coefficient over the temperature range 900–1070°C is about $12{\cdot}0\times10^{-6}\,\mathrm{deg}^{-1}$. The temperature variation of the (peak) intensities of diffracted powder lines for silver is in agreement with Debye–Waller theory, after applying a correction due to Paskin, and corresponds to a Debye temperature of 197°K. Corresponding results for α-titanium indicate that the Debye temperature is about 270° ± 30°K. Analysis of the line shapes of cold-worked titanium indicates an appreciable density of basal plane stacking fault.

§ 1. Introduction and Lattice Spacing Measurements

This work is a preliminary investigation into the determination of Debye temperatures by measurements of x-ray intensity in a high temperature diffractometer. Such measurements are of especial interest in metals such as iron and manganese which have more than one stable structure, since they assist in the division of the enthalpy and entropy into lattice, magnetic and electronic terms. Silver was chosen as a typical example of a well-behaved cubic metal, having a known lattice spacing–temperature relation. Titanium was used as a more severe test of the performance of the instrument, but an important secondary purpose was to determine the lattice spacing–temperature relations of this metal more accurately. The predictions of some of the current theories of martensite crystallography depend rather critically on the parameters of the two phases at the transition temperature.

The high temperature diffractometer has been described elsewhere (Spreadborough and Christian 1959), and the lattice spacings of silver at temperatures up to 850°C were in very good agreement with accepted values. Some difficulties were experienced in preventing surface contamination of titanium, and experiments were made with both powder specimens and solid specimens machined to the shape of the specimen holder; good quality iodide titanium was used throughout. Despite many precautions, and very low pressures, the powder specimens were found to contaminate appreciably in the temperature range 700–900°C, and in one such specimen the hexagonal form was retained up to 960°C. The impurities, presumably nitrogen and oxygen, produced some line broadening; the a and c parameters increased slightly, and c/a increased considerably. The change in c/a between 700° and 900° is especially evident

for powder specimen 2 in table 1. The solid specimens did not seem to be affected at all after heating in the α range, but some slight contamination was apparent after experiments at up to 1100°c in the β region. This impurity had no measurable effect on line sharpness, and the surface appeared clean and bright, but there were changes in the parameters at room temperature, and the hardness had increased slightly. After one set of exposures entirely in the α range, the mean hardness was 85 V.P.N. Another sample used for exposures in the β region had an initial hardness of 102 V.P.N. and a final hardness of 190 V.P.N. Both this hardness increase and the lattice spacing changes shown in table 1 are consistent with about 0·2–0·5 wt. % nitrogen plus oxygen in the surface layers.

The main results on the α and β parameters are shown in tables 1 and 2. Lattice spacings were determined by a standard extrapolation procedure, and

Table 1. Lattice Parameter Results for α-Titanium

Treatment	a (kx)	c (kx)	c/a	Temp. of meast (°c)	Vol atom^{-1} (kx^3)
Solid No. 1					
cold worked	2·9447	4·670(3)	1·586(0)	22	17·53(5)
ann. at 600°c	2·9610	4·699(1)	1·587(0)	600 ± 2	17·84(0)
down to 400°c	2·9554	4·689(3)	1·586(7)	406 ± 3	17·73(5)
Powder No. 1					
heated to 600°c	2·9589	4·695(8)	1·587	601 ± 2	—
Powder No. 2					
rough values	2·956(5)	—	1·587	500 ± 5	—
heated to 600°c	2·9586	—	1·587(0)	597 ± 1	—
heated to 700°c	2·9616	—	1·587(2)	703 ± 2	—
heated to 965°c	3·01(0)	—	1·60(0)	965 ± 5	—
Solid No. 3					
ann. at 600°c	2·9435	4·671(3)	1·587	9	17·52(5)
heated to 950°c	2·9440	4·678(0)	1·589	9	17·55(6)
heated to 374°c	2·9554	4·693(2)	1·588	374 ± 2	17·75(6)
heated to 581°c	2·9608	4·704(7)	1·589	581 ± 3	17·85(8)
heated to 699°c	2·9646	4·713(4)	1·590	699 ± 1	17·93(7)
after measuring β, back to room temp.	2·9445	4·684(7)	1·591	9	17·58(7)

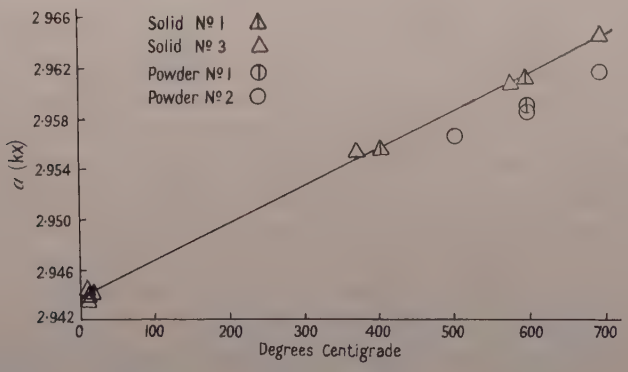

Figure 1. Variation of a parameter with temperature for α–titanium.

the accuracy of the measurements is estimated to be within $\pm 0{\cdot}0005$ kx for a and $\pm 0{\cdot}001$ kx for c. Figure 1 shows the temperature variation of the a parameter of the α phase, and figure 2 the parameter of the β phase. It is rather surprising that in the α phase, the powder results are a little below those of the solid specimens, since oxygen and nitrogen increase the parameter slightly. As already noted, the higher temperature results refer to slightly impure specimens, but it is believed that they are more accurate than any previous determinations. The mean coefficients of expansion of the α phase over the range 0–600°c were

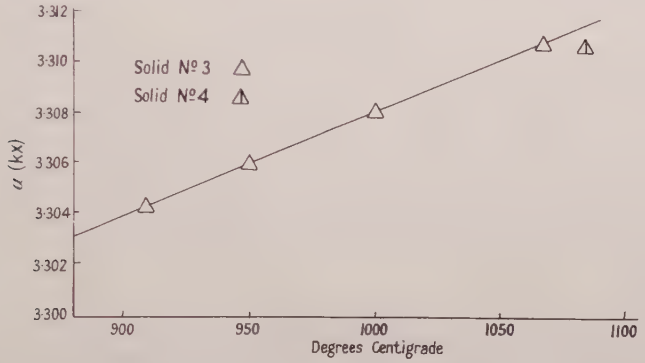

Figure 2. Variation of lattice parameter of β-titanium with temperature.

Table 2. Lattice Parameter Results for β-Titanium

Specimen	a (kx)	Temp. of meast (°c)	Atomic volume
	3·3107	1067 ± 3	18·14(4)
Solid No. 3	3·3082	1000 ± 2	18·10(3)
	3·3062	951 ± 1	18·07(0)
	3·3044	908 ± 1	18·04(0)
Solid No. 4	3·3107	1084 ± 2	18·14(4)

$9{\cdot}55 \pm 0{\cdot}5 \times 10^{-6}\,\mathrm{deg}^{-1}$ for the a parameter and $10{\cdot}65 \pm 0{\cdot}7 \times 10^{-6}\,\mathrm{deg}^{-1}$ for the c parameter; the expansion coefficients do not vary with temperature to within the experimental error. These values are about 15 and 25% respectively lower than the expansion coefficients given by Berry and Raynor (1953) from x-ray measurements, but they support the conclusion of Berry and Raynor that c/a increases with temperature; some results of Brocklehurst, quoted by McHargue and Hammond (1953), indicated the opposite result. The coefficient of expansion of the β phase in the range 900–1070°c is about $12 \times 10^{-6}\,\mathrm{deg}^{-1}$, and the extrapolated room temperature parameter of β-titanium (3·272 kx) is in reasonable agreement with that obtained by extrapolating parameter values from retained β phase titanium alloys ($3{\cdot}276 \pm 0{\cdot}003$ kx) (Levinger 1953). The change of volume associated with the α–β transition is very small, and is estimated to be between $-0{\cdot}15\%$ and $-0{\cdot}30\%$.

§ 2. Temperature Variation of Diffracted Intensity for Silver

If it is assumed that there is a single Debye characteristic temperature Θ which does not vary with temperature, and if the variation of Bragg angle with

temperature due to lattice expansion is neglected, the Debye–Waller theory leads to an expression

$$\frac{\lambda^2}{\sin^2\theta}\ln\left(\frac{\rho_T}{\rho_1}\right)=\frac{12\,h^2}{mk\,\Theta^2}\left\{T_1\phi\left(\frac{\Theta}{T_1}\right)-T\phi\left(\frac{\Theta}{T}\right)\right\} \qquad \ldots\ldots(1)$$

where ρ_1, ρ_T are the integrated intensities of a Bragg reflection at temperatures T_1 and T, ϕ is the Debye integral function, and the other symbols have their usual meanings. If the lines are sharp, and the angular range over which the intensity is appreciable is nearly constant, it is reasonable to take the integrated intensities as proportional to the intensities of the $K\alpha_1$ peaks. The accurate measurement of a peak intensity is rather easier than is that of an integrated intensity, since small temperature variations during the scanning of a line can introduce appreciable errors into the latter. The use of peak intensities is not justified if there is grain growth, or change of line shape for any other reason, but very careful measurements now being made at Oxford by Dr. C. W. Haworth show that I_T/I_0 is almost always very nearly equal to ρ_T/ρ_0 if the structure is first stabilized by a high temperature anneal. The results in this paper are all obtained from peak intensities.

Using copper Kα radiation, the peak intensities I_T for the three highest angle lines of silver were measured at various temperatures, after a preliminary high temperature anneal to stabilize the grain size. From equation (1), it follows that $(\lambda/\sin\theta)^2\log_{10}(I_T/I_1)$, where I_1 is the peak intensity at a standard temperature $T_1=289°\text{K}$, should vary linearly with T, since $\{\phi(\Theta/T)+\Theta/4T\}$ is only very slightly greater than unity for all temperatures T greater than Θ. The observed decrease in intensity is greater than the theoretical decrease, as has been found by other workers in tests of the Debye–Waller theory at high temperatures. The main error in equation (1) arises from the neglect of volume changes with temperature; the equation refers to constant volume conditions, but the measurements are made at constant pressure. One way of correcting for the volume changes is to introduce the concept of an effective Debye temperature, varying with temperature, as was suggested by Zener and Bilinsky (1936). More recently, Paskin (1957) has published a similar method, which is easier to apply in practice. His treatment leads to a Debye temperature Θ_T which is related to the Debye temperature at absolute zero Θ_0 by the equation

$$\Theta_T/\Theta_0=(V_0/V_T)^\gamma \qquad \ldots\ldots(2)$$

where V_T, V_0 are the atomic volumes at temperatures $T°$, $0°\text{K}$ respectively and γ is the Grüneisen constant. The equation corresponding to (1) then becomes

$$\frac{\lambda^2}{\sin^2\theta}\ln\left(\frac{\rho_T}{\rho_1}\right)=\frac{12h^2}{mk\Theta_1{}^2}(T_1-T') \qquad \ldots\ldots(3)$$

where we have assumed that T is sufficiently large for $\{\phi(\Theta/T)+\Theta/4T\}$ to be taken as unity. The modified temperature T' in this equation is defined by the relation

$$T'/T=(V_T/V_1)^{2\gamma}$$

V_1 being the atomic volume at the reference temperature T_1.

For the calculation of T', values of V_T from the experimental lattice spacing–temperature curve were used, and γ was taken as 2·40 (Slater 1939). Figure 3 shows the effect of plotting $(\lambda/\sin\theta)^2\log(I_T/I_1)$ against T' instead of T,

The use of Paskin's correction places the experimental points on a straight line, from the slope of which $\Theta_1 = 191 \pm 8°\text{K}$.

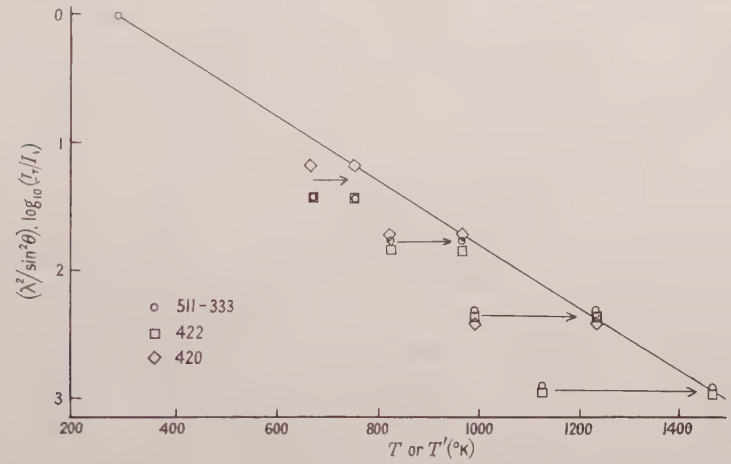

Figure 3. Effect of applying Paskin's method to silver results. The arrows indicate the change from T to T', resulting in a straight line plot.

The Debye temperature Θ_1 is related to the Debye temperature at 0°K by equation (2), which gives $\Theta_0 \simeq 197°\text{K}$. This is somewhat lower than the Debye temperature of 225°K deduced from specific heat measurements (Corak, Garfunkel, Satterthwaite and Wexler 1955). In a theoretical calculation of the x-ray Debye temperature for a face-centred cubic lattice, based on the known vibrational spectrum, Blackman (1957) finds $\Theta = 189°\text{K}$. If the vibrational spectrum has the Debye form, Θ from x-ray measurements should be equal to Θ from specific heat measurements; in general, the effect of the actual spectrum is to lower the x-ray value in comparison with the specific heat value.

§ 3. Mean Square Displacements of Atoms in Silver

For a Bravais lattice with random displacements of the lattice points from their mean positions, the diffracted intensity in a Bragg reflection is reduced by a factor $\exp(-2M)$ where $2M = (4\pi \sin\theta/\lambda)^2 \overline{u_s^2}$ and $\overline{u_s^2}$ is the mean square displacement of a lattice point in a direction normal to the diffracting planes. In the simple cubic structures, having one atom on each lattice point, the Debye–Waller theory gives an expression for M in terms of the temperature T, from which $\overline{u_s^2}$ may be calculated if Θ is known. A direct experimental measurement of $\overline{u_s^2}$ is not possible, since the x-ray results give only the difference in M at two different temperatures. However, the error in $\overline{u_s^2}$ resulting from an incorrect Θ may be reduced if the procedure given by James (1948) is followed. His equations (5.96) and (5.97) give $\overline{u_s^2}$ in terms of three quantities, β, γ and δ, of which γ contains known constants and δ is a small term which may be calculated with an approximate value of Θ. The quantity β is then obtained from the experimental intensity results. For cubic crystals, the thermal expansion is isotropic, so that $\overline{u_s^2}$ does not depend on direction and the mean square of the total displacement is given by $\overline{u^2} = 3\overline{u_s^2}$. Table 3 shows values of $(\overline{u^2})^{1/2}$ for silver

calculated from the experimental results in this way, and also directly from the assumption $\Theta = 191°\text{K}$.

Table 3. Values of r.m.s. Total Displacement for Silver

Temperature (°K)	300	500	800	1100
$(\overline{u^2})^{1/2}$ from James' procedure (Å)	0·18	0·22	0·27	0·32
$(\overline{u^2})^{1/2}$ assuming $\Theta = 191°\text{K}$ (Å)	0·15	0·17	0·22	0·25

The values of $(\overline{u^2})^{1/2}$ calculated directly from the experimental intensities by James' procedure are about 25% higher than those calculated from an effective Debye temperature obtained by Paskin's method. Although James' method reduces the error caused by an incorrect Θ, it makes no other allowance for the effects of thermal expansion. Thus the most reliable way of finding $\overline{u^2}$ may be to use Paskin's method to obtain Θ, and then calculate M from this value of Θ. This view is confirmed to some extent by the results for the constant β. A theoretical value of β may be obtained from the known elastic constants of silver by means of Waller's equation (James 1948, eqn (5.99)), and is $\beta \simeq 1{\cdot}3 \times 10^{-21}$. This agrees reasonably well with β calculated from $\Theta = 191°\text{K}$ $(1{\cdot}88 \times 10^{-21})$, and less well with β obtained directly from the intensity change $(3{\cdot}05 \times 10^{-21})$. The magnitude of the $\overline{u^2}$ values in table 3 are such that the r.m.s. atom displacements in silver are roughly 5–6% of the interatomic distance at room temperature and 8·5–11% of this distance at 850°C.

§ 4. Temperature Variation of Diffracted Intensity for α–Titanium

The x-ray data on solid specimen 3 (table 1) were used to measure the decrease in intensity in the $K\alpha_1$ peak at 375°, 580° and 700°C, referred to the annealed specimen at 9°C. Measurements were made on the $(12\bar{3}3)$, $(30\bar{3}2)$, $(30\bar{3}0)$, $(11\bar{2}4)$ and $(12\bar{3}1)$ lines, but only those from the two latter strong reflections were sufficiently accurate for quantitative calculations. There is some difficulty in applying Paskin's method, since Grüneisen's constant is not known for titanium, but this is obviated by the small coefficient of expansion, which reduces the difference between T' and T and makes it insensitive to γ. Within the limited accuracy attainable, there is no difference in the intensity ratios of the two lines used, despite the difficulties in applying the usual Debye–Waller theory to a non-cubic structure with more than one atom in the unit cell. The results were plotted in the same way as figure 3, making separate assumptions that $\gamma = 2$, 3 or 4. From the limiting slopes obtained in this way, it is estimated that the effective value of Θ is $270° \pm 30°\text{K}$. The value obtained from low temperature specific heat measurements is 280°K (Estermann, Friedberg and Goldman 1952).

The results for β-titanium could not be interpreted on the basis of the Debye–Waller theory, probably because of bad particle statistics or other effects caused by grain growth (De Wolff, Taylor and Parrish 1959).

§ 5. Stacking Faults in Titanium

Mogard and Averbach (1958) report that they found no indication of stacking faults in cold-worked zirconium. In the present work, however, it was noticed that cold-worked powder patterns of titanium show anomalous broadening effects qualitatively similar to those produced by basal plane stacking faults.

The profiles of the $\{11\bar{2}4\}$ line (which is not affected by stacking fault) and of the neighbouring $\{12\bar{3}1\}$ line from a heavily deformed solid specimen were measured accurately, and analysed by the Fourier method used by Anantharaman and Christian (1956). A deformation stacking fault parameter of $\alpha \simeq 0{\cdot}10$ was obtained; this is very high, and comparable with unpublished results obtained for hexagonal cobalt nickel alloys. Smith (1959, private communication) has observed basal plane stacking faults in thin film transmission electron micrographs of titanium, thus giving some support to our x-ray results.

§ 6. Conclusion

The results for silver show that the Paskin correction to the Debye–Waller theory is in reasonable agreement with experiment for a face-centred cubic metal. For hexagonal metals, the position is uncertain; the present results enable an approximate Debye temperature to be deduced, but more work is needed to establish the validity of this procedure.

Acknowledgments

This work was partially financed from a research grant made to the Department of Metallurgy, Oxford, by the British Non-Ferrous Metals Research Association. We should also like to thank Dr. C. W. Haworth for helpful discussion, and Professor W. Hume-Rothery for his interest. One of the referees kindly drew our attention to the paper by De Wolff *et al.*

References

Anantharaman, T. R., and Christian, J. W., 1956, *Acta Cryst., Camb.*, **9**, 479.
Berry, R. L. P., and Raynor, G. V., 1953, *Research, Lond.*, **6**, 21s.
Blackman, M., 1957, *Handbuch der Physik*, Vol. VII/1, *Crystal Physics* (Berlin: Springer), p. 325.
Corak, W. S., Garfunkel, M. P., Satterthwaite, C. B., and Wexler, A., 1955, *Phys. Rev.*, **98**, 1699.
De Wolff, P. M., Taylor, J. M., and Parrish, W., 1959, *J. Appl. Phys.*, **30**, 63.
Estermann, I., Friedberg, S. A., and Goldman, J. E., 1952, *Phys. Rev.*, **87**, 582.
James, R. W., 1948, *Optical Principles of Diffraction of X-Rays* (London: Bell).
Levinger, B. W., 1953, *Trans. Amer. Inst. Min. (Metall.) Engrs*, **162**, 195.
McHargue, C. J., and Hammond, J. P., 1953, *Acta Met.*, **1**, 700.
Mogard, J. H., and Averbach, B. L., 1958, *Acta Met.*, **6**, 552.
Paskin, A., 1957, *Acta Cryst., Camb.*, **10**, 667.
Slater, J. C., 1939, *Introduction to Chemical Physics* (New York: McGraw-Hill).
Spreadborough, J., and Christian, J. W., 1959, *J. Sci. Instrum.*, **36**, 116.
Zener, C., and Bilinsky, S., 1936, *Phys. Rev.*, **50**, 101.

Observations on the Development of Electroplating Deposit Structures on Single Crystals of Copper

By V. R. HOWES†
Department of Industrial Metallurgy, University of Birmingham

MS. received 21*st April* 1959, *in final form* 15 *June* 1959

Abstract. Results of step height measurements of layer structures on electrodeposits, on a copper single crystal surface with orientation close to a (100) plane, are shown by frequency distribution curves for increasing deposition times. Platelet layer width measurements are given for the same times. The results are associated with the concept of bunching. Observations are also described of a secondary topographical structure, detected by auxiliary microscope techniques, on the surfaces of the normal platelet layers; these are seen to be differentially tilted, curved and covered with micro-layers.

§ 1. Introduction

Many studies of the growth of crystals have shown that this occurs by the successive spreading of thin layers over the crystal faces. That this method of growth also applies in electrodeposition was first indicated by Volmer (1922) and more recent observations have been made by Wranglen (1955) and by Pick and Wilcock (1958). With similar conditions of plating as in this last work, Storey (1957) has studied the effect on the process of such variables as base orientation, current density and temperature. The quantitative results and the detailed study of the plating structures described here form one of several extensions to this work that are being currently investigated.

The preparation and plating conditions in these experiments were as follows. The cathode specimen was a cut surface, at a particular crystallographic plane, of a copper single crystal, previously grown in a Bridgman type furnace. After mounting and mechanically polishing, the specimen surface was electropolished in a solution of 50% orthophosphoric acid immediately before electroplating was begun. For the electrodeposition the anode was of polycrystalline oxygen free high conductivity copper, the current density being 10 mA cm^{-2} in a normal solution of copper sulphate and sulphuric acid ($\frac{1}{2}$M . $CuSO_4 + \frac{1}{2}$M . H_2SO_4) at a temperature of 25°C. The single crystal surfaces used all had orientations close to the (100) plane of the cubic crystal, since it had already been shown by Storey (1957) that the most coarse platelet-layer structures were then obtained, consisting of platelets with surfaces in the (100) crystallographic plane (to a first approximation) and having edges predominantly in ⟨110⟩ directions but with smaller edges in ⟨100⟩ directions, and this type of structure is the most easily accessible for a first detailed microscopic study.

This investigation has special reference to development of the plating structure with time, and for this purpose four plating times of 15, 30, 45 and 60 minutes were chosen for study, one specimen being used for all four times, being

†Now at Department of Metallurgy, Technical University of Norway.

repolished and re-prepared again for plating between each experiment. The specimen was specially mounted for repolishing so that change in orientation between experiments was avoided; this was checked by an x-ray photograph taken for the newly prepared surface before each plating. The electrolyte solution was made up from Analar chemicals using thoroughly cleaned glassware, and everything immersed into it afterwards was first given a prolonged rinse in running distilled water to prevent contamination. A standardized electroplating test was used to check the solution; if the appearance of the deposit—extremely sensitive to impurities present—did not conform to that usually found, the solution was rejected. The same electrolyte solution was used in all the experiments described; it was checked for reproducibility between each plating experiment, and quantitative reproducibility was also obtained when a repeat experiment was done for 30 minutes' deposition again after several intermediate platings.

§ 2. Quantitative Measurement

2.1. *Experimental*

The specimen surface used in this series of experiments (specimen A) had the orientation as shown in figure 1, and this gave the typical platelet layer structure with (100) crystallographic surfaces for 60 minutes' deposition seen in figure 2 (*a*) (Plate), the indicated direction being the ⟨110⟩ direction in the (100) plane. This regular structure developed gradually with time, the platelet size and regularity increasing continuously; this development is illustrated by a comparison of figure 2 (*a*) with figure 2 (*b*), which shows the structure obtained after only 15 minutes' deposition on the same specimen under identical conditions; much larger magnification had to be used in order to resolve the smaller structure.

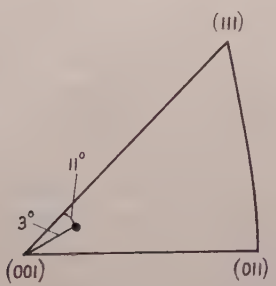

Figure 1. Orientation of surface of specimen A.

For the four plating times already specified, measurements were made on this specimen's surface of the step heights between platelet-layers and of the average widths of the layers. Step heights were measured by the profile technique of Tolansky (1951) with calibration against a standard before and after each series of measurements; ten consecutive measurements were made, traversing the surface in a direction at right angles to the step edges, at each of five positions on the surface spaced symmetrically 1 mm apart; thus 50 measurements were made for each plating time. Average widths of the platelet-layers were calculated from measurements of the distance across 10 to 20 layers at each of nine positions on the surface 1 mm apart for each plating time.

2.2. *Step Height and Step Width Measurements*

These results are shown in figure 3 in the form of frequency curves of the distribution of measured step heights for each plating time; N is the number of times the values of step height H were obtained. The points A on the ordinates show the average value of step height for each plating time, and the points X on the abscissae show the number of steps found that had height values below the resolution of the measuring technique ($0{\cdot}1\,\mu$).

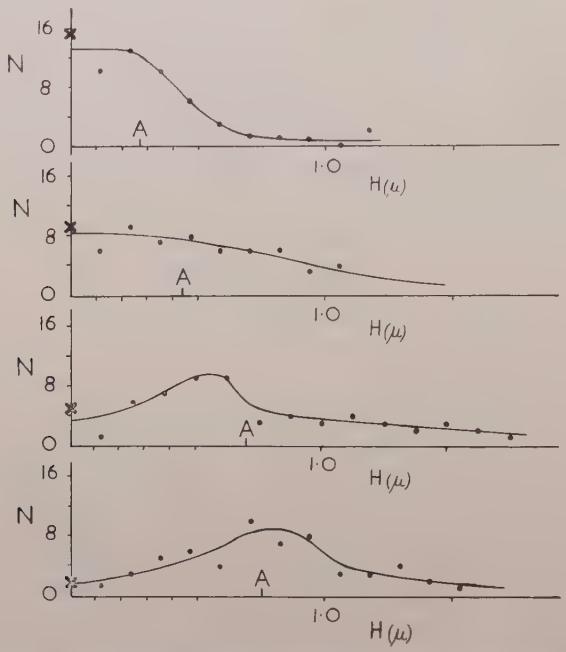

Figure 3. Frequency distribution curves of measured step heights of platelet layers for electrodeposits on specimen A.

It is immediately seen that the number of small step heights decreases rapidly with plating time, a correlating increase in the number of larger step heights and in the largest step height values occurring to give a broader step height distribution. This development continues giving a clear maximum in the distribution curve for 45 minutes' plating which has broadened and shifted to a higher value of step height after 60 minutes' plating.

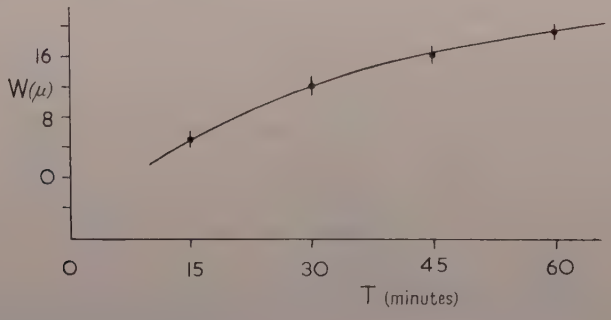

Figure 4. Variation of step widths of platelets of deposits with time.

The positions of the points A illustrate that the average step height value increases with plating time but that the rate of increase gets less with time.

Figure 4 shows the variation of average step width W with plating time T, the error range being plus or minus twice the standard error of the mean. The values of W are seen to increase with time but the rate of increase gets less, this notably corresponding to the variation of average step height with plating time as already described.

These variations in step heights and width with time can only be the result of bunching of the growth layers, i.e. the development of surface growth by the catching up and meeting of growth layers with others spreading in the same direction across the surface.

§ 3. Secondary Structure on the Normal Platelet Layers

3.1. *Detection and Development*

During the investigation described above, a secondary structure was detected and then consistently found for all the plating times and on all the specimens observed. Not seen by normal microscopy, it was studied with phase contrast and multiple beam interferometry techniques. The illustrations given are of the surface of specimen A, and also of the surface of another single crystal specimen with face orientation exactly on a crystallographic (100) plane, as indicated by back reflection Laue photograph patterns and the symmetry of the deposit structure itself (to be referred to as specimen B).

Figure 5 (*a*) (Plate) shows a region of the surface of specimen B after electroplating for 45 minutes, figure 5 (*b*) shows the identical region but with phase contrast illumination showing up the secondary structure consisting of diffuse lines occurring singly and in networks. This photograph shows typical secondary structure which is reproducible in general appearance, but not in detail, for any one plating time.

However, the general appearance does change with plating time as can be seen in figures 5 (*c*) and (*d*). In the former, after only 15 minutes' deposition on to specimen B, the secondary structure appears as small circles occurring on individual large platelet tops; whereas after 30 minutes on the same specimen small circles and linear networks are seen as in the latter photograph, giving a definite appearance of an intermediate stage between that seen at 15 and 45 minutes. The appearance after 60 minutes' plating did not change from that after 45 minutes except that the secondary structure lines became even more profuse. These changes in appearance of the secondary structure were found to be quite general for all the single crystal specimens observed—as indeed were all the observations reported in this work—but these were limited to specimens having the coarse platelet-layer structure associated with surface orientations close to the (100) plane of the crystal.

3.2. *Height Changes on the Platelet Surfaces*

Once found, the secondary structure was further studied by interferometry, and figure 6 (*a*) (Plate) shows a multiple beam interferogram of the surface of specimen B after 60 minutes' plating. Since the step heights between platelets are relatively large (as seen from the light profile measurements already described), the interference fringes are not generally related from platelet to platelet; however undulations and irregularities in the fringes clearly show height variations on

individual platelet tops in the range of 200–1000 Å. It was at once established that these height variations correspond to the secondary structure by increasing the fringe dispersion until a contrast effect within the very broad fringes thus obtained showed up the structure at the same positions as the sharp fringe variations. It would seem from these observations that the observed secondary structures are of the form of non-sharp micro-steps on the platelet surfaces.

It is also seen in figure 6 (*a*) that the fringes on the platelets, apart from variations, are generally not straight but curved showing that the surfaces are non-flat. In addition the changes, from platelet to platelet, in both the general direction and the dispersion of the fringes indicate that the platelet surfaces are differentially tilted one with respect to another; measured variations in fringe dispersion show that differential tilt angles up to 2° occur. The surface curvatures are more clearly seen with the high dispersion high magnification multiple beam fringes seen in figure 6 (*b*) for the same electrodeposit as above; here complete ring fringes are found which indicate dome-shaped platelet tops.

Similar fringe variations, curvatures and tilts were found on the platelet surfaces of deposits on specimen A, as can be seen for example in the interferogram of figure 6 (*c*), obtained after 60 minutes' plating.

3.3. *Origin of the Secondary Structure*

The small circles seen in figure 5 (*c*) for a 15 minute deposit suggest that *surface nucleation* of the micro-layer secondary structure has occurred on the largest platelets at the early plating times. A second source of the micro-layers is seen in figure 5 (*e*) showing the appearance of a 45 minute deposit on specimen A; here it is seen that often the secondary structure on the platelet surfaces is associated with small projections at the platelet edges, as at points marked X in the photograph. Such projections are a common feature of the plating structures observed, although becoming less frequent at the longest plating time; also they have been found without exception to be of two types, in plan they appear triangular on ⟨110⟩ platelet edges and rectangular on ⟨100⟩ platelet edges. Although the reason for the growth of these projections is not known, it would seem that the cause can also initiate *edge-nucleation* of the secondary structure micro-layers.

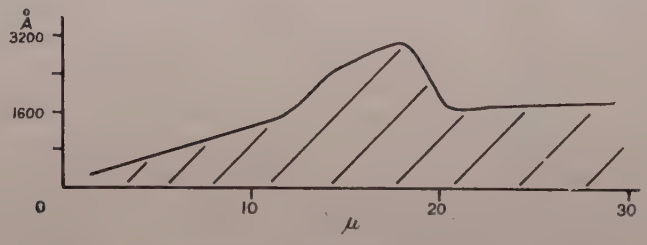

Figure 7. Calibration of interferogram of figure 6 (*d*).

A third origin of the secondary structure, and the most important at the longer plating times, is the merging of platelets or layers, i.e. the development of surface growth by the meeting of growth platelets or layers with others spreading in the opposite direction across the surface. Merging is continuously occurring in all layer growth development and examples can be seen of it in all the photographs shown. The height differences between merging platelets, or even the tilt or curvature differences alone, give rise to small remnant steps which then

appear as secondary structure micro-layers on the surfaces, as seen for example at point Y in figure 5 (*f*), showing a 30 minute deposit on specimen B.

An example of exactly how merging influences the surfaces of platelets is seen in figure 6 (*d*), which is an interferogram taken at high magnification, by an extension of the method reported by Tolansky and Emara (1955), using fringes of equal chromatic order. The fringes illustrate a topographical section at the line marked X in figure 6 (*e*) where merging of one platelet with another has occurred. The calibration of this interferogram, seen in figure 7, shows that this merging has given a height disturbance on the platelet surface of the order of 1200 Å; also further evidence of differential tilting and surface curvature can be observed.

§ 4. Discussion

The deposit structures that have been observed are derived from the character of the earliest stages of growth when platelets were first formed. Surface geometrical irregularities on an atomic scale, adsorbed or inherent impurities, strains and lattice faults in the surface of the crystal must all influence the initiation of the platelets and their consequent spread to give the wide range of step heights found as the plating time increases. Once a distribution of step heights is in existence, however small, the range of different values will be extended continuously by the processes of merging and bunching.

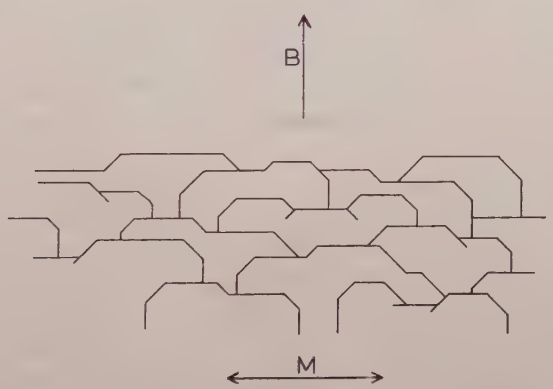

Figure 8. Illustration of bunching (B) and merging (M).

These two processes of crystal growth by layer spreading have been illustrated in this experimental investigation, and the relationship between them, for the growth of a typical platelet layer structure as found on a surface with orientation somewhere near to a (100) plane, is shown diagrammatically in figure 8 where B indicates bunching and M indicates merging. On such a surface platelets form with (100) top surfaces at a slight tilt to the specimen surface, and as these spread outwards they meet and merge to give layers. The layers so formed spread in a direction influenced both by the tilt direction of the surface with respect to the crystallographic (100) plane, and by the ⟨110⟩ directions in the surface, which are the directions of the dominant edges of individual platelets. Figure 8 shows a stage in the development of the layers, where it is seen that bunching, as already defined, occurs in the direction of spread of the layers,

while merging occurs at right angles to this direction; indeed it is by the latter process that layers are formed from individual platelets. It is to be noted that in the case of specimen B, having a surface exactly on a (100) crystallographic plane, the growth process is more complicated since then bunching and merging can both occur in all directions and there is no main direction of spread.

An explanation for the occurrence of bunching, as a result of adsorbed impurities on the growing surface, has been given by Frank (1958). But although such impurities do exist and must be of some influence on the process, it is thought that for the present results, once different values of step heights are obtained—a point already discussed—then this must be the dominant factor for further bunching, since small steps should move faster than large steps under similar conditions. The process is then more like that analysed by Chernov (1957), for which the average step heights and widths are both proportional to the square root of the time of deposition. The experimental values of widths shown in figure 4 closely follow this proportionality although agreement is not so good for the measured values of average step height. The distribution curves can also be explained qualitatively on this basis, since then bunching will occur predominantly where small and large steps are consecutive. Thus a rapid decrease in the number of small step heights found on plating surfaces with increasing deposition time, and a steady increase in the number of larger step heights obtained, is exactly what would be expected.

The secondary structure has so far only been observed on specimen surfaces with orientations close to the (100) crystallographic plane, but the observed changes of the phenomena with deposition time would lead one to expect that the main criteria for the occurrence of secondary structure are initially that the individual platelets reach a certain size, and finally that merging of similar platelets occurs.

It appears, from observations after 15 minutes' plating, that growth on the *tops* of platelets, as opposed to that at the edges, starts with surface nucleation occurring when the platelets have become larger than a certain size, these small growth layers then spreading out over the separate platelets. At later times, merging of platelets gives a second source of micro-layers, so that both small circles and non-circular secondary structures are seen, as for 30 minutes' deposition. At still later times the necessity for surface nucleation to occur is avoided by the profusion of micro-layers already on the surface due to the merging that becomes increasingly common with further growth; thus at 45 and 60 minutes, although the profusion of secondary structures has increased, there are no circular features as seen earlier. With reference to the necessity for nucleation, it is well known that crystal growth occurs most easily at kinks in layer edges rather than by the formation of new surface nuclei. However, there is a limit to the distance that new material can diffuse to get to an edge, this limiting distance depending very much on the type of growth occurring and on the particular conditions of this growth. Thus if distances exceeding this limit are obtained on flat surfaces produced during growth then surface nucleation again becomes a probability.

The new observations of the tilts and curvatures of platelet surfaces together with the secondary structure gives rise to an interesting possibility that these are indirect evidence of sub-microscopic steps on the growth surface. Supposing growth to occur by the spreading of fundamental layers too small to be seen by

any technique, then surface curving and tilting could be the observable indication of an array of these layers, as shown diagrammatically in figure 9. An apparent tilt on the surface would be obtained by the presence of sub-microscopic layers as in figure 9 A, while a curvature would be given as in figures 9 B and C. In addition, the observable secondary structure micro-layers could be the result of either the merging of platelets with surface curvatures, giving remnant small non-sharp steps, or the extended bunching of the fast moving fundamental layers, in the manner described by Frank (1958), after surface or edge nucleation, as indicated in the diagram of figure 9 D. Both these last postulates would explain the diffuseness of the secondary structure lines as seen with phase contrast, why they do not improve in visibility with increased lateral magnification, and why attempts made to observe them with the high magnification and extended depth of focus of the electron microscope have so far failed.

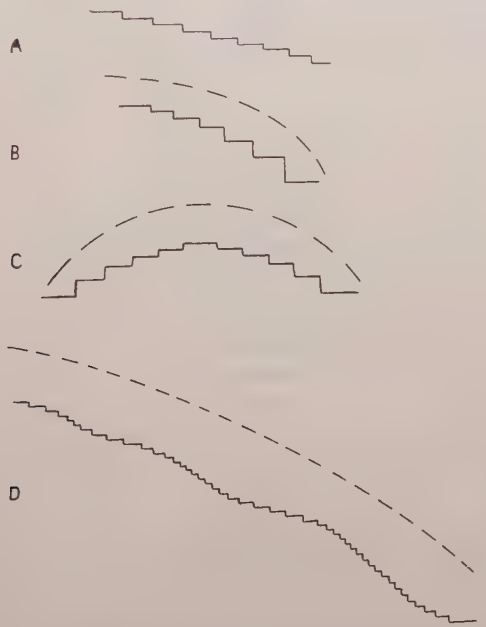

Figure 9. Illustration of surface changes on platelets due to possible sub-microscopic layers.

Finally, one other observation is relevant to the above mentioned possibility. Under the conditions of the experiments that have been described, solitary single straight-sided platelets are quite often observed on the electrodeposits, although most common at the early plating times. These attain considerable heights above the average platelet level without any visible secondary structure on their surfaces, and are quite distinct from the surrounding deposit, as can be seen for the three examples shown in figure 6 (*f*) for a 15 minute deposit on specimen A. The presence of sub-microscopic layers would seem to be a most likely explanation for the growth mechanisms (but not the initial development) of these particular platelets.

Acknowledgments

The author would like to thank Dr. H. J. Pick for useful discussion of the work. Thanks are also due to Messrs. Joseph Lucas Limited for financial support and to Professor E. C. Rollason for providing laboratory facilities.

References

Chernov, A. A., 1957, *Dokl. Akad. Nauk S.S.S.R.*, **117,** 983.
Frank, F. C., 1958, *Growth and Perfection of Crystals* (New York: Wiley).
Pick, H. J., and Wilcock, J., 1958, *Trans. Inst. Met. Finishing*, **35.**
Storey, G. G., 1957, *M.Sc. Thesis*, University of Birmingham.
Tolansky, S., 1951, *Z. Electrochem.*, **56,** 263.
Tolansky, S., and Emara, S. H., 1955, *J. Opt. Soc. Amer.*, **45,** 792.
Volmer, M., 1922, *Z. phys. Chem.* (A), **102,** 267.
Wranglen, G., 1955, *Trans. Roy. Inst. Technol.* (Stockholm), 94.

Proton–Proton Elastic Interactions at 930 MeV

By J. D. DOWELL, W. R. FRISKEN, G. MARTELLI† AND B. MUSGRAVE
Department of Physics, University of Birmingham

Communicated by P. B. Moon ; MS. received 7th May 1959

Abstract. The elastic scattering of 930 MeV protons by protons present in a propane bubble chamber is investigated. The method of isolating elastic p–p events from background contaminations is discussed. An estimate is made of the scanning efficiency and the elastic cross section is found, from track length measurements, to be $21{\cdot}6 \pm 2{\cdot}5$ mbn, in good agreement with the values obtained by other authors. The angular distribution of the scattered particles is also given and compared with the predictions of two high energy models.

§ 1. Introduction

During an analysis of the interactions in a propane bubble chamber of 930 MeV protons from the Birmingham proton synchrotron, some results have been obtained on p–p elastic scattering.

Measurements of p–p elastic and differential cross sections near this energy have been performed by Duke *et al.* (1955), Smith, McReynolds and Snow (1955) and more recently by Batson *et al.* (1959). With the exception of the latter results, the most significant information has been obtained for centre-of-mass angles greater than 30°. The measurements of Duke *et al.* were limited by poor statistics and those of Smith *et al.* involved a normalization to the results of Sutton *et al.* (1955) at 437 MeV.

The present results supplement the existing information, and also illustrate the possibility of isolating free hydrogen events in a propane bubble chamber (Chretien *et al.* 1957).

The experimental arrangement is shown in figure 1. A beam of 950 MeV protons, energy selected by the fringing field of the synchrotron and focused by a quadrupole system, emerges through a lead collimator into the laboratory. A second lead collimator, placed close to the chamber, confines the tracks to the central region so as to reduce scattering from the walls. Because of energy losses, the mean energy of a proton producing an interaction in the propane is 930 ± 20 MeV.

The chamber has a useful volume of 9 in. × 3 in. × $2\frac{1}{2}$ in. About 5000 pairs of stereophotographs (stereoangle 16°) were scanned for events. The investigation has been limited mainly to those events whose geometry could give unambiguous information for their analysis. The p–p elastic events fall into this category, and can be selected with fairly high accuracy, the only limitation being due to errors in angular measurements. When possible, ranges and relative ionization densities have been used to derive auxiliary information.

† On leave of absence from the University of Pisa, Italy.

The coordinates of the events were measured on full-size reprojections, and the accuracy of a single coordinate measurement has been estimated to be to $\pm 0{\cdot}2$ mm. Scattering and azimuthal angles and their errors have been computed electronically.

More detailed information about the experimental technique and the methods of analysis employed are given in a separate paper (Dowell, Frisken, Martelli and Musgrave, to be published). The plate shows a typical p–p event.

§ 2. Selection of Events

In elastic free p-p collision the trajectories are coplanar and the scattering angles θ_1 and θ_2 (figure 2) satisfy the relativistic equation

$$\cot\theta_1 \cot\theta_2 = \frac{E}{2M} \qquad \ldots\ldots (1)$$

where E is the total energy of the system and M is the mass of the proton (all quantities are referred to the laboratory system).

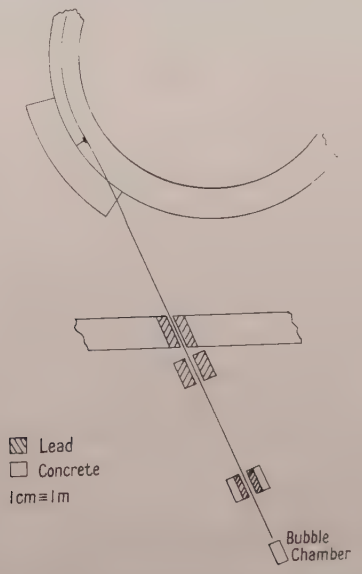

Figure 1. Experimental arrangement.

In a propane bubble chamber, because of the magnitude of the measurement errors, the main source of contamination comes from quasi-elastic interactions of protons with bound protons in carbon (Dowell, Frisken, Martelli and Musgrave 1960). To assist the separation of these two types of events, three further quantities have been used:

(i) The angle χ between the tracks of the two final particles, defined by

$$\cos\chi = \cos\theta_1 \cos\theta_2 + \sin\theta_1 \sin\theta_2 \cos(\phi_1 - \phi_2)$$

where ϕ_1 and ϕ_2 are the azimuthal angles of the final particles. For a coplanar event $\phi_1 - \phi_2 = 180°$, and $\chi = \theta_1 + \theta_2$.

(ii) The difference $\Delta\theta$ between the computed opening angle and the opening angle which would be obtained for an elastic collision, i.e.

$$\Delta\theta = \chi - \left\{\theta_1 + \cot^{-1}\left(\frac{E}{2M}\tan\theta_1\right)\right\}.$$

(iii) The angle α made by the incident particle with the plane containing the two scattered particles. This is given by

$$\sin\alpha = \frac{\sin\theta_1 \sin\theta_2 \sin(\phi_1 - \phi_2)}{\sin\chi}.$$

These three quantities have been computed electronically for each event.

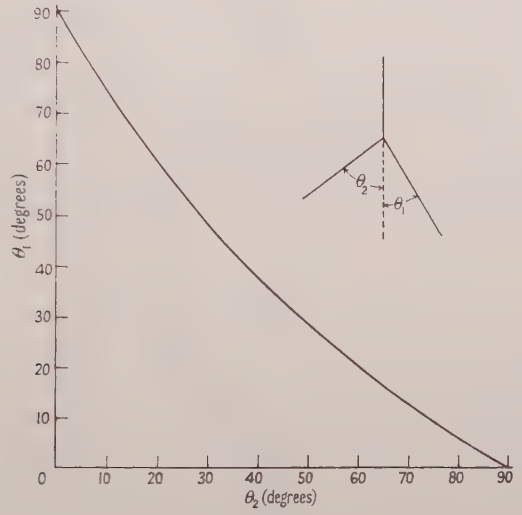

Figure 2. Relation between the scattering and the recoil angles in proton–proton elastic scattering at 930 MeV.

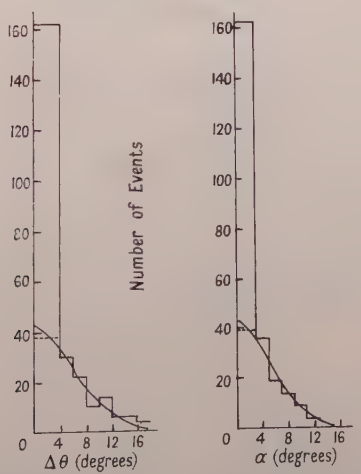

Figure 3. Distribution in $\Delta\theta$ for all coplanar events.

In order to separate the p–p elastic events from the background contamination, the two prong events have been divided as follows: (*a*) events for which $\theta_1 \leqslant 10°$; (*b*) events for which $\theta_1 > 10°$.

The first group includes events where angular measurements become less accurate with decreasing θ_1, but where range and relative ionization density may be used as an additional means of identification. Thus, an event with $\theta \leqslant 10°$

was classified as elastic if the range of the recoil was consistent with an elastic interaction. In cases where both particles left the chamber, relative ionization measurements have been used to exclude meson events. Forty-one p–p elastic collisions have been found in this region.

In the second group the accuracy does not vary appreciably with angle. Events which, within the experimental errors, were found to be coplanar (the limits being approximately $-3^\circ \leqslant \alpha \leqslant 3^\circ$), were examined for angular correlation (equation (1)). It was found that a limit of $\pm 4^\circ$ for $\Delta\theta$ would include more than 95% of the events which could be elastic. The distribution in $\Delta\theta$ for all coplanar events is shown in figure 3. A Gaussian curve has been extrapolated into the region $\Delta\theta \leqslant 4^\circ$. To check the consistency of the method the distribution in α for all events with $\Delta\theta \leqslant 4^\circ$ has also been plotted, and gives substantially the same result (figure 3). In this way 124 events have been selected, out of a total of 162 possible elastic events.

§ 3. Scanning Efficiency

Events where the secondary tracks have large azimuthal angles may be missed, particularly if they occur when many other tracks are present. Figure 4 shows azimuthal distributions of events in the various angular intervals (the interval 0°–5° has not been plotted because of intrinsic inaccuracy in measuring the large recoil angle of the slow proton). Booth *et al.* (1958) found no significant asymmetry in the azimuthal distribution for elastic p–p scattering at this energy.

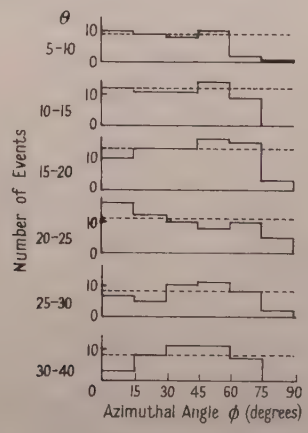

Figure 4. Azimuthal distributions of events, for various scattering angles.

The scanning efficiency has been estimated by assuming no losses for $\phi \leqslant 60^\circ$ and by extrapolating the average numbers in this region into the region $60^\circ \leqslant \phi \leqslant 90^\circ$. The values of scanning losses obtained in this way are given in the table. It is assumed that the losses for $\theta \leqslant 5^\circ$ are the same as for the interval 5°–10°. The possibility of an additional undetected loss at small angles cannot be ruled out, although a second scanning failed to reveal any further events.

Region(deg)	5–10	10–15	15–20	20–25	25–30	30–35	35–40
% loss	27	21	12·5	7·5	12·5	17	17

§ 4. Elastic Cross Section

The elastic cross section has been found from track length measurements. To ensure that the total track length was accurately determined, only those photographs showing less than about 15 incident protons were used. A mean free path of 217·6 cm was found for two prong events on a total track length of 311·15 m. The total number of events analysed in the experiment was 747, out of which 165 were elastic.

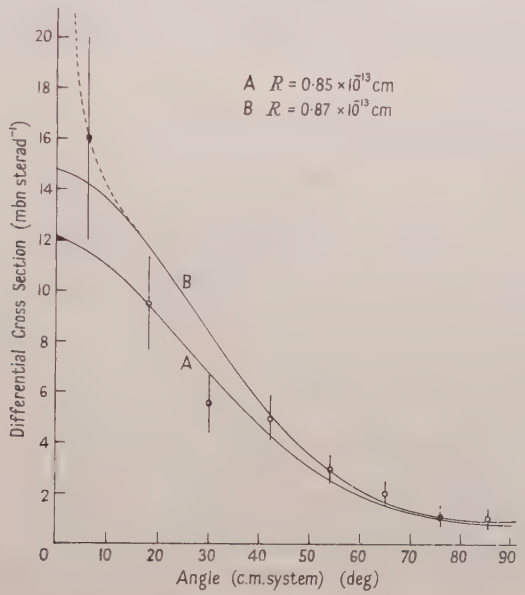

Figure 5. The proton–proton differential cross section at 930 MeV compared with that for the black disc model.

The density of expanded propane at 60°c (the average working temperature) was taken to be 0·429 g cm^{-3}, which gives a partial hydrogen density of 0·078 g cm^{-3}. The value obtained for the elastic cross section was thus $21{\cdot}6 \pm 2{\cdot}5$ mbn (the quoted error is the statistical uncertainty). This assumes no scanning losses during the track length measurements. The angular distribution normalized to this cross section, and corrected for scanning inefficiency, is plotted in figure 5.

§ 5. Discussion of Results

The value of $21{\cdot}6 \pm 2{\cdot}5$ mbn obtained for the elastic cross section falls among those found by other authors near this energy (Duke *et al.* 1955, Smith, McReynolds and Snow 1955, Batson *et al.* 1959). It should be noted, however, that the assumption that no scanning losses were present during this measurement, may not be completely justified, and the value obtained might be as much as 10% too low.

The angular distribution for angles greater than 30° is in good agreement with the results of Smith, McReynolds and Snow (1955) and Batson *et al.* (1959). However the present values of the differential cross section for smaller angles are significantly lower than those found by the latter authors.

If one treats the results in the black disc approximation (Fernbach, Serber and Taylor 1949) with

$$\sigma(\theta)=\frac{\sigma_{el}}{\pi}\left[\frac{J_1(kR\sin\theta)}{\sin\theta}\right]^2$$

the best fit is obtained for a radius $R=0{\cdot}85\times10^{-13}$ cm, where $kR=2{\cdot}85$ (cf. figure 5, curve A). This corresponds to a total cross section ($\sigma_T=2\pi R^2$) of 45 mbn. A second curve (B) corresponding to the experimentally measured total cross section of 48 mbn (Chen, Leavitt and Shapiro 1956) is also shown for comparison. The contribution of Coulomb scattering has been evaluated using the Mott formula

$$\sigma_c(\theta)=\frac{\eta^2}{4k^2}\left[\sin^{-4}\tfrac{1}{2}\theta+\cos^{-4}\tfrac{1}{2}\theta-2\cos^{-2}\tfrac{1}{2}\theta\sin^{-2}\tfrac{1}{2}\theta\cos\left(2\eta\ln\tan\tfrac{1}{2}\theta\right)\right]$$

where (Breit 1955)

$$\eta=\frac{e^2}{\hbar c}\left[1+\frac{E_L}{Mc^2}\right]\left[\frac{E_L}{Mc^2}\left(2+\frac{E_L}{Mc^2}\right)\right]^{-1/2}$$

and is shown in figure 5 as a broken curve added to curve B.

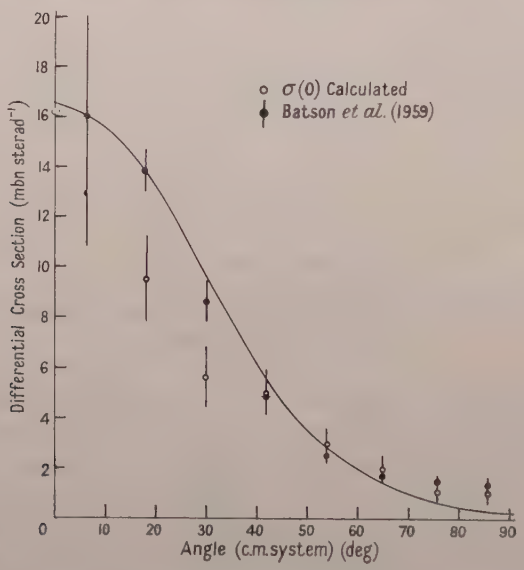

Figure 6. The proton–proton differential cross section at 930 MeV compared with that for the hard core model (Brown 1958).

Recently Brown (1958) has proposed a model with a repulsive core, and an external attractive and absorptive potential of Gaussian form. This model has been compared with both our points and those of Batson *et al.* (1959) (see figure 6). A limiting value at 0° has been calculated from the relation

$$\sigma(0^\circ)\geqslant\left(\frac{k\sigma_T}{4\pi}\right)^2.$$

The best fit has been obtained using a core radius of $0{\cdot}52\times10^{-13}$ cm and a mean radius for the external part of $0{\cdot}77\times10^{-13}$ cm. It appears that the model predicts too little large angle scattering. Since the model is likely to be more realistic

than the black disc, this provides strong evidence for the existence of an appreciable spin–orbit force at this energy.

§ 6. Acknowledgments

The authors are indebted to Professor P. B. Moon for his interest in this research. They wish to thank Dr. G. E. Brown and the members of the diffusion chamber group for making available their results prior to publication. Particular thanks are due to Dr. A. P. Batson for programming the data for electronic computation. The continued and valuable technical advice and assistance of Mr. G. Young and Mr. R. Joines is gratefully acknowledged.

References

Batson, A. P., Culwick, B. B., Hill, J. G., and Riddiford, L., 1959, *Proc. Roy. Soc.* A, **251,** 218.

Booth, N. E., Hereford, F. L., Huq, M., Hutchinson, G. W., Law, M. E., Segar, A. E., and White, D. H., 1958, *Nucl. Phys.*, **7,** 284.

Breit, G., 1955, *Phys. Rev.*, **99,** 1581.

Brown, G. E., 1958, *Phys. Rev.*, **111,** 1178.

Chen, F. F., Leavitt, C. P., and Shapiro, A. M., 1956, *Phys. Rev.*, **103,** 211.

Chretien, M., Leitner, J., Samois, N. P., Schwarz, M., and Steinberger, J., 1957, *Phys. Rev.*, **108,** 383.

Dowell, J. D., Frisken, W. R., Martelli, G., and Musgrave, B., 1960, *Proc. Phys. Soc.*, in the press.

Duke, P. J., Lock, W. O., March, P. V., Gibson, W. M., McEwen, J. G., Hughes, I. S., and Muirhead, H., 1955, *Phil. Mag.*, **2,** 204.

Fernbach, S., Serber, R., and Taylor, T. B., 1949, *Phys. Rev.*, **75,** 1352.

Smith, L. W., McReynolds, A. W., and Snow, G., 1955, *Phys. Rev.*, **97,** 1186.

Sutton, R. B., Fields, T. H., Fox, J. G., Kane, J. A., Mott, W. E., and Stallwood, R. A., 1955, *Phys. Rev.*, **97,** 783.

Cross Sections for some (n, pn) Reactions with Heavy Nuclides

By J. F. BARRY, R. F. COLEMAN, B. E. HAWKER and J. L. PERKIN
Atomic Weapons Research Establishment, Aldermaston, Berks.

Communicated by K. W. Allen; MS. received 26th May 1959, in final form 10th June 1959

Abstract. The (n, pn) cross sections of five heavy nuclides for 14·5 MeV neutrons have been measured using activation methods. The variation of both the (n, pn) and (n, p) cross sections of ^{186}W with neutron energy in the range 13 to 22 MeV has also been investigated.

All the cross sections found have been compared with those calculated using the direct interaction theory of Brown and Muirhead.

§ 1. Introduction

The understanding of the nature of (n, pn) and (n, np) reactions with medium or heavy weight target nuclides and neutrons of about 14 MeV is hampered by the lack of experimental evidence.

The most probable mechanism for the (n, np) reaction involves the initial emission of a neutron either directly or from a compound nucleus, followed by the emission of a proton from the residual compound nucleus. The emission of a proton in competition with the usually much higher probability of neutron emission under these conditions is only possible in special circumstances. These occur when the binding energy of the residual nucleus after neutron emission is greater for neutrons than for protons and its excitation energy is such that only proton or γ-ray emission is possible. Allan (1958) examined the reaction $^{63}Cu(n, np)^{62}Ni$ and March and Morton (1958) the reaction $^{54}Fe(n, np)^{53}Mn$, both of which are examples of this type of mechanism.

The most likely mechanism for the (n, pn) reaction consists of a direct (n, p) reaction followed by the emission of a neutron either directly or from the residual compound nucleus. Possible examples of this type of reaction were investigated by Cohen, Hyder and White (1956) who found upper limits for the (n, pn) cross sections of four nuclides for 14·5 MeV neutrons. No conclusions could be drawn from this work as these limits were higher than the values they calculated using both the statistical theory of the compound nucleus and the direct interaction theory of Austern, Butler and McManus (1953).

In a recent experimental survey of (n, p) cross sections with heavy nuclides and 14·5 MeV neutrons, Coleman *et al.* (1959) had considerable success in predicting the cross sections measured with the direct (n, p) reaction theory of Brown and Muirhead (1957). This success encouraged the present authors to measure some (n, pn) cross sections and compare these with an extension of the same theory.

§ 2. Experimental Details

2.1. *Choice of Target Nuclides*

The choice of heavy target nuclides suitable for (n, pn) cross section measurements by activation methods is severely limited. It was essential in every case

to separate chemically the (n, pn) reaction products from the target material after irradiation in order to remove some of the activity of the products of other reactions with much higher cross sections. The (n, pn) product in this separated fraction must be such that it could not be formed by an (n, p) reaction with an isotope of the same target element. Its half-life should not only be convenient to measure but, because of the low levels of activity expected, should be a factor of at least three or four different from that of any other (n, p) or (n, pn) product produced. Only five nuclides were found to fulfil these requirements namely ^{108}Pd, ^{128}Te, ^{130}Te, ^{142}Ce and ^{186}W. Isotopically enriched target elements for three of these nuclides (^{128}Te, ^{130}Te and ^{142}Ce) were used in order to reduce the intensity of the (n, p) products of the other isotopes present and thus increase the precision with which the (n, pn) product was counted.

In the work described here the (n, pn) cross sections of these five nuclides were measured for 14·5 MeV neutrons. In addition, one of these nuclides was selected in order to measure the variation of the (n, pn) cross section in the neutron energy range 13–22 MeV. ^{186}W was chosen for this purpose because its (n, p) cross section could be measured conveniently by the same method and could be compared with the predictions of the direct interaction theory of Brown and Muirhead.

2.2. *Neutron Irradiations*

2.2.1. *Irradiations with* 14·5 *MeV neutrons.*

The (D, T) reaction was used to obtain neutrons in the energy range 13 to 22 MeV. For the 14·5 MeV neutron cross section determinations a tritiated zirconium target was bombarded with 500 kev deuterons. The neutron output was maintained at about 10^{10} per sec during the course of the irradiations. Samples for irradiation consisted of some 50 mg of material sandwiched between aluminium discs and were placed close to the back of the tritium target. The ^{27}Al(n, α)^{24}Na reaction was used to monitor the neutron flux in this close position. In order to calibrate the ^{24}Na activity of the aluminium discs in terms of neutron flux, a separate experiment was performed in which the aluminium discs were irradiated in positions of known geometry with respect to the tritium target. The neutron output from this target was found by counting the associated α-particles from the (D, T) reaction. The accuracy of the flux determined in this way was estimated to be about 3%.

2.2.2. *Irradiations with* 13 *to* 22 *MeV neutrons.*

The measurement of the (n, p) and (n, pn) cross sections of ^{186}W over the energy range 13 to 22 MeV involved the positioning of the target material (tungsten metal) at some distance from the tritium target to ensure some degree of neutron energy resolution. This meant that the amount of target material had to be increased to about 12 g in order to obtain sufficient activity from the smaller neutron flux in this position. The weight of the aluminium discs for monitoring this flux also had to be increased for the same reason. Five of these were placed at regular intervals throughout the target material which was packed into a cylindrical container 1·8 cm long and 1·6 cm in diameter. In this way a value for the mean flux throughout the target material was obtained.

Neutrons of 13 to 15 MeV were produced using the tritiated zirconium target already described. Neutrons of 17 to 22 MeV were obtained by increasing the

deuteron beam energy. Large beam currents and a tritium gas target had to be used however in order to obtain a sufficient yield of neutrons. It was found possible to use beams as high as 5 to 10 μA by cooling the nickel foil entrance window to the tritium cell. This was done with a double foil helium cooled window similar to that described by Nobles (1957). The tungsten samples were irradiated a few centimetres from the gas cell and in the forward direction. The spread in energy of the neutrons passing through the sample was calculated from the angular distribution measurements for the (D, T) reaction (Bame and Perry 1957).

Corrections were applied to the neutron fluxes calculated from the activities of the aluminium discs for the variation of the $^{27}Al(n,\alpha)^{24}Na$ reaction cross section with neutron energy. The results of Mani, McCullum and Ferguson (to be published) for the neutron energy range 12 to 21 MeV were used.

2.3. *Chemical Separations and Counting Techniques*

2.3.1. *Chemical yields and counting techniques.*

Standard techniques were used in the chemical separations performed on each target element examined. These are described briefly in §§ 2.3.2. to 2.3.5. With the exception of tungsten, the methods used to obtain the chemical yield and to count the reaction products were similar. The final solution containing the separated reaction product was divided into two portions, one for the measurement of activity and the other for the determination of the chemical yield of the process. This yield was determined by a suitable colorimetric or microtitration method. The activity of the solution was measured by evaporating on a 20 μg cm^{-2} plastic film and counting in a 4π proportional counter. Since the source weighed less than 0·5 mg the correction for self-absorption of β-particles was, in all the cases examined, negligible compared with the other experimental errors.

2.3.2. *Palladium.*

The irradiated palladium was dissolved in aqua regia and 1 mg of rhodium and rutherium carriers was added. The rhodium was separated by passing a 6M hydrochloric acid solution through an anion exchange column on to which the palladium and most of the ruthenium was absorbed. The remaining ruthenium was removed by evaporating to dryness with perchloric acid. Finally, the residue was dissolved in hydrochloric acid.

2.3.3. *Tellurium.*

The tellurium was dissolved in aqua regia and mixed with 1 mg of tin and antimony carriers. The tellurium was separated by reducing it to the elemental state with sulphur dioxide and hydrazine. The antimony was then precipitated by hydrogen sulphide from a fluoride solution in which tin is strongly complexed.

2.3.4. *Cerium.*

The irradiated ceric oxide was dissolved in nitric acid with 1 mg of barium and lanthanum carriers. The cerium was extracted by methyl iso-butyl ketone and the lanthanum precipitated from the aqueous solution as hydroxide. This precipitate was then dissolved in dilute acid.

2.3.5. *Tungsten.*

About 12 grammes of irradiated tungsten were dissolved rapidly in acid solution (3M sulphuric acid, 4M nitric acid and 6M hydrofluoric acid) containing a known quantity of ^{182}Ta tracer. The tantalum was extracted with methyl iso-butyl ketone and then back extracted with a 6M sulphuric acid solution saturated with boric acid. This volume of the solution was adjusted to 10 ml and transferred to a liquid Geiger counter. The decay of ^{186}Ta and ^{185}Ta the (n, p) and (n, pn) products of ^{186}W was measured; background activity from the longer lived isotope ^{184}Ta was subtracted and finally the residual activity due to the ^{182}Ta tracer was counted. From the ratio of the activities of the tracer before and after separation the chemical yield was determined.

The liquid counter was calibrated for ^{182}Ta by standardizing a solution of ^{182}Ta using a 4π proportional counter and then counting portions of this solution in the liquid counter in exactly the same way as for the cross-section measurement. The counter was similarly standardized for ^{185}Ta and ^{186}Ta using nuclides of similar β energy, namely ^{32}P and ^{90}Y.

§ 3. Results and Discussion

3.1. *Experimental Results*

The values found for the five (n, pn) cross sections measured with 14·5 MeV neutrons are shown in table 1. In table 2 are the results obtained for the variation of the (n, p) and (n, pn) cross section of ^{186}W with neutron energy. These are also shown graphically in figure 2.

Table 1. Cross Sections for (n, pn) Reactions with 14·5 ± 0·4 MeV Neutrons

Target Nuclide	Q value	Cross section (mbn) Experimental $E_n = 14{\cdot}5 \pm 0{\cdot}4$	Calculated $E_n = 14{\cdot}5$	Calculated $E_n = 15{\cdot}0$
^{108}Pd	−10·04	4·0 ±0·8	1·5	2·5
^{128}Te	− 9·89	0·33 ± 0·05	0·04	0·08
^{130}Te	−10·68	0·17 ± 0·02	0·01	0·10
^{142}Ce	− 8·87	1·0 ±0·2	0·08	0·20
^{186}W	− 8·48	0·11 ± 0·05	0·02	0·05

Table 2. Cross Sections for the Reactions ^{186}W(n, p)^{186}Ta and ^{186}W(n, pn)^{185}Ta

Incident neutron energy E_n (MeV)	13·7 ±0·25	14·5 ±0·3	14·85 ±0·15	18·0 ±1·0	19·7 ±1·3	21·2 ±1·0
σ (n,p) (mbn)	1·0 ± 0·2	1·4 ± 0·3	2·8 ± 0·5	9·6 ± 2·0	14·5 ± 3·0	13·6 ± 2·7
σ (n,pn) (mbn)	< 0·04	0·11 ± 0·05	0·3 ± 0·15	4·7 ± 1·5	14·6 ± 3·0	17·1 ± 3·0

3.2. *Calculation of the (n,p) and (n,pn) Reaction Cross Sections*

The calculated cross sections shown in both the tables and figure 2 were obtained using the direct (n, p) reaction theory of Brown and Muirhead (1957). With this theory an energy spectrum for the emitted protons can be obtained for any given target nuclide and incident neutron energy (see example in figure 1).

Each spectrum has a high energy peak and extends to a maximum energy of $E_n + Q$ where E_n is the energy of the incident neutron and Q is the energy released in the reaction. To calculate direct (n, p) cross sections a low energy cut-off of magnitude $E_n - q$ must be imposed, where q is the binding energy of the last proton in the target nucleus. This ensures that the residual nucleus after proton emission is not left with sufficient excitation to emit a further neutron either directly or later on from a compound nucleus if formed.

To calculate direct (n, pn) cross sections only the protons emitted with energies less than $E_n - q$ were taken into account. A second low energy limit to exclude those protons with sufficiently low energy to make possible (n, p2n) reactions was applied to the spectra calculated for the higher neutron energies investigated. The fractions of the proton spectrum found below this second limit were, however, very small.

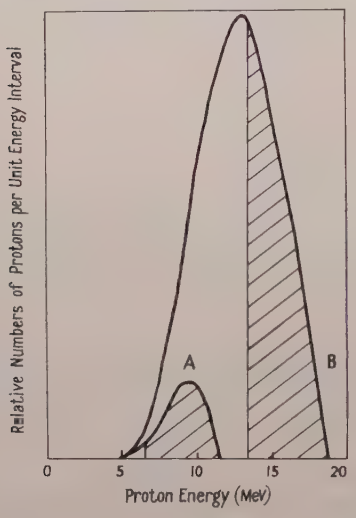

Figure 1. Calculated energy spectra of protons from the reactions $^{186}W(n,p)^{186}Ta$ and $^{186}W(n,pn)^{185}Ta$ for incident neutrons of : A, 15 MeV, and B, 22 MeV. Protons in the shaded areas are from (n, p) reactions. Those in unshaded areas are from (n, pn) reactions.

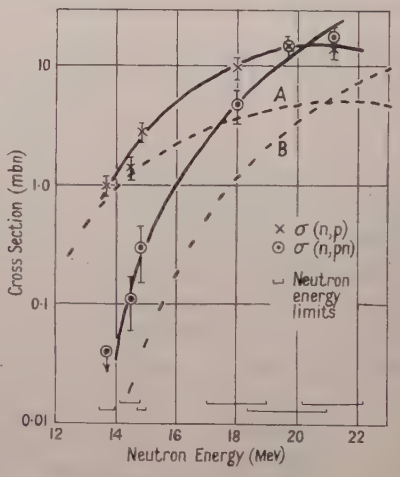

Figure 2. The variation of the cross sections for the reactions $^{186}W(n,p)^{186}Ta$ and $^{186}W(n, pn)^{185}Ta$ with neutron energy. The broken curves show the predicted variation of : A, the (n, p), and B, the (n, pn) cross sections using direct interaction theory.

Although the emission of a second proton from the residual compound nucleus can be neglected under the present conditions, there is still the possibility that a second proton could be emitted directly with the first, and this would invalidate the (n, pn) cross section calculations made. Brown and Muirhead have investigated the probability of direct emissions from second collisions of the incident neutron and have found this to be negligible.

3.3. *Comparison of the Experimental and Theoretical Cross Sections*

A comparison between the experimental and theoretical results can be made if it is assumed that the cross sections measured are in fact due solely to (n, pn)

reactions. The activation method of detection used cannot of course distinguish between (n, pn), (n, np) or (n, d) reactions.

From the results for the variation of the cross section of the $^{186}W(n, pn)^{185}Ta$ reaction with neutron energy it can be seen that the cross sections measured in the region of 14·5 MeV are very dependent on neutron energy. These remarks will also apply to the other four (n, pn) reactions measured at this neutron energy as they have similar thresholds. The calculated values in tables 1 and 2 show a similar dependence and are very sensitive to the magnitude assumed in the theory for the penetrability of protons through the nuclear boundary.

In these circumstances therefore the agreement between experiment and theory can be taken as satisfactory. The agreement is almost as good as that obtained for direct (n, p) reaction cross sections by Coleman *et al.* (1959) using the same theory.

The results for both the (n, p) and (n, pn) cross sections for ^{186}W represent a much more comprehensive test of this theory. In figure 2 the calculated excitation functions for these cross sections have the same general shape as that found experimentally although the absolute values are too low by a factor of three or four. The neutron energy at which the two cross sections become equal is predicted correctly and the calculated ratio of the two cross sections in the energy region where they are varying more slowly agrees with the experimental results to within 50%. Thus within the limits of experimental error and the simplifications made in the theory, the (n, p) and (n, pn) cross sections found are consistent with the direct mechanism envisaged by Brown and Muirhead. The possibility however that some of the activity attributed to (n, pn) reactions was in fact due to (n, np) or (n, d) reactions, cannot be excluded.

3.4. *Possible (n, np) Reactions*

Although the cross section for the initial stage of the (n, np) reaction is three orders of magnitude greater than that for the (n, pn) reactions studied, the emission from the compound nucleus of the proton in the second stage is about five orders of magnitude less likely than neutron emission. The contribution to the measured cross sections by (n, np) reactions should therefore be small.

3.5. *Possible (n, d) Reactions*

It has not been found possible to calculate the magnitude of the cross section of (n, d) reactions which could occur in the present experiments. Some indirect estimate of this magnitude can be obtained however from the published data for (p, pn) and (p, d) reactions.

Cohen *et al.* (1954 and 1958) found that the (p, pn) and (p, d) cross sections for heavy nuclides and 23 MeV protons are of the order of 60 and 30 mbn respectively. These results can be compared with the value of approximately 30 mbn found in the present work for the (n, pn)(+(n, d)) cross section for ^{186}W and neutrons of the same energy. This comparison is possible because the thresholds for these reactions and the penetrabilities of the coulomb barriers for the different incident particles are similar.

Preliminary calculations using Brown and Muirhead's theory have shown that the ratio of the (p, pn) to (n, pn) cross sections just quoted should be

approximately 2. This suggests that the contribution to the measured (n, pn) cross sections by (n, d) reactions is small.

Acknowledgments

We would like to thank Dr. G. S. Mani, Mr. G. J. McCallum and Dr. A. T. G. Ferguson for making available to us their $^{27}Al(n, \alpha)^{24}Na$ cross-section measurements.

The isotopically enriched elements used in these experiments were supplied by the Atomic Energy Research Establishment, Harwell.

References

Allan, D. L., 1958, *Nucl. Phys.*, **6**, 464.
Austern, N., Butler, S. T., and McManus, H., 1953, *Phys. Rev.*, **92**, 350.
Bame, S. J., and Perry, J. E., 1957, *Phys. Rev.*, **107**, 1616.
Brown, G., and Muirhead, H., 1957, *Phil. Mag.*, **2**, 473.
Cohen, A. V., Hyder, S. B., and White, P. H., 1956, *Nucl. Phys.*, **1**, 278.
Cohen, B. L., Rubin, A. G., and Fulmer, C. B., 1958, *Comptes Rendus du Congrès International de Physique Nucléaire* (Paris: Dunod), p. 392.
Cohen, B. L., Newman, E., Charpie, R. A., and Handley, T. H., 1954, *Phys. Rev.*, **94**, 620.
Coleman, R. F., Hawker, B. E., O'Connor, L. P., and Perkin, J. L., 1959, *Proc. Phys. Soc.*, **73**, 215.
March, P. V., and Morton, W. T., 1958, *Phil. Mag.*, **3**, 143.
Nobles, R., 1957, *Rev. Sci. Instrum.*, **28**, 962.

RESEARCH NOTES

Flame Spectra: the Effect of Deuteration on the Hydrocarbon Flame Bands

By G. N. SPOKES and A. G. GAYDON
Chemical Engineering Department, Imperial College, London

MS. received 1st *July* 1959

§ 1. Introduction

The hydrocarbon flame bands are a system of bands extending from 2400 Å to 4000 Å found in the emission spectrum of flames of all hydrocarbons. They were first studied in detail by Vaidya (1934), who suggested that the emitter was the molecule HCO. Various other emitters have been proposed, including CH_2 (Bell 1937) and CH . OH (Smith 1940). The excitation of the bands in the fluorescence spectrum of formaldehyde subjected to very short wave ultraviolet radiation (Dyne and Style 1947) indicates that the emitter must be either HCO or formaldehyde. Vaidya (1951) has studied the isotope shift when deuterium is substituted for hydrogen. That there is a shift shows that there must be at least one hydrogen atom in the molecule responsible for the bands. Ramsay (1953) and Herzberg and Ramsay (1956) have obtained in absorption quite a different band system which is also attributed to the HCO molecule. This absorption is found at $\lambda\lambda$ 6138·2 and 5624·1 Å when glyoxal, aldehydes and formates are flash photolysed. Detection of absorption in the region of the main hydrocarbon flame bands has not been possible because the parent compound usually absorbs strongly at these wavelengths.

One of us (Gaydon 1957) has reported that flames of acetylene mixed with deutero-acetylene showed much overlapping band structure which appeared to be merely a superposition of the bands obtained with acetylene alone and deutero-acetylene alone. This observation would seem to indicate that only one hydrogen atom is present in the emitter of the flame bands. Confirmation of this, however, was needed and we have now studied flames of mixtures of deuterated, undeuterated and partly deuterated acetylenes.

§ 2. Experimental

Flames of very rich mixtures of various fuels (Spokes 1959) have been found to give clear strong hydrocarbon flame bands without the so-called B bands (Vaidya 1934). The absence of the B bands leads to clarity in the appearance of the spectrum which makes observation and measurement easier. The intensity of emission from these rich flames is, however, low, making exposure times for the deuterated mixtures prohibitively long. Hornbeck and Herman (1951, 1954) have described a burner for running flames at low temperatures, which gives strong emission without B bands. We have used a similar burner; an alumina tube, 6 inches long and of 1 inch diameter, was used, the end being heated by a bunsen burner. Air was used in place of oxygen, and the fuel–oxygen ratio was consequently higher than in the experiments of Hornbeck and Herman. Fuel and air flows were about 30 cm^3 sec^{-1} and 1000 cm^3 sec^{-1} respectively.

With a Hilger E517 quartz Raman spectrograph, it was possible to obtain a good spectrum in the region 2400–2700 Å in three minutes on Ilford Zenith plates. The resolving power of the spectrograph is quite good in this region (about 15 000) and the isotope shift is easily seen. Interference from other molecular spectra is not serious at these wavelengths, although very weak OH 2608 Å emission has been noted on some plates.

The various mixtures of acetylenes were made by adding carefully a mixture of water and heavy water to calcium carbide of commercial quality. The gas, which appeared to be of adequate purity to give the usual spectrum, was collected in a rubber bag.

Acetylenes were prepared from the following mixtures of water and heavy water: (*a*) H_2O alone, (*b*) 2 H_2O : D_2O, (*c*) H_2O : 2 D_2O, (*d*) D_2O alone.

§ 3. Results

If a molecule containing more than one hydrogen atom were responsible for the hydrocarbon flame bands, a new system of bands would appear in the spectra of flames of acetylenes produced by mixtures (*b*) and (*c*). No such new system has been observed. The spectra of the mixtures (*b*) and (*c*) are found to be a superposition of hydrocarbon and deuterocarbon flame bands with approximately correct intensities. Vaidya's assignment of the hydrocarbon flame bands to the HCO radical is thus strongly supported. Formaldehyde which contains two hydrogen atoms is eliminated.

Prints of the spectra are shown in the plate. Shading has been necessary in the printing process, and this has resulted in some unevenness of reproduction. All negatives are considerably more dense at about 2700 Å than at about 2400 Å.

Long exposures (up to one hour) on the flame, using ultra-violet sensitive plates (Ilford Q2) showed some bands of the Fourth Positive system of CO between λλ 2337·9 Å and 2173·0 Å. It is rather surprising that a spectrum requiring an excitation energy of over 8 ev should occur in a relatively low temperature flame.

§ 4. A Possible Array for the DCO System

We have measured a few additional bands of the DCO system and, using these, together with more accurately measured bands observed on larger dispersion by Hornbeck and Herman, we have arranged most of the strong bands into the vibrational array shown in the table. A few other fragments of arrays using the same intervals have been formed, but their relation to the main array is uncertain.

Vibrational Array for DCO Bands

v'													
0	33158	1818	31340	1805	29535	1783	27752	1779	25973	1743	24230		
	975		997		993		981		986		968		
1	34133	1796	32337	1809	30528	1795	28733	1774	26959	1761	25198		
			941	1797	953		962		966		952		
2			33278		31481	1786	29695	1770	27925	1775	26150	1755	24395
							963		953		967		963
3							30658	1780	28878	1761	27117	1759	25358
													943
4													26301

The vibrational intervals of around 1800 and 980 cm^{-1} presumably correspond to the C=O vibration in the lower and upper states, and are similar, allowing for anharmonic terms, to the intervals in the formula given by Vaidya (1951), but the actual arrangement of bands in the array appears to be different.

For HCO the main array uses only slightly larger vibrational intervals. Without knowing the other vibrational frequencies and their isotopic shift, it is not possible to use the present data definitely to assign an origin to the band system or to assign values of v'' with certainty.

References

Bell, J., 1937, *Proc. Roy. Soc.* A, **158**, 429.
Dyne, P. S., and Style, D. W. G., 1947, *Disc. Faraday Soc.*, **2**, 159.
Gaydon, A. G., 1957, *The Spectroscopy of Flames* (London: Chapman and Hall), p. 118.
Herzberg, G., and Ramsay, D. A., 1956, *Proc. Roy. Soc.* A, **233**, 34.
Hornbeck, G. A., and Herman, R. C., 1951, *Industr. Engng Chem.*, **43**, 2739.
—— 1954, *Energy Transfer in Hot Gases*, Nat. Bur. Stand. Circular, **523**, 9.
Ramsay, D. A., 1953, *J. Chem. Phys.* **21**, 960.
Smith, E. C. W., 1940, *Proc. Roy. Soc.* A, **174**, 110.
Spokes, G. N., 1959, *Seventh Symposium on Combustion* (London: Butterworths), p. 229.
Vaidya, W. M., 1934, *Proc. Roy. Soc.* A, **147**, 513.
—— 1951, *Proc. Phys. Soc.* A, **64**, 428.

Ageing Effect in Evaporated Films of Zinc Sulphide

By LEE SANG SOO†

Technical Optics Section, Physics Department, Imperial College, London

Communicated by W. T. Welford; MS. received 26th March 1959, in final form 29th April 1959

Earlier work on the application of dielectric thin solid films to optical purposes has been mainly in the production of interference devices and few attempts have been made to measure instability or ageing after the films are prepared. However, recently this instability has acquired great importance due to effects such as the shift of the predetermined position of the pass band of an interference filter and broadening of the band.

Magnesium fluoride films have been observed to age (Greenland and Billington 1950) but zinc sulphide films have been found to be very stable to within one unit of the second decimal place of the refractive index (Hall and Ferguson 1955), and it has been suggested that the instability of a system of MgF_2 and ZnS films such as the all-dielectric interference filter is due to the irregular instability of the former.

To investigate possible changes in ZnS films, it is necessary to use a very sensitive method of measurement, as the changes are apparently so small, the apparatus, described elsewhere in detail (Lee Sang Soo 1959), is a modified form of Rayleigh refractometer with photoelectric detection. It measures the difference in phase between light transmitted through the film under test and through the

† Now at College of Liberal Arts and Sciences, Seoul National University, Republic of Korea.

same geometrical thickness of air, with a probable deviation of about $\pm\lambda/7000$, by detecting the amplitude of the fundamental frequency component introduced to the system by oscillating the double slit Fraunhofer diffraction pattern in a small amplitude of the order of one-tenth of a fringe, which makes the expansion to a Taylor series possible.

The samples of ZnS used in the present investigation are as follows :

Material	Impurity (%)	Producer
A	0·004 (0·001% of each of Sn, Mg, Si and Mn)	Levy and West Ltd.
B	0·16 (0·04% of each of Sn, Mg, Si and Cd)	Levy and West Ltd.
C	2·5 (0·5% of each of Ca, Mg, Cd, Mn and Pb)	Hopkin and Williams Ltd.

and the analytical data are to be found in Musset's thesis (1957).

Throughout the present investigation the specimens were all prepared under the same optimum conditions found after repeated trials so as to eliminate any differences between specimens, namely the speed of the deposit was approximately

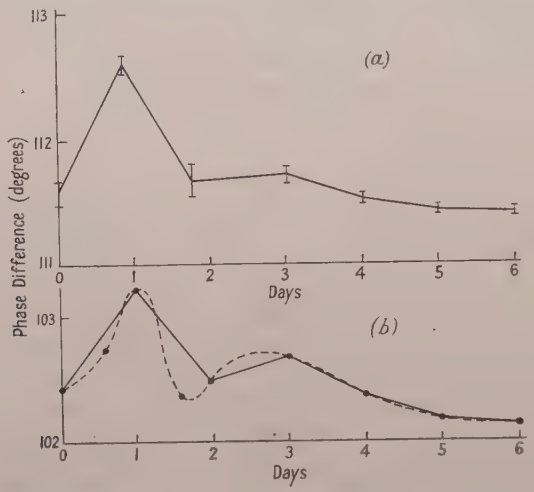

The ageing effect of ZnS impurity 0·004% (optical thickness of the film $\sim\lambda/2$).

90 Å min^{-1} which is near to Rood's suggestion of 100 Å min^{-1} and the material charged in the molybdenum boat was thoroughly baked before evaporation, following Hall and Ferguson's (1955) report. No specimen developed the common defects in ZnS films which are a milky bloom and spots. The thickness of the film was controlled visually by observing the sequence of interference colours and $\lambda/2$ thickness was used to obtain equal amplitudes on the two slits of the interferometer; otherwise some disadvantages occur in measurement.

The results which follow were all obtained with a probable deviation in each measurement of less than $\pm 0{\cdot}15$ degree from at least five complete measurements, and during the period of a series of measurements for about a week, the film under test was kept in position in the apparatus to eliminate possible error due to resetting.

The phase differences were measured in degrees and the results from material A, the purest one, are given in the figure, the points being obtained in most cases at intervals of a day. Graph (*a*) shows features which are typical of all experiments, the initial rise and then gradual drop to a final value near to the initial value.

Graph (*b*) is from another specimen of the same material and additional points were taken in the first two days in which the curve varies most significantly according to the smooth curve. It can be seen that corresponding points of (*a*) and (*b*) agree well. The results from materials B and C gave similar but more pronounced peaks and results obtained are summarized as follows :

Material	A	B	C
Impurity (%)	0·004	0·16	2·5
Main peak occurs after (days)	1	$1\frac{1}{2}$	$2\frac{1}{3}$
Total ageing period (days)	5 to 6	6 to 7	8
Height of the peak (degrees)	0·9	1·7	2·6
Slow hump for (days)	3	$3\frac{1}{2}$	4

From this table it is seen immediately that the ageing effect increases with the increasing impurity, but it is by no means simply related to the original impurity of the material evaporated. This may suggest that the well-known decomposition and hydrolysis of zinc sulphide during the progress of evaporation must be taken into account in clarifying the ageing effect of the film.

Acknowledgment

My sincere thanks are due to Dr. W. T. Welford for suggesting the problem and for his advice and encouragement throughout.

References

Greenland, K. M., and Billington, C., 1950, *Proc. Roy. Soc.* B, **63**, 359.
Hall, J. F., and Ferguson, W. F. C., 1955, *J. Opt. Soc. Amer.*, **45**, 74.
Lee Sang Soo, 1959, *Thesis*, University of London.
Musset, E. A., 1957, *Thesis*, University of London.

Electric Conduction in Semiconductors

By H. Fröhlich† and G. L. Sewell‡

† Department of Theoretical Physics
‡ Mathematical Institute, University of Liverpool

MS. received 1*st June* 1959

Electric conduction in semiconductors with high mobility μ is well understood. Difficulties arise, however, in the case of semiconductors with low mobility as has been pointed out on various occasions by A. F. Joffé (e.g. Joffé 1956). In the present note we shall show that the usual theory actually is invalid in these cases, and we shall give a qualitative survey of the modes of conduction in such semiconductors. According to Joffé, typical values for mean free path l and velocity v according to the usual theory would be 10^{-9} cm sec^{-1} and 10^{-7} cm sec^{-1} respectively, values which, as he emphasizes, are incompatible with Heisenberg's uncertainty relation. This argument must be somewhat modified because the above value for v is obtained from a mean kinetic energy $3kT/2$ (T = temperature) on the assumption that the effective mass m^* is equal to the electronic mass m. Also since μ and not l is normally

measured, the requirements of the uncertainty relation in the usual semiconductor theory (assuming absence of degeneracy) can be expressed as

$$\frac{3}{2}kT > \frac{\hbar}{\tau} = \frac{e\hbar}{m^*\mu} \qquad \ldots\ldots(1)$$

where $\tau = l/v$ is the relaxation time, $\hbar/\tau$ the energy uncertainty and

$$\mu = e\tau/m^*. \qquad \ldots\ldots(2)$$

Express μ in $\mathrm{cm^2\,sec^{-1}\,v^{-1}}$; then (1) implies that

$$\frac{m^*}{m} > \frac{2}{3}\frac{e}{300}\frac{\hbar}{mkT\mu} \simeq \frac{20}{\mu}\frac{300}{T}. \qquad \ldots\ldots(3)$$

Joffé's values for l and v correspond to

$$\mu \sim 10^{-1}\,\mathrm{cm^{-2}\,sec^{-1}\,v^{-1}}.$$

Inequality (3) appears in the first place as a condition which the effective mass must satisfy in order to permit discussion of semiconductors in terms of the conventional theory. However, equations (1) and (2) are correct only if m^*/m is not too large. Large values of m^*/m entail narrow bands and the usual theory breaks down whenever the band width W is less than $k\theta$ (θ = Debye temperature). For remembering that $\mathbf{v} = (1/\hbar)(\partial E(\mathbf{K})/\partial \mathbf{K})$ is the velocity of a state of wave vector $\mathbf{K}$ and band energy $E(\mathbf{K})$, the maximum velocity in a band is of the order

$$v_{\max} \simeq Wa/\hbar \simeq sW/k\theta \qquad \ldots\ldots(4)$$

where s is the velocity of sound and a the lattice distance. Whenever

$$v_{\max} < s, \qquad \text{i.e. } W < k\theta \qquad \ldots\ldots(5)$$

then absorption or emission of single acoustic phonons becomes impossible in view of energy and wave vector conservation. In this case, therefore, the usual $\mu \propto T^{-3/2}$ law becomes invalid. Furthermore, equation (2) also breaks down. For on the assumption of an appropriate scattering mechanism described by a relaxation time $\tau(K)$, the current density j in the say i direction is in the usual way obtained as

$$j = -\frac{e^2F}{\hbar^2}\int\left(\frac{\partial E}{\partial K_i}\right)^2 \tau\frac{\partial f}{\partial E}\,d\mathbf{K} = \frac{e^2F\overline{n\tau v_i^2}}{kT}, \qquad \ldots\ldots(6)$$

where F is the field, f the (Maxwell) distribution and n the number density of electrons. The bar indicates appropriate averaging. Thus

$$\mu = \frac{e\tau\overline{v_i^2}}{kT} \simeq \frac{e\tau}{kT}\frac{W^2a^2}{\hbar^2} \qquad \ldots\ldots(7)$$

provided $W < kT$, because then $\overline{v^2}$ is of the order $v_{\max}{}^2$. In this case the uncertainty relation requires $W > \hbar/\tau$, or

$$\mu > \frac{ea^2}{\hbar}\frac{W}{kT}, \qquad \text{if } W < kT. \qquad \ldots\ldots(8)$$

Before discussing a number of modes of scattering we wish to point out that very narrow bands are well feasible in particular in dealing with substances such as oxides where atomic wave functions tend to overlap relatively little. In the first place through application of Bloch's tight binding approximation this would not lead to a drastic reduction of band width. It is necessary, however, to consider displacement of ions due to localized wave functions and hence to include in the overlap integrals not only electronic but also ionic contributions.

The latter may lead to a very drastic reduction of band width. Details of this have been worked out by Sewell (1958) after a sketch by Fröhlich (1957) where it is shown that occurrence of dielectric loss of the Debye type due to electrons (observed in oxides and similar substances) can be understood only in terms of very small overlap integrals corresponding to extremely narrow bands. This latter thus provides some experimental evidence for very high effective mass.

In discussing now modes of scattering in bands whose width W is less than kT it will first be observed that electrons can in this case be represented by nearly localized wave packets. Nevertheless, for some purposes it is useful to employ extended wave functions. In considering first scattering by impurities it is important to realize that perturbation theory cannot be employed because in general W will be small compared with the magnitude of the potential of the impurity. Short range repulsive potentials will normally lead to a scattering cross section A of the order of the geometrical cross section because of the relatively large wave vectors of the electrons (order π/a). This leads to a mean free path of the order $1/An_i$, n_i being the number density of impurities. Since the velocity is of the order v_{max}, equation (4), we find the mobility μ_i from equation (7),

$$\mu_i \simeq \frac{e}{kT}\frac{Wa}{\hbar}\frac{1}{An_i}. \qquad \ldots\ldots(9)$$

It will be noticed that condition (8) holds provided $n_i < 1/Aa$, a trivial condition.

In turning now to scattering by lattice vibrations, again it is of importance to realize that it would be wrong to treat the electron–phonon interaction as perturbation. Instead use can be made of the narrowness of the bands which permits the lattice displacements to follow the electronic motion in a nearly adiabatic way. Starting, for example, from localized electronic wave functions for which interactions with lattice displacements can be treated in a nearly exact way (cf. Sewell 1958) the remaining energy terms lead to electronic transitions to neighbouring sites. The matrix elements for these can be classified according to the change in phonon quantum numbers connected with such transitions; no change leads simply to formation of the band as indicated above. To deal with a more definite model we shall assume that interaction with optical modes is principally responsible for the reduction of the band width to W. Matrix elements for emission and absorption of acoustic phonons are then found proportional to W but in contrast to the case of wide bands they may even in first order involve more than one phonon. For a z-phonon process they are found proportional to g^z where the important factor g is the ratio of two lengths: the acoustic mode contribution to the displacement of an ion through an electron on a neighbouring site, and the magnitude of the ion's zero point displacement. By appropriate summations these matrix elements can be coordinated to extended wave functions, but this concept is useful only if $g < 1$ (unless $T \ll \theta$) because otherwise electronic jumps connected with phonon processes become more important than those without. For $g < 1$ then, since single-phonon processes are prohibited by energy-wave vector conservation, the main contribution arises from two-phonon (absorption of a phonon with wave vector $\mathbf{w}_1$, quantum number n_1; emission of a phonon $\mathbf{w}_2$, n_2) process. These matrix elements are found of the order

$$M_2 \simeq \frac{1}{N} W g^2 a (w_1 w_2 n_1 (1+n_2))^{1/2} \qquad \ldots\ldots(10)$$

where N is the total number of atoms. For $T > \theta$, i.e. $n_1 \propto T$, $1+n_2 \propto T$, these

processes occur with a probability proportional to W^2T^2. Equation (7) then shows that the corresponding mobility μ_L becomes proportional to T^{-3}, but is independent of W,

$$\mu_L \simeq \frac{ea^2}{\hbar}\frac{1}{g^4}\left(\frac{\theta}{T}\right)^3, \quad \text{if} \quad g<1,\ T>\theta,\ W<k\theta. \qquad \ldots\ldots(11)$$

For $T \ll \theta$ the cube has to be replaced by the eighth power but impurity scattering will then be predominant.

The above case is realized when interaction with acoustic modes is relatively weak ($g<1$) but when interaction with optical modes is sufficiently strong to reduce the band width to $W<k\theta$ so that the usual $T^{-3/2}$ law becomes invalid. At $T=\theta$, equation (11) leads to $\mu_L > 1\,\mathrm{cm^2\,sec^{-1}\,v^{-1}}$ (using $a \simeq 3\times10^{-8}$ cm), and comparison with condition (8) shows that no contradiction with the uncertainty relation arises. Note that $g=\frac{1}{4}$ would lead to $\mu_L \simeq 300$.

Quite a number of cases have been reported in the experimental literature which might find their explanation in terms of equation (11). Thus Joffé (1957) and Putley (1952) find for PbTe, PbSe, or PS either a T^{-3} or a $T^{-5/2}$ law. It must be pointed out that the experiments do not always permit a clear distinction between the two; also impurity scattering is probably not negligible so that the T^{-3} law should be approached for rather pure samples only.

It is evident now that empirical values of μ_L below or of the order of $1\,\mathrm{cm^2\,sec^{-1}\,v^{-1}}$ must correspond to the case of strong interaction with acoustic phonons, i.e. $g>1$. At sufficiently high temperatures scattering by optical modes may also become important. As mentioned above the use of extended wave functions is not a useful concept in this case, except for very low temperatures, because the jumping of a localized electron to a neighbouring site will almost certainly be accompanied by multi-phonon processes (most likely an equal number of absorptions and emission involving very little energy change). We have so far considered this jumping conductivity only for two-phonon processes where it leads to a mobility

$$\mu_J \simeq \frac{ea^2}{\hbar}\left(\frac{W}{k\theta}\right)^2 g^4\left(\frac{T}{\theta}\right), \qquad T \gg \theta. \qquad \ldots\ldots(12)$$

This type of conduction—i.e. transfer of an electron from a lattice site to its neighbour with the help of lattice vibrations—does of course exist even if $g<1$. In this case it leads however to currents which are smaller by a factor $g^8(W/k\theta)^2 \ll 1$ than the usual conduction currents, and therefore are negligible. Clearly this is reversed when g is sufficiently larger than unity. In this case, however, two-phonon processes are probably negligible compared with multi-phonon processes and a new approach is therefore preferable. It seems likely that such multi-phonon processes essentially can be described in terms of thermal fluctuations leading to temporary reductions of the potential barrier surrounding a localized electron and hence to a mobility which increases strongly with temperature. In this event Fe_2O_3 and NiO might provide examples for Morin (1954) found here mobilities which increase strongly with temperature but are always well below $1\,\mathrm{cm^2\,sec^{-1}\,v^{-1}}$.

References

Fröhlich, H., 1957, *Arch. Sci., Genève*, **10**, 5.

Joffé, A. F., 1956, *Proceedings of the International Conference on Electron Transport, Canad. J. Phys.*, **34**, 1393.

—— 1957, *Semiconductor Thermoelements and Thermoelectric Cooling* (London: Infosearch), pp. 140–141.

Morin, F. J., 1954, *Phys. Rev.*, **93**, 1195, 1199.
Putley, E. H., 1952, *Proc. Phys. Soc.* B, **65**, 388.
Sewell, G. L., 1958, *Phil. Mag.*, **36**, 1361.

A Strong Absorption System in Type I Diamonds

By F. A. RAAL
Diamond Research Laboratory, Johannesburg, S. Africa

MS. received 19*th June* 1959

Robertson, Fox and Martin (1934) suggested the existence of two types of diamond, Type II having a transparency in the ultra-violet down to 2250 Å compared with about 3000 Å in Type I.

Nayar (1942) showed that there is no complete cut-off at 3000 Å in the spectrum transmitted by the Type I variety and that the cut-off could be extended progressively towards shorter wavelengths by reducing the thickness of the specimen. It was subsequently shown by Custers and Raal (1957) that, if sufficiently thin specimens are employed, Type I diamonds can be made to transmit down to 2220 Å which is also the limit for Type II diamonds. They concluded, in agreement with other investigators, that this limit constitutes the fundamental absorption edge of diamond. In Type I diamonds a secondary absorption edge is superimposed on this fundamental absorption which, according to Kaiser and Bond (work being published) is due in a large measure to the presence of nitrogen as an impurity in substitutional sites in these particular diamonds.

Clark, Ditchburn and Dyer (1956) made a very thorough study of the absorption spectra of diamonds. Type II diamonds were shown to have no sharp absorption bands and little change was observed on varying the temperature.

Type I diamonds, on the other hand, exhibit eight distinct sets of absorption bands which are numbered N_1, $N_2 \ldots N_8$. It was shown by the authors that a definite correlation exists between certain sets of bands and they suggested that the natural absorption bands of Type I diamonds be classified as:

Group A, consisting of N_5, N_6, N_7, N_8 and the secondary absorption edge;
Group B, composed of N_2, N_3 and N_4.

Group A bands are strongly temperature dependent while Group B bands are quite sharp even at room temperature. Also Group A bands do not appear to have systems of ancillary lines similar to those associated with the principal bands of Group B from which it was concluded that two independent absorption centres A and B are responsible for the absorption bands observed in Type I diamonds.

The region below 3000 Å was not explored by them although the existence of a band located at about 2355 Å was established for one diamond of intermediate type. This band, as well as one at approximately 2300 Å, was first observed by Robertson *et al.* (1934) and later confirmed by Bai (1944) and Ramanathan (1946). It was suggested by the last two workers that the intensity and breadth of the bands are directly correlated with the intensity of luminescence of the diamond, i.e. the N_3 absorption band system since, as was shown by Dyer and Matthews

(1958), the fluorescence emission spectrum at 4150 Å for diamond is approximately the mirror image of the absorption band system at this wavelength. Champion and Humphreys (1957) contradicted the existence of any such correlation. The present experiments were done to verify the existence of these bands by a different method and to find out if any correlation with the known Type I band systems exists.

Very thin parallel-sided slabs of Type I diamond were necessary for the investigation since only with these could the transmission be extended beyond the required wavelength. To obtain these thin plates presented a major experimental obstacle since, whereas Type II diamonds can be cleaved readily into thin plates, Type I diamonds, not being laminar, are inclined to shatter and give pieces with curved surfaces quite unsuitable for optical work. Several thin parallel-sided plates varying in thickness from 0·04 mm to 0·50 mm were finally obtained by means of a special polishing process.

Light absorption measurements were made at room temperature on an adapted model DU Beckman spectrophotometer. The instrument has wavelength settings reproducible to 0·5 Å in the ultra-violet region and great accuracy could be obtained by using the most sensitive range of the instrument. The thin plates were used for measurements up to 3000 Å but, beyond this, slabs of about 1 mm thickness were used to increase the accuracy of the measurements.

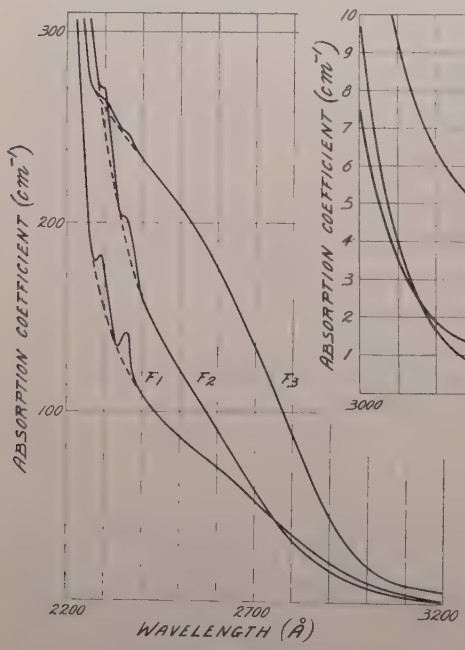

Figure 1. Absorption coefficients of diamonds F_1, F_2 and F_3 in the range 2200–3200 Å.

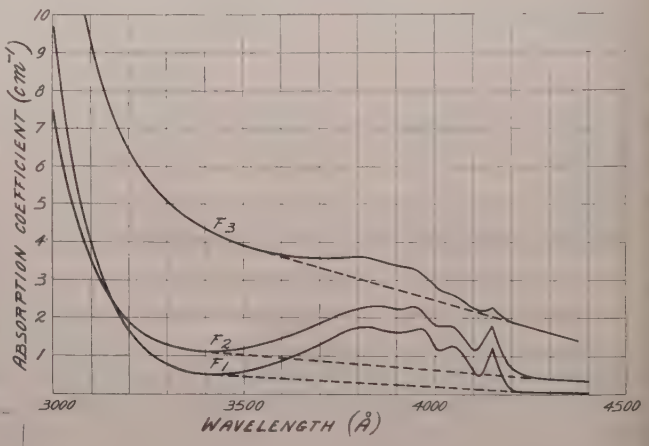

Figure 2. Absorption coefficients of diamonds F_1, F_2 and F_3 in the range 3000–4500 Å.

The absorption coefficients of three diamonds F_1, F_2 and F_3 having different degrees of fluorescence are plotted as a function of the wavelength in figures 1 and 2.

The existence of bands at 2290–2310 Å and 2350–2370 Å is plainly evident from figure 1 in full agreement with Robertson *et al.* (1934) and the Indian

school (Bai 1944, Ramanathan 1946). Comparison of the integrated areas of these bands revealed that they bear a constant ratio to each other even though the absolute values differ over a wide margin from specimen to specimen. It is reasonable to assume, therefore, that they belong to one and the same system which we shall designate N_9.

In figure 2 the N_3 band system which is associated with the fluorescence of diamond is depicted for F_1, F_2 and F_3 respectively. F_1 and F_2 are strongly blue fluorescent while F_3 fluoresces blue only weakly. The bands at about 3840, 3940, 4030 and 4150 Å which form the greater part of the N_3 system are clearly in evidence. Measurements of the integrated areas between the continuum (dotted lines) and the N_3 and N_9 band systems are consistent with the existence of correlation between these systems. The ratio of the strength of N_9 to that of N_3 is approximately 2 : 1 and N_9 thereby constitutes the strongest natural absorption band system found in Type I diamonds to date.

Acknowledgments

The author wishes to thank Messrs. Industrial Distributors (1946) Ltd., for permission to publish this note and is grateful to Dr. J. F. H. Custers, Director of Research, for his advice and interest.

References

Bai, K. S., 1944, *Proc. Indian Acad. Sci.* A, **19,** 253.
Champion, F. C., and Humphreys, D. L. O., 1957, *Proc. Phys. Soc.* B, **70,** 320.
Clark, C. D., Ditchburn, R. W., and Dyer, H. B., 1956, *Proc. Roy. Soc.* A, **234,** 363.
Custers, J. F. H., and Raal, F. A., 1957, *Nature, Lond.*, **179,** 268.
Dyer, H. B., and Matthews, I. G., 1958, *Proc. Roy. Soc.* A, **243,** 320.
Nayar, P. G. N., 1942, *Proc. Indian Acad. Sci.*, **15,** 293.
Ramanathan, K. G., 1946, *Proc. Indian Acad. Sci.* A, **24,** 137.
Robertson, R., Fox, J. J., and Martin, A. E., 1934, *Phil. Trans. Roy. Soc.* A, **232,** 463.

Decomposition of 3×3 Matrices

By P. ROMAN
Department of Theoretical Physics, The University, Manchester, England

MS. received 28*th May* 1959

As is well known, the four-element Pauli algebra $1, \tau_1, \tau_2, \tau_3$, which is generated by the three elements τ_i, enables one to express any 2×2 matrix as a linear combination of the elements of this algebra. Similarly, 4×4 matrices can be decomposed in terms of the sixteen-element Dirac algebra which is generated by the four Dirac matrices γ_α.

In the following we shall develop an algebra which allows the expansion of any 3×3 matrix. Such a device can be useful for many physical applications; the problem which has actually led us to develop this method is that of the decomposition of the correlation matrix of an arbitrary electromagnetic field (Roman 1959).

The familiar analogue (see, for example, Votruba 1951) of the Pauli spin matrices for the case of spin one is, in a suitable representation,

$$\xi_1=\frac{1}{\sqrt{2}}\begin{bmatrix}0&1&0\\1&0&1\\0&1&0\end{bmatrix},\quad \xi_2=\frac{1}{\sqrt{2}}\begin{bmatrix}0&-i&0\\i&0&-i\\0&i&0\end{bmatrix},\quad \xi_3=\begin{bmatrix}1&0&0\\0&0&0\\0&0&-1\end{bmatrix}. \qquad \ldots\ldots(1)$$

These satisfy the angular momentum commutations relations

$$\xi_1\xi_2-\xi_2\xi_1=i\xi_3 \text{ and cycl.,} \qquad \ldots\ldots(2)$$

and their eigenvalues are $+1$, 0, -1. It has long been known that, besides (2), they also satisfy the Kemmer relations

$$\xi_i\xi_k\xi_l+\xi_l\xi_k\xi_i=\xi_i\delta_{kl}+\xi_l\delta_{ki}, \qquad (i, k=1, 2, 3). \qquad \ldots\ldots(3)$$

Using these relations, it can be seen that the three elements ξ_i $(i=1, 2, 3)$ generate a 35-element algebra. This 'three-dimensional' Kemmer algebra has been discussed, with all other Kemmer algebras, in a paper by Kemmer (1943). The algebra is semi-simple, and has four commuting elements. Hence, from the generalized theorem of Frobenius and Schur, which states that

$$n=n_1^2+n_2^2+\ldots+n_r^2,$$

where n is the number of elements, r the number of commuting elements, and n_s the dimension of the sth irreducible representation, it follows that the algebra in question has four inequivalent irreducible representations of dimension 1, 3, 3 and 4 respectively. One of the two three-dimensional 'twin representations' for the generating elements is given by (1); the other differs only in sign.

Both the three- and four-dimensional representations have been used extensively in problems connected with the isobaric properties of elementary particles (see, for example, Votruba 1951, Votruba and Lokajíček 1958).

It is clear that any 3×3 matrix can be decomposed into a linear combination of the 35 elements generated by the three 3×3 matrices ξ_i or $-\xi_i$. We search for a 'minimal algebra', however, which serves the same purpose. This algebra must consist of nine elements. To find it, consider the three matrices

$$\sigma_1\equiv\xi_3, \qquad \sigma_2\equiv\frac{1}{\sqrt{2}}(\xi_1+i\xi_2), \qquad \sigma_3\equiv\frac{1}{\sqrt{2}}(\xi_1-i\xi_2). \qquad \ldots\ldots(4)$$

By direct calculation we find that the linearly independent products which can be formed of these three generators are

$$\sigma_1^2\equiv\sigma_4, \qquad \sigma_2\sigma_3\equiv\sigma_5, \qquad \sigma_1\sigma_3\equiv\sigma_6, \qquad \sigma_2^2\equiv\sigma_7, \qquad \sigma_3^2\equiv\sigma_8.$$

All other double (and, consequently, all other higher order) products can be expressed as linear combinations of the 3×3 unit matrix and the eight matrices $\sigma_1, \ldots, \sigma_8$. Thus we have arrived at the nine-element algebra

$$\left.\begin{aligned}
\sigma_0&=\begin{bmatrix}1&0&0\\0&1&0\\0&0&1\end{bmatrix}, \quad \sigma_1=\begin{bmatrix}1&0&0\\0&0&0\\0&0&-1\end{bmatrix}, \quad \sigma_2=\begin{bmatrix}0&1&0\\0&0&1\\0&0&0\end{bmatrix},\\
\sigma_3&=\begin{bmatrix}0&0&0\\1&0&0\\0&1&0\end{bmatrix}, \quad \sigma_4=\begin{bmatrix}1&0&0\\0&0&0\\0&0&1\end{bmatrix}, \quad \sigma_5=\begin{bmatrix}0&0&0\\0&0&-1\\0&0&0\end{bmatrix},\\
\sigma_6&=\begin{bmatrix}0&0&0\\0&0&0\\0&-1&0\end{bmatrix}, \quad \sigma_7=\begin{bmatrix}0&0&1\\0&0&0\\0&0&0\end{bmatrix}, \quad \sigma_8=\begin{bmatrix}0&0&0\\0&0&0\\1&0&0\end{bmatrix}.
\end{aligned}\right\} \ldots(5)$$

We notice that this algebra has only one element which commutes with all others, namely the unit matrix σ_0. Further, by applying the criterion $\det G \neq 0$, where $G=(G_{AB})=\mathrm{Tr}\,(\sigma_A\sigma_B)$ (see, for example, Kemmer 1939), we find that this algebra is semi-simple. Consequently, by the above-mentioned theorem of Frobenius and Schur, the algebra has just one irreducible representation and this is a three-dimensional one. Therefore, up to equivalence, the representation (5) is unique.

It is, however, useful to find a Hermitian representation. This can be obtained by constructing the linear combinations

$$\rho_0\equiv\sigma_0,\quad \rho_1\equiv\sigma_1,\quad \rho_2\equiv(\sigma_2+\sigma_3),\quad \rho_3\equiv i(\sigma_2-\sigma_3),\quad \rho_4\equiv\sigma_4,$$
$$\rho_5\equiv(\sigma_5+\sigma_6),\quad \rho_6\equiv i(\sigma_5-\sigma_6),\quad \rho_7\equiv(\sigma_7+\sigma_8),\quad \rho_8\equiv i(\sigma_7-\sigma_8).$$

Explicitly, we have

$$\left.\begin{aligned}
\rho_0&=\begin{bmatrix}1&0&0\\0&1&0\\0&0&1\end{bmatrix},\quad \rho_1=\begin{bmatrix}1&0&0\\0&0&0\\0&0&-1\end{bmatrix},\quad \rho_2=\begin{bmatrix}0&1&0\\1&0&1\\0&1&0\end{bmatrix},\\
\rho_3&=\begin{bmatrix}0&i&0\\-i&0&i\\0&-i&0\end{bmatrix},\quad \rho_4=\begin{bmatrix}1&0&0\\0&0&0\\0&0&1\end{bmatrix},\quad \rho_5=\begin{bmatrix}0&0&0\\0&0&-1\\0&-1&0\end{bmatrix},\\
\rho_6&=\begin{bmatrix}0&0&0\\0&0&-i\\0&i&0\end{bmatrix},\quad \rho_7=\begin{bmatrix}0&0&1\\0&0&0\\1&0&0\end{bmatrix},\quad \rho_8=\begin{bmatrix}0&0&i\\0&0&0\\-i&0&0\end{bmatrix}.
\end{aligned}\right\}\quad\ldots\ldots(6)$$

Clearly, any 3×3 matrix $A=(a_{rs})$ can be decomposed by our algebra into the form

$$A=\sum_{\alpha=0}^{8} r_\alpha\rho_\alpha. \qquad\ldots\ldots(7)$$

For the nine coefficients r_α we find:

$$\left.\begin{aligned}
r_0&=a_{22},\\
r_1&=\tfrac{1}{2}(a_{11}-a_{33}),\\
r_2&=\tfrac{1}{2}(a_{21}+a_{12}),\\
r_3&=\frac{i}{2}(a_{21}-a_{12}),\\
r_4&=\tfrac{1}{2}(a_{11}+a_{33}-2a_{22}),\\
r_5&=\tfrac{1}{2}(a_{21}+a_{12}-a_{32}-a_{23}),\\
r_6&=\frac{i}{2}(a_{21}-a_{12}-a_{32}+a_{23}),\\
r_7&=\tfrac{1}{2}(a_{31}+a_{13}),\\
r_8&=\frac{i}{2}(a_{31}-a_{13}).
\end{aligned}\right\}\quad\ldots\ldots(8)$$

If the matrix A is Hermitian then all coefficients r_α will be real. If A is symmetric then

$$r_3=r_6=r_8=0.$$

If A is antisymmetric then

$$r_0=r_1=r_2=r_4=r_5=r_7=0.$$

References

Kemmer, N., 1939, *Proc. Roy. Soc.* A, **173**, 91.
—— 1943, *Proc. Camb. Phil. Soc.*, **39**, 189.
Roman, P., 1959, *Nuovo Cim.*, Ser. X, **13**, 974.
Votruba, V., 1951, *Phys. Rev.*, **85**, 141.
Votruba, V., and Lokajíček, M., 1958, *Report* P-191, Joint Institute for Nuclear Research, Dubna.

Nucleon Polarization from Charge-exchange Reactions in Deuterium

By R. J. N. Phillips

Theoretical Physics Division, Atomic Energy Research Establishment, Harwell, Didcot, Berks.

Communicated by W. M. Lomer; *MS. received 3rd June* 1959

This note considers the polarization of fast neutrons emerging in the forward direction ($\theta=0$) from high-energy d(p, n) reactions when the incident protons are polarized, and the polarization at small angles when the incident beam is unpolarized. Our results apply equally to the 'mirror' reaction d(n, p). The impulse approximation (Chew 1950, 1951, Chew and Wick 1952) is used, neglecting multiple scattering, to relate these effects to nucleon–nucleon phase shifts.† Numerical examples are given for the inter-nucleon potentials of Gammel and Thaler (1957) and Signell and Marshak (1958); we find that the neutron polarization differs appreciably from that in the corresponding free p–n scattering; this difference is due to the action of the Pauli principle in the residual two-proton system.

Let us label the bombarding proton, the struck neutron and the second proton by suffices 1, 2 and 3 respectively. Then for transitions from an initial proton momentum $\mathbf{k}_1$ and deuteron state ϕ to a (fast) neutron momentum $\mathbf{k}_2'$ and final two-proton state ψ, the impulse approximation replaces the true three-body t-matrix‡ by the n–p t-matrix, according to

$$\langle \mathbf{k}_2', \psi | t | \mathbf{k}_1, \phi \rangle$$

$$\simeq \int d\mathbf{k}_1' \, d\mathbf{k}_3' \, d\mathbf{k}_2 \, d\mathbf{k}_3 \, \psi^*(\mathbf{k}_1', \mathbf{k}_3') \langle \mathbf{k}_1' \mathbf{k}_2' | t_{\mathrm{np}} | \mathbf{k}_1 \mathbf{k}_2 \rangle \times \delta(\mathbf{k}_3' - \mathbf{k}_3) \phi(\tfrac{1}{2}[\mathbf{k}_2 - \mathbf{k}_3]) \delta(\mathbf{k}_2 + \mathbf{k}_3), \quad \ldots\ldots (1)$$

$$\simeq \langle t_{\mathrm{np}} \rangle \int d\mathbf{k}_1' \, \psi^*(\mathbf{k}_1', \mathbf{k}_1 - \mathbf{k}_2' - \mathbf{k}_1') \phi(\mathbf{k}_1' + \mathbf{k}_2' - \mathbf{k}_1), \quad \ldots\ldots (2)$$

in an obvious notation, suppressing spin for brevity.

Equation (1) expresses the impulse approximation proper. In equation (2) the matrix element of t_{np} has been taken outside the integral, to be evaluated at the maximum of the remaining integrand§; this further approximation is

† Similar calculations, for elastic nucleon–deuteron scattering, have been made by Castillejo and Singh (1959) and Sawicki and Watanabe (1959).

‡ We mean the scattering matrix without the energy-conserving δ-function.

§ For the case of small momentum transfer $\mathbf{k}_1 - \mathbf{k}_2'$, which proves to be dominant, this integrand peaks at small values of k_1' and k_2. However, this peak has considerable width, and equation (2) is not a trivial approximation.

always made for convenience in practice. If we specialize the two-proton eigen function ψ to have total momentum $\mathbf{K}$ and internal quantum numbers λ, labelling spin, angular momentum and energy (which is of course related to K^2 by conservation laws), the integral in (2) can be written

$$\delta(\mathbf{k}_1-\mathbf{k}_2'-\mathbf{K})\int d\mathbf{x}\,\psi_\lambda^*(\mathbf{x})\phi(\mathbf{x})\exp(i\tfrac{1}{2}\mathbf{K}.\mathbf{x}). \qquad \ldots\ldots(3)$$

To calculate the outcome of the reaction we must sum over a complete set of ψ_λ for each $\mathbf{K}$. However, for forward and near-forward reactions the overlap integral (3) very strongly favours the smallest values of K and an S-wave for ψ_λ, which is therefore spin singlet by the Pauli principle. Chew (1950, 1951) and Gluckstern and Bethe (1951) call attention to this; it is easy to understand, remembering the strong S-state attraction which almost binds the p–p system. We therefore give $\langle t_{\mathrm{np}}\rangle$ its value for free n–p scattering at the incident energy and the corresponding angle; because of the Pauli principle, however, we have to consider only transitions which leave the two protons in a singlet state.

For convenience we assume a pure S-state deuteron wave function, since the space and spin parts then separate and the polarizations we calculate do not depend on the former. This further approximation introduces very little error roughly estimated at about 1% †.

The t-matrix elements for elastic nucleon–nucleon scattering at given energy and angle are often written as a 4×4 matrix in spin space, $M_{\mu\nu}$ (e.g. Wolfenstein 1956). We use the singlet–triplet representation in which the suffices $\mu, \nu = \mathrm{S}, 1, 0, -1$ represent the singlet and three triplet spin states of the two-nucleon system. Spin is quantized along the incident beam.

If the incident protons have transverse and longitudinal components of polarization P_{t} and P_{l}, respectively, and the deuterons are unpolarized, we find that the neutrons emerging forward have corresponding components of polarization $\alpha_{\mathrm{t}}P_{\mathrm{t}}$ and $\alpha_{\mathrm{l}}P_{\mathrm{l}}$, where

$$\left.\begin{aligned}\gamma\alpha_{\mathrm{t}} &= -|M_{11}-M_{00}|^2-|M_{11}+M_{\mathrm{ss}}|^2+\tfrac{1}{2}|M_{00}+M_{\mathrm{ss}}|^2\\ \gamma\alpha_{\mathrm{l}} &= -|M_{00}+M_{\mathrm{ss}}|^2+\tfrac{1}{2}|2M_{11}-M_{00}+M_{\mathrm{ss}}|^2\\ \gamma &= \;\;|M_{11}-M_{00}|^2+|M_{11}+M_{\mathrm{ss}}|^2+\tfrac{1}{2}|M_{00}+M_{\mathrm{ss}}|^2\end{aligned}\right\}. \qquad \ldots\ldots(4)$$

The n–p M-matrix is evaluated at centre-of-mass angle 180°. α_{t} and α_{l} are to be compared with the 'triple-scattering' parameters $D(\mathrm{p,n})$ and $A'(\mathrm{p,n})$ of Wolfenstein (1954, 1956) which take their places in free p–n scattering, where there are no restrictions from a 'spectator' proton and the Pauli principle. D and A' are given at 180° centre-of-mass angle by

$$\left.\begin{aligned}I_0D &= \tfrac{1}{2}\mathscr{R}M_{11}(M_{00}-M_{\mathrm{ss}})^*\\ I_0A' &= \tfrac{1}{2}|M_{11}|^2+\tfrac{1}{8}|M_{00}-M_{\mathrm{ss}}|^2-\tfrac{1}{8}|M_{00}+M_{\mathrm{ss}}|^2\\ I_0 &= \tfrac{1}{2}|M_{11}|^2+\tfrac{1}{4}|M_{00}|^2+\tfrac{1}{4}|M_{\mathrm{ss}}|^2\end{aligned}\right\}. \qquad \ldots\ldots(5)$$

The table shows numerical values for these parameters, calculated from the phase shifts given by Gammel and Thaler (1957) and Signell and Marshak (1958) at bombarding energies from 40 to 160 Mev. The column for zero energy is included only to confirm the trends suggested by the other figures: our approximation has no physical significance here. α_{l} is the most sensitive to

† For small $\mathbf{K}$, the D-wave part of ϕ contributes mainly through a D-wave ψ_λ. For larger $\mathbf{K}$ it contributes more through an S-wave ψ_λ. In both cases the overlap integral is small.

corrections: the small values shown for most of the range reflect a near-cancellation of large terms.

Potential		Signell–Marshak			Gammel–Thaler	
E (Mev)	0	40	100	150	90	156
α_t	−0·33	−0·49	−0·60	−0·52	−0·54	−0·58
D	0·48	−0·19	−0·45	−0·39	−0·38	−0·50
α_l	−0·33	−0·02	0·19	0·04	0·08	0·16
A'	0·48	0·18	0·27	0·12	0·17	0·20

Let us now consider neutrons emerging at a small laboratory angle θ, small enough for triplet p–p final states to be greatly inhibited. Then for unpolarized incident protons the neutron polarization is β, where

$$\gamma\beta = \sqrt{2}\mathscr{R}i(M_{10} - M_{01})(M_{00} + M_{ss} - 2M_{1-1})^*. \quad \ldots\ldots(6)$$

It is to be compared with the free p–n polarization P_{pn}, where

$$I_0 P_{pn} = \frac{1}{2\sqrt{2}}\mathscr{R}i(M_{10} - M_{01})(M_{11} + M_{00} - M_{1-1})^*. \quad \ldots\ldots(7)$$

Strictly, γ and I_0 here contain extra terms involving M_{10}, M_{01} and M_{1-1} not given in (4) and (5), but these terms are of order θ^2 and may be ignored. In both (6) and (7) M is taken at the centre-of-mass angle $\pi - 2\theta$ (non-relativistically), and the polarization vector is parallel to $\mathbf{k}_i \times \mathbf{k}_f$ where $\mathbf{k}_i$ and $\mathbf{k}_f$ are the initial and final relative p–n momenta. As an illustration we take the Signell–Marshak phase shifts at 100 Mev, for which

$$\beta = -0{\cdot}21\theta, \qquad P_{pn} = -0{\cdot}27\theta \quad \ldots\ldots(8)$$

to first order in θ (radians).

According to Chew and Wick (1952) the impulse approximation introduces errors of order a/kR^2, where a is the two-body scattering amplitude (here meaning some average), k is the incident proton's relative wave number and R is the average nucleon separation in the deuteron ($\sim 3{\cdot}2 \times 10^{-13}$ cm). This quantity is about 5% at 150 Mev and 15% at 40 Mev. These authors also state that multiple scattering corrections may be of order 3% at 200 Mev, rising to 16% at 50 Mev. The accuracy of substituting a mean value for $\langle t_{np} \rangle$ in equation (2) depends on how smoothly t_{np} varies with energy; rough estimates for the examples considered give an error from this cause of about 5% at 100 Mev, and perhaps 10% at 50 Mev. Arguments of Chew (1951) suggest that the neglect of final two-proton triplet states is a fair approximation for neutron angles $\theta < 10°$. Within such limits our formulae should have quantitative significance.

It should be possible to test some of our conclusions experimentally, with one or other of the mirror reactions d(p, n) and d(n, p). The small-angle polarization measurement appears the easiest; the example shown in equation (8) gives $\beta = -0{\cdot}03$ and $P = -0{\cdot}04$ at $\theta = 8°$ and 100 Mev, seemingly within reach of present techniques. To compare the transverse polarization parameters α_t and D (p, n; 180°) requires essentially triple-scattering experiments. None of the latter involving neutrons has yet been performed, but these are among the least difficult. To measure the longitudinal polarization parameters α_l and A' (p, n; 180°) requires triple-scattering experiments with magnetic precessing of the nucleon spin between successive scatterings, which are more difficult.

Measurements of α_t, α_l and β might in principle be used to supplement n–p scattering data, to help to determine unique phase shifts. However, nucleon nucleon experiments of no greater difficulty will probably be sufficient, and would suffer from no theoretical uncertainties.

Our conclusions also suggest a possible application. The d(p, n) reaction may be used to generate a nearly monoenergetic neutron beam from a proton beam. If the protons were partly transverse-polarized, like those from a linear accelerator with a polarized ion source for instance, our examples would predict an appreciable transverse neutron polarization.

Acknowledgments

The author is grateful to Dr. J. S. Bell and Dr. E. J. Squires for helpful discussions. He is also indebted to Dr. L. Castillejo and Dr. L. S. Singh, who have independently reached similar conclusions, for information about their results (unpublished).

References

Castillejo, L., and Singh, L. S., 1959, *Nuovo Cim.*, **11**, 131, 136.
Chew, G. F., 1950, *Phys. Rev.*, **80**, 196.
—— 1951, *Ibid.*, **84**, 710.
Chew, G. F., and Wick, G. C., 1952 *Phys. Rev.* **85**, 636.
Gammel, J. L., and Thaler, R. M., 1957, *Phys. Rev.*, **107**, 291, 1337.
Gluckstern, R. L., and Bethe, H. A., 1951, *Phys. Rev.*, **81**, 761.
Sawicki, J., and Watanabe, S., 1959, *Nuclear Phys.*, **10**, 151.
Signell, P. S., and Marshak, R. E., 1958, *Phys. Rev.*, **109**, 1229.
Wolfenstein, L., 1954, *Phys. Rev.*, **96**, 1654.
—— 1956, *Ann. Rev. Nucl. Sci.*, **6**, 43.

The Scattering of Fast Charged Particles VI: The Multiple Scattering of 10 MeV Electrons and Positrons in Nuclear Emulsions

By K. Phillips and C. Ambasankaran†
Research Department, Metropolitan-Vickers Electrical Co. Ltd., Manchester

MS. received 28th May 1959

§ 1. Introduction

Several investigators have used nuclear emulsions to study the multiple scattering of fast particles and the methods have been widely adopted to the energy and mass determination of cosmic-ray particles. The Bristol University group has been particularly active and has carried out a series of exhaustive researches in these fields, see Gottstein *et al.* (1951) and other papers. Most of the previous work has been concentrated on developing the techniques of energy determination and also on the measurement of the scattering constant of the emulsion and its variation with cell size. Two notable exceptions are the investigations by Voyvodic and Pickup (1952) and Hisdal (1952). The former studied the angular distribution of the scattering deflections for electron pairs

† Now at the Tata Institute, Bombay.

produced by Be γ-rays and compared the distribution with the theory of Williams (1939, 1940). Some differences with this theory were found at the larger angles but the authors mention, however, that the apparent experimental 'excess' can be accounted for by the theories of Molière (1947, 1948) and Snyder and Scott (1949). The other paper by Hisdal described measurements on the multiple scattering of 0·59 MeV electrons. The experimental mean of these results was found to be significantly lower than the value given by Molière's theory.

More recently, Heymann and Williams (1956) have measured the multiple scattering in nuclear emulsions of electrons and positrons with energies up to 2·5 MeV and found significant differences from the theoretical scattering constant and also in the angular distribution. A comparison of the scattering of positrons and electrons in this energy range has already been carried out by Phillips and Allen (1959) using a cloud chamber. A detailed examination of the angular distribution was found to be too tedious by this method and it is the aim of this work to make an accurate comparison of the multiple scattering distribution for 10 MeV electrons and positrons.

§ 2. Experimental Arrangement

The electrons used in this experiment were accelerated by means of a betatron and were scattered out of the glass donut by means of a platinum target attached to the end of the injector gun. They were bent by the magnetic field of the betatron magnet out of the main x-ray beam which was blocked off by means of a 7 ft thick barytes concrete wall. The electrons were then selected and deflected into 400 micron thick G5 emulsions, contained in a thin-walled light-tight box, by means of a 90° spectrometer magnet. The calibration of the magnet was known with an accuracy to $\pm 3\%$ and areas of the plate were chosen so that the energy spread was less than $\pm 5\%$. The positrons used were the positive component of electron pairs produced in a 0·005 in. thick lead target by the high energy x-ray beam which was collimated into a fine pencil beam. A series of visual checks was made on the positrons by means of a Wilson cloud chamber in a magnetic field placed at the back of nuclear plates. This gave a definite indication of the sign of the particles and was considered necessary since it seems inadvisable to allow the whole experiment to depend on the adjustment of the direction of flow of the spectrometer current. Another confirmatory fact which also indicated that the particles in the plates were positrons and not electrons was shown by the fact that several of the tracks appeared to stop in the emulsion indicating possible annihilation.

In order to reduce any distortion in the emulsion to a minimum, a low temperature development technique was used, pre-soaking at 2°c and development at 6°c. All the measurements were carried out using a Cooke, Troughton and Simms type M 4005 nuclear research microscope with a $\times 95$ oil immersion objective and a binocular $\times 6$ eye-piece one of which contained a graticule. The coordinate method of Fowler (1950) was used to measure the scattering. For every track, the coordinates of the point of entry and departure in the emulsion were noted together with the angle of inclination into the emulsion and also the angle with respect to a fixed fiduciary line representing the direction of the incoming beam of particles. If, during the traversal of the emulsion, the angle of the inclination to this fiduciary became greater than 20° then no more

measurements were made on the track since large errors in the measurement of the deflection are likely to occur. The plates were quarter-plate size and only tracks which entered near the centre of the emulsion were measured in order to reduce any distortion effects which are generally more pronounced near the edges of the plates. Two other conditions of acceptance were that the tracks had to be at least 1 mm long and must have entered the emulsion at an angle of less than 10° to the fiduciary line. The measurements of the track deviation were made for cell lengths of 40 microns. An attempt was made to measure every individual deflection to within 0·2 division (0·27 micron) on the graticule. Measurements were made on 300 positron and 300 electron tracks resulting in a total of about 30 000 second differences for both distributions. The resulting mean energy of each distribution, based on the theoretical scattering constant of 21·7, was 10·3 MeV for the electrons and 9·7 MeV for the positrons. These values lie within the estimated energy spread of the spectrometer magnet.

§ 3. The Results and Comparison with Molière's Theory

The angular distribution of the projected angles given by Molière is

$$F(\phi)\,d\phi = \frac{2}{\pi^{1/2}}\left[f^0(\phi) + \frac{f^1(\phi)}{B} + \frac{f^2(\phi)}{B^2} + \ldots \right] d\phi$$

the f functions being tabulated and defined in terms of the parameter

$$\chi_i^2 = 4\pi N e^4 Z(Z+1)\frac{dx}{p\beta^2},$$

with dx equal to the cell length.

This angular distribution is modified due to the contribution from spurious scattering introduced by reading errors and effects due to non-linearities in the microscope stage. The corrections have been calculated by Menon, O'Ceallaigh and Rochat (1951) and involve replacing the parameter B and Ω_b by B^* and $\Omega_b{}^*$ with

$$\ln \Omega_b{}^* = \ln \Omega_b + B\left(\frac{\text{noise}}{\text{signal}}\right)^2$$

where Ω_b is defined as the number of collisions suffered by the particle.

The theory of Molière does not however take into account any effects due to the spin orbital interaction. Spencer and Blanchard (1954) have applied a method for summing slowly converging series of Legendre polynomials and used the single scattering cross section α^2 approximation to refine the theory of Molière for electrons. They point out that the equivalent result could be obtained by multiplying Molière's results by the ratio of the exact single scattering cross section to the cross section used by Molière. The scattering cross section for the α^4 approximation has been calculated by Allen, Phillips and Whittaker (1957) for positrons and electrons for angles less than 30°, but this cross section has to be modified for projected angles.

The Molière distribution together with the modified form are given in figures 1 and 2 for electrons and positrons together with the experimental histograms normalized at the mean value of the scattering angle. The experimental results and the theoretical results for both the electrons and positrons show excellent agreement over the whole range except for scattering near the zero degrees. Here the experimental results are lower than predicted by theory and

this discrepancy may be considered to be due to a somewhat larger value of the noise than estimated.

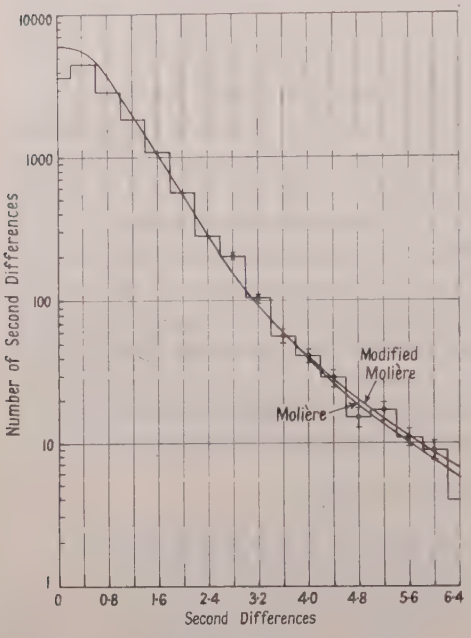

Figure 1. Angular distribution of electrons with a mean energy of 10·3 MeV compared with the theoretical distribution of Molière.

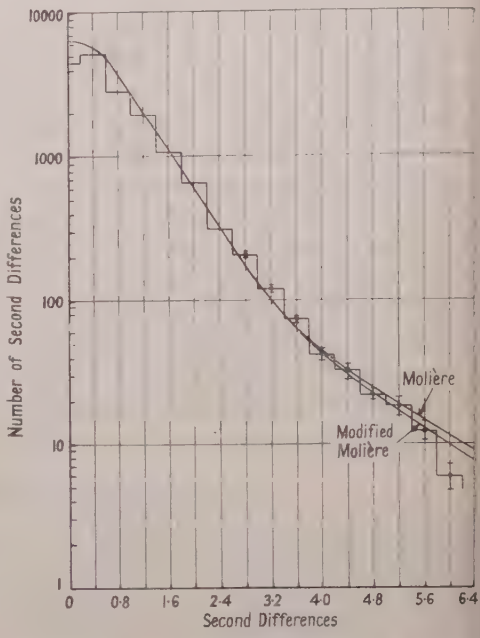

Figure 2. Angular distribution of positrons with a mean energy of 9·7 MeV compared with the theoretical distribution of Molière.

One source of correction which may cause some difference at the large angles is the 'Flachekammer' or flat-chamber effect. This is necessary in order to account for electrons which are scattered at large angles and may go out of the emulsion. If this happens the track length may be comparatively short and owing to the artificially imposed experimental condition that the track must be longer than 1 mm then tracks which undergo large scatters may be omitted. Therefore the observer will tend to select tracks which do not have large angle scatters, this resulting in a reduction in the experimental distribution at large angles. This problem has been considered by O'Ceallaigh and MacCarthaigh (1944) in connection with cloud chambers. Another method of estimating the number of tracks lost, due to scattering out of the emulsion, is to adopt the method used by Allen *et al.* (1956) for the correction of large angle single scattering.

The average fraction of tracks which lie in the conical scattering envelope which are not measurable is

$$\bar{a}=\frac{2}{\pi d}\left[d\cos^{-1}\left(\frac{d}{r}\right)-\left\{r^2-\frac{d^2}{r^2}\right\}^{1/2}+r\right]$$

where d is the depth of the emulsion (400 microns), $r=b\sin\theta$ where θ is the scattering angle, and where b is taken to be the minimum acceptable length of track which in the present case is 1 mm.

If $d<r$, then $b>d/\sin\theta$, i.e. $b>1000$ microns for $\theta=10°$, so even though the electron is scattered through a large angle near the surface of the emulsion it will still be accepted for measurement.

If $d \geqslant r$ then the $\cos^{-1}(d/r)$ term can be neglected and with $d^2/r^2 \geqslant 1$, $\bar{a} \simeq 0{\cdot}03$. The correction is then at the most 3%. By considering different values of $(1-d^2/r^2)^{1/2}$ values of $\bar{a}$ and b can be calculated and, in all the cases of $b<1$ mm, $\bar{a}$ is always less than a few per cent. For scattering angles less than 10° the correction will be correspondingly smaller.

§ 4. Conclusions

There is good agreement between the experimental multiple scattering histogram and the theoretical distribution calculated from Molière's theory for both the electrons and positrons. In the single scattering region there is a tendency for the experimental results to be higher in the case of the electrons and lower for the positrons indicating a somewhat better agreement with the theory of Molière modified to take into account a more accurate single scattering law. However, the experimental probable errors are larger than the differences and more experimental work will have to be done before any significant conclusions may be drawn about this single scattering region. An interesting feature of this work is the agreement between the mean energy of the electrons and positrons deduced from the multiple scattering measurements with the mean energy estimated from the magnetic spectrometer setting. This tends to confirm the work of Husain (1955) that the experimental value of the scattering constant is in good agreement with the theoretical value of 21·7 deduced from Molière's theory. Furthermore, this result suggests that any difference between the multiple scattering of positrons and electrons is likely to be less than $\pm 5\%$. This is in agreement with the theoretical results of Mohr (1954) who showed that the differences will be about 1% for the 10 Mev electrons and positrons.

It is interesting to note however that the electron distribution does not show a significant excess in the single scattering region as found by Hanson *et al.* (1951). The present results are not necessarily inconsistent with the findings of these workers since their experiments were carried out using gold foils at 15·7 Mev and the excess may only be noticeable at the higher values of Z.

Acknowledgments

The authors wish to thank Sir Willis Jackson, Director of Research and Education, Metropolitan-Vickers Electrical Co. Ltd., for permission to publish.

References

Allen, K. R., Lipsicas, M. M., Major, D., and Phillips, K., 1956, *Proc. Phys. Soc.* A, **69**, 141.
Allen, K. R., Phillips, K., and Whittaker, F., 1957, *Proc. Phys. Soc.* A, **70**, 536.
Fowler, P. H., 1950, *Phil. Mag.*, **41**, 169.
Gottstein, K., Menon, M. G. K., Mulvey, G. H., O'Ceallaigh, C., and Rochat, O., 1951, *Phil. Mag.*, **42**, 708.
Hanson, A. O., Lanzl, L. H., Lyman, E. M., and Scott, M. B., 1951, *Phys. Rev.*, **84**, 634.
Heymann, F. F., and Williams, W. F., 1956, *Phil. Mag.*, **1**, 212.
Hisdal, E., 1952, *Phil. Mag.*, **43**, 790.
Husain, A., 1955, *Proc. Phys. Soc.* A, **68**, 45.
Menon, M. G. K., O'Ceallaigh, C., and Rochat, O., 1951, *Phil. Mag.*, **42**, 932.
Mohr, C. B. O., 1954, *Proc. Phys. Soc.* A, **67**, 730.
Molière, C., 1947, *Z. Naturf.*, **2a**, 133.
—— 1948, *Ibid.*, **3a**, 78.
O'Ceallaigh, C., and MacCarthaigh, M. D., 1944, *Proc. Roy. Ir. Acad.* A, **50**, 13.

PHILLIPS, K., and ALLEN, K. R., 1959, *Proc. Phys. Soc.*, **74**, 257.
SNYDER, H. S., and SCOTT, W. T., 1949, *Phys. Rev.*, **76**, 220.
SPENCER, L. V., and BLANCHARD, C. J., 1954, *Phys. Rev.*, **93**, 114.
VOYVODIC, L., and PICKUP, E., 1952, *Phys. Rev.*, **85**, 91.
WILLIAMS, E. J., 1939, *Proc. Roy. Soc.* A, **169**, 531.
—— 1940, *Phys. Rev.*, **58**, 292.

1·12 MeV Level in ^{18}F

BY K. W. ALLEN, D. ECCLESHALL AND M. J. L. YATES
Atomic Weapons Research Establishment, Aldermaston, Berks.

MS. received 28th May 1959, in final form 19th June 1959

THE energy level structure of mass 18 nuclei is of particular interest in view of the detailed shell model calculations of Elliott and Flowers (1955). These authors have obtained the positions of the even parity levels assuming a Rosenfeld mixture for the force between the extra-core particles, and taking proper account of configurational mixing. Assuming that the strength of the nuclear force between the extra-core particles is about the same as in the deuteron, a feature of the theoretical results is the occurrence of the level sequence 1^+, 3^+, 5^+ in ^{18}F; the ground state is 1^+, while the predicted separation of the 3^+ and 5^+ levels is about 0·2 MeV at an excitation of about 1 MeV.

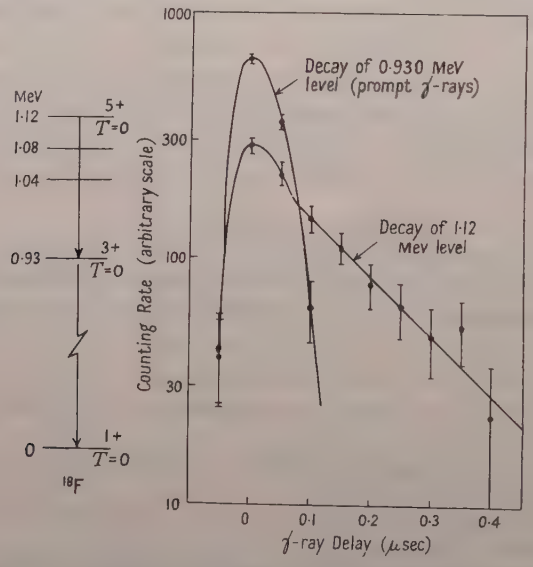

Figure 1. The ^{18}F level scheme and the time delay curves showing the lifetime of the 1·12 MeV level.

Recent work in our laboratory and elsewhere (Kuehner, Almqvist and Bromley 1958, Rao *et al.* 1959) has been directed to the study of the low-lying levels in ^{18}F. Hinds and Middleton (1959) have located accurately some 40 levels in ^{18}F by magnetic analysis of the disintegration particles in the reaction

$^{16}O(^3He, p)^{18}F$ and $^{19}F(^3He, \alpha)^{18}F$. They observed four levels in the neighbourhood of 1 MeV (figure 1) and they also measured the angular distribution of the proton groups leading to these levels for bombarding energies close to 6 MeV. Although the interpretation of the angular distributions of the protons is not completely clear, there are strong indications that the formation of the 1·12 MeV level requires the transfer of four units of orbital angular momentum from the bombarding particle, suggesting an assignment of 5^+. The following experiments were therefore undertaken to study the decay of this level.

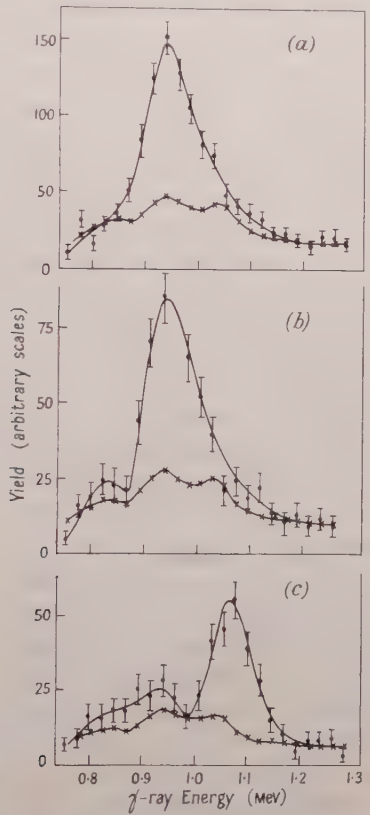

Figure 2. The γ-ray energy spectra for the decay of various levels in ^{18}F; (*a*) decay of 0·930 MeV level (prompt γ-rays); (*b*) decay of 1·12 MeV level (delayed γ-rays); (*c*) decay of 1·08 MeV level (prompt γ-rays). The curves drawn through the crosses indicate the background present in each run.

A beam of 5 MeV ^3He ions was focused on to a quartz target about 40×10^{-6} g cm^{-2} thick. Protons from the reaction $^{16}O(^3He, p\gamma)^{18}F$ emerging at 90° to the incident beam were analysed in a 180° double focusing magnet and detected in a CsI(Tl) crystal. The protons leading to the states in ^{18}F at 1 MeV excitation had an energy of about 5 MeV and were observed with an energy resolution (full width at half height) of approximately 45 kev. Gamma rays emerging in approximately the opposite direction to the protons were detected in a $1\frac{3}{4}$ in. diameter × 2 in. thick NaI(Tl) crystal situated 1 in. from the target. Preliminary experiments showed that the lifetime of the 1·12 MeV state was of the order of $0{\cdot}1 \times 10^{-6}$ second.

A γ-ray pulse height spectrum, gated by coincidences between protons and γ-rays which lost more than 800 kev in the NaI crystal, could be displayed on a

100 channel kicksorter. The coincidence unit also gated the output from a time to pulse height converter (time sorter) which was fed by amplified and limited fast pulses from the two detectors. Coincidence resolving times of 0·1 and $0{\cdot}2 \times 10^{-6}$ second were used. Some of the γ-ray pulse height spectra obtained when the magnet was set to observe the proton groups corresponding to the excitation of the various levels in ^{18}F are shown in figure 2. Also shown are the background curves which were obtained by substituting a pulse generator for the proton counter. Curves 2 (*a*) and (*b*) show that 0·93 MeV γ-rays are associated with the protons going to both the 0·93 MeV and the 1·12 MeV levels. Curve 2 (*b*), showing the decay of the 1·12 MeV level, was obtained with a resolving time of $0{\cdot}1 \times 10^{-6}$ sec by selecting γ-ray pulses delayed by $0{\cdot}2 \times 10^{-6}$ second. Other results taken at this magnet setting but with coincidence delays at the 'prompt' setting showed no evidence for a γ-ray of 1·12 MeV. There were, however, a few γ-rays of 1·08 MeV due to overlapping of the proton groups, a consequence of the modest proton energy resolution used. Curve 2 (*c*) shows the 1·08 MeV γ-ray associated with the decay of the 1·08 MeV level; 1·04 MeV γ-rays were also observed in coincidence with protons leading to the 1·04 MeV level.

A time sorter spectrum was obtained with each of the above curves. The time resolution was sufficient to show that the lifetimes of the 0·93 and 1·08 MeV levels are less than 10^{-8} second.

The best measurement of the lifetime of the 1·12 MeV level was obtained by comparing the ungated time sorter spectrum associated with the protons going to the 1·12 MeV level with the ungated time spectrum obtained with protons feeding the 0·93 MeV level. In order to keep the random coincidence background within bounds for this run, the gain of the γ-ray counter had to be reduced, and this resulted in a poorer prompt resolution curve. The results after subtracting background are shown in figure 1. The lifetime deduced from the slope of the curve for delays greater than 0·1 μsec is $(0{\cdot}190 \pm 0{\cdot}045) \times 10^{-6}$ second. The early portion of the delay curve is complicated by the presence of prompt γ-rays from the 1·08 MeV level which was not completely resolved from the 1·12 MeV level.

These experiments show conclusively that the 1·12 MeV level decays by cascade through the 0·93 MeV level. The measured lifetime is almost exactly equal to the value of $0{\cdot}2 \times 10^{-6}$ sec calculated by J. P. Elliott (private communication) for a 190 keV E2 transition, assuming the same degree of enhancement as that required for the 200 keV E2 transition in ^{19}F. It is therefore very likely that the ground state, 0·93 MeV and 1·12 MeV levels form the 1^+, 3^+, 5^+ sequence predicted theoretically.

Acknowledgments

We are grateful to Mr. V. Shepherd and the Van de Graaff operating staff for their co-operation throughout the experiment and to Mr. A. R. D. Norman for his assistance with the measurements.

References

Elliott, J. P., and Flowers, B. H., 1955, *Proc. Roy. Soc.* A, **229**, 536.
Hinds, S., and Middleton, R., 1959, *Proc. Phys. Soc.*, **73**, 721.
Kuehner, J. A., Almqvist, E., and Bromley, D. A., 1958, *Phys. Rev. Letters*, **1**, 260.
Rao, D., Young, T. E., Spencer, R. R., Beckner, E. H., and Phillips, G. C., 1959, *Bull. Amer. Phys. Soc.* [II], **4**, 96.

LETTERS TO THE EDITOR

Paramagnetic Resonance of Yb^{3+} in Yttrium Gallium Garnet

We have observed the paramagnetic resonance of approximately 1% Yb^{3+} in crystals of $Y_3Ga_5O_{12}$. Since the structure of this compound is very similar to that of the rare earth iron garnets (Keith and Roy 1954, Bertaut and Forrat 1956, Geller and Gilleo 1957), the results are of interest in connection with the magnetic properties of $Yb_3Ga_5O_{12}$, $Yb_3Fe_5O_{12}$, and the effects of rare earth impurities in $Y_3Fe_5O_{12}$ (Dillon and Nielsen 1959). These are discussed further in the subsequent letter (Wolf 1959).

The crystals were grown from a PbO flux using the method of Nielsen (1958) and they were oriented by optical and x-ray methods. Measurements were made at 9 Gc/s, using a standard video spectrometer, at temperatures of 4°, 20° and 90°K. No appreciable difference was observed between the spectra at 4° and 20°K, but above 20°K the lines began to broaden, indicating that the spin–lattice relaxation time was becoming comparable with 10^{-10} sec at about 90°K. Below 20°K the line width was constant at about 35 gauss, indicating that even with only a 1% concentration of Yb there was still some residual interaction broadening.

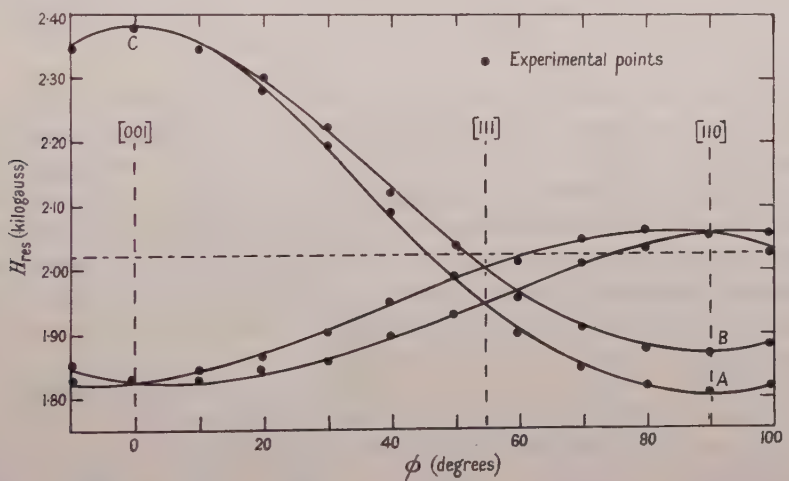

Variation of resonance field with angle in a (110) plane at 9·677 Gc/s. Full lines: curves calculated from g values given in text; chain line: field corresponding to $g = 3\Lambda$.

When a magnetic field was applied in a general direction relative to the crystal axes six main lines were clearly resolved, together with a large number of smaller lines which were later identified as the hyperfine structure due to ^{171}Yb and ^{173}Yb. In order to simplify the interpretation of the spectrum, a crystal was mounted with the $[1\bar{1}0]$ direction normal to the magnetic field and measurements were made of the resonance field as a function of the angle between the [001] axis and the field. The results are shown in the figure. It can be seen that in general only four lines were now observed, which coalesced to two along the [001] and [111] axes and to three along [110]. It was found that the positions of the two lines which cross at [110] were extremely sensitive to slight misalignments of the crystal, a tilt of 4° producing splittings of the order of 100 gauss. These could be removed by careful reorientation.

The energy levels of a Yb^{3+} ion in the garnet structure have been considered by Ayant and Thomas (1959). Making the approximation that the crystal field arising from the eight nearest O^{2-} ions has perfectly cubic symmetry, they predicted that the ground state would be a degenerate doublet well below the other states. In a magnetic field this splits like a spin of $S=\frac{1}{2}$ with an isotropic g value equal to 3Λ, where Λ is the Landé factor which is equal to 8/7 for the $^2F_{7/2}$ term of Yb^{3+}. From the figure it is clear that the splitting is not quite isotropic but that the general order of magnitude is close to 3Λ. To allow for the effect of deviations from cubic symmetry we can introduce an empirical g tensor for each ion with principal values (g_x, g_y, g_z) and from the spectrum determine the orientation of the axes relative to the crystal. Alternatively we can use the crystal structure to determine the relation between the 24c $Yb–O_8$ complexes which occur in each unit cell. Both methods show that there are six magnetically inequivalent rare earth ions in the unit cell whose g tensors are identical apart from orientation, and whose axes are given by $(\mp 1/\sqrt{2}, 1/\sqrt{2}, 0)$; $(\mp 1/\sqrt{2}, 1/\sqrt{2}, 0)$; $(0, 0, 1)$, together with cyclic permutations relative to the cubic axes. The points marked A, B and C in the figure therefore correspond to the principal g values which are:

$$A:\ g_x=3{\cdot}85\pm0{\cdot}05,\quad B:\ g_y=3{\cdot}71\pm0{\cdot}05,\quad C:\ g_z=2{\cdot}91\pm0{\cdot}05.\dagger$$

From these we can calculate the variation of H_{res} with angle and obtain the solid curves shown in the figure. The small discrepancies between these curves and the experimental points are mainly due to some slight residual misalignment of the crystal.

No attempt was made to analyse in detail the spectrum of subsidiary lines which from their intensity and general structure were ascribed to nuclear hyperfine structure effects. This was confirmed by comparing approximate values of A/g with those found by Cooke and Park in ytterbium acetate. An exact evaluation of the hyperfine interaction constants would require a high order perturbation calculation since at 9 Gc/s $h\nu$ is not very much larger than the hyperfine structure.

Similar experiments are now in progress with other rare earths diluted in $Y_3Ga_5O_{12}$ and it is hoped to present the results in the near future.

This work was carried out during the tenure by one of us (W. P. W.) of an I.C.I. Research Fellowship, and it was partially supported by the United States Air Force Cambridge Research Centre through the European Office of Research and Development Command. A grant from the General Electric Company is gratefully acknowledged. We should also like to thank Mr. E. Daintree for help with some of the experiments.

The Clarendon Laboratory,
Oxford.
10th July 1959.

D. Boakes.
G. Garton.
D. Ryan.
W. P. Wolf.

† *Note added in proof.*—From a more accurate re-determination we now find that

$$g_x=3{\cdot}73_0\pm0{\cdot}010,\ g_y=3{\cdot}60_5\pm0{\cdot}010,\ g_z=2{\cdot}85_0\pm0{\cdot}015,$$

in excellent agreement with the values found independently by Carson and White (Conference on Magnetism and Magnetic Materials, Detroit, November 1959), who used a frequency of 34 Gc/s. We are grateful to these authors for drawing our attention to the previous small discrepancy, which was due to a systematic error in our measurements, and not to any intrinsic difference in higher order effects at the two frequencies.

Ayant, Y., and Thomas, J., 1959, *C.R. Acad. Sci., Paris*, **248**, 387.
Bertaut, F., and Forrat, F., 1956, *C.R. Acad. Sci., Paris*, **242**, 382.
Cooke, A. H., and Park, J. G., 1956, *Proc. Phys. Soc.* A, **69**, 282.
Dillon, J. F., Jr., and Nielsen, J. W., 1959, *Phys. Rev. Letters*, **3**, 30.
Geller, S., and Gilleo, M. A., 1957, *J. Phys. Chem. Solids*, **3**, 30.
Keith, M. L., and Roy, R., 1954, *Amer. Mineral.*, **39**, 1.
Nielsen, J. W., 1958, *J. Appl. Phys.*, **29**, 390.
Wolf, W. P., 1959, *Proc. Phys. Soc.*, **74**, 665.

Magnetic Properties of Rare Earth Ions in Garnets

In the previous letter (Boakes *et al.* 1959) paramagnetic resonance experiments were reported on Yb^{3+} ions diluted in yttrium gallium garnet. In this letter we shall discuss some of the implications of these results on the magnetic properties of isostructural $Yb_3Ga_5O_{12}$, $Yb_3Fe_5O_{12}$ and $Y_3Fe_5O_{12}$ with small impurities of rare earths.

From the measured g-values we can calculate directly the susceptibility and saturation magnetization to be expected in pure $Yb_3Ga_5O_{12}$. Assuming that the Yb–Yb interaction is small (Pauthenet 1959) and that dilution does not alter the crystal field appreciably, we find that the susceptibility.

$$\chi_M = \frac{N\beta^2}{12kT}(g_x^2+g_y^2+g_z^2) = \frac{1{\cdot}095}{T},$$

is in reasonable agreement with the Curie constant 1·07 reported by Cohen and Ducloz (1959).

The saturation magnetization in large magnetic fields M_s is more difficult to estimate since, even though the crystals have overall cubic symmetry, M_s will not be isotropic on account of deviations from cubic symmetry at the magnetic ions. So far this effect has not been observed since magnetic moment measurements are nearly always made on polycrystalline samples. We can estimate an order of magnitude for the anisotropy to be expected by calculating M_s for two principal directions [100] and [111]. For [100]

$$M_s = \tfrac{1}{6}N\beta\,[\sqrt{2}(g_x^2+g_y^2)+g_z] = 1{\cdot}699\,N\beta \qquad \ldots\ldots(1)$$

while for [111]

$$M_s = \frac{N\beta}{4}\left[\left(\frac{2g_x^2+g_z^2}{3}\right)^{1/2}+\left(\frac{2g_y^2+g_z^2}{3}\right)^{1/2}\right] = 1{\cdot}708\,N\beta. \qquad \ldots\ldots(2)$$

With the g-values as found for Yb^{3+} the anistropy is therefore rather small and M approximately follows the same Brillouin function in all directions. However, other rare earth ions may have much more anisotropic g-values and M_s could then vary by as much as a factor of two. This effect should be readily observable even in a powder since M would then deviate considerably from the Brillouin function.

One class of ions for which the deviation in g from cubic symmetry should be more pronounced than for Yb^{3+} are those for which the predominantly cubic crystal field leads to a fourfold degenerate Γ_8 ground state (Bleaney 1959). The axial and rhombic distortions which remove this degeneracy then give rise to an admixture of the states in first order, rather than in second order as for Yb^{3+}.

The anomalous magnetization curves reported by Pauthenet (1959) for erbium and dysprosium gallium garnets may be due to this effect.

When rare earth ions are included in ferrimagnetic iron garnets they are subjected to relatively strong exchange effects from the Fe^{3+} ions and these will give rise to an anisotropy in the magnetic moment similar to that described above. However, in contrast to an applied magnetic field, the magnitude of the effective exchange field will not be independent of the direction of the Fe^{3+} sub-lattices. If the exchange interaction is small compared with the crystal field and we consider only low temperatures so that the Fe^{3+} sub-lattices are completely aligned by their strong mutual interactions, the problem is reduced to the sum of interactions of effective spins $s=\frac{1}{2}$ with ions in a non degenerate state $|S=5/2, S_z=5/2\rangle$, where z denotes the direction of the Fe^{3+} magnetization. Corresponding to the usual molecular field approximation of isotropic exchange, but allowing for the fact that the exchange will be different for different orbital states, this interaction may be expressed formally as

$$\mathscr{H}_e = \sum_{\text{all ions}} \mathbf{H}_e . G . \mathbf{s} \qquad \ldots\ldots (3)$$

where H_e is an *isotropic* exchange field in the direction of z, and G is an anisotropic tensor which in most cases has the same axes as the magnetic g tensor. In an applied field H the direction of z can be found by minimizing the free energy which comprises the magnetic interaction of both the Fe^{3+} and rare earth sub-lattices with H plus the anisotropic part of (3). However, if the total contribution to the anisotropy energy from (3) is not too large, we can assume that z will be approximately parallel to H. We can then find a closed expression for the contribution to the saturation magnetic moment from the rare earth ions. Thus at $T=0°K$

$$M_0 = \sum \frac{N_i\beta}{2} \frac{l_i^2 G_x g_x + m_i^2 G_y g_y + n_i^2 G_z g_z}{(l_i^2 G_x^2 + m_i^2 G_y^2 + n_i^2 G_z^2)^{1/2}} \qquad \ldots\ldots (4)$$

where the summation runs over all sets of magnetically inequivalent ions, N_i is the number of ions in each set and $(l_i\, m_i\, n_i)$ are the direction cosines of z relative to the axes of each G. If G is proportional to g, equation (4) reduces to the normal paramagnetic case, as illustrated in equations (1) and (2).

In the case of Yb^{3+}, for which g is not very anisotropic, it is likely that G will also be relatively isotropic so that M_s in any direction will be close to the average value of $\frac{1}{2}N\beta(\bar{g}) = 1{\cdot}697\, N\beta$. This value is consistent with the small magnetic moment ($0{\cdot}25\, N\beta$) of $Yb_3Fe_5O_{12}$ at low temperatures (Pauthenet 1958), which indicates that the moment of $3Yb^{3+}$ ions is almost equal to that of (3–2) antiparallel Fe^{3+} ions. Since the magnetic moment of the Fe^{3+} ions is isotropic we might therefore expect that the net magnetization of a single crystal of $Yb_3Fe_5O_{12}$ would show up any small anisotropy in the magnetic moment of the rare earth ions. However, in practice this type of magnetic moment anisotropy may be difficult to observe directly, since equation (3) also implies a large anisotropy in the energy. This would make it hard to achieve technical saturation without using very large magnetic fields.

From equation (3) the anisotropy energy at $T=0°K$ is given by

$$F = -\sum_{\text{ions}} \tfrac{1}{2} H_e (l_i^2 G_x^2 + m_i^2 G_y^2 + n_i^2 G_z^2)^{1/2}. \qquad \ldots\ldots (5)$$

If we assume, as suggested by the values of g, that G is approximately axially

symmetric about one of the three cubic axes and that the anisotropy in G is small this reduces to

$$F \simeq -\frac{NH_eG_\perp}{6}\sum_{\alpha=l,m,n}\left(1+\frac{G_\parallel{}^2-G_\perp{}^2}{G_\perp{}^2}\alpha^2\right)^{1/2}$$
$$\simeq -\frac{NH_eG}{2}\left[1-\frac{1}{6}\left(\frac{\Delta G}{G}\right)^2(l^4+m^4+n^4)+\ldots\ldots\right] \qquad \ldots\ldots(6)$$

where $\Delta G = G_\parallel - G_\perp = G_z - G_x$. The last term may be identified with a conventional cubic anisotropy term K_1 if

$$K_1 = -\frac{NH_eG}{6}\left(\frac{\Delta G}{G}\right)^2 \sim -10^8\left(\frac{\Delta G}{G}\right)^2 \text{erg cm}^{-3},$$

taking the exchange energy per rare earth ion to be of the order of $50\boldsymbol{k}$. This expression shows why rare earth ions can have a profound effect on the anisotropy since even if $\Delta G/G$ is as small as 0·1, K_1 is still of order 10^6 erg cm^{-3}.

For certain rare earth ions we may have $G_z \gg G_x$ or G_y and the expansion in equation (6) is then not valid. However, in that case we can use (5) directly and find

$$F = -\frac{NH_eG_\parallel}{6}(|l|+|m|+|n|) \sim -10^8 \text{ erg cm}^{-3}.$$

Such an anisotropy would be extremely large and it could not be expressed in terms of the usual expansion in K_1 and K_2. The striking anisotropy results recently found by Dillon and Nielsen (1959) for small rare earth impurities in yttrium iron garnet may be due to a term of this kind.

Throughout this analysis we have assumed that crystal field splittings are large compared with exchange effects and that each rare earth ion is in a doublet ground state. If there are other low-lying levels we may expect more complex effects.

The author wishes to thank Dr. J. F. Dillon, Jr, and Dr. J. W. Nielsen for making available to him the results of their experiments prior to publication. This work was carried out during the tenure of an I.C.I. Research Fellowship.

The Clarendon Laboratory, W. P. Wolf.
Oxford.
10th July 1959.

Bleaney, B., 1959, *Proc. Phys. Soc.*, **73**, 937.
Boakes, D., Garton, G., Ryan, D., and Wolf, W. P., 1959, *Proc. Phys. Soc.*, **74**, 663.
Cohen, J., and Ducloz, J., 1959, *J. Phys. Radium*, **20**, 403.
Dillon, J. F., Jr, and Nielsen, J. W., 1959, *Phys. Rev. Letters*, **3**, 30.
Pauthenet, R., 1958, *Ann. de Phys.*, **3**, 424.
—— 1959, *J. Phys. Radium*, **20**, 388.

The Absorption Edge of Arsenic–Sulphur–Selenium Mixtures

Arsenic trisulphide (Frerichs 1953), a stable glass at room temperature, is a well-known infra-red optical material transmitting to beyond 13 microns. Its absorption edge has been studied by Rekalova (1952), using thin single

crystals, and by Doyle (1956) and Schlosser (1957), using evaporated layers. The triselenide is similar to the trisulphide in many respects. Dewulf (1954) has investigated the infra-red optical properties of the pentasulphide and pentaselenide, and shown that these might be still more satisfactory than As_2S_3 for infra-red components.

We have found that all four compounds can be evaporated without appreciable decomposition. The transmission of As_2S_3, As_2Se_3 and As_2S_5 layers about one micron thick on glass substrates is shown in figure 1, and compared with that of a layer of amorphous selenium. The oscillations in transmission are due to interference. The absorption edges of As_2Se_3 and As_2Se_5 almost coincide and for clarity the As_2Se_5 curve is omitted from figure 1. The results for As_2S_3 agree with those previously reported.

Mixtures of As_2Se_3 and As_2S_3 were also prepared and evaporated. The two compounds appeared miscible in all proportions, and the absorption edge moved progressively towards the red as the proportion of the selenide was increased (figure 2). Similar results were obtained with mixtures of As_2Se_5 and As_2S_5 (figure 3).

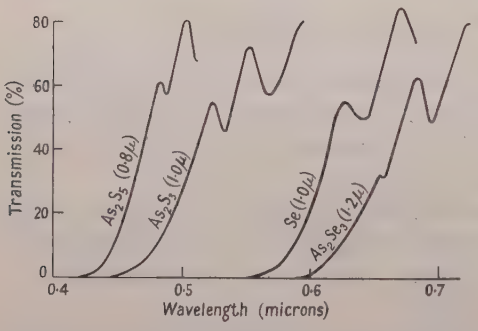

Figure 1. Transmission of arsenic sulphides and selenides compared with selenium.

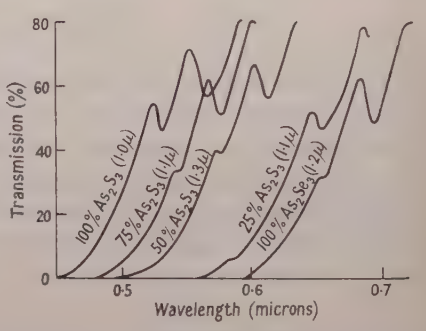

Figure 2. Transmission of mixtures of arsenic trisulphide and triselenide.

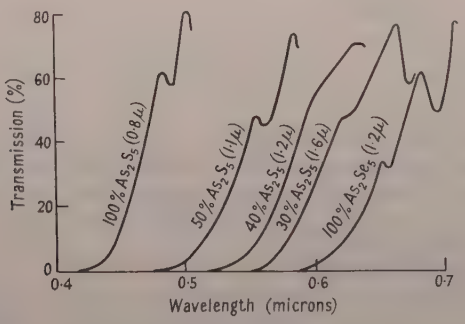

Figure 3. Transmission of mixtures of arsenic pentasulphide and pentaselenide.

The stability of all layers was good when they were kept at room temperature but the As_2S_3–As_2Se_3 layers showed a slight tendency to crystallize when heated to 40°C and exposed to a powerful source of light. The As_2S_5–As_2Se_5 layers showed no change after this test. Stable optical filters with a cut-off anywhere between the yellow and the deep red can therefore be made using these materials.

Acknowledgment is made to Mr. N. Graydon for his help in these measurements, and to the Admiralty for permission to publish.

Services Electronics Research Laboratory,
Baldock,
Herts.
7th July 1959.

C. Hilsum.

Dewulf, G., 1954, *Rev. Opt. (théor. instrum.)*, **33**, 513.
Doyle, W. P., 1956, *Proc. Phys. Soc.* B, **69**, 865.
Frerichs, R., 1953, *J. Opt. Soc. Amer.*, **43**, 1153.
Rekalova, G. I., 1952, *J. Tech. Phys., Moscow*, **22**, 143.
Schlosser, H., 1957, *J. Appl. Phys.*, **28**, 512.

The Control of Resistivity in Pulled Silicon Crystals

The control of the impurity concentration along pulled crystals is important where material within certain closely defined resistivity limits is required. The impurity distribution along a crystal is determined by the effective segregation coefficients of the impurities present, loss by evaporation and by contamination from the crucible material and surroundings. With the high purity quartz available and careful design of the apparatus, contamination can be reduced to negligible limits for silicon with resistivity below about 200 Ω cm. Thus the impurity distribution is determined by the other two factors. Boron can be used to make uniform p-type material. The segregation coefficient is near unity, and crystals with a near uniform resistivity distribution can be readily grown. For n-type material the commonly used donor impurities, arsenic and phosphorous, have segregation coefficients of 0·3 and 0·35 respectively. This leads to considerable variation in resistivity over the useful region of the crystal. The loss by evaporation for crystals pulled in an atmospheric pressure of inert gas is small.

Bradshaw and Mlavsky (1956) have shown how the evaporation of impurities in vacuum can be used to control the resistivity and produce p–n junctions. In this laboratory we have controlled the resistivity by pulling crystals in a reduced pressure of ambient gas such that the segregation of impurity from the solid to the liquid is balanced by the evaporation of impurity from the surface of the melt.

Consider a crystal pulling system with the following characteristics : diameter of crucible D, diameter of growing crystal d, impurity concentration in melt after volume v has grown C, pressure of ambient gas p, segregation coefficient of impurity k, growth rate x, rate of evaporation of impurity from melt surface r. Suppose that in time Δt an amount Δv is grown, then the concentration in this volume is kC, and an amount $kC\Delta v$ of impurity is removed from the melt by segregation.

The amount of impurity evaporating from the surface of the melt in this time is

$$\tfrac{1}{4}r\pi(D^2-d^2)\Delta t.$$

For the concentration in the melt to remain constant a quantity $C\Delta v$ must be removed, hence

$$C\Delta v = kC\Delta v + \tfrac{1}{4}\pi r(D^2-d^2)\Delta t.$$

Now $\Delta v = \tfrac{1}{4}\pi d^2 \Delta t x$, hence $r = \dfrac{(1-k)Cx}{D^2/d^2-1}$.

It will be seen from this result that (*a*) if a value of r can be obtained which satisfies this condition a constant impurity concentration will result, (*b*) the important control parameters are the ratio of crucible diameter to crystal diameter, the desired impurity concentration, the rate of growth of the crystal and the pressure of the ambient gas (controlling r).

A more general analysis, and the assumption that the rate of evaporation is controlled by diffusion of the impurity through a thin surface layer, leads to a modification of the normal freezing equation

$$C=kC_0(1-g)^{k-1}$$

to

$$C=kC_0(1-g)^{k+A-1}$$

where

$$A=\frac{1}{x}\left(\frac{D^2}{d^2}-1\right)\frac{D_0}{a}.$$

C is the concentration after a fraction g of the crystal has grown, C_0 is the initial concentration in the melt, D_0 the diffusion coefficient of impurity through a boundary layer, and a the thickness of boundary layer. Putting in the condition for a uniform concentration we find

$$r=f(p)=\frac{D_0C}{a}=\frac{(1-k)xC}{D^2/d^2-1}.$$

Experimentally a value of pressure for a particular set of conditions was found by varying the ambient pressure and measuring the resultant resistivity variation. For low pressures the impurity is removed and the resistivity increases along the crystal; for high pressures a segregation approaching normal is obtained. At a certain pressure a near uniform distribution results. The melting, seeding and initial crystal growth are carried out at atmospheric pressure of argon. When the required crystal diameter is achieved, the pressure is reduced and maintained constant during the run. Pressure control is not very critical. The ratio D/d is more significant and it is important to maintain the crystal diameter constant. The effect of small changes in crystal diameter can be reduced by increasing the crucible diameter.

Typical values for an arsenic doped crystal to give a resistivity of $3{\cdot}0 \pm 0{\cdot}3\ \Omega$cm over the useful part of the crystal are: $D=5$ cm, $d=2$ cm, $p=4$ cm Hg, $x=10$ cm hr^{-1}.

The authors wish to thank the Directors of Mullard Limited, for permission to publish this note. We also wish to thank Dr. M. Smollett for helpful discussions.

Research Department,
Mullard Southampton Works,
Southampton.
25th June 1959.

A. Trainor.
P. T. Harris.

Bradshaw, S. E., and Mlavsky, A. I., 1956, *Report of the Meeting on Semiconductors* (London : Physical Society), p. 21.

Low Temperature Resistivity of Plutonium and Neptunium

A specimen of plutonium metal and one of neptunium have been cooled to 0·75°K and their electrical resistivities measured. Neither showed superconductivity at this temperature, the residual resistance of the plutonium sample being 14×10^{-2} and that of the neptunium sample being $3{\cdot}1 \times 10^{-2}$ of the room temperature value. Details of this work will be published later.

Atomic Energy Research Establishment, Harwell, Berks. — J. A. Lee.
Clarendon Laboratory, Oxford. — G. T. Meaden. K. Mendelssohn.
20th July 1959.

CORRIGENDUM

The β-decay of ^{239}Np, by R. D. Connor and I. L. Fairweather (*Proc. Phys. Soc.*, 1959, **74**, 161).

Table 1: The errors given in the column headed '$\log_{10} ft$' in fact apply to the entries given in the previous column headed 'Relative intensity (%)'.

REVIEWS OF BOOKS

Ancillary Mathematics, by H. S. W. Massey and H. Kestelman. Pp. xvi + 990. (London : Sir Isaac Pitman and Sons, 1959.) 75*s*.

It seems to be generally agreed nowadays that students of physics and chemistry need to learn a lot of mathematics, not only at school but also during their first two years at a university. However desirable a knowledge of mathematics may be in all other branches of physics it becomes essential in quantum mechanics, the teaching and application of which is occupying more and more of the honours syllabus. So much of the quantum theory appears a deplorable fudge when taught in terms of simple physical pictures so-called, that the student with his wits about him rightly rejects it as absurd. On the other hand, the amount of mathematics he needs in order to understand at least the principles of quantum mechanics is really not very great: certainly it is within his powers to learn it in two years. The present book sets out to supply the student of physics

and chemistry with a basic knowledge of mathematics with the subsequent teaching of quantum mechanics as one of the principal objects in mind. The topics treated include the concept of number, the differential and integral calculus, series, analytic geometry, complex number, vector analysis, differential equations, Fourier series, and the calculus of variations; and there is a much more systematic application to physical problems than is customary in such texts (which partly accounts for its length), or than would appear from the above list. One suspects that there may be fierce controversy about the choice of topics, partly occasioned by taste and prejudice, partly with an eye to future applications. The present reviewer, with his eye mainly on the teaching of quantum mechanics to physicists, would have preferred to have seen a fuller discussion of eigenvalue problems instead of the substantial sections on analytic geometry; and he would have wanted a section on matrices (although he is at his wit's end to suggest what this might displace). On the whole he would have preferred a somewhat broader syllabus treated with less emphasis on detail. But that is partly taste and partly, no doubt, prejudice. What he must admit is that, given the topics, they are treated with sufficient thoroughness to bring about understanding without at the same time producing the normal bewildered reaction of a physicist faced with the austere rigours of pure mathematics; that the text is admirably illustrated with examples both mathematical and physical; and that each chapter ends with an impressive and searching list of exercises for the serious student. He is also bound to admit that a physics or chemistry student who had mastered the content of this book by the end of his second year would be a much easier student to teach in his third year than one who had not. B. H. FLOWERS.

Nuclear Explosions and their Effects, by D. S. KOTHARI, with a Foreword by JAWAHARLAL NEHRU. Pp. xvi+340. (Delhi: The Publication Division, Ministry of Information and Broadcasting, Government of India, 1958.) 25*s*.

The second edition maintains the high standard set by the first edition. The book is complementary to *The Effects of Nuclear Weapons* prepared by S. Glasstone for the United States Department of Defence and Atomic Energy Commission.

The two books, taken together, give a balanced and factual account of the physical effects of nuclear weapons, and a dispassionate account of some of the biological effects. The American book is much more complete on the physical data. These are based on direct physical measurement and therefore are unlikely to need revision at some future date. The Indian book has more on the biological side, but is written from the point of view of a physicist. Since there is a very large scientific effort all over the world on the medical side of radiation and fall-out problems, the Indian book, being later, has more data.

While the book does not present any new data, it does collect together a great deal of information which is presented logically, clearly and in good grammatical style. The authors have searched widely through the literature and have made their selections without prejudice. The source of their information is given in footnotes, together with many helpful comments and brief explanations.

For those interested in the subject, this book and the American book are highly recommended. W. G. PENNEY.

(*a*) × 150

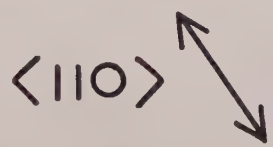

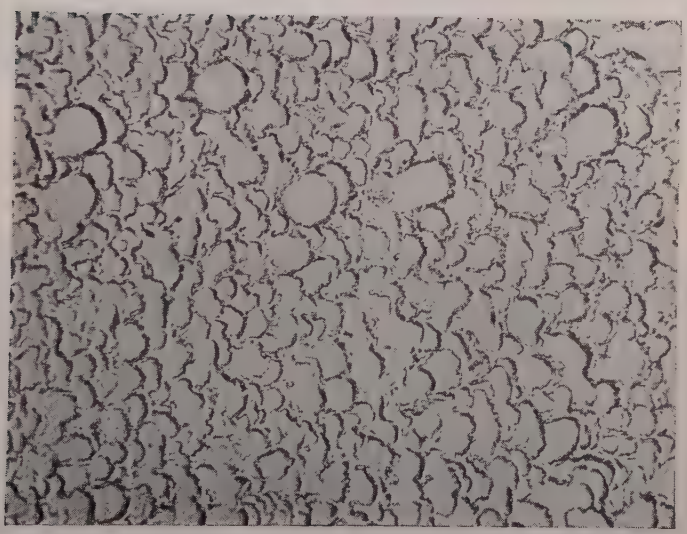

(*b*) × 600

Figure 2. Platelet layer structures on specimen A, (*a*) 60 minutes deposit, (*b*) 15 minutes deposit.

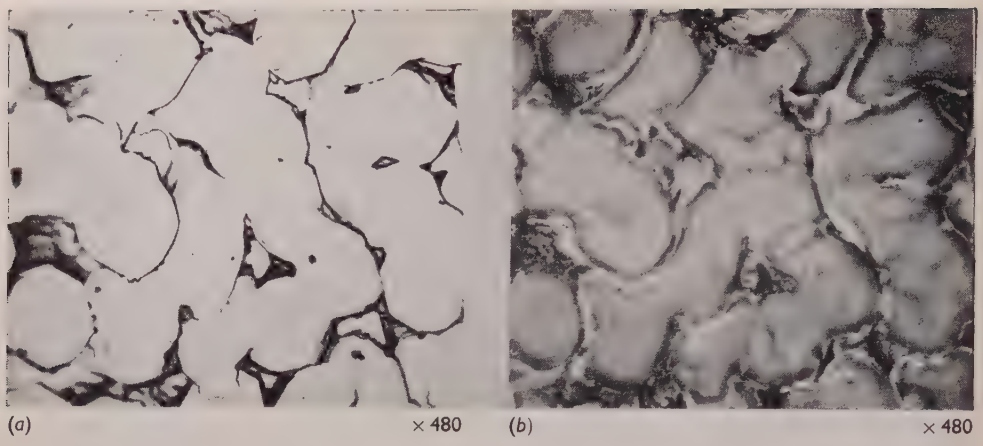

Figure 5. Details of secondary structure on platelets of deposits.

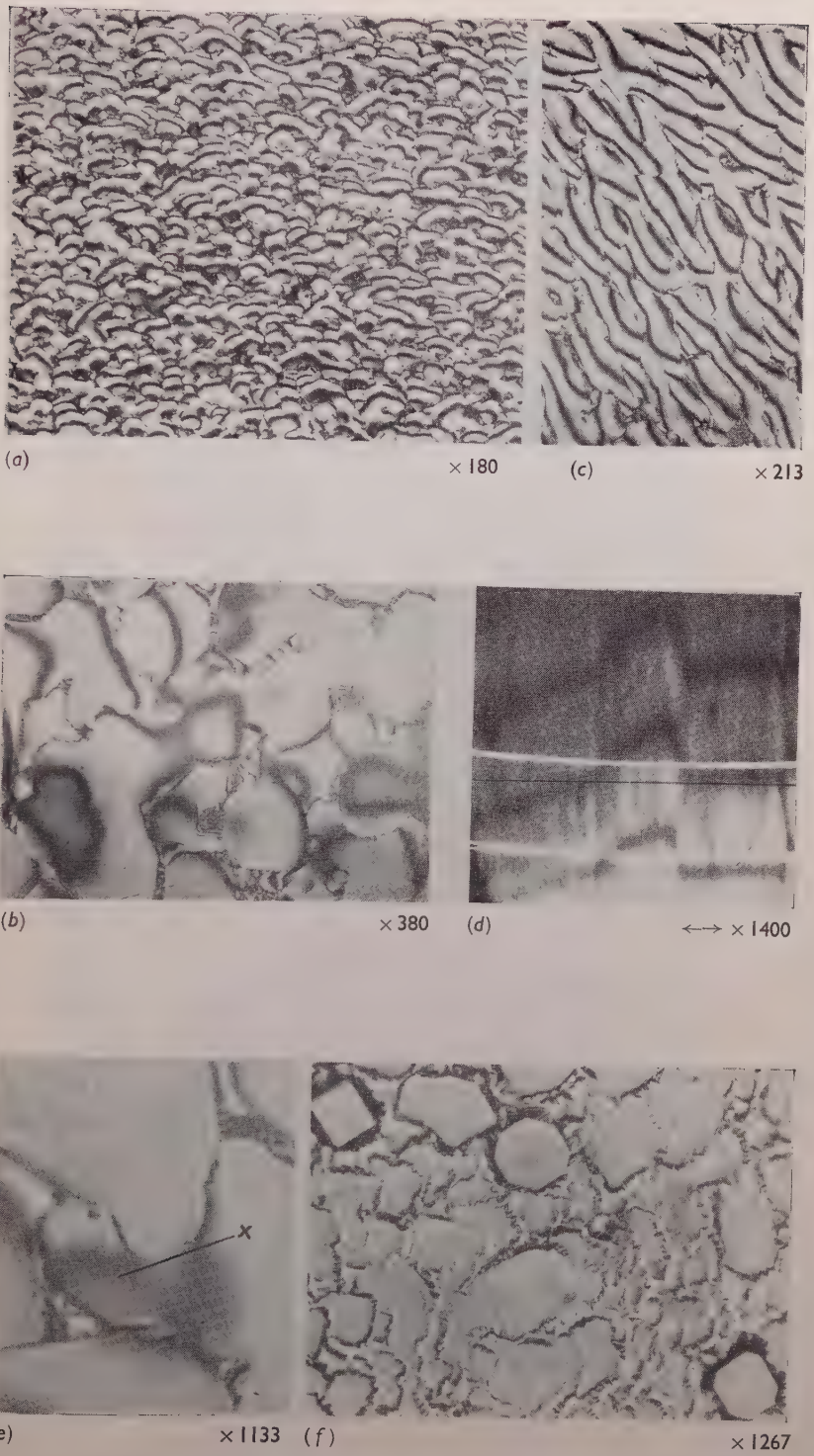

Figure 6 (*a*)–(*e*). Interferograms of platelet surfaces of deposits. (*f*) Individual single platelets on specimen A.

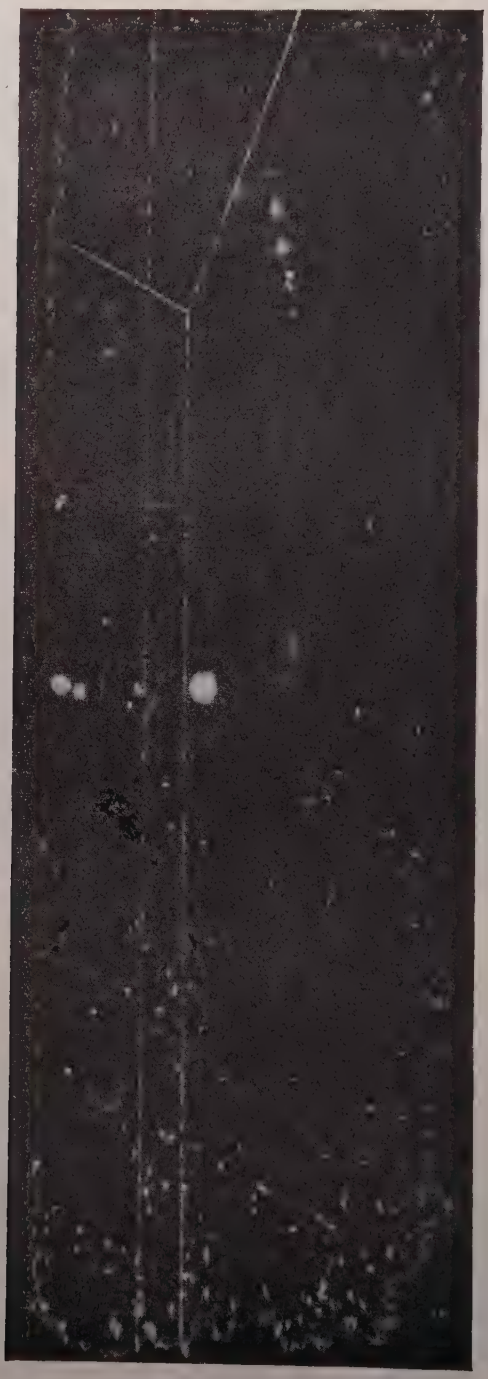

A typical proton–proton event.

(*a*) H/D = ∞; (*b*) H/D = 2; (*c*) H/D = 1/2; (*d*) H/D = 0.

An X-ray Study of the Factors causing Variation in the Heats of Solution of Magnesium Oxide

By D. K. THOMAS† and T. W. BAKER
Atomic Energy Research Establishment, Harwell, Didcot, Berks.

MS. received 6*th November* 1956, *in final form* 11*th June* 1959

Abstract. Line breadths in the x-ray diffraction patterns of a series of magnesium oxide specimens prepared by dehydrating brucite at different temperatures, were determined using a Geiger counter diffractometer. Analysis showed that the broadening was primarily due to small crystallite size and permitted correlation of the differing heats of solution of various preparations of magnesium oxide with their mean crystallite sizes.

§ 1. Introduction

Magnesium oxide prepared by controlled dehydration of brucite has a heat of solution in aqueous hydrochloric acid which can vary by 2 kcal g mol^{-1} and which depends upon the temperature and duration of dehydration.

This fact has received considerable attention in the past, and two explanations have been put forward (Fricke and Lucke 1935, Kahler 1949, Taylor and Wells 1938, Weissenbach 1951). One suggests that the increased energy content is due to micro-stresses set up in the magnesium oxide lattice during the dehydration process, and the other that it is a crystallite size effect.

Both lattice strains and small crystallite size produce a broadening of the x-ray diffraction lines, and this broadening bears different theoretical relationships to the Bragg angle and wavelength of x-rays employed.

The following relationships exist (Scherrer 1918, von Laue 1926, Bragg 1919, Peiser, Rooksby and Wilson 1955) between β_p the particle size broadening, β_s that due to lattice strain, θ the Bragg angle and λ the x-ray wavelength:

$$\beta_p = \frac{K\lambda}{\epsilon \cos\theta} \qquad \ldots\ldots (1)$$

$$\beta_s = \eta \tan\theta. \qquad \ldots\ldots (2)$$

K is a constant known as the 'shape factor', ϵ is the measure of particle size and η is the 'strain function'.

§ 2. Materials

The five samples of magnesium oxide used were obtained by dehydrating brucite at 1380°, 1000°, 700°, 500° and 380°c. Their heats of solution in aqueous hydrochloric acid were determined calorimetrically (Livey 1957) and were quoted as 36·21, 36·45, 36·82, 37·42 and 37·47 kcal g mol^{-1} respectively.

§ 3. Experimental Procedure

The diffractometer measurements were made with a fully stabilized, rectified, and smoothed Philips P.W.1010 x-ray generator. The radiation used was crystal

† Now at Research Association of British Rubber Manufacturers, Shawbury, Shrewsbury.

reflected and asymmetrically focused copper K_{α_1}. The detector was a Mullard MK 118 Geiger counter connected to standard scaling units (Smallman 1957).

Specimens were prepared by mixing the magnesium oxide powder with a weak solution of 'Durofix' in amyl acetate until it was of paste-like consistency. The paste was then transferred to a metal specimen holder and allowed to dry out. Care was taken to ensure that the sample was well packed into the holder and that the surface was as smooth as possible and flush with the surface of the holder.

Each diffraction line was scanned in detail, counts being taken every two minutes of arc over the background and at one minute intervals over the peaks. All specimens were spun during measurements.

§ 4. Experimental Results

Table 1 gives the angular breadths of the diffraction lines in degrees measured at half-maximum intensity. The accuracy of measurement is of the order of 3%.

Table 1

	Temperature of dehydration of samples (°C)				
line (*hkl*)	1380	1000	700	500	380
111	0·220	0·266		0·466	0·783
200	0·240	0·271	0·383	0·540	0·803
220	0·250	0·280	0·433	0·553	0·849
311	0·308	0·317	0·500	0·633	0·883
222	0·291	0·300	0·516	0·620	0·916
400	0·320	0·366	0·555	0·733	
331	0·383		0·650		
420	0·388		0·696	0·850	1·41
422	0·452		0·850	1·130	1·70

§ 5. Discussion

5.1. *Correction for Instrumental Broadening*

To obtain the intrinsic broadening β from the experimentally observed line width B an allowance must be made for the instrumental broadening b. Instrumental broadening is generally due to a number of factors, such as the widths of the slits defining the x-ray beam, the size and form of the specimen, the spectral distribution of the radiation, and the doublet nature of the K_α characteristic. The latter was avoided in this determination by using only K_{α_1}. It has become standard practice to take the instrumental breadth as that given by unstrained particles of quartz of a size greater than 1000 Å. Birks and Friedmann (1946), when looking into the problem of allowing for instrumental broadening found that a specimen of magnesium oxide which had been prepared at 1000°C gave lines almost as sharp as those given by quartz powder of particle size above 1000 Å. In view of this, and since the 1380°C sample gave an almost normal heat of solution, it was employed in this investigation as the standard for instrumental broadening. This offered the additional advantage that the correction is given at the Bragg angles concerned, thus avoiding the necessity for interpolation.

Several theoretical relationships have been used for evaluating the intrinsic breadth from the experimentally observed line broadening.

Scherrer (1918) used

$$\beta = B - b \qquad \ldots\ldots (3)$$

while Warren and Biscoe (1938) suggested

$$\beta^2 = B^2 - b^2. \qquad \ldots\ldots (4)$$

Alexander (1954) used a graphical method derived by the convolution principle. Providing the intensity distribution were known, there would be no difficulty in approximating the proper relationship. Equation (3) assumes a Cauchy distribution. Jones (1938) showed that equation (4) was valid for a Gaussian distribution. Under the experimental conditions obtaining, the intensity distribution of the x-ray diffraction lines approximates more closely to the Cauchy than the Gaussian (Williamson and Smallman 1954). Alexander's method which applies specifically to diffractometers of modern design, gives results falling between the other two and lying more closely to the Scherrer formula. For this reason it is employed for evaluating the particle sizes.

For differentiating between particle size and lattice strain the Scherrer relationship is used, but that of Warren and Biscoe could be applied equally well.

5.2. *Measurement of Line Breadths*

The two definitions of x-ray line breadths that have been widely used are
(i) The half-breadth, which is the angle between the two positions at which the intensity is one-half the peak value.
(ii) The integral breadth given by

$$\frac{\text{intensity integrated with respect to angle}}{\text{intensity at peak}}.$$

The former is the most easily measured, whereas the latter is more completely identifiable with the mathematical theory.

Visual examination of the profiles concerned in this investigation indicated that the broadening that took place was of a form that would be taken into account by measurement of half-breadths. If for example, the broadening was of a type that predominantly affected the base of the curve, then a half-breadth measurement would not give a proper indication of the change. In this case, however, the broadening appeared to affect the profile over its total height.

Tests were carried out using both methods of measurement on the 380°C and 1380°C specimens. These showed that the differences were within the experimental error. The areas for the integral breadths were measured by planimeter and gave a larger scatter of points on the ($\beta_{1/2}\cos\theta$, $\sin\theta$) plot (figure 1) than the half-breadths. For this reason, together with their comparative ease of measurement, half-breadths are used in this paper.

5.3. *Differentiating between the Effects*

A convenient graphical method of expressing the relationship shown in equations (1), (2) and (3), is to plot $\beta\cos\theta$ against $\sin\theta$, in which case a horizontal straight line is obtained if the specimen has a small crystallite size and no strain, whereas a straight line passing through the origin is obtained if there is strain but the crystallites are large. Mazur (1949) and Hall (1949) have previously employed

a similar graphical method and state that departures from linearity are unlikely to be very marked, especially if the broadening were predominantly due to one factor. Table 2 shows the results treated in this manner.

Table 2

	$\beta \cos\theta$ Temperature of dehydration (°C)				
Line (*hkl*)	1000	700	500	380	$\sin\theta$
111	0·0369		0·227	0·527	0·3173
200	0·0372	0·142	0·287	0·532	0·3654
220	0·0250	0·156	0·258	0·512	0·5187
311	0·0365	0·181	0·287	0·493	0·6074
222	0·0170	0·183	0·264	0·494	0·6344
400	0·0272	0·163	0·284		0·7320
331		0·176			0·7976
420		0·185	0·274	0·597	0·8178
422		0·173	0·286	0·539	0·8961

These are plotted in figure 1 and show that the best plot for each specimen is a horizontal line within the limits of experimental error. Thus the line broadening in the x-ray powder diffraction pattern of the magnesium oxide

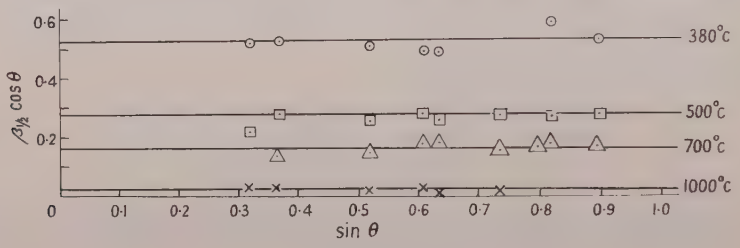

Figure 1.

specimens is predominantly due to small crystallite size. A small strain contribution to the broadening could be masked by the scatter of the points, although the contribution can only be small, amounting to 20% of the total broadening in the most pronounced case, the 380°c specimen.

5.4. *Determination of Crystallite Size*

Measurements of the broadening of x-ray diffraction lines is regarded as one of the most accurate indirect methods of determining crystallite sizes of less than 1000 Å, and results thus obtained have been favourably compared with those determined by rates of solubility (Taylor and Wells 1938), sedimentation experiments (Taylor and Wells 1938), electron microscopy (Birks and Friedman 1946) and nitrogen adsorption measurements (Zettlemoyer and Walker 1947).

From the experimental point of view the accuracy of a crystallite size determination is mainly dependent upon the certainty with which the pure diffraction breadth β can be measured.

Estimates have demonstrated the need for keeping the ratio of b to B smaller than about 0·50 for precise work, and this condition can be realized to a certain extent by the proper choice of the experimental conditions referred to above. As the particle size approaches 1000 Å, the ratio of b to B inevitably increases

into the unfavourable range above 0·50 in spite of the best possible adjustment of experimental conditions. At 380°c the mean value is 0·29 while at 500°c it becomes 0·45. For the specimens prepared at 700°c and 1000°c it falls well inside the unfavourable region and therefore the values obtained for the crystallite sizes would be expected to be less precise in these cases.

Further uncertainty is introduced into the absolute crystallite sizes due to the degree of indeterminacy associated with the shape and size distribution factors in the specimen, i.e. the uncertainty in the value of K in equation (1).

Two procedures are available for determining K depending upon whether the dimension ϵ in the crystallite size equation is defined as the effective thickness of the crystallite in a direction perpendicular to the reflecting planes (ϵ_{hkl}), or as the cube root of the volume of the crystallite ($\epsilon v^{1/3}$). Defining ϵ as ϵ_{hkl} and β as the angular width at half maximum intensity, Scherrer (1918), Bragg (1919), Murdock (1930), Warren (1938) and others obtained values of K in the neighbourhood of 0·90. Assuming the particles to be of spherical shape and cubic structure Patterson (1936) obtained a value of $K=1{\cdot}11$; subsequently $K=0{\cdot}95$ has been regarded as a satisfactory approximation of the true value (Klug and Alexander 1954, Zettlemoyer and Walker 1947).

Using the value $\lambda(K_{\alpha_1})=1{\cdot}5405$ Å the mean particle sizes were reckoned using the graphical method of Alexander as discussed above. The values obtained are shown in table 3.

Table 3

Temperature of preparation (°c)	380	500	700	1000
Mean particle size (Å)	144 ± 5	267 ± 10	448 ± 50	2350 ± 150

The errors cited are random only and are evaluated from a 3% uncertainty in the half-breadths. Absolute values would have to take account of the uncertainties in correcting for K and for instrumental broadening. The systematic error in allowing for the latter is likely to be the greatest and a probable value is 20% for the smaller sizes increasing to 100% for the larger values.

§ 6. Particle Size and Energy Content

The relationship between energy content and particle size in magnesium oxide has been treated in detail by Weissenbach (1951). He defines the surface energy as the difference in the energy content between a finely powdered substance and the same substance in the coarsely crystalline state. Calculation based on the assumption that the magnesium oxide powder consisted of cube-shaped particles of uniform size which were bounded by (100) faces yielded the following approximate formula relating energy content and particle size

$$\Delta E=111\frac{1}{n}+1035\frac{1}{n^2}-1944\frac{1}{n^3}+1350\frac{1}{n^4}\,\text{kcal mol}^{-1}$$

n being the number of atomic diameters in the particle edge.

The first term is the surface energy corresponding to the (100) face, whereas the second term can be considered on the basis of the factor $1/n^2$ as the edge energy. The edge energy only becomes appreciable below $n=40$, and when $n<20$ there is a 'loosening' of the lattice which can no longer be accounted for

by the edge and surface energies alone. A particle size of $n = 50$ (~ 100 Å) would have an internal energy of about 2·6 kcal mol^{-1}, but for smaller sizes the loosening of the lattice begins to be appreciable.

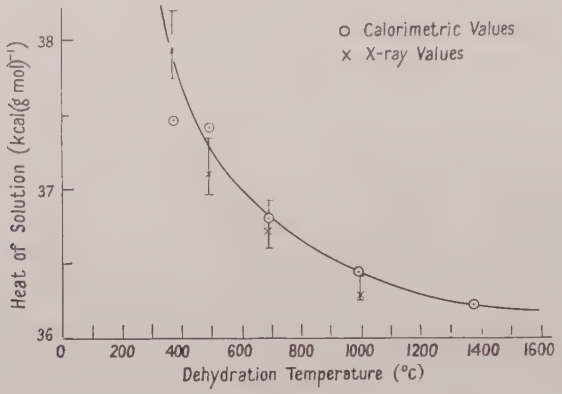

Figure 2.

The values of ΔE obtained on substituting the above crystallite sizes in the Weissenbach relationship are shown in figure 2 where they are plotted together with the experimentally determined calorimetric values, against temperature of preparation. Good agreement is obtained and on this basis the crystallite sizes as obtained from the line breadth measurements account satisfactorily for the variations in heat of solution exhibited by the magnesium oxide specimens.

§ 7. Conclusion

The factors most likely to cause variation in the heats of solution of magnesium oxide are susceptible to differentiation by x-ray methods. Such methods show that the phenomenon is predominantly a crystallite size effect. The crystallite sizes obtained in this manner can be satisfactorily related to the differing heats of solution by means of the Weissenbach relationship.

Acknowledgments

We are indebted to Dr. R. E. Smallman for the use of his diffractometer and much useful discussion. Our thanks are also due to Mr. C. J. Harris and Mr. W. E. Spindler for help with the experimental work. We should also like to express our gratitude to Dr. H. M. Finniston, for his advice and encouragement. The problem was suggested by Dr. D. T. Livey.

References

Alexander, L. E., 1954, *J. Appl. Phys.*, **25**, 155.
Birks, L. S., and Friedman, H., 1946, *J. Appl. Phys.*, **17**, 687.
Bragg, W. L., 1919, *Crystalline State* (London: Bell), Vol. 1, 189.
Fricke, R., and Lücke, J., 1935, *Z. Elektrochem.*, **41**, 174.
Hall, W. H., 1949, *Proc. Phys. Soc.* A, **62**, 741.
Jones, F. W., 1938, *Proc. Roy. Soc.* A, **166**, 16.
Kahler, F., 1949, *Berg-u-Hüttenm*, **94**, 83.
Klug, H. P., and Alexander, L. E., 1954, *X-ray Diffraction Procedures* (New York: John Wiley), pp. 512–516.
von Laue, M., 1926, *Z. Kristallogr.*, **64**, 115.
Livey, D. T., 1957, *Trans. Brit. Cer. Soc.*, **56**, 217.

Mazur, J., 1949, *Nature, Lond.*, **164,** 358.
Murdock, C. C., 1928, *Phys. Rev.*, **31,** 304.
—— 1930, *Ibid.*, **35,** 8.
Patterson, A. L., 1936, *Phys. Rev.*, **49,** 884.
Peiser, H. S., Rooksby, H. P., and Wilson, A. J. C., 1955, *X-ray Diffraction by Polycrystalline Materials* (London: Institute of Physics), p. 415.
Scherrer, P., 1918, *Cottinger Nachrichten*, **2,** 98.
Smallman, R. E., 1957, *Phil. Mag.*, **2,** 669.
Taylor, K., and Wells, 1938, *J. Res. Nat. Bur. Stand.*, **21,** 133.
Warren, B. E., 1938, *Z. Kristallogr.*, **99,** 448.
Warren, B. E., and Biscoe, J., 1938, *J. Amer. Ceram. Soc.*, **21,** 49.
Weissenbach, B., 1951, *Radex Rdsch.*, **6,** 257.
Williamson, G. K., and Smallman, R. E., 1954, *Acta Cryst.*, **7,** 574.
Zettlemoyer, A. C., and Walker, W. C., 1947, *J. Phys. Chem.*, **51,** 763.

Measurements of Atomic Velocity Distributions in Hg and HgO by the Nuclear Resonant Scattering of Gamma Rays

By D. C. CHAMPENEY and C. A. MILLER
University of Birmingham

Communicated by P. B. Moon; MS. received 2nd June 1959

Abstract. With a technique based on the nuclear resonant scattering of gamma rays, the thermal velocity distributions of the mercury atoms in mercury at 296°K and in mercuric oxide at 77°K have been measured. In agreement with theoretical predictions, the distributions are found to be Maxwellian in shape but corresponding to a distribution appropriate to an effective temperature higher than the actual one.

§ 1. Introduction

The conditions necessary for the observation of nuclear resonant scattering, and their dependence on the thermal motions of the nuclei in the source and scatterer, have been discussed by Moon (1951) on the assumptions that the nuclei recoil freely during emission or absorption of photons, and that the nuclear velocity distributions in source and scatterer are the same as in a gas (Maxwellian). He obtained the result that if a source, emitting gamma rays by de-excitation from nuclear levels of energy E_0, is moving bodily with a velocity U cm sec^{-1} towards a scatterer containing similar nuclei, then the amount of radiation resonantly scattered per unit solid angle through angle θ may be represented by an effective nuclear cross section

$$\sigma(\theta)=3{\cdot}6\times10^{-3}\frac{f(\theta)}{4\pi}\frac{I\Gamma_\gamma}{E_0{}^3\Gamma}\frac{g_a}{g_b}\left(\frac{A}{T}\right)^{1/2}\exp\left[-3\times10^{-9}\frac{A}{T}\left(\frac{32E_0}{A}-U\right)^2\right]. \quad \ldots\ldots(1)$$

In this equation I is the isotopic abundance of the resonantly scattering isotope, A its atomic weight, g_a and g_b are the multiplicities of the excited and ground states respectively, T is the mean of the temperatures of the source and scatterer in degrees K, $f(\theta)$ is the angular distribution factor normalized so as to be equal to unity for isotropic scattering, Γ is the total width of the excited state, and Γ_γ is the partial width for gamma decay to the ground state. E_0, Γ and Γ_γ are expressed in electron volts, $\sigma(\theta)$ in cm^2 sterad^{-1}.

In principle, then, an experiment measuring $\sigma(\theta)$ as a function of U enables one to verify whether or not the velocity distributions are Maxwellian.

This treatment relies on the fact that the nuclear resonance is very sharp, and that the energies lost or gained as a result of nuclear recoil at the emission and absorption of photons can be sufficient to throw the system off resonance. Considerations of energy and momentum conservation show, however, that if the nuclei have an initial relative approach velocity of E_0/mc (where m is the mass of the atom and c the velocity of light) then the losses balance the gains and the system is exactly on resonance. The experiment envisaged above thus measures a quantity

proportional to the numbers of pairs of atoms which have relative approach velocities within a small range round the value E_0/mc.

In the present experiments a radioactive source of ^{198}Au emitting gamma rays from the de-excitation of the 412 kev level of ^{198}Hg was used, set in motion by fixing it to the tips of a high speed rotor. Scatterers of mercury at room temperature and mercuric oxide at 77°K were used.

Descriptions of experiments of this type using the same source have been published by Davey and Moon (1953) and by Moon and Storruste (1953). The emphasis in these experiments was on the determination of Γ from the amount of scattering observed at the optimum rotor speed, equation (1) being assumed valid. With increase in accuracy of the technique it has become possible to measure the shape of the curve accurately enough to obtain from it information about the velocity distribution. Knapp's results (1957) were the most accurate to date, and he pointed out that there appeared to be certain irregularities in the results obtained with a mercuric oxide scatterer which might be the result of a breakdown of equation (1) resulting from the nuclei being in a solid and not a gas. Knapp considered the effects to be on the verge of his experimental accuracy, and the experiments described here are an extension of his work. To enhance any irregularities due to solid state effects, the oxide scatterer in the present experiments was cooled in liquid nitrogen.

§ 2. Apparatus

A scale plan of the apparatus is given in figure 1. A is the rotor, initially having approximately 100 mc of ^{198}Au on each tip. B is the scatterer of mercury or compressed mercuric oxide powder in the shape of an ellipse 7 cm high in a Perspex holder. For the cold scatterer experiments this was immersed in liquid nitrogen C

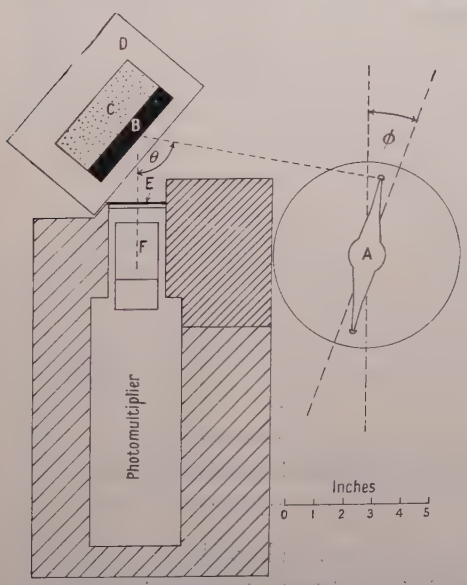

Figure 1. Scale plan of the apparatus.

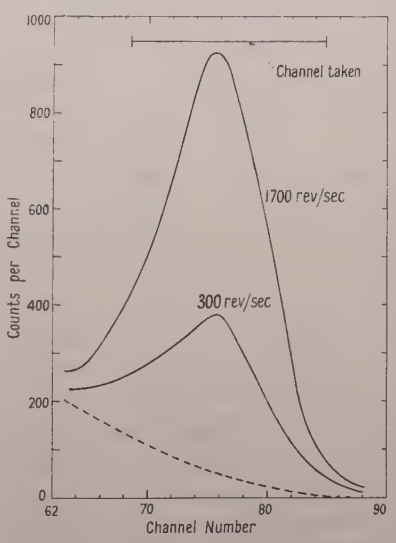

Figure 2. Typical spectra of the scattered radiation in eight-minute counts, with the estimated background shown by dotted line.

held in a 'Styrofoam'† holder D designed to reduce the amount of unwanted Compton and Rayleigh scattering off the cooling system to a minimum. The mean scattering angle θ was 100° so that the ratio of resonant to Rayleigh scattering was a maximum. E was a 1·5 mm thick sheet of lead which preferentially absorbed the lower energy Compton scattered radiation. F was a NaI scintillation crystal and light guide used in conjunction with a pulse height analyser having one hundred half-volt channels.

The amount of resonant scattering at any rotor speed was determined by measuring the numbers of counts within a fixed channel on either side of the 412 kev peak of the spectrum, and subtracting from this the corresponding number of counts at low rotor speed when resonant scattering was negligible. The spectrum was calibrated for each measurement using a ^{198}Au calibration source. Typical spectra are shown in figure 2.

The counting circuit was gated so that it counted only whilst the rotor was within the angle ϕ of figure 1, ϕ being 20°. This reduced the spread in component of source velocity towards the scatterer and also reduced the background counting rate. A correction of 1% in the speed was necessary to allow for the finite size of ϕ and for the angle subtended at the source by the scatterer.

§ 3. Results

The resonant counting rate is plotted as a function of rotor speed in figure 3 for the two different scatterers. In all 200 eight-minute counts were taken. After correcting for the decay of the source (the results are quoted in terms of a total activity of 200 mc) the readings have been grouped together within 50 rev/sec speed intervals and for each group a single point plotted at the mean speed and mean counting rate. The errors given represent the root mean square deviations of the individual points within a group from the smooth curve. Since there were only about four points within each group these errors are somewhat arbitrary.

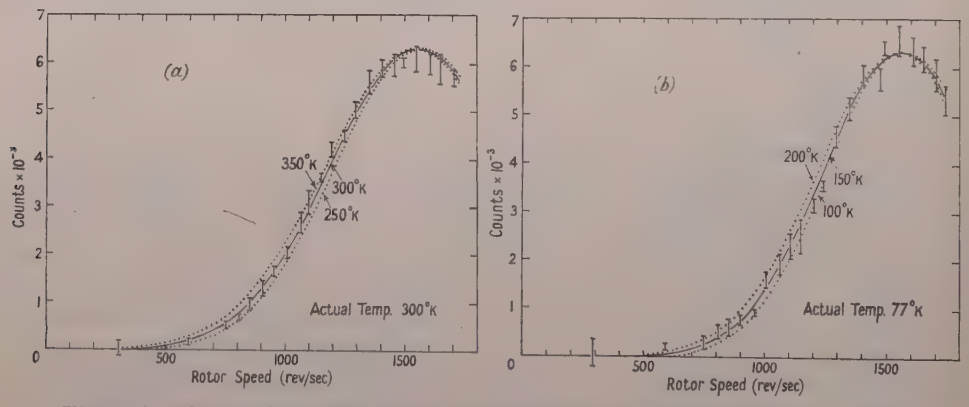

Figure 3. Comparison of the resonant counting rates with theoretical curves for (*a*) mercury, and (*b*) mercuric oxide scatterers.

In comparing these points with a theoretical curve a knowledge of the rotor as well as the scatterer temperature is necessary. The rotor warmed due to induction heating during the acceleration and then cooled by radiation during the subsequent gradual slow down. Experiments carried out with a clamped rotor

† Trade mark of the Dow Chemical Company.

subjected to the drive indicated that at the maximum speed of about 1700 rev/sec the rotor would have been at about 60°c, and that it would have cooled to about 40°c at 1500 rev/sec and about 30°c at 1200 rev/sec. These figures are based on the assumption that the rate of warming is proportional to the square of the difference in angular speeds of the rotor and driving field. The theoretical curves referred to below have been calculated on this basis. The 1% correction due to the finite value of ϕ has also been included in the theoretical curves. Thus whereas for ideal geometry the peak should occur at 1548 rev/sec we expect the curves of figure 3 to have peaks at 1563 rev/sec.

§ 4. Discussion

A calculation more rigorous than that leading to equation (1) should take into account the fact that the atoms are bound in a crystal lattice. Calculations of this type have been made by Lamb (1939) for the analogous case of neutron resonance absorption in a solid. The nature of the results depends on the relative magnitudes of $2(R\bar{\epsilon})^{1/2}+\Gamma$ and $\boldsymbol{k}\theta$ where R is the recoil energy loss, $\bar{\epsilon}$ is the mean atomic thermal energy per vibrational degree of freedom of the crystal, Γ is the total half value width of the resonance level, $\boldsymbol{k}$ is Boltzmann's constant and θ is the Debye temperature of the solid. For the case of gamma rays R is equal to $E_0^2/2\boldsymbol{mc}^2$. In the present case $\Gamma \sim 2{\cdot}1\times10^{-5}$ ev and may be neglected in comparison with the other terms.

If $(R\bar{\epsilon})^{1/2} \gtrsim 2\boldsymbol{k}\theta$ then the result is given by the free atom approximation, except that the temperature used in equation (1) must be replaced by effective temperatures defined by $\boldsymbol{k}T_{\text{eff}}=\bar{\epsilon}$. This effect may be regarded as arising from the zero-point motion of the atoms, and has been mentioned by Metzger (1956, 1958, 1959) and by Moon, Shute and Sood (1958).

If $(R\bar{\epsilon})^{1/2} \lesssim \frac{1}{2}\boldsymbol{k}\theta$ then the recoil may not be regarded as free and equation (1) is not valid. The extension of Lamb's theory to the resonant absorption of gamma rays under these conditions with supporting experiments has been described by Mössbauer (1958 a, b, 1959) with further confirmatory experiments by Craig *et al.* (1959) and by Lee *et al.* (1959). Mössbauer finds a resonance curve shape as given by the effective temperature concept together with a sharp line of width Γ occurring at zero speed, with height strongly dependent upon temperature.

The Debye temperature of mercuric oxide as estimated by comparing its molecular heat at 100°K with the classical value of $6R$ is 350°K. The specific heat does not vary with temperature as in the simple Debye theory so that this figure is only approximate, the corresponding figures deduced from the specific heats at 50°K and 300°K being 250°K and 450°K respectively. Assuming the value 350°K for θ, then the effective temperature corresponding to a real temperature of 77°K is 142°K.

Using this figure, we find for the case of the oxide scatterer at 77°K that $(R\bar{\epsilon})^{1/2}=2{\cdot}5\boldsymbol{k}\theta$, so that we expect the effective temperature concept to be valid. Conditions in the source are such that its effective temperature should equal its real temperature.

The full and dotted lines in figure 3 are theoretical curves based on various values of effective temperature substituted into equation (1). The liquid mercury fits best onto the 300°K curve, showing its velocity distribution to be the same as in a gas at the same temperature to within say ±30°K. The mercuric oxide results are best represented by an effective temperature within the range 150°K ± 50°K.

Within the experimental accuracy this is in agreement with the theoretical value. In further agreement with Lamb's theory there seems to be no evidence for marked irregular structure.

Acknowledgments

The authors would like to thank Professor P. B. Moon for suggesting the problem, and for his continued interest in the work. One of us (C.A.M.) acknowledges financial support from the Department of Scientific and Industrial Research.

References

Craig, P. P., Dash, J. G., McGuire, A. D., Nagle, D., and Reiswig, R. D., 1959, *Phys. Rev. Letters*, **3**, 221.
Davey, W. G., and Moon, P. B., 1953, *Proc. Phys. Soc.* A, **66**, 956.
Knapp, V., 1957, *Thesis*, University of Birmingham.
Lamb, W. E., 1939, *Phys. Rev.*, **55**, 190.
Lee, L. L., Jr., Meyer-Schutzmeister, Schiffer, J. P., and Vincent, D., 1959, *Phys. Rev. Letters*, **3**, 223.
Metzger, F. R., 1956, *Phys. Rev.*, **103**, 983.
—— 1958, *Ibid.*, **110**, 123.
—— 1959, *Progr. Nucl. Phys.*, **7**, 54.
Moon, P. B., 1951, *Proc. Phys. Soc.* A, **64**, 76.
Moon, P. B., Shute, G. G., and Sood, B. S., 1958, *Phys. Rev. Letters*, **1**, 47.
Moon, P. B., and Storruste, A, 1953, *Proc. Phys. Soc.* A, **66**, 585.
Mössbauer, R. L., 1958 a, *Z. Phys.*, **151**, 124.
—— 1958 b, *Naturwissenschaften*, **45**, 539.
—— 1959, *Z. Naturf.*, **14 a**, 211.

The Radiative Capture Cross Section of ^{232}Th for Neutrons in the Energy Range 300 to 1200 keV

By J. F. BARRY, L. P. O'CONNOR and J. L. PERKIN
Atomic Weapons Research Establishment, Aldermaston, Berks.

Communicated by K. W. Allen; MS. received 10th June 1959, in final form 10th July 1959

Abstract. A redetermination of the (n,γ) cross section of ^{232}Th in the energy region 300 to 1200 kev has been made by an activation method. A discrepancy existed between the level structure of this nucleus obtained directly from inelastic scattering measurements and the level structure deduced by Lane and Lynn in their interpretation of radiative capture cross section measurements. The energy dependence of the radiative capture cross section used by Lane and Lynn showed a plateau extending between the neutron energies of 250 and 650 kev followed by a sharp drop. The present measurements show that this plateau actually extends up to about 900 kev so that the (n,γ) cross section is no longer inconsistent with the level structure of ^{232}Th deduced from inelastic scattering measurements.

§ 1. Introduction

The radiative neutron capture cross sections of ^{232}Th and ^{238}U do not show the steady decrease with increasing neutron energy expected according to the orthodox statistical theory. Lane and Lynn (1957) have explained this anomalous behaviour in terms of the energy level structure of these two nuclides. At certain excitation energies, the density of low-lying levels available for inelastic scattering will decrease owing to the rotational nature of the levels. The radiative capture process is able to compete more effectively with inelastic scattering in such an energy region, so that the (n,γ) cross section will level off or even increase with increasing neutron energy.

At the time the calculations were made, the energy level structure of ^{232}Th had not been determined experimentally. Lane and Lynn therefore postulated levels at 425 and 500 kev in order to explain the measurements of Hanna and Rose (1959). However, the recent work of Batchelor and Towle (1959), who studied the levels of ^{232}Th by inelastic neutron scattering, did not reveal levels in the region of 400 to 500 kev. In view of the excellent agreement obtained between theory and experiment for ^{238}U, it was therefore felt worth while to redetermine the radiative capture cross section of ^{232}Th in the energy region 300 to 1200 kev.

After the work reported here had been completed more American data became available in the compilation of Hughes and Schwartz (1958). These data are in good agreement with our own measurements and are consistent with the energy levels of ^{232}Th obtained by Batchelor and Towle.

§ 2. Method

^{233}Th, the end product of the (n,γ) reaction in ^{232}Th, emits β particles with a maximum energy of 1·23 Mev and has a half-life of 22·1 minutes. It was measured by counting the β-particles in an end window Geiger counter. Comparison of the activities produced at different neutron energies for the same neutron flux gives the relative values of the cross sections at these energies.

The β-particle activity due to ^{233}Th produced in the irradiations was some orders of magnitude smaller than that due to the natural daughters of thorium. Therefore the natural element was chemically purified to remove most of the daughters before each run. Lead, radium and actinium were removed from a solution of 400 mg of thorium by repeated precipitation of the hydroxy-peroxide of thorium in 0·4 M nitric acid solution after the prior removal of lead and bismuth by sulphide precipitation. Thorium was finally precipitated as oxalate and ignited to ThO_2.

A known weight of this oxide was packed into a polystyrene container of internal dimensions 2 cm diameter by 0·075 cm depth and irradiated with neutrons from the T(p, n)^{3}He reaction at 0° to the proton beam. It was then counted through the 0·025 cm polystyrene wall in an end window Geiger counter with a geometry of about 30%. The activity was followed for about six half lives by which time only a background due to the grow-in of natural daughters remained. Several points on the grow-in curve were obtained throughout the day in between each irradiation. This was subtracted to obtain the ^{233}Th decay curves.

After normalizing to a fixed count on the neutron monitor, the activities obtained after irradiation at different neutron energies were proportional to the cross sections at these energies.

Neutrons were obtained by bombarding tritium gas at approximately atmospheric pressure in a 1 in. long cell with protons from the Aldermaston 6 Mev Van de Graaff generator. The neutrons were monitored with a long counter (Hanson and McKibben 1947). Corrections were applied to the relative neutron flux measured during each irradiation for the variation of the long counter efficiency with energy and for the anisotropic output from the target. The lowest energy points were also corrected for displacement of the effective centre of the gas target resulting from the increased proton energy loss ($5\frac{1}{2}$% correction at 300 kev), and for the effects of the lower energy neutron group which is produced at bombarding energies close to the T(p, n)^{3}He reaction threshold. This low energy group is present when the velocity of the centre of mass in the laboratory system of coordinates is greater than the velocity of the emitted neutron in the centre-of-mass system. Thus neutrons emitted in a backward direction in the centre-of-mass system are actually emitted in a forward direction with reduced velocity in the laboratory system.

§ 3. Uranium Calibration

To fix the absolute scale of the cross-section curve, use was made of the well-established cross section for radiative capture in ^{238}U in this energy region (Hughes and Schwartz 1958). ^{238}U contained in a sample of identical size and weight to the ^{232}Th sample was irradiated in the same neutron flux and the ^{239}U produced was counted in the same experimental arrangement. The maximum

β-particle energy and half-life of ^{239}U have similar values to those of ^{233}Th. Thus the ratio of the radiative capture cross sections of ^{232}Th and ^{238}U is, after small corrections, given by the ratio of their activities after irradiation.

It was necessary to use metal depleted in ^{235}U because of β-particle activity produced by fission of this isotope during the irradiation. Uranium containing about 0·02% by weight of ^{235}U was obtained from the Atomic Energy Research Establishment, Harwell. The activity obtained after neutron irradiation decayed with the half-life of ^{239}U and there was no indication of fission product activity from the small amount of ^{235}U present.

Chemical purification was again required to remove the natural daughters of the uranium. Thorium and protoactinium were removed daily to the extent of more than 99·9% from about 400 mg of uranium. This was done by the chromatographic separation of uranyl nitrate on a cellulose column from a 1% nitric acid–ether solution, a technique introduced by Burstall and Wells (1951). The bulk of the fission products of ^{235}U were also removed by this method. The purified nitrate was ignited to U_3O_8, which was used in the irradiations.

In each irradiation the thorium was nearer to the neutron source than was the uranium so that a correction, calculated at 4·5% had to be applied. This value was confirmed experimentally by means of a second irradiation with the thorium and uranium sample positions reversed.

The effect of β-particle absorption and scattering in the two samples was checked by impregnating the original weights of the recently purified oxides with known activities of ^{210}Bi (maximum β-particle energy 1·15 MeV). For the thorium sample this was done by co-precipitation of the oxalates and for the uranium by mixed slurrying. The specific count rates of the sources were compared using the original counting geometry and were found to agree within the experimental error of 5%.

§ 4. Results and Conclusions

The thorium cross section values are shown in the table and are plotted, together with all the other available data, in the figure. The absolute values were obtained by comparison of the activities of thorium and uranium from the 600 kev irradiation and by using a value of 132 mbn for the uranium (n,γ) cross section at that energy.

Cross Section of the Reaction $^{232}Th(n,\gamma)^{233}Th$

Neutron Energy, E_n (kev)	300	400	500	600	700	800	900	1000	1100	1200
Spread in E_n (kev)	±90	±80	±75	±73	±69	±67	±66	±65	±64	±62
Cross section (mbn)	206	190	172	195	187	172	173	120	120	118
Standard deviation (mbn)	±17	±11	±11	±12	±12	±11	±10	± 8	± 8	± 8

The errors shown include possible errors in the neutron flux corrections as well as counting statistics. The neutron energy limits shown are the maximum and minimum energies effective in any given irradiation.

The points agree with those obtained in America and imply that the measurements of Hanna and Rose are probably in error above 650 kev. The flat portion of the curve continues up to 800 or 900 kev before falling off,

confirming the position of the levels found by Batchelor and Towle at 760, 820 and 1090 kev, with no indication of levels about 450 kev.

This group of levels corresponds to the levels found by Cranberg and Levin (1958) and Batchelor and Towle (1959) at 730, 980 and 1060 kev in ^{238}U. As ^{232}Th and ^{238}U are both even–even nuclei far removed from a closed shell this similarity between their level structures is to be expected.

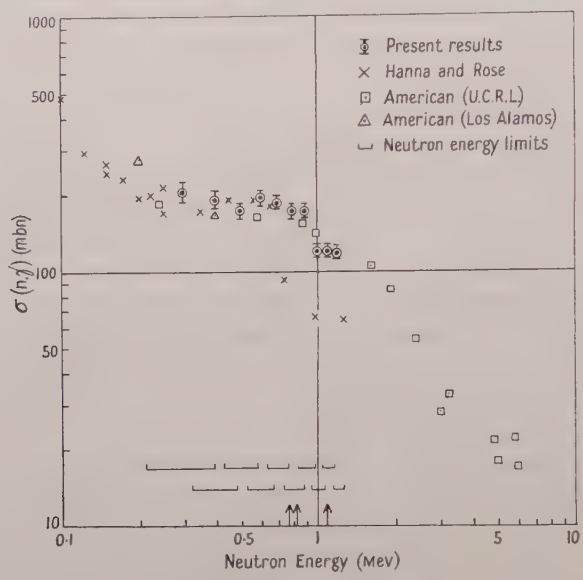

Cross-section values for the reaction ^{232}Th(n, γ)^{233}Th. The arrows indicate the positions of the levels found by Batchelor and Towle.

Acknowledgments

We are indebted to the Atomic Energy Research Establishment, Harwell, for the supply of isotopically enriched uranium.

References

Batchelor, R., and Towle, J. H., 1959, *Proc. Phys. Soc.*, **73**, 193.
Burstall, F. H., and Wells, R. A., 1951, *Analyst*, **76**, 396.
Cranberg, L., and Levin, J. S., 1958, *Phys. Rev.*, **109**, 2063.
Hanna, R. C., and Rose, B., 1959, *J. Nucl. Energy*, **8**, 197.
Hanson, A. O., and McKibben, J. L., 1947, *Phys. Rev.*, **72**, 673.
Hughes, D. J., and Schwartz, R. B., 1958, *U.S. Atomic Energy Commission Report*, BNL 325 (2nd Edn) (Washington: U.S. Government Printing Office).
Lane, A. M., and Lynn, J. E., 1957, *Proc. Phys. Soc.* A, **70**, 557.

Isotope Shift in the CdI Intercombination Resonance Line λ 3261 A

By F. M. KELLY and E. TOMCHUK
Department of Physics, University of Manitoba, Winnipeg, Canada

MS. received 2nd June 1959, in final form 3rd July 1959

Abstract. The isotope shifts in the intercombination resonance line of CdI have been measured. The line was excited in an atomic beam by electron bombardment and the high resolution obtained with a Fabry–Perot interferometer. The shifts between even isotopes decrease with increasing neutron number and the odd isotopes lie close to the next lighter even isotope showing a pronounced odd–even staggering. The relative shifts are in agreement with those of other Cd lines.

§ 1. Introduction

Cadmium has six stable even isotopes and two stable odd isotopes so that it is ideal for isotope shift studies. The relative abundances of the naturally occurring isotopes (Bainbridge and Nier 1950) are given in table 1.

Table 1

Isotope	106	108	110	111	112	113	114	116
Abundance (%)	1·22	0·88	12·4	12·8	24·1	12·3	28·8	7·6

Isotope shifts in the intercombination resonance line λ3261 ($5s^2\ {}^1S_0 - 5s5p\ {}^3P_1$) were first measured by Brix and Steudel (1950) who used the absorption of six atomic beams in series. They measured the relative separations of isotopes 110, 112 and 114.

In this experiment an atomic beam was excited by electron bombardment and λ3261 was observed in emission. The isotope shifts between 106, 110, 111, 112, 113, 114 and 116 were observed.

Isotope shifts for cadmium have also been measured by several authors in the spark line λ4416 ($4d^{10}\,5p\ {}^2P_{3/2} - 4d^9\,5s^2\ {}^2D_{5/2}$). The most recent measurements are those of Kuhn and Ramsden (1956) who used enriched isotopic samples and a hollow cathode cooled with liquid hydrogen. They measured the shifts between all of the stable isotopes.

In the heavy elements the isotope shifts can be explained by the field or volume effect. For the light elements isotope shifts arise from the two mass effects. The normal mass effect can be accounted for by a reduced mass calculation. The specific mass effect which arises from the interaction between the electrons is difficult to calculate. Both mass effects decrease with increasing mass number but it is not certain where the specific effect becomes negligible. The shifts reported here were measured to redetermine the ratios of Kuhn and Ramsden using a different line to check the possible influence of a residual specific mass effect.

The spins of both the odd isotopes are known to be $\frac{1}{2}$ and the nuclear magnetic moments are negative (Strominger, Hollander and Seaborg 1958). Then

each odd isotope gives rise to two components in λ3261 Å. The weaker component has the higher wave number.

§ 2. Experimental Arrangement

An atomic beam light source essentially similar to that described by Crawford *et al.* (1950) was constructed. The beam of cadmium atoms was produced by evaporating cadmium from a wire wound iron furnace heated by an electrical current. The collimation of the beam was 14, so that the source line width was $0{\cdot}002\,\mathrm{cm}^{-1}$.

The beam was excited by electron bombardment with low speed electrons. The line λ3261 was isolated with a Hilger medium quartz spectrograph and the high resolution was supplied by a quartz Fabry–Perot interferometer mounted externally to the spectrograph. Spacers of 3 and 5 cm were used.

The interferometer plates were coated with aluminium films each of which had a transmission coefficient of about 0·03 in the visible region. This corresponds to a reflection coefficient of about 0·85 at a wavelength of 3200 Å (Burridge, Kuhn and Pery 1953). Eastman 103aO plates were used. The exposure times varied between ten minutes and one hour.

§ 3. Results

The 5 cm etalon gave good resolution for the four most abundant even isotopes. The four components to be expected for the odd isotopes were thrown in the inter-order space and three components were observed. One of these three was due to a superposition of two components. The components are named according to the mass number of the isotope of origin. The two components from each of the odd isotopes are designated as s or w to indicate the strong and weak components.

With the 5 cm spacer the components 113w and 111s were not resolved. With a 3 cm spacer the components 111s and 113s were well separated and could be easily measured. However the resolution was not as high, and, there was interference between the two weak components of the odd isotopes and the even components, so that measurements of the even components from these plates were not used in the calculations. The results of the measurements are summarized in table 2.

Table 2

Isotope pair	No. of fringes measured	Etalon spacer (cm)	Separation ($\times 10^{-3}\,\mathrm{cm}^{-1}$)
114, 116	81	5	$9{\cdot}3 \pm 0{\cdot}3$
112, 114	301	5	$13{\cdot}5 \pm 0{\cdot}4$
110, 112	98	5	$16{\cdot}3 \pm 0{\cdot}5$
112, 113s	88	5	$26{\cdot}1 \pm 0{\cdot}4$
112, 111w	69	5	$51{\cdot}5 \pm 0{\cdot}4$
112, 113w+111s	69	5	$44{\cdot}0 \pm 0{\cdot}4$
112, 106	24	3	$51{\cdot}7 \pm 1{\cdot}7$
113s, 111s	164	3	$19{\cdot}8 \pm 0{\cdot}3$

Theoretical intensity curves were plotted to estimate the displacement of the peak of 116 due to the presence of the much stronger component due to 114. The correction was estimated to be $0{\cdot}0002\,\mathrm{cm}^{-1}$ and has been included in table 2. Similar corrections were applied to other components which were close together

in the observed patterns. The errors quoted in table 2 are probable errors obtained by multiplying the average deviations from the means by 0·68. Some twenty exposures with each spacer were measured five times by each of two observers with a comparator. The number of fringes measured is given in table 2.

The shifts between the various even isotopes are given directly by table 2. However, the centres of gravity of the components due to the odd isotopes must be calculated before the relative isotope shifts can be estimated.

From table 2, $\Delta\nu(112, 111w) = 151{\cdot}5$. 111w is overlapped one order in the pattern. Also from table 2, $\Delta\nu(112, 113s) = 100{\cdot}0 - 26{\cdot}1 = 73{\cdot}9$. From the 3 cm etalon measurements $\Delta\nu(113s, 111s) = 19{\cdot}8$ so that $\Delta\nu(112, 111s) = 54{\cdot}1$. The total magnetic hyperfine structure splitting for 111 is the sum of $\Delta\nu(112, 111w)$ and $\Delta\nu(112, 111s)$ and is 205·6.

For isotope 113, $\Delta\nu(112, 113s)$ is measured directly from the 5 cm patterns and is 73·9. The direct measurements also give $\Delta\nu(112, 113w + 111s) = 44{\cdot}0$. From the information concerning isotope 111, 111s lies 1·9 to the higher frequency side of the measured centre of gravity of 113w and 111s in the 5 cm patterns. Then, weighting 111s and 113w according to known relative abundances and statistical weights, 113w lies 3·9 to the low-frequency side of the centre of gravity of 113w and 111s. Thus, in the 5 cm pattern 113w is 40·1 to the high-frequency side of 112 and $\Delta\nu(112, 113w) = 140{\cdot}1$. Then, the magnetic hyperfine structure for 113 is $73{\cdot}9 + 140{\cdot}1 = 214{\cdot}0$. The unit in these separations is $10^{-3}\,\mathrm{cm}^{-1}$.

A check on the accuracy of these results can be made by a comparison with the ratio of the nuclear magnetic moments from other determinations. From our measurements

$$\frac{\mu 113}{\mu 111} = \frac{14{\cdot}0}{205{\cdot}6} = 1{\cdot}041.$$

This agrees well with the nuclear induction measurements of Proctor and Yu (1950) which give a ratio of 1·046 for these two nuclear moments.

From the above measurements the centres of gravity of the odd isotopes can be placed relative to the even ones and we find

$$\Delta\nu(112, 113) = 2{\cdot}4 \pm 1{\cdot}3 \times 10^{-3}\,\mathrm{cm}^{-1}$$
$$\Delta\nu(110, 111) = 1{\cdot}8 \pm 1{\cdot}6 \times 10^{-3}\,\mathrm{cm}^{-1}$$

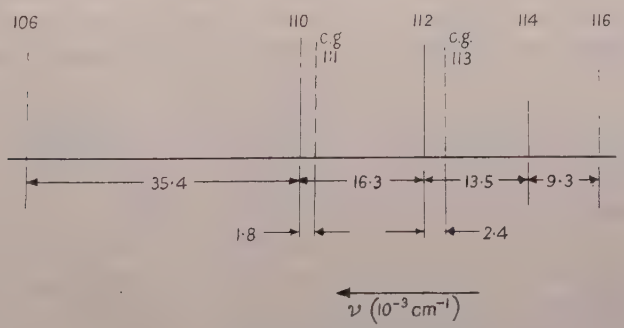

Isotope shifts in CdI λ 3261.

The order of the isotopes is regular. A summary of our observed shifts is given in the figure.

§ 4. Isotope Shift

The observed isotope shifts in $\lambda 3261$ need to be adjusted for the normal mass shift. Table 3 gives the values of the shifts when the normal mass effect has been taken into account.

Table 3

Isotope pair	114, 116	112, 114	110, 112	106, 110	111, 113
Isotope shift $\times(10^{-3}\ \mathrm{cm}^{-1})$	$11{\cdot}8\pm0{\cdot}4$	$16{\cdot}1\pm0{\cdot}4$	$19{\cdot}0\pm0{\cdot}5$	$40{\cdot}8\pm2{\cdot}1$	$19{\cdot}5\pm2{\cdot}4$

Following Kuhn and Ramsden the relative shifts between the various isotopes are calculated using $\Delta\nu(110, 112)=1{\cdot}00$. In table 4 the results are compared.

Table 4

Isotopes	Relative shift	
	This paper	Kuhn and Ramsden
$(106, 110)\frac{1}{2}$	1·07	1·04
108, 110	–	1·00
110, 112	1·00	1·00
111, 113	1·03	1·03
112, 114	0·85	0·93
114, 116	0·62	0·65

These ratios agree within experimental error with those of Kuhn and Ramsden (1956) except for the ratio (112, 114). In this case the observed difference is 9% whereas the sum of the experimental errors is 7%. However we have made visual measurement only so that there may be a small and unknown systematic error in our results. To this extent the results of Kuhn and Ramsden are confirmed.

§ 5. Magnetic Moment

The measurement of the magnetic hyperfine structure of the odd isotopes enables a calculation of the nuclear magnetic moments. From the formula for intermediate coupling (Breit and Wills 1933) we obtain $\mu(113)=-0{\cdot}55$ n.m. and $\mu(111)=-0{\cdot}52$ n.m. These values are about 12% lower than the results from nuclear induction (Proctor and Yu 1950).

The spectroscopic values calculated in this way may be expected to be low for we have used the value of a_{5s} determined from data for Cd II whereas in fact the 5s electron is screened by the 5p electron. A reduction of a_{5s} by 10% to allow for the screening to the 5p will bring the two values into agreement.

Acknowledgments

The research reported here was supported by a grant from the National Research Council of Canada. One of us (E.T.) is indebted to the Northern Electric Company of Canada for a research scholarship.

References

Bainbridge, K. T., and Nier, A. O., 1950, *Nuclear Science Series, Preliminary Report* No. 9 N.R.C. U.S.A.

Breit, G., and Wills, L. A., 1933, *Phys. Rev.*, **44**, 470.

Brix, P., and Steudel, A., 1950, *Z. Phys.*, **128**, 260.

Burridge, J. C., Kuhn, H., and Pery, A., 1953, *Proc. Phys. Soc.* B, **66**, 963.

Crawford, M. F., Schawlow, A. L., Kelly, F. M., and Gray, W. M., 1950, *Canad. J. Phys.*, A, **28**, 558.

Kuhn, H. G., and Ramsden, S. A., 1956, *Proc. Roy. Soc.* A, **237**, 485.

Proctor, W. G., and Yu, F. C., 1950, *Phys. Rev.*, **76**, 1728.

Strominger, D., Hollander, J. M., and Seaborg, G. T., 1958, *Rev. Mod. Phys.*, **30**, 585.

The Decay of Arsenic 80

By R. E. MEADS and J. E. G. McILDOWIE
Clarendon Laboratory, Oxford

MS. received 25th May 1959

Abstract. Arsenic 80 has been produced by the ^{80}Se (n, p)^{80}As reaction induced by 14 Mev neutron irradiation of natural Se and enriched ^{80}Se samples. The β^- decay to ^{80}Se ($t_{1/2} = 15{\cdot}3$ sec) has been investigated by scintillation spectrometry using β–γ and γ–γ coincidence techniques. The γ-ray spectra are interpreted in terms of levels in ^{80}Se at 0·66, 1·44, 1·52, 1·77, 1·88, 2·30, 2·50 and 3·01 Mev. The β-transitions to the ground and first excited states of ^{80}Se (log *ft* values 5·8 and 5·9 respectively) are probably allowed, giving spin 1^+ for the ground state of ^{80}As.

§ 1. Introduction

An activity probably due to the decay of ^{80}As was first observed by Ythier and Hermann (1954), using chemical separation techniques following fast neutron irradiation of Se. They found an activity of half-life < 1 minute, which was assigned to ^{80}As produced by the ^{80}Se (n, p) ^{80}As reaction. The 2^+ first excited state of the daughter nucleus ^{80}Se has been observed at 0·65 Mev in Coulomb excitation using 6 Mev α-particles (Temmer and Heydenburg 1956).

§ 2. Experimental Methods

In the present work ^{80}As was again produced by the ^{80}Se (n, p)^{80}As reaction, samples of natural Se and enriched ^{80}Se being irradiated with 14 Mev neutrons from 400 kev deuteron bombardment of a thick titanium tritide target. The target was water cooled, permitting deuteron beams up to 200 μA without unduly rapid target deterioration. In order to avoid inducing activities in the scintillation counters due to the high neutron flux in the vicinity of the target, they had to be placed some distance away, and a pneumatic transit tube 40 feet in length was employed to convey the samples, in polythene cells, between the target and counters. The transit time was 3 seconds.

γ-ray measurements were made using two 4 in. × 4 in. cylindrical NaI(Tl) crystals, supplied by the Harshaw Chemical Company, mounted on E.M.I. type 6099 A photomultipliers. The ungated spectra from one of the crystals were displayed by a Hutchinson–Scarrott type 75-channel pulse-height analyser. For the coincidence work, spectra from the same crystal coincident with a gating pulse were similarly displayed. The gating pulse was generated when a coincidence with 0·2 μsec resolution occurred between the two counters, together with the further requirement that the height of the pulse from the second counter lay within limits defined by a single channel pulse height analyser. This enabled the spectra of γ-rays in coincidence with another γ-ray of defined energy to be examined.

For the γ-ray measurements a sample irradiation time of 30 seconds followed by an equal counting period was employed. The cycle was automatically controlled using a rotary selector switch operated by pulses at 1 sec intervals obtained from a clock.

Spectra of β-particles were observed using a 'Nuclear Enterprises' type NE 102 2 in. × 2 in. plastic phosphor mounted on an E.M.I. type 6097 A photomultiplier. The β-sources were made by mixing selenium powder to a paste with polystyrene and benzene, and mounting a layer 2 mm thick on the end of a polystyrene holder suitable for use in the transit tube. The shortness of the half-life and the poor counting rates obtainable precluded the use of sources sufficiently thin to measure the actual shape of the β spectrum so that the measurements were confined to the determination of end points. For calibration purposes, similar sources were made using other materials.

§ 3. Results

3.1. *Assignment of Activity*

By far the most intense short-lived activity produced by fast neutron irradiation of selenium is due to the decay of the isomeric state at 0·16 Mev in ^{77}Se (half-life 17·5 sec). There is also a group of γ-rays due to an activity of much longer half-life which correspond in energy to those observed by Schram *et al.* (1957,

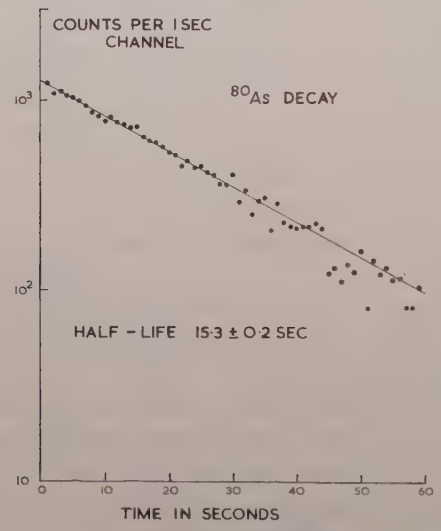

Figure 1. Half-life measurement on ^{80}As decay. This was made on the 0·66 Mev γ-ray, using a time-pulse height convertor in conjunction with the 75 channel analyser. A background subtraction (as for figure 2) was carried out.

unpublished data, see Strominger, *et al.* 1958, van Lieshout 1958, private communication) in the decay of ^{78}As. In addition to these there are a number of γ-rays corresponding to another activity of short half-life which are assigned to the decay of levels in ^{80}Se populated by ^{80}As β-decay. The most intense of these has an energy of 0·66 Mev, in reasonable agreement with Temmer and Heydenburg (1956) for the first excited state of ^{80}Se. Half-life measurements made with this γ-ray indicate a value of 15·3 ± 0·2 sec for ^{80}As decay (figure 1). The use of a 98% enriched ^{80}Se sample (1·8 g, supplied by the

Harwell Electromagnetic Separator Group) confirms that this activity is produced from ^{80}Se, as the other activities mentioned are greatly reduced in intensity when the enriched sample is used.

3.2. *γ-ray Spectra*

We now summarize the results of the γ-ray measurements. It was essential to use the enriched ^{80}Se sample here, to avoid confusion due to γ-rays from other activities. γ-rays of energies $0{\cdot}66 \pm 0{\cdot}01$, $1{\cdot}22 \pm 0{\cdot}01$, $1{\cdot}64 \pm 0{\cdot}01$, $1{\cdot}77 \pm 0{\cdot}03$, and $2{\cdot}35 \pm 0{\cdot}03$ MeV were observed in the ungated spectra (figure 2), together with a broad peak at 0·8 MeV which consists of more than one component. The relative intensities of these γ-rays were calculated by comparing them with standard γ-ray spectra and by the use of tables (Miller *et al.* 1958, Wolicki *et al.* 1956) of total efficiencies and photofractions for the sodium iodide crystals employed.

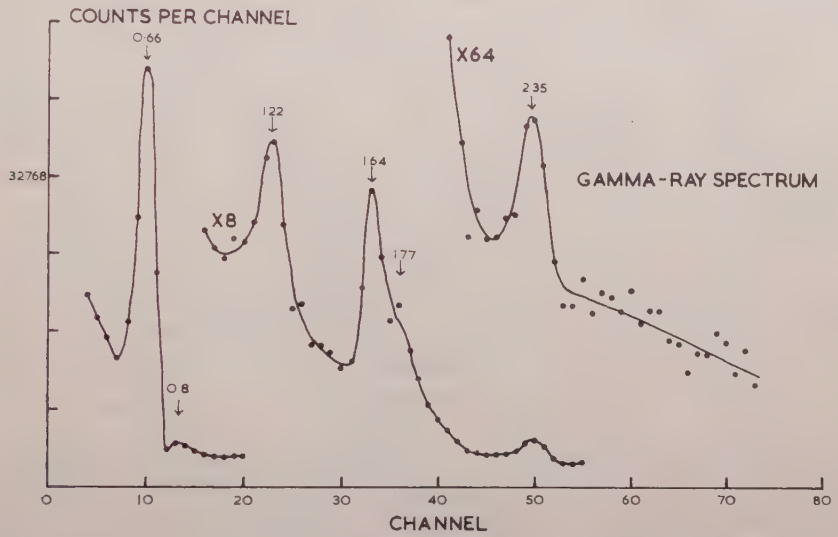

Figure 2. Ungated γ-ray spectrum. A background correction was made from a second run with an empty sample holder in the transit tube.

In making γ–γ coincidence measurements it was necessary to show that coincidences observed were not merely due to bremsstrahlung. For example, in determining what γ-rays were in coincidence with the 0·66 MeV line, three spectra were taken, with the energy window set to accept radiation of 0·57, 0·66 and $0{\cdot}73 \pm 0{\cdot}02$ MeV respectively. The results were normalized to a fixed count in a neutron monitor. (BF_3 counter in paraffin.) The neutron flux was maintained at a constant level during each run. This meant that the total activity observed was the same in each case. The count rate in the 0·8 MeV region and for the peaks at 1·22, 1·64 and 2·35 MeV was much greater when the window was set at 0·66 MeV than when it was displaced to either side of the peak. The spectrum in coincidence with 0·66 MeV also showed a weak peak at $1{\cdot}84 \pm 0{\cdot}03$ MeV which was not resolved in the ungated spectrum. A repeat spectrum confirmed the presence of this peak (figure 3).

The results confirm that these γ-rays are truly in coincidence with the 0·66 MeV γ-ray, as coincidences with the bremsstrahlung would merely show an

increase in rate as the energy setting of the window is reduced. The γ-ray at 1·77 MeV is not coincident with 0·66 MeV radiation. The relative intensities of the γ-rays in coincidence with the 0·66 MeV line is substantially the same as in the ungated spectrum, except that the 2·35 MeV peak is reduced to about half its previous intensity. This could be explained by assuming that half the counts in the ungated 2·35 MeV peak were due to the decay of the proposed level at 2·30 MeV direct to the ground state.

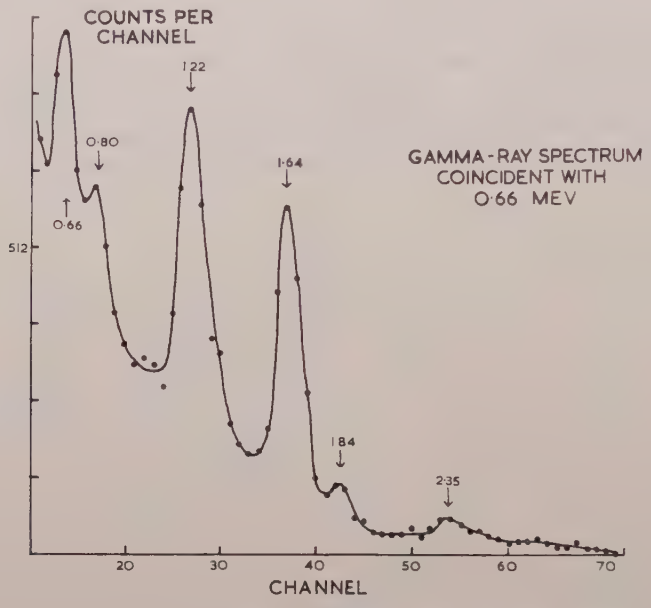

Figure 3. γ-ray spectrum coincident with 0·66 MeV radiation.

A number of other coincidence spectra were taken, with the window set at 0·78, 0·86, 1·22, 1·64 and 2·35 MeV. The results for 1·22, 1·64 and 2·35 MeV show only the 0·66 MeV γ-ray, indicating that none of these γ-rays form part of a triple cascade, but that they go direct to the 0·66 MeV level. This shows the presence of levels at 1·88, 2·30 and 3·01 MeV, as shown on the level scheme. The 1·84 MeV γ-ray is attributed to the decay of a level at 2·50 MeV, but owing to its weakness, and proximity to the strong 1·64 MeV peak, it was not possible to confirm this. The broad peak at 0·8 MeV was further examined by obtaining a spectrum in coincidence with 0·66 MeV with improved statistics and a narrower energy coverage (figure 4). This, together with the spectra in coincidence with 0·78 and 0·84 MeV, is consistent with its being made up of a doublet with about these latter two energies, both in coincidence with 0·66 MeV but not mutually coincident. If these were in coincidence with each other, (forming a triple cascade from the 2·30 MeV level through a level at about 1·5 MeV) there would be a considerable enhancement of the 0·78 MeV peak when the window was set to 0·86 MeV, and vice versa, and the intensity of the enhanced peak would be the same as that of the 0·66 MeV γ-ray, neglecting spurious coincidences. No such enhancement was found. The small number of counts present in these peaks can be attributed to coincidences with the high energy tail of the 0·66 MeV γ-ray appearing in the window, and with bremsstrahlung. The γ-rays were attributed to the decay of levels at 1·44 and 1·52 MeV.

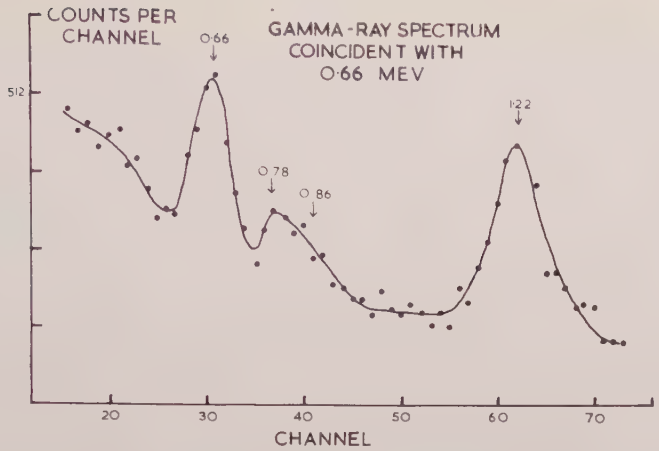

Figure 4. γ-ray spectrum coincident with 0·66 MeV radiation. This gives the region below 1·4 MeV in greater expansion, showing the shape of the peak at 0·8 MeV.

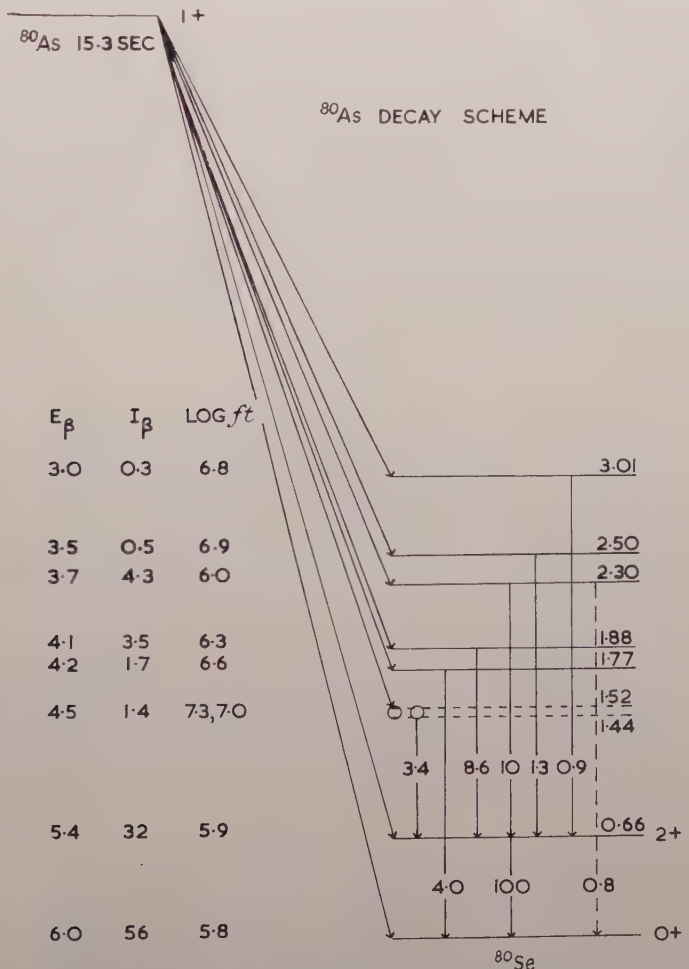

Figure 5. ^{80}As decay scheme. The energies of excited states in MeV, and γ-ray relative intensities are shown, together with a table of properties of the β branches against the appropriate daughter states.

3.3. *β-ray Measurements*

Measurements on the β-spectrum gave an end-point of $6{\cdot}0 \pm 0{\cdot}2$ MeV. Calibration sources were made by neutron irradiation of oxalic acid ($^{16}O(n, p)^{16}N$, $E_{max} = 10{\cdot}4$ MeV) and polytetrafluorethylene ($^{19}F(n, p)^{19}O$, $E_{max} = 4{\cdot}5$ MeV) samples. The 11·5 MeV β-rays from $^{11}B(n, p)^{11}Be$ were used as an additional check on the linearity of the counter up to the 10 MeV region. The spectrum of β-rays in coincidence with 0·66 MeV γ-radiation shows a displacement corresponding to the difference in energy of the transitions to the ground state and to the first excited state in ^{80}Se, indicating that the highest energy β branch goes to the ground state. The β branching ratios to the various excited states in ^{80}Se could be calculated from the γ-ray results, assuming that the upper levels are independently excited in the β-decay and not by γ-cascades, but it was necessary to make further measurements to determine the proportion of β-radiation going to the ground state. To obtain this, the total count of β-particles with energy greater than 2·5 MeV was compared with the simultaneous count, using the same energy discrimination, of β-particles coincident with the photopeak of the 0·66 MeV γ-ray in a fixed counter geometry with a calculable γ-detection efficiency. From the ratio of these two quantities the required ground state fraction of the total β counts could be deduced if the relative efficiencies of the β counter for particles in the various branches was also known. These efficiencies were deduced from standard β-spectra by calculating the fraction of the total count above the 2·5 MeV bias setting.

The calculated efficiency of the γ-counter and the expected coincident rate were checked using the double γ-cascade in the decay of ^{60}Co with a source of calibrated strength.

The β branching ratios and log *ft* values for all the observed transitions are shown in figure 5.

§ 4. Discussion

The measured log *ft* values of 5·8 and 5·9 for the β-transitions to the ground and first excited states of ^{80}Se suggest that these are allowed transitions. This would establish the ground state spin of ^{80}As as 1^+. The corresponding transition in the decay of 90 min ^{78}As to the ground state of ^{78}Se has a much higher log *ft* value of 7·6 (Steinberg and Engelkemeir 1950). This latter transition is unique first forbidden and gives a spin 2^- for the ground state of ^{78}As. The ground state spins of the other odd–odd As isotopes of lower mass number than 78 have also been shown to be 2^-. This corresponds to a shell model configuration with $2p_{3/2}$ proton shell complete and a single additional proton if the $1f_{5/2}$ state. This couples, with an odd neutron in the $1g_{9/2}$ state, which is being filled as N increases, to give spin 2^- in accordance with Nordheim's 'strong' coupling rule (Nordheim 1951).

In order to obtain a spin 1^+ for ^{80}As a configuration may be assumed in which the protons in the $1f_{5/2}$ shell tend to pair leaving a hole in the $2p_{3/2}$ state. Similar pairing of $1g_{9/2}$ neutrons leaves a hole in the $2p_{1/2}$ state. Coupling of the $2p_{3/2}$ hole with the $2p_{1/2}$ hole would give a spin 1^+. Another, less probable, configuration would leave the odd proton and the odd neutron in the $2p_{1/2}$ shell. The presence of both nucleons in the same shell could have the effect of depressing its energy relative to that of the $1f_{5/2}$ shell which is normally below it.

Several other nuclei in this region have similar configurations, for example ^{78}Br, ^{80}Br and ^{82}Rb. In the first two of these a state with the alternative configuration (spin 2^-) has been observed at low excitation (Way *et al.* 1955, Strominger *et al.* 1958). In addition there are several cases known of even-odd nuclei, e.g. ^{77}Se having a ground state $1/2^-$ corresponding to a $2p_{1/2}$ neutron and a low-lying metastable level of spin $7/2^+$ due to the coupling of $1g_{9/2}$ neutrons. In the case of ^{79}Se the situation is reversed, the ground state having a spin $7/2^+$ and the first excited state, spin $1/2^-$.

The second excited state of ^{80}Se occurs at an energy the ratio of which to the first excited state energy is approximately 2·2, corresponding well to the expected value for the second vibrational state of an even–even nucleus in this region (Scharff-Goldhaber and Weneser 1955). The observed doublet at about 1·5 Mev may correspond to the 0^+ and 2^+ components of the expected 0^+ 2^+ 4^+ triplet. In the β-decay from a 1^+ state one would not expect to see the 4^+ state but would expect the 0^+ and 2^+ states to be populated with comparable probabilities. The fact that no ground state γ-transition from these levels is observed agrees with the suggestion that they arise from a two-phonon excitation.

Angular correlation measurements on γ-cascades through the 0·66 Mev level were impractical owing to poor counting rates, so that information on the spins of the higher states of ^{80}Se could not be obtained.

Acknowledgments

We are most grateful to Professor B. Bleaney for the use of the facilities of his laboratory, and to Professor D. H. Wilkinson for helpful discussions and encouragement. One of us (J. E. G. McI.) is indebted to the Ministry of Education for Northern Ireland for a Research Studentship.

References

Miller, W. F., Reynolds, J., and Snow, W. J., 1958, *A.E.C. Report*, ANL-5902, Argonne National Laboratory.

Nordheim, L. W., 1951, *Rev. Mod. Phys.*, **23**, 322.

Scharff-Goldhaber, G., and Weneser, J., 1955, *Phys. Rev.*, **98**, 212.

Steinberg, E. P., and Engelkemeir, D. W., 1950, *National Nuclear Energy Series* (McGraw-Hill), Vol. **9**, 566.

Strominger, D., Hollander, J. M., and Seaborg, G. T., 1958, *Rev. Mod. Phys.*, **30**, 585.

Temmer, G. M., and Heydenburg, N. P., 1956, *Phys. Rev.*, **104**, 967.

Way, K., King, R. W., McGinnis, C. L., and van Lieshout, R., 1955, *A.E.C. Report* TID-5300, Washington.

Wolicki, E. A., Jastrow, R., and Brooks, F., 1956, *Naval Research Laboratory Report*, NRL 4833, Washington.

Ythier, C., Hermann, G., 1954, *Z. Elektrochem.*, **58**, 630.

The Current Sheet in a Gas Discharge

By N. J. PHILLIPS†
Department of Physics, Imperial College, London

Communicated by R. Latham; MS. received 22nd April 1959, in revised form 1st July 1959

Abstract. A simple theory of the trapping of gas in a 'fast-pinch' gas discharge is given. In the early stages of a gas discharge, a sheet of current flows near the walls of the discharge tube. This sheet subsequently collapses on to the cold gas inside it, with the consequent compression of the gas. It is shown that the efficiency of the trapping of the cold gas within the sheet during the collapse stage increases with the initial gas density.

§ 1. Introduction

Much interest is centred around the possibility of producing high temperature conditions in gases by means of the pinch effect. This effect is due to the confinement of the gas by the interaction of the current flowing through the gas with its associated magnetic field.

Most experiments take the form of discharges through cylindrical tubes of gas at low pressure. If the gas is initially pre-ionized to some extent, then the electric field will at first be confined to a thin skin at the surface of the gas. The free electrons from the pre-ionization will then be accelerated in the field and collide with neutral atoms. At this point the free electrons will ionize some of the neutrals by impact and the surface of the gas may be made highly conducting before there is appreciable penetration of the surrounding magnetic field into the gas. This highly conducting sheet then experiences forces due to the interaction of the current and the magnetic field and collapses with the result that the gas within is compressed. The gas inside will be mainly composed of cold neutral atoms and it is our purpose to find out whether these atoms leak through the sheet as it collapses.

The theory predicts that the temperature of the electrons in the sheet and the initial gas density are important factors in determining the efficiency of the trapping process.

§ 2. The Collapse Stage of the Discharge

The model of the collapse which we shall consider is that of a cold gas pinched by the collapsing current sheet. We shall assume that in the early stages of the discharge most of the matter at the inner surface of the current sheet is un-ionized. An atom which passes into the current sheet will suffer interactions with the ions and electrons in the sheet and it is these interactions which determine whether or not the atom is held by the sheet or passes out through the sheet.

The sheet itself is composed of ionized matter and if this ionization is to be maintained then the temperature of the charged particles in the sheet must be sufficiently high. Thus the most important event which occurs when a neutral atom passes into the sheet must be the ionization of this neutral. Of course the

† Now at A.W.R.E., Aldermaston, Berks.

atom may first be excited before being ionized, but for simplicity, we shall assume that when an atom passes into the sheet then it is either ionized before any other event takes place or suffers no serious disturbance of its original motion. If the atom is ionized, it will be held in the sheet by the combination of electric and magnetic fields. It is not clear that the charged products of the ionization process would be reflected back into the middle of the discharge. It seems more plausible that the electron formed, subsequently contributes to the current and remains in the sheet and that the ion is held by electrostatic forces. Thus the thickness of the current sheet should increase as more material is stuck to it.

Let us suppose that the sheet is moving with a speed which is much greater than the thermal speeds of the cold atoms. This is the so called 'fast-pinch' model. Following the model of Rosenbluth (1956) we can describe the collapse process in the following manner.

The sheet collapses on to the particles which are sitting there and sweeps them up. No shock wave will be transmitted into the gas if the atoms are stuck to the sheet after ionization. In the initial stages of the discharge, we can assume that the radius of curvature of the sheet is so large that we can consider the sheet locally as a plane and transforming to a suitable coordinate system, bring it to rest.

From momentum balance we then have the relation

$$B^2/8\pi = nm(\dot{r})^2 P \qquad \ldots\ldots (2.1)$$

where $\dot{r}$ is the sheet velocity, B the confining magnetic field, n the number density of neutrals, m the mass of the neutral and P the probability that a given neutral is held by the sheet.

§ 3. The Behaviour of Neutral Atoms in the Sheet

A section of the sheet is shown in the figure. Let the sheet have thickness d

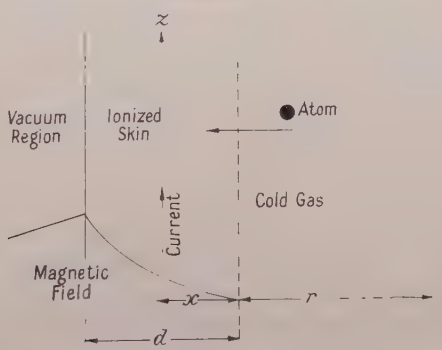

Section of current sheet ($r \gg d$).

and let us denote the velocity distribution function for electrons and ions in the sheet by f_e and f_i respectively.

Let us define

$$\langle q \rangle_v = \frac{\int q(v) f(\mathbf{v}, x)\, d\mathbf{v}}{\int f(\mathbf{v}, x)\, d\mathbf{v}} \qquad \ldots\ldots (3.1)$$

where q is some quantity dependent on the particle velocity and x is a coordinate measured from the inner surface of the sheet normally outwards.

We then define

$$\langle q\rangle_{v,x}=\frac{\int_0^d \langle q\rangle_v n(x)\,dx}{\int_0^d n(x)\,dx}, \qquad \ldots\ldots(3.2)$$

where

$$n(x)=\int f(\mathbf{v},x)\,d\mathbf{v}. \qquad \ldots\ldots(3.3)$$

The probability that an incoming atom suffers an interaction after a displacement dx into the sheet is then

$$\frac{dx}{\dot r}\left[n_e(x)\langle\sigma_{ea}g_{ea}\rangle_v+n_i(x)\langle\sigma_{ia}g_{ia}\rangle_v\right] \qquad \ldots\ldots(3.4)$$

where σ_{ea} and σ_{ia} are the electron–atom and ion–atom interaction cross sections and g_{ea}, g_{ia} are the corresponding relative speeds before impact.

If interactions result in ionization and not serious deflection of the neutral before ionization, then if n_{ai} atoms are incident on the inner surface of the sheet, the number of these which reach the neighbourhood of a point x within the sheet without ionization is

$$n_a=n_{ai}\exp\left\{-\int_0^x\frac{dx}{\dot r}\left[n_e(x)\langle\sigma_{ea}g_{ea}\rangle_v+n_i(x)\langle\sigma_{ia}g_{ia}\rangle_v\right]\right\}. \qquad \ldots\ldots(3.5)$$

Thus the probability of escape of atoms from the outer surface of the sheet is $\exp(-\Pi)$, where

$$\Pi=\int_0^d\frac{dx}{\dot r}\left[n_e(x)\langle\sigma_{ea}g_{ea}\rangle_v+n_i(x)\langle\sigma_{ia}g_{ia}\rangle_v\right]. \qquad \ldots\ldots(3.6)$$

The sheet itself though certainly not electrically neutral at all points within it must be neutral overall so that

$$\int_0^d n_i(x)\,dx=\int_0^d n_e(x)\,dx. \qquad \ldots\ldots(3.7)$$

Thus we may write

$$\Pi=\frac{\langle\sigma_{ea}g_{ea}\rangle_{v,x}+\langle\sigma_{ia}g_{ia}\rangle_{v,x}}{\dot r}\int_0^d n_e(x)\,dx. \qquad \ldots\ldots(3.8)$$

An enlightening transformation of this expression may be made by the use of the following results:

When the current flows axially, the total current through the sheet may be written in the form

$$I=2\pi r\int_0^d n_e(x)\langle v_{ez}\rangle_v\,dx\,e/c \qquad \text{e.m.u's}$$

$$=2\pi r\left(\frac{e}{c}\right)\langle v_{ez}\rangle_{v,x}\int_0^d n_e(x)\,dx. \qquad \ldots\ldots(3.9)$$

Thus we have

$$\Pi=\frac{[\langle\sigma_{ea}g_{ea}\rangle_{v,x}+\langle\sigma_{ia}g_{ia}\rangle_{v,x}]cI}{\langle v_{ez}\rangle_{v,x}2\pi r\dot r\,e}. \qquad \ldots\ldots(3.10)$$

When the magnetic field is due to an axial flow of current we have the relation

$$B = \frac{2I}{r} \qquad \ldots\ldots (3.11)$$

and when the probability P is close to unity we can write from equation (2.1)

$$\frac{I^2}{4\pi^2 r^2 \dot{r}^2} = \left(\frac{\rho}{2\pi}\right), \quad \rho = nm. \qquad \ldots\ldots (3.12)$$

Thus in the case in which the neutrals are securely held by the current sheet, we have from equations (3.10) and (3.12)

$$\Pi = \frac{c\Sigma}{e}\left(\frac{\rho}{2\pi}\right)^{1/2}, \qquad \ldots\ldots (3.13)$$

where

$$\Sigma = \frac{\langle \sigma_{ea} g_{ea} \rangle_{v,x} + \langle \sigma_{ia} g_{ia} \rangle_{v,x}}{\langle v_{ez} \rangle_{v,x}}. \qquad \ldots\ldots (3.14)$$

Thus the condition for good trapping, i.e. $\Pi \gg 1$, shows us that the efficiency of trapping increases with the gas density.

In most circumstances, the electron drift velocity will be much greater than the relative speeds of atoms and ions. Furthermore, in order to avoid runaway electrons, we must keep the electron drift speed below the electron thermal speed in the sheet. The generalized cross section Σ illustrates that the effect of runaway electrons is such as to lower Π through the dependence of the electron–atom ionization cross section on the electron velocity. Thus runaway electrons whilst enhancing the pinch effect, increase the porosity of the sheet.

The electron velocity $\mathbf{v}_e$ may be written in the form

$$\mathbf{v}_e = \mathbf{v}_{ed} + \mathbf{v}_{et}, \quad \mathbf{v}_{ed} = \langle v_{ez} \rangle_v, \qquad \ldots\ldots (3.15)$$

where $\mathbf{v}_{ed}$ is the drift velocity and $\mathbf{v}_{et}$ is the thermal velocity. The relative speed of the electrons and atoms is

$$\mathbf{g}_{ea} = \mathbf{v}_e - \dot{\mathbf{r}} \simeq \mathbf{v}_e,$$

since in general an individual electron moves much faster than the sheet. Thus in the non-runaway condition we may write approximately

$$\Pi = \frac{\langle \sigma_{ea} v_{et} \rangle_{v,x} c}{\langle v_{ez} \rangle_{v,x} e}\left(\frac{\rho}{2\pi}\right)^{1/2}. \qquad \ldots\ldots (3.16)$$

To calculate Π numerically, we need to know the electron velocity distribution in the sheet. However, certain general deductions can be made from the formula (3.16). Firstly, we can only really increase Π by increasing ρ for a given gas. Secondly, the difference between a light gas which is difficult to ionize such as helium and an easily ionized relatively heavy gas such as argon should be easily detectable by experiment. A rough numerical estimate of the density required to make $\exp(-\Pi)$ about 1% has been made taking $v_{ez} = v_{et}$ approximately and σ to be the ionization cross section by electron impact at 50 ev in argon, hydrogen and helium. Values of σ were obtained from Massey and Burhop (1952). The required densities are given in the table below:

	ρ g cm^{-3}
A	$1{\cdot}7 \times 10^{-7}$
H_2	$1{\cdot}8 \times 10^{-6}$
H_e	$3{\cdot}2 \times 10^{-5}$

We see that the difference between helium and argon is very appreciable. In fact, due to the difference between $\langle v_{\mathrm{et}} \rangle$ and $\langle v_{cz} \rangle$, the value of ρ required to effect this efficiency will be reduced in the ratio $(\langle v_{cz} \rangle / \langle v_{\mathrm{et}} \rangle)^2$ and the figures given above are somewhat too large.

Finally, we note that if the collapse velocity is sufficiently large, it may be possible to bring the ions into play via the term $\langle \sigma_{\mathrm{ia}} g_{\mathrm{ia}} \rangle$ in Σ.

§ 4. Conclusion

We have considered a special model of the collapsing fast-pinch discharge in which a particular type of trapping mechanism is proposed. Heavy gases which ionize easily are the best to use from the trapping point of view.

It should be possible to check the theory roughly by experimental measurement in say helium and argon.

A more refined treatment of the problem must contain the effect of the slowing down of neutrals in the sheet before ionization. The present treatment is simply meant to illustrate the main physical processes involved.

Acknowledgments

I should like to thank Dr. R. Latham and members of the High Temperature Group at Imperial College for helpful advice and I should also like to thank the Department of Scientific and Industrial Research for a Maintenance Grant.

References

Rosenbluth, M., 1956, *Los Alamos Technical Report*, LA 1850.

Massey, H. S. W., and Burhop, E. H. S., 1952, *Electronic and Ionic Impact Phenomena* (Oxford: University Press).

The Polarization of Protons Elastically Scattered from Oxygen at 8·7 MeV

By M. A. AL-JEBOORI, M. S. BOKHARI,
B. HIRD and A. STRZAŁKOWSKI
Nuclear Physics Research Laboratory, The University of Liverpool

Communicated by H. W. B. Skinner; MS. received 2nd June 1959

Abstract. A polarized proton beam has been obtained by inserting an internal graphite target in the cyclotron and using the polarization properties of the reaction $^{12}C(d, p)^{13}C$. By scattering this beam from an ice target, the elastic scattering polarization from oxygen was determined at a number of angles. The results show some similarity to the predictions of the optical model but there is evidence of a rapid variation of the polarization with energy.

§ 1. Introduction

Elastic proton scattering cross sections are usually fitted by optical model calculations. The agreement between experiment and the model has been steadily improved by adding more parameters to the complex potential. The edge of the well has been rounded (Woods and Saxon 1954) and a spin–orbit potential has been added, usually as a surface term (Feshbach 1958). When the parameters associated with these modifications are suitably chosen, it is possible to reproduce fairly accurately the differential cross sections, at least away from backward angles. However, with so many variables, some of which only affect the differential cross section slightly, a range of solutions is often possible.

A further source of experimental information for determining optical parameters is to measure the polarization produced by scattering. In contrast to the cross section, the polarization depends sensitively on the spin dependent part of the potential and it seems from the work of Erickson and Cheston (1958) that the real and imaginary parts of the spin–orbit potential usually produce very different effects on the angular distribution of the polarization. It may therefore be possible to determine each of them uniquely. The radial dependence of the spin–orbit term, on the other hand, seems to have little influence.

This paper describes measurements of the polarization produced in the elastic scattering of protons by oxygen, the first results of an experimental technique developed to measure polarization angular distributions in the 10 MeV energy region.

§ 2. Experimental Arrangement

A polarized proton beam was obtained using the deuteron stripping reaction $^{12}C(d, p)^{13}C$. The polarization of the ground state group is known to reach nearly 50% at an angle of about 45° (Bokhari *et al.* 1958). The polarized protons obtained in this way were scattered from a second target where the left–right asymmetry was measured with counter telescopes.

In all the polarizations we use the sign convention that the direction $(\mathbf{K}_{in} \times \mathbf{K}_{out})$ is positive, where $\mathbf{K}_{in}$ and $\mathbf{K}_{out}$ are the wave vectors of the incident and emitted particles respectively.

§ 3. The Polarized Proton Beam

To obtain the maximum proton yield, the internal circulating deuteron beam of the 37 in. cyclotron was used, a graphite target being placed inside one of the dees of the cyclotron (figure 1). This target was supported on an arm which projected through a hole cut in the dee edge and was attached in such a way that it could be pivoted about a point near the hole. A wide range of target positions was therefore possible. Adjustments in the target position could be made from outside the cyclotron tank by pushing on the arm with a retractable rod.

The hole in the dee acted also as the first slit in the proton selecting system. The ground state group protons emitted at about 45° emerged through it and were focused by the fringe field of the cyclotron and an external wedge magnet

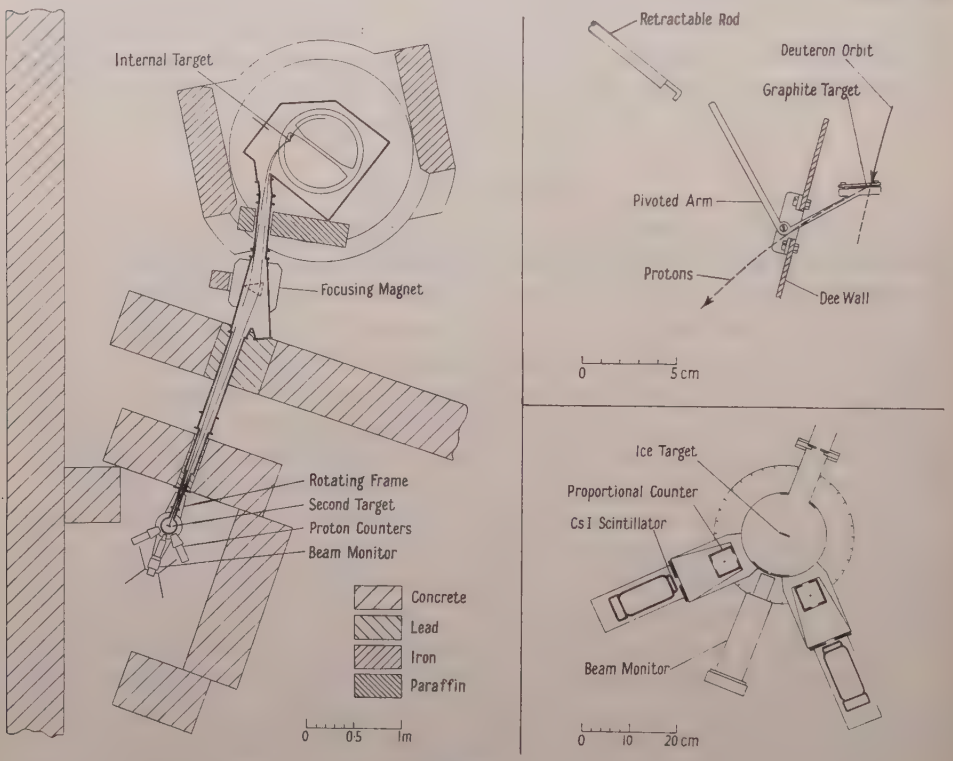

Figure 1.

to an image four metres from the cyclotron. The flux of protons obtained in the region of the focus was 5×10^5 per second in an area of 9 mm × 2 cm.

The internal target consisted of a self-supporting strip of pile graphite approximately 25 mg cm^{-2} thick. It became white hot when bombarded by the beam, but usually lasted 200 hours before requiring replacement. The thickness of the target did not affect the beam energy spread because of the strong energy selection occurring in the focusing system, it merely had to be thin enough to prevent energy overlap of the first excited state group.

Each time an internal target was changed and the focusing conditions optimized, the polarization of the proton beam was calibrated by filling the second scattering chamber with helium and measuring the asymmetry in the

scattering at 40°. Measured in this way the polarization varied from one target to another but was always between -40% and -50% in agreement with previous results.

The helium elastic scattering polarization was calculated from the phase shifts given by Putnam, Brolley and Rosen (1956) at an energy of 9·48 MeV and a value of $-33{\cdot}5\%$ was obtained. Since it is difficult to estimate the accuracy of these calculated polarizations, we have not included this source of error in our results†.

It was found that there was considerable deuteron contamination of the proton beam. Since the energy selection and focusing are by magnetic fields, deuterons of half the proton energy, which are scattered from the target, are also focused on to the second target. Measurements with this experimental arrangement must therefore be confined to targets where there is a clear energy separation of elastic scattered protons from those produced by stripping in the second target. In the case of oxygen, the $^{16}O(d, p)^{17}O$ reaction Q value is low enough to exclude this process completely from the counter pulse height distributions.

§ 4. Measurement of the Scattering Asymmetry

Protons scattered left and scattered right at the same angle were recorded simultaneously. Each counter telescope consisted of a thin CsI scintillator mounted behind an argon filled proportional counter. The scintillation pulses coincident with pulses in the proportional counter were recorded on a 50-channel pulse height analyser. With this arrangement, the background was confined to small pulse heights, so that the short runs, without the second target, were sufficient in making the background correction. The energy threshold of each counter system for the detection of proton coincidences was about 6 MeV, of which 1 MeV represented the energy lost in the proportional counter. Energy resolution was sufficiently good for the scattered proton peak to be accounted for by the spread in the incident beam energy and by the target thickness. The angular resolution of each counter was $\pm 1{\cdot}5°$.

The two counter systems, the target chamber and the beam defining slits were all mounted on a frame which enabled the entire system to be rotated about the incident proton direction. Half the running time was spent with the frame upside down. By taking the product of the two ratios of counts left to counts right, which were obtained with the frame in the two positions, the scattering asymmetry is obtained independent of the counter efficiencies, and with first order errors in the geometry eliminated. To minimize the effects of drifts in the counting system, the system was turned over each hour throughout the run.

§ 5. The Ice Target

A solid oxygen target was prepared in the form of ice; protons scattered from the hydrogen having too small an energy to be detected by the counters at any of the angles of measurement. A thin flake of ice was obtained by surface freezing a dish of distilled water and cutting out a suitable area. The flake was then attached to a metal frame cooled with solid CO_2. Thermal radiation to this target was reduced by having a large area of cooled metal inside the target chamber.

† This polarization is about 6% smaller than the value given graphically by Brockman (1958).

The average target thickness prepared in this way was 1 MeV. This arrangement meant unfortunately that protons emitted from one face of the flake could not reach the counters. Measurements near 90° scattering angle were therefore

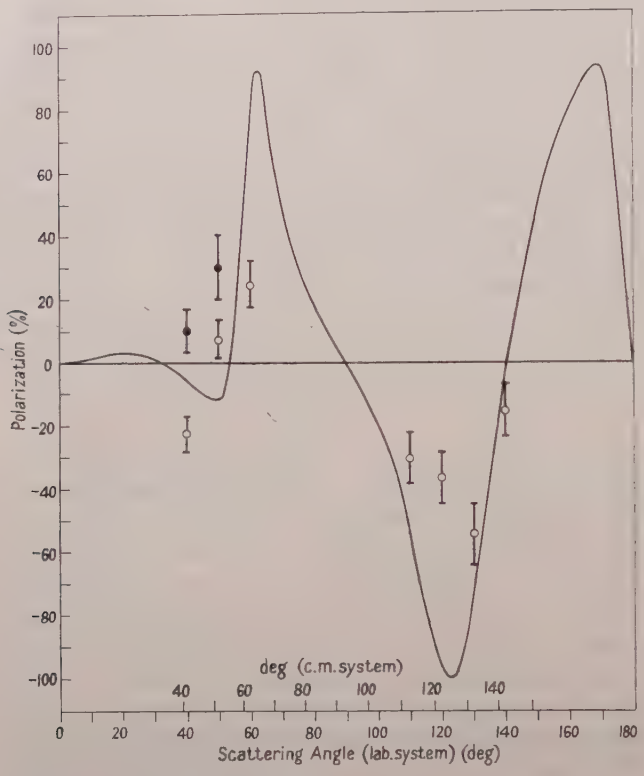

Figure 2. The elastic scattering polarization of protons on oxygen. The hollow points were measured with a polarized proton beam of energy $(8{\cdot}9\ ^{+0{\cdot}1}_{-0{\cdot}2})$ MeV and polarization $-41\pm8\%$. The solid points were measured with a proton beam of energy $(8{\cdot}7\pm0{\cdot}5)$ MeV and polarization $-48\pm6\%$. The line is a theoretical optical model calculation of Bjorklund and Fernbach for 10 MeV protons scattered by a potential with parameters $a=0{\cdot}65\times10^{-13}$ cm, $b=1{\cdot}2\times10^{-13}$ cm, $r_0=1{\cdot}25\times10^{-13}$ cm, $V_{CR}=46{\cdot}2$ MeV, $V_{CI}=11{\cdot}0$ MeV, $V_{SR}=9{\cdot}48$ MeV.

difficult and were not attempted. For the measurements at backward angles, the metal frame was turned round so that the proton beam passed through the target in the opposite direction. An 0·00025 in. thick Mylar window between the target chamber and the cyclotron prevented water vapour from reaching the cyclotron vacuum.

§ 6. Results

The table gives the experimental results. In figure 2 they are compared with a theoretical calculation by Bjorklund and Fernbach (private communication) of the polarization produced by scattering 10 MeV protons from a coulomb potential and a nuclear potential of the type,

$$V_{CR}\rho(r)+iV_{CI}q(r)+V_{SR}(\hbar/\rho c)^2r^{-1}\frac{d\rho}{dr}\boldsymbol{\sigma}\cdot\mathbf{L},$$

where the radial shapes of the potentials have the forms

$$\rho(r)=\left[1+\exp\left(\frac{r-R_0}{a}\right)\right]^{-1},$$

$$q(r)=\exp-\left(\frac{r-R_0}{b}\right)^2, \text{ and } R_0=A^{1/3}r_0.$$

The polarization, measured at the two angles which are shown as solid circles, was obtained with a proton beam of average energy 8·7 MeV and a spread such that the beam fell to half intensity at $\pm 0{\cdot}5$ MeV. A change in the target position and focusing conditions later produced the same beam intensity but with less energy spread ($8{\cdot}9^{+0{\cdot}1}_{-0{\cdot}2}$) MeV. This beam was used to obtain the results shown as open circles.

(1)	(2)	(3)		(4)		(5)
		L	R	L	R	
40°	$8{\cdot}9^{+0{\cdot}1}_{-0{\cdot}2}$	557	574	394	588	$-22{\cdot}3\pm 5{\cdot}4$
50°	,,	406	346	242	246	$+7{\cdot}5\pm 6{\cdot}6$
60°	,,	330	227	197	179	$+24{\cdot}3\pm 7{\cdot}7$
110°	,,	239	252	156	268	$-30{\cdot}7\pm 8{\cdot}6$
120°	,,	272	329	181	307	$-37{\cdot}0\pm 8{\cdot}5$
130°	,,	270	261	125	375	$-54{\cdot}2\pm 10{\cdot}0$
140°	,,	236	213	149	222	$-15{\cdot}4\pm 8{\cdot}3$
40°	$8{\cdot}7\pm 0{\cdot}5$	443	322	381	446	$+9{\cdot}9\pm 6{\cdot}8$
50°	,,	257	166	276	260	$+30{\cdot}2\pm 10{\cdot}7$

(1) Angle in lab. system; (2) energy of bombarding protons (MeV); (3) number of counts with the frame upright; (4) number of counts with the frame inverted; (5) polarization (%).

§ 7. Discussion

The large change in the polarization, produced by a change in the energy spread of the beam, seems to indicate that the polarization, if measured with better energy resolution, would be a rapidly fluctuating function of the energy. This is clearly inconsistent with the shape scattering predictions of the optical model, but could be produced if considerable compound elastic scattering were present. The polarization would then be different from each of the compound levels which lies within the range of energies covered by the beam. In the present experiment the number of these levels must have been insufficient to give complete statistical averaging. For this particular target, considerable compound elastic scattering is to be expected, since the compound nucleus which is formed, ^{17}F, is stable against neutron emission, and there are few other low lying levels in ^{16}O to compete when it decays by proton emission.

In view of the compound elastic contribution to the polarization, it seems somewhat surprising that, even at backward angles the shape of the angular distribution is consistent with the optical model prediction.

Acknowledgments

The authors wish to thank Professor Fernbach and Professor Cheston for communicating unpublished work. One of us (A. S.) thanks the Polish Academy of Sciences for a grant. M. A. A. wishes to acknowledge the receipt of a scholarship from the Iraq Government.

References

Bokhari, M. S., Cookson, J. A., Hird, B., and Weesakul, B., 1958, *Proc. Phys. Soc.*, **72**, 88.

Brockman, K. W., Jr., 1958, *Phys. Rev.*, **110**, 163.

Erickson, G. W., and Cheston, W. B., 1958, *Phys. Rev.*, **111**, 891.

Feshbach, H., 1958, *Annu. Rev. Nuclear Sci.*, **8**, 49. (This review includes extensive references.)

Putnam, T. M., Brolley, J. E., and Rosen, L., 1956, *Phys. Rev.*, **104**, 1303.

Woods, R. D., and Saxon, D. S., 1954, *Phys. Rev.*, **95**, 577.

On the Magnetic Susceptibility and Anisotropy of Trivalent Vanadium Alum under the Crystalline Electric Field having predominantly Cubic Symmetry with a Small Trigonal Symmetry

By A. S. CHAKRAVARTY
Department of Magnetism, Indian Association for the Cultivation of Science, Calcutta 32, India

Communicated by M. H. L. Pryce; MS. received 28th April 1959, in final form 12th June 1959

Abstract. On the assumption that the cubic field for V^{3+} is not strong enough to break down the Russell-Saunders (l–l) coupling, the magnetic susceptibility of V^{3+} has been calculated in a generalized way using Abragam and Pryce's Hamiltonian and wave functions. The susceptibility expression contains four parameters α, α' (the effective crystalline Landé factors), Δ (the trigonal field orbital parameter) and λ (the crystalline spin–orbit coupling constant). An excellent agreement with the experimental results of Van den Handel and Siegert and Dutta Roy are obtained by taking $\alpha = 1{\cdot}10$, $\alpha' = 1{\cdot}35$, $\Delta = -1390\ \text{cm}^{-1}$, $D = 4{\cdot}8\ \text{cm}^{-1}$ and $\lambda = 64\ \text{cm}^{-1}$. The reduction of λ from its free ion value $104\ \text{cm}^{-1}$ is due to the inclusion of the covalency factor. ($f^2 = 0{\cdot}62$, arising from overlap of the 3d-orbital wave functions of V^{3+} with the σ- and π-wave functions of the surrounding oxygen.) The values of α, α' and Δ are consistent with reasonable values of the cubic and trigonal field parameters.

§ 1. Introduction

Siegert (1937) deduced the theory of magnetic susceptibility of vanadium ammonium alum under a crystal field having cubic symmetry with a small superimposed trigonal field (Lipson and Beevers 1935), assuming that the cubic field is so strong as to break down not only the L–S coupling but also the l–l coupling. To explain the experimental data of Van den Handel and Siegert (1937) on the basis of this theory Siegert assumed a splitting of the lowest two close-lying levels of about $4{\cdot}8\ \text{cm}^{-1}$ and the trigonal field orbital separation of about $600\ \text{cm}^{-1}$, but then the calculated value of the temperature independent susceptibility K_c comes out as about twice the experimental value, and the spin–orbit coupling constant λ has to be taken about 40% lower than the free ion value of $+104\ \text{cm}^{-1}$. Apparently, these two findings require explanation and it seems desirable to look more critically into the theory as also to check the experimental results. The break down of Russell–Saunders l–l coupling does not seem to be well justified (Van Vleck 1939) since it is very probable that in these V^{3+} salts the binding is only partially covalent in nature (Owen 1955). Moreover, Siegert neglected the contribution to magnetic moment from the upper orbital and spin levels.

We have, therefore, calculated the susceptibility of V^{3+} salts, taking into consideration the admixture from upper orbital levels retaining l–l coupling following a more general theory of Abragam and Pryce (1951). The advantage

of this theory is that in the susceptibility we can take into account the contribution of the orbital upper levels in a straightforward manner. The ground state of a free V^{3+} ion is $3d^2\,{}^3F$. There is another term ${}^3P$ arising from the same configuration $3d^2$ of the free ion about $9\,300\,cm^{-1}$ higher (Owen 1955). Besides these there is no term of sufficient importance lying in the neighbourhood. The x-ray analysis of Al^{3+} and Cr^{3+} alums (Lipson and Beevers 1935, Klug 1940) shows that the field on the trivalent cation arises from a trigonally distorted octahedron of six water molecules surrounding the ion. The trigonal axis of each ion coincides with one of the four body diagonals of the unit cube which contains four such ions. Then the predominant cubic field having a positive coefficient (Gorter 1932) splits up the ${}^3F$ state into a degenerate orbital triplet Γ_4 lying lowest and another orbital triplet Γ_5 and an orbital singlet Γ_2 lying successively above it (Bethe 1929, Van Vleck 1932). The comparatively small trigonal field component now splits up each of the two triplets into a singlet and a doublet of which the singlet must be lower if the susceptibility is found to obey the Curie law with an approximate 'spin only' value of the moment (Van Vleck 1939) which is actually the case. Further, the effect of the spin–orbit coupling on the orbital levels each with the three-fold spin degeneracy is to split them up into three non-degenerate and three doubly degenerate spin levels and to cause an admixture between them. We now proceed to find out the fine structure levels of the Stark pattern under the crystalline field in the following section.

§ 2. The Fine Structure

The basic orbital triplet states given by Abragam and Pryce (1951) are

$$|1\rangle = -(\phi_x' + i\phi_y')/\sqrt{2}$$
$$|0\rangle = \phi_z'$$
$$|-1\rangle = (\phi_x' - i\phi_y')/\sqrt{2}$$

and the appropriate effective Hamiltonian is

$$\mathscr{H} = \Delta(1 - l_z'^2) - \alpha\lambda l_z' S_z - \alpha'\lambda(l_x' S_x + l_y' S_y)$$

where Δ stands for the energy difference between ϕ_z' (singlet) and ϕ_{xy}' doublet, α and α' are effective Landé factors dependent on admixtures of excited orbitals in the axial and perpendicular directions of the $V^{3+}.6H_2O$ group and λ stands for the spin–orbit coupling constant of V^{3+} in the crystal.

The fine structure levels are classified by m ($= \pm 2,\ \pm 1,\ 0$), the eigenvalues of $l_z' + S_z$. The secular matrix for $\mathscr{H}$ breaks up into

$$\begin{bmatrix} \alpha\lambda & -\alpha'\lambda & 0 \\ -\alpha'\lambda & \Delta & -\alpha'\lambda \\ 0 & -\alpha'\lambda & \alpha\lambda \end{bmatrix} \qquad (m=0),$$

$$\begin{bmatrix} 0 & -\alpha'\lambda \\ -\alpha'\lambda & \Delta \end{bmatrix} \qquad (m=\pm 1),$$

$$\begin{bmatrix} \Delta & -\alpha'\lambda \\ -\alpha'\lambda & 0 \end{bmatrix} \qquad (m=\pm 1),$$

$$-\alpha\lambda \qquad (m=\pm 2).$$

The eigenvalues are, therefore,

$$E_0=\tfrac{1}{2}\{\Delta+\alpha\lambda-S_0\} \qquad E_3=\alpha\lambda$$
$$E_1=\tfrac{1}{2}\{\Delta-S_1\} \qquad E_4=-\alpha\lambda$$
$$E_2=\tfrac{1}{2}\{\Delta+S_1\} \qquad E_5=\tfrac{1}{2}\{\Delta+\alpha\lambda+S_0\}$$

where

$$S_0=[(\Delta-\alpha\lambda)^2+8\alpha'^2\lambda^2]^{1/2}, \qquad S_1=[\Delta+4\alpha'^2\lambda^2]^{1/2}.$$

In the above expressions for the electronic energy levels in the basic orbital triplet, we have neglected the spin–spin interaction term because its effect is very small in the case of V^{3+}, the value of the coefficient ρ of this term being $0{\cdot}24\pm0{\cdot}05$ (Pryce 1950).

The corresponding eigenstates are thus,

$$\phi_0=a|1,-1\rangle+b|0,0\rangle+a|-1,1\rangle,$$
$$\phi_1=c|1,0\rangle+d|0,1\rangle,$$
$$\phi_1'=c|-1,0\rangle+d|0,-1\rangle,$$
$$\phi_2=d|1,0\rangle-c|0,1\rangle,$$
$$\phi_2'=d|-1,0\rangle-c|0,-1\rangle,$$
$$\phi_3=\frac{1}{\sqrt{2}}|1,-1\rangle-\frac{1}{\sqrt{2}}|-1,1\rangle,$$
$$\phi_4=|1,1\rangle,$$
$$\phi_4'=|-1,-1\rangle,$$
$$\phi_5=\frac{1}{\sqrt{2}}b|1,-1\rangle-\sqrt{2}a|0,0\rangle+\frac{1}{\sqrt{2}}b|-1,1\rangle.$$

The number of independent coefficients in the above expressions are reduced to only four by virtue of the symmetry existing in the $m=0$ states and of the orthogonality of the states, together with the normalizing conditions $2a^2+b^2=1$, $c^2+d^2=1$.

It should be noticed here that only in the case when the sign of Δ is negative the lowest state is a singlet ($m=0$) and immediately above it a doublet ($m=\pm1$) the remaining levels being well separated above these. We then proceed to calculate the magnetic susceptibility considering only the lowest two levels $m=0$ and $m=\pm1$. The contribution from the other levels will be negligible, since the next higher levels are of the order of 1300 cm^{-1} above the lowest triplet, as will be seen later.

§ 3. The Magnetic Susceptibility

The first order Zeeman terms can be obtained by finding $\langle\phi_i|\mathscr{H}_m|\phi_j\rangle$ where $i,j=0,\pm1$.

When $i=j$,

$$\mathscr{H}_m=\mathscr{H}_0+\beta(-\alpha l_z'+2S_z)H_z$$

and when $i\neq j$,

$$\mathscr{H}_m=\mathscr{H}_0+\beta\left[-\frac{\alpha'}{2}H_+L_--\frac{\alpha'}{2}H_-L_++H_+S_-+H_-S_+\right]$$

where $\mathscr{H}_0$ is the unperturbed Hamiltonian and β is the Bohr magneton. The second order Zeeman energy terms can be obtained from above by solving a

secular determinant for ϕ_0 and $\phi_{\pm 1}$, in the usual way. Thus we arrive at the perturbation energy terms for the crystalline levels when the external field is present.

If we now expand, the energy in powers of the field strength H, we get

$$W_i = W_i^{(0)} + W_i^{(1)}H + W_i^{(2)}H^2 + \ldots$$

where the first term is the unperturbed energy, the second and third terms are the first order and second order Zeeman energy terms, respectively.

Then, the paramagnetic gramme-ionic susceptibility is given by the well-known formula (Van Vleck 1932):

$$K = N\frac{\sum_i [(W_i^{(1)2}/kT) - 2W_i^{(2)}] \exp(-W_i^0/kT)}{\sum_i \exp(-W_i^0/kT)}.$$

Performing the above calculations up to the second order we finally obtain for the mean gramme-ionic susceptibility K which is the same for the crystal per gramme-ion, χ,

$$\tfrac{1}{3}(K_1 + K_2 + K_3) = K = \chi = \frac{8N\beta^2}{3k}\frac{(A^2/4T) + (2B^2k/D)[\exp(D/kT) - 1]}{2 + \exp(D/kT)} + K_c \qquad \ldots\ldots (1)$$

where

$$A^2 = (2d^2 - \alpha c^2)^2$$

$$B^2 = \left(ac + bd - \frac{\alpha'}{2}bc - \frac{\alpha'}{2}ad\right)^2$$

$$D = \tfrac{1}{2}(S_0 - S_1 - \alpha\lambda)$$

where K_c is the susceptibility coming from the high frequency contributions. Actual calculation of K_c is shown in a later section. Figure 1 gives the variation of $10^2 KT$ with T obtained theoretically by us using the values:

$$A^2 = 3{\cdot}842, \quad B^2 = 0{\cdot}810, \quad D = 4{\cdot}800\ \text{cm}^{-1}, \quad \text{and} \quad K_c = 248{\cdot}2 \times 10^{-6},$$

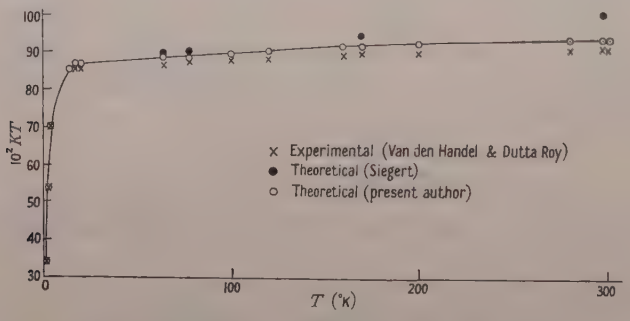

Figure 1. Variation of 10^2 KT with temperature.

so as to give fit with the experimental points of Van den Handel and Siegert (1937) and of Dutta Roy (Thesis, 1958), as may be seen in figure 1 which also shows the points obtained on Siegert's theory. The above values are unique

though the fits might be made somewhat better by a trial and error calculation, but in view of what has been said in §§ 5 and 6, such labour would not serve very useful purpose for the present.

Now by trial we choose such values for α, α', Δ and λ as will give the above values for A^2, B^2 and D. We find approximately that

$$\Delta = -1390 \text{ cm}^{-1}, \quad \alpha = 1{\cdot}105, \quad \alpha' = 1{\cdot}350, \quad \lambda = +64 \text{ cm}^{-1}. \qquad \text{(Set I)}$$

It is very interesting to remark that, supporting Siegert's finding, the value of λ required to give a fit has to be taken 40% less than the 'free ion' value 104 cm^{-1} (Laporte 1928), the reason for which will be discussed in detail in a subsequent section. But the important difference is that Δ obtained here is more than twice the value given by Siegert.

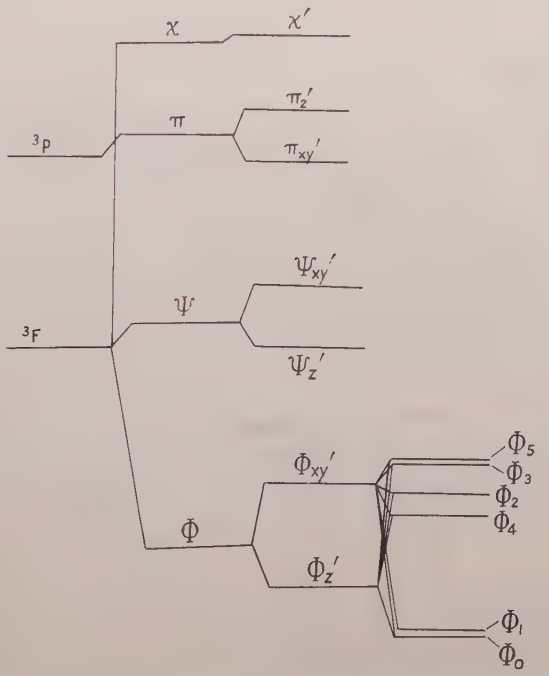

Figure 2. The energy level diagram for V^{3+} ion under the predominantly cubic with a small trigonal electric field and the effect of L–S coupling on the lowest ϕ-orbital states.

Figure 2 shows the diagrammatic position of the energy levels, for the above values of the parameters, with the approximate energies:

ϕ_0	$-1400{\cdot}15$ cm^{-1}	ϕ_2	$5{\cdot}35$ cm^{-1}
ϕ_1	$-1395{\cdot}35$	ϕ_3	$70{\cdot}72$
ϕ_4	$-70{\cdot}72$	ϕ_5	$80{\cdot}87$.

We shall now find out the theoretical expression for K_c, the high frequency contribution to susceptibility and the g-values and evaluate them for the above choice of the parameters.

§ 4. Calculation of Susceptibility arising from High Frequency Elements (K_c)

In this calculation we consider the effect of the next four upper levels on the basic levels ϕ_0 and $\phi_{\pm 1}$ as a result of magnetic perturbation. Proceeding in a similar manner as in the case of susceptibility, we get

$$K_c = \frac{N\beta^2}{3} B \cdot \left[\left\{ \frac{16(c-\frac{1}{2}\alpha' d)^2}{E_4 - E_1} + \frac{4c^2 d^2 (\alpha+2)^2}{E_2 - E_1} + \frac{4(c+\frac{1}{2}d)^2}{E_3 - E_1} + \frac{\frac{1}{2}(2bc - 4ad + 2ac - bd)^2}{E_5 - E_1} \right\} + \left\{ \frac{16(ad - bc - \frac{1}{2}\alpha' bd + \frac{1}{2}\alpha' ac)^2}{E_2 - E_0} + \frac{4(\alpha+2)^2 a^2}{E_3 - E_0} \right\} \exp(D/kT) \right]$$

where

$$B = \frac{1}{2 + \exp(D/kT)}.$$

When the values of the coefficients are substituted, K_c takes the form

$$K_c = \frac{N\beta^2}{3} \cdot \frac{0{\cdot}004631 + (0{\cdot}005041)\exp(6{\cdot}9/T)}{2 + \exp(6{\cdot}9/T)}$$
$$= 276{\cdot}8 \times 10^{-6}$$

since the terms of higher order than unity in the exponentials are too small for serious consideration.

This value is in very good agreement with the value of $K_c = 248{\cdot}2 \times 10^{-6}$ found from the experimental investigations of Van den Handel and Siegert (1937) and Dutta Roy (Thesis).

§ 5. The g-values

When the magnetic field is applied along the z direction (i.e. along the axis of symmetry) and x direction of the V^{3+} ion respectively, we have by definition

$$g_{\parallel} = \langle \phi_1 | -\alpha l_z' + 2S_z | \phi_1 \rangle$$
$$g_{\perp} = \sqrt{2} \langle \phi_1 | -\alpha' l_x' + 2S_x | \phi_0 \rangle.$$

Performing the calculation, we get

$$g_{\parallel} = (2d^2 - \alpha c^2)$$
$$g_{\perp} = 2\left(ac + bd - \frac{\alpha'}{2} bc - \frac{\alpha'}{2} ad \right).$$

For the specified values of the parameters, we get $g_{\parallel} = 1{\cdot}96$, $g_{\perp} = 1{\cdot}80$, in complete agreement with Van den Handel and Siegert's and Dutta Roy's investigations. Resonance data on $g_{\parallel}$ and $g_{\perp}$ are not yet available and hence a direct check on these values cannot be obtained.

§ 6. A Discussion on the Cubic and Trigonal Electric Field Parameters in V^{3+}

We mentioned (1958) a set of probable values for these basic parameters α, α', Δ and λ which would fit the experimental susceptibility of V^{3+} alum, as given below:

$$\Delta = -400\,\text{cm}^{-1}, \quad \alpha = 1{\cdot}25, \quad \alpha' = 0{\cdot}60, \quad \lambda = 104\,\text{cm}^{-1}. \qquad \text{(Set II)}$$

In addition to the fact that here λ is exactly the free ion value, this set of values also fulfils our susceptibility requirements $g_{\parallel}=1{\cdot}98$, $g_{\perp}=1{\cdot}82$ and $D=4{\cdot}8\ \mathrm{cm}^{-1}$. But on further investigations it was found that these values of α and α' cannot be justified with any reasonable values for the anisotropic field parameters H and I (Abragam and Pryce 1951) with the cubic field parameter $G=39\,000\ \mathrm{cm}^{-1}$ and ^{3}P-level parameter in crystal. $E_p=9300\ \mathrm{cm}^{-1}$ (obtained from the optical absorption data, Hartmann and Schlafer 1951). In the case of Co^{2+} under a cubic and a small tetragonal field Abragam and Pryce have given a probable set of values for H and I, namely $H=3600\ \mathrm{cm}^{-1}$, $I=3400\ \mathrm{cm}^{-1}$ with $G=23\,100\ \mathrm{cm}^{-1}$, $E_p=11\,500\ \mathrm{cm}^{-1}$. These values have been found out from an analysis of the g-values obtained from paramagnetic resonance experiments by means of trial and error. These values of H, I, G and E_p then fix the value of Δ (the energy difference between ϕ_{xy}' and ϕ_z') and the admixtural coefficients ϵ, τ, ρ, ϵ', τ', σ which are related to α and α' by

$$\alpha=\tfrac{3}{2}\epsilon^2-\sqrt{5}\epsilon\rho-\tfrac{1}{2}\rho^2-\tau^2$$

$$\alpha'=\tfrac{3}{2}\epsilon\epsilon'+\tfrac{1}{2}\sqrt{5}\epsilon'\rho+2\sigma\rho-\tau\tau'$$

for trigonal symmetry (Abragam and Pryce 1951).

The theoretical expression for susceptibility in case of Co^{2+} under a tetragonal field, taking the values for the parameters given by Abragam and Pryce ($\alpha=1{\cdot}128$, $\alpha'=1{\cdot}503$, $\Delta=1090\ \mathrm{cm}^{-1}$, $\lambda=-180\ \mathrm{cm}^{-1}$), calculated by us (unpublished) as well as by Uryu (1956) gives excellent agreement with the experimental susceptibility values given by Bose (1948) which shows that the values of H, I and Δ in Co^{2+} must be quite reasonable.† It should be remembered here that though the method indicated by Abragam and Pryce cannot decide uniquely and separately the magnitudes of H and I, it is adequate to give a fairly reasonable value of $H+I$ in those cases where g-values are known from resonance measurements. But, unfortunately, no resonance data for the g-values in the case of V^{3+} alum are available yet. Since V^{3+} is trivalent and the 3d-electron radius relatively large because of small Z_{eff} compared with divalent Co^{2+} one would expect differences in the field parameters.

Let us now examine our present set of parameters (Set I) to see whether these are consistent with reasonable values of H and I, G and E_p being given by optical absorption measurements (Hartmann and Schlafer 1951). The values of Δ, α and α' for particular values of H and I have been calculated in the following manner.

For example, taking $G=39\,000\ \mathrm{cm}^{-1}$, $E_p=9300\ \mathrm{cm}^{-1}$, $H=3500\ \mathrm{cm}^{-1}$, $I=3400\ \mathrm{cm}^{-1}$, figure 2 gives diagrammatically the positions of the orbital energy levels with the following approximate values (cm^{-1}) χ, 22 610; π_z', 11 930; π_{xy}', 11 550; ψ_{xy}', 3812; ψ_z', 3567; Φ_{xy}', $-13\,210$; Φ_z', $-14\,560$. The perturbed wave functions Φ_{xy}' and Φ_z' (given by Abragam and Pryce) are

$$\Phi_x'=\epsilon\phi_x-\tau\pi_x-\rho\psi_y$$

$$\Phi_y'=\epsilon\phi_x-\tau\pi_x+\rho\psi_y$$

$$\Phi_z'=\epsilon'\phi_z-\tau'\pi_z-\sigma\chi.$$

† The calculation in the trigonal case has not been made yet owing to lack of sufficient experimental data.

For the above eigenvalues for Φ_{xy}' and Φ_z' the coefficients are given by

$$\epsilon = 0{\cdot}9335, \quad \tau = 0{\cdot}3538, \quad \rho = 0{\cdot}06027,$$
$$\epsilon' = 0{\cdot}9747, \quad \tau' = 0{\cdot}2225, \quad \sigma = 0{\cdot}00557.$$

From these values we finally get $\alpha = 1{\cdot}10$, $\alpha' = 1{\cdot}35$. The table gives the variation of Δ for different sets of values for H and I along with known cubic field parameters $G = 39\,000$ cm^{-1} and $E_p = 9300$ cm^{-1}, given by optical absorption measurements (Hartmann and Schlafer 1951). We see from table 1 that though each

Table 1

H (cm^{-1})	I (cm^{-1})	Φ_{xy}' (cm^{-1})	Φ_z' (cm^{-1})	Δ (cm^{-1})	α	α'
6000	5800	−13090	−15400	−2310	0·925	1·39
5000	3000	−13490	−14130	−1640	1·05	1·351
3500	3400	−13210	−14560	−1350	1·10	1·35
3400	3100	−13260	−14430	−1170	0·70	1·168

set of Δ, α, α' corresponds to reasonable values for H and I only the set shown in the calculation is the one which fits the experimental magnetic behaviours. Too much quantitative significance should not, however, be attached to the values for H and I, but these values do give an approximate idea regarding the magnitudes of α and α' since a slight change of H and I though causing a relatively large change of Δ gives only a small variation in the values of α and α', as will be seen from table 1. After these calculations were made we have been informed by Professor Pryce that our value of Δ agrees well with the value obtained directly by Pryce and Runciman (1958) for V^{3+} in Al_2O_3 which shows that our choice of H and I is quite reasonable.

§ 7. The Spin–Orbit Coupling Constant in Crystal

The fact that in order to get agreement of the theory with the experimental values it is essential to use a value of λ about 40% lower than its free ion value suggests that it may not be correct to treat the complex $[V(H_2O)_6]^{3+}$ on a purely ionic model. Such discrepancies between experiment and theory have been observed by Siegert (1937) in V^{3+}, Abragam and Pryce (1951) in Cu^{2+} and Griffiths and Owen (1952) in Ni^{2+}. Owen (1955) has shown that by postulating a certain amount of overlap of the 3d-wave functions of the paramagnetic ion with the σ- and π-wave functions of the attached oxygens, the above discrepancy can be accounted for. The magnitude of the 'covalency factor' depends on the strength of bonding. For example, in Ni^{2+} salts (Griffiths and Owen 1952, Bose *et al.* 1958), λ in the crystal is found to be smaller by about 10–20% from its free ion value, as against 40% for V^{3+}, so that the apparent reduction of λ in the crystal is greater in the case of M^{3+} ions than for M^{2+} ions. Both the σ- and π-types of bonding, corresponding to the overlap of $d\gamma$-orbits of the central ion with $\psi(\sigma)$ orbits of the attached oxygen atoms and of $d\epsilon$-orbits with the $\psi(\pi)$-orbits respectively are probably important in the case of V^{3+}. From Owen's discussion, it is probable that in V^{3+} as in Cr^{3+}, the total observed covalency factor 0·6 may be made up of the σ-bonding factor approximately 0·75 and the π-bonding factor approximately 0·8 (Owen and Stevens 1953, Stevens 1953).

Conclusion

Superiority of the present theory lies in better plausibility of the assumption regarding the (l–l) coupling, greater generality, better fit with susceptibility at *all* temperatures and agreement of the value of Δ with optical absorption spectra (Pryce and Runciman 1958).

Acknowledgements

My most sincere thanks are due to Professor A. Bose for suggesting the problem and for his constant advice and encouragement during the progress of this work and to S. K. Dutta Roy for making available his excellent data on V^{3+} alums (Thesis). My sincere thanks are due to Dr. D. K. Roy of the Saha Institute of Nuclear Physics, Calcutta, for his many valuable suggestions and stimulating discussions in developing the paper and Miss G. Bhowmik for her help in the calculations. I am very grateful to Professor M. H. L. Pryce for his many valuable suggestions.

References

Abragam, A., and Pryce, M. H. L., 1951, *Proc. Roy. Soc.* A, **205,** 135, **206,** 173.
Bethe, H., 1929, *Ann. Phys., Lpz.*, 3, **133,** 760.
Bose, A., 1948, *Indian J. Phys.*, **22,** 276.
Bose, A., Mitra, S. C., and Datta, Sunil K., 1958, *Proc. Roy. Soc.* A, **248,** 153.
Chakravarty, A. S., 1958, *Indian J. Phys.*, **32,** 447.
Dutta Roy, S. K., 1958, *D.Phil. Thesis*, Calcutta University.
Gorter, C. J., 1932, *Phys. Rev.*, **42,** 437.
Griffiths, J. H. E., and Owen, J., 1952 , *Proc. Roy. Soc.* A, **213,** 459; *Proc. Phys. Soc.* A, **65,** 951.
Hartmann, H. von, and Schlafer, H. L., 1951, *Z. Naturf.*, **6 A,** 760.
Klug, H. P., 1940, *J. Amer. Chem. Soc.*, **62,** 2992.
Lipson, H., 1935, *Proc. Roy. Soc.* A, **151,** 347.
Lipson, H., and Beevers, C. A., 1935, *Proc. Roy. Soc.* A, **148,** 664.
Laporte, O., 1928, *Z. Phys.*, **47,** 761.
Owen, J., 1955, *Proc. Roy. Soc.* A, **227,** 183.
Owen, J., and Stevens, K. W. H., 1953, *Nature, Lond.*, **171,** 836.
Pryce, M. H. L., 1950, *Phys. Rev.*, **80,** 1107.
Pryce, M. H. L., and Runciman, W. A., 1958, *Disc. Faraday Soc.*, **26,** 34.
Siegert, A., 1937, *Physica*, **4,** 138.
Stevens, K. W. H., 1953, *Proc. Roy. Soc.* A, **219,** 542.
Uryu, N., 1956, *J. Phys. Soc. Japan*, **11,** No. 7, 770.
Van den Handel, J., and Siegert, A., 1937, *Physica*, **4,** 871.
Van Vleck, J. H., 1932, *The Theory of Electric and Magnetic Susceptibilities* (Oxford: University Press).
—— 1939, *J. Chem. Phys.*, **7,** 61.

APPENDIX

In the case of V^{3+} we have taken the expressions for α and α' given by Abragam and Pryce for Co^{2+} under cubic and a small trigonal symmetry since in both these cases the matrix elements for the crystal field are identical.

In the case of Co^{2+} the appropriate matrix elements for the crystal field between different ^4F and ^4P orbital states are found out from those for a single electron in an f-state, by multiplying with appropriate conversion factors converting the charge densities (expanded in terms of spherical harmonics of different orders not greater than four) for a single electron in an f-state into those for Co^{2+}. The conversion ratios are the same in both the cases (Co^{2+} and V^{3+}) for the second

and fourth order terms excepting the zeroth order which, fortunately, does not appear in the secular determinants and hence we get the same expressions for α and α' in our case also. The following table gives the conversion ratios calculated by Abragam and Pryce and the present author for Co^{2+}. From table 2 we notice, however, that the ratios calculated by us are opposite in sign to those obtained by Abragam and Pryce, excepting for the zeroth order terms. This discrepancy, however, will not affect the results of Abragam and Pryce and hence ours since the secular determinants will remain unchanged, in these two special cases.

Table 2

Order of Spherical Harmonics	For f-state		For p-state		For f- and p-states coupled	
	(1)	(2)	(1)	(2)	(1)	(2)
Zeroth Order	3	3	3	3	–	–
Second Order	$-\frac{3}{7}$	$+\frac{3}{7}$	1	-1	$\frac{4}{\sqrt{21}}$	$-\frac{4}{\sqrt{21}}$
Fourth Order	$\frac{11}{7}$	$-\frac{11}{7}$	–	–	$-\frac{3}{\sqrt{21}}$	$+\frac{3}{\sqrt{21}}$

(1) Abragam and Pryce's results; (2) author's results.

Geometrical Optical Calculation of Frequency Response for Systems with Coma

By A. S. MARATHAY†
Physics Dept., Imperial College, London

MS. received 19*th September* 1958, *in final form* 25*th June* 1959

Abstract. The usefulness of the geometrical optical treatment of frequency response is considered here for the case of coma, an aberration having odd symmetry. Calculations of frequency response and phase shift using this treatment have been made, for different orientations of incoherent line objects, in the presence of Seidel coma in different focal planes. Similar calculations have been made for higher order coma in the Gaussian focal plane. Results are also given according to a mixed treatment of frequency response. The results are compared with diffraction calculations made by Goodbody. It appears from these results that the mixed treatment leads to a smaller value of the response than that given by diffraction theory, and that the geometrical optical treatment will give errors less than about 5% when the wave-front aberration exceeds about 1·5 times the Strehl type of tolerance.

§ 1. Introduction

The use of frequency response techniques for optical image assessment (in incoherent light) may be described as follows. The image of a self-luminous (or incoherently illuminated) object consisting of a sinusoidal variation of intensity is itself a sinusoidal distribution of intensity having a scale determined by the ordinary magnification. The contrast in the image of such a sine-wave grating is less than that in the object, and the image may be displaced laterally from its ideal position. The ratio of the contrast in the image to that in the object $T(R,\psi)$ is the contrast modulation and the lateral shift (in angular measure) $\theta(R,\psi)$ is a phase-shift. These terms are used by analogy with corresponding quantities occurring in the analysis of electrical circuits. The variables (R,ψ) specify the spatial frequency of the grating R and the angle ψ between the direction of the lines of the grating and the meridian plane of the optical system. $\psi=0$ denotes, therefore, that these lines are in the radial direction from the axial point of the image plane. The contrast modulation and the phase-shift may be combined into a single complex number, $D(R,\psi)=T(R,\psi)\exp[i\theta(R,\psi)]$, which is the frequency response of the system.

The image quality at a given part of the image formed by an optical system may be represented by curves of the frequency response as a function of spatial frequency for different orientations ψ of the line objects. The computation of frequency response curves using diffraction theory is lengthy and, since many such curves are often required for a given lens system, it is desirable to have simpler approximate methods of obtaining them. A possibility of this kind is offered in the treatment of frequency response using the geometrical optical approximation

†Now at Itek Corporation, Boston, Mass.

(Hopkins 1957 a). Bromilow (1958) has used this method to study the influence of spherical aberration on frequency response, and has made comparisons with results obtained from diffraction theory. A similar study is described here for the case of coma.

§ 2. The Geometrical Optical Treatment of Frequency Response

To facilitate comparison between the geometrical and diffraction treatments it is convenient to express the frequency response in terms of a reduced spatial frequency s and reduced coordinates (x_0, y_0) in the exit pupil plane. These latter are given by $x_0 = X_0/h$, $y_0 = Y_0/h$, in which (X_0, Y_0) are ordinary coordinates and h is the radius of the aperture. If $n \sin \alpha$ is the numerical aperture of the optical system, measured in the image space, the reduced spatial frequency s is defined by $s = \lambda R/n \sin \alpha$ where R is the spatial frequency in the image. To calculate the frequency response for a structure having a direction ψ the aberrations of the system may be referred to a new set of axes (x, y) rotated through an angle ψ from the old axes (x_0, y_0). If $W(x, y)$ is the resulting wave-front aberration, the frequency response according to geometrical optics is given by the formulae

$$D(s, \psi) = \frac{g(s, 0)}{g(0, 0)} \qquad \ldots\ldots (1)$$

$$g(s, 0) = \iint_A [\tau(x, y)]^2 \exp\left[i \frac{2\pi}{\lambda} s W_x(x, y) \right] dx\, dy. \qquad \ldots\ldots (2)$$

The double integration extends over the whole area of the pupil, denoted here by A; $\tau(x, y)$ is the real amplitude at any point (x, y) in the pupil and $W_x(x, y)$ is the first derivative with respect to x of the wave-front aberration $W(x, y)$. Apart from a constant factor, $W_x(x, y)$ is simply the component of the transverse ray aberration normal to the direction of the line structure.

The calculation of frequency response according to diffraction theory requires the formula (Hopkins 1956)

$$g(s, 0) = \iint_S \tau(x + \tfrac{1}{2}s, y)\tau(x - \tfrac{1}{2}s, y) \exp\left[i \frac{2\pi}{\lambda} s V(x, y;\ s) \right] dx\, dy \qquad \ldots\ldots (3)$$

to be used in place of (2) above. Here the double integration is over the common area, denoted by S, of the two pupils centred at $(\frac{1}{2}s, 0)$ and $(-\frac{1}{2}s, 0)$. The argument of the exponential function involves the quantity $V(x, y;\ s)$, which is defined by

$$V(x, y;\ s) = W_x(x, y) + \frac{1}{3!}\left(\frac{s}{2}\right)^2 W_x^{\mathrm{III}}(x, y) + \frac{1}{5!}\left(\frac{s}{2}\right)^4 W_x^{\mathrm{V}}(x, y) + \ldots \qquad \ldots\ldots (4)$$

where W_x, W_x^{III} ... etc. denote successive derivatives of the wave-front aberration $W(x, y)$, the series terminating at a point determined by the degree of the wave-front aberration function considered. The geometrical optical treatment neglects all terms in the expression of $V(x, y;\ s)$ except the first. From this it appears that the geometrical treatment should give closer approximation to diffraction theory at low frequencies, in which case the higher terms in $V(x, y;\ s)$ become less significant and the areas A and S become less different. Also a better agreement is expected for pupils of uniform transparency, when $\tau(x, y) = 1$, so that

$$\tau(x + \tfrac{1}{2}s, y)\tau(x - \tfrac{1}{2}s, y) = [\tau(x, y)]^2.$$

Only the lower frequencies have good image contrast in the presence of larger aberrations, so that the geometrical optical approximation is expected to be useful for such cases. On the other hand the slope of the geometrical optical response curve at $s=0$ is zero, but that given by diffraction theory is $-2/\pi$. The geometrical treatment will thus overestimate the response at low frequencies. Moreover, $D_0(s, \psi)$, the frequency response in the absence of aberration, is always equal to unity in the geometrical optical treatment, so that the relative response defined by

$$M(s, \psi)\exp[i\theta(s, \psi)] = \frac{D(s, \psi)}{D_0(s, \psi)} \qquad \ldots\ldots(5)$$

is identical with the response itself in this treatment. If $D_0(s, \psi)$ is calculated according to the diffraction theory, $M(s, \psi)$ according to the geometrical optical treatment, a value of $D(s, \psi)$ given by (Hopkins 1957 a)

$$D(s, \psi) = D_0(s, \psi)M(s, \psi)\exp[i\theta(s, \psi)] \qquad \ldots\ldots(6)$$

may be used. Results according to this mixed treatment of frequency response are given later for the case of coma.

§ 3. Method of Integration

For the evaluation of the integral a numerical method suggested by Hopkins (1957 b) was used. The (x, y) plane is divided into rectangles of sides $2\epsilon_x$, $2\epsilon_y$. The rectangle (p, q) is centred at the point (x_p, y_q) with $x_p=(2p)\epsilon_x$, $y_q=(2q)\epsilon_y$. The argument of the exponential function in (2) is then replaced by the first terms in the Taylor series expansion about (x_p, y_q), and the mean value of the integrand over the given rectangle is found. The contributions of all rectangles whose centres lie within the region of integration are then summed. This leads to the following formula for the frequency response according to geometrical optics, (1) and (2) above, for the case of a pupil of uniform transparency, $\tau(x, y)=1$:

$$\left.\begin{aligned} &D(s, \psi) = \frac{4\epsilon_x\epsilon_y}{A}\sum_p\sum_q e^{iZ}\frac{\sin X}{X}\frac{\sin Y}{Y} \\ &\text{where} \\ &Z=\frac{2\pi}{\lambda}sW_x(x, y), \qquad X=\frac{2\pi}{\lambda}sW_x^{\text{II}}(x, y)\epsilon_x, \\ &Y=\frac{2\pi}{\lambda}sW_{x,y}^{\text{II}}(x, y)\epsilon_y, \quad W_{xy}^{\text{II}}(x, y) \text{ denotes } \frac{\partial^2 W}{\partial x\partial y}; \end{aligned}\right\} \qquad \ldots\ldots(7)$$

the factor $4\epsilon_x\epsilon_y/A$ is equal to $1/N$, N being the number of rectangles whose centres lie in the pupil area. It is important to note that an error of 0·01 in obtaining the contribution of each elementary rectangle will give rise to a final error of only this amount in the value of $D(s, \psi)$. The errors in the evaluation of the integral by this method will be due to neglecting higher terms in the Taylor expansion of the exponential function in (2) and in approximating the true boundary of the pupil by a zig-zag. Results obtained by Goodbody (1958) for different mesh sizes suggest that a mesh size of $2\epsilon_x=2\epsilon_y=0{\cdot}1$ will seldom lead to errors in excess of 0·02. In the present work this size of mesh was used and the contribution of each rectangle was computed using five decimal places and the final result rounded off to three places.

For Seidel coma and defect of focus the wave aberration in the unrotated axes is given by

$$W_0(x_0, y_0) = w_{20}(x_0^2+y_0^2)+w_{31}(x_0^2+y_0^2)y_0.$$

Rotation of the axes through an angle ψ transforms this expression to the form

$$W(x, y) = w_{20}(x^2+y^2) + w_{31}(x^2+y^2)(x\sin\psi + y\cos\psi). \quad \ldots\ldots (8)$$

Substitution from (8) in (7) gives for the quantities Z, X and Y occurring there:

$$\left.\begin{aligned} Z &= 2\pi(sw_{31})[\beta_{23}\,.\,2x_p + (3x_p{}^2 + y_q{}^2)\sin\psi + 2x_p y_q\cos\psi] \\ X &= \epsilon_x 2\pi(sw_{31})[2\beta_{23} + 6x_p\sin\psi + 2y_q\cos\psi] \\ Y &= \epsilon_y 2\pi(sw_{31})[2x_p\cos\psi + 2y_q\sin\psi] \end{aligned}\right\} \quad \ldots\ldots (9)$$

in which w_{31} is expressed in terms of the wavelength λ as unit of length, and where $\beta_{23} = w_{20}/w_{31}$ is used to denote the plane of focus. Knowing these quantities the normalized frequency response is evaluated using the summation in (7).

In the presence of higher order circular coma the aberration function (8) becomes

$$\begin{aligned} W(x, y) = {} & w_{20}(x^2+y^2) + w_{31}(x^2+y^2)(x\sin\psi + y\cos\psi) \\ & + w_{51}(x^2+y^2)^2(x\sin\psi + y\cos\psi) \end{aligned}$$

and the parameters

$$\beta_{25} = \frac{w_{20}}{w_{51}} \quad \text{and} \quad \beta_{35} = \frac{w_{31}}{w_{51}}$$

are then used to denote the amount of defocusing and the amount of primary coma respectively. Expressing w_{51} in terms of the wavelength λ as unit of length, the quantities Z, X and Y take the following forms:

$$\left.\begin{aligned} Z = {} & 2\pi(sw_{51})[2x_p\beta_{25} + \beta_{35}\{(3x_p{}^2 + y_q{}^2)\sin\psi + 2x_p y_q\cos\psi\} \\ & + (x_p{}^2 + y_q{}^2)\{(5x_p{}^2 + y_q{}^2)\sin\psi + 4x_p y_q\cos\psi\}] \\ X = {} & \epsilon_x 2\pi(sw_{51})[2\beta_{25} + \beta_{35}\{6x_p\sin\psi + 2y_q\cos\psi\} \\ & + 4\{x_p(5x_p{}^2 + 3y_q{}^2)\sin\psi + y_q(3x_p{}^2 + y_q{}^2)\cos\psi\}] \\ Y = {} & \epsilon_y 2\pi(sw_{51})[\beta_{35}\{2y_q\sin\psi + 2x_p\cos\psi\} \\ & + 4\{y_q(3x_p{}^2 + y_q{}^2)\sin\psi + x_p(x_p{}^2 + 3y_q{}^2)\cos\psi\}] \end{aligned}\right\} \quad \ldots\ldots (11)$$

these values being used as before in the summation in (7).

The modulus of the response $T(s, \psi) = |D(s, \psi)|$ and the phase shift

$$\theta(s, \psi) = \arg\{D(s, \psi)\}$$

were obtained from the real and imaginary parts of the double summation in (7). The lateral shift of the image of the spatial frequency component with respect to the ideal image is given by

$$\delta u = -\frac{\theta(s, \psi)}{2\pi s}$$

a formula which applies equally to the diffraction and geometrical optical treatments.

For the azimuth $\psi = 0$ the direction of the line structure is parallel to the axis of symmetry of the coma pattern. In consequence the imaginary part is identically zero, so that the phase shift $\theta(s, \psi)$ is zero for this case. Accordingly only the real part of the formula in (7) has to be computed over one quadrant. In all other cases it is necessary to compute both the real and imaginary parts of (7) over the first and fourth quadrants of the (x, y) plane. In obtaining these frequency response curves, according to the geometrical optical treatment, about nine values of the variables sw_{31} or sw_{51} were used in each case.

§ 4. Results

The comparison of the geometrical optical and diffraction treatments of frequency response given by Bromilow (1958) considered the case of spherical aberration, which is an aberration term having even symmetry in x and y. The present comparison is for coma, which is an aberration term having odd symmetry, and for which tolerance formulae give more severe tolerances. The case of coma might therefore constitute a somewhat more severe test of the usefulness of the geometrical optical treatment of frequency response.

The parameter β_{23} was given successively the values zero, denoting the Gaussian plane of focus, and $+1$ corresponding to an amount of defocusing. The modulus $T(s, \psi)$ of the response is the same in planes of focus at equal distances on either side of the Gaussian focal plane so that the case $\beta_{23} = -1$ need not be treated separately. For these two cases the frequency response $D(s, \psi)$ has been calculated for the azimuths $\psi = 0, \pi/4, \pi/2$, using for each case values of the product sw_{31} equal to $0{\cdot}1, 0{\cdot}2, \ldots 1{\cdot}2$. The modulus of the frequency response so obtained, $T(s, \psi)$, was then plotted against sw_{31}. The advantage of plotting the response curves as a function of sw_{31} in the geometrical treatment is that a single curve then applies to different values of the aberration coefficient w_{31} (in terms of wavelength λ as the unit of length) merely by choosing the correct scale for s.

The resulting frequency response curves are given in figures 1 and 3. In figure 1 the curve for $\psi = \pi/2$, in which case the line structure is perpendicular to the axis of symmetry of the coma pattern, shows a lower response for all frequencies than the curve for $\psi = 0$; on the other hand the curve for $\psi = \pi/4$ indicates a lower response than that for $\psi = 0$ for the low frequencies, but gives a higher response for the higher frequencies. When $\beta_{23} = +1$, however, the curve for $\psi = \pi/2$ starts below that for $\psi = 0$, but shows greater response for the higher frequencies. The broken curves are calculated by the mixed treatment of frequency response for the case $w_{31} = 1\lambda$. There would be a different response curve according to the mixed treatment for each different value of w_{31}. These are not shown in the figure to avoid confusion. These curves always lie below the corresponding curves of the purely geometrical optical treatment since

$$D_0(s, \psi) < 1 \quad \text{for} \quad s > 0.$$

The curves of figures 1 and 3 are compared with those from diffraction theory obtained by Goodbody (private communication) in figures 2 (*a*), (*b*), (*c*) and 4 (*a*), (*b*) respectively. These show that the geometrical treatment does, in fact, overestimate the response for low frequencies: for higher frequencies the curves oscillate about those of the diffraction theory. The frequency response obtained according to the mixed treatment is in better agreement with diffraction theory for the low frequencies, and underestimates the response for higher frequencies. The Strehl type tolerance on Seidel coma is $|w_{31}| \leqslant 0{\cdot}63\lambda$. The curves of these figures show that when $|w_{31}| \geqslant 1\lambda$, i.e. when the aberration exceeds about 1·5 times the Strehl type of tolerance, the mixed treatment always gives a lower result than diffraction theory, and that the geometrical treatment is in better agreement with diffraction theory. This is not the case for the curves corresponding to $w_{31} = 0{\cdot}63\lambda$. This particular comparison was not made by Bromilow for spherical aberration, but it is of importance as showing that the mixed treatment errs on the safe side. The insets in these curves give the phase shift $\theta(s, \psi)/2\pi$ as calculated using the geometrical treatment and from diffraction theory.

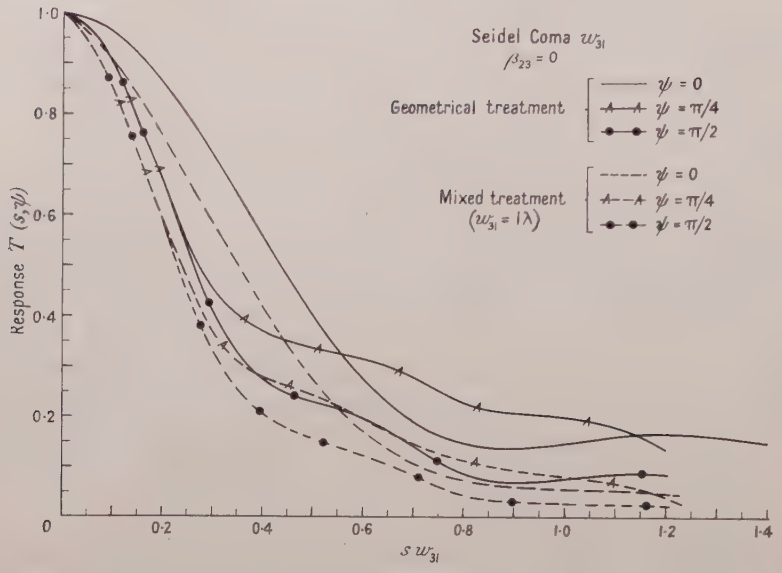

Figure 1. The geometrical optical response $T(s, \psi)$, for Seidel coma, is plotted as a function of (sw_{31}) in the Gaussian focal plane for the azimuths $\psi = 0$, $\pi/4$ and $\pi/2$.

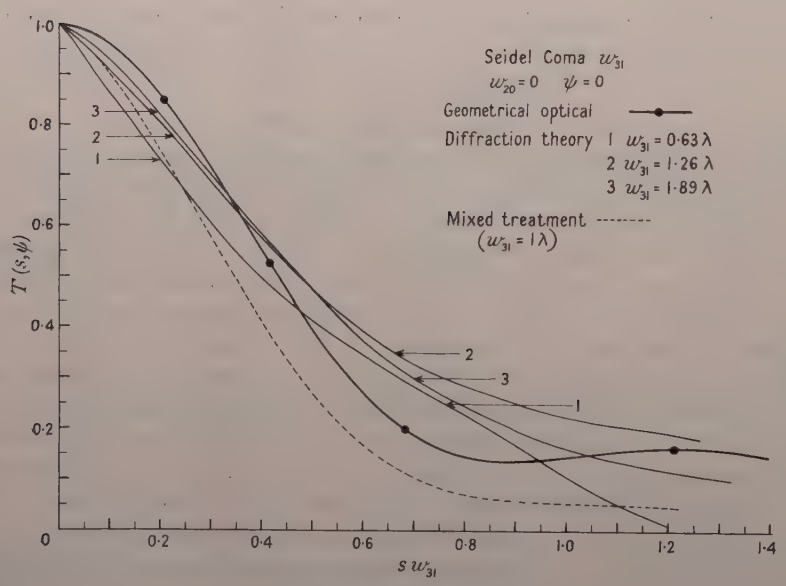

Figure 2 (*a*).

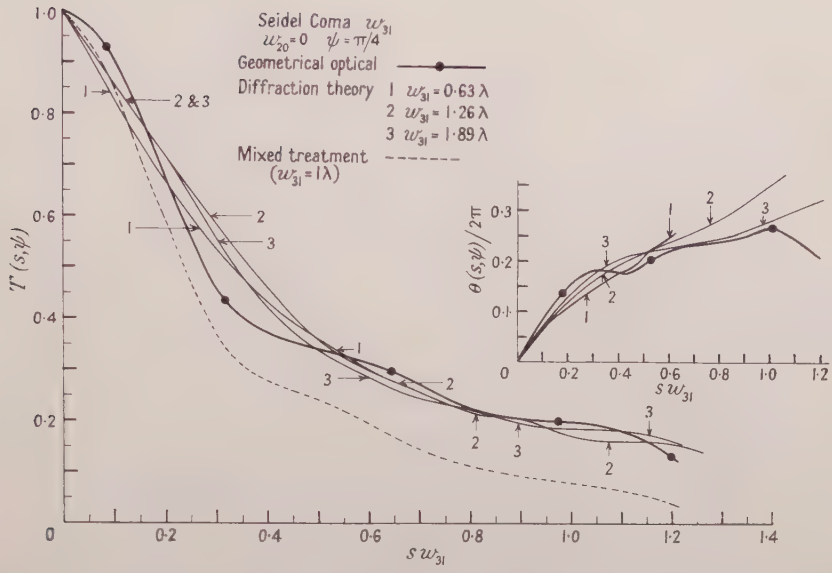

Figure 2 (*b*).

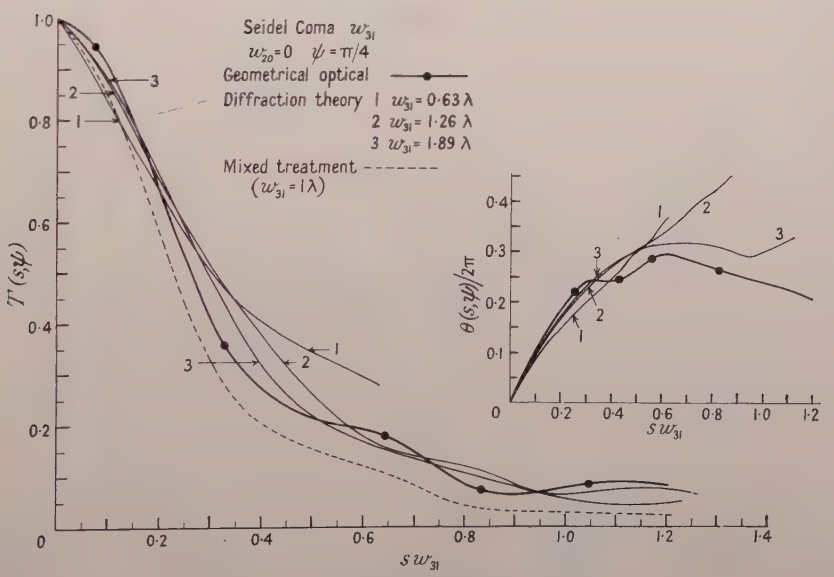

Figure 2 (*c*).

Figures 2 (*a*), (*b*) and (*c*). Comparison of the geometrical and diffraction treatments in the Gaussian focal plane, for Seidel coma, with azimuths $\psi=0$, $\pi/4$ and $\pi/2$. The phase shift $\theta(s,\psi)/2\pi$, using the geometrical and diffraction treatments, is plotted against (sw_{31}), for comparison, in the insets of figures 2 (*b*) and (*c*).

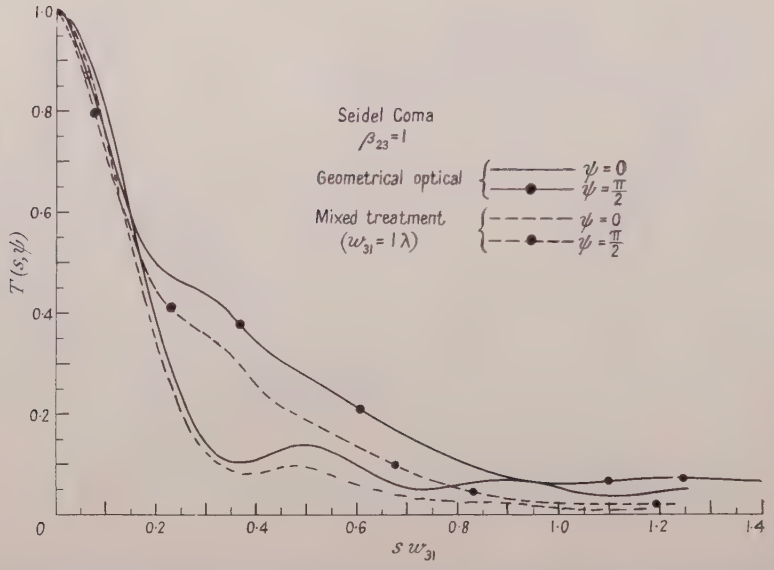

Figure 3. The geometrical optical response $T(s, \psi)$, for Seidel coma, is plotted as a function of (sw_{31}) in the focal plane determined by $\beta_{23}=+1$ for azimuths $\psi=0$ and $\pi/2$.

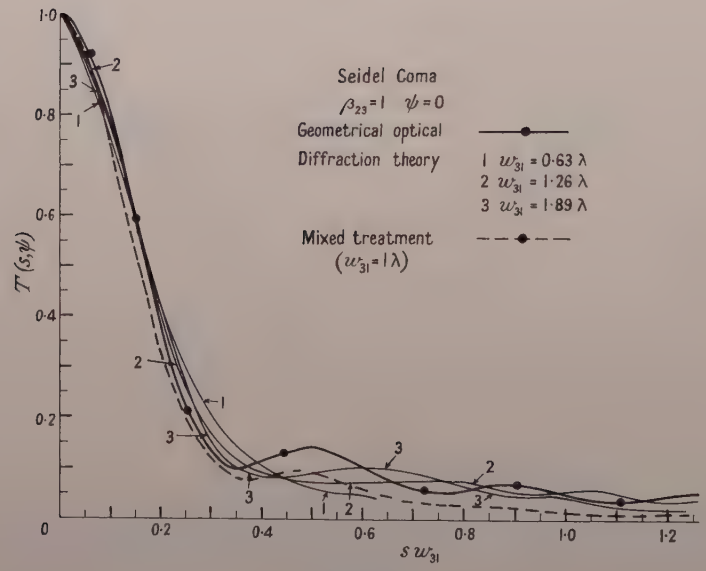

Figure 4 (*a*).

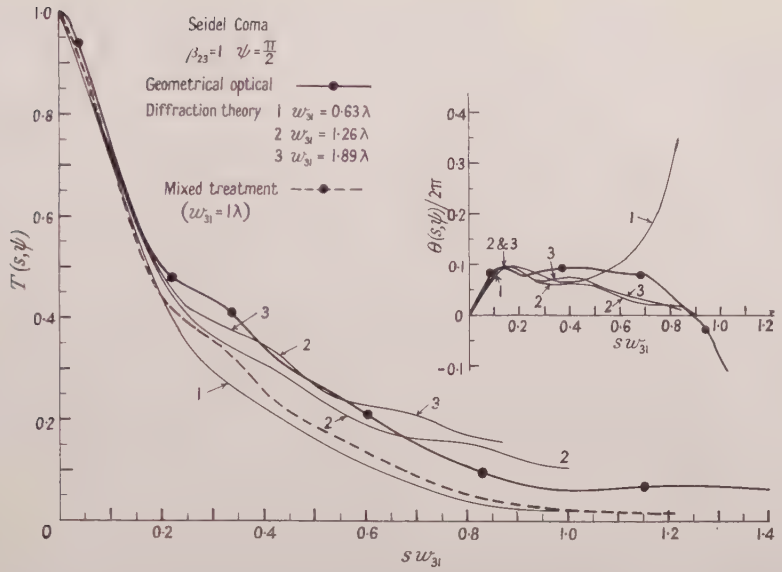

Figure 4 (*b*).

Figures 4 (*a*) and (*b*). Comparison of the geometrical and diffraction treatments, in the focal plane determined by $\beta_{23}=+1$, for Seidel coma with azimuths $\psi=0$ and $\pi/2$. The phase shift $\theta(s,\psi)/2\pi$ using the geometrical and diffraction treatments is plotted against (sw_{31}), for comparison, in the inset of figure 4 (*b*).

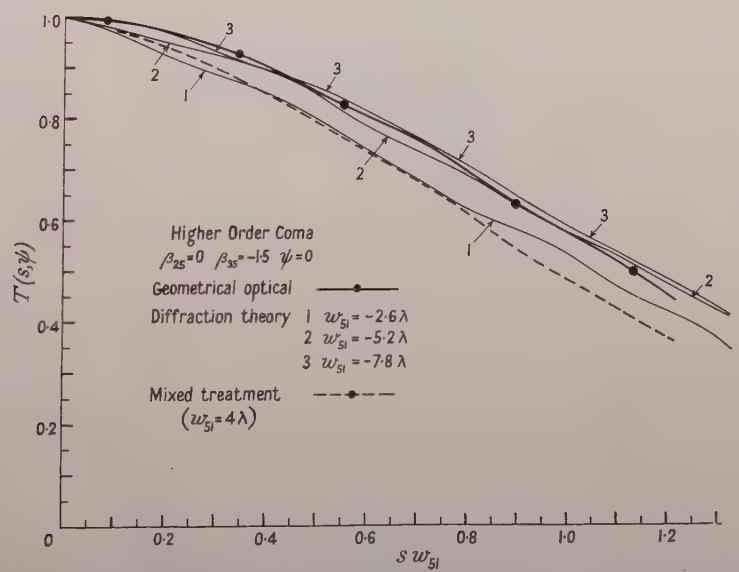

Figure 5. The frequency response $T(s,\psi)$, using the geometrical and diffraction treatments, is plotted against (sw_{51}) for a value of $\beta_{35}=w_{31}/w_{51}=-1{\cdot}5$ which will optimize the low-frequency response in the Gaussian focal plane.

4.1. *Higher Order Coma* (w_{51})

In this case the frequency response $D(s, \psi)$ has been calculated in the Gaussian focal plane $\beta_{25}=0$ for the state of correction represented by $\beta_{35}=-1{\cdot}5$, which will optimize the low-frequency response according to the tolerance theory of Hopkins (1957 a). Here sw_{51} was used as the variable and the response was calculated for the azimuth $\psi=0$ for $sw_{51}=0{\cdot}1, 0{\cdot}2, \ldots 1{\cdot}2$ so that this single curve again serves for different values of the aberration w_{51} (in terms of wavelength λ as the unit of length) by merely choosing the proper scale of s. The comparison of the geometrical and mixed treatments with the diffraction theory is given in figure 5. There would, in fact, be a different response curve according to the mixed treatment for each different value of w_{51}. The results again show that the mixed treatment underestimates the response for higher frequencies. The Strehl type tolerance for higher order circular coma is $|w_{51}| \leqslant 2{\cdot}6\lambda$, that is approximately four times that of w_{31}. The curves of figure 5 show that when $|w_{51}| \geqslant 4\lambda$, i.e. when the aberration exceeds about 1·5 times the Strehl type of tolerance, the mixed treatment gives a lower response than diffraction theory, and that the geometrical treatment is in better agreement. This is not the case for the curve corresponding to $w_{51}=2{\cdot}6\lambda$.

These results support the findings of Bromilow, namely that the geometrical treatment is a useful approximation and will give errors less than $\pm 0{\cdot}05$ when the wave aberration exceeds 1·5 times the Strehl type of tolerance. Considerably less computation is involved in the geometrical treatment than is required by the diffraction theory. It appears, therefore, that the geometrical treatment of frequency response will be useful for many studies of image quality.

Acknowledgment

I am grateful to Dr. H. H. Hopkins for suggesting this problem and for useful discussions.

References

Bromilow, N. S., 1958, *Proc. Phys. Soc.*, **71**, 231.
Goodbody, A. M., 1958, *Proc. Phys. Soc.*, **72**, 411.
Hopkins, H. H., 1956, *Proc. Phys. Soc.* B, **69**, 562.
—— 1957 a, *Ibid.*, **70**, 1162.
—— 1957 b, *Ibid.*, **70**, 449.
—— 1957 c, *Ibid.*, **70**, 1002.
Miyamoto, K., 1958, *J. Opt. Soc. Amer.*, **48**, 57, 567.

Aplanatic Lenses

By A. K. HEAD
Division of Tribophysics, Commonwealth Scientific and Industrial Research Organization, University of Melbourne, Australia

MS. received 20*th May* 1959, *in final form* 13*th July* 1959

Abstract. A differential equation is obtained for the shape of an aspherical lens which is aplanatic for an object at infinity. Numerical integration of this equation for a range of lenses shows the variation in the shape and properties of such a lens for a range of adjustable parameters. A differential equation is also derived for the shape of a lens which exactly corrects the spherical aberration and coma of an arbitrary optical system.

§ 1. Introduction

In two previous papers (Head 1957, 1958) an analysis has been given of optical systems containing two aspherical mirrors such that the complete system is exactly aplanatic. In this paper the optical systems considered contain a lens with two aspherical surfaces such that the complete system is exactly aplanatic. The simplest system is just a lens which forms an image of an object at infinity; this is examined in § 2. In § 3 the general problem is analysed.

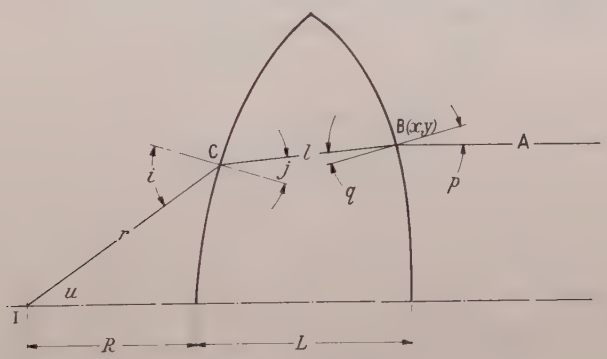

Figure 1.

§ 2. The Aplanatic Lens with One Focus at Infinity

We consider an axially symmetric lens of refractive index n and ask what shapes the front and rear surfaces of the lens must be in order that: (*a*) a beam of parallel light along the axis of the lens is brought exactly to a point focus and (*b*) the sine condition is satisfied exactly implying that the lens is free from primary coma. Figure 1 shows an axial section of the lens and the path ABCI of a typical ray through the lens. The rear face is specified by polar coordinates (r, u) about the image point I and the front face by cartesian coordinates (x, y) about I as origin. The angles i, j, p, q are measured from the normals to the faces. The

length of BC is denoted by l and the angle BC makes with the axis by k. The four adjustable constants which specify the lens are its focal length f, refractive index n, the distance R from I to the pole of the rear face, and the axial thickness L. Then the lens is specified by the following equations:

$$k=u-i+j=p-q, \quad \ldots\ldots(1)$$

$$\sin i=n\sin j, \quad \ldots\ldots(2)$$

$$\sin p=n\sin q, \quad \ldots\ldots(3)$$

$$l\sin k=y-r\sin u, \quad \ldots\ldots(4)$$

$$l\cos k=x-r\cos u, \quad \ldots\ldots(5)$$

$$y=f\sin u \quad \text{(sine condition)}, \quad \ldots\ldots(6)$$

$$r+nl-x=(n-1)L \quad \text{(optical path)}, \quad \ldots\ldots(7)$$

$$\frac{1}{r}\frac{dr}{du}=\tan i, \quad \ldots\ldots(8)$$

$$\frac{dx}{dy}=-\tan p. \quad \ldots\ldots(9)$$

From these equations we find an expression for $\tan i$ which involves only r and u. Substituting this in (8) then gives a first-order differential equation between r and u which specifies the shape of the rear face of the lens.

Eliminating x between (5) and (7) gives

$$l(n-\cos k)=(n-1)L-r(1-\cos u) \quad \ldots\ldots(10)$$

and eliminating y between (4) and (6) gives

$$l\sin k=(f-r)\sin u. \quad \ldots\ldots(11)$$

On dividing (11) by (10), l is eliminated giving

$$\frac{\sin k}{n-\cos k}=\frac{(f-r)\sin u}{(n-1)L-r(1-\cos u)}. \quad \ldots\ldots(12)$$

Now the left-hand side of (12) is just $\tan q$ so

$$q=\arctan\left[\frac{(f-r)\sin u}{(n-1)L-r(1-\cos u)}\right]. \quad \ldots\ldots(13)$$

From (1)

$$j=p-q-u+i$$

and substituting this in (2) gives

$$\sin i=n\sin(p-q-u+i)$$
$$=n\sin(p-q-u)\cos i+n\cos(p-q-u)\sin i,$$

i.e.

$$\tan i=\frac{n\sin(p-q-u)}{1-n\cos(p-q-u)}. \quad \ldots\ldots(14)$$

Thus,

$$\frac{dr}{du}=\frac{nr\sin(p-q-u)}{1-n\cos(p-q-u)} \quad \ldots\ldots(15)$$

is the required differential equation where

$$p=\arcsin(n\sin q) \quad \text{from (3)}$$

and q is given as a function of r and u by (13).

In a similar manner it can be shown that the differential equation for the front face is

$$\frac{dx}{dy} = \frac{n \sin(u-i+j)}{1-n\cos(u-i+j)} \qquad \ldots\ldots(16)$$

where

$$u = \arcsin(y/f), \qquad \ldots\ldots(17)$$

$$i = \arcsin(n \sin j), \qquad \ldots\ldots(18)$$

$$j = \arctan\left[\frac{x\sin u - y\cos u}{(n-1)L - y\sin u + x(1-\cos u)}\right]. \qquad \ldots\ldots(19)$$

These differential equations are of a complicated form and it has not been possible to solve them analytically. The only known solutions are for the very special case $n=-1$ when they reduce to the equations for the Schwarzschild–Chretien two-mirror telescope. However, the equations are very suitable for numerical integration by a digital computer and the following lenses were obtained using the computer CSIRAC. These results could have been obtained by the methods of Wassermann and Wolf (1949) or Vaskas (1957). However, the computer programme would have been more complicated, involving the simultaneous integration of a pair of coupled differential equations.

It is not necessary to integrate both the differential equations (15) and (16), and the equation (15) for the rear face was chosen as being the simpler to programme. When a point on the rear face had been found, the corresponding point on the front face was given by

$$y = f\sin u \qquad \ldots\ldots(6)$$

$$x = \{rn\cos u - r\cos(p-q) + (n-1)L\cos(p-q)\}/\{n-\cos(p-q)\} \qquad \ldots\ldots(20)$$

the latter equation being obtained by eliminating l between (5) and (7).

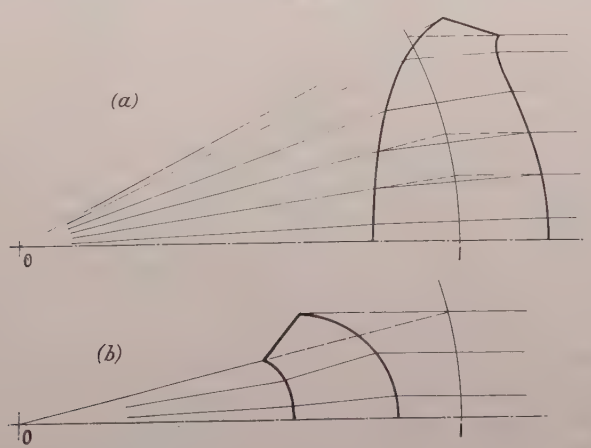

Figure 2. (*a*) Martin's lens: $R=0{\cdot}8$, $L=0{\cdot}4$, $n=1{\cdot}5$, $f=1$.
(*b*) Burch's lens: $R=\frac{1}{2}(\sqrt{5}-1)$, $L=(\sqrt{5}-2)$, $n=\frac{1}{2}(\sqrt{5}+1)$, $f=1$.

Martin (1944) has computed some aplanatic lenses by expanding (1)–(9) as infinite series. One of the lenses he describes is given by $R=0{\cdot}8$, $L=0{\cdot}4$, $n=1{\cdot}5$, $f=1$. Our numerical integration of this lens is shown in figure 2 (*a*) which also illustrates the geometrical interpretation of the sine condition, that the point of intersection of the incident and emergent rays lies on a circle of

radius f. The maximum aperture of this lens ($u_{max}=27{\cdot}9°$) is reached when the emerging ray is tangential to the rear face.

The lens $R=\frac{1}{2}(\sqrt{5}-1)$, $L=(\sqrt{5}-2)$, $n=\frac{1}{2}(\sqrt{5}+1)$, $f=1$ is shown in figure 2 (b). Burch (1943) has shown that this lens, in the approximation of fourth power figuring, is not only aplanatic but also anastigmatic and with no curvature of field. The maximum aperture of this lens ($u_{max}=13{\cdot}6°$) is seen to be limited by tangential incidence on the front face.

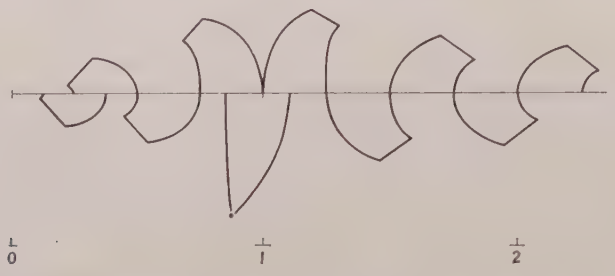

Figure 3. Ten lenses with $L=0{\cdot}25$, $n=1{\cdot}5$, $f=1$ and various R.

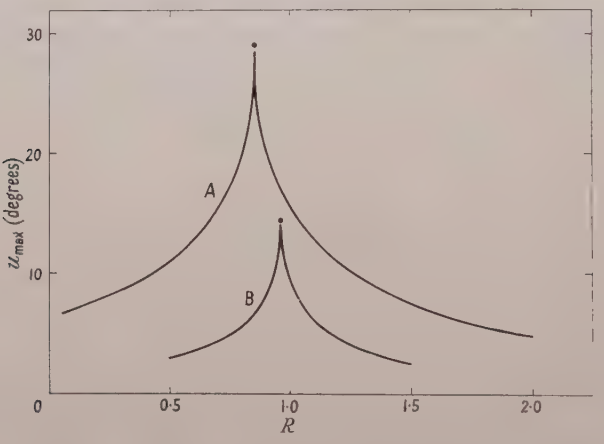

Figure 4. A. Variation of maximum aperture with R for $L=0{\cdot}25$, $n=1{\cdot}5$, $f=1$.
B. As A but $L=0{\cdot}0625$.

A series of ten lenses is shown in figure 3. These lenses all have their focus at O, focal length $f=1$, refractive index $n=1{\cdot}5$, and glass thickness $L=0{\cdot}25$ but differ in their value of R. Curve A of figure 4 shows the variation of u_{max} with R for this series of lenses. It will be seen that the maximum aperture is limited by the front face if R is small and by the rear face if R is large. The transition between these two types is a lens whose maximum aperture is reached when the front and rear faces meet, i.e. the lens runs out of glass. At such a point $l=0$ in (4)–(8) giving

$$r=f$$

and

$$\cos u_{max}=1-\frac{(n-1)L}{f} \qquad \ldots\ldots(21)$$

and this gives the maximum possible aperture for a lens of given n, L and f. The closest approach to such a lens which has been obtained is shown in figure 3 and is for $R=0{\cdot}8528$. The dot in figure 3 is the position given by (21) for the tip of the maximum aperture lens and the dot at the cusp of curve A of figure 4

is the aperture of this lens, the cusp having been drawn at the point for the lens $R=0{\cdot}8528$. The computations indicate that the maximum aperture lens lies between $R=0{\cdot}8527$ and $R=0{\cdot}8528$, but it is possible that these limits are slightly in error. The reason is that at the point given by (21) both numerator and

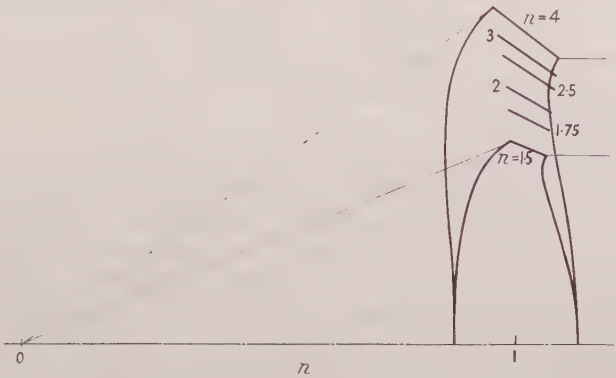

Figure 5. Six lenses with $R=0{\cdot}875$, $L=0{\cdot}25$, $f=1$ and various n.

denominator of (13) are zero and so q is indeterminate. Thus numerical integration in the neighbourhood of this point is of low accuracy. A similar series of lenses with $f=1$, $n=1{\cdot}5$, $L=0{\cdot}0625$ were computed and their apertures are given in curve B of figure 4 with the dot indicating the maximum possible aperture given by (21), this occurring in the neighbourhood of $R=0{\cdot}9626$. The effect of varying the refractive index is shown in figure 5 where all lenses have $R=0{\cdot}875$, $L=0{\cdot}25$ and $f=1$. In this figure only the two lenses for $n=1{\cdot}5$ and $n=4$ are shown in full, and for intermediate values only the limiting ray through the lens is shown.

§ 3. The General Case

The general case of an arbitrary optical system to which an aspherical lens is added so that the complete system is aplanatic, can be analysed in a similar manner to the simple lens of § 2. If the arbitrary optical system is specified by the three functions $\theta(\phi)$, $X(\phi)$, $P(\phi)$ (Head 1958), then the rear face of the lens is specified by the differential equation

$$\frac{dr}{du}=\frac{nr\sin(p-q-u-\theta)}{1-n\cos(p-q-u-\theta)} \qquad \ldots\ldots(22)$$

where

$$q=\arctan\left[\frac{X(\phi)\sin\theta-r\sin(\theta+u)}{K-P(\phi)-X(\phi)\cos\theta-r\{1-\cos(\theta+u)\}}\right]$$

$p=\arcsin(n\sin q)$, $K=$constant optical path length through complete system, and $\sin\phi=m\sin u$ (sine condition).

This differential equation is also of suitable form for numerical integration. Some of the simpler optical systems which it covers are:

(i) An aplanatic lens working between finite foci. In the simple case of a lens of unit magnification, there are some obvious solutions where each face is a cartesian oval. These give some analytical solutions to (22) but appear to be very special cases and give no hint of how the general solution might be obtained.

(ii) The correction of the coma of a parabolic reflector by an aspherical lens.

(iii) The aplanatic combination of a spherical reflector and an aspherical lens. If the lens is before the reflector, then the lens is similar to a Schmidt plate but figured on both sides.

References

Burch, C. R., 1943, *Proc. Phys. Soc.*, **55,** 433.
Head, A. K., 1957, *Proc. Phys. Soc.* B, **70,** 945.
—— 1958, *Ibid.*, **71,** 546.
Martin, L. C., 1944, *Proc. Phys. Soc.*, **56,** 104.
Vaskas, E. M., 1957, *J. Opt. Soc. Amer.*, **47,** 669.
Wassermann, G. D., and Wolf, E., 1949, *Proc. Phys. Soc.* B, **62,** 2.

Radial Hydromagnetic Oscillations

By G. B. F. NIBLETT and T. S. GREEN
Atomic Weapons Research Establishment, Aldermaston, Berks.

Communicated by K. W. Allen; MS. received 15th May 1959, in final form 27th July 1959

Abstract. This paper discusses the radial hydromagnetic oscillations of a plasma confined by an axial magnetic field. Oscillations of this type have recently been observed experimentally in this laboratory and typical high speed streak photographs are presented and analysed. On the assumption that the plasma is confined in a thin cylindrical annulus, the non-linear equation of motion can be integrated analytically. The calculated period of the oscillations is independent of amplitude and is found to be in good agreement with experimental results. Damping of the oscillations by diffusion of the magnetic field is discussed and reference made to the possible significance of the oscillations as a means of transferring energy irreversibly to the ions.

§ 1. Introduction

In recent years there has been considerable interest in the initial dynamic processes occurring in the high current pinch effect. Several theoretical and experimental investigations have been reported on the initial collapse and subsequent oscillations of a gas column which carries a large axial current and which is compressed by the interaction between this current and its own azimuthal magnetic field (Cousins and Ware 1951, Rosenbluth 1954, Kurchatov 1956, Andrianov *et al.* 1956, Leontovich and Osovets 1956, Burkhardt and Lovberg 1958). In the course of similar experiments using an azimuthal gas current and external axial magnetic field to compress the plasma (Niblett 1959) high frequency oscillations have been observed which are believed to be radial hydromagnetic oscillations of a cylindrical annulus of plasma trapped between external and internal magnetic fields. The purpose of this paper is to describe the experimental observation of these oscillations, to discuss their characteristics, and to point to their possible significance as a means of putting energy into the ions of the plasma by means of a cyclic relaxation process (magnetic pumping).

§ 2. Experimental Arrangement

The experimental arrangement is shown schematically in figure 1. A wide single-turn coil encircles a quartz tube containing gas at a pressure of about a hundred microns weakly ionized by means of a low power radio-frequency system. The coil is connected to a low inductance condenser bank by means of a switch. When this switch is closed the rising current in the coil induces an azimuthal current in the gas and the magnetohydrodynamic interaction between the external field and the gas current results in rapid compression of the plasma. The oscillations have been observed by photographing the hot luminous plasma using a streak camera with a writing speed of up to twenty millimetres per microsecond which views the discharge axially through a narrow diametral slit.

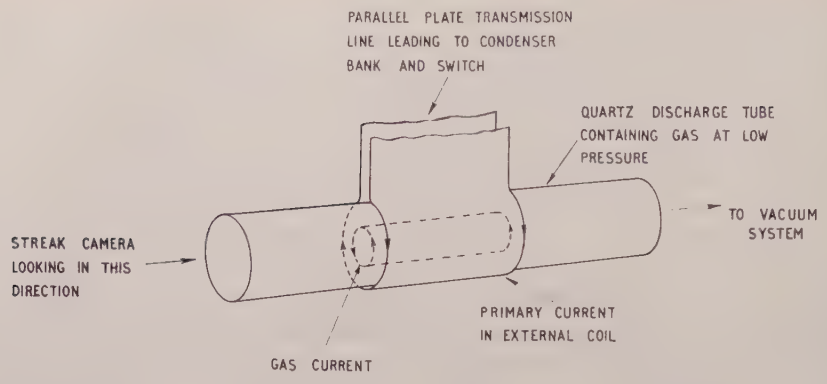

Figure 1. Diagram showing experimental arrangement.

Experiments have been performed on two different scales. On the larger scale a coil 50 cm long and 17 cm in diameter encircled a thick-walled quartz tube of internal bore 16 cm. The discharge was produced by connecting the coil to the Atomic Weapons Research Establishment low inductance condenser bank MAGGI (Fitch and McCormick 1959) which provides 45 000 joules of electrical energy at 30 kv and uses 200 spark gap switches in parallel. The total circuit inductance was 60 mμH of which the bank (including switches) contributed about 5 mμH. On the smaller scale a discharge was produced using a coil 10 cm wide wrapped around a tube 4 cm in diameter and connected to a small bank supplying 4500 joules also at 30 kv. The total inductance was 65 mμH of which the bank and single switch contributed 40 mμH.

Typical streak photographs of the oscillations are shown in figure 2 (Plate) in which (*a*) is a photograph taken with the large coil using deuterium at an initial pressure of 80 microns and (*b*) is a photograph with the small coil using deuterium at 120 microns. The time scale is shown beneath each photograph and the mean period of the oscillations differs in the two experiments by a factor of about five. The profile of the oscillations clearly differs from a sine wave being much sharper at the turning point near the axis than away from the axis.

§ 3. Model of the Oscillations

The streak photographs suggest the model of the oscillations shown in figure 3 in which a thin cylindrical annulus of plasma is confined between axial magnetic fields. During the initial growth of the gas current the field from the external coil is able to penetrate the weakly ionized gas and as the conductivity rises this field is trapped and subsequently compressed by the implosion of the current sheath. The imploding plasma overshoots the radius r_e at which the external field and the trapped field are equal and oscillates about this equilibrium position.

The assumption that the plasma is confined in a thin shell enables the oscillations to be analysed by means of elementary dynamics. The model assumes that the plasma is highly conducting and hence that there is no significant diffusion of the field into the plasma. The collection of the gas in a shell is predicted by the 'snow-plough' model of the implosion process (Rosenbluth 1954) in which the gas particles are assumed to adhere to the current-carrying sheath and travel in with it. The gas in the centre of the tube will be sufficiently highly conducting to travel with the compressed lines of force and so will not experience any E field

to further ionize or heat it. There will of course be a gradual mutual diffusion of plasma and magnetic field and under these conditions (Tuck 1958) the period of the oscillations will be dependent on the plasma characteristics.

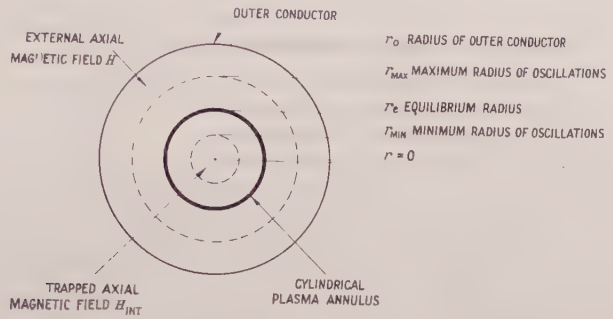
OUTER CONDUCTOR
EXTERNAL AXIAL MAGNETIC FIELD H
r_0 RADIUS OF OUTER CONDUCTOR
r_{MAX} MAXIMUM RADIUS OF OSCILLATIONS
r_e EQUILIBRIUM RADIUS
r_{MIN} MINIMUM RADIUS OF OSCILLATIONS
$r = 0$
TRAPPED AXIAL MAGNETIC FIELD H_{INT}
CYLINDRICAL PLASMA ANNULUS

Figure 3. Cross section of model of radial hydromagnetic oscillations. For perfect field trapping $H_{\text{int}} = H(r/r_e)^{-4}$.

On the assumption of high electrical conductivity the annulus of plasma carries two azimuthal currents: a current in its outer surface in the opposite sense to the current in the external coil; and a current on the inner surface which varies with the trapped field and which flows in a direction determined by this field. In general the oscillations occur at high compression and with an amplitude small enough to make wall effects negligible so that the oscillations do not themselves modify significantly the external magnetic field.

§ 4. Equation of Motion

On the assumptions that all the particles are trapped within a thin annular shell as shown in figure 3 and that the external magnetic field H is constant during the period of one oscillation, the equation of motion can be written

$$\frac{d}{dt}\left(Nm_i\frac{dr}{dt}\right) = -\left[2\pi r\frac{H^2}{8\pi} - 2\pi r\frac{H_{\text{int}}{}^2}{8\pi}\right] \qquad \ldots\ldots(1)$$

where H_{int} is the internal magnetic field, r is the radius of the annulus and N is the line density of ions of mass m_i in the annulus. At the equilibrium position, $r = r_e$, the internal field is equal to the external field and if trapping is perfect then

$$(H_{\text{int}})^2 r^4 = H^2 r_e{}^4 \qquad \ldots\ldots(2)$$

i.e.

$$(H_{\text{int}})^2 = H^2\beta^{-4} \qquad \ldots\ldots(3)$$

where $\beta = r/r_e$. The equation of motion then becomes

$$\frac{d^2\beta}{dt^2} = -\frac{\alpha^2}{4}\beta(1-\beta^{-4}) \qquad \ldots\ldots(4)$$

where $\alpha^2 = H^2/Nm_i$. Equation (4) is the equation of a non-linear radial oscillation remarkable in that the period is independent of amplitude. Integration gives

$$\beta^2 = k^2 + (k^4-1)^{1/2}\sin\alpha t; \qquad k \geqslant 1 \qquad \ldots\ldots(5)$$

where k is a constant of integration which determines the amplitude of the

oscillations. The period τ is

$$\tau = \frac{2\pi}{\alpha} = 2\pi\left(\frac{Nm_i}{H^2}\right)^{1/2}. \qquad \ldots\ldots(6)$$

It is easily shown that $k = [\frac{1}{2}(\beta_{max}^2 + \beta_{min}^2)]^{1/2}$ where β_{max} and β_{min} are the maximum and minimum radial excursions of the annulus from the axis of the tube and are related by the expression

$$(\beta_{max})^2(\beta_{min})^2 = 1. \qquad \ldots\ldots(7)$$

Equation (5) is plotted in figure 4 to show the wave profile for k values of 1·05, 1·60 and 3·00. As k approaches 1 the profile approaches that of a simple harmonic oscillation about the equilibrium radius. As k gets larger the profile becomes increasingly different from a sine wave and the annulus spends an increasing proportion of its period at radii greater than the equilibrium radius.

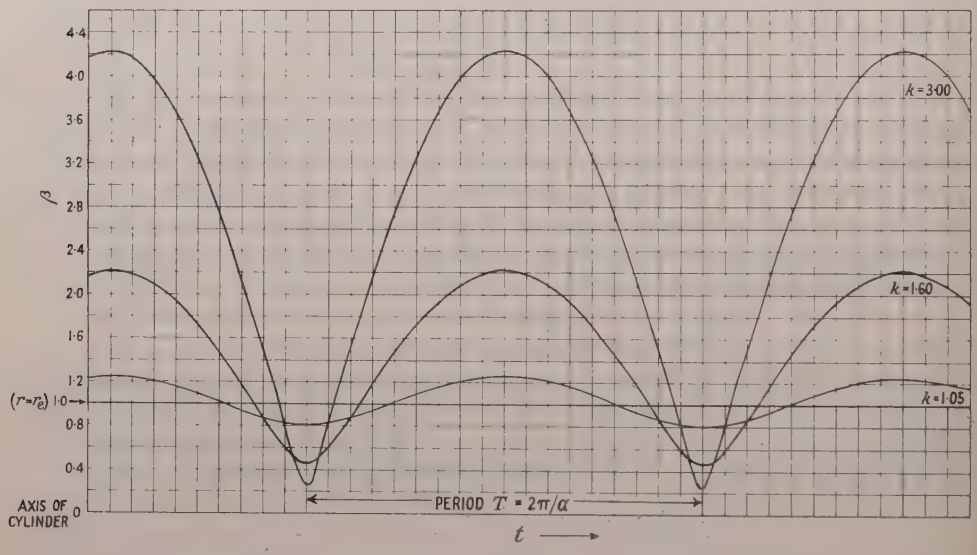

Figure 4. Theoretical wave profile of the oscillations.

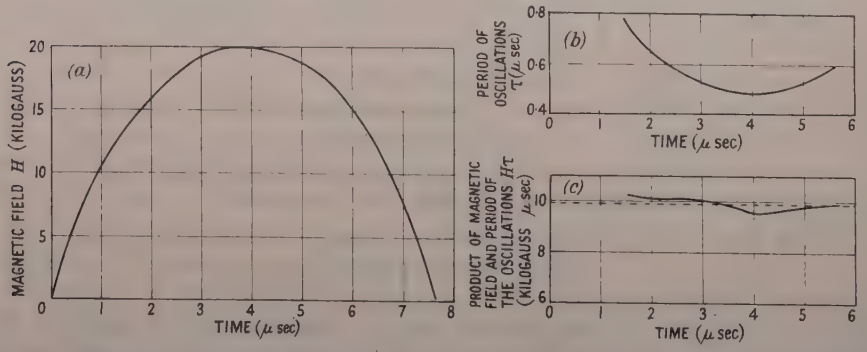

Figure 5. These curves were obtained from analysis of the oscillations shown in figure 2 (*a*). Curve (*a*) shows the variation of magnetic field with time and curve (*b*) presents the measured variation of the period τ of the oscillations with time. The product $H\tau$ (curve (*c*)) is approximately constant and its value (broken line) provides an estimate of Nm_i using the derived relation $\tau = 2\pi\,(Nm_i/H^2)^{1/2}$.

It is found experimentally that the period varies inversely with the magnetic field as predicted by equation (6) and is consistent with the assumption that all the gas is collected in the annulus by the imploding current sheath. The analysis of the oscillation of figure 2 (*a*) is shown in figure 5 in which the curve (*a*) shows the time-variation of the external field and (*b*) exhibits the variation of τ with time. Curve (*c*) shows that the product $H\tau$ is constant and the corresponding value of Nm_i agrees to within 10% with the total mass of gas per unit length originally within the tube.

§ 5. Damping by Field Diffusion

Figure 6 (Plate) is a streak photograph of a discharge in air at an initial pressure of 120 microns taken with the small scale system at 10 kv. Under these conditions the plasma temperature is much lower than for the discharges in deuterium shown in figure 2 and it is believed that the absence of oscillations is determined by resistive losses which are accompanied by diffusion of the magnetic field through the plasma. The peak field for this discharge is $1{\cdot}1 \times 10^4$ oersteds and the corresponding period calculated from equation (6) is about one microsecond.

Figure 6 is interpreted as follows. On the first half-cycle the external field penetrates the weakly ionized gas before the gas current has fully developed and this field is subsequently trapped by the advancing current sheath and compressed until the internal magnetic pressure is equal to the external pressure. Since the plasma temperature is low the oscillations are damped by resistive effects and the photograph suggests that the field diffuses through the plasma in about two microseconds. On the second half-cycle the current grows more rapidly in the now highly ionized gas; hence no field is trapped and the imploding plasma proceeds unimpeded to the centre of the tube.

An estimate of the plasma temperature can be made from the implosion velocity if it is assumed that conventional hydrodynamic shocks exist. At the temperatures and densities of figure 6 this assumption is reasonable since the collision mean free path is about 10^{-3} cm, much less than the dimensions of the apparatus. The velocity of the leading edge of the light trace is approximately 2·5 centimetres per microsecond and the corresponding equilibrium temperature behind a shock moving at that velocity into undisturbed air at a pressure of 120 microns is about 30 000°K and the shocked air will have on average roughly one free electron per atom. It is therefore of interest to estimate the time for field diffusion through plasma at this temperature.

The diffusion problem is conveniently treated in one dimension though this approximation is strictly valid only when the distance the magnetic field diffuses is small compared with the radius of the plasma surface. In cylindrical geometry diffusion occurs more rapidly so that the one-dimensional treatment will overestimate the diffusion time. From Maxwell's equations, neglecting the displacement terms, the diffusion is described by the differential equation

$$\frac{\partial H}{\partial t} = \frac{1}{4\pi\sigma\mu}\frac{\partial^2 H}{\partial x^2} \qquad \ldots\ldots (8)$$

where x is distance perpendicular to an infinite plane surface of conductivity σ and permeability μ. Equation (8) may be solved to give the skin depth x for diffusion of field through a conductor as a function of time when a field is suddenly

applied to the boundary of the conductor at time $t=0$. Using as a criterion of skin depth the distance over which magnetic pressure, proportional to H^2, changes by a factor of two, gives

$$x=0{\cdot}15\sqrt{\frac{t}{\sigma}} \qquad \ldots\ldots(9)$$

where the permeability of the plasma is taken to be unity.

The conductivity of a plasma is given as a function of temperature by (Spitzer 1956):

$$\sigma=\frac{1{\cdot}53\times10^{-13}T^{3/2}}{\ln\Lambda\, Z}\ \text{e.m.u.} \qquad \ldots\ldots(10)$$

where Z, the degree of ionization (number of free electrons per nucleus), is greater or equal to one, and $\ln\Lambda$ is a slowly varying function of the plasma density and temperature. Taking $\ln\Lambda$ to be 10 and substituting for σ in equation (9) gives

$$x=1{\cdot}21\times10^{6}\sqrt{\frac{tZ}{T^{3/2}}}. \qquad \ldots\ldots(11)$$

Equation (11) expresses the skin depth x as a function of time and temperature. The estimated thickness of the plasma annulus in figure 6 is 0·5 cm and assuming the temperature to be 30 000°K gives one microsecond as the diffusion time, i.e. the diffusion time is about equal to the calculated period of the oscillations. These figures are all approximate; but the evidence tends to sustain the hypothesis that figure 6 is a photograph of an oscillation damped by the diffusion of magnetic field. Since significant diffusion takes place in a time equal to one period, the damping is not far from critical.

§ 6. Magnetic Pumping

The oscillations are accompanied by a cyclic magnetic compression of the plasma and thus could represent a form of magnetic pumping. By pumping with a period of the order of, or shorter than, the ion–ion self-collision time, i.e. the characteristic time for an ensemble of ions with a non-Maxwellian velocity distribution to relax towards a Maxwellian, it is possible to transfer energy irreversibly to the ions. This process can of course only contribute the energy stored in the oscillatory motion unless some means of re-exciting the oscillations can be found. The mechanism might be termed variable-γ heating as it depends on the variation of the plasma specific heat ratio during the compression cycle.

Schlüter (1957) has considered a particular form of variable-γ heating in which an oscillatory magnetic field within the plasma is used to transfer energy to the ions. By calculating the e-folding time as a function of field amplitude and the frequency of ion–ion collisions Schlüter demonstrates that the process is an efficient one. His analysis shows that the e-folding time is sensitive to the amplitude of the magnetic field variations and is independent of the frequency of the oscillations provided this is greater than the ion collision frequency.

The radial oscillations provide a simple means of achieving a large amplitude of field variation; for example with $k=1{\cdot}05$ (a modest value) the internal field varies by a factor greater than two. The ion–ion self-collision time t_c for deuterium ions is (Spitzer 1956),

$$t_c=\frac{1{\cdot}61T^{3/2}}{n} \qquad \ldots\ldots(12)$$

where T is the temperature in °K, n is the ion density and $\ln\Lambda$ is again ten. For $T = 10^6$ °K and $n = 10^{18}$ the collision frequency is 6×10^8 sec^{-1}. It should not be difficult to produce a discharge in which α $(= (H^2/Nm_i)^{1/2})$ reaches this value; in recent experiments at the Atomic Weapons Research Establishment values of α of 3×10^8 sec^{-1} have been obtained. It is therefore considered that radial hydromagnetic oscillations of this type can provide a sufficient field variation and can be generated at sufficiently high frequency to contribute effectively to the heating of the ions.

§ 7. Conclusion

Experimental observations of radial oscillations have been presented and shown to give agreement with simple theory on the assumption that all the gas is collected by the collapsing current sheath. This result suggests that the oscillations may be used for diagnostic purposes; measurement of the period can be combined with measurement of the current in the coil to calculate the mass of gas contributing to the oscillations.

Photographs taken under conditions such that a low temperature plasma is produced suggest that resistive effects damp the oscillations and this hypothesis is supported by an estimate of the diffusion time and of the plasma temperature from the implosion velocity.

Finally, it is suggested that excitation of these oscillations at a frequency of the order of the ion–ion collision frequency might heat the plasma ions by a form of magnetic pumping.

The experimental study of these oscillations is continuing at the Atomic Weapons Research Establishment, Aldermaston.

Acknowledgments

This work was carried out in the Atomic Weapons Research Establishment fusion group directed by S. C. Curran and K. W. Allen, and forms part of an experimental study of the rapid compression of plasma using external axial magnetic field carried out in collaboration with H. A. B. Bodin and N. J. Peacock. The authors are grateful to R. A. Fitch for helpful criticism.

References

Andrianov, A. N., Artsimovich, L. A., Bazilevskaya, O. A., Prokhorov, Yu-G., and Filippov, N. V., 1956, *Atomnaya Energiya*, **3**, 76.

Burkhardt, L. C., and Lovberg, R. H., 1958, Paper and Supplement I, *Geneva Conference on the Peaceful Uses of Atomic Energy*.

Cousins, S. W., and Ware, A. A., 1951, *Proc. Phys. Soc.* B, **64**, 159.

Fitch, R. A., and McCormick, N. R., 1959, *Proc. Instn Elect. Engrs*, A, **106**, 117.

Kurchatov, I. V., 1956, *Nucl. Engng*, **1**, 103.

Leontovich, M. A., and Osovets, S. M., 1956, *Atomnaya Energiya*, **3**, 81.

Niblett, G. B. F., 1959, *Proc. Instn Elect. Engrs*, A, **106**, 152.

Rosenbluth, M., 1954, *Los Alamos Scientific Report*, LA 1850.

Schlüter, A., 1957, *Proceedings of the Third International Congress on Ionization Phenomena in Gases*, Venice, p. 942.

Spitzer, L., 1956, *Physics of Fully Ionized Gases* (London, New York : Interscience Publishers).

Tuck, J. L., 1958, Paper P1860, *Geneva Conference on the Peaceful Uses of Atomic Energy*.

The Properties and Behaviour of some Artificial Ice Nuclei

By B. J. MASON and A. P. van den HEUVEL
Imperial College, London

MS. received 16th February 1959, in revised form 27th May 1959

Abstract. Reasons for the discordant results obtained by different workers on the ice-nucleating properties of chemical aerosols are discussed and, in an attempt to resolve these differences, the ability of a variety of pure, inorganic crystals to nucleate supercooled water clouds in both diffusion- and mixing-cloud chambers, and also large drops of highly purified water, has been carefully investigated. For a finely dispersed, insoluble substance, closely similar threshold nucleation temperatures were obtained with all three techniques. The results for finely powdered metallic oxides were less reproducible and were peculiar in that the activity of the particles, always slight, did not increase markedly as the temperature was lowered below the threshold value. Also, their potency was reduced by wetting of their surfaces.

A number of substances, e.g. CdI_2, NH_4F and I_2, normally inactive in a water cloud because of their solubility, initiate ice-crystal formation in an atmosphere sub-saturated relative to water but supersaturated relative to ice. Insoluble nuclei may act as either 'freezing' or 'sublimation' nuclei depending on the temperature. Thus silver iodide nuclei act between $-4°C$ and $-12°C$ only if the air surpasses water saturation but, at lower temperatures, they act as sublimation nuclei provided the supersaturation relative to ice exceeds 12%; lead iodide shows a similar behaviour but requires a critical supersaturation of 15% below $-15°C$. The efficiency of ice-forming nuclei may be interpreted partly, but not wholly, in terms of the particles possessing low-index crystal faces in which the atomic spacings differ from those in either the basal or prism faces of ice by not more than a few per cent. That such geometrical considerations alone are insufficient becomes apparent from experiments in which epitaxial deposits of ice crystals have been formed on large, single crystals of seven different substances.

§ 1. Introduction

In recent years a number of papers have appeared from several different laboratories reporting on the ice-nucleating ability of a wide variety of chemical compounds introduced either as smokes, sprays, or as fine dusts into supercooled clouds formed in expansion-, diffusion-, or mixing-cloud chambers. Except in the case of silver iodide, which is generally agreed to be the most effective of the substances tested so far, the results obtained by the different workers are very conflicting; for example, substances reported as highly effective by one laboratory are found to be inactive by another.

After some very careful experiments, performed in very clean apparatus and using highly pure air and chemicals, Mason and Hallett (1956, 1957) concluded that some of the earlier results must have been spurious because of the presence, in the air or the chemicals, of small traces of silver or free iodine, leading to the

formation of silver iodide; if all such trace impurities were removed many of the substances hitherto claimed as highly efficient nucleators were then found to be inactive. The same authors also pointed out the dangers of the conventional method of inferring the onset of ice-crystal formation solely from the appearance in the cloud of twinkling particles because crystalline particles of the seeding agent itself may glitter and be optically indistinguishable from ice crystals. Furthermore, no reliance could be placed on the results of tests on unstable compounds, such as some of the iodides, which may decompose either at room temperature or during the dispersion process to produce free iodine.

Mason and Hallett tested a considerable number of substances which had been reported effective by other workers but found only AgI (−5°c), CuS (−6°c), PbI_2 (−7°c), Cu_2I_2 (−15°c), V_2O_5 (−15°c) to be definitely active, about one particle in 10^4 forming an ice crystal at the temperatures indicated when introduced into a supercooled water cloud in *both* a diffusion- and a mixing-cloud chamber. The inactivity of small particles of a wide range of highly soluble salts was attributed to their going into solution. In fact it was demonstrated that, while ice sublimed directly on to iodine crystals at temperatures below −14°c in an atmosphere supersaturated relative to ice but sub-saturated relative to water, on entering a water cloud, the minute iodine crystals quickly dissolved and lost their ice-nucleating ability.

In order to investigate, in more detail, the degree to which the nucleating ability of chemical aerosols may be influenced by the environmental humidity, and to search for other relevant factors which may also account for the discrepancies in the results of different workers, the experiments now to be described were carried out.

§ 2. Nucleating Properties of Insoluble Inorganic Compounds

Tests were carried out in both a mixing- and a diffusion-cloud chamber. The mixing-cloud chamber consisted of a sealed glass vessel immersed in a thermostatically controlled refrigerator, this system being preferred to the usual open-top cold chamber because it could be kept scrupulously clean and free from contamination by atmospheric aerosols. A 5-litre 'Pyrex' flask, after being carefully cleaned, is placed in the refrigerator, flushed with clean, filtered air until cooled to the required temperature, and then sealed. After the air in the flask has reached a steady temperature as indicated by suitably disposed thermocouples, the material under test is introduced as a fine aerosol through a side tube, and a supercooled cloud is formed by evaporation from electrically heated, water-soaked gauze. The appearance of ice crystals can be detected by their glittering in a light beam traversing the chamber, but it proved much more convenient and reliable to use the supercooled-film technique described by Mason and Hallett (1957).

A film stretched across a wire hoop, about 2 in. in diameter, made by dipping the latter into a 50/50 mixture of 'Stergene' and water, is suspended inside the test flask. When tiny ice crystals fall on the supercooled film they grow quite rapidly and produce much larger crystals which are easily seen and counted. In order to detect large numbers (about a hundred) of crystals on a single film, it was necessary to retard the rate of ice-crystal growth. Very suitable films for this purpose were made from equal parts of 'Stergene', sucrose, and water, and remained stable for several hours. The films can be used successfully down

to temperatures of -18°C but, at appreciably lower temperatures, they soon become nucleated by the metal supporting ring. An estimate of the concentration of ice crystals in the cloud may be made from the rate of appearance of crystals on the film; one crystal appearing every 5 seconds corresponds to a concentration of about 10 per litre under the particular conditions of this experiment.

Most of the insoluble substances to be tested, having been ground in a pestle and mortar, were stored in polythene bottles fitted with outlet tubes through which they were dispersed into the test chamber by squeezing the bottle after shaking. By waiting a few minutes between shaking the bottle and dispersing the powder, the larger particles were allowed to settle out and the great majority of particles entering the flask were between $0{\cdot}2\mu$ and 1μ radius. The experimental procedure was to determine the highest temperature at which ten crystals appeared on the film within 50 seconds of introducing the nucleant. With a total particle concentration of about 100/cm^3 in the flask, this threshold temperature corresponded to that at which about one particle in 10^4 became an active nucleus.

The results for a number of stable, insoluble or only very slightly soluble substances having threshold temperatures of -15°C or above, are shown in table 1. The threshold temperatures at which a similar level of activity appears in a diffusion-cloud chamber of the type described by Mason and Hallett (1956) are also shown in this table. In all cases, the threshold temperatures obtained in the mixing- and diffusion-cloud chambers are in close agreement.

To determine whether or not these powdered materials would nucleate *bulk* water at the same temperatures at which they produce ice crystals in a supercooled cloud, aqueous suspensions containing 1% by weight of the material were made using highly purified water, one-millimetre drops of which could be readily supercooled to -20°C. Millimetre drops of such a suspension, hanging from a fine thermocouple, were placed in a small cooling chamber, cooled at the rate of 1–5°C min^{-1}, and their freezing temperatures determined. The standard deviation of the freezing temperatures of 20 drops of a particular suspension was rarely greater than 1°C, the mean temperature (see row 11 of table 1) agreeing very well with the threshold temperature at which the substance nucleated a droplet cloud in the mixing-cloud and diffusion-cloud chambers.

§ 3. The Behaviour of Metallic Oxides

The results of tests on the nucleating ability of a number of metallic oxides were, in all cases except that of Ag_2O, less clear-cut and reproducible than for the substances listed in table 1.

All the oxides shown in table 2, dispersed in finely powdered form, were active to the extent that one particle in 10^4 or 10^5 produced an ice crystal in both mixing- and diffusion-cloud chambers at temperatures above -15°C, but showed no appreciable increase in activity at temperatures below the quoted threshold value. In the diffusion chamber, an insignificant number of ice crystals appeared at temperatures above -40°C unless very heavy concentrations ($>10^5$ particles/cm^3) of powder were introduced; under these conditions about 1 crystal per cm^3 appeared at the temperatures shown in table 2. The failure to observe, with less than one-tenth of these concentrations of aerosol, more than an occasional ice crystal, led Mason and Hallett (1956) to report SnO, MnO_2 and NiO of only 'general purpose' quality as probably inactive. In their experiments, a very

Table 1. The Ice-Nucleating Properties of some Chemical Compounds

		Insoluble					Soluble				
Substance	Ice	AgI	CuS	HgI_2	Ag_2S	Ag_2O	PbI_2	NH_4F	CdI_2	V_2O_5	I_2
Crystal symmetry	Hex.	Hex.	Hex.	Tetrag.	Mono-clinic	Cubic	Hex.	Hex.	Hex.	Orthorhombic	
Lattice spacings (Å)											
(a)	4·52	4·58	3·80	4·36	4·20	4·72	4·54	4·39	4·24	11·48	4·78
(b)				4·36	6·93					4·36	7·25
(c)	7·36	7·49	16·43	12·34	9·50		6·86	7·02	6·84	3·55	9·77
Solubility (g/100cm^3)	—	8×10^{-6}	Insol.	3×10^{-3}	2×10^{-5}	Insol.	4×10^{-2}	v.sol.	79·8/0°C	0·5	3×10^{-2}
Threshold nucleation temp. (°C)											
Mixing chamber—soap film		−4	−6	−8	−8	−11	−6	−9	−12	−15†	−14
Diffusion chamber		−5	−5	−8	−8	−12	−7	—	—	−17†	—
Bulk water		−4	−7	−7	−9	−10	−6	—	—	—	—
Orientation on single crystals		−4	−5	—	—	—	−6	—	−12	−12	−12
Threshold temperatures of other workers:											
Hosler (1951)		−6	—	−18	−4	—	−4	—	−15	—	−12
Mossop (1956)		−6	—	−17	—	—	−7	—	—	—	—
Pruppacher & Sanger (1955)		−4	−4	−13	−4	−6	−5	x	−15	−6	x
Mason & Hallett (1956,1957)		−5	−6	x	—	—	−7	—	x	−15	−14
Fukuta (1958)		−3	−7	−12	−7	−5	−1	−13	−12	—	x

†A much lower degree of activity is observed at about −10°C.
x Tested and found inactive.

Table 2. Nucleating Properties of Metallic Oxides

Substance	Al_2O_3	CdO	CuO	Cu_2O	Mn_3O_4	NiO	SnO_2
Threshold nucleation temp. (°c):							
Mixing chamber—							
soap film (1 in 10^4)	−12	< −16†	− 7	− 6	−10	< −16†	− 7
Diffusion chamber (1 in 10^5)	− 8	− 9	− 7	− 6	− 8	−11	− 8
In aqueous suspension			< −15	−10	−14	< −17	< −16
On surface of water drops	− 6	− 9	− 6	− 7	− 7	−10	− 7

†Very slight activity, about 1 in 10^5, at −10°c.

slight degree of activity may have been due to impurities, but these have been practically eliminated in the present work by using spectroscopically pure oxides, the specifications of which are shown in table 3.

Table 3. Purity of Nucleating Materials

The following spectroscopically pure materials were supplied by Johnson Matthey & Co. Ltd., who quote the impurity content in parts per million as follows:

Al_2O_3	Nil	NiO	Fe 6, Si 8, Al 2, Na 2
CdO	Pb 7, Na 2, Zn 2	SnO_2	Na 3, Bi 2
CuO	Si 2	V_2O_5	Fe 3, Si 3
Mn_3O_4	Mg 7, Si 3	Ag_2O	Fe 2, Si 3

The concentrations of other impurities did not exceed 1 part/10^6.

AgI was produced by sparking of ' spec-pure ' silver (Fe 3, Al 1, Pb 1; Cd, Cu, Li, Mg, Mn all <1) in iodine vapour. I_2 crystals were produced by sublimation from the vapour. CuS was specially prepared and ground and contained less than 1 part/10^6 of Ag and Pb.

The remaining nucleating substances, which showed a high and reproducible degree of activity and for which expitaxial growth of ice was directly observed, at the same threshold temperature, on single crystals of the substance, were of ' Analar ' quality.

It appears that the nucleating ability of these ' spec-pure ' oxides is lowered if they first become centres of condensation in the highly-supersaturated atmosphere of the diffusion chamber, and that only when the supersaturation is reduced by the introduction of high concentrations of particles do they appear to be as effective as in the mixing chamber where the air is barely water-saturated.

Evidence that nucleation efficiency of the oxide particles is reduced on being immersed in bulk water is also provided by the fact that millimetre size drops of aqueous suspensions of the oxides, each containing about 10^5 particles, froze at considerably lower temperatures than the corresponding threshold temperatures observed in cloud chambers—in contradistinction to the results obtained for the insoluble substances of table 1. On the other hand, if roughly the same number of oxide particles was sprayed on the surface of the water drop, instead of being immersed in it, the freezing temperatures were several degrees higher (see table 2) and very similar to the threshold temperatures recorded for the diffusion chamber.

The reasons for the rather peculiar behaviour of metallic oxides is not clear. Certainly only a very small fraction of the particles which, under the microscope, are of irregular shape with few well-defined crystal faces, act as effective ice nuclei —perhaps only those which have a face for which the epitaxial misfit is small (see table 4), and which have especially favourable sites for nucleation. Their loss of potency after immersion in bulk water may, perhaps, be associated with their tendency to form hydration compounds.

§ 4. The Behaviour of Soluble Nuclei

The discovery by Mason and Hallett (1957) that sub-microscopic iodine crystals initiate the sublimation of ice in an ice-supersaturated atmosphere at temperatures below -14°c, but lose this property when introduced into a water-supersaturated atmosphere by going into solution, suggested that a number of other salts found to be inactive in the water-supersaturated environment of a diffusion chamber should be tested under sub-water-saturated conditions.

The tests were carried out in much the same way as for the insoluble nuclei but the particles were introduced into the flask by atomizing saturated solutions, allowing the droplets to fall through relatively dry air in which the majority crystallized before entering the test flask (which now contained no visible cloud), and allowing the crystals to fall on the soap film. Again the highest temperature at which about one particle in 10^4 nucleated the film was determined. The results are shown separately in table 1 and will be discussed later.

§ 5. Epitaxy of Ice on Nucleogenic Crystals

The most direct evidence of a particular crystal acting as an ice nucleus is afforded by the direct observation of epitaxial growth of ice on its surfaces. The growth of ice on those substances for which reasonably good crystal faces of sufficient size may be obtained has therefore been studied.

Oriented deposits of ice crystals have been observed on the basal (0001) faces of hexagonal AgI (-4°c), PbI_2 (-6°c), CdI_2 (-12°c) and CuS (-6°c) on the (010) face of orthorhombic HgI_2, on the (100) face of V_2O_5 (-12°c) and on the (001) face of orthorhombic iodine. On the other hand, only randomly oriented ice crystals have been observed on the basal face of hexagonal CdS in which the atomic spacing differs by only 10% from that of ice.

A detailed account of these experiments will appear elsewhere; the results are quoted here only in confirmation of the nucleation tests.

§ 6. Discussion of Nucleation Experiments

The observed ice-nucleating ability of a particular aerosol will be determined not only by the properties of the particles themselves but also by the experimental conditions under which they are tested. Discrepancies between the results obtained by different workers may arise from differences in one or more of the following factors:

(i) The criterion adopted for the onset of nucleation in terms of the fraction of particles which become activated, and the reliability of the technique used for ice-crystal detection.

(ii) The concentrations and size of the nuclei; these will govern the number of particles which enter the observational space and the time for which they remain there.

(iii) The volume of the test space and hence the total number of nuclei observed during a test. Small volumes will fail to detect low ice-crystal concentrations at the threshold of activity.

(iv) The time for which the particles are subjected to the prevailing temperature and supersaturation before disappearing from view. For example, nuclei requiring a few seconds to produce ice crystals of detectable size would appear inactive in a rapid expansion chamber having a sensitive time of only a fraction of a second,

(v) The magnitude of the prevailing supersaturation which may determine the time-lag for nucleation and whether or not the nuclei act as centres of condensation before reaching sub-freezing temperatures.

(vi) The solubility and rate of solution of the nuclei in water.

(vii) The crystalline and surface structure of the particles; it is currently believed that the nucleating ability of a particle is determined largely by the similarity of the atomic arrangement in its surface layers to that of ice, and that the presence of steps or other favourable sites is necessary to allow nucleation at low supersaturations. The proportion of particles having suitable faces may well be governed by their method of preparation. Furthermore, as we have seen, discordant results may arise from the presence of trace impurities, the decomposition of the substance under test, or the use of inadequate detection methods.

Bearing in mind that discrepancies may arise for one or more of the above reasons, we shall now compare the threshold nucleation temperatures obtained in our experiments with those of other workers.

Silver iodide.

There is substantial agreement among all investigators on the activity of this substance. Threshold temperatures ranging from $-3°C$ to $-6°C$, with a preference for $-4°C$, have been quoted, the lower values having been obtained with expansion chambers having small observational volumes and small sensitive times.

Cupric sulphide.

There is general agreement that the threshold temperature lies between $-4°C$ and $-7°C$ with a preference for $-6°C$.

Mercuric iodide.

Using a powder, our three different techniques all yield threshold temperatures of $-7°C$ or $-8°C$, which are considerably higher than those reported by Hosler ($-18°C$), Pruppacher and Sänger ($-13°C$), Mossop ($-17°C$), and Fukuta ($-12°C$). This rather large discrepancy may have arisen because three of these authors produced their aerosol by vaporizing the compound from a heated wire whereby partial decomposition and transformation to the orthorhombic yellow form may have occurred. Birstein and Anderson (1955) and Mason and Hallett (1956) found similarly produced smokes to be inactive above $-20°C$.

Silver sulphide and silver oxide.

We find these substances to be initially active at about $-8°C$ and $-11°C$ respectively—at rather lower temperatures than the range $-4°C$ to $-7°C$ reported by Fukuta and Pruppacher and Sänger. It seems that the differences are too large to be attributed to differences in observation and technique; perhaps small traces of iodine, leading to the formation of silver iodide, may have been responsible for the high activity observed by these authors.

Oxides of aluminium, cadmium, copper, manganese and tin.

These oxides all show a similar behaviour in that a small fraction of the particles become effective ice nuclei at temperatures between $-6°C$ and $-12°C$, but their activity does not increase appreciably thereafter with falling temperature. The threshold temperatures quoted in table 2 are in reasonable agreement with those reported by Pruppacher and Sänger and by Fukuta except that we find SnO_2 to be rather more effective than did Fukuta and CuO to be active at $-7°C$

rather than -12°c (Pruppacher and Sänger) or -4 c (Fukuta). The slight degree of activity shown by 'general purpose' quality MnO_2 and SnO may be due to traces of Mn_3O_4 and SnO_2 respectively.

Soluble nuclei.

As far as the soluble compounds are concerned, Mason and Hallett's discovery that crystalline iodine will behave as a sublimation nucleus at temperatures below -14°c is confirmed and epitaxial deposits of ice crystals at special sites on the (001) face have been observed at -12°c. Crystals of highly soluble ammonium fluoride and cadmium iodide act as sublimation nuclei below -9°c and -12°c respectively, these temperatures being in fair agreement with those reported by Fukuta. The results obtained with evaporated sprays of alkali iodides were not clear cut. Sodium iodide was found to be inactive at temperatures down to -16°c in disagreement with several other workers who have quoted threshold temperatures as high as -12°c. Potassium iodide and ammonium iodide caused nucleation of the soap-film detector below -13°c, but perhaps by the release of free iodine which, in the case of NH_4I, was clearly demonstrated by the simultaneous introduction of a silver aerosol when copious numbers of ice crystals were produced at -6°c through the production of silver iodide.

Lead iodide.

The nucleation efficiency of very small lead iodide particles depends to what extent they become previously involved in condensation and dissolution. Our experiments confirm those of Schaefer (1954) in showing that if a lead iodide smoke is introduced into a sub-water-saturated environment so that condensation and dissolution is avoided, ice crystals appear at temperatures below -6°c or -7°c. On the other hand, if they have to spend some 30 sec or so in traversing the highly-supersaturated region of a diffusion chamber before reaching the supercooled region, their nucleating ability is destroyed.

Most authors quote a threshold temperature between -5°c and -7°c, the exception being Fukuta who claims $-1{\cdot}3$°c. We are unable to confirm this last figure, and suggest that Fukuta may have been misled by the fact that lead iodide aerosol glitters very much like an ice-crystal cloud in a sub-water-saturated environment, even at positive temperatures.

Vanadium pentoxide.

Dispersed as a fine powder, this substance shows very slight activity at about -10°c and thereafter no appreciable increase until the temperature falls below -15°c. The existence of these two threshold temperatures appears to be associated with the orientation of the prism plane of ice on the (100) face of V_2O_5 at the higher temperature, and the orientation of the basal ice plane on the (001) face at the lower temperature.

In attempting to relate the nucleating ability to some physical property of the particles, it is natural to compare their crystal structures with that of ice. In previous discussions, considerable emphasis has been laid on the fact that the most effective nucleators, e.g. silver iodide, lead iodide, and cupric sulphide, are all hexagonal crystals with atomic spacings in the basal plane very similar to those in ice.

The present work shows that a number of non-hexagonal crystals are also potent nucleators but for all those active at temperatures above -15°c it is possible to find a low index face on which the atomic spacings differ from those of ice by not

more than a few per cent. If, in calculating the minimum misfit, one permits the matching of atomic rows in the ice and substrate lattices in ratios of up to 3 : 1, the values shown in heavy type in table 4 are the misfits in the two most favoured of the three mutually perpendicular directions, $(1\bar{2}10)$, $(10\bar{1}0)$, (0001), of the ice lattice. Although epitaxy is usually discussed in terms of the misfit in only the most favourable direction, it seems reasonable to regard the formation of two dimensional nuclei in terms of the misfits in two mutually perpendicular directions in the manner of Pashley (1956). And, because the nucleation of ice crystals usually occurs at steps on the substrate surface (Bryant, Hallett and Mason 1960), the misfit in the third mutually perpendicular direction may also be relevant and therefore all three misfits are listed in table 4. In the case of the simple inorganic structures, a reasonable correlation appears to exist between the threshold nucleation temperature (which enters explicitly into the expression for the critical radius of the ice nucleus) and the sum of the misfits in the three mutually perpendicular directions. A much poorer correlation obtains for the metallic oxides. Thus it appears that ice-nucleating ability of a crystalline substrate is only partly determined by geometrical factors.

§ 7. Effect of Supersaturation on the Activity of Ice Nuclei

It has long been argued whether nuclei can form ice crystals by the direct deposition (sublimation) of ice from the vapour phase or whether the vapour condenses first as a liquid which subsequently freezes. In order to avoid the difficulties of drawing a sharp theoretical distinction between these two possibilities when an adsorbed water layer, perhaps only a few molecules thick, is initially involved, it has become the practice to define, empirically, a *sublimation nucleus* as one which produces an ice crystal in an atmosphere super-saturated relative to ice but sub-saturated relative to liquid water, and to designate it as a *freezing nucleus* if it becomes active only when the air is cooled below the dew point. But such a distinction is not entirely satisfactory because it may be sufficient for the liquid to exist either as a thin film, which the nucleus may acquire at relative humidities below 100 per cent if its surface is hygroscopic or otherwise suitable for multi-layer adsorption, or to form in the pores of the particle by capillary condensation.

In any case, the few available experimental data on the supersaturation conditions necessary for nucleation are conflicting. While Fournier d'Albe (1949) and Mossop (1956) using expansion-cloud chambers, and Weickmann (1947) condensing water on to nuclei supported on a chilled metal plate, claimed that the great majority of ice nuclei act only if the air is cooled to the dew point and in the presence of liquid water, Schaefer (1954) reported that particles of silver and lead iodides act as 'sublimation' nuclei in a sub-water-saturated atmosphere at temperatures lower than about $-5\,^{\circ}$C, and a similar behaviour was observed by Mason and Hallett (1957) for iodine at temperatures below $-15\,^{\circ}$C. Furthermore, Birstein (1954) claims to have observed ice crystals within one minute of introducing powdered silver iodide into a cold chamber with ice-coated walls and with no water cloud present.

However, no detailed measurements have been made to determine, as a function of temperature, the minimum supersaturations required to activate ice nuclei, and it was to fill this gap that the following experiments were performed. The nuclei were introduced into a diffusion-cloud chamber of the type described

Table 4. Data on Substances Active as Ice Nuclei at Temperatures above −16 c

Substance	Crystal symmetry	Lattice constants (A) a	b	c	Substrate plane	% Misfit between substrate and ice lattice in directions: $(1\bar{2}10)$	$(10\bar{1}0)$	(0001)	Threshold temp. (°C)
Ice	Hex.	4·52		7·36					
					(*a*) Insoluble substances				
AgI	Hex.	4·58		7·49	(0001)	$+\mathbf{1{\cdot}3}_{(1:1)}$	$+\mathbf{1{\cdot}3}_{(1:1)}$	$+1{\cdot}8_{(1:1)}$	−4
CuS	Hex.	3·80		16·43	(0001)	$-2{\cdot}8_{(3:2)}$	$+2{\cdot}8_{(1:2)}$	$+11{\cdot}5_{(2:1)}$	−6
HgI_2	Tetrag.	4·36	4·36	12·34	(001)	$-3{\cdot}5_{(1:1)}$	$+\mathbf{11{\cdot}5}_{(1:2)}$	$-16{\cdot}2_{(2:1)}$	−8
	O. Rhombic	4·67	13·76	7·32	(010)	$+3{\cdot}3_{(1:1)}$	$-6{\cdot}4_{(1:1)}$	$-6{\cdot}5_{(2:1)}$	
Ag_2S	Monoclinic $\beta=55°$	4·20	6·93	9·50	(010)	$-7{\cdot}1_{(1:1)}$	$-0{\cdot}3_{(1:1)}$	$-5{\cdot}9_{(1:1)}$	−8
Ag_2O	Cubic	4·72			(001)	$+\mathbf{4{\cdot}4}_{(1:1)}$	$-9{\cdot}5_{(2:3)}$	$-\mathbf{3{\cdot}8}_{(2:3)}$	**−11** (prisms)
					(*b*) Soluble substances				
PbI_2	Hex.	4·54		6·86	(0001)	$+\mathbf{0{\cdot}4}_{(1:1)}$	$+\mathbf{0{\cdot}4}_{(1:1)}$	$+6{\cdot}8_{(1:1)}$	−6
NH_4F	Hex.	4·39		7·02	(0001)	$-2{\cdot}9_{(1:1)}$	$-2{\cdot}9_{(1:1)}$	$-4{\cdot}6_{(1:1)}$	−9
V_2O_5	O. Rhombic	11·48	4·36	3·55	(100)	$-3{\cdot}5_{(1:1)}$	$-2{\cdot}1_{(3:2)}$	$-\mathbf{3{\cdot}5}_{(1:2)}$	−10 (prisms)
					(001)	$-3{\cdot}5_{(1:1)}$	$-\mathbf{2{\cdot}1}_{(3:2)}$	$-3{\cdot}5_{(1:2)}$	−15 (plates)
CdI_2	Hex.	4·24		6·84	(0001)	$-6{\cdot}2_{(1:1)}$	$-6{\cdot}2_{(1:1)}$	$-7{\cdot}1_{(1:1)}$	−12
I_2	O. Rhombic	4·78	7·25	9·77	(001)	$+\mathbf{5{\cdot}8}_{(1:1)}$	$-16{\cdot}3_{(3:2)}$	$-\mathbf{1{\cdot}5}_{(1:1)}$	**−12 (prisms)**
						$+\mathbf{5{\cdot}8}_{(1:1)}$	$-7{\cdot}3_{(1:1)}$	$-11{\cdot}6_{(3:2)}$	**−14 (plates)**
					(*c*) Metallic Oxides				
Cu_2O	Cubic	4·25			(100)	$-\mathbf{6{\cdot}0}_{(1:1)}$	$+\mathbf{8{\cdot}7}_{(1:2)}$	$+15{\cdot}5_{(1:2)}$	−6
CuO	Monoclinic $\alpha=99°$	4·65	3·41	5·11	(001)	$+2{\cdot}9_{(1:1)}$		$-\mathbf{7{\cdot}35}_{(1:2)}$	**−7 (prisms)**
					(010)	$+2{\cdot}9_{(1:1)}$	$-2{\cdot}0_{(2:3)}$		**(plates)**
SnO_2	Tetrag.	4·72	4·72	3·16	(001)	$+\mathbf{4{\cdot}4}_{(1:1)}$	$-14{\cdot}2_{(1:2)}$	$-\mathbf{3{\cdot}8}_{(2:3)}$	−8
α–Al_2O_3	Rhombohed.	5·13	$\alpha=\beta=\gamma=55°6'$		Any face	$+\mathbf{13{\cdot}5}_{(1:1)}$	$+\mathbf{7{\cdot}7}_{(1:2)}$		−8
Mn_3O_4	Tetrag.	5·75	5·75	9·42	(100)	$+\mathbf{4{\cdot}2}_{(2:1)}$	$+\mathbf{10{\cdot}3}_{(2:3)}$	$+17{\cdot}2_{(2:3)}$	−8
CdO	Cubic	4·69			(100)	$+\mathbf{3{\cdot}8}_{(1:1)}$	$-10{\cdot}0_{(2:3)}$	$-\mathbf{4{\cdot}4}_{(2:3)}$	−9
NiO	Cubic	4·17			(100)	$-\mathbf{7{\cdot}7}_{(1:1)}$	$+\mathbf{6{\cdot}6}_{(1:2)}$	$+13{\cdot}3_{(1:2)}$	**−11**

by Hallett and Mason (1958). The chamber, cooled at the bottom by dry ice and with its top at room temperature, encloses a thermally stratified, convectively stable atmosphere in which steady-state conditions are readily achieved. Inside the chamber are suspended two horizontal, plane-parallel sheets of ice facing one another. Water vapour from the upper, warmer plate diffuses downwards through the chamber towards the lower, colder plate, the supersaturation regime in between being largely determined by the temperatures of the source and sink, the position and vertical separation of which can be varied. If the chamber is sealed and left for some hours, the atmospheric aerosols, having become centres of condensation, are progressively removed by sedimentation, leaving clean particle-free air. Under these conditions the profile of water-vapour concentration between the plates can be computed knowing the temperatures of the source and sink; the temperature profile being measured with a thermocouple, the supersaturation of the air at any level can then be calculated (see Hallett and Mason 1958).

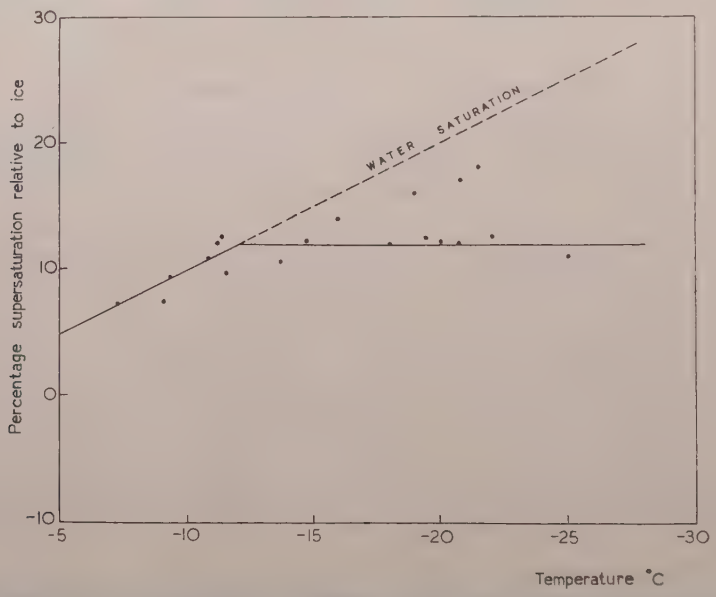

The temperature and supersaturation conditions under which silver iodide smoke produces ice crystals in a diffusion-cloud chamber. The dots represent conditions under which ice crystals were observed.

The chamber having reached equilibrium, with the temperatures of the two ice plates adjusted to produce the required temperature and supersaturation profiles, a small quantity of the silver-iodide smoke, produced by heating the pure crystals on a nichrome wire in a dry nitrogen atmosphere, was introduced and allowed to enter the space between the ice plates through a small hole in the upper plate. The level at which ice crystals were first observed glittering in an intense beam from a mercury arc lamp was noted and the temperature at this level measured. Similar observations were made for differing conditions between the plates and the results plotted on a temperature–supersaturation diagram, as shown in the figure, where the indicated temperatures are in error by not more than $\pm \frac{1}{2}$°C and the corresponding error in supersaturation is not more than $\pm 2\%$.

These data show clearly that, at temperatures below -12°C, silver iodide can initiate ice-crystal formation in an atmosphere subsaturated relative to

liquid water provided that the supersaturation with respect to ice exceeds a critical value of 12%. At temperatures between -5°c and -12°c, however, the air has to become water saturated before ice crystals appear; this may be a consequence of the fact that, at temperatures above -12 °c, the critical supersaturation of 12% cannot be reached without passing water saturation as indicated by the dashed line in the figure. The fact that ice crystals appear in the absence of visible water droplets suggests that, for the silver iodide nuclei to act, it is not necessary for them to enter, or to be captured by, pre-existing supercooled droplets but rather that the adsorption of a thin film of water ($<0{\cdot}1\mu$) is sufficient. An aerosol of lead iodide showed a very similar behaviour but with a critical supersaturation of 15% being required at temperatures below -15°c.

Very similar results have also been obtained by Bryant, Hallett and Mason (1960) from measurements on the critical supersaturations and temperatures required to produce the growth of oriented ice crystals on single crystals of silver iodide, cupric sulphide, lead iodide and cadmium iodide, for which the critical supersaturations are 12, 13, 15 and 22% occurring at -12, -13, -15 and -21°c respectively.

Thus, at temperatures below the critical, the particles just mentioned may be said to act as sublimation nuclei while, at higher temperatures, they apparently first become centres of condensation and act by initiating the freezing of the supercooled water.

The failure to observe nucleation in rapid cloud chamber expansions before reaching water saturation may be attributed to the crystals having insufficient time to grow to visible size during the very short sensitive times of the chambers. Indeed it is interesting to recall that Findeisen (1942), by making a very slow expansion, did observe some atmospheric ice nuclei to become operative *before* water-saturation was reached.

Acknowledgments

This work was carried out as part of the Imperial College Interdepartmental Research Programme on the Physics and Chemistry of Water. The financial support of the Department of Scientific and Industrial Research and The Rockefeller Foundation is gratefully acknowledged.

References

Birstein, S. J., 1954, *U.S.A.A.F., Geophysical Research Directorate, Geophys. Res. Papers*, No. 32.

Birstein, S. J., and Anderson, C. E., 1955, *J. Met.*, **12**, 68.

Bryant, G. W., Hallett, J., and Mason, B. J., 1960, *J. Phys. Chem. Solids*, **12**, in the press.

Findeisen, W., 1942, *Met. Z.*, **59**, 349.

Fournier d'Albe, E. M., 1949, *Quart. J. Roy. Met. Soc.*, **75**, 1.

Fukuta, N., 1958, *J. Met.*, **15**, 17.

Hallett, J., and Mason, B. J., 1958, *Proc. Roy. Soc.* A, **247**, 440.

Hosler, C. L., 1951, *J. Met.*, **8**, 326.

Mason, B. J., and Hallett, J., 1956, *Nature, Lond.*, **177**, 681.

—— 1957, *ibid.*, **179**, 357.

Mossop, S. C., 1956, *Proc. Phys. Soc.* B, **69**, 165.

Pashley, D. W., 1956, *Advanc. Phys.*, **5**, 173.

Pruppacher, H. R., and Sänger, R., 1955, *Z. für angew. Math. und Phys.*, **6**, 407.

Schaefer, V. J., 1954, *J. Met.*, **11**, 417.

Weickmann, H., 1947. *Die Eisphase in der Atmosphäre, Reports and Translations* 716 (Völkenrode), Ministry of Supply, London.

Conduction Processes in Condensed Aromatic Hydrocarbons

By D. C. NORTHROP
Services Electronics Research Laboratory, Baldock, Herts.

MS. received 6th April 1959, in final form 13th July 1959

Abstract. Conductivity has been measured as a function of temperature for evaporated hydrocarbon films and for hermetically sealed single crystal specimens. A model is proposed which explains why the activation energy for conduction corresponds to a spectral region of low absorption. The model is consistent with the exciton theory of fluorescence and photoconductivity. The conduction levels are pictured as being localized in polarized regions of the lattice.

§ 1. Introduction

Although there is now a considerable body of results on conduction in hydrocarbons, the physical processes involved remain obscure. One important feature which makes interpretation difficult is the unexpectedly large variation in conductivity between one specimen and another and between different methods of measurement. Many specimens also exhibit long term drifts in current and non-linear characteristics which might be either real physical properties of the materials, or merely products of the experimental method. The results presented here may be divided into two groups. Firstly, evaporated films are used to determine the characteristics of some of the higher molecular weight hydrocarbons; they exhibit many of the undesirable characteristics mentioned above. The other measurements use single crystal specimens grown from the melt in contact with the electrode system. These are far better behaved than anything previously reported. Although comparatively few compounds can be treated in this way the results are valuable in showing what features of other methods are significant.

§ 2. Experimental

Evaporated films carrying evaporated metal electrodes may be prepared by the method described by Northrop and Simpson (1956 a). Figure 1 is a diagram of the specimen geometry. By placing the upper electrode entirely on the hydrocarbon and earthing the lower electrode it is possible to eliminate both bulk and surface currents in the Pyrex substrate. Electrical contact is made to the specimen whilst it is inside a massive copper container which can be maintained at any temperature between 15 °C and 150 °C by electrical heating. A thermocouple junction in the enclosure measures the specimen temperature. An average specimen is about 10 microns thick, so that a 1·5 volt dry battery produces a field of the order 10^3 volts cm^{-1}. The resulting conduction current is measured using an Ekco 1709 c vibrating reed electrometer having a current sensitivity of 10^{-15} amp.

These specimens exhibit current drifts which may continue for many hours. On applying the field, for example, a period of 24 hours is often required before an equilibrium current is established. A change in specimen temperature of 10°C necessitates waiting about an hour before the current settles down again. There

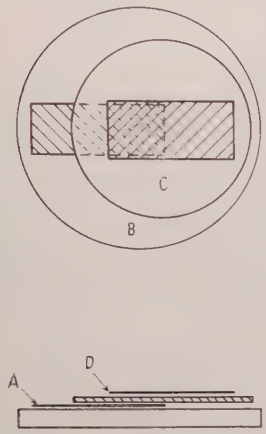

Figure 1. The evaporated conductivity specimen. A, lower electrode; B, Pyrex disc; C, hydrocarbon film; D, upper electrode.

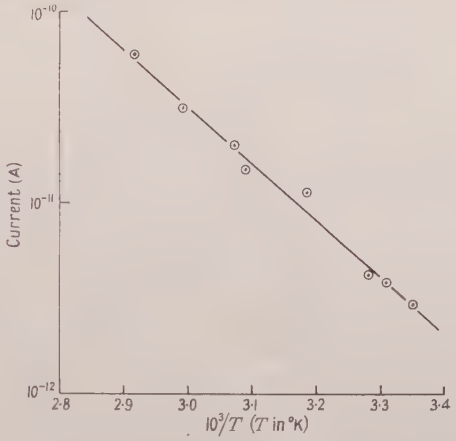

Figure 2. Conductivity of evaporated violanthrene.

is also a permanent change in conductivity on heating the specimen, which is probably due to annealing. Provided each specimen is first cycled to a temperature higher than the maximum used in the measurements, then results are reproducible on successive runs. A typical current–temperature plot is that for violanthrene shown in figure 2. Experimental scatter is low, and the points fit accurately to an equation of the form

$$\sigma = \sigma_0 \exp\left(-\frac{E}{2\boldsymbol{k}T}\right) \qquad \ldots\ldots(1)$$

where σ is the specific conductivity at absolute temperature T, $\boldsymbol{k}$ is Boltzmann's constant, and σ_0 and E are characteristic parameters of the hydrocarbon. Values of E, calculated from the slope of the graph are well reproduced from one specimen to another, lying within the expected experimental error $\pm 5\%$. The same is not true of σ_0 however; currents through apparently identical specimens may differ by as much as two orders of magnitude. Possible reasons for this variation will be given later. It is evident however that this method is not a good one for determining σ_0. In table 1 are listed the values of E found for a number of hydrocarbons and compares with ${}^1E_1$ the first singlet excitation energy of the free molecule taken from the absorption spectra of Clar (1952). Differences between these quantities are tabulated for future reference. The most important feature of the results is the smallness of the values of E. In all cases they are much lower than the energy of the first allowed optical transition, corresponding to spectral regions of low absorption. This behaviour is by no means similar to the inorganic intrinsic semiconductors to which the hydrocarbons have sometimes been compared, and requires an entirely new outlook on the conduction mechanism.

Table 1

Hydrocarbon	E	$^1E_1$	$^1E_1 - E$
Coronene	2·55	3·60	1·05
Ovalene	2·0	2·80	0·8
Violanthrene	1·18	2·48	1·30
Iso-violanthrene	1·20	2·49	1·29
Pyranthrene	1·71	2·67	0·96
Dinaphthopyrene	1·60	2·70	1·10
Hexacene	1·3	—	—

The current drifts and lack of reproducibility of σ_0 values, together with the non-ohmic behaviour observed by some workers (cf. Mette and Pick 1953) raise serious doubts about the interpretation of these experimental data. For this reason a further set of experiments has been undertaken using a different kind of specimen. This consists of a thin film of hydrocarbon crystallized from the melt between two Pyrex or silica flats, each of which carries a transparent (Nesa) electrode. The practical details of their preparation is given by Northrop and Simpson (1958). Figure 3 is an exploded view showing the specimen geometry. Comparatively few compounds can be treated in this way; in fact specimens have been successfully prepared in only five cases, but this is adequate to show what features of the earlier work are true bulk properties of the hydrocarbons.

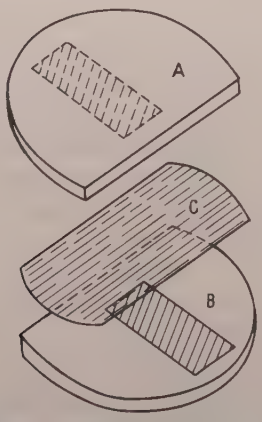

Figure 3. Exploded view of single crystal conductivity specimen. A, upper Pyrex flat with Nesa electrode facing down; B, lower Pyrex flat with Nesa electrode facing up; C, hydrocarbon film.

The general behaviour of the specimens is far more satisfactory. Equilibrium currents are quickly established on changing the temperature or the applied electric field, and moreover the currents are reproducible from one specimen to another. Conduction is strictly ohmic up to fields of about 10^5 volts cm^{-1}, as is illustrated by the current–voltage plot for anthracene shown in figure 4. The detailed results for the five compounds are shown in figure 5, from which it is immediately obvious that equation (1) is obeyed. Table 2 is an analysis of these curves. The deduced values of E and σ_0 are compared with those determined earlier for evaporated films of the same materials (Northrop and Simpson 1956 a). Also given are the molecular singlet energy $^1E_1$ and the difference between this and activation energy E.

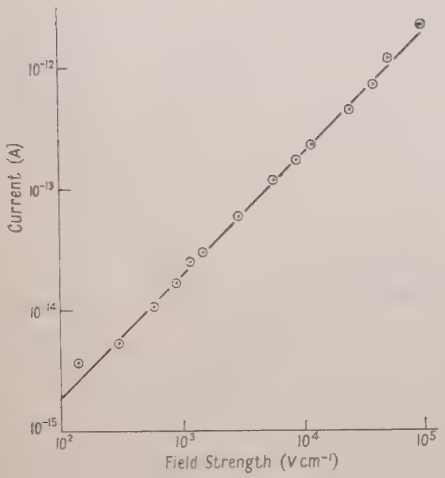

Figure 4. Current voltage characteristic for anthracene; single crystal specimen.

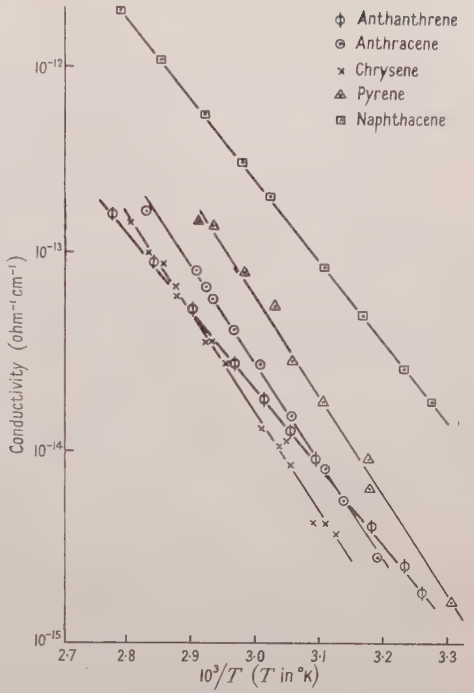

Figure 5. Conductivity of single crystal films.

Table 2. Comparison between Evaporated and Single Crystal Films

Compound	Evaporated films		Single crystal films			
	E (ev)	σ_0(ohm^{-1} cm^{-1})	E (ev)	σ_0(ohm^{-1} cm^{-1})	$^1E_1$ (ev)	$^1E_1 - E$ (ev)
Anthracene	1·93	2×10^{-2}	1·95	1·6	3·30	1·35
Anthanthrene	1·60	1×10^{-4}	1·58	0·5	2·85	1·27
Chrysene	2·20	4×10^{-1}	2·04	13·0	3·87	1·83
Naphthacene	1·70	5×10^{-1}	1·64	0·2	2·61	0·97
Pyrene	2·02	1	2·06	69	3·70	1·64

The obvious deductions to be made at this stage are (i) the normal behaviour of hydrocarbon crystals is ohmic with short electrical time constants; (ii) the activation energies derived for evaporated films are in close agreement with those found for single crystal films. Both are presumably physically significant; (iii) specific conductivities determined for evaporated films are too low. Since those of single crystal films are reproducible within experimental error it is assumed they are correct.

Discussion of the experimental results is based on these three conclusions.

It is suggested that the main practical difficulty is one of making contact to the specimen. The evaporated lead electrodes may have an effective area of contact much smaller than their apparent dimensions. This would lead to low values of the specific conductivity if the apparent dimensions were used. Results

would not be reproducible because the actual dimensions do not bear a fixed relation to the apparent ones. A second consequence of low contact areas would be high local current densities. The long time necessary to establish a steady current could therefore be due to an ageing process of some kind. Single crystal films apparently give a good area contact.

§ 3. The Conduction Model

The conductivity of the hydrocarbons has been observed under equilibrium conditions and has been shown to be ohmic, so that the parameter E derived from these data using equation (1) must be the energy gap between the ground state and the conduction state of the crystal. Figure 6 is a schematic energy level diagram showing the conduction level in relation to the lowest optical excited

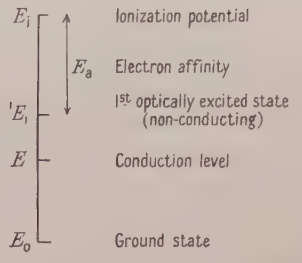

Figure 6. Energy level diagram.

state $^1E_1$ and the ionization potential E_i of a hydrocarbon molecule in the environment of its crystal lattice. As would be expected for a weakly bound molecular crystal the optically excited levels of the crystal are similar to those of the constituent molecules, being only slightly perturbed by the crystal bonding energy. E_i and $^1E_1$ have exact counterparts in the molecular energy level scheme, but the conduction level E does not derive in any obvious way from this scheme. In addition the first optical transition $^1E_1$ has been shown to lead to a non-conducting exciton state (Northrop and Simpson 1956b, Simpson 1956). Any successful model of the dark-conduction process must therefore be capable of explaining (*a*) how the conduction state is related to the optically excited states of the crystal, (*b*) why the exciton state $^1E_1$ does not decay to the conduction state E by a monomolecular process: the transition is clearly possible energetically. The following is an attempt to derive such a model from general consideration of the (one-electron) energy states E_i and $^1E_1$, and the properties of the lattice.

The energy required to remove an electron from one neutral molecule in the ground state and to place it on another some distance away is $E_i - E_a$, where E_a is the electron affinity. The lattice around the positive and negative ions so produced will now relax to a new minimum energy configuration and in so doing will lower the total energy of the system by E_p. If the charges are now supposed free to move the activation energy for conduction is given by

$$E = E_i - E_a - E_p. \qquad \ldots\ldots (2)$$

It can be seen from figure 6 that the ionization potential, the electron affinity and the first optical excitation energy are related by the equation

$$E_i - E_a = {}^1E_1. \qquad \ldots\ldots (3)$$

Combining equations (2) and (3) gives

$$E_p = {}^1E_1 - E. \qquad \ldots\ldots (4)$$

This is the quantity tabulated in the final columns of tables 1 and 2 which takes a range of values between about 1 and 2 electron volts for the hydrocarbons under investigation. The polarizability of a hydrocarbon crystal is expected to be quite large (Pople 1957, private communication) so that the experimental values for E_p are not unreasonable. The charge carriers are therefore polarons; under the action of an externally applied field both positive and negative charges can move, each taking its polarization with it. Low mobilities are to be expected, and this is borne out by the estimate of $5 \times 10^{-3}\,\mathrm{cm^2\,volt^{-1}\,sec^{-1}}$ made from observations of photoconductivity (Northrop and Simpson 1958).

Because of the lattice polarization associated with each charge carrier, direct optical excitation to such a conducting state is unlikely. Monomolecular decay of the optically excited levels such as ${}^1E_1$ to the conducting state is equally unlikely, because the lifetime of the optical states ($\sim 10^{-8}$ second) is not large enough to allow the required degree of polarization to be built up thermally. There is in fact a potential barrier between the two levels which is much greater than $\boldsymbol{k}T$.

Northrop and Simpson (1958) showed that although the first excited state ${}^1E_1$ is a non-conducting absorption in the fundamental band, it is nevertheless accompanied by weak photoconductivity. They also proved quantitatively that this is consistent with random encounters between mobile excitons resulting in ionization. In other words the energy made available by one excited molecule is sufficient to release an electron over the potential barrier around a second excited molecule.

No attempt has been made to include in this description the behaviour of impurities in influencing conductivity. The above model does not lead one to expect any correlation between activation energies for conduction and any energy gap in the hydrocarbon molecule. Earlier work has shown however that the energy required to liberate charge carriers from impurity molecules is closely correlated with the lowest triplet excited state of these molecules (Northrop and Simpson 1956 a). This is not entirely surprising since impurity molecules are known to behave in many ways like isolated centres in a neutral matrix. It is not clear how the impurity triplet level couples to the lattice to produce free charge carriers, although ionization of the triplet state is more probable than that of the singlet because of its much longer lifetime.

Acknowledgments

The author warmly thanks Dr. O. Simpson for his encouragement and helpful criticism. Acknowledgment is made to the Admiralty for permission to publish this paper.

References

Clar, E., 1952, *Aromatische Kohlenwasserstoffe*, 2nd edn (Berlin: Springer).
Mette, H., and Pick, H., 1953, *Z. Phys.*, **134**, 566.
Northrop, D. C., and Simpson, O., 1956 a, *Proc. Roy. Soc.* A, **234**, 124.
—— 1956 b, *Ibid.* A, **234**, 136.
—— 1958, *Ibid.* A, **244**, 377.
Simpson, O., 1956, *Proc. Roy. Soc.* A, **238**, 402.

The Angular Distribution of some Proton Groups from the Reaction $^{16}O(^3He, p)^{18}F$

By S. HINDS and R. MIDDLETON
Atomic Weapons Research Establishment, Aldermaston, Berks.

Communicated by K. W. Allen; MS. received 16th June 1959, in final form 22nd July 1959

Abstract. The angular distribution of five proton groups from the reaction $^{16}O(^3He, p)^{18}F$ have been measured at incident energies of 5·9 and 9·16 MeV. An attempt has been made to explain the observations by a double stripping process and some tentative spin and parity assignments have been made.

§ 1. Introduction

A considerable amount of experimental work has been directed at ^{18}F since the publication of the independent particle model calculations of Elliott and Flowers (1955) and the collective model calculations of Redlich (1958).

The energy levels of ^{18}F are now well established. The energies of the first twelve excited states have been determined by Rao, Young, Spencer, Beckner and Phillips (1959) from the magnetic analysis of the protons from the $^{16}O(^3He, p)^{18}F$ reaction. More recently Hinds and Middleton (1959a), also using magnetic analysis, have measured the energies of 40 states from the reactions $^{16}O(^3He, p)^{18}F$ and $^{19}F(^3He, \alpha)^{18}F$. These values have been used in the present paper and are slightly different from the preliminary values communicated to Ajzenberg-Selove and Lauritsen (1959).

Until recently, little was known of the properties of the states, primarily because there are few convenient reactions from which they could be determined. There is no convenient deuteron stripping reaction leading to ^{18}F from which at least parities could be deduced. However, there are two inverse stripping reactions which might prove useful, namely $^{19}F(p, d)^{18}F$ and $^{19}F(d, t)^{18}F$. These have been investigated by Bennett (1958) and El-Bedewi and Hussein (1957) respectively, but in neither case was it possible to resolve the multiplet of states occurring at about 1 MeV.

The $^{20}Ne(d, \alpha)^{18}F$ reaction is also of particular interest since as only $T=0$ levels will be strongly excited, the $T=1$ levels may be deduced by comparing the energy spectrum with that from the $^{16}O(^3He, p)^{18}F$ reaction. However, the necessity for using a gas target has prevented high resolution studies and Middleton and Tai (1951) report only one group of α-particles corresponding to a state at $1{\cdot}05 \pm 0{\cdot}03$ MeV.

The most useful data concerning the low-lying states of ^{18}F have come from measurements made on the γ-rays from the reactions $^{14}N(\alpha, \gamma)^{18}F$ and $^{16}O(^3He, p\gamma)^{18}F$ (Kuehner, Almqvist and Bromley 1958, Allen, Eccleshall and Yates 1959). A summary of these results is presented in figure 3.

In this communication are reported the results of angular distribution measurements made on five proton groups from the reaction $^{16}O(^3He, p)^{18}F$

at incident energies of 5·9 and 9·16 MeV. Following the course of a previous communication on the $^9Be(^3He, p)^{11}B$ reaction (Hinds and Middleton 1959 b), an attempt has been made to interpret the results on the basis of a double stripping reaction mechanism. Spin and parity assignments have been made and although these remain consistent with the theoretical predictions of Elliott and Flowers, they are at slight variance with the results of Kuehner *et al.*

§ 2. Experimental Procedure

The Aldermaston Van de Graaff generator has been used on several occasions to accelerate singly charged ^3He particles to energies of about 6 MeV. Recently the yield of doubly charged particles has been considerably increased by inserting a gas stripper a short way down the accelerating tube. With this arrangement, which will be described in detail at a later date, analysed beams of about 0·5 μA at energies up to 10·2 MeV have been obtained. The results reported in this communication at an incident energy of 9·16 MeV were obtained using the doubly charged beam from the gas stripper.

The targets were prepared by evaporating pure silica and consisted of self-supporting films of about 30 to 40 $\mu g\,cm^{-2}$. To prevent the accumulation of electrostatic charge on the target, a thin film of gold was evaporated on one surface to provide a conducting layer. The proton energy spectra were measured with the broad-range magnetic spectrograph described in a previous article (Hinds and Middleton 1959 b). Several exposures were made at angles ranging from $7\frac{1}{2}°$ to 118° at bombarding energies of 5·9 and 9·16 MeV, the target remaining fixed and inclined at an angle of 45° to the incident beam. Relative exposure strengths were measured by integrating the total beam passing through the target and into a Faraday cup. A check was maintained on the stability of the target during bombardment by counting with a scintillation counter the protons emitted at 90° from the $^{16}O(^3He, p)^{18}F$ reaction. Exposure strengths were adjusted according to target thickness and were within the range 100 to 500 microcoulombs.

§ 3. Results

The angular distributions of four proton groups from the $^{16}O(^3He, p)^{18}F$ reaction measured at incident energies of 5·9 and 9·16 MeV are shown in figure 1. All angular distributions at a given bombarding energy are correctly normalized, but relative magnitudes at different energies are not preserved. Similar measurements have also been made by the authors at an incident energy of 5·7 MeV but extending only to an angle of 70°. These results were very similar to those obtained at 5·9 MeV and were briefly reported at the Paris Nuclear Physics Conference 1958.

The proton group corresponding to the 1·076 MeV state was very weak and it was difficult to distinguish it from spurious groups from the $^{28}Si(^3He, p)^{30}P$ reaction. However, tentative angular distributions were obtained and are shown in figure 2. The arbitrary units of cross section are similar to those used in figure 1.

The curves shown in figure 1 were calculated from an approximate expression for a double stripping process derived by H. C. Newns (to be published, see also Hinds and Middleton 1959 b) viz.

$$\sigma(\theta) \propto \left(\exp \frac{-K^2}{4\gamma^2}\right) \sum_L |A(L) j_L(ka)|^2.$$

The exponential factor depends upon the internal motion of the ^3He particle and

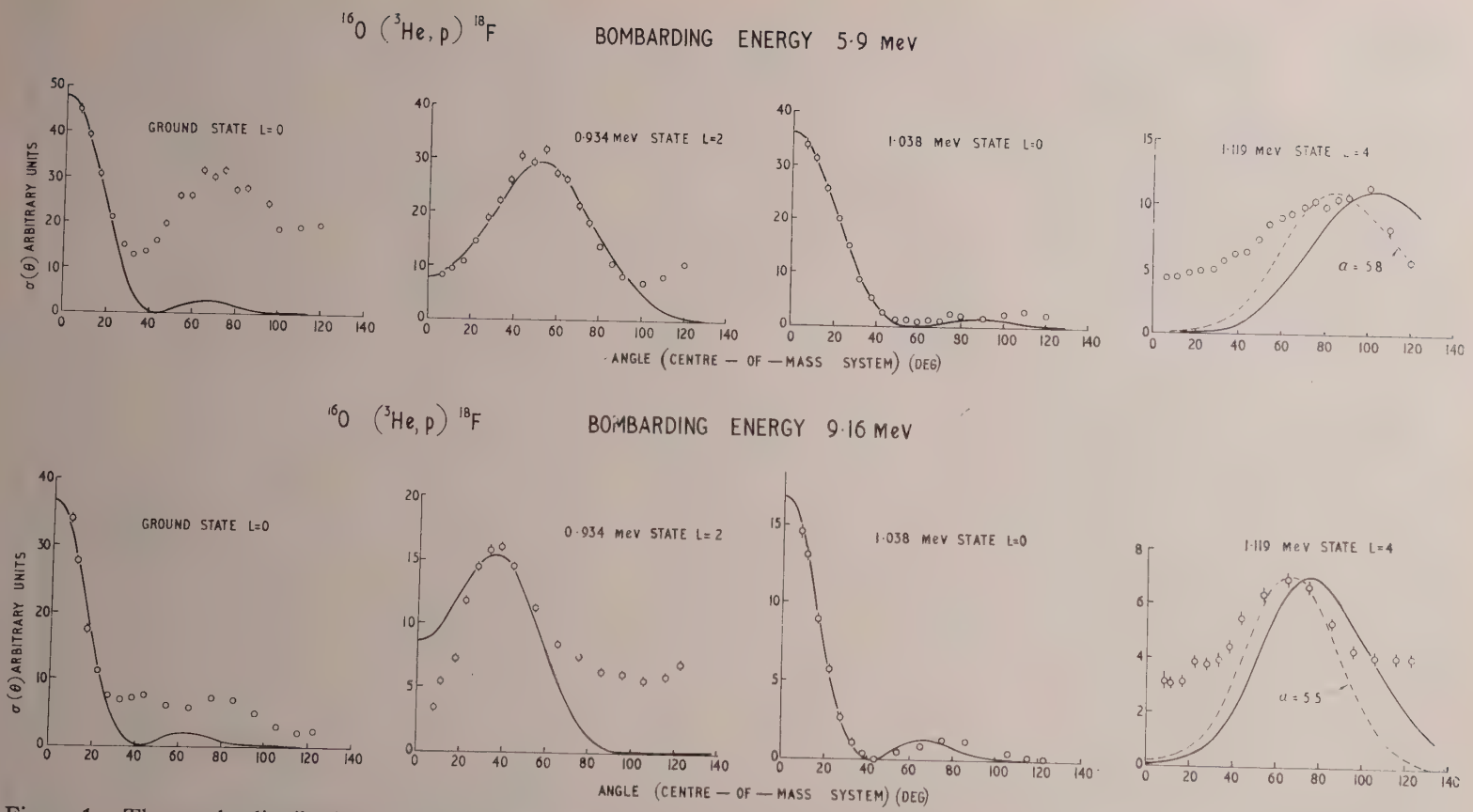
^{16}O (^{3}He, p) ^{18}F BOMBARDING ENERGY 5·9 Mev
GROUND STATE L=0
0·934 Mev STATE L=2
1·038 Mev STATE L=0
1·119 Mev STATE L=4
a = 5·8
σ(θ) ARBITRARY UNITS
ANGLE (CENTRE — OF — MASS SYSTEM) (DEG)
^{16}O (^{3}He, p) ^{18}F BOMBARDING ENERGY 9·16 Mev
GROUND STATE L=0
0·934 Mev STATE L=2
1·038 Mev STATE L=0
1·119 Mev STATE L=4
a = 5·5
σ(θ) ARBITRARY UNITS
ANGLE (CENTRE — OF — MASS SYSTEM) (DEG)

Figure 1. The angular distributions of four proton groups from the reaction $^{16}O(^{3}He, p)^{18}F$ measured at incident energies of 5·9 and 9·16 Mev. The curves have been calculated from a double stripping theory.

is analogous to the $G(K)$ factor encountered in deuteron stripping. It has little effect on the shape of the angular distribution which is mainly determined by the spherical Bessel function $j_L(ka)$. Unlike deuteron stripping, for a zero spin initial nucleus, two values of L are allowed by the selection rules. However, the contribution from one value is generally negligible, but this depends upon the configuration of the final state.

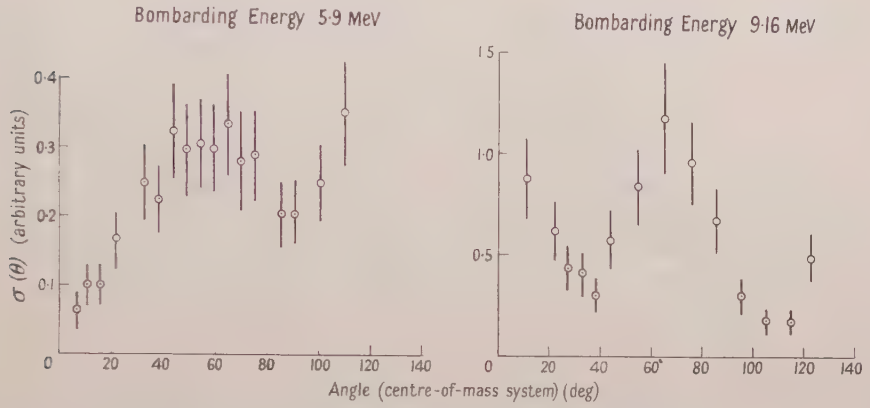

Figure 2. The angular distribution of the proton group corresponding to the 1·076 MeV excited state of ^{18}F, measured at bombarding energies of 5·9 and 9·16 MeV.

The radius of interaction a was chosen to give best agreement and except where otherwise indicated was equal to 4·8 fermi, which is the Gamow radius, i.e. $1{\cdot}7 + 1{\cdot}22A^{1/3}$ fermi. It will be noticed that slightly increased radii had to be used to fit the $L = 4$ curves to the 1·119 MeV state angular distributions. Although agreement could be obtained with $L = 3$ and a smaller radius, the former L-value is preferred since there is evidence that the 1·119 MeV state has even parity. Allen, Eccleshall and Yates (1959) have observed an E2 γ-ray transition between the 1·119 and 0·934 MeV states and there is evidence that the latter has even parity (Kuehner *et al.* 1958).

§ 4. Discussion

The L-value assignments obtained on the assumption of a double stripping process are shown in figure 3, together with the parities and possible spins, J_f^a. It may be noted that since the ground state of ^{18}F is known to have spin 1^+, $L = 2$ is allowed by the selection rules in addition to $L = 0$. At 5·9 MeV the ground state angular distribution exhibits a strong secondary maximum at about 70° which can be fitted with an $L = 2$ component, although a small radius must be used. However, calculations by Newns (private communication) using the Elliott and Flowers wave function for the ground state of ^{18}F indicate that the intensity of the $L = 2$ component should be negligible and probably undetectable. This is consistent with our observations at 9·16 MeV, where there is little evidence of a secondary maximum. A possible explanation of the secondary maximum observed at 5·9 MeV is that it arises from interference between the direct and compound nucleus contributions. This might be expected to occur in a ^3He reaction with oxygen since the binding energy of the ^3He particle in the compound nucleus ^{19}Ne is 8 MeV, which is unusually low.

In figure 3 the possible spins of the 0·934 MeV states are shown as 1, 2 or 3^+. It may be reasoned that since no $L=0$ component was observed, the 1^+ assignment is inadmissible. Since an $L=0$ transition is intrinsically much stronger than an $L=2$ transition, this is a more sensitive test than the case of the ground state. Similar reasoning can be used to exclude the 3^+ assignment for the 1·119 MeV state.

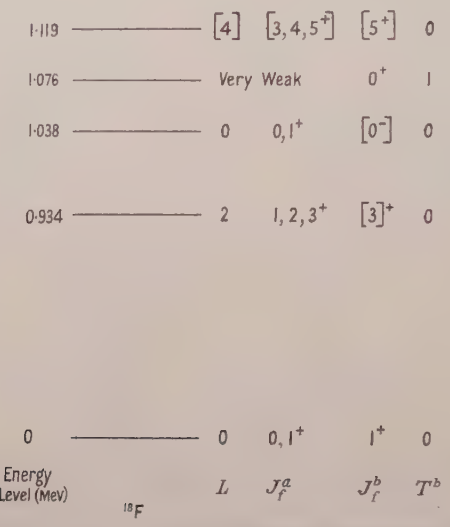

Figure 3. Energy levels of ^{18}F. L orbital angular momentum from double stripping, $J_f{}^a$ spin and parity predictions from double stripping, $J_f{}^b$ spins and parities from Kuehner *et al.*, T^b isotopic spin from Kuehner *et al.*

The spins, parities and isotopic spins obtained by Kuehner *et al.* from an investigation of the γ-rays accompanying the ^{16}O(^{3}He, p)^{18}F and ^{14}N + α reactions are shown in columns $J_f{}^b$ and T^b of figure 3. It is apparent that there is disagreement concerning the parity of the 1·038 MeV state. Also, since the 0^+ state may be identified with the first $T=1$ state, the present investigation would indicate that the 1·038 MeV state has $T=1$ rather than the 1·076 MeV state reported by Kuehner *et al.*

The extremely weak transition to the 1·076 MeV state observed in the present investigation is consistent with this state having odd parity and probably arises from excitation of the ^{16}O core. Such a configuration cannot be excited by a stripping process and consequently the transition to it would be expected to be very weak. It is not particularly surprising for such a configuration to occur at 1 MeV excitation in ^{18}F since a state of similar configuration is thought to occur in ^{19}F at 112 kev (Elliott and Flowers 1955).

The available evidence concerning the low-lying even parity state of ^{18}F, indicates that the 3^+ and 5^+ states predicted by Elliott and Flowers are those at 0·934 MeV and 1·119 MeV excitations respectively. The identification of the 0^+, $T=1$ state is in doubt but it is certainly either the 1·038 MeV or 1·076 MeV excited states. This uncertainty may be resolved from an investigation of the ^{20}Ne(d, α)^{18}F reaction which will strongly excite only the $T=0$ states.

Acknowledgments

We would like to thank Dr. K. W. Allen for his continued interest and advice and for his many suggestions concerning the installation of the gas stripper

We are also indebted to Mr. V. Shepherd and Dr. A. C. Rivière for their invaluable assistance in the latter project. Our thanks are also due to Dr. H. C. Newns for communicating the results of his work on the double stripping process prior to publication and to Mr. D. A. Procter and Mr. H. Marchant for assisting with the exposures.

References

Ajzenberg-Selove, F., and Lauritsen, T., 1959, *Nucl. Phys.*, **11,** 1.
Allen, K. W., Eccleshall, D., and Yates, M. J. L., 1959, *Proc. Phys. Soc.*, **74,** 660.
Bennett, E. F., 1958, *Bull. Amer. Phys. Soc.*, [II], **3,** 26.
El-Bedewi, F. A., and Hussein, I., 1957, *Proc. Phys. Soc.* A, **70,** 233.
Elliott, J. P., and Flowers, B. H., 1955, *Proc. Roy. Soc.* A, **229,** 536.
Hinds, S., and Middleton, R., 1959 a, *Proc. Phys. Soc.*, **73,** 721.
—— 1959 b, *Ibid.*, **74,** 196.
Kuehner, J. A., Almqvist, E., and Bromley, D. A., 1958, *Phys. Rev. Letters*, **1,** 260.
Middleton, R., and Tai, C. T., 1951, *Proc. Phys. Soc.* A, **64,** 801.
Rao, D. A. A. S. N., Young, T. E., Spencer, R. R., Beckner, E. H., and Phillips, G. C., 1959, *Bull. Amer. Phys. Soc.* [II], **4,** 96.
Redlich, M. G., 1958, *Phys. Rev.*, **110,** 468.

RESEARCH NOTES

The Sintering of Bismuth Telluride

By W. R. GEORGE, R. SHARPLES and J. E. THOMPSON
Nelson Research Laboratories, English Electric Co., Stafford

MS. received 19*th May* 1959, *in revised form* 29*th June* 1959

THE use of bismuth telluride and its alloys for refrigeration has been discussed by a number of authors. Wright *et al.* (1958) have obtained a cooling drop of 65°C using p- and n-type bismuth telluride.

Zone refined material is somewhat fragile, and from the point of view of commercial applications it is preferable to have a more robust bar. One way that has been considered to overcome this difficulty is to use sintered material, and this note records some changes in type that have occurred with p-type bismuth telluride. Changes of type on sintering have been reported already by Birkholz (1958) on certain doped compounds of Bi_2Te_3.

p-type zone refined bismuth telluride was made from bismuth and tellurium (purity 1 in 10^6), with iodine doping, by melting the stoichiometric proportions in a closed evacuated tube and subsequent zone refining. The material was crushed to 100-mesh size and the resulting powder compacted at various pressures. The samples were sintered at temperatures up to the melting point.

The results of the sintering experiments are shown in the figure, where the value of $d\epsilon/dT$ (the thermoelectric power) is plotted against the sintering temperature. The sintering time was constant at 16 hr. The parameter $d\epsilon/dT$ is representative of the basic properties of the sintered bismuth telluride, since

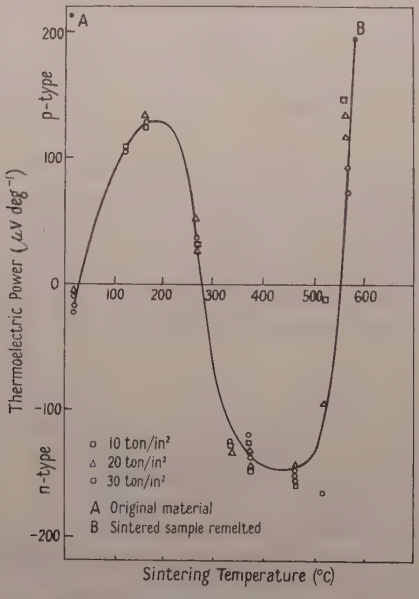

The variation of the thermoelectric power of bismuth telluride with sintering temperature.

it is uninfluenced by porosity and the area of contact between the sintered particles, as is the case with thermal conductivity and electrical resistivity. The first noteworthy point is that the results obtained were repeatable and the second that there is a continuous change in $d\epsilon/dT$. Some slight dependence on the compacting pressure can be observed.

The change of type could not be attributed to loss of one or other component or contaminant pick-up from the gas stream, since the samples were vacuum sealed in quartz tubes before heat treatment. Moreover, the samples were gradually slit down in thickness and the measured values were constant throughout the bar. This is not always the case, when sintering in a gas stream such behaviour can be noted sometimes.

A tentative explanation of the changes in sign can be given. The first change from p-type to n-type on crushing and pressing at room temperature is due to the effects of strain and an increase in dislocation density, which disappears as the sintering temperature is raised. However, before the recovery is complete the sintering process begins to take place at about 150 °C. This sintering process is complex, though one possible mechanism of sintering that has been proposed is of spherical particles in contact being united gradually by diffusion of lattice vacancies from this contact area into the material, and atomic diffusion in the reverse direction to form a bridge joining the particles. The vacancy concentration will be in excess of that due to thermal excitation alone. Cabrera (1950) has considered a similar process in detail and a critical discussion is given on sintering by Bernard (1959). Such an increase in vacancy concentration will result in the material becoming n-type, since the vacancies are thought to act as hole traps. Evidence has been presented by Crawford and Cleland (1954) that in indium antimonide antimony vacancies act as hole traps, whereas an indium vacancy acts as a hole trap in p-material and an electron trap in n-material. At higher temperatures, the sintering process is more complete and vacancies become more mobile and can be eliminated at the surface of the bar or at grain boundaries—as proposed by da Silva (1951) and Barnes (1952). Thus, at higher temperatures, the properties of the sintered material will revert to those of the original refined bismuth telluride, and indeed on melting the reversion is complete. As can be seen from the figure, this later stage only takes place at temperatures close to the melting temperature.

Further work is proceeding on the explanation given here of the change of type by measurements of the variation with temperature of thermoelectric power, thermal conductivity, electrical resistivity and Hall coefficient for the sintered samples. Measurements are also being made on fast neutron irradiated samples from BEPO to determine the energy levels of any vacancy traps and this will be reported in due course.

Acknowledgments

Thanks are expressed to Mr. V. A. Hughes and Dr. R. F. Weil for many helpful discussions, and to Mr. J. K. Brown, Director of Research, for permission to publish this work.

References

Barnes, R. S., 1952, *Phil. Mag.*, **43**, 1221.
Bernard, R. G., 1959, *Powder Metallurgy*, No. 3, 86.
Birkholz, U., 1958, *Z. Naturf.*, **13a**, 180.

Cabrera, N., 1950, *Trans. Amer. Inst. Min. (Metall.) Engrs*, **188**, 677.
Crawford, J. H., and Cleland, J. W., 1954, *Phys. Rev.*, **95**, 1177.
da Silva, L. C., and Mehl, R. F., 1951, *J. Metals*, **3**, 155.
Wright, D. A., Goldsmid, H. J., and Sheard, A. R., 1958, *Brit. J. Appl. Phys.*, **9**, 365.

Heat Transfer by Forced Convection

By D. V. GOGATE and H. S. DESAI
Physics Department, M.S. University of Baroda

MS. received 10*th March* 1959

§ 1. Introduction

This note is concerned with the study of heat interchange between a solid body (metal sphere) and a moving fluid. It is an extension to higher Reynolds numbers of the work described in a previous paper (Gogate, Patil and Desai 1956). The main point that emerges from the present study is that the rate of heat exchange undergoes a relatively sudden change in the region of $(Re) = 10^5$, this being the region where the nature of the flow undergoes a change.

In § 2 a brief description of the apparatus is given and the results are described in § 3. After giving the relation between heat transfer, friction-drag force and the drag coefficient, the values of drag coefficient are exhibited for different Reynolds numbers. The nature of the change of flow for Reynolds numbers in the region of 10^5 is briefly described and its relation to the experimental results described in this note is then discussed in § 4.

§ 2. Experimental Arrangement

The apparatus used in this investigation was a slight modification of that used in the previous experiments (Kapadnis and Gogate 1952, Gogate, Patil and Desai

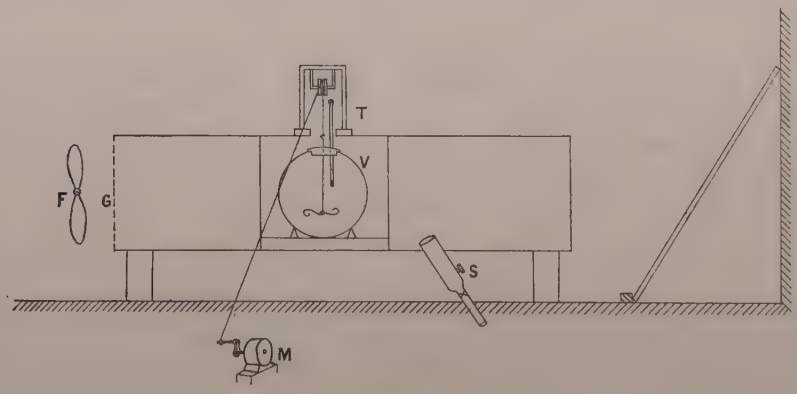

Figure 1.

1956). A spherical copper vessel V (figure 1) containing hot water was placed in a small wind tunnel at a distance of about 34 cm from an electric fan F and a stream of air proceeding from the fan was directed on to this vessel through the wind tunnel

after allowing it to pass through a wire grid G situated at a distance of about 9 cm from the fan. The wind tunnel consisted of a rectangular wooden case 165 cm long with a square cross section 38 cm × 38 cm and open at both ends. The top of the vessel was closed with a lid having two holes in it. Through one hole passed a sensitive thermometer T and through the other a stirrer was kept working up and down by means of a string connected to an eccentric arrangement attached to the shaft of a low speed electric motor. The speed of the air stream could be varied by changing the strength of the current in the circuit of the d.c. fan F and the air velocity was measured by means of a sensitive three cup anemometer. The latter was placed exactly in the place of the vessel V before and after every set of observations for the rate of cooling of the vessel. Special care was taken to avoid reflected air streams from the front wall by using tilted screens at different angles. These screens helped in diffusing and directing upwards the oncoming air streams. The temperature of the water in the vessel was measured by focusing a small telescope S on the vertical thermometer T passing through the lid of the vessel. This procedure eliminated the possibility of affecting the temperature of the vessel by the breath of the observer. The usual precautions were taken to minimize the heat losses due to conduction, radiation and evaporation. Losses due to natural convection were determined separately in still air and all subsequent observations were corrected accordingly.

§ 3. Results

A number of cooling curves were obtained for the vessel using different values of air velocity and the rates of fall of temperature $d\theta/dt$ for different mean temperatures θ were calculated. These values of $d\theta/dt$ were used to calculate the total heat losses by the vessel at different temperatures and air velocities.

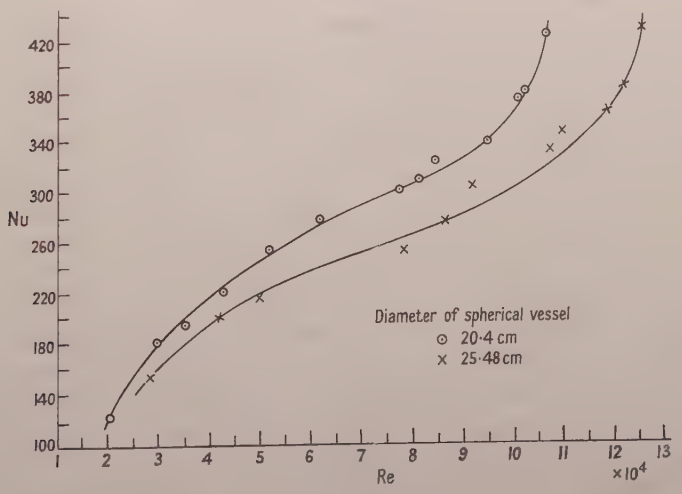

Figure 2.

To study the relation between heat transfer and the velocity of the air stream, a graph was plotted (figure 2) between the dimensionless quantity $Hl/k\Delta\theta$ known as the Nusselt number (Nu) and another dimensionless variable $\rho Vl/\mu$ known as the Reynolds number (Re) where H is the total heat loss due to forced convection, l the linear dimension of the vessel used, k the thermal conductivity of air, $\Delta\theta$ the temperature difference between the vessel and the surroundings, ρ the density and

μ the viscosity of air at the temperature of the experiment. It is clear from figure 2 that for values of (Re) up to nearly 8×10^4, the curve is concave to the (Re) axis but as we approach the value of (Re) near about 10^5, the curve changes its form and becomes convex towards the (Re) axis. This change from concavity to convexity towards the (Re) axis of the curve giving the relation between (Nu) and (Re) has been confirmed by experiments with spheres of different sizes as is evident from the two curves in figure 2. This shows that the convective process of heat exchange undergoes a relatively sudden change near $(\mathrm{Re}) = 10^5$.

§ 4. Discussion

We know that the skin drag-coefficient C_f which is defined in aerodynamics as $2F/\rho V^2$ is given by (Fishendon and Saunders 1952)

$$C_f = \frac{2F}{\rho V^2} = \frac{2HV}{C\theta} \cdot \frac{1}{\rho V^2} = 2\,(\text{Stanton number})$$

where H represents the amount of heat-transfer per second, F is the friction drag force, θ the temperature difference between the surface of the vessel and the main fluid stream, C the specific heat of the fluid at constant pressure, V the velocity of the fluid stream and ρ its density at the temperature of the experiment. In figure 3, we have plotted C_f against the Reynolds number (Re). It will be

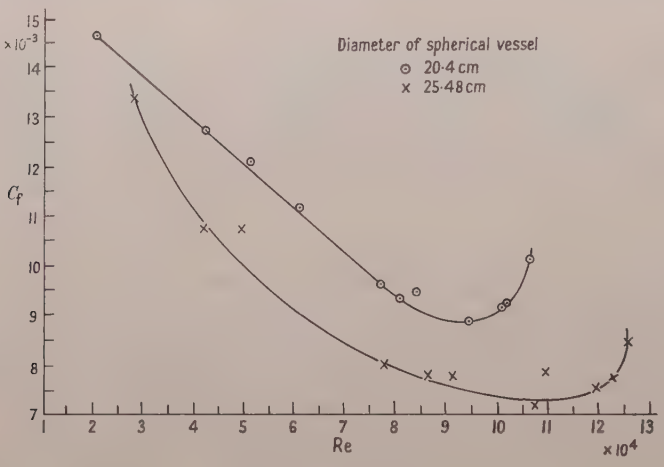

Figure 3.

observed that the value of C_f goes on decreasing rather rapidly with increasing (Re), attains a minimum value for $(\mathrm{Re}) \sim 10^5$ and then it begins to increase again with increasing (Re). This behaviour of C_f as a function of (Re) is associated, as is well known (Goldstein 1938), with a change in the nature of the flow pattern as Re approaches its critical value which is, in general, of the order of 10^5; by the critical value of (Re) we refer to the value for which C_f is minimum. For low Reynolds numbers the flow in the boundary layer is laminar and it changes into turbulent flow when the Reynolds number exceeds the critical value. This value depends, to some extent, on the shape of the body and also on the nature of the surface, i.e. whether it is smooth or rough. Experiments on the direct determination of the drag coefficient of a sphere placed in wind tunnels have shown (Goldstein 1938) that in the case of a sphere the critical Reynolds number is comparable with $(2\text{–}5) \times 10^5$.

We thus find, as is to be expected from the correspondence between the mechanisms of drag and convective heat loss, that the phenomenon of critical (Re) also finds expression in heat exchange through the process of convection. It would be of interest to extend the experiments described in this note to the case of heat exchange between a solid body and a flowing liquid.

ACKNOWLEDGMENT

We are grateful to Prof. D. S. Kothari of Delhi University for helpful discussions.

REFERENCES

FISHENDON, M., and SAUNDERS, O. A., 1950, *An Introduction to Heat Transfer* (Oxford : Clarendon Press).

GOGATE, D. V., PATIL, H. N., and DESAI, H. S., 1956, *J. Maharaja Sayajirao University, Baroda*, **V**, 39.

GOLDSTEIN, S., 1938, *Modern Developments in Fluid Dynamics*, Vol. II, edited by S. Goldstein (Oxford : Clarendon Press).

KAPADNIS, D. G., and GOGATE, D. V., 1952, *Indian J. Phys.*, **24**, 172.

The Effect of the Direction of a Transverse Magnetic Field on the Electronic Component of Ultrasonic Absorption in a Lead Single Crystal

BY L. MACKINNON, A. MYERS AND M. T. TAYLOR

Department of Physics, The University, Leeds

MS. received 29th June 1959

THIS note reports briefly some observations on ultrasonic absorption in a lead single crystal at 4·2°K when a magnetic field was applied perpendicular to the direction of propagation of the ultrasound. Such absorption is electronic in origin and from the results of experimental investigations into it, additional information may be derivable about the electrons in the metal; it is for this reason that the study was undertaken.

Longitudinal and shear sound waves at frequencies between 10 and 70 Mc/s have been propagated in a [100] direction through a lead crystal. Lead has a face-centred cubic structure. Magnetic fields of up to 4690 oersteds have been applied transverse to the direction of the sound, and their orientation relative to the other crystal axes has been varied.

The lead single crystal was grown from spectroscopically standardized lead rods (Johnson, Matthey and Co., Laboratory No. 10596, Catalogue No. J.M.560) of purity greater than 99·995% lead. The orientation was determined by back-reflection Laue X-ray photographs with an accuracy to $\pm 2°$. The technique of ultrasonic observation was substantially that described in an earlier paper (Mackinnon and Myers 1959), differing only in that an improvement in supply voltage stability allowed working without a comparison pulse.

X and Y cut quartz plates, of $\frac{1}{2}$ in. diameter and 10 Mc/s fundamental frequency, were used throughout and operated on odd harmonics as required. In the case of shear waves, the shear vibration direction relative to the lead crystal axes has been varied, the axes of vibration of transmitting and receiving quartz

plates always being parallel to one another. The path distance in the lead crystal was 2·5 cm, longitudinal waves taking 11·3 μsec and shear waves 19·0 μsec to travel this distance.

A representative set of results is shown in the figure; the caption gives the necessary details. Measurements were taken at 10° intervals as the magnet was rotated; there was no evidence of any finer detail in the anisotropy which would have necessitated smaller intervals. Further measurements have been carried out at other frequencies and at lower temperatures (down to 1·2°K). It was found that, in general, the anisotropy becomes less pronounced at lower frequencies and slightly more pronounced at lower temperatures. Changes in the form of the anisotropy have been noted and are consistent with the product of sound wavelength and magnetic field being the relevant variable. These changes include, for example, the appearance of slight minima at magnetic fields lower than those illustrated in the direction of the principal maxima of curves (*c*), and other similar effects.

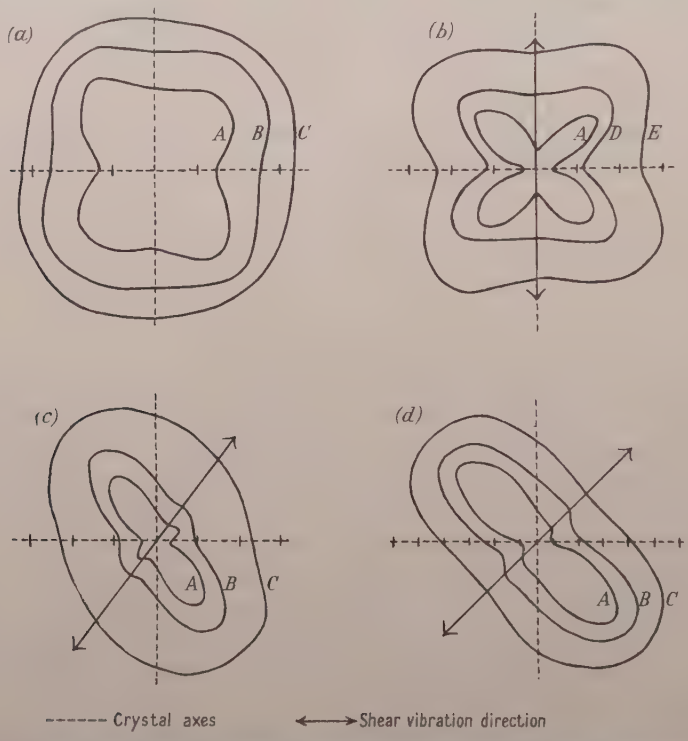

The relative attenuation for an ultrasonic wave plotted radially in the direction of an applied transverse magnetic field for fields of $A = 4690$ Oe, $B = 4030$ Oe, $C = 3060$ Oe, $D = 4315$ Oe and $E = 3560$ Oe. (*a*) longitudinal waves at 69 Mc/s, (*b*), (*c*), (*d*) shear waves at 49 Mc/s. The angles between the shear vibration and cube axes are 0°, 37° and 45° for (*b*), (*c*) and (*d*) respectively. The attenuation units (indicated on the horizontal axes) are 2 dB over 2·3 cm path. A 69 Mc/s longitudinal wave has the same wavelength as a 41 Mc/s shear wave.

The magnetic fields are always greater than the critical field for the superconducting transition. Ideally, the absorption in the superconducting state could be taken as a reference level, but it has not yet been possible to obtain this in every case owing to the effect of frozen-in moments.

When the variation of absorption with magnetic field strength was studied, the absorption in the normal state decreased monotonically for all magnet settings with increasing magnetic field, the absence of oscillations indicating that the electron mean free path could not be much greater than the sound wavelength (Kjeldaas and Holstein 1959). Therefore the anisotropy observed here corresponds to conditions different from those in the observations reported recently by Morse and Gavenda (1959) on longitudinal waves in copper where the electron mean free path was relatively long.

It may be noted that (*a*) the observed anisotropy is rather more marked in all cases when the absorption is low (i.e. in the higher fields), and (*b*) in the case of shear waves there would appear to be two factors controlling the absorption, namely the direction of the magnetic field relative (i) to the crystal axes and (ii) to the shear vibration.

The lack of the expected symmetry in some of these curves is most probably due to slight misalignment in orientation. It is not yet known if there is any rotation of the plane of polarization of the shear waves.

Until the general theory of these effects has been developed more fully, any suggestion as to the kind of information which may be obtainable from these results would be of little value. However, the observations which have so far been made appear to be sufficiently new and striking to make it desirable to place them on record.

Acknowledgments

The authors are grateful to Professor E. C. Stoner and to Dr. F. E. Hoare for their helpful comments.

References

Kjeldaas, T., Jr, and Holstein, T., 1959, *Phys. Rev. Letters*, **2**, 340.
Mackinnon, L., and Myers, A., 1959, *Proc. Phys. Soc.*, **73**, 291.
Morse, R. W., and Gavenda, J. D., 1959, *Phys. Rev. Letters*, **2**, 250.

Some Angular Distribution Measurements on the Reactions $^{16}O(^{3}He, d)^{17}F$ and $^{16}O(^{3}He, \alpha)^{15}O$

By S. Hinds and R. Middleton

Atomic Weapons Research Establishment, Aldermaston, Berks.

Communicated by K. W. Allen; *MS. received* 10*th June* 1959

§ 1. Introduction

During a recent study of the $^{16}O(^{3}He, p)^{18}F$ reaction at energies of 5·9 and 9·16 Mev, evidence was obtained favouring the direct reaction process. On this basis it would also be expected that the $^{16}O(^{3}He, d)^{17}F$ and the $^{16}O(^{3}He, \alpha)^{15}O$ reactions proceed predominantly via a direct process, particularly since only one particle is involved in the transfer as opposed to two in the former reaction. In this communication are presented the results of some angular distribution measurements of the α-particles and deuterons from the bombardment of oxygen with 5·70, 5·89 and 9·16 Mev ^{3}He particles.

The $^{16}O(^3He, \alpha)^{15}O$ reaction has previously been investigated by Bromley, Kuehner and Almqvist (1959) at incident energies up to 3·1 MeV. The excitation function of the ground state α-particle group, measured at 90°, exhibits pronounced resonances and the angular distributions observed below 2·6 MeV are approximately symmetrical about 90°. At slightly higher energies a marked asymmetry appears in the angular distributions which suggests that the direct reaction mechanism is a rapidly increasing competitive process. This conclusion appears to be confirmed by the measurements made by Holmgren (1957) on the $^{13}C(^3He, \alpha)^{12}C$ reaction at incident energies of 2·0 and 4·5 MeV.

Few investigations of the (^{3}He, d) reaction have been reported, but the inverse reaction and particularly the related (d, t) reactions, have been studied. Since the majority of the latter results are consistent with an inverse stripping reaction mechanism (Newns 1952), there is good reason for believing that stripping plays a major role in the (^{3}He, d) process. This is confirmed by measurements made by the authors (Hinds and Middleton 1959 a) on the $^9Be(^3He, d)^{10}B$ reaction at an incident energy of 5·7 MeV.

The results presented in this communication were obtained from the nuclear plates previously used to study the $^{16}O(^3He, p)^{18}F$ reactions and a description of the experimental procedure has been reported by Hinds and Middleton (1959 b, c). The angular distributions of the ground state α-particle group have been measured at incident energies of 5·70, 5·89 and 9·16 MeV and of the first and second excited states at 9·16 MeV. Measurements of the latter at the lower energies were complicated by the presence of a number of strong elastically scattered ^{3}He groups. Tentative angular distributions of the first and second excited states have been obtained at 5·70 MeV and were reported at the Paris Nuclear Physics Conference, 1959. These are similar to those obtained at 9·16 MeV and since they extended only to 70°, are not presented here.

§ 2. Results and Discussions

2.1. *The $^{16}O(^3He, \alpha)^{15}O$ Reaction*

The α-particle angular distributions measured at an incident energy of 9·16 MeV are shown in figure 1. Although the unit of cross section is arbitrary, it is the

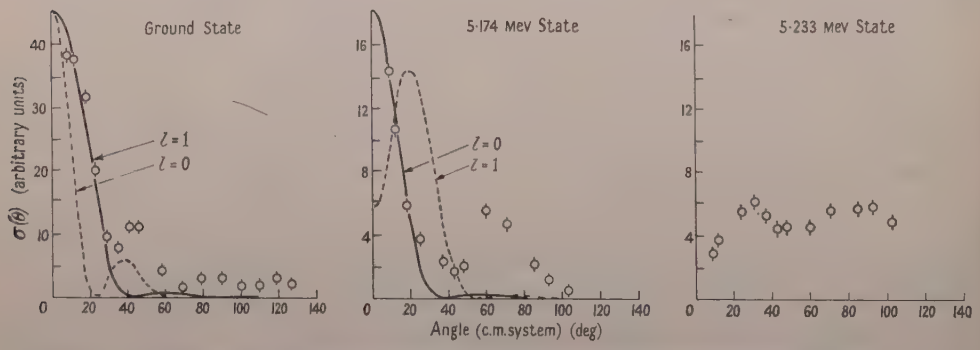

Figure 1. The angular distributions of the α-particle groups corresponding to the ground, first and second excited states of ^{15}O from the $^{16}O(^3He, \alpha)^{15}O$ reaction measured at an incident energy of 9·16 MeV. The curves were calculated from Born approximation pick-up theory.

same as that used in a previous communication (Hinds and Middleton 1959 b) on the $^{16}O(^3He, p)^{18}F$ reaction at the same energy. The curves shown in the

figure were calculated from a form of Born approximation pick-up theory reported by Newns (1952, also private communication). In all cases the radius of interaction was the same and equal to 4·8 fermi, the Gamow radius.

On the basis of a simple pick-up process the $l=1$ transition observed leading to the ground state of ^{15}O is consistent with this state having a predominant configuration of s^4p^{11}, assuming ^{16}O to be s^4p^{12}. Similarly, the configuration of the first excited state may be inferred to be predominantly s^3p^{12}. The second excited state does not appear to be formed by a pick-up process and must therefore have a configuration containing particles in states other than the s and p present in ^{16}O. A possible configuration would be $s^4p^{10}d$.

The above assignments are consistent with the observations of Sharp and Sperduto (1955) on the $^{14}N(d, p)^{15}N$ reaction leading to the mirror nucleus ^{15}N, if it is assumed that the closely spaced first and second excited states are inverted. These authors report that the first excited state is formed by stripping and the angular distribution is of the $l=2$ type. This is consistent with the state having the same configuration as the second excited state of ^{15}O, namely $s^4p^{10}d$. The angular distribution of the group leading to the second excited state, however, did not show stripping, which is consistent with a configuration of s^3p^{12} similar to that of the first excited state of ^{15}O.

Theoretical treatment of the mass 15 system (Elliott and Flowers 1957, Halbert and French 1957) indicate that a low-lying state with a predominant configuration of $s^4p^{10}d$ is expected. A state is also expected of configuration s^3p^{12} or $s^4p^{10}s$ or of a mixture of both. The former is preferred since the $s^4p^{10}s$ configuration cannot be directly formed from ^{16}O by a simple pick-up process.

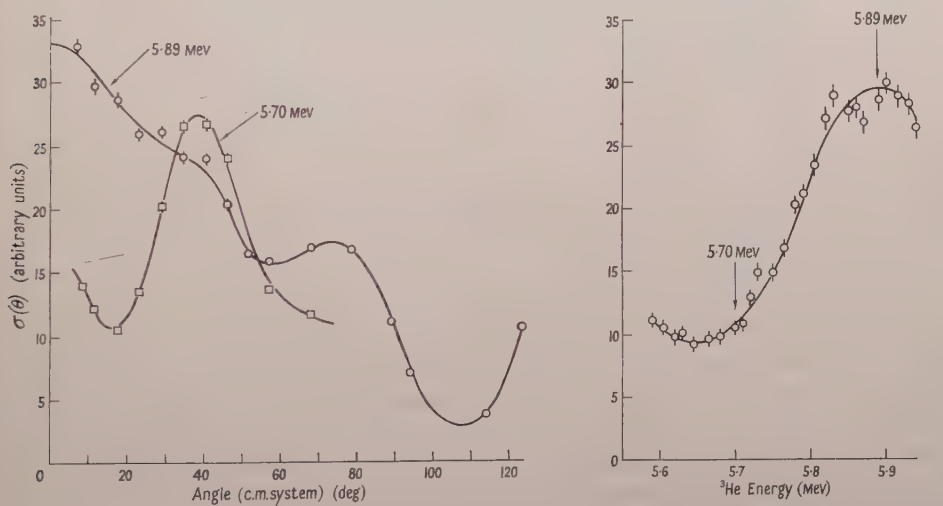

Figure 2. In the left-hand figure are shown the angular distributions of the ground state α-particle group from the $^{16}O(^3He, \alpha)^{15}O$ reaction measured at energies of 5·70 and 5·89 Mev. On the right-hand side is shown the excitation function observed at 15°.

The ground state angular distributions measured at energies of 5·70 and 5·89 Mev are shown in figure 2 together with the excitation function measured at 15°. The unit of cross section is the same as that of the protons from the $^{16}O(^3He, p)^{18}F$ reaction measured at 5·9 Mev (Hinds and Middleton 1959 b). It will be noticed that the excitation function shows resonance effects and that the

angular distributions measured at 5·70 and 5·89 MeV are very different. This suggests that at energies up to 6 MeV, compound nucleus formation still competes strongly with the direct process. The strong energy dependence of the angular distribution is probably due to interference. This is particularly likely since the excitation energy of the compound nucleus ^{19}Ne is unusually low.

The present results suggest that at 9 MeV the $^{16}O(^3He, \alpha)^{15}O$ reaction proceeds predominantly via a direct process and that tentative spin and parity assignments can be made from the angular distributions. At 6 MeV, however, this is not the case. This is perhaps surprising since measurements made of the protons from the $^{16}O(^3He, p)^{18}F$ reaction at this energy appeared to be consistent with a predominantly direct process.

2.2. *The $^{16}O(^3He, d)^{17}F$ Reaction*

The angular distribution of the deuteron group leading to the gound state of ^{17}F is shown in figure 3. This was measured at an incident energy of 9·16 MeV and is plotted using the same units of cross section as figure 1. The experimental

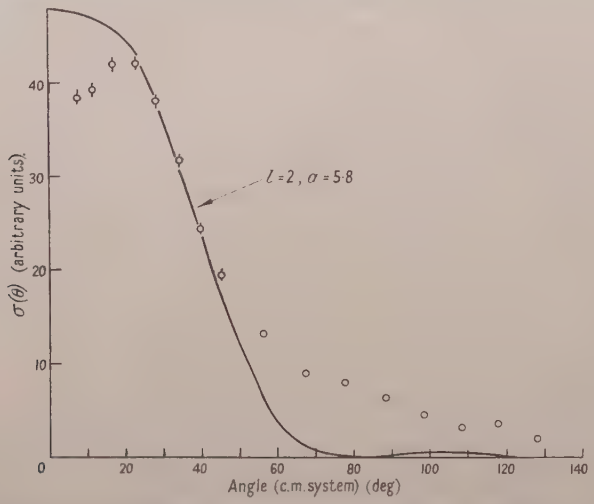

Figure 3. The angular distribution of the ground state deuterons group from the $^{16}O(^3He, d)^{17}F$ reaction observed at an incident energy of 9·16 MeV. The curve was calculated from Born approximation stripping theory.

points have been fitted with a Born approximation stripping curve calculated from the theory of Newns (1952). Best agreement was obtained with $l=2$ and a radius of 5·8 fermi, which is equal to the Gamow radius plus one fermi. The $l=2$ assignment is consistent with the known spin and parity of $^{17}F(5/2^+)$ and the l-value reported by Middleton, El-Bedewi and Tai (1953) for the corresponding transition in the $^{16}O(d, n)^{17}F$ reaction.

The mechanism of the $^{16}O(^3He, d)^{17}F$ reaction at an incident energy of 9·16 MeV appears to be predominantly stripping. This confirms previous conclusions drawn from observations made on the $^9Be(^3He, d)^{10}B$ reaction at an incident energy of 5·7 MeV.

Acknowledgments

We would like to thank Dr. K. W. Allen for his encouragement and advice, and also Dr. H. C. Newns for much useful discussion.

REFERENCES

BROMLEY, D. A., KUEHNER, J. A., and ALMQVIST, E., 1959, *Paris Nuclear Physics Conference Proceedings* (Paris: Dunod), p. 355.
ELLIOTT, J. P., and FLOWERS, B. H., 1957, *Proc. Roy. Soc.* A, **242**, 57.
HALBERT, E. C., and FRENCH, J. B., 1957, *Phys. Rev.*, **105**, 1563.
HINDS, S., and MIDDLETON, R., 1959 a, *Proc. Phys. Soc.*, **74**, 196.
—— 1959 b, *Ibid.*, **74**, 762.
—— 1959 c, *Ibid.*, **73**, 727.
HOLMGREN, H. D., 1957, *Phys. Rev.*, **106**, 100, 102.
NEWNS, H. C., 1952, *Proc. Phys. Soc.* A, **65**, 916.
MIDDLETON, R., EL-BEDEWI, F. A., and TAI, C. T., 1953, *Proc. Phys. Soc.* A, **66**, 95.
SHARP, R. D., and SPERDUTO, A., 1955, *Massachusetts Institute of Technology Report*, May 1955.

The Energy Levels of ^{21}Ne

BY S. HINDS AND R. MIDDLETON

Atomic Weapons Research Establishment, Aldermaston, Berks.

Communicated by K. W. Allen; *MS. received* 11*th June* 1959

THE energy levels of ^{21}Ne have previously been measured up to 3 MeV excitation energy by Sperduto (1951) and Ahnlund (1954 a, b). In both cases magnetic analysis was used and the reactions investigated were ^{23}Na(d, α)^{21}Ne and ^{20}Ne(d, p)^{21}Ne respectively. Low resolution measurements have also been made up to an excitation energy of 6·72 MeV by Middleton and Tai (1951) and Burrows *et al.* (1956). In the present communication the positions of 67 levels are reported from an investigation of the ^{19}F(^{3}He, p)^{21}Ne reaction.

Singly charged ^{3}He was accelerated in the Aldermaston Van de Graaff generator to an energy of 5·87 MeV and used to bombard a thin target containing ^{19}F. The target was prepared by evaporating a thin layer of calcium fluoride on a thin backing of carbon and gold. Proton energy spectra were measured at angles of observation of 15°, 30° and 45° with the broad-range magnetic spectrograph previously described by Hinds and Middleton (1959).

A typical proton energy spectrum, obtained at an angle of 15° and with a field strength of 11 039 gauss is shown in the figure. Groups arising from the ^{19}F(^{3}He, p)^{21}Ne reaction are labelled numerically and were identified from the impurity groups by their characteristic variation of energy with angle. Groups arising from target impurities are labelled by the symbol for the residual nucleus, the subscript referring to the appropriate excited state. At this particular angle, group 1 was obscured by a very intense group of elastically scattered singly charged ^{3}He particles which prevented it from being measured in the normal way. However, it was possible, by using a high-power objective, to count some of the tracks, enabling its position to be accurately determined but not its relative intensity. The result of these measurements is shown in the inset figure.

A separate exposure was made at 90° to determine the energies of the elastically scattered ^{3}He particles from gold, calcium, fluorine and carbon. From these the mean beam energy was calculated to be $5{\cdot}870 \pm 0{\cdot}010$ MeV which leads to a Q-value for the ^{19}F(^{3}He, p)^{21}Ne reaction of $11{\cdot}902 \pm 0{\cdot}015$ MeV. This agrees

with the value of 11·907 MeV expected from the mass defects listed by Ajzenberg and Lauritsen (1955).

In column (1) of the table are listed the energy levels measured during the present investigation; the experimental error is ± 10 kev except for the levels quoted to only two decimal places and for these an error of ± 20 kev is possible. In columns (2)–(5) are listed the levels determined from other investigations.

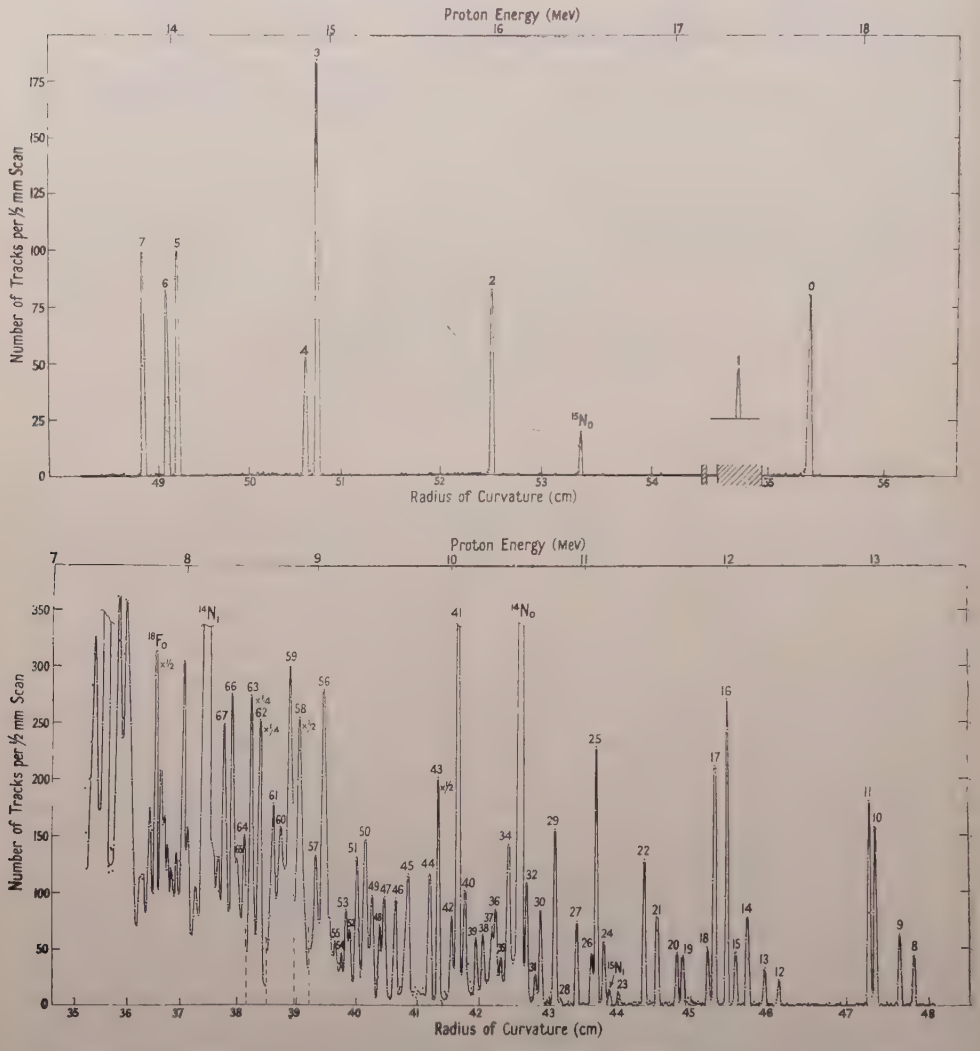

An energy spectrum of the protons from the $^{19}F(^3He, p)^{21}Ne$ reaction measured at an incident energy of 5·87 MeV and at an angle of observation of 15°.

Agreement is good for the low-lying levels but many of the higher excited states are shown to be multiplets. This is not surprising since most of the previous work was done using the ^{20}Ne(d, p) reaction and the energy resolution was impaired by the use of a gas target.

It may be noted that there is a steady increase in the proton background in the spectrum beyond group 28. This probably arises from a number of broad virtual states which are known to occur in ^{21}Ne above 6·756 MeV. In the present

^{21}Ne Level Energy (MeV)

Group Number	(1)	(2)	(3)	(4)	(5)
0	0	0	0	0	0
1	0·352	0·35	0·33	0·349	0·343
2	1·736	1·73	1·68		1·735
3	2·789	2·78	2·79	2·788	
4	2·864				2·852
5	3·664				
6	3·733		3·73		
7	3·883				
8	4·433				
9	4·525	4·58			
10	4·681		4·71		
11	4·727	4·81			
12	5·334				
13	5·427	5·43	5·44		
14	5·541				
15	5·624	5·63			
16	5·683		5·74		
17	5·770	5·78			
18	5·813	5·89			
19	5·986				
20	6·029	6·10			
21	6·170				
22	6·259				
23	6·446				
24	6·543				
25	6·597				
26	6·633				
27	6·743	6·72	6·66		
28	(6·85)				
29	6·898				
30	7·002				
31	7·039				
32	7·104				
33	7·148†				
34	7·225				
35	7·29				
36	7·326				
37	7·354				
38	7·413				
39	7·461				
40	7·547	(6)			
41	7·597				
42	7·644				
43	7·740				
44	7·805				
45	7·964†	7·966			
46	8·058	8·056			
47	8·137				
48	8·174				
49	8·229				

Group Number	(1)	(6)
50	8·275	
51	8·345†	8·356
52	8·39	
53	8·424	
54	8·457	
55	8·50	
56	8·576†	
57	8·642	
58	8·768	
59	8·840	
60	8·908	
61	8·959	
62	9·061	
63	9·136	
64	9·19	
65	9·25	
66	9·276	
67	9·339	

(1) Present investigation of the ^{19}F(^{3}He, p)^{21}Ne reaction. The experimental error on all levels is ± 10 kev, except for those accurate to two decimal places for which an error of ± 20 kev is possible; (2) Burrows, Green, Hinds and Middleton (1956); (3) Middleton and Tai (1951); (4) Ahnlund (1954 a, b); (2)–(4) from investigations of the ^{20}Ne(d, p)^{21}Ne reaction; (5) Sperduto (1951) from the ^{23}Na(d, α)^{21}Ne reaction; (6) Cohn and Fowler, sharp levels only from ^{20}Ne(n, n)^{20}Ne.

† Level is possibly a doublet.

investigation, only relatively narrow levels have been observed and many of the broad states reported by Cohn and Fowler (1958) determined from neutron resonance scattering were not detected. In column (6) of the table are listed the levels reported by Cohn and Fowler having a width less than 10 kev. These agree surprisingly well with the present results particularly since the masses of ^{20}Ne and ^{21}Ne are involved in the calculation of the latter. It is surprising that a level at 7·622 Mev and width of 14 kev reported by Cohn and Fowler was not detected.

Acknowledgments

We are grateful to Dr. K. W. Allen for his interest and advice. We would like to thank Mr. D. A. Procter and Mr. H. Marchant for their assistance in making the exposures and Mrs. N. Neville, Mrs. M. Smith and Mr. P. Bampton for scanning the nuclear plates.

References

Ahnlund, K., 1954 a, *Ark. Fys.*, **7**, 155.
—— 1954 b, *Ibid.*, **9**, 39.
Ajzenberg, F. and Lauritsen, T., 1955, *Rev. Mod. Phys.*, **27**, 77.
Burrows, H. B., Green, T. S., Hinds, S., and Middleton, R., 1956, *Proc. Phys. Soc.* A, **69**, 310.
Cohn, H. O., and Fowler, J. L., 1958, *Bull. Amer. Phys. Soc.*, [II], **3**, 18.
Hinds, S., and Middleton, R., 1959, *Proc. Phys. Soc.*, **74**, 196.
Middleton, R., and Tai, C. T., 1951, *Proc. Phys. Soc.* A, **64**, 801.
Sperduto, A., 1951, *Massachusetts Institute of Technology Prog. Report* (May 1951).

Comments on Faragó's Treatment of Spin Precession in Crossed Magnetic and Electric Fields†

By V. L. Telegdi and R. Winston

The Enrico Fermi Institute of Nuclear Studies, The University of Chicago, Chicago, Illinois

Communicated by N. Kemmer; *MS. received* 14*th May* 1959, *in final form* 17*th August* 1959

It is well known that a Dirac particle with $g \neq 2$ gradually changes its polarization from longitudinal to transverse (or vice versa) when moving on a circular orbit in a magnetic field. The rate of this change in polarization, Ω, is given in terms of the orbital angular velocity ω by $\Omega/\omega = \gamma(v)(\frac{1}{2}g - 1)$, where $\gamma(v) \equiv (1-v^2)^{-1/2}$, $\mathbf{v}$ being the velocity of the particle.

Faragó has recently proposed (Faragó 1958‡) to measure the anomaly $a = (\frac{1}{2}g - 1)$ by observing the change of polarization when the particle moves in the laboratory on a trochoidal orbit in crossed magnetic and electric fields. To derive Ω/ω for this case, or rather the fractional change in polarization per loop of the trochoid, he appeals to the fact that there exists a frame in which the motion takes place in a circle, i.e. in which the electric field has been transformed.

† Research supported by a joint programme of the Office of Naval Research and the United States Atomic Energy Commission.

‡ In terms of Faragó's notation, our $\Omega = \omega_L - \omega$; while his frame S' corresponds to our frame S^0. We put $\hbar = 1$ and $c = 1$, whereas Faragó retains these constants.

away. In that frame, as noted above, the answer is known; Faragó applies certain arguments involving clocks in relativity to derive the result in the laboratory frame.

It is a straightforward matter to derive Ω for Faragó's experiment formally from first principles (cf. Bargmann, Michel and Telegdi 1959). One finds, in the notation of this reference,

$$\Omega = \frac{e}{m}\left[a(H - Ev_x) + \frac{Ev_x}{\gamma^2 - 1} \right]. \qquad \ldots\ldots (1)$$

It is easy to verify that Faragó's contention that Ω/ω (ω = orbital angular velocity) is an invariant, i.e. has the same numerical value as in the (primed) frame where the field is purely magnetic, is incorrect. In fact this ratio, like ω itself, varies along the loops of the trochoidal orbit.

Statements about the change in polarization per trochoidal loop can readily be made by integrating equation (1) over an orbital period. It is, however, illuminating to examine Faragó's slightly incorrect reasoning more closely†. One finds that an argument running along very similar lines to his, but using legitimate relativistic concepts, leads to a correct result in agreement with the integration of equation (1). This argument is given here.

We shall admit as a 'clock' into special relativity any observable that is periodic in time, provided the periodicity occurs at the same space point in some inertial frame (the proper frame of the clock in question). We consider the motion of a charged particle endowed with spin through homogeneous electromagnetic fields; let this motion be confined to a plane and periodic in the sense that $\mathbf{v}(t+T) = \mathbf{v}(t)$ for all t. The question then is: what clocks can be constructed out of the dynamical variables involved, and which are their respective proper frames?

(*a*) *Orbit clock: periodicity of the velocity.*

There exists a unique inertial frame S^0, of velocity

$$\frac{1}{T}\int_t^{t+T} \mathbf{v}(t)\, dt,$$

in which the periodic orbit appears closed. Since $\mathbf{v}$ is to be measured at the particle's instantaneous position, S^0 is the proper frame of this orbit clock. Let its period in S^0 be denoted by T^0.

(*b*) *Polarization clock: periodicity of the polarization.*

Ω, the rate of change from longitudinal to transverse polarization, is a function of the velocity and field vectors only, and may be written as $\Omega = d\phi/dt$, ϕ being an angle variable connected with the decomposition into longitudinal and transverse polarization (Bargmann, Michel and Telegdi 1959). Periodicity of the polarization means that the particle, at fixed velocity $\mathbf{v}$, is observed in the same state of polarization at times t and $t + T_p$. In the rest frame of the polarization clock—if such a clock exists—these two observations must be made at the same space point. Hence this frame must again be S^0, where the orbit is a closed one. To meet our definition of a clock, the polarization must at a point on the orbit in S^0 come back to itself with a period $T_p{}^0$. Thus one has to

† One of the main objections to Faragó's reasoning is that angular velocities cannot in general be used in legitimate relativistic clock arguments.

have $T_p{}^0 = NT^0$ (N = positive integer) for the polarization clock to exist if we assume (as may be done without loss of generality) $T_p{}^0 > T^0$. If such a degeneracy of the two periods indeed arises, then there exists a polarization clock, and $T/T_p = 1/N$ is a Lorentz invariant. From the periodicity of Ω it follows that $\Delta\phi$, a quantity which measures essentially the change in polarization per loop of trajectory, is the same for each loop. Clearly, by continuity, $\Delta\phi$ is independent of frame.

If N were indeed an integer (which is generally not true in any situation of physical interest!), then Faragó's argument could be phrased as follows in terms of the above considerations:

In S^0: $T^0/T_p{}^0 = \gamma(v')a$, $H^0 = H'$, $E^0 = E' = 0$, circular orbit, $v^0 = v'$.

In S: $T/T_p = \gamma(v')a = 1/N$; $E \neq 0$, trochoidal orbit with velocity $\mathbf{v}$ dependent on position. With reference to any orbit point (regardless of $\mathbf{v}$ at that point) the change in polarization per loop $\Delta\phi/2\pi$ is just $\gamma(v')a$.

Even when N is not an integer, i.e. when there exists no polarization clock in our sense, it turns out that $\Delta\phi$ is still the same per loop in any inertial frame. This interesting fact enables one to take over the above result, $\Delta\phi/2\pi = \gamma(v')a$, for the situations of actual physical interest. Hence the conclusions of the present analysis do not affect Faragó's implied evaluation of his experiment.

This important property of $\Delta\phi$ can be seen by appealing to the continuity of Lorentz transformations and to the fact that the statement 'the particle has returned to the same state of polarization at a given velocity' is independent of observer (although the state of polarization and the velocity are *not*). If N is an integer, then $\Delta\phi^0/2\pi$ (observed in S^0) is given by $(K/L) + \epsilon$, where ϵ can be made arbitrarily small by observing the polarization through a sufficiently large number L of orbital turns (K is the nearest integer to $L\Delta\phi^0/2\pi$, the change in polarization per L orbital turns). In an inertial frame S, in which S^0 moves with a velocity $\mathbf{u}$, one may have only $\Delta\phi/2\pi = \Delta\phi^0/2\pi + f(\mathbf{u})$. We wish to show that $f(\mathbf{u}) = 0$. If $f(\mathbf{u})$ were equal to a constant, then this constant would have to be equal to zero, as $f(0) = 0$. If f really depended on $\mathbf{u}$, then one could find a $\mathbf{u}$ such that $f(\mathbf{u}) = -\epsilon$, i.e. find an observer for whom $\Delta\phi = (K/L)2\pi$. Thus for this observer the polarization would return precisely to its initial state periodically at some orbital point, in contrast to what happens in the frame S^0. Thus one must have $f(\mathbf{u}) = 0$ for all $\mathbf{u}$, and $\Delta\phi$ is a Lorentz invariant.

One can also verify the Lorentz invariance of $\Delta\phi$ in a more formal way by using the polarization four-vector $\mathbf{s}$ (Bargmann, Michel and Telegdi 1959). For plane motion, $\mathbf{s}$ can at all times t be decomposed as

$$\mathbf{s}(t) = \mathbf{e}_t(t)\cos\phi(t) + \mathbf{e}_t(t)\sin\phi(t). \qquad \ldots\ldots (2)$$

Since the motion is periodic in $\mathbf{v}$ with a period T one has a 'periodic basis', i.e.

$$\mathbf{e}_t(t+T) = \mathbf{e}_t(t); \quad \mathbf{e}_t(t+T) = \mathbf{e}_t(t). \qquad \ldots\ldots (3)$$

Clearly

$$\mathbf{s}(t)\,.\,\mathbf{s}(t+T) = \cos[\phi(T+t) - \phi(t)] = \cos\Delta\phi \qquad \ldots\ldots (4)$$

$$\Delta\phi = \text{Lorentz invariant } (\text{mod } 2\pi).$$

To conclude, we compute $\Delta\phi$ by actually evaluating

$$\Delta\phi = \int_0^T dt\Omega \qquad \ldots\ldots (5)$$

where Ω is given in (1), and T is the period of the trochoidal orbit.

The decomposition

$$\Omega = \frac{d\phi}{dt} = \Omega_1 + \Omega_2 = \frac{e}{m} a(H - Ev_x) + \frac{e}{m} \frac{Ev_x}{\gamma^2 - 1} \qquad \ldots\ldots (1')$$

is a natural one, inasmuch as Ω_2 is independent of **a**. To see its significance, we next express Ω_1 and Ω_2 in terms of the (primed) variables of the frame S^0. With the notation

$$\gamma(v) = \gamma, \gamma(v') = \gamma', \gamma(u) = \gamma(E/H) = \Gamma, \gamma = \Gamma\gamma'(1 + uv_x') \qquad \ldots\ldots (6)$$

one has

$$\Omega_1 \gamma = (e/m) H' a \gamma' = \omega' \gamma'^2 a = \Omega' \gamma' \qquad \ldots\ldots (7)$$

so that (5) may be written as

$$\Delta\phi = \int_0^{T'} dt' \Omega' + \int_0^{T'} dt' (\Omega_2 \gamma / \gamma') = \Delta\phi + \alpha. \qquad \ldots\ldots (8)$$

As the integral α is independent of **a**, one could anticipate already at this state that α must be $0 \pmod{2\pi}$ for all a. Using (6),

$$\alpha = \int_0^{T'} dt' \frac{\Omega_2 \gamma}{\gamma'} = \tfrac{1}{2}\omega' \int_0^{T'} dt' \left[\frac{\Gamma + \gamma'}{\Gamma\gamma'(1 + uv_x') + 1} + \frac{\Gamma - \gamma'}{\Gamma\gamma'(1 + uv_x') - 1} \right]$$

$$\tfrac{1}{2}(\alpha_+ + \alpha_-) \qquad \ldots\ldots (9)$$

with the substitutions $v_x' + iv_y' = v' e^{i\theta'} = v'z$, $\omega'\, dt' = -i dz/z$, $\Gamma\gamma' uv' = 2b$, we evaluate $\alpha_\pm$ in equation (9) over $|z| = 1$:

$$\alpha_\pm = -i \int dz (\Gamma \pm \gamma')[bz^2 + (\Gamma\gamma' \pm 1)z + b]^{-1}$$

$$= -ib^{-1} \int dz (z + z_1^{\pm})^{-1} (z + z_2^{\pm})^{-1} (\Gamma \pm \gamma')$$

where

$$z_{1\,(2)}^{\pm} = \frac{(\Gamma\gamma' \pm 1) + (-)|\Gamma \pm \gamma'|}{2b} \qquad \text{and } z_1 z_2 = 1,$$

$$\alpha_\pm = 2\pi(\Gamma \pm \gamma')/|\Gamma \pm \gamma'|.$$

Hence

$$\alpha = \begin{cases} 0 & u < v' \\ 2\pi & u > v' \end{cases}$$

which implies that $\Delta\phi = \Delta\phi' \pmod{2\pi}$.

APPENDIX

In the laboratory (L) the spin of the particle moves with a (varying) angular velocity

$$\omega_L = \omega_L(R)/\gamma + \omega_T \qquad \ldots\ldots (A\,1)$$

where

$\omega_L(R)$ = spin precession frequency in instantaneous rest frame R,

$= g(e/2m)H(R)$,

ω_T = Thomas precession frequency of R in L $= -(\gamma - 1)\omega$.

Also

$$H(\mathrm{R}) = \gamma(H - Ev_x)$$
$$\omega = (e/m\gamma)(H - Ev_x/v^2) \qquad \ldots\ldots(\mathrm{A}\,2)$$

so that

$$\Omega \equiv \omega_{\mathrm{L}} - \omega = \frac{e}{m}\left[a(H - Ev_x) + \frac{Ev_x}{\gamma^2 - 1}\right], \qquad \ldots\ldots(\mathrm{A}\,3)$$

which is the same as equation (1).

References

Bargmann, V., Michel, L., and Telegdi, V. L., 1959, *Phys. Rev. Lett.*, **2**, 435.
Faragó, P. S., 1958, *Proc. Phys. Soc.*, **72**, 891.

Domain Structures on Thin Sheets of Magnetoplumbite

By E. D. Isaac

Department of Physics, University of Nottingham

Communicated by L. F. Bates; *MS. received 6th August* 1959

§ 1. Introduction

The domain structure of single crystals of the hexagonal iron oxide compound, magnetoplumbite, $PbFe_{12}O_{19}$, has previously been reported by Bates *et al.* (1959). It was shown to consist of 180° domains in the bulk of each crystal with complex patterns of undulatory walls and closed loops on the basal planes. The closed loops are presumed to mark the intersections of spikes of reverse magnetization with the surface. A typical pattern obtained on the basal plane of a large crystal is shown in figure 1 (Plate).

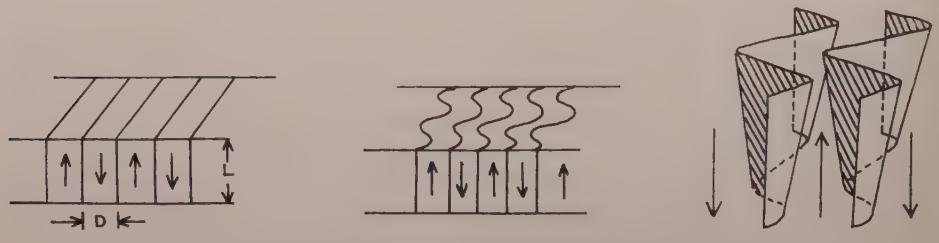

(*a*) (*b*) (*c*)

Figure 2.

Simpler patterns of undulatory walls, termed 'rick-rack' patterns, were reported by Roberts and Bean (1954) on the basal plane surfaces of manganese bismuthide, and Goodenough (1956) made calculations of the various energy terms involved for several observed and predicted basal plane structures. He found that the simple 180° slab-domain model of Kittel, figure 2 (*a*), is energetically more favourable than the 'rick-rack' structure shown in figure 2 (*b*). This led him to suggest that where such a 'rick-rack' structure exists, the amplitude of the 'rick-rack' waves decreases regularly with depth of penetration into the crystal as shown in figure 2 (*c*). Here, he maintains that the decrease of energy

due to the smaller wall area more than compensates for the increase of energy due to the divergence of magnetization through the walls.

In this manner, Goodenough has accounted for the observed rick-rack patterns and further, has shown that for specimens even thinner in the axial direction, the most stable configuration is that of simple 180° slab domains. Such a structure has been observed by Kooy (1958) in platelets of barium ferrite less than 1 μ thick, using a polarized light technique. It is of interest to observe such patterns since direct measurement of the domain spacing and specimen thickness will then enable an estimate of the domain wall energy to be made.

Kittel (1949) has calculated that for equally spaced parallel strips of magnetic poles of alternating sign, the magnetic energy σ_m is given by $\sigma_m = 0{\cdot}8525 I_s^2 D$ per unit area where I_s is the spontaneous magnetization and D the width of a strip. The total energy W corresponding to unit surface area of the crystal (figure 2 (*a*)) is

$$W = \sigma_w + \sigma_m$$

where σ_w is the wall energy per unit area of wall, i.e.

$$W = \sigma_w \frac{L}{D} + 1{\cdot}705\, I_s^2 D$$

and this is a minimum with respect to the domain width D when

$$\frac{\partial W}{\partial D} = -\left(\frac{\sigma_w L}{D^2}\right) + 1{\cdot}705 I_s^2 = 0$$

or

$$D = \left[\frac{\sigma_w L}{(1{\cdot}705 I_s^2)}\right]^{1/2}.$$

§ 2. Experimental Procedure

The single crystal of magnetoplumbite used in the present experiments was bounded by two plane parallel surfaces which were basal planes of the hexagonal structure. Four axial plane surfaces were obtained by cutting the crystal at right angles to the basal planes with a thin carborundum wheel. The resulting rectangular block measured approximately 0·5 cm × 0·6 cm × 0·7 cm.

The saturation magnetization of magnetoplumbite at room temperature was found from an (I, H) curve measured on this crystal and was approximately 345 e.m.u.

One of the basal plane surfaces of the rectangular block was glued to the finely polished surface of a brass mount using cold-setting Araldite. The crystal was then cleaved leaving a section of magnetoplumbite, some 25 μ thick, glued to the mount. Bitter figures were obtained using the dried-on films of a water-soluble colloid (Craik and Griffiths 1957), as this colloid had been found to give better resolution in this case than other well-known colloid solutions.

Figure 3 (Plate) shows the domain structure in the basal plane of the 25 μ thick section. It consists of a rick-rack pattern of undulatory walls and is similar to that seen by Roberts and Bean. The specimen was ground on $\frac{1}{4}\mu$ diamond compound so that its thickness was gradually reduced. When the thickness of the specimen was estimated to be about 6 μ, application of the colloid gave a pattern similar to that of figure 4 (Plate), i.e. straight 180° walls, as predicted by Goodenough. Each light and dark band in the picture represents the intersection

of a domain with the basal plane surface. The domain wall spacing is approximately $1{\cdot}2\mu$ and substitution of this value in the above equation gives $\sigma_w = 5\ \text{erg cm}^{-2}$.

Acknowledgments

The author is indebted to Professor L. F. Bates for his constant guidance, to Dr. A. W. Simpson of Plessey Company Limited for the provision of the crystal used, and to the Electrical and Allied Industries Research Association for financial support and permission to publish.

References

Bates, L. F., Craik, D. J., Griffiths, P. M., and Isaac, E. D., 1959, *Proc. Roy. Soc.* **A, 253**, 1.

Craik, D. J., and Griffiths, P. M., 1957, *Proc. Phys. Soc.* B, **70**, 1000.

Goodenough, J.B., 1956, *Phys. Rev.*, **102**, 356.

Kittel, C., 1949, *Rev. Mod. Phys.*, **21**, 541.

Kooy, C., 1958, *Philips Technical Review*, **19**, No. 10, 286.

Roberts, B. W., and Bean, C. P., 1954, *Phys. Rev.*, **96**, 1494.

LETTERS TO THE EDITOR

Light Beats as Indicators of Structure in Atomic Energy Levels

Light emitted in the decay of atoms from different energy levels is incoherent. Suppose, however, that the atoms are subject to an oscillatory field capable of inducing transitions between a pair of excited energy eigenstates. The state of atoms initially excited to one or other of these eigenstates will become a coherent mixture of both. One might expect that this coherence would be reflected in coherence between radiations of different frequencies emitted when the excited atoms decay spontaneously. This would manifest itself as a modulation of the optical radiation (i.e. light beats) at the frequency of the oscillatory field.

We have observed this modulation in the resonance radiation 2537 Å emitted in the decay of level 6^3P_1 in mercury. In a magnetic field H the three eigenstates $|m_J\rangle = |1\rangle, |0\rangle, |-1\rangle$ are separated in energy by two equal intervals, $g_J\beta H = \hbar\omega$. We refer to the even isotopes only, although natural mercury was used in the experiments. Under the simultaneous influence of H and a magnetic field H_1 oscillating in a plane perpendicular to H at a radio frequency ω_0 near ω, modulation frequencies ω_0 and $2\omega_0$ are to be expected if the direction of observation is suitably chosen.

The apparatus is similar to that used by Brossel and Bitter (1952) for observing 'double resonance' in the level 6^3P_1, except that the photoelectric current which records the intensity of the fluorescent radiation is applied to a narrow-band amplifier tuned to one of the harmonics of the oscillator frequency. Audio-frequency modulation of the magnetic field, and phase-sensitive detection are employed. Oscillators at a fixed frequency about 14 Mc/s are used, and the magnetic field varied through the various resonances.

The components of the photoelectric current which are detected are those which arise from the light beats and those which form part of the noise spectrum. The former are proportional to the depth of modulation of the fluorescent radiation: the latter depend on its intensity, which varies with magnetic field to produce the double resonance intensity signal as observed by Brossel and Bitter. The two effects are distinguishable in the following ways: (i) the shapes of the resonance curves are different, (ii) the intensities of the two types of signal depend in different ways on the polarization of the exciting radiation and the direction of observation. When the two signals occur together, the modulation signal alone is obtained by normalization and subtraction.

Resonance curves are obtained which are symmetrical (or anti-symmetrical) about $H = H_0 = \hbar\omega_0/g_J\beta$, and about $H = H_0/2$, where ω_0 is the frequency of the oscillatory field. The observations, which to date are exploratory only, are summarized in the following table.

If the light beats are a consequence of coherence between the original eigenstates, one might expect the amplitude of the beats to be related to the cross products $(a_1^*a_0 + a_1a_0^*)$, etc., where the coefficients a are defined in the expansion of the excited state, $|\rangle = a_1(t)|1\rangle + a_0(t)|0\rangle + a_{-1}(t)|-1\rangle$. These cross products have been evaluated, assuming that the states are subject to no perturbation other than the radio-frequency interaction, for initial conditions appropriate

(1)	(2)	(3)	(4)	(5)
Perpendicular to H	ω_0	$H_0/2$	L	See footnote ‡
	ω_0	†No resonance detected at H_0		
	$2\omega_0$	H_0	L	$\|1\rangle$ and $\|-1\rangle$
Approximately $\tan^{-1}\sqrt{2}$ to H	ω_0	$H_0/2$	L	See footnote ‡
	ω_0	H_0	D	$\|\rangle 1$ and $\|\rangle 0$; $\|0\rangle$ and $\|-1\rangle$
	$2\omega_0$	H_0	L	$\|1\rangle$ and $\|-1\rangle$
Parallel to H	ω_0	†No beats detected		
	$2\omega_0$	†No beats detected		

(1) Direction of observation; (2) detector tuning; (3) value of field at resonance; (4) line shape, the phase-sensitive method of detection displayed the derivative of L(Lorentz-type) and of D (dispersion-type) curves; (5) interpretation: coherent decay from the states.

to the method of excitation of the atoms. The cross products contain terms which oscillate at frequencies ω_0, $2\omega_0$, whose amplitudes, as functions of magnetic field, are broadly in agreement with the observations. In particular, the dispersion-type curve recorded in line 5 of the table is predicted. The absence of signal in those cases marked † is to be expected as a consequence of the orthogonality of the polarization vectors.

Unexpected resonances occur at fields $H_0/2$ both in the unmodulated component of the fluorescent light, and in the component modulated at frequency ω_0 (see footnote ‡).

We wish to distinguish the light beats observed here from those observed by Forrester, Gudmundsen and Johnson (1955). In that experiment, each atom was radiating a sharp frequency (to the extent that we can assume incoherent excitation in the light source, and also, very long lifetimes), and the beat frequency between pairs of atoms could range over the combined Doppler widths of two spectral lines. In our experiments, sharp beat frequencies are present in the radiation from each atom, and these appear in the ensemble with a much more favourable ratio of signal to noise.

Modulation of light has also been observed by Bell and Bloom (1957). The phenomenon depended on radio-frequency mixing in the ground states. The modulation was observed in absorption.

The coherence exhibited in our experiments is that which is exhibited in an entirely different way in the experiments of Guiochon, Blamont and Brossel (1957) and of Barrat and Brossel (1958) on the multiple diffusion of resonance radiation.

Clarendon Laboratory,
Oxford.
8th June 1959.

J. N. Dodd§.
W. N. Fox.
G. W. Series.
M. J. Taylor.

‡ *Note added in proof.*—Since the manuscript was submitted it has been confirmed that the resonances at $H_0/2$ occur only when the atoms are excited by a coherent mixture of σ and π radiation, produced by setting a polarizer at 45° to the magnetic field. The occurrence of these resonances, together with that of the others, can now be understood in terms of a theory of the light beats which is being prepared for publication.

§ On leave of absence from the University of Otago, New Zealand.

Barrat, J. P., and Brossel, J., 1958, *C.R. Acad. Sci., Paris*, **246**, 2744.
Bell, W. E., and Bloom, A. L., 1957, *Phys. Rev.*, **107**, 1559.
Brossel, J., and Bitter, F., 1952, *Phys. Rev.*, **86**, 308.
Forrester, A. J., Gudmundsen, R. A., and Johnson, P. O., 1955, *Phys. Rev.*, **99**, 1691.
Guiochon, M. A., Blamont, J. E., and Brossel, J., 1957, *J. Phys. Radium*, **18**, 99.

Dipolar Ferromagnetism in Dysprosium Ethyl Sulphate

Measurements of the magnetic properties of dysprosium ethyl sulphate at temperatures below 1°K show that this substance undergoes a transition at $0{\cdot}13_6 \pm 0{\cdot}01$°K, below which the magnetic susceptibility is independent of temperature. We attribute this transition to the onset of ferromagnetism produced by the very strong magnetic dipole–dipole coupling between the Dy^{3+} ions.

Experiments reported earlier (Cooke, Edmonds, McKim and Wolf 1959) have shown that in the helium range of temperatures the Dy^{3+} ions occupy a doublet state having g-values 10·8 parallel to the crystal axis and approximately zero perpendicular to it. Because of the very high value of $g_{\parallel}$, magnetic dipole interaction is particularly strong in this salt, and accounts for the observed departure of the susceptibility from Curie's law and for the magnetic specific heat anomaly, other effects such as exchange interaction and nuclear hyperfine splitting being small in comparison. Four types of experiment have been made below 1°K. The susceptibility–temperature relation has been found using the susceptibility of a cerium magnesium nitrate crystal in thermal contact with the specimen to measure the temperature. The susceptibility–entropy relation has been found by a series of demagnetizations from known initial conditions. The specific heat has been measured using electrical heating and also relaxation and gamma-ray heating. Finally, relaxation effects have been studied above and below the Curie point by measuring the susceptibility ballistically and in alternating fields of different frequencies.

The crystal structure of the rare earth ethyl sulphates is such that the main magnetic dipole interaction is between ions which lie in lines parallel to the crystal axis. Because of the very small value of $g_{\perp}$ in the dysprosium salt, the magnetic ions can be considered to have their moments always along the crystal axis, without any moment perpendicular to the axis, exactly as in the classical Ising model. This fact is important when considering possible ordered configurations and also greatly simplifies calculations of interaction effects. It is found that the variation of the entropy and the magnetic susceptibility down to the Curie point can be accounted for by an exact calculation of the interaction of nearest neighbours along the crystal axis (Kramers and Wannier 1941) together with approximate calculations of the interaction of more distant neighbours.

To arrive at a model of the ordered state below the transition, we first postulate that the ions are ordered in chains parallel to the axis, since the coupling between nearest neighbours in such chains is over seven times greater than the interaction with any other class of neighbour. Viewed perpendicular to the crystal

axis, the chains form a hexagonal array, each chain having three nearest neighbours. A molecular field calculation for a very long ellipsoid (70:1 axial ratio) showed that at any ion the molecular field due to a nearest neighbour chain is overwhelmingly larger (some 100 times) than that due to any more

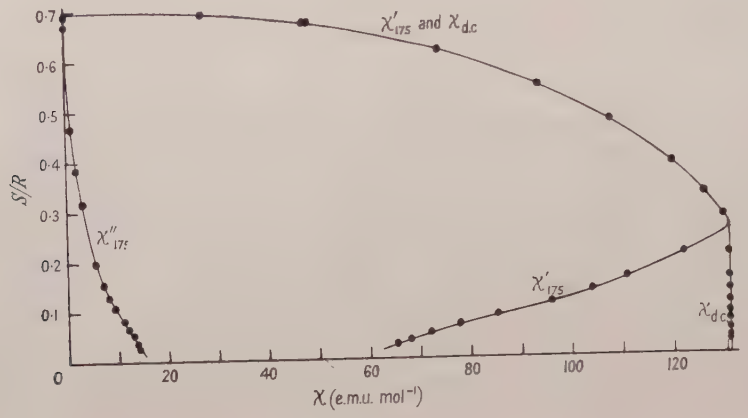

Magnetic entropy of specimen of dysprosium ethyl sulphate plotted against magnetic susceptibility, as measured by ballistic galvanometer method ($\chi_{d.c.}$), and against in-phase and out-of-phase components of magnetic susceptibility at 175 c/s. (χ'_{175} and χ''_{175}).

distant chain, and is in a direction to favour parallel (i.e. ferromagnetic) ordering of the chains. We conclude then that the ordered state is ferromagnetic. This conclusion will also hold for a short specimen, save that it will break up into domains (Kittel 1951). Calculation shows that the energy of the domain walls is small and is not particularly sensitive to the type of domain formed. For our specimens the thickness of a domain will be approximately 10^{-4} cm. Application of a small magnetic field will give a resultant magnetic moment, the volume susceptibility of a specimen being $1/N$, where N is the demagnetizing factor of the specimen. Because the domains are so thin, the surface energy is small, and it is found that this value of susceptibility should hold independent of temperature and magnetic field up to the saturating field, $H_s = NM_s$. Here M_s is the spontaneous magnetization of the domains, which tends to 84 gauss cm^{-3} at 0°K.

These conclusions are in excellent agreement with the experimental results. Measurements have been made on two specimens, a sphere (demagnetizing factor 4·18) and an ellipsoid of demagnetizing factor 2·78. The inverse susceptibilities observed at the transition points were $4{\cdot}1_2$ and $2{\cdot}7_3$. The results for the ellipsoidal specimen are shown in the diagram, in which the magnetic susceptibility, as measured by a ballistic galvanometer method, is plotted against entropy remaining after demagnetization. Within an error of 0·3% the susceptibility was constant below the transition point. No remanence was detected. The susceptibility as measured by an alternating field method showed a considerable frequency dependence below the transition point and also a large out-of-phase component (see diagram). These effects are ascribed mainly to relaxation processes connected with domain wall movements, but the non-zero

value of the out-of-phase susceptibility above the transition indicates that short range ordering processes may also be important.

We wish to thank Dr. R. J. Elliott, Mr. B. R. Heap and Mr. P. J. Armstrong for their help with some of the theoretical problems. The molecular field calculation was made at the University Computing Laboratory by courtesy of the Director, Dr. H. L. Fox. We wish to thank Dr. J. S. Rollett and Dr. L. J. Challis for their guidance with the programming.

Clarendon Laboratory,
Oxford.

14th July 1959.

A. H. Cooke.
D. T. Edmonds.
C. B. P. Finn.
W. P. Wolf.

Cooke, A. H., Edmonds, D. T., McKim, F. R., and Wolf, W. P., 1959, *Proc. Roy. Soc.* A, **252**, 246.
Kittel, C., 1951, *Phys. Rev.*, **82**, 965.
Kramers, H. A., and Wannier, G. H., 1941, *Phys. Rev.*, **60**, 252.

The Electrical Resistivity of Oxygen Deficient Nickel Ferrite

In a recent publication one of us (Parker 1958) has pointed out that semiconducting materials which have ordered magnetic spin arrangements below the Curie temperature may be divided into two main groups from the point of view of their electrical conduction. Materials in the first group exhibit no anomalies in their electrical resistivity ρ at the Curie temperature. The temperature dependence of resistivity of such materials may be described by the usual semiconductor equation.

$$\rho = A \exp(\epsilon/KT) \qquad \ldots\ldots(1)$$

with A and ϵ constant for a given material over a temperature range which includes the magnetic transformation temperature. This behaviour has been termed 'type I' by Parker. Materials of the second group obey equation (1) only above the Curie point and exhibit quasi-metallic conduction (with positive values of $d\rho/dT$) in the temperature range in which they are spontaneously magnetized. This has been referred to as 'type III' conduction. Materials in this latter group exhibit therefore large anomalies in resistivity in the temperature range around the Curie point.

It was further pointed out by Parker that the great volume of published data conforms to the following empirical rule. Type I conduction is generally associated with materials with Curie point resistivities ρ_C greater than about $4\Omega\,\text{cm}$, type III with materials where ρ_C is less than $0{\cdot}6\Omega\,\text{cm}$. Materials with $4\Omega\,\text{cm} > \rho_C > 0{\cdot}6\Omega\,\text{cm}$ show either type of conduction or they may have a resistance–temperature curve which corresponds to a transition from type I to type III and this has been termed 'type II' conduction.

The theoretical aspects of conduction of electricity in transition metal oxides have been considered recently by Parker and Tredgold and the results of this investigation will be reported later. The most important conclusion reached in this study is that exceptions should be found to the empirical rule of Parker (1958) by a careful choice of material. In particular it is predicted by Parker and Tredgold that low resistivity nickel ferrite ($NiFe_2O_4$) and cobalt ferrite ($CoFe_2O_4$) should always conform to type I conduction. In order to test this prediction we have prepared specimens of nickel ferrite with very low resistivities by firing them under low pressure conditions. It is well known (Snoek 1947) that under such conditions a loss of about 0·1% of oxygen occurs and that the consequential creation of Fe^{2+} ions in the ferrite lattice causes a drop in resistivity of several orders of magnitude.

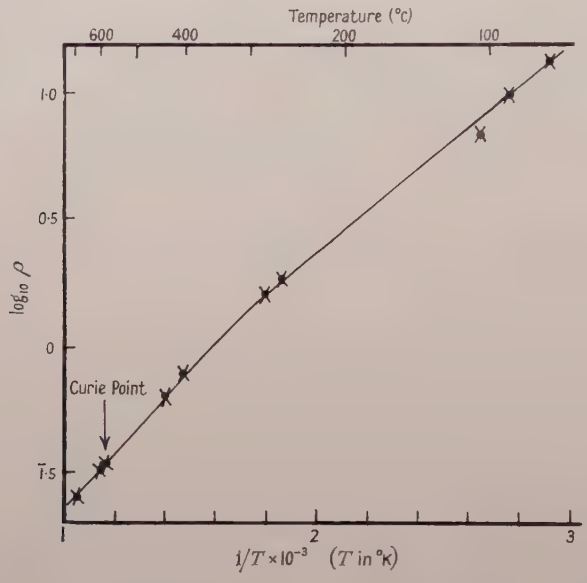

We have prepared a nickel ferrite by firing a mixture of NiO and Fe_2O_3 at 1220°c for 12 hours under pressure of about 0·1 mm of oxygen. The resulting ferrite has a high density (5·15 g cm^{-1}) and a Curie point resistivity of only 0·3Ω cm, as compared with about 100Ω cm for the corresponding stoichiometric compound (Parker 1958).

As $\rho_C = 0{\cdot}3\,\Omega$ cm is well below the value for which type III conduction might have been expected from the empirical rule, the material is very suitable for a test of the theory of Parker and Tredgold. Careful resistivity measurements were made by a four-terminal method at d.c. and a bridge method at a.c. No dispersion in resistivity was found and the material may therefore be assumed to be homogeneous (Koops 1951). The measurements were extended over a temperature range to include the Curie point, 585°c. The results obtained are shown in the figure. It will be noted that there is a slight change in the slope of the graph at a point corresponding approximately to a temperature of 140°c. This is a commonly observed behaviour in ferrites (see for example van Uitert 1956) and has not yet been explained. Equation (1) is obeyed with $A \simeq 0{\cdot}02$ and 0·09 Ωcm, and $\epsilon = 0{\cdot}18$ and 0·15 ev respectively above and below 140°c. There

is no anomaly at the Curie point and the material therefore exhibits type I conduction as predicted by Parker and Tredgold.

It is perhaps of interest to point out that our values for A and ϵ correspond very closely to those reported recently by Jonker (1959) for iron-rich cobalt ferrites. Such agreement is not unexpected as the two materials have the same crystal structure and the high conductivity in each case derives from the presence in the crystal lattice of a number of divalent iron ions.

The authors which to acknowledge the facilities and encouragement given to them by Professor E. R. Andrew and Dr. D. Wooller.

Department of Physics,
University College of North Wales,
Bangor.
18th August 1959.

R. Parker.
H. Lord.

Jonker, G. H., 1959, *J. Phys. Chem. Solids*, **9**, 165.
Koops, C. G., 1951, *Phys. Rev.*, **83**, 121.
Parker, R., 1958, *Phil. Mag.*, **3**, 853.
Snoek, J. L., 1947, *New Developments in Ferromagnetic Materials* (Amsterdam, New York: Elsevier).
van Uitert, L. G., 1956, *J. Chem. Phys.*, **24**, 306.

CORRIGENDUM

A Simple Method of Calculating Moiré Patterns, by G. L. Rogers (*Proc. Phys. Soc.*, 1959, **73**, 142).

The author's attention has been drawn to prior work by a number of Australian physicists. In a much more thorough examination they develop the moiré pattern from a superlattice calculated in exactly the same way as the difference vector. References to their work are :

Cowley, J. M., and Rees, A. L. G., 1958, *Rep. Progr. Phys.* **21**, 165 (London: Physical Society)
Dowell, E. C. T., Farrant, J. L., and Rees, A. L. G., *Proceedings of International Conference on Electron Microscopy*, London, July 1954, p. 279.
—— First Regional Conference, Tokyo, 1956, p. 320.

REVIEWS OF BOOKS

The Physical Metallurgy of Magnesium and its Alloys, by G. V. Raynor. Pp. ix+531. (London, New York, Paris, Los Angeles: Pergamon Press, 1959.) 75*s*.

This book is a most excellent account of what is known of the metal magnesium and its alloys. Professor Raynor's special grasp of the significance of the electronic structure and its interaction with crystal structure gives a unifying approach to his subject which is most welcome. The whole book will therefore appeal to physicists who want to find out either what magnesium does in some circumstance, and why, or what physical metallurgists do, and why. It will obviously become the standard book on magnesium, and it is a great relief to find such a book equipped with an index which really is adequate to its task of guiding one through 500 pages on the physical, mechanical and alloying properties of magnesium. The book is pleasantly printed and illustrated with many well thought out diagrams. W. M. LOMER.

Basic Physics of Atoms and Molecules, by U. Fano and L. Fano. Pp. xv+414. (New York : Wiley; London : Chapman and Hall, 1959.) 80*s*.

The aim of this book is surely unattainable. It sets out to present a clear concept of quantum mechanics without previous knowledge of physical theory or mathematics. This is attempted by presenting a set of key experiments which display the quantum nature of matter on the atomic scale, and arguing inductively to the formulation of quantum laws and the uncertainty principle. On p. 168 at last we reach the Schrödinger equation and the explanation of the meaning of a partial derivative. The remainder of the book introduces in a similar way the notions of electron spin, the exclusion principle, molecular bonding and metallic bonds. The short section on crystals and plasticity is very badly out of date and misleading.

The reviewer finds it difficult to believe that a book like this is as simple to learn from as one which rests on deductive reasoning from accepted axioms justified *a posteriori*. However, Dr. Fano believes it will be of value to biologists and others whose science has included little mathematics. I hope he is right, for the need on purely cultural and educational grounds is great. W. M. LOMER.

The Growth and Perfection of Crystals, edited by R. H. Doremus, B. N. Roberts and D. Turnbull. Pp. xvii+609. (London: Chapman and Hall; New York: John Wiley, 1959.) 100*s*.

In August 1958, an international conference was held at Cooperstown, New York, sponsored jointly by the U.S. Air Force Office of Scientific Research, and the General Electric Research Laboratory. This volume represents the proceedings of the conference, which was attended by about sixty scientists, including fifteen from overseas.

Following an introductory lecture, given, most appropriately, by F. C. Frank, the proceedings of the conference fall into five sections. Each section begins with a review article which summarizes the present state of knowledge on the appropriate topic, and this is followed by a group of papers, numbering between five and ten, presenting the results of new or recent work.

The first section on ' The growth of whiskers ' is introduced by F. R. N. Nabarro and P. J. Jackson with an exhaustive review covering not only what they call ' proper whiskers '—those grown direct from a massive solid phase—but also many other forms of filamentary growth. The treatment is comprehensive and, as far as possible in a rapidly developing subject, critical, covering both experimental and theoretical work. The second review by S. S. Brenner, is on ' The properties of whiskers and crystal imperfections ' and about half of it is concerned with their mechanical properties. This is to be expected in view of the fact that the current interest in the subject springs largely from the demonstration, in 1952, of the very great mechanical strength of some whiskers. The review covers very thoroughly the work done since this observation was made and includes some unpublished work by the author.

The topic of ' The growth of crystals of pure materials and of the solvents of solutions ' is dealt with by B. Chalmers. His account consists essentially of a summary of his own extensive contributions to this subject and it is unfortunate that the reproduction of a wrong diagram (figure 6) makes it needlessly difficult to follow the argument. The discussion which took place at the conference is reproduced, with a minimum of editing, after each paper. This practice certainly enlivens the printed volume, and the discussion on Chalmers contribution, by Frank and others, is particularly illuminating.

The complementary section on ' The growth of crystals from solution ' is introduced by N. Cabrera and D. A. Vermilyea. Like its predecessor, this is not a comprehensive review of present knowledge on the subject but a coherent account of the authors' own approach to the theoretical problem, linked to the experimental observations at appropriate points.

The final section, on the Crystallization of polymers, is introduced by two reviews, the first by L. Mandelkern dealing with ' Crystallization kinetics in polymeric systems ' and the second by A. Keller on ' The morphology of crystalline polymers '. In style, these fall somewhere between the opposite tendencies of the first two pairs. Both are restricted rather than widespread in their scope: but both represent a critical survey of the whole field they set out to cover.

It is impossible in a short notice even to mention the 35 papers on more specialized subjects which constitute the remainder of the volume, and it would be invidious to single out any few. Most of them are, by their very nature, more specialized in their appeal than the introductory reviews and are the kind of publication one would expect to find in any learned periodical. The value of a volume such as the one under review is that it collects them all within one cover. In the present instance an even more important point is that the book was published within five months of the date of the conference. This truly remarkable achievement on the part of the editors was made possible by the use of a photo-offset reproduction process from typed copies of the papers. The resulting clarity of text and quality of reproduction of the numerous photographs leaves nothing to be desired. The volume is one which no active worker in the field which it covers can afford to be without, and which is likely to be the standard work on its subject for some years to come. It weighs more than two kilogrammes.

N. THOMPSON.

Extensive Air Showers, by W. GALBRAITH. Pp. xvi+211. (London: Butterworths Scientific Publications, 1958.) 40*s*.

During the last two decades cosmic-ray physicists have made many detailed studies of the interaction in the earth's atmosphere of the ultra-high-energy

proton component of cosmic radiation. In their own jargon the results of these very high-energy interactions are known as extensive air showers. The study of these showers, which are mainly, but not entirely, huge electron–photon cascades, is of interest for two main reasons.

The showers are produced by primary particles of very great energy, up to 10^{19} ev or possibly even greater energies. The primary particles make nuclear collisions in the upper layers of the atmosphere and mesons are produced. The electron–photon cascades arise from the decay of the π^0-meson component of the secondary particles. The nuclear physicist can only study these ultra-high-energy collisions using the cosmic radiations, the energies are far higher than those attainable using proton synchrotrons.

From observations on the extensive air showers, information has been obtained on the energy spectrum of the primary cosmic rays. This data is of great importance in understanding the astrophysical processes in which the cosmic rays are produced. Thus the subject of Dr. Galbraith's book is of interest to astrophysicists as well as nuclear physicists interested in ultra-high-energy phenomena.

The first chapter is devoted to a theoretical account of the generation of air showers. Both the photon–electron and the nuclear cascades are discussed briefly and finally formulae for the lateral spread of extensive air showers are quoted. The theory is not given in detail but rather a useful outline is provided which will be of considerable value to young research workers.

The remaining chapters are mainly devoted to experimental results on the structure of the air showers, including the weak component of penetrating particles. Some discussion is included, however, on the search for time variations in the rate of extensive air showers and a brief mention is made of theories of the origin of cosmic radiation. The last chapter is concerned with the properties of Čerenkov radiation produced by extensive air showers.

This book will be of great value to experimental physicists starting research in cosmic-ray physics. In the view of the reviewer it is rather too specialized and includes too much experimental detail to be of great interest to the general reader.

C. C. BUTLER.

Progress in Nuclear Energy: Physics and Mathematics, Vol. 2, edited by D. J. Hughes, J. E. Sanders and J. Horowitz. Pp. vii+375. (London, New York, Paris, Los Angeles: Pergamon Press, 1958.) 90*s*.

The book contains eight articles, dealing with various experimental and theoretical topics in reactor physics.

The first two chapters are concerned with the measurements of cross section data. The information on fast neutron data presented in the first article is still incomplete for accurate calculations of some fast reactor systems. However, this chapter does contain a very good section on the measurement of fast neutron flux, the errors involved in the various types of measuring apparatus are thoroughly discussed. The second article gives an adequate review of the thermal and resonance energy cross section measurements of some heavy nuclei, other than ^{239}Pu, ^{233}U and ^{235}U. There is a discussion of the formula to use for the fluctuations of the reduced neutron widths of levels. This is of interest in the calculations of resonance escape probability for the unresolved resonances and is discussed in a later article.

The third chapter deals with the measurement and theory of reactor spectra. The review of the experimental measurements is quite comprehensive and deals with thermal, intermediate and fast reactor assemblies. The theoretical section deals mainly with the calculation of spectra which are independent of position. There is only a qualitative discussion of such important problems as the energy distribution of thermal neutrons as a function of position. However, this is understandable as the methods of calculation are being developed at the present time.

There is an article on the standardization of neutron sources, including a section on the intercomparison of the various standard neutron sources.

The next chapter deals with diffusion measurements using pulsed neutron sources. It contains an excellent description of this recently developed technique for the measurement of the thermal neutron absorption cross sections and the diffusion coefficient in a scattering medium. A very clear account of the theory is given, including a description of the diffusion cooling phenomenon.

The sixth chapter is concerned with the calculation of the resonance escape probability in thermal reactors. This article is to be welcomed as it contains a discussion of the American and Russian work on this subject, and the differences in the empirical theories which became apparent at the 1955 Geneva Conference. The article includes a description of some analytical approaches which may result in an improvement of the theory.

The seventh chapter deals with a number of topics. Various methods for the numerical solution of partial differential equations in (r, z) geometry are discussed, and a formal explanation of Kron's method is given. Calculations of heterogeneous systems are then discussed. The application of these methods to a practical problem is discussed and the results compared with experiment. It is evident that the predictions using the methods described are not accurate enough to determine all the properties of the chosen reactor.

The last chapter deals with Monte Carlo methods in transport problems. This article is intended for the mathematician. From a practical point of view other methods are probably better suited for the solution of some of the reactor problems described at the end of this article.

This book reviews a wide cross section of reactor physics work. It contains excellent material and should be welcomed. J. H. TAIT.

The Physics of Elementary Particles, Investigations in Physics No. 9, by J. D. JACKSON. Pp. x+135. (Princeton: University Press; London: Oxford University Press, 1958.) 30*s*.

This is an admirable addition to this already well-established series. The physics of elementary particles in the sense in which the term is used here is a subject that did not exist fifteen years ago except for the one chapter of 'classical' β-decay. Today it has the place in physics occupied earlier by pre-fission nuclear physics—the vast, newly opened field of knowledge posing entirely unforeseen problems to the investigator and, apparently, leading far away from matters of practical applicability. Past experience makes one wonder how long this detachment from the rest of reality will last.

A book of the size of this one cannot do more than give a broad introduction to this, by now, vast field. To do this is the author's avowed intention and he accomplishes his task most satisfactorily with an approach that balances

experiment and theory in the manner we have learnt to expect from the best American expositors. The book is divided into the three parts: I. The interaction of pions and nucleons, II. K-mesons and hyperons and III. Decay processes. To anyone seeking his bearings within the field covered annually by the ' Rochester ' Conferences the book will serve as an admirable introduction. References up to May 1958 are included. N. KEMMER.

Introduction to Monopulse, by DONALD R. RHODES. Pp. x+119. (New York, London, Toronto: McGraw-Hill Book Company, 1959.) 42*s.* 6*d.*

Monopulse is a system of radar, first conceived almost at the same time as radar itself by various inventors. It is the method of locating an object by two or three simultaneous lobes instead of by sequentially emitted beams. During the War, for certain reasons, only the sequential method was developed, but since that time monopulse appears to have gained importance. Its great advantage is, of course, that it eliminates ' jitter ' through scintillation of the target or by the rapid motion of the glint from one point of the target to another. This book is an excellent introduction to the subject, comprehensive to the point at which military secrecy prevents the publication of details. In particular the theoretical explanations are handled in an exemplary manner by the author, who is the Head of the Basic Research Department of an important American company. D. GABOR.

Noise in Electron Devices, edited by L. D. SMULLIN and H. A. HAUS. Pp. xvi+413. (Massachusetts: M.I.T. Technology Press; New York: John Wiley; London: Chapman and Hall, 1959.) 96*s.*

Based on a course given at M.I.T. in 1955, this book consists of seven articles by six authors. In the first article C. F. Quate gives, in 43 pages, a lucid account of our present knowledge of shot noise from thermionic cathodes. This article is a delight to read and fills a long standing gap in the literature. The second article by A. van der Ziel surveys flicker noise in vacuum tubes. The less satisfactory state of the subject is to some extent reflected in the article whose 31 pages are packed with valuable information but, as the author remarks, the exact mechanism of the noise has not yet been established. In 61 pages T. E. Talpey presents virtually everything the electronic engineer needs to know about noise in grid control tubes. This is a most informative and useful article.

H. A. Haus (73 pages) and R. W. Peter (88 pages) discuss the general properties of noise in electron beams and the design of low noise travelling wave tubes. These two competent and exhaustive articles alone will make the book a necessity for the microwave tube designer.

In the final two chapters A. van der Ziel (31 pages) and W. H. Fonger (60 pages) deal with noise in semiconductors and transistors. They provide a thorough discussion of the sources of semiconductor noise and the factors influencing the design of low noise transistor amplifiers.

The editors are to be congratulated on having assembled such an excellent and thoroughly professional book on a subject not notably well served by the existing literature. The articles by Quate, Talpey and van der Ziel (flicker noise) will be valuable to anyone concerned with the design of low noise amplifiers using conventional tubes, while specialists in the appropriate fields will undoubtedly welcome the remaining articles. F. N. H. ROBINSON.

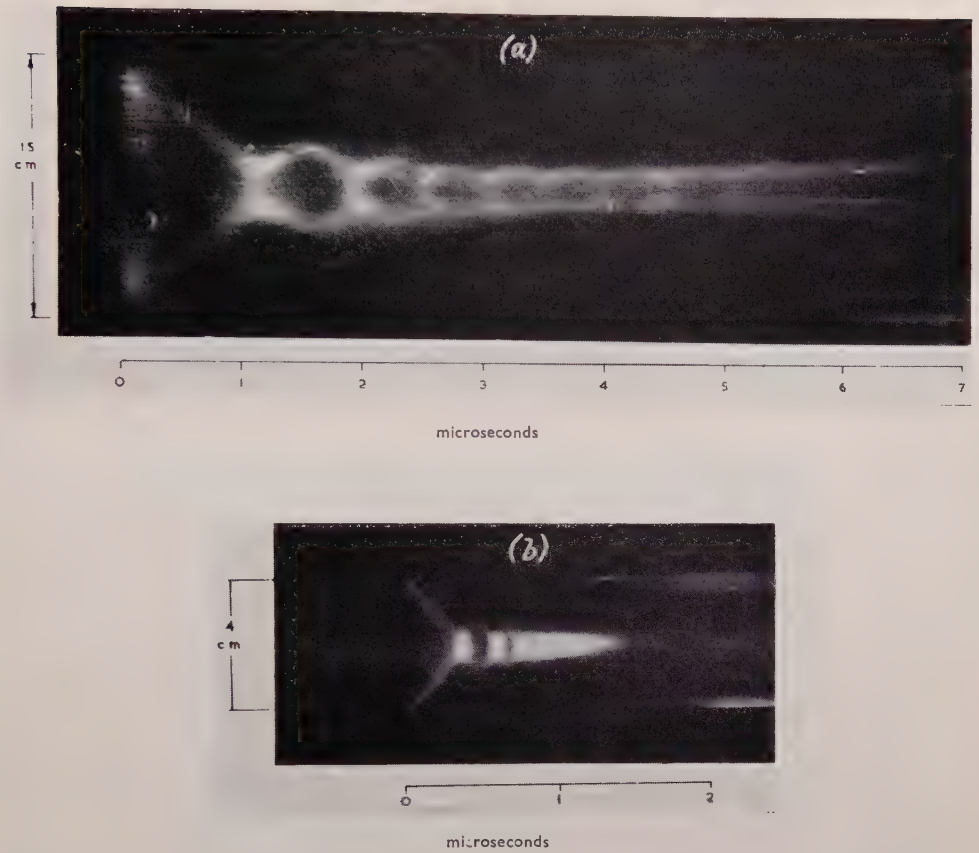

Figure 2. Streak photographs of radial hydromagnetic oscillations in discharges in deuterium: (*a*) experiment in 15 cm bore tube; (*b*) experiment in 4 cm bore tube.

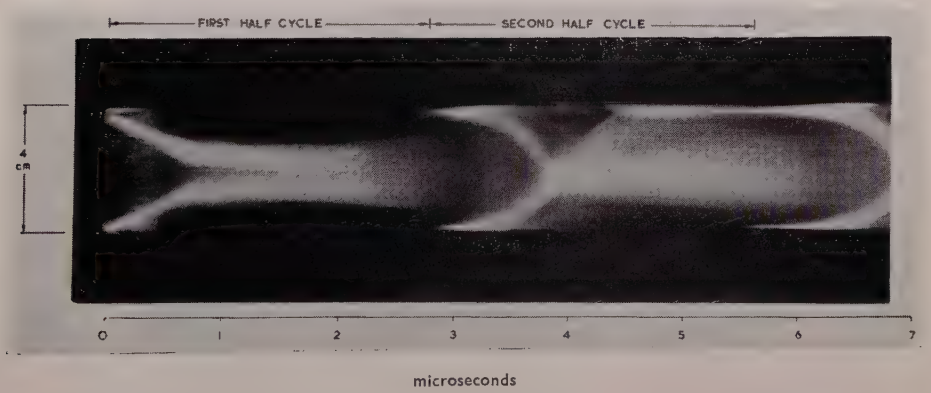

Figure 6. Streak photograph of a discharge in air using 4 cm bore tube.

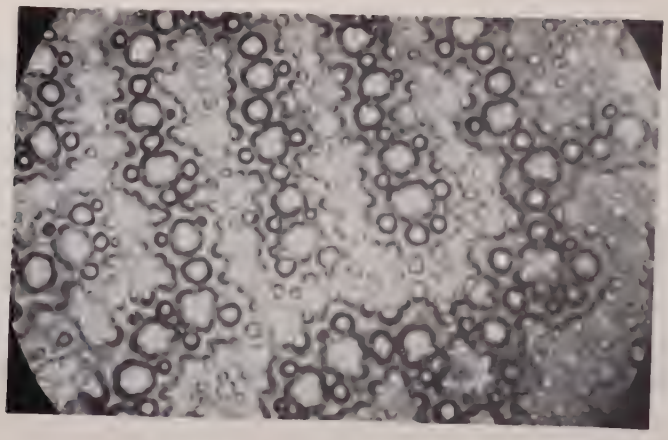

Figure 1.

30μ

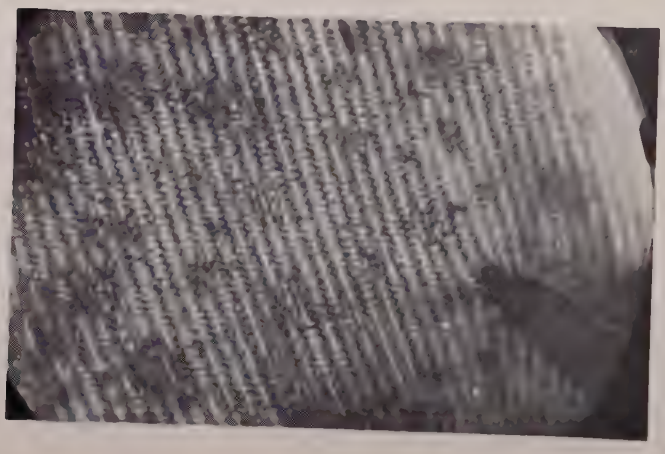

Figure 3.

30μ

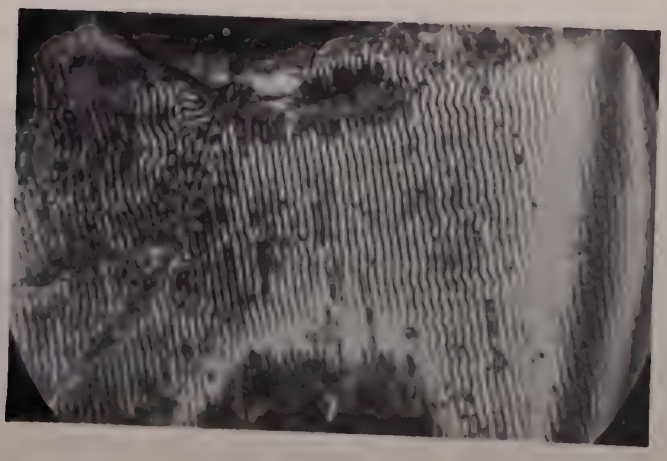

Figure 4.

30μ

PROCEEDINGS OF THE PHYSICAL SOCIETY

1959—VOL. 74

SUBJECT INDEX

PAGE

Absorption edge of arsenic–sulphur–selenium mixtures (L) 667
Absorption of microwaves in ethyl chloride 401
Absorption system in type I diamonds (R) 647
Absorption, *see also* Ultrasonic
Ageing effect in evaporated films of ZnS (R) 641
Alloys, GaSb–InSb system, optical energy gap variation 244
Alloys, iron–chromium, magnetic susceptibilities 290
Alloys, Ni–Co, electronic specific heats 417
Alpha particles in water and water vapour, range–energy relations and stopping power 585
Alpha particles, scattering by helium 529
Angular distribution of (d, p) stripping reactions 517
Angular distributions, *see also* Reactions
Anisotropy and magnetic susceptibility of trivalent vanadium alum 711
Antiferromagnetics, asymptotic behaviour of Mayer cluster series 432
Arsenic 80, decay 693
Arsenic mixtures, absorption edge (L) 667
Atomic velocity distributions in Hg and HgO by nuclear resonant scattering of γ–rays 680
Atmosphere, upper, *see* Upper atmosphere

Band systems, application of r-centroid concept (R) 133
Beryllium, bombardment by ^{3}He 196
Beta decay, double, electron coincidence spectrum in 350
Beta decay of ^{239}Np . . . . . 161, corr. 671
Binding, ionic, in cadmium telluride (L) 490
Bismuth telluride, magnetic susceptibility 599
Bismuth telluride, sintering (R) 768
Bombardment of ^{9}Be with 5·7 Mev ^{3}He, protons, deuterons and tritons from . . 196
Bonding in cadmium telluride (L) 489
Bosons, charged, vacuum polarization due to (R) 480
Breakdown, and ionization and attachment coefficients in dry air 33
Breakdown voltage of air gaps, influence of humidity 297

Cadmium telluride, bonding in (L) 489
Cadmium telluride, ionic binding in (L) 490
Cavity, resonant, coupling of spin system to 561
Colloid centres in LiH, electron spin resonance 540
Colour centres, in LiH, properties 540
Coma, systems with, geometrical optical calculation of frequency response . . 721
Conduction, electric, in semiconductors (R) 643
Conduction processes in condensed aromatic hydrocarbons 756
Conductivity, thermal, *see* Thermal conductivity
Cosmic ray showers, extensive, penetrating component 554
Cross sections, electron collision, in helium 473
Cross sections, photoelectric, use of fractional parentage coefficients in calculation (R) 136
Cross sections, radiative capture, of ^{232}Th for neutrons in energy range 300–1200 kev 685
Cross sections, *see also* Reactions
Crystal structure, *see under* Mayer
Crystals, silicon, pulled, control of resistivity (L) 669

PAGE
Crystals, single, of CdS, reflection spectrum (L) 138
Crystals, single, of copper, development of electroplating deposit structures . . 616
Crystals, single, LaF_3, containing Gd^{3+}, electron spin resonance . . . 249
Crystals, single, lead, effect of magnetic field on ultrasonic absorption (R) . . 774
Crystals, yttrium acetate, principal g values of Yb^{3+} ions 513
Crystals, *see also* Magnetocrystalline
Current pulses, generation of pairs at variable intervals (R) 378
Current sheet in gas discharge 700

Decay of arsenic 80 693
Decay of ^{144}Ce 449
Decay of ^{147}Pm (R) 478
Diamond, pressure crack figures, critical stress for 48
Diamond, semiconducting, Hall coefficient and magnetoresistance . . . 363
Diamonds, type I, absorption system in (R) 647
Dielectric liquids, monatomic, thermal conductivity 208
Diffraction by opaque strip (R) . . . . . corr. 140
Digital computer, electronic, lens designing by: II 316
Discharge, hot-cathode, noise spectra of probe in 42
Discharge, low pressure plane symmetric 145
Discharge, spark, early stages of spark channel expansion 309
Domain structures on thin sheets of magnetoplumbite (R) 786
Domain wall energy, direct measurement 170

Electrodeposits, growth on copper single crystals 616
Electromagnetic fields, scalar representation: II 269
Electromagnetic fields, scalar representation: III 281
Electron attachment coefficients in oxygen, dry air, humid air and water vapour . 297
Electron coincidence spectra in double beta decay 350
Electron guns, trajectory plotting in. 177
Electron spin resonance of colloid centres in LiH 540
Electron spin resonance of Gd^{3+} in lanthanum fluoride 249
Electron spin resonance for polycrystalline substances (L) 491
Electronic configurations f^n, matrix elements of tensor operators for . . . 330
Emulsions, nuclear, multiple scattering of electrons and positrons (R) . . . 655
Energy levels, atomic, light beats as indicators of structure (L) 790
Energy levels of ^{21}Ne (R) 777
Energy levels, 1·12 Mev, in ^{18}F (R) 660
Entropy of non-equilibrium ideal quantum gas (R) 486
Equilibrium of double layer 368
Ethyl chloride, absorption of microwaves in 401
Expansion, adiabatic, of water vapour, production of ice crystals 11
Expansion, lattice theory 17

Faraday effect, infra-red, determination of effective electron mass in GaAs by (R) . 131
Ferrites, maganese, Co-substituted, magnetic anisotropy 505
Ferrites, nickel, oxygen deficient, electrical resistivity (L) 793
Ferromagnetism, dipolar, in dysprosium ethyl sulphate (L) 791
Films, evaporated, of ZnS, ageing effect (R) 641
Films, helium, thickness (R) 217
Flame spectra, effect of deuteration on hydrocarbon bands (R) 639
Fluctuations of photon beams: distribution of photo-electrons 233
Fluorescence, *see under* Scintillators
Fluorine 18, 1·12 Mev energy level (R) 660
Frequency response for systems with coma, geometrical optical calculation . . 721

Gallium arsenide, determination of effective electron mass by infra-red Faraday effect (R) 131

PAGE
Garnet, magnetic properties of rare earth ions in (L) 665
Garnet, paramagnetic resonance of Yb^{3+} in yttrium gallium (L) 663
Gas discharge, current sheet in 700
Gas, lattice model 444
Germanium surfaces, recombination relaxation effects in 395
Graphite, electronic structure 604
Graphite π-band, self-consistent calculation 385

Hall coefficient and magnetoresistance in semiconducting diamond . . . 363
Heat transfer by forced convection (R) 771
Heats of solution of magnesium oxide, variation, x-ray study 673
Helium, double charge transfer and mobility of He^{2+} ions 457
Helium, electron collision cross sections 473
Helium films, thickness (R) 217
Humidity, influence on breakdown voltage of air gaps 297
Hydrocarbons, aromatic, conduction processes 756
Hydrogen, atomic, electron loss from passage of fast H^- ions 463

Ice crystals, production by large adiabatic expansions of water vapour . . . 11
Ice nuclei, artificial, properties and behaviour 744
Immersed body, equilibrium of double layer surrounding 368
Indium antimonide, p-type, properties II: photoelectric properties and carrier lifetime 81
Interaction, electron–lattice, in metals 545
Interactions, elastic, proton–proton, at 930 MeV 625
Ionization in air, and breakdown 33
Ions, potassium, mobility in nitrogen and neon at 294°K 497
Iron and silicon–iron, magnetothermal effects 53
Iron ditelluride, magnetic susceptibility: I 65
Iron ditelluride, magnetic susceptibility: II 75
Isotope shift in CdI intercombination resonance line λ 3261 Å 689
Isotope shifts in rare gases, interpretation 424

Lattice expansions and Debye temperatures of Ti and Ag 609
Lattice model of gas 444
Lattice theory of expansion 17
Lens designing by electronic digital computer: II 316
Lenses, aplanatic 731
Light beats as indicators of structure in atomic energy levels (L) . . . 789
Light, forward scattering by spheres according to geometrical optics . . . 105
Low temperature resistivity of plutonium and neptunium (L) 671

Magnesium oxide, variation in heats of solution, x-ray study 673
Magnetic susceptibility and anisotropy of trivalent vanadium alum . . . 711
Magnetic susceptibility of bismuth telluride 599
Magnetic susceptibility of $FeTe_2$: I 65
Magnetic susceptibility of $FeTe_2$: II 75
Magnetic susceptibilities of iron–chromium alloys 290
Magnetism, *see also* Domain
Magnetocrystalline anisotropy of Co-substituted manganese ferrite . . . 505
Magnetothermal effects in iron and silicon–iron 53
Matrices, 3×3, decomposition (R) 649
Matrix elements of tensor operators for electronic configuration f^n . . . 330
Mayer cluster series in antiferromagnetic problem, asymptotic behaviour . . 432
Mayer method, application to melting problem 183
Meissner effect, gauge invariance and electron correlations 340
Melting problem, application of Mayer method 183
Metals, electron–lattice interaction 545
Microwaves, absorption in ethyl chloride 401

PAGE
Mobility of potassium ions in nitrogen and neon at 294°K 497
Moiré patterns, calculating (L) . . . . . corr. 795

Neutrons, radiative capture cross section of ^{232}Th for 685
Noise spectra of probe in hot-cathode discharge 42

Oscillations, radial hydromagnetic 737

Paramagnetic resonance of Yb^{3+} in yttrium gallium garnet (L) 663
Paramagnetic resonance, *see also* Cavity
Particles, fast charged, scattering: multiple scattering of fast electrons and positrons in xenon 257
Photoelectric effect, selective 27
Photon beams, fluctuations: distribution of photo-electrons 233
Pions, neutral 92
Pions, neutral, spin 124
Plasma oscillations, radial hydromagnetic 737
Polarization, effect on elastic scattering of positrons by H atoms 101
Polarization, nucleon, from charge-exchange reactions in deuterium (R) . . 652
Polarization of protons elastically scattered from oxygen at 8·7 MeV . . . 705
Polarization, vacuum, due to charged bosons (R) 480
Polycrystalline substances, electron spin resonance for (L) 491
Positrons, elastic scattering by H atoms, effect of polarization 101
Proton magnetic resonance in liquid *iso*-butyl bromide 408
Protons, excitation of N_2 and O_2 by 87
Protons, *see also under* Polarization

Quantum gas, non-equilibrium ideal, entropy (R) 486

r-centroids of molecular transitions, equilibrium internuclear separations and oscillator turning points (R) 133
Rare earth ions, in garnets, magnetic properties (L) 665
Rare gases, isotope shifts, interpretation 424
Reaction $^{16}O(^3He, p)^{18}F$, angular distribution of proton groups from . . . 762
Reactions, charge-exchange, in deuterium, nucleon polarization (R) . . . 652
Reactions, (n, pn), with heavy nuclides, cross sections 632
Reactions $^{16}O(^3He, d)^{17}F$ and $^{16}O(^3He, \alpha)^{15}O$, angular distribution measurements (R) 775
Reactions, *see also* Stripping
Recombination relaxation effects in Ge surfaces. 395
Resistivity, control in pulled silicon crystals (L) 669
Resistivity, electrical, of oxygen deficient nickel ferrite (L) 793
Resistivity, low temperature, of plutonium and neptunium (L) 671
Resonance, *see under* Electron, Electron spin, Electron spin resonance, Proton magnetic resonance

Scalar representation of electromagnetic fields: II 269
Scalar representation of electromagnetic fields: III 281
Scattering, elastic, from oxygen, polarization of protons 705
Scattering, elastic, *see also under* Positrons
Scattering of alpha particles by helium 529
Scattering of fast charged particles: multiple scattering of fast electrons and positrons in xenon 257
Scattering of fast charged particles—VI: multiple scattering of 10 MeV electrons and positrons in nuclear emulsions (R) 655
Scattering of light, forward, by spheres according to geometrical optics . . 105
Scattering, nuclear resonant, of γ-rays, and measurements of atomic velocity distributions 680
Scattering, p–p, spin correlation coefficient for 90° c.m. scattering angle (R) . . 482

PAGE

Scintillators, plastic, response to protons (R) 483
Self-consistent field theory, applied to graphite π-band 385
Semiconductors, electric conduction in (R) 643
Semiconductors, *see also under* Bismuth, Diamond, Germanium, Indium
Silver, lattice expansion and Debye temperature 609
Sintering of bismuth telluride (R) 768
Skin effect, inverse 576
Spark channel expansion, early stages 309
Spark channels, generation of pairs of current pulses (R) 378
Specific heats, electronic, of Ni–Co alloys. 417
Spectra excited in N_2 and O_2 by protons 87
Spectra, spark, selective pressure broadening and Stark effect 97
Spectra, *see also* Flame
Spectrum, reflection, of CdS (L) 138
Spin Hamiltonian of Γ_8 quartet . . . . . corr. 493
Spin precession in crossed magnetic and electric fields (R) 782
Spin system, coupling to cavity mode 561
Stark effect and selective pressure broadening 97
Stripping reactions, (d, p), angular distribution 517
Superconductivity, Meissner effect, gauge invariance and electron correlations . 340
Superconductivity, susceptibility of superconducting spheres 153
Susceptibility, magnetic, *see under* Magnetic Susceptibility
Susceptibility of superconducting spheres 153

Thermal conductivity of monatomic dielectric liquids 208
Titanium, lattice expansion and Debye temperature 609
Trajectory plotting in electron guns 177
Turbulence in upper atmosphere, measurements 1

Ultrasonic absorption, electronic component in lead single crystal, effect of magnetic field (R) 774
Upper atmosphere, measurements of turbulence in 1

Water and water vapour, α-particles in, range–energy relations and stopping power 585

X-ray emission spectra of graphite, interpretation 604
X-ray measurements of lattice expansion and Debye temperatures of Ti and Ag 609

Yttrium acetate, principal g values of Yb^{3+} ions in 513

INDEX TO AUTHORS (WITH TITLES)

PAGE

Agarwal, B. K.: Thickness of helium films (R) 217

Al-Jeboori, M. A., Bokhari, M. S., Hird, B., and Strzałkowski, A.: Polarization of protons elastically scattered from oxygen at 8·7 MeV 705

Allaby, J. V., Ashmore, A., Diddens, A. N., and Eades, J.: Measurement of spin correlation coefficient C_{nn} in p–p scattering at 320 MeV, for 90° centre of mass scattering angle (R) 482

Allen, K. R., with Phillips, K.: Scattering of fast charged particles: V—Multiple scattering of fast electrons and positrons in xenon 257

Allen, K. W., Eccleshall, D., and Yates, M. J. L.: 1·12 MeV level in ^{18}F (R) . . 660

Ambasankaran, C., with Phillips, K.: Scattering of fast charged particles: VI—Multiple scattering of 10 MeV electrons and positrons in nuclear emulsions (R) 655

Archard, G. D.: Trajectory plotting in electron guns 177

Armstrong, B. H.: Use of fractional parentage coefficients in calculation of photo-electric cross sections (R) 136

Ashmore, A., with Allaby, J. V., Diddens, A. N., and Eades, J.: Measurement of spin correlation coefficient C_{nn} in p–p scattering at 320 MeV, for 90° centre of mass scattering angle (R) 482

Baker, J. M., with Jones, D. A., and Pope, D. F. D.: Electron spin resonance of Gd^{3+} in lanthanum fluoride 249

Baker, T. W., with Thomas, D. K.: X-ray study of factors causing variation in heats of solution of magnesium oxide 673

Banbury, P. C., with Lindley, D. H.: Recombination relaxation effects in germanium surfaces 395

Barry, J. F., Coleman, R. F., Hawker, B. E., and Perkin, J. L.: Cross sections for some (n, pn) reactions with heavy nuclides 632

Barry, J. F., O'Connor, L. P., and Perkin, J. L.: Radiative capture cross section of ^{232}Th for neutrons in the energy range 300 to 1200 kev 685

Bate, R. T., and Willardson, R. K.: Hall coefficient and magnetoresistance in semiconducting diamond 363

Bates, L. F., and Davis, P. F.: Direct measurement of domain wall energy . . 170

Bates, L. F., and Sansom, D. J.: Magnetothermal effects in iron and silicon–iron 53

Bellamy, E. H., with Evans, H. C.: Response of plastic scintillators to protons (R) 483

Bellamy, E. H., with Prentice, J. D., and Williams, W. S. C.: Spin of neutral pion 124

Blackman, M.: Lattice theory of expansion 17

Bleaney, B.: Spin Hamiltonian of Γ_8 quartet . . . . . corr. 493

Boakes, D., Garton, G., Ryan, D., and Wolf, W. P.: Paramagnetic resonance of Yb^{3+} in yttrium gallium garnet (L) 663

Bokhari, M. S., with Al-Jeboori, M. A., Hird, B., and Strzałkowski, A.: Polarization of protons elastically scattered from oxygen at 8·7 MeV 705

Boot, A. R., with Eisenschitz, R.: Thermal conductivity of monatomic dielectric liquids 208

Bromley, D. A., with Nicholls, R. W., and Reeves, E. M.: Excitation of N_2 and O_2 by 1/2 and 1 MeV protons 87

Bunn, P. B., with Walling, J. C.: Electronic specific heats of some nickel–cobalt alloys 417

Butcher, A. C., and McNamee, J. M.: Scattering of alpha particles by helium . 529

Cade, R.: Equilibrium of double layer 368

Cassels, J. M., Jones, D. P., Murphy, P. G., and O'Neill, P. L.: Neutral pions 92

PAGE

Chakravarty, A. S.: Magnetic susceptibility and anisotropy of trivalent vanadium alum under crystalline electric field having predominantly cubic symmetry with small trigonal symmetry 711
Champeney, D. C., and Miller, C. A.: Measurements of atomic velocity distributions in Hg and HgO by nuclear resonant scattering of gamma rays . . . 680
Christian, J. W., with Spreadborough, J.: Measurement of lattice expansions and Debye temperatures of titanium and silver by X-ray methods . . . 609
Coleman, R. F., with Barry, J. F., Hawker, B. E., and Perkin, J. L.: Cross sections for some (n, pn) reactions with heavy nuclides 632
Connor, R. D., and Fairweather, I. L.: β-decay of ^{239}Np . . . 161, corr. 671
Cooke, A. H., Edmonds, D. T., Finn, C. B. P., and Wolf, W. P.: Dipolar ferromagnetism in dysprosium ethyl sulphate (L) 791
Crompton, R. W., and Elford, M. T.: Mobility of potassium ions in nitrogen and neon at 294°K. 497

Davis, P. F., with Bates, L. F.: Direct measurement of domain wall energy . . 170
Desai, H. S., with Gogate, D. V.: Heat transfer by forced convection (R) . . 770
Dickinson, N., with Kellermann, E. W.: Structure of extensive cosmic ray air showers: Penetrating component 554
Diddens, A. N., with Allaby, J. V., Ashmore, A., and Eades, J.: Measurement of spin correlation coefficient C_{nn} in p–p scattering at 320 MeV, for 90° centre of mass scattering angle (R) 482
Dodd, J. N., Fox, W. N., Series, G. W., and Taylor, M. J.: Light beats as indicators of structure in atomic energy levels (L) 789
Dowell, J. D., Frisken, W. R., Martelli, G., and Musgrave, B.: Proton–proton elastic interactions at 930 MeV 625
Doyle, W. T.: Selective photoelectric effect 27
Doyle, W. T., Ingram, D. J. E., and Smith, M. J. A.: Electron spin resonance of colloid centres in lithium hydride 540
Dutta, A. K.: Analysis of soft X-ray emission spectroscopy of graphite and appropriate electronic picture of it 604

Eades, J., with Allaby, J. V., Ashmore, A., and Diddens, A. N.: Measurement of spin correlation coefficient C_{nn} in p–p scattering at 320 MeV, for 90° centre of mass scattering angle (R) 482
Eccleshall, D., with Allen, K. W., and Yates, M. J. L.: 1·12 MeV level in ^{18}F (R) 660
Edmonds, D. T., with Cooke, A. H., Finn, C. B. P., and Wolf, W. P.: Dipolar ferromagnetism in dysprosium ethyl sulphate (L) 791
Eisenschitz, R., and Boot, A. R.: Thermal conductivity of monatomic dielectric liquids 208
Elford, M. T., with Crompton, R. W.: Mobility of potassium ions in nitrogen and neon at 294°K. 497
Ellison, J. McK., and Peetz, C. V.: Forward scattering of light by spheres according to geometrical optics 105
Evans, H. C., and Bellamy, E. H.: Response of plastic scintillators to protons (R) 483
Evans, J. A., with Woolley, J. C., and Gillett, C. M.: Optical energy gap variation in GaSb–InSb system 244

Fairweather, I. L., with Connor, R. D.: β-decay of ^{239}Np . . . 161, corr. 671
Ferguson, A. F., and Moiseiwitsch, B. L.; Double charge transfer and mobility of He^{2+} ions in helium 457
Finlayson, D. M., Llewellyn, J. P., and Smith, T.: Magnetic susceptibility of iron ditelluride, Part II 75
Finn, C. B. P., with Cooke, A. H., Edmonds, D. T., and Wolf, W. P.: Dipolar ferromagnetism in dysprosium ethyl sulphate (L) 791
Fox, W. N., with Dodd, J. N., Series, G. W., and Taylor, M. J.: Light beats as indicators of structure in atomic energy levels (L) 789
Freeman, N. J.: Decay of ^{144}Ce 449

PAGE

Frisken, W. R., with Dowell, J. D., Martelli, G., and Musgrave, B.: Proton–proton elastic interactions at 930 MeV 625
Fröhlich, H., and Sewell, G. L.: Electric conduction in semiconductors (R) . . 643

Gabathuler, E., with Stewart, D. T.: Electron collision cross sections in helium 473
Garton, G., with Boakes, D., Ryan, D., and Wolf, W. P.: Paramagnetic resonance of Yb^{3+} in yttrium gallium garnet (L) 663
Gaydon, A. G., with Spokes, G. N.: Flame spectra: effect of deuteration on hydrocarbon flame bands (R) 639
George, W. R., Sharples, R., and Thompson, J. E.: Sintering of bismuth telluride (R) 768
Gillett, C. M., with Woolley, J. C., and Evans, J. A.: Optical energy gap variation in GaSb–InSb system 244
Gilson, J. G.: Vacuum polarization due to charged bosons (R) 480
Gogate, D. V., and Desai, H. S.: Heat transfer by forced convection (R) . . 770
Goodman, C. H. L.: Bonding in cadmium telluride (L) 489
Green, T. S., with Niblett, G. B. F.: Radial hydromagnetic oscillations . . 737
Greenhow, J. S., and Neufeld, E. L.: Measurements of turbulence in upper atmosphere 1

Haines, M. G.: Inverse skin effect 576
Harper, P. G.: Electron–lattice interaction in metals 545
Harris, P. T., with Trainor, A.: Control of resistivity in pulled silicon crystals (L) 669
Harrison, E. R., and Thompson, W. B.: Low pressure plane symmetric discharge 145
Hawker, B. E., with Barry, J. F., Coleman, R. F., and Perkin, J. L.: Cross sections for some (n, pn) reactions with heavy nuclides 632
Head, A. K.: Aplanatic lenses 731
van den Heuvel, A. P., with Mason, B. J.: Properties and behaviour of some artificial ice nuclei 744
Hilsum, C.: Absorption edge of arsenic–sulphur–selenium mixtures (L) . . 667
Hilsum, C.: Properties of p-type indium antimonide. II: Photoelectric properties and carrier lifetime 81
Hinds, S., and Middleton, R.: Angular distribution of some proton groups from reaction ^{16}O (^{3}He, p) ^{18}F 762
Hinds, S., and Middleton, R.: Energy levels of ^{21}Ne (R) 779
Hinds, S., and Middleton, R.: Investigation of protons, deuterons and tritons from bombardment of ^{9}Be with 5·7 MeV ^{3}He 196
Hinds, S., and Middleton, R.: Some angular distribution measurements on reactions $^{16}O(^{3}He, d)^{17}F$ and $^{16}O(^{3}He, \alpha)^{15}O$ (R) 775
Hird, B., with Al-Jeboori, M. A., Bokhari, M. S., and Strazlkowski, A.: Polarization of protons elastically scattered from oxygen at 8·7 MeV 705
Honda, T., and Nagasaki, M.: Angular distribution of (d, p) stripping reactions 517
Howes, V. R.: Critical stress for production of pressure crack figures on diamond faces 48
Howes, V. R.: Observations on development of electroplating deposit structures on single crystals of copper 616

Ingram, D. J. E., with Doyle, W. T., and Smith, M. J. A.: Electron spin resonance of colloid centres in lithium hydride 540
Isaac, E. D.: Domain structures on thin sheets of magnetoplumbite (R) . . 786

Jakeways, R., and Rosser, W. G. V.: Decay of ^{147}Pm (R) 478
Jarmain, W. R., with Nicholls, R. W.: On *r*-centroids of molecular transitions, equilibrium internuclear separations and oscillator turning points (R) . . 133
Jones, D. A., Baker, J. M., and Pope, D. F. D.: Electron spin resonance of Gd^{3+} in lanthanum fluoride 249
Jones, D. P., with Cassels, J. M., Murphy, P. G., and O'Neill, P. L.: Neutral pions 92
Josephson, B., Jr., with Stevens, K. W. H.: Coupling of spin system to cavity mode 561

PAGE

Judd, B. R.: Matrix elements of tensor operators for the electronic configurations f^n 330

Kellermann, E. W., and Dickinson, N.: Structure of extensive cosmic ray air showers: Penetrating component 554
Kelly, F. M., and Tomchuk, E.: Isotope shift in CdI intercombination resonance line λ 3261 Å 689
Kuffel, E.: Electron attachment coefficients in oxygen, dry air, humid air and water vapour 297

Landsberg, P. T.: Entropy of non-equilibrium ideal quantum gas (R) . . . 486
Lee, J. A., Meaden, G. T., and Mendelssohn, K.: Low temperature resistivity of plutonium and neptunium (L) 671
Lee Sang Soo: Ageing effect in evaporated films of zinc sulphide (R) . . . 641
Lempicki, A.: Reflection spectrum of CdS (L) 138
Lindley, D. H., and Banbury, P. C.: Recombination relaxation effects in germanium surfaces 395
Llewellyn, J. P., with Finlayson, D. M., and Smith, T.: Magnetic susceptibility of iron ditelluride. Part II 75
Llewellyn, J. P., and Smith, T.: Magnetic susceptibility of iron ditelluride. Part I 65
Longhurst, R. S.: Diffraction by opaque strip . . . . . corr. 140
Lord, H., with Parker, R.: Electrical resistivity of oxygen deficient nickel ferrite (L) 793
Luszczynski, K., and Powles, J. G.: Proton magnetic resonance in liquid *iso*-butyl bromide 408

McDowell, M. R. C., and Peach, G.: Electron loss from fast negative ions of atomic hydrogen passing through atomic hydrogen 463
McIldowie, J. E. G., with Meads, R. E.: Decay of arsenic 80 693
Mackinnon, L., Myers, A., and Taylor, M. T.: Effect of direction of transverse magnetic field on electronic component of ultrasonic absorption in lead single crystal (R) 773
McNamee, J. M., with Butcher, A. C.: Scattering of alpha particles by helium 529
McWeeny, R., with Peacock, T. E.: Self-consistent calculation of graphite π band 385
Maissel, L. I.: Selective pressure broadening and Stark effect 97
Mandel, L.: Fluctuations of photon beams: Distribution of photo-electrons . 233
Mansfield, R.: Magnetic susceptibility of bismuth telluride 599
Marathay, A. S.: Geometrical optical calculation of frequency response for systems with coma 721
Martelli, G., with Dowell, J. D., Frisken, W. R., and Musgrave, B.: Proton–proton elastic interactions at 930 Mev 625
Mason, B. J., and van den Heuvel, A. P.: Properties and behaviour of some artificial ice nuclei 744
Mason, B. J., with Maybank, J.: Production of ice crystals by large adiabatic expansions of water vapour 11
May, R. M., and Schafroth, M. R.: Susceptibility of superconducting spheres 153
Maybank, J., and Mason, B. J.: Production of ice crystals by large adiabatic expansions of water vapour 11
Meaden, G. T., with Lee, J. A., and Mendelssohn, K.: Low temperature resistivity of plutonium and neptunium (L) 671
Meads, R. E., and McIldowie, J. E. G.: Decay of arsenic 80 693
Mendelssohn, K., with Lee, J. A., and Meaden, G. T.: Low temperature resistivity of plutonium and neptunium (L) 671
Middleton, R., with Hinds, S.: Angular distribution of some proton groups from reaction $^{16}O(^3He, p)^{18}F$ 762
Middleton, R., with Hinds, S.: Energy levels of ^{21}Ne (R) 779
Middleton, R., with Hinds, S.: Investigation of protons, deuterons and tritons from bombardment of ^9Be with 5·7 Mev ^3He 196

PAGE

Middleton, R., with Hinds, S.: Some angular distribution measurements on the reactions $^{16}O(^{3}He, d)^{17}F$ and $^{16}O(^{3}He, \alpha)^{15}O$ (R) 775
Miller, C. A., with Champeney, D. C.: Measurements of atomic velocity distributions in Hg and HgO by nuclear resonant scattering of gamma rays . . 680
Moiseiwitsch, B. L., with Ferguson, A. F.: Double charge transfer and mobility of He^{2+} ions in helium 457
Moss, T. S.: Extent of ionic binding in cadmium telluride (L) 490
Moss, T. S., and Walton, A. K.: Determination of effective electron mass in GaAs by infra-red Faraday effect (R) 131
Moussa, A. H.: Effect of polarization on elastic scattering of positrons by hydrogen atoms 101
Murphy, P. G., with Cassels, J. M., Jones, D. P., and O'Neill, P. L.: Neutral pions 92
Musgrave, B., with Dowell, J. D., Frisken, W. R., and Martelli, G.: Proton–proton elastic interactions at 930 MeV 625
Myers, A., with Mackinnon, L., and Taylor, M. T.: Effect of direction of transverse magnetic field on electronic component of ultrasonic absorption in lead single crystal (R) 773

Nagasaki, M., with Honda, T.: Angular distribution of (d, p) stripping reactions 517
Neufeld, E. L., with Greenhow, J. S.: Measurements of turbulence in upper atmosphere 1
Newmann, M. M., and Stevens, K. W. H.: Magnetic susceptibilities of iron–chromium alloys 290
Niblett, G. B. F., and Green, T. S.: Radial hydromagnetic oscillations . . . 737
Nicholls, R. W., and Jarmain, W. R.: r-centroids of molecular transitions, equilibrium internuclear separations and oscillator turning points (R) . . . 133
Nicholls, R. W., Reeves, E. M., and Bromley, D. A.: Excitation of N_2 and O_2 by 1/2 and 1 MeV protons 87
Northrop, D. C.: Conduction processes in condensed aromatic hydrocarbons . 756
Nunn, M., and Wynne, C. G.: Lens designing by electronic digital computer: II 316

O'Connor, L. P., with Barry, J. F., and Perkin, J. L.: Radiative capture cross section of ^{232}Th for neutrons in the energy range 300 to 1200 kev . . 685
O'Neill, P. L., with Cassels, J. M., Jones, D. P., and Murphy, P. G.: Neutral pions 92

Palmer, R. B. J., and Simons, H. A. B.: Experimental determination of range–energy relations for alpha particles in water and water vapour, and stopping power of water and water vapour for alpha particles at energies below 8·78 MeV . 585
Park, J. G.: Principal g values of ytterbium ions in yttrium acetate, a triclinic crystal 513
Parker, R., and Lord, H.: Electrical resistivity of oxygen deficient nickel ferrite (L) 793
Peach, G., with McDowell, M. R., C.: Electron loss from fast negative ions of atomic hydrogen passing through atomic hydrogen 463
Peacock, T. E., and McWeeny, R.: Self-consistent calculation of graphite π band 385
Pearson, R. F.: Magnetocrystalline anisotropy of cobalt-substituted manganese ferrite 505
Peetz, C. V., with Ellison, J. McK.: Forward scattering of light by spheres according to geometrical optics 105
Perkin, J. L., with Barry, J. F., Coleman, R. F., and Hawker, B. E.: Cross sections for some (n, pn) reactions with heavy nuclides 632
Perkin, J. L., with Barry, J. F., and O'Connor, L. P.: Radiative capture cross section of ^{232}Th for neutrons in energy range 300 to 1200 kev 685
Phillips, K., and Allen, K. R.: Scattering of fast charged particles: V—Multiple scattering of fast electrons and positrons in xenon 257
Phillips, K., and Ambasankaran, C.: Scattering of fast charged particles: VI—Multiple scattering of 10 MeV electrons and positrons in nuclear emulsions (R) 655
Phillips, N. J.: Current sheet in gas discharge 700
Phillips, R. J. N.: Nucleon polarization from charge-exchange reactions in deuterium (R) 652

PAGE

Pope, D. F. D., with Jones, D. A., and Baker, J. M.: Electron spin resonance of Gd^{3+} in lanthanum fluoride 249
Powles, J. G., with Luszczynski, K.: Proton magnetic resonance in liquid *iso*-butyl bromide 408
Prasad, A. N.: Measurement of ionization and attachment coefficients in dry air in uniform fields and the mechanism of breakdown 33
Prentice, J. D., Bellamy, E. H., and Williams, W. S. C.: Spin of the neutral pion 124

Raal, F. A.: Strong absorption system in type I diamonds (R) 647
Reeves, E. M., with Nicholls, R. W., and Bromley, D. A.: Excitation of N_2 and O_2 by 1/2 and 1 Mev protons 87
Rogers, G. L.: Simple method of calculating Moiré patterns . . . corr. 795
Roman, P.: Decomposition of 3×3 matrices (R) 649
Roman, P.: Scalar representation of electromagnetic fields: III 281
Rosen, S. P.: Electron coincidence spectrum in double beta decay 350
Rosser, W. G. V., with Jakeways, R.: Decay of ^{147}Pm (R) 478
Ryan, D., with Boakes, D., Garton, G., and Wolf, W. P.: Paramagnetic resonance of Yb^{3+} in yttrium gallium garnet (L) 663

Sansom, D. J., with Bates, L. F.: Megnetothermal effects in iron and silicon–iron 53
Schafroth, M. R., with May, R. M.: Susceptibility of superconducting spheres 153
Searl, J. W., Smith, R. C., and Wyard, S. J.: Electron spin resonance for polycrystalline substances (L) 491
Series, G. W., with Dodd, J. N., Fox, W. N., and Taylor, M. J.: Light beats as indicators of structure in atomic energy levels (L) 789
Sewell, G. L.: Meissner effect, gauge invariance and electron correlations . . 340
Sewell, G. L., with Fröhlich, H.: Electric conduction in semiconductors (R) . 643
Sharples, R., with George, W. R., and Thompson, J. E.: Sintering of bismuth telluride (R) 768
Simons, H. A. B., with Palmer, R. B. J.: Experimental determination of range–energy relations for alpha particles in water and water vapour, and stopping power of water and water vapour for alpha particles at energies below 8·78 Mev 585
Singh, Chater: Noise spectra of probe in hot-cathode discharge 42
Smith, M. J. A., with Doyle, W. T., and Ingram, D. J. E.: Electron spin resonance of colloid centres in lithium hydride 540
Smith, R. C., with Searl, J. W., and Wyard, S. J.: Electron spin resonance for polycrystalline substances (L) 491
Smith, T., with Finlayson, D. M., and Llewellyn, J. P.: Magnetic susceptibility of iron ditelluride. Part II 75
Smith, T., with Llewellyn, J. P.: Magnetic susceptibility of iron ditelluride. Part I 65
Somerville, J. M.: Method of generating pairs of millimicrosecond current pulses separated by variable interval (R) 378
Somerville, J. M., and Williams, J. F.: Early stages of spark channel expansion 309
Spokes, G. N., and Gaydon, A. G.: Flame spectra: effect of deuteration on hydrocarbon flame bands (R) 639
Spreadborough, J., and Christian, J. W.: Measurement of lattice expansions and Debye temperatures of titanium and silver by X-ray methods 609
Srivastava, G. P.: Absorption of microwaves in ethyl chloride 401
Stevens, K. W. H., and Josephson, B., Jr.: Coupling of spin system to cavity mode 561
Stevens, K. W. H., with Newmann, M. M.: Magnetic susceptibilities of iron–chromium alloys 290
Stewart, D. T., and Gabathuler, E.: Electron collision cross sections in helium . 473
Stone, A. P.: Interpretation of isotope shifts in rare gases 424
Strzałkowski, A., with Al-Jeboori, M. A., Bokhari, M. S., and Hird, B.: Polarization of protons elastically scattered from oxygen at 8·7 Mev 705

Taylor, M. J., with Dodd, J. N., Fox, W. N., and Series, G. W.: Light beats as indicators of structure in atomic energy levels (L) 789

PAGE

Taylor, M. T., with Mackinnon, L., and Myers, A.: Effect of direction of transverse magnetic field on electronic component of ultrasonic absorption in lead single crystal (R) 773
Telegdi, V. L., and Winston, R.: Comments on Faragó's treatment of spin precession in crossed magnetic and electric fields (R) 782
Temperley, H. N. V.: Application of Mayer method to melting problem . . 183
Temperley, H. N. V.: Asymptotic behaviour of Mayer cluster series in antiferromagnetic problem 432
Temperley, H. N. V.: Can ' lattice ' model of gas describe both liquefaction and solidification? 444
Thomas, D. K., and Baker, T. W.: X-ray study of factors causing variation in heats of solution of magnesium oxide 673
Thompson, J. E., with George, W. R., and Sharples, R.: Sintering of bismuth telluride (R) 768
Thompson, W. B., with Harrison, E. R.: Low pressure plane symmetric discharge . 145
Tomchuk, E., with Kelly, F. M.: Isotope shift in CdI intercombination resonance line λ 3261 Å 689
Trainor, A., and Harris, P. T.: Control of resistivity in pulled silicon crystals (L) 669

Walling, J. C., and Bunn, P. B.: Electronic specific heats of some nickel–cobalt alloys 417
Walton, A. K., with Moss, T. S.: Determination of effective electron mass in GaAs by infra-red Faraday effect (R) 131
Willardson, R. K., with Bate, R. T.: Hall coefficient and magnetoresistance in semiconducting diamond 363
Williams, J. F., with Somerville, J. M.: Early stages of spark channel expansion 309
Williams, W. S. C., with Prentice, J. D., and Bellamy, E. H.: Spin of neutral pion 124
Winston, R., with Telegdi, V. L.: Comments on Faragó's treatment of spin precession in crossed magnetic and electric fields (R) 782
Wolf, E.: Scalar representation of electromagnetic fields: II 269
Wolf, W. P.: Magnetic properties of rare earth ions in garnets (L) 665
Wolf, W. P., with Boakes, D., Garton, G., and Ryan, D.: Paramagnetic resonance of Yb^{3+} in yttrium gallium garnet (L) 663
Wolf, W. P., with Cooke, A. H., Edmonds, D. T., and Finn, C. B. P.: Dipolar ferromagnetism in dysprosium ethyl sulphate (L) 791
Woolley, J. C., Evans, J. A., and Gillett, C. M.: Optical energy gap variation in GaSb–InSb system 244
Wyard, S. J., with Searl, J. W., and Smith R. C.: Electron spin resonance for polycrystalline substances (L) 491
Wynne, C. G., with Nunn, M.: Lens designing by electronic digital computer: II 316

Yates, M. J. L., with Allen, K. W., and Eccleshall, D.: 1·12 Mev level in ^{18}F (R) . 660

INDEX TO REVIEWS OF BOOKS

PAGE

Allen, James S.: *The neutrino* 224
Atkins, K. R.: *Liquid helium* 223

Bell, C. G., and Hayes, F. N.: *Liquid scintillation counting* 225
Bers, L.: *Mathematical aspects of subsonic and transonic gas dynamics* 495
Blanc-Lapierre, A., Casal, P., and Tortrat, A.: *Méthodes mathématiques de la mécanique statistique* 144
Bowden, F. P., and Yoffe, A. D.: *Fast reactions in solids* 381
Brosze, O: *Leitfaden zur Berechnung von Schallvorgängen* 381

Centre National de la Recherche Scientifique: *Colloque National de Magnétisme* (commémoratif de l'oeuvre de Pierre Weiss) 220
Cox, D. R.: *Planning of experiments* 228
Cusack, N.: *The electrical and magnetic properties of solids* 229

Dekker, A. J.: *Solid state physics* 219
Delcroix, J. L.: *Introduction à la théorie des gaz ionisés* 222
Doremus, R. H., Roberts, B. N., and Turnbull, D., (Eds): *The growth and perfection of crystals* 796

Endt, P. M., and Demeur, M., (Eds): *Nuclear reactions* 496

Fano, U., and Fano, L.: *Basic physics of atoms and molecules* 796
Finkelnburg, W.: *Einführung in die Atomphysik* 143
Flügge, S., (Ed.): *Handbuch der Physik.* Vol. 7/2. *Kristallphysik* II . . . 141
Flügge, S., (Ed.): *Handbuch der Physik.* Vol. 26. *Light and matter* II . . 141
Flügge, S., (Ed.): *Handbuch der Physik.* Vol. 38/1. *External properties of atomic nuclei* 219
Flügge, S., (Ed.): *Handbuch der Physik.* Vol. 51. Astrophysics II: *Stellar* structure 232
French, A. P.: *Principles of modern physics* 221

Galbraith, W.: *Extensive air showers* 797
Goodier, J. N., and Hodge, P. G., Jr.: *Elasticity and plasticity* (Surveys in applied mathematics, Vol. I) 225
Grivet, P., and Blaquiere, A.: *Le bruit de fond* 223

Hughes, D. J., Sanders, J. E., and Horowitz, J., (Eds): *Progress in nuclear energy: Physics and mathematics*, Vol. 2 798

Institute of Metals: Monograph and Report Series No. 23: *Vacancies and other point defects in metals and alloys* 227

Jackson, J. D.: *The physics of elementary particles, investigations in physics* No. 9 799
Joos, Georg: *Theoretical physics* (3rd Edn) 384
Jury, E. I.: *Sampled-data control systems* 224

Kothari, D. S.: *Nuclear explosions and their effects* 672

Landau, L. D., and Lifshitz, E. M.: *Quantum mechanics* (*Non-relativistic theory*) . 142
Lawson, W. D., and Nielsen, S.: *Preparation of single crystals* 144
Lehnert, B. (Ed.): *Electromagnetic phenomena in cosmical physics: Report of symposium No. 6 of the International Astronomical Union* 494
Lipson, H., and Taylor, C. A.: *Fourier transforms and x-ray diffraction* . . 494

PAGE

Massey, H. S. W., and Kestelman, H.: *Ancillary mathematics* 671
McConnell, J.: *Quantum particle dynamics* 227

Nijgh, G. J., Wapstra, A. H., and Van Lieshout, R.: *Nuclear spectroscopy tables* . 226

O'Connell, D. J. K.: *The green flash and other low sun phenomena* 226

Powell, L. S.: *Physics.* Vol. I. *Mechanics, heat and sound.* Vol. II. *Electricity and magnetism.* Vol. III. *Light* 221
Popper, K. : *The logic of scientific discovery* 230

Ratcliffe, J. A.: *The magneto-ionic theory and its applications to the ionosphere* . 228
Raynor, G. V.: *The physical metallurgy of magnesium and its alloys* 796
Rhodes, Donald R.: *Introduction to monopulse* 800

Segrè, E., (Ed.): *Annual review of nuclear science.* Vol. 8 230
Sandorfy, C.: *Les spectres electroniques en chimie theorique* 496
Smullin, L. D., and Haus, H. A., (Eds): *Noise in electron devices* 800

Treloar, L. R. G.: *The physics of rubber elasticity* (2nd Edn) 380

Weinberg, A. M., and Wigner, E. P.: *The physical theory of neutron chain reactors* . 382
White, G. K. : *Experimental techniques in low temperature physics* 382
Whitrow, G. J.: *The structure and evolution of the universe* 384

Printed in England
Taylor & Francis, Ltd., Red Lion Court, Fleet Street, London, E.C.4

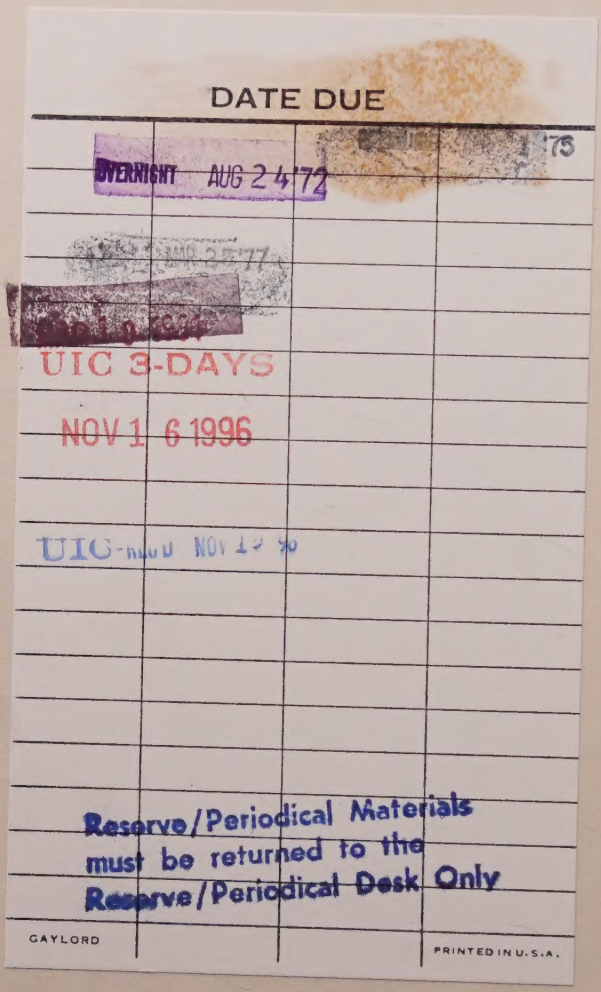
DATE DUE
OVERNIGHT AUG 24 '72
UIC 3-DAYS
NOV 1 6 1996
Reserve/Periodical Materials
must be returned to the
Reserve/Periodical Desk Only
GAYLORD
PRINTED IN U.S.A.

THE UNIVERSITY OF ILLINOIS AT CHICAGO
3 8198 314 312 578